19th
2 Days International Conference

on

"Hydraulics, Water Resources, Coastal and Environmental Engineering(HYDRO 2014 International)"
December 18-20, 2014

Organized by
Department of Civil Engineering, MANIT Bhopal
Maulana Azad National Institute of Technology Bhopal
(Madhya Pradesh) India Pin -462051
Web : www.manit.ac.in

In association with

1. International journal of scientific engineering and Technology (ISSN : 2277-1581)

Website : www.ijset.com and email : editor@ijset.com

2. International journal of Engineering Research ISSN:2319-6890)(online),2347-5013(print)
Website : www.ijer.in and email : editor@ijer.in

Indexing of journals : google scholar, Index Copernicus, DOAJ, endnote, OALIB and many more

Editorial Board

Computation of Combined Discharge of Centrifugal Pumps in Series And Parallel Connections

Deepak Singh[1], Vishwas Mahara[2] and Arkaja[3]
1 & 3. M. Tech. students, Civil Engg. Deptt., College of Technology, GBPUA&T Pantnagar, 263145, Distt. Udham Singh Nagar (Uttarakhand), India Email:
kumaindeepaksingh@gmail.com & arkajakandari@gmail.com
2nd. M. Tech. students, Mechanical Engineering. Deptt., Thapar University, Patiala (Punjab), India
Email: vishwas.mhra.89@gmail.com

ABSTRACT: *Centrifugal pumps are employed to pump water for irrigation and water supply. In general, single stage centrifugal pumps have limitations to meet the pressure and discharge requirements of systems. The pumps are connected in series to meet the higher pressure head requirements and in parallel for higher discharge. When identical pumps are connected in series the discharge remains same while pressure head is multiplied with number of stages. Similarly for parallel connections of the identical pumps the head remains same whereas discharge is multiplied by number of stages. While selecting operating conditions of discharge and pressure, it is important to run the pump at its higher efficiency. Normally, the characteristics of centrifugal pumps and system head curves are graphically plotted to select the operating conditions for the pump. This may be a tedious process and time consuming. In this paper, mathematical equations have been developed to compute the combined discharge of centrifugal pumps connected in series and parallel to meet the system head requirements. The performance data of the centrifugal pumps relating discharge, head and power were used to develop the characteristic curves' equations of the identical pumps connected in series or parallel. The system head curve equations were developed by considering the elevation difference between the source and the delivery point, the frictional head loss and velocity head for a particular pipe size. Mathematical equations for combined discharge were derived by equating the nonlinear equations of the characteristic curves and the system head curves. The constants of the equations representing characteristic curves and system head curves were obtained by curve fitting in EXCEL software. The combined discharge can be easily computed by substituting the values of the constants in the developed equations. The applicability of the developed equations is illustrated with the help of example problems. The method will be quite useful for field engineers working in irrigation and water supply departments.*
Keyword: Centrifugal pump, Characteristic curves, system head curve, pump connection in series and parallel.

1. INTRODUCTION

A waterworks pumping station can be located according to the positions of source of water and the delivery point. The pumping station may be equipped with a number of centrifugal pumps to provide certain head to meet demand of flow rate for water

supply or irrigation (Garg, 2008). The pumps can be placed below or above the level of water of the source. A single stage centrifugal pump may have limitations to meet the requirements of either the pressure or discharge or both. To meet the requirements of higher pressure head and discharge, the pumps are connected in series and in parallel, respectively. Two or more number of identical pumps connected in series deliver the same discharge as delivered by a single pump, whereas the pressure head is increased to the pressure head of a single pump multiplied by number of pumps. In series connection of centrifugal pumps, the discharge of the first pump enters the suction of the second pump and the discharge of the second pump enters the suction of the third pump and so on. In parallel connection of centrifugal pumps, the discharge is multiplied by number of parallel connections of the identical pumps and the head is equal to that of a single pump (Church and Lal 1973).

The manufacturers of the pumps normally supply the test results of the pumps that can be used to prepare the characteristic curves of the pumps. The characteristic curves are obtained by combined plotting of pressure head, efficiency and power on vertical axis against the discharge of the pump on horizontal axis. Depending on the pipe size and length, elevation difference between source of water and the delivery point, the system head curve is prepared. The system head curve is superimposed on the characteristic curve, to determine its intersection with the head-discharge curve of the pump as operating point of the pump. This graphical procedure may be tedious and time consuming especially when characteristic curves are to be prepared for pumps connected in series and parallel based on the characteristic curves of a single pump. In this paper, mathematical equations have been developed to compute the combined discharge of centrifugal pumps connected in series and parallel to meet the system head requirements.

2. METHODOLOGY

The frictional head loss in a pipeline can be computed by Darcy-Weisbach equation as:

$$h_f = f L \frac{v^2}{2gd} \qquad (1)$$

Where h_f is loss of head due to friction in pipe line in (m); f is the friction co-efficient; L is the length of pipe line (m); v is the mean velocity of flow in pipeline (m/s); d is the diameter of pipeline; g is the acceleration due to gravity in (m/s^2)
This equation can be written in discharge form as:

$$hf = k \frac{L Q^2}{d^5} \qquad (2)$$

Where, Q is discharge in pipe line (L/s). The value of k can be calculated as:

$$k = 8 \times 10^{-6} \times \frac{f}{g\pi^2} \qquad (3)$$

2.1 System Head Curve: Neglecting velocity head the system head curve can be represented as (Lal .J.):

$$H = h + h_f \qquad (4)$$

Where h is the static head. Substituting the value of h_f from equation 2 in to equation 4 it can be written as:

$$H = h + \frac{k L Q^2}{d^5} \qquad (5)$$

2.2 Pump Characteristic Curve: Pump has a definite head-discharge relationship known as pump characteristic curve that can be represented as (Mahar and Singh, 2014):

$$H = AQ^2 + BQ + C \qquad (6)$$

Where A, B and C are the constant. For a single stage centrifugal pump, the operating point in terms of discharge can be determined by equating equation 5 and equation 6 as:

$$AQ^2 + BQ + C = h + \frac{kLQ^2}{d^5} \qquad (7)$$

Rearranging above equation:

$$aQ^2 + bQ + c = 0 \qquad (8)$$

Where a, b and c are the constants and their values can be determined as:

$$a = \frac{KL}{d^5} - A \qquad (9)$$

$$b = -B \qquad (10)$$

$$c = h - C \qquad (11)$$

The value of Q from equation 8 can be found as:

$$Q = \frac{-b \pm \sqrt{(b^2 - 4ac)}}{2a} \qquad (12)$$

2.3 Two Pumps Connected in Series

When two identical pumps are connected in series, the characteristic curve will be changed by doubling the head for each discharge point on the X-axis. Since the system head curve remains the same for the pumps connected in series, the combined characteristic curve for two pumps in series can be equated as:

$$A_1 Q^2 + B_1 Q + C_1 = h + \frac{kLQ^2}{d^5} \qquad (13)$$

Where A_1, B_1 and C_1 are constants for the combined characteristic curve and their values are equal to twice the values of A, B and C, respectively.
After rearranging above equation:

$$a_1 Q^2 + b_1 Q + c_1 = 0 \qquad (14)$$

Where the values of a_1, b_1 and c_1 can be calculated as:

$$a_1 = \frac{kL}{d^5} - A_1 \qquad (15)$$

$$b_1 = -B_1 \qquad (16)$$

$$c_1 = h - C_1 \qquad (17)$$

The value of Q from equation 14 can be found as:

$$Q = \frac{-b_1 \pm \sqrt{(b_1^2 - 4a_1 c_1)}}{2a_1} \qquad (18)$$

2.4 Two Pumps Connected in Parallel

When two identical pumps are connected in parallel, the characteristic curve will be changed by doubling the discharge for each head point on the Y-axis. Since the system head curve remains the same for the pumps connected in parallel, the combined characteristic curve for two pumps in parallel can be equated as:

$$A_2 Q^2 + B_2 Q + C_2 = h + \frac{kL}{d^5} Q^2 \qquad (19)$$

Where A_2, B_2 and C_2 are constants for the combined characteristic curve and their values can be obtained by plotting the values graphically. After rearranging above equation:

$$a_2 Q^2 + b_2 Q + c_2 = 0 \qquad (20)$$

Where the values of a_2, b_2 and c_2 can be calculated as:

$$a_2 = \frac{kL}{d^5} - A_2 \qquad (21)$$

$$b_2 = -B_2 \qquad (22)$$

$$c_2 = h - C_2 \qquad (23)$$

The value of Q from equation 20 can be found as:

$$Q = \frac{-b_2 \pm \sqrt{(b_2^2 - 4a_2 c_2)}}{2a_2} \qquad (24)$$

3. DESIGN EXAMPLE AND DISCUSSION

The applicability of the developed methodology is demonstrated with the help of an example. The data related to the example are taken from Jain (200…).

3.1 Example

A centrifugal pump has the discharge and head data as given in Table 1. It is required to deliver water through a 500 m long, 15 mm diameter pipeline having a friction factor equal to 0.025. The static lift is 15 m. Neglecting minor losses, determine the discharge flowing through the pipeline when two pumps are connected in series and in parallel at the operating point of the pumps.

Table1. Head-Discharge data for a centrifugal pump

Discharge(L/s)	0	10	20	30	40	50
Head (m)	25.3	25.5	24.5	22.2	18.7	12.0

3.2 SOLUTION

The system head curve was obtained by using the given data in equation 5 as:

$$H = 15 + 0.002066 \times 10^{-6} \frac{L}{d^5} Q^2 \tag{25}$$

The constants of pump characteristic curve represented by equation 6 were obtained by using given data in EXCEL as $A = -0.007$, $B = 0.142$ and $C = 25.08$. The values of constants in equation 8 were obtained as: $a = 0.0206$, $b = -0.142$ and $c = -10.08$. Using these values in equation 12, the value of discharge for the single pump was obtained as 25.83 L/s.

3.2.1 Series Connection

When two identical pumps were connected in series, the values of constants A_1, B_1 and C_1 were obtained as -0.015, 0.284 and 50.16, respectively. The values of constants a_1, b_1 and c_1 were obtained as 0.0286, -0.284 and -35.16, respectively. Using these values in equation 18, the combined discharge was obtained as 40.38 L/s. The values of discharge for single stage and two stages were also obtained graphically using EXCEL as shown in Figure1. It can be seen from Figure1 that the values of discharge for the two cases are same as obtained by using equations 12 and 18, respectively. This verifies the accuracy of the developed equations.
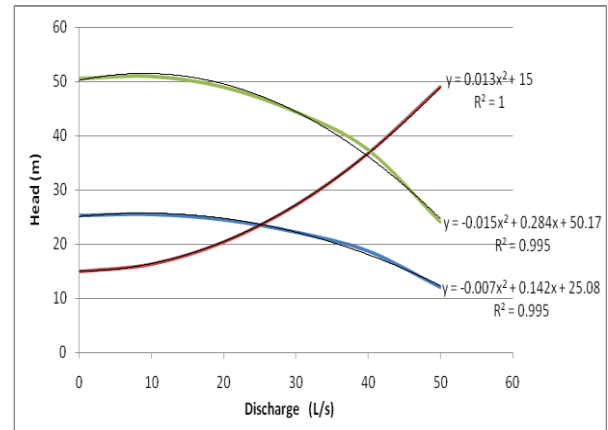
Figure1. Graphical solution for centrifugal pumps connected in series.

3.2.2 Parallel Connection

When two identical pumps were connected in parallel, the values of constants A_2, B_2 and C_2 were obtained as -0.002, 0.071 and 25.08, respectively. The values of constants a_2, b_2 and c_2 were obtained as 0.0156, -0.071 and -10.08, respectively. Using these values in equation 24, the combined discharge was obtained as 27.80 L/s. The value of discharge for two pumps connected in parallel was also obtained graphically using EXCEL as shown in Figure2. It can be seen from Figure2 that the value of discharge for this case is the same as obtained by using equations 24. This further establishes the accuracy of the developed equations.
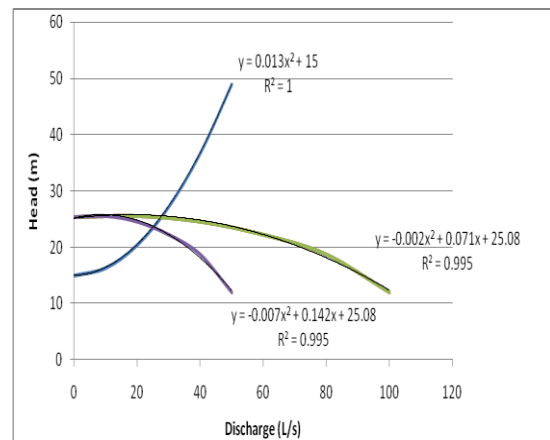
Figure 2. Graphical solution for centrifugal pumps connected in parallel.

4. CONCLUSIONS

Mathematical equations have been developed for determining the discharge of two identical centrifugal pumps connected in series and in parallel for pumping water from a source to a delivery point through a pipeline. The equations can be easily used for given data related to pump performance and pipeline. The developed methodology will be helpful to field engineers working in water supply and irrigation departments.

REFERENCES

i.   Church, A. H. and Lal, J. (1973). Centrifugal pumps and blowers. Metropolitan Book Co. Pvt. Ltd. Delhi -6, India.
ii. Garg, S.K. (2008) Water Supply Engineering, Khanna Publishers, New Delhi.
iii. Jain, A.K.(2007) Fluid Mechanics and Hydraulic Machines, Khanna Publishers, New Delhi.
iv. Lal, Jagdish (1995) Hydraulic Machines Metroplitan Book Co. Private Ltd. publishers, New Delhi-110002
v.   Mahar, P. S. and Singh, R. P. (2014). "Optimal design of pumping mains considering pump characteristics". Journal of Pipeline Systems Engineering and Practice, Vol. 5 (1) p.p. 04013010-1,6.

A Gis Based Groundwater Vulnerability Assessment Of Contamination Using Drastic Model

Manish Kumar Sinha[1], Vivek Verma[2], Dr. M. K. Verma[3]

[1]P.G. Research Scholar, Department of Civil Engineering, NIT Raipur 492010, Chhattisgarh, India.
Email: manishsinha200389@gmail.com.
[2]B. Tech. Scholar, Department of Civil Engineering, SSIPMT Raipur 492015, Chhattisgarh, India.
Email: vivekverma10@gmail.com.
[3]Professor, Department of Civil Engineering, NIT Raipur 492010, Chhattisgarh, India.
Email: mkseem670@gmail.com.

ABSTRACT: *Geographic information system (GIS) emerges as one of the leading tools in the field of hydrogeological science that helps in assessing, monitoring, analysing and conserving groundwater resources. Groundwater is a finite resource, which is being overexploited due to increase in demand over the years leading to decrease in its potentiality. In the present study, DRASTIC model has been used to prepare groundwater vulnerable zone in Kharun sub basin; which is a major tributary of Seonath River situated in Chhattisgarh state. The main objective is to determine susceptible zone for groundwater pollution by integrating hydrogeological layers in GIS environment. The final output of the map shows that the DRASTIC Index value varies from 65 to 151, depending on the equal index value interval the zones is divided in four classes. Around 82% of the area falls under low and moderate risk of pollution zone. This study produces a very comprehensive indication of vulnerability to groundwater contamination. The knowledge about high vulnerable zone is important for local authorities to manage and monitor groundwater resources in Kharun sub basin.*

Key words:Aquifer, DRASTIC Index, vulnerability, groundwater, Geographic Information System.

1.   INTRODUCTION

Groundwater is a natural resource in most countries, particularly for those in arid and semi-arid areas, due to its relatively low susceptibility to pollution in comparison to surface water (Jamrah et al., 2008). It is the major source of freshwater available for all socioeconomic development. But the existence of groundwater is under great stress of degradation both in quality and quantity. Due to increase in population, lack of awareness among the people, and improper management of this valuable resource lead to depletion in potential and deterioration of the quality. Therefore, it is very important to have proper understanding of the aquifer system and hydrogeological setting of the area for development and safe exploitation of groundwater.The quality of groundwater plays an important role in the scarcity problem. So, it has to be protected from the increasing threat of subsurface contamination.Furthermore, the quality of groundwater is generally under a considerable potential of contamination especially in agriculture as well as urban areas with intense activities that involve the use of fertilizers and pesticides (Lake et al., 2003; Thapinta and Hudak, 2003; Chae et al., 2004). This necessitates for a definite strategy and guidelines which would focus on specific part of a groundwater management, i.e. the protection of groundwater from contamination. Thus groundwater quality monitoring becomes necessary for proper assessment and management of groundwater. Keeping in view of above facts a study on groundwater vulnerability has been made in present paper.

1.1 DRASTIC Model

The DRASTIC method was developed as a means of creating an index to rank sites (area) in terms of their vulnerability to contamination. The aim of this study is to prepare groundwater vulnerability map. The DRASTIC model consists of seven hydrogeological parameters which help in defining groundwater regime and its vulnerability towards pollution. The seven thematic parameters are **D**epth to aquifer,Net **R**echarge,**A**quifer media,**S**oil media,**T**opography (Slope),**I**mpact of vadose zone, andHydraulic **C**onductivityof an aquifer generated in the GIS environment. Each parameter has been assigned different weight and rating value on its relative behaviour towards groundwater pollution and its rating value varies from 1 to 10 (Aller et al., 1987). The DRASTIC Index is computed by summation of the products of rating and weights of each factor as follows:

$$\text{DRASTIC Index} = \sum_{i=1}^{7} (W_i \times R_i)$$

$$= D_r.D_w + R_r.R_w + A_r.A_w + S_r.S_w + T_r.T_w + I_r.I_w + C_r.C_w$$

Where,
W = Weight of parameter
R = Rating of each parameter
It has been evaluated with respect to the others for determine the relative significance of each range with respect to pollution potential.The DRASTIC method assumes that:
i)   Any contaminant is introduced at the ground surface;
ii)   The contaminant is flushed into the groundwater by precipitation;
iii)   The contaminant has the mobility of water.

The use of DRASTIC model was first started in France towards the end of the 1960s to develop awareness of groundwater contamination. The objective of this model is to delineate the zones which are more prone to contamination from anthropogenic activity. It was developed by the US Environmental Protection Agency for the entire USA (Aller et al., 1987). Many researchers have used this concept in the field of groundwater for assessing aquifer vulnerability, Evans and Mayers, 1990; Kim and Hamm, 1999; Rupert, 2001; Al-Adamat et al., 2003; Babikeri et al., 2005; Rahman, 2007; Xiaahu Wen et al., 2008; Chitsazan et al., 2009.

2.   STUDY AREA

The area under study, i.e. Kharun river basin, is bounded with Chhattisgarh Plain province in Chhattisgarh region. Kharun river originated near petechua village with its latitude 20°33'30" N to 21°33'38" N and longitude 81°17'51" E to 81°55'25" E. Kharun river basin has total area of 4191sq.km., the basin is covered by 13 topographic sheets of survey ofIndia. Kharun river basin is bounded by three districts of the Chhattisgarh. The major part of the basin is contributed byDurg district, some part of the basin is in Dhamtari, and Raipur district. The average annual rainfall over the basin is 1400mm. The monsoon brings over 80% of the annual rainfall between the months of June to October, with the highest precipitation occurring in July & August. Groundwater is the major source for all purposes and is being exploited mainly through dug wells & bore wells under moderate & shallow depth for drinking & irrigation purposes.

3.   DATA USED AND METHODOLOGY

A number of published map and reports were used for the purpose of thematic layers generation as input. Table 1 shows the type of data along with details and sources of data to be procured. The methodology adopted for the present study is shown in Figure 2.

*Preparation of Geo-spatial database:*This work begins with creation of a database for the quantitative evaluation of vulnerability, including: topography, geology, and hydrology data. GIS is used to convert these maps to raster files. The conversion consists in the fragmentation of a map into a series of pixels with defined size (100m.×100m.). A numerical value is attributed to each pixel. The resulting grid corresponds to support the seven DRASTIC parameters. Thus, the vulnerability is calculated for each pixel implicating a high resolution. The

GIS is also used to generate the groundwater vulnerability map by overlaying the seven thematic maps. Figure 2 summarizes the GIS preprocessing and manipulation techniques used to create the seven input data layers for the DRASTIC index.
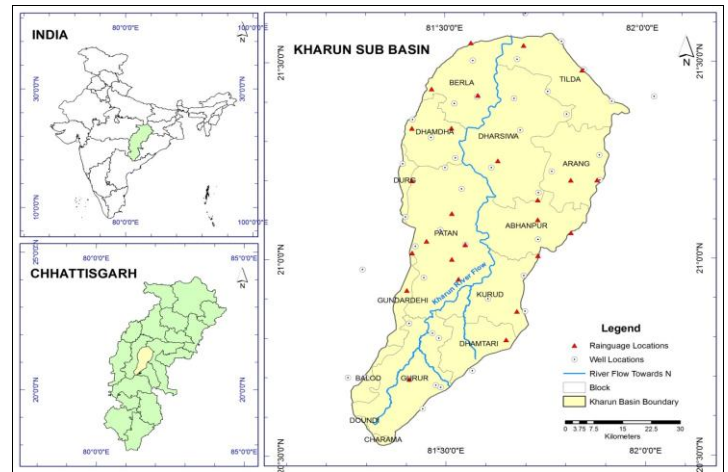
Figure 1: Location map of Kharun sub Basin (Study Area)

Table 1: Data used for layer generation of DRASTIC parameter

S.No.	Data	Details & Duration	Sources
1.	Topographic sheets (Base map preparation)	[64G - 6, 7, 8, 10, 11, 12, 14, 15, 16 & 64H - 5, 6, 7, 10] in the scale 1:50,000	Survey of India, Raipur.
2.	Bore well Data (Water Table)	7 Years from (2006-2012)	WRD, Raipur, Chhattisgarh.
3.	Recharge Data	Average of 7 Years (Water Level Fluctuation method based)	CGWB, Raipur.
4.	Aquifer Data	(District Resource Map) and Pumping test Data	Chhattisgarh Council of Science and Technology
5.	Soil Map	(District Planning Map Series) In the scale 1:2,50,000	Chhattisgarh Council of Science and Technology
6.	Water Quality Data	(2010-2012)	Chhattisgarh Council of Science and Technology

*Depth to water table:*Depth of water table is one of the most important factors because it determines the thickness of material through which infiltrating water travel before reaching the aquifer. Instead of considering pre-monsoon and post-monsoon season's data separately the mean value of the water table is used. These point data were interpolated using IDW (Inverse Distance weight) method in ArcGIS® 9.2 software and divided into four classes which areshown in Figure 3(a). Thereafter, the converted raster data is use for further weighting and rating operation. The depth of water table interval range, DRASTIC rating, weight, and resulting index are shown in Table 2. Areas with high water tables are vulnerable because pollutants have short distances to travel before contacting the groundwater. So, the deeper the groundwater smaller the rating value.

*Net Recharge:*Groundwater table get recharged by two sources; firstly the rain water and secondly by other sources like seepage from water bearing structures etc. Though the major contribution comes from rain water, whichis utilized partly in filling the soil moisture deficiency and part of it is percolated down reaching the water table. This phenomenon of water reaching the water table is known as the recharging of aquifer by rainfall water. Net recharge map is shown in Figure 3(b).

*Aquifer media:*The aquifer media refers to the consolidated and unconsolidated rock, which serves as a storage of water. The aquifer is defined as a rock formation which will yield sufficient quantities of water for use. The shallow aquifers occur within a depth of 50m from the earth's surface (Rahman, 2008). Groundwater yield depends upon the size and interconnectivity of the secondary porosity, i.e., fractures. In the DRASTIC model material properties of the saturated zone have been considered as the model parameter media but in this study yield of existing well in the area have been used. Its range varies from 10 LPM (litre per minute) to 800 LPM. The well yield is suggestive of permeability of the saturated zone; therefore, the higher the yield, the higher is the permeability. In the DRASTIC model analysis, the higher yield has been assigned more rating than the less as shown in Table 2.

*Soil media:*Soil being the top most layer of unsaturated zone overlying the aquifer is one of the important factors for the determination of groundwater pollution zone. It is the nature of porosity and permeability of the soil media, responsible for the rate of infiltration in to the aquifer. In the study area four types of soil found such as clay loam, loamy black soil, sandy clay loam and sandy loam based on USGS Agriculture soil classification system. Based on the presence of clay (Aller et al., 1987), its rating has been assigned because it reduces the permeability of soil and rate of infiltration of solvent.

*Topography:*Topography refers to slope of an area. Areas with low slope tend to retain water for longer period of time. This allows a greater infiltration or recharge of water and a greater potential for contaminant migration. Areas with steep slopes, having large amounts of runoff and smaller amounts of infiltration are less vulnerable to groundwater contamination. The digital elevation model (DEM) was used to extract the slope of the study area. Within the study area, most of the regions have a gentle slope, smooth slope in the range of 0–22.19% have been mapped.

*Impact of vadose zone:*Unsaturated zone above the water tableis referred to as the vadose zone.It controls the passage and attenuation of the contaminated material to the saturated zone. The layer that most restricts the flow of water will be used. It means that attenuation of groundwater is due to porosity of the media. The map to Impact of vadose zone was obtained by sub-surface geology map was imported in digital formatgeo-referenced and on-screen digitization was done to create a representation of the different geological units. The geological sections were then used to encode the geological units according to the DRASTIC model rating system. The coarse (saturated or unsaturated)

media was assigned a high rating value compared to the fine media types.

*Hydraulic Conductivity:*Hydraulic conductivity is the ability of the aquifer to transmit water. It controls the rate of contaminant movement and dispersion from the injection point. For assessing the hydraulic conductivity, the scaled values based on pumping tests data have been used 47 wells were selected for calculating the transmissivity by pumping test. Aquifer map is used for estimate hydraulic conductivity map and the higher conductivity has been assigned more rating than the lesser one. Because Hydraulic conductivity of the soil media determines the amount of water percolating to the groundwater through the aquifer. For highly permeable soils, the pollutant travel time is decreased within the aquifer.
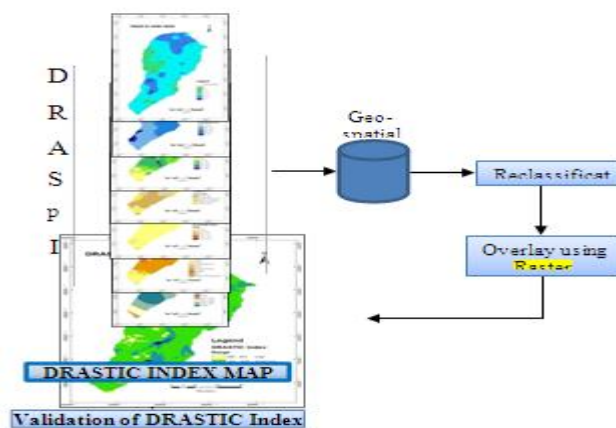
Figure 2: Methodology used

Table 2: DRASTIC rating and weight for the various hydrogeological parameter

Parameter	Depth to Water table (m.)	Net Recharge (mm./year)	Aquifer Media (Lit./min.)	Soil media	Topography (% slope)	Impact of vadose zone	Hydraulic Conductivity (m./day)
Weight	5	4	3	2	1	5	3
Rating	Range	Range	Range	Range	Range	Range	Range
10	< 1.5	> 250	400-800		<4.44		> 0.0305
9							
8	1.5 – 3				4.45 – 8.88		0.0243 – 0.0304
7						Alluvium, Laterite	
6	3.0 – 4.5	200 – 250		Sandy Loam	8.89 – 13.32	Limestone & dolomite	0.0182 – 0.0242
5		150 – 200	200-400	Sandy Clay Loam		Shale with limestone & Dolomite, Arenite, Shale, Sandstone	
4	4.5 – 6	100 – 150			13.33 – 17.75		0.0121 – 0.0181
3		< 100	100-200	Loamy Black			

				Soil								< 50			Granite	
2	> 6		50-100	Clay Loam	17.76 – 22.19		< 0.0120									
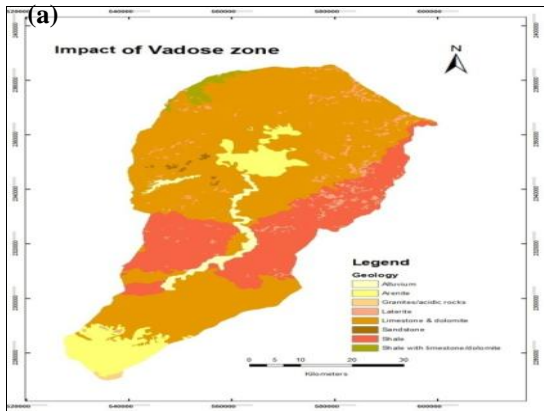
Figure 3(a): Depth to water table map
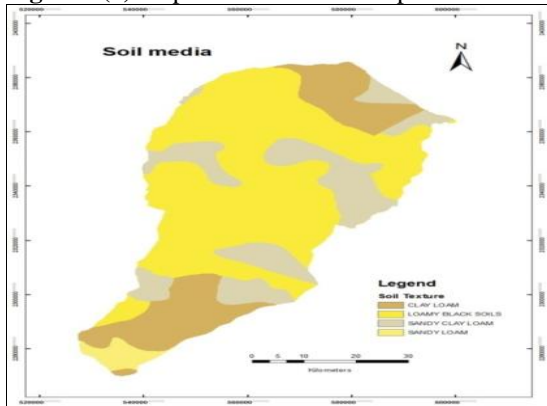
Figure 3(b): Net Recharge map
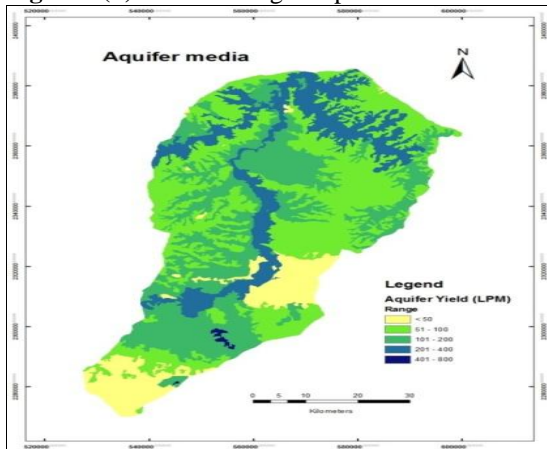
Figure 3(c): Aquifer media map
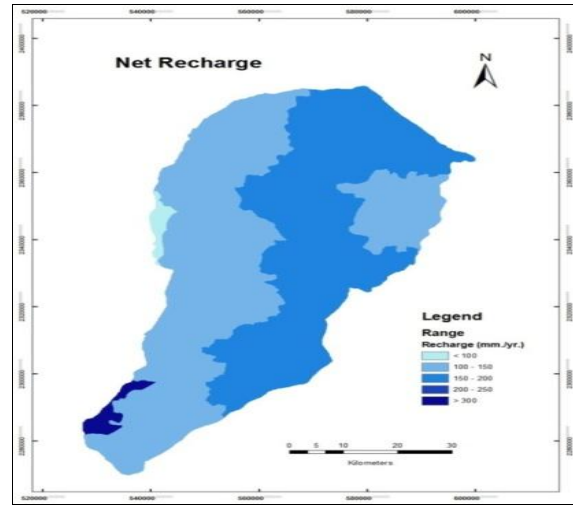
Figure 3(d): Soil media map
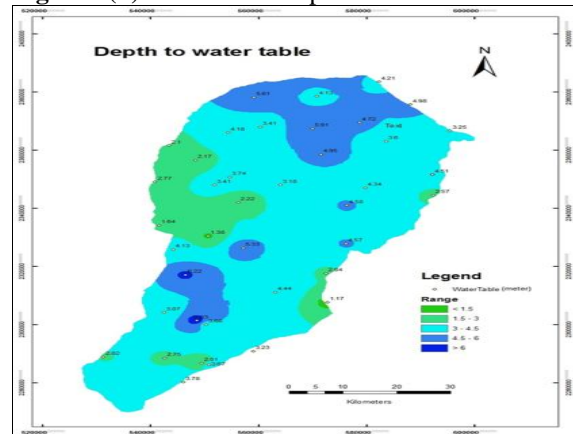
Figure 3(e): Topography map
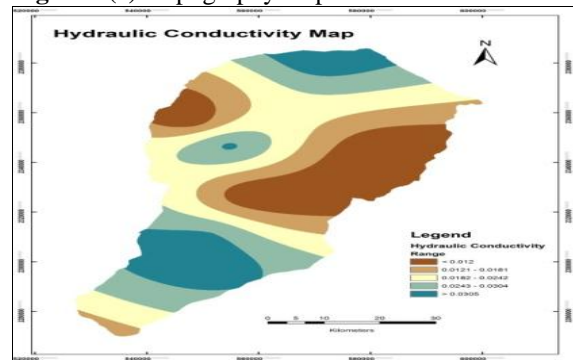
Figure 3(f): Impact of vadose zone
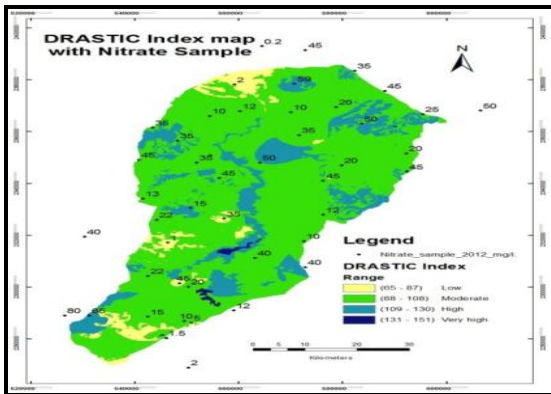
Figure 3(g): Hydraulic Conductivity map
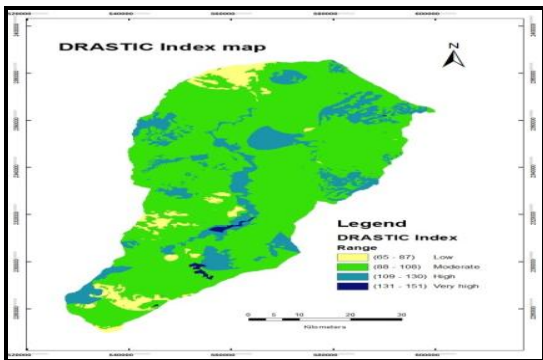
Figure 3(h): DRASTIC Index map
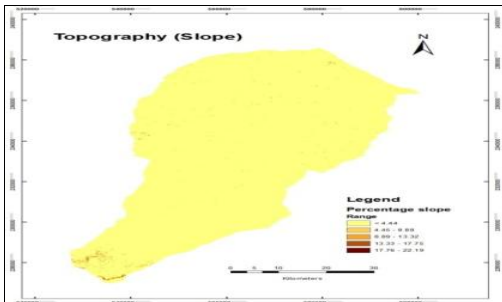
Figure 3(i): DRASTIC Index map with NO$_2$

4. DRASTIC MODEL RESULT

The final DRASTIC vulnerability index map is computed by multiplying their weights and overlay the prepared raster files (parameter map) on raster calculator tool in ArcGIS. The final output DRASTIC index map is obtained as shown in Figure 3(h). The calculated DRASTIC index identifies areas, which are likely susceptible to groundwater contamination relative to each other. The resulting maximum DRASTIC index value is 151 and minimum is 65. The higher DRASTIC index value shows, the greater the relative groundwater contamination potential. The DRASTIC vulnerability index values divided into four categories according to (Foster et al, 2002).The result shows that more than 82.88% (Table 3) of the area is under low and moderate zone of vulnerability. Hence Kharun sub basin is at moderate risk in terms of pollution potential. These areas are

mainly in the north-east; central and southern part of the basin. The physical factors like gentle slope and shallow water table are the major factor supporting the chances of getting shallow aquifer contaminated. Further "high" and "very high vulnerable zone" is approximately 17.11%, showing north (some portion of Tilda block) south east and central area of the Kharun sub basin, which is lies on Tilda block with high index value as 117 due to Parsada Tank (high recharge and high aquifer yield), this land is agriculture land having two seasoned crop which shows the possibility of leaching of pesticides used in agricultural activity and very high index value as 131. This "very high vulnerable zone" is due to stone crusher at Dhansuli-1 in Tilda block and source of water is Pindraon Tank which serves to enter the contaminants from surface to groundwater zone. In Dharsiwa block the high vulnerable index value varies from 103 to 125, because of the agriculture activity in surrounding riegion near Kharunriver along with area ofPatan, Abhanpur, Kurud and Dhamtari block. These areas are 76.71% of agricultural lands were, traditional agriculture activities started since very long time the leaching of pesticides from surface to groundwater is obvious due to high net recharge in this zone 200-250 mm/yras shown in Figure 3(b). Raipur city lies in Dharsiwa block and the major problem that is seen in the Kharunriver is the pollution due to dumping of municipals solid waste at Kharun river bank. The area is gently undulated & flat terrain, during the pre-monsoon the solid waste gets settled and the waste water getsleached from surface to groundwater and polluting groundwater body. Berla, Durg, and major part of Gurur block having low and moderate DRASTIC index value. The Balod block of the study area completely shows high vulnerability index varies from 109-129, due to high groundwater recharge in the zone through Tandula reservoir and shallow water bodies.

Table 3: Vulnerability DRASTIC Classes

Range	Class	Percentage Area	Area(sq.km)
65 – 87	Low	8.10	341.5
88 – 108	Moderate	74.78	3128
109 – 130	High	16.61	697
131 – 151	Very high	0.51	24.5
Total area			**4191**

Model validation with nitrate samples:A validation of the DRASTIC method is vital as it is an empirical model; thus, nitrate concentrations were applied to validate the results of the DRASTIC model. Nitrate is not naturally found in groundwater, but it usually enters via the surface. The correlation between the DRASTIC index and the nitrate concentrations in groundwater was investigated to check the efficiency of using this approach to assess groundwater vulnerability. The first nitrate sample was obtained in 2010 and the second nitrate sample was obtained in 2012 to determine the correlation between DRASTIC index and agriculture

activity. Visual observation of nitrate sample (2012) overly on DRASTIC index map (Figure 3(i)) shows that high nitrate concentration lies in the "very high" and "high zone" groundwater pollution potential areas, which have a good correlation with DRASTIC index. Therefore, the results of vulnerability assessment using the DRASTIC model are confirmed. The resulting DRASTIC index shows mean value 100.30 and standard deviation 9.64. After the loading first sample of nitrate on DRASTIC index map the mean value is converted to 125.49 and standard deviation is 17.59. This result shows the values will be changes such a way that the mean value is increases which is indicate the presence of nitrate contamination and further adding a second nitrate sample map shows increasing the mean value to 128.37 and standard deviation is 15.66. The change in mean value indicate the growth of nitrate concentration in 2010 to 2012 due to agriculture activity and the decrement in standard deviation shows conversing of spatial distribution of nitrate sample data (the nitrate concentration is spreading to the other areas due to over exploitation of groundwater).

5.   CONCLUSION

The Kharun sub basin is located in a semi-arid region. Where the groundwater is a very important source of domestic water supply, the evaluation of groundwater quality is crucial. Therefore, a study was carried out to assess the groundwater vulnerability of the Kharun sub basin using the DRASTIC model in a GIS environment.The DRASTIC vulnerabiliy index ranges between 65 and 151. Based on this index value the study area is classified into four class low, moderate, high and very high. The results of this study show that 24.5 sq.km (0.51%) of the study area has very high pollution potential, 697 sq.km (16.61%) area has high pollution potential, 3128 sq.km (74.78%) area has moderate pollution potential, and the remaining 342 sq.km (8.10%) of the study area has no risk for groundwater pollution. In addition, the majority of the area consists of agricultural land where pesticides and fertilizers are commonly used. Given the above mentioned considerations, nitrate is well correlated with the DRASTIC vulnerability maps for model validation. The application and validation of DRASTIC model in Kharun sub basin provides a satisfactory assessment of the vulnerability of groundwater to contamination. According to susceptible zones identified in the Kharun sub basin, for future it would be conveniently utilized by the water resource management departmentdecision makes for proper management to mitigate the quality of groundwater resources and source of contaminant.

REFERENCES

i.   Al-Adamat R.A.N., Foster I.D.L., and Baban S.M.J. (2003) "Groundwater vulnerability and risk mapping for the Basaltic aquifer of the Azraq basin of Jordan using GIS, Remote sensing and DRASTIC." Applied Geography, 23:303–324.

ii.   Aller L, Bennet T, Leher JH, Petty RJ, Hackett G, (1987) "DRASTIC: A standardized system for evaluating groundwater pollution potential using hydrogeological settings." EPA 600/2-87-035; 622.

iii.   Babiker I, Mohamed M, Hiyama T, Kato K (2005) "A GIS based DRASTIC model for assessing aquifer vulnerability in Kakamigahara Heights, Gifu Prefecture, Central Japan."Sci Total Environ 345(1–3):127–140.

iv.   Chitsazan, M., and Y. Akhtari. (2009). "A GIS-based DRASTIC model for assessing aquifer vulnerability in Kherran Plain, Khuzestan, Iran." Water Resources Management 23, no. 6:1137.

v.   Evans BM, Mayers WL (1990)"A GIS-based approach to evaluating regional groundwater pollution potential with DRASTIC." J Soil Water Conserv 1990; 45:242– 5.

vi.   Foster, S., Hirata, R., Gomes, D., D'Elia, M., Paris, M., (2002) "Groundwater Quality Protection" The World Bank Washington, D.C. 25071, ISBN:0.8213-4951-1.

vii.   Jamrah, A., AL-Futaisi, A., Rajmohan, N. & AL-Yaroubi, S. (2008) "Assessment of groundwater vulnerability in the coastal region of Oman using DRASTIC index method in GIS environment. Environmental monitoring and assessment," 147, 125-138.

viii.   Kim, Y. J., & Hamm, S. (1999) "Assessment of the potential for groundwater contamination using the DRASTIC/EGIS technique, Cheongju area, South Korea." Hydrogeology Journal, 7(2), 227–235.

ix.   Lake, I.R., Lovett, A.A., Hiscock, K.M., Betson, M., Foley, A., Su¨nnenberg, G., Evers, S., Fletcher, S., (2003)"Evaluating factors influencing groundwater vulnerability to nitrate pollution: developing the potential of GIS." Journal of Environmental Management 68 (3), 315–328.

x.   Rahman A (2008) "A GIS based DRASTIC model for assessing groundwater vulnerability in shallow aquifer in Aligarh, India."ApplGeogr 28(2008): 32–53.

xi.   Rupert, M.G. (2001)"Calibration of the DRASTIC groundwater vulnerability mapping method."Groundwater 39, no. 4: 625.

xii.   Xiaahu Wen., et al. (2008)"A GIS based DRASTIC model for assessing shallow groundwater vulnerability in the Zhangy Basin, north western China." Environmental Geology, 57, 1435–1442.

Spatial Variability Analysis Of Rainfall In Indian Himalayas Of Uttarakhand Region

Madhuri Kumari[1*]   Ashoke Basistha[2]   Oinam Bakimchandra[3]   C. K. Singh[4]

[1] Department of Natural Resources, TERI University, New Delhi

Department Civil Engg., Amity School of Engineering & Technology, Amity University Uttar Pradesh, Noida, U.P - 201313, India

[2] Hydro Power & Water Resources, Lahmeyer International (India) Pvt. Ltd.

Intec House, 37, Institutional Area, Sector 44, Gurgaon – 122002, India

[3] Department of Civil Engineering, School of Engineering, Shiv Nadar University, Gautam Budh Nagar, Uttar Pradesh - 201314, India

[4] Department of Natural Resources, TERI University, New Delhi-110070, India
Email: madhurikumari@gmail.com

ABSTRACT: With increasing thrust in water sector, water resources management has gained focus in India. More effective and integrated water resource management needs information on the present and future status of spatio-temporal variability of precipitation which is generally

presented as precipitation map or a precipitation model. This implies that the accuracy of spatial interpolation technique for generating the precipitation map from the data available from point location is very important. Reliable estimation of rainfall distribution in mountainous regions poses a great challenge not only due to highly undulating surface terrain and complex relationships between irregular topography and precipitation, but also due to non-availability of abundant rainfall measurement points. The large variability in altitude, slope and aspect may increase variability by means of processes such as rain shading and strong winds. This study presents a comparison of different spatial interpolation methods used for spatial analysis of rainfall in complex terrain of Indian Himalayas in Uttarakhand region. To understand the role of topography in explaining the geographical phenomenon of rainfall, elevation and slope are incorporated as covariables in geostatistical model. Further, the study area is divided into three different regions based on variation in the elevation of topography and accuracy of different spatial interpolation methods is analyzed for subdivided regions.
Keywords: Spatial interpolation methods, Geostatistics, Mountainous region, Complex terrain, Indian Himalayas

1. INTRODUCTION

Reliable estimation of rainfall distribution in mountainous regions poses a great challenge owing to complex relationships between irregular topography and precipitation. Moreover, the data availability in such region is also very sparse. The large variability in altitude, slope and aspect increases the variability of rainfall by means of processes such as rain shading and strong winds. For exploring the spatial variability of rainfall in complex terrains, geostatistical interpolation methods are preferred over deterministic methods as it allows incorporation of secondary attributes. When the sparsely sampled observations of the rainfall data is complemented with data of secondary attributes which are more densely sampled over the study area, the estimate of spatial variability of rainfall improves. The elevation, slope, aspect, slope-aspect ratio, atmospheric circulation pattern, proximity to moisture sources and climatological variables like temperature, humidity, and wind speed are some of the important co-variables that influence the rainfall.

Different deterministic methods such as Thiessen polygon and inverse distance weighted (IDW) (Thiessen 1911; Dingman 2002) estimates rainfall values at unknown points by using the values of surrounding observations. However, these methods do not account for spatial dependencies of data. The geostatistical techniques are becoming more popular as it considers the spatial dependencies of observations on neighboring data. It includes kriging and cokriging interpolation methods. These methods have been increasingly preferred over conventional methods (Goovaerts 2000; Sarangi et al. 2005; Carrera-Hernandez and Gaskin 2007, Mair et al.

2011) as it allows inclusion of secondary information like elevation, weather radar data and are found to perform better in complex terrain with sparse data (Basistha et al. 2008; Moral 2010; Mair et al. 2011).

The objective of this study is to compare three different spatial interpolation methods namely IDW, ordinary kriging (OK) and ordinary cokriging (OCK) used for spatial analysis of rainfall in complex terrain of Indian Himalayas in Uttarakhand region. To understand the role of topography in explaining the phenomenon of rainfall, elevation and slope are incorporated as covariables in geostatistical model of OCK. Further, the study area is divided into three different regions based on variation in the elevation and accuracy of these spatial interpolation methods is analyzed for subdivided regions. The performance of the interpolation methods are compared using cross-validation.

2. STUDY AREA AND DATA USED

The study area is located in Uttarakhand state of India which covers an area of 53,484 km^2. It lies between 28°42′N to 31°28′N and 77°35′E to 81°05′E coordinates. The variation of altitude is from 175 m to 7,409 m above mean sea level as per digital elevation model (DEM) of GTOPO 32. Uttarakhand is divided into four physiographic zones (Joshi 2004). The plain area in the foothills is known as Terai (finer alluvium deposits) and Bhabar (deposits of pebbles) region where elevation range is 175-600 m. The elevation range of second zone is 600–1200 m and is known as Shivaliks. The third zone is known as Lesser Himalayas comprising of areas with elevation range of 1200–3000 m. The elevation range of fourth zone is 3000–7500 m and is known as Greater Himalayas. The annual rainfall in this region varies between 948 mm and 2,986 mm.

For this study, normal annual rainfall data of 80 rain gauge stations is used. The data is average of 50 years annual rainfall data from 1901–1950. The topographical variables namely, elevation and slope are extracted from GTOPO32 which is the digital elevation model (DEM) of 1 km spatial resolution. Fig. 1 shows the spatial variability of elevation and rainfall data of study area.
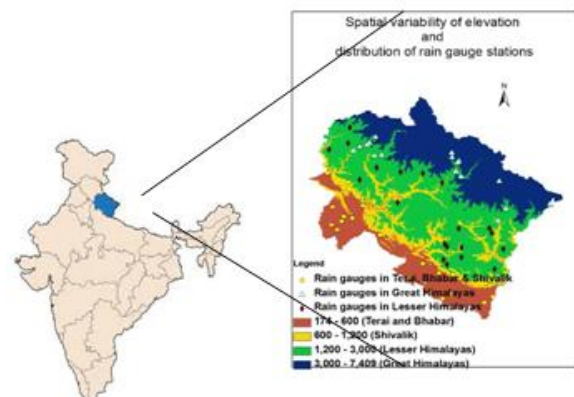
Figure 1. Spatial variability of elevation and distribution of rain gauge stations in Uttarakhand

3. METHODOLOGY

To understand the spatial variability of rainfall in complex terrain, the study region is subdivided into smaller regions. Following methodology is adopted for exploring the performance of different interpolation methods used to map the rainfall variability in Indian Himalayas of Uttarakhand.

1.   Study region is divided into smaller regions based on the elevation and district boundary.

2.   Co-variables of elevation and slope is extracted from DEM.

3.   Correlation of the co-variables with rainfall is studied. For understanding the correlation between topographical variables and rainfall phenomenon, complete data is initially considered followed by the data of subdivided region.

4.   Deterministic interpolation method of IDW and geostatistical interpolation methods of OK and OCK is applied for generating rainfall map. In OCK, both elevation and slope is used as covariables.

The performance of spatial interpolation methods is evaluated based on root mean square error (RMSE) value. Figure 2 represents the flow chart of methodology adopted for the study.

As rainfall is influenced by the topography of the area, it was decided to subdivide the rainfall data based on elevation variation of Uttarakhand region. The extent of study area is divided into three different parts depending on the elevation which is overlaid with district boundaries. In accordance to this, the rainfall data was clustered into Shivalik, Lesser Himalayas and Greater Himalayas regions. Figure 3 represents the clustering of rainfall data into 3 different clusters.
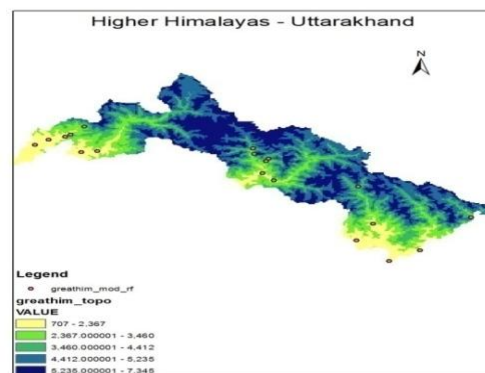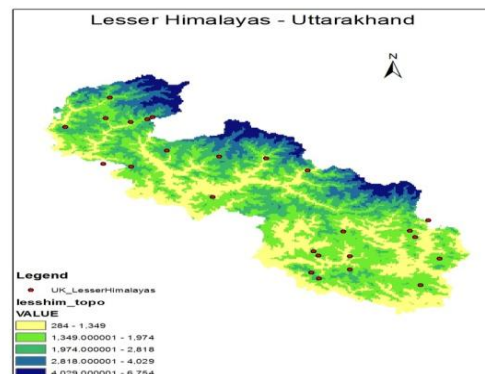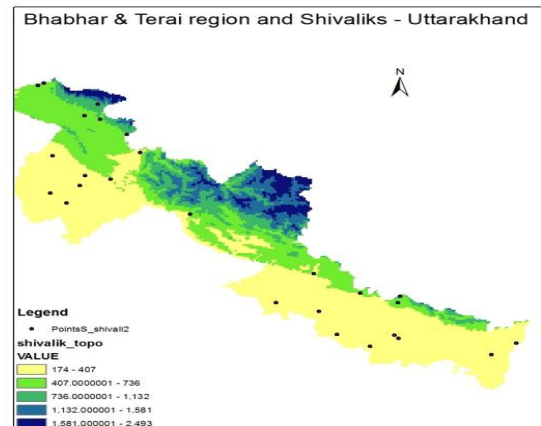
Figure 2. Study methodology – Flowchart

3.1 Division of study region

Figure 3. Clustering of rainfall data into 3 subdivided regions of UttarakhandTable 1 provides the statistical details of these cluster.

Table 1. Geography based clustering of rainfall data in Uttarakhand

	Cluster		
	1	2	3
Region	Bhabhar & Terai region + Shivaliks	Lesser Himalayas	Greater Himalayas
Elevation Range (m)	175-1200	1200-3000	3000-7500
Mean Normal Annual Rainfall of Cluster (mm)	1632.1	1625.6	1386.6
Standard Deviation	496.95	471.88	685.88
No. of rain gauge stations in Cluster	33	28	19

3.2 Extraction of co-variables from DEM

Terrain plays an important role in modulating various atmospheric processes. It is imperative to analyze the terrain effect and extract various topographical attributes that influences the rainfall as a first step towards modeling this atmospheric process. The topographical attributes are computed from digital elevation model (DEM). Those attributes that can be directly computed from DEM are known as primary attributes such as elevation, slope, aspect, plan and profile curvature. The compound or secondary attributes involves combination of primary attributes and constitutes physically based or empirically derived indices. For the current study two primary topographical attributes namely elevation and slope is computed from DEM of GTOPO32. Table 2 shows the statistics of elevation and slope distribution in Uttarakhand region.

Table 2. Elevation and slope variability in study region

Sl. No	Region	Elevation Range (m)	Slope range (degrees)
1	Complete (Uttarakhand state)	174-7409	0-50
2	Terrai & Bhabar + Shivalik	174-2493	0-21
3	Lesser Himalayas	284-6754	0-47
4	Greater Himalayas	707-7409	0-50

3.3 Correlation of covariables and rainfall

Correlation analysis is performed to examine the relationship between the dependent variable (response variable) rainfall and the independent variables (explanatory variables) elevation and slope. One of the measure of correlation is Pearson's coefficient of correlation (r) which has a value between -1 and +1. A correlation coefficient of +1 indicates that two variables are perfectly related in a positive linear sense; a correlation coefficient of -1 indicates that two variables are perfectly related in a negative linear sense, and a correlation coefficient of 0 indicates that there is no linear relationship between the two variables. It is not always necessary that the variables are related linearly. For this study, relationship between rainfall and elevation and slope was analyzed using value of r.

3.4 Application of spatial interpolation methods

Three different spatial interpolation methods namely IDW, OK and OCK was applied for mapping spatial variability of rainfall in Indian Himalayas of Uttarakhand region. To understand the role of topography in explaining the phenomenon of rainfall, elevation and slope are incorporated as covariables in geostatistical model of OCK. Table 3 list different scenarios that was used for the study.

Table 3. Scenarios for spatial interpolation of rainfall

Scenarios	Deterministic/Geostatistical	Secondary variables	Methods of Simulation
Scenario 1	Deterministic	None	IDW
Scenario 2	Geostatistical	None	OK
Scenario 3		Elevation	OCK(E)
Scenario 4		Slope	OCK(S)
Scenario 5		Elevation + Slope	OCK(E,S)

3.5 Comparison of interpolation methods

In this study, evaluation of spatial interpolation methods was based on exhaustive cross validation. Leave-one-out cross validation (LOOCV) was used where one rainfall data is removed at a time from the data set and the value is estimated from remaining data. The common diagnostic statistics used for assessing the accuracy of the interpolation method is root mean square error (RMSE). The method yielding smaller RMSE is considered to be an optimal method.

$$\text{RMSE} = \sqrt{\frac{1}{n} \sum_{i=1}^{n} \left(z_{i,act} - z_{i,est} \right)^2}$$

(1)

Where,
n = number of samples
$z_{i,act}$ = measured value of ith sample
$z_{i,est}$ = predicted value of ith sample

4. RESULTS AND ANALYSIS

The normal annual rainfall data collected over 80 rain gauge stations were explored to understand the data distribution pattern. The statistics of the data as presented in Table 4 indicates normal distribution of complete data set and Shivalik region data set. The data set of Lesser Himalayas region is right skewed and that of Greater Himalayas is left skewed.

Table 4. Descriptive Statistics of normal annual rainfall (mm) data used for study

Type	No. of Points	Min	Max	Mean	Median	S.D	CSK	Kurtosis
Complete	80	429.3	2986	1528.8	1419.1	549.01	0.42	2.9
Terrai & Bhabar + Shivalik	33	740.8	2986	1652.6	1613	504.2	0.49	3.03
Lesser Himalayas	28	1044.8	2849.1	1668.1	1611	491.48	0.94	3.02
Great Himalayas	19	429.3	2599.3	1407.8	1522.8	649.85	-0.03	2.07

Min = minimum value; Max = maximum value; S.D = standard deviation; CSK= coefficient of skewness

The correlation between rainfall and secondary variable namely, elevation and slope was analysed for 4 different sets of data and the result is presented in Table 5. No evident correlation is found between rainfall and slope for complete rainfall data set ($r < 0.1$). In Shivalik region, correlation coefficient of 0.79 indicates good correlation of rainfall and elevation. Similarly, the correlation coefficient of 0.43 indicates correlation of rainfall with slope in this region. In Lesser Himalayas, the correlation between rainfall and elevation is 0.4. In Greater Himalayas, there is no correlation between rainfall and topographical variables of elevation and slope. The correlation of rainfall and slope is not significant ($r < 0.4$) in most of the cases but being derivative of elevation, it was incorporated as secondary variable for comparative study.

Table 5. Correlation analysis matrix

Pearson's Correlation Coefficient (r)		
Region	Elevation	Slope
Complete	-0.10	-0.09
Shivalik	**0.79**	**0.43**
Lesser Himalayas	**0.40**	0.29
Greater Himalayas	-0.11	-0.06

For rainfall mapping IDW, OK and OCK were evaluated based on RMSE value. The error statistics of different scenarios is graphically represented in Figure 4.
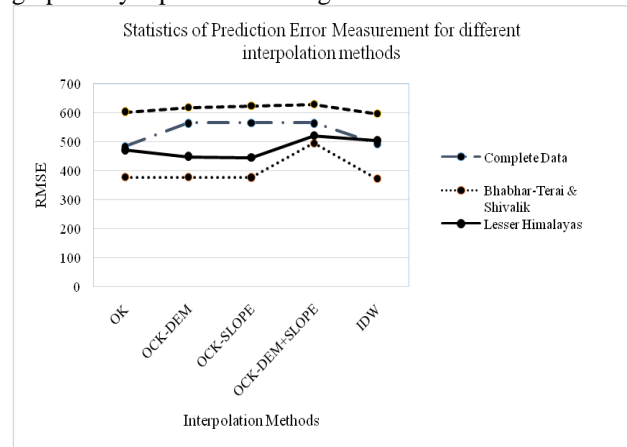
Figure 4. Error statistics (RMSE) for different scenarios applied to study region

From the cross-validation result, it is evident that the inclusion of elevation or slope as auxiliary variables improves the prediction of rainfall in the region where the correlation is good ($r>0.4$). The prediction error is relatively less with incorporation of slope as compared to elevation in OCK. The reason for this can be attributed to the fact that derivative of elevation responds better to stationary model. When elevation and slope is considered together then the result is not very promising as both the variables are not independent. IDW and OK performs better than OCK for cases where no significant correlation exists between dependent variable (rainfall) and independent variable (elevation, slope). In Shivalik and Lesser Himalayas region OCK performs better than IDW and OK as $r>0.4$.

4. CONCLUSIONS

In this study, spatial interpolation of rainfall was performed using normal annual rainfall data derived from 80 rain gauge stations in Indian Himalayas of Uttarakhand region. For mapping the spatial variability of rainfall three methods were used namely IDW, OK and OCK. The aim was to compare the performance of geostatistical methods OK and OCK with deterministic method IDW. The study region was divided into three different regions based on the elevation extracted from DEM to understand the spatial distribution pattern of rainfall. The result indicates that the estimates of rainfall improves by considering secondary information like elevation and slope when the correlation between these variable and rainfall is good ($r>0.4$). Due to sparse data set in Greater Himalayas, it is difficult to capture the spatial variability and comparative result of interpolation method may not be truly indicative.

REFERENCES:

i. Anders, A., Gerard, H.R., Bernard, H., David, R.M., Noah, J.F. and Jaakoo, P., 2006. Spatial patterns of precipitation and topography in the Himalaya. Geological Society of America. Special Paper 398.

ii. Barros and Lang, 2003. Monitoring the Monsoon in the Himalayas: Observations in Central Nepal, June 2001, Monthly Weather Review, 131(7): 1408–1427.

iii. Basistha, A., Arya, D.S., Goel, N.K., 2007, Spatial Distribution of Rainfall in Indian Himalayas – A Case Study of Uttarakhand Region, Vol: 22(10):1325-1346.

iv. Burrough, P.A. 2001. GIS and geostatistics: essential partners for spatial analysis. Environmental and Ecological Statistics 8: 361–377.

v. Bookhagen, B.: Appearance of extreme monsoonal rainfall events and their impact on erosion in the Himalaya, Geomatics, Natural Hazards and Risk,Vol. 1, No. 1, 37–50, 2010.

vi. Buytaert, W., Celleri, R., Willems, P., De Beivre, B., and Wyseure, G., 2006. "Spatial and temporal rainfall variability in mountainous areas: A case study from the south Ecuadorian Andes." J. Hydrol. (Amsterdam, Neth.), 329, 413–421.

vii. Carrera-Hernández, J.J., Gaskin, S.J., 2007. Spatio temporal analysis of daily precipitation and temperature in the Basin of Mexico, Journal of Hydrology, Volume 336, Issue 3-4, p. 231-249.

viii. Chang, Kang-tsung.: Introduction to Geographic Information System, Tata McGraw-Hill

ix. Daly, C., Neilson, R.P., Phillips, D.L. 1994. A statistical topographic model for mapping climatological precipitation over mountain terrain. Journal of Applied Meteorology 33: 140–158.

x. Diodato, N. 2005. The influence of topographic co-variables on the spatial variability of precipitation over small regions of complex terrain. International Journal of Climatology 25: 351–363.

xi. Dirks, K.N., Hay, J.E., Stow, C.D., Harris, D. 1998. High-resolution studies of rainfall on Norfolk Island, Part II: interpolation of rainfall data. Journal of Hydrology 208(3–4): 187–193.

xii. Goovaerts, P. 1999. Using elevation to aid the geostatistical mapping of rainfall erosivity. Catena 34(3–4): 227–242.

xiii. Goovaerts, P. 2000. Geostatistical approaches for incorporating elevation into the spatial interpolation of rainfall. Journal of Hydrology 228: 113–129.

xiv. Hengl, T., Heuvelink, G.B.M., Stein, A. 2003. Comparison of kriging with external drift and regression-kriging. Technical Note, International Institute for Geo-information Science and Earth Observation (ITC), Enschede, http://www.itc.nl/library/Academic output.

xv. Hijmans, R.J, Cameron, S.E., Parra, J.L., Jones, P.G., and Jarvis, A.: Very high resolution interpolated climate surfaces for global land areas, Int. J. Climatol., 25, 1965–1978, 2005.

xvi. Isaaks, E.H., Srivastava, R.M. 1989. An Introduction to Applied Geostatistics. Oxford University Press: Oxford.

xvii. Joshi, S.C. (2004) Uttaranchal: environment and development – a geo-ecological overview. Gyanodaya Prakashan, Nainital, Uttarakhand, p 426.

xviii. Krishna Murthy, B. R. and Abbaiah, G.: Geostatistical analysis for estimation of mean rainfalls in Andhra Pradesh, India, International Journal of Geology, Issue 3, Vol. 1, 2007.

xix. Mair, A. and Fares, A., 2011. Comparison of Rainfall Interpolation Methods in a Mountainous Region of a Tropical Island, Journal of Hydrologic Engineering, Vol. 16, No. 4.

xx. Moral, F.J., 2010. Comparison of different geostatistical approaches to map climate variables: application to precipitation, International Journal of Climatology. 30: 620–631.

xxi. Sarangi, A., Cox, C.A., Madramootoo, C.A., 2005, Geostatistical Methods for Predication of Spatial Variability of Rainfall in a Mountainous Region. Transactions of the ASAE, Vol. 48(3): 943-954.

xxii. Teegavarapu, R. and Chandramouli, V.: Improved weighting methods, deterministic and stochastic data-driven models for estimation of missing precipitation records, J. Hydrol., 312, 191–206, 2005.

xxiii. Thiessen, A. H. 1911. Precipitation averages for large areas. Monthly Weather Review 39(7): 1082-1084.

xxiv. Verworn, A., U. Haberlandt (2011): Spatial interpolation of hourly rainfall effect of additional information, variogram inference and storm properties,Hydrol. Earth Syst. Sci.,15,569-584, 2011.

xxv. Viviroli, D. and Weingartner, R.: The hydrologic significance of mountains: from regional to global scale, Hydrology and Earth System Sciences, 8(6), 1016-1029, 2004.

Evaluation of Remote Sensing Based Newly Developed Rain Detection Index Over Indian Region

Shruti Upadhyaya[1] and RAAJ Ramsankaran[1*]
[1]Department of Civil Engineering, Indian Institute of Technology Bombay, Powai, Mumbai 400 076
[*]Corresponding Author: Email:
ramsankaran@civil.iitb.ac.in

ABSTRACT : *Estimating accurate rainfall is very much needed for proper management of water resources. In case of scarcity in rain gauge stations as prevailing in most developing countries, accurate estimation becomes near impossible. To overcome this limitation, satellite data can be used which provides an alternate solution. However, there are still lots of challenges involved in satellite based rainfall estimations. One such challenge is to accurately detect the rain and no-rain pixels in a satellite image. As a solution, a new index i.e., TIRt<260K and TIRt -WVt<19K (Upadhyaya and Ramsankaran, 2014) has been developed for detecting rain and no-rain pixels in Kalpana-1 satellite images. This article presents the results of an evaluation study of the above mentioned index over Indian region. This study has been conducted for the south west monsoon season of the year 2013 using TRMM-2A25 rainfall rates as reference dataset. The newly developed index's performance has been checked by comparing with two most popular rain detection methods used for Indian regions i.e. Simple TIR threshold used in Global Precipitation Index (GPI) technique and Roca method used in Insat Multi Spectral Rainfall Algorithm (IMSRA). Performance of the above considered indices has been analyzed by considering various categorical statistics like Probability of Detection (POD), Probability of no-rain detection (POND), Accuracy, Bias, False Alarm Ratio (FAR) and Heidke Skill Score (HSS). The obtained results clearly show that the new index performs much better than the earlier indices.*
Keywords: Rain Detection Index, Kalpana-1 data, India, Roca method, Simple TIR Threshold

1. INTRODUCTION:

Rainfall is considered to be the most important input for hydrologic modelling, stream flow modelling, near real time flood forecasting, climate studies etc. Hence, accurate measurement/ estimation of which becomes the key task. This can be achieved either through dense network of rain gauges over the study area or with the well distributed Doppler Weather Radars (DWR). It is very difficult to achieve both in developing countries like India, as it becomes too expensive to

establish and maintain huge network of gauges/DWR. Instead as an alternative, satellite data which is freely available with good spatial and temporal resolutions can be used.

Satellite rainfall estimation (SRE) techniques can be broadly categorized into three categories: First are the techniques that use Visible (VIS) and Infrared (IR) Sensor data. These sensors are mounted over geostationary satellites and provide data at very high temporal resolution e.g. Kalpana-1 satellite provides images at every 30min. Secondly, few other techniques use microwave (MW) sensors data mounted over low earth orbiting (LEO) satellites and has very coarse temporal resolution (E.g. NOAA AMSU sensor's repetitive coverage is only once in 12hrs) and third kind of technique combines both the previous techniques. VIS/IR images provide only cloud top information, they does not penetrate the clouds and hence, are indirect means of rainfall estimation. Whereas, microwave radiations penetrate the cloud and can estimate rainfall more accurately but has poor temporal resolution. Hence, combined techniques are evolved in recent decades (Ba and Gruber, 2001; Haile et al. 2010; Mishra et al. 2009, 2010, etc.), which combines the advantages of both the methods i.e. high temporal resolution of VIS/IR techniques and better accuracy of microwave techniques. A detailed review of various methods of rainfall estimation using satellite data is available in Upadhyaya and Ramsankaran, 2013.

For any SRE algorithm which involves VIS/IR data, the major limitation is proper rain area detection which is the initial step towards SRE (Kidder and Vonder Haar, 1995). If the rain area is not properly delineated then it may lead to over/under estimation of rainfall area or it may oversight a complete rainfall event. Since decades, many indices have been developed to separate these rain and no-rain area, popular of them are developed by Arkin and Meisner (1987), Ba and Gruber (2001), Haile et al. (2010), Roca et al. (2002), etc. Most of these indices are developed for a particular region and cannot be applied directly to the Indian region without proper validation. Very recently, a new index has been developed by Upadhyaya and Ramsankaran, 2014 for Indian region. However, before applying this index for operational purpose, more validation studies have to be performed. Considering this, a study has been made to validate the new index by considering the rain area detected by TRMM 2A25 (microwave based rainfall estimates) as reference data. In addition, a comparative performance study of the new index against the most widely used Global Precipitation Index (GPI) technique developed by Arkin and Meisner (1987) and the cloud classification technique developed by Roca et al. (2002) which is widely used in rainfall estimation algorithms over Indian regions (Mishra et al. 2009 and 2010 and Prakash et al. 2010) has been reported in this article. Study area boundary considered in the present work is from Latitude: 37°.1 N – 8°.076 N and Longitude: 68°.1167E- 97°.4167E.

2. DATASETS:

2.1 Kalpana-1 Data

Kalpana-1 satellite is a dedicated Indian meteorological geostationary satellite launched by GSLV and operating since 24th Sept 2002. This geostationary satellite carries onboard a Very High Resolution Radiometer (VHRR) along with other instruments. This sensor operates in three wavelengths band namely VIS (0.55μm-0.75μm), TIR (10.5μm-12.5μm), and WV (5.7μm-7.1μm). In WV and TIR, spatial resolution is 8 Km where as in VIS band spatial resolution is 2 Km. Temporal resolution of the satellite is 30 min. The images are provided in HDF5 format and can be downloaded free of cost from MOSDAC (http://www.mosdac.gov.in).

2.2 TRMM PR - 2A25 Data

The TRMM PR -2A25 is the orbital data product of TRMM satellite which gives the instantaneous surface rainfall rates for the swath of PR. The 2A25 products represent snapshot of rainfall rates with a horizontal resolution of 5 km and a temporal frequency of one or two observations per day depending on the latitude. The 2A25 products and other TRMM products can be downloaded free-of-charge following the links at (http://daac.gsfc.nasa.gov/precipitation/). The data is provided in the HDF4 format. This data is considered as reference dataset in various studies (Haile et al. 2010, Mishra et al. 2009 and 2010, Prakash et al. 2010) and hence, in the present analysis also it is considered as reference dataset as it is available freely.

Considering the importance of South–West (S–W) monsoon rainfall for India, in this study, the S-W monsoon data of the year 2013 has been used for validation and comparison of the newly developed rain index with the other rain area detection approaches mentioned above.

3. METHODOLOGY:

The methodology involves 3 major steps as shown in Fig 1. First step is to collocate the Kalpana-1(K-1) and TRMM 2A25 data. This is an important step because K-1 data is the geostationary data available over complete India at every 30 min interval whereas TRMM 2A25 is an orbital data which crosses certain part of India once or twice a day, so the validation accuracy is entirely dependent on with what accuracy the both datasets are matched. If TRMM 2A25 pixel rain rate is greater than zero then it is considered as raining pixel else it is identified as no-rain pixel. Once the collocated dataset is prepared then second step is to apply rain area detection indices over the collocated dataset. Last step is to form a contingency matrix and estimate various categorical statistics to find the best performing index over India.

Collocation is a method of obtaining K-1 pixels which are captured at approximately same place and same time as that of

TRMM 2A25 pixels. This has been achieved by finding the nearest captured K-1 image initially (less than 10 min) whenever TRMM passes over India and then finding the pixels at same location as that of TRMM pixels. In house computer programs have been developed to extract the collocated pixels in K-1 images.
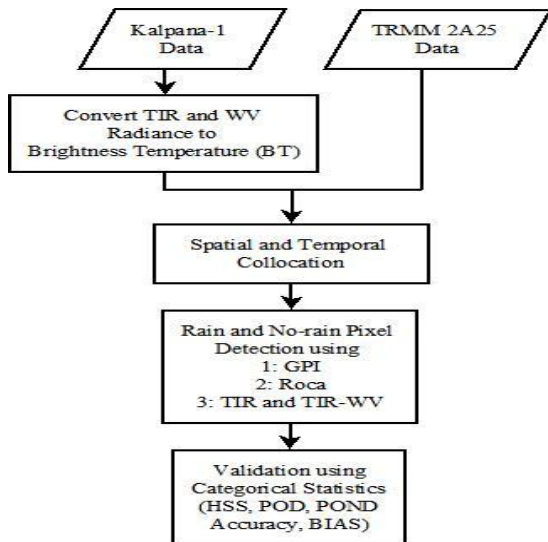
Figure 1: Flowchart of the methodology

3.1 Rain Detection Indices

In the present article, performances of three rain detection indices have been compared. The considered indices are described in the following section.

1-   Global Precipitation Index (GPI):

This index is also popularly known as simple threshold method. Arkin and Meisner (1987) used TIR channel (10.5µm-12.5µm) (TIR_t) and defined a threshold of 235K for TIR Brightness Temperature (TIR BT). If the pixel is having TIR BT less than the threshold then it is considered as raining else it is neglected as non-raining pixel. This is the oldest and most popularly used index. The assumption behind the use of TIR threshold is that the raining pixels are associated with colder TIR BT.

2-   Roca Cloud Classification:

An empirical method developed by Roca et al. (2002) for Indian Ocean region has also been evaluated in this study. This empirical technique has been widely used in India which is evident from the studies of Mishra et al. (2009) and (2010) and Prakash et al. (2010) wherein they have developed a rain rate estimation algorithm suitable for Indian land region called Insat Multi-Spectral Rainfall Algorithm (IMSRA) using the above mentioned Roca cloud classification method. The rain area

detection scheme adopted in IMSRA is given in Table 1. Here, the pixels which satisfy the mid to upper level clouds and low level clouds criteria are considered as raining and remaining pixels are classified as no-rain pixels.

Table 1. Roca Cloud Classification Scheme used in IMSRA algorithm

Cloudiness Class	Test
Clear sky	If $TIR_t > 282°$ and Standard deviation$\leq0.5°K$
Cloudy sky	Otherwise
Middle-to upper-level clouds	If $TIR_t \leq270°K$
Low-level clouds	Cloudy and if $TIR_t > 270°K$ and $WV_t > 246°K$
Semitransparent thin cirrus clouds	Cloudy and if $TIR_t > 270°K$ and $WV_t \leq246°K$

3- TIR_t and TIR_t-WV_t (The New Index by Upadhyaya and Ramsankaran, 2014)

The simple threshold index alone may not be the sufficient criteria for rain area detection, as some clouds like cirrus appear cold in TIR image but does not produce rain. Hence, along with simple threshold, other indices has to be used which can detect these thin cirrus clouds, this is the basis of Multi Index Rain Detection (MIRD) approach suggested by *Upadhyaya and Ramsankaran, 2014*. Also, the threshold value used by Arkin and Meisner (1987) may not be suitable for other regions but most of the rainfall estimation algorithms use same threshold of 235K. So to approach these snags, Upadhyaya and Ramsankaran (2014) developed an index TIR_t and TIR_t-WV_t with a threshold value of 260 K for TIR_t and 19 K for TIR_t-WV_t, for Indian land region. It is noteworthy to mention that though the mentioned index is developed for Indian region but the MIRD approach can be applied to different areas to find the best rain detection index for that particular region.

3.2 Categorical Statistics

To evaluate the effectiveness of these indices, various categorical statistics have been used. For a quick reference, they are briefly described in this section along with their importance.
The categorical statistics can be defined by using a standard 2 X 2 contingency table. The Table 2 shows a sample contingency matrix between the rain detected by a selected method in reference to the rain detected by the standard rainfall data, in this case it is TRMM-2A25.

Table 2. Contingency matrix

		Observed (TRMM-2A25)	
Forecast (Any cloud detection index)	Class	Yes (Rain)	No (No-Rain)
	Yes (Rain)	Hits(h)	False alarms(f)
	No (No-Rain)	Misses(m)	Correct Negatives(z)

- *hits (h)* is the number of pixels for which both the selected Rain Detection Index (RDI) and the TRMM-2A25 has

detected as rainfall and therefore indicates the number of pixels correctly classified as rainy by the RDI.

- *False alarms (f)* is the number of pixels for which rainfall is detected only by the selected RDI but not by the TRMM-2A25 and it indicates the number of pixels incorrectly classified as rain by the selected RDI.
- *Misses (m)* is the number of pixels for which rainfall is not detected by the selected RDI while it is detected by the TRMM-2A25 and it indicates the number of pixels incorrectly classified as non-rainy by the selected RDI.
- *Correct Negatives (z)* is the number of pixels for which rainfall is not detected by both the selected RDI and the TRMM-2A25, which indicates the number of pixels correctly classified as non-rainy by the selected RDI.

Based on the above contingency matrix, the various categorical statistics are defined as follows (Table 3):

Table 3: List of categorical statistics

STATISTICS	FORMULAE	RANGE	BEST VALUE	DESCRIPTION
Accuracy	$\dfrac{h+z}{h+m+z+f}$	0 to 100%	100%	Percent of pixels that were correctly classified
Bais	$\dfrac{f+h}{m+h}$	$-\infty$ to $+\infty$	1	Index underestimates or overestimates the number of rainy pixels
POD	$\dfrac{h}{m+h}$	0 to 1	1	Fraction of times the reference rainy pixels are correctly detected by the selected index
POND	$\dfrac{z}{z+f}$	0 to 1	1	Fraction of times the reference non-rainy pixels are correctly detected by the selected index
FAR	$\dfrac{f}{f+h}$	0 to 1	0	Fraction of times the no-rain pixels are incorrectly detected by the selected index
HSS	$\dfrac{C-E}{N-E}$	-1 to 1	1	Measures forecast accuracy relative to that of a random chance

FAR: False Alarm Ratio, HSS: Heidke Skill Score, ACC: Accuracy, POD: Probability of Detection, POND: Probability of No-Rain Detection

Where:
$$E = [(h+f)(h+m)+(f+z)(m+z)]/(h+m+z+f)$$
, $C = h+z$ and N= $(h+f+m+z)$.

As all the statistics gives different information each, only one cannot be used for choosing the optimal index. Hence, optimal

RDI is one, which gives better categorical statistics i.e. large value of HSS, POD, POND, Accuracy, small values of FAR and BIAS approximately equal to 1. Following the methodology given in Fig.1, all the categorical statistics has been found for the entire S/W monsoon season of 2013 for all three cloud rain area detection methods and the obtained results has been given in the next section.

4. RESULTS AND DISCUSSION:

As a first step, the collocation between TRMM 2A25 and K-1 data has been carried out for the months June, July, August and September for the year 2013 and the collocated pixels are extracted. Next, the validation dataset has been prepared by considering equal proportion of rain and no-rain pixels so that the results would not be biased towards the proportion in the dataset. The entire S-W monsoon months collocated dataset size is more than 25,000 pixels in each month, which is sufficiently large to carry out the statistical analysis. Based on these collocated pixels, categorical statistics for each month has been estimated separately and are shown in Fig.2a-f.

BIAS is the ratio of the number of rainy pixels detected by a RDI to the total number of rainy pixels present in TRMM-2A25. BIAS greater than 1 implies that the RDI overestimates the number of rainy pixels while a BIAS of less than 1 implies the RDI underestimates. The results of BIAS for all three considered RDI's is shown in Fig. 2a. It can be observed from Fig. 2a that the Roca method always over estimates the number of rainy pixels, whereas GPI method always estimates less number of rainy pixels. The new TIR_t and TIR_t-WV_t index gives the best result for the month of June and July but slightly underestimates for the other two monsoon months.
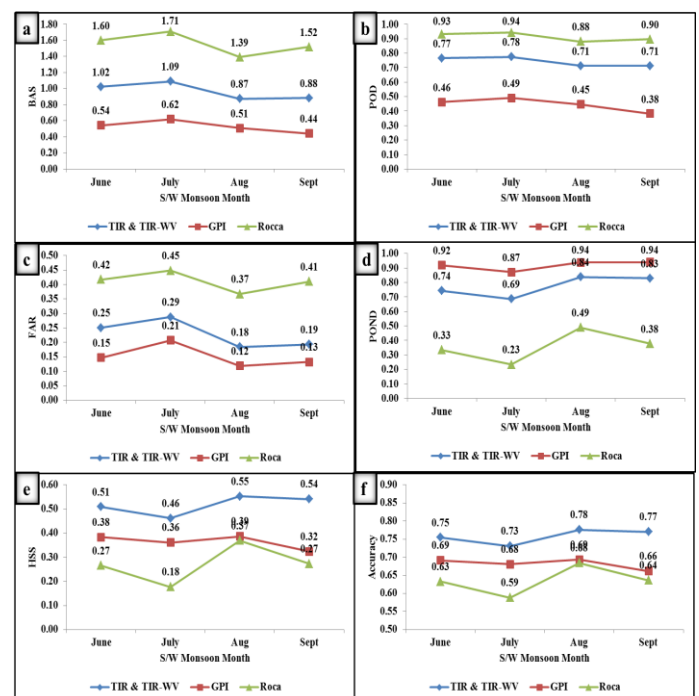
Figure 2: Categorical statistics for different S/W monsoon months and for different cloud detection indices for the year 2013. a) BIAS b) POD c) FAR d) POND e) HSS f) Accuracy

The POD (Probability of Detection) is the ratio of the number of correct rain pixels detected by a RDI to the total number of rain pixels available in TRMM-2A25. A POD = 1 indicates that the selected RDI correctly detects all the rain pixels. The POD of three RDI's is shown in Fig. 2b. From this it can be observed that the Roca method is able to detect more number of raining pixels than the other two indices. TIR_t and TIR_t-WV_t index performs considerably well but GPI method performs very poor, it could not detect more than 50% of raining pixels.

The FAR (False Alarm Ratio) is the ratio of the number of incorrect rainy pixels detected by a RDI to the total number of rainy pixels detected by that RDI and it indicates the fraction of times the selected index falsely detects rainy pixels compared to TRMM-2A25. From Figure 2c it can be observed that FAR of Roca method is very high indicating that large number of raining pixels are falsely detected. FAR of GPI is least but its POD is very low to consider this index as best. FAR of TIR_t and TIR_t-WV_t is fairly good.

Similar to the POD, there is another statistics called POND (Probability of no-rain detection). POND can be defined as the ratio of the number of correct no-rain pixels detected by a RDI to the total number of no-rain pixels present in TRMM-2A25. POD alone cannot be used for evaluation, it has to be used along with POND because the RDI should detect both rain and no-rain pixels with better accuracy. If it fails in anyone also then the index is not performing well for the study region. From Fig. 2d it can be observed that the GPI method is able to detect maximum number of no-rain pixels correctly but it fails in detecting raining pixels. In a similar way, though Roca method is able to detect most of the raining pixels, it fails miserably in detecting no-rain pixels. The index TIR_t and TIR_t-WV_t performance is consistent in detecting both rain and no-rain pixels in all the monsoon months.

HSS measures forecast accuracy relative to that of a random chance. HSS=1 for (m= 0) and (f = 0) which indicates that the selected index did not incorrectly classify any pixel. The HSS values obtained for the 2013 monsoon months for the three RDI's is shown in Fig. 2e. In terms of HSS TIR_t and TIR_t-WV_t index performs exceptionally well compared to the other two indices. Roca method performs poor.

Accuracy is the ratio of the correctly detected pixels to the total number of pixels. It gives an overall accuracy of what percent of pixels were correctly classified; it may be rain or no-rain pixels. In simple terms, it gives combined information of both POD and POND. From Fig. 2f it can be observed that the accuracy for TIR_t and TIR_t-WV_t index is highest for all monsoon months whereas least accuracy is obtained for Roca method.

To conclude TIR_t and TIR_t-WV_t index performs comparatively better than the other two popularly used indices over India with highest HSS and Accuracy and fairly good FAR and with almost equal probability for detecting both rain and no-rain pixels.

5. CONCLUSIONS:

In the present article the new cloud detection index TIR_t and TIR_t-WV_t developed by Upadhyaya and Ramsankaran, 2014 has been evaluated with other two popularly used indices in India i.e. GPI and Roca method. The analysis has been carried out using various categorical statistics and the results clearly show that the new index performs better than the other indices. But, the results are validated by considering entire India as one region which has highly varying topography and climate. Hence, further analysis has to be carried out to check the performance of the index in different homogeneous spatial locations of India. Also, analysis has to be carried out using different satellite data with higher spatial resolution and at different spatial scales to check whether the performance of indices remains consistent or not.

REFERENCES:

i.   Arkin, P. A., and Meisner, B., 1987: The relationship between large-scale convective rainfall and cold cloud over the Western Hemisphere during 1982-1984. Monthly Weather Review 115: 51-74.

ii.   Ba, M., and Gruber, A., 2001: GOES Multispectral Rainfall Algorithm (GMSRA). Journal of Applied Meteorology 40: 1500–1514.

iii.   Haile, A.T., Rientjes, T.H., Gieske, A., Gebremichael, M., 2010: Rainfall estimation at the source of the Blue Nile: A multispectral remote sensing approach. International Journal of Applied Earth Observation and Geoinformation. 12S:76-83

iv.   Iguchi, T., Kozu, T., Meneghini, R., Awaka, J., Okamoto, K., 2000: Rain-profiling algorithm for the TRMM precipitation radar. Journal of Applied Meteorology 39:2038–2052.

v.   Kidder, S. Q., and Vonder Haar, T. H., 1995: Satellite Meteorology: An Introduction. Academic Press, San Diego 307-355.

vi.   Meneghini, R., Iguchi, T., Kozu, T., Liao, L., Okamoto, K., Jones, J., and Kwiatowski, J., 2000: Use of the surface reference technique for path attenuation estimates from the TRMM Precipitation Radar. Journal of Applied Meteorology 39: 2053–2070.

vii.   Mishra, A., Gairola, R. M., Varma, A. K., and Agarwal, V. K., 2010: Remote sensing of Precipitation over Indian land and oceanic regions by synergistic use of multi-satellite sensors. Journal of Geophysical Research 115: D08106

viii.   Mishra, A.K., Gairola, R.M., Varma, A.K., Agarwal, V.K., 2009: Study of intense rainfall events over India using Kalpana-IR and TRMM precipitation radar observations. Current Science 97: 689-695.

ix.   Prakash, S., Mahesh, C., Gairola, R.M., Pal, P.K., 2010: Estimation of Indian summer monsoon rainfall using Kalpana-1 VHRR data and its validation using rain gauge and GPCP data. Meteorology and Atmospheric Physics 110: 45–57.

x.   Roca, R., M. Viollier, L. Picon, and M. Desbois, 2002: A multisatellite analysis of deep convection and its moist environment over the Indian Ocean during the winter monsoon. Journal of Geophysical Research 107: 8012.

xi.   Upadhyaya, S. and Ramsankaran, RAAJ., 2014: Multi-Index Rain Detection: A New Approach for Regional Rain Area Detection from Remotely Sensed Data, Journal of Hydrometeorology (In Press). doi: http://dx.doi.org/10.1175/JHM-D-14-0006.1

xii.   Upadhyaya, S. and Ramsankaran, RAAJ., 2013: Review of Satellite Remote Sensing Data Based Rainfall Estimation Methods. Proceedings of HYDRO 2013 International. 897:905

Identifying Potential Sites For Groundwater Recharge Using Integrated Remote Sensing And Gis Techniques In Hirakud Canal Command Area (India)

Satiprasad Sahoo[1] Anirban Dhar[2]

[1]M.S Research Scholar, School of Water Resources, Indian Institute of Technology Kharagpur, Kharagpur-721302, India.

[2]Assistant Professor, Department of Civil Engineering, Indian Institute of Technology Kharagpur , Kharagpur-721302, India.

Email: satispss@gmail.com and anirban@civil.iitkgp.ernet.in

ABSTRACT : *Groundwater depletion is a common problem in most of the states (INDIA). The western part of Odisha is facing drinking water crisis almost every year due to large scale deforestation, unplanned use of irrigation water, unscientific or poor water management strategy. Hirakud command area, situated in the western part of Odisha, comes under Mahanadi river basin. In the present work, an analysis has been performed to delineate and classify possible groundwater potential zones in the Hirakud command area using integrated remote sensing and GIS techniques. Groundwater recharge potential depends on geological and hydrological characteristics of land surface. The groundwater potential zone index (GWPZI) map is generated by using Analytic Hierarchy Process (AHP) along with different influencing features, e.g., land use land cover, soil type, geology. All the feature layers have been integrated through GIS analysis and the groundwater potential zones have been delineated. Three zones have been identified for Hirakud command area (poor: 18.79%, moderate: 45.59%, and good: 35.61%).*
Keywords: Groundwater Potential, Analytic Hierarchy Process, Remote Sensing, GIS

1. INTRODUCTION:

Identification of groundwater potential zone is a general technique for qualitative assessment. Satellite remote sensing provides efficient data and effective platform for groundwater mapping. Hydrogeological investigation is required for better understanding of the groundwater conditions. As remote sensors cannot detect groundwater directly, the presence of groundwater is inferred from different surface features derived from satellite imagery, e.g., geology, soils, land use/ land cover (Jha and Peiffer, 2006). Rao et al. (2009) carried out hydrogeological mapping for evaluation of groundwater potential in Madhurawada, India using GIS and remote sensing techniques. Shahid and Nath (2002); Madrucci et al. (2008) and Chowdhury et al. (2009) have used MCDA techniques (i.e., analytic hierarchy processes) for processing the weights assigned to different features and their sub features. Several studies are available in the direction of groundwater potential zoning both in India and abroad, e.g., Jaiswal and others 2003; Solomon and

Quiel 2006; Krishnamurthy and Srinivas (1995); Saraf and Choudhary (1998); Kumar (1999); Krishnamurthy et al. (2000); Murthy (2000); Srivastava and Bhattacharya (2000); Shahid et al. (2000); Khan and Moharana (2002); Sreedevi et al. (2005). GIS is broadly used in decision making, processing, interpretation and overlaying information layer (Kao and Lin, 1996). In the present study, an AHP based groundwater potential zone index mapping technique is applied to Hirakud command area.

2. MATERIAL AND METHODS:

2.1 Study area:

Hirakud command area is situated in the western part of Odisha (North Latitudes 20º 53': 21º 36' and East Longitudes 83º 25': 84º10'), INDIA. The study area includes five blocks (administrative units) of Sambalpur District, Six blocks of Bargarh District, two blocks of Suvarnapur District and one block of Bolangir District covering a total area of 2260 km².

2.2 Data used:

To identify the groundwater potential zones in the study area, 10 thematic maps (geology, soil, LULC, drainage density, recharge rate, rainfall, slope, relief (elevation), Normalized Difference Vegetation Index (NDVI), groundwater depth are prepared through satellite imagery and conventional data. Relief, slope and drainage density maps are prepared from the CARTOSAT 1 data. Land use land cover map and NDVI for the study area are generated from the Landsat 7 Enhanced Thematic Mapper Plus (LANDSAT 7 ETM+). Soil and geology maps are prepared from NBSS & LUP and Geological Survey of India.

2.3 Methodology:

Groundwater potential zone (GWPZ) identification is generally performed by standard index approach. All feature layers (e.g., soil type, geology) are converted into raster format. Then, individual feature layers are reclassified into sub-features and ranks are assigned accordingly. Finally, feature maps are integrated using a weighted linear combination approach in the GIS platform to generate potential index map. Potential index can be calculated as

$$GWPI_{i,j} = \sum_{k \in F} W_k \left(\sum_{l \in S_k} w_l^k \, \chi_{A_l^k} \left(C_{i,j}^v \big|_k \right) \right)$$

where index (i, j) denotes row column location of a pixel; F denotes the set of all features, k denotes element of feature set; S_k denotes set of sub-features for k[th] feature; l denotes element of sub-feature set; W_k normalized weight of kth feature; w_l^k normalized weight of lth sub-feature for k[th] feature; $C_{i,j}^v \big|_k$ denotes the class value of the cell (i, j) for k[th] feature; A_l^k denotes the sub-feature interval; $\chi_{A_l^k}$ denotes

the indicator function for l^{th} sub-feature of kth feature. It takes 1 for $C_{i,j}^{v}\big|_{k} \in A_{l}^{k}$ and zero otherwise. Analytic Hierarchy Process (AHP) can be applied for estimation of W_{k} and w_{l}^{k} . In AHP (Saaty, 1980), 1-9 scale (i.e., extremely unimportant, strongly unimportant, unimportant, moderately unimportant, equally important, moderately important, more important, strongly important, extremely important) is adopted for constructing judgment matrices.

3. RESULTS AND ANALYSIS

Groundwater potential zones in Hirakud command area is determined based on feature layers of geology, soil type, elevation, slope, rainfall, drainage density, groundwater recharge, land use & land cover, Normalized Differential Vegetation Index and depth to groundwater table. Individual features are described in the following sub-sections.

3.1 Geology (GG):
Geological formation has a very important role in groundwater recharge process. Recharge amount increases with higher value of permeability and high water storage capacity. In the present study area four types (Figure 1) of geology, namely (a) Conglomerate, shale and sandstone (b) Granite gneiss, migmatite, augeogneiss (c) Quartz garnet sillimanite schist and gneiss graphite, calc silicate, leptynite, metabasic rocks (d) Gabbro, norite and anorthosite, are found. Conglomerate is a coarse-grained clastic sedimentary rock. Sandstone is a medium-grained clastic sedimentary rock composed of abundant sand – sized fragments. Shale is a laminated rock. Conglomerate, shale and sandstone have very good percolation capacity.

3.2 Soil Type (ST):
Soil is an important factor for the delineation the groundwater potential zones. Soil characteristics invariably control penetration of surface water into the aquifer system and they are directly related to rates of infiltration, percolation and permeability. Soil map (NBSS & LUP) of the study area is scanned, rectified and geometrically corrected. Different attributes of soil such as texture, hydrologic soil groups are assigned to these polygons. The thematic layer on soil map for the study area reveals five soil (Figure 1) classes, namely (i)fine (ii)fine loamy (iii)fine, loamy skeletal (iv) fine, montmorillonitic and (v)loamy skeletal.

3.3 Elevation (EL):
The relief directly reflects (Figure 1) the terrain ruggedness, which is characterized by steeper topographic gradient as well as hydraulic gradient as the relief increases. The study area can be divided into five classes: (i) 0- 75 m, (ii) 75- 93 m (iii) 93- 109 m (iv) 109-156 and (v) 156-304.The lower relief areas are characterized by softer lithologies permitting more recharge to groundwater whereas higher relief areas have comparatively hard lithologies forming higher runoff.

3.4 Slope (SL):

Slope (Figure 1) is one of the factors controlling the infiltration of groundwater into subsurface. Thus it is an indicator for the suitability for groundwater prospect. The study area divided into five classes: (a) 0∘-2.63∘, (b) 2.63∘- 7.64∘ and (c) 7.64∘- 22.12∘ (d) 22.12∘- 47.13∘ and (e) 47.13∘-72.26∘. In the gentle slope area the surface runoff is slow, allowing more time for rainwater to percolate. However, high slope area facilitates high runoff, allowing less residence time for rainwater.

3.5 Rainfall (RF):

Rainfall is the most vital input in the hydrological cycle. Its fluctuation in quantity and distribution strongly influence surface and subsurface water resources. Rainfall is the major source of recharge. It determines the amount of water that would be available for percolation into the groundwater system. The rainfall map (Figure 1) is divided into five classes: (a) 0- 267 mm, (b) 267- 432 mm (c) 432- 506 mm (d) 506- 589mm and (e) 589- 752 mm. High rainfalls are favorable for high groundwater potential (assigned higher priority).

3.6 Drainage Density (DD):
Drainage density (Figure 1) in the study area ranges from 0 to 4.65 km/km2 . The study area is divided into five classes: (i) 0- 0.70 kmkm2, (ii) 0.70- 1.36 km/km2 (iii) 1.36- 2.09 km/km2 (iv) 2.09- 2.99 km/km2 and (v) 2.99- 4.65 km/km2. Thus, the lesser the drainage density, the higher is the probability of recharge.

3.7 Groundwater Recharge (RR):

Groundwater is recharged naturally by rain and to a smaller extent by surface water. A GIS based hydrologic model, SWAT (Soil and Water assessment Tool) is applied for Hirakud command area, Odisha. Meteorological data (rainfall, temperature, relative humidity, solar radiation and wind speed) for 12 years (1997- 2008) has been used to run the model. Most of the input data (DEM, Soil texture, LULC, Slope) for the model are extracted from various map and satellite images using remote sensing and GIS techniques. The average annual (1997-2008) ground water recharge in Hirakud command area obtain by the SWAT model is found to vary form 0 to 70.30 cm year-1. The study area can be divided into five recharges (Figure 1) classes: (i) 0 – 24.70 cm year-1, (ii) 24.70 – 40.20 cm year-1, (iii) 40.20 – 47.20 cm year-1 (iv) 47.20- 55.30 cm year-1 and (v) 55.30- 70.30 cm year-1 .

3.8 Land Use &Land Cover (LULC):

Land use is the utilization representation of the land for different purposes, e.g., farming, mining, lumbering. Land cover describes the physical state of the land surface as in cropland or forest. The term land cover originally referred to the kind and state of vegetation, but it has broadened in subsequent usage to include human structures such as buildings or pavement and other aspects of the natural environment, such as soil type, biodiversity, and surface and groundwater. Land use and land cover (Figure 1) are interpretable by Enhanced Thematic Mapper Plus (ETM+) satellite image. LULC analysis is performed by

unsupervised classification techniques. There are six LULC patterns identified in the entire study area namely water bodies (5.41%), forest land (10.06%), agriculture land (74.82%) ,Barren land/Wastelands (6.48%), builtup, urban (0.65%) and builtup, rural (2.59%).
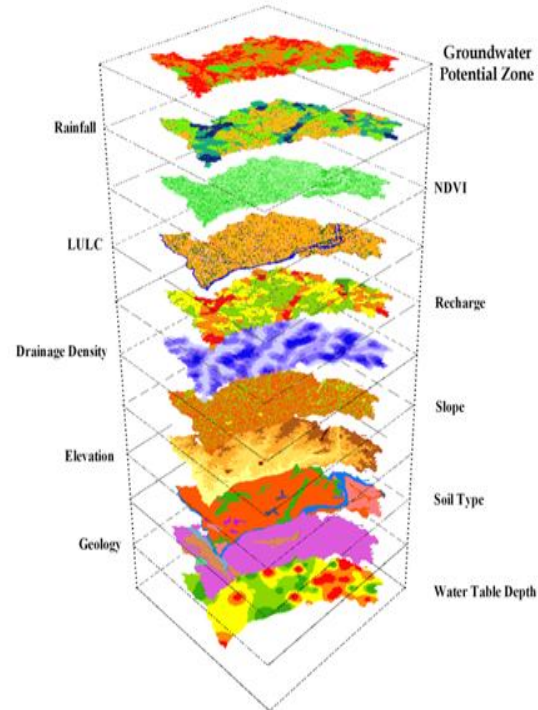
Figure 1: Overlay analysis of groundwater potential zone map
3.9 Normalized Difference Vegetation Index (NDVI):

Enhanced Thematic Mapper Plus (ETM+) sensor data can be processed to extract information of vegetation distribution. The study area can be divided into five (Figure 1) classes: (i) (-) 0.66 – (-) 0.05, (ii) (-) 0.05 - 0.07 (iii) 0.07- 0.15 (iv) 0.15- 0.24 and (v) 0.24-0.58. Theoretically, NDVI values are represented as a ratio ranging in value from -1 to 1. However, in practice extreme negative values represent water, values around zero represent bare soil and values over 6 represent dense green vegetation. Normalized Differential Vegetation Index (NDVI) is used in this exercise for the extraction of information. Satellite imagery is downloaded from the Global Land Cover Facility (GLCF).

3.10 Groundwater Depth or Depth to Groundwater Table (GD):

Average depths to groundwater table (Figure 1) values are utilized for determination of groundwater potential zones. The study area can be divided into five classes :(a) 0.58- 1.60 m bgl , (b) 1.60- 2.07 m bgl ,(c) 2.07- 2.54 m bgl, (d) 2.54-3.06 and (e) 3.06-4.93.

3.11 Groundwater potential zoning

Suitable weights are assigned to the ten features (Figure 1) and their individual sub-features after assessing their hydrogeological importance in causing groundwater occurrence in the study area. Normalized weights for individual attributes (Table 1) are obtained from Saaty's analytical hierarchy process (AHP).

Table 1: Pair-wise comparison matrix developed for AHP based groundwater potential zoning

Parameters	LULC	ST	GG	RR	DD	RF	SL	EL	NDVI	GD	Normalized Weight
LULC	3/3	3/8	3/9	3/7	3/5	3/4	3/4	3/3	3/2	3/6	0.0593
ST	8/3	8/8	8/9	8/7	8/5	8/4	8/4	8/3	8/2	8/6	0.1581
GG	9/3	9/8	9/9	9/7	9/5	9/4	9/4	9/3	9/2	9/6	0.1779
RR	7/3	7/8	7/9	7/7	7/5	7/4	7/4	7/3	7/2	7/6	0.1383
DD	5/3	5/8	5/9	5/7	5/5	5/4	5/4	5/3	5/2	5/6	0.0988
RF	4/3	4/8	4/9	4/7	4/5	4/4	4/4	4/3	4/2	4/6	0.0791
SL	4/3	4/8	4/9	4/7	4/5	4/4	4/4	4/3	4/2	4/6	0.0791
EL	3/3	3/8	3/9	3/7	3/5	3/4	3/4	3/3	3/2	3/6	0.0593
NDVI	2/3	2/8	2/9	2/7	2/5	2/4	2/4	2/3	2/2	2/6	0.0395
GD	6/3	6/8	6/9	6/7	6/5	6/4	6/4	6/3	6/2	3/6	0.1106

Similar approach is applied to obtain normalized weights for individual sub-features. After obtaining normalized weights for individual features and sub- features expression (1) is utilized to calculate the GWPI for the study area. Final integration of attributes yields a GWPI map (Figure 2).
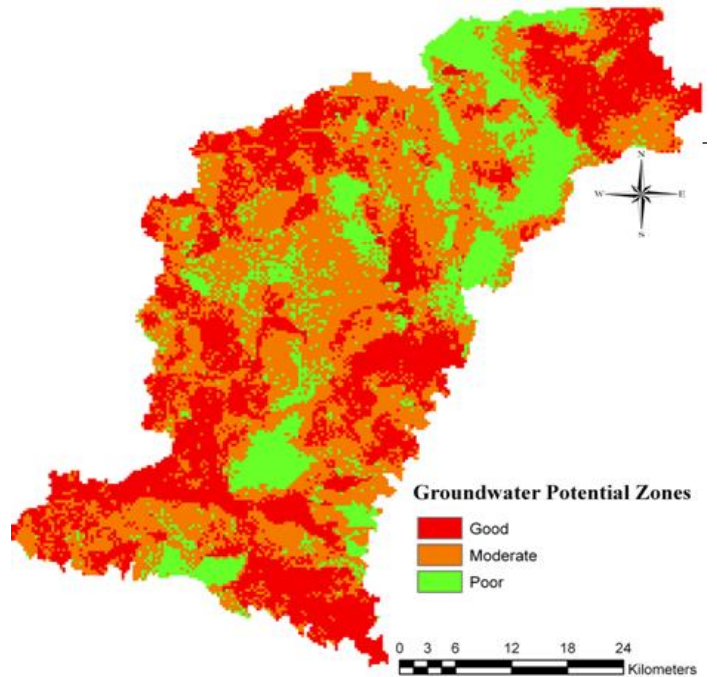
Figure 2: Groundwater Potential Zones map of the study area

The resulting map has been classified into three groundwater potential zones namely: poor, moderate and good covering

18.79%, 45.59%, and 35.61%, area, respectively. The GWPI reveals the overall groundwater quantity scenario in the study area.

4. CONCLUSIONS

The utility of geospatial technologies in estimating the groundwater potential in Hirakud canal command area has been demonstrated. Groundwater quantity assessment is performed on the basis of groundwater potential zone index (GWPZI) map. The GWPZI map is generated by using AHP method along with different features, e.g., LULC, ST, GG, RR, DD, RF, SL, EL, NDVI, GD. Three zones have been identified for Hirakud command area. The results obtained are meaningful considering the water table depth in the aquifer.

REFERENCES

i. Chowdhury, A., Jha, M. K.,Chowdary, V. M., and Mal, B. C.(2009). Integrated remote sensing and GIS based approach for assessing groundwater potential in West Medinipur district, West Bengal, India. International Journal of Remote Sensing, 30 (1), 231-250.

ii. Jaiswal, R.K., Mukherjee, S., Krishnamurthy, J. and Saxena, R. (2003). Role of remote sensing and GIS techniques for generation of groundwater prospect zones towards rural development: An approach. International Journal of Remote Sensing, 24, 993–1008.

iii. Jha, M.K., Peiffer, S. (2006). Applications of remote sensing and GIS technologies in groundwater hydrology: past, present and future. BayCEER, Bayreuth, Germany, 201.

iv. Kao, J. J., & Lin, H. Y. (1996).Multifactor spatial analysis for landfill siting. Journal of Environmental Engineering, 122(10), 902–908.

v. Khan, M.A. and Maharana, P.C.(2002).Use of remote sensing and GIS in the delineation and characterization of groundwater prospect zones. Photonirvachak, Journal of Indian Society of Remote Sensing, 30, 131–141.

vi. Krishnamurthy, J. and Srinivas, G.(1995). Role of geological and geomorphological factors in groundwater exploration: A study using IRS LISS data. International Journal of Remote Sensing, 16, 2595–2618.

vii. Krishnamurthy, J., Mani, A.N., Jayaram, V. and Manivel, M., (2000). Groundwater resources development in hard rock terrain: An approach using remote sensing and GIS techniques. International Journal of Applied Earth Observation and Geoinformatics, 2, 204–215.

viii. Kumar, A. (1999).Sustainable utilization of water resources in watershed perspective – A case study in Alaunja watershed, Hazaribagh, Bihar. Photonirvachak, Journal of Indian Society of Remote Sensing, 27, 13–22.

ix. Madrucci ,V., Taioli, F., and Araujo, C. C.D.(2008).Groundwater favorability map using GIS multicriteria data analysis on crystalline terrain, Sa˜o Paulo State, Brazil. Journal of Hydrology, 357, 153– 173.

x. Murthy, K.S.R.(2000). Groundwater potential in a semi-arid region of Andhra Pradesh: A GIS approach. International Journal of Remote Sensing, 21, 1867–1884.

xi. Rao, N. S. (2009).Fluoride in groundwater, Varaha River basin, Visakhapatnam District, Andhra Pradesh, India. Environmental Monitoring and Assessment, 152(1-4), 47-60.

xii. Saraf, A.K. and Choudhury, P.R. (1998).Integrated remote sensing and GIS for groundwater exploration and identification of artificial recharge sites. International Journal of Remote Sensing, 19, 1825–1841.

xiii. Shahid, S., Nath, S.K. and Ray, J.(2000).Groundwater potential modeling in softrock using a GIS. International Journal of Remote Sensing, 21, 1919–1924.

xiv. Solomon, S. and Quiel, F. (2006). Groundwater study using remote sensing and geographic information system (GIS) in the central highlands of Eritrea. Hydrogeology Journal, 14, 729–741.

xv. Sreedevi, P.D., Subrahmanyam, K. and Ahmed, S. (2005). Integrated approach for delineating potential zones to explore for groundwater in the Pageru River basin, Kuddapah District, Andhra Pradesh, India. Hydrogeology Journal, 13, 534–545.

xvi. Srivastav, P. and Bhattacharya A.K.(2000).Delineation of groundwater potential zones in hard rock terrain of Bargarh District, Orissa using IRS, Journal of Indian Society of Remote Sensing, 28(2-3), 129–140

Lessons Learnt From The Manual Dredging Of A Minor Port In Northern Malabar

P K Abdulla[1]   C Dinil Sony[2]
[1&2]Scientist, Centre for Water Resources Development and Management, Kunnamangalam, Kozhikode, Kerala, 673571, India
Email: [1.]pka@cwrdm.org; [2.]dsc@cwrdm.org

ABSTRACT: Dredging incur heavy expenditure on ports; the dredged materials can be used for reclamation, beach nourishment, landscaping and in construction industry. Three medium ports and 17 minor ports/fishing harbours owned and operated by the State government exist along 560 km long Kerala coast which is mainly sandy in nature. Dredged material contains significant portion of sand. Government of Kerala initiated manual dredging at Azheekkal port with many objectives; maintain navigation channel, avoiding the revenue expenditure on dredging, minimize/stopping illegal mining by issuing permits for manual dredging with proper license fees, ensure the availability of sand at reasonable price for the construction industry, provide alternate employment to the local community during lean periods, generate additional income through manual dredging, etc. are a few among them. Study revealed that 95% of the dredged material is sand; almost equal percentage in medium and fine sand category. Study also revealed that envisaged objectives, particularly channel clearing and avoiding the revenue expenditure on dredging could not be achieved due to unscientific method in the implementation of this project. Unscientific methods for dredging and separation of dredged materials has caused adverse impacts on river ecosystem; whereas employment generation, better availability of sand, boost to the construction industry, boosted trade in the local market and increase in the port revenue are a few positive impacts. Implementation of manual dredging in a scientific manner can mitigate these adverse impacts. Total ban on dredging during the breeding season of the marine species, zoning the area and specify duration of dredging for each zone and keeping buffer zones near the banks are some of the mitigate measures.

Keywords: construction industry; sand; minor port; impacts; sand washing; marine species.

1. INTRODUCTION

Dredging is unavoidable for the development of ports. Operation of ports often requires maintenance dredging which costs good portion of its revenue; cost of dredging depends on the nature of the sediment, type of the dredgers, distance to the disposal sites, etc. Disposal site for the dredged material will be generally in the open sea or part of the estuary such that the materials will not recirculate to the area of interest. Depending on the nature of the sediments; dredged materials can be used for reclamation, beach nourishment, landscaping and in construction

industry. Twelve major ports and many medium/ minor ports are located on 7200 km long Indian coastline; major portion of the dredged materials (both capital and maintenance dredging) from these ports is often disposed in the sea/estuary, while only a portion is utilized for reclamation and beach nourishment. One major, 3 medium and 17 minor ports are located along 560 km long Kerala coast; which is mainly sandy in nature and the dredged materials from these ports generally contains significant portion of sand which is an essential raw material for the construction industry. Considering the usefulness of the dredged materials in the construction industry and also to avoid the revenue expenditure incurred for mechanized dredging of the port, Government of Kerala initiated manual dredging at selected minor ports with the involvement of the cooperative societies of the local people who are generally involved in fishing activities. Providing employment to the local people particularly during the lean period, stopping illegal sand mining by issuing permits with proper license fee and generation of additional revenue for the port are a few factors vetted in favour of the manual dredging of minor ports. This paper discusses the lessons learnt from the manual dredging programme implemented at Azheekkal port; a minor port in Kerala.

1.1 Study area:

The minor port of Azheekkal in Kannur district, northern Kerala is located at 11°56'38"N latitude and 75°18'36"E longitude on the southern bank of Valapattanam river about 5 km upstream of its confluence with the Lakshadweep sea. Azheekkal fishing harbour having independent basin is situated midway between the port and the inlet. Kuppam river joins with the Valapattanam river on the northern side and is on opposite to the fishing harbour. The drainage areas for Valapattanam and Kuppam rivers are 1867 km^2 and 539 km^2 respectively, of which 546 km^2 and   70 km^2 lies in Karnataka State.   Average annual runoff from Valapattanam and Kuppam rivers are 4779 Mm³ and 1516 Mm³, about 85% of these runoff are contributed by the southwest monsoon. Valapattanam is famous for its timber and allied industries, many plywood factories including the Western India Plywood Ltd, the largest integrated wood-processing complex in the country are located along the bank of this river. Industries associated with shipping and fishing are also exist along the banks of this river.

1.2 Port facilities:

Presently the port is having 305 m long wharf. Light house at Azheekkal is located at the entrance to the port. Because of its position, port is well protected from the turbulence from the Arabian Sea.   To keep the inlet in position and to improve the navigability through the inlet, breakwaters are constructed at the inlet which also improved the tranquility conditions in the port. The port is well connected by road; NH 66 (Panaval-Kanyakumari) passes very close to the port (Fig.1). The port is located in micro tidal zone; the tidal range is about 1m only.
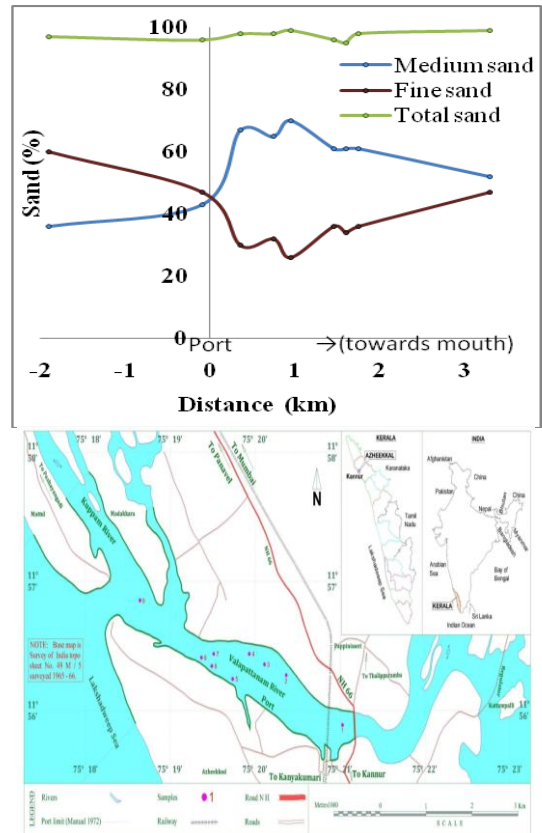
Figure 1. Location map of Azheekkal port

2. MATERIALS AND METHODS

Bed sediments and water samples are analysed for grain size and physico-chemical properties. Available hydrographic charts for different years are used. Perceptions of the local people staying around the sand ghats on manual dredging are gathered through household social survey.   Activities associated with manual dredging are studied.

3. ANALYSIS AND RESULTS

3.1 Sediment samples:

Sediments sampled from different locations from the port area (Fig. 1) are analysed for particle size distribution, both dry and wet sieving was carried out to estimate the amount of fine materials (silt and clay) adhered to the sand particles. Percentages of fine sand (0.075mm to 0.425mm), medium sand (0.425mm to 2.0mm) and coarse sand (2.0mm to 4.75mm) are obtained from the gradation curves. Variations of fine, medium and total sand available in sediments sampled at different points along the river course are shown in Fig 2, which indicates that percentage of particles in the medium sand category increases towards the downstream. However, percentage of particles in medium sand category is relatively low near the entrance. It is seen that sediment samples contain only insignificant portion of silt and clay.   Sediment samples contain more than 95% sand which is mainly in medium and fine sand category.   Gradation

curves for a typical sediment sample are given in Fig. 3. As seen from the figure, the variation between the gradation curves for wet and dry sieving is very little indicating that the amount of fine materials adhered to the sand particles is insignificant, the maximum is only 3%. Physio-chemical parameters for selected sediment sample are given in Table 1.
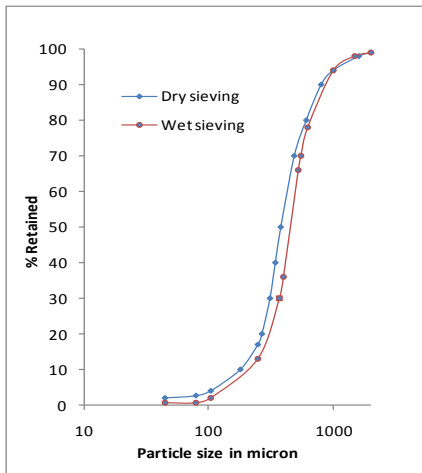
3.2 Water samples:

Water samples from 5 locations in Valappatanam river (Fig. 1), are analysed for various physico-chemical parameters as per the standard procedure; the results of which are given in Table 1. All water samples exceed the tolerance limits for inland surface water when used as raw water for public water supplies and bathing ghats as specified by Bureau of Indian Standards. Most of the timber and plywood industries are located within a distance of 8 km from the river mouth and these industries uses the river for saline seasoning of the timber and as their stockyard. Industrial and coir retting activities enhanced the pollution level in the river which ultimately leads in crossing above specified standard.

3.3 Hydrographic surveys:

For the operation, dredging and developmental works of the port, hydrographic surveys are carried out by the Hydrographic Survey Wing of the Port Department at regular intervals within the port limits. Manual dredging activity at the port is started in the year 2011; hydrographic survey carried out prior to the manual dredging is in November 2010. During the period of manual dredging hydrographic survey was carried out during January 2012; portion of the hydrographic chart around the port area is given in Fig. 4. Features of the port channel (Valapattanam river) changes at many locations along its course, hence comparison between the hydrographic charts of 2010 and 2012 are made. Comparison of cross sectional areas at ten locations (Fig. 4) where the channel features changes significantly or the effect of manual dredging is prominently visible are presented in Figs 5a to 5j. From the Figs 5a to 5c, it can be seen that for the reaches on the downstream portion of the fishing harbour, the areas of the cross section of the river has decreased during 2010-12; the reduction varies between 3% and 12%. Portion of the waterway between the fishing harbor and

300 m downstream of port wharf had undergone only nominal changes in the area of cross section (Figs 5d, 5e, 5f, 5g and 5h). Area of cross section of waterway decreased at section Nos. 5 and 7; whereas it is increased at section Nos. 6 and 8. The percentage change in the area of cross sections in both cases is between 1.5% and 3%. Area of cross section of the waterway remains the same at section No: 4. A long shoal exists between the fishing harbour and the port wharf (from section No. 5 to 8) forming two channels in the river; the port channel is narrow; whereas the wider channel is away from the port wharf which is not favourable for the port. It can be seen from the sections (Figs 5e, 5f, 5g and 5h) that there is no appreciable change for the northern channel; whereas southern channel (port channel) is silted and become shallow and narrow. On the upstream side of the port wharf there is a significant increase in the area of cross section of the waterway, the increase is about 33% for section No: 9 and 60% for section No: 10 (Figs. 5i and 5j). Deepening of river bed is throughout the entire width of the river for the later section; whereas it is mainly in the mid portion for the earlier section. These facts indicate that the manual dredging is not effectively implemented near the port channel and operating area of the port.

Table 1. Physio-chemical parameters for selected sediment sample

Sl. No	Parameters	Water					Sediment
		1	2	3	7	9	1
1	pH	6.30	6.79	6.50	6.83	6.87	7.1
2	Electrical conductivity (μS/cm)	26100	27700	30400	33100	31400	2901
3	Total Dissolved Solids (mg/l)	15600	16800	17300	19200	19500	
4	Chloride (mg/l, mg/kg)	13667	12813	11455	18819	16229	9610
5	Total Alkalinity (mg/l, mg/kg)	4100	7920	2160	2160	1440	504
6	Total Hardness (mg/l)	10400	10400	4000	5600	6400	
7	Sulphate(mg/l, mg/kg)	22	36	39	20	21	395
8	Calcium(mg/l, mg/kg)	2240	640	640	640	1280	800
9	Magnesium(mg/l, mg/kg)	1166	2138	583	972	778	437
10	Sodium (mg/l, mg/kg)	5560	5880	6120	6510	6430	2870
11	Potassium (mg/l, mg/kg)	270	290	310	340	330	215
12	Salinity (ppt)	17	19	19	21	22	
13	Total organic carbon (%)						0.5

3.4 Social survey:

Perception of the local people on manual dredging are collected through a social survey during January 2012 using prepared performa. Randomly selected 338 households located around the sand ghats on both banks of the rivers are covered under the survey. Though the guidelines for issuing permit for manual dredging is to limit for the cooperative societies of the local

people who are generally involved in fishing and coir retting activities, only 8% of the sample population had memberships in any of the societies associated with the manual dredging; whereas only 10% of the sample population are involved in the manual dredging activities. Majority of the workforce engaged in the manual dredging activities belongs to other States; details of their whereabouts are known neither to the societies engaging them in dredging activities nor to the local people. Generally they are accommodated in congested conditions with insufficient facilities poses health, social and cultural problems. Local people had apprehensions about the increased vehicular traffic mainly due to the sand laden trucks which often ply during wee hours of the night. They are concerned about the negative impacts if any to the river environment caused by the manual dredging and also on the infrastructure particularly on the roads with multi axle trucks.
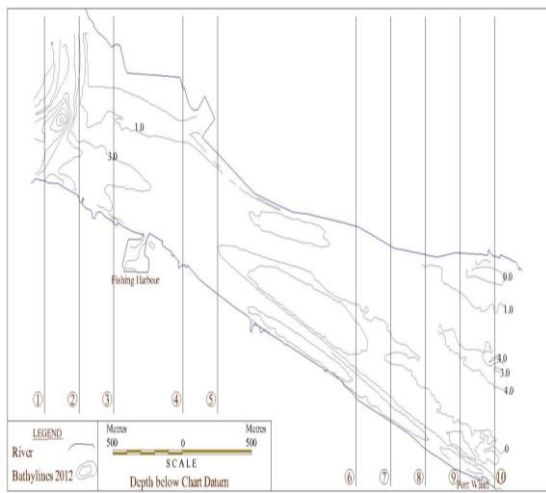
Figure 4. Hydrographic chart of the study area

3.5 Separation lime shell and sand:

Besides sand, dredged materials from the port contain lime shells and little amount of clay. The process of separating lime shell and sand is practiced at many sand ghats located on the river banks. Dredged material is pumped as slurry to temporary wells located on the river banks through large meshed sieve which will remove the lime shell. The sand particles will be settled in the open wells, whereas the fine particles (clay) recirculate to the river along with the overflow. In addition to fine particles, dredged materials from different stretches of the river contain residual chemicals of the plywood industries; separation process of lime shell and sand practiced at few sand ghats can results in concentration of residual chemicals and fine particles near the vicinity of the same. Separation is a continuous process, over a period of time the fine particles and residual chemicals will get deposited on the river bed which will affect the sediment quality, fish breeding, micro-organisms present in the river bed, make the river bed impervious and further deterioration of the water quality; ultimately all these will affect the river environment adversely.

3.6 Manual dredging practice

During the flourishing time of the manual dredging (January 2012), licenses were issued to 11 cooperative societies for carrying out the manual dredging at Azheekkal port. Workforces of these societies vary between 95 and 298; total workforce for all the societies put together is 1998. Country boats having valid license under Kerala State Harbour Craft Rules 1970 only are permitted for manual dredging, number of vessels used by these societies varies between 4 and 35;
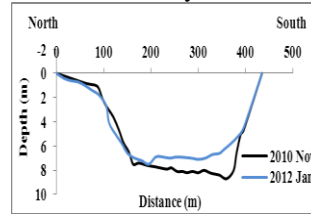
Fig 5a. Comparison of cross section at section No.1   **Fig 5f.** Comparison of cross section at section No.6
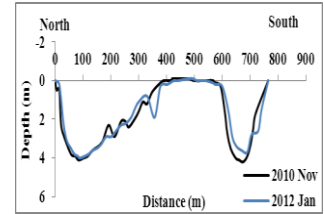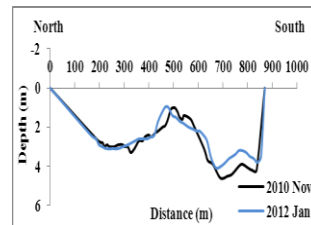
Fig 5b. Comparison of cross section at section No.2   **Fig 5g.** Comparison of cross section at section No.7
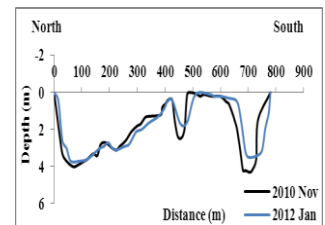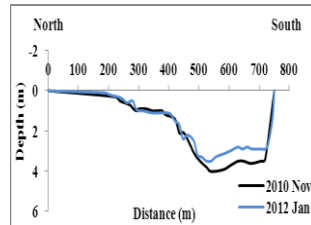
Fig 5c. Comparison of cross section at section No.3   **Fig 5h.** Comparison of cross section at section No.8
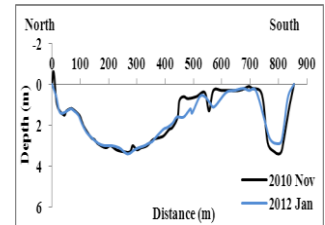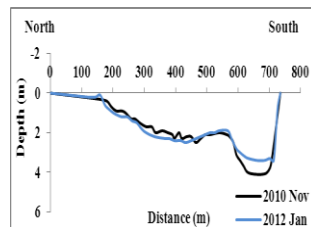
Fig 5d. Comparison of cross section at section No.4   **Fig 5i.** Comparison of cross section at section No.9
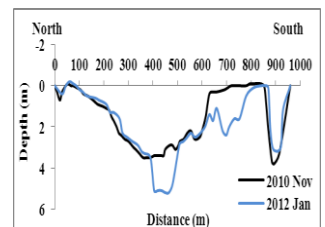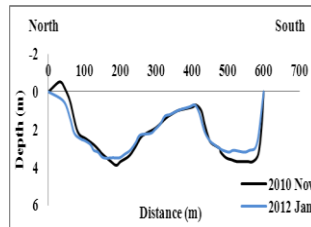
Fig 5e. Comparison of cross section at section No.5   **Fig 5j.** Comparison of cross section at section No.10
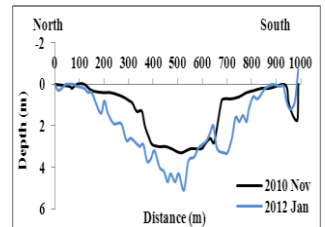
total number of vessels with all the societies is 229. These 11 cooperative societies associated with the manual dredging activities operate from 19 jetties located on both banks of the river; carried out manual dredging wherever they feel to fetch maximum profit. Continuous disturbances to the bed cause removal/destruction of benthos, habitat reduction and even the complete disappearance of well-developed benthic communities around the area. Certain marine species are more sensitive to disturbances due to dredging than others; recovery of the disturbed habitats depends on the nature of the new sediments, nature of re-colonizing species, current, extent of disturbance, etc.

4. DISCUSSIONS

Manual dredging at selected ports are initiated with noble objectives. Fulfillment of the objectives of any project depends on how it is implemented. An attempt is made to assess the extent of fulfillment of different objectives envisaged for the introduction of the manual dredging at Azheekkal port and are summarized in Table 2.

Table 2. Fulfillment of the envisaged objectives of the manual dredging

Objectives envisaged	Achievement	Non fulfillment
Channel clearing		Unscientific dredging practices caused deterioration of the port channel both in terms of width and depth
Avoid expenditure on maintenance dredging		Unscientific dredging practices caused deterioration of the port channel both in terms of width and depth
Involvement of cooperative societies of the local people	Only cooperative societies are entrusted with the manual dredging	Limited involvement of local community in these cooperative societies. Only 8% of the household covered under the survey are having membership in these cooperative societies.
Employment to the local people in the manual dredging programme		Limited employment for local community in manual dredging. Only
		10% of the sample population are associated with manual dredging.
Stopping illegal sand mining	To a great extent	
Availability of sand for construction industry	To a great extent	
Generation of additional revenue for port	Sand sale price (30%) Vehicle pass Fee for sand ghats Registration of Society with port Registration of boats Land rent (if used)	

Manual dredging and associated activities can cause both beneficial and adverse impacts, on the environment and in the society. Following are a few effects caused by different components of the activities.

Dredging: Unscientific (continuous and haphazard) dredging causes removal/reduction/ destruction to the benthos and disappearance of developed benthic community. Changes in the hydrodynamics (flow pattern) of the river may cause changes in the erosion/deposition pattern; change in the bathymetry will alter the sediment transport regime and also affect the breeding of the aquatic species.

Separation of lime shell and sand: Unscientific separation of lime shell and sand on the bank of the river adversely affect the breeding of the aquatic species, micro-organism, further deterioration of water/ sediment quality and make river bed impervious; all these causes adverse impacts on the river environment.

Infrastructure: Large numbers of sand laden trucks, particularly multi axle trucks plying are adversely affect the roads.

Social: Accommodating the workforce from other states in congested condition with insufficient facilities cause social, health and cultural problems. Whereabouts of these workforces are not known to the societies engaging them or to the local people.

Boost to the construction industry and in the local trade, increasing purchasing capacity of the local people, relief to the scarcity of sand, increased employment opportunities are some of the positive effects. Engagement in the manual dredging, construction industries, transportation of construction materials, local trade are a few employment avenues.

The best way for the conservation of any species is to maintain ideal conditions for its breeding. A total ban on the dredging activity during the breeding period of aquatic species is essential to ensure minimal disturbances for this period. Deployment of all societies engaged in the manual dredging to a single zone can ensure the localization of the disturbances while most part of the estuary will remain undisturbed/with least disturbances, which will provide space with minimum disturbances for aquatic flora and fauna. Manual dredging in a disciplined and phased manner in the demarcated zones is to be strictly enforced. Dredging near the banks other than in front of is a waterfront structure should not be allowed. Improvements of the roads to the jetties, imposing traffic regulation for the trucks are required for better functioning. Institutional mechanism should be strengthened through additional manpower, equipment and interdepartmental cooperation to ensure disciplined manual dredging and for stopping the illegal mining of sand. Sand washing should be strictly prohibited on the banks of the river.

Physiochemical properties of sediment samples indicate similar pattern as that of the water samples. Timber mills and plywood industries on the river bank and effluent from these industries are the major source of pollution.

Illegal sand mining is a practice in most of the States, often this causes law and order problem; here also illegal mining is practiced. It is learnt that after the introduction of manual dredging at Azheekkal port, the illegal sand mining is reduced significantly. Presence of salt in the sand dredged from the port is the main drawback to use this sand for a few item of construction work, particularly for the reinforced cement concrete work.

5. CONCLUSION

Envisaged objective of the manual dredging from Azheekkal port limits can be achieved only if the programme is implemented in a scientific manner. A total ban on manual dredging should be imposed during the breeding period of aquatic species. At any time all societies engaged with dredging should be deployed into a single zone which can ensure minimal disturbances within the port limit and cause least adverse impacts on aquatic species. Washing of sand on the banks of the river should be strictly prohibited.

ACKNOWLEDGEMENTS

Selection of Fender System

S.N. Das[1]   S. Kulkarni[2]   M.D. Kudale[3]
[1] Research Officer, CWPRS, Pune,411024, India
[2] Chief Research Officer, CWPRS, Pune,411024, India
[3] Joint Director, CWPRS, Pune, 411024, India
Emil: sndas_cwprs@rediffmail.com

ABSTRACT : *The principal function of marine fender system is to prevent vessel or berth structure from being damaged during ship berthing or during ship moored to jetty. The fenders should have high energy absorbing capacity with exerting manageable reaction force on quay and on ship's hull. Thus selection of marine fender is an important aspect as it determines the safety and efficiency of port operations. A Quick Fender Selection Method (QFSM), based on conversion of ship berthing energy into potential energy of the fender, has been applied for the determination of suitable fender to be installed at Multi User Liquid Terminal jetty at Cochin Port. The Super Cone Fender of 2 m height is capable of absorbing the berthing energy of 80000 DWT Oil Tanker. A ship-fender relation intended as a guideline for selection of fenders for various types of ship is discussed in the paper.*

Keywords: Ship berthing, QFSM, berthing energy, ship-fender relation, fender selection

1. INTRODUCTION

Fender acts as interface between a ship and face of a berth structure. The main function of a fender is to absorb certain amount of kinetic energy of a berthing ship through fender compression and transform remaining part of the kinetic energy into reaction forces which both the ship and the berth structure can sustain safely. Therefore, a fender system must be able to stop the berthing ship gently without damaging the ship, the berth structure and the fender itself. In the early days, vessels were made of wood and run by wind and human efforts. At that time timber (first generation fender) was used as fenders. Afterwards, old vehicle tyres (second generation fender) were used as fenders; but the old tyres absorbs little energy. With the advancement of ship building technology and necessity for mass transportation system, vessels were made to propel by steam engines or diesel engines, and hulls were constructed by steel in place of wood. Cylindrical type rubber fenders (third generation fender) were the first purpose designed fenders developed in 1940, which allowed vessels to berth directly at the wharves. However the cylindrical fender use to get damaged easily and had high reaction forces. To overcome these difficulties, V-shaped buckling type fenders (fourth generation fenders) were developed around 1960. It offered better durability and energy absorption capacity with lower reaction force compared to cylindrical fenders. The research and development work continued in search of ideal fenders dedicated to berthing of small boats to super tankers. Modern marine fenders of fifth generation have been evolved for modern ports and terminals, diverse vessels, high valued and hazardous cargo. These fenders are highly sophisticated units, produced with the aid of computerized design, engineering expertise and advanced

manufacturing process. These fenders also ensure the enhancement of safety and efficiency of port operation, and hence reduced the downtime.

2. CATEGORIES OF FENDERS

Fender systems can be categorized primarily the way by which they absorb or dissipate kinetic energy. Some categories of fender systems (PIANC, 1984) are given in Table 1.

Table 1. Categories of Fender

Mode of absorption of ship's kinetic energy		Fender type
Conversion to potential energy by gravity force		Gravity
Conversion to potential energy by buoyancy force		Floating body
Conversion to potential energy by elastic deformation	Compression	Spring Bush End loaded rubber Pneumatic Foam filled
	Compression/ bending	Side loaded rubber Buckling
	Shear	Shear
	Compression / shear	Rubber / steel sandwich
	Torsion	Torsion
	Bending	Flexible pile
Dissipation of heat energy		Hydraulic
Dissipation by plastic deformation		Steel corrugated unit

Many fenders as mentioned in Table 1 are not in use and hence replaced by more efficient fenders. The gravity, buoyancy, spring, bush and end loaded fender have been used successfully in the recent past. But, these fenders are not the optimum fender for a modern port providing safe berthing even in normal environmental conditions for large vessels. Shear fenders do not have sufficient energy absorption capacity. The rubber and steel sandwich fenders are replaced mostly by less expensive and more efficient buckling fenders. Torsion fenders are not so efficient and popular to be used widely. Fender like gravity, floating body, hydraulic, steel corrugated etc., are expensive to install, difficult to maintain and not designed for stringent mooring requirement of modern vessels. For modern ships and marine terminals the buckling type fenders and pneumatic fenders are serving the purpose. Henceforth, fender indicates only modern marine fender of fifth generation which are used for recent vessels. The shapes and performance characteristics of these fenders are given in Table 2.

3. DESCRIPTION OF VARIOUS MODERN FENDERS

The performance of a fender depends on the manufacturing process, material compound formulation and mixing, embedded steel surface, wrapping or moulding. The description and application of some modern fenders are described below:
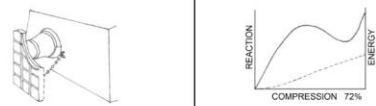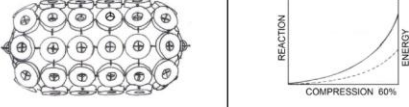
Super Cell Fenders (SUC)

The Super Cell Fender has high energy absorption capacity and low tilt compression performance. In the front it is equipped with frame pad which greatly reduce the face pressure on ship panel and generates low friction force. This fender requires less maintenance and long usage life.

Super Cone Fenders (SCN)

Super Cone Fenders are the latest generation of "cell" fenders having excellent energy absorption capacity with low reaction force. The conical shape keeps the body stable under all combinations of axial, shear and angular loading, making it ideal for berths where large berthing angles and heavy impacts need to be accommodated. Optional overload stops can be moulded inside the cone to prevent over compression.

Table 2. Types of modern fenders, their shapes and performances

Parallel Motion Fenders (PMF)

Parallel Motion fender systems use a non-tilt torsion arm mechanism which keeps the frontal panel vertical all the time irrespective of impact level and allows the panel to rotate freely to fit with large berthing angles. Forces are evenly spread to reduce contact pressure. These fenders are high energy absorption capacity with reaction forces 30~60% lower than conventional fenders.

V-Shaped Fenders (VSF, UPi)

Conventional cylindrical type fenders absorb energy through compressive deformation while V-shaped fenders materialized a revolutionary improvement of energy absorption by adding compressive deformation to buckling deformation. The V-shaped fenders consist of pairs of elements with and without frontal pad to make a simple but highly versatile design.

Pneumatic Fenders (PNU)

Pneumatic Fenders are ideal for permanent and semi-permanent port applications where there is a solid faced quay structure. Their low reaction and large contact area make them ideal for "soft" vessels. Optional chain tyre net units are ideal for heavy duty and exposed locations. Special mooring guide systems can be provided at locations having very high tidal range, to prevent the fenders from drifting off.

Foam fenders (FOM)

Foam fenders are unsinkable and robust due to their thermo-laminated closed cell polyethylene foam core. They have a tough outer skin of reinforced polyurethane elastomeric material. The foam filled fenders provide good energy absorbing capacity with low reaction force.

4. FENDER SELECTION CRITERIA

The major factors while selecting fender systems are:

1.   The fender system must have sufficient energy absorption capacity to absorb the kinetic energy of the berthing vessel or moored vessel.
2.   The force exerted by a fender on the ship's hull as well as berthing structures should be within limit.
3.   Special attention must be paid while selecting fenders for vessels with unusual hull configuration or protrusions.
4.   The fender system must accommodate all the vessels during full range of water levels.

5. QUICK FENDER SELECTION METHOD (QFSM)

A Quick Fender Selection Method (QFSM) is based on conversion of ship berthing energy into potential energy of the fender. QFSM consists of four modules of input data namely, ship data, berthing facility, environmental conditions and berthing data. These are used to compute ship berthing energy using empirical formulae and laboratory tested coefficients. The energy absorption capacity of a fender must be higher than that of berthing energy and it must perform in accordance with tidal levels and hull pressure. The flowchart (Fig. 1) depicts the fender selection process.
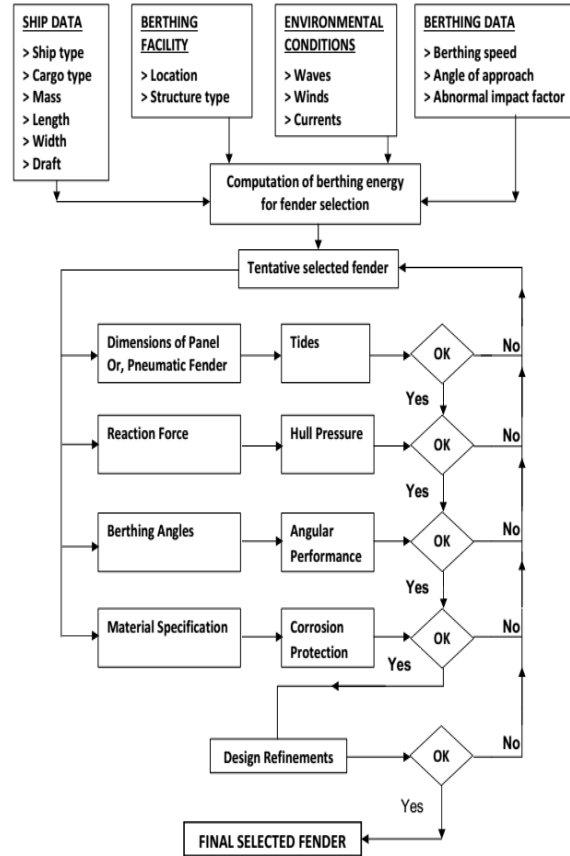
Figure 1. QFSM Flow Chart

5.1 Computation of design energy

Computation of design energy to be absorbed by the fender is of prime importance in the selection of fender system. The design energy for a vessel of mass M (ton) approaching towards a berth with a speed of v (m/s) is computed using following formula (Report of Working Group: PIANC, 2002):

$$E_d = \frac{1}{2}Mv^2 C_e C_m C_s C_c$$

(1)

Where E_d is the design energy to be absorbed by fender (kNm), C_e is the eccentricity factor, C_m is the virtual mass factor, C_s is the softness factor and C_c is the berth configuration factor.

6. APPLICATION OF QFSM

Cochin Port proposed to develop Multi User Liquid Terminal jetty located in the exposed area near the entrance of the harbour

to cater Oil Tankers ranging between 10,000 DWT and 80,000 DWT, and LPG Vessels ranging between 5,400 DWT and 55,000DWT. The computed berthing energy for abnormal impact of the largest vessel i.e., 80,000 DWT Oil Tanker with approach velocity of 0.4 m/s is 3126 kNm. This energy can be absorbed by a Super Cone Fender of 2 m height having maximum energy absorption capacity of 3330 kNm (CWPRS Report No. 5070, 2014).

Finally, QFSM has been applied to different types of ships in order to get an overview of the fender selection. The data of these ships are given in the Table 3. The environmental conditions (EC), ship's speed (SS), abnormal impact factor (AIF), computed berthing energy, maximum reaction force for designed fender, hull pressure and proposed fender for specific ships are described in the Table 4.

Table 3. Ship Data

Sh	DWT	Mass (ton)	LOA	LB	Beam (m)	Depth (m)	Block	Max.	Hull Pressure
General	5000	7690	111	104	16.9	9.4	0.61	6.6	400-700
	10000	14800	137	129	20.5	11.6	0.62	8.3	400-700
	20000	28400	170	161	24.9	14.3	0.63	10.4	400-700
	40000	54500	211	200	30.2	17.6	0.64	13.0	<400
Bulk car	10000	13300	132	124	19.2	10.6	0.66	7.7	<200
	20000	25700	161	152	23.8	13.0	0.70	9.4	<200
	50000	61100	209	200	32.3	17.1	0.71	12.4	<200
	70000	84000	231	221	32.3	18.9	0.80	13.7	<200
Containe	7000	10700	123	115	20.3	9.8	0.58	7.2	<300
	15000	22200	166	156	25.0	13.3	0.58	9.0	<300
	30000	43000	218	205	30.2	17.5	0.57	11.1	<300
	60000	83200	286	271	36.5	23.0	0.56	13.8	<300
Oil tank	20000	27700	158	151	25.8	12.8	0.69	9.6	<300
	50000	66400	211	204	32.3	17.6	0.75	12.6	<300
	70000	91600	235	227	38.0	19.9	0.72	13.9	<350
	100000	129000	263	254	42.5	22.5	0.73	15.4	<350
Ro/Ro sh	1000	2190	73	66	14.0	6.2	0.60	3.5	BELTED
	5000	9670	131	120	20.7	12.5	0.54	6.4	
	15000	26700	196	180	27.2	20.3	0.51	9.6	
	30000	50600	252	233	32.2	27.6	0.49	12.4	
Ferry	1000	1230	67	61	14.3	5.5	0.37	3.4	BELTED
	5000	5970	119	110	21.4	9.0	0.42	5.5	
	10000	11800	153	142	25.4	11.1	0.44	6.8	
	20000	23300	196	183	30.2	13.8	0.46	8.3	
Gas c	20000	34800	179	169	28.4	16.5	0.61	11.0	<200
	50000	78000	237	226	37.2	22.8	0.70	12.3	<200
	70000	105000	263	251	41.2	25.7	0.77	12.3	<200

Ship Type	DW	EC	SS	AIF	Com m	Max reaction per unit	Hull pressure	Proposed fender	
a r	100000			14400 0	294	281	45.8	29.2	0.85 12.3 <200

Table 4. Computed Berthing Energy and Proposed Fender

Ship Type	DW	EC	SS	AIF	Com m	Max reaction per unit	Hull pressure	Proposed fender	
General cargo	5000	F	0.2	1.75	132	440	220	400-700	SCN600H
	10000	M	0.45	1.75	1311	1970	197	400-700	SCN1300H
	20000	U	0.45	1.75	2560	3278	273	400-700	SCN1600H
	40000	U	0.45	1.75	5003	2980	248	<400	PMF1800H
Bulk carrier	10000	F	0.2	1.75	235	566	57	<200	CSS1000H
	20000	M	0.3	1.75	1024	1667	167	<200	CSS1600H
	50000	U	0.45	1.50	4669	5690	144	<200	PNU4.5X1 0.5
	70000	U	0.45	1.50	6902	3680	191	<200	PMF2000H 2C
Container carrier	7000	F	0.2	2.00	199	558	279	<300	SCN700H
	15000	M	0.3	2.00	931	1503	251	<300	SCN1200H
	30000	U	0.45	1.75	3567	6612	220	<300	PNU3.3x1 0.5
	60000	U	0.2	1.50	1178	2560	224	<300	PNU2.5x5. 5
Oil tanker	20000	F	0.12	1.75	172	633	181	<300	UPi800H
	50000	M	0.3	1.75	2690	5121	171	<300	PNU3.3x1 0.5
	70000	U	0.2	1.50	1360	1542	257	<350	UPi2000H
	100000	U	0.2	1.50	1915	1785	298	<350	UPi2500H
Ro/Ro ship	1000	F	0.2	2.25	40	220	110	BELTED	UPi400H
	5000	M	0.45	2.25	945	1818	303		UPi1150H 2mL
	15000	U	0.45	2.00	2436	4545	325		UPi1150H 5mL
	30000	U	0.45	2.00	4805	6720	480		UPi1700H 5mL
Ferry	1000	F	0.2	2.25	20	197	657	BELTED	BETA250H
	5000	M	0.45	2.25	519	1224	204		UPi1000H 2mL
	10000	U	0.6	2.00	1651	3570	340		UPi1000H 5mL
	20000	U	0.45	2.00	1862	4270	407		UPi1000H 5mL
Gas carrier	20000	F	0.12	1.75	214	627	179	<200	SCN700H
	50000	M	0.3	1.50	2472	5121	171	<200	PNU3.3x1 0.5
	70000	U	0.2	1.25	1217	1846	185	<200	SCN1300H
	100000	U	0.2	1.25	1668	1555	156	<200	PMF1300H

EC=Environmental condition   SS= Ship speed in m/s
AIF=Abnormal impact factor
F = Favourable, M =   Moderate, U = Unfavourable

A ship–fender matrix relation is obtained for different tidal range, berth types and its location as given in Table 5. The set of

fenders selected are not unique; equivalent fenders satisfying the conditions may also work.

Table 5. Ship – fender matrix

Ship Type	Range of DWT in thou	Environ		Tidal Range	Berth		Berth Locat		Propose		Propose
		F	M	U	(0-2)	(2-5)m	Solid	Pi	P	OS	
General cargo	5-10	✓			✓		✓		✓		SCN1300H,
	10-20		✓			✓		✓	✓		SCN1600H,
	20-40			✓		✓		✓	✓		PMF1800H,
Bulk carrier	10-20	✓			✓		✓		✓		SUC1600H,
	20-50		✓			✓		✓	✓		PNU4500X105
	50-70			✓		✓		✓	✓		PMF2000H – 2CONE
Container carrier	7-15	✓			✓		✓		✓		SCN1200H,
	15-30		✓			✓		✓	✓		PNU3300x105
	30-60			✓		✓		✓	✓		PNU2500x550
Oil tanker	20-50	✓				✓		✓	✓		PNU3300x105
	50-70		✓		✓			✓		✓	UPi2000H, 3x2
	70-100			✓	✓			✓		✓	UPi2500H, 3x2
Ro/Ro ship	1-5	✓			✓		✓		✓		UPi1150H
	5-15		✓			✓		✓	✓		UPi1150H
	15-30			✓		✓		✓	✓		UPi1700H
Ferry	1-5	✓			✓		✓		✓		UPi1000H
	5-10		✓			✓		✓	✓		UPi1000H
	10-20			✓		✓		✓	✓		UPi1000H
Gas carrier	20-50	✓				✓		✓	✓		PNU3300x105
	50-70		✓		✓			✓		✓	SCN1300H,
	70-100			✓	✓			✓		✓	PMF1300H,

PH = Protected harbour, OS = Open sea

7. CONCLUSIONS

QFSM can be used conveniently as an efficient tool for fender selection. The essence of the study is a "Ship-fender matrix" derived from application of QFSM to various ships. This can be useful as a guideline to port and harbour engineers and planners for the selection of fender.

REFERENCES

i. *Report of the international commission for improving the design of fender system, PIANC 1984*
ii. *Guidelines for the design of fender systems: Report of Working Group 33 of the Marine*
iii. *Navigation Commission, PIANC 2002*
iv. *Ship mooring analysis for the proposed MULT jetty at Cochin Port, Technical Report No. 5070,*
   November 2014, CWPRS, Pune, India

Determination of Effect Of Stacking Sequence On Strength Evaluation Of Composite Propeller Blade

M.L.PavanKishore[1] R.K. Behera[2]

[1]National Institute of Technology, Rourkela 769008, India
[2] National Institute of Technology, Rourkela 769008, India
Email: kishoremamdoor9@gmail.com

ABSTRACT : Because of the complexity of the geometry, material system application of various boundary conditions the strength evaluation of marine propeller blade cannot be predicted accurately. The strength capabilities of marine propeller blade made with composite are very much dependent on the material properties of ply orientations and stacking sequence. The study of the proposed work mainly focuses to evaluate the dynamic characteristics of a composite propeller blade. The effect of stacking sequence, ply orientations will be studied. The solution to the dynamic analysis of the propeller blade will be obtained by using finite element based numerical solver Ansys. Each layer will be modeled separately. The proposed study will reveal some interesting features of the propeller blades. In this study the parameters determined are used in strength predictions.
Keywords: Ansys, Finite Elements, Mesh, Mode shapes

1. INTRODUCTION

During the past years most of the marine propeller blades are fabricated from the materials of cast iron, members of steel, Bronze. Comparatively two principal materials which has changed over the years [1] and replaced the above stated materials are high tensile brass and Nickel aluminum bronze, Manganese aluminum bronze. Early in the years 1960's High tensile brass accounted for 64%.In 1980 Nickel aluminum Bronze has gained complete dominance over the other material accounting for 82% of the propellers. From strength and stiffness point of view for a given blade to minimize inertia, to reduce gyroscopic loads and to avoid fatigue the blade should be as light as possible. Blades made of these materials are subjected to excessive weight, corrosive environment and reduced fatigue life. Because of these limitations most of the blades operating under water conditions are fabricated with composite materials.

Popularity of these composite materials in the present scenario is mainly because of their high specific strength and stiffness. [2]The composites are gaining wide acceptance, particularly in marine ,aerospace for their low weight, high strength to weight ratios and their capabilities to withstand high temperatures being used in applications such as radomes, surfing blades, gas and steam turbine blades, gears of locomotives, conveyer belts,

pump impellers in mineral slurry processing. Visualizing their importance of composites a lot of work has been done to evaluate various types of polymers and their composites. Most of these works have carried out over wide range of glass, carbon, graphite, Kevlar, fibers in the form of tape, fabric, chopped materials as reinforcement. Taylor [3] considered a propeller blade as a cantilever rigid at the boss. A theoretical study to determine the vibrations of a pre twisted cantilever blading was done by [4]. The blading is pre twisted linearly about the centroidal axis of its cross section up to an angle of π/2c and is considered to be mounted en casted at the root. White [5] employed greens functions to derive the conditions of orthogonally for a uniform pre twisted blade executing bending-bending vibrations. Diprima and Handle [6] solved the equation of motion of a pre twisted cantilever blade by the Rayleigh Ritz principle. Hi-Royuki Matsunaga [7]analyzed the stresses and displacements in the laminated composite beams subjected to lateral pressures by using the method of power series expansion of displacement components. [8] Presented a paper using the combined classical momentum and blade element theory to design the wind turbine blade aerodynamic shape. [9] Conducted mechanical property test and vibration characteristics test of carbon fiber reinforced plastics specimens that can be adopted as new, marine propeller materials [10] determined the vibration characteristics of pre twisted metal matrix composite blade using beam and plate theories. Sabeel &Vijayangan [11] studied the effect of stacking sequence on tensile, flexural and inter laminar shear properties of glass-fiber reinforced isothalic polyester composites and reported that incorporation of glass in fiber composites enhances the properties of resulting hybrid composites and layering sequence significantly affects the flexural and inter laminar shear strength. Miyazaki & Takeda [12] studied the effect of above the effect of matrix materials, reinforcement fibers, interface strength between matrix materials and fibers impact angle, particle velocity on the solid particle erosion behavior of short glass carbon fiber reinforced nylon 60 resin. Pipes, R. B. and Pagano, N. J [13] studied the mechanism of shear transfer and response with in a composite symmetric laminate by treating with classical elasticity theory under uniform axial condition. Chuijin Yang, Jubing [14] Studied the effects of inter laminar stresses of a plate subjected to uniform axial strain condition combining the first shear theory with layer wise theory. [15] Andrew Makeev used a simple approximate method for predicting the effects of inter laminar stresses in composite laminates subjected to axial tension and torsion loads. Detailed stacking sequence on particular specific layer orientation of a laminate under uniaxial and fatigue loadings over laminate strength was given by Pagano, N. J., and Pipes, R. B [16]

2. PROPELLER BLADE MODELING

The selection of element type becomes an important parameter for modeling of a laminate for the propeller blade. Since blade being a complex geometry modeled with composite and metallic materials with aero foil shape having pretwist and varying thickness along its length
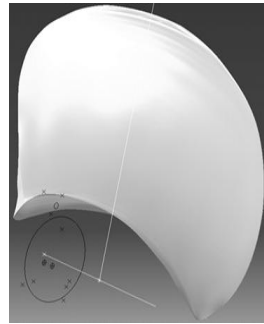
Figure 1. Single surface Propeller Blade
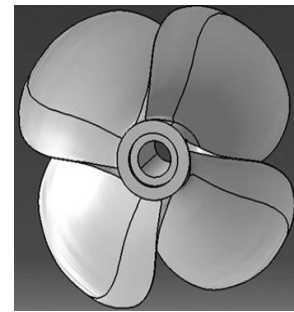
Figure 2. Solid Model of Propeller Blade

2.1Element types
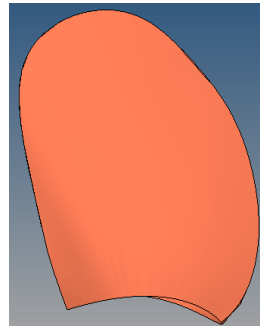
Figure 3. Single Propeller Blade
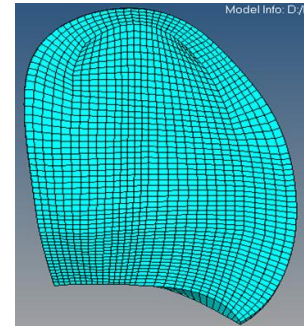
Figure 4. Meshed Propeller Blade

For analysis of composite laminates using numerical analysis like Ansys various element types are defined for 2d modeling shell99, shell91, shell181 are used. For 3d modeling solid46, solid191 are used. In this research work the modeling of propeller blade concerned as three dimensional shell181 element is used. Shell 181 element having 4 nodes which each node having six degrees of freedom supports modeling of composite structures.

2.2. Materials

A four bladed propeller with three dimensional models shown in figure is considered for study. The propeller blade is modeled with different materials.Since the propeller is right handed propeller Isotropic material Nickel Aluminum Bronze is used as the base material for both blades and hub. Later the blade materials are replaced with composite materials. The composite blade is made of number of plies of orthotropic materials; the principal material lines of a ply may be oriented at an arbitrary angle with respect to the x-axis. Glass fiber is used as reinforcement in the form of unidirectional fibers with epoxy resin as a matrix. The mechanical propeller of composite are tabulated in table[2] considering the constituent of composite to the linear elastic and generally orthotropic therefore the concept of engineering constants are used to describe them elastically. Certain elastic properties are required as input parameters for the analysis. The input parameters are shown in the table.

Table 1. Material properties for Metallic propeller

Material used	NAB
Young's modulus	121.5[Gpa]
Poisson's ratio	0.34
Density	7.55[g/cc]
Hardness	152-190 [BHN]

Table2. Material properties of composite blade

Mat erial	E_x [Gpa]	E_y [Gpa]	Ez [Gpa]	NU xy	NU yz	NU zx	G_{xy} [Gpa]	G_{yz} [Gpa]	G_{zx} [Gpa]	density g/cc
S-Glass	22.92	22.92	12.4	0.12	0.2	0.2	4.7	4.2	4.2	1.8

3. ANALYSIS OF PROPELLER BLADE

The blades were discretized using finite elements as shown in the fig. The element type chosen for analysis is shell 181 for isotropic material and composite (orthotropic material).The element solid 45, solid 46 has 8 nodes, associated for 3d modeling; possess 3 degrees of freedom at each node. The choice of element type depends on the application of structural model and the results are to be calculated.

4. RESULTS & DISCUSSIONS

4.1. Static Analysis

Table3. Comparison of NAB vs. Composite Propeller

	NAB	S-Glass epoxy
Deflection	2.78535	0.20819
x-component stress	103.386	1.30743
y-component stress	479.207	4.53431
z-component stress	74.7087	0.99693
I Principal stress	74.7087	4.56388
II Principal stress	161.337	2.08901
IIII Principal stress	0.63050	0.00703
Vonmises	423.471	4.21451
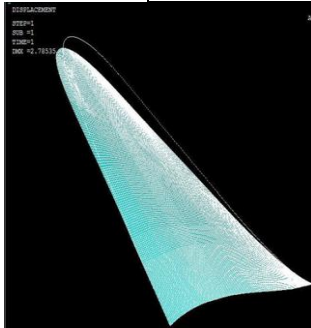
Figure 5. Deflected shape of NAB blade   **Figure 6.** Deflected shape of Composite blade
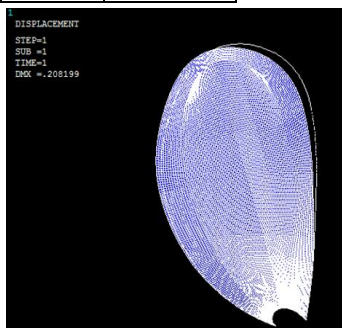
Table4. Composite with various stacking sequences for deflection and Inter laminar stresses

Stacking Sequence	Deflection	Inter Laminar stresses	
		Min	Max
$(45_2/0_4/90/45/0_2/-45/0/90)_{sym}$	0.20819	-82.5270	77.1046
$(0/45/-45)_7(0/90)_2$	0.21708	-83.5047	77.9270
$(45/-45/0)_7(0/90)_2$	0.22701	-83.4314	78.0294
$(45/0/-45)_7(0/90)_2$	0.22185	-83.2624	77.8298
$(-45/0/45)_7(0/90)_2$	0.23259	-86.3005	80.7387

4.2. Modal Analysis
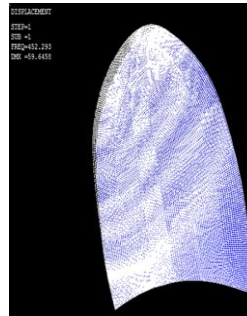
Figure 7. I Mode shape of NAB   **Figure 8.** I Mode shape of Composite
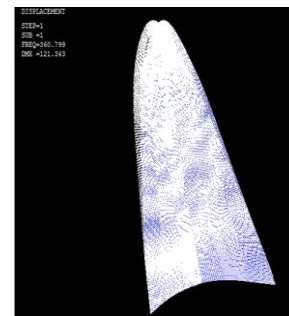
Table5. Comparision of Natural frequencies of NAB vs. Composite

Mode No	NAB	S-Glass epoxy
1	452.29	360.80
2	1483.9	1188.3
3	1692.0	1352.9
4	3104.1	2495.2
5	4139.7	3288.9
6	5745.9	4543.1
7	6272.5	4898.9
8	6758.8	5613.7
9	7616.9	5940.9
10	8581.4	6891.4

SNo	SQ-1	SQ-2	SQ-3	SQ-4	SQ-5
1	360.80	355.72	347.77	351.51	347.77
2	1188.3	1178.4	1165.3	1171.9	1165.3
3	1352.9	1355.2	1366.2	1306.9	1366.2
4	2495.2	2484.1	2439.3	2460.5	2439.3
5	3288.9	3307.1	3323.8	3316.6	3323.8
6	4543.1	4494.1	4432.2	4462.3	4432.2
7	4898.9	4909.0	4892.7	4899.9	4892.7
8	5613.7	5396.2	5385.5	5390.5	5385.5
9	5940.9	5956.6	5951.0	5953.8	5951.0

| 10 | 6891.4 | 6794.3 | 6739.1 | 6765.1 | 6739.1 |

4.3. Harmonic analysis
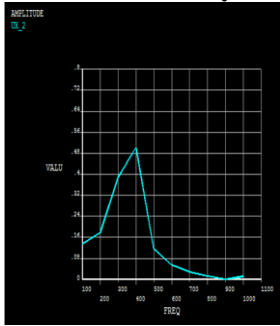
Figure 9. X-component of displacement for NAB
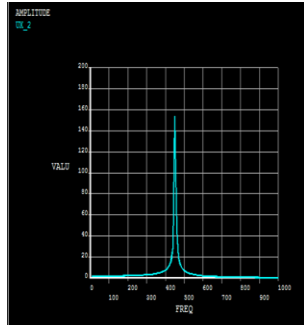
Figure 10. X-component of displacement for Composite

Table6. ComparisonofNaturalfrequenciesforComposite with various stacking sequences
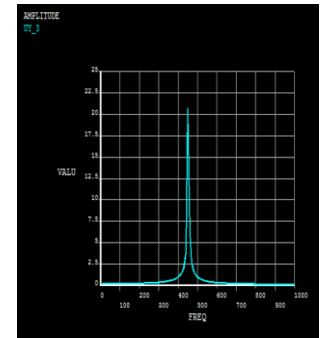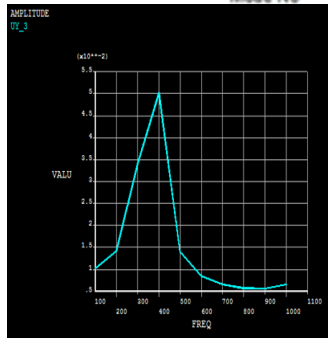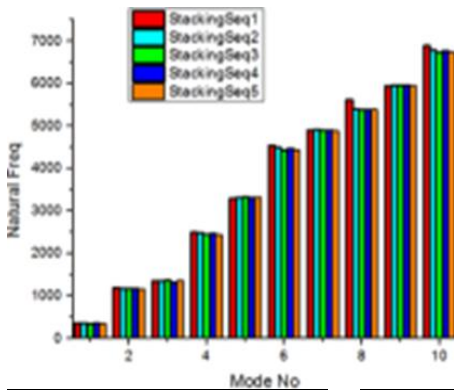
Figure 11. Y-component of displacement for NAB

Figure 12. Y-component of displacement for Composite

Figure 13. Z-component of displacement **Figure 14.** Z-component of displacement for for NAB Composite

5. CONCLUSIONS

The strength evaluation of a single bladed metallic propeller replaced with composite material was analyzed in terms of its stress evaluation and dynamic characteristics determination. Five different balanced laminate stacking sequences with each 25 ply ups are used for analyzing the composite material. The following are the conclusions are made from the results.

From table1 the maximum deflection for metallic blade is about 2.78535mm and the vonmises stress is 423.471Mpa.

From table2 the deflections for various stacking sequences are analyzed and the stacking sequence 1 produced the less deflection and minimum inter laminar stress and stacking sequence 5 produced the maximum.

Table3 &4 predicts the free vibration characteristics of the both metallic and composite materials. From table3 &4 metallic propeller blade with Nab as the base material has the highest operating frequency.

The application of various stacking sequences on composite blade achieved close results to metallic one and the percentage difference between metallic and composite is 0.203 to 0.232%.

From table4 of all the stacking sequences considered for analysis the stacking sequence1 has less deflection, inter laminar stresses and high operating frequencies. With further increase in number of layers the blade can be made much stiffer than metallic one

The Harmonic analysis results for NAB propeller shows that resonance occurs in the frequency range of 400-500Hz in U_x, U_y,U_z directions and for composite 300-400Hz,so the propeller may be operated in frequency range other than 400-500 for NAB and 300-400 for composite.

With further change in number of layers and layup sequences the strength characteristics of the blade operating in underwater conditions may be improved without modifying the shape.

REFERENCES:

i.   Carneige.W. Vibrations of pre twisted cantilever blading, Proceedings of the Institution of Mechanical engineers 1959 173:343

ii.   Chuijin Yang, Jubing Chen& Shexu Zhao. The Inter laminar Stress of Laminated Composite under Uniform Axial Deformation, Modeling and Numerical Simulation of Material Science, 2013, 3, 49-60.

iii.   ITTC Guide for measured Mile Trials. Rep. of Perf.Comm. Proc. 12th ITTC, Rome, 1969.

iv.   Diprima, R.C. and Handle man, G.H., Vibration of twisted beams, Q. appl. Math. 12, p.241 (1954)

v.   Matsunaga H., Inter laminar Stress Analysis of Laminated Composite Beams According to Global Higher-Order Deformation Theories,CompositeStructures,Vol55, No. 1, 2002, pp.105-114.

vi.   Miyazaki N., Takeda T. 1993. Solid particle erosion of fiber reinforced plastics, Journal of Composite Materials, Vol.27, pp. 21–31.

vii.   Mohammad Nabi S & Ganeshan N, Comparison of Beam and Plate theories for free vibration of metal matrix composite pretwisted blades. Journal of Sound and Vibration (1996) 189(2), 149-160.

viii.   Pipes, R. B. and Pagano, N. J., Inter-laminar stresses in composite laminates under uniform axial extension, J. composites Mater. 4,538, 1970

ix.   Sabeel A.K., Vijayarangan S. 2008. Tensile, flexural and inter laminar shear properties of woven jute and jute-glass fabric reinforced polyester composites, Journal of Materials Processing Technology, Vol.207, No.1-3, pp. 330-335.

x.   Sheng-An Liu, Chen-Yee Hung, Chun-Ying Lee, Vibration analysis of Pre twisted rotating composite wind mill blade by FEM.

xi.   Subramanian, P., (2006), Dynamic analysis of laminated composite beams using higher order theories and finite elements, Composite Structures, Vol. 73, pp. 342353.

xii.   Taylor, D.W, The speed and power of ships, Washington, 1933.

xiii.   Toshio Yamatogi, Hideaki Murayama, Kiyoshi Uzawa, Takahiro Mishima, Yasuaki Ishihara, Study on Composite Material Marine Propellers, Journal of the JIME Vol.46. No.3 ©JIME 2004.

xiv.   white,W.T. An integral equation approach to problems of vibrating beams Franklin Ins.,245,pp.25 and 117(1948)

Importance Of Site Speicific Design For The Coastal Protection Measures

A.V.Mahalingaiah[1], B.R.Tayade[2], and M.D.Kudale[3]

1   Chief Research Officer, CWPRS, Pune 411024,
2   Research Officer, CWPRS, Pune 411024,
3   Joint Director, CWPRS, Pune 411024,

Email: mahalingaiah_av@cwprs.gov.in, maha_av@yahoo.co.in

ABSTRACT : Coastline is an interface between the ocean and the land. It is dynamic morphological entity, which responds to the external forces exerted by waves, tides and near shore currents and resultant sediment movement. Coastal erosion is recession of the shoreline and loss of land area due to action of waves, currents and wind. Human interference also contributes to the adverse effects along the coastline, including the erosion. The physical regime of the Indian coastline is characterized by different types of coastal features. In order to mitigate the coastal erosion, the coastal protections are provided and are broadly classified as soft and hard solutions, and also combination of both. The site specific measures to combat erosion are required to be evolved based on evaluation of coastal environment conditions prevailing at the site, availability of material and equipment and resourcefulness of execution team. As such, the site specific protection measures are evolved based on coastal environment of the different coastal regime. Some site specific coastal protection measures evolved in the form of seawall, offshore reefs and groynes with geo-tubes, beach nourishment, etc., are described in the paper, which emphasize the importance of site specific solutions.

Keywords: Seawall, Gabions, Tetrapods, Geotubes, Beach Nourishments, Submerged reef

1. INTRODUCTION

The physical regime of the Indian coastline is characterized by different types of coastal features like promontories, Sand spits, Barrier beaches, Embayment, Estuaries and offshore Islands etc. The morphological changes near shore region are entirely due to waves, tides and other environmental parameters, which cause changes in the coastline in the form of recession or advancement. In the most part of Indian coast, the erosion observed is seasonal in nature, i.e. beach gets eroded during monsoon and regains its original profile during fair weather season. The magnitude and nature of erosion changes from place to place. However, at some places, erosion is of permanent nature and there is a need to protect on priority. The causes of coastal erosion are broadly classified as natural and human causes. The natural causes are due to increased rate of net littoral drift, extreme wave and storm surge conditions, loss of sand into canyons, sea level rise, deflation, subsidence and variation in supply of sand from rivers due to droughts. The human causes due to interruption to littoral drift by constructing structures such as breakwaters, navigational channels, dredging and disposal of sand, removal of sand from the beach, obstruction to natural supply of sand from rivers, encroachment with construction of vertical wall on beach.

In order to mitigate the coastal erosion, the coastal protections are provided and are broadly classified as soft and hard solutions, and also combination of both. The soft solutions are mainly, plantation of vegetation, stabilsation of dunes, beach nourishment, sand bypassing, flood proofing, zoning, retreat etc. The hard solutions are mainly, construction of seawall /revetment, groynes, offshore breakwaters, detached seawalls etc. The coastal resources are over exploited with the increase in coastal population, which have resulted in threatening of not only our coastal resources but also the entire eco-system of the coastal belts. The protection does not only stop the erosion of the coast but also saves the cultivable land being inundated and protects important structures and valuable properties along the coast. The methodology/solutions need to be evolved with thorough understanding of the various coastal processes, with due consideration to the environmental aspects as well as should be easily constructible in minimum period of time. The solutions evolved for protecting the coastline will vary considerably depending on the extent of erosion and environmental conditions. In predominant littoral zone, the groynes field is useful, whereas in vertical cliff type erosion where there is no chance of stabilsation of beach, the seawalls/ revetments are proposed. It was felt necessary to develop site specific methods for coastal protection considering site conditions, cost, and time

and construction equipments. As such, specific site solutions for effective coastal protection measures are evolved and successfully implemented at various sites along the coast of India. Some coastal protection measures are described in the paper, which depict the importance of site specific solutions for coastal protection.

2. METHODS OF COASTAL PROTECTIONS

The coastal protections with hard solutions are mainly construction of seawall /revetment, groynes, offshore breakwaters, detached seawalls etc. The seawalls are relatively massive rubblemound or vertical monolithic structures constructing parallel to the shoreline and prone to damage due to scouring at toe. The revetments are similar to seawalls constructing parallel to the shoreline and sloped in such a way as to match the natural slope of the shoreline profile, which are exposed to lower level of attack of waves and does not feature back-slope armour. The Groynes are normally constructed in a series, perpendicular to the shoreline to traps sediments by interrupting or reducing long-shore drift and may cause down-drift erosion. The bulkheads primarily retain the land and earthen dikes primarily prevent the flooding. Offshore reefs/detached seawalls are normally constructed parallel to the shoreline in a series for breaking the waves before they reach shoreline and to trap the sediments by providing calm area on leeside. The submerged reefs/perched beaches/sills, detached structures are constructed parallel to the shoreline to trap sand. They differ from submerged offshore breakwaters in having wider crown and useful when used in front of seawalls or revetments.

A typical seawall consists of armour layer on slope with a supporting toe as shown Fig.1. The toe protection is supplemental to armour layer provided in front of structure, which prevents waves from scouring and undercutting it. The computations for the unit weight of armour using Hudson's formula as shown below:
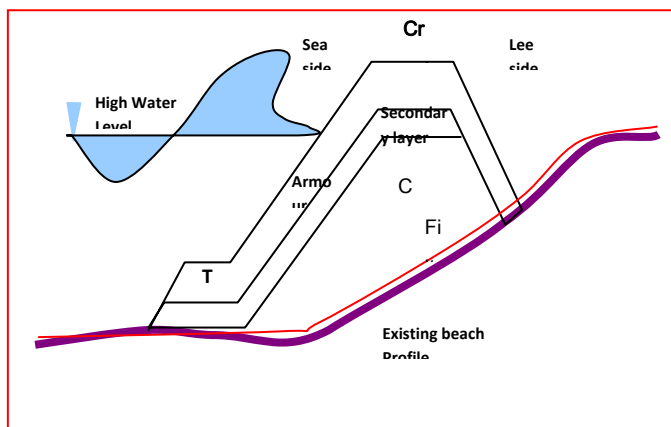
Fig.1: A typical rubblemound seawall

$$W = \frac{w_r . H_b{}^3}{K_D \times (Sr-1)^3 \cot\theta}$$

Where, W = Weight of armour unit (kg), wr= Unit weights of

armour block (kg/cum),
H = Wave height at the proposed structure (m)
Sr = Specific gravity of the armour units
Θ = Angle of armour slope measured with the horizontal,
K_D = Stability coefficient

The detached breakwater is constructed parallel to shore as a coastal protection measures, which leads to formation of Salient and Tombola on lee side. Some important parameters in the design of offshore detached breakwater are as listed below:

L_B = Length of detached breakwater
x = detached breakwater distance from the shoreline
x_{80} = Surf-zone width (Approx. 80% of littoral transport take place landward to this line)
$L_B * = L_B / x$
$X* = x/X80$
$L_B * < 0.6$ to 0.7 - Formation of Bell shaped Salient
$L_B * > 0.9$ to 1.0 - Formation of Tombola

The coastal protections with soft solutions are mainly, plantation of vegetation, stabilsation of dunes, beach nourishment, sand bypassing, flood proofing, zoning, retreat etc. The artificial beach nourishment is a natural eco-friendly way to combat coastal erosion, preserves flora & fauna and supports recreational opportunities, controls flooding, in which sand is added to existing beach. Planting of appropriate species of vegetation to assist in the stabilization of dunes, bluffs or banks. Geo-synthetic tubes / bags filled with sand can be used as groins, submerged reefs/detached seawalls for beach protection.
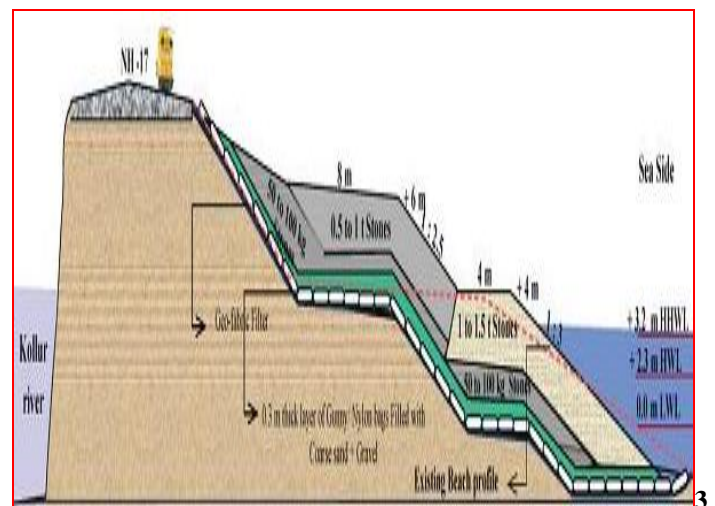
. SITE SPECIFIC SOLUTIONS OF COASTAL PROTECTION MEASURES

A coastal protection measure in a given situation depends on the three primary conditions viz. i) problems (coastal erosion, beach degradation or flooding), ii) morphological conditions (type of coastal profile and coastline) and iii) land use (Infrastructure/habitation, recreation agriculture etc.). The conventional method of coastal protection by providing massive seawalls has some limitations viz. non availability of suitable construction material & machines, no space for movement of construction equipment at site and non availability of sufficient beach width. In order to overcome these, the various site specific coastal protection measures are examined and evolved. The site specific solutions are in the form of seawall with higher toe-berm, detached seawalls, offshore reefs, seawall with concrete stepped crest slab, concrete piles for bank protection, artificial beach nourishment, offshore reefs with artificial beach nourishment, groyne field, sand bypassing, revetment with heavy stones pitching, bank protection with stones pitching etc. Design of few sites specific solutions for the coastal protections are discussed below:

3.1 Seawall with higher Toe-Berm

If the beach profile is with composite slope, the hydraulic stability of structure should be confirmed for individual part of the structure. The stability of the toe is essential, else failure of the toe will lead to failure of the whole structure. The utility of the toe can be enhanced by providing flatter slope of toe face, or by providing horizontal berm on the seawall face at a level close to the design water level. However, this toe is exposed to the direct wave attack, since the waves are breaking on the toe berm or toe slope. Seawall/revetments without toe will not serve the purpose as the wave force will cause damage to the seawall/revetments. In view of these constraints at the coastal erosion site along the National highway near Maravanthe in Karnataka, the erosion problem was solved using a seawall with higher toe-berm (Fig.2 & 3). The toe berm is kept at higher level than the design Highest High Water Level (HHWL). A flatter toe slope is provided to protect the armour and crest vis a vis the highway by absorbing the brunt of the breaking wave energy on toe berm itself, reducing the up rush and prevent overtopping or splashing of the water on to the highway embankment.

Fig.2(a): Severe Erosion at Maravanthe.   Fig. 2(b): Coast after construction of seawall.

Fig.3: Cross-section of seawall with higher toe-berm.

A 4 m wide toe-berm with 1.0 to 1.5 t stones on 1:3 slope is provided above HHWL. The toe takes the brunt of the breaking

waves and subsequently reduces the up rush. The construction of the seawall at Maravanthe was completed as per CWPRS recommendations (TR No. 4316, 2006) and has withstood well (Fig.9). Sand is accumulated on the toe slope and sufficiently wide beach is also formed in front of the seawall. Thus the concept of seawall with differential toe helps in reducing the overtopping of the waves on the crest vis a vis provides better protection to the coastal highways.

3.2 Toe Protection to the Vertical Wall
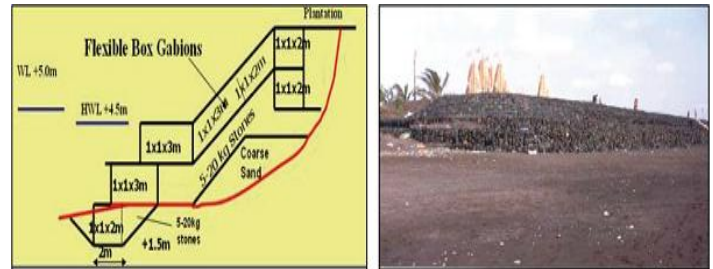
A historical Somnath temple is located on the west coast of India in Saurashtra, Gujarat. Recently, a part of the retaining wall on the seaside of the temple suffered damage due to action of sea waves. A rubble mound slope was suggested at the toe of the vertical wall, which prevents scouring and undermining of the vertical wall (Fig 4).

Fig.4 (a): Retaining wall at Somnath temple   Fig.4 (b): Wave flume tests for toe protection

The vertical walls constructed along the coast with rocky bed slope at several places in Mumbai (ie. Priyadarshini park, Worli, Dadar Chaityaboomi, etc.) suffered damages due to wave action. A toe protection in the form of seawall with tetrapods in the armour is suggested as shown in Fig.5 & 6 at these sites. This solution with tetrapods in the armour is useful from aesthetics point of view in the city like Mumbai.

Fig.5: Toe protection in the form of seawall to vertical wall.

Fig.6: Seawalls with tetrapods in the armour.

3.3 Seawalls with Stone-Filled Gabions

The coastline at Tithal near Valsad was under the threat of severe erosion for many years. Swami Narayan temple near the coast was in danger as the boundary wall of the temple is located very close to the coast. It was proposed to construct seawall with stone filled flexible gabions to provide immediate protection to the temple. The coastal protection work was completed in very short time using the local labours. The construction of protection works has been maintained regularly. The section is stable and beautiful beach has been formed in front of the structures, due to better dissipation of wave energy on the stone filled gabions (Fig.7)
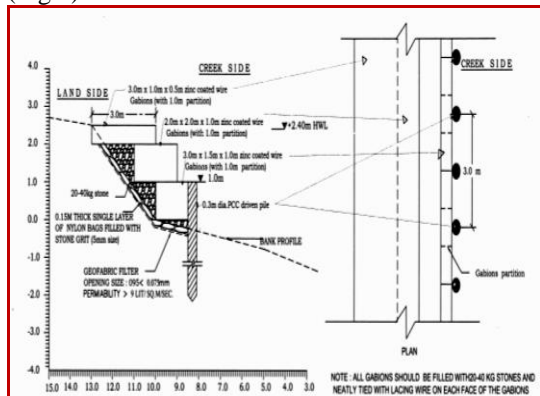
Fig.7: Seawall with stone filled Gabions at Tithal.

3.4 Bank Protection in the Creek

Pankhol Juwa is an Island located well inside the creek on north side of Malvan, Maharashtra. The loose soil of the bank has tendency to slide and wash away due to the tidal currents and flow during monsoon. The bank profiles are very steep and space required for construction is substantially less. Since the site is situated well inside the creek, locally generated waves, tide and currents are considered for design. In view of the site condition, it was decided to design protection measures in the form of PCC driven piles with conventional bank protection technique (Fig.8). PCC driven piles of 0.3m diameter at 1.5 m spacing are suggested and top of the piles is fixed at el. +1.0m. The gabions (zinc coated wire) filled with 20 to 40 kg trap stones are placed in between the piles and bank slope. The piles would hold the gabions on steeper slope.
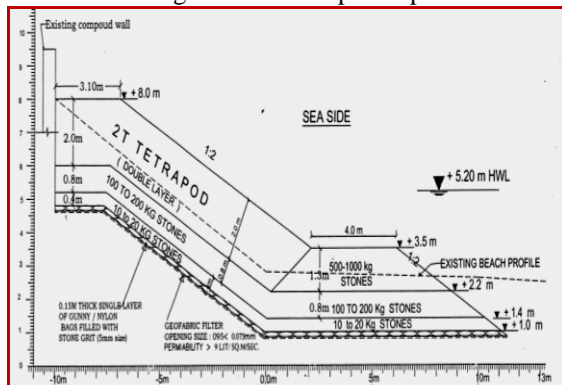
Fig. 8: PCC piles for bank protection.

3.5 Seawall with stepped crest slab

A beautification plan on the beach with coastal protection against waves has been proposed for tourism places at Shrivardhan, Dahanu and Kelwa beaches, in Maharashtra. It was decided to incorporate beautification components consistent with the proposed coastal protection work. A rubble mound seawall consisting of 0.5 to 1.0 t stones with 1:2.5 slope in the armour layer was proposed to sustain the wave attack. L-shaped PCC parapet wall was suggested at top with a layer of PCC blocks resting on soling layer (Fig.9). The armour stones are to be placed in pitching fassions from asthetic point of view and ramps at suitable interval are proposed for access to the Beach
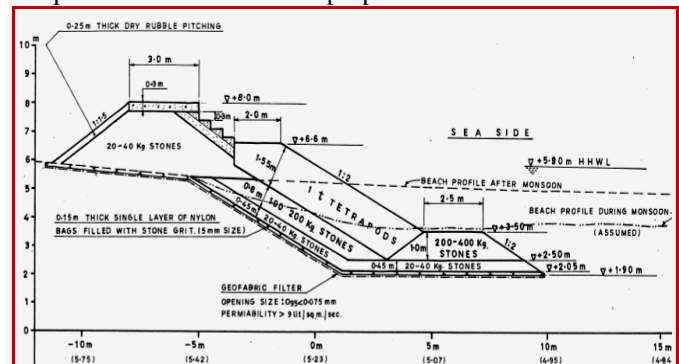
Fig.9: Seawall with stepped crest slab.

3.6 Artificial Beach Nourishment and Submerged Reefs with Geo-tubes

The sand filled geo-tubes with submerged reefs, groynes are proven to be economical alternative for coastal protection. The Geo-tubes are made up with woven polypropylene fabrics with fibrillated yarns. Requirement of the beach width is the main criterion for deciding the alignment or the depth contour of the offshore reefs. The submerged reef combined with sand nourishment helps rapidly stabilization of the beach. As such, the offshore reefs could be of dual purpose viz. allowing overtopping of the hydraulic loading for the formation of the salient/tombola at high water level and holds nourished/deposited sand on the beach against down rush. Generally, the emergent offshore reefs for the purpose of holding sand are constructed at the nearshore region without gap and special attention has to be provided for the turbulence

created by the breaking of waves. Ultimately, crest elevation and the alignment location of the offshore breakwater play a key role in deciding the design cross -sectional details. Use of the geo-tube as an offshore breakwater for holding the nourished sand is the new trend adopted in India instead of the conventional rubblemound offshore structure. Effort should be taken to extend life span of the offshore geo-tubes up to the permanent beach stabilization. They can be appropriately covered with sand. The tubes are susceptible to damage due to the rocky bed or can be easily tampered.

The submerged reefs with geo-tubes have been provided at INS-Amla, Mumbai (Fig.10). A continuous row of the 3.0 m dia and 1.0 m dia geo-tubes are provided at a distance of about 50 m away from the existing compound wall at the bed level of +1.0 m. The tidal range in this area is about 5.2 m and with this top portion of goe-tube is kept at Mean Sea level of +2.6 m. It was expected to act as intermediate submerged reef and would help in arrested the nourished sand on the beach. The nourishment beach carried out with well graded coarse sand. Over a couple of seasons a wide beautiful beach has been created and part of these submerged reefs are buried with sand. Similarly, submerged reef with geo-tubes are provided at Dahanu and sand deposit take place in the next season.
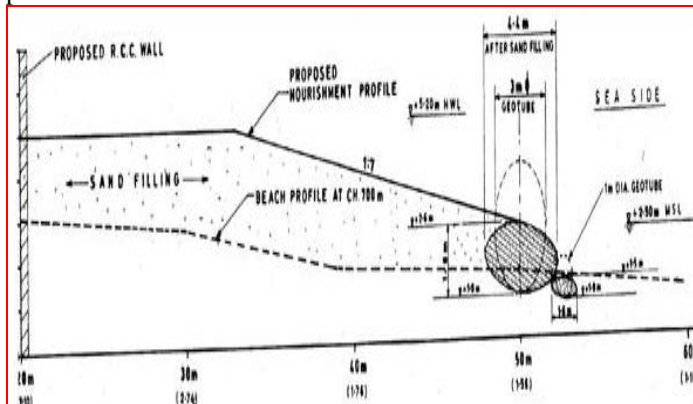
Fig.10: Artificial beach nourishment and submerged reef with Geo-tubes.

3.7 Shoreline Management Scheme

Major morphological impact felt after development of Ennore port, as this coastal region is having high longshore littoral drift. It is observed from the studies that, the annual northward and

southward transports are of the order of 0.60 million cum & 0.10 million cum with net and gross transports being 0.50 million cum and 0.70 million cum. respectively. The northward transport is more dominant and hence the net transport is towards north. Also it is observed that the major northward transport occurs in SW monsoon period. In order to protect the eroding coastline & accommodate the dredged sand to meet the requirement of additional area, eco-friendly multipurpose solution of shoreline management is planned with combination of sand bypassing and beach nourishment to combat erosion on downdrift side. Sand trap is suggested at the entrance in the protection zone of the breakwater from which sand would be dredged throughout the year. The dredged sand would be bypassed on the northern shoreline by deploying a pipeline from a berth extending along the northern coast.

Groynes are also employed in combination with shoreline protection in order to develop a beach. These may be either permeable or non permeable so that portion of the alongshore drift is trapped on the updrift side, thereby causing advancement of the shoreline. Groyne field is a system of series of groynes placed at regular intervals along the beach, which is found to be effective to protect and nourish a long stretch of coastline. The alignment of groynes is determined at angle between 90o to 100o to the shoreline for the effective sand trapping. The spacing of groynes would be 4 to 5 times the length of the groynes with beach fill in between. The length of the groyne field extending up to 40% of breaker zone width is more effective. A layout of groyne field consisting of 10 groynes of 40 m length each has been suggested on the north side of northern breakwater (Fig.11). Sand-filled geo-tubes of 3m diameter are to be placed perpendicular to the shoreline to form a groynes field. This eco-friendly solution would protect the coastline as well as meet the requirements of the port for disposal of dredged material.
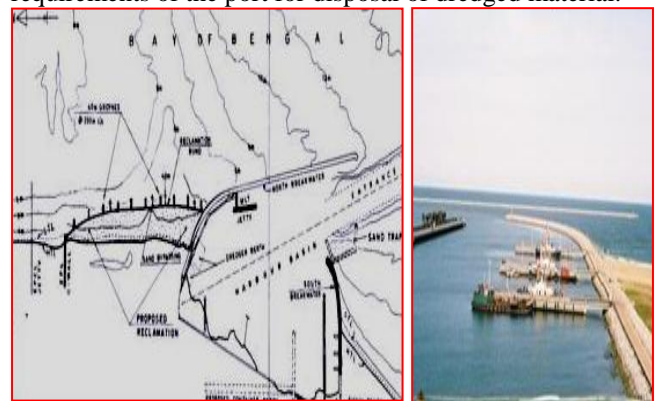
Fig.11: Shoreline management scheme at Ennore Port

3.8 Other Specific Coastal Protection Measures in India

The site specific solutions have been evolved at number of locations for coastal protection along the Indian coast. Rubblemound seawalls with stones/tetrapod in the armour have been adopted at Paradip, Mumbai, Maravanthe, Mangalore, Alleppy and seawalls with flexible Gabions at Tithal, Varsoli, Ankaleshwar. Groins and detached seawalls with stones/geo-

tubes have been used at Udwada, Dahanu and Shankarpur. Artificial beach nourishment is successfully carried out through sand bypassing systems at Visakhapatnam and Paradip Ports. Low cost protection schemes are found successful at Lakshadweep & Minicoy Islands.

4.0 CONCLUDING REMARKS

The site specific solution for the coastal protections are evolved based on the prevailing site conditions. Following conclusions are drawn from the studies and performance of these solutions in the prototype:

➢ The concept of seawall with higher toe-berm helps in reducing the overtopping of the waves on the crest and provides better protection to the coastal highways.

➢ The tourism sites could be developed by providing seawalls with stepped crest slab and offshore reefs for formation of beautiful beach.

➢ The historical monuments under the threat of severe erosion could be saved by providing immediate site specific solution in the form of rubblemound seawall.

➢ The toe protection to vertical wall reduces the scour due to reflection of waves and protects the structures adjacent to coast with wave action.

➢ A eco-friendly multipurpose solution consisting of sand bypassing system, reclamation, a reclamation bund and series of groynes could be adopted to combat the erosion and create additional area for Port facilities.

➢ A concept of artificial beach nourishment and submerged reefs with Geo-tubes can be adopted as successful coastal protection project, which provides an eco-friendly solution by restoring the beach.

ACKNOWLEDGEMENT

REFERENCES

i. CWPRS Technical Report No. 4316 (2006). Desk & Wave Flume Studies for Strengthening of Existing Seawall & Evolving Shore Protection Works NH-17 at Maravanthe, Karnataka

II. CWPRS Technical Report No.4658 (September 2009), Desk studies for shoreline management for the proposed phase-II development at Ennore port, Tamilnadu.

iii. Mahalingaiah A.V., Kudale M.D., "Eco-friendly solution of coastal protection by shoreline management for port development in littoral zone" proceedings of National Conference on Hydraulics and Water resource (Hydro-2011) Dec 2011.

iv. Shore protection Manual (SPM, 1984). CERC, U.S.Army Corps of Engineers, Vicksburg, U.S.A

Geotextiles In Coastal Protection And Coastal Engineering

Ashis Mitra

Visva-Bharati University, Department of Silpa-Sadana, Textile Section, Sriniketan, Birbhum, 731236, India
Email: mitra.ashis1@gmail.com

ABSTRACT: *Invention of geotextiles forms a bridge between civil engineering and textile technology. There are numerous geopolymeric materials which are used in civil engineering and other geotechnical applications, but probably the most important are geotextiles, which are permeable textile materials or fabrics used for various geotechnical applications. Geotextiles were one of the first textile products used in human history. The application geotextiles is large and has expanded very rapidly worldwide especially during the last decade. With the rapidly growing advancement of technology, geotextiles have invaded a large variety of domains and won trust and esteem around the world because of their inherent advantages like easiness and flexibility of use, softness (as compared to monolithic and rock constructions), rapidity of installation and long term efficacy. Geotextiles offer a safe and economical solution to everyday engineering challenges and construction requirements. Used as replacement of natural materials, geotextile products perform a wide range of functions such as erosion control, soil stabilization, filtration, drainage, separation and reinforcement requirements. Geotextile bags, tubes and containers made with geotextiles are playing a major role in hydraulic, coastal, offshore engineering and river protection works. The use of geotextiles can save money by considerably reducing construction times, material costs and the costs of maintaining structures. The global geotextile market is enjoying strong growth but it is also highly competitive. This review paper highlights the constructional and functional aspects of this emerging branch of technical textiles, and emphasizes the potential role of various geotextile products in coastal protection and coastal engineering.*

Keywords: Geotextiles, Geosynthetics, Groins/Groynes, Dykes, Revetment, Levees, Breakwaters.

1. INTRODUCTION:

Geotextiles were one of the first textile products in human history. Excavations of ancient Egyptian sites show the use of mats made of grass and linen. Geotextiles have been used for thousands of years. Geotextiles were used in roadway construction in the days of the Pharaohs to stabilize roadways and their edges. These early geotextiles were made of natural fibres, fabrics or vegetation mixed with soil to improve road quality, particularly when roads were made on unstable soil [1, 2].

Geotextiles were first applied into civil construction projects in the 1960s in the USA and Europe in drainageand separation applications for road construction. The technology rapidly

developed from that point onwards with the First International Conference on Geotextiles held in Paris in 1977. Due to the need for greater knowledge and understanding of the material, the International Geosynthetics Society (IGS) was founded in 1982 [3].

The use of geotextiles has now grown to such an extent that virtually every civil construction project undertaken includes a geosynthetic of some description. The marine and coastal environment is an extremely harsh environment to use what is a relatively thin light weight material, where the geotextile will be subjected to abrasion from armour rock and marine sediment, large dynamic flow conditions from both tidal action and wave impact. As such, geotextiles used in coastal and marine must be able to withstand conditions which are far more aggressive than the original road construction applications.

2. GEOTEXTILES:

2.1 Construction and raw materials:

Geotech segment comprises of technical textile products used in geotechnical applications pertaining to soil, rock, earth etc. This class of product s is loosely called Geotextiles. However, geotextiles particularly refer to flat, permeable, polymer-synthetic or natural textile materials which can be non-woven, woven, knitted or knotted materials. They are used in contact with soil or rock and/or any other geotechnical materials in civil engineering earthworks and building constructions. In fact, geotextiles is one of the members of the geosynthetic family which comprises of geogrids, geonets, geotextiles, geomembranes, geosynthetic clay linters, geopipe, and geocomposites [1-4].

Geotextiles are made from polypropylene (PP), polyester (PET), polyethylene (PE), polyamide (nylon), polyvinylidene chloride (PVC), and fiberglass, and their GSM varies from under 40 to over 3000 which is mainly used in landfill end uses. PP and PET are the most widely used. Sewing thread for geotextiles is made from Kevlar or any of the above polymers [4-5]. Different fabric composition and construction are suitable for different applications.

To survive aggressive underground environments, geotextiles must be resistant to various forms of attack, such as mechanical, chemical and biological. Chemical attack may be initiated directly by acidic and alkaline soils or indirectly by the active wastes present in the landfills. Depending on the type of chemical compound, changes in the polymer structure can be brought about by oxidation, chain scission, cross linking, swelling or dissolution of the polymers, volatilization or extraction of ingredients of the polymeric compound, or an increase in the crystallinity of the polymer. In addition the service temperature may accelerate the effects of chemical degradation.

2.2 Types, desired characteristics and functions:

In general, the vast majority of geotextiles are made from polypropylene or polyester and formed into the following fabric categories [2,4]:
- Woven monofilament
- Woven multifilament
- Woven slit-film monofilament
- Woven slit-film multifilament
- Nonwoven continuous filament heat bonded
- Nonwoven continuous filament needle-punched
- Nonwoven staple needle-punched
- Nonwoven resin bonded
- Other woven and nonwoven combinations
- Knitted.

The non-woven geotextiles provide planar water flow in addition to stabilization of soil. Typical applications include i) access road and rail building, ii) dam, canal and pond lining, iii) hydraulic works, sewer lines, iv) asphalt pavement overlays, v) soil stabilization and reinforcement, vi) soil separation, vii) drainage, viii) landfill, ix) filtration, x) weed control, xi) sport surfaces, xii) drainage channel liners, xiii) sedimentation and erosion control, etc. Woven geotextile looks like burlap. It is a fabric made of two sets of parallel strands systematically interlaced to form a thin, flat fabric. The strands are of two kinds - slit film which are flat, or monofilaments which are round. Woven geotextiles are generally preferred for applications where high strength properties are needed, but where filtration requirements are less critical and planar flow is not a consideration [4, 5]. Woven geotextiles are mainly used in coastal works, embankment and in or near dams, waterways, and woven geogrids for reinforcement. Both woven and knitted geotextiles are beneficially used for a wide range of both cohesive and non-cohesive soils and they support quick formation of a natural soil filter. They facilitate dissipation of pore pressures and, thanks to their strength characteristics and low elongation, they improve mechanical properties of soil and enable the construction of reinforcing ground structures in this way [5].

The desired characteristics of woven geotextiles are: i) Ability to resist clogging, ii) Excellent elongation at break, iii) Excellent water permittivity, iv) Good grab tensile strength, v) Good puncture resistance, vi) Trapezoidal tear strength, vii) UV resistance, viii) Very good Mullen burst, etc. [1].

There are mainly four segments of Geotech family namely, i) Geogrid, ii) Geonet, iii) Geomembrane, and iv) Geocomposites.

Geotextiles perform one or more basic functions in a structure like filtration, drainage, separation, erosion control, sediment control, reinforcement, and (when impregnated with asphalt) moisture barrier. In any one application, a geotextiles may be performing several of these functions.

3. ROLE OF GEOTEXTILE IN COASTAL PROTECTION AND OFF-SHORE ENGINEERING

Due to sea or river current, fine soils of the bank start migrating causing erosion. Conventional design of cementing the banks is not a solution due to hydraulic pressure of the soil. Only feasible solution is the application of geotextiles or geosynthetics. Geotextiles allow water to pass through but resist the fine soil migration.

Coastal
pro

Figure 1. **Geotextile preventing coastline erosion**

tection measures are designed to protect inland flooding and minimise the erosion of the coastline caused by the constant motion of the sea. Geotextiles protect the coast line as their flexibility and permeability ensure withstanding of the impact of waves and currents, preventing erosion and washing out of lines (Fig. 1).

Geosynthetics are used in various coastal protection applications such as filters in dykes and dams, for foundations under groynes and breakwaters, as well as by using geotextile containers as structural elements in groynes, seawalls, breakers or for bed and embankment stabilisation.

Woven geotextile containment systems in tubular forms filled with locally available sand/slurry are formed in-situ on land or in water to protect shore and marine environments. Geotextile Tubes are used as a cost-effective alternative to mitigate erosion on coastal shorelines, riverbanks, and lakes using readily available materials for infill. Geotextile Tubes filled with dredged materials or sand and strategically placed will dissipate the wave energy, as well as provide structural support against other erosive forces. Geotextile Tubes can be set in place along shorelines and river fronts either to be left exposed to battle the elements, or incorporated into the environment as part of a manmade dune or riverbank. They can also be placed in the water to serve as jetties and groins [6].

4. GEOTEXTILES/GEOSYNTHETICS ——— HOW IT WORKS:

Coastal and marine environments are susceptible to erosion, which is caused by the action of waves, tides, currents and other water motion. The consequence of erosion can range from a simple loss of surface soil to the wholesale undermining and collapse of structures. To positively influence the morphology and prevent erosion at designed locations a variety of measures are used. Generally, these measures fall into one of three categories:

- *Geometrical measures*, where the shape of the structure and adjacent profile is altered in order to reduce the water forces below a minimum threshold.
- *Stabilisation measures*, where the exposed structure is protected from erosion by stabilising the susceptible soil. Examples include the provision of revetments, etc.
- *External measures*, where the exposed structure is protected from erosion by the provision of a protection structure, placed at some distance. Examples include breakwaters, etc.

TenCate® and Terrafix® Geosynthetics, for example, with filtration, containment or reinforcement functions, are used as integral components in the design and construction of a variety of coastal and marine structures such as revetments, scour protection layers, levees, dykes, groynes (or groins), jetties and breakwaters. These Geosynthetics are easy to install beneath the water surface, in difficult conditions, and once in place provide continued performance [7].

5. SOME COASTAL AND MARINE STRUCTURES AS MEASURES OF COASTAL PROTECTION AND COASTAL ENGINEERING [6-14]

5.1 Stabilisation of dykes:

Needle-punched geotextiles (like Terrafix®) are used to protect the coastline when used in the toe area of sea walls and dykes. They improve the construction efficiency if the sea currents cause surface erosion or unacceptable soil displacement. The three-dimensional, labyrinth-like pores and channels of Terrafix® nonwovens are not only similar to the soil structure itself, but, if correctly designed, also increase the stability of the revetment against impact stress caused by the motion of the sea.

A geotextile with a minimum mass per unit area of 600 g/m² is necessary wherever type II or III armor rock with individual weights $\leq$ 60 kg are placed directly on geotextiles, or where concrete revetments for high-stress applications have been installed. Where individual stone weights exceed 60 kg, geotextiles with yet a higher mass per unit area is recommended. In the case of low-stressed dykes, filter geotextiles (like Terrafix®) with a minimum mass of 500 g/m² and minimum thickness of 4.5 mm serve to encapsulate and stabilise the sand core from erosion. When flooding occurs, they prevent washout of the sand and ensure the stability of the dyke. Top soil as well as concrete blocks can act as an effective cover layer over the geotextile [7].

5.2 Coastal revetments ——— preventing shoreline erosion:

Revetments are often used to protect coastlines. Coastal revetments may be deployed to protect toes of coastal cliffs, bluffs, dunes, etc, They may also serve other purposes such as limiting wave overtopping or wave reflections. Natural sand dunes may be found at the landward extent of an active beach and can offer some form of protection against wave attack under extreme tidal or surge conditions. When natural dunes do not

exist or when they do not provide sufficient protection, rock revetment structures may be built hidden within covered sand for beach aesthetics and recreation purposes. During a storm event, the front sand cover may be eroded but the exposed revetment would prevent further damage from occurring. After the storm event, the sand cover is then replaced [6-8].

TenCate® and Terrafix® Geotube Systems, for example, are commonly used as a very cost effective alternative to hidden revetments in the sand dune zone.

5.3 Levees and flood control dykes ———— preventing rising sea levels from flooding inland areas:

There are many reasons for sea levels to rise above inland areas. Tides result in regular rise and fall in sea levels. Although the typical tidal range in the open ocean is about 0.6 m, coastal tidal ranges can vary between zero to over 10 m in height, depending on the coastal geography and location. Due to global warming, the mean sea level is expected to gradually rise with time. Water levels can also rise as a result of waves and surges.

To protect flooding of low lying areas flood control dykes or levees are constructed along estuaries and coastlines. The top of flood control dykes or levees should be higher than the design high water level plus a safety freeboard. In addition the levees should be designed to prevent seepage through the core structure. As such the levee is either constructed with earth or consists of at least one zone of fine-grained soil to act as a hydraulic barrier to seepage water [6, 7, 9].

5.4 Estuarial barriers and barrages:

Estuarial Barriers & Barrages ———— allow river discharges while holding back rising sea levels. Tides cause sea levels to rise and fall in constant cycles. Tidal effects are experienced in coastal and river delta areas. Estuarial barriers and barrages are special dam structures that are designed to hold back the sea during high sea levels while allowing river discharges during normal sea levels. The primary objective of such structures is usually flood prevention. Such constructions are usually extremely challenging and techniques often project specific. TenCate® geotextiles are used as components in prefabricated systems for filtration and reinforcement functions [6-7].

5.5 Coastal groynes (or groins):

Groynes are finger-like hydraulic structures that jut perpendicularly out of coastlines. Their engineering function is to interrupt or reduce longshore sediment transport. This interruption will produce accretion updrift of the groynes and produce concomitant erosion downdrift of the groynes. Groynes are usually constructed in groups otherwise referred to as groynefields. When constructed in concert with beach restoration, the groyne field will act to reduce future beach maintenance and nourishment requirements. The sectional requirement of a groyne structure is the same as that of a basic dyke structure. Geotextiles are used as a filter layer to prevent

sand beneath from being eroded away. Alternatively, Geotube Systems may be used to construct coastal groynes [6-7, 9 11-12].

5.6 Land reclamations ———— retaining reclamation fill:

The shortage of land along certain coastlines requires land to be reclaimed from the sea. Reclamation dykes are cofferdam units that retain fill while providing protection against wave attack during construction, prior to placement of long term armour protection cover. Conventionally, the cofferdam units are constructed of rock fill material in much the same way as the rock fill core of groynes, jetties, etc. Depending on the grading of the rock fill material, geotextiles may be laid on the inner side of the reclamation dyke to prevent washout of sand fill through the rock fill dyke. Geotextiles may also be laid over the sea side of the reclamation dyke prior to placement of the armour protection. Alternatively, Geotube Systems and Geocontainer Systems may be used to replace the rock fill reclamation dyke [6-7, 9-14].

5.7 Creating islands ———— preventing shoreline erosion:

Artificial islands are constructed for a variety of reasons. They may provide land for development of prime residential and commercial properties; create eco-friendly habitats and sanctuaries; act as barrier islands to protect coastal habitats,etc. Reclamation dykes are used to form the shorelines of the islands in very much the same way as land reclamation techniques. Geotextiles may be laid on the inner side of the reclamation dyke to prevent washout of sand fill through the rock fill dyke. Geotextiles may also be laid over the sea side of the reclamation dyke prior to placement of the armour protection. Alternatively, Geotube Systems and Geocontainer Systems may be used to replace the rock fill reclamation dyke [6-7, 9-12].

5.8 Coastal breakwaters ———— sheltering and preventing erosion of coastal development:

Coastal breakwaters are marine structures that have the primary function of sheltering a coastal development by preventing longshore currents from causing erosion and reducing wave energies impacting a shoreline. They are connected to the shoreline like groynes and jetties but differ in function and massiveness. Like groynes and jetties they impact the littoral functions but coastal breakwaters differ with the additional function of forcing waves to break offshore. Coastal breakwaters also tend to have special end details in the sea e.g. fishtailed, L-shapes or T-shaped that are designed to eliminate problems of downdrift erosion and promote the formation of beaches. Geotextiles are used as filter layers for the construction of coastal breakwaters. Geotextiles can also be prefabricated onshore into a large panel of fascine mattress that can be floated out to sea. This panel of fascine mattress can then be ballasted into position on the seabed by dropping rock onto the floating fascine mattress. Alternatively, Geotube Systems, Geocontainer Systems and Geobag Systems may be used to replace the rock fill core of breakwaters [6-7, 9, 11].

5.9 Offshore breakwaters ———— reducing wave energies impacting shorelines:

Offshore breakwaters are marine structures that have the primary function of reducing wave energies impacting a shoreline. Offshore breakwaters reduce wave energies by partially reflecting some wave energy seawards as well as forcing some wave energies to be expensed through wave breaking on the structure before such destructive waves can reach the shoreline. Offshsore breakwaters are generally constructed parallel to shorelines. Offshore breakwaters are sometimes designed to be permanently submerged and are often designed to retain a perched or artificial beach. As offshore breakwaters tend to involve construction in relatively deep waters, the installation of geotextiles can often be challenging. Geotextiles can be specially designed to make installation in deep waters a simple and efficient task. Construction of this marine structure is just similar to that of coastal breakwaters [6-7, 9, 11-14].

Figure 2. **Installation of geotextile tubes**

6. COASTAL PROTECTION/COASTAL ENGINEERING APPLICATIONS:

6.1 Applications in our country:

The below is mentioned a few real-life projects on application of geotextile products for coastal protection and off-shore engineering works:

- Installation of geotextile bags and geotextile tubes along the coast line of the Bay of Bengal from Shankarpur to Haldia, West Bengal (Fig. 2).
- Application of Geotextile tubes at the coastal area of INS Hamla, Malad (W), Mumbai.
- Application of geotextile tubes to protect sea wall of Uppada, Andhra Pradesh.
- Reclamation bundh using imported geotextile containers at Adani Port, Gujarat (Fig. 3).

6.2 Coastal protection/engineering applications in abroad [6-7]:

Figure 3. **Reclamation bandh using geotextile container**

Figure 4. **Coastal revetment, CT, USA**

Figure 9. **Kerteh breakwater, Malaysia**

Figure 8. **Bengkulu breakwater, Indonesia**

Figure 7. **Geotube groyne**

Figure 5. **Flood control dyke, Germany**

• Coastal Revetment, CT, USA ——The town of East Lyme in CT, USA wanted to connect two separate beaches facing the Atlantic Ocean with a new elevated pedestrian and bike path. This elevated pedestrian and bike path would also serve as a buffer to an existing high speed train line that was located beside it. A coastal revetment was constructed to protect the new coastline. The armour layer of the coastal revetment consists of approximately 1.8 m of large heavy rip rap. TenCate geotextiles were used as filter layer underneath the rip rap [Fig.

Figure 6. **Eastern Scheldt Barrier, The Netherlands**

Flood Control Dykes, Germany —— The Big Flood of 1953 that affected the Netherlands also caused flooding and severe damages to land and property in northern Germany. As a result, a 7 km long flood control coastal dyke was constructed beginning in 1992. The 8.8 m high dykes facing the North Sea at Leybucht would keep inland areas of up to 31 km from flooding during extreme events. TenCate geotextiles were used as filtration layer beneath the rock armour protection for the dyke as well as for the bed protection in the inlet-outlet channel. Geotube systems were used as reclamation dyke to raise the earthworks platform above high water levels [Fig. 5].

• Eastern Scheldt Barrier, The Netherlands ——The Eastern Scheldt Barrier is part of the Delta Project to protect the Netherlands against a repeat of the big flood of 1953. The Eastern Scheldt Barrier with a length of 8 km, seals of an estuary with a tidal volume of 2.2 billion m3. TenCate geotextiles are supplied for the fabrication of foundation mattresses for the 65 prefabricated reinforced concrete piers, each with the height of a 12-storey building and weighing 18,000 tonnes [Fig. 6].

• Bald Head Island, NC, USA —— The South Beach of Bald Head Island in North Carolina experienced severe coastline erosion. Geotube systems were used to construct a field 14 coastal groynes for long term protection of 3.7 km of South Beach shoreline. The Geotube groynes had a circumference of 2.75 m and were underlain with a 7.3 m wide scour protection apron [Fig. 7].

• Bengkulu Breakwater, Indonesia —— The Port of Bengkulu in Indonesia completed in 1985 is protected with two

rubble mound breakwaters with approximate crest lengths of 390 m and 420 m. The heads of the breakwaters were constructed with blocks weighing up to 10 tons. A total of 110,000 m^2 of TenCate geotextiles were used for the project [Fig. 8].

• Kerteh Breakwater, Malaysia —— The onshore operation base for Peninsular Malaysia's offshore petroleum production is situated along Kerteh Bay. Coastal erosion threatened the school and housing facilities, as well as a golf course. Offshore breakwaters together with beach nourishment was the solution of choice as this option would allow the recreational beach to be fully accessible without imposing rock structures along the shoreline. TenCate geotextiles were prefabricated onshore into large panels of fascine mattresses. These large panels of fascine mattresses were then floated offshore and sunk into position by ballasting with bedding stones [Fig. 9].

8. CONCLUSION:

Geotextiles or geosynthetics are a special branch of technical textiles which possess high potentiality in various geotechnical and civil engineering applications including road construction, railway track-bed stabilization, soil stabilization, erosion control, reinforcement, separation and drainage. The application is large and has expanded very rapidly worldwide especially during the last decade. Supported by the technological boom, geotextiles has invaded a large variety of domains, and won trust and esteem around the world because of their inherent advantages like easiness and flexibility of use, softness (as compared to monolithic and rock constructions), rapidity of installation and long term efficacy. The use of geotextiles can save money by considerably reducing construction times, material costs and the costs of maintaining structures. Apart from the regular applications, the use of geotextiles in coastal and marine applications has grown significantly since the early applications. This paper highlights the applications of geotextiles or geosynthetics in the form of geocontainer, geobag, geomat, geotube etc in various coastal and marine structures including dykes, revetments, groins/groynes, breakwaters, sea walls, estuarial barriers and barrages and so on as measures of coastal protection and coastal engineering works. Some of the real-life ventures in our country and abroad have also been reported to give some awareness regarding the immense possibilities of these specialist engineering materials. It must be remembered that due to the unique nature of many of the coastal and marine structures mentioned above, the installations are application specific and require sound understanding of the nature of problem to be solved, the behavior of material to be used in real world, the optimum utilization of machineries involved without creating so much environmental impact etc. Actual field trials are always recommended prior to final application of these kinds.

REFERENCES:

i. Basant T., and Jahan S. (2012). Engineering use of textiles in geotextiles, Textile Review, November, 2012. http://www.technical textile.net.

ii.   Tholkappian E.; Geotextile degradation under different environ conditions; ITJ, July (2010).

iii.   Hornsey W.P., Geotextiles in specialist marine applications: An Australia perspective over 32 years. http://www.geofabrics.com.au/documents/Specialist-marine-applications-of-geosynthetics-in-Australia.pdf

iv.   Geotextiles: The Fabric of Erosion Control. http://www.multigeo.com.

v.   Civil engineering and geotextiles. http://www.edana.org/content.

vi.   PIANC MarCom Working Group, "The Application of Geosysthetics in Waterfront Areas", ISBN: 978-87223-188-1, 2011. http://www.piacn.org

vii.   Tencate; Geosynthetics for Coastal and Marine Engineering. http://www.tencate.com /amer/Images/ BRO_marine_tcm29-31781.pdf.

viii.   Nielsen A.F., and Mostyn G., Consideration in applying geotextiles to coastal revetments, In: Australian Geomechanics Society Sydney Chapter Symposium, October 2011.

ix.   Saathoff F. (2003): "Geosynthetics in geotechnical and hydraulic engineering. Geotecnical Engineering Handbook", vol. 2: Procedures, First Ed., Ernst & Sohn, pp 507-597.

x.   GEOfabrics Limited. (2005). Designing Rock & Rip-rap Structures with Geotextiles. Leeds, West Yorkshire. http://www.geofabrics.com/downloads/downloads.htm?category=21&back=3.

xi.   Deptt. of the Army & the Air Force; Engineering use of Geotextiles; Army TM; July (2010).

xii.   Koerner, Robert M. (2000). A Brief Overview of Geosynthetics and Their Major Applications: United States Universities Council on Geotechnical Education and Research. http://www.ce.ncsu.edu/ usucger/ Teaching%20Aids.html.

xiii.   Oumeraci, H & Recio, J (2010). "Geotextile sand containers for shore protection", Chapter 21 in Handbook of Coastal and Ocean Engineering ed. KC Young, World Scientific.

xiv.   Heibaum, M., Fourie A., Girard H., Kurunaratne G.P. et al. (2008): "Hydraulic Applications of Geosynthetics", Procedings of the 8th International Conference on Geosynthetics (8ICG), Yokohama, Japan, September 18-22, 2006.

Importance Of Modeling In Fixing Orientation Of Bund At The Mouth Of Narrow Steeply Graded Creek For Safe Berthing In Macro Tidal Region

A.A. Purohit[1], M. M. Vaidya[2], A. Basu[3], K.A. Chavan[4]
1. Chief Research Officer, Central Water and Power Research Station, Pune-411024, India   2 & 3 Research Officer, Central Water and Power Research Station, Pune-411024, India   4 Research Assistant, Central Water and Power Research Station, Pune-411024, India

purohit_aa@cwprs.gov.in;
vaidya_mm@cwprs.gov.in;basuanimesh12@gmail.com;
ka_chavan@yahoo.com

ABSTRACT: *The physical hydraulic modeling tool is being used for past several decades to solve a number of complex fluid flow problems in the field of coastal engineering. The phenomena such as flow separation, formation of eddy, effect of marine structure on flow pattern, hydrodynamics at the confluence of two unsteady flows with steeply graded bathymetry etc. are the various types of complex flows and needs to be properly simulated and studied to assess effect of new development in such regions. The development of deep draft container terminal at the mouth of Nhava creek wherein a flow from shallow creek (1m above CD) suddenly meets at 90^0 to the deepest navigational channel (-14m CD) of Jawaharlal Nehru port wherein such flow exist. The presence of steep gradient of 1:10 results in more complex unsteady flow field with dynamic eddies. Evolving hydraulic design of terminal facility in such region requires site specific field data on tides, currents and proper simulation of flow in the model. The study of such complex flow in the region of macro tidal region is feasible and can be visualised in scaled physical tidal model with automatic tide generator and advanced data recording techniques. Evolving engineering solution for safe berthing by finalising orientation/alignment of guide bund at the mouth of creek requires true simulation and diversion of flow away from proposed terminal. However, it should not affect the operability of existing waterfront facilities in nearby regions. Using physical tidal model of Mumbai port, the flow conditions are studied for 10^0 and 18^0 orientations of 160m long guide bund at the mouth of Nhava creek. The studies reveal that physical model provides excellent information on flow visualisation (movement of eddy) during flood/ebb tide. The maximum strength of current at Nhava Creek entrance for $18^\bullet$ increases by about 34% and 41% during flood & ebb tide respectively with that of 10^0, indicating that 10^0 orientation is suitable for achieving desirable flow conditions at the proposed terminal. Also reclamation in Nhava Creek is not only useful for efficient storing of containers but also its typical shape does not affect hydrodynamics of Nhava Creek as well as its entrance. The timing at which the fishing vessels should ply in & out of Nhava Creek mouth after development can be scheduled effectively depending on current strength and water depth.*

Keywords: *Creek, berth, eddy, Guide bund, hydrodynamics, Macro tide, unsteady flow*

1. INTRODUCTION:

Among the various developing countries in Asia like China, Malaysia etc, India is also developing its infrastructural facilities in the form of waterfront structures like major/minor ports, power plants etc. at an exponential rate due to the rapid modernization and globalization in the world. These developments of waterfront structures in the form of jetties/wharfs/stack-yards etc. are being built by many private companies/joint ventures to cope up the present demands and future needs due to liberalization policy of the Government. The existing major ports are also keeping the pace of new developments at par with the private companies.

The major ports like Mumbai and Jawaharlal Nehru (JN) situated in Thane Creek on the west coast of India are having access through wide entrance in the Arabian Sea. These ports are called as natural ports and does not face the problem of wave tranquility in view of their locations either on leeside of Salsette Island or well inside in the Thane Creek. However, due to the presence of macro- semidiurnal type of tidal phenomenon (tidal range of 5m) in the region with ultra wide estuarine entrance of about 10 km and water area extending 30-40 km north in Thane estuary, it contributes to large exchange of water mass in and out of creek during flood/ebb phase of the tide. The suspended sediment concentration being high in Mumbai harbour area due to cohesive (clay) nature of sediment and reduction in tidal flux

due to the large reclamations carried out for the developments of new suburbs on eastern side of creek, it has resulted increase in siltation rates at various waterfront facilities. As such, siltation in addition to the effect of tidal currents governs the hydraulic design of waterfront facilities. Also in view of scarcity of land and waterfront area for development of new terminal facilities, deeper draft vessels being built all over the world requiring higher depths as well as existence of shallower depths in the nearby region, limits the expansion of existing facilities. Considering all above aspects and to handle large volume of shipping traffic at Mumbai, Port Authorities are forced to carry out new developments either off the shore or near to the navigational channel, wherein deeper depths exist.

The JN port being developed well inside the Creek along the navigational channel in Elephanta deep and nearby area being consisting of tidal flats, future development in offshore area is not feasible. Hence, in order to cope up the demand of deep draft container carriers (14-16 m depth), development on the north side of existing waterfront facilities is the alternative. The port in order to enhance its infrastructural facilities has opted for development along the existing navigational channel in line with the existing facilities at the mouth of Nhava Creek as in Figure-1. The other side of the channel towards Elephanta Island cannot be used in view of archeological importance.
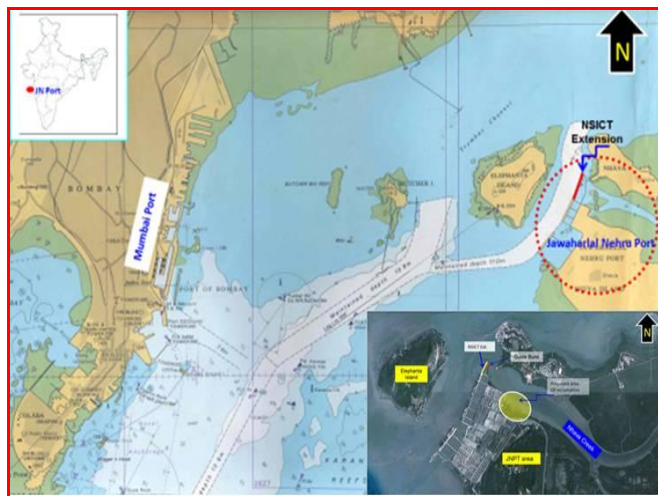
Figure1. Location of proposed container terminal at mouth of Nhava creek

2. COMPLEXITY AT THE MOUTH OF NHAVA CREEK:

The hydraulic design of proposed 330m long container terminal at mouth of Nhava creek and finalisation of its alignment is really a challenging job due to various complexities in the flow prevailing at the proposed location. Also providing stack yard facility for storing of containers can only be feasible inside the Nhava creek due paucity of space and approach. The major complexity at the entrance of Nhava Creek is shallower depths (+1 m CD) suddenly meeting artificially deepened navigational channel (-14 m CD) at Elephanta deep. The presence of such steeply graded bathymetry (1:10) causes meeting of secondary flow from the Nhava creek to the main channel flow at an angle of 90° as in Figure 2. It creates formation of dynamic eddies

during the ebb tide. So, the presence of such complex flow field at the entrance of Nhava creek will pose a serious problem on safe berthing of container vessels near the proposed terminal as the flow will pass beneath the berth during flood and ebb current as well as entry of fishing boats into the Nhava creek.

Hence extension of the existing guide bund by about 160 m on north and fixing its orientation (10^0 OR 18^0 clockwise) needs to be assessed so that at proposed terminal ship can be berthed safely irrespective of flood/ebb phase of tide, there will be easy entry of fisher boats in/out of Nhava creek as well as no problem to the existing berthing facility of ONGC on Nhava island further north of proposed terminal. The maximum orientation of bund by 18^0 clockwise and length of bund by 160 m is considered due to limitation of width available at the entrance to the Nhava creek.

Figure 2. View of proposed developement at the confluence of Nhava Creek

The simulation of flow condition in such complex scenario and evolving engineering solution in the form of construction of bund, fixing its length, orientation under time varying hydraulic phenomenon wherein flow is reversible (flood/ebb) is possible by studying the phenomenon on scale hydraulic model. The visualization of flow phenomenon such as formation of multiple eddies, its location with respect to time/phase of tide and interpretation of result is challenging job. Hence in order to obtain solution for finalising orientation of guide bund studies were conducted on physical model of Mumbai port [scale-1:400(H); 1:80 (V)], to achieve favorable flow condition for safe berthing of vessels at the proposed container terminal.

3. FIELD DATA FOR MODEL STUDY:

The field data collected on oceanographic parameters such as tides and current at proposed development in JN Port area was used to simulate flow condition in the model. The measured field data on tide at Apollo Bundar as well as current near mouth of Nhava creek is shown in Figure-3(A) and (B) respectively and was used to simulate the hydrodynamic condition in the model to study the flow pattern at proposed development of container terminal.
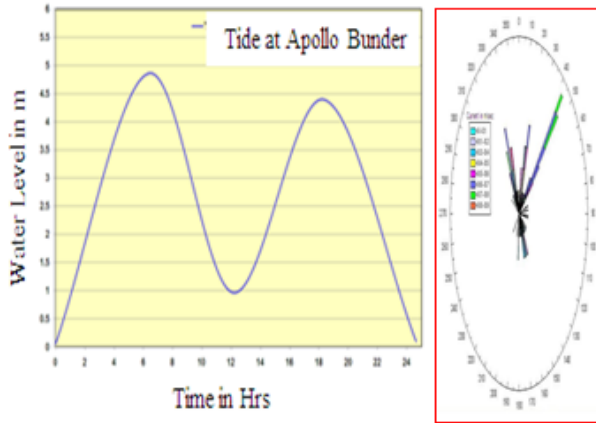
Figure 3(A). Tide during Spring condition creek   **Figure3(B).** Current at Mouth of Nhava

4. PRINCIPLES OF HYDRAULIC MODELING:

The hydraulic scale models are used to solve complex hydrodynamic flow problems which vary not only in space but also with time and are not amenable to mathematical analysis. These scale models are based on laws of similarity and the forces acting on fluid. Based on laws of similarity and dimensional analysis the major force which governs the flow is simulated so that flow in model behaves in similar fashion as that in prototype. In case of tidal flow, since the gravitational and inertial forces are dominant compared to other type of forces such as viscous force, surface tension force etc, the flow governed by tidal phenomenon in model is simulated based on the principles of Froude's law.

$$Froude\ Number = \frac{Inertia\ Force}{Gravitional\ Force}$$

$$F_n = \frac{\rho V^2 L^2}{\rho\, gL^3} = \frac{V^2}{g\,L}$$

$$F_{proto} = F_{model}$$

$$\frac{V_m^2}{V_p^2} = \frac{l_m}{l_p}; \ V_r^2 = V_m^2 / V_p^2 = 1 \qquad ---- \qquad \text{(Hudson, R.Y etal,}$$

1979)

Where, F_n is the Froude's number; V_m, L_m and V_p, L_p are the velocity and characteristic length scale in model and proto respectively. When very large area has to be reproduced in the model, then depth reproduced by geometrically similar model scales becomes too small transforming turbulent flow (in proto) into laminar flow (in model) besides causing difficulties in measurements as well as difficulties in achieving practicable smoothness. In order to overcome these difficulties, often distorted model i.e. Length Scale (L_r) different than depth scale (d_r) is used in simulating tidal flow phenomenon. In such cases equality of Froude number in model and proto leads to $V_r =$

$(d_r)^{0.5}$. These models are used only when vertical acceleration is negligible.

For the present hydraulic model, the horizontal length scale is 1:400 and the vertical length scale is 1:80. Form Froude similitude criteria the time scale for this distorted model will be.

$$T_r = \frac{L_r}{d_r^{0.5}} = \big(1\sec(Model) : 44.42\sec(Prototype)\big)$$

5. DESCRIPTION OF PHYSICAL MODEL:

The Physical modelling technique is being used at CWPRS for the past six decades in the field of coastal engineering to finalise the layout of Ports, navigational channels, alignment of jetties, shape of reclamations etc. These models are namely tidal models, wave models or wave flume models to assess hydraulic stability of marine structures. These models works on the principle of Fraud's law of similitude as gravitational forces are dominant in the physical processes compared to other type of forces mentioned above. The numerous advantages in having a permanent physical model for major port establishments are:

❖ Model in the long run is beneficial and economical for future developments likely to take place in the region.

❖ Various proposals can be tested speedily by making minor modifications and alterations in model and input variables such as generation of tide can be controlled easily.

❖ The complex flows like formation of eddies/ separation or bifurcation of flow, simulation of combined flows like tide and river discharges in estuarine region and its effect on future development etc. provides a clear picture about hydrodynamic processes to helps engineers/modelers to take appropriate decisions which can guide the project Authority.

The Mumbai port model at CWPRS is a distorted tidal model having scales of 1/400(H) and 1/80(V). The model covers Thane estuary, Panvel creek, Dharamtar creek and part of Arabian Sea. The model is covered by a shed of size 70 m X 45 m, representing an area of about 28 km X 18 km in proto. The location of proposed terminal at JN port in physical model is shown in Figure 4.

Figure 4. Location of proposed container terminal studied on Mumbai port model

5.1 Generation of tides:

The type of tide prevailing at Mumbai being semi-diurnal, a typical tidal cycle is of 12 hrs. and 25 minutes (proto) is reproduced in 17 minutes; 8½ minutes of flood and 8½ minutes of ebb in the model. A re-circulating system with a discharge of about 1.5 Cumecs is used for generation of tides. A well-equipped Automatic Tide Generating (ATG) system generates tides of required amplitude and period. The system consists of radial gates mounted on a single common shaft connected to a stepper motor through gear box. The operation of gate (clockwise/counter clockwise) is controlled by the computer having data acquisition and control interface. The Figure.5 shows the pictorial representation of the system and the reproduced tide.
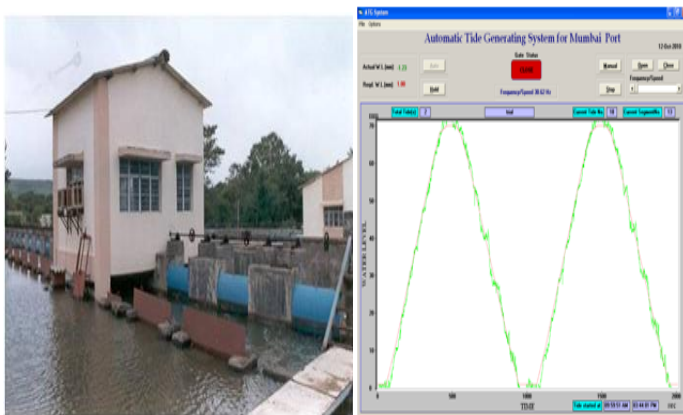
5.2 Model calibration and tests:

A tidal model is said to be calibrated when the flow conditions in model are in proportion to that in prototype and this is possible by comparing water levels and current (magnitude/direction) in model with prototype. The model was calibrated for a tidal data measured and comparison of typical pseudo tide during spring is shown in Figure 6. The velocity measurements were also carried out by digital image processing technique. In this technique, paper confetti was spread on the water surface. The confetti moves with flow velocity. Photographs of the flow were taken at fixed duration, for a known exposure time, by using digital camera. The displacement of confetti in known time gives magnitude of velocity while its direction can be found with respect to North. The model tide have 95-98% matching with prototype tide and in view of model being laid with latest bathymetry, velocity field has also been found to be in good agreement with site.
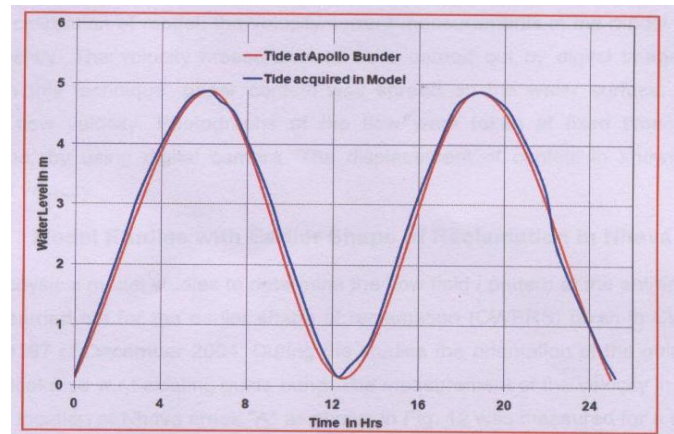
Figure 6. Comparison of proto and model tide at Apollo Bundar

The Hydraulic model studies were carried out for prevailing hydrodynamic condition in order to visualize the flow field/pattern near the proposed 330m long container terminal and current strength/direction at the entrance of Nhava creek. The studies were performed on model with two different orientations of guide bund (extension length 160m) viz. 10° and 18° clockwise w.r.t. the existing bund as shown in Figure 7(A) & (B). The studies include proposed reclamation inside the Nhava creek as a stack yard. The suitable orientation of bund for safe berthing of ship at proposed terminal irrespective of phases (flood/ebb) tide is finalised based on the flow conditions at hour interval every.
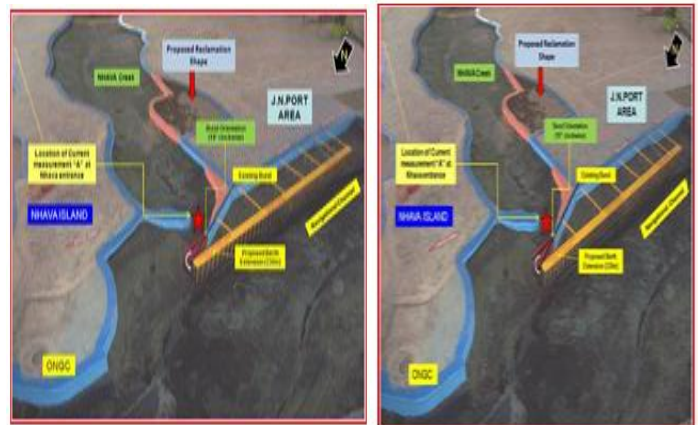
Figure 7(B. Guide bund with 180 clockwise   **Figure 7(A).** Guide bund with 10^0 clockwise

The information on current strength as well as flow pattern was obtained by digital image processing techniques at the entrance of Nhava creek and terminal location respectively.

6. DISCUSSIONS OF RESULTS:

The model studies carried out to assess the flow field at the entrance of Nhava creek and at proposed container terminal/ONGC facility north of JN port for the orientation of

160 m long guide bund at an angle of 10° and 18^0 during fourth hour are presented in Figures 8(A) to 8(D).

Figure 8(A). Flow during 4th hour flood (10°)

Figure 8(B). flow during 4th hour flood (18°)

Figure 8(C). Flow during 4th hour ebb (10°) Figure 8(D). Flow during 4th hour ebb (18°)
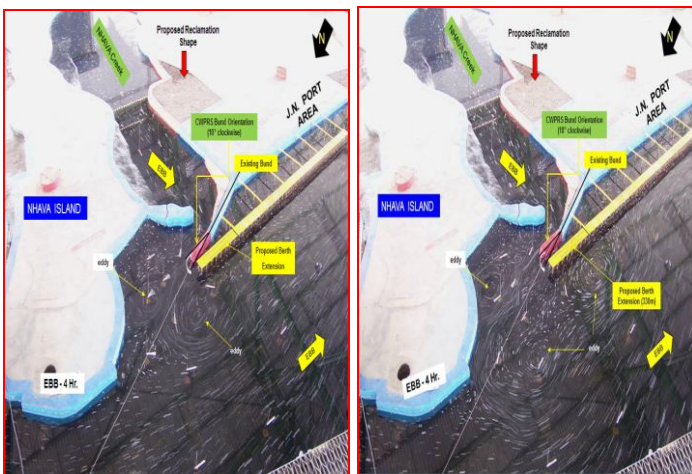
Flow pattern observed during various phases of tide (flood/ebb) at every one hour interval (prototype) reveals that during flood tide flow almost remains parallel to the proposed 330 m berth, for the entire flood period for 10° & 18° orientations. During various phases of ebb tide, eddies are seen to be formed in varying intensity at the locations of proposed berth, entrance of Nhava creek and ONGC for 18° orientation. While for 10° eddy of weaker strength during 1st hour of ebb at terminal and formation of circulation in Elephanta deep away from berth is seen to be formed. However this will not hamper safe berthing of ships at proposed terminal. The comparison of current strength measured at the entrance of Nhava creek at every one hour interval (during flood/ebb) for 10° and 18° orientation is shown in Figure 9.
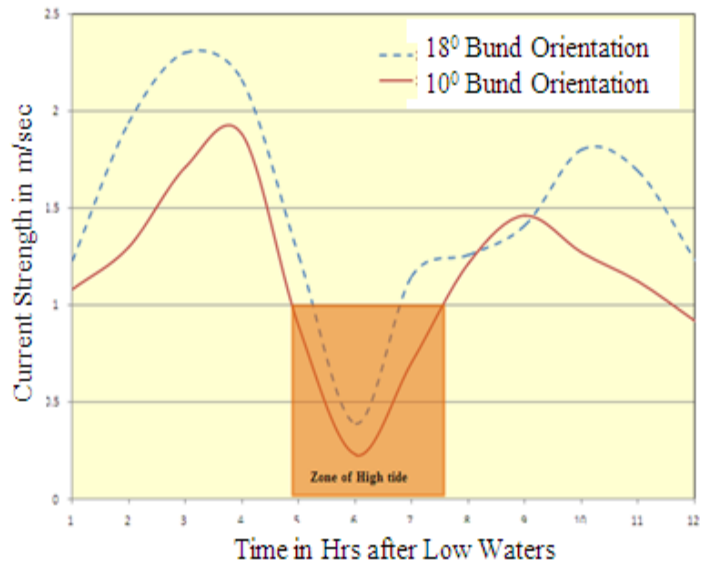
Figure 9. Comparison of current at entrance of Nhava creek for 10^0 & 18^0 orientation

The hydraulic model study also reveals that the maximum strength of current at Nhava Creek entrance for 18° increases by about 34% and 41% during flood & ebb tide respectively with that of 10^0, indicating that 10^0 orientation is suitable for smooth entry of fishing boat in/out of Nhava creek during high tide zone as shown in Figure 9.

7. CONCLUDING REMARK:

Based on studies carried out, the following broad conclusions can be drawn, which also highlights the importance of modeling tool in fixing orientation of bund in narrow steeply graded Creek:

➢   Physical model provides excellent information on flow visualisation (movement of eddy) during flood/ebb tide as well

as velocity field to fix the orientation of bund for achieving desirable flow conditions at the proposed terminal in complex hydrodynamic conditions.

➢ Reclamation in Nhava Creek is not only useful for efficient storing of containers but also its typical shape does not affect hydrodynamics of Nhava Creek as well as its entrance.

➢ The timing at which the fishing vessels should ply in & out of Nhava Creek mouth after development can be scheduled effectively (zone of high tide) depending on current strength and water depth.

➢ Flow pattern observed for the two alternative cases during flood/ebb tide indicates that the orientation of guide bund at an angle of 10° clockwise with respect to the existing guide bund provides desirable flow conditions for safe berthing of vessels at proposed terminal without affecting operability at ONGC compared to that for 18°.

ACKNOWLEDGEMENT

REFERENCES:

i.   CWPRS technical report No. 5080 of June 2013

ii.   Hudson RY, Herrmann FA, Sager RA, Whalin RW, Keulegan GH, Chatham CE and Hales LZ(1979), Coastal Hydraulic Models, Special Report No.5, US Army Engineer Waterways Experiment Station, Vicksburg, Mississippi.

Underwater Seismic Reflection Survey Using Chirp Sonar For The Development Of Port

M.S. Chaudhari, V.Chandrashekhar, Vivek Bagade and R.S. Ramteke
Central Water and Power Research Station, Khadakwasla, Pune-411024
Tel.9120-24103481 Fax. 9120-24381004
mukund_chaudhari@yahoo.co.in

ABSTRACT: *High resolution seismic reflection profiling was carried out deploying dual frequency echo sounder and chirp sub bottom profiler system from a precisely positioned survey vessel along ten traverses to delineate the sub surface stratigraphy and bed rock topography for the development of Haldipur port. The results of the survey revealed four to five sub surface reflectors including sea bed. The depth of sea bed with respect to chart datum in the area surveyed varied from 1.1 m to 10.3 m and rock depth ranged between 25.7 m to 43.8 m. The strata inferred seismically along these traverses corroborated well with those from the boreholes drilled in the area. The survey also revealed the occurrence of acoustic masking. Sub-bottom reflectors are seen to be affected by gas masking in the records. The acoustic masking in the record indicates the gas charged sediments. Fine grained sediments contain appreciable quantities of interstitial gas bubbles which are responsible for the anomalous seismic signatures. This could be due to shallow hydrocarbon gases derived mostly from biogenic degradation of organic matter accumulated under palaeo-estuarine conditions. The behavior of the gas charged sediments create a potential hazard for the offshore civil engineering construction and its development. When gas gets trapped and accumulate under the impermeable layer, the resulting gas pressure goes up to such a level that the blowout can occur during drilling. Similarly, gas escaping naturally to the surface in extreme cases causes the collapse of structures due to undermining of the foundation. Hence, these findings are very important in the design of breakwaters and other offshore marine structures for the development of the port.*
Key Words: Underwater Seismic Reflection, Chirp Sonar, Gas charged Sediments

1. INTRODUCTION

It is proposed to develop a deep water all weather port with artificial harbor protection at Haldipur in the vicinity of Honavar port with a view to optimizing the trade potential of Northern Karnataka's agro and mineral rich hinterland. The port shall be developed for handling deep drafted vessels up to 20 m, which shall be an alternative between Mumbai and Mangalore port. To decide the feasibility of any project before proceeding with the execution of the project it is desirable to carryout geological survey for mapping sediments and rock types. This subsurface strata information can be obtained by borehole drilling, borehole video recording and sea bed sampling but these methods are expensive and time consuming, also the information derived corresponds to point and covers small area of the strata which may or may not hold for the nearby area. On the other hand, geophysical methods are non invasive, non contact type and give continuous sub surface strata information. Shallow underwater seismic reflection technique provide information on sediment thickness and rock topography which is important in assessing the quality and in calculating the quantity of the material to be dredged (Dobinson & Mc Caun,1990, Conway et.al.,1984) for the development of the navigation channel.

This paper presents the results of chirp sonar survey and dual frequency echo sounder survey carried out from a precisely position survey vessel at the proposed Haldipur port. Data from the few boreholes drilled in the survey area was used to calibrate and to geologically define different sub surface acoustic reflectors.

2. STUDY AREA

The study area lies in the shallow waters off Honavar port in the west cost of India. (Fig. 1). The area lies between latitude 14º 17' 17.98" to 14º 22' 8.99" and Longitude 74º 17' 6.28" to 74º 24' 55". In the study area water depths ranges from 1.1 m to 10.3 m and is dominated by gently westward slope and it lies off the mouth of Indravati river.
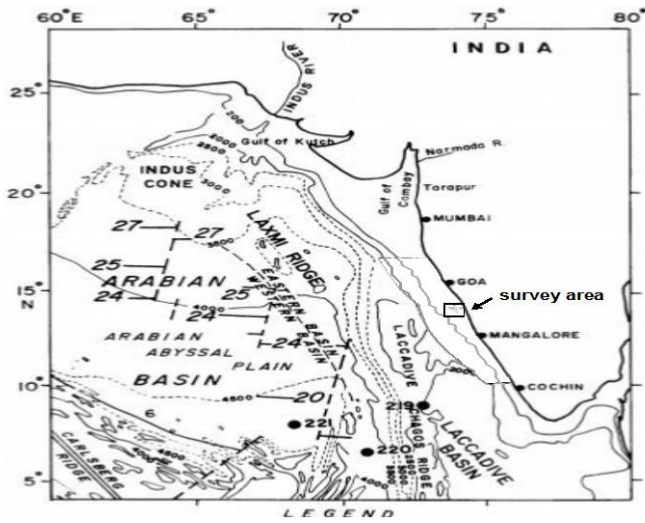
Figure 1. Map showing Location Plan of survey area

Underwater seismic reflection technique was deployed to decipher subsurface stratigraphy including rock topography in the survey area. In seismic reflection technique, the acoustic waves reflected at the geological interfaces, such as sea-floor, stratigraphic or lithologic and geotechnical boundaries are recorded continuously. The reflection of waves is a function of the change in acoustic impedance (product of density and velocity) of the sea-floor as well as the underlying subsurface strata. The quantum of reflected energy will decide whether a particular layer will be detected and hence recorded. The reflected energy is a function of the thickness of the subsurface layer, the sharpness of the geological boundary or the physical interface. The reflection coefficient `R' of a normal incident ray for a geological boundary is evaluated by

$$R = \frac{\rho_2 V_2 - \rho_1 V_1}{\rho_2 V_2 + \rho_1 V_1}$$

where ' ρ ' and 'V' are the bulk densities and velocities on either side of the boundary. More the value of `R' , more compact or hard is the boundary.

If acoustic impedance of the two layers on either side of the boundary (even though the layers are geologically different) is the same, then acoustic energy will not get reflected from the boundary (Sheriff, R.E., 1977). This means that, though two layers are geologically different, they appear as one as far as acoustic properties are concerned and hence will not be differentiated on the chirp sonar record. On the other hand the greater the impedance contrast, the stronger will be the reflected energy. The physical and elastic characteristics of the water column and the underlying solids comprising bed and sub-sea bed, determine the amount of wave energy that will be absorbed and thus attenuated. This property of the water column and the underlying material controls the depth of investigation and in

turn the depth from which the reflected energy will return to the surface.

Underwater seismic reflection survey was conducted with digital chirp sonar sub-bottom profiler model X-star and SB 0512i Tow-fish manufactured by M/s Edge Tech. Chirp sonar system, the acronym for which is Compressed High-Intensity Radar Pulse, use a calibrated Frequency Modulated (FM) pulse that provides nearly constant resolution with depth and produces high resolution images of sea bed as well as of sub-sea bed. In chirp sonar wide band FM pulses are used that sweep over the frequency range of 500 Hz to 12 kHz. The wide band width ensures that sediment layers ~7 cm thick can be resolved. Chirp sonar is a multiplexed system. The tow-fish consists of four transmitters and four receivers. Upon receipt of a key pulse from the surface unit, the tow fish transmits high voltage electrical signals and the sub-bottom reflections are measured at the hydrophone receiving array, the output of which is amplified by a programmable gain amplifier before being digitized by a 16-bit A/D converter. This digitized signal is processed using matched filter and cross-correlation techniques. The chirp sonar has many different ranges of frequency bands within the maximum frequency band 500 Hz to 12 kHz stored inside it and any of these bands can be selected remotely depending on the depth of interest, the vertical and horizontal resolutions required to be achieved and geological strata encountered in the area of investigation. In the present survey tow fish with frequency band of 500 Hz to 8 kHz was used and towed about 3 m behind the survey vessel. The reflected signals from the sea bed were recorded continuously and displayed on the monitor.

Kongsberg dual frequency echo-sounder with output frequencies 38 kHz and 200 kHz was used to record water depths precisely. Position fixing and navigation of the survey vessel was conducted by deploying Sokkia Global Positioning System with beacon receiver. 'Sokkia' GPS is a satellite based system and uses signal broadcast frequency of 1575 MHz   ±10 MHz with position measuring accuracy of ± 2 m for the moving survey vessel.

4. DETAILS OF INVESTIGATIONS

Chirp sonar and dual frequency echo-sounder surveys were conducted along 10 traverses covering approx. 35 line Km. The lengths of these traverses varied between 2.95 Km and 4.0 Km. Out of these ten profiles, seven traverses CD, EF, GH, IJ, KL, MN and OP were taken from shore to sea while three cross traverses ST, UV and XW were conducted across the parallel lines to verify and confirm the findings of the survey. Fig. 2 shows the layout map of all the 10 traverses.

The position co-ordinates of the survey vessel were taken every 30 seconds and the fixes were also noted every 30 seconds on the seismic record. The depths of various acoustic reflectors, deciphered on the chirp sonar records were then calculated at those fixes. The depth-sections with respect to chart datum depicting various subsurface layers were then drawn along these traverses after correcting the sea bed depth for tidal variations.
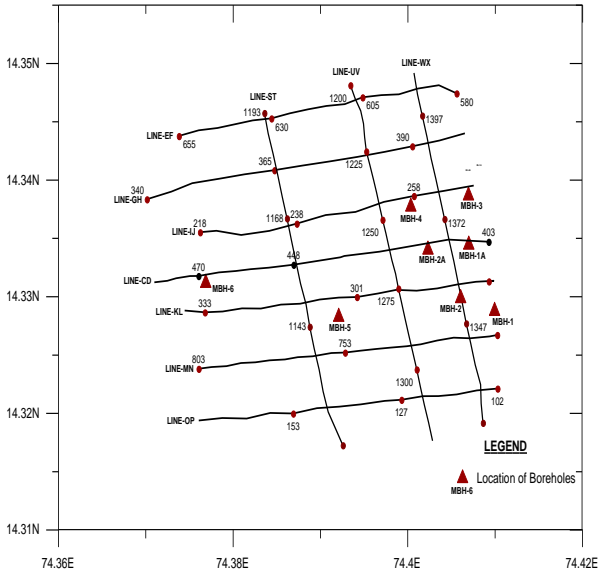
Figure 2. Layout of Seismic

5. RESULTS AND DISCUSSION

In the area surveyed, the depth sections with respect to chart datum along all the traverses show, in general, four to five subsurface reflectors including sea bed. The first reflector in all the cases was interpreted as sea bed i.e. boundary between water and sea bed, while the last reflector was inferred to be representing rock topography i.e. boundary between sediment and rock. The reflectors in between represent sediment layers of different grain size, clay content and compactness i.e. silt, clay, sandy or silty clay, clay with gravel, stiff/very stiff clay. However, at some places along these traverses, sediments also occur in the form of pockets and lenses. The geological identification of the reflectors is based on the data of boreholes drilled in the survey area.

Two way reflection times recorded in milliseconds were converted into depths in meters by multiplying with the velocity of the water 1550 m/s and of sediments 1700-2050 m/sec. This inference of value of velocity is based on the experience of working at various sites in India, as also on the velocities of the sediments reported in the literature (Wadhwa, R.S., et al, 2007). The difference in the depths of first and second reflector will yield the thickness of first sediment layer. Similarly, the difference in the depths of second and third reflector will yield the thickness of second sediment layer and so on.

The depth section with respect to chart datum along traverse CD conducted from shore towards sea shows, four subsurface reflectors including sea bed. However, along this traverse, one isolated pocket of sediments have been inferred, the lateral and vertical extent of which is shown in the depth-section (Fig.3).

It is seen from this depth-section that depth to sea-bed with respect to chart datum varies from 2.2 m to 10.3 m, it being shallowest at fix 404 and deepest at fix 479. The rock levels with respect to chart datum along this depth section range between

25.7 m and 40.4 m. The depth section depicts five reflectors (including sea-bed) at fix 404 and continues to be five up to fix 422. Then further down, one reflector disappears up to fix 473. The rock level in borehole MBH-2A with respect to chart datum was 27.0 m while the reflector representing rock for traverse CD at fix 419 which was close (27.5 m) to this borehole was inferred to be at 27.8 m indicating a good match between the two. The correlation of depth to rock determined seismically and that inferred in the borehole MBH-2A drilled nearby is shown in the same figure. The other two boreholes MBH-1A (near fix 409) and MBH-6 (near fix 469) drilled near traverse CD did not show any rock as the same were terminated at 19.5 m and 12.5 m respectively. The seismically evaluated rock levels at fixes 409 and 469 of traverse CD were 27.5 m and 38.8 respectively.

From the results of ten seismic traverses conducted, contour maps of sea bed and rock depth were obtained. The depth to sea bed with respect to chart datum varies from 1.1 m to 10.3 m (Fig.4). Sea bed has gentle slope towards west. Fig. 4 also shows the features of gas charged sediments where sub-bottom details are lost due to effects of gas bubble within the sediment pore spaces. The rock depth with respect to chart datum varies 25.7 m to 43.8 m (Fig.5).
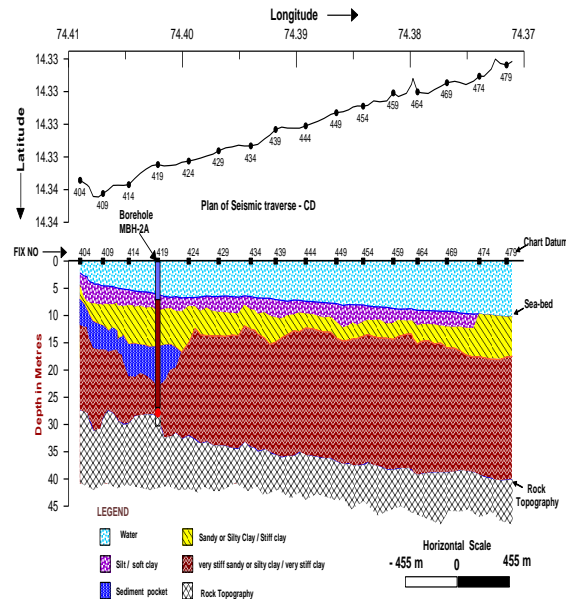
Figure 3. Depth-Section along
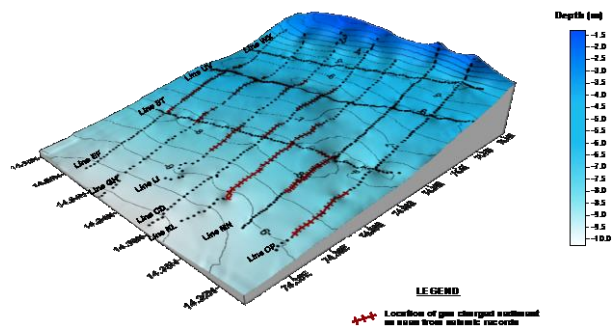
Figure 4. Topography of sea bed along with depth contours with respect to chart datum
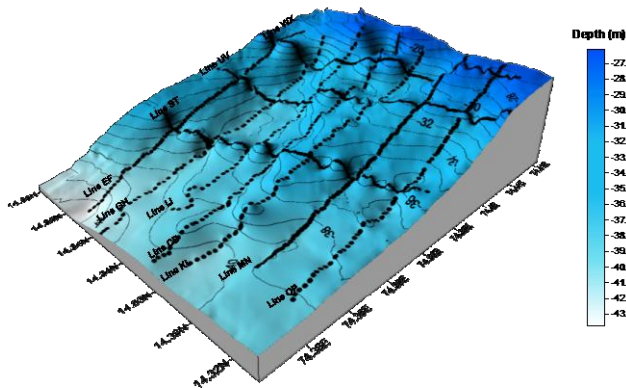
Figure 5. Topography of Rock –depth along with contours with respect to chart datum
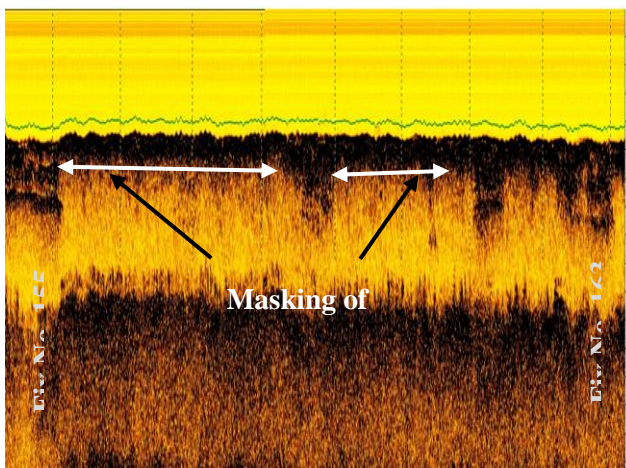
Figure 6. Typical seismic record obtained in traverse OP from fixes 155 to 163

From the seismic records it is observed that, at certain fixes subsurface layers keeps disappearing due to presence of gas charged sediments on the sea floor. These gas charged sediments does not pass seismic energy downward and as most of the seismic energy gets reflected disappearances of subsurface layers is seen in the seismic record. Discontinuity of sub-bottom reflection is commonly seen associated with gas masking features (Ramana, M.V., et al, 2006). Fine grained sediments contain appreciable quantities of interstitial gas bubbles which are responsible for the anomalous seismic signatures. This could be due to shallow hydrocarbon gases derived mostly from biogenic degradation of organic matter accumulated under palaeo-estuarine conditions. It is found that these anomalous features are confined only to the seismic records and are not seen

in the corresponding echograms. This reveals that the anomalous features due gas charged sediments are localized within sediments. The behavior of the gas charged sediments create a potential hazard for the offshore civil engineering construction and its development. When gas gets trapped and accumulate under the impermeable layer, the resulting gas pressure goes up to such a level that the blowout can occur during drilling. Similarly, gas escaping naturally to the surface in extreme cases causes the collapse of structures due to undermining of the foundation (Subba Raju, L.V., et al, 1996). Hence, these findings are very important in the design of breakwaters and other offshore marine structures for the development of the port. Typical seismic record obtained in traverse OP from fixes 155 to 163 is shown in Fig. 6.

6. CONCLUSIONS

Results of the chirp sonar and dual frequency echo-sounder surveys revealed that in the area surveyed the subsurface comprises four to five acoustic reflectors. These acoustic reflectors were interpreted as sea-bed, i.e. silt, clay, sandy or silty clay, clay with gravel, stiff/very stiff clay and rock topography. The geological identification of the different sediment reflectors is based on the data of boreholes drilled in the survey area. It is observed that along the same traverse the number of acoustic reflectors varied. From the varying number of subsurface reflectors along the same traverse, it was inferred that, the sediments occur in the form of thin to thick pockets and lenses. The level of sea-bed with respect to chart datum varied between 1.1 m to 10.3 m and rock level ranged between 25.7 m and 43.8 m. The strata inferred seismically along the traverses correlate well with those from the boreholes drilled nearby. Seismic records of the survey area also revealed the occurrence of acoustic masking. The acoustic masking in the record indicates the gas charged sediments. The gas charged sediments create a potential hazard for the offshore civil engineering construction and its development. Hence, these findings are very important in the design of breakwaters and other offshore marine structures for the development of the port.

7. ACKNOWLEDGEMENTS

8. REFERENCES

i.   Conway, B.W., Mc Caun D.M., Sarginson, M. and Floyd, R.A., 1984, A geophysical survey of the Crouch/ Roach river system in South Essex with special reference to buried channels, Quarterly Journal of Engineering Geology, 17, p 269-282
ii.   Dobinson, A., and Mc Caun, D.M., 1990, Application of marine seismic surveying methods to engineering geological studies in near-shore environment, Quarterly Journal of Engineering Geology, 23, p 109-123.

iii.   Ramana, M.V., Ramprasad, T.,Desa, M.,Sathe, A.V., and Sethi,A.K.,2006, Gas hydrate-related proxies inferred from multidisciplinary investigations in the Indian offshore areas, Vol 91, No.2, p 183-189.

iv.   Sheriff, R.E., 1977, Limits on resolution of seismic reflections and geologic details derivable from them in Seismic Stratigraphy - Applications to hydro carbon exploration, Mem. 26. Payton, C.E., Ed., American Association of Petroleum Geologist, Tulsa, 3

v.   Subba Raju, L.V., and Wagle, B.G., 1996, Gas-charged sediments in shallow waters off Redi along the central west coast of India, Current Science, Vol.71, No.5, p 416-418.

vi.   Trabant, P.K., 1984, Applied high resolution geophysical method – offshore geoengineering hazards, International Human Resources Development Corporation, Boston, USA, pp 265

vii.   Wadhwa, R.S., Rani, C.K., Chaudhari, M.S, Raja Mukhopadhyay and Ghosh.N., 2007, Chirp Sonar Survey for development of Jawaharlal Nehru Port, Vol.11, No. 4, p 181-187.

Experimental Study On The Behaviour Of An Interface System Connecting Between Two Offshore Structures

Gowri Shankar C[1]   B.V. Mudgal[2]   Ashwani Vishwanath[3]

[1]Assistant Professor, Saveetha School of Engineering, Chennai-602105, India
[2] Professor, Centre for Water Resources, Anna University, Chennai-600025, India
[3]Scientist-B, National Institute of Ocean Technology, Chennai-600100, India
Email: gowrishankar1805@gmail.com

ABSTRACT: *The study is primarily concerned with experimental study of the response of an interface system which interconnects the semi-submersible platform and a spar for a large scale desalination plant of capacity 10 million litres per day, based on Low Temperature Thermal Desalination Technology (LTTD) which is to be operated offshore. A physical model of scale ratio 1:100 was used. Among all the configurations analysed, the configuration for four corner columns of size 60 mm x 57.5 mm x 140 mm with deck size of 360 mm x 320 mm x 60 mm and ring pontoon of size 360 mm x 110 mm x 100 mm in transverse direction gave good heave response with a peak natural period of 0.8 sec for model which can be scaled up for prototype using Froude scaling. The configuration of the spar model tested is of the size of 100 mm diameter and 600 mm depth where a ball and socket joint is placed at the top of the spar to interconnect it with the semi-submersible. Therefore the above configuration has been chosen for model making and experimental analysis. The model was tested in a wave flume which includes Free Oscillation test and Motion Response analysis for with and without the interface systems. The motion response results obtained from the experimental study infer that a ball and socket arrangement on the semi-submersible could produce a better performance and safe operating conditions.*
Keywords: LTTD, YCM, Spar, Semi-submersible, significant wave height, wave period, RAO

1. INTRODUCTION:

One of the most vital and abundant natural resource on the planet earth is water. But only 0.3% of the world's total amount of water can be used as clean drinking water. As natural fresh water reserve is limited, sea water can be utilized as an important source of drinking water by employing effective methods of desalination. National Institute of Ocean Technology (NIOT), Chennai is in the planning stage for setting up a large scale Low Temperature Thermal Desalination plant (LTTD) with 10 million liters per day (MLD) capacity located offshore. The plant is to be operated in severe ocean environment which induces severe motion of the platform. Hence a suitable offshore structural system has been designed with reference to the concept called Truss Pontoon Semi-submersible (TPS) developed by Chakrabarti et al., (2007) for installing the desalination plant which must have good station keeping characteristics. In the present study, a new concept based on the well-known soft yoke principle has been developed whereby the yoke structure has the dual function of mooring the semi-submersible to a permanently moored spar platform and of supporting the rigid pipe system which transfers the hot and cold water for the desalination plant. The new configuration which will now on be referred to as Yoke Connection Mechanism (YCM) is designed as a temporary mooring which can be disconnected in wake of extreme operating environments. Several soft yoke systems have been constructed by oil industries in the past for the shallow waters of West Africa and South East Asia. Soft yoke systems are complex articulated (jointed) systems.

1.1 Hydrodynamic behaviour:

A floating body on the surface of the sea is always in oscillatory motion. The components of linear body motions that a floating body experiences along coordinate direction with respect to center of gravity of the floating body are called surge the linear longitudinal (front/back) motion, sway the linear lateral (side-to-side) motion, and heave the linear vertical (up/down) motion. Whereas the angular displacements about the respective axes are roll the rotation of a vessel about its longitudinal (front/back) axis, pitch the rotation of a vessel about its transverse (side-to-side) axis and yaw the rotation of a vessel about its vertical axis as shown in Figure 1.1. Among the six components of motion, heave, pitch, roll motion are important as they affect the stability of the platform. Hence, the heave natural period, pitch natural period and roll natural period are taken as the main deciding criteria for finalizing the configuration of the semi-submersible.
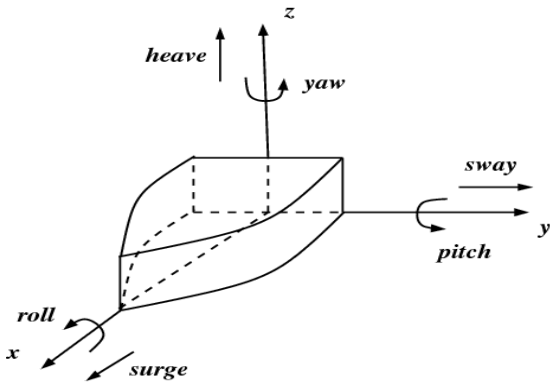
Figure1.1 Six degrees of freedom

1.2 Platform configurations:

The platform configurations chosen for the offshore desalination plant include the semi-submersible which houses the complete desalination plant and the spar which supports the 800 meter deep cold water pipes. There is an inter connection mechanism between these platforms which is similar to the inter connection mechanism developed by Arango et al., (2002) where a yoke was designed to connect a Floating Production, Storage and Offloading (FPSO) to the spar platform. This enhances the functionality of the system as shown in Figure 1.2.
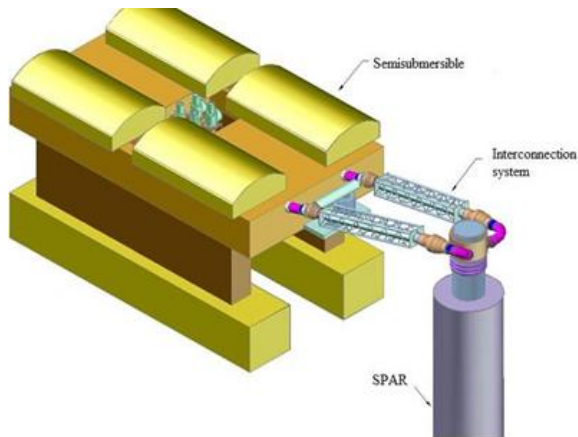
Figure 1.2 Conceptual Interconnection System
(Source: National Institute of Ocean Technology)

1.3 Response Amplitude Operator (RAO):

The Response Amplitude Operator (RAO) is an engineering statistic, or set of such statistics, that are used to determine the likely behaviour of a floating structure when operating at sea. It is the ratio between amplitude of response motion to the amplitude of wave. Response amplitude operators are usually obtained from models of proposed designs tested in a model basin, or from running specialized CFD computer programs, often both.

2. MATERIAL AND MODEL MAKING

The prototype has to be scaled down to suitable scale ratios to adopt into wave flume at the laboratory. All linear dimensions will have the same scale ratio in an undistorted model. Scaling down the prototype has to be done by Froude scaling because gravity forces are predominant. Wave flume dimensions, wave characteristics and beach profile are important in scaling down the prototype. In hydraulic structures and for wave motions studies the gravity effect is usually predominant in the prototype. The flow is fully turbulent and hence viscous and surface tension effects are negligible in the prototype. Froude number Fr, characterizing the ratio of the inertia force to gravity force is chosen for similitude. Equating the Froude number of the model and the Froude number of the prototype ensures that the gravitational and inertial forces are in the same proportion.

Table 1. Scaled Down Dimension of Semi-Submersible Model

Description	Prototype		Model	
1.Pontoon				
Length	36	m	360	mm
Breadth	10	m	100	mm
Height	10 m		100 mm	
Acrylic thickness			5 mm	
2.Column				
Length	9	m	90	mm
Breadth	5.75	m	57.5	mm
Height	14 m		140 mm	
Acrylic thickness			4 mm	
3. Deck				
Length	36	m	360	mm
Breadth	32	m	320	mm
Height	06 m		60	mm
Acrylic thickness			3 mm	
4.Total weight	9434 ton		9.43 kg	
5. Centre of Gravity	8.79 m		87.9 mm	
6. Metacentric Height				
Longitudinal direction	1.38	m	13.8 mm	
Transverse direction	1.01 m		10.1 mm	

The material chosen for the model is acrylic which has a density of 1300 kg/m³. Mild steel plates of 16 mm and 25 mm thickness were placed in the pontoon and 3 mm thick plate was placed on the deck in order to match the payloads of the prototype. The ballasting of pontoon to replicate the existing scenario was done by placing mild steel plates in the transverse pontoon with respect to CG. The spar is of 100 mm in diameter and 600 mm in height is also made up of acrylic and is fixed over a mild steel plate. The ball and socket joint, inter-connecting rod are made up of aluminum which is fixed over the spar.

Figure 2.1 Interconnected Spar and Semi-submersible Model

2.1 Wave flume:

Experiments were carried out in the wave flume of the PG Hydraulics Laboratory of Centre for Water Resources, Anna University. The wave flume is 30 m in length, 1 m in width and 1 m in depth. One end of the flume has a wave generator. At the other end, 40 mm aggregate is spread in a slope of 1:8 so that the waves don't reflect but break due to the beach effect. This holds good only for water depth up to 0.6 m. The waves are generated by the to and fro motion of the paddle which is connected to the crank. The crank is connected to the motor by a belt. By turning the wheel, the rpm of the motor can be controlled. This helps in varying the period of oscillation of the waves.

Figure 2.2 Wave Flume

2.2 Accelerometer:

The accelerometer used is MEMS 3 axis + or − 2g/6g digital output low voltage linear accelerometer evaluation board based on the LIS3LV02DL. The special features of the accelerometer are Graphical user interface, USB connector, control switches, MEMS sensor, LED indicators and ST7 – USB microcontroller. The STEVAL – MKI005V1 is an evaluation kit designed to provide the user with a complete, ready to use platform for evaluation of the LIS3LV02DL, a lower power 3 axis linear accelerometer with digital output. The device includes a sensing element and an IC interface capable of translating information from the sensing element into a measured signal that can be used for external applications. In additions to the MEMS sensor, the

evaluation board utilizes an ST7 –USB microcontroller which functions as a bridge between the sensor and with the sensor and the PC, on which it is possible to use the graphical user interface included with the kit or dedicated software routines for customized applications. The accelerometer has the frequency of 7 Hz. The accelerometer is fixed at the top of the model above the CG.

2.3 Data acquisition:

Data acquisition is set to collect data for a specified period of time at a specified frequency. During data collection data acquisition system displays the time for the test together with a graphical display of the channels being acquired in real time. At any time the acquisition can be retained or aborted to get data without any error one or two channels shall be selected. The collected data set is saved to a file named within the project.

3. EXPERIMENTAL INVESTIGATIONS

3.1 Free oscillation test:

Free motion test was carried out in order to measure the natural heave, roll and pitch periods of the model. To carry out the heave oscillation test the model is given a gentle push through the centre of deck where vertical axis passes through CG and immediately released. The model is allowed to oscillate and the data is acquired till the oscillation stops. The free heave oscillations were recorded by the accelerometer. The same procedure is followed for roll and pitch oscillation test except that the push is given at the center point of deck, where the lateral axis passes through CG and the data is acquired. The typical record of free oscillation test for heave, roll and pitch are shown below in Figure 3.1, Figure 3.2 and Figure 3.3 respectively.
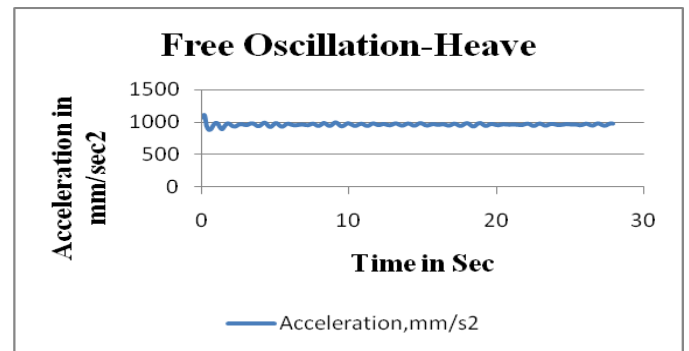
Figure 3.1: Typical record of Free Oscillation test for Heave

T_m =Heave natural period in sec   = Duration of time for no of cycles/No of cycles

$$= 0.8 \text{ sec}$$

$$T_p = T_m * (\lambda)^{(1/2)} =$$
$$0.8*(100)^{(1/2)}$$

$$= 8 \text{ sec}$$

Damping Ratio   = 0.28 %

Free Oscillation-Roll
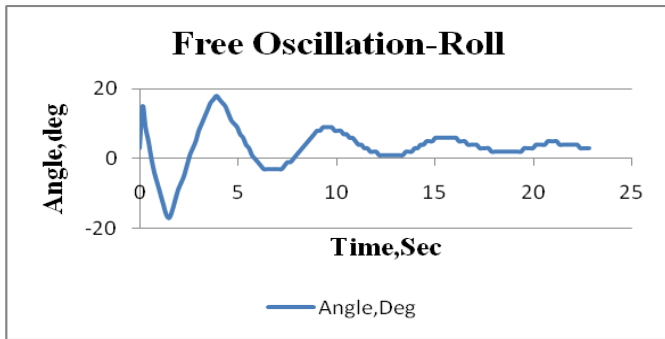
Figure 3.2: Typical record of Free Oscillation test for Roll

T_m =Roll natural period in sec = Duration of time for no of cycles/No of cycles

= 5.65 sec

$T_p = T_m*(\lambda)^{(1/2)}$ = 5.65*(100)^{(1/2)} = 56.5 sec

Damping Ratio = 4.675 %

Free Oscillation-Pitch
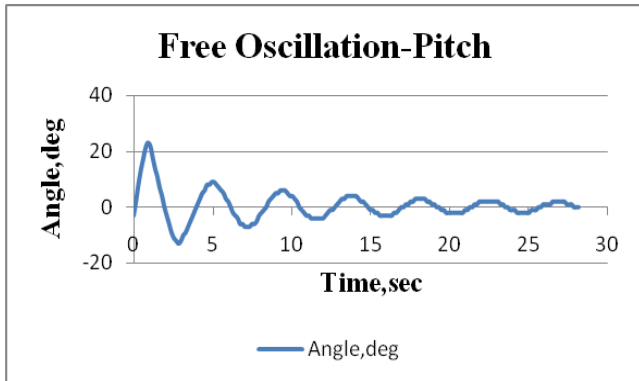
Figure 3.3: Typical record of Free Oscillation test for Pitch

T_m =Pitch natural period in sec = Duration of time for no of cycles/No of cycles

= 4.3 sec

$T_p = T_m*(\lambda)^{(1/2)}$ = 4.3*(100)^{(1/2)} = 43 sec

Damping Ratio = 5.20 %

3.2 Motion response of the semi-submersible without the interface system:

Experiments were conducted for 6 different time periods in the range of 1.33 s to 2.11 s (prototype wave period corresponds between 13.3 sec to 21.1 sec). Throughout the experiments the water depth of the flume was maintained at 0.6m. The test was carried out without the interlinked setup for different wave heights and wave periods and the RAO's of the semi-submersible are calculated and compared with the numerical analysis results from Saravanan (2008). The values tabulated are shown in the table 2

Table 2. Heave, Roll, Pitch RAO's for Different Wave Periods [Semi-submersible without the interface system]

Wave period of model (s)	Wave period of prototype (s)	Heave RAO (m/m)	Roll RAO (deg/m)	Pitch RAO (deg/m)
1.33	13.3	0.50	0.12	0.64
1.40	14.0	0.93	0.36	0.13
1.55	15.5	1.15	0.38	0.16
1.64	16.4	2.27	0.50	0.20
1.73	17.3	2.08	0.42	0.28
2.11	21.1	1.59	0.27	0.53

3.3 Motion response of the semi-submersible with the interface system:

The motion response analysis were carried out with the inference from Li et al., (2006) who investigated the motion performance of the soft yoke mooring FPSO system. The spar and the semi-submersible platform are interconnected with the proposed interface mechanism of ball, socket and bellow joints. The test was carried out with the interlinked setup for different wave heights and wave periods and the RAO's of the semi-submersible is calculated. The values tabulated are shown in the table 3.

Table 3. Heave, Roll, Pitch RAO's for Different Wave Periods [Semi-submersible with the interface system]

Wave period of model (s)	Wave period of prototype (s)	Heave RAO (m/m)	Roll RAO (deg/m)	Pitch RAO (deg/m)
1.33	13.3	0.64	0.047	0.38
1.40	14.0	0.85	0.065	0.24
1.55	15.5	1.18	0.08	0.21
1.64	16.4	2.34	0.061	0.36
1.73	17.3	2.13	0.12	0.10
1.33	13.3	0.64	0.047	0.38

3.4 Average angular displacements at the rotational joint of the spar:

Glanville et al., (1991) gave the details of the concept, construction and installation of spar platform. Experiments were carried out to find out the average angular displacements at the rotational joint of the spar where the ball and socket arrangements are provided. The test was carried out with the interlinked setup for different wave heights and wave periods and the values are tabulated as shown in the table 4.

Table 4. Average Angular Displacements for Roll and Pitch [With ball-and-socket joint at the spar end]

Wave period of model (s)	Wave period of prototype (s)	Average Angular Displacements for Roll (deg)	Average Angular Displacements for Pitch (deg)
1.33	13.3	7.01	11.76
1.40	14.0	5.85	4.04
1.55	15.5	6.46	11.29
1.64	16.4	6.06	9.17
1.73	17.3	6.33	9.87

Computational Fluid Dynamics Turbulent Flow Over An Elliptical Cylinder

Manish Rawat[1], Dinesh kumar soni [2], Dr. Rajesh Gupta[3]

[1] PG Student, Department of Mechanical Engineering, Maulana Azad National Institute of Technology, Bhopal, MP, India 462051
[2] PG Student, Department of Mechanical Engineering, Maulana Azad National Institute of Technology, Bhopal, MP, India 462051
[3] Associate Professor, Department of Mechanical Engineering, Maulana Azad National Institute of Technology, Bhopal, MP, India 462051

4. CONCLUSIONS

Initially from the free oscillation test the natural periods for heave, roll and pitch of the semi-submersible platform are 0.8s, 5.65s and 4.3s for the model and 8s, 56.5s and 43s for the prototype respectively. The damping ratio of the semi-submersible for heave, roll and pitch are 0.28%, 4.675% and 5.20% respectively. The highest motion responses of the free floating semi-submersible platform are 2.27m/m, 0.50deg/m and 0.64 deg/m for heave, roll and pitch at a wave period of 1.64s, 1.64s and 1.33s respectively.The RAO's of the semi-submersible with the interface system was found to have an increase in the heave direction and a small decrease in the roll and pitch directions respectively. The results obtained from the experimental studies was compared and validated with the results obtained through the numerical analysis by Kiran (2011). The average angular displacements at the rotational joints of the spar was found to have higher displacing angles. This is because the loads from the semi-submersible platform are directly getting transmitted to the spar through the interface system.

REFERENCES:

i.   Arango, M., Armstrong, J., and Burris, D. (2002), Design of a Yoke System for a close coupled Spar/FPSO floating production system for the Gulf of Mexico, International Student Offshore Design Competition- 2002, Ocean Engineering, Civil Engineering Department, Texas A&M University.

ii.   Chakrabarti, S. K., Barnett, J., Kanchi, H., Mehta, A., and Yim, J. (2007), Design analysis of a truss pontoon semi-submersible concept in deep water. Ocean Engineering, vol.34, pp. 621-629.

iii.   Glanville, R.S., Paulling, J.R., Halkyard, J.E., Lehtinen, T.J. (1991), Analysis of the spar floating drilling production and storage structure, Offshore Technology Conference, (OTC-6701), pp. 57–68.

iv.   Kiran (2011), Numerical Analysis of the Hydrodynamic Behaviour of Interconnected Spar and Semi-Submersible Platforms, M.Tech Thesis, Ocean Engineering, Indian Institute of Technology Madras.

v.   Li, X., Yang, J., and Xiao, L. (2006), Research on Motion Response of Soft Yoke Mooring FPSO System. In ISOPE-2006: Sixteenth (2006) International Offshore and Offshore and Polar Engineering Conference Proceedings, San Francisco, California, USA.

vi.   Saravanan R. (2008), Hydrodynamic analysis of floating offshore platform for large scale desalination, M.Tech Thesis, IIT Madras.

Abstract:- *Unsteady Reynolds-Averaged Navier–Stokes(URANS) equations with a standard high Reynolds number k- ε turbulence model is used to investigate numerically variation in value of Reynolds no (Re= 0.5×10^6, 1×10^6, 2×10^6 and 3.6×10^6, based on the free stream velocity and cylinder diameter) around a 2D elliptical cylinder. Present study shows the evaluation of coefficient of drag along the outer surface of elliptical cylinder with minor to major axis ratio of 0.4, 0.6 and 0.8 for different types of velocity inputs e.g. uniform, parabolic, triangular and plain shear velocity profiles. The results for circular cylinder in cross flow having uniform velocity are compared with previous data. The drag coefficient of elliptical cylinders is lower than a circular cylinder. By making the streamlined cylinders more slender reductions in drag may be increased. Over the range of Reynolds number considered, an elliptical cylinder with an axis ratio equal to 0.6 reduces drag coefficient approximately by 40 percent compared to that of a circular cylinder. Although the k- ε model is known to yield less accurate predictions of flows with strong anisotropic turbulence, satisfactory results for engineering design purposes are obtained for high Reynolds number flows around an elliptical cylinder in the supercritical and upper-transition flow regimes.*

Introduction:- The phenomenon of flow separation and bluff body wakes has long been intensely studied because of its fundamental significance in flow physics and its practical importance in aerodynamic and hydrodynamic applications. Flow behind a circular cylinder has become the canonical problem for studying such external separated flows. Engineering applications, on the other hand, often involve flows over complex bodies like wings, submarines, missiles, and rotor blades, which can hardly be modeled as a flow over a circular cylinder. In such flows, parameters such as axis ratio, Reynolds number and initial velocity profile can greatly influence the nature of separation and coefficient of drag. A fundamental study of flow over a complex non-canonical object would therefore significantly augment our current under-standing of such flows. Due to the complicated nature of the flow,

theoretical and experimental analysis is typically limited to flow at very low Reynolds number. Numerical simulations provide a promising approach to analyzing this problem. Elliptical cylinders ranging from a circular cylinder to a flat plate with changes in axis ratio and provide a richer flow behavior characteristic. There have been a few numerical simulations of flows over elliptic cylinders. Among the few numerical results reported in the open literature are those of yoshihiro mochimaru[2] and Zhihua Li et al.[3].

Yoshihiro mochimaru[2] investigates the effect of Reynolds number and axis ratio on the coefficient of drag and flow streamline prediction for the flow at higher Reynolds number up to 10^5. Zhihua Li et al.[3] applied Kω-SST model to study the effect of axis ratio on drag coefficient at Re up to 10^4. In the absence of comprehensive experimental data for elliptic cylinders for Re $\geq 5 \times 10^5$, the present results are in most cases compared against corresponding experimental and numerical data for circular cylinders. Catalano et al. [1] applied 3D Large Eddy Simulation (LES) with wall modeling as well as URANS using the standard k- ε model of Launder and Spalding [8] with wall functions, for 0.5×10^6 <Re< 4×10^6. Singh and Mittal [4] performed their studies for 100 <Re < 1×10^7 using a 2D LES method. Most of the results appear to yield satisfactory agreements with experimental data.

Mathematical formulation:- The Reynolds-averaged equations for conservation of mass and momentum are given by

$$\frac{\partial u_i}{\partial x_i} = 0$$

$$\frac{\partial u_i}{\partial t} + u_j \frac{\partial u_i}{\partial x_j} = -\frac{1}{\rho}\left(\frac{\partial p}{\partial x_i}\right) + \nu \frac{\partial^2 u_i}{\partial x_j^2} - \frac{\partial \overline{\acute{u_i}\acute{u_j}}}{\partial x_j}$$

Where i, j =1, 2. Here x_1 and x_2 denote the horizontal and vertical directions, respectively; u_1 and u_2 are the corresponding mean velocity components; P is the dynamic pressure; and ρ is the density of the fluid. The Reynolds stress component, $\overline{\acute{u_i}\acute{u_j}}$, is expressed in terms of a turbulent viscosity ν_T and the mean flow gradients using the Boussinesq approximation,

$$-\overline{\acute{u_i}\acute{u_j}} = \nu_T \left(\frac{\partial u_i}{\partial x_j} + \frac{\partial u_j}{\partial x_i}\right) - \frac{2}{3}k\delta_{ij}$$

Where k is the turbulent kinetic energy and δ_{ij} is the Kronecker delta function.
A standard high Reynolds number k–ε turbulence model (see e.g. Launder and Spalding, 1972; Rodi, 1993) is used in the present study; the model has been applied previously on vortex shedding flow by Majumdar and Rodi (1985). The k and ε equations are given by:

$$\frac{\partial k}{\partial t} + u_j \frac{\partial k}{\partial x_j} = \frac{\partial}{\partial x_j}\left(\frac{\nu_T}{\sigma_k}\frac{\partial k}{\partial x_j}\right) + \nu_T\left(\frac{\partial u_i}{\partial x_j} + \frac{\partial u_j}{\partial x_i}\right)\frac{\partial u_i}{\partial x_j} - \varepsilon$$

$$\frac{\partial \varepsilon}{\partial t} + u_j \frac{\partial \varepsilon}{\partial x_j} = \frac{\partial}{\partial x_j}\left(\frac{\nu_T}{\sigma_\varepsilon}\frac{\partial \varepsilon}{\partial x_j}\right) + C_1 \frac{\varepsilon}{k}\nu_T\left(\frac{\partial u_i}{\partial x_j} + \frac{\partial u_j}{\partial x_i}\right)\frac{\partial u_i}{\partial x_j} - C_2 \frac{\varepsilon^2}{k}$$

Where $\nu_T = C_\mu(k^2/\varepsilon)$.
The following standard model coefficients have been adopted:
(C_1 =1.44, C_2=1.92, C_μ= 0.09, σ_k= 1.0, σ_ε= 1.3).

Numerical solution procedure, computational domain and boundary conditions:- The Reynolds-averaged equations for conservation of mass and momentum, in conjunction with a standard high Reynolds number k -ε model. A pressures based solver with 1st order discretization in time and 2nd order in spatial is used in this numerical simulation. The geometric size of the rectangular computational domain and the boundary conditions imposed for all simulations are shown in Fig. 1. The size of the whole computational domain is 27D ×14D, where D is the diameter of base circular cylinder. The upper and lower boundaries are located at a distance 7D from the centre of the cylinder; this ensures that these boundaries have no effect on the flow around the cylinder. The flow inlet is located 7D upstream from the centre of the cylinder, and the flow outlet is located 20D downstream from the centre of the cylinder. These distances are sufficient to eliminate the far field effects on the flow upstream and downstream of the cylinder.
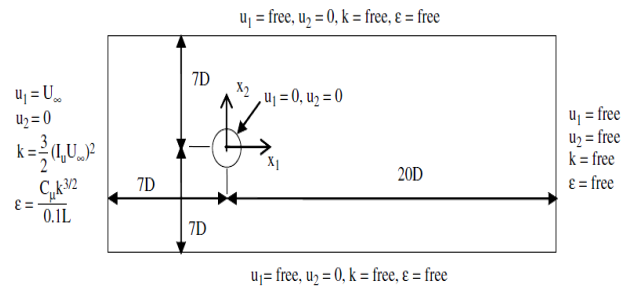
Fig. 1. Computational domain and the imposed boundary conditions
The boundary conditions used for the numerical simulations are as follows:

(i)   Uniform flow is specified at the inlet with $u_1 = U_\infty$, $u_2 = 0$. The free stream inlet turbulence values for kinetic energy $\left(k = \left(3/2\right)(I_u U_\infty)^2\right)$ and   turbulent   dissipation $\left(\varepsilon = \left(C_\mu k^{3/2}\right)/(0.1L)\right)$, proposed by Tutar and Hold [5], have been imposed.

(ii)   Along the outflow boundary, u_1, u_2, k and ε are specified as free boundary conditions in a finite element context. This means that a traction-free velocity–pressure boundary condition is applied for u_1, u_2 and P, while the flux is set equal to zero for k and ε.

(iii)   Along the upper and lower boundaries, u_1, k and ε are free, while u_2 is set equal to zero.

(iv)   No-slip condition is applied on the cylinder surface with $u_1= u_2 =0$ and standard near-wall conditions are applied for k and ε near the cylinder wall (see e.g. Rodi , 1993) as

$$k = \frac{u_*^2}{\sqrt{C_\mu}} \ , \qquad \varepsilon = C_\mu^{\frac{3}{4}}\frac{k^{\frac{3}{2}}}{k h_p}$$

where hp is the radial distance between the first node and the wall, k = 0.41 is the von Karman constant, and u* is the wall friction velocity obtained from the logarithmic (log) law.

$$\frac{u_{tan}}{u_*} = \frac{1}{k}\ln\left(\frac{9h_p u_*}{\nu}\right)$$

is applicable for $\frac{h_p u_*}{\nu} \geq 30$ Where u_{tan} = tangential velocity to the wall.

Results and discussion:- The computations have been performed at Re= 0.5 ×10⁶, 1 ×10⁶, 2×10⁶ and 3.6×10⁶, covering the supercritical to upper-transition flow regimes. The objective is to evaluate the coefficient of drag variations with minor to major axis ratio for different type of velocity input by using a standard high Reynolds number k -ε model around an elliptical cylinder and compared with published experimental data and numerical results of circular cylinder (minor to major axis ratio equal to 1).The presentation which follows is structured to first validate the numerical approach and then to highlight the effect of axis ratio, λ_o, and various velocity profiles on drag coefficient.

Validation of Numerical Approach:- The numerical approach is validated by comparing average values of drag coefficient to prior data for a circular cylinder with $\lambda_o = 1$. The overall drag coefficient is plotted as a function of Re in Fig. 2.
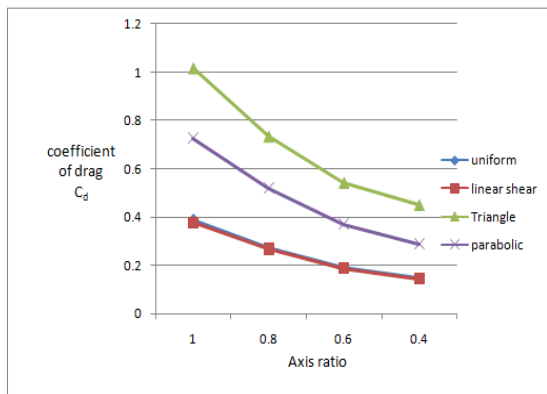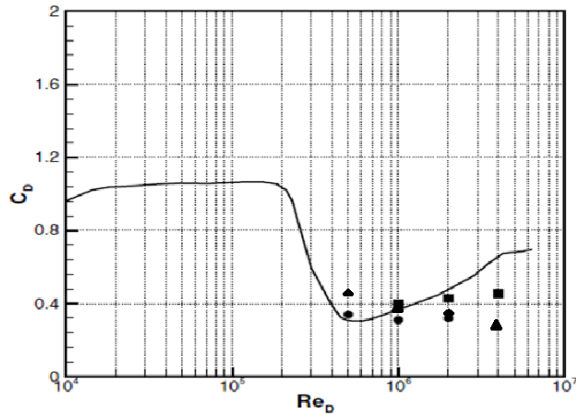
Fig. 2. Drag coefficient as a function of the Reynolds number.
Fig. 3. Coefficient of drag variation with axis Achenbach (1968); (●) LES; (■) URANS (♣) present simulation.   ratio at Re = 10⁶.

The measured data were obtained for a free stream turbulence intensity of 0.8% and turbulent length scale of 0.0045 per unit diameter. The predicted drag coefficient for $0.5\times10^6 \leq Re \leq 2\times10^6$ agrees with the experimental and other numerical result but small discrepancies between the present results and the

results reported by Catalano et al.[3] are seen at 3.6×10⁶. The present computed C_D decreases slightly as the Reynolds number increases, whereas the URANS and LES results reported by Catalano et al [1]. exhibit a slight increase of C_D. This might be caused by different implementations of the wall function. The comparisons are shown in Table 1 for Re =1×10⁶.

Parametric study:- Attention is first turned to the effect of streamlined cylinder shape (axis ratio, λ_o) and different types of velocity profiles on coefficient of drag. Numerical results for elliptical cylinders with $\lambda_o = 0.4$, 0.6 and 0.8 at $0.5\times10^6 \leq Re \leq 3.6\times10^6$ are compared with the circular cylinders ($\lambda_o = 1$). The results are interpreted to determine the conditions under which the shaped cylinder is feasible from the perspective of reducing drag in turbulent cross flow. The impact of Re within the range considered is significant for elliptical cylinders. For streamlined shapes, C_D decreases as the cylinders are slenderized, i.e. λ_o is decreased. For example, for an elliptical cylinder, C_D at $\lambda_o = 0.4$ is 25% lower than that at $\lambda_o = 0.6$ and 60% lower than the

Re = 1× 10⁶ (supercritical regime)	C_D
Present simulation	0.39
Muk Chen Ong et al. k-epsilon	0.5174
Catalano et al. [1] 3D LES	0.31 –0.35
Catalano et al. [1] URANS	0.41
Singh and Mittal [4] 2D LES	0.591
Published experimental data	0.21–0.63

circular cylinder. Significant reductions in drag compared to that of the circular cylinder are possible for $\lambda_o \leq 0.6$. To illustrate this point, consider elliptical cylinders with $\lambda_o = 0.6$ at Re = 1×10⁶ as shown in fig. 3; drag is reduced by 45% compared to the circular cylinder for any type of input velocity profile.For any streamlined cylinder, coefficient of drag for triangular and parabolic velocity input is greater than the uniform and shear velocity input as shown in fig. 3. C_D curve for uniform and shear velocity overlaps each other. Coefficient of drag for shear velocity has slightly smaller value than uniform velocity. C_D for triangular velocity profile is 3 times and for parabolic profile is 1.75 times approximately as compared to uniform velocity. The variations of coefficient of drag at various axis ratios with Reynolds number for different types of velocity profile are shown in fig. 4. This shows that C_D decreases as the Reynolds number increases at all axis ratio for any type of initial velocity profiles. These results show better agreement with experimental and numerical results.

(1) Uniform flow.   (3) Parabolic velocity profile.
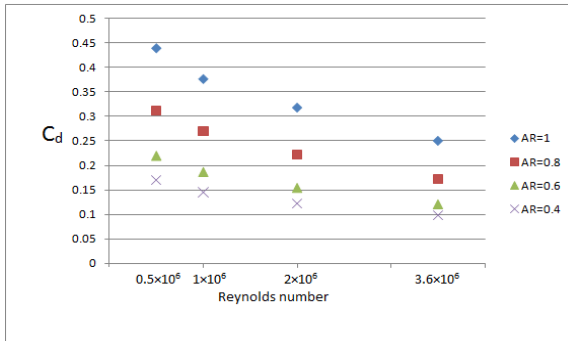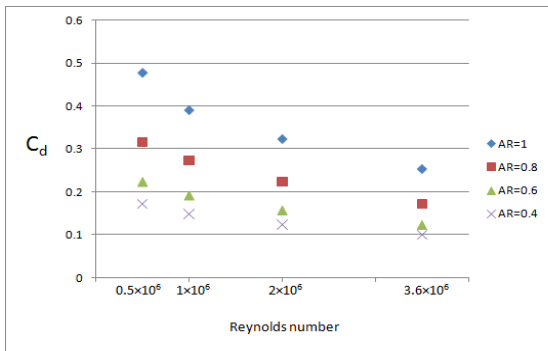
(2) Shear velocity profile. (4) Triangular velocity profile.
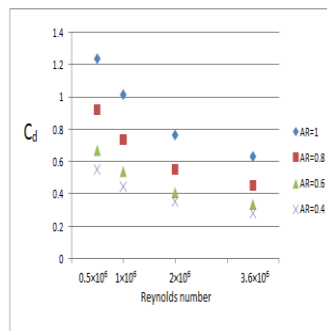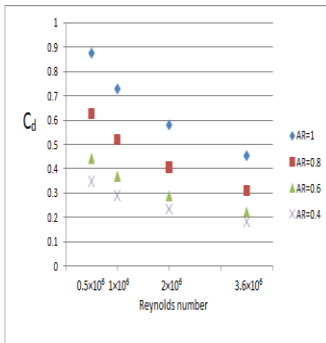
Overall, the standard high Reynolds number k -ε model gives satisfactory predictions of the drag coefficient around a 2D circular and elliptical cylinder in the range Re =$0.5×10^6$ to $3.6×10^6$. This is based on comparing the results with the published experimental data and numerical results. The results of the present study are encouraging for CFD-based engineering applications, e.g. submarine and wings because the URANS with the standard high Reynolds number k-ε model requires less computational effort compared with LES and DNS.

Conclusion:- The numerical study of the drag around elliptical cylinders in cross flow with various input velocity profiles for $0.5×10^6$ ≤ Re ≤ $3.6×10^6$ demonstrate the effects of using streamlined cylinders rather than circular cylinders in different engineering applications. Minor-to-major axis ratios ($λ_o$) equal to 0.4, 0.6 and 0.8, are considered for elliptical cylinder. Drag coefficient decreases, as the cylinders are made more slender, i.e. $λ_o$ is decreased. Compared with a circular tube, the drag coefficient is reduced by 40 to 45% by the use of an elliptical cylinder with $λ_o$ = 0.6 for any type of velocity profile.

References:-
i.   Pietro Catalano, Meng Wang, Gianluca Iaccarino, Parviz Moin, 2003. Numerical simulation of the flow around a circular cylinder at high Reynolds numbers. International Journal of Heat and Fluid Flow 24 (2003) 463–469.
ii.   yoshihiro mochimaru, 1992. numerical simulation of flow past an elliptical cylinder at moderate and high Reynolds numbers, using a spectral method. 11th Australasian fluid mechanics conference, Dec 1992.
iii.   Zhihua Li, Jane Davidson and Susan Mantell, Numerical simulation of flow field and heat transfer of Streamlined cylinders in crossflow. ASME Summer Heat Transfer Conference, 2005
iv.   Singh SP, Mittal S. Flow past a cylinder: shear layer instability and drag crisis. Int J Numer Meth Fluids 2005;47:75–98.
v.   Tutar M, Hold AE. Computational modeling of flow around a circular cylinder in sub-critical flow regime with various turbulence models. Int J Numer Meth Fluids 2001;35:763–84.
vi.   Rodi W. Turbulence models and their application in hydraulics. A state-of-the-art review. IAHR Monograph Series. 3rd ed. Rotterdam, Netherlands: A.A. Balkema; 1993.
vii.   Majumdar S, Rodi W. Numerical calculation of turbulent flow past circular cylinder. In: Proceedings of the 7th turbulent shear flow symposium; 1985. p. 3.13–25. Stanford, USA.
viii.   Launder BE, Spalding DB. Mathematical models of turbulence. London: Academic Press; 1972.
ix.   Achenbach E. Distribution of local pressure and skin friction around a circular cylinder in cross-flow up to Re= $5×10^6$. J Fluid Mech 1968; 34(4):625–39.

An Integrated ISPH Model For Surface And Ground Water Interaction

Gourabananda Pahar[1] and Anirban Dhar[2]
[1]Research Scholar, Department of Civil Engineering, Indian Institute of Technology Kharagpur, Kharagpur-721302, India
gpahar@civil.iitkgp.ernet.in,
[2] Assistant Professor, Department of Civil Engineering, Indian Institute of Technology Kharagpur, Kharagpur-721302, India
anirban@civil.iitkgp.ernet.in

ABSTRACT: *An Incompressible Smoothed Particle Hydrodynamics (ISPH) model is proposed to simulate interaction between free-surface flow and flow through porous media. SPH is a pure Lagrangian method, which can take complex interface/boundary into account without any special front-tracking treatment. Unsteady 2D Navier-Stokes type momentum and incompressible mass conservation equations are used as governing equations for the porous media. The viscous term varies linearly with velocity to introduce extra resisting force. Standard SPH solves the flow equations considering water as a weakly compressible fluid thus taking an equation of state based on sound velocity. The proposed method utilizes a two-step semi-implicit method. Predictor step determines the velocity field without considering divergence-free characteristic of the flow. Corrector step gives the actual pressure by solving Pressure Poisson Equation (PPE). ISPH model improves the computational efficiency of the standard SPH formulation and reduces the artificial pressure fluctuation given by the standard weakly compressible SPH. A 2D dam break with a block of porous media is simulated by the suggested algorithm to test the capability of the model for capturing the free surface and wall boundary conditions. A quintic kernel is used for less computational cost and higher accuracy for nonlinear effects. The non-slip boundary is*

simulated by placing a few layers of dummy particles to provide compact support for the boundary particles. The simulation results show that the ISPH flow model can produce accurate solution in coastal hydrodynamic problems.

Keywords: Flow through Porous Media, Smoothed Particle Hydrodynamics, Non-Darcian Flow, Surface water-Groundwater Interaction

1. INTRODUCTION:

Traditionally, water resources flow models have focused on individual simulation of surface water or ground water. In reality, all surface water bodies (e.g. streams, lakes, wetlands, coastal areas and estuaries) often hydraulically interact with ground water aquifers. Moreover, interaction between surface and ground water affects both their quantity and quality. Influent or effluent conditions occur due to the relative difference between surface water and ground water levels. The nature of flow thorough ground changes its nature depending upon the different characteristic properties of the material. It is difficult to solve a multiphase flow through complex porous media. In the present work an Incompressible Smoothed Particle Hydrodynamics (ISPH) model is proposed for simulating the interaction between free-surface flow and flow through porous media.

Considerable amount of research is available in the area of groundwater and surface water interaction. Erduran et al. (2009) have modeled ground and surface water interaction by introducing source-sink terms into the continuity equations. Vertical discharge is considered as the source/sink discharge for sub-surface flow equations. 2-D depth averaged Navier-stokes equations and extended Darcy's equation have been used for modeling water interchange between coastal area and the ocean, with the hydrostatic pressure being assumed to apply for surface as well as groundwater flow. The CFL stability conditions are loosely satisfied by the model. A coupled model of surface and groundwater is also developed using the finite difference based modeling software like the MIKE SHE and MIKE 11 by Thompson et al. (2004), where between the surface water and groundwater bodies, seepage exists and the water table exit point is allowed to be considered isolated from the driving head. The flux gradient and the source/sink terms are balanced by the surface gradient method.

Eulerian formulation can produce proper results for integrated free-surface and groundwater flows with certain assumptions. A Fully Lagrangian method is needed to take care of the interface conditions. In the present work, Smoothed Particle Hydrodynamics (SPH), a fully Lagrangian method, has been adopted. Surface water can be simulated using Navier-Stokes equation, whereas flow through porous media is governed by the Brinkman Equation. A semi-implicit predictor corrector scheme has been used to treat resisting terms and pressure quantity. Water has been treated as fully incompressible fluid unlike standard SPH formulation.

2. METHODOLOGY

Computational Fluid Dynamics (CFD) has always given its priority on grid-based methods. However, these methods share limitation of treating advective terms, which can be partially subdued by using higher order upwinding. Only, pure lagrangian model can treat the advective term exactly, as the frame follows the fluid particles throughout the simulation. Smoothed Particle Hydrodynamics (SPH), invented by Monaghan *et al.* (1977) and Lucy (1977) for simulating astrophysical problems, is one of the most popular mesh-free methods. SPH can be applied readily in Civil Engineering applications for its capability of capturing free surfaces and taking irregular boundaries into effect with seeming ease.

In SPH, Integral interpolation theory transforms the partial differential equations into an integral form. The fluid domain is represented by a set of irregularly spaced nodal points represents the fluid domain, where physical properties (e.g., mass, density, velocity, position, pressure) are concentrated. The properties of the points will change due to the interactions with neighboring particles over time. These nodal points can move according to the governing equation, thus making the technique a Lagrangian meshless method.

2.1. Smoothed Particle Hydrodynamics

Any particle property *f* can be written as a Convolution product of *f* with the Dirac delta function. In SPH formulation, Dirac delta function can be approximated by a kernel function estimated over a support domain.

$$f(s,t) = \int f(s^i,t)\delta(|s - s^i|)ds^i$$

(1a)

$$f(s,t) = \int_v W(s^i - x,h)f(x,t)dv$$

(1b)

Where, the integral is over the domain *v* and *dv* is the element of volume which depends on the dimensionality of the problem and W is the weighting function also called smoothing kernel in SPH.

The size of the kernel is determined by the parameter *h*, which determines a domain of influence around. In *2D* that domain is an area of radius *nh*, where n depends on the kernel definition. Although *h* is a constant in the simplest applications of SPH, the parameter can depend both on time and space as described in Monaghan (1992).

$$f(s,t) = \int_v W(s^i - x,h)f(x,t)dv$$

(2) For computational purposes, the integrals are approximated numerically by a summation of contributions from the surrounding particles in the domain.

$$f(s,t) = \sum_v W(s - x,h)f_j v_j$$

(3)

Where,

$$\sum_v W(s - x,h)v_j = \rho$$

v = the volume associated with particle *j*,

m = mass of particle j (fixed),

ρ_j = varying density of the particle j.

Basic gradient and divergence can be directly written as,

$$\nabla f(s,t) = \sum_v f_j \nabla W(s-x,h)v_j$$

(4a)

$$\nabla . f(s,t) = \sum_v f_j . \nabla W(s-x,h)v_j$$

(4b)

However, these basic operators can create large problematic errors. Through simple algebraic manipulations, expressions for conserving linear momentum can be formulated as following.

$$\nabla f(s,t) = -\sum_v (f_i - f_j)\nabla W(s-x,h)v_j$$

(4c)

Nodal particles near the boundary will have a truncated support domain. The kernel and its gradients need to be normalized at those points. Bonnet and Lok (1999) suggested a correction method to preserve the angular momentum in gradient and divergence operators. In the present work, the discretized form of governing equations involves the kernel as well as its derivatives, both first and second orders, which has been corrected using Taylor's expansion.

In the classical SPH formulation, when solving the Navier-Stokes equations the fluid is treated as quasi-compressible fluid. If water is being simulated, then an artificial equation of state is used by Monaghan (1992). Alternatively some authors like Shao *et al.* (2003) have considered incompressible formulations solving a pressure Poisson equation.

2.2. Governing Equations

The isotropic flow of a viscous Newtonian fluid through porous media is governed by Darcy's law.

$$U = -\frac{K}{\mu}\frac{\partial P}{\partial X_i}$$

(5)

Where,

U = Average seepage velocity,

μ = Dynamic viscosity,

P = Pressure,

X = space variable.

Brinkman (1949) introduced an estimated of viscous force for fluid flowing through a dense swarm of particles. The equation for flow through porous media can be written as per Auriault (2008),

$$\frac{\partial P}{\partial X_i} = -\frac{\mu}{K}\vec{U}_i + \mu^e \Delta \vec{U}_i$$

(6)

Where,

μ^e = effective viscosity

For transient flow of viscous Newtonian flow through porous media, following Wooding the Governing Equation can be written as

$$\rho \frac{D\vec{U}}{Dt} = \rho \vec{g}_i - \frac{\partial P}{\partial X_i} - \frac{\mu}{K}\vec{U}_i + \mu^e \Delta \vec{U}_i$$

(7a)

For Surface Water, the momentum equation can be written as

$$\rho \frac{D\vec{u}}{Dt} = \rho \vec{g}_i - \frac{\partial P}{\partial X_i} + \mu \Delta \vec{u}_i$$

(7b)

Where, $\vec{u}$ = velocity of the surface-water flow.

In standard SPH, water is considered to be a weakly compressible fluid. An equation of state involving sound speed is used to calculate pressure. Gomez (2010) has shown that Realistic speeds of sound cannot be used for computational purposes since the associated time step imposed by the Courant-Freidrich-Lewy criteria will be too small. However, the equation of state will produce very noisy pressure variation.

Lee *et al.* (2008) has shown that ISPH can produce better results for dam break flow than Weakly Compressible SPH (WCSPH). For incompressible flow, no direct relation can be established between Pressure and the velocity. By taking the divergence of the momentum equation, and enforcing solinoidal velocity condition, pressure at the unknown time level can be found out using Pressure Poisson Equation (PPE).

2.3. Solution Procedure

Incompressible fluid can be simulated in SPH using Divergence-free velocity field and Density Invariance. Shao *et al.* (2003) stated that the velocity can be represented in terms of density fluctuation. Then the Density variation can be solved using Pressure Poisson Equation. To produce a divergence-free velocity field, a semi-implicit projection method in SPH was first proposed by Cummins and Rudman (1999). The method uses a second-order time-marching scheme. Both density and mass of the nodal particles are kept constant throughout the time.

Here, a divergence free velocity field Predictor-Corrector algorithm has been used. In predictor step, the momentum equation can be discretized by a summation of contributions from the surrounding particles in the domain. But the acceleration will be free of pressure gradient of the time known time level.

$$\frac{D\vec{v}}{Dt} = n_e \vec{g}_i - \frac{\mu}{\rho}n_e K^* . \vec{u}_i^n + n_e \mu^e \sum_j 2 \frac{V_j}{\rho_j}\frac{(\vec{u}_i^n - \vec{u}_j^n)r_{ij}.\nabla w_{ij}}{(r_{ij}^2 + 0.001h^2)}$$

(8)

Where,

$K^* = K^{-1}$

v = actual velocity

n_e = effective porosity

Intermediate velocity will be determined using velocity at known time level and the acceleration.

$$\vec{u}_i^* = \vec{u}_i^n + \frac{d\vec{v}}{dt}.\Delta t$$

(9a)

Then particle position will be updated with intermediate velocity.

$$\vec{r}^{*} = \vec{r}^{n} + \vec{v}_{i}^{*}.\Delta t$$

(9b)

Intermediate velocity can be projected onto a divergence-free velocity field and a curl free pressure gradient field. Pressure Poisson equation can be obtained by taking divergence of the momentum equation.

For flow through porous media,

$$n_e \Delta P_i = \nabla u_i^{*}$$

(10a)

For free surface flow,

$$\Delta P_i = \nabla u_i^{*}$$

(10b)

The PPE for porous media can be discretized in the same manner as a laplacian operator.

$$\sum_j n_e \frac{V_j}{\rho_j}(P_j - P_i).\nabla^2 w_{ij} = \frac{1}{\Delta t}\sum_j V_j(\vec{u}_j^{*} - \vec{u}_i^{*}).\nabla w_{ij}$$

(10c)

The velocity gradient term has been discretized approximately to avoid checker board effect on pressure. Actual velocity at unknown time level can be found out from the momentum equation by taking the obtained pressure gradient into account.

$$\vec{u}_i^{n+1} = \vec{u}_i^{*} - \Delta t \sum m_j V_j n_e \frac{-P_i + P_j}{\rho_i \rho_j}\nabla w_{ij}$$

(11)

Then the particle position will be updated using a second order time marching scheme.

$$\vec{r}_i^{n+1} = \vec{r}_i^{n} + \Delta t\left(\frac{\vec{u}_i^{n} + \vec{u}_i^{n+1}}{2}\right)$$

(12)

In case of surface water, the resistance term containing intrinsic permeability will be removed. The effective viscosity will be replaced with original viscosity.

2.4. Boundary Conditions

For Dirichlet boundary condition, the pressure can be found out by solving PPE for specified velocity field. In FDM, near a no-slip boundary, the same order of the discretization can be maintained by introducing a high order backward differencing. However, in SPH, the support domain of the particles nearby wall can become truncated, resulting to erroneous estimation of kernels and kernel derivatives. The result may lead to penetration of particles. This phenomenon can be prevented in various manners, for example, by introducing dummy particles, or mirror particles or some extensive repulsive forces.

At the boundary, Dummy particles, suggested by Hosseini (2007) are regularly distributed in the initial state and have zero velocity throughout the whole simulation. Koshizuka (1998) proposed a few layers of dummy particles as an extension of the

edge particles surrounding the no-slip boundaries to ensure the kernel compact support for particles located close to those boundaries. The number of dummy particle layers is decided from the radius of the compact support. They will carry an identical pressure to edge particles normal to the wall. This also makes the coding simpler to implement while parallelizing the process. The only difference with fluid particles is that wall particles are not displaced from their original position at the end of the time step.

Free Surface particles have a smaller domain than a full kernel support. This property has been used to find out the free surface particles and assigning zero pressure at them while solving PPE.

2.5. Time Step

For WCSPH, time-step is fixed based on the corresponding sound speed of the fluid. However, ISPH makes the time step more flexible. Cummins *et al*. (1999) has stated that the time step criteria may vary depending upon the resolution and viscosity. For high-resolution viscous simulation, the diffusion criterion is more rigorous than CFL condition.

$$\Delta t_{CFL} = \sigma \frac{h}{u_{ref}}$$

Where,

u_{ref} = the maximum velocity at that time step.
h = the smoothing length/ initial particle distance and σ is a constant (<0.1).In the present work it is set as 0.05.

3. Results and Analysis

A 2D dam break in porous media is simulated by the suggested algorithm to test the capability of the model for capturing the free surface and wall boundary conditions.
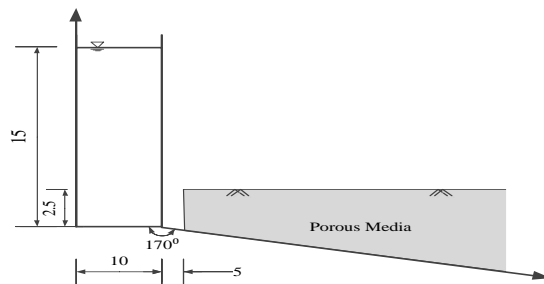
Figure 1: Initial Configuration of Water Column with Porous media on an inclined floor

The non-slip boundary is simulated by placing 4 layers of dummy particles to provide compact support for the boundary particles. Free surface particles are identified by evaluating a unit scalar at each particle node. If the value of the scalar falls below 0.85, it is to be considered as a free surface particle.

3630 particles are used to simulate the dam-break. A quintic Wendland (1995) Kernel has been chosen to capture the non-linear effects of the flow. And it also offers a certain balance between computation overhead and accuracy.

$$W(r,h) = \frac{7}{4\pi h^2}\left(1 - \frac{r}{2h}\right)^4\left(\frac{r}{h} + 1\right) \qquad \text{For} \quad 0 \le r \le 2h$$

The intrinsic permeability tensor is assumed to be

$$W(r,h) = \begin{bmatrix} 10^{-8} & 0 \\ 0 & 0.5x10^{-8} \end{bmatrix} m^2/s$$

Effective viscosity has been assumed to be equal to the dynamic viscosity of water. Porosity is taken as 0.5. The velocity and pressure variation with different time instants are shown below.

3.1. Velocity Distribution

Velocity Distribution for three different time intervals are shown in Figures 2(a)-2(c).
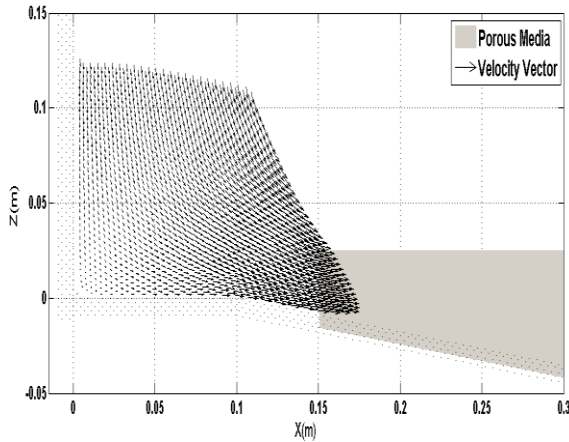
Figure   2(a):   Velocity   Profileat t=0.08
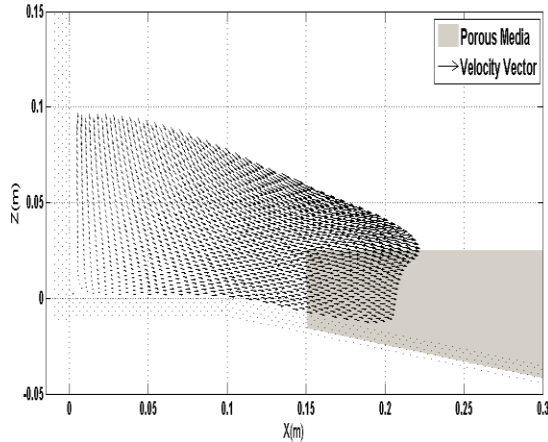
Figure 2(b): Velocity Profile at t=0.154s
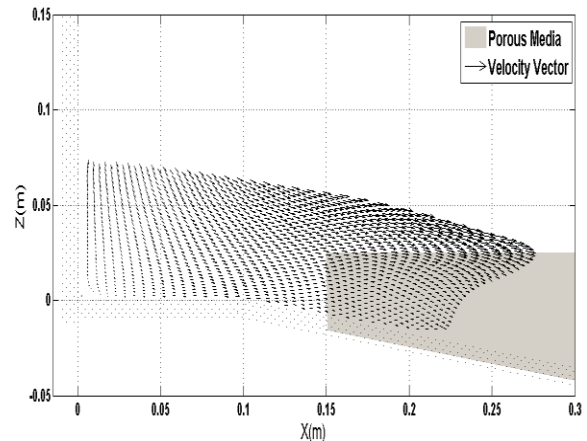
Figure 2(c): Velocity Profile at t=0.22s

3.2. Pressure Distribution

Corresponding pressure distribution of the particles at above mentioned time intervals are shown in Figures 3(a)-3(c).
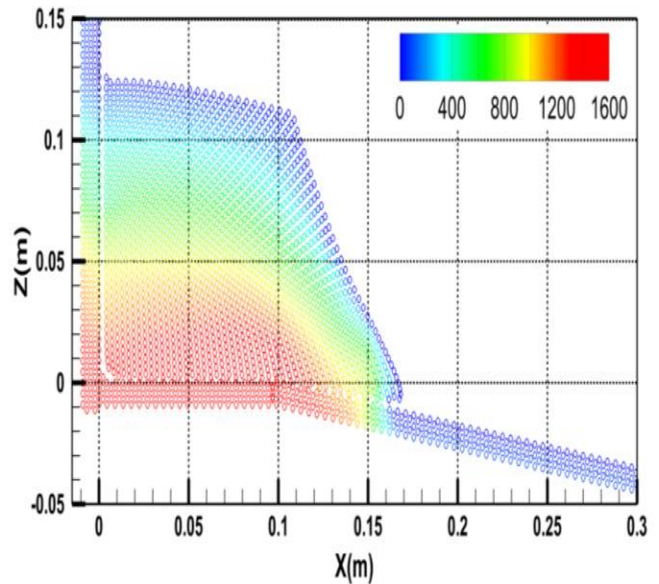
Figure 3(a): Pressure (Pa) Distribution at t=0.0873s
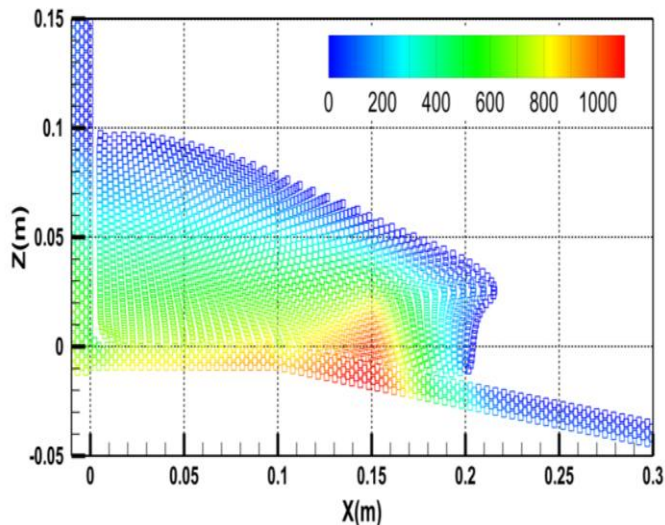
Figure 3(b): Pressure (Pa) Distribution at t=0.154s

The velocity is very high for free surface flow. In porous media, velocity decreases rapidly with depth. SPH does not need any specialized front tracking treatment for surface and groundwater flow. In both cases, free surface has been identified using kernel property and gauge pressure is assigned on them. For a pure surface-water dam-break, the pressure decreases rapidly as the water starts to move (Figure 3a). Figure 3(b) and 3(c) show an accumulation of pressure at *x=0.15m.* This rising pressure occurs due to the impact at the porous block. Velocity also starts to decrease while passing through the porous media. The viscous and flow resistance terms are treated in known time level. The intermediate velocity field is independent of pressure gradient of previous time level. This full pressure projection is capable of avoiding error accumulation than incremental pressure projection.
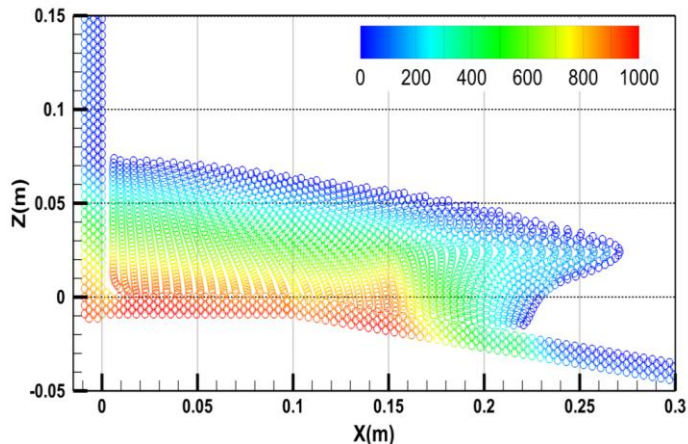
Figure 3(c): Pressure (Pa) Distribution at t=0.22s

4. CONCLUSIONS

Flow through porous media has been solved using Brinkman Equation with the above mentioned formulation. The simulation produces intuitively correct results. The model has considered as a 2D flow through porous media. Model can be extended in lateral direction with suitable modifications. Dummy boundary particles have been used to formulate boundary condition. However, a hybrid model of dummy and mirror particles is capable of producing better results. Multiphase flow simulation through can be formed using different porosity and permeability parameters for different regions. The different flows can be interconnected easily based on the ground geometry to develop an integrated model. The Semi-Implicit pressure projection can produce very good pressure variation compared to WCSPH. SPH simulations take longer time than Eulerian grid-based methods. However, the implementation is easy and it can take irregular boundaries and interfaces without any special treatment.

REFERENCES:

i.   Auriault, J.-L. (2008) On the Domain of Validity of Brinkmans Equation. Transport in Porous Media 79, 2, (215-223).
ii.   Bonet, J., and Lok, T.S. (1999) Variational and momentum preservation aspects of Smooth Particle Hydrodynamic formulations. Computer Methods in Applied Mechanics and Engineering 180, 1-2,(97-115).
iii. Brinkman, H. C. (1949) A Calcultion of the Viscous Force Exerted by a Flowing Fluid on a Dense Swarm of Particles. Journal of Applied Sciences Research A1, (27-34).
iv.   Cummins, S. J., and Rudman, M. (1999) An SPH projection method. Journal of Computational Physics 152-2, (584-607).
v.   Erduran K. S., Kutija V, Macalister C. (2005). Finite volume solution to integrated shallow surface-saturated ground water flow, International journal for numerical methods in fluids, 49(763-783).
vi.   Gingold, R., and Monaghan, J. (1977) Smoothed particle hydrodynamics- theory and application to non-spherical stars. Monthly Notices of the Royal Astronomical Society 181, (375-389).
vii. Gomez-Gesteira, M., Rogers, B. D., Dalrymple, R. a., and Crespo, A. J. (2010) State-of-the-art of classical SPH for free-surface flows. Journal of Hydraulic Research 48, (6-27).
viii. Hosseini, S., Manzari, M., and Hannani, S. (2007) A fully explicit three-step SPH algorithm for simulation of non-Newtonian fluid flow. International Journal of Numerical Methods for Heat & Fluid Flow 17, 7 (715-735).
ix.   Koshizuka, S., Nobe, A., and Oka, Y. (1998) Numerical Analysis of BreakingWaves Using the Moving Particle Semi-Implicit Method. International journal of Numerical Methods in fluids 769: (751-769).
x.   Lee, E.-S., Moulinec, C., Xu, R., Violeau, D., Laurence, D., and Stansby, P. (2008) Comparisons of weakly compressible and truly incompressible algorithms for the SPH mesh free particle method. Journal of Computational Physics 227, 18, (8417-8436).
xi.   Lucy, L. B. A numerical approach to the testing of the fission hypothesis. The Astronomical Journal 82, 12 (December 1977).
xii. Monaghan, J. (1992) Smoothed Particle Hydrodynamics. Annu. Rev. Astron. Astrophys 30, (543-74).
xiii. Monaghan, J. Simulating Free Surface Flows with SPH. Journal of Computational Physics 110 (1994), (399-406).
xiv. Shao, S., and Lo, E. Y. (2003) Incompressible SPH method for simulating Newtonian and non-Newtonian ows with a free surface. Advances in Water Resources 26, 7, (787-8000).
xv.   Thompson J., Sørenson, H., Refstrup G, and Refsgaard H., (2004) A.Application of the coupled MIKE SHE/MIKE 11 modelling system to a lowland wet grassland in southeast England. Journal of Hydrlogy 293, (151-179).
xvi. Wendland, H. (1995) Piecewise polynomial, positive definite and compactly supported radial functions of minimal degree. Advances in Computational Mathematics 4, 1 (389-396).
xvii. Wooding, R. A. (1957) Steady state free thermal convection of liquid in a saturated permeable medium. Journal of Fluid Mechanics 2, (273-285).
xviii. Xu, R., Stansby, P., and Laurence, D. (2009) Accuracy and stability in incompressible SPH (ISPH) based on the projection method and a new approach. Journal of Computational Physics 228, 18, (6703-6725)

Study Of Drought Characteristics In Mid-Climatic Regions

R.P.Pandey, Ravi V. Galkate and Rakesh Kumar
National Institute of Hydrology, Roorkee-247667

ABSTRACT:*Primary purpose of this study is to establish relationship between climatic parameters and the drought characteristics. Droughts are usually defined by relative deficiency of moisture (precipitation, streamflow, water storages etc.) with reference to their central tendency (mean, or predefined threshold). To characterize droughts in mid-latitudinal regions a new classification of climate has been used to demarcate the climatic spectrum into dry and wet regions based on the ratio of mean annual potential evapotranspiration (E_p) to mean annual precipitation (E_p/P_a). Long-term annual rainfall series for 110 stations for the period from 1901 to 2007 located in different climatic regions of India were analyzed to identify drought years and drought events. Potential evapotranspiration rates were computed using 30 years of daily meteorological data from various stations. The relationships indicated the frequency of meteorological droughts to be greatly governed by the E_p/P_a ratio. Average drought return period varied from 2 to 3 years in arid regions (with $12 > E_p/P_a > 5$), 3 to 5 years in semiarid regions (with $5 > E_p/Pa > 2$) and 5 to 9 years in sub-humid regions (with $2 > E_p/P_a > 3/4$). Further, the relations clearly indicated drought frequency to decrease exponentially with decrease in the mean annual deficit ($E_p - P_a$). Similar relations of E_p/P_a ratio with duration and intensity of drought were derived. The incidence of drought events of 2 and 3 consecutive years was found to be relatively more frequent in areas with E_p/P_a ratios of 4.5-7.0 and 7.5- 8.5, respectively. The analysis revealed that the areas with greater E_p/P_a ratio faced relatively more frequent severe intensity droughts than did the others. A comparison of these inferences was found consistent with those for Australia, Brazil, United States, Ukrain & Kazakstan, Moracco etc. Since the relationships closely followed the drought frequency behaviour in similar climatic regions elsewhere, these results are expected to be rationally useful. Influence of elevation, of distance from mountain/major hills and of distance from sea coast could be observed on drought intensity and drought persistence (i.e. duration). Typically, it was found from the data that stations, falling in regions located at relatively short distance from sea (ds) and mountain, and having $P_a \approx E_p$, hardly faced drought events of severe/extreme intensity, and droughts of 2 or more consecutive years hardly persisted in such areas. The study revealed that, besides the climatic parameters, drought characteristics at a place are also influenced by the distance from sea and mountain barrier as well. The results of the study are expected to enhance the understanding for a systematic analysis of drought characteristics and may help in evolving appropriate drought management strategies.*

Keywords: Drought frequency, drought severity, precipitation-evapotranspiration ratio, climatic region,

INTRODUCTION

Droughts are driven by the regional climatic conditions. The most common climatic elements which govern regional drought characteristics (i.e. frequency, duration and severity) are precipitation and temperature, and hence the evapotranspiration. The other important feature of climate that influence regional drought characteristics is the distribution of rainfall over the year and hence, the length of wet season. Droughts are random, cyclic, and regional climatic phenomenon (Alley, 1984). Drought at a given location or region is defined as a deficiency of actual moisture supply which consistently falls short of climatically expected moisture supply over months, seasons or years. The prolonged deficiency or short-supply of water relative to normal availability poses threat to normal life pattern, agriculture and regional economy. Impacts of drought are wide ranging, and therefore, it can be interpreted in many ways. Meteorological drought refers to a precipitation anomaly which leads to a marked deficiency of precipitation in a given period. Hydrological drought is associated with marked depletion in streamflow, groundwater levels and storages in fresh water bodies, in an amount sufficient to affect their normal uses. Agricultural drought refers to short-term soil moisture deficiency in an area which normally receives sufficient moisture to sustain crops and livestock (Karl and Young, 1987).

Regions with higher variability of rainfall and runoff are more vulnerable to droughts (Kundzewicz and Kaczmarek, 2000). The water scarcity occurs primarily due to inconsistency of variables that constitute the processes of hydrologic cycle. A drought is characterized by its frequency, duration, severity, and areal extent, which vary across the climatic spectrum (Gregory, 1989; Ponce et al, 2000; Pandey and Ramasastri 2001). Frequency, duration, and severity are governed by regional climatic parameters (Dracup et al. 1980; Ponce et al., 2000; Pandey and Ramasastri, 2001) and morphological factors (Paulson et al., 1980; Mimikou et al., 1993; Lana and Burgueno, 1998). A number of climatic and hydrologic variables, such as precipitation, evapotranspiration, streamflow, moisture content in the air, and similar other variables have been widely used in literature for characterizing regional droughts (Sharma, 1997; Shin and Salas, 2000). Recent droughts in many parts of the world have raised the need develop better understanding of regional drought characteristics and their relationship with regional climatic, morphological, and other hydrological parameters. Being natural recurring phenomena, droughts cannot be prevented, but their adverse impact can be minimized with proper prediction of its regional characteristics and planning of mitigation strategies. To cope with adverse impacts of drought, it is important to develop capabilities to predict its characteristics for a given place/region, i.e. its duration (how long will it last?), its severity (how severe will it be?), and its frequency (how often will it recur?). Prediction of regional drought characteristics in relation to climatic parameters can encourage for appropriate proactive planning to cope with drought.

The mid-climatic regions of India refer to the plateau regions encompassing the States of Andhra Pradesh, Karnataka,

Maharashtra, Madhya Pradesh, Chhattisgarh, Bihar, Jharkhand, Uttar Pradesh, parts of Orissa, Tamilnadu, and West Bengal, plus arid regions including Rajasthan, Gujarat and part of Haryana. The occurrence of drought is normally linked with the amount, distribution, and time of onset and withdrawal of monsoon rainfall in India. Since, the monsoon rainfall is highly erratic and unevenly distributed, drought conditions prevail almost every year in one or the other part of the country. This leads to uncertainty in agriculture system and unstable economy in considerable sections of the society.

In this study precipitation, evapotranspiration, and morphologic factors have been have been analyzed to develop relationship between climatic parameters and the drought characteristics in different climatic regions in India. The basic assumption for drought characterization is that the main cause of drought is a precipitation deficit compared to the long-term average precipitation in an area over the analyzed period of time. Using long term records of mean annual precipitation and mean annual potential evapotranspiration, drought frequency, duration and severity are related with climatic parameters in the arid, semiarid and sub-humid climatic regions in India. It is believed that the knowledge of the affinity of drought characteristics with regional climatic parameters forms the essence in planning of management strategies for coping with drought catastrophe in a given region.

BRIEF DESCRIPTION OF DOCUMENTED EXPERIENCES ON DROUGHT

Drought-prone areas in India broadly fall in central plains (in the States of Uttar Pradesh, Madhya Pradesh, Chhattisgarh, Bihar, Jharkhand, West Bengal, and Orissa, in peninsular plateau in South (Andhra Pradesh, Karnataka, Maharastra, and Tamil Nadu), in desert regions in west (Rajasthan & Gujarat) and a few pockets in Haryana, Himanchal Predesh and Jammu & Kashmir. Regions with annual rainfall ranging from 400-750 mm and from 750-1125 mm have greater inter-annual variability and therefore, more vulnerable to drought. DMI (1999) analysed 100 years of rainfall behaviour and reported that the meteorological causes of drought vary according to the climate of the affected region. The frequency of occurrence of below normal rainfall in arid, semi-arid and dry sub-humid areas is 54 to 57 per cent, while severe and rare droughts occur once in every 8 – 9 years in arid and semi-arid zones (DMI, 1999). In semi-arid and arid climatic zones, about 50 per cent of the severe droughts cover generally 76 percent of area of the country. In this region, rare droughts of most severe intensity occurred on an average once in 32 years and almost every third year was a drought year. During the last century, droughts in the years 1917-1918, 1965-1966 and 1986-1987, 1996-97, and 2002 were the most severe, affecting a high percentage of India's population (Samra 2004). Patel & Iyar (1987) indicated that droughts recur most frequently in Gujarat, eastern Rajasthan and Rayalseema, followed by south interior Karnataka, eastern Uttar Pradesh, Vidarbha, and Madhya Pradesh. The major factors responsible for the drought distress in most parts of

India are deficient rainfall, inadequate conservation of water, inadequate water management strategy, and indiscriminate exploitation of the ground water by industries and agricultural sectors and large scale deforestation for various purposes.

DETAILS OF LONG-TERM METEOROLOGICAL DATA USED

Long-term annual rainfall records for 110 rainfall stations spread over 15 drought prone States of India have been used to derive relationships of climatic parameters with drought characteristics. The data used in the study includes annual rainfall records for a total length ranging from 35 to 106 years for the period between 1901 to 2006. The details of the data used are given in Table 1. The locations of the selected raingauge stations throughout India are shown in Fig. 1. The years for which rainfall data were not available or missing have not been included in the analysis. Details of missing data and latitude longitude and range of EP/Pa ratio is shown in Appendix I. To estimate potential evapotranspiration rates, 30-35 years of daily meteorological data from various stations were used. The meteorological data used for estimation of evapotranspiration includes maximum temperature, minimum temperature, wind speed, humidity, and sunshine hours. The estimates of potential evapotranspiration was obtained using the Penman (1963) method, and results compared with the potential evapotranspiration estimates given by India Meteorological Department (IMD) (Rao et al., 1971) to authenticate the rationality of the computed values.

Table 1: Details of selected raingauge stations and length of

Sl. No	Name of stations in various states	Station no. as shown in location map (Fig. 1)	Length of rainfall records and period	Range of E_p/P_a Ratio
	(1)		(3)	(5)
1.	**Karnataka State :** Belgaum, Bellary, Bijapur, Gulbarga, Raichur, Mysore, Chikmanglure, Tumkur, BangaloreNorth, Hassan, Mandya, Chitradurg	1 - 13	79 - 88 yrs 1901-1988	1.097 to 3.373
2	**Madhya Pradesh :** Betul, Dhar, Jhuabua, Khaegoan, Sidhi, Shahdol, Umaria, Devas, Datia, Sajapur, Damoh, Panna, Chhattarpur, Tikamgarh , Hatta and Sagar	14 - 23 and 96 - 101	67 - 87 yrs 1901-2006	1.130 to 2.149
3.	**Orissa :** Bhavanipatna, Nawapara, Phulwani, Bolangir, and Boudh	24 - 28	67 - 93 yrs. 1901-2006	1.04 0 to 1.434
4	**Andhra Pradesh :** Anantpur, Cuddappa, Kurnool, Mahboobnagar, Prakasam, and Chittoor	29 - 34	76 - 85 yrs. 1901-1985	1.905 to 3.316
5	**West Bengal :** Bankura, Midnapur, and Purulia	35 - 37	60 - 81 yrs. 1901-1981	0.960 to 1.078
6	**Bihar :** Nawada, Gaya, Munger, Rohtas, Aurangabad, Bhojpur, and Palamu	38 - 44	65 - 79 yrs. 1901-1980	1.169 to 1.608
7	**Maharastra :** Bhir, Solapur (North), Satara, Ahmednagar, Nanded, Aurangabad, Hulsi, Pune, Osmanabad, and Nasik	45 – 53 and 106	62 -78 yrs. 1901-1980	0.929 to 2.642
8	**Gujrat :** Ahmedabad, Mahmedabad, Rajkot, Bharuch, Jafrabad, Surendranagar, Bhavnagar, Jamnagar, Kalol, and Bhuj, Jaiselmer, Jhunjhunu.	54 - 63	68 - 87 Yrs. 1901-1980	1.721 to 5.392
9	**Rajasthan :** Nagaur, Jalor, Bhinmal, Udaipur, Jodhpur, Pali, Dungarpur, Barmer, Bikaner, Churu, Ajmer, Kota, Bansawara, Bhilwara and Bitu	64 - 76 and 102-105	86 - 88 yrs. 1901-1988	2.151 to 10.875
10	**Haryana :** Rohtak, Rewari, and Gurgaon,	77 - 79	74 -75 yrs. 1901-1978	2.528 to 3.659
11	**Uttar Pradesh :** Varanasi, Jalaun, Banda, Hamirpur, Allahabad, and Mirzapur	80 - 85	69 - 80 yrs. 1901- 1980	1.470 to 1.991
12	**Jammu & Kashmir :** Kishtwar, Bhadarwah, and Udhampur,	86 - 88	59 - 73 yrs. 1901-1981	0.568 to 1.033
13	**Tamilnadu :** Salem, Tiruneveli, Dharmapura, Kanyakumari, Ramnathpuram, Madurai, and Coimbatore	89 - 95	74 - 80 yrs. 1901-1980	1.034 to 3.273
14	**Chhattisgarh :** Raipur, Bilaspur, Ambikapur and Jagdalpur	107-110	36-38 yrs 1970-2005	1.15 to 1.50
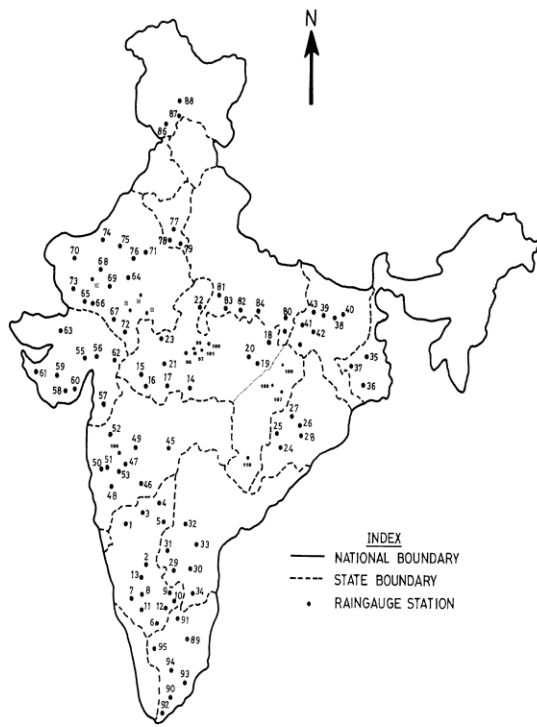
Fig. 1: Location of selected raingauge stations in different parts of India

CLASSIFICATION CLIMATIC REGIONS

Thornthwaite (1948) presented a climatic classification based fundamentally on balance between incoming and outgoing heat and moisture at the earth's surface. In this classification, Thornthwaite considered potential evapotranspiration (PE) as key climatic constituent equal in importance to precipitation (P). Using a simple concept of water balance, the potential evapotranspiration was compared with the precipitation and the periods of moisture deficiency (D) and excess (S) were obtained to express relative moistness or aridity of a climate. Finally, an annual/seasonal moisture adequacy index, I_m, was derived from the following relationships (Eqs.1 & 2).

$$I_m = \frac{100(S - D)}{PE}$$

(1)

If the soil moisture is assumed to be constant, the equation is simplified to:

$$I_m = \frac{100P}{PE} - 1$$

(2)

The moist and dry climates are thus separated by the moisture index of zero. Based on I_m, the world climatic system was categorized into nine classes (Table 2).

Table 2: A rational classification of climate by Thornthwaite (1948)

Sl No.	Climate Class	Class code	Moisture adequacy index, I_m
1	Perhumid	A	100 and above
2	Humid	B_4	80 to 99.9
3	Humid	B_3	60 to 79 9
4	Humid	B_2	40 to 59.9
5	Humid	B_1	20 to 39.9
6	Moist subhumid	C_2	0 to 19.9
7	Dry subhumid	C_1	- 19.9 to 0
8	Semiarid	D	- 39.9 to - 20
9	Arid	E	- 60 to - 40

The climatic spectrum could be characterized using the ratio of mean annual potential evapotranspiration (E_p) to mean annual precipitation (P_a) (WMO, 1975; Ponce et al., 2000). Pandey and Ramasastri (2002) proposed a new climatic classification based on the ratio of mean annual precipitation (P_a) to the mean annual evapotranspiration (E_p). To depict the relationship of regional drought characteristics (duration, severity and frequency) with climatic parameters, the climatic spectrum was divided into eight regions as shown in Table 3 (Pandey and Ramasastri, 2002). the ranges of estimated values of mean annual potential evapotranspiration for mid-latitudinal regions, across the climatic spectrum, were utilized to determine suitable limits of E_p/P_a ratios for demarcation of climatic classless as given in Table 3.

Table 3: Delineation of climatic regions based on Ep/Pa ratio.

Sl. No.	Climatic regions	E_p/P_a ratio
1	Superarid	$E_p/P_a \geq 30$
2	Hyperarid	$30 > E_p/P_a \geq 12$
3	Arid	$12 > E_p/P_a \geq 5$
4	Semiarid	$5 > E_p/P_a \geq 2$
5	Subhumid	$2 > E_p/P_a \geq 3/4$
6	Humid	$3/4 > E_p/P_a \geq 3/8$
7	Hyperhumid	$3/8 > E_p/P_a \geq 3/16$
8	Superhumid	$E_p/P_a < 3/16$

Above limits of P_a/P_g and E_p/P_a values are indicative of general trends, and not necessarily be regarded as exact values separating the climatic regions. For E_p/P_a ratio, the values vary between 30 and 3/16, decreasing gradually and are derived based on experience (Rao, et al. 1971; Abbi, 1974; WMO, 1975; Ponce, 1995). This type of climatic classification was derived

specifically for drought characterization across the climatic regions. Also, the above classification closely matches with other existing classifications given by Bull (1991), Dutt (1986), Stern et al. (1999) and Ponce *et al.*(2000).

DESCRIPTION OF APPROACH AND ANALYSIS

The climatic parameters used in this study refer to mean annual precipitation and mean annual potential evapotranspiration. Since the time unit is a year, the minimum duration of a meteorological drought is one year and the minimum drought return period may be two years. In the present study, the annual rainfall series for 35–106 years for each of the given stations was analysed using percentage annual rainfall departure from normal (PARD) to identify the drought years and the drought events. Using the definition given by IMD, a meteorological drought year is marked as PARD ≤ -25%. Plots of percentage annual rainfall departure from mean were prepared for identification of drought years and the drought events. The sample plots of PARD for Damoh station in Madhya Pradesh and Bijapur in Karnataka are shown in Fig. 2a & Fig.2b. Similar plots of PARD for various stations located in different climatic regions were prepared to identify drought years/events.
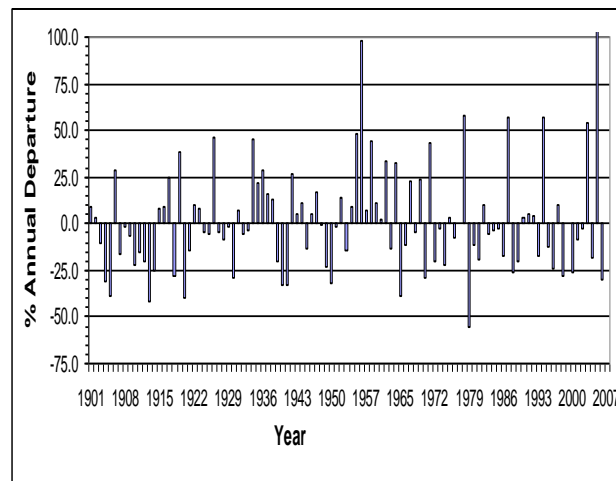
Fig. 2a: Plot of percentage annual rainfall departure from mean for Damoh, Madhya Pradesh
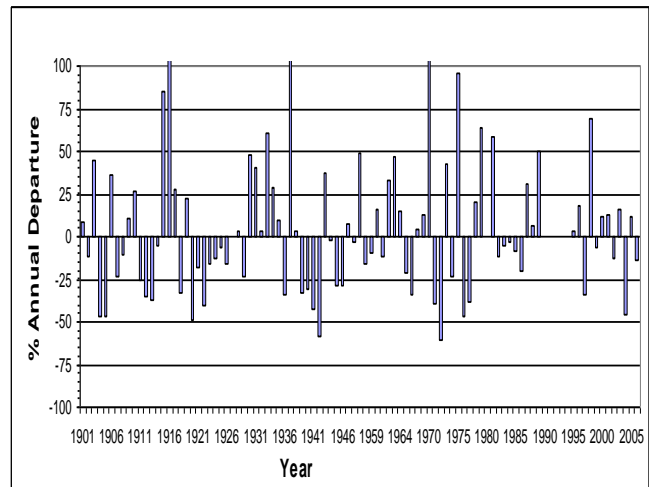
Fig.2b: Plot of percentage annual rainfall departure from mean for Bijapur, Karnataka.

The average drought return period (T) has been obtained as numbers of years of rainfall records analyzed divided by the number of meteorological drought years. The years for which rainfall records were missing at a given station, were not accounted in the analysis while estimating total number of years of records analyzed for a given station. Drought severity (S) ascribes to the magnitude to which actual precipitation is lesser than the mean or a predefined threshold value. In this study, Drought severity (S) for a given place during a drought year with actual rainfall, P_{id}, and with mean annual rainfall, P_a, has been obtained as follows:

$$S = \frac{p_{id} - p_a}{p_a}$$

(3)

The precipitation P_{id} in a drought year is always less than P_a at a given place (i.e. $P_{id} < P_a$), and therefore, equation 3 estimates the negative values of S, While studying the applicability of various drought indices in India, Dash (2006) proposed a new classification for severity as Mild (S_{ml}) = -0.25 ≥I> -0.35; Moderate (S_m) = -0.35 ≥S > to -0.45, Severe (S_s) = -0.45 ≥I> -0.60, and Extreme (S_e) S≤-0.60. This classification of S has been utilized for further analysis of drought severity in this study. Out of the total estimated drought events at a given station, over the period of record analyzed, the percent probabilities of occurrence of drought events of different severity classes were estimated. For the purpose of simplicity in presentation, S_{ml} and S_m were combined into a single class (i.e. S_m), and percent probabilities of occurrence of three major categories (i.e. S_m, S_s, and S_e) were computed. The results have been compared with the documented experiences in various countries.

RESULTS AND DISCUSSION

Relationship of Drought Frequency with Climatic Parameters

Percentage annual rainfall departures from normal were estimated from long-term annual rainfall series for each of the

given stations to identify the drought years and the drought events. The average drought return period for each station was thus computed from the number of years of rainfall records at a given station divided by number of meteorological drought years (i.e. the number of years for which annual rainfall was less than 75% of its mean value). The drought frequency (F) refers to reciprocal of return period (T) (i.e. F=1/T). Since the ratio of mean annual potential evapotranspiration to mean annual precipitation (E_p/P_a) may never be zero, both power and exponential regression models were applied to relate the E_p/P_a ratio with the average drought frequency (i.e. in terms of return period) (Fig. 3). The power type regression showed better correlation ($R^2 = 0.68$) than did the logarithmic or exponential type regression. Figure 3 shows that the frequency of meteorological droughts has a significant relationship with the Ep/Pa ratio. Average drought frequency (expressed in terms of return period) varies from 2 to 3 years in arid regions (with 12 $> E_p/P_a \geq 5$), 3 to 5 years in semiarid regions (with 5 $> E_p/P_a \geq 2$), and 5 to 9 years in subhumid regions (with 2 $> E_p/P_a \geq 3/4$). In Fig. 4, the average drought frequency was correlated with the ratio of mean annual deficit to mean annual precipitation. Since the mean annual deficit ($E_p - P_a$) may be zero or less than zero, the relationship between the average drought return period and the ratio of mean annual deficit ($E_p - P_a$) to mean annual precipitation (P_a) was derived using an exponential regression model.

Fig. 3 reveals that the average return period decreases with increase in the E_p/P_a ratio. In the arid and semiarid regions, it decreases gradually from 2.5 years on an average to 5 years for a long range of E_p/P_a ratio of 2–10. However, in wet sites (sub-humid regions), it increases sharply from 5 years to 9 years for a short range of E_p/P_a ratio of 0.75–2.0. Fig.3 clearly indicates that the drought frequency decreases exponentially with the increase of wetness.

In arid regions ($E_p/P_a \geq 5$) the average drought frequency is found to be once in every 2–3 years (Fig.3). This indicates that those regions, in which the mean annual potential evapotranspiration is more than five times the amount of mean annual precipitation, would experience drought on an average every 2–3 years. In the semiarid regions, the mean annual potential evapotranspiration is two to five times the total amount of mean annual rainfall. In these semiarid areas, where the total annual rainfall is of the order of about half of the local mean annual potential evapotranspiration (i.e. $E_p/P_a \approx 2$), droughts occur once in every 5 years (Fig. 3). In areas with E_p/P_a ratios between 2.0–3.0 and 3.0–5.0, droughts recur every 4–5 and 3–4 years, respectively (Fig. 3).
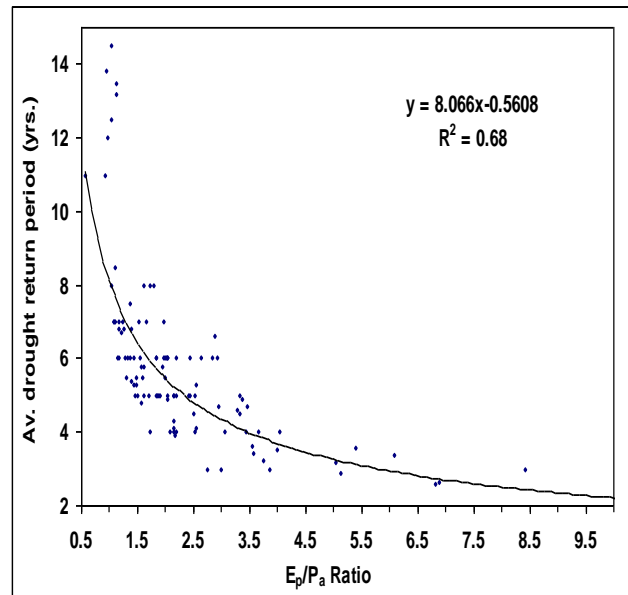
Fig. 3: Relationship of average drought return period with E_p/P_a ratio.
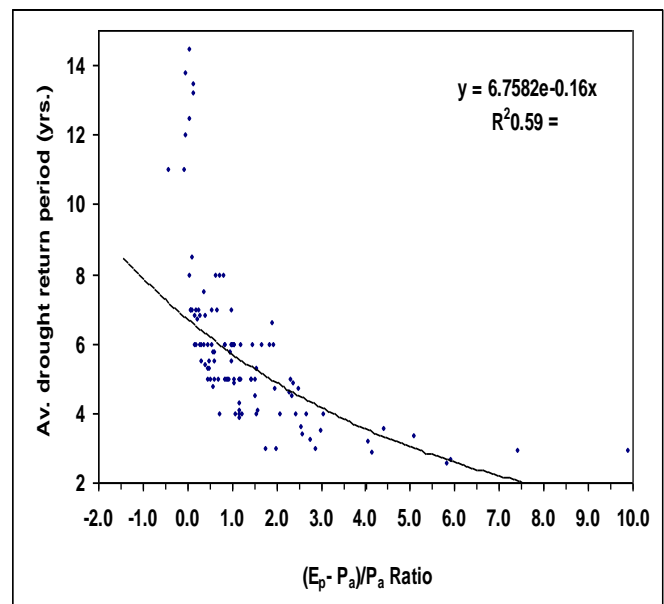
Fig. 4: Relationship of average drought return period with (E_p–P_a)/P_a ratio.

In sub-humid areas ($0.75 \leq E_p/P_a < 2$), the average drought frequency is once in 5–10 years (Fig. 3). The areas which receive mean annual rainfall nearly equal to their mean annual potential evapotranspiration (i.e. $E_p/P_a \approx 1$) experience drought every 8 years (Fig. 3). Further, if the area belongs to the further wet side of the climatic spectrum, (i.e. $0.5 \leq E_p/P_a < 1$), the drought frequency is of the order of once in 9–11 years. However, it can also be seen from analysis (Fig. 3) that a few stations in sub-humid regions, namely, Midnapur and Bankura in West Bengal, Phulbani in Orissa and Belgaum in Karnataka State, whose mean annual rainfall nearly equals the local mean annual potential evapotranspiration, experienced

less frequent droughts. The average frequency of drought at these stations was once in every 14, 13, 12 and 11 years, respectively. This typically indicated the possibility of some influence of other physical/regional/morphological factors particularly in respect of presence of orograpgraphic barrier (distance of station from mountains/ major-hills, h_s) and distance from sea (d_s). It may also be one of the possible reasons restricting the value of correlation coefficient of above relationships to moderately significant (i.e., $R^2 = 0.68 \& 0.59$).

In Figure 4, the average drought frequency was correlated with the ratio of mean annual deficit to mean annual precipitation ($R^2 \approx 0.56$). Similar to Fig 3, the relationship shown in Fig. 4 reveals that the average frequency of drought decreases exponentially with decrease in the ratio of mean annual deficit (E_p–P_a)/mean annual precipitation.

A comparison of the above inferences with drought data and experiences elsewhere indicates that the results are rationally comparable. For instance, in Brazil, in Sarido, which belongs to an arid region with $E_p/P_a \approx 5.8$, and in semiarid Caatinga and Saritao, where the E_p/P_a ratio varies from 2.2 to 4.8 (Ponce, 1995a), droughts recur approximately once in every 3 and 5 years, respectively.

However, in sub-humid Agreste and Mata, where the E_p/P_a ratio varies between 1.3 and 2.0 and between 0.7 and 1.1, respectively, the drought conditions occur every 8–12 years on an average (Ponce, 1995a; Magalhaes & Magee, 1994). For sub-humid climatic regions in the upper midwest United States with mean annual precipitation of about 1500 mm (NOAA, 1980), the average return period of drought is reported as approximately 10 years (Klugman, 1978). French (1987) analysed long-term series of annual rainfall for Georgetown in South Australia, where the mean annual rainfall is 475 mm. The records from 1874 to 1985 show 20 drought events, i.e. an average frequency of once in 5.5 years. Swearingen (1994) reported that Morocco, which belongs to the semiarid climatic region (P_a = 400–500 mm), experienced approximately 25 years of drought during the period from 1901 to 1994, i.e. an average drought frequency of once in 3.5 years. Thus, the relationships proposed broadly follow the drought frequency behaviour in similar climatic regions in other parts of the world. It is hoped that these relations may be useful for further critical analysis of drought in different climatic regions.

Influence of Morphological Factors on Drought Characteristics

According to Lana & Burgueno (1998), besides morphological factors orography affects the drought characteristics significantly. In view of this, an attempt was made to assess relevance of drought characteristics with the distance of major orographic barriers (d_h), distance from sea coast (d_s) and elevation of the place from mean sea level (m.s.l.). Multiple regressions were applied to determine significance of these factors in description of frequency, duration, and intensity of meteorological droughts using long-term data for 110 stations.

Some influences of elevation could be observed in drought intensity and of distance from sea coast on drought persistence (i.e. duration). However, no specific pattern could be established among them. From the spreadsheet analysis of long-term meteorological drought, it was seen that the stations which are close to sea, and are situated near some mountain/major hill did not face drought events of severe and extreme intensity (Table 4).

Table 4: List of stations which never faced drought events of severe & extreme severity

Sl. No.	Station	Ep/Pa	Data length, years	Total No. of drought events	No. of events with duration > 1 yr	No. of events with S_s & S_e intensity	Approx. Altitude (w.r.t. msl), m	Distance from sea coast km	Distance from major hill/mountain km
1	Tumkur Karnataka	1.84	77	12	0	0	300	252	150
2	Bangalore Karnataka	1.66	80	11	0	0	1200	280	95
3	Mandya Karnataka	2.0	79	14	0	0	800	195	90
4	Hassan Karnataka	1.62	76	8	1	0	1000	135	50
5	Tirunelveli Tamilnadu	1.96	76	13	1	0	40	52	40
6	Salem Tamilnadu	1.8	78	9	1	0	300	178	12
7	Madurai Tamilnadu	1.03	78	6	0	0	100	98	45
8	Agastheswara Kanyakumari Tamilnadu	1.19	76	9	0	0	30	10	15
9	Belgaum Karnataka	1.10	77	6	1	0	700	90	40
10	Hulsi Maharashtra	0.9	77	9	1	0	1200	114	On hills

It was found from the data that stations which are located at relatively shorter distance from sea and have $P_a \approx E_p$ did not faced persistent droughts of 2 or more consecutive years. Regions with Ep/Pa<1.2, d_s<100 km, and d_h<100 km hardly ever faced persistent droughts or the drought events of severe and extreme intensity. For example, Madurai and Kanyakumai in Tamilnadu (Ep/Pa<1.2, ds<100 km and d_h<100) have respectively experienced 7 and 9 drought events during 1901- 2001, but none of them persisted for two or more consecutive years. Further, the stations which are within 100 to 150 km from ocean (100<d_s<150) and have close distance (d_h< 100 km) from mountain/major hill seldom faced the drought events of severe and extreme intensity, and also the occurrences of persistent droughts events were very few. Thus, beside the climatic parameters, drought characteristics at a given location are influence by distance from sea coast and mountain barrier.

SUMMARY AND CONCLUSSIONS

The average drought frequency can be significantly

described using dimensionless climatic parameters derived as the ratio of mean annual potential evapotranspiration to mean annual precipitation (E_p/P_a) and the ratio of mean annual deficit to mean annual precipitation (($E_p - P_a)/P_a$). The study revealed that the frequency and intensity of meteorological droughts have notable relationship with the E_p/P_a ratio. Average drought frequency (i.e. yr^{-1}) is seen to decrease gradually from dry to wet regions, from once in two to three years in the arid regions ($12 > E_p/P_a \geq 5$), three to five years in the semiarid regions ($5 > E_p/P_a \geq 2$) and five to nine years in the sub-humid regions ($2 > E_p/P_a \geq 3/4$). In semiarid to sub-humid regions with Ep/Pa ratios between 3.5 and 0.5, the drought frequency decreases exponentially with increase in wetness. Also, identical relationship is obtained between the average drought frequency (F) and the ratio of mean annual deficit to mean annual precipitation [($E_p-P_a)/P_a$]. The relationship obtained between the average drought return period and the ratio of mean annual deficit to mean annual precipitation (($E_p - P_a)/P_a$) also indicates the drought frequency to increase with increase in mean annual deficit.

The probability of occurrence of a severe or extreme intensity drought increases gradually from wet to dry regions, the case is however reverse for moderate intensity droughts. Thus, it can be concluded that the areas located in arid and semiarid climatic regions are prone to suffer from relatively more intense meteorological droughts than areas in the sub-humid climatic region. The occurrences of severe droughts are much rare in the regions with E_p/P_a ratio less than 1.2. The extreme drought events are almost unnoticed in the regions with E_p/P_a ratio less than 1.20. This again confirms that the climatic region with lesser mean annual deficit is less susceptible for intense droughts.

The results were compared with drought experiences in other countries and were found to be in conformity with them. The relations presented in this paper can be used as a sensible tool for prediction of regional drought characteristics and planning of appropriate drought management strategies for different climatic regions in India.

REFERENCES

i. Abbi, S.D.S. (1974) Hydrometeorological studies in India. Preprints, International Tropical Meteorology Meeting, American Meteorological Society East African Metorological Department, World Meteorological Organization, January 31-February 7, 1974, Nairobi, Kenya.

ii. Alley, W.M. (1984) The Palmer Drought Severity Index: Limitations and Assumptions. Journal of Climate and Applied Meteorology, 23(7), 1100-1109.

iii. Bull, W. B. (1991) Geomorphic response to climatic change. Oxford University Press, New York.

iv. Byun, H.R and Wilhite D.A. (1999) Objective quantification of drought severity and duration. Journal of Climate, 12(2), 747-756.

v. Dash B.B. (2006) Objective estimation of drought severity and associated parameters. M.Tech. dissertation, Dept. of Water Resources Development and Management, Indian Institute of Technology, Roorkee (India), p-65.

vi. DMI (1999) Urban risk assessment tools, a preliminary status report part-A. Disaster Mitigation Institute, Ahmedabad – 380 009.

vii. Dracup, J.A., Lee, K.S. and Paulson, E. G. Jr. (1980) On the definition of droughts. Water Resources Research, 16(2), 297-302.

viii. Dutt, D. K. (1986) Management of ground water under drought conditions, Jal Vigyan Sameeksha, High Level Technical Committee on Hydrology, NIH, Roorkee, 111-128.

ix. French, R. J., 1987. Adaptation and adjustments in drought prone areas: An overview South Australian Study. Planning for Drought, Toward a Reduction of Societal Vulnerability, D.A. Wilhite et al., eds., Westview Press, Boulder, Colorado.

x. Gregory, S. (1989) The changing frequency of drought in India, 1871-1985. The Geographical Journal, 155(3), 322-334.

xi. Karl, T. R., and Young, P. J. (1987) The 1986 Southeast drought in historical perspective. Bulletin American Meteorological Society, 68(7), 773-778.

xii. Kogan, F. N. (1995) Droughts of the late 1980s in the United States as derived from NOAA polarorbiting satellite data. Bulletin of the American Meteorological Society, 76(5), 655-668.

xiii. Kogan, F. N. (1997) Global drought watch from space. Journal of the American Meteorological Society, 78(4), 621-636.

xiv. Klugman, M. R. (1978) Drought in the Upper Midwest, 1931-1969. Journal of Applied Meteorology, 17(10), 1425-1431.

xv. Kundzewicz, Z.W. and Zdislaw Kaczmarek (2000) Copping with hydrological extremes. Jour. of Water International. International Water Resources Association, 15(1), 66-75.

xvi. Lana, X and Burgueno A. (1998) Spatial and temporal characterization of annual extreme droughts in Catalona (North Spain). International Journal of Climatology, 18, 93-110.

xvii. Lugo, A. E. and Morris G. L. (1982) Los sistemas ecologicos y la humanidad (The ecological systems and humanity). Organizacion de los Estados Americanos, Monografia No. 32, Washington, D.C., in Spanish.

xviii. Magalhaes, A. and Magee P. (1994) The Brazilian Nordeste (Northeast). In: Drought Follows the Plow (ed. By M. H. Glantz), Cambridge University Press, Cambridge, UK., pp.59–76.

xix. Mimikaou M.A., Kouvopoulos Y.S. and Hadjissavva P.S. (1993) An analysis of multiyear droughts in Greece. Water Resources Development Jour. 9(3), 281-291.

xx. Pandey, R. P. and Ramasastri K. S. (2002) Incidence of droughts in different climatic regions. Hydrological Sciences Journal, August especial issue 47(S), pp. S31-S40.

xxi. Pandey, R. P. and Ramasastri K. S. (2001) 'Relationship between the common climatic parameters and average drought frequency. Hydrological Processes Journal, 15(6), 1019-1032.

xxii. Patel, V.B and Iyer D.R.S. (1987) Water Resources projects and strategies for water management for drought affected areas including drinking water supplies based on Gujarat experience. All-India seminar on strategies for drought proofing and management, water Management Forum, Institution of Engineers (India), Ahmedabad, 6-7 Feb. 1987, pp. 1-22.

xxiii. Paulson, E.G.Jr., Sddeghipour J. and Dracup J.A. (1985) Regional frequency analysis of multiyear droughts using watershed and climatic information. Journal of Hydrology, 77, pp. 57-76.

xxiv. Penman, H.L. (1963) Vegetation and hydrology. Tech. comm. no. 53, commonwealth Bureau of soils, Harpenden, Eng., p.-125.

xxv. Ponce, V. M. (1995) Management of droughts and floods in the semiarid Brazilian Northeast-The case for conservation. Jour. of Soil and Water Conservation, 50(5), 422-431.

xxvi. Ponce, V. M., Pandey R.P. and Sezan Ercan (2000) Characterization of drought across climatic spectrum. Journal of Hydrologic Engineering, ASCE, 5(2), 222-224.

xxvii. Rao, K.N., George C. J. and Ramasastri K. S. (1971) Potential evapotranspiration over India, IMD Scientific Report No. 136, Meteorological Office Pune-5.

xxviii. Samra, J.S. (2004) Review and analysis of drought monitoring declaration and management in India. Working paper no 84. International Water Management Institute, Colombo, Shri Lanka. pp. 1-40.

xxix. Sharma, T.C. (1997) A drought frequency formula. Hydrological sciences Journal, 42(6), 803-814.

xxx. Shin Hyun-Suk and Salas J.D. (2000) Regional drought analysis based on Neural Networks. Jour. of Hydrologic Engg., ASCE, 5(2), 145-155.

xxxi. Stern, H., de Hoedt G. and Ernst J. (1999) Objective classification of Australian climates. 8th Conf. on Aviation, Range and Aerospace Meteorology, Amer. Meteor. Soc., Dallas, Texas, 10-15 Jan., 1999.

xxxii. Swearingen, W. (1994) Northwest Africa. Drought follows the plow, M. H. Glantz, (eds.), Cambridge University Press, Cambridge, England, 117-134.

xxxiii. *Thornthwaite, C. W. (1948) An approach toward a rational classification of climate. The Geographical Review vol. 38, 55-94.*
xxxiv. *WMO, (1975) Drought and agriculture. Technical Note No. 138, World Meteorological Organization No. 392, Geneva, Switzerland.*

Drought Assessment And Forecasting: A Case Study Of Dharoi Sub Basin

J.K.Solanki[1]   Dr. Falguni Parekh[2]

[1]*PG Student, Water Resources Engineering and Management Institute (WREMI), Faculty of Technology and Engineering, The Maharaja Sayajirao University of Baroda, Samiala-391410*
Email: jalpa_solanki_8276@yahoo.co.in
[2]*Offg. Director & Associate Professor, Water Resources Engineering and Management Institute (WREMI), Faculty of Technology and Engineering, The Maharaja Sayajirao University of Baroda, Samiala-391410*
Email: fpparekh@gmail.com

ABSTRACT :*Drought is natural hazard that results from lower levels of precipitations than what is considered normal. When this phenomenon extends over a season or a longer period of time, precipitation is insufficient to meet the demands of human activities and the environment. Predicting future dry events in a region is an important first step for finding sustainable solutions to water management and risk assessment of drought occurrences. Drought is a normal recurrent feature of climate occurring in all climatic zones and it originates from a deficiency of precipitation over a given period of time: short time scales (months) characterize meteorological drought, while longer time scales hydrological drought. A useful index for drought monitoring, based only on monthly precipitation data is the Standardized Precipitation Index (SPI), has been proposed to monitor dryness and wetness on multiple time scales (McKee, 1993).The present approach examines the SPI drought index in application for the Dharoi sub basin and it is evaluated accordingly by historical precipitation data (1968-2010) for 3 meteorological stations. The Standardized Precipitation Index (SPI) is forecasted and compared using feed forward neural Network System (ANN) with rainfall and SPI values as inputs. SPI 3 and SPI 12 are the SPI values that will be forecasted over lead times of 1 and 6 months. The model is evaluated using performance indices, RMSE and Coefficient of Determination (R^2) for training and validation. The best model has R^2 values varies between 0.85 - 0.93. SPI Index is a useful tool to assess the severity of drought and ANN can be used to forecast the drought situation for Dharoi sub basin.*

Keywords: Artificial Neural Network, Drought Assessment, Drought Forecasting, Standardized Precipitation Index, Trend Analysis.

1. INTRODUCTION

Drought can be a disastrous natural phenomenon that can have significant impact on agricultural, hydrological and environmental sphere. Once drought duration and severity have been found objectively and then it is forecasted over different lead times, hence it is possible to plan for the transport of water in known quantities to drought affected areas, either from other water resources or from water stored during monsoon periods. These deficits may cause low crop yields for agriculture, unreplenished ground water resources, depletion inlakes /reservoirs, and shortage of drinking water and, reduced fodder availability etc. In addition to adversely impacting the hydroelectric industry, as well as causing deficits in the drinking water supply which can negatively affect local populations.

Drought forecasting is an effective tool for water resource managements well as an effective tool for the agricultural industry. Conceptual definition helps people to understand the concept of drought. For example, drought is a prolonged period of deficient precipitation resulting in extensive damage to crops, further resulting in loss of yield. Conceptual definitions may also be important in establishing drought policy. An operational definition of drought helps people to identify the beginning stage, ending stage and degree of severity of a drought. This definition is usually made by comparing the current situation to the historical average, often based on a 30 years or more period of record. These operational definitions can also be used to analyse drought rate of recurrence, severity and duration for a given historical period.

One of the major challenges of agricultural systems is how to mitigate the impacts of droughts. Drought impact on agricultural systems, economically as well as environmentally. From an environmental perspective, droughts can deprive crops and soils of essential precipitation as well as increase the salt content in soils and irrigation systems. To mitigate the impacts of drought an effectively and timely monitoring system is required. Effective monitoring of droughts can aid in developing an early warning system.

An objective of evaluation of the drought condition in a particular area is the first step for planning water resources in order to prevent and mitigate the impacts of future occurrences of drought. The evaluation and forecasting of drought is made possible by the use of drought indices. There are several drought indices that are commonly used, such as the Palmer Index, the Crop Moisture Index and the Standardized Precipitation Index (SPI). The Palmer Index and the SPI are traditionally the most popular indices for forecasting drought due to their standardization. For the purposes of comparing drought conditions from different areas, which often have different hydrological balances, the most important characteristic of a drought index is its standardization. Standardization of a drought index ensures independence from geographical position as the index in question is calculated with respect to the average precipitation in the same place. There are two main definitions of drought: conceptual and operational. American scientists McKee, Doesken and Kleist developed the Standardized Precipitation Index (SPI) in 1993. It is just as effective in analysing wet periods/cycles as it is in analysing dry periods/cycles. At least 20-30 years of monthly value is needed and with 50-60 years (or more) being optimal and preferred

outputs. In this study, the Standardized Precipitation Index (SPI) has been used for drought severity and forecasting of SPI in Dharoi sub basin.

2. MATERIAL AND METHODS

The Sabarmati River is a river of western India and one of the biggest rivers of north Gujarat. River Sabarmati is one of the major west flowing river of Gujarat which originates from Dhebar Lake in Aravalli Range of the Udaipur District of Rajasthan and meets the Gulf of Cambay of Arabian Sea after travelling 371 km. from the origin. The Sabarmati basin has a maximum length of 300 km. and maximum width of 105 km. The total catchment area of the basin is 21674 km^2 out of which, 4124 km^2 lies in Rajasthan state and the remaining 18550 km^2 in Gujarat state.

Sabarmati River basin is situated in the mid-sothern part of Rajasthan. To its east lie the Banas and Mahi basins, to its north the Luni basin and to its west the West Banas basin. Its southern boundary is the border with Gujarat state. The total catchment area of the basin is 4164 km^2. Sabarmati river basin extends over parts of Udaipur, Sirohi, Pali and Dangarpur districts. Orographically, the western part of the basin is marked by hilly terrain belonging to the Aravali chain. East of the hills lies a narrow alluvial plain with a gentle eastward slope.

The Sabarmati river basin is often divided into three smaller sub-basins: Dharoi sub-basin, Hathmati sub-basin, and Watrak sub-basin. The Dharoi sub-basin is the uppermost of the three as shows in Figure 1. The catchment area of Dharoi Sub Basin in Gujarat is shown in below Figure 2 and which is marked by yellow line.

Area selected for the present study is the Dharoi sub basin which is the part of Sabarmati river basin. The area covering upper sub-basin and the catchment of the main river up to Dharoi dam is designated as Dharoi sub-basin. Constructed in 1978, Dharoi dam is located about 165 km upstream Ahmadabad in village Dharoi of Mehsana district. This covers drainage area of the main river up to Dharoi dam.

In Dharoi sub basin there are six Rain gauge stations existed but among them three rain gauge station's data is selected for the year 1968 to 2010 (42 years). Monthly Precipitation data are considered for each year of the three stations namely Hadad, Dharoi and Khedbrahma.

Figure 1. Sabarmati river with sub basins
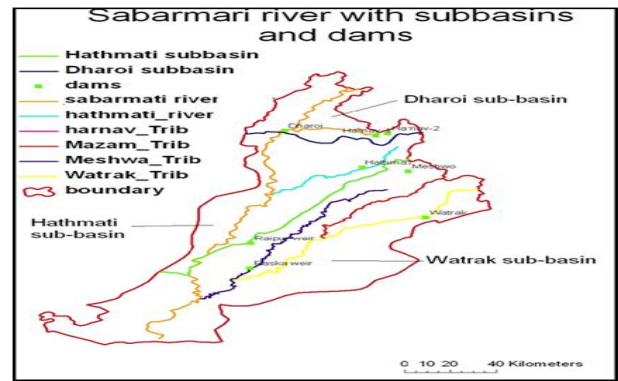
Figure 2. Dharoi Sub Basin in Gujarat State

The methodology section includes the SPI has been calculated and then forecast over two separate lead times using ANN. The model inputs are previous rain and drought indices. The Standardized Precipitation Index (SPI) is forecasted and compared using feed forward neural Network System (ANN) with rainfall and SPI values as inputs. The model is evaluated using performance indices, RMSE and Coefficient of Determination (R^2) for training and validation data sets. In this study, for all the ANN models the cross validation technique has been used to partition the data sets; 60% of the data has been used to train the models, while the remaining 40% of the data to validate the models. The training set has been used to compute the error gradient and to update the network weights and biases.

3. RESULTS AND ANALYSIS

Table 1. Drought severity for the years of 1968 – 2010 for Dharoi sub basin.

Station	Drought Years	Drought Severity	Average Rainfall
	2002, 2004, 2010	Moderate Dry	More than 100 mm
Hadad	1982, 1986, 1987 1999, 2000	Severe Dry	30 mm to 100 mm
Dharoi	1987, 2009, 2010	Moderate Dry	More than 100 mm
	1999, 2000, 2002	Severe Dry	30 mm to 100 mm

	1989, 2006	Moderate Dry	More than 100 mm
Khedbrahma	2003, 2005	Severe Dry	30mm TO 100mm
	1987,1988	Extreme Dry	Less than 30 mm

Table 1. shows the drought severity years for three stations of Dharoi sub basin. According to SPI values and average rainfall, drought can be classified in three categories shown in Table 1. If the average rainfall value is more than 100 mm and SPI calculated is in between -1 to -1.49, then these years can said to be moderate dry in the years of 2002, 2004 and 2010 of Hadad station. If the average rainfall value is between 30 mm to 100 mm and SPI calculated is in between -1.5 to -1.99, then these years can said to be severe dry in the years of 1999, 2000 and 2002 of Dharoi station. Similarly if the average rainfall value is below 30 mm and SPI calculated is above -2, then those years can said to be extreme dry in the years of 1987 and 1988, then these years categorized as extreme dry of khedbrahma station. Drought severity class has been carried out in reference of below Table 2 which was developed by McKee et al in 1993.

Table 2. Drought classification based on SPI (McKee et al 1993)

SPI values	Class	SPI values	Class
>2	extremely wet	-1 to –1.49	moderately dry
1.5 to 1.99	very wet	-1.5 to-1.99	severely dry
1.0 to 1.49	moderately wet	< -2	extremely dry
-0.99 to 0.99	near normal		

Fig 3 & 4 shows the SPI calculated for 5 month rainfall totals for the monsoon season of India (June-July-Aug-Sept-Oct) from 1971 to 2010 for Hadad station. It shows the drought severity for that particular year. Similarly the SPI is calculated from 1971 to 2010 for Dharoi and khedbrahma stations .

Figure 3. SPI calculated for Hadad station (1971-1990
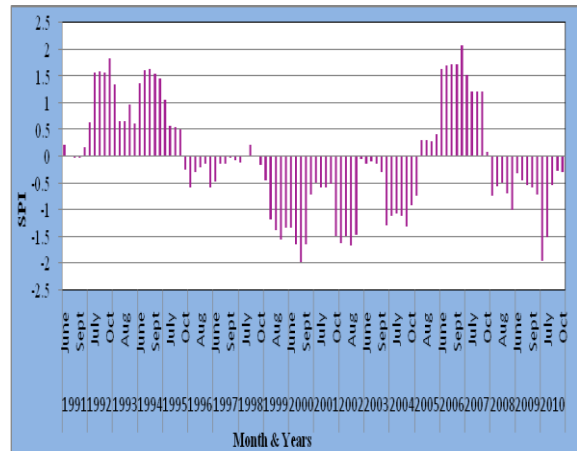
Figure 4. SPI calculated for Hadad station (1991-2010)

3.1 Drought Forecasting

Results are obtained after modelling the SPI values in feed forward neural Network System (ANN toolbox, MATLAB). Analysis of the predicted SPI and observed SPI have been carried out. Training and validation are also given to justify the results. The meteorological parameter considered in this study is the precipitation data (mm). In this study, SPI 3 and SPI 12 have been forecasted over lead times of 1 and 6 months to determine the effectiveness of the models over short and long-term lead times. The models to effectively forecast SPI 3 and SPI 12 over different lead times have been evaluated in this section. The forecast results for the best models in the Dharoi sub basin are presented for all three stations. The performance results of the models for each station are presented in Table 3 and 4. The results presented are based on the Training and validation data sets.

Table3. Forecast Results of ANN models for Training

Model Type	Hadad				Dharoi				Khedbrahma			
	SPI 3		SPI 12		SPI 3		SPI 12		SPI 3		SPI 12	
	R^2	RMSE	R^2	RMSE	R^2	RMSE	R^2	RMSE	R^2	RMSE	R^2	RMSE
ANN L1	0.36	0.78	0.24	0.850	0.42	0.745	0.17	0.946	0.50	0.700	0.13	0.700
ANN L6	0.84	0.36	0.56	0.640	0.90	0.309	0.56	0.761	0.91	0.287	0.44	0.359

Explanation: L1-1 month forecast lead time; L3- 3 month forecast lead time.

.
Table 4. Forecast Results for ANN models for Validation

Model Type	Hadad				Dharoi				Khedbrahma			
	SPI 3		SPI 12		SPI 3		SPI 12		SPI 3		SPI 12	
	R^2	RMSE	R^2	RMSE	R^2	RMSE	R^2	RMSE	R^2	RMSE	R^2	RMSE
ANN L1	0.44	0.68	0.29	0.94	0.50	0.701	0.02	0.909	0.36	0.733	0.19	0.692

ANN L6	0.85	0.33	0.56	0.737	0.93	0.256	0.28	0.807	0.91	0.247	0.06	0.812

Explanation: L1-1 month forecast lead time; L3- 3 month forecast lead time.

Figure 5 to 10 illustrates the relationship between the observed SPI and the predicted SPI for 1 and 6 month lead times at Hadad, Dharoi and Khedbrahma stations for training and validation data set. It shows that the SPI 3 has best forecast results for 6 month lead time. The results indicate that SPI 3 is more effective than SPI 12 forecast in this study.
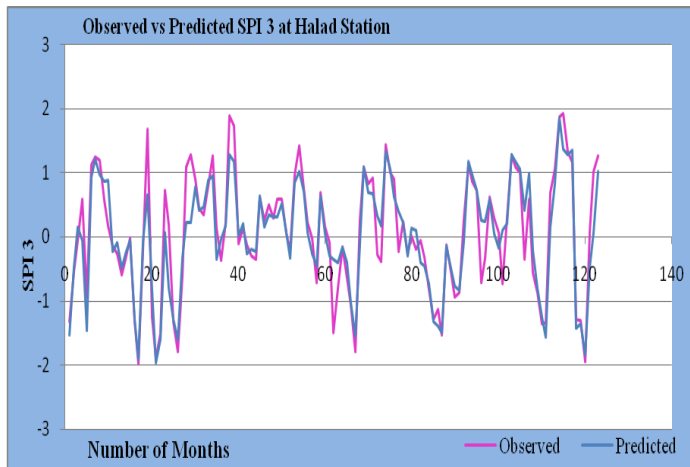
Figure 5. SPI 3 forecast results for the best ANN model at the Hadad Station for 6 months lead time for training.
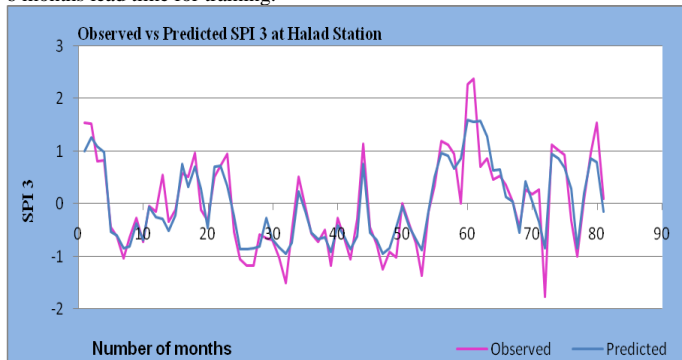
Figure 6. SPI 3 forecast results for the best ANN model at the Hadad Station for 6 months lead time for validation
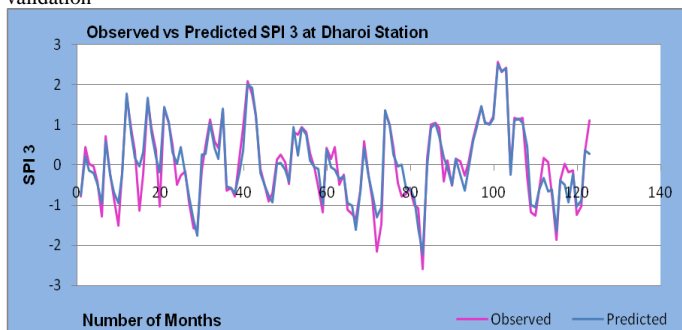
Figure 7. SPI 3 forecast results for the best ANN model at the Dharoi Station for 6 months lead time for training.
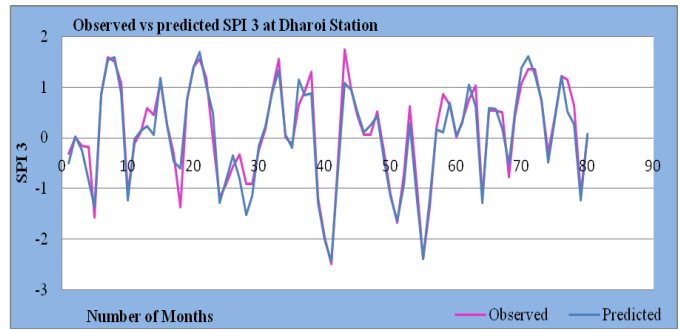
Figure 8. SPI 3 forecast results for the best ANN model at the Dharoi Station for 6 months lead time for validation
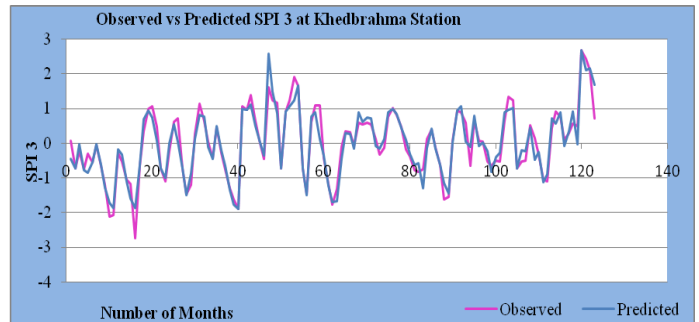
Figure 9. SPI 3 forecast results for the best ANN model at the Khedbrahma Station for 6 months lead time for training.
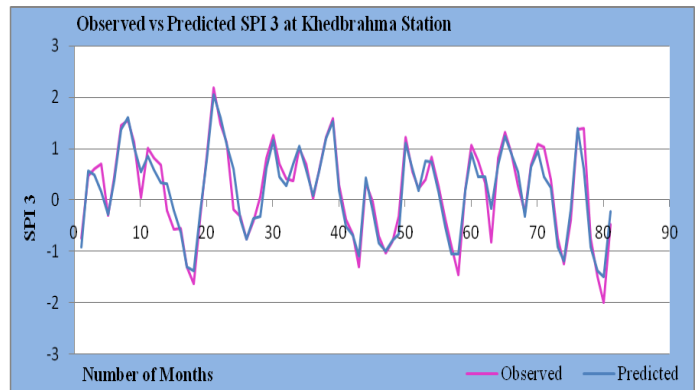
Figure 10. SPI 3 forecast results for the best ANN model at the Khedbrahma Station for 6 months lead time for validation

3.2 SPI 3 Forecasts

This section presents the results from the validation data sets. The SPI3 forecast results for the Hadad station in terms of R^2 are 0.443 and 0.851 for lead times of 1 and 6 months, respectively. For Dharoi station in terms of R^2 are 0.507 and 0.931 for lead times of 1 and 6 months respectively. For Khedbrahma station in terms of R^2 are 0.368 and 0.919 for lead times of 1 and 6 months respectively. The R^2 value between 0.7–0.9 indicates a high degree of correlation, a value between 0.5–0.7 indicates a moderate degree of correlation and a value between 0.3–0.5 indicates a low degree of correlation. The forecast results for SPI 3 are better than the forecast results for SPI 12 in all cases.

3.3 SPI 12 Forecasts

The SPI 12 forecast results for the Hadad station in terms of R^2 are 0.292 and 0.563 for lead times of 1 and 6 months, respectively. For Dharoi station in terms of R^2 are 0.023 and 0.286 for lead times of 1 and 6 months respectively. For Khedbrahma station in terms of R2 are 0.196 and 0.063 for lead times of 1 and 6 months respectively.

Figure 11, 12 and 13 shows the trend analysis of SPI for Hadad, Dharoi and Khedbrahma stations.
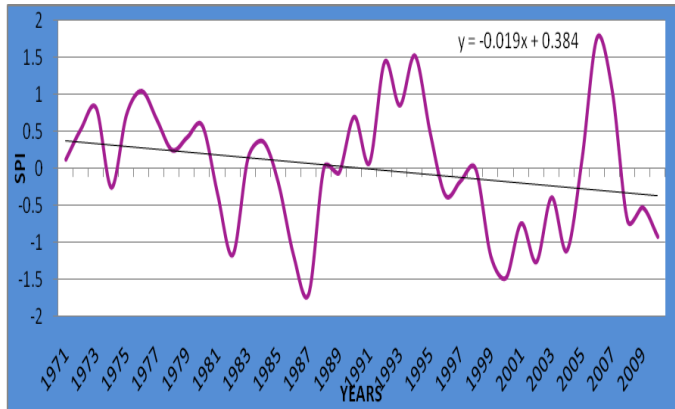
Figure 11. Trend analysis of SPI value for Hadad Station.
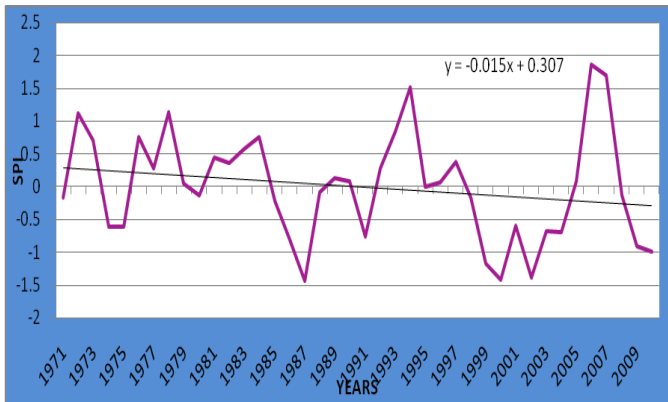
Figure 12. Trend analysis of SPI value for Dharoi Station.
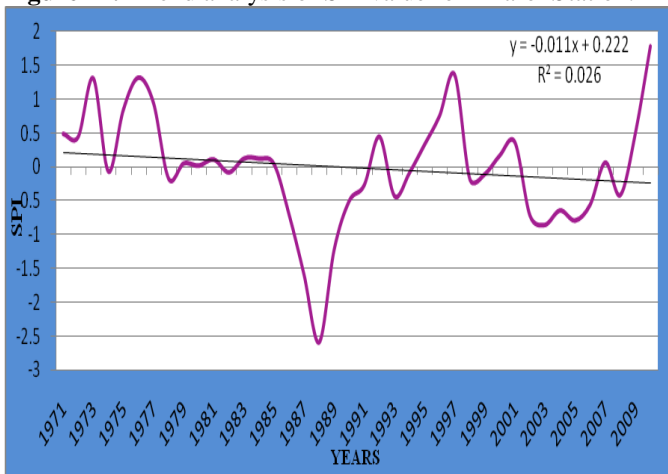
Figure 13. Trend analysis of SPI value for Khedbrahma Station.

The SPI value has been calculated from 1, 3, 6, 12, 24 and 36 months time scales. From graph 11, it is observed that, SPI Index is following decreasing trend from the years 1971-1991. From 1991 to 2010, SPI 3 value shows negative values which indicates that area is under drought condition and the severity of drought condition is increasing from 1991 to 2010.From graph 12, it is observed that, SPI Index is following decreasing trend from the years 1971-1988. From 1988 to 2010, SPI 3 value shows negative values which indicates that area is under drought condition and the severity of drought condition is increasing from 1988 to 2010.From graph 13, it is observed that, SPI Index is following decreasing trend from the years 1971-1985. From 1985 to 2010, SPI 3 value shows negative value which indicates that area is under drought and the severity of drought condition is increasing from 1985 to 2010.

4. CONCLUSIONS

- This study has tried to assess the drought severity and the models are developed to forecast the drought of the Hadad, Dharoi and Khedbrahma Stations of Dharoi sub basin for the year of 1968 to 2006. Although SPI permits comparisons over space and time better than any other index.

- From this study, all the 3 stations of Dharoi sub basin has different rainfall pattern, hence the severity of drought may vary with the intensity of rainfall. While reviewing the year 1987, it's being analyzed that drought severity found Severe, Moderate & Extreme dry conditions at Hadad, Dharoi & Khedbrahma Stations respectively. For all the station, the irrigation requirement can be evaluated based on the rainfall deficits & its severity for the given year.

- This study tries to determine the most effective model to forecast the SPI drought index in the Dharoi sub basin. The model shows greater correlation between observed and predicted for SPI 3 compared to SPI 12. SPI 3 shows lower values of RMSE compared to the SPI 12 in this study. Hence, the forecasts result for SPI 3 is more accurate than the results for SPI 12. Also better results are obtained for 6 month lead time compared to 1 month lead time. The model is evaluated using performance indices, RMSE and Coefficient of Determination (R^2) for training and validation. The best model is obtained for SPI 3 with six month lead time and has R^2 values varies between 0.85 - 0.93 for a lead time of six months.

- From the trend analysis of SPI, it is concluded that Dharoi sub basin is under severe drought condition from year 1991-2010. There is scarcity of water in sub basin and alternative resources may be planed and managed to satisfy the irrigation demand of the area.

- SPI Index is a useful tool to assess the severity of drought and ANN can be successfully used to forecast the drought situation for this study area.

REFERENCES:

i. *Alireza,S., Mohammad,H.(2012) Drought Prediction in Karoon Watershed using Meteorological Variables, International Research Journal of Applied and Basic Sciences Vole, 3 (9):(1760-1768)*

ii. *Belayneh, A., Adamowski, J. (2012) Standard Precipitation Index Drought Forecasting Using Neural Networks, Wavelet Neural Networks, and*

Support Vector Regression, Applied Computational Intelligence and Soft Computing Volume.

iii. Belayneh, A., Adamowski, J. (2013) Drought forecasting using new machine learning methods, Journal of Water and Land Development, No. 18 (I–VI), 2013: 3–12.

iv. Cancelliere, A., Di Mauro G.,Bonaccorso,B., Rossi, G.(2007) Drought forecasting using the Standardized Precipitation Index, Water Resour Manage 21:801–819

v. Karavitis C.A., Alexandris S., Tsesmelis D.E., Athanasopoulos G. (2011) Application of the Standardized Precipitation Index (SPI)in Greece, Water 2011, 3, 787-805

vi. Keskin, M.E.,Terzi, O, Taylan, E.D., Kuçukyaman, D.(2011) Meteorological drought analysis using artificial neural networks, Scientific Research and Essays Vol. 6(21), 4469-4477.

vii. Kumar, M.N., Murthy, C.S.,SeshaSai, M. V. R., Roy,P. S(2009) On the use of Standardized Precipitation Index (SPI) for drought intensity assessment, Meteorological applications, 16: 381–389.

viii. Mckee T.B., Doesken N.J., Kleist J. (1993) The Relationship of Drought Frequency And Duration to Time Eighth Conference on Applied Climatology, Anaheim, California scales.

ix. Mishra, S.S., Nagarajan, R.(2012) Forecasting Drought in Tel River Basin using Feed-forward Recursive Neural Network, International Conference on Environmental, Biomedical and Biotechnology,vol.41, 122-126

x. Morid, S., Smakhtin, V., Bagherzadeh,K..(2007) Drought forecasting using artificial neural networks andtime series of drought indices, International journal of climatology, 27,2103–2111

xi. Khadr,M., Morgenschweis, G., Schlenkhoff, A.(2009), Analysis of Meteorological Drought in the Ruhr Basinby Using the Standardized Precipitation Index, World Academy of Science, Engineering and TechnologyVol:3 , 09-21.

xii. Panu, U.S., Sharma, T. C.(2002) Challenges in drought research: some perspectives and future directions, Hydrotogical Sciences-Journal—des Sciences Hydrologiques, 47(S), S19-S30

xiii. Paulo, A.A , Pereira, L.S.(2007) Prediction of SPI Drought Class Transitions UsingMarkov Chains, Water Resour Manage, Vol 21: 1813–1827

xiv. Rafiuddin, M., Dash, B.K., Khanam, F.(2011), Diagnosis of Drought in Bangladesh using Standardized Precipitation Index, International Conference on Environment Science and Engineering, vol.8: 184-187.

Drought Analysis Using Artificial Neural Network: A Case Study

P.S. Wable[1], S. Sharama[2] and M.K. Jha[3]
Agricultural and Food Engineering Department, Indian Institute of Technology,
Kharagpur – 721 302, West Bengal, India
[1]*pawan.wable@agfe.iitkgp.ernet.in,* [2]*zepo1in@gmail.com,*
[3]*madan@agfe.iitkgp.ernet.in*

ABSTARCT: *In recent decades, drought is occurring frequently in various parts of world and causing water shortage, reduced agricultural production and detrimental impacts on vegetation, animals and people. Drought simulation helps to mitigate the impacts of drought. Standardized Precipitation Index (SPI) which is one of the meteorological drought index was used for drought analysis. The drought was simulated using Artificial Neural Network (ANN) for ChinchondiPatil raingauge station located at Ahmednagar district, Maharashtra, India for the period of 25 years (1985-2009). For simulation of drought, the Multilayer Perceptron (MLP) ANN model was developed for simulating different SPIs (SPI-3, SPI-6, SPI-9, SPI-12 and SPI-24) with rainfall as a input. The performance of the developed ANN models was evaluated using statistical and graphical indicators.*

Comparison of the calculated values and the model simulated results showed better agreement only for SPI-12 and SPI-24. In case of SPI-12, RMSE (Root Mean Square Error) and NSE (Nash-Sutcliffe Efficiency) values were found to be 0.042 and 0.998 for the training, whereas 0.188 and 0.962 for testing periods, respectively. However, for SPI-24, RMSE and NSE values were found to be 0.219 and 0.946 for the training, and 0.270 and 0.853 for testing periods, respectively.Therefore, the developed ANN models can be applied for simulating hydrological droughts in the study area.
Keywords: Standardized precipitation index, Artificial neural network, Drought simulation

1. INTRODUCTION

Drought is a deficiency in precipitation over an extended period and even its shorter duration with high intensity deficit may be the basis of destruction. It has caused water shortages, reduction of agricultural production and detrimental impacts on vegetation, animals and people. It is a natural frequent feature of climate and can occur in almost all climatic zones. Droughts have been known as an environmental disaster and due to which many hydrologist, environmentalist, agricultural scientist have become aware of it. The spatial extend of drought and impacts, as compare to other natural hazard such floods and hurricanes, are larger and non-structural, respectively (Obasi, 1994). Globally, 22% of the economic damage caused by natural disasters and 33% of the damage in terms of the number of persons affected can be credited to drought (Keshavarz *et al.*, 2013).

In India, large parts are under frequent droughts. The drought-prone areas of the country are mainly north-western and central part (Ramakrishna *et al.*, 2005). Over 68% of India is vulnerable to drought in which the 'chronically drought-prone areas' encompass around 33% and receive less than 750 mm of rainfall, while 'drought-prone areas' encompass around 35% and receive a rainfall of 750-1125 mm (PACS, 2000). In Maharashtra state also every year or other part of this state is affected by drought or drought like condition affecting drinking water availability and water for irrigation (EIS, 2006). To address the challenges due to increasing drought occurrences and to mitigate it, effective strategies for drought management are essential.

In recent decades, several drought indices have been derived to analyze the conditions of drought viz., Standardized Precipitation Index (SPI), Palmer Drought Severity Index (PDSI), Crop Moisture Index, etc. However, among those, the most commonly used meteorological drought index is Standardized Precipitation Index (SPI) as it requires only rainfall data and can be calculated for different time scales (McKee *et al.*, 1993). For effective mitigation of drought, its simulation is playing an important role. Artificial neural networks (ANN) a modelling technique have been successfully applied in hydrology due to its advantage of handling non-linearity and non-stationarity in the time series (Mishra and Singh, 2011). Some studies have been reported on the application of ANN on drought forecasting (e.g., Morid *et al.*, 2007; Keskin *et al.*,

2011). The current study was undertaken to simulate drought in a semi-arid region of Maharashtra (India) using ANN technique.

2. MATERIALS AND METHODS

2.1 Calculation of Standardized Precipitation Index

The study area selected for the drought analysis was semi-arid region of upper Bhima River basin in western Maharashtra. The daily rain gauge station data of ChinchondiPatil rainguage station for duration of 25 years (1985-2009) was used. This station is located at 18° 58' N latitude and 74° 57' E longitude with elevation of 652 m above MSL. The rainfall data of this station was procured from Hydrology Project (HP), Nashik.

To calculate SPI values, initially long term rainfall series is fitted to gamma distribution and the cumulative distribution was transformed to standard normal distribution so as SPI has mean 0 and variance 1. The SPIs were computed for different time steps viz.,1 month (SPI-1), 3 months(SPI-3), 6 months(SPI-6), 9 months(SPI-9), 12 months(SPI-12) and 24 months(SPI-24).The SPI drought indices for this study have been calculated on the basis of these rainfall data and using SPI Calculator provided by National Drought Mitigation Center, University of Nebraska Lincoln (http://drought.unl.edu//MonitoringTools/DownloadableSPIProgram.aspx).

2.2 Artificial Neural Network modeling

An ANN is type of biological inspired computational model, which is based on the functioning of the human brain (Haykin, 1994). ANN finds the relationship between inputs and outputs but not giving any knowledge about the concerned actual processes (Jha and Sahoo (2014); it is in essence based on pattern recognition. Artificial neuron, the basic unit of ANN, simulates the two basic functions of biological neurons: first it computes the weighted sum of all the inputs fed into it and this computed sum is then passed through an activation function/non-linear filter to generate the output. Activation function acts as a normalising function, such that the output is between certain values (usually 0 and1, or -1 and 1). Sigmoid activation function, most commonly used activation function, was used between input layer, hidden layer and output layer (Ochoa-Rivera, 2008). Multilayer Perceptron which is widely used network architecture in hydrological modeling was applied in this study (Nayak *et al*., 2006). For training, Levenberg-Marquardt back propagation algorithm was chosen because of its efficiency and reduced computational time in training models (Adamowski and Chan, 2011).

In order to train and test the developed ANN models, total available data were divided into two sets. For the period 1985-2009, the 50% data were used for training and remaining 50% of the data were used for testing. Neural network simulations were carried out with the help of the Neural Builder Wizard of NeuroSolutions (version 5.0) software. The neural networks were trained using optimum number of neurons in the hidden

layer for 1000 epochs. The training was stopped, when the initial defined criterion of threshold value of 0.001 was reached. One hidden layer has been considered in this study. Only rainfall time series data were used as the model input. Number of nodes in the output layer depends on the number of target variables. Only one target variable SPI for different time steps was used. The determinationof hidden neurons was done by using trai and error method.Thereafter, the ANN models were examined for their generalization properties using testing datasets.

2.3 Evaluation of the developed ANN models

The performance of the developed models was assessed by using both statistical and graphical indicators. Two goodness-of-fit statistics were used in this study namely, Root Mean Square Error (RMSE) and Nash-Sutcliffe Efficiency (NSE). In case of graphical indicators, the match between calculated and simulated SPIs was visualized.

3. RESULT AND ANALYSIS

3.1 Determination of optimal number of hidden neurons

For optimizing number of hidden neurons in the hidden layer, trial and error method was used. The number of hidden neurons was changed from 1 to 25 and corresponding MSE values given by model were noted. The model was developed for different time periods of SPIs viz., SPI-3, SPI-6, SPI-9, SPI-12 and SPI-24. The number of hidden neurons which gave the least value of MSE during training was taken as optimal number of hidden neuron as shown in Fig. 1 for SPI-12. This figure (Fig.1) shows that lowest MSE is for 17 hidden neurons. Afterwards, testing was done using the weights which were determined for the optimal number of hidden neurons during training. The optimal number of hidden neurons for simulation of different time periods of SPIs is summarized in Table 1. For Chinchondipatil rainfall station, the number of hidden neurons ranged from 15-17.
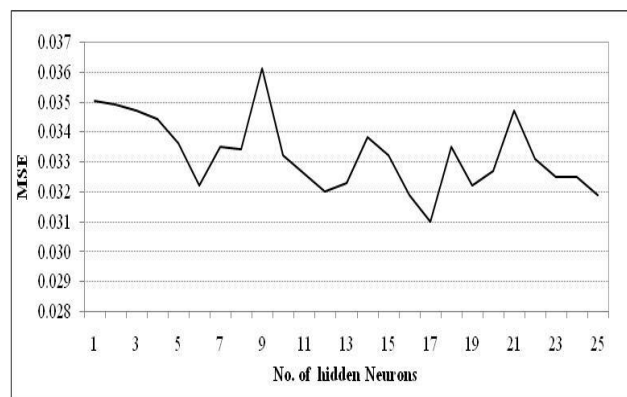
Figure 1. Plot of MSE vs number of hidden neurons for SPI-12 at Chinchondipatil raingauge station.

Table 1. Optimal number of hidden neurons for Chinchondipatil rainguage station

SPI	No. hidden neurons
SPI-3	15
SPI-6	15
SPI-9	15
SPI-12	17
SPI-24	15

3.2 Training and Testing Results of ANN Modeling

The two goodness-of-fit tests were conducted during training and testing period using RMSE and NSE as shown in Table 2. During training, better fit was obtained for SPI-12 and SPI-24 with NSE value above 0.9 as compare to other SPIs. Similarly, the error value was least (RMSE= 0.042) for SPI-12 and followed by SPI-24 and other showing more error values ranges from 0.456 to 0.684. In case of testing, the SPI-12 and SPI-24 showed higher NSE values and lower error values (RMSE) compared to other SPIs.

Besides the quantitative evaluation, the efficacy of the ANN techniques in forecasting different SPIs was assessed by graphical indicator. Comparison of calculated and forecasted SPIs using developed model was performed using: (a) simultaneous plots of calculated and simulated time series plots; (b) scatter plot with 1:1 line. Fitting for SPI-6, SPI-12 and SPI-24 during training period are shown in the Fig. 2(a, b), Fig. 4(a, b), and Fig. 6(a, b) while fitting during testing period are shown in Fig. 3(a, b), Fig. 5(a, b) and Fig.7 (a, b), respectively. The graphs are shown only for SPI-6, SPI-12 and SPI-24. From these figures, it is clearly revealed that there is a good match for both training and testing for SPI-12 and SPI-24 compared to other SPIs. Scatter plot also indicated higher value of r^2 or better fit for SPI-12 and SPI-24 compared to other SPIs.

A comparison of testing and training result, it was found that training results were better. Hence, based on both statistical and graphical indicators it was found that SPI-12 and SPI-24 simulated well which indicated better imitation of hydrological drought in the study area which was similar to results found by other researchers (Mishra and Desai,2005**;** Belayneh and Adamowski, 2012).

Table 2. Summary of goodness-of-fit statistics for the developed ANN model

SPI	Datasets	RMSE	NSE
SPI-3	Training	0.660	0.330
	Testing	0.849	0.155
SPI-6	Training	0.684	0.531
	Testing	0.823	0.215

SPI-9	Training	0.456	0.778
	Testing	0.644	0.600
SPI-12	Training	0.042	0.998
	Testing	0.188	0.962
SPI-24	Training	0.219	0.946
	Testing	0.270	0.853
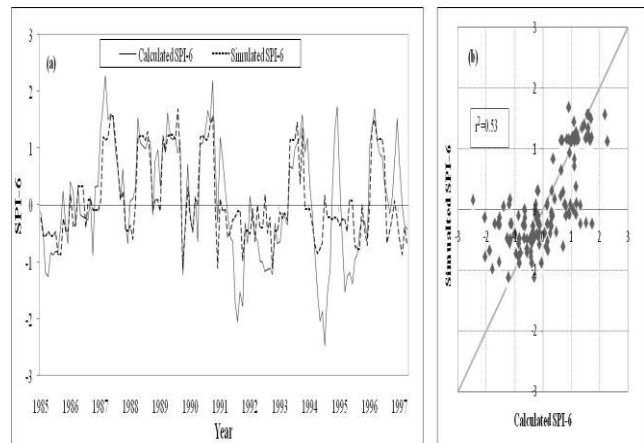
Figure 2. Comparison of calculated and simulated SPI-6 at ChinchondiPatil raingauge station during training period (1985-1997): (a) calculated and simulated time series plots; (b) scatter plot with 1:1 line.
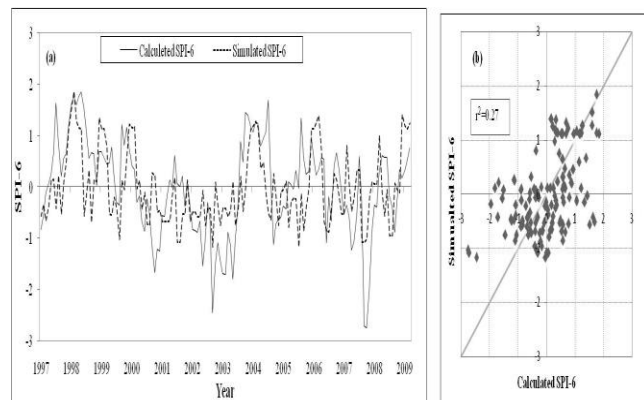
Figure 3. Comparison of calculated and simulated SPI-6 at ChinchondiPatil raingauge station during testing period (1997-2009): (a) calculated and simulated time series plots; (b) scatter plot with 1:1 line.
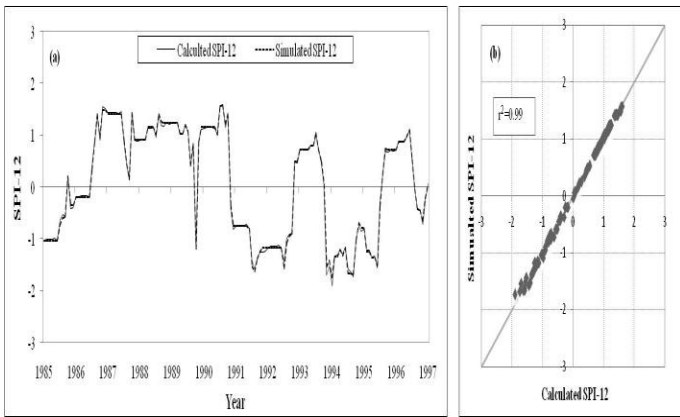
Figure 4. Comparison of calculated and simulated SPI-12 at ChinchondiPatil raingauge station during training period (1985-1997): (a) calculated and simulated time series plots; (b) scatter plot with 1:1 line.
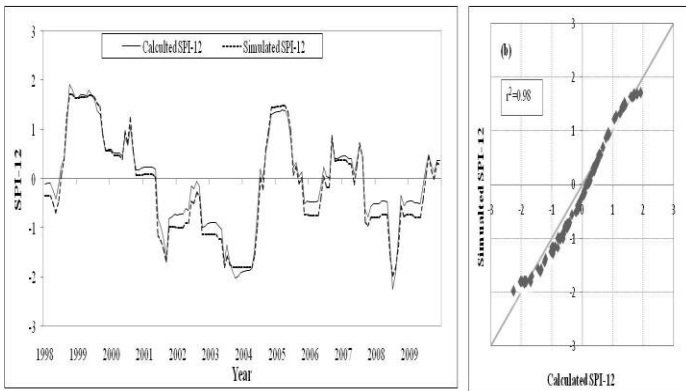
Figure 5. Comparison of calculated and simulated SPI-12 at ChinchondiPatil raingauge station during testing period (1998-2009): (a) calculated and simulated time series plots; (b) scatter plot with 1:1 line.
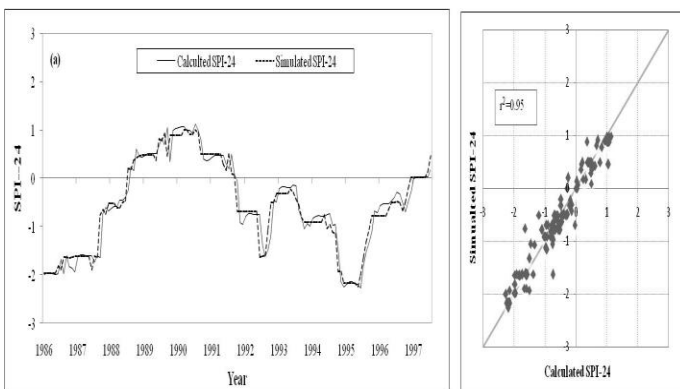
Figure 6. Comparison of calculated and simulated SPI-24 at ChinchondiPatil raingauge station during training period (1986-1997): (a) calculated and simulated time series plots; (b) scatter plot with 1:1 line.
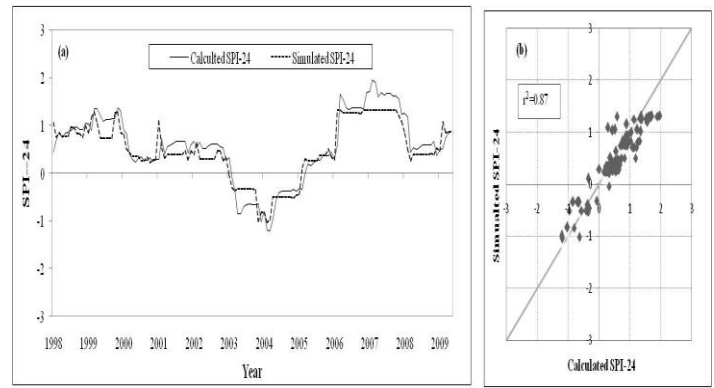
Figure 7. Comparison of calculated and simulated SPI-24 at ChinchondiPatil raingauge station during testing period (1998-2009): (a) calculated and simulated time series plots; (b) scatter plot with 1:1 line.

3. CONCLUSIONS

In this study, analysis of drought was performed using ANN for ChinchondiPatil rainguage station, Western Maharashtra (India). The statistical and graphical indicators indicated that the performances of the ANN models in simulating long-term droughts (SPI-12 and SPI-24) were reasonable. It can be concluded that the developed ANN models are capable of simulating hydrological droughts satisfactorily in the study area. The results of this study provide preliminary guidelines for future studies in this direction. Also they are useful for decision makers and water managers of the study area.

REFERENCES

i.   Adamowski J, and Chan HF (2011) A wavelet neural network conjunction model for groundwater level forecasting. Journal of Hydrology 407.1 (2011): 28-40

ii.   Belayneh A, Adamowski, J (2012) Standard Precipitation Index drought forecasting using neural networks, wavelet neural networks, and support vector regression. Applied Computational Intelligence and Soft Computing, Article ID 794061, 13 pages.

iii.   EIS (2006) Disaster Management in Maharashtra. Environmental Information System (EIS), Environmental Department, Environmental Information System (ENVIS) Newsletter, Government of Maharashtra, India, 1: 1-10

iv.   Haykin S (1994) Neural Networks. Macmillan College Publishing Company, Inc., New York

v.   Jha MK and Sahoo S. (2014) Efficacy of neural network and genetic algorithm techniques in simulating spatio-temporal fluctuations of groundwater. Hydrological Processes: DOI: 10.1002/hyp.10166

vi.   Keshavarz M, Karami E, Vanclay F, (2013) The social experience of drought in rural Iran. Journal of Land Use Policy 30:120–129.

vii.   Keskin ME., Terzi O., Taylan ED. and Kucukyaman, D (2011) Meteorological drought analysis using artificial neural networks. Scientific Research and Essays 6(21): 4469-4477.

viii.   McKee TB, Doesken NJ and Kleist J (1993) The relationship of drought frequency and duration to time scales. Proceedings of the 8th International Conference on Applied Climatology, Boston, MA, 179-184 pp.

ix.   Mishra AK and Desai VR. (2005). Spatial and temporal drought analysis in the Kansabati River Basin, India. International Journal of River Basin Management 3(1): 31-41

x.   Mishra AK, and Singh VP (2011) Drought modeling–A review. Journal of Hydrology 403(1): 157-175

xi.   Morid S, Smakhtin V, Bagherzadeh K (2007) Drought forecasting using artificial neural networks and time series of drought indices. International Journal of Climatology 27 (15), 2103-2111

xii.   Nayak P, Rao YRS, Sudheer KP (2006) Groundwater level forecasting in a shallow aquifer using artificial neural network approach. Water Resources Management 20 (1): 77–90

xiii.   Obasi, GOP (1994) WMO's role in the international decade for natural disaster reduction. Bulletin of the American Meteorological Society 75(9): 1655-1661

xiv.   Ochoa-Rivera JC (2008) Prospecting droughts with stochastic artificial neural networks. Journal of Hydrology 352(1): 174-180

xv.   PACS (2000) Drought in India: Challenges and Initiatives. Report of Poorest Areas Civil Society (PACS) Programme 2001-2008, New Delhi, India

xvi.   Ramakrishna YS, Rao GGSN, Vijayakumar P and Kesava Rao AVR. (2005) Droughts and their impact. In: K.D. Sharma and K.S. Ramasastri (editors), Drought Management, Allied Publishers, New Delhi, India, pp. 147-156.

Study Of Regional Meteorological Drought Characteristics In Rajasthan

Kumar Amrit[1], R.P.Pandey[2] and S.K.Mishra[1]

[1] Department of Water Resources Development & Management, IIT Roorkee

[2] National Institute of Hydrology, Roorkee

ABSTRACT: *Drought is a normal recurring feature of climate occurring due to less than average rainfall at a place during a given period of time, which consequently leads to short-term water deficit and economic loss. Drought characteristics refer to frequency, severity, i.e. magnitude of deficiency, and its duration. In this study, long term monthly rainfall records of 1901-2012 were used for 31 districts of Rajasthan State, which is one of the chronic water deficit States in India. The maximum rainfall deficit was 96.5% of mean rainfall in 1918 in Jaisalmer district. Besides, 1904, 1911, 1915, 1938, 1968, 1969, 1974, 1987 and 2002 also experienced huge rainfall deficit. The most severe drought event of Standard Precipitation Index (SPI) equal to -3.08 occurred in 1918. Based on SPI and Effective Drought Index (EDI) that was computed for the years 1901-2012, the northern, western, south-western, and central parts of Rajasthan had an average drought frequency of once in 3 years while the eastern, north-eastern, southern, and south-eastern parts had droughts of once in 4 years. Only Bharatpur and Chittorgarh districts exhibited average drought frequency of once in 5 years.*

Keywords: Drought frequency, Severity, Meteorological drought, SPI, EDI.

INTRODUCTION

Drought is a natural calamity, occurring due to less than average rainfall over a given period of time at given space which consequently leads to short-term water deficit and economic loss. It is an environmental disaster which attracts the attention of environmentalist, hydrologists, geologists, meteorologists, ecologists and agricultural scientists. Droughts occur when there is reduction in the amount of rainfall received over an extended period of time, such as a season or a year leads to the problems like crop failure, lowering of water table, depletion of water storage in reservoirs, reduced fodder availability and shortage of drinking water etc. The demand of water has been increased many fold due to rapid increase in population and industrial development. The happening of frequent water shortages have become a common problem in various parts of India. It is widely believed that the climate change and contamination of fresh water are also responsible for the water scarcity. In literature drought is defined in different ways. A drought is a period dominated by abnormally dry weather that lasts long enough to produce a serious imbalance in the water cycle (Zhang et al., 2012). Drought has no single definition which is acceptable everywhere. Droughts occur more frequently in the north-western, central and peninsular regions of India. Pandey et. al. (2001) studied relationship between common climatic parameters and average drought frequency in different climatic regions of India indicating that the average drought frequency decreases gradually from arid to sub humid regions. Pandey et. al. (2008) studied the various indices for drought characterization in KBK districts in Orissa, India. They compared percent of normal (PN), standard precipitation index (SPI) and effective drought index (EDI) and found that the ratio of annual precipitation to potential evapotranspiration is below 0.6 (Pa_e/PET< 0.6) in a drought year. The study reveals that the EDI is better for the identification and quantification of drought severity in the region. The researchers have used various indices viz. deciles index (DI), China-Z index (CZI), modified CZI (MCZI), PN, Z-Score, SPI and EDI for quantification of drought severity in various parts of the world and suggested that the SPI, CZI and Z score provides identical assessments of drought situation (Chumo et. al.,2011; Mishra and Singh 2012; Morid et. al.,2006). Tabari et. al (2014) studied the temperature and precipitation based aridity indices in Iran using monthly data of temperature and precipitation of 40 years (1966-2005). In this study they calculated two indices viz de Martonne aridity index(I_{DM}) and the Pinna combinative index(I_P). They found the value of I_{DM} ranged from 2 to 68 across the Iran. The higher value of I_{DM} implies humid, very humid and extremely humid climate. The I_P values less than 10 denotes the dry climate. Based on Pinna index about 96% area of the Iran classified as arid and semi-arid regions while according to de Martonne index it is about 88%. Further, it is reported that the I_{DM} is more appropriate than I_P for climatic classification (Tabari et. al. 2014). Yan-jun et. al (2012) studied the drought evolvement characteristics based on standardized precipitation index in the Huaihe river basin in China and found that the drought frequency and drought intensity have increased at the beginning of 21st century while the area of drought get decreased. The study also revealed that the occurrence of mild and moderate drought were more while the severe drought rarely occurs in the basin.

The major objective of the study is to assess the frequency, severity and the persistency of drought events in different districts of Rajasthan which may be helpful in devising strategies to deal with droughts and planning for mitigation.

STUDY AREA AND DATA USED

Rajasthan is the largest state located in western part of India encompassing area of about 342,239 km^2. Rajasthan is one of the hottest states of India. In Rajasthan, climatic conditions vary throughout the year. Rajasthan weather is usually hot and dry, yet one can see four distinct seasons in this state. These can be classified as Summers, Monsoons, Autumn (Post-monsoon) and Winters. Summer starts in April and extend up to June. During the summer the temperature varies 32^{0}C to 45^{0}C and sometimes it rise up to 48^{0}C. Monsoon season starts in July and extend up to September and it receives nearly 90% of the annual rainfall during the monsoon season.
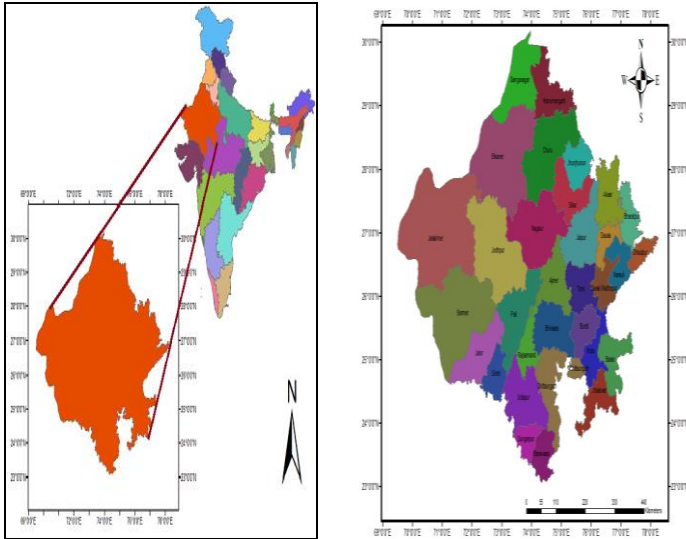
Figure-1 Location and district map of Rajasthan

For the study of long-term meteorological drought characteristics in Rajasthan, the monthly rainfall data 112 years (1901-2012) of 31 districts of the state has been used. The data were obtained from the India Meteorological Department, Pune for the year 1901-2000 and rest from year 2001 -2012 obtained from the website of Rajasthan water resource department. Some of the missing data of a given station was estimated as mean of the rainfall of the surrounding station. The data of Karauli district was not sufficient so it is excluded from analysis. The documented drought events in literature have been referred for comparison and verification of results.

METHODOLOGY

The Standardized Precipitation Index (SPI) (McKee et. al.,1993) has been used to analyze past drought events during the period from 1901 to 2012. The advantages of using SPI index are first, it is based on only on precipitation so, its evaluation is relatively easy and second, that the drought can be described on multiple time scales such as 1 month, 3 months, 4 months, 6 months, 12 months, 24 months etc. The SPI can be computed when long term time series of monthly rainfall data of at least 30 years are available. Mathematically, the SPI is based on the cumulative probability of a given rainfall event occurring at a station. The historic rainfall data of a station is fitted to gamma distribution, as the gamma distribution has been found to fit the precipitation

distribution quite well. This is done through a process of maximum likelihood estimation of the gamma distribution parameters, α and β. The rainfall data of 112 years are analyzed in SPI program for different time scale. In this study the 4-month time scale values for the month of October are taken, to evaluate the seasonal drought. On the basis of SPI values drought are classified as moderate, severe and extreme. Classification of drought on the basis of SPI values are given in Table-1.

Table-1: Classification of SPI (McKee et al.,1993)

SPI Value	Type of Drought
-1 to -1.49	Moderate
-1.5 to -1.99	Severe
-2.0 or above	Extreme

Effective drought index (Byun and Wilhite, 1999) is based on a new concept of effective precipitation which is summed value of daily precipitation with a time dependent reduction function. The daily water accumulation is considered in Effective drought index (EDI) with a weighting function for the time passage. The EDI has some advantages over other indices (Kim and Byun, 2006; Morid et. al. 2006; Mishra and Singh 2011; Pandey et al. 2008). First, it is the only index that was specifically designed to calculate daily drought severity. This enables rapid detection of drought and precise measurement of short-term drought. Second, by utilizing a calculation method that places greater emphasis on recent precipitation, it more accurately calculates the current level of available water resources. Finally, because it calculates the total precipitation period, considering the continuity of the drought period during the entire calculation process, it is distinguishable from existing drought indices that only provide a calculation for a limited period (e.g., 12 months). Therefore, it becomes possible to diagnose prolonged droughts that continue for several years (Byun and Wilhite, 1999). The EDI values also helps in classification of drought as given in the Table-2.

Table-2. Classification of EDI (Byun and Wilhite, 1999)

EDI value	Type of Drought
< -0.7 to -1.5	Moderate
<-1.5 to -2.0	Severe
< -2.0 or less	Extreme

The percentage departure of annual and seasonal rainfall from corresponding mean have been applied for identification of onset, termination, and quantification of severity of drought events. The percentage departure of the seasonal rainfall from the corresponding mean of every year for each district is calculated using IMD criteria. The IMD defined drought as a period of year or season when the deficiency of rainfall is more than 25% of the corresponding mean. On the basis of percentage departure from the mean, the seasonal drought can be classified as moderate, severe and extreme. The classification give below in Table-3.

Table-3. Classification of drought on the basis of percentage departure frainfall from mean (Pandey et al. 2008).

Percentage departure from mean (%)	Type of Drought

< -24.5 to -44	Moderate
< -44 to -60	Severe
< -60 or less	Extreme

RESULTS

The occurrence of deficit rainfall in the state often leads to critical water shortage and hardness to the society. The Standardized Precipitation Index (SPI), Effective Drought Index (EDI) and percentage departure of annual and seasonal rainfall from corresponding mean have been applied for identification of onset, termination and quantification of severity of drought events.

The percentage departure from the seasonal mean method reveals that the average return period of drought in Rajasthan varies from 3 year to 4 year. The north, north-west, west, south- west and some part of central Rajasthan including the district, Ganganaga, Hanumangarh, Churu, Bikaner, Jaisalmer, Barmer, Jalore, Sirohi, Pali, Jodhpur, Nagaur etc. have drought frequency of once in 3 years while the north-east, east, south east and southern part of the state consisting of the districts, Alwar, Dhaulpur, Dausa, Jaipur, Ajmer, Sawaimadhopur, Bundi, Kota, Tonk , Baran , Jhalawar, Bhilwara, Rajasmand, Udaipur, Banswara and Dungarpur here the average drought frequency is once in 4 years. There are only two districts Bharatpur and Chittorgarh where the average drought frequency had been once in 5 years. The magnitude of deficit has been found maximum of 96.5% of mean rainfall for the district of Jaisalmer in year 1918 besides this there had been huge rainfall deficits in the following years 1904, 1911, 1915, 1938, 1968, 1969, 1974, 1987 and 2002. The spatial distribution of return period of drought in different district of Rajasthan state is shown in Fig.2.
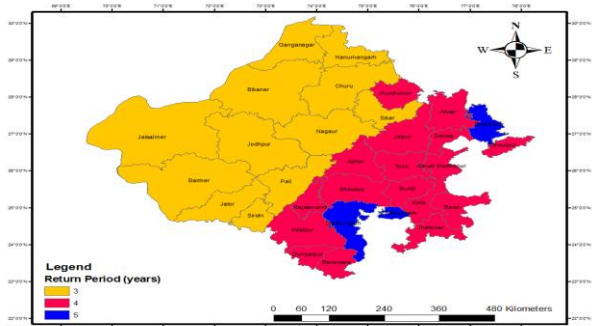
Figure-2 spatial distribution of return period of drought in different district of Rajasthan state

In this study the maximum persistence of drought in different districts has been analyzed. The maximum drought persistence in major part of the state range between 3 to 4 consecutive years. The maximum drought persistence in Bhilwara, Baran, Tonk, Chittorgarh and Udaipur districts had been estimated 2 consecutive years. The drought persisted in other parts of the Rajasthan for 3 or more consecutive years. The drought persisted for 5 consecutive years in Hanumangarh (2000-2004), Alwar (1937-1941), Dausa (1937-1941) and Jhunjhunu (2002-2006) districts. The estimates indicate that the drought persisted for 6 consecutive years in Dungarpur (1964-1969) and Ganganagar

(1934-1939) districts. The map showing spatial distribution of maximum drought persistence in various districts is presented in Fig.3.
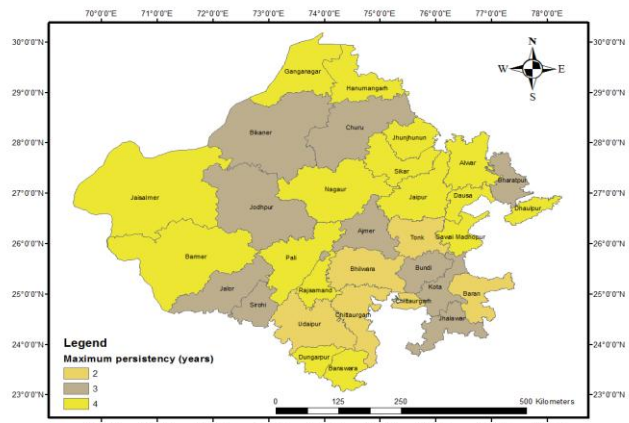
Figure-3 showing the spatial distribution of maximum drought persistence in various districts.

From the Fig.2 and Fig.3 it can be seen that area with less return period of drought having maximum drought persistence for 3 to 4 consecutive years.

The return period of drought in different districts have been computed using Effective Drought index (EDI). The estimates using EDI indicate that in Hanumangarh, Bikaner, Churu, Jaisalmer, Baran, Kota, Bhilwara districts of the Rajasthan state has the average frequency of once in 3 year. The average drought frequency of once in 4 years had been estimated in the Barmer , Jalore, Sirohi, Udaipur, Chittorgarh, Nagaur and Ajmer districts. The return period of drought had been estimated as 5 years in Rajasmand and Bharatpur districts, while the drought occurs once in 6 years in Sikar, Bundi and Dhaulpur districts. The map showing the spatial distribution return period of drought event obtained using EDI in different districts is presented in Fig.4.
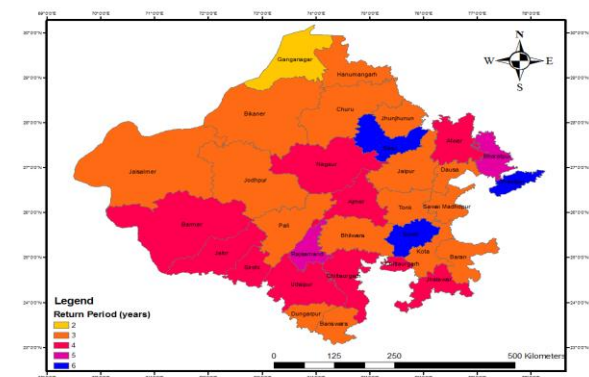
Figure-4 showing the spatial distribution return period of drought event obtained using EDI.

From Fig.2 and Fig.4 it is evident that the return period of drought computed using EDI is comparable and it is in good agreement with the estimates obtained using percentage departure from mean. The return period of drought varies from 3 to 4 years in most of the parts of the state.

Standardized Precipitation Index (SPI) is applied to assess onset and termination of drought events for 4 months time scale. To quantify the return period of seasonal droughts the SPI values below -0.99 have been investigated for the month of October. According to estimates of SPI the average frequency of drought in different districts range between once in 5 years to once in 8 years. The map showing drought return period in various districts obtained using SPI is presented in Fig.5. The estimates of drought return period using SPI appears to be different from estimates obtained using the rainfall departure method and EDI. This indicates that the SPI may not provide reasonable assessment of seasonal drought characteristics for the state of Rajasthan in India. On the other hand the estimates of drought return period using EDI are acceptable. This reveals that the EDI may provide better assessment of regional drought characteristics in the state of Rajasthan.
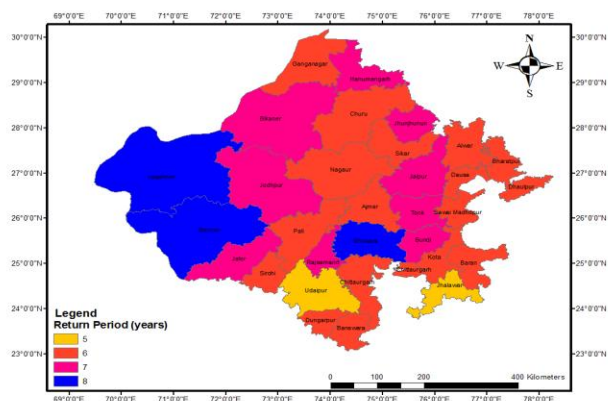
Figure-5 showing drought return period in various districts obtained using SPI.

The average frequency of severe drought events in Alwar, Banswara, Barmer, Bhilwara, Bikaner, Bundi, Churu, Dausa, Dungarpur, Ganganagar, Jaipur, Jaisalmer, Jalore, Jodhpur, Kota, Sikar, sirohi, Tonk, Nagaur, Rajasmand and Hanumangarh range between once in 5 years to once in 10 years. In other districts of Rajasthan state the return period of severe drought had been estimated to more than 10 years. The study indicated that the extreme drought events have also occurred in the state from time to time. The return period of extreme drought events had been estimated as 9 years for Barmer and Jaisalmer districts, and 10 years for Ganganagar. In rest of the districts, return period of extreme drought had been more than 10 years.

The analysis indicates that there have been numerous events of persistent drought events for 2, 3 and 4 consecutive years in different districts. The return period of persistent drought for 2, 3, and 4 consecutive years have been analyzed for different districts and the details are given in Table 4.

Table- 4 showing return period of drought in different districts

District	No. of years data anlysed	Return period of moderate drought	Return period of severe drought	Return period of extreme drought	No. of 2 year or more persistent drough	Return period of 2 year or more persisten drought	No. of 3 year or more persistent drought	Return period of 3 year or more persistent drought	No. of 4 year or more persistent drough	Return period of 4 year or more persistent drought
Ajmer	112	4	12	37	4	28	1	112	-	-
Alwar	112	4	10	56	4	28	1	112	1	112
Banswara	112	4	9	56	5	22	2	56	1	112
Barmer	112	3	5	9	11	10	2	56	1	112
Bharatpur	112	5	11	56	3	37	1	112	-	-
Bhilwara	112	4	10	22	4	28	0	-	-	-
Bikaner	112	3	10	16	10	11	2	56	-	-
Bundi	112	4	9	22	2	56	1	112	-	-
Chittorgarh	112	5	12	56	3	37	0	-	-	-
Churu	107	3	8	21	6	18	2	54	-	-
Dausa	112	4	9	56	2	56	2	56	1	112
Dholpur	112	4	11	56	5	22	1	112	1	112
Dungarpur	112	4	10	112	3	37	2	56	1	112
Ganganagar	107	3	6	10	7	15	2	54	2	54
Jaipur	112	4	9	37	4	28	1	112	1	112
Jaisalmer	112	3	5	9	8	14	4	28	1	112
Jalore	112	3	4	16	10	11	2	56	-	-
Jhalawar	112	4	28	0	2	56	1	112	-	-
Jhunjhunu	112	4	9	22	8	14	2	56	-	-
Jodhpur	112	3	6	19	9	12	4	28	-	-
Kota	112	4	14	112	4	28	1	112	-	-
Pali	112	3	6	16	10	11	3	37	2	56
Sawai madhopur	112	4	10	28	5	22	2	56	1	112
sikar	112	3	6	19	6	19	3	37	1	112
Sirohi	112	3	7	12	12	9	3	37	-	-
Tonk	112	4	9	22	3	37	0	-	-	-
Udaipur	112	4	12	112	6	19	0	-	-	-
Nagaur	110	3	7	12	6	18	2	55	2	55
Rajasmand	112	4	7	16	5	22	2	56	1	112
Baran	112	4	12	37	4	28	0	-	-	-
Hanumangarh	107	3	10	21	7	15	4	27	3	36

SUMMARY AND CONCLUSIONS

The meteorological drought events in different districts of Rajasthan State were analyzed using long-term rainfall records of 112 years (1901-2012). The analysis revealed that the major part of the State has the average drought frequency ranging from once in 3 years to once in 4 years. There are only two districts namely Bharatpur and Chittorgarh where the average drought frequency had been once in 5 years. The estimates of drought return period obtained using EDI were comparable with those of percentage departure from mean method. EDI was found to have provided a reasonable assessment of drought characteristics in the State of Rajasthan. The estimates of drought return period and drought persistence using SPI were quite different from that if EDI and percentage departure from mean method. There had been several persistent drought events for 2, 3, and 4 consecutive years in different districts; the first of which was quite frequent and it is one of the unique features of hydrologic extremes in the region.

REFERENCES

i. Byun H. R. and Wilhite Donald A., 1999. Objective Quantification of Drought Severity and Duration. Journal of Climate. 12, pp. 2747–2756.

ii. Chumo J. K., Ng'etich W. K., Ucakuwun E. K., Sharma T. C. and Rao M. S. 2011. Using Indices to Study Drought Variability in The Lake Victoria Basin, International Journal of Current Research 3, pp.361-364.

iii. Hisdala H., Tallaksen Lena M., 2003. Estimation of regional meteorological and hydrological drought characteristics: a case study for Denmark. Journal of Hydrology 281, pp. 230–247.

iv. Kim, Y.W., Byun, H.R., 2006. On the causes of summer droughts in Korea and their return to normal. Journal of Korean Meteorological Society 42, pp. 237– 251.

v. McKee T.B., Doesjen, N.J and Kelist, J. 1993. The relationship of drought frequency and duration to time scales, 8th AMS Conference on Applied Climatology, Anaheim CA.,

American Meteorological Society, pp.179-184, January17-22, 1993, Boston.

vi. Mishra Ashok k, Singh V. P. 2010. A review of drought concepts, Journal of hydrology, 391, pp. 202-216.

vii. Mishra Ashok k, Singh V. P. 2011. Drought modeling- A review, Journal of hydrology, 403, pp. 157-175.

viii. Mishra Ashok K, Singh V. P. 2012. Simulating hydrological drought properties at different spatial units in United States based on wavelet-Bayesian regression approach. Earth Interactions, 16,pp.1-23.

ix. Morid Saeid, Smakhtin Vladimir, Moghaddas Mahnosh 2006. Comparison of seven meteorological indices for drought monitoring in Iran, International Journal of Climatology 26, pp. 971-985.

x. Pandey R.P., Ramasastri K.S 2001. Relationship between the common climatic parameters and average drought frequency. Hydrological Processes. 15, pp. 1019-1032.

xi. Pandey R.P., Dash B.B., Mishra S. K. and Singh Ranvir, 2008. Study of indices for drought characterization in KBK districts in Orissa, India. Hydrological Processes 22, pp.1895–1907.

xii. Pandey R.P., Ramasastri K.S 2002. Incidence of droughts in different climatic regions, Hydrological Sciences Journal, 47, pp. S31-S40.

xiii. Pandey R.P., Pandey Ashish, Galkate Ravi V., Byun H.R, Mal Bimal C., 2010. Integrating Hydro-Meteorological and Physiographic Factors for Assessment of Vulnerability to Drought, Water Resource Management, 24, pp. 4199-4217.

xiv. Tabari H., Talaee Hosseinzadeh P., Nadoushani S.S. Mousavi, Willems Patrick, Marchetto Aldo, 2014. A survey of temperature and precipitation based aridity indices in Iran, Quaternary International xxx pp. 1-9.

xv. Yan-jun, L., Xiao-dong, Z., Fan, L., & Jing, M. 2012. Analysis of Drought Evolvement Characteristics Based on Standardized Precipitation Index in the Huaihe River Basin. Procedia Engineering, 28, pp.434–437.

Zhanga Qiang, Xiao Mingzhong, Singh Vijay P. & Li Jianfeng 2012. Regionalization and spatial changing properties of droughts across the Pearl River basin, China. Journal of Hydrology 472–473, pp.355–366.

Modeling Of Potential Evaporation For A Humid River Basin Located In Western Ghats Of India

B. Venkatesh
Scientist, National institute of Hydrology,
Hanuman Nagar, 2nd Stage, Belgaum, Karnataka – 590 019.
India
bvenki30@yahoo.com

ABSTRACT: *Potential evapotranspiration is an important index of hydrologic budget at different spatial scales and it is a critical variable for understanding regional biological processes. Several models have been used in computing reference evapotranspiration. This study aims at identifying a suitable alternative method to FAO-56 PM method for estimating the PET in Western Ghats region covering Northern part of Karnataka. In the present analysis, performances of 3 radiation based methods (Makkanik, Turc and Priestly-Taylor) and 2 temperature based (FAO-56 based Hargreaves and Hamon) methods were compared with the FAO-56 PM method using the daily climatic data of Santibestwad station located in Malaprabha basin. The data for a period of 3 (2010-2012) years pertaining to temperature, wind speed, humidity minimum and maximum temperature were used. ET_0 estimation of all these equations were statistically compared for daily time step. Among the ET_0 methods evaluated, estimates obtained by the TURC (temperature based) method was closest to the FAO-56 PM method at daily time step. In order to provide simpler ET_0 estimation tools, a regression equations were developed for preferred FAO-56 PM ET_0 estimates in terms of ET_0 estimates by the simpler methods and validated for each climate. Overall, these results indicated that, the simpler equations have yielded better estimates of ET_0 with smaller error for daily time step in this part of Western Ghats.*

Keywords: Evapotranspiration, Western Ghats, Hargreves, Turc, regression equation

1. INTRODUCTION

Evaporation from a watershed is one of the major components of the hydrological cycle. Although there is an adequacy of the network established for measuring precipitation, only very few measurements of the evapotranspiration (ET_0) were made. Direct measurements of ET_0 at watershed level are rather difficult and therefore needs to be estimated by indirect methods. Two different kinds of indirect methods are used to calculate ET_0 from a watershed. The first kind is one which uses the water balance of watershed to estimate actual ET_0. The accuracy of ET_0 estimates by this method depends on the quality of runoff and precipitation data. There are approximately 50 methods or models available to estimate PET, but these methods or models give inconsistent values due to their different assumptions and input data requirements, or because they were often developed for specific climatic regions. Equations for determining evapotranspiration can be grouped into several categories including the energy budget, empirical, semi empirical and combination. Most of the equations were developed for use in specific studies and were appropriate for use in climates similar to where they were developed. The classical empirical equations are often used in Regional Climate models not only for reconstructing past climate situations but for future climate change scenarios. Some of these equations have been applied to open-water surfaces and water bodies. The numerous equations for estimation of evapotranspiration have a wide range of data requirement.

The generalization and data availability are often the two major factors influencing the estimation of PET as most of the empirical methods were originally developed on the past local climate conditions. Firstly, due to inherent limitation of empirical equations and the complicate mechanism of ET

process, the generalization of the empirical methods must be checked and calibrated before applying to local areas. Secondly, the data requirements for different methods vary from location to location. This is especially true in mountainous region where climate change from one location to other location.

Mountain areas are assumed to be the main sources of runoff generation for many rivers system. Therefore, there have been many studies carried out to understand the possible impact of changing land covers and climatic scenarios on runoff generation mechanisms in the mountainous regions especially in Himalayas and Western Ghats regions. In the Western Ghats region, unlike the studies related to understanding the spatial and temporal variation of rainfall, no in-depth studies have been

Keeping in view of the above, the present study aims at comparing five empirical methods with FAO56-PM method as standard criteria for two stations of different climatic conditions. This work would help in understanding and parameterizing different ET models to the climate prevailing in the Western Ghats region. The empirical methods chosen include one combination method (Penman-Monteith), two radiation based (Makkink, and Priestley-Taylor) and three temperature based (Hargreaves, Hamon, and Turc) methods have been analyzed in present report.

2.0 STUDY AREA AND DATA AVAILABILITY

The station characteristics and the length of available for the selected station is described in the Table 1.

Table 1 Details of Santibestwad station

Station	District	Taluk	Latitude (North)	Longitude (East)	Altitude (mamsl)	Climate	Data Period
Santibestwad	Belgaum	Belgaum	15 46 30	74 20 51	762	Sub-Humid	2009-2012

The study area is shown in Figure1
Santibestwad station situated on the leeward side of the Western Ghats at an elevation of 762m from MSL. The station experiences a very high temperature of about 38°C with a average relative humidity of 90%. A plot of the data used for computation of ET values are presented in Figure.2.

carried out to generalised the Evapotranspiration models to the region. In the recent time, there is a dramatic change in the land cover has been reported. The change in the land cover might influence the variation of Evapotranspiration in the region and thus the water balance component. In this changing land cover and climatic scenarios, it assumes a greater importance to identify a suitable alternative method to the FAO-56 Penman-Monteith method, which would help in understanding and parameterising the changes that occur at the scale of the hydrological cycle and the consequences for water resources. The concept of a reference evapotranspiration (*ETo*) can be used to estimate the climatic effect on evapotranspiration and represents the evapotranspiration from a hypothetical reference surface.
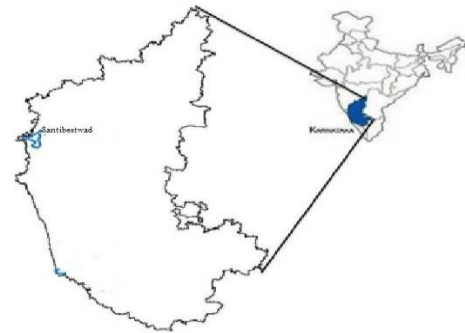
Fig.1. Location of hydro-meteorological stations used in the study
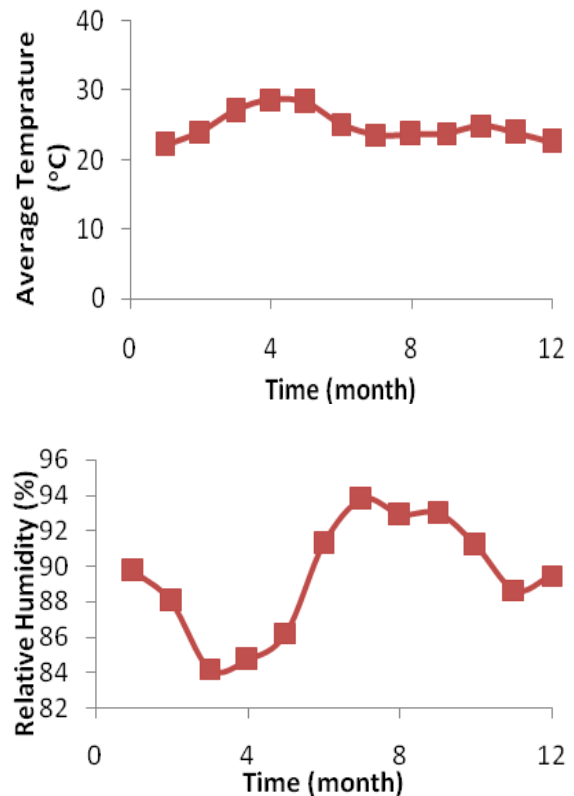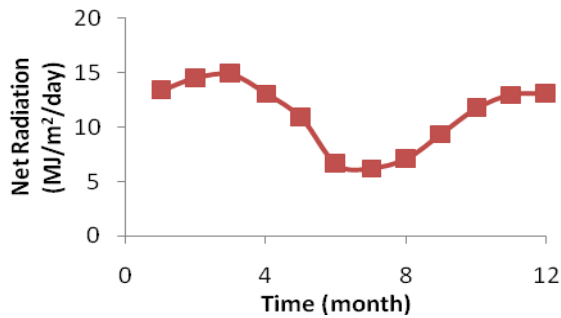
Fig 2 Input Parameters used in the calculation of ET_0

3.0 METHODOLOGY

Table 1 lists details of the climate station considered in the analysis. The station is maintained by the Water Resources Department of Govt. of Karnataka. This station is equipped with standard ground-based instruments; alcohol and wet-bulb thermometers, sunshine recorder, cup anemometer, and mercury thermometers. Readings are taken twice a day at 0830 and 1730 hrs. Data is scrutinized and subjected to quality checks prior to supply to users. For each station, the data set used in this study comprised daily values of maximum air temperature (Tmax), minimum air temperature (Tmin), maximum relative humidity (RHmax), minimum relative humidity (RHmin), actual hours of sunshine (n), 24 h wind speed (u_2) at 2 m height, and pan evaporation depth ($e$pan). Site details required in ET_0 calculations are: altitude (z) above mean sea level, height (zw) at which wind speed is measured, latitude and longitude of the station. Individual data records for each station were converted in to the utilizable format for the computation of ET_0. Climatic variables as per procedures described in FAO56-PM have been calculated as the first step. Further all the other nine methods have been implied for all the eight stations.

3.1 ET_0 METHODS AND CALCULATIONS

ET_0 estimation methods included in the comparative analysis are listed in Table 2 Other than the FAO-56 PM combination method that was used as the benchmark method, five other ET_0 estimation methods included in the analysis are: Makkink, Hamon, Hargreaves, Priestley–Taylor and Turc. The details of each of the method is given in Table 2 and data required for computing ET_0 in Table 3.

Table 2 Details of PET methods

Methods	Basic equation	Developed for
Combination group		
FAO56 -Penman- Monteith	$ET_0 = \dfrac{0.408*\Delta*(R_n-G)+\gamma*((900*U_2)/(T+273))(e_s-e_a)}{\Delta + \gamma*(1+0.34*U_2)}$	Daily
Solar Radiation, Temperature group		
Makkink	$ET_0=0.61*(\Delta/(\Delta+\gamma))*(R_s/2.45)-0.12$	Daily
Priestly- Taylor	$ET_0= \alpha*(\Delta/(\Delta+\gamma))*Er$	Daily

Temperature Group		
Hamon	$ET_0= \dfrac{29.8*N*e_s(T)}{(T+273.2)}$	Daily
Turc	RH < 50 percent $ET_0=0.013*(T/(T+15))*(R_s+50)*(1+(50-RH)/70)$ RH > 50 percent $ET_0=0.013*(T/(T+15))*(R_s+50)$	Daily
Hargreaves	$ET_0=0.0023*(T+17.8)*(T_{max}-T_{min})0.5 *R_a$	Daily

*The meaning and units of symbols in the six empirical PET methods, if not expressed explicitly, are the same to those of Penman-Monteith method.

Table 3 Data requirement for various methods

Sl. no	Methods	Type	Temperature	Radiation	Relative Humidity	Others
1	Penman- Monteith	Combination	T_{mean} (daily)	R_n, R_a	-	U_2, e_s, e_a, γ , Δ
2	Makkink	Radiation	T_{mean} (daily)	R_{ns}	-	Δ
3	Priestly-Taylor	Radiation	T_{mean} (daily)	R_n, R_a	-	
4	Hamon	Temperature	T_{mean} (daily)	-	-	Day time length, calibration coefficient
5	Turc	Temperature	T_{mean} (daily)	R_{ns}	RH_{mean} (daily)	
6	Hargreaves	Temperature	T_{max},T_{min}	R_a	-	

4. RESULTS AND DISCUSSIONS

The data available from 2010 to 2012 for all the stations considered in this study were used to estimate the Evapotranspiration by 6 ET_0 methods on daily basis. In order to compare the results, the mean daily ET_0 values were obtained by averaging daily results across the period of record are Tabulated in Table 4, and mean monthly values of ET_0 are tabulated in Table. 5.

Table 4. Mean daily ET_0 estimates

Stations	Combination Group	Radiation, temperature Group	Temperature

	PM	MK	PT	T	HRG	HM
Santibe stwad	2.98	2.93	4.13	3.62	4.52	3.77

*PM-FAO56-PM, MK-Makkink, PT-Priestley Taylor, HM-Hamon, T-Turc, HRG-Hargreaves.

Table. 5 Mean Monthly ET_0 estimates for all the stations

Station	Method	Evapotranspiration values (mm)											
		Jan	Feb	March	April	May	June	July	Aug	Sept	Oct	Nov	Dec
Santibestwad	PM	3.63	4.1	4.59	4.19	3.30	1.60	1.19	1.51	2.20	3.28	3.69	3.64
	MK	3.58	3.96	4.18	3.69	3.06	1.70	1.56	1.78	2.44	3.14	3.54	3.56
	PT	4.88	5.45	5.84	5.26	4.33	2.54	2.32	2.65	3.53	4.48	4.87	4.79
	Tu	4.27	4.69	4.96	4.47	3.79	2.33	2.17	2.40	3.09	3.8	4.26	4.26
	HRG	5.63	6.41	6.86	6.07	4.65	2.88	2.32	2.69	3.48	4.66	4.89	5.36
	HM	3.01	3.47	4.25	4.82	4.85	4.14	3.75	3.69	3.58	3.66	3.36	5.4

Fig.3 . Temporal variation of Evapotranspiration at Santibestwad Station

Comparison of different PET estimation methods are based on both temporal character and spatial similarities. Among the three groups of empirical PET methods, Makkinik and Turc method show a similarity in the temporal variation with FAO56 PM method (Figure 3). Wheras, the Hamon based method showed the dis-similarity. Comparisons between the FAO56-PM method and the other methods are particularly relevant, given the popularity of the latter method among Indian practitioners. This is more clearly evident from the scatter plots shown in Figure 4, in which daily comparisons for the individual days of record are shown.

The Co-efficient of determination were calculated for each individual methods across all the stations with the FA056-PM method. From Table 8 it's seen that Hargreaves, Makkink, Turc and Priestley-Taylor methods have noticeable correlation with the P-M method. Various performance statistics were computed for each station on the basis of individual comparisons between daily ET_0 estimated by the FAO-56 PM method and each of the other methods. Methods were ranked separately on the basis of SEE, STDEV, and R^2 values. Since each statistic highlights a different aspect of model performance, an "overall" rank number calculated as the average of rank numbers from the three statistics was also computed for each method. From these results Table 8, it is evident that for a given ET_0 method, considerable differences exist in rank numbers derived from the performance statistics and, therefore, the overall rank may prove useful in selecting the best method.

2012	Pre-Monsoon	607.36	910.12	795.86	573.61	687.08	615.51
	Monsoon	188.94	349.59	313.91	209.28	284.78	459.53
	Post-Monsoon	327.83	472.68	425.72	310.5	375.42	312.3

A comparison of the ET values computed for FAO-56 PM method for Santibestwad reveal that, the higher ET_0 amounts are observed. during the monsoon and post-monsoon months. This is may be due to the difference in the temperature and humidity (Figure.2) at these stations. It is seen from the Figure 2 that, the temperature and humidity are higher during the post-monsoon season at Santibestwad. Further, it can be noticed from the Figure 5, that, July month is recorded the lowest value for the station. It is observed that the FAO-56 PM and Makkanik method have the temporal similarities in almost all months.

Fig 5 Comparison of all the Six methods for Santibestwad stations.

4.2 REGRESSION EQUATION

The daily ET_0 values estimated by each empirical method and Penman-Montheith method are used to develop a regression relationship, where the FAO-56 PM ET_0 values considered as the dependent variable and the alternative simpler method as the independent variable. Equations ere developed for only those methods which were ranked among the top three on the basis of daily SEE values (Table.8). A part of the available climatic data was used for developing the relationship and the remaining part was used for validating the developed equations. The performance of the equations were assessed in terms of SEE and R^2 values obtained in the validation phase through the comparison of daily PM ET_0 values estimated by FAO-56 procedures and those obtained from the regression equations.

The forms of the established regression equations and their associated validation performance statistics are listed in Table.8. Figure. 4 show a scatter plot of these comparisons for each of the three top methods for each of the climatic stations considered for analysis. On comparing these statistics with the one listed in the Table.8, it can be seen that in all cases the developed regression equation perform much better than the original equations in yielding daily ET_0 estimates comparable to the FAO-56 PM method.

Fig 4 Comparison between Monthly ET_0 estimates by FAO-56 PM for Santibestwad station with other empirical methods respectively: Hargreaves; Preistley-Taylor; Makkink ; Turc; and Hamon.

4.1 SEASONAL VARIATION OF ET VALUES

The Seasonal ET values for three distinct seasons of the Western Ghats are computed for both the stations and are Tabulated in Tables 6 and Table 7. From these tables it is noticed that, there is a distinct difference between the values of ET in each of the season. The lowest amount is noticed during the Monsoon season in all the methods as these months (June, July, Aug and Sept) are colder compared to that of other months. The humidity is higher during these months with very little sunshine hours. Similar is the trend during the Post-monsoon months (Oct, Nov, Dec and Jan). However, the pre-monsoon months have higher ET values.

Table. 7: Seasonal values of ET for Santibestwad Station

Year	Season	PM	Har	PT	Mak	Turc	Hamon
2010	Pre-Monsoon	594.34	892.43	752.92	531.03	643.33	648.51
	Monsoon	209.23	359.08	357.56	243.53	321.35	473.45
	Post-Monsoon	307.47	418.62	421.68	301.94	366.09	306.24
2011	Pre-Monsoon	596.08	883.49	787.16	570.25	681.92	591.09
	Monsoon	195.57	329.33	337.31	229.92	306.71	453.34
	Post-Monsoon	340.19	480.1	452.71	330.08	395.75	309.39

Table 8. Regression Statistics for Daily ET$_0$ Comparisons with FAO-56 PM method

Station	Method	Regression Equation	SEE (mm/day)	STDEV (mm/day)	R^2	Overall Rank
Santibestwad	Har	0.703X-0.200	0.435	0.796	0.753	4
	PT	0.893X-0.732	0.866	1.05	0.922	4
	Mak	1.132X-0.335	0.299	0.269	0.911	2
	Turc	1.074X-0.904	0.211	0.257	0.917	1
	Hamon	0.277X+1.937	0.730	1.406	0.019	5

Table 9. Recommended methods for ET$_0$ estimation for the stations considered for analysis

Stations	Recommended methods
Santibestwad	TURC

From the analysis it is found that, the TURC method performs (Table.9) better under both climate and there fore it is recommended as the empirical methods for estimating the ET$_0$ values for these stations.

5.0 SUMMARY

The present study was aimed at identifying an alternative method of ET$_0$ estimation for data deficit region of Western Ghats by using the observed data of Santibestwad in Karnataka. The observed data for 3 years starting from 2010 to 2012 were used to estimate the ET$_o$ values using 5 different methods were compared with FAO-56 PM method. Following observation are made based on the results obtained through the analysis;

1.   At both the station, the Hargreaves method forms the upper bound and Makkanik method formed the lower bound of ET$_0$ values.
2.   The performance statistics shows that, the TURC method performed better at both the stations. However, the temporal variation indicates that, the method is always estimated higher value than FAO-56 PM method

In conclusion, it can be stated that, considering the data requirement and the performance of different methods for estimating the ET$_0$ vlaues, the TURC method is best suited for both the stations.

REFERENCES

i.   Allen RG, Pereira LS, Raes D, Smith M, (1998), "Crop evapotranspiration. Guidelines for computing crop water requirements", Irrigation Drainage Paper no.56, FAO, Rome, Italy, pp 300.

ii.   Doorenbos J, Kassam AH, (1979) Yield response to water. FAO Irrigation and Drainage Paper No. 33, Food and Agriculture Organisation, Rome Italy, 193pp.

iii.   Irmak, S., Allen, R.G., and Whitty, E.B., (2003) Daily gras and alfalfa-reference evapotranspiration estimates and alfalfa-to-grass evapotranspiration ratios in Florida, Journal of Irrigation and Drainage Engineering, **129(6)**, 440-448.

iv.   Jensen, M.E., Burman, R.D., and Allen, R.G., (1990) Evapotranspiraiton and Irrigation Water Requirement, ASCE manuals and reports on Engineering Practice, No.70, ASCE, New York.

v.   Mohan S, (1991) Intercomparison of evapotranspiration estimates. Hydrological Science Journal, 36(5), 447-460.

vi.   Nandagiri L, Kovoor GM, (2006) Performance Evaluation o Reference Evapotranspiration Equations across a range of Indian Climates, Journal of Irrigation and Drainage Engineering, ASCE, **132(3)**, 238-249.

vii.   Xu C-Y, Singh VP, (2001) Evaluation and generalization of radiation based methods for calculating evaporation. Hydrological Processes, 15: 305-319.

viii.   Zhao C, Nan Z, Cheng G, (2005) Evaluating methods of estimating and modeling spatial distribution of evapotranspiration in the Middle Heihe river basin, China. American Journal of Environmental Science, 1(4), 278-285.

Trend Assessment For Extrem Rainfall Indices In The Upper Mahanadi With Reference To Climate Change

R.K. Jaiswal[1]   H.L. Tiwari[2] A.K. Lohani[3]
[1]Scientist, GPSRC, National Institute of Hydrology, WALMI Campus, Bhopal (M.P.) India
[2]Astt. Professor, Maulana Azad National Institute of Technology, Bhopal (M.P.)
[3]Scientist, National Institute of Hydrology, Jal Vigyan Bhavan, Roorkee (Uttarakhabd) India
E-mail of Corresponding Author: rkjaiwal_sagar@yahoo.co.in

ABSTRACT: *Assessment of climatic variability is an important aspect in water resources management, adaptability and reducing impact on agriculture production due to changing climate. The intergovernmental panel on climate change (IPCC) in their various reports indicated that the global temperature is increasing due to emission of greenhouse gases, industrialization, change in lifestyle and land-use/ land-cover change. These and natural forces have contributed to change in earth's climate over 20th century by warming of land and ocean surface temperature, changing in spatial and temporal pattern of precipitation, rising in sea levels and increase in frequency and intensity of Al Nino. Various studies in the past have confirmed that global temperature is rising continuously since start of industrial age that may impact surface runoff, groundwater, availability of water, water quality, crop production and livelihood of society. Precipitation being the primary input in hydrological cycle needs to be investigated for possible climate change using GCMs/RCMs or statistical analysis. In the present study, an attempt has been made to identify significant trends in monthly, seasonal rainfall and different extreme rainfall indices proposed by World Meteorological Organization (WMO) and Expert Team on Climate Change Detection and Indices (ETCCDI) considering suitability for Indian rainfall conditions in six rain gauge stations namely Ambagarh, Bhanpura, Balod, Dhamtari, Kanker and Murumsilli of upper Mahanadi catchment. The river Mahanadi is an important river for water resources development in Chhattisgarh State of India and availability of water may adversely be affected due to possible change in precipitation regime. For identification of trends, long term rainfall data from 1960 to 2012 have been used to compute extreme rainfall indices including maximum one-day rainfall (RX1D), maximum 5-days rainfall (RX5D), heavy*

precipitation days (R7.5cm), very heavy precipitation days (R12.5cm), moderate wet days (R75P), very wet days (R95P), precipitation friction due to moderate wet days (R75PTOT), precipitation friction due to very wet days (R95PTOT) and simple daily intensity index (SDII). The Mann Kendal's and Spearman Rho's test were used to identify significant trend in extreme rainfall indices at 5 % significant level. The results of analysis indicated that simple daily intensity index indicated no significant trends in any rain gauge stations while rising trend in very heavy precipitation days (R12.5cm) in most of the station. Dhamtari and Murumsilli stations showed significant rising trend in moderate wet days and very wet days related extreme indices, while extreme indices series of Bhanpura and Balod stations were found random without any significant trend.

Keywords: Climate change, extreme rainfall indices, Mann Kendal's test, Spearman Rho's test, R75TOT (precipitation friction due to moderate wet days), R95TOT (precipitation friction due to very wet days)

1. INTRODUCTION

Various reports of Intergovernmental panel on climate change (IPCC) confirmed that the global temperature is rising due to increasing concentration of greenhouse gases causing negative effects on water resources, environment, health, agriculture, ecology etc. The atmospheric concentrations of green house gases have increased since 1750 due to human activities, primarily the combustion of fossil fuels and changes in land-use/land-cover (Trenbert et al 2007). Increase in land and ocean surface temperature, spatial and temporal change in rainfall, sea levels rise, increase in frequency and increased intensity of extreme events are very likely due to human intervention and other natural forces (IPCC 2002). The latest report of IPCC included another aspect of change in precipitation regime and expected more sever wet extreme in many areas where mean precipitation projected may decreased, resulting more flooding in Asian monsoon and other tropical region (IPCC 2007). The temperature and precipitation are the most commonly used meteorological variables to assess the climate change with the help of statistical tests and/or circulation model results. The distribution of precipitation varies spatially and temporally governed primarily due to atmospheric circulation, moisture availability and terrain effects (Wang & Zhou, 2005; Xuet al, 2007) needs to be investigated for future floods and droughts scenarios due to inevitable climate change conditions.

The parametric and non-parametric tests are commonly used to assess the possible trends in long term series of climatic variables by many researchers throughout the world (Serra et al 2001; Partal and Kahya 2006; Boroujerdy 2008; Sabohi 2009; Shirgholami and Ghahraman 2009; Al Buhairi 2010; Karpouzos *et al* 2010; Roshan *et al* (2011); Croitoru *et al* 2012; Bavani et a. 2012 etc.). Parthasarathy & Dhar, 1974 analyzed trend in annual rainfall for the period 1901–1960 in central India and the adjoining parts of the peninsula and concluded a positive trend existed in central India while some part of eastern India

experienced a decreasing trend. Modarres & Dasilva (2007) investigated annual rainfall and monthly rainy days of twenty rain gauge stations in Iran for assessing the impact of climate change using Mann Kendall test and found no significant climatic change in precipitation regime. Jain & Kumar, 2012 reviewed various studies on trend analysis of temperature and rainfall and concluded that there were no clear trend in annual, seasonal and monsoon rainfall on country scale but some pockets experienced a significant long term trend in rainfall. Kumar et al, 2010 conducted trend assessment on rainfall for 30 sub-divisions in India, found Chhattisgarh sub-division exhibited a significant downward trends out of 15 sub-divisions showing decreasing trend in annual rainfall.

Guhathakurta et al, 2011 carried out a study on extreme rainfall events and flood risk due to impact of climate change in India using records of 6000 stations from 1901-2005. The frequency analysis was carried out to analyze the changing probability of extreme events to determine change in flood risk and results showed significant decrease trends over central India and many parts of north India, while increasing trend were witnessed over peninsular India. Bavani et al (2012) applied parametric (linear regression analysis) and non-parametric (Mann-Kendall test) approaches on long –term annual temperature and precipitation from 1968 to 2008 in west Azerbaijan of Iran and observed an abrupt change around 1998. The temperature series showed an increasing while precipitation series indicated a falling trend. From the review of literature, it has been observed that limited studies have been carried out in the past on extreme events of precipitation and other variables although there were enough evidences of increasing extreme events due to climate change worldwide. In the present study, nine different rainfall extreme indices of precipitation considering the rainfall behavior in Indian monsoon has been computed for six rain gauge stations in upper Mahanadi catchment. The trends in these series were determined with the help of Mann-Kendall and Spearman rho's tests for detection of significant trend due to possible climate change.

2. STUDY AREA AND DATA USED

2.1 Study Area

River Mahandi is an important river of Chhattisgarh state amongst the twelve major river basins in India. It is the prime source of water for domestic, industrial, irrigation, power generation in the state. The river rises at an elevation of about RL 442.00 m. above msl at latitude $20^{\circ}20^{'}$N and longitude $82^{\circ}0^{'}30^{''}$E near Nagri village. Initially the river flows in west direction up to Kanker, where it takes a sharp turn to northeast direction. After the confluence with one of its major tributary Seonath, the river takes an easterly course and continues to flow in this direction till it leaves Chhattisgarh state and enters Orissa state of India. The basin lies between longitude 83°30'E and 84°50'E and latitude 19°20'N and 23°35'N. The total length of the river is 851 km and the catchment area of the river is about 1, 41, 589 km^2. The river has 25 major tributaries with catchment area exceeding 250 km^2 out of which 18 lies wholly in

Chhattisgarh. The river Seonath is the longest tributary which is 383 km long and lies partly in Chhattisgarh and Maharashtra with a catchment area of 30, 523 km^2. The Mahanadi basin is saucer shaped basin has boundary on north by the Baghelkhand plateau (Sarguja and Sahdol district) and central India hills; on the south and east by the Dandakarnya plateau and the Eastern ghats and on the west by Satpura Maikal ranges. The basin is fed by both south west and south east monsoon. The rains commence by second week of June and last till the end of September. Average annual rainfall is 1420 mm. About 90% rainfall occurs during the monsoon month (June to September) and the balance 10% is distributed in the winter and summer months.

Figure 1. Base map of the study area
2.2. Data Used

In the analysis, rainfall data from 1960 to 2012 of Kanker and Murumsilli, 1970 to 2012 of Gangrel, Ambagarh, Balod and Bhanpura in upper Mahanadi catchment have been used for computation of trends in extreme rainfall indices.

3. METHODOLOGY

The methodology for assessment of impact of climate change rainfall consists of computation of time series of nine extreme precipitation indices from the list of extreme indices suggested by World Meteorological Organization (WMO, 2006) and Expert Team on Climate Change Detection and Indices (ETCCDI) on the basis of suitability under Indian condition (Joshi & Rajivan, 2006). Mann-Kendal and Spearman rho's tests were applied in these series of indices to determine significant trend.

3.1 Extreme Rainfall Indices

3.1.1 Heavy precipitation days (R7.5cm)

The heavy precipitation days are the number of days with rainfall more than 7.5 cm in a period/year. Let R_{ij} be the daily rainfall on i^{th} day of jth period/year, the heavy precipitation days (R7.5cm$_j$) may be the count of the days where precipitation is more than 7.5 cm.

$$RX7.5cm_j = Count\lfloor R_{ij} > 7.5\ cm \rfloor$$

(1)

3.1.2 Very heavy precipitation days (R12.5cm)

The very heavy precipitation days are the number of days with rainfall more than 12.5 cm in a period/year. Let R_{ij} be the daily rainfall on i^{th} day of jth period/year, the heavy precipitation days (R12.5cm$_j$) may be the count of the days where precipitation is more than 12.5 cm.

$$RX12.5cm_j = Count\lfloor R_{ij} > 12.5\ cm \rfloor$$

(2)

3.1.3 Maximum one-day rainfall (RX1D)

The maximum one-day rainfall (RX1D) is the highest rainfall in one day period. Let R_{ij} be the daily rainfall on i^{th} day of jth period/year, the maximum one-day rainfall for j^{th} period (RX1D$_j$) will be:

$$RX1D_j = Max\lfloor R_{ij} \rfloor$$

(3)

3.1.4 Maximum 5-days rainfall (RX5D)

The maximum 5-day rainfall may be defined as the highest rainfall amount in five-day period. Let, R_{kj} be the total rainfall k^{th} interval of 5-days for j^{th} period/year. Here, k is the last day of 5-day interval. The $RX5D_j$ for a period j can be defined as:

$$RX5D_j = Max\lfloor R_{kj} \rfloor$$

(4)

3.1.5 Moderate wet days (R75P) and very wet days (R95P)

The moderate wet days (R75P) are the number of days having rainfall more than 75 percentile of the long period. Let R_{wj} be the precipitation series of wet day (R_{wj}>1mm) in $j= 1,2,3---n$ period/year. The probability analysis of R_{wj} is used to compute 75 percentile (R_{w75}). Now, moderate wet day will be the count of the days where rainfall is greater than R_{w75} in R_{wj} series.

$$R75P_j = Count\lfloor R_{wj} > R_{w75} \rfloor$$

(5)

Similarly, very wet days (R95P) are the number of days having rainfall more than 95 percentile of the long period and can be written as:

$$R95P_j = Count\lfloor R_{wj} > R_{w95} \rfloor$$

(6)

where, R_{w95} is the 95 percentile of R_{wj} series.

3.1.6 Precipitation friction due to moderate wet days (R75PTOT) and very wet days (R95PTOT)

The precipitation friction of moderate wet days (R75PTOT) may be defined as the ratio of sum of precipitation greater than 75 percentile value (R_{w75}) to the total seasonal rainfall for a period/year. Let R_{ij} be the daily precipitation on i^{th} day of jth period/year, the $R75PTOT_j$ can be computed as:

$$R75PTOT_j = \sum_{i=1}^{n}[R_{ij}: R_{ij} > R_{w75}]/R_{TOT}$$

(7)

Similarly, the friction of precipitation due to very wet days ($R95PTOT_j$) may be the ratio of sum of precipitation greater than 95 percentile value (R_{w75}) to the total seasonal rainfall for a period/year can be computed as:

$$R95PTOT_j = \sum_{i=1}^{n}[R_{ij}: R_{ij} > R_{w95}]/R_{TOT}$$

(8)

where, n is the number of days and R_{TOT} is the total seasonal rainfall in a period/year .

3.1.7 Simple daily intensity index (SDII)

The simple daily intensity index (SDII) is the mean precipitation amount on wet days. Let, R_{wj} be the daily precipitation on wet day (precipitation ≥1 mm) in j^{th} period and W be the number of rainfall days. The $SDII_j$ for j^{th} period/year may be computed using following equation:

$$SDII_j = \frac{\sum R_{wj}}{W}$$

(9)

3.2 Statistical Tests for Trend Analysis

3.2.1 Mann-Kendal's test

Mann Kendal's test is a non parametric test does not require the data to be normally distributed and this test has low sensitivity to abrupt breaks due to inhomogeneous time series (Tabari, 2011). This test has been recommended widely by the World Meteorological Organization for public application (Mitchell et al., 1996). Furthermore, Al Buhairi (2010), Marvomatis & Stathis (2011), Tabari et al 2011, Tabari and Marofi (2011), Salarijzi et al. (2012) have used this test for evaluating the trend in climatological, hydrological and water resources data. In this test, each value in the series is compared with others, always in sequential order. The Mann Kendal's statistic can be written as:

$$S = \sum_{i=1}^{n} \sum_{j=1}^{i-1} sign(x_i - x_j)$$

(10)

where, n is the total length of data, x_i and x_j are two generic sequential data values, and function $sign(x_i$-$x_j)$ assumes the following values.

$$sign(x_i - x_j) = \begin{bmatrix} 1, & if\ (x_i - x_j) > 0 \\ 0, & if\ (x_i - x_j) = 0 \\ -1, & if\ (x_i - x_j) < 0 \end{bmatrix}$$

(11)

Under this test, the test statistic S is approximately normally distributed with the mean $E(S)$ and the variance $Var(S)$ can be computed as follow:

$$E(S) = 0$$

(12)

$$Var(S) = \frac{1}{n}[n(n-1)(2n+5) - \sum_t t(t-1)(2t+5)]$$

(13)

where, n is the length of time series, and t is the extent of any given tie and Σt denotes the summation over all ties number of values. The standardized test statistics Z for this test can be computed by the following equation:

$$Z = \begin{bmatrix} \frac{S-1}{\sqrt{Var(S)}}, & if\ S > 0 \\ 0, & if\ S = 0 \\ -1, & if\ S < 0 \end{bmatrix}$$

(14)

According to this test, the null hypothesis H_0 states that the depersonalized data is a sample of n independent and identically distributed random variables, there is no trend in the data and no correlation between considered variable and time, each ordering of the data set is equally likely.

3.2.2 Spearman's rho test

The Spearman's rho test is a non-parametric methods proposed and applied in the literature for trend analysis (EPA, 1973; Kolaz and Swinford, 1989; Sadmani et al 2011 etc). This is one of the non-parametric tests widely used for studying populations that take on a ranked order. If there is no trend and all observations are independent, then all rank orderings are equally likely. In this test, the difference between order and rank (d_i) for all observations $x_1, x_2, x_3, \ldots x_n$ can be used to compute and Spearman's ρ, variance $Var(\rho)$ and test statistic (Z) using following equations.

$$\rho = 1 - \frac{6\sum d_i^2}{n(n-1)}$$

(15)

$$Var(\rho) = \frac{1}{(n-1)}$$

(16)

$$Z = \frac{\rho}{\sqrt{Var(\rho)}}$$

(17)

The null hypothesis is tested in this test considering statistic is normally distributed.

4. RESULTS AND ANALYSIS

4.1 Extreme Indices

In order to develop a uniform perspective about the impact of climate change, World Meteorological Organization (WMO) has suggested a set of 50 indices (http://www.wmo.int) and Expert Balod, 52.4 mm to 247 mm at Dhamtari, 49.5 mm to 258 mm at Kanker and 55 mm to 279.6 mm at Murmsilli RG station.

Team on Climate Change Detection and Indices (ETCCDI) suggested a core set of 27 indices (http://www.clivar.org/organization/etcdi/etccdi.php) for temperature and precipitation. In the present study, a series of extreme precipitation indices namely *RX1D, RX5D, R7.5cm, R12.5cm, R75P, R95P, R75PTOT, R95PTOT* and *SDII* were computed for Ambagarh, Bhanpura, Balod, Dhamtari, Kanker and Murumsilli rain gauge stations. The statistics related to time series of these indices have been presented in Table 1. From the analysis of statistics, it was observed that maximum one-day rainfall (*RX1D*) varies from 63 mm to 210 mm at Ambagarh, 76.2 mm to 291.2 mm at Bhanpura, 45 mm to 192.4 mm at

Table 1. Sample statistics in precipitation extreme indices series

Indices	R7.5cm	R12.5cm	RX1D	RX5D	R75P	R95P	R75TOT	R95TOT	SDII
Ambagarh									
Minimum	0	0	63	123.4	9	1	0.15	0.02	4.2
Maximum	5	3	210	419	31	13	0.47	0.26	11.1
Mean	2.1	0.4	112.2	220.1	17.7	7.7	0.3	0.1	7.2
Std. Dev.	1.28	0.65	34.6	65.9	5.87	3.12	0.09	0.07	1.8
Bhanpura									
Minimum	1	0	76.2	137.6	6	2	0.11	0.04	5.4
Maximum	12	8	291.2	589.3	36	19	0.53	0.28	15.8
Average	3.8	1.4	165.9	299.7	20.2	9.6	0.33	0.16	9.7
Std. Dev.	2.5	1.8	71.4	121.8	7.4	4.2	0.10	0.06	2.9
Balod									
Minimum	0	0	45	84	10	3	0.21	0.07	1.4
Maximum	5z	3	192.4	403.5	34	17	0.53	0.27	11.1
Average	2.12	0.42	107.0	199.6	17.15	8.7	0.34	0.17	6.27
Std. Dev.	1.58	0.75	38.7	78.4	4.91	3.51	0.07	0.06	2.32
Dhamtari									
Minimum	0	0	52.4	102.4	10	5	0.23	0.09	3.9
Maximum	5	2	247	345.3	47	34	0.60	0.43	10
Average	2.0	0.3	106.5	195.3	25.3	15.8	0.41	0.26	6.7
Std. Dev.	1.5	0.7	38.0	58.5	8.2	6.7	0.09	0.08	1.5
Kanker									
Minimum	0	0	49.5	96.6	10	4	0.22	0.06	3.7
Maximum	6	5	258	493.5	42	29	0.55	0.43	13
Average	2.14	0.59	126.1	232.9	24.6	15.4	0.40	0.25	7.2
Std. Dev.	1.59	1.02	48.03	88.4	7.9	6.7	0.1	0.11	1.9
Murumsilli									
Minimum	0	0	55	98.8	8	2	0.18	0.06	3.2
Maximum	6	4	279.6	539	44	31	0.58	0.46	12.3
Average	2.5	0.9	131.1	235.5	25.5	15.2	0.40	0.24	7.7
Std. Dev.	1.8	1.0	52.2	94.8	7.7	6.6	0.09	0.09	2.0

4.2 Trend Analysis

For trend analysis of extreme indices, Mann-Kendal and Spearman rho's tests were applied to determine significant trend at 95% level of confidence. The test statistics and trend at 95% confidence has been presented in Table 2. To test for either

increasing or decreasing monotonic trend at *p* significance level, the null hypothesis is rejected if the absolute value of *Z* is greater than *Z(1-p/2)*; where *Z(1-p/2)* is obtained from the standard normal cumulative distribution tables (Partal and Kahya, 2006; Modarres and Silva, 2007). From the analysis, it has been observed that Mann-Kendal and Spearman's rho tests gave the identical results in most of the series of extreme

Table 2. Test statistics and trends of different indices

Extreme Indices	Mann-Kendal's test		Spearman rho's test		Final result
	Test statistics	Trend	Test statistics	Trend	
Station: Ambagrah					
R7.5cm	2.18	Rising	2.80	Rising	Rising
R12.5cm	1.99	Rising	3.55	Rising	Rising
RX1D	0.88	No Ternd	0.78	No Trend	No Trend
RX5D	-0.26	No Ternd	-0.36	No Trend	No Trend
R75P	-0.67	No Ternd	-0.13	No Trend	No Trend
R95P	-0.92	No Ternd	-0.56	No Trend	No Trend
R75TOT	-0.47	No Ternd	-0.32	No Trend	No Trend
R95TOT	-0.28	No Ternd	-0.10	No Trend	No Trend
SDII	0.71	No Ternd	0.78	No Trend	No Trend
Station: Bhanpura					
R7.5cm	-0.53	No Trend	0.44	No Trend	No Trend
R12.5cm	-0.08	No Trend	1.28	No Trend	No Trend
RX1D	-0.70	No Trend	-0.69	No Trend	No Trend
RX5D	-0.08	No Trend	-0.21	No Trend	No Trend
R75P	-0.42	No Trend	-0.22	No Trend	No Trend
R95P	-1.17	No Trend	-0.59	No Trend	No Trend

R75TOT	0.11	No Trend	0.42	No Trend	No Trend
R95TOT	-0.47	No Trend	-0.23	No Trend	No Trend
SDII	-0.65	No Trend	-0.64	No Trend	No Trend
Station: Balod					
R7.5cm	-1.08	No Trend	-0.08	No Trend	No Trend
R12.5cm	0.99	No Trend	0.33	No Trend	No Trend
RX1D	-0.42	No Trend	-0.50	No Trend	No Trend
RX5D	-0.59	No	-0.51	No Trend	No Trend

		Trend			
R75P	-0.47	No Trend	-0.23	No Trend	No Trend
R95P	-1.39	No Trend	-1.03	No Trend	No Trend
R75TOT	0.20	No Trend	0.32	No Trend	No Trend
R95TOT	-1.14	No Trend	-0.76	No Trend	No Trend
SDII	-0.37	No Trend	-0.21	No Trend	No Trend

ndices. Heavy precipitation days (*R7.5cm*) and very heavy precipitation days (*R12.5cm*) time series at Ambagarh rain gauge station showed a significant rising trend at 95% confidence level, while all other indices were found random. No time series of Bahnpuar and Balod RG station indicated any significant trend, while Kanker RG station depicted a rising trend in very heavy precipitation days (*R12.5cm*) time series. Dhamtari RG station showed a rising trend in *R12.5cm, R75P, R95P, R75PTOT* and *R95PTOT* time series. The time series of *R12.5cm, R75PTOT* and *R95PTOT* at Murumsilli confirmed a significant rising trend. A linear trend lines have been fitted on time series which confirmed significant trend. The graphs showing trends in few times series of extreme indices in these rain gauge stations have been presented in Fig. 2.

5. 0 CONCLUSIONS

Assessment of climatic variability is an important aspect in water resources management, adaptability and agriculture production due to changing climate. The impact of climate change is imperative that can be assessed by statistical tests and climatic models to develop mitigation measures and adaptation strategies. In the present study, nine extreme indices of precipitation namely maximum one-day rainfall *(RX1D),*

maximum 5-days rainfall *(RX5D)*, heavy precipitation days *(R7.5cm)*, very heavy precipitation days *(R12.5cm)*, moderate wet days *(R75P),* very wet days *(R95P)*, precipitation friction due to moderate wet days *(R75PTOT),* precipitation friction due to very wet days *(R95PTOT)* and simple daily intensity index *(SDII)* were investigated with the help of statistical Man-Kendal and Spearman's rho trend tests for six rain gauge stations in upper Mahanadi catchment. From the analysis, it may be concluded that all the extreme indices series of Bhanpur and Balod were distributed random and no trend was reported in any of the series. The trend analysis of *R12.5cm* indicated that number of precipitation days with more than 12.5 cm rainfall showed significant rising trend at Ambagarh, Dhamtari, Kanker and Murumsilli station which attributed to higher incidences of extreme rainfall possibly due to climate change. Dhamtri rain gauge stations signified positive trend in maximum number of extreme indices including very heavy precipitation days *(R12.5cm)*, moderate wet days *(R75P),* very wet days *(R95P)*, precipitation friction due to moderate wet days *(R75PTOT)* and precipitation friction due to very wet days *(R95PTOT)*. The simple daily intensity index *(SDII)* which is indicative of normal distribution of rainfall did not show any trend in all six rain gauge stations in spite of positive trend in extreme rainfall in few rain gauge stations in the region.

6.0 REFERENCES

i. Al Buhairi MH (2010) Analysis of monthly, seasonal and annual air temperature ariability and trends in Taiz city - Republic of Yemen. Journal of Environ Protection 1: 401-409

ii. Bavani AM, Goodarzi E, Zohrabi N (2012) Detection of climatic variables trend using parametric and non-parametric statistical tests (A case study of west Azerbaijan, Iran). Technical Journal of Engineering and Applied Sciences 2(5): 557-564

iii. Boroujerdy PS (2008) The analysis of precipitation variation and quantiles in Iran. 3rd IASME/WSEAS International Conference on Energy & Environ, University of Cambridge UK Feb 23-25: 2008

iv. Croitoru A, HolobacaI H, Catalin LC, Moldovan F, Imbroane A (2012) Air temperature trend and the impact on winter wheat phenology in Romania. Climate Change 111(2): 393-41

v. Environmental Protection Agency (1973) The national air monitoring program: air quality and emissions trends -annual report. US Environmental Protection Agency, Office of Air Quality Planning and Standards, Research Triangle Park, North Carolina (450/1-73-001a and b)

vi. Guhathakurta P, Sreejitha OP, Menon PA (2011) Impact of climate change on extreme rainfall events and flood risks in India. Journal of Earth System and Sciences 102(3): 359-373

vii. Intergovernmental Panel on Climate Change (2002) Climate change and biodiversity: IPCC Technical Paper V. http:// ipcc.ch/pdf/technical papers/Climate_change_boidiversity_en.pdf

viii. Intergovernmental Panel on Climate Change (2007) Summary for Policymakers. Climate Change 2007: The Physical Science Basis. Contribution of Working Group I to the Fourth Assessment Report of the Intergovernmental Panel on Climate Change, Eds: Solomon S, Qin D, Manning M, Chen Z,

Marquis M, Averyt KB, Tignor M, Miller HL. Cambridge University Press, Cambridge: 1-18

i. ain SK, Kumar V (2012) Trend analysis of rainfall and temperature data for India. Current Sciences 102(1): 37-49

ii. Joshi UR, Rajivan M (2006) Trends in precipitation extremes over India. National Climate Centre Report No. 3/2006, Indian Meteorological Department, Pune, India: 3-7

iii. Karpouzos DK, Kavalieratou S, Babajimopoulos C (2010) Trend analysis of precipitation data in Pieria Region (Greece). European Water 30: 31-40

iv. Kumar V, Jain SK, Singh Y (2010) Analysis of long-term rainfall trends in India. Hydrological Sciences 55: 484–496

v. Modarres R, DaSilva V (2007) Rainfall trends in arid and semi-arid regions of Iran. Journal of Arid Environment 70: 344-355

vi. Partal T, Kahya E (2006) Trend analysis in Turkish precipitation data. Hydrological Process 20: 2011–2026

vii. Parthasarathy B, Dhar ON (1974) Secular variations of regional rainfall over India. Quartery Journal of Research, Meteorological Society 100: 245–257

viii. Portnyagin YI, Merzlyakov EG, Solovjova TV, Jacobi C, Kurschner D, Manson A, Meek C (2006) Long-term trends and year-to-year variability of mid-latitude mesosphere/lower thermosphere winds. J Atmos Sol Terr Phys 68 1890–1901 doi:10.1016/j.jastp.2006.04.004

ix. Radziejewski M, Bardossy A, Kundzewicz ZW (2000) Detection of change in river flow using phase randomization. Hydrological Sciences 45(4): 547–558

x. Ravindran PN, Nirmal Babu K, Sasikumar B, Krishnamurthy KS (2000) Botany and Crop Improvement of Black pepper, (in) Black pepper 23 142 (Eds.) Ravindran P N. Harwood academic publishers

xi.   Rodionov SN (2004) A sequential algorithm for testing climate regime shifts. Geophysics Research Letter 31 L09204 doi:10.1029/2004GL019448

xii.   Roshan GH, Khoshakh LF, Azizi G, Mohammadi H (2011) Simulation of temperature changes in Iran under the atmosphere carbon dioxide duplication condition. Iranian Journal of Environment, Health, Sciences & Engineering 8: 139-152

xiii.   Sabohi R (2009) Trend analysis of climatic factors in great cities of Iran. International Journal of Climate Change 18: 34-43

xiv.   Sadmani M, Safar M, Roknian M (2012) Trend analysis in reference evaporation using Mann Kendal and Spearman' rho test in arid regions of Iran. Water Resources Management 26(1):211-224

xv.   Salarijazi M, Ali Mohammad AA, Adib A, Daneshkhan A (2012) Trend and change-point detection for the annual stream-flow series of the Karun River at the Ahvaz hydrometric station. African Journal of Agricultural Research 7(32): 4540-4552

xvi.   Serra C, Burgueno A, Lana X (2001) Analysis of maximum and minimum daily temperatures recorded at Fabra observatory (Barcelona, NE Spain) in the period 1917–1998. Journal of Climate 21: 617–636

xvii.   Shirgholami H and Ghahraman B (2009) Study of time trend changes in annual mean temperature of Iran. Journal of Sciences, Technology, Agriculture & Natural Resources 23: 44-53

xviii.   Tabari H, Marofi S (2011) Changes of pan evaporation in the west of Iran. Water Resources Management (25): 97–111

xix.   Tabari H, Marofi S, Aeini A, Talaee PH, Mohammadi K (2011) Trend analysis of reference evapotranspiration in the western half of Iran. Agricultural Forest Meteorology 151: 128-136

xx.   Wang Y, Zhou L (2005) Observed trends in extreme precipitation events in Chins during 1961-2001 and the associated change in large-scale circulation, Geophysics Research Letter, 32: L09707

xxi.   World Meteorological Organization (2005) Guidelines on analysis of extremes in a changing climate in support of informed decision for adaptation, Climate data monitoring WCDMP No. 72, Geneva Switzerland

xxii.   Xu ZX, Li JY, Takeuchi K, Ishidaria H (2007) long term trend of precipitation in china & its association with El Nino-southern oscillation. Hydrological Processes 21: 61-71

R.G. station: Kanker (*R12.5cm*)

R.G. Station: Dhamtari (*RX1D*)

R.G. Station: Ambagarh (*R7.5cm*)

R.G. Station: Murumsilli (*R75PTOT*)
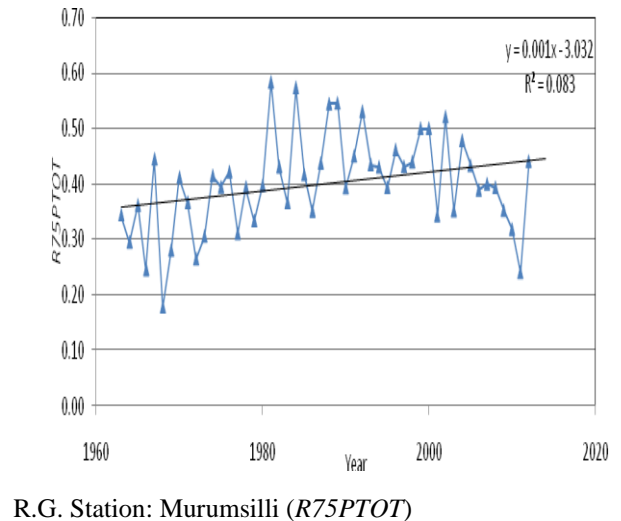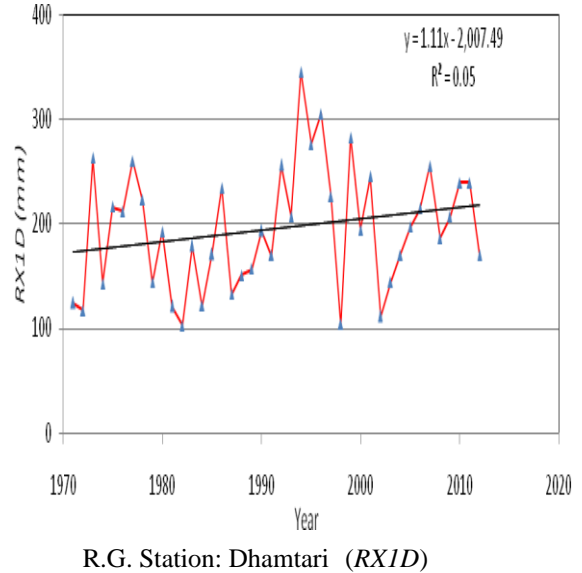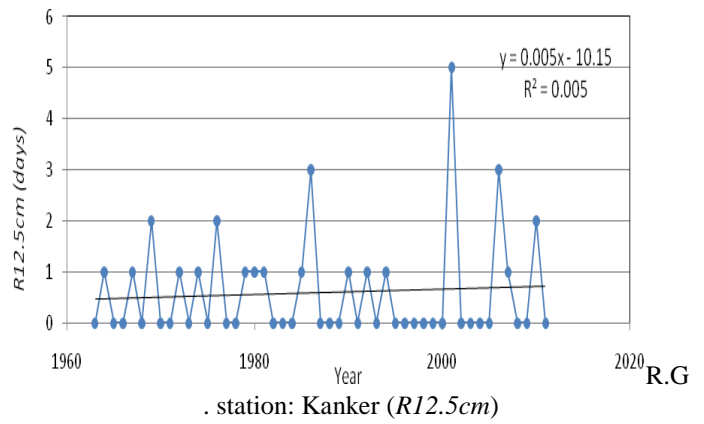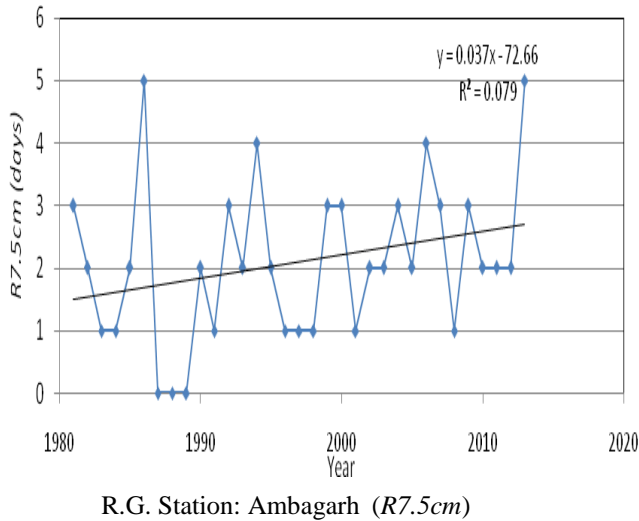
Figure 2. Trend lines showing rising trend for few extreme indices

Impact Of Climate Change On Rainfall And Temperature Trends: A Pragmatic Analysis Of Scenarios For Tea Growing Regions Of North Eastern India

Rupanjali D. Baruah[1*], R.M. Bhagat[2], S.Roy[3], L.N. Sethi[4]

[1]*Research Scholar, Department of Information Technology, Assam University, Silchar-788011, India, (rupanjali.debbaruah@gmail.com)*

[2] *Deputy Director (Research)/Chief Scientist, Tea Research Association, Tocklai Tea Research Institute, Jorhat (Assam) 785008, India*

[3]*Associate Professor, Department of Information Technology, Assam University, Silchar-788011, Assam, India.*

[4]*Associate Professor, Department of Agricultural Engineering, Assam University, Silchar (Assam), India*

ABSTRACT: *North Eastern India is typified by a monsoonal climate. Traditionally, tea grows well in this hot humid region due to plentiful rainfall and sunshine. However, the climate change triggered by global warming and coupled with large scale deforestation has disturbed the major component of the hydrological cycle i.e. precipitation, as well as the prevailing temperature, which are the most important factors for the growth and production of tea. As these changes are taking place both in space and time, hence this is a spatio-temporal phenomenon and requires both statistical and spatial analysis. Archived datasets, available at the Tocklai Tea Research Institute, Jorhat, Assam, India for seven locations (ranging from 30 -96 years) in tea growing regions of North East India were analyzed for climate trends. The trends indicate a total annual rainfall decrease of up to 220 mm over a period of 90 years, with highly erratic distribution observed in recent years. The increase in minimum temperature (T_{min}) for the corresponding period has been observed to be around 1.4^0C. These trends were compared with the data obtained from the general circulation models downscaled to regional climate models (wherever available) for baseline scenarios. The comparison of trends matches well, but some numerical abrasions were observed. Middle level (2020-2050) and future scenarios (2071-2100) for rainfall and temperature were also obtained from these climate models for various tea growing regions of North Eastern India. The outputs indicated that the total annual rainfall will fall while temperature (both T_{max} & T_{min}) will increase much above current levels for both middle level and future scenarios. However, large spatial variability in both the parameters (rainfall and temperature) was observed for various tea growing regions perhaps due to orographical features of the region. Since the statistical significance depends largely upon the length of time series, the study points towards further analysis in spatio- temporal domain.*
Keywords: Climate change, climate scenarios, spatio-temporal domain, tea growing region.

1. INTRODUCTION

Climate change is a broad concept that has received many different meanings and interpretations in the recent past. The general idea is that weather and climate patterns are changing significantly due to known, unknown and surmised causes. This usually means that at places, the average daily temperature is increasing, that rainfall patterns are changing, both in space and time and that extreme events periodicity has increased. Since these changes are taking place in both space and time, hence the concept of climate change is a spatio-temporal phenomenon.

North Eastern India is typified by a monsoonal climate. Traditionally tea grows well in this hot-humid region due to plentiful rainfall and sunshine. There is increasing evidence of late that climate change has disturbed the hydrological cycle i.e. precipitation, as well as the prevailing temperature, which are the most important factors for growth and production of tea. While tea production is fragmented between the garden owners (small units compared to total area under tea production), and production system flow between zones and where there is a high degree of communal ownership, hence requires a different non conventional approach for their management (Bhagat and Singh, 2007a). It is thus important that the programmatic needs for information for sustainable tea production in North Eastern India must direct data collection. However, at this stage, it may not be possible to develop individual garden level data for the entire North Eastern India. Different data reduction techniques, involving statistical and neutral network analysis, can be used to identify characteristic sites of niche based (clustering Gardens) tea production on which to concentrate the research efforts. At the moment, however, no scaled and geo-referenced datasets are available for quick decision making. This happened because our information needs for decision making were simple and limited. There are some static datasets available for tea in the form of manually produced geographic information, maps and charts. These data can be accessed, but cannot be quickly compiled for multi-sector and problem oriented analysis. This results in long delays in decision making and increase the response time for the planners and decision makers. While in effective crop planning quick decision making (e.g. application of nutrients, application of pesticides for control of pest/diseases/weeds) is a pre-requisite (Dutta et.al., 2010).

Initial climate trends in North eastern India show a marked decrease in rainfall and increase in minimum temperature with large variability both in space and time (Bhagat et al., 2010). Although these datasets can be doubted, in particular when further data are added, or when a more refined scale is considered, the evidence is large and more convincing. Further, addition of data of a highly abnormal year brings about marked changes in statistical averages, thus upsetting the long term trends. Convincingly, however, it is imperative if at times deviation from the long term trends is also determined to see the extremities of climate and weather patterns. The present study was initiated with the objectives to study (a) the long term trends of rainfall and temperature in tea growing regions from archived datasets available at the Tocklai Tea Research Institute, Jorhat, Assam and (b) future trends developed for

middle level and long term future IPCC scenarios for the same regions of North Eastern India.

2. MATERIAL AND METHODS

The archived datasets for rainfall and temperature (T_{max} and T_{min}) available at the Tocklai Tea Research institute, Jorhat, Assam, India for seven locations (Tocklai, Jorhat, South Bank, Assam; Dikom, Upper Assam; Silcoorie, Cachar, Assam; Thakurbari, North Bank, Assam; Darjeeling, West Bengal; Bengdubi, Terai, West Bengal; Nagrakata, West Bengal) for different periods in Assam and West Bengal (Fig.1) tea growing regions of North eastern India were used for the analysis as base level data. For the sake of brevity, all the analyzed data for all locations are although discussed but not presented in this paper, except the Tocklai, Jorhat, Assam data.
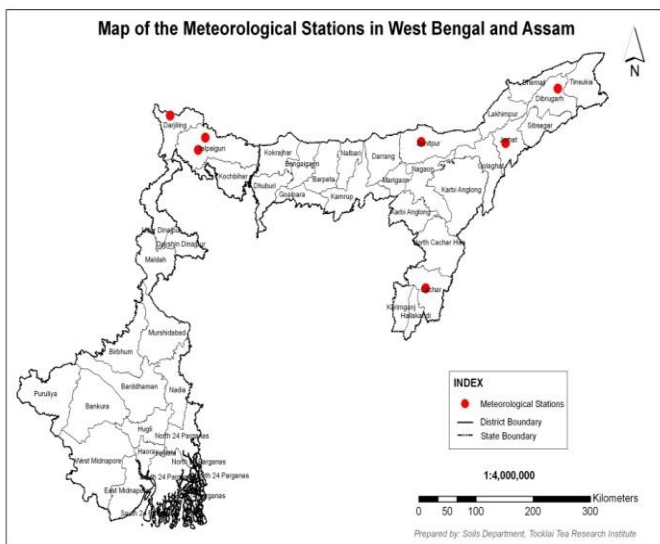
Figure 1. Locations of TRA met stations in Assam and West Bengal

2.1 Data capture and Trend analysis

Trend is defined as the general movement of series over an extended period of time or it is the long term change in the dependant variable over a long period of time Webber and Hawkins, (1980). In the present case trend is determined by the relationship between the two variables as rainfall and time, temperature and time. The statistical method generally used is regression analysis and co-efficient of determination (R^2). However, as a first step to check the data homogeneity, the time series were plotted on a linear scale. Inspection of plots, show few changes in the time series, which is related to missed data gaps. Although very few such gaps were observed for some of the meteorological stations; was mainly either due to malfunction of gauges and or due to regional unrest (when data could not be collected). However, it was not related to any serious non-homogeneity and any changing points could be contained within the respective period. Trend analysis of time series consists of the magnitude of trend and statistical significance. In the present case the time series (rainfall, T_{max} and T_{min}) were taken as annual and seasonal (main active

growth production season, dormant season) to observe any changes occurring annually or seasonally and how these impact the tea plants both in the active growth and dormant seasons. Time series data were also examined for shorter periods, where there were abnormal trends (or trend reversal) and deviations from long term normal to observe whether such abnormal trends interfere with normal management practices in the tea gardens. If assumption is made of a linear trend (as in present case) in time series, the analysis becomes easy and more diagnostic. Hence, regression analysis was carried out directly on time series. A linear equation Y=mX+c, defined by intercept 'c' and slope 'm' (trend) is fitted by regression. The linear trend value represented by the slope 'm' of the simple least square regression line provides the rate of rise /fall in the rainfall, T_{max} and T_{min}. Further, magnitudes of the trends of increasing or decreasing total mean rainfall, T_{max} and T_{min} were derived and tested by Mann –Kendall test (Mann (1945) trend test and the slope of the regression line using the least square method as stated above.

The non-parametric Man-Kendall test for identifying randomness against time or trends in time series data compares the relative magnitudes of sample data rather than the data values themselves (Longobardi and Villani, 2009; Deshmukh and Lunge, 2013). Also, no particular distribution of data is required. If X_1, X_2 .... X_n is the sequence of measurement representing 'n' data points where X_j represents the data points at time j. Then the Mann-kendall test statistic (S) is given by

$$S = \sum\sum \text{sign} (X_j - X_k), J=2,3.... n; k=1,2.....j-1$$

$$\text{Where} \quad \text{sign} (X_j - X_k) = 1 \text{ if } X_j - X_k > 0$$
$$= 0 \text{ if } X_j - X_k = 0$$
$$= -1 \text{ if } X_j - X_k < 0$$

A high (positive) value of 'S' is an indicator of an increasing trend and a low (negative) value indicates a decreasing trend. Further, it is necessary to compute the probability associated with 'S' and the sample size 'n', to statistically quantify the significance of trend (Deshmukh and Lunge, 2013). It has been documented that for a sample size > 8, the statistics 'S' is approximately normally distributed (Mondal, *et al*, 2012)

$$\text{Var } S = [n(n-1)(2n+5) - \sum t_p(t_p -1)(2t_p+5)]/18, p=1,2......q$$

Where, tp is the number of ties up to sample p (or p^{th} value) and q is the number of tied values. Then standardised statistical test (test statistics Z) is computed as:

$$Z = S-1/\sqrt{\text{Var} (S)} \text{ if } S>0$$
$$= 0 \text{ if } S=0$$
$$= S+1/\sqrt{\text{Var} (S)} \text{ if } S<0$$

Z here follows a standard normal distribution. A positive (negative) value of Z signifies an upward (downward) trend. An attempt was made to plot the trends of future climate (Rainfall, T_{max} and T_{min}) as obtained from the regional climate modelling system of IPCC and derived from the Network Project on Climate Change (NPCC) of Indian Council of Agricultural Research (ICAR), New Delhi, India, archived data sets for TRA, Jorhat, Assam Centre. The data are plotted only for the South Bank (precisely Jorhat) region of Assam.

3. RESULTS AND DISCUSSION

Seven met stations data showed a general decrease in rainfall in the tea growing regions of Assam and West Bengal (Fig. 2). However, a detailed study of the long term data indicated large variability both in space and time. Increased frequency of too much and too less rainfall (data not shown), respectively leading to flood and drought like situations have become common, inducing production shortfalls in tea (Dutta, 2010). The linear regression trends for rainfall, T_{max} and T_{min} with their linear regression equations and co-efficient of determination are respectively presented in Fig 2, 3 & 4 and summarised in table 1. In South bank region, a decrease of more than 200 mm has been observed over a period of 96 years. Such trends have also been observed in other tea growing regions, although with a varying magnitude (Bhagat, et al., 2010). Cachar has shown the highest rate of decrease, while Terai and Darjeeling have shown marginal increase. Linear regression equations for rainfall (Table 1) also indicated these data trends with respect to rainfall at various production zones.

In addition, the distribution of rainfall has also undergone a drastic change (data not shown). There is a complete absence of winter rains recently in many tea growing areas and the early weather rainfall (March – April) also is absenting now. The rainfall is now mostly concentrated from June to September.
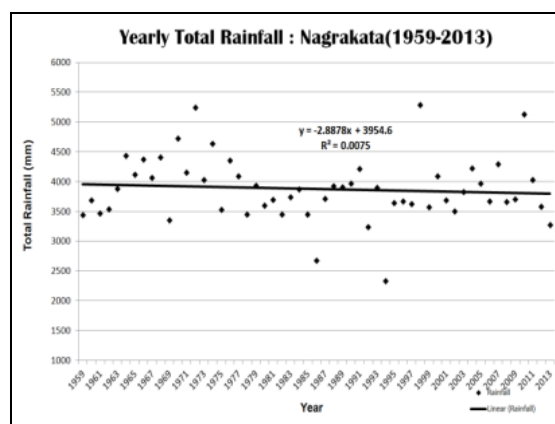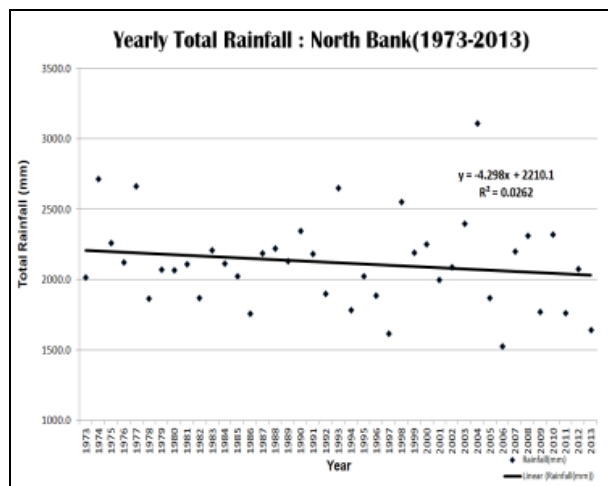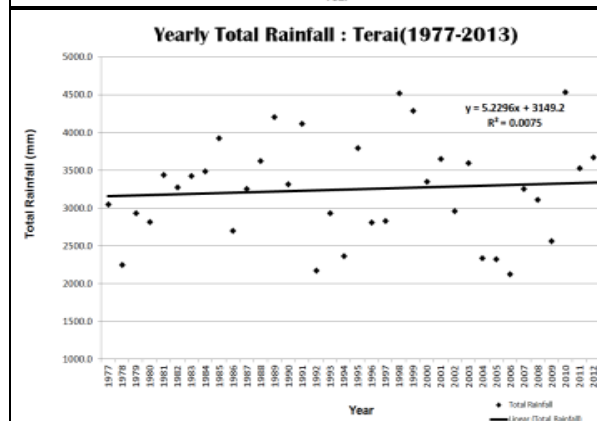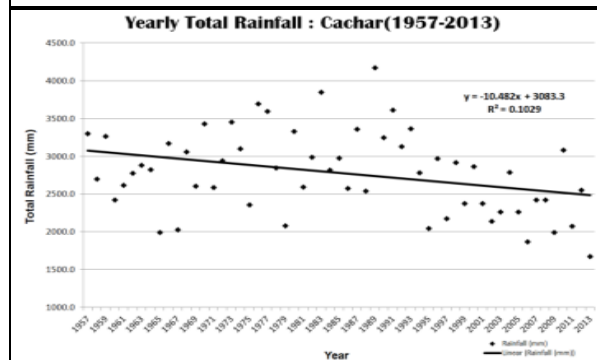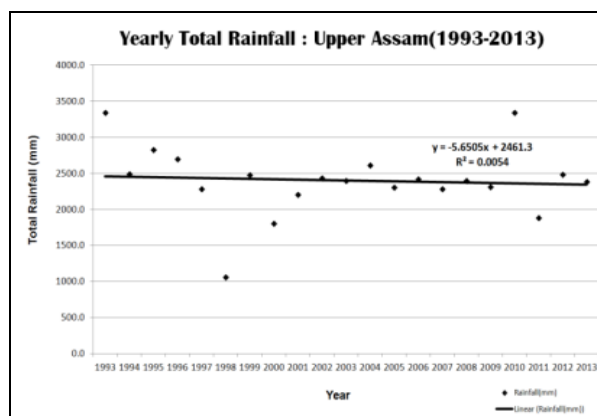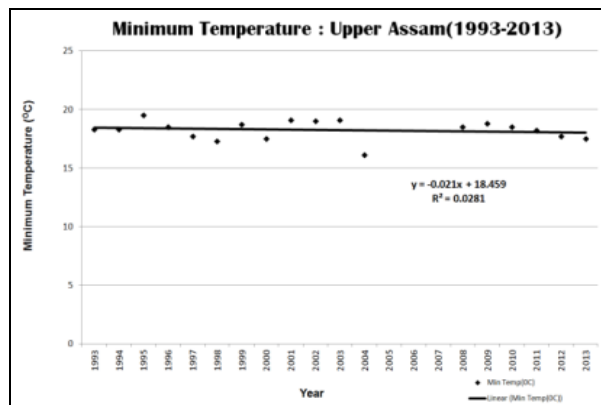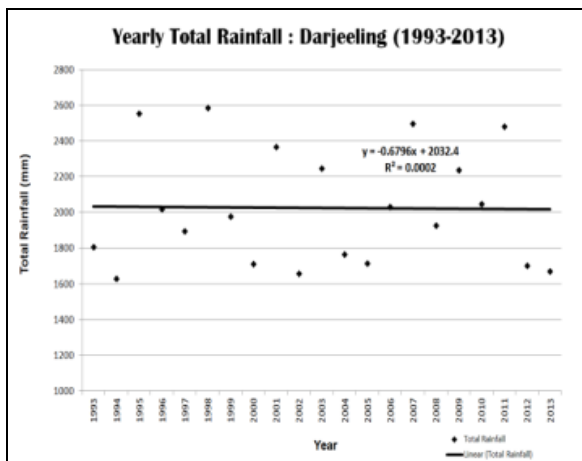
Figure 2. Rainfall trends at seven locations in Assam and West Bengal

It has been observed that in general minimum temperature (T_{min}) is increasing at various locations in Assam and West Bengal (Fig. 3). A steep increase has been observed in South Bank, while no significant increase is observed in Upper Assam. However, in many individual years there is rise in minimum temperature in Upper Assam, which however, seems masked in long term averages. Almost similar trend is observed in maximum temperature also. In line with earlier studies (Bhagat et al. 2009), this study also indicated (data not shown) that the number of days with temperature >30^0C or >35^0C have increased in the last about thirty years which may also be detrimental for tea production, since tea is known to produce best and thrive better between 13 -30^0C (Dutta et al, 2012).
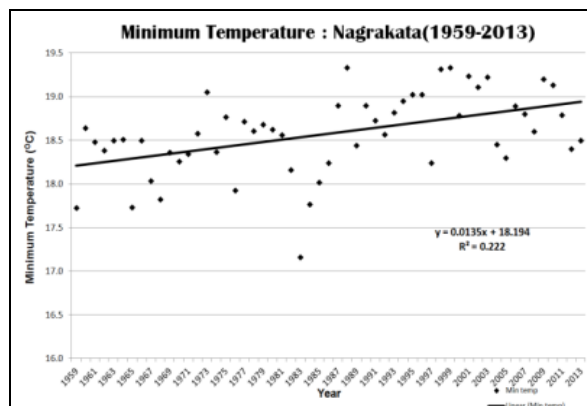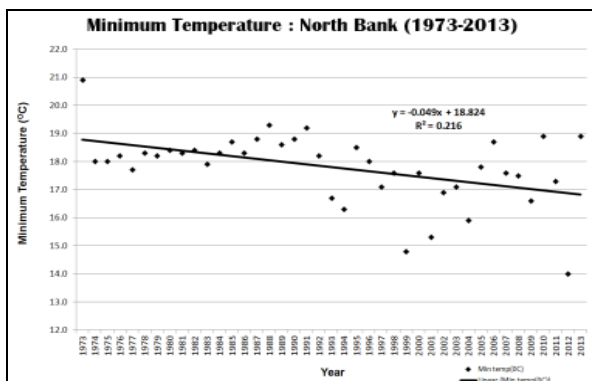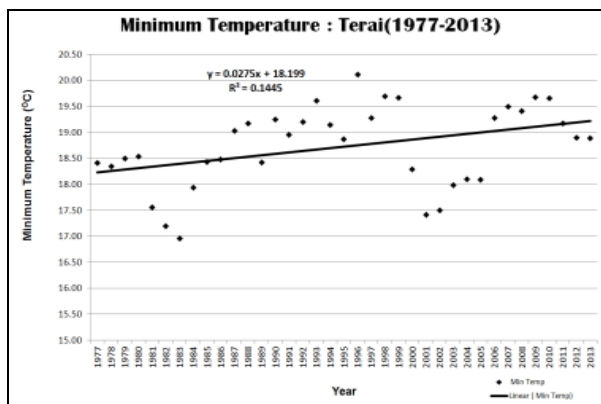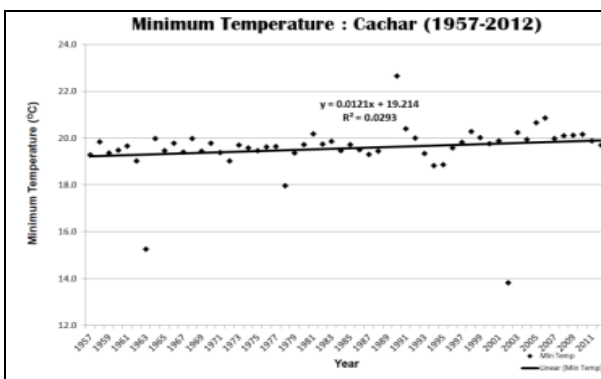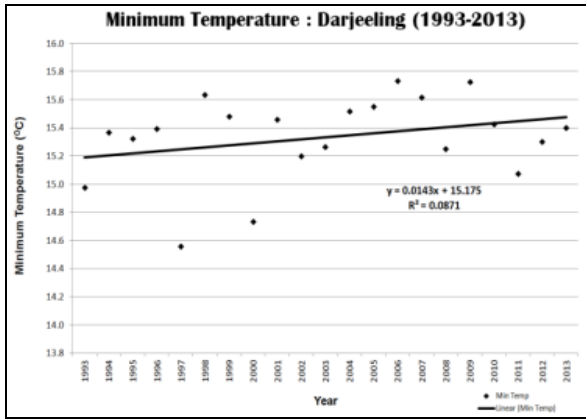
Figure 3. Minimum temperature (T_{min}) trends at seven locations in Assam and West Bengal

Table 1. Linear regression equations for rainfall (mm), T_{max} (^{0}C) and T_{min} (^{0}C) for all met stations

Name of met station	Rainfall, Regression line	R^2	T_{min}, Regression line	R^2	T_{max}, Regression line	R^2
South Bank (Assam)	Y=2.7573X+2149.5	0.0803	Y=0.017X+17.987	0.6283	Y=0.0013X+28.186	0.003
North Bank (Assam)	Y= -4.298X+2210.1	0.0262	Y=-0.049X+18.824	0.216	Y=0.0046X+29.285	0.0088
Upper Assam (Assam)	Y= -5.650X+2461.3	0.0054	Y=-0.021X+18.459	0.0281	Y= -0.0084X+28.369	0.0112
Cachar (Assam)	Y= -10.482X+3083	0.1029	Y=0.0121X+19.214	0.0293	Y=0.0247X+29.483	0.1129
Terai (West Bengal)	Y= 5.2296+3149.2	0.0875	Y=0.0275X+18.199	0.1445	Y= -.0104X+30.06	0.018
Nagrakata (West Bengal)	Y= -2.887X+3954.6	0.0075	Y=0.0135X+18.194	0.222	Y=0.0042X+28.577	00031
Darjeeling (West Bengal)	Y= -0.6796+2032.4	0.0002	Y=0.0143X+15.175	0.0871	Y=0.034X+22.575	0.2503

An attempt was made to plot the future climate scenarios (Fig 4, 5) for rainfall and temperature (T_{max} and T_{min}). The scenarios were plotted for middle level (2021-2050) and long term future (2070-2100). This was done since tea is a long term crop and

once planted it normally stays in fields for 40 -50 years and in extreme cases up to even 80 -100 years also. These scenarios indicate a general built up in rainfall as well as increase in both T_{max} as well as T_{min}. The data are presented here only for South Bank (Tocklai, Jorhat, Assam), although similar trends were observed for other tea production regions in Assam and West Bengal.
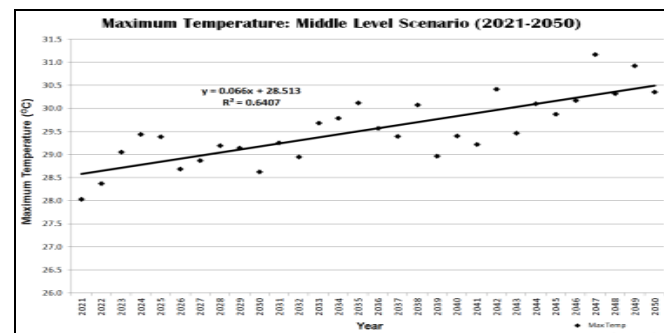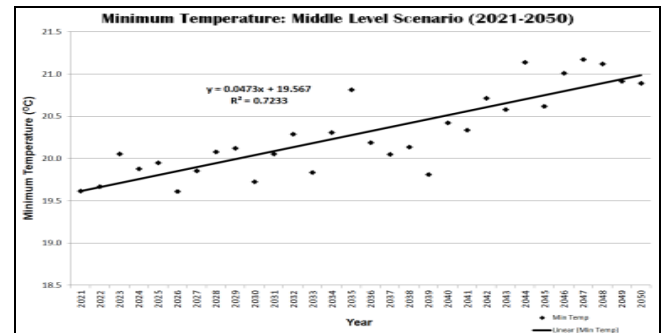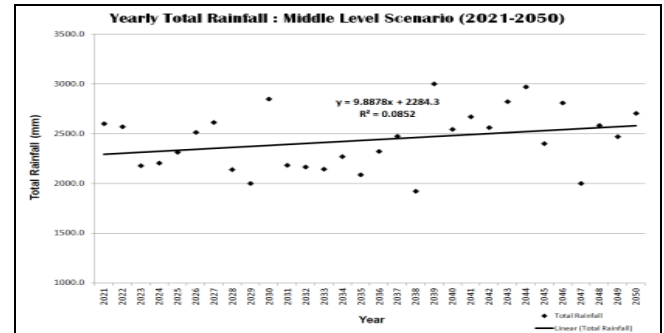
Figure 4. Middle level (2021-2050) scenarios for rainfall T_{min} and T_{max} (IPCC A2) for South Bank (Tocklai)
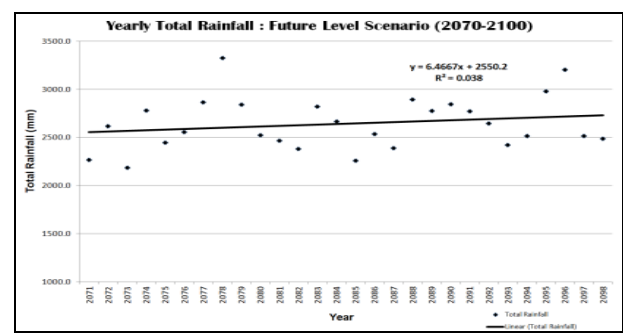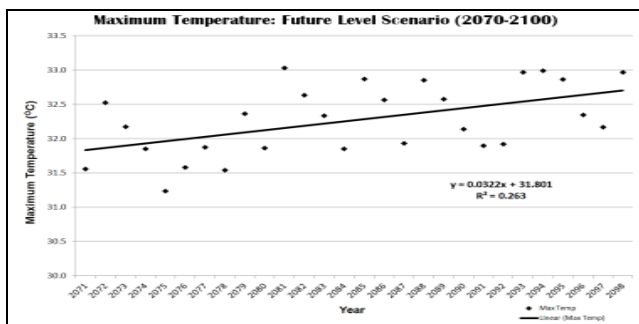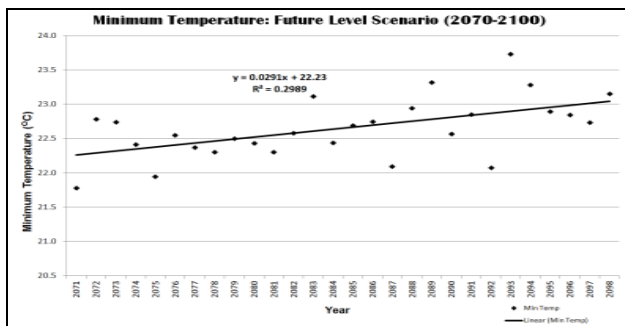
Figure 5. Future scenarios (2071-2100) for rainfall T_{min} and T_{max} (IPCC A2) for South Bank
(Tocklai)

Specifically, trend analysis indicated that although rainfall has decreased on long term basis, of course with variations as compared with long term normals, but if there is a segmented analysis performed on recent data (e.g. twenty years intervals), then general rainfall trend is reversing at many locations. This somehow matches with the future climate scenarios (Fig 4, 5). Additionally, when the data for recent twenty years (1993-2013) were subjected to Mann-Kendall trend test, the rainfall seems either stable or no trend was observed, with single exception of Cachar, where it appeared to be decreasing (Table 2). However, T_{max} was either increasing or stable at all locations except Terai, where it appeared decreasing. T_{min}, did not show any decreasing trend, it was either increasing, stable or no trend was observed. This analysis opens up further investigation areas for analysis as to whether the twenty years interval is too short for such an analysis or the sampling points should be further increased on a much larger time series. Also, it may still be worthwhile to analyse the data on a decadal basis to further narrow down on recent trends.

Table 2. Mann Kendall trend test performed for all tea production zones met data

Sampling Place	Rainfall			T_{max}			T_{min}		
	Co-eff. Of Var.	Mann-Kendall Statistic (S)	Trend	Co-eff. Of Var.	Mann-Kendall Statistic (S)	Trend	Co-eff. Of Var.	Mann-Kendall Statistic (S)	Trend
South Bank	0.15	-36	Stable	0.02	74	Increasing	0.02	5	No trend
North Bank	0.18	-26	Stable	0.02	-42	Stable	0.08	21	No trend
Upper Assam	0.20	-34	Stable	0.02	-13	Stable	0.05	-22	Stable
Cachar	0.18	-52	Decreasing	0.02	-11	Stable	0.07	66	Increasing
Terai	0.22	14	No trend	0.03	-158	Decreasing	0.04	-10	Stable
Nagrakata	0.16	16	No trend	0.01	-13	Stable	0.02	-39	Stable
Darjeeling	0.16	-2	Stable	0.02	73	Increasing	0.02	38	No trend

4. CONCLUSION

A general trend of decrease in rainfall and increase in T_{max} and T_{min} was observed in tea growing regions of North Eastern India on long term data. However, for recent data of shorter intervals i.e. twenty years, the trends changed which appeared to continue at some locations for future climate, as obtained for middle level and long term future climate scenarios. The temperature trends for both T_{max} and T_{min} were increasing on long term and short term basis as well as for future middle level and long term future scenarios. The time series need further analysis on different sampling points and on a spatio-temporal scale.

REFERENCES

i. *Bhagat RM, Singh S (2007) Mapping agricultural indicators of Himachal Pradesh and their trends. International J. Agril. Sci.3(2): 274-276*
ii. *Bhagat RM, Baruah RD, Saikia M, Hazarika M (2009) Long term climate trends in tea growing areas of North Eastern India, Two & Bud 56: 21-31*
iii. *Bhagat RM, Baruah RD, Safique S (2010) Climate and tea [Camellia sinensis (L.) O. Kuntze] production with special reference to North Eastern India: a review. J. Environ. Res. Develop. 4(4):1017-1028*
iv. *Deshmukh DT, Lunge HS (2013) A study of temperature and rainfall trends in Buldana district of Vidharbha India. Int. J. Scientif. & Tech. Res., 2(2):67-73*
v. *Dutta R, Stein A, Smaling E, Bhagat RM, Hazarika M (2010) Effect of plant age and environmental and management factors on tea yield in North East India. Agron. J., 102(4): 1-12*
vi. *Dutta R, Smaling EMA, Bhagat RM, Tolpekin VA, Stein A (2012). Analysis of factors that determine tea productivity in North Eastern India: A combined statistical and modeling approach. Experimental Agriculture 48(1):64-84*
vii. *Longobardi A, Villani P (2009). Trend analysis of annual and seasonal rainfall time series in the Mediterranean area. Int. J. Climatol. (www.interscience.wiley.com) DOI:10.1002/joc.2001*
viii. *Mann HB (1945). Nonparametric tests against trend. Econometrica, 13:245-259*
ix. *Mondal A, Kunduu S. Mukhopadhyay A (2012). Rainfall trend analysis by Mann-Kendall test: A case study of North eastern part of Cuttack District, Orrisa. Int. J. Geology, 2(1):70-78.*
x. *Webber J, Hawkins C (1980). Statistical analysis applications to business and Economics. Harper and Row, New York, 1980*

Fine Resolution Precipitation Projections For Tapi River Basin

SadhanaSingh[1] ,S Kannan[2], P.V.Timbadiya[3]

[1]PG Student, Civil Engineering Department, S.V. National Institute of Technology-Surat, Gujarat, India.
[2]Assistant Research Officer, Central Water and Power Research Station, Pune, Maharashtra, India.
[3]Assistant Professor, Civil Engineering Department, S.V.National Instiute of Technology-Surat, Gujarat, India.
Email: sadhana.civil10@gmail.com
kannan_s@cwprs.gov.in
pvtimbadiya@ced.svnit.ac.in

ABSTRACT: *Study of regional-scale hydrology of any river basin due to impacts of climate change has gained the attention of researchers in the recent past. The global climate models, widely used tools for assessing the impacts of climate change, usually projects the hydrological variables of interest at a large-scale, which necessitates the use of downscaling techniques. The present study aims to downscale the daily precipitation using the kernel-regression (KR) based downscaling method for the Tapi River basin at a very fine resolution of $0.25^\bullet \times 0.25^\bullet$. The KR based downscaling method first simulates the rainfall state of the region from the large scale atmospheric variables using the supervised classification and regression tree, and then projects the multisite rainfall amount using a non-parametric kernel regression estimator, conditioned on the estimated rainfall state. The impacts of climate change under the two future emission scenarios (RCP 4.5 and RCP 8.5) on daily precipitation patterns are evaluated in this study. The predictors used in this study were air temperature at surface, 500 and 850 hpa, specific humidity at surface, 500 and 850 hpa, zonal and meridional wind at surface, 500 and 850 hpa, mean sea level pressure (MSLP) and geopotential height at surface from the NCEP/NCAR reanalysis and from Canadian Centre for Climate Modelling and Analysis (CCCMA) General Circulation Model (GCM). It is found that projections obtained by KR model matches well with that of the observed rainfall, which proves the strength of this model in comparison to the other downscaling models. The projected rainfall series from the model for both future scenarios are analysed in terms of cumulative distribution function, wet and dry spell length probabilities, state to state transition probabilities and the occurrences of extreme rainfall events. For future projections, extreme events are likely to increase in the near future while decrease for far future.*
Keywords:Climate change, CART, Kernel Regression, APHRODITE.

1. INTRODUCTION

Global warming, due to enhanced greenhouse emissions have significant effects on the hydrological cycle. Human activities have significant effects in increasing the greenhouse gases. Greenhouse gases along with the increasing temperature have significant impacts in changing climate. Climate change may be due to natural internal processes or external forcings, or to persistent anthropogenic changes in the composition of the atmosphere or in land use [IPCC, 2013].The GCMs are the most widely used tools available for assessing the future impacts of climate change. They are good in simulating the large climate variables accuratelybut fail to simulate the small scale hydrological variables accurately [Ghosh and Mujumdar, 2006]. The output given by the different GCMs cannot be directly used for hydrologic impact assessment because of their coarse resolution. The objective of the downscaling is to overcome this scale mismatch and to use the skill in atmospheric forecasts at local scales. The downscaling in terms of hydrology can be defined as a method that predicts regional-scale hydrologic variables of interest (e.g. rainfall and stream flow) based on large-scale climatological variables (e.g. mean sea level pressure, temperature, specific humidity etc.,) simulated by a GCM [Mujumdar and Kumar, 2013].There are two approaches currently available for performing downscaling i.e. dynamical and statistical.The dynamical downscaling is the use of high-resolution regional climate models (RCMs) to provide simulated climate outputs at finer resolutions [Fowler et al., 2005; Rupa Kumar et al., 2006 and Krishna Kumar et al., 2011]. The statistical downscaling, also known as empirical downscaling, derives a statistical or empirical relationship between the variables simulated by the GCMs, called predictors, and station-scale hydrologic variables, called predictand. They have been preferred in hydrologic impact assessment because they provide good fits to observed data while being computationally inexpensive, provide quick results, and their domain of application can be easily transferred from one region to another [Mehrotra and Sharma., 2005, 2006; Raje and Mujumdar., 2009; Ghosh and Mujumdar., 2006; Ghosh., 2010].Statistical downscaling methodologies can further be broadly be classified as weather generators [Hughes and Guttorp.,1994; Charles *et al,.* 1999], weather typing [Gangopadhyay and Clark., 2005; Willems and Vrac., 2011; Salvi et al., 2011; Kannan and Ghosh 2013], and transfer functions [Wilby et al., 2003;Tatli et al,. 2005; Ghosh and Mujumdar., 2006].

Kannan and Ghosh [2011] addressed the problem of multisite downscaling using the common rainfall state of the river basin. The rainfall state is generated using an unsupervised data classification technique k-means clustering coupled with a supervised data classification technique, (CART). For the current study, the kernel regression model coupled with an unsupervised data classification k-means clustering developed by Kannan and Ghosh [2013] is used for the rainfall projections. The organisation of the paper is as follows.

A) The selection of the GCM and data related details along with study area are given in the section 2.

B) Theanalysis and results obtained from thestudy are presented in section 3

C) Summary, followed by the conclusions are given in section 4.

2. STUDY AREA &DATASOURCES

The Tapi basin is situated in the northern part of the Deccan Plateau and extends over an area of 65,145 km^2 which is nearly 2% of the total geographical area of thecountry. The catchment area up to Ukai dam is 62,225 km^2. Nearly, 80% of the basin lies in State of Maharashtra. The basin lies between east longitudes of 72° 38′ to 78° 17' and north latitudes of 20° 5' to 22° 3'.The TapiRiver is the second largest west flowing river of Indian Peninsula.The Tapi River has 14 major tributaries having a length more than 50 km. The Purna and the Girna Rivers together account for nearly 45% of the Tapi basin area. An index map of the Tapi Basin is shown in the Figure 1 below.

The selection of a particular GCM is the most important step for the success of any downscaling technique. For the present study, the GCM developed by Canadian Centre for Climate Modelling and Analysis (CCCMA) from the latest developed (CMIP5) is used.
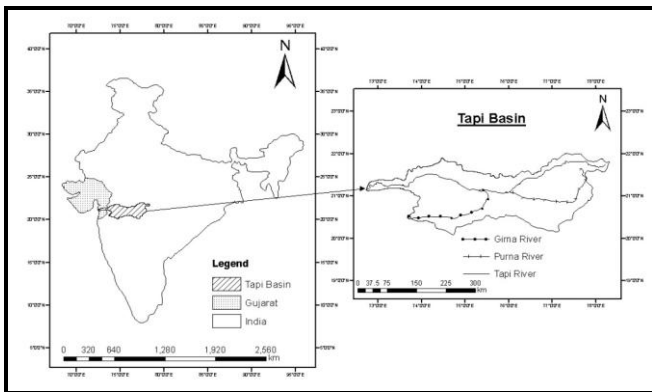
Figure 1 Index Map of Tapi Basin

Predictors: The selection of predictors relies on 1) the data for the particular predictor should be available for the desired period, 2) predictors should be capable of simulating the predictand well and, 3) predictors should show a good correlation with the predictand [Wilby et al., 1999]. For the present work, NCEP/NCAR reanalysis-I provides daily reanalysis data on six climatic predictor variables including geopotential height, air temperature, mean sea level pressure, specific humidity, zonal wind speed and meridional wind speed. The geopotential height and mean sea level pressure are taken only at the surface whereas air temperature, specific humidity, zonal and meridonal wind are taken at surface, 500 hpa and 850 hpa. The predictors are selected based on the previous studies carried out taking daily precipitation as the predictand [Kannan and Ghosh, 2013, Salvi et al, 2013, Raje and Mujumdar, 2009].The output from CanESM2 developed by Canadian Centre for Climate Modelling and Analysis, Canada (CCCMA) is used for downscaling precipitation for future emission scenarios RCP 4.5 and RCP 8.5.

Predictand: The daily precipitation data at a grid spacing of 0.25°×0.25° fromAsian Precipitation Highly-Resolved Observational Data Integration towards Evaluation of the Water Resources(APHRODITE)[Yatagai*et al*.; 2009] is used as predictand for the present study. The 0.25°×0.25° gridded daily

precipitation data were obtained from APHRODITE for all India for the period 1951–2007 (http://www.chikyu.ac.jp).

3. RESULTS AND ANALYSIS

The present part describes the analysis carried out for predictor variables to make them to use as inputs in downscaling models and how they are used for training and projections.The downscaling of daily rainfall projections at a very fine scale involves the process of selection of spatial extent, bias correction, principal component analysis (PCA), and modeling of rainfall occurrence and then modeling of rainfall amount. The modeling of rainfall occurrence includes identification of rainfall states and projection of future rainfall state projections. The selection of spatial extent is done by plotting the Pearson correlation coefficientbetween the key predictor variables and the average rainfall data of theTapi basin for the region between the latitudes 5°-40° N and longitudes 60°-120°E. After analyzing the contour plots, the selection of spatial extent for downscaling is taken as 10°N-35°N and 65°E-95°E corresponding to latitudes and longitudes respectively. The contour plot of predictor variables at surface is shown in Figure 2.
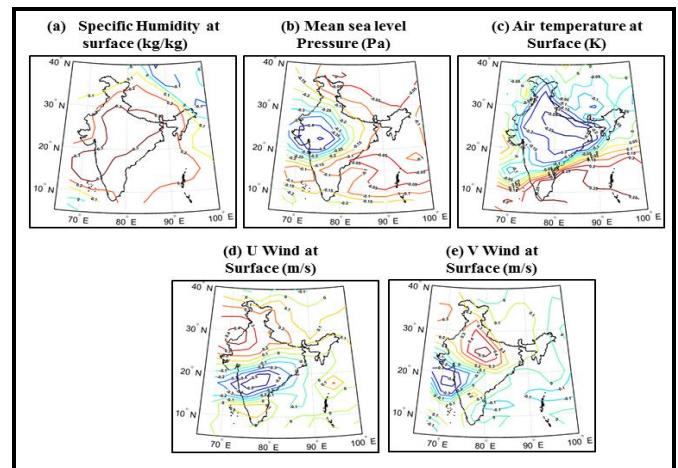
Figure 2 Contour plot of Pearson correlation coefficient between surface predictor variables and the basin average rainfall

After selecting the spatial extent for performing downscaling, bias correction is carried out by standardization/normalization [Wilby et al., 2004] for reducing the systematic biases in the means and variances of various GCM predictors, with respect to that of NCEP/NCAR predictors. The total dimension of the standardized data available data available for modeling is 858 (6 variables at 143 grid points). The Principal Component Analysis (PCA) is performed next to convert the highly correlated multidimensional predictor into a set of uncorrelated variables with reduced dimensionality. For the present study, the standardized predictor containing 858 dimensions are reduced to a predictor set containing 134 dimensions without ignoring the important information contained in the original data. For identification of rainfall state, the methodology developed by Kannan and Ghosh [2011], which uses an

unsupervised data classification technique, viz. k-means clustering solves the problem. The optimum number of cluster is worked out based on the cluster validity indices such as Dunn's index, Davies-Bouldin index, and Silhouette index and is found out to be 3.They are named as "Almost Dry", "Medium" and "High" on the basis of rainfall amounts represented by the cluster centroids. Figure 3 shows cluster centroids as computed using k-means clustering technique for three clusters.
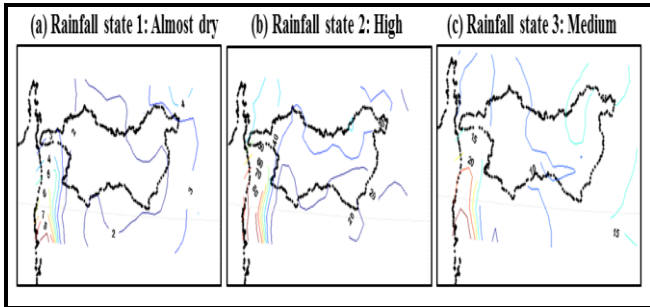
Figure 3 Cluster centroids computed by K-means clustering technique for cluster 3

Modeling the rainfall occurrence with CART: The present study uses three models for training and validation of the CART model.The CART model results are tested on the basis of skill measures based on contingency table, such as, success rate of model prediction (SRMP) and heidke skill score (HSS). For testing the association between observed and forecasted rainfall occurrences, χ^2 goodness-of-fit statistic is used. From the results of computed SRMP (percentage), HSS and χ^2 goodness-of-fit statistic for the three CART models under the consideration, it is found that the results of Model-III validation runs are fairly good as compared to Model-I and Model-II and is used for future rainfall state projections. Figure 4 presents the

Figure 5 and Figure 6 presents the correlation plots of the mean and standard deviation for the observed rainfall, KR Model, KRWS model and the rainfall projections from CCCMA using the kernel regression method conditioned on weather states. Figure 7 gives the correlation plots for R^2 values for kernel regression model with and without conditioning on weather states.

plots of changes in "almost dry-almost dry", "high-high" and "medium-medium" rainfall state transition probabilities obtained for model outputs for all the experiments.
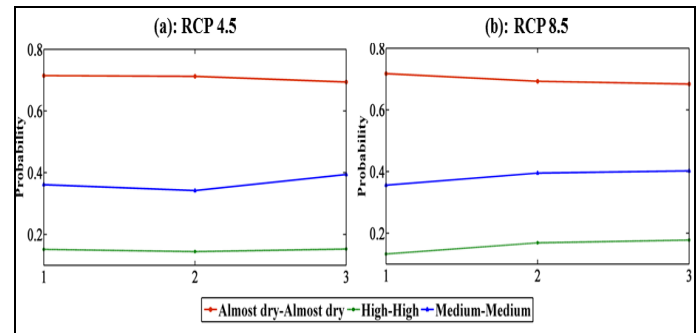
Figure 4 Plot of state-state transition probabilities for (a) CCCMA RCP 4.5
(b) CCCMA RCP 8.5

Modeling the multisite rainfall amount: For modeling the multisite rainfall amount, a recent nonparametric kernel regression based downscaling model developed by [Kannan and Ghosh, 2013] is used in the present work.The two models used in the present study are Kernel regression without conditioning on weather states (KRWS) and Kernel regression conditioned on weather states (KR). The validation of KR model over the baseline period is carried in terms of comparison of statistics, calculation of basin averaged wet days and rainfall amount, basin averaged wet/dry spell length and their conditional probabilities and in terms of their ability to capture temporal and spatial dependence.

Wet Days					Rainfall				
	5	50	95	Mean		5	50	95	Mean
Observed					Observed				
Jun	3	7	15	8	Jun	75.1	161.0	257.9	159.9
Aug	4	9	17	9	Aug	108.7	169.1	255.9	181.3
Sep	1	6	12	5	Sep	66.0	130.4	233.5	136.1

Jul	1	14	18	12	Jul	60.2	247.9	333.6	243.5
Aug	8	13	15	12	Aug	156.9	227.8	295.7	227.2
Sep	0	6	16	7	Sep	31.3	139.7	312.5	153.5
Modeled With State					**Modeled With State**				
Jun	4	8	13	8	Jun	108.4	193.9	236.6	181.8
Jul	1	13	17	12	Jul	86.2	239.5	299.4	228.3
Aug	8	13	17	12	Aug	144.9	227.0	364.7	235.1
Sep	0	6	14	6	Sep	57.7	148.2	311.4	161.2
Modeled Without State					**Modeled Without State**				
Jun	2	9	15	9	Jun	115.4	173.2	229.3	180.0
Jul	5	11	16	11	Jul	139.3	189.1	293.5	197.8
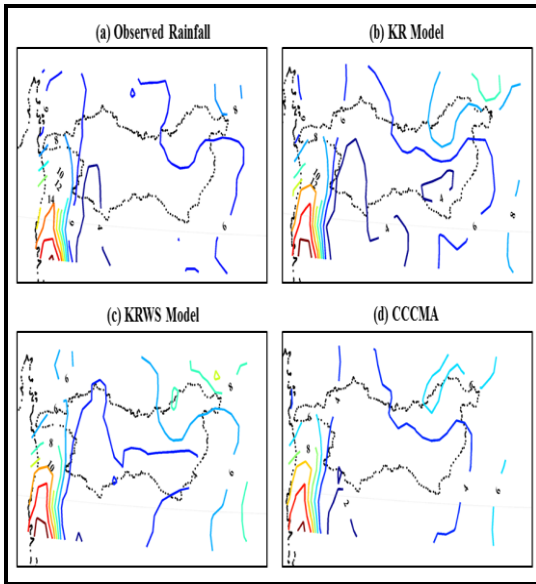
Figure 5 Correlation plots of mean for validation period(a) Observed rainfall (b) KR Model (c) KRWS Model (d) CCCMA
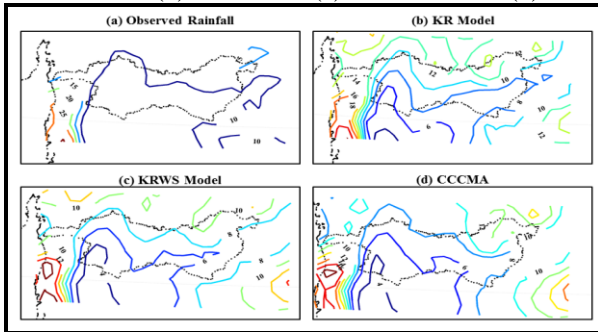
Figure 6 Correlation plots of standard deviation for validation period(a) Observed rainfall (b) KR Model (c) KRWS Model (d) CCCMA
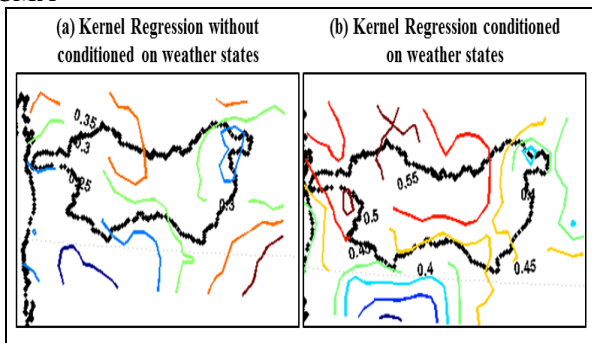
Figure 7 Correlation plots of R^2 value obtained by kernel regression model (a) without conditioning on weather states (b) with conditioning on weather states

For planning and management of water resources, characteristics of wet spells (WSs) and intervening dry spells (DSs) are extremely useful [Mehrotra and Sharma, 2010]. Singh and Ranade [2010] have worked out a Daily Mean Rainfall DMR of 12.1 mm/day for theTapi Basin. Table 2 gives a comparison of both observed and downscaled monthly and

monsoon wet days and rainfall amounts over the study region. It can be observed that the performance of KR model performs better than KRWS for both in capturing the number of wet days and simulating the total rainfall amount.

Table 2 Observed and Downscaled (5th, Median (50th), and 95th Percentile estimates) Monthly wet days for the Testing Period: 1996-2005

Sustained periods of wet and dry spells form the basis of reservoir design and operation and agricultural studies [Mehrotra and Sharma, 2010]. For the present study, the KR model is evaluated for dry/wet spell lengths probabilities and conditional probabilities, in terms of their ability to check, whether the shape and distribution of wet/dry spell length and also the conditional probabilities of predictandare captured by the downscaling model for validation period (1996-2005).

Figure 8 compares the cumulative distribution obtained from basin-averaged observed rainfall series with those obtained with five models used in present study. Among two methods KR and KRWS, it is observed that KR model shows minimum deviation from that observed rainfall and therefore KR method is selected for rainfall projections.
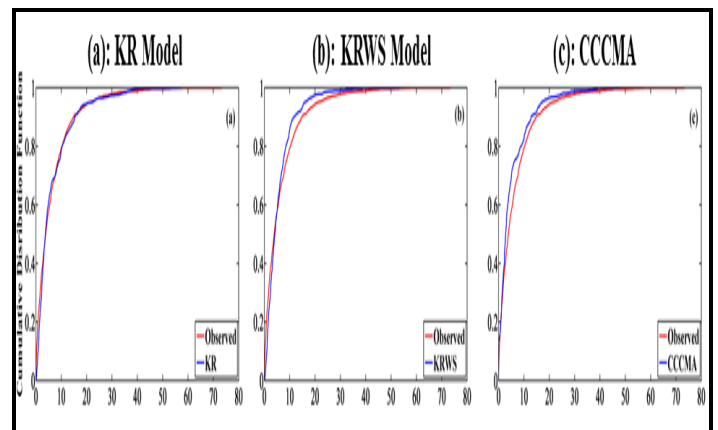
Figure 8 Cumulative distribution function of basin averaged rainfall. (a) KR (b) KRWS (c) CCCMA. The KR method is finally selected for CCCMA projections with historical experiment outputs.

The projected rainfall from both the KR and KRWS models are evaluated in terms of their ability to capture both temporal and spatial dependence. Figure 9 (a) shows the plots of basin averaged wet and dry spell length probabilities for the observed rainfall and the rainfall predicted by the model for the validation period and a close match of KR model is observed with that of the observe case whereas a noticeable deviation can be observed in case of KRWS model.Figure 9 (b) presents the scatter plots of cross correlation coefficients obtained from observed and model simulated rainfall series for both the KR and KRWS model. From the scatter plot, it can be inferred that the spatial structure of rainfall field is captured well by the KR model.
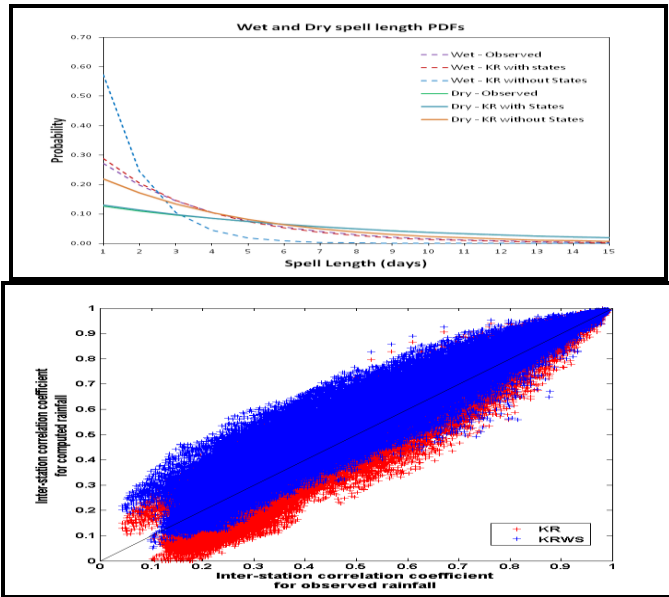
Figure 9(a)Basin-averaged Wet and Dry spell length probabilities for observed, KR and KRWS simulations. (b)Inter station correlation coefficient for observed rainfall compared with rainfall simulated by KR and KRWS model.

After analyzing the KR model and KRWS model in terms of their ability to capture basin averaged wet days and rainfall amount, basin averaged wet/dry spell length probabilities and spatial and temporal variability, the KR model is found better than KRWS model and is therefore selected for future rainfall projections.The KR model along with standardized and dimensionally reduced data corresponding to RCP 4.5 and RCP 8.5 experiments of CCCMA outputs conditioned on the rainfall states is used for the projection of the future JJAS (June, July, August and September) daily rainfall. For investigating the changes of the global warming on the precipitation characteristics, three time slices (2011-2040, 2041-2070 and 2071-2100) have been selected in the future.

The changes in the precipitation characteristics are evaluated in terms of changes in shape of wet and dry spell length, and conditional probabilities. Further, the 50-year return period of extreme daily rainfall for both the future scenarios RCP 4.5 and RCP 8.5 are also analyzed.Figure 10 presents the plots of wet and dry spell length probabilities obtained from model results of CCCMA for both the scenarios RCP 4.5 and RCP 8.5 respectively.
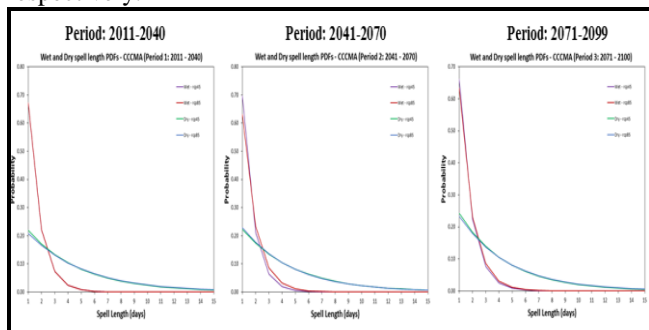
Figure 10 Wet and dry spell length probabilities for CCCMA for (a) 2011-2040, (b) 2041-2070 and (c) 2071-2100

The CDFs are obtained with model generated rainfall series for both RCPs i.e. RCP 4.5 and RCP 8.5 for examining the changes in the frequency of high/low rainfall occurrence. Figure 11 presents the CDF plots obtained for RCP 4.5 and RCP 8.5. The CDFs are further analyzed using the probability-probability plots.Figure 12(a) show the p-p plots for three time slices (2011-2040, 2041-2070 and 2071-2100) and can be observed that a significant and a slight change in the shape of CDF for high rainfall values is observed during 2071-2100 and 2041-2070 respectively.
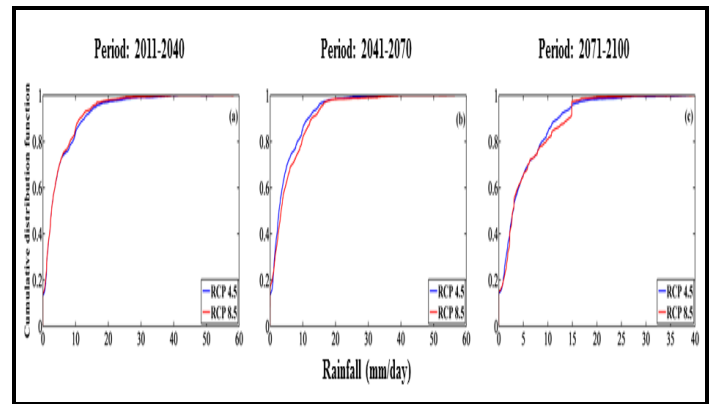
Figure 11 CDF of daily rainfall for near and far future for CCCMA projections (a) 2011-2040 (b) 2041-2070 (c) 2071-2100
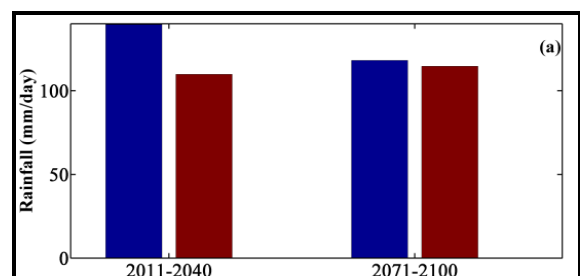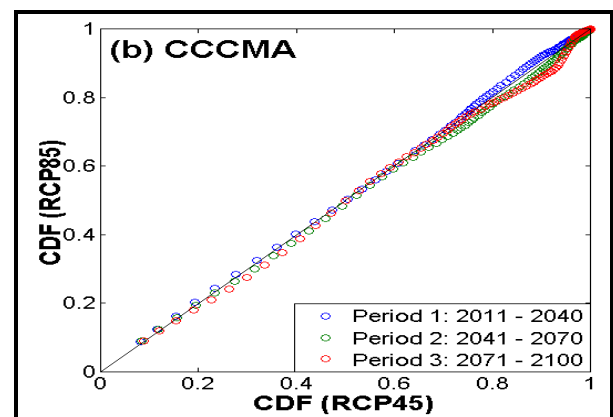
Figure 12(a) p-p plot of CDF of daily rainfall for (2011-2040), (2041-2070) and (2071-2100) for CCCMA. (b)50-year return

period of extreme daily rainfall for near future (2011-2040) and far future (2071-2100) for CCCMA

The extreme events will increase as a result of warming environment [Goswami et al., 2006]. Figure 12(b) compares results for trends for extreme daily rainfall for 50 - year return period for both the future scenarios for two time periods during 2011-2040 and 2071-2100. From the figure12 (b), it can be observed that, RCP 4.5 exhibit a decreasing trend while there is no change for RCP 8.5 projections for both the time period. Moreover, it can be seen that for far future RCP 4.5 and RCP 8.5 have a very slight difference in their projections.

4. CONCLUSIONS

In the present work, the rainfall is projected for the Tapi basin at a very fine resolution of (0.25° × 0.25°) up to 21st century. The present work is performed using the methodology developed by Kannan and Ghosh [2013] using the latest developed CMIP-5 experiments GCM model CCCMA.The present methodology uses projection of the rainfall state of the basin using the k-means clustering and CART. It is generally observed that almost dry rainfall state is having no significant trend, however, medium and high rainfall state tends to increase in future. In context of downscaling of rainfall amounts the present work uses of kernel density estimate. The kernel regression model conditioning on the rainfall state of the basin is found to be better in comparison to kernel regression without conditioning on weather state and is therefore used for rainfall projection for observed period and for future rainfall projections under scenarios RCP 4.5 and RCP 8.5 from CCCMA. The KR model conditioned on rainfall state of the basin is found to be better than other downscaling models developed in the past in capturing the problem of cross correlation.It is generally observed that almost dry rainfall state is having no significant trend however medium and high rainfall state tends to increase in future.

For future scope of work, a better weather typing scheme may be used in future to identify the exact weather state of region. There is also scope for improving the kernel bandwidth formula in this study. The present work uses a single GCM CCCMA model for assessing the future impacts of climate change. The uncertainty cannot rely using the single GCM Model, so there is scope to perform the same work using the multiple GCM models.

REFERENCES

i. Charles, S. P., Bates, B. C., and Hughes, J. P. (1999). "A spatiotemporal model for downscaling precipitation occurrence and amounts". *Journal of Geophysical Research: Atmospheres (1984–2012)*, 104(D24), 31657-31669.

ii. Fowler, H. J., Blenkinsop, S., and Tebaldi, C. (2007). "Linking climate change modelling to impacts studies: recent advances in downscaling techniques for hydrological modeling". *International Journal of Climatology*, 27(12), 1547-1578.

iii. Gangopadhyay, S., Clark, M., andRajagopalan, B. (2005). "Statistical downscaling using K-nearest neighbors". *Water Resources Research*, 41(2).

iv. Ghosh, S. (2010). "SVM-PGSL coupled approach for statistical downscaling to predict rainfall from GCM output". *Journal of Geophysical Research*, 115, D22102, doi: 10.1029/2009JD013548.

v. Ghosh, S., and Mujumdar, P. P. (2006). "Future rainfall scenario over Orissa with GCM projections by statistical downscaling". *Current Science*, 90(3), 396-404.

vi. Goswami, B. N., Venugopal, V., Sengupta, D., Madhusoodanan, M. S., and Xavier, P. K. (2006). "Increasing trend of extreme rain events over India in a warming environment". *Science*, 314(5804), 1442-1445.

vii. Hughes, J. P., Guttorp, P., and Charles, S. P. (1999). "A non-homogeneous hidden Markov model for precipitation occurrence". *Journal of the Royal Statistical Society: Series C (Applied Statistics)*, 48(1), 15-30.

viii. Stocker, T. F et al. (2013). "Climate change 2013: The physical science basis".*Intergovernmental Panel on Climate Change, Working Group I Contribution to the IPCC Fifth Assessment Report (AR5) (Cambridge Univ Press, New York)*.

ix. Kannan, S., andGhosh, S. (2011). "Prediction of daily rainfall state in a river basin using statistical downscaling from GCM output". *Stochastic Environmental Research and Risk Assessment*, 25(4), 457-474.

x. Kannan, S., andGhosh, S. (2013). "A nonparametric kernel regression model for downscaling multisite daily precipitation in the Mahanadi basin". *Water Resources Research,* 49(3), 1360-1385.

xi. Krishna Kumar, K., S. K. Patwardhan, A. Kulkarni, K. Kamala, K. K. Rao, and R. Jones (2011), simulated projections for summer monsoon climate over India by a high-resolution regional climate model (PRECIS), *Current. Science*, 101(3).

xii. Mehrotra, R., and Sharma, A. (2006). "Conditional resampling of hydrologic time series using multiple predictor variables: A *K*-nearest neighbour approach". *Advances in water resources*, 29(7), 987-999.

xiii. Mehrotra, R., and Sharma, A. (2010). "Development and application of a multisite rainfall stochastic downscaling framework for climate change impact assessment". *Water Resources Research*, 46(7).

xiv. Mehrotra, R., and A. Sharma (2005), A nonparametric nonhomogeneous hidden Markov model for downscaling of multisite daily rainfall occurrences, *Journal of Geophysical. Research.* 110, D16108, doi: 10.1029/2004JD005677.

xv. Mujumdar, P, P and Kumar, N, D. (2013). "Floods in Changing Climate: Hydrologic Modelling". *International Hydrology Series*, Cambridge.

xvi. Raje, D., andMujumdar, P. P. (2009). "A conditional random field–based downscaling method for assessment of climate change impact on multisite daily precipitation in the Mahanadi basin". *Water Resources Research*, 45(10).

xvii. Salvi, K., andGhosh, S. (2013). High-resolution multisite daily rainfall projections in India with statistical downscaling for climate change impacts assessment. *Journal of Geophysical Research: Atmospheres*, *118*(9), 3557-3578.

xviii. Singh, N., andRanade, A. (2010). "The wet and dry spells across India during 1951-2007". *Journal of Hydrometeorology*, 11(1), 26-45.

xix. Tatli, H., NüzhetDalfes, H., andSibelMenteş, Ş. (2004). "A statistical downscaling method for monthly total precipitation over Turkey". *International Journal of Climatology*, 24(2), 161-180.

xx. Wilby, R. L., S. P. Charles, E. Zorita, et al. (2004), The guidelines for use of climate scenarios developed from statistical downscaling methods. Supporting material of the Intergovernmental Panel on Climate Change (IPCC), prepared on behalf of Task Group on Data and Scenario Support for Impacts and Climate Analysis (TGICA).

xxi. Wilby, R. L., Tomlinson, O. J., and Dawson, C. W. (2003). Multi-site simulation of precipitation by conditional resampling. *Climate Research*, 23(3), 183-194.

xxii. Willems, P., and Vrac, M. (2011). "Statistical precipitation downscaling for small-scale hydrological impact investigations of climate change". *Journal of Hydrology*, 402(3), 193-205.

xxiii. Yatagai, A., Arakawa, O., Kamiguchi, K., Kawamoto, H., Nodzu, M. I., and Hamada, A. (2009). "A 44-year daily gridded precipitation dataset for Asia based on a dense network of rain gauges". *Sola, 5*, 137-140.

Study Of Climate Change Impact On Reservoir Storage Capacity Using Hydrograph- A Case Study Of Gangapur Dam, Nashik District, India

Kadbhane S.J.[1]Dr. Manekar V.L.[2]

[1]Research fellow, Water Resource Department, SVNIT Surat, Gujarat,395 007, India.

[2]Associate Professor, Water Resource Department, SVNIT Surat, Gujarat, 395 007, India.

Email:sharad_kadbhane@rediffmail.com,
vivek_manekar@yahoo.co.in

ABSTRACT: *Climate change has showing the critical impact on water resources and reservoir storages. In absence of gauging system on rivers it is difficult to collect the discharge for hydrological and climate change studies in river basin. According to IPCC some of the studies have detected significant trends in some indicators of river flow, and some have demonstrated statistically significant links with trends in temperature or precipitation; but no globally homogeneous trend has been reported.To study the climate change impact on such basin it is advantageous to use the dam storage and overflow data. For this study month wise precipitation data observed by Indian water portal and day wise precipitation and discharge data collected by Maharashtra Irrigation Department, Nashik division from July to October months particularly for Gangapur dam, upper Godawari basin, Nashik district has been used. Hydrographical analysis has been carried out by using above mentioned data for the period of 1971 to 2012. After studying the hydrographs of above mentioned years it has been found that rainfall and discharge event shows 20 to 80% variations year by year, also there is a 10 to 20% reduction in rainfall intensities during last two decades as compare to previous decades and rainfall duration has shown significant impact on reservoir storage capacity. It has been conclude that use of reservoir storage and overflow data is the better option for hydrographical study in the absence of stream gauging data to observe climate change impac*t.*

Keywords: Climate change, reservoir storage, hydrology, hydrographical study, river basin.

1. INTRODUCTION

Climate change has showing the critical impact on water resources and reservoir storages. It is necessary to find out theactual runoffthrough stream with rainfall occur.Measurement of actual runoff is difficult in absence of gauging system. Hydrological and climate change studies in river basinrequires accurate data of all hydrological parameters.Accurate hydrograph simulation is an essential basis for floodforecasting, hazard mitigation, and water resource managementamid an increasing need for such activities, given the increasingoccurrence of global warming and population growth (Vörösmartyet al).Calibration of rainfall-runoff models for catchmentswith ephemeral streamflow regimes can be difficult because they tend to have infrequent runoff events withgenerally narrow peaks, limiting the information contained within a streamflow time series.

Inaddition, for most catchments, while streamflow dataof high temporal resolution are available, only dailyrainfall data exist. This limits application of discrete time rainfall-runoff models to a daily time step, whilethe observed flow peaks are typically only a few hoursin duration (Chapman TG.). Consequently, most of the informationcontained within the recorded streamflow is not used.However, ephemeral streamflow catchments lend themselves to direct estimation of the unit hydrograph response curve, as most peaks are well-separated, havinglittle or no overlap with preceding or subsequent flowevents. This enables the higher temporal resolution datacontained within the streamflow record to be used,thereby increasing the amount of information available(compared to daily data) and revealing the shape ofthe unit hydrograph more clearly(Croke BFW).The earth has experienced a significant change of warming overthe past 100 years. A temperature rise will lead to an increased volume of ice-melt water, and further result in the increase of discharge of headstream from mountainous areas, plus the increasedvolume of precipitation. Flood control and agriculture water arehighly related to the discharge change affected by climate change(Yanlong Kong et al).Runoff prediction has been an active area ofresearch in surface water hydrology and will remainso in the foreseeable future because of the uncertainties associated with both the meteorological andhydrological parameters causing extreme floodevents.

A reasonable prediction of runoff not onlyprovides useful information for management of waterresources, but also reduces losses to life and propertycaused by extreme events. Predicted runoff is alsovital for the economic analysis of flood managementalternatives. With increasing population and economic activity in floodplains and along major rivers theimportance of accurate runoff prediction is increasing.Several techniques have been developed to predictrunoff ranging from empirical or statistical relationships to detailed mathematical models. While empirical or statistical relationships can provide magnitudeand frequency of floods, they are not capable ofgenerating a runoff hydrograph with complete information on timing of peak, volume of flood and shapeof hydrograph, especially slope of rising and fallingsides of hydrograph. Though frequency analysis ofpast flood peaks can provide information on the risk, itis limited by its lack of consideration of the forcingfactors producing floods(Sajjad Ahmad et. al.).

Nashik is one of the agriculture producer districts among the India and is a food bank of Mumbai as well as largest table grape exporter in India. There are seventeen major, medium, minor dams located in Nashik district which supply the water foe agriculture, but from the last decade climatic changes shows adverse effect on storage level of dams and it directly impact on agricultural activity. It is need to study those effects on dam storages since few previous years. In this paper climate change impact has been study particular for Gangapur dam by using hydrograph.

2. MATERIAL AND METHODS

2.1 Use of Hydrograph in Study Area

Runoff hydrograph at the outlet of an urban catchmentdepends on the space-time variation of rainfall, the rainfall-runoff process over the catchment area, and the hydrograph routing in pipes. With the help of computers, complexmodels can be used to simulate detailed runoff hydrographsand provide flow rates and hydraulic gradient lines at thevarious nodes of the sewer network(Crobeddu E. 2007).A hydrograph is the hypothetical response of a watershed (in terms of runoff volume and timing) to aninput of rainfall. As a hydrograph is applicable only to the direct runoff component of a hydrograph (i.e., surface runoff), a separate determination of the base flow component is required. A hydrograph is specific to particular watershed, and specific to a particular length of time corresponding to the duration of the effective rainfall. In this study hydrograph is plotted for every year for the months July to October. There can be many hydrographs, each one corresponding to a different duration of effective rainfall. In this study time is taken in day.

2.2 A Technique for Deriving an Average Event Hydrograph from Storage Croke B. approach

Consider a small length of stream (∂x) over a small time element (∂t) for which there is no flux of water into or out of the channel (i.e. the only flux is along the channel). Conservation of mass requires that

$$\frac{\partial Q(x,t)}{\partial x} = -\frac{\partial A(x,t)}{\partial t} - l(x,t) \quad\dots\dots\dots\dots\dots(1)$$

where $Q(x, t)$ is the discharge, $A(x, t)$ is the flow cross section area and $l(x, t)$ is the loss of water due to evapo ration and infiltration into the streambank (for porous channels) at position x at time t. The evaporative loss from the stream is given by

$$l_e(x,t)=E(x,t)w(x,t)\dots\dots\dots\dots\dots\dots\dots\dots(2)$$

where $E(x, t)$ is the evaporation per unit width, and $w(x, t)$ is the width of the water surface. The infiltration loss can be written as:

$$l_i(x,t)=I(x,t)P(x,t)\dots\dots\dots\dots\dots\dots\dots\dots(3)$$

where $I(x, t)$ is the infiltration per unit wetted streambed, and $P(x, t)$ is the wetted perimeter. The value of $I(x, t)$ will depend on the surface of the saturated zone in the porous material adjoining the channel, and so a mass balance equation is needed to derive this function. This will not be considered here as the functional form of $l(x, t)$ will not be specified. In this discussion, the following notation will be used:

$$\frac{\partial y}{\partial t}=\dot{y}, \quad \frac{\partial y}{\partial x}=y', \quad \frac{\partial^2 y}{\partial t \partial x}=\dot{y}_x\dots\dots\dots\dots\dots\dots\dots\dots(4)$$

Typically, the PDE in Eq. (1) is simplified to an ODE:

$$Q(x,t)=-\alpha(x)\dot{Q}\dots\dots\dots\dots\dots\dots\dots\dots\dots\dots\dots\dots\dots(5)$$

for which the solution is an exponential:

$$Q(x,t)=\beta(x)exp[-\alpha(x)(t-\delta)]\dots\dots\dots\dots\dots\dots\dots\dots(6)$$

where $\beta(x)$ is the decay constant, δ is the time when flux into the channel stopped (rainfall + runoff + inter flow + baseflow) and $\beta(x)$ is the flow at time δ.
Here we will investigate what assumptions are required for this simplification, and the implications of these assumptions. The discharge $Q(x, t)$ is given by $v(x, t)A(x, t)$ where $v(x, t)$ is the

effective streamflow velocity, averaged across the stream cross-section (note that since Q, v and A are all positive, monotonically decreasing functions of t for all x, this implies that v and A decay more slowly than Q). Thus, Eq. (1) can be written as

$$Q' = -\frac{1}{v}\dot{Q} + \frac{Q}{v^2}\dot{v} - l\dots\dots\dots\dots\dots\dots\dots(7)$$

This can be rearranged to give:

$$\dot{Q} = -Q' + Q\frac{\dot{v}}{v} - lv\dots\dots\dots\dots\dots\dots\dots..\dots.(8)$$

Combining Eq. (8) with Eq. (5) gives the dependence of a on Q and v:

$$\alpha = v\frac{Q'}{Q} + \frac{\dot{v}}{v} + \frac{l}{A}\dots\dots\dots\dots\dots\dots\dots\dots\dots\dots\dots(9)$$

The solution is an exponential when a is independent of time (i.e. $\dot{\alpha}= 0$). Using the form for Q given in Eq. (6) gives:

$$\dot{z} = \dot{v}\left[\frac{\beta'}{\beta} - (t - \delta)\alpha'\right] - v\alpha' + \frac{v\dot{v} - \dot{v}^2}{v^2}\dots\dots\dots\dots(10)$$

where $z(x, t)= l(x, t)/A(x, t)$. This sets a particular relationship between Q, v and α, which implies that only a specific channel structure can result in an exponential decay. The complex, highly variable nature of natural stream channels thus means that if Eq. (A.6) has the correct functional form (and assuming the mass balance equation is correct), the decay coefficient a is likely to be time-dependent and a single constant-coefficient exponential decay is not appropriate for such systems.

An alternate approach is to integrate Eq. (1) with respect to x to obtain the streamflow at position L along the stream $Q(L, t)$:

$$Q(L,t) = \int_0^L Q'dx = -\int_0^L\left[\frac{1}{v}\dot{Q} - \frac{\dot{Q}}{v^2}\dot{v} + l\right]dx\dots\dots\dots\dots\dots\dots(11)$$

By using above methods analysis has been done for the avilable data of gangapur dam.

2.3 Detail of Gangapur Dam

Gangapur dam have locate at Latitude 20°38', Longitude 73°19', and it is earthen dam constructed from 1954 to 1963. The total catchment area of the dam is 357.4 Sq.kmand average annual rainfall is 1240 mm.The total dam length is 3810 m. and maximum height of the dam is 36.57m. The total Gross storage of the dam is 215.88 MCM and total live storage is 203.76 MCM, Submergence Area 2231Ha. The length of the waste weir is 102 m. There are total 9 radial gates of size (9.15x6.10 m.) having the discharge capacity of 2294 Cumec. The dam has two canals, the left bank canal is 64 Km. long and right bank canal is 30 Km. long. The total irrigable area of this dam is 15960 Ha. Due to deposition of silt storage capacity of Gangapur Dam reduced to 5630 mcft also due to increase in residential zone (civilization) in command area of Nashik Right Bank canal is closed and now since 2006.Thatland is given to Nashik Municipal Corporation for laying pipeline for drinking water from Gangapur Dam. The water from Gangapur Dam is used for irrigation through Nashik Left Bank canal Godawari canal in Nashik district, domestic purpose of Nashik Municipal Corporation and

industrial purpose M.I.D.C. Satpur, Thermal Power station Eklhare.
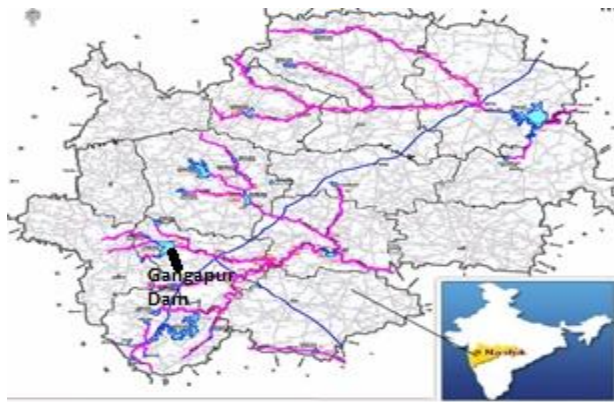
Figure 1. Location map of Gangapur Dam
2.4 Data Collection

For this study month wise precipitation data of Nashik District generated by Indian water portal and date wise precipitation and storage data collected by Maharashtra Irrigation Department, Nashik division from July to October months particularly for Gangapur dam, upper Godawari basin, Nashik district have been used. Hydrographical analysis has been carried out by using above mentioned data for the period of 1971 to 2013.

3. RESULTS AND ANALYSIS

3.1 Hydrograph of Gangapur Dam Catchment

By collecting the day wise data of precipitation in mm and water inflow in damin million cubic meters (considering as stream flow) hydrographs are plotted for every year. Rainfall is mainly in 1st July to 15th October in Nashik district, so by considering 1st July as first day and 15th October is 107th day, hydrographs have been plotted. The hydrographs of decade 1971-80,1981-90 and 1991-2000 areas shown in fig.2,3 and 4.
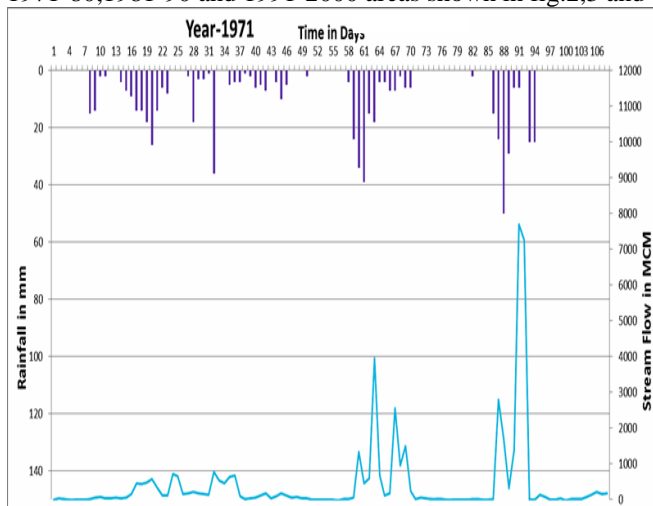
Figure 2. Hydrograph of Gangapur Dam of Deacade 1971-80
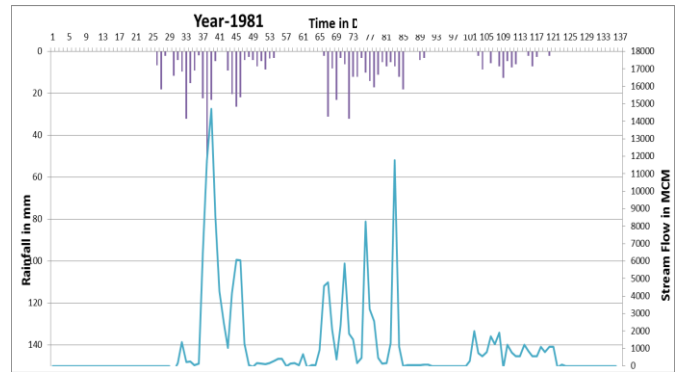
Figure 3. Hydrograph of Gangapur Dam of Deacade 1981-90
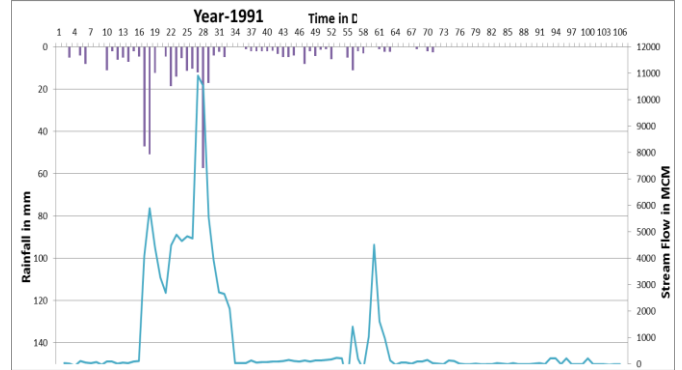
Figure 4. Hydrograph of Gangapur Dam of Deacade 1991-2000

After studying all hydrograph since 1971, it has been observe thatduration of rainfall events get decrease year by year and due to that runoff get decrease and evaporation and infiltration losses are increases, this conditions directly effect on dam storage. After studying the hydrographs of above mentioned years it has been found that rainfall and discharge event shows 20 to 80% variations year by year.

3.2 Rainfall Intensity in Nashik District

In Nashik average rainfall since 1971 is about 1240mm as per data available with Indian water portal. The amount of rainfall below average is taken –ve, above average is taken +ve, and considering this data graph has been plotted as below:
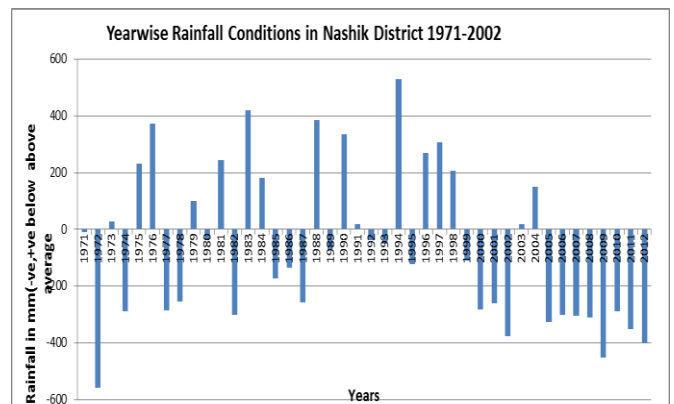
Figure 4. Rainfall below and above average since1971

After sudying above graph carefully, since 1971to 1999 rainfall is near to avrege at maximum time but from 1999 rainfall decrese significantly. So it is nothing but the sign of climate change impact on percipitation, and near about 10-20% reduction in rainfall.

3.1 Gangapur Dam Storage conditions

Once rainfall deceases, runoff gets reduced and it effect on dam storage. Fig.5 is plotting with help of dam storage data collected from Maharashtra irrigation department, Nashik region.Gangapur dam average storage since 1971 is about 89% as per available data.The% dam storage below average is taken -ve, above average is taken +ve, and considering this data, graph has been plotted as below:
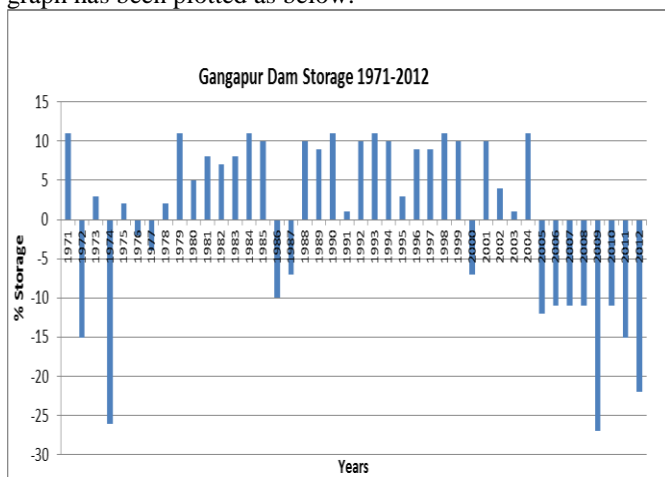
Figure 5. Storage of Gangapur dam below and above average since1971

After sudying above graph carefully since 1971to 1999 dam storage is below and above than avrege at maximum time but from 1999 dam storage decrese significantly. So it is nothing but the sign of climate change impact on runoff and dam storage, observe near about 10-35% reduction in dam storage.

4. CONCLUSIONS

After studying the hydrographs of above mentioned years, it has been found that rainfall and discharge event shows 20 to 80% variations year by year, also there is a 10 to 20% reduction in rainfall intensities during last two decades as compare to previous decades and rainfall duration has shown significant impact on reservoir storage capacity. Since 1971to 1999 dam storage is above and below than avrege at maximum time, but from 1999 dam storage decrese about 10-35%.So it is the sign of climate change impact on runoff and dam storage. It has been conclude that use of reservoir storage and overflow data is the better option for hydrographical study in the absence of stream gauging data to observe climate change impacts.

REFERENCES:

i. Ahmadi M, Hadded OB, Marino MA (2014) Extraction of flexible multi-objective real time reservoir operation rule. Water Resources Management 28(1): 131-147

ii. Vörösmarty CJ, GreenP, Salisbury J, Lammers RB(2000) Global waterresources: vulnerability from climate change and population growth. Science289:284–288.

iii. Chapman TG. (1996) Unitgraph Identification from streamflow data. Hydrol Processes10:773–82.

iv. Croke BFW (2006) A technique for deriving an average event unithydrograph from streamflow—only data for ephemeralquick-flow-dominant catchments. Advances in Water Resources 29:493–502.

v. Yanlong Kong, Zhonghe Pang(2012) Evaluating the sensitivity of glacier rivers to climate change basedon hydrograph separation of discharge.Journal of Hydrology 434–435:121–129

vi. Sajjad Ahmad,Slobodan P,Simonovic, (2005) An artificial neural network model for generating hydrographrom hydro-meteorological parameters.Journal of Hydrology 315:236–251

vii. Croke B.F.W.(2006)A technique for deriving an average event unit hydrograph from streamflow -only data for ephemeralquick-flow-dominant catchments. Advances in Water Resources 29:493–502

viii. CrobedE, Bennis du, Rhouzlane S.S (2007). Improved rational hydrograph method.Journal of Hydrology 338:63– 72

ix. Obrien J O Brien, Bruce D-Misstear, Laurence W. Gill, Jenny L. Deakin , Ray Flynn (2013) . Developing an integrated hydrograph separation and lumped modelling approach to quantifying hydrological pathways in Irish river catchments. Journal of Hydrology 486: 259–270

x. Jakeman AJ, Littlewood IG, Whitehead PG. (1990) Computation of theinstantaneous unit hydrograph and identifiable component flowswith application to two small upland catchments. J Hydrol117:275–300.

Statistical Downscaling Of Temperature In Godavari River Sub Basin

V. R. Saraf[1] and D. G. Regulwar[2]
[1]Research Scholar, Dept. of Civil Engg, Government College of Engineering, Aurangabad, Maharashtra State, India. E-mail: vrsaraf@yahoo.com

[2] Associate Professor, Dept. of Civil Engg, Government College of Engineering,Aurangabad, Maharashtra State, India. E-mail: regulwar@gmail.com

ABSTRACT: *The climate impact studies in hydrology often rely on climate change information at fine spatial resolution. Because generalcirculation models (GCMs) operate on a coarse scale, the output from a GCM has to be downscaled to obtain the information relevant tohydrologic studies.Statistical downscaling methods describe a statistical relationship between large-scale atmospheric variables such as temperature,humidity, precipitation, etc., and local-scale meteorological variables like precipitation.In this paper, SDSM was used todownscaled the monthly temperature in Godavari river basin.The predictor variables are extracted from: (i) the National Centre for Environmental Prediction (NCEP) reanalysis dataset for the period 1961–2003; and (ii) the simulations from the third-generation Hadly centre Coupled Climate Model (HadCM3)and Coupled Global Climate Model (CGCM3) for emission scenarios A2, B2and A1B for the period 1961–2100. The scatter-plots and cross-correlations are used for verifying the reliability of the*

simulation.The results showthat the temperature is projected to increase in future for almost all the scenarios. It was concluded that Statistical downscaling using SDSM can be implemented to downscale coarse-scale atmospheric parameters to monthly temperature at station scale by using the above parameters as inputs in the study area.

Keywords:*Climate change, SDSM,maximum and minimum temperature,IPCC SRES scenarios.*

1.INTRODUCTION:

The General Circulation Models (GCMs) are the most advanced tools that are available for the simulation of future climate (Anandhi et al., 2008). These models are capable of predicting climate, hundreds of years into future considering the GHG concentrations in the atmosphere. GCMs as the most credible tools designed to simulate time series of climate variables, considering the concentrations of GHGs (Ghosh and Mujumdar 2008). Although GCMs are among the most advanced tools for predicting the futureclimate, they are incapable of producing outputs at a finer spatial resolution, needed for most hydrologic studies. The spatial resolution of a present day GCM is coarse, which is in the order of a few hundred kilometers (Anandhi et al., 2008). The coarse resolution does not allow the direct use of GCM predictions at the catchment scale.Using downscaling techniques, GCM outputs can be changed into surface variables in the scale of the basin under study (Wilbyet al.2002*). According to Tisseuil et al. (2010), downscaling bridges the large scale atmospheric conditions with local scale climatic data.There are different methods for creating local climate scenarios from GCM climate scenarios. Downscaling techniques are broadly classified into two categories as dynamic downscaling and statistical downscaling. In dynamic downscaling a Regional Climatic Model (RCM) is nested in a GCM. The RCM is an atmospheric physics based model to which boundary conditions are provided with the output of a GCM. The major drawback of dynamic downscaling is its complexity and high computation cost (Anandhi et al., 2008). The other problem with dynamic downscaling is the propagation of systematic bias from GCM to RCM (Salathe 2003). Statistical downscaling methods construct statistical relationships between the large scale GCM outputs (predictors) and the catchment scale climate variables (predictands). The basic advantage of statistical downscaling is that it is computationally less demanding compared to dynamic downscaling.

According to Wilby and Wigly (2000), statistical downscaling is based on few assumptions. These assumptions are that the predictor-predictand relationships are valid under future climatic conditions, and predictor variables and their changes are well characterised by GCMs. In general, statistical downscaling techniques are classified into three main categories as weather classification, regression models and weather generators. Weather classification methods classify large scale atmospheric variables of GCMs into finite number of states and relate them to basin scale climate variables. Regression methods build up linear or nonlinear functions

between predictors and predictands. Weather generators produce a synthetic series of climate data, while preserving statistical attributes of the observations of climate variables (Fistikoglu and Okkan,2011)

The present study make use of SDSM downscaling model.SDSM was created as a tool for downscaling statistically by Wilby et al.(2002).The base of the model is a linear multiple regression and is used to predict the climate parameters such as precipitation and temperature in long time regarding climate large scale signals. In classifying different downscaling models, statistical downscaling model is one of the best models.(Wilbyet al.2002,Khanday et al 2008).In this model, a linear multiple regression is created between the large scale predictor variables (independent variables) and the predictant variables (precipitation or temperature) as dependent variables for each month of the year. Suitable large scale predictors are selectedby correlation analyses between the predictor variables and partial correlation in the area under study.The prediction of climate change model was carried out for scenarios, A2,B2 and A1B, among the presented scenarios in SRES(IPCC 2007)

Temperature is an important parameter for climate change impact studies. A proper assessment of probablefuture temperature and its variability is to be made for various hydro-climatology scenarios. In a transient simulation, anthropogenic forcing, which are mostly decided based on IPCC climate scenarios, are changed gradually in a realistic pattern. The objective of this study is to downscale mean monthly maximum temperature (T max) and minimum temperature (T min) using SDSM on a river sub basin scale in an arid region from simulations of CGCM3 and HadCM3 for latest IPCC scenarios. The scenarios which are studied in this paper are relevant to IPCC's fourth assessment report (AR4) which was released in 2007 (IPCC, 2007)

2. STUDY REGION:

Godavari rises in the Sahyadris near Triambakeswar, about 80 km from the shore of Arabian Sea, at an elevation of 1,067 m in the Nasik district of Maharashtra. After flowing for about 1,465 km in a general south-easterly direction through Maharashtra and Andhra Pradesh, Godavari falls into the Bay of Bengal north of Rajahmundry.The basin lies between latitudes 16^0 16' 0" N and 23^0 43` N longitudes 73^0 26' E and 83^0 07' E.The basin extends over an area of 312,813 km², which is nearly 10% of the total geographical area of the country.It is bounded on the north by the Satmala Hills, the Ajanta Range and the Mahadeo Hills, on the east and south by the Eastern Ghats and on the west by the Western Ghats**.**The study area of the research is the upper Godavari basin in Maharashtra state in India The mean monthly T max in the upper Godavari basin varies from 29.64 to 38.60 and mean annual T max is 32.45. The mean monthly T min ranges from 14.38 to 25.12 based on decadal (1961–2000) observed values.

3. DATA EXTRACTION:

3.1. Reanalysis data

The monthly mean atmospheric variables were derived from the National Center for Environmental Prediction(NCEP/NCAR) reanalysis dataset for the period of January1961 to December 2003. The data have a horizontal resolution of $2.5^o \times 2.5^o$ and seventeenconstant pressure levels in the vertical.

3.2 GCM data

The Canadian Center for Climate Modeling and Analysis(CCCma) providesGCM data for a number of surface and atmospheric variablesfor the CGCM3 T47 version which has a horizontalresolution of roughly 3.75^o x3.75^o,and a vertical resolution of 31 levels. CGCM3 is the thirdversion of the CCCma Coupled Global Climate Model and third-generationHadly centre Coupled Climate Model (HadCM3), whichhas a spatial resolution of 2.5° x 3.75°.

3.3 Observed data was obtained from IMD for the period of 1961-2008.

4. SELECTION OF PREDICTORS:

In SDSM, screening of predictor variables is conducted through linear correlation analysis and scatter plots (between the predictors and predictand variables) and by investigating the percentage of variance explained by each predictand–predictor pair. Appropriate predictors are chosen by considering whether the identified variables and relationships are physically sensible for the particular experiment and study site

For identification of the best predictor all 26 atmospheric variables in the grid boxes (completely covering the entire study area) were selected as potential predictors. Subsequently, the most sensitive predictors for each predictand were identified through the screening(Wang & Yang 2011). The predictor variables applied in this study areSurface Zonal Velocity (ugl),850hPa Zonal Velocity(8_ugl),850hPa Geopotential(p850),temp forCGCM3 and Surface Vorticity (zas), 850hPa Geopotential(p850),surface specific velocity (humas),temp for Hadcm3 (at the 95% confidence level).

a)
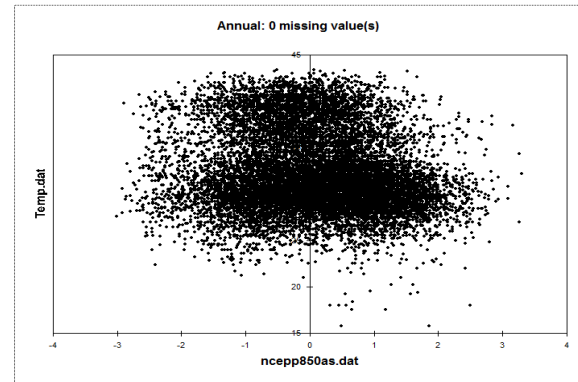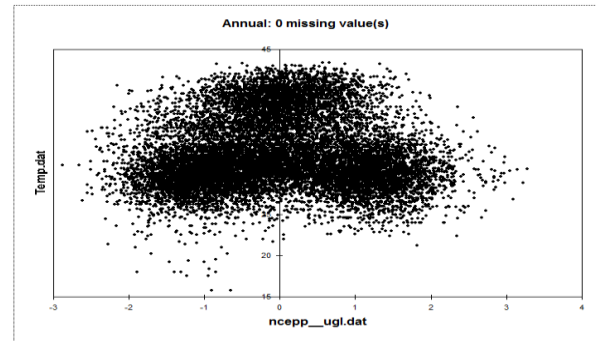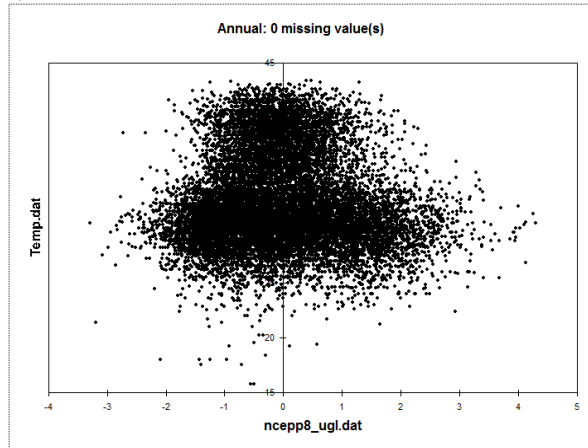
b)
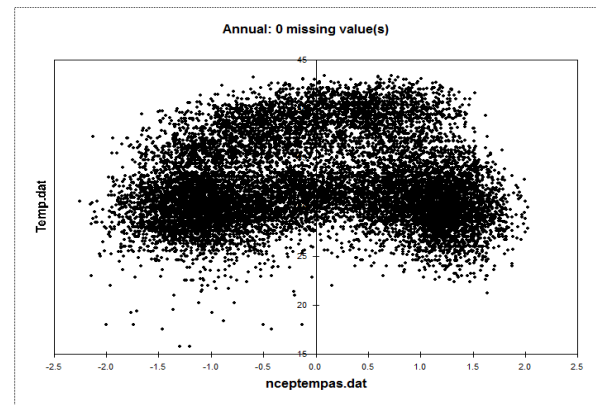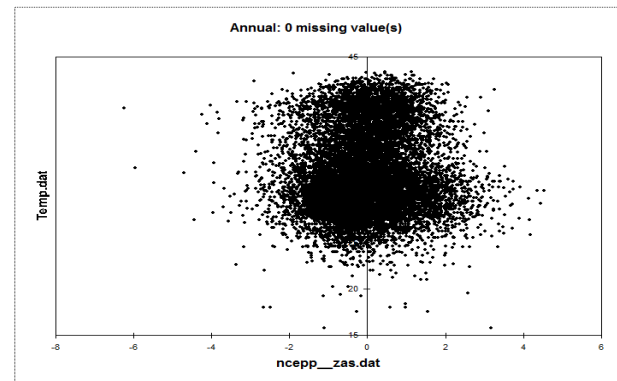
Figure 1: Scatter plots prepared to investigate dependence structure between probable predictor variables in NCEP data and the observed Temperature. (a) denotes plots for CGCM3 , while (b) denotes plots for HadCm3.

5.CALIBRATION AND VALIDATION:

The model was calibrated and validated using observations (1961–1980) and (1981–2000), respectively. The predictor variables were from the NCEP reanalysis data. The predictands were from the observed surface variables. Table 1 showed the performance in the validation period (1981–2000).

Table 1: Performance assessment for predictands in validation(1981–2000)

GCM	Item	Durbon Watson	SE	RS
CGCM3	Daily mean maxi temperature (_C)	0.627	2.260	0.042
	Daily mean Mini temperature (_C)	0.473	2.251	0.059
HadCM3	Daily mean maxi temperature (_C)	0.481	2.253	0.059
	Daily mean Mini temperature (_C)	0.627	2.260	0.627

6.RESULTS AND DISCUSSION:

The daily maximum and minimum temperature data of upper Godavari (Maharashtra) for the period of 1961-2003 was used in order to carry out the present study. SDSM input files were produced and the downscaled data of the three parameters were simulated for a 90 year period (2011-2099).

The present study investigates the effects of different scenarios of SDSM in upper Godavari. The weather parameters are estimated by A2 and B2 scenarios for HadCm3 and A2 and A1B scenario for CGCM3 in future time periods as following :
1. The first time period : (2011-2039)
2. The second time period : (2040-2069)
3. The third time period : (2070-2099)

The results of estimated weather parameters in different scenarios are presented in (Tables 2 andTable 3).

Table 2 : Observed and estimated maximum monthly temperature means in future timeperiods of different scenarios (°C)

a)Maximum temperature

Hadcm3_A2

	Jan	Feb	Mar	April	May	June	July	Aug	Sep	Oct	Nov	Dec	Annual
Observed 61-2000	34.7	39.3	42	43.4	43.4	42.6	36.6	35.8	37	37.6	34	37	43.4
2011-40	36.86	41.80	45.19	45.58	48.54	42.52	36.14	36.13	37.48	37.82	35.28	35.11	49.01
2041-2070	37.41	42.51	44.79	45.62	48.53	41.92	36.52	35.82	37.74	37.57	35.61	35.45	48.53
2071-2099	37.51	42.67	42.1	46.02	47.11	41.12	36.16	35.58	37.53	37.83	35.56	35.58	47.2

(continuation fragment at top of right column: 9 | 9 | 4 | 9 2 6)

Hadcm3_B2

	Jan	Feb	Mar	April	May	June	July	Aug	Sep	Oct	Nov	Dec	Annual
Observed 61-2000	34.7	39.3	42	43.4	43.4	42.6	36.6	35.8	37	37.6	34	37	43.4
2011-40	37.1	42.05	45.06	45.71	49.07	42.98	36.9	35.82	37.97	37.5	35.16	35.41	49.07
2041-2070	37.15	42.30	45.27	45.66	48.81	42.43	36.29	35.85	37.44	37.42	35.20	35.72	48.81
2071-2099	37.76	42.4	45.10	45.78	47.55	42.17	36.25	35.70	37.67	37.62	35.46	35.46	47.57

CGCM3_A2

	Jan	Feb	Mar	April	May	June	July	Aug	Sep	Oct	Nov	Dec	Annual
Observed 61-2000	34.7	39.3	42	43.4	43.4	42.6	36.6	35.8	37	37.6	34	37	43.4
2011-2040	36.98	41.37	44.15	45.38	49.00	44.43	37.72	35.11	37.19	37.61	35.19	35.49	49.00
2041-2070	36.93	41.87	44.49	45.56	48.68	44.58	37.99	35.12	37.38	37.51	35.37	35.67	48.85
2071-2099	36.98	41.77	44.52	45.58	48.58	45.10	37.72	34.94	37.28	37.78	35.37	35.36	48.58

CGCM3_A1B

	Jan	Feb	Mar	April	May	June	July	Aug	Sep	Oct	Nov	Dec	Annual
Observed 61-2000	34.7	39.3	42	43.4	43.4	42.6	36.6	35.8	37	37.6	34	37	43.4
2011-2040	36.85	41.44	44.46	45.39	49.33	44.28	37.62	35.26	37.31	37.56	35.26	35.61	49.33
2041-2070	37.03	41.60	44.35	45.10	48.73	44.39	37.36	34.95	37.66	37.61	35.16	35.47	47.73
2071-2099	37.11	41.52	44.80	45.55	48.63	44.98	37.44	35.07	37.26	37.84	35.16	35.43	48.64

Table 3 : Minimum temperatureObserved and estimated minimum monthly temperature means in future time periods of different scenarios (°C)

Hadcm3_A2

	Jan	Feb	Mar	Apr	May	Jun	July	Aug	Sep	Oct	Nov	Dec	Annual
Observed 61-2000	21.60	25.50	28.80	31.80	31.80	29.90	25.20	24.80	24.40	24.40	23.10	20.10	31.80
2011-2040	21.11	25.99	29.11	31.74	30.30	27.11	24.90	24.24	27.40	27.55	24.38	20.05	31.76
2041-2070	21.25	26.28	29.28	31.94	30.19	26.71	24.83	24.41	27.61	24.51	30.79	31.95	

Time Period													
2071-2099	20.96	26.62	29.78	32.57	30.14	26.75	24.82	24.09	27.42	27.65	25.13	20.65	32.62
Hadcm3_B2													
Observed 61-2000	21.60	25.50	28.80	31.80	31.80	29.90	25.20	24.80	24.40	24.40	23.10	20.10	31.80
2011-2040	21.09	25.72	28.92	31.52	30.45	26.91	24.75	24.29	27.40	27.21	24.03	20.71	31.67
2041-2070	21.13	26.28	29.31	31.79	30.21	26.81	24.80	24.19	27.48	27.76	24.21	20.92	31.82
2071-2099	20.69	26.34	29.31	32.29	30.26	26.68	24.71	24.23	27.57	27.63	24.18	20.66	32.29
CGCM3_A2													
Observed 61-2000	21.60	25.50	28.80	31.80	31.80	29.90	25.20	24.80	24.40	24.40	23.10	20.10	31.80
2011-2040	21.00	25.73	29.17	31.44	30.79	27.29	25.70	24.02	26.00	27.81	24.25	20.82	31.72
2041-2070	21.04	26.10	29.33	31.42	30.69	27.44	25.75	24.15	25.72	28.18	24.06	20.72	31.58
2071-2099	21.23	26.44	29.45	31.42	30.34	27.57	25.69	24.18	25.19	28.73	24.36	20.07	31.59
CGCM3_A1B													
Observed 61-2000	21.60	25.50	28.80	31.80	31.80	29.90	25.20	24.80	24.40	24.40	23.10	20.10	31.80
2011-2040	21.08	25.93	29.38	31.12	30.63	27.20	25.76	24.14	25.89	27.88	24.26	20.66	31.27
2041-2070	21.30	25.71	29.65	31.12	30.45	27.50	25.64	24.11	25.60	28.15	24.64	20.85	31.42
2071-2099	21.43	25.98	29.55	31.15	30.53	27.33	25.90	24.14	25.58	28.58	24.45	20.50	31.30

temperature shows increasing trend in Hadcm3 in A2 and B2 scenario for second and third time period.

Maximum temp for Hadcm3_B2 senario

Maximum temp for CGCM3_A2 scenario

Maximum temp for CGCM3_A1B scenario

Minimum temp for HadCm3_A2 scenario
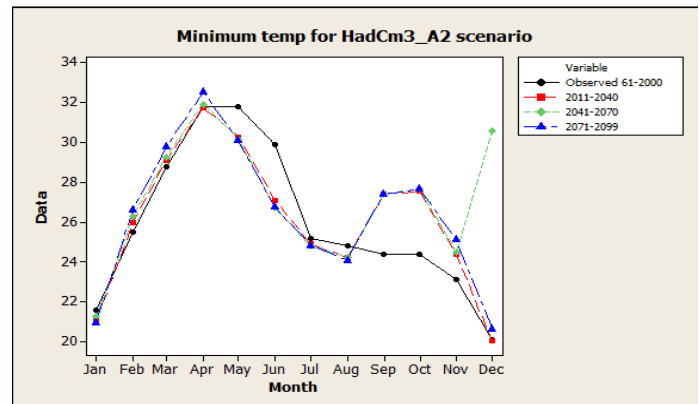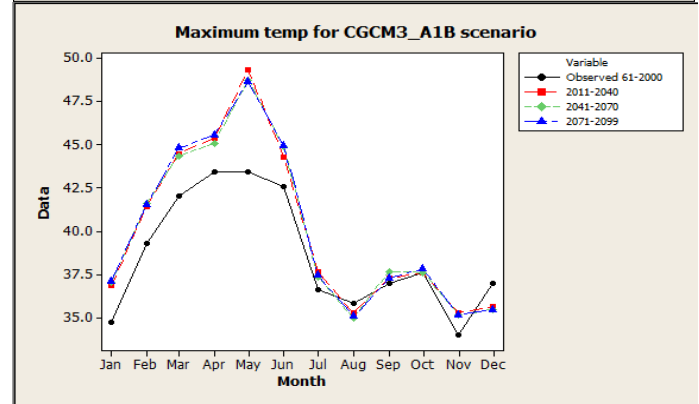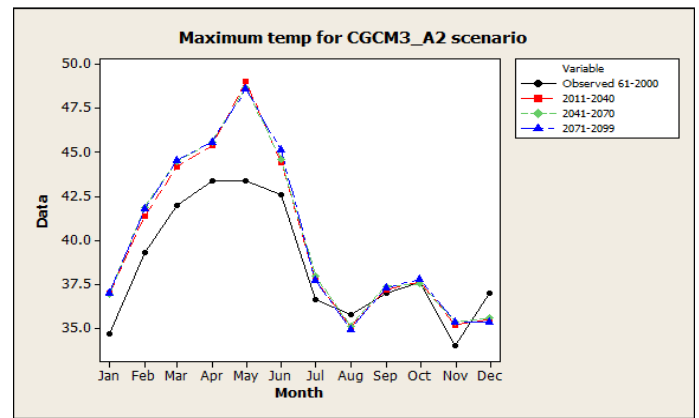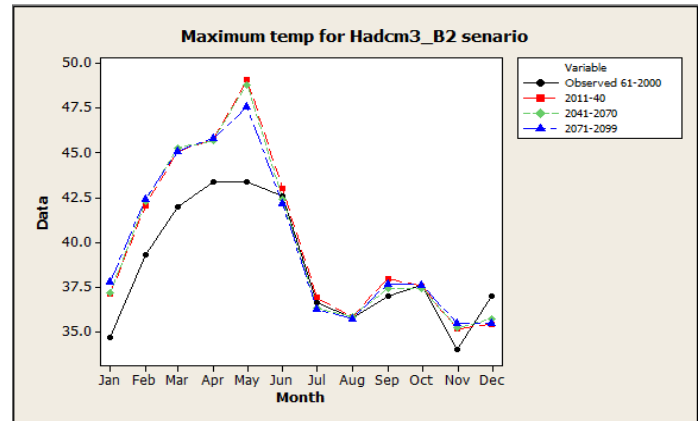
In the first time period the increase in maximum temperature in A2 and B2 scenarios for both GCM are the same. The maximum yearly temperature will increase 5.6 °C in A2 and B2 scenarios and for A1B scenario it will 5.9°C. Minimum yearly temperature will show increasing as well as decreasing trend . Annual minimum temperature in the first time period decreases by 0.04°C and 0.09°C in HadCm3 and CGCM3 for A2 scenarios. In the second and third time period the maximum temperature increase in all scenario will be less than A2 scenario for both HadCm3 and CGCM3 , Minimum
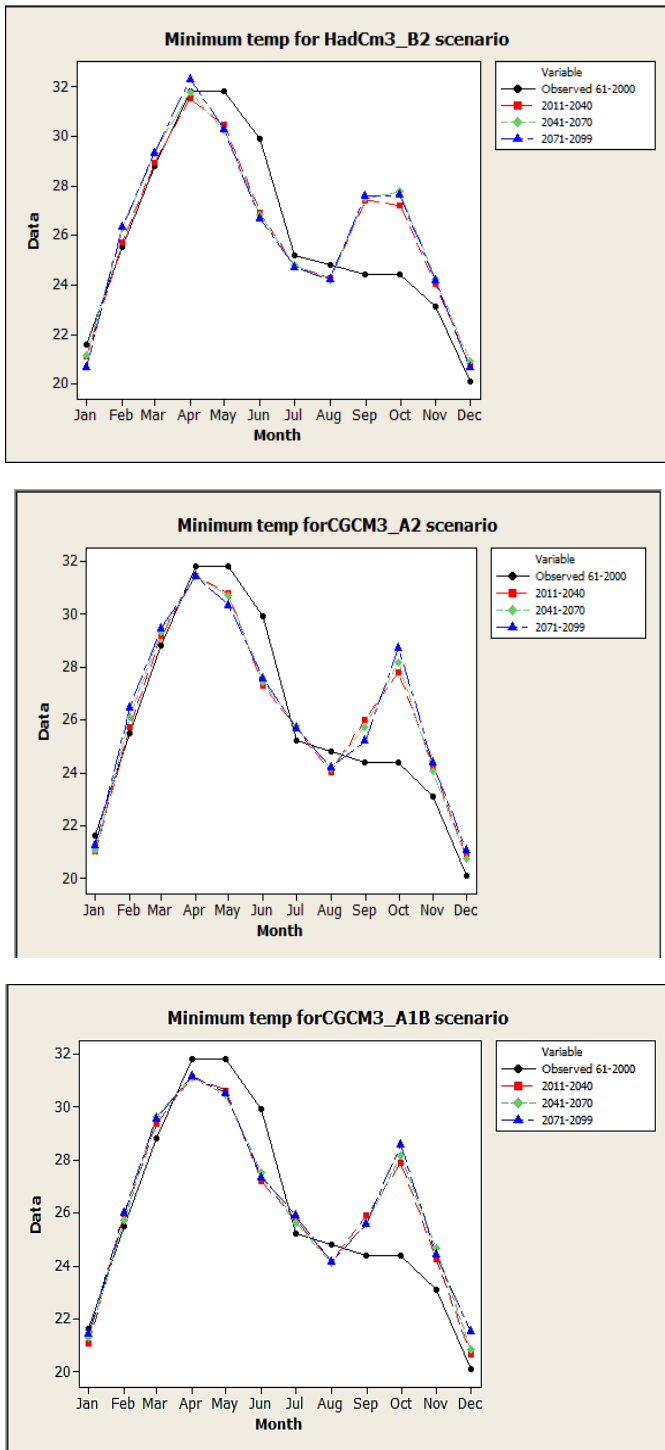
Figure 2: Variation in maximum and minimum temperature between the period (1961–2000) and the period (2011–2099) under the A2,B2,and A1B scenario.

7.CONCLUSION:

Awidely used decision support tool known as the SDSM was applied to downscale Tmax and Tmin in upper Godavari sub-basin under A2,B2 and A1B scenario.Historical data of 40 years (1961-2000) was used to construct a strong statistical

relationship between large-scale and local scale variables .The downscaled data(2011-2099) was divided into three periods:2011-2040(2020s).2041-2070 (2050s), and 2071-2099(2080s) and compared with the baseline period (1961-1980) to observed the changes. The results shows considerable increase in Tmax in all scenario as compared to Tmin.Tmax almost show same trend in all scenario in both GCM, it shows increasing trend but in Dec it shows decreasing trend.Tmin not shows any fix trend .In summer it shows decrease in temperature but in winter there will be increase in minimum temperature.

REFERENCE:

i.   Aavudai Anandhi,V.V. Srinivas ,Ravi Nanjundiah and Nagesh Kumar(2008).''Downscaling Precipitation to River Basin in India for IPCC SRES Scenarios using Support Vector Machine'', International Journal of Climatology,vol 28, pp 401-420

ii.   Ahmad Rajabi and SaeidShabanlou(2012), "Climate index change in future by SDSM in Kermanshah, Iran", Journal of Environmental research and development Vol. 7,pp37-44.

iii.   AWood,   L.R.Leung,   V.Sridhar and.P.Lettenmaier(2004).''Hydrological Implication of   Dynamical and Statistical Approaches to Downscaling Climate   Model Outputs'', Climate Change,vol 62, pp 189- 216.

iv.   B.C. Hewitson,(1996),''Climate Downscaling: Techniques and Applications'', Climate Research,vol-7,pp85-95 .

v.   Clement Tisseuil , Mathieu Vrac , SovanLek, Andrew J. Wade(2010),'' Statistical downscaling of river flow'', Journal of Hydrology,vol 385 ,pp279–291

vi.   Eric P. Salathe J.R.(2003).''Comparision of Various Precipitation Downscaling Methods for the Simulation of Streamflow in a Rainshadow River Basin'',International Journal of   Climatology,vol 23, pp 887-901.

vii.   IPCC,(2007),Climate Change, Fourth Assessment Report of the Intergovernmental Panel on Climate Change**.**

viii.   JAMES MURPHY(1998),'' An Evaluation of Statistical and Dynamical Techniques for Downscaling Local Climate'', Journalofclimate,vol l2,pp2256-2284

ix.   ] S.Kannan and Subimal Ghosh(2013).''A Nonparametric Kernal Regression Model for   Downscaling Multisite Daily Precipitation in the Mhanadi Basin'',Water Resources   Research,vol 49,pp1-26.

x.   M.Y Khanday. and JavedA(2008),'' Impact of Climate Change on Land use/Land Cover Using Remote Sensing and GIS in Chopan Watershed,Guna, Madhya Pradesh, India''. J. Environ. Res. Develop., vol 2(4), pp568-579.

xi.   Manish Kumar Goyal and C.S.P Ojha and Donald H Burn(2012).'' Nonparametric Statistical Downscaling of Temperature, Precipitation and Evaporation in Semiarid Region in India'',Journal of Hydrologic Engineering ASCE,vol 17,pp 615-627

xii.   Manish Kumar Goyal and C.S.P Ojha(2012).''Downscaling of Surface Temperature for   Lake Catchment in an Arid Region in India using Linear Multiple Regression and Neura Network'', International Journal of Climatology,vol 32, pp 552-566

xiii.   Okan Fistikoglu and Umut Okkan(2011).''Statistical Downscaling of Monthly Precipitation using NCEP/NCAR Reanalysis Data for Tahtali River Basin in Turkey'',Journal of Hydrologic engineering ASCE

xiv.   P.P.Mujumdar and Subimal Ghosh(2008)." Modeling GCM and Scenario uncertainty using a possibilistic approach:Application to Mahananadi river basin'',Water resources research ,vol 44.

xv.   Scott Spak1, Tracey Holloway, Barry Lynn, Richard Goldberg(2007),**"**A Comparison of Statistical and Dynamical Downscaling for Surface Temperaturein North America**"**, J. Geophys. Res., vol112,

xvi.   Subimal Ghosh(2010),''SVM-PGSL Coupled Approach for Downscaling to Predict Rainfall from GCM output'',Journal of Geophysical Research,vol 115,pp 1-18

xvii.   Wilby, R. L., and Wigley, T. M. L. (1997). "Downscaling General CirculationModel Output: AReview of Methods and Limitations." Prog. Phys.Geogr., vol21,pp 530–548

xviii.   Wilby, R. L., Charles, S. P., Zorita, E., Timbal, B., Whetton, P., andMearns, L. O. (2004). "The Guidelines for Use of Climate ScenariosDeveloped from Statistical Downscaling Methods." Supporting materialof the Intergovernmental Panel on Climate Change (IPCC), preparedon behalf of Task Group on Data and Scenario Support for Impacts andClimate Analysis.

xix.   Wilby RL, WigleyTML(2000)," Precipitation Predictors for Downscaling:Observed and General Circulation Model Relationships", International Journal of Climatology,vol**20**(6),pp 641–661.

xx.   Wilby R.L., Dawson C.W., and Barrow E.M(2002),"SDSM- A Decision SuportTool for theAssessment of Regional Climate ChangeImpacts", J. Environ. Mod.Soft.,vol**17**(2), pp147-159**.**

xxi.   Wilks, D. S., and Wilby, R. L.(1999),"The weather generation name: Areview of stochastic weather models." Prog. Phys. Geogr.,vol 23, pp329–357.

xxii.   Xiaoyan Wang,Tao Yang Quanxi Shao, Kumud Acharya,Weiguang Wang (2012)."Statistical Downscaling of Extremes of Precipitation and Temperature and Construction of their Future Scenarions in an Elevated and Cold Zone",Stoch Environ Res Risk Assess Springer,vol 26,pp 405-418.

Statistical Downscaling Of Gcm And Generation Of Future Hydrological Scenario

S.Rajan[1], B.R. Nikam[2*], S.P. Aggarwal[3] and V. Garg [2]

[1]M.Tech. Student, Water Resources Department, Indian Institute of Remote Sensing (ISRO), Dehradun-248001, India
[2] Scientist/Engineer 'SD', Water Resources Department, Indian Institute of Remote Sensing (ISRO), Dehradun-248001, India
[3] Head, Water Resources Department, Indian Institute of Remote Sensing (ISRO), Dehradun-248001, India
*email: bhaskarnikam@iirs.gov.in

ABSTRACT: General Circulation Models (GCMs) are regarded as credible tools that use transient climate simulations to generate time series of the climate. However GCMs are only available at a coarse-resolution. Most hydrological models require climatic information at a finer resolution. Downscaling has been thus considered an important component of climate change impact assessment. This research performs daily downscaling using two statistical techniques, namely the Least Square-Support Vector Machine (LS-SVM) and Multivariate Kernel Regression (KR) to downscale CMIP5 GCM output to obtain simulations of local climate variable for the monsoon month of August, 2040. A robust methodology was established after conducting numerous experiments. The calibration and validation was done based on the observed daily station data from Indian Meteorological Department (IMD). The study also undertakes a rigorous evaluation and comparison of the two downscaling techniques. Included in the research is a list of the best evaluation techniques for measuring the efficiency of downscaling models. Further, future hydrological regime was generated using Variable Infiltration Capacity (VIC) model, a macroscale semi-distributed hydrological model. Though literature suggests that KR techniques are better suited for daily simulations, the study indicates that the LS-SVM was able to simulate peak rainfall events more effectively, whereas KR was seen to mainly give mean values for simulation period. KR was observed to model individual rainfall events better than SVM. The sum of total daily rainfall and the Nash-Sutcliffe coefficient were determined to be the most suitable downscaling evaluation measures. The downscaled precipitation data indicates an increase in monthly precipitation of August from 239.67 mm (year 2005) to 264.51 mm (year 2040). The generation of hydrological regime for the future indicated a runoff of 29057.71 m^3/s at the outlet of the Ganga basin for the month of August, 2040.

1. INTRODUCTION

The fourth assessment report (AR4) of the Intergovernmental Panel on Climate Change (IPCC, 2007) has listed the various climate scenarios and its drivers. The rising demand for water and the possible decline in future water resources due to climate change, will pose a significant challenge to water resources planners (Chiew et al., 2010). Therefore, a proper assessment of probable future precipitation and its variability over time should be included in climate change studies (Anandhi et al., 2008). Such studies can be carried out with the use of climate models and hydrological models (Chen et al., 2012). GCM, a computer based model following the laws of physics and thermodynamics, is regarded as the most credible tool to simulate time series of the climate (Ghosh and Majumdar, 2008). However, GCMs are only available at a coarse grid resolution of 1º to 2°. The GCM outputs cannot be used as direct inputs to certain impact assessment models such as hydrological models. The inconsistency between the spatial scale of the GCMs and the hydrological models makes it essential to perform downscaling .Thus, downscaling is performed to bridge the gap between the large-scale GCMs and the information required to assess the impacts of climate change on the small scale study area. Spatial downscaling has three primary assumptions (Tripathi et al., 2006); the GCM should be able to simulate the atmospheric features that influence regional climate effectively, the climatic variables involved in downscaling should not exhibit sub-grid variations, and finally, the variables considered for downscaling should be a direct model output and not an output of model parameterizations.

Downscaling, or translation across scales can be broadly classified into two types: Dynamic Downscaling and Statistical Downscaling. Dynamic downscaling involves nesting a regional climate model into an existing GCM (Jenkins and Barron, 1996). It can be understood as a regional climate model (RCM) embedded in a GCM (Tripathi et al., 2006). Statistical downscaling involves translation using statistical regression to link local variables to particular drivers in GCMs. The regression function is known as transfer function and is derived from long term observational data. The transfer function needs to be established depending on the nature of the predictand to be downscaled. Precipitation is considered

difficult to downscale, especially on a daily time-scale since it is a non-smooth field unlike surface pressure, vertical and horizontal winds and exhibits high sub-grid variability. The more the ability of the transfer function to capture non-linear aspects of the circulation-local climate relationship, the more efficient it is considered. A wide range of transfer functions have been explored in the past; Regression-based techniques (Hessami et al., 2008, Alsornsingchai and Srinilta, 2011; Joshi et al., 2013), Artificial Neural Network (ANN) (Tatli et al., 2004), Support Vector Machine (SVM) (Sachindra et al., 2011, Najfi et al., 2011), Relevance Vector Machine (RVM) (Ghosh and Majumdar, 2008) and Canonical Correlation Analysis (CCA) (Landman et al. 2001; Huth, 2002; Busuioc et al., 2007).

Furthermore, the formation and intensification of the hydrological regime due to the impacts induced by different hydro-meteorological parameters by climate change also needs to be studied and analyzed. The main aim in such a study would be to utilize the downscaled GCM output to drive hydrological models to obtain time series hydro-meteorological parameters, Several researches in the past have tried to amalgamate the impact of climate change through downscaling and its implications on the hydrological regime. Dibike and Caulibaly (2005) used a stochastic and regression based downscaling technique to simulate two hydrological models for the generation of future streamflow. Chen et al. (2012) attempted to compare and evaluate various GCMs, statistically downscale using Smooth Support Vector Machine (SSVM) and Statistical Downscaling Model (SDSM) and use the corresponding downscaled inputs into the Xin-anjiang and HBV hydrological models.

In this study, statistical downscaling of precipitation on a daily time step has been explored for particular sites. A comparative study of the downscaling models has been conducted to obtain the better suited model for daily downscaling. The study also determines statistical measures for evaluating the performance of these models. And finally, hydrological regime for the future has been generated with the downscaled local scale variable. The technique route in the study has been shown in Figure1.
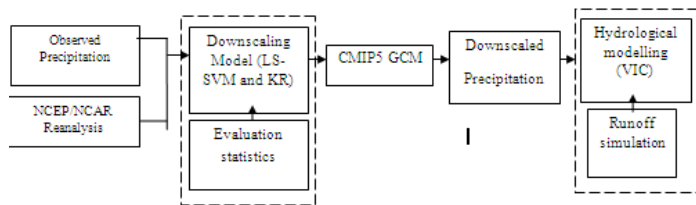
Figure 1. The technique route in this study

2. STUDY AREA

The largest river basin of India, the Ganga Basin, is selected as the region of study (Figure 2). The Ganga basin outspreads in India, China, Nepal and Bangladesh over an area of 10,86,000 Sq.km. It covers almost 11 states namely Madhya Pradesh, Rajasthan, Bihar, West Bengal, Uttarakhand, Jharkhand, Haryana, Chhattisgarh, Himachal Pradesh and the Union Territory of Delhi draining an area of 8,61,452 Sq.km, which is nearly 26% of the total geographical area of the country. The study encompasses four stations across the Ganga basin in India; namely, Kota, New Delhi, Patna and Indore. The study area lies between 73° 38' E to 88° 9' E longitudes and 22° 45' N to 31° 45' N latitudes. The *Farakka* barrage located in West Bengal is considered as the outlet for the Ganga Basin located at 87.9333° E longitude and 24.8047° N latitude. The basin is bounded by the Himalayas in the north, Aravalli in the west, Vindhyas and Chotanagpur plateau in the south and Brahmaputra Ridge in the east. The length of the Ganga is around 2525 Km.

The predominant soil types in the basin are sandy, loamy, clay and their combinations such as sandy loam, salty clay loam and loamy sand soils etc.

The climate of the basin is generally temperate with great variation in both rainfall and temperature. The climate in the northern part of the basin is primarily influenced by the Himalayas where winters are cold and summers are moderate. The average rainfall in the basin is between the ranges of 550-2500 mm. 80% of the rainfall can be attributed to the south-western monsoon from July to October. The Upper Ganga encompassing Uttarakhand and Uttar Pradesh receives an average rainfall of 760-1000 mm. The central plains of Bihar receive 1500-1600 mm with the Lower Ganga receiving the maximum rainfall of around 2540 mm in the delta regions of West Bengal. The temperature range in the basin varies temporally and geographically; from 3-4 ° C in winters in some parts to 40 ° C in summers in some others. The temperature varies in the basin from 2-3 ° C in January making it the coolest month of the year to 45-47 ° C in May or June making it the warmest.
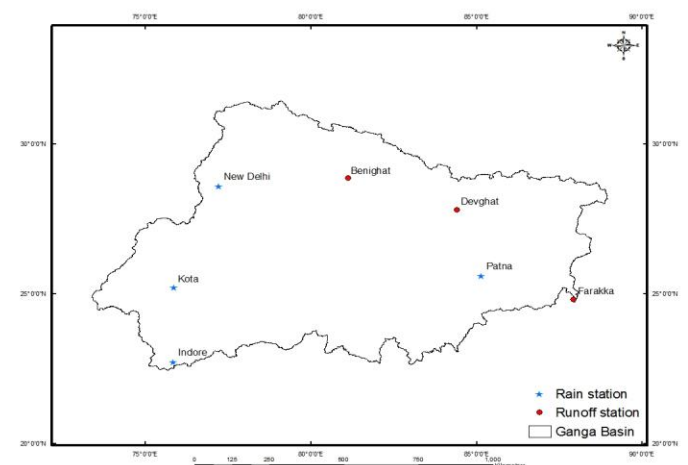
Figure 2. The location of the study area

3. MATERIAL AND METHODS

Four hydro-meteorological stations; Kota, New Delhi, Patna and Indore with daily rainfall and three discharge gauging

stations; Benighat, Devghat and Farakka are selected in this study. The four hydro-meteorological rain stations (as shown in Figure 2) are used to establish a statistical downscaling model and the three runoff stations are used for performing calibration and validation of the macroscale hydrological VIC model. The station data of daily rainfall are acquired from the IMD and are considered as the station level climatic data. The daily NCEP/NCAR Reanalysis data is used for the calibration of the downscaling model from 1975-2011. RCP 4.5 of the daily CMIP5 (Coupled Model Intercomparison Project 5) data with its appropriate predictors (as shown in Table 1) in the atmospheric realm are considered for the validation and the prediction using statistical downscaling model for 2012 and 2040 respectively. The CMIP5 GCM is used to generate regional climate scenarios by statistical downscaling, which in turn is used to drive the hydrological model for simulating the hydrological responses to a changed climate. The calibration for the macroscale hydrological model VIC is performed for 2005 and the validation periods are selected to be 1985 and 1995. The downscaling processes is performed at a daily time step following the generation of the hydrological regime for the future at a grid resolution of 25 km X 25 km. Seven large-scale climate factors are used in this study as listed in Table 1.

Table 1. Large-scale climate factors for the statistical downscaling methods in the study

Long Name	Units	Remark	Variable name	Standard Name
Air Temperature	K		Ta	air_temperature
Relative Humidity	%	This is the relative humidity with respect to liquid water for T> 0 C, and with respect to ice for T<0 C.	Hur	relative_humidity
Specific Humidity	1		Hus	specific_humidity
Sea Level Pressure	Pa			Air_pressure_at_sea_level
Northward Wind	ms^{-1}	Near-surface (usually, 10 meters) northward component of wind.	Va	northward_wind
Eastward Wind	ms^{-1}	Near-surface (usually, 10 meters) eastward component of wind	Ua	eastward_wind
Geopotential Height	m		Zg	geopotential_height

3.1 Statistical downscaling methods

Establishing a statistical downscaling relationship, involves the transfer functions to estimate an empirical relationship between the observed small scale station level variables and the large scale atmospheric variables. This mathematical function is then used to drive the CMIP5 daily simulations. Various statistical downscaling models have been attempted and explored in the recent past. This study involves two statistical downscaling models; Least Square-Support Vector Machine (LS-SVM) (Tripathi et al., 2006; Raje and Majumdar, 2011;Sachindra et al., 2011) and Multivariate Kernel Regression (KR) (Kannan and Ghosh, 2013). The first model is a simple variant of the Support Vector Machine (SVM), a machine learning technique based on the fundamental principles of statistical learning theory and structural risk minimization (Haykin, 2003), while the second belongs to the class of non-parametric smoothing techniques involving regression analysis. In order to determine the technique better suited for statistical downscaling, various statistical measures are adopted to draw comparisons between the observed and the simulated rainfall. Further, the result of the more suitable downscaling technique is used as input in the macroscale semi-distributed hydrological model VIC, to estimate the water balance components for a future period. This step is crucial in order to understand the future hydrological scenario of the basin.

3.1.1 Overview of LS-SVM

Support Vector Machine, originally conceptualized by Vapnik (1998), is a kernel based neural network technique (Tripathi et al., 2006) that works on the statistical learning theory and structural risk minimization (Haykin, 2003). The SVM has gained immense popularity over traditional techniques of neural network such as multi-layer back propagation neural network in applications including pattern recognition and classifications etc. The statistical learning theory (Vapnik and Chervonekis, 1974) attempts to set an upper limit on the generalization error by trading off between the training error of the machine and the capacity of the machine to help learn a training set without any error. This ensures a global optimum solution for the output. The SVM algorithm maps the training set into a high-dimensional feature space from a lower dimensional input space and then in that space attempts to locate a plane that separates the classes concerned. The Statistical Learning Theory governs the selection of the hyperplane leading to maximum generalization, while estimating the functions for regression, function estimation or classification.

In the present study, a popular version of the SVM, known as LS-SVM has been used for function estimation and establishment of the downscaling model. The version was proposed by Suykens and Vandewalle (1999). The LS-SVM is a more simplified version of the SVM, preserving the original qualities of SVM (Zhou et al., 2011), yet manages to maintain efficient costs with a good ability to generalize (Sachindra et al., 2011). Unlike the SVM that finds solution by using complex quadratic programming, the LS-SVM solves a set of linear equations. In SVM, the mapping is performed with the help of a kernel function that implicitly maps the data to a higher infinite dimensional plane. This kernel function ensures flexibility and adaptability in the model. There are several kernels that can be used in SVM. These include linear, polynomial, radial basis function (RBF) and sigmoid function. RBF is the most commonly used kernel because of its ability to have a 'localized and finite response' across the entire 'range of x-axis' (Tripathi et al, 2006). The selection of the kernel plays a very crucial role in the performance of LS-SVM.

The LS-SVM regression model has two tuning parameters γ and σ^2 where γ is the regularization parameter which determines the magnitude for penalty of the soft margin and σ^2 which is the kernel parameter for the RBF kernel selected (in case of the RBF, σ is the width of the kernel). Though the number of kernel parameters may vary from kernel to kernel, the regularization parameter always remains the same for any kernel used. The detailed derivation of LS-SVM has been given in Annexure-1.

3.1.2 Overview of KR

The second technique used in the study is the non-parametric KR model that uses the weighted sum of the observed predictands. The estimator is often used as a powerful tool for smoothing, image and signal processing. However, this method is computationally expensive when used for multivariate cases. The efficiency of the model can be improved only when the neighbors are used within an effective range around a regression point. Therefore, the identification of points with a given range determines the efficacy of the model. Thus, kernel regression belongs to a non-parametric smoothing technique where the weighted sum of all the observations is used along with the kernel density function weights as mentioned in Nadayara (1964). The kernel bandwidth is a free parameter that is produced using the Asymptotic Mean Integrated Square Error (AMISE) method and exhibits a strong influence on the performance of the estimate.

The Nadayara-Watson kernel regression algorithm based on the Gaussian kernel (described in Aneexure-1) was used for the current research. The default bandwidth was eventually derived from the optimum bandwidth of the Gaussian kernel density function.

3.2 Evaluation criteria for Downscaling Models

Khan and Coulibaly (2010) adopted different evaluation statistics for assessing statistical downscaling models for downscaling daily rainfall. The study however attempts to evaluate the models on the basis of each season (DJF: Winter; MAM: Spring, JJA: Autumn; SON: Summer).
However, the current study employs statistics that compares the simulated with the observed rainfall. The measures used in the study assess how close the simulated rainfall is to the observed rainfall on a daily time scale. Each of the statistical performance indices has been calculated for the model outputs. Finally, a comparison has been drawn between the two transfer functions. The study has also determined the best performance indices to evaluate downscaling models.

The first method assesses the performance of the model on the independent test dataset through visual interpretation by plotting the observed data and the simulated data. The sum of the total daily rainfall for the simulated period and the sum of the total rainfall for the observed period has also been compared, to understand the performance of the model.

Conceptually, the observed and the simulated rainfall should be equal. Additionally, Root Mean Square Error (RMSE), commonly known as the Root Mean Square Deviation (RMSD) has been used to measure the difference between the values predicted by the model and the values observed. The individual differences between the values are known as residuals. The RMSE aggregates these residuals to measure the predictive power of the model. Correlation coefficient has also been used as another measure to indicate the strength and the direction of the linear relationship between two variables. The measure ranges between +1 to -1. A correlation of +1 show a perfectly increasing linear relationship and -1 show a perfectly decreasing linear relationship, whereas, a correlation coefficient of 0 indicates a lack of a linear relationship between the variables. The popular Nash Sutcliffe (N-S) Coefficient (Nash and Sutcliffe, 1970), commonly used to assess the predictive power of hydrological models and quantitatively assess the efficiency of any model, has been used to estimate the match between model output and observational data. The Percent Bias (PBIAS) (Gupta et al, 1999) and the RMSE-Observations standard deviation ratio (RSR) have also been computed to understand the percentage measure of the average tendency of the simulate data with respect to the observed data as well as to calculate the ratio of RMSE to the standard deviation of the measured data respectively. The above listed measures have been computed to determine the performance measure that best represents the efficiency of a model on the basis of its simulated output.

3.3 Generation of future hydrological scenario

Once the small scale climate variable for the future is obtained, the intensification of the hydrological regime due to hydrological impacts of climate change also needs to be subsequently addressed. Thus, the outcome of the selected downscaling model was used to drive a hydrological model to generate the hydrological regime for a time period in the future. The exercise will help assess the changing scenario of the hydrology in the future.

The fundamental purpose of modeling the hydrology is to gain an overall understanding of the complex hydrological system and its dynamics in order to provide reliable information to water resource managers and policy makers (Bhattacharya et al., 2013). But most impact models require high-quality reliable data as inputs. Remote sensing has in this regard shown great promise in providing an abundance of data and information due to its unrestricted spatial and temporal coverage. SWAT (Soil and Water Assessment Tool), MIKE-SHE, HEC-HMS (Hydrologic Engineering Centre-Hydrologic Modelling System) are some of the physically based distributed hydrologic models that accept satellite-borne products as inputs. But most of these models do not consider horizontal complexity and spatial heterogeneity of soil, topography, vegetation etc, all of which plays a significant role in governing surface runoff (Garg et al., 2012). However, VIC, a two layer semi distributed model, takes into consideration sub-grid

variability in soil infiltration capacity and vegetative classes into consideration.

3.3.1 Variable Infiltration Capacity (VIC) Model

Variable Infiltration Capacity (VIC) model developed by Gao et al. (2009) is a semi-distributed macroscale hydrological model that works on both water and surface energy mode within a grid cell and captures sub-grid variation effectively. The model, developed to study the surface energy, hydrological fluxes at scales ranging from 'large river basins to the entire globe' (Garg et al., 2012). It computes vertical energy and moisture fluxes specific to each grid by considering soil and vegetation parameters. The uses inputs from both space-borne sources as well as ground-based inputs. Primary characteristics of the model includes subgrid variability in land surface vegetation classes, soil moisture storage capacity and drainage from the lower soil moisture zone also known as baseflow as a non-linear flow; and the inclusion of topography that allows for orographic precipitation and temperature resulting in a more realistic simulation of the mountainous terrain. The model accepts multiple soil layers with variable infiltration and non-linear baseflow. It involves representation of sub grid variability in soil infiltration capacity and mosaics of vegetation classes at the grids. The inclusion of vegetation characteristics in the model makes it suitable to study the impact of LULC dynamics on the local hydrology of a region.

VIC model requires four mandatory input files; namely, the Vegetation parameter file, Vegetation Library file, Soil parameter file and Forcing file. Information of the grid-wise vegetation characteristics are input into the model as the Vegetation parameter file and the Vegetation Library file. Some of the variables used in these files are root depth, root fraction, LAI, ALBEDO, roughness length, displacement height, architectural resistance, minimum stomatal resistance etc. The above mentioned input files are input into the model in the form of the Global Parameter file which modifies the input characteristics to activate the water balance model and to specify the paths of the input and the output files. VIC utilizes the infiltration formula used in the Xinanjang model (that assumes precipitation in excess of the infiltration capacity as surface runoff) and the Penman-monteith formula for the computation of evapotranspiration. The baseflow is calculated as a derivation of the function of soil moisture in the lowest layer of the soil using the Arno non-linear baseflow formula. The governing equations of the model can be found in Gao et al., (2009).

4. RESULTS AND ANALYSIS

4.1 Calibration and validation of LS-SVM and KR

The statistical relationship between the large-scale circulation factors and the rainfall in the hydro-meteorological stations is established using LS-SVM and KR. The calibration period for the model is 1975-2011 (for a period of approximately 35 years), and the evaluation period is for the month of August in

2012. The evaluation period is a period of one month (August) since the prediction period was set for the monsoon month of August, 2040. The selection of atmospheric domain is the primary step for downscaling, since the climate at any point on the ground is governed by the atmospheric domain above it. The present study performs downscaling upto a single site on a daily basis. The selection of the most probable and potential predictors, forms the next crucial step. This required screening of large-scale variables having a reasonable relationship with rainfall. Karl Pearson's coefficient of correlation was employed to identify the predictors that influenced rainfall at the particular site. The screening of the predictors was followed by a process to reduce the systematic biases in the mean and variance of the GCM in relation to the reanalysis data, known as Bias Correction. Though, Bias correction can be done in the form of re-gridding, quartile-based corrections or by standardization of the data (Wilby et al. 2004), the current study only uses standardization to remove the systematic biases.

LS-SVM and KR were established by utilizing the NCEP/NCAR reanalysis data and the observed station rainfall data for each station. In case of the calibration for the LS-SVM, the two tuning parameters were changed iteratively using the leave-one-out cross validation. The optimization routing for fine tuning was done using the simplex algorithm with the RBF kernel. Model validation was performed on an independent dataset with the optimal values of the tuning parameters fixed at the time of calibration. The model that simulated the rainfall closest to the observed values of rainfall was determined to be the optimum model (as shown in Figure 3). Though LS-SVM was seen to simulate the peaks sufficiently well, it was seen to be unsuccessful in modeling the high anomalous rainfall event of the simulation period. In order to get a true estimate of the performance of the model, the highest rainfall event(s) was accommodated from the computation using a frequency distribution histogram. Also, after multiple iterations, it was evaluated that the best model was established using only the rainy days for the entire baseline period.
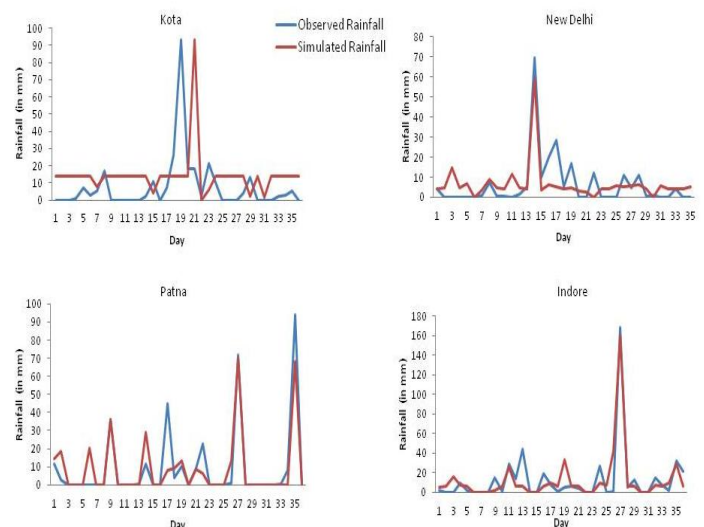
Figure 3. Observed rainfall and LS-SVM predicted rainfall

Numerous statistical measures were calculated as performance indices to estimate the efficiency of the downscaling model. N-S Coefficient and sum of total daily rainfall were observed to be the most reliable evaluation measures. Table 2 shows the optimum values of hyperparameters and the best performance measures to assess the efficiency of a downscaling model.

Table 2. Hyperparameters and computation of performance indices for Indore

γ, σ^2	100, 0.5
Nash-Sutcliffe coefficient	0.81
Total rainfall observed	446.7
Total rainfall simulated	442.86

The calibration of the KR model was done through the selection of the appropriate bandwidth. This formed an important step in the kernel estimation method. The initial value of the kernel bandwidth (h) was obtained from the predictor and the predictand of the training period. The value was eventually adjusted to get the best performance from the model. The simulations of KR displayed that the values obtained from the model were mainly mean values of rainfall. However, it was observed that the number of rainfall events was identified accurately in the KR model.

4.2 Evaluation Criteria for downscaling models

Various statistical measures have been calculated for the results of SVM for the four stations. This was done to get a clearer understanding of the performance of different downscaling models and to determine the best performance indices while evaluating them. Table 3 lists the different statistical measures used to evaluate the efficiency of downscaling.

Table 3. Evaluation statistics of statistical downscaling

	Kota	New Delhi	Patna	Indore
Sum$_{obs}$	268	214.2	329.7	446.7
Sum$_{sim}$	341.0626	223.4682	319.3387	451.8585
RMSE	17.6922	7.3253	9.001	12.3378
Pearson Correlation	0.1489	0.8184	0.9209	0.905
N-S Coefficient	-0.2126	0.6633	0.7705	0.8124
PBAIS	-27.2622	-4.3269	3.1426	-1.1548
RSR	1.0858	0.5721	0.4289	0.4270

The sum of the total amount of rainfall over the period of simulation was seen to be an important indicator of the performance of the model. The N-S Coefficient gives the relative magnitude of noise as compared to information. The coefficient for all the four stations was within the acceptable range representing a good match of the simulated to the

observed. The best N-S Coefficient was observed for Indore (0.81) and the lowest for Kota (-0.2126). The optimal value of PBIAS is considered to be 0. A negative value indicates overestimation bias while a positive value indicates an underestimation bias. Clearly, results of Kota show a high overestimation bias, making it less accurate than the other stations. Only Patna shows an underestimation bias. RSR usually ranges from 0 to higher values. A low value of RSR indicates a good model simulation. Ideally, the value of NS Coefficient should be greater than 0.50 and RSR should be lesser than 0.70. All stations other than Kota were seen to satisfy the following condition.

4.3 Parameter Optimization of VIC

VIC accurately generated the water balance components, namely; Precipitation (mm), Runoff (mm), Baseflow (mm) and Evaporation (mm) for the calibration period (2005), the validation period (1985 and 1995) and simulated the hydrological regime for August, 2040. VIC considers 10 calibrating parameters out of which 6 parameters are considered more important than the rest; namely, Variable Infiltration curve parameter (b_{infilt}), Fraction of maximum velocity baseflow where baseflow occurs (D_s), Fraction of maximum soil moisture where non-linear baseflow occurs(W_s), D_m, d_1 and d_2 . Keeping the depth of soil layers un-altered, other parameters are calibrated. Model input parameters only represent the physical properties of the basin and may contain certain errors. Hence, calibration is required.

On the generation of the water balance components, the model was calibrated by adjusting the soil properties.The model was simulated by considering initial values of calibrating parameters. Keeping the results of the initial iteration as reference, the remaining parameters were increased or decreased until the best match between the observed and simulated was obtained at b_{infilt}=0.4, D_s=0.01 and W_s=0.08. It was observed that after calibration the imbalance in the water balance component was solved to a great extent. The error term was seen to reduce from 70.79 mm before calibration to 39.02 mm after calibration. The validation of the model was done on an annual and monthly basis and for the month of August of the validation years as shown in Table 4.

Table 4. Water Balance components for August in the calibration and validation period (in mm)

Year	Precipitation	Runoff	ET	Baseflow	Error Term
1985 (Validation Year)	277	107	110	48	11.14
1995 (Validation Year)	340	124	113	47.89	55.11
2005 (Calibration Year)	239	89	100.35	35.53	14.37

However, the primary validation of results was conducted based on the streamflow simulated by the routing module of VIC. The resultant runoff generated after routing was compared with the observed runoff value (at different sites) obtained from Global Runoff Data Centre (GRDC) as shown in Figure 4.
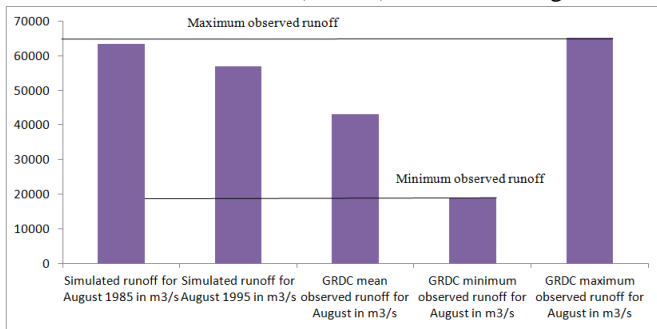
Figure 4. Validation for the month of August at Farakka (Outlet)

After calibration, VIC was run to generate hydrological components. Subsequently, routing was performed to simulate runoff for August, 2040. Figure 5 shows the projected hydrological components averaged over the area of the basin for August, 2040.
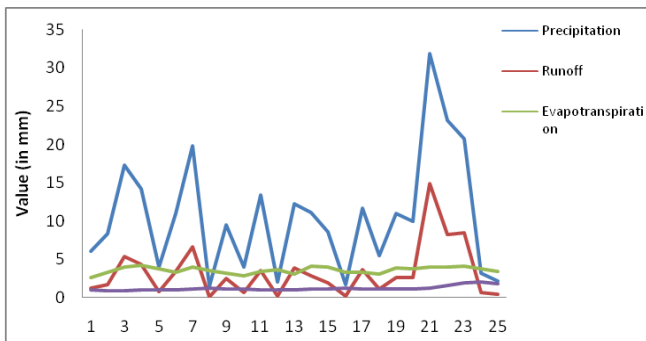
Figure 5. Water balance components of the Ganga basin for August, 2040

Following the determination of the hydrological components, runoff was computed at the outlet of the basin (Farakka) for the same time period .The runoff computed was computed to be 86.80 mm/year for August, 2040 (Figure 6).
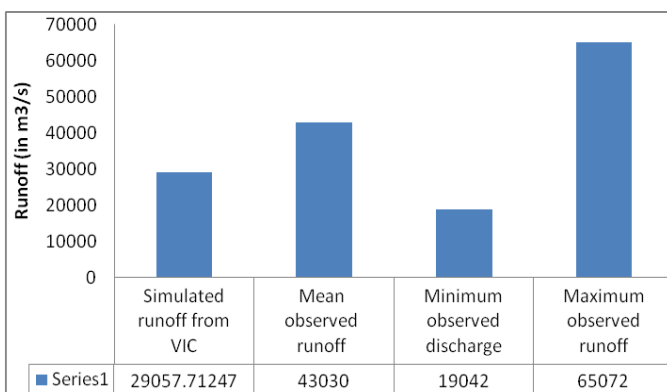
Figure 6. Simulated runoff for August 2040 for Farakka

Normal and projected water balance components have been shown in Figure 7. It was realized after analysis, that total rainfall for August 2040 was projected to be higher than the rainfall in 2005. The runoff and evapotranspiration was seen to be on a decline. Baseflow was also seen to be consistently on the fall. The results support the simulated runoff of Farakka for August (Figure 6), indicating an overall decline in the runoff in 2040 at the outlet.

	Precipitation	Runoff	ET	Baseflow	Error Term
Aug-85	277.95	107.70	110.13	48.97	11.14
Aug-95	340.49	124.71	113.69	47.99	54.10
Aug-05	239.68	89.41	100.36	35.53	14.38
Aug-40	264.52	82.49	90.25	31.42	60.36
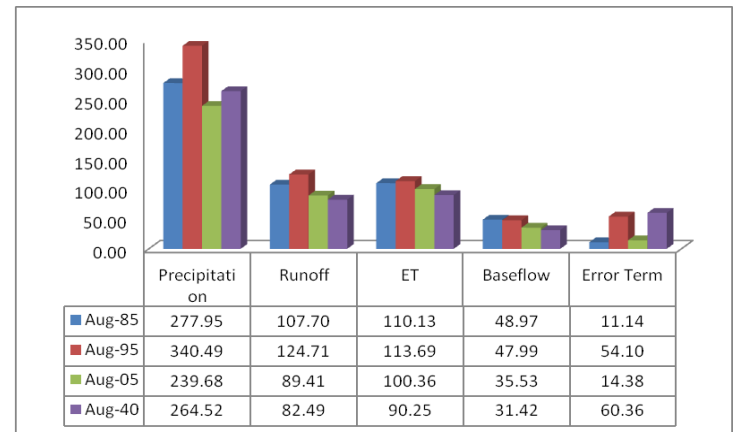
Figure 7. Normal and Projected water balance components

It is noticed that though the error term is very small for the validation period of August 2005 and calibration period of August 1985, the error term is substantially high for August 1995. This however is estimated so, due to the high precipitation in 1995 as compared to the precipitation in August 1985 and August 2005. The simulated water balance components for August 2040 shows a large error term (imbalance) of 60.36 mm. Thus, the large error term for August 2040 is an indicator that a larger time period needs to be considered while performing calibration of the VIC model.

5. CONCLUSIONS

The research focused on exploring two statistical downscaling techniques, drawing comparisons between them and determining the evaluation criteria to assess the performance of a downscaling model; followed by the determination of the water balance components at every grid and streamflow at specific locations for a future period. This however was performed by driving the hydrological model with the downscaled rainfall.

The study successfully attempts to downscale rainfall for the monsoon month of August, 2040. It is evident from the study that LS-SVM performs better than KR in simulating daily rainfall due to its ability to capture peaks and extreme rainfall events. The regression technique was observed to be incapable of modeling peaks and was seen to give only mean values. Whereas, KR was observed to model individual rainfall events

to a higher degree of accuracy. In the kernel regression method, the selection of an appropriate bandwidth was noted to be the most crucial step in the kernel estimation method since the bandwidth (h) acted as the smoothing parameter for the kernel regression. It can be concluded that the most suitable model was established by considering only the rainy days of the baseline period. The experiments displayed that both the models were unsuccessful in simulating the highest rainfall event in the same month, since such deviant events are beyond the scope of the training set. Nash-Sutcliffe coefficient and the total sum of the rainfall were both estimated to be the best measures in evaluating the performance of the downscaling model. The other statistical measures adopted tended to mislead to a great extent. The highest value of Nash-Sutcliffe was seen to be 0.8124 for Indore. The RMSE for Indore was however seen to be 12.337, thereby indicating that RMSE was a poor indicator of the efficiency of a model.

Downscaled precipitation was successfully used to force the VIC model for hydrological simulation over the Ganga basin. VIC was calibrated and validated for Farakka, Devghat and Benighat annually, monthly and for the specific month of August to ensure that the model is suited for simulating for the same month. The hydrological components for August, 2040 were generated. Precipitation was determined to be on the rise while runoff and baseflow was seen to decline. The evaporation however, did not show any large variation. The runoff for Farakka in August 2040 was estimated to be 29057.71 m3/s. The high value of error term in the water balance equation for the month of August, 2040 indicated the need to calibrate for a larger number of years. Recommendations in regard to downscaling will encompass the inclusion of inter-station correlation between the rainfall values of the stations. PCA operation must be conducted on the training set to reduce the redundant data that mostly tends to mislead the calibration of the downscaling model. Future work will also include attempts to improve the calibration of the hydrological model for more number of years and more stations using reliable observed discharge data. For areas such as the Ganga basin, where a substantial part lies in the snow-capped mountainous regions, the accommodation of snowmelt will give a better account of the fluxes of the region.

5. REFERENCES

i.   Aksornsingchai, P.,Srinilta, C. (2011). Statistical Downscaling for Rainfall and Temperature Prediction in Thailand. In, International MultiConference of Engineers and Computer Scientists Hong Kong

ii.   Anandhi, A., Srinivas, V. V.,Nanjundiahb, R. S., Kumara D.N. (2008). Downscaling precipitation to river basin in India for IPCC SRES scenarios using support vector machine. Int. J. Climatol, 28, 401–42

iii.   Bhattacharya, T., Aggarwal, S.P.,Garg, V. (2013). Estimation of Water Balance Components of Chambal River Basin Using a Macroscale Hydrology Model International Journal of Scientific and Research Publications, 3(2)

iv.   Busuioc, A., Tomozeiub, R. ,Cacciamani, C (2007). Statistical downscaling model based on canonical correlation analysis for winter extreme precipitation events in the Emilia-Romagna region. Int. J. Climatol.

v.   Chen, H., Chong, Y.X.,Guo, S. (2012). Comparison and evaluation of multiple GCMs, statistical downscaling and hydrological models in the study of climate change impacts on runoff. Journal of Hydrology, 434, 36–45

vi.   Chiew, F.H.S., Young, W.J., Cai, W., Teng, J. (2010). Current drought and future hydroclimate projections in southeast Australia and implications for water resources management. Stochastic Environmental Research and Risk Assessment, 602-612

vii.   Dibike, Y.B.,Coulibaly, P. (2005). Temporal Neural Networks for Downscaling Climate Variability and Extremes. In, International Joint Conference on Neural Networks. Montreal, Canada

viii.   Gao, H., Tang, Q., Shi, X., Zhu, C.,Bohn, T., Su, F., Sheffield, J., Pan, M., Lettenmaier, D.,Wood, E. F. (2009). Water Budget Record from Variable Infiltration Capacity (VIC) Model.

ix.   Garg, V., Khwanchanok ,A., Gupta, P.K., Aggarwal, S.P., Kiriwongwattan, K.,Thakur,P.K.,Nikam,B.R. (2012). Urbanisation Effect on Hydrological Response: A Case Study of Asan River Watershed, India. Journal of Environment and Earth Science, 2(9)

x.   Ghosh,S., Mujumdar, P.P.(2008). Statistical downscaling of GCM simulations to streamflow using relevance vector machine. Advances in Water Resources, 31, 132-146

xi.   Gupta, H.V., Sorooshian, S., Yapo, P.O. (1999). Status of automatic calibration for hydrologic models: comparison with multilevel expert calibration. J. Hydrol, 4, 135–143

xii.   Haykin, S. (2003). Neural Networks: A comprehensive foundation. Fourth Indian Reprint, Pearson Education, 842

xiii.   Hessami M., G., P., Ouarda, B.M.J, Hilaire, A.S. (2008). Automated regression-based statistical downscaling tool. Environmental Modelling & Software, 20.456-467

xiv.   Huth, R. (2002). Statistical downscaling of Daily Temperature in Central Europe. American Meteorological Society, 15, 1731-1742

xv.   Jenkins, G.S.,Barron, E.J. (1996). General circulation model and coupled regional climate model simulations over the eastern United States: GENESIS and RegCM2 simulations.

xvi.   Joshi, D., Hilaire, A. S. , Daigle, A., Ouarda, B.M.J. (2013). Databased comparison of Sparse Bayesian Learning and Multiple Linear Regression for statistical downscaling of low flow indices. Journal of Hydrology, 488, 136–149

xvii.   Kannan, S., Ghosh, S. (2013). A non parametric kernel regression model for downscaling multisite daily precipitation in Mahanadi Basin. Water Resource Research, 49, 1360-1385

xviii. Khan, M.S., Coulibaly, P., 2010. Assessing hydrologic impact of climate change with uncertainty estimates:bayesian neural network approach. J Hydrometeorol. 11(2), 482-495

xix.   Landman, W.A., Mason, S.J., Tyson,P.D., Tennant, W.J. (2001). Statsitical downscaling of GCM simulation to Streamflow. Journal of Hydrology, 252, 221-236

xx.   Nadayara, E.A. (1964). Estimating Regression Theory. (pp. 186-190)

xxi.   Nash, J.E., Sutcliffe, J. V. (1970). River flow forecasting through conceptual models, Part I—A discussion of principles. J. Hydrol., 10, 282–290

xxii.   Raje, D., Majumdar, P. P. (2011). A comparison of three methods for downscaling daily precipitation in the Punjab region. Hydrol. Process.

xxiii. Sachindra, D.A., Huanga,F., Barton, A.F.,Pereraa, B.J.C. (2011). Statistical Downscaling of General Circulation Model Outputs to Catchment Streamflows. In, 19th International Congress on Modelling and Simulation. Perth, Australia

xxiv.   Suykens, J.A., Vandewalle, J. (1999). Least squares support vector machine classifiers. Neural Process (pp. 293–300)

xxv.   Tatli, H., Dalfes, H.N., Mentes, S. (2004). A statistical downscaling method for monthly total precipitation over Turkey. International Journal of Climatology, 24, 161–180

xxvi.   Tripathi, S., Srinivas, V.V. ,Nanjundiah, R.S. (2006). Downscaling of precipitation for climate change scenarios: A support vector machine approach. Journal of Hydrology, 330, 621-640

xxvii. Vapnik, V.N. (1998). Statistical Learning Theory. John Wiley & Sons

xxviii. Vapnik, V.N., Chervonenkis, A.Y. (1974). Theory of Pattern Recognition: Statistical Problems of Learning. In. Moscow, Nauka

xxix.   Wilby, R.L., Charles, S.P., Zorita, E., Timbal, B., Whetton, P. ,Mearns, L.O. (2004). Guidlines for Use of Climate Scenarios Developed from Statistical Downscaling Methods.

xxx.   Zhou, J., Shi, J., Li, G. (2011). Fine tuning support vector machines for short-term wind speed forecasting. Energy Conversion and Management.

Annexure -1
Derivation of Least Square –Support Vector Machine and Kernel Regression

i)   Derivation of LS-SVM

Given a training set of N data points $\{y_k, x_k\}_{k=1}^N$, where $x_k \in R^n$ is the k-th input pattern and $y_k \in R$ is the k-th output pattern, the classifier can be constructed using the SVM in the form:

$$y(x) = sign\left[\sum_{k=1}^N \alpha_k y_k K(x, x_k) + b\right]$$

(1)

Here, α_k are called support values and b is the scalar bias constant. The $K(\cdot, \cdot)$ is the kernel, which can either be a linear SVM or a polynomial SVM of degree d or a Radial Basis Function (RBF), where κ θ, and σ are constants.

The problem of classifying two binary classes is defined as follows:

$$\begin{cases} w^T \varphi(x_k) + b \geq +1 & \text{if } y_k = +1 \\ w^T \varphi(x_k) + b \leq -1 & \text{if } y_k = -1 \end{cases}$$

(2)

This may also be written as the following:

$$y_k[w^T \varphi(x_k) + b] \geq 1, \quad k = 1,..., N$$

(3)

$\varphi(\cdot)$ is a nonlinear function mapping of the lower dimensional input space to a higher dimensional feature space.

Then, LS-SVM classifiers

$$\min_{w,b,e} J_{LS}(w,b,e) = \tfrac{1}{2} w^T w + \gamma \tfrac{1}{2} \sum_{k=1}^N e_k^2$$

(4)

are subjected to the equality constraints (Least Square-Support Vector Machine)

$$y_k[w^T \varphi(x_k) + b] = 1 - e_k, \quad k = 1,..., N$$

(5)

The Lagrangian is defined as the follows:

$$L(w,b,e;\alpha) = J_{LS} - \sum_{k=1}^N \alpha_k \left\{y_k[w^T \varphi(x_k) + b] - 1 + e_k\right\}$$

(6)

with Lagrange multipliers $\alpha_k \in R$ (also called support values which are primarily involved in training).

The Lagrange's multiplier is a strategy to find the local maxima and the minima of a function subject to equality constraints.

Next, the conditions for optimality are:

$$\begin{cases} \frac{\partial L}{\partial w} = 0 & \rightarrow & w = \sum_{k=1}^N \alpha_k y_k \varphi(x_k) \\ \frac{\partial L}{\partial b} = 0 & \rightarrow & \sum_{k=1}^N \alpha_k y_k = 0 \\ \frac{\partial L}{\partial e_k} = 0 & \rightarrow & \alpha_k = \gamma \, e_k \\ \frac{\partial L}{\partial \alpha_k} = 0 & \rightarrow & y_k[w^T \varphi(x_k) + b] - 1 + e_k = 0 \end{cases}$$

(7)

for $k = 1,...,N$.

On the elimination of w and e we can get:

$$\begin{bmatrix} 0 & Y^T \\ Y & ZZ^T + \gamma^{-1}I \end{bmatrix} \begin{bmatrix} b \\ \alpha \end{bmatrix} = \begin{bmatrix} 0 \\ 1_v \end{bmatrix}$$

(8)

Where,

$$Z = [\varphi(x_1)^T y_1;...; \varphi(x_N)^T y_N], Y = [y_1;...; y_N], 1_v = [1;...;1], e = [e_1;...; e_N]$$

and $\alpha = [\alpha_1;...;\alpha_N]$.

Following which, Mercer's condition is applied to the matrix $\Omega = ZZ^T$ with

$$\begin{aligned} \Omega_{kl} &= y_k y_l \varphi(x_k)^T \varphi(x_l) \\ &= y_k y_l K(x_k, x_l) \end{aligned}$$

(9)

ii)   Derivation of KR

To find the relationship between X & Y, a density estimator for Y given X is constructed. This density estimate shows the conditional expectation of Y on X.

It is known that the conditional expectation of Y on X is

$$\hat{Y} = E(Y \mid X = x)$$

(10)

The regression equation mentioned below:

$$Y_i = \alpha + \sum_{i=1}^n \beta_i X_i + \varepsilon_i = \hat{Y} + u_i$$

(11)

Becomes

$$Y_i = E(Y \mid X = x_i) + u_i$$

(12)

The conditional moment $m(x_i)$ (conditional expectation of Y on X) in the linear least squares case is,

$$\hat{Y}_i = E(Y \mid X = x_i) = \alpha + \sum_{i=1}^n \beta_i X_i = m(x_i)$$

(13)

Using the concept of conditional moment, the regression equation becomes

$$Y_i = m(x_i) + u_i$$

(14)

In non-parametric statistics, instead of estimating $m(x_i)$ with parameters that describe a linear relationship between X and Y, a *kernel* density function is used to estimate the conditional moment at an x^*. This estimate is seen to be smoother than other methods of nonparametric density estimation after which the function below must be satisfied:

$$\int_{-\infty}^{\infty} K(\psi)\, d\psi = 1$$

(15)

Where, $\quad \psi = \dfrac{(x_i - x^*)}{h}$

h = bandwidth (also known as window width)

In the case where the uniform kernel density function is used (i.e., where each observation in the range is equally weighed with a value of 1), the conditional moment is

$$\hat{m}(x^*) = \frac{\sum_{i=1}^{n} y_i}{n}$$

(16)

Thus, kernel regression belongs to a non-parametric smoothing technique where the weighted sum of all the observations is used along with the kernel density function weights as follows:

$$E(Y/X) = m(x) = \int yf(y/x)dy = \frac{\int yf(y,x)dy}{\int x(x)}$$

(17)

Where m(x) is the conditional expectation function X, Y is the predictand, f(Y/X) is the conditional probability density function (p.d.f.) of Y given X=x.

iii)   Percent Bias (PBIAS)

The PBIAS has also been calculated between the observed and simulated. The PBIAS expressed as percentage measure the average tendency of the simulated data to be larger or smaller than their corresponding observed values.
The equation for the measure is as follows:

$$PBIAS = \left[\frac{\sum_{i=1}^{n}(Q_i^{obs} - Q_i^{sim}) * 100}{\sum_{i=1}^{n} Q_i^{obs}} \right]$$

(18)

Where, Q_i^{obs} indicates observed value and Q_i^{sim} simulated value and n is the total number of days in the series. Optimal value for PBIAS is considered to be 0. Positive values indicate underestimation bias. Negative values indicate overestimation bias.

iv)   RMSE-observations   standard   deviation   ratio (RSR)

First proposed by Moriasi et al., 2007, the RSR standardizes the observations-standard deviation and is calculated as the ratio of RMSE and the standard deviation of measured data.

$$RSR = \frac{RMSE}{STDEV_{obs}}$$

(19)

RSR has an optimal range of 0 to a large positive value. Lower the RSR, lower the RMSE, the better the model.

Estimation Of Cropwater Demand For Wheat At Hissar, Haryana Using Cropwat Software

Nivedita Singh[1] and K.K. Singh[2]
[1]PhD student, Civil Engineering Department, NIT Kurukshetra, Haryana, India
e-mail: niveditasinghrana@gmail.com
[2]Professor, Civil Engineering Department, NIT Kurukshetra, Haryana, India
e-mail:k_k_singh_2000@yahoo.com

ABSTRACT: *CROPWAT 8.0 is a computer based model for calculation of crop water requirement, irrigation water requirement, irrigation schemes and water management. CROPWAT model reference evapotranspiration (ET_0) calculates using Penman-Montieth formula, which requires climate data such as temperature, humidity, wind speed and sunshine hour. In the present study CROPWAT 8.0 is used to estimate the crop water demand and the irrigation requirement from climate, crop and soil data of Hissar district, Haryana. Total geographical area of Hissar is about 404 Ha out of which cultivable area is 340 Ha. 80 % of the total area consist of sandy lom soil. Major source of irrigation is canal. The climate of Hisar has tropical monsoonal climate and is characterized as arid type of climate. The total crop water requirement of wheat crop in the rabi season for the years 2008 and 2009 using field method i.e. E pan method are 246.9 mm and 250 mm respectively. Using CROPWAT 8 one gets the total crop water requirements in the rabi season for the years 2008 and 2009 as 241.7 mm and 253.1 mm respectively, which are close to observed values. The total irrigation requirements of years 2008 and 2009 in the rabi season are 231.9 mm and 229.5 mm respectively. Hence, CROPWAT can be used as decision support system, which is a useful tool to help meteorologist and irrigation engineers to carry out the standard estimations for Evapotranspiration, Irrigation scheduling and crop water studies.*

Keywords: Reference evapotranspiration, Crop water requirement, Irrigation requirement.

1.   INTRODUCTION

Water is a very valuable resource and needs to be conserved and managed very efficiently. Intensive competition of water among wide range of users, changing economics, increasing environmental concern, changing public value and other trends in modern times are putting pressure on irrigation. India has an estimated 142 (Mha) cultivated area of which about 57 Mha is irrigated and the remaining 85 Mha is rain fed. The cropping intensity is stagnating at 1.35, which could be increased with increase irrigation and mechanization. The rapid population growth has increased urbanization. More mouths mean more water for foodgrains production, more water for drinking, more water for household/ sanitation; while industrialization has also raised the demand of more water for manufacturing, commercial and service sectors. Environmental flows to replenish depleted river flow are being released in a number of developed countries, and in some developing countries. The resulting total of these demands put far greater pressure on water resources and efficient water uses. Lin and Hung (1995) used the evaporation pan to estimate the transpiration potential of crops, and the potential evapotranspiration was estimated by Penman equation. Shih and Ho (1997) conducted field experiments at the HsuehChia Experimental Station to estimate the crop coefficient and actual evapotranspiration for soybean. Cavero et al. (2000) applied CROPWAT model to simulate maize grain yield reduction caused by water stress under semi-arid conditions. Furthermore, many researcher used CROPWAT for various works such as Naheed and Mahmood (2011); Waseem (2010); Jamshid (2003); Karanjal (2008), Doorenbos and Pruitt (1976); Allen et al (1998), Smith (1991, 1992). In the present study, an attempt has been made to determine the crop water demand of wheat crop during rabi season in the Hissar district using CROPWAT, which is less data intensive, fast and accurate. The other adavantage with CROPWAT is that it can help in irrigation scheduling and canal water management.

2.   STUDY AREA

The Hissar district lies at the 29° 5'5"N *latitude* and 75° 45'55"E *longitudes*. Total geographical area of Hissar (shown in Figure 1) is about 404 Ha out of which cultivable area is 340 Ha. 80 % of the area consist of sandy lom soil. Major source of irrigation is canal. The climate of Hisar has tropical monsoonal climate and is characterized as arid type of climate. It has four seasons during the year viz., Summer (March to May), SW Monsoon (June to September), Post-Monsoon (October to November) and Winter (December to February) season. The main characteristics of climate of in the district are its dryness, extremes of temperature and scanty rainfall. Around 75 to 80 per cent of the annual rainfall is received during SW Monsoon season (June to September) with 50 per cent coefficient of variation (CV). The average annual rainfall is around 450 mm. The average number of rainy days (day with rainfall = 2.5 mm is called a rainy day) per annum are 27±5 days out of which 19 falls during SW Monsoon period. The maximum temperature in summer months between 40 to 44°C and the minimum temperature between 4 to 6°C in winter months are normal for

the place. Relative humidity varies from 5 to 100 per cent during the year at Hisar. Sunshine from October to April are generally sunny months receiving more than 70 per cent of the total possible sunshine hours. February to May and September to December months receive an average of more than 8 hours per day of bright sunshine. Whereas, January ,July, August and December recorded little less sunshine viz., 6 to 7 hours per day because of cloudiness due to rain bearing weather systems. Monthly mean wind speed values are varying between 4 and 10 kms per hour. Evaporation during the summer months remains above 12 mm/day. However, during rainy and winter seasons, average value of evaporation remains around 6.8 and 4.0 mm/day, respectively.

Figure 1. Location Map of Study Are

3.   DATA AND METHODOLOGY

Daily meterological data include rainfall, maximum temperature, minimum temperature, relative humidity, wind speed and sunshine hour were collected for the period of 2008-2009 for Rabi season from the Hissar meterological department of Haryana Agricultural University, Hissar. Crop data and soil data collected from the literature(site:www.*agriharyana.nic.in)*

CROPWAT has four modules viz. Climate module, Rain module, Crop module and Soil module.

It uses Penman - Monteith method to calculate reference evapotranspiration (ET$_o$) given by Allen et al., 1998.   The mathematical expression of the same is presented below:

$$ET_0 = \frac{0.408(R_n-G)+\gamma\frac{900}{T+273}u_2(e_s-e_a)}{\Delta+\gamma(1+0.34u_2)}$$

(1)

Where ET_o is crop reference evapotranspiration (mm day^{-1}), R_n is net radiation at the crop surface (MJ m^{-2} day^{-1}), G is soil heat flux density (MJ m^{-2} day^{-1}), T is mean daily air temperature at 2 m height (°C), u_2 is wind speed at 2 m height (m s^{-1}), e_s is saturation vapour pressure (kPa), e_a is actual vapour pressure (kPa), e_s - e_a is saturation vapour pressure deficit (kPa), Δ is slope of vapour pressure curve (kPa °C^{-1}), and γ is psychrometric constant (kPa °C^{-1}). In application having 24-h

calculation time steps, G is presumed to be 0 and e_s is saturation vapour pressure (kPa).

If crop water requirement is designated as ET_c and K_c represents crop coefficient then crop water requirement can be estimated using the relationship as below

$$ET_c = ET_0 * K_c \quad (2)$$

Effective rainfall can be calculated using USDA soil conservation services formulae

$$P_{eff} = P_{month} \times \frac{125 - 0.2 \times P_{month}}{125}; \quad \text{for} \quad P_{month} \leq 250mm \quad (3a)$$

$$P_{eff} = 125 + 0.1 \times P_{month}; \quad \text{for} \quad P_{month} > 250mm \quad (3b)$$

The irrigation requirement (IR) is estimated by the equation

$$IR = ET_c - P_{eff} \quad (4)$$

Figure 2 shows the flowchart depicting CROPWAT methodology for estimation of crop-water requirement and irrigation water requirement.
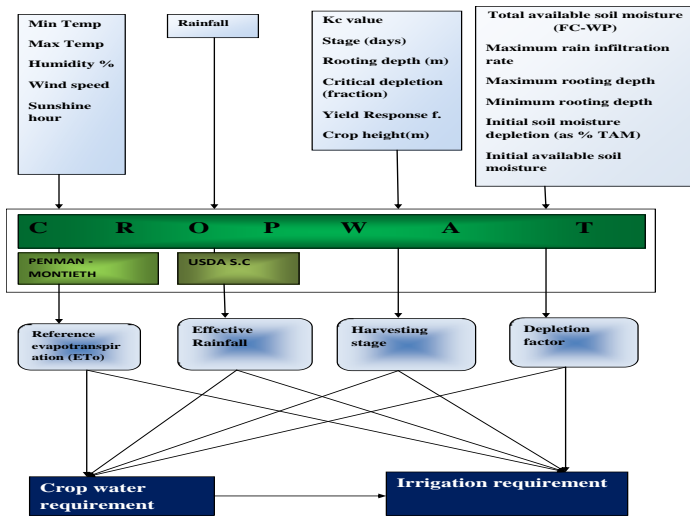
Fig 2. Flowchart depicting CROPWAT methodology for estimation of crop water and irrigation water requirements

4. Result and Discussion

The 2 year rabi season meteorological data were used in CROPWAT model to calculate crop-water demand. Crop-water requirements of wheat during rabi season are 241.7 mm and 231.9 mm in the years 2008 and 2009 respectively. The irrigation requirements of wheat are 253.1 mm and 229.5 mm for the years 2008 and 2009.
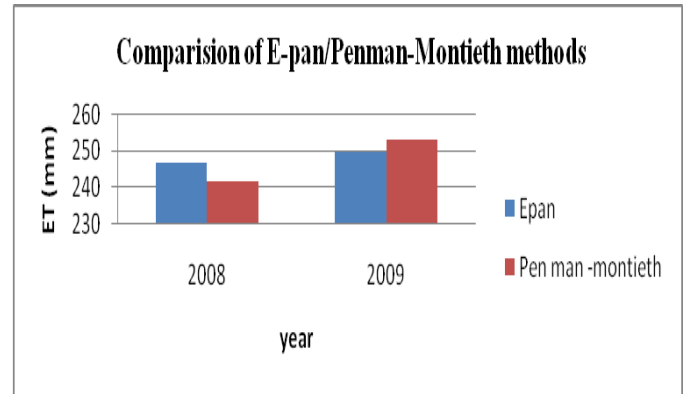
Figure. 3 Comparision of methods
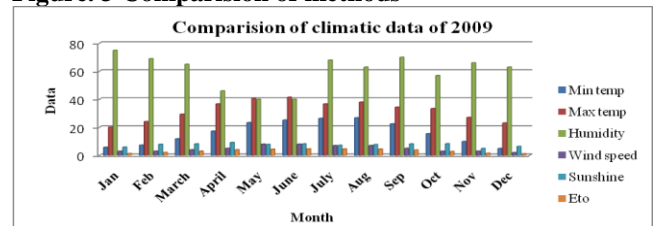
Month	Decade	Stage	Kc coeff	ETc mm/day	ETc mm/dec	Eff rain mm/dec	Irr. Req. mm/dec
Nov	2	Init	0.58	0.92	0.9	0.3	0.9
Nov	3	Init	0.58	0.82	8.2	0.0	8.2
Dec	1	Init	0.58	0.78	7.8	0.0	7.8
Dec	2	Deve	0.62	0.71	7.1	0.8	6.3
Dec	3	Deve	0.82	0.91	10.0	0.0	10.0
Jan	1	Deve	1.03	1.13	11.3	3.2	8.1
Jan	2	Deve	1.23	1.50	15.0	0.0	15.0
Jan	3	Mid	1.37	1.64	18.1	0.0	18.1
Feb	1	Mid	1.38	1.77	17.7	0.9	16.8
Feb	2	Mid	1.38	2.71	27.1	0.0	27.1
Feb	3	Late	1.37	3.13	25.1	0.0	25.1
Mar	1	Late	1.21	3.43	34.3	0.0	34.3
Mar	2	Late	0.95	2.85	28.5	0.0	28.5
Mar	3	Late	0.68	2.34	25.7	0.0	25.7
Apr	1	Late	0.49	1.60	4.8	3.9	0.0
					241.7	9.1	231.9

Crop Water Requirements — ETo station Hissar, Crop wheat, Planting date 20/11

Month	Decade	Stage	Kc coeff	ETc mm/day	ETc mm/dec	Eff rain mm/dec	Irr. Req. mm/dec
Nov	2	Init	0.58	0.83	0.8	0.0	0.8
Nov	3	Init	0.58	0.81	8.1	0.0	8.1
Dec	1	Init	0.58	0.75	7.5	0.0	7.5
Dec	2	Deve	0.62	0.70	7.0	0.0	7.0
Dec	3	Deve	0.82	0.92	10.1	0.0	10.1
Jan	1	Deve	1.03	1.13	11.3	0.0	11.3
Jan	2	Deve	1.23	1.51	15.1	8.9	6.3
Jan	3	Mid	1.37	2.15	23.7	0.0	23.7
Feb	1	Mid	1.38	2.54	25.4	5.9	19.4
Feb	2	Mid	1.38	2.71	27.1	0.0	27.1
Feb	3	Late	1.37	3.31	26.5	0.0	26.5
Mar	1	Late	1.21	3.31	33.1	0.0	33.1
Mar	2	Late	0.94	2.94	29.4	0.0	29.4
Mar	3	Late	0.67	2.11	23.3	4.0	19.2
Apr	1	Late	0.48	1.59	4.8	6.6	0.0
					253.1	25.4	229.5
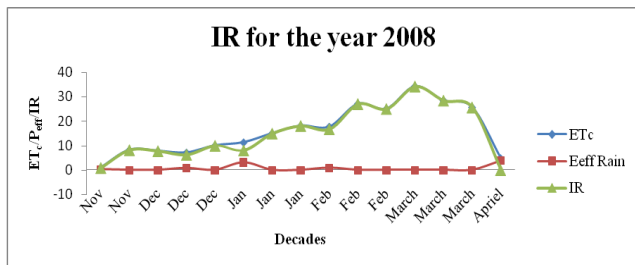
Figure 4. Cropwater demands in Rabi season for the years 2008 and 2009 using CROPWAT

Figure 5. The trend of Cropwater demand, Irrigation requirement and Effective rainfall for the year 2008.

The crop grown in a hot climate need more water per day than the same crop in cooler climate. There are, however, apart from sunshine and temperature, other climatic factors such as relative humidity, wind speed, etc. also influence the crop-water need. During dry region, the crop water need is higher than humid area. In windy climates, the crops will use more water than in calm climates. From the above, it is clear that the climatic parameters are changed, then water requirement will change. Effective rainfall also effect on crop-water requirement. If effective rainfall is more crop-water requirement is less or if effective rainfall is less than crop-water requirement is more.

Figure 6. The trend of Cropwater demand, Irrigation requirement and Effective rainfall in 2009.
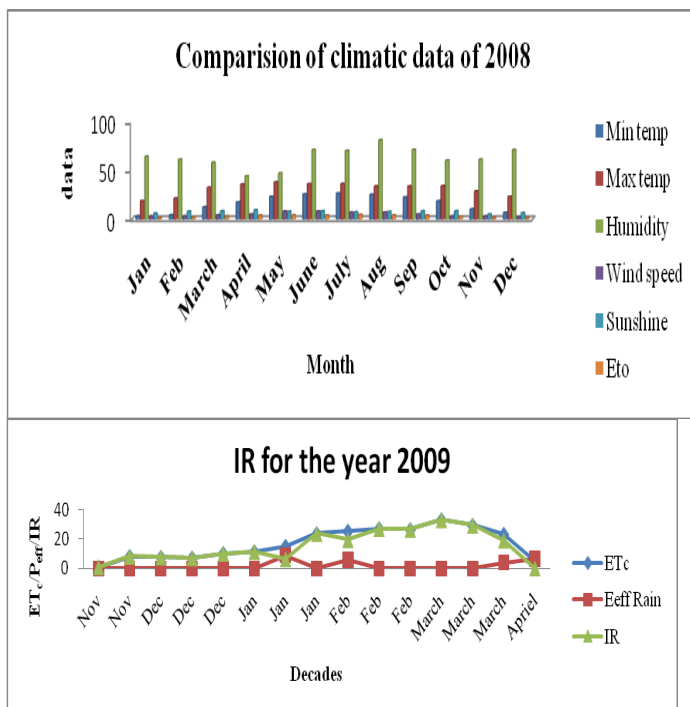
Figure 7. Comparision of climatic parameters in 2008.

Figure 8. Comparision of climatic parameters in 2009.

5.   CONCLUSION

In the present study CROPWAT model was used for calculation of crop-water demand of wheat. Two years rabi season meteorological data were used in the study and it is found that crop-water requirement changes according to climatic parameter. Crop-water requirement of wheat is low in the year 2008 and high in the year 2009.The result reveals that the ET_0 estimated from limited data i. e. daily air temperature, relative humidity and wind speed through CROPWAT have good agreement with that of ETo estimated from the field observation. Thus, to estimate the crop ET and the irrigation requirement for wheat crop CROPWAT model is best suited. CROPWAT is easy to handle, less time consuming, more accurate and less prone to error. Hence, CROPWAT can be used as decision support system, which is a useful tool to help meteorologist and irrigation engineers to carry out the standard estimations for Evapotranspiration, Irrigation scheduling and crop water studies.

REFERENCES

i.   Allen, RG, Pereira, LS, Raes, D, Smith M (1998) FAO56: Crop Evapotranspiration— Guidelines for Computing Crop Water Requirements. FAO of UN, Rome, Italy.

ii.   Cavero, J, Farre, I, Debaeke, P, Maci JM, (2000) Simulation of maize yield under water stress with the EPIC phase and CROPWAT models. Agron. J. 92:679–690.

iii.   Doorenbos, J, Pruitt WO (1976) Guideline for predicting CROPWATer requirements. FAO Irrigation and Drainage Paper No. 24, FAO, Rome

iv.   Jamshid Y (2003) The integration of satellite images, GIS and CROPWAT model to investigation of water balance in irrigated area, thesis report, Internatinal institute for Geo- information Science and Earth observation ENSCHEDE, NETHERLAND.

v.   Karanjal, FK (2008)CROPWAT Model analysis of crop water requirement use in Six districts in Kenya, research project report, 1-41.

vi.   Lin, CF, Hung, JT (1995)An approach to the coefficients of crop water requirement for a simple evaporationpan. Chinese Agric. Assoc. Rep. 176:1–9.

vii.   Naheed, G, Mahmood, A (2011) Water Requirement of Wheat Crop in Pakistan. Pakistan Journal of Meteorology 6: 89-95.

viii.   Shih, CC, Ho, SS (1997) Crop coefficients of soybean evapotranspiration in Taiwan. TaiwanWater Conserv 45(2): 1–12.

ix.   Smith, M (1991) CROPWAT: Manual and Guidelines. FAO of UN, Rome, Italy.

x.   Smith, M (1992) CROPWAT, a computer program for irrigation scheduling and management, FAO Irrigation and Drainage Paper 46, FAO, Rome. pp.127.

xi.   Waseem, R (2010)Validation of CROPWAT 8.0 for estimation of reference evapotranpiration using limited climatic data under temperate condition of Kashmir. Research Journal of Agricultural Science 1(4):338-340

xii.

Design Of Multi Reservoir Multi Junction Water Transmission System For Water Supply Schemes

B.A.Konnur[1]   R.K. Rai[2]

[1]Government College of Engineering, Karad, PIN: 415 124
India
[2] Government College of Engineering, Amravati, PIN: 444 604
India
Email: bakonnur@gmail.com

ABSTRAC: *In the last century, treated water was available to the rural population only if individual direct pipelines could reach them. But, the introductions of Regional Water Supplies Schemes (RWSS) have considerably improved the status of treated water supply to large rural population which once considered economically not viable to implement. In RWSS, a water transmission pipeline system is designed such that the combination of treated water from various source reservoirs is transported via a common pipeline and then branch to village service reservoirs at different locations and elevations for distribution. Such transmission system is termed as Multi Reservoir Multi Junction Water Transmission System (MRMJWTS) in which reservoirs either contribute or remove a portion of the overall flow in a transmission network. MRMJWTS is the backbone of RWSS. The major share of the capital investment in a RWSS goes to such water transmission network. Even though, these networks are basically branched networks, their configuration is not simple because of wide geological area that they cover. Further, they involve long distance pipelines having large diameters. Through efficient design of water transmission network, engineers shall be able to optimize pipeline resources, minimize cost, and run the water supply system at peak levels.*

MRMJWTS involve number of junctions and flow in each connected pipe depends on the elevation of a hydraulic grade line at junction which is variable. For such case of flow which originates or ends in more than one elevation or boundary condition, simple analytical processes are unable to solve for flow or velocity. Methodologies for the design of such type of network have been addressed by a number of researchers. Proposed paper briefly reviews the methods available in the literature that can be applied for designing MRMJWTS. Alternate method of solving MRMJWTS is discussed with an example.
Key Words: Rural water supply, Water transmission lines, Continuity equation, Friction factor, Design parameters

1. INTRODUCTION:

A typical rural water supply scheme in India draws water from one or more deep bore wells through electric pumps and has storage and distribution facilities like overhead tanks, public stand posts etc. Since bore wells can be drilled within the villages or close to habitations, the cost of pumping and conveying water to the habitations is minimal. The progressive depletion of groundwater sources in the country mainly due to

exploitation of this source for irrigation made it necessary to consider surface water based water supply schemes as the long term solution to the problem of rural water supply in many dry areas. It is needless to say that such an approach would call for heavy investment of resources in the sector, particularly in the dry and backward areas. Water Supply Schemes based on surface water sources like rivers involved huge capital expenditure on intake structures and pipelines besides requiring treatment facilities to render water safe for human consumption. Traditionally, treated water was available to the rural population only if individual direct pipelines could reach them. So supply of treated water based on surface sources to rural population was considered economically not viable to implement. But the introductions of water supply planning on a regional scale in the form of Regional Water Supply Schemes (RWSS) have considerably improved the status of treated water supply to large rural population (Bhave2006).

The RWSS covers large areas serving a number of villages in a group which mar situated geographically at considerable distance. To meet water supply needs in a given region, it becomes necessary to obtain water from different sources in the region or outside it. So in RWSS, a water transmission pipeline system is designed such that the combination of treated water from various sources is transported via a common pipeline and then branch to village service reservoirs at different locations and elevations for distribution. Water transmission network is the backbone of RWSS. The major share of the capital investment in a RWSS goes to the water transmission network. Through efficient design of water transmission network, engineers shall be able to optimize pipeline resources and minimize cost of water supply infrastructure.

2. DESIGN OF WATER TRANSMISSION NETWORKS:

Water transmission network is like a tree trunk and branch structure, where tree trunk feeds the branches and in turn branches feed sub branches. The water flow path in single input water transmission network is unique. But in multi input branched transmission systems, the flow direction in some of the pipes interconnecting the reservoirs can change due to the spatial or temporal variation in water demand. Reservoirs either contribute or remove a portion of the overall flow in transmission network. The flow in pipe system assumed to be steady and then so-called steady-state network analysis problem is solved for a given set of boundary conditions (i.e., tank levels, nodal demands, pipe hydraulic resistances, pump characteristics, and minor losses), resulting in the pipe flows and nodal heads. In any pipe network analysis problem all of the physical features of the network are known, and the solution process endeavors to determine the discharge in every pipe and the pressure, etc. at every node of the network. Diameters of all pipes, their lengths and their roughnesses are assumed to be known, as well as where reservoirs, pumps, pressure reduction valves, and other fittings are located. Design of pipe networks; on the other hand, try to select the diameters of pipes, the capacities of pumps, the water surfaces elevations of reservoirs, and so on. Thus, a design problem is

distinguished from an analysis problem by the choice of the variables that are regarded as unknown. Design pipe networks are usually more challenging to solve than are analysis problems, and design problems usually require the simultaneous solution of a larger system of equations than do analysis problems. A thorough understanding of the techniques of analysis for large networks that are composed of known physical features is a prerequisite to the understanding of the design of networks.

During precomputer era elaborate and often complicated analytical methods were required to obtain numerical answers to transmission network problems. The oldest systematic method for solving design problem in a pipe network is the Hardy Cross method. Since then methodologies for the design of water transmission network have been addressed by a number of researchers (Karmelli 1968, Watanatada 1973, Liang 1997, Hossein 2006). Some of these methods are;

i.   Newton-Raphson Method
ii.   Linear Theory Method
iii.   Gradient Method
iv.   Non Linear Programming Method
v.   Global Gradient Method
vi.   Dynamic Programming Method
vii.   Integer Programming

Over the past quarter century, the Newton–Raphson method has proven to be superior in solving the nonlinear equations and now networks of 2500 pipes or more can be analyzed successfully with a desktop computer. In Linear Theory method, the looped energy equations are modified to be linear for previously known discharges and solved iteratively. The process is repeated until the two solutions are close to the allowable limits. Other methods make use of mathematical programming techniques in identifying solutions. All these methods are characterized by the simultaneous solution of the network equations and solve a system of nonlinear equations whose size is a function of the topological representation of the network. In these methods, the pipe diameters and the input heads are assumed to obtain the average pipe velocities and discharges in pipes. The average pipe velocities are checked against the maximum allowable average velocity. The pipe diameters and the input heads are revised several times to ensure that the average pipe velocities do not exceed the allowable limits. Such designs attempt only to satisfy basic hydraulic constrains viz. continuity principle and work energy principle. In turn they address only the functional and to some extent safety requirements. Two other important requirements viz. cost and reliability of systems are overlooked by these methods (Swamee 2008).

3. MULTI RESERVOIR MULTI JUNCTION WATER TRANSMISSION SYSTEMS:

The grid of transmission mains along with their accessories that convey water from one reservoir to another reservoir situated at various locations in a water supply system is known as water transmission network. A multisource multi junction water transmission network is a grid of transmission mains consists of two or more interconnected reservoirs. These reservoirs are connected by intermediate junctions. Schematic diagram of four reservoir two junction water transmission system is shown in Figure 1. The pipes on the main line are assigned number 1, 2 and 3 starting from the end of the system. The lowest reservoir is assigned number 1 and highest reservoir is assigned the number equal to the number of first pipe. The junctions on the main line are assigned j_1 and j_2. The intermediate reservoirs are assigned 2' and 3'. Lengths of the pipes are denoted by L_1, L_2, L_3, L_2' and L_3' Similarly discharges and diameters are denoted by Q_1, Q_2, Q_3, Q_2, Q_2' and $D_1, D_2, D_3, D_2', D_3'$ respectively. The water elevations of the reservoirs are assigned H_1, H_2', H_3' and H_3 starting from lowest reservoir. Reservoirs in MRMJWTS either contribute or remove a portion of the overall flow in transmission network. Accordingly they are teemed as either supplying reservoir or receiving reservoir. There are no intermediate withdrawals of water in a water transmission network.
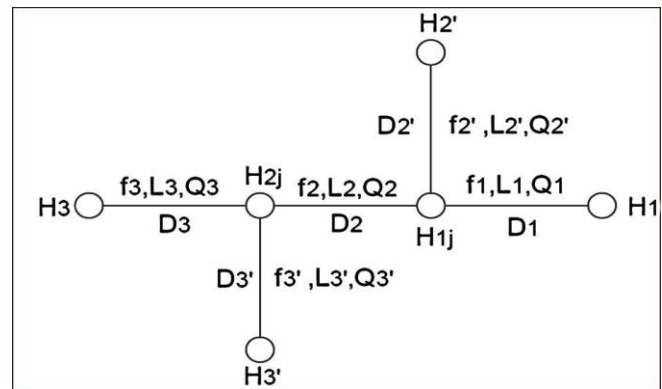
Figure 1. Four reservoir two junction water transmission system

Water transmission systems for regional water supply are multi source branch systems because of insufficient water from a single source and reliability considerations. In such systems two or more reservoirs are connected by a junction and are termed as Multi Reservoir Multi Junction Water Transmission Systems (MRMJWTS). In multi input branched transmission systems, the flow direction in some of the pipes interconnecting the source reservoirs are not unique and can change due to the spatial or temporal variation in water demand. The location of the input reservoirs, pumping stations and supply reservoirs can vary based on the availability of land and topography of the area. Because of these complexities, in MRMJWTS the number of design variables becoming too large to handle efficiently by design techniques discussed earlier. In order overcome these difficulties various optimisation techniques have been effectively tried by researchers in recent times (Deb 1974, Chipulankar 1983).
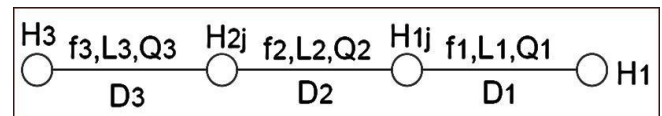
Figure 2. Typical flowpath selected from MRMJWTS

The design of transmission network deals with finding diameters of the pipes for given elevation of the reservoirs knowing various parameters such as discharge, velocity, length, material and age of the pipes. The designer must
have better idea of the spatial and temporal distribution of demand, routes along which the pipes will be actually laid and the field data regarding different lengths and levels. A.K.Dev in 1971 developed a method of optimum analysis of branched pipe networks which could be solved with the help of a desk calculator. The procedure involves initially solving all the single branches in the network containing pipes in series only (not branching). This is followed by combining two single branches at a time and modifying the coefficients calculated previously for the same. Further, this linking of pair of branches (or modified combined pairs) is continued two at a time with recalculation of coefficients each time for all the linked branches till the whole network is covered. In real life situations as the number of branches increase, the process of necessarily linking only two branches at a time involves increasing number of computational steps and reevaluations for same branches to obtain the final solution. Chipulankar and Khanna proposed a optimisation algorithm for multibranch pipe network system using Lagrangian multiplier technique in the year 1983.

4. COST OPTIMISATION OF MRMJWTS:

Providing a solution merely satisfying the functional and safety requirements is not enough. Water transmission networks have a large number of feasible solutions due to trade off between pumping head, pipe sizes, and the quantity of earth cutting and filling. In the water transmission system, the components sharing costs are pumps and pumping stations, pipes of various commercially available sizes and materials, storage reservoirs, pipe laying costs and recurring costs such as energy usage; operation and maintenance of the system components. Therefore, there is an ample scope for the cost saving through proper combination of these feasible solutions. Water is carried over long distances through transmission network having large diameter pipelines. Considerable amount of a water supply project funds are used in the water transmission network; therefore, one cannot overlook the cost considerations in designing a water transmission network. The cost of such system has to be reduced to a minimum consistent with functional and safety requirements and also reliability considerations. Optimization approach for the design of water transmission network considering cost factors have been addressed by a number of researchers [9]. An attempt is made in this paper to use an optimization approach for the design of MRMJWTS based on Lagrange Multiplier Technique.

In MRMJWTS, entire network is decomposed in to number of transmission mains by identifying flow path for each branch. For given input reservoir, number flow path will be equal to the number of receiving reservoirs in the system. Hence there will be three flow paths for the transmission network shown in

Figure 1. They are 3-3', 3-2' and 3-1. The flow path 3-2 is shown in the Figure 2. Consider each of these flow path as a independent water transmission main consisting of n number of branches denote by length L_i and diameter D_i.

If F is cost of completed transmission main denoted by selected flowpath, the objective function to be minimized for pumping main is (Swamee 2008);

$$F = k_m \sum_i^n L_i D_i^{\ m} \tag{1}$$

k_m as pipe cost coefficient, m is an exponent,

If H is required head at reservoir, Darcy Weisbach head loss equation can be represented as constraint equation;

$$\sum_i^n \frac{8 f_i L_i Q_i^2}{\pi^2 g D_i^5} - z_0 + H + z_L = 0 \tag{2}$$

Z_0 and Z_L are the elevations of first and last reservoirs respectively.

The Lagrangian function of the problem is,

$$F_1 = k_m \sum_1^n L_i D_i^{\ m} + \lambda \left(\sum_1^n \frac{8 f_i L_i Q_i^2}{\pi^2 g D_i^{\ 5}} - z_0 + H + z_L \right)$$

For simplicity considering constant value for friction factor f_i and differentiating above Lagrangian function with respect to D_i,

$$k_m m \sum_1^n L_i D_i^{m-1} + \frac{8 \lambda Q_i^2}{\pi^2 g} \sum_1^n f_i L_i (-5 D_i)^6 = 0$$

$$D_i = \left(\frac{40 \lambda f_i Q_i^2}{\pi^2 g m k_m} \right)^{\frac{1}{m+5}} \tag{3}$$

$$\therefore D_1 = \left(\frac{40 \lambda f_i Q_1^2}{\pi^2 g m k_m} \right)^{\frac{1}{m+5}} \tag{4}$$

From equations 3 and 4,

$D_i =$

$$D_1 \left(\frac{f_i Q_i^2}{f_s Q_s^2} \right) \qquad (5)$$

Substituting value of D_i in equation 2,

$$D_1 = (f_1 Q_1^2)^{\frac{1}{m+5}} \left[\frac{8}{\pi^2 g (z_0 - z_L - H)} \sum_1^n L_i (f_i Q_i^2)^{\frac{m}{m+5}} \right]^{\frac{1}{5}}$$

Substituting value of D_l in equation 5,

$D_i =$

$$(f_i Q_i^2)^{\frac{1}{m+5}} \left[\frac{8}{\pi^2 g (z_0 - z_L - H)} \sum_1^n L_i (f_i Q_i^2)^{\frac{m}{m+5}} \right]^{\frac{1}{5}} \qquad (6)$$

In equation 6, initially arbitrary value of f_i is used to obtain D_i^*. Knowing diameter, an improved value of f_i can be obtained. Using this value of f_i, an improved value of D_i^* can be calculated. The process is repeated until two successive values of D_i^* are very close.

It can be seen that equation 6 is applicable to a single flow path. Some pipes can be common to more than one flow path. Hence values of optimum diameter D_i^* for such pipes are calculated separately for each flow path. In order to satisfy minimum terminal pressures and maintain the desired flows, the maximum pipe diameter values of D_i^* are selected in final solution. Continuous pipe sizes thus obtained are converted to nearest commercial pipe diameters for adoption. Continuing with the same process diameters of all the branch pipes from various flow paths are calculated. Finally knowing diameters of all branches, equation 1 is used to calculate the total cost of water transmission line. Care is to be taken to consider all pipes of transmission network for calculating total cost.

5. DESIGN EXAMPLE:

Design data for the four reservoir two junction transmission network represented by Figure 1 is given in Table 1.
Table 1. Design data for four reservoir two junction transmission network

Pipe	Length L (m)	Discharge Q (m³/s)	Friction factor f
3	5000	1.00	0.03
3'	2000	0.15	0.03
2	3000	0.85	0.03
2'	1000	0.15	0.03
1	3000	0.70	0.03

Elevations of reservoir level H_3, $H_{3'}$, H_2 and H_1 are considered as 100m, 80m, 65m and 60m respectively. Pressure head at all reservoirs are neglected. Pipe 1 is common to all three flow paths, hence D3 is calculated separately for all three paths using equation 6 and it's maximum value 0.938m is rounded

off to the next available commercial size i.e.0.950m. Similarly the values of 3', 2, 2' and 1 are calculated as 0.500m, 0.850m, 0.400m and 0.800m.

The cost of the pipeline is calculated by using equation 1. In order to determine k_m and m values cost of CI pipes for various diameters are considered from schedule of rates published by Maharashtra Jeevan Pradhikaran, Amravati region for the year 2012-13. The cost of fixtures and fastening is considered as 10% of the cost of pipe. Cost of lying is also considered separately. By plotting the variations in cost of pipes versus diameter in excel, the best fit of the curve is obtained. By using power form of the equation the value of the K_m and m are estimated at 32623 and 1.405 respectively. Knowing length and diameters of each pipe the cost of the four reservoir two junction transmission network is obtained as Rs3348 lakhs.

6 CONCLUSIONS:

Conventional design practice of water transmission system in vogue provides a feasible design satisfying only functional requirements. Providing a solution merely satisfying the functional requirements is not enough. The design procedure discussed in the paper reduces the cost of water transmission system to a minimum consistent with functional and safety requirements. Introduction of multiple reservoirs in the system take care of reliability considerations also. However empirical cost function is used to obtain total cost of transmission network. Hence there is a need to study effect of change in length, change in discharge and change in water elevation to know the limitations of method discussed. Finally for the purpose of validation of the method, there is a need to carry out comparison of this method with other mathematical methods. There is a scope to improve this design procedure to incorporate other components sharing costs such as pumps and pumping stations, storage reservoirs, pipe laying costs and recurring costs such as energy usage; operation and maintenance of the system components.

REFERENCES:

i. Bhave, P. R., and Gupta, R. (2006), Analysis of Water Distribution Networks, Narosa Publishing House, New Delhi
ii. Chipulankar, A. V., and Khanna, P. (1983), Optimal Design of Branched Water Supply Networks, Journal of Environmental Engineering, Vol. 109, No. 3, pp. 604-618
iii. Deb A.K, "Least Cost Design of Branched Pipe Network System" Journal of Environment Engineering Division, ASCE, Vol 100, No. EE4, Proc. Paper 10711, Aug, 1974, pp 821-835
iv. Hossein, M. V. S., and Alireza, M. (2006), Optimization of Water Distribution Networks Using Integer Linear Programming, Journal of Hydraulic Engineering, Vol. 132, No. 5, pp.501-509
v. Karmeli D and Gadish Y. Design of optimal water distribution network Journal of pipeline devision ASCE Vol. 94 Oct 1968 pp 1-10)
vi. Liang T. Design of Conduit System by Dynamic Programming, Journal of Environmental Engineering Division ASCE Vol 97No. HY3 March 1997
vii. MJP, "Schedule of Rates for Maharashtra Jeevan Pradhikaran Works for the year 2012-2013", Maharashtra Jeevan Pradhikaran, Nagpur-Amravati Region, Nagpur, 2012
viii. Robinson R.D. &Austin D.A. Cost Optimisation of Rural Water Systems, Journal of Hydraulic Division, ASCE Vol.102,No.HY 8, Aug 1976

ix. Swamee, P. K., and Sharma, A. K. (2008), Design of Water Supply Pipe Networks Wiley Interscience

x. Watanatada T. Least Cost Design of Water Distribution System, Journal of Hydraulic Engineering Division, ASCE, Vol 99, No.HY 9, Sept 1973

Identification Of Groundwater Pollution Source Through Inverse Modeling

Jyoti Chaubey[1]   Deepak Kashyap[2]

Research Scholar, Department of Civil Engineering, IIT Roorkee,Roorkee 247667, India
Email: jyotidce@iitr.ernet.in
Professor, Department of Civil Engineering, IIT Roorkee, Roorkee 247667, India
Email: dkashfce@iitr.ernet.in

ABSTRACT:*Groundwater pollution source identification plays an important role in risk assessment studies and in designing the groundwater remediation measures. The present study involves development and illustration of an inverse problem model for identification of pollution source characteristics. The model, based upon linked simulation optimization approach, invokes a finite difference based simulator and a Sequential Unconstrained Minimization Technique (SUMT) based optimizer. The model arrives at such pollution source characteristics that provide the closest match between observed and the simulated concentration field. The estimated pollution source characteristics include source location and strength. The model has been illustrated for a hypothetical study area with known boundary conditions and flow/transport parameters. Two dimensional steady state flow and transport was considered and pollutant sources were assumed to release conservative pollutant at uniform rate throughout the activity period. Objective of the optimizer was to minimize the sum of squares of difference between observed and simulated concentration with respect to the unknown pollution source characteristics. For model illustration, observed concentration felidwas generated by the simulation model assuming the source flux to be known. Subsequently generated concentration field was employed for solving the identification problem, masking the assumed source flux.Model is validated by demonstrating a close enough match between source flux values emanating from the model and the source flux assigned while generating the concentration field. Three monitoring networks with varying density of monitoring wells were considered. The developed model gave satisfactory results of the source flux and source location. Monitoring network with dense observed concentration field datacould identify the source characteristics better as compared to the monitoring network with sparse data.*
Keywords: Groundwater pollution, source identification, simulation, optimization, monitoring network.

1. INTRODUCTION

Identification of groundwater pollution source plays an important role in risk assessment studies, in designing the groundwater remediation measures and in groundwater development studies. Pollution source identification problem is essentially an inverse problem in the context of groundwater solute transport modeling. This inverse problem is solved for obtaining source characteristics for a given set of spatial and temporal concentration and head fields.

Several methods have been reported to solve this inverse problem. These methods can be broadly classified as Optimization approaches (Mahar and Dutta 2000, 2001; Gorelick 1983; Datta et al. 2009, Aral et al. 2001, Singh et al. 2004, Singh and Datta 2006, Ayvaz 2010, Jha and Dutta 2013), Analytical solutions, Deterministic direct methods, Probabilistic and Geostatistical simulation approaches (Bagtzoglou et al. 1991, 1992),Backward Modeling Technique (Wilson and Liu 1994).

Among the solution approaches, optimization is one of the most widely used solution approaches for source identification problem.Optimization approach consists of the integration of both simulation and optimization models. Simulation model solves the governing flow and transport equations for given initial and boundary conditions. It is then integrated with the optimization model which aims to find the best results to achieve a given set of objectives. Optimization model aims at selecting that set of simulated potential sources (location, magnitude and release history) which results in simulated concentrations representing the closest match with local groundwater solute concentration data.

Simulation model can be incorporated into an optimization model as constraints (Mahar and Dutta 2000,2001) or as concentration response matrix (Gorelick 1982, 1983)or it could be linked externally with an optimization model (Datta et al. 2009, Aral et al. 2001, Singh et al. 2004, Singh and Datta 2006,Ayvaz 2010,Jha and Dutta 2013).
Present study is based linked simulation optimization approach for solving the inverse problem of pollution source identification. Source characteristics in the present context comprise source location and source flux. The model invokes a finite difference based simulator and a Sequential Unconstrained Minimization Technique (SUMT) based optimizer. Two different scenarios of observed concentration data availability have been considered, depending upon the concentration data availability. The effect of monitoring networks on the identification of source characteristics is also studied.

2. METHODOLOGY

In linked simulation optimization approach, initial solution (source flux) is given to the optimizer, which is used as input in the simulation model to generate the simulated concentration

distribution. The simulated concentrations at designated observation locations are matched with the observed concentrations at various time intervals at those locations. This residual is used to calculate the objective function value, which is utilized by optimization algorithm to improve the candidate solution. The process continues till an optimal solution is obtained. Schematic representation of the process is shown in Figure-1.
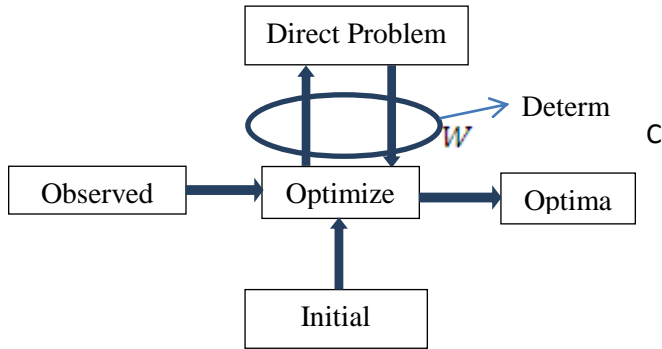
Figure-1: Schematic representation of Linked Simulation Optimization approach

2.1. Governing Equations

Simulation model in the present study is based on the following partial differential equation governing the two-dimensional, transient transport of contaminants in groundwater (Bear, 1972),

$$\frac{\partial}{\partial x}\left(D_{xx}\frac{\partial C}{\partial x}\right) + \frac{\partial}{\partial x}\left(D_{yy}\frac{\partial C}{\partial y}\right) - \frac{\partial}{\partial x}(uC) - \frac{\partial}{\partial y}(vC) + W = R\frac{\partial C}{\partial t}$$

1

where, D_{xx} and D_{yy} are hydrodynamic dispersion coefficients, u and v are velocities along x and y direction respectively, W is the pollution source flux, R is the retardation factor of the pollutant involved, C is concentration of contaminants dissolved in groundwater. The velocities in Eqn. 1 are given by,

$$u = \frac{\frac{\partial h}{\partial x}T_{xx}}{b*n} \text{and} v = \frac{\frac{\partial h}{\partial y}T_{yy}}{b*n}$$

2

where, b is aquifer thickness, n is effective porosity of the aquifer, h is nodal head, T_{xx} and T_{yy} are transmissivities in x and y direction respectively. Dispersivity could be taken as $D_{xx} = \alpha_L|u|$ and $D_{yy} = \alpha_T|v|$ where, α_L is longitudinal dispersivity and α_T is transverse dispersivity.

The necessary head fields for computing velocity vector are simulated by solving following differential equation governing

the transient, two dimensional horizontal flow of groundwater through a non-homogeneous, anisotropic, saturated aquifer.Iterating Alternative Direction Implicit Explicit (IADIE) finite difference scheme has been applied for solving Eqn. 1, to generate concentration fields.

2.2. Model formulation

The objective of the problem is to determine the source location and flux given a set of potential source locations and observed concentration distribution. Although the source location is not known a priori, it may be possible to delineate the area that is prone to pollution. The nodes lying therein are termed herein as potential source locations. Since the potential source locations are assigned, the source flux values become the decision variables. Mathematically the objective of the optimization model can be described as:

Minimize $Z = \sum_{i \in I}\left(C_i^{obs} - C_i^{simu}\right)^2$

with respect to W_j(It may be noted that C_i^{simu} and hence Z would be a function of W_j)

subject to $W_j \geq 0$ j=1,2….,m

where C_i^{obs} is observed concentration at node i , C_i^{simu} is simulated concentration at node i, W_j is source flux,$i \in I$ where I is the set of nodes at which observed concentration data are available and m is the number of potential source locations.

Sequential Unconstrained Minimization Technique (SUMT) technique was employed to solve the above posed optimization problem.

3. MODEL ILLUSTRATION

For demonstrating the model applicability, observed concentration field data is needed. However in the present context, observedconcentration field data was not available. To overcome this deficit, observed concentration field data was generated by solving the solute transport equation for assumed source flux values and known source location. This generated data was then used as an input to the linked simulation optimization model, masking the assumed source flux values and known source location.

3.1. Study Area and Database

The model developed has been illustrated by a hypothetical two dimensional study area, shown in Figure-2. The north and south boundaries are considered impervious boundaries while east and west boundaries are considered to be constant head boundaries. Two pollution sources (S1 and S2) are there in the study area, the location of which is shown in the Figure-2. A pond is located in the area, which is free from

contamination.The flow and transport parameters used in the simulation model are given in Table 1.
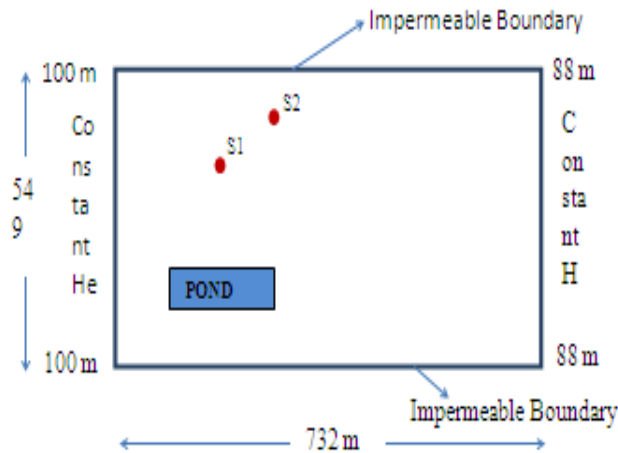
Figure-2: Study Area

Table-1:Simulation model Parameters

Parameters	Value
T_{xx} (m^2/d)	26.35
T_{yy} (m^2/d)	26.35
Grid spacing in x direction, Δx (m)	91.5
Grid spacing in y direction, Δy (m)	91.5
Longitudinal dispersivity, α_L (m)	40.0
Transverse dispersivity,α_T (m)	9.6
Δt (days)	90
Saturated Thickness, b (m)	30.5
Effective porosity, ϕ	0.2
Pond Recharge (L/s)	2.15
Source flux (S1 and S2) (g/s)	31.7

3.2 Generation of Concentration Field

3.2.1 Generated Concentration Field

The study area has been divided into grids of size 91.5×91.5 m each.Single time step of 90 daysis taken for the study. Initial concentration of pollutant is assumed to be zero in the groundwater. Pollution sources are assumed to release conservative pollutant at a uniform rate throughout the activity period. The corresponding steady state concentration field was generated by solving the solute-transport equation numerically, employing the parameters and the assumed source flux listed above. The generated concentration field comprising nodal concentration is depicted in the Figure-3.
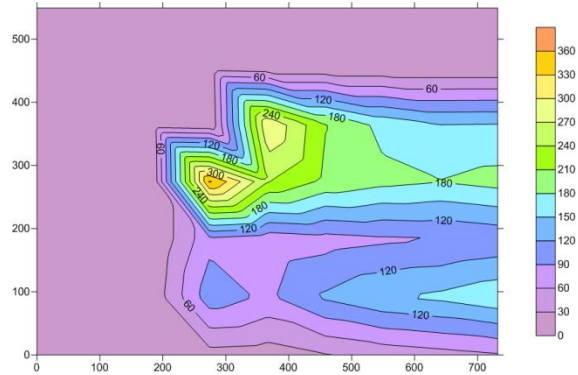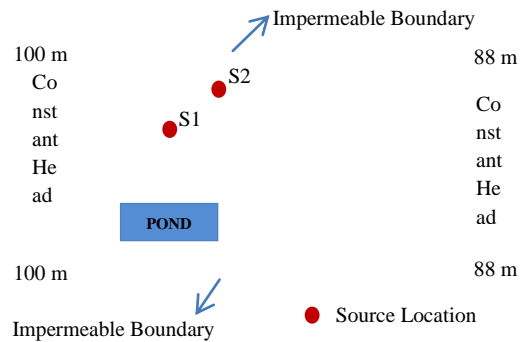
(a)   (b)

Figure-3 (a) Finite Difference Grid for the Concentration generation (b) Observed Concentration field generated by using known source fluxes(Dimensions along x and y axis are in m and concentration is in mg/l)

3.2.2 Concentration Networks

In practice monitoring of concentration data of various polluting species is expensive and tedious. Hence obtaining the observed concentration data at all the nodes of study area is practically not possible. As suchthree Monitoring networks with varying density of monitoring wellsare considered for the present application. The first monitoring network (MN1) comprises sixty three uniformly distributed locations, coinciding with the grid involved for generating the concentration field (Figure-3(a)). For rest two Monitoring networks it is assumed that the observed concentration data is available at few monitoring locations. Second monitoring network (MN2) comprises four monitoring wells located far away from the sources, coinciding with the second last corners of each side in the grid involved for generating the concentration field.Third monitoring network (MN3) also comprises four monitoring wells located in the vicinity of the pollution sources. The concentration data for the monitoring wells incorporated in the monitoring networks are derived from the generated concentration field. Monitoring networks MN2 and MN3 are shown in Figure-4.

3.3 Model Runs

The objective of the optimization problem is to determine the source location and flux, employing the given observed concentration field data. Potential source locations (termed as "SL")are shown in Figure-5. Simulation-optimization model was run for a given initial set of source fluxes as an initial solution of the optimization problem.
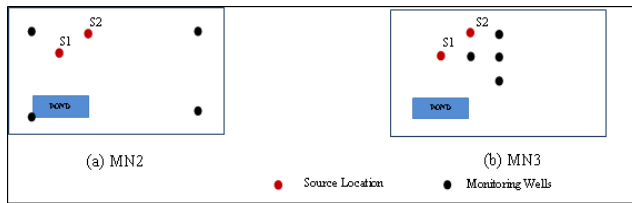
Figure-4Various Monitoring networks
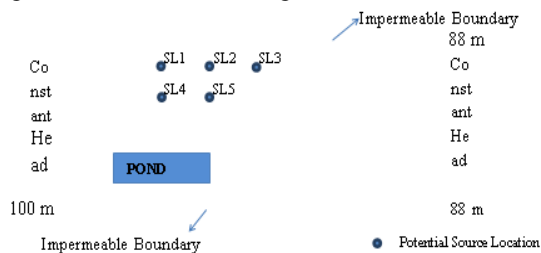
Figure-5 Potential Source Location

4. RESULTS AND ANALYSIS

The linked simulation-optimization model was run and the source flux values obtained for all the Monitoring Networks have been listed in Table-2. Pollution source locations identified by various monitoring networks has been shown in Table-3.Table-4 shows the number of simulation model run to arrive at the optimal solution.Model is validated by demonstrating a close enough match between source flux values emanating from the model and assigned source flux while generating the concentration field.

Table-2 Source fluxes assigned and obtained for various Monitoring networks; Model runs for different Monitoring Networks

Source Location	Pollutant flux (g/s)			
	Assigned	Model Simulated		
		MN1	MN2	MN3
SL1	0.0	0.55	0.0009	0.63
SL2	31.7	31.03	31.16	29.68
SL3	0.0	0.009	0.96	0.98
SL4	31.7	31.33	30.34	30.26
SL5	0.0	0.0004	4.35	0.93

Table-3 Source Location Identification

Monitoring Networks	Pollution Source Locations	Source Locations Identified
MN1	SL2 and SL4	SL1,SL2 and SL4
MN2	SL2 and SL4	SL2,SL3,SL4 and SL5
MN3	SL2 and SL4	SL1, SL2,SL3,SL4 and SL5

Table-3 Model runs for different Monitoring Networks

Model Runs	Monitoring Network		
	MN1	MN2	MN3
	2836	553	2504

From the results it is evident that the model is generally able to identify the source characteristics, i.e. the location of the pollutant sources and source flux. From the results it can be inferred that model performed better (model obtained source fluxes closer to the actual flux values and could identify the source location)for MN1, where data at all the nodes are considered known for the solution. MN 2 could capture the sources well except for the source SL5. It is interesting to note that MN2 consisted of the monitoring wells located far away from the sources (at the second last corner points); still it successfully captured the source characteristics. Monitoring network comprising wells located far from pollution sources performed better as compared to the monitoring network comprising wells located in the vicinity of pollution source locations. Superfluous (though small) sources were also identified, which could be because of the numerical errors or due to inadequate convergence during optimization.

5. CONCLUSION

The linked simulation-optimization model developed could generally able to identify the source characteristics: location and flux, for the given study area. With dense data availability, uncertainty in the identification of the source characteristics reduces; the source flux values obtained are closer to the values assumed. With the sparse data availability,(i.e. observed concentration data available at few selected locations) uncertainty in the identification of source characteristics is increased.

REFERENCES:

i.   Aral M, Guan J, Maslia M (2001) Identification of contaminant source location and release history in aquifers. Journal of Hydrologic Engineering 6(3): 225–234

ii.   Atmadja J, Bagtzoglou AC (2001) Pollution source identification in heterogeneous porous media. Water Resources Research 37 (8): 2113-2125

iii.   Atmadja J, Bagtzoglou AC (2001) State of Art Report on Mathematical Methods for Groundwater Pollution Source Identification. Environmental Forensics 2: 205-214

iv.   Ayvaz MT (2010) A linked simulation–optimization model for solving the unknown groundwater pollution source identification problems. Journal of Contaminant Hydrology 117: 46–59

v.   Bagtzoglou AC, Dougherty DE, Tompson AFB (1992) Application of particle methods to reliable identification of groundwater pollution sources. Water Resource Management 6(1): 15–23

vi.   Bagtzoglou AC, Tompson AFB, Dougherty DE (1991) Probabilistic simulation for reliable solute source identification in heterogeneous porous media. Water resources engineering risk assessment 189–201

vii.   Chadalavada S, Datta B, Naidu R (2011) Uncertainty based optimal monitoring network design for a chlorinated hydrocarbon contaminated site. Environment Monitoring Assessment 173(1–4): 929–940

viii.   Datta B, Chakrabarty D, Dhar A (2009) Simultaneous identification of unknown groundwater pollution sources and estimation of aquifer parameters. Journal of Hydrology 376(1–2): 48–57

ix.   Dhar A, Datta B (2010) Logic-based design of groundwater monitoring network for redundancy reduction. Journal of Water Resource Planning and Management 136(1): 88–94

x.   Jha M, Datta B (2013) Three-Dimensional Groundwater Contamination Source Identification Using Adaptive Simulated Annealing.Journal of Hydrologic Engineering 18(3): 307-317

xi.   Gorelick SM (1982) A Model For Managing Sources of Groundwater Pollution.Water Resource Research 18(4): 773–781

xii.   Gorelick SM, Evans BE, Remson I (1983) Identifying sources of groundwater pollution: An optimization approach. Water Resource Research 19(3): 779–790

xiii.   Mahar PS, Dutta B (2000) Identification of Pollution Sources in Transient Groundwater Systems. Water Resources Management 14: 209–227

xiv.   Mahar PS, Datta B (2001) Optimal Identification of Ground-water Pollution Sources and Parameter Estimation. Journal of Water Resource Planning and Management 127(1):20-29

xv.   Singh R, Datta B, Jain A. (2004) Identification of unknown groundwater pollution sources using artificial neural networks. Journal of Water Resource Planning and Management 130(6): 506–514

xvi.   Singh R, Datta B (2006) Identification of groundwater pollution sources using ga-based linked simulation optimization model. Journal of Hydrologic Engineering 11(2): 101–109

xvii.   Wilson JL, Liu J (1994) Backward tracking to find the source of pollution.Waste Management From Risk to Remediation 1(10): 181–199

Chlorine Decay Simulation Of A Typical Water Distribution System: A Case Study

Neetta S Kumar[1]   Dr. P.G Jairaj[2]
1M.Tech Student, Dept of Civil Engineering, College of Engineering Trivandrum
2Professor, Dept. of Civil Engineering, College of Engineering Trivandrum
Email: neetta8181@gmail.com, jairaj_pg@yahoo.com

ABSTRACT :Deterioration of water quality is a serious issue as water passes through a distribution network. The water supplied to the users must have the desired residual chlorine until it reaches the end users. If sufficient residual chlorine is not available, the chance of microbial contamination exists, thereby making the water non potable. The present study aims to analyse the decay of residual chlorine within a distribution system, by determining the amount of chlorine available at point of consumption, thereby ensure better protection for the consumer. The simulation model was formulated with the chlorine decay was modelled through a first order kinetic law. Hydraulic and water quality analysis were performed for a period of 3 days, in which residual chlorine decay for constant and variable water demand situations were analysed. The residual chlorine at various pipes in the networks was simulated with respect to time. The optimum amount of chlorine that should be injected into the system for the typical cases was also arrived out of the study.

Keywords: Simulation, Chlorine decay, Water distribution network

1. INTRODUCTION:

The quality of treated water deteriorates, after leaving the treatment plant, as water travels through a water distribution system (WDS). Deterioration of water quality in distribution networks has a great impact on human health. The water supplied to the users must have the desired residual chlorine till it reaches the point of consumption. In the absence of sufficient residual chlorine, the chance of microbial contamination is high or in other words residual chlorine concentration is taken as an indicator of microbial contamination. Mugur and Carmen (2012) showed how chlorine residuals can vary throughout the day at different locations in a water distribution network designed for a town with 50,000 inhabitants. Castro and Mário (2003) conducted a study on chlorine decay in Lousada network and concluded that the pipe wall reaction is more significant than that of bulk fluid reactions in chlorine decay in a water distribution network. The effect of variation in demand and the significance of injection of chlorine to a distribution network are not addressed in the earlier works reported.

In the present study, the decay of residual chlorine within a distribution system has been analyzed, by determining the amount of chlorine available at point of consumption. The modeling procedure was applied to two water distribution networks, one having 8 nodes and 8 pipes and the other with 64 nodes 63 pipes. The effect of demand pattern on the decay of residual chlorine concentration is also considered in the study. The optimum amount of chlorine that should be injected into the system for different cases of injection is also determined so as to have proper disinfection of water distribution network. The details pertaining to the methodology used, distribution network studied, specific analysis carried out and results of the study are discussed in subsequent sections. The effect of variation in demand and the significance of injection of chlorine to a distribution network are not addressed in the earlier works reported and they are discussed in the present study.

2. METHODOLOGY

The present study deals with the simulation of chlorine decay while it travels through a water distribution system, and consisting of pipes, nodes, pumps, valves, reservoirs and tanks. The analysis of such a system includes both hydraulic water quality analysis.

2.1 Hydraulic Analysis

Hydraulic analysis involves, determining the discharge and pressure at which water is to be delivered at the consumption point. It involves continuity equation of flow and energy equation wherein the head loss that occur in the pipe is considered. For the hydraulic analysis of the system, properties of the components of the system namely, pipes, nodes, reservoirs, tanks, pumps, values etc are known. The pipe

properties include length, diameter and pipe wall roughness coefficient. Hazen- William's roughness coefficient is commonly used for the analysis. Nodal properties are consumption demand and the elevation at each node. For the reservoir, only the elevation is required. In the case of storage tank, its elevation, initial water level, final water level and its diameter are given to the model. If the network considered is a pumped one, pump's design flow and the head imparted by the pump should be known.

In the hydraulic analysis of water distribution system, by knowing all the properties of network components, the flow characteristics of the system were obtained. The analysis was performed over single period as well as extended period. In extended period analysis, the variation of flow characteristics over a period of time was analyzed. The demand pattern varies over the course of the day and hence in order to make the analysis more realistic, the variation in demand pattern is also considered.

2.2 Mechanism of chlorine decay

Once the hydraulic analysis of the system is completed, water quality analysis can be performed so that the decay of chlorine concentration while it travels through the distribution network was analyzed. Chlorine is usually injected at the source node which may be a treatment plant or a reservoir. The amount of chlorine added at the source node should be sufficient to provide proper disinfection over the entire system so that sufficient amount of residual chlorine will be present when it reaches the end user and at the same time it should not be at larger concentration which may impart a bad taste and can also cause health hazards.

For a non conservative substance like chlorine, the principle of mass conservation within a differential section of a pipe can be written as:

$$\frac{\partial C(x,t)}{\partial t} = -u\frac{\partial C(x,t)}{\partial x} + E\frac{\partial^2 C(x,t)}{\partial x^2} \pm K_R \partial C(x,t)$$

(1)

Considering the first order reaction of chlorine with other substance the conservation of mass is given by Equation (1) in which $C(x, t)$ is concentration of chlorine at location x at time t, u is the velocity in the pipe and E is the coefficient of longitudinal dispersion, $K_R[C (x,t)]$ is the reaction rate constant, which is the sum between the rate of reaction in bulk flow and the rate of pipe wall reaction, in which negative sign is used to reflect the decrease in chlorine concentration due to decay rate.

The first term in this equation represents the rate of change of chlorine within a differential section of pipe, the second term accounts for advection flux of the chlorine in which negative sign reflects an increasing concentration within the control volume if the mass inflow rate is greater than the outflow rate, the third term accounts for dispersive flux of chlorine and fourth term gives the chlorine reaction and it is negative.

Dispersion of chlorine is negligible if the velocity is high and the dispersion coefficient is very low in such a case the third term can be neglected. In the present study, only advection and reaction of chlorine in the system are considered.

The mechanism of chlorine decay in pipe has two dimensions. The first one is the reaction of chlorine with substances present in water, known as bulk decay. Bulk fluid reactions can also occur within tanks. The second dimension is the reaction of chlorine with substances present on pipe wall, known as wall decay. The wall decay in distribution network is predominant where significant corrosion is present.

a) Bulk Reactions

The reactions of chlorine occurring in the bulk flow is modelled with n-th order kinetics, where the instantaneous rate of reaction R (mass/volume/time) is assumed to be concentration-dependent according to

$$R = k_b C^n$$

(4)

where k_b is the bulk reaction rate coefficient, C = reactant concentration (mass/volume), and n is the reaction order. k_b has units of concentration raised to the (1-n) power divided by time. It is positive for growth reactions and negative for decay reactions.

b) Wall Reactions

The rate of water quality reactions occurring at or near the pipe wall was considered to be dependent on the concentration in the bulk flow by using an expression of the form:

$$R = (A/V)\ k_w\ C^n$$

(5)

where k_w = a wall reaction rate coefficient and (A/V) = the surface area per unit volume within a pipe (equal to 4 divided by the pipe diameter). The latter term converts the mass reacting per unit of wall area to per unit volume basis. First-order k_w values ranges from 0 to of 1.5 m/day.

The hydraulic analysis and the simulation of chlorine decay discussed were applied in two water distribution networks wherein the variation in demand and the effect of wall reaction on chlorine decay were considered. The details of analysis carried out in the water distribution networks are explained in subsequent sections.

3. ANALYSIS OF THE PROBLEM

The simulation study on the selected networks was done using the software EPANET, in which the chlorine decay was modelled using a first order kinetic law. The analysis was performed for fixed and variable demand pattern. The effect of

reaction of chlorine with the pipe wall material on the decay of residual chlorine was also analysed.

3.1 Data Used

The present study deals with the simulation of chlorine decay in two water distribution networks. The first case study was done on a simple distribution network given in the EPANET 2.0 Users Manual. It consists of a source reservoir (e.g., a treatment plant clear well) from which water is pumped into a two-loop pipe network which is shown in Figure1. There is also a pipe leading to a storage tank that floats on the system. It also consists of a pump which can deliver 46 m of head at a flow of 136.26 m^3/hr, and the tank having a diameter of 18m, 1.1 m water level, and a maximum level of 6.1 m. The second water distribution network selected for the study is a real case study of Kadinankulam Grama Panchayat, Trivandrum, which is shown in Figure2. The distribution system consists of a surface well of 6m diameter. Water is pumped from the well to an overhead tank with a capacity of four lakh litres, 12 m above the ground level, by means of 30 HP pump. The source of supply is located midway in the network. The total number of consumer connections is 900 of which nearly 850 are household connections. The minimum head required at each node in the network is considered as 8m. The network consists of 63 pipes, which are made of PVC material and 64 nodes with 13 loops as given in Figure 2. The total water demand is estimated to be 260.97 litres/minute. Hazen-Williams roughness coefficients given for the pipe is taken as 100 and 150 for case studies 1 and 2 respectively.
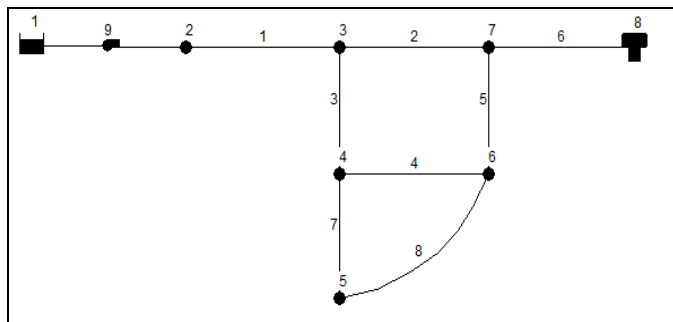
Figure.1 WDS used in Case Study 1

3.2 Hydraulic Analysis

During the analysis of the selected water distribution networks, hydraulic analysis was carried out as the first step. For the extended period hydraulic analysis, the properties of nodes and pipes of the network are supplied to the model and the flow characteristics of all pipes and nodes are obtained for the period of simulation selected in the study.
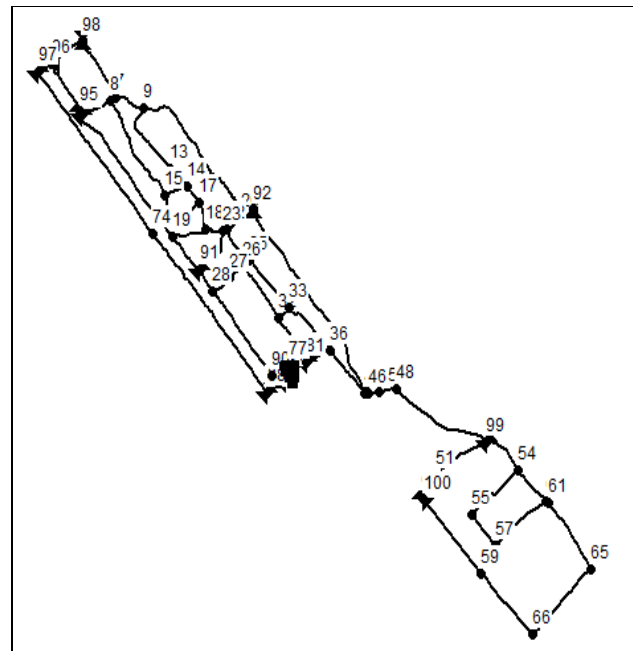
Figure.2 WDS of Kadinankulam Grama Panchayat

3.3 Simulation of chlorine decay

Once the hydraulic analysis was performed on the distribution network, modelling procedure of chlorine decay was carried out. The analysis was performed for a period of 3 days in which constant and variable demand patterns were considered. In the first case study, a variable water demand over 72 hours was taken with a 4 hours flow pattern time step thus making the demand changing at six different times of a day. But in the second case, 2 hour pattern time step was taken. The hydraulic time step and the water quality time step were taken as 1 hour and 0.05 minute for both case studies so as to ensure accurate prediction of chlorine concentration. Chlorine was injected into the system through nodal points at specified concentration in mg/l. The decay of chlorine is governed by the values of reaction coefficients k_b and k_w. The bulk flow decay coefficient, k_b was taken as 1day^{-1}. Since the pipes in the two networks, being analysed were made of PVC material, the reaction of chlorine with the pipe wall was absent. Hence the value of k_w was taken as zero. All reaction coefficients were inserted as negative values to model the disinfectant concentration decay. Analysis of fixed water demand was carried out for maximum, minimum and average demand pattern. For the simulation of fixed demand pattern, the multiplier value given to the model during the entire period of simulation was 1.5, 0.5 and 0.85 for maximum, minimum and average demand condition respectively in which chlorine was injected at the tank with a concentration of 1 mg/l. In the present study, three cases pertaining to variable demand were considered which are indicted by Case 1, Case 2 and Case 3 representing the point of injection of chlorine at *source, intermediate nodes and overhead tank* respectively.

4. RESULTS AND DISCUSSIONS

In the present study, simulation of chlorine decay was performed in two water distribution networks labelled as Case study1 and Case study 2, during fixed and variable demand situations.

4.1 Case study 1

For the variable water demand situation, hydraulic and water quality analysis were performed over a 3 days period of time and the time dependent flow rate as well as time dependent rate of reaction and chlorine residual concentration in the network were obtained so that the optimum amount of chlorine that should be injected at the source node in order to obtain adequate level of residual chlorine throughout the distribution network was determined by trial and error. According to U.S. Environmental Protection Agency, the dosage, contact time and other factors in the chlorination process have to be adjusted so that a concentration of 0.1 to 0.3 mg/l chlorine remains after 30 minutes' contact. For the case of continuous chlorine injection at the source node with a concentration of 1 mg/l, the residual chlorine concentration in each node was simulated with respect to time and it was obtained that the residual chlorine at all the selected nodes is higher than the permissible limit and the maximum decay of chlorine has occurred at nodes 6 and 7and is approximately equal to 50% of the initial chlorine concentration. This may be due to the feeding of water to the nodes (6 and7) from the tank (node 8) where the chlorine concentration may be low. When the concentration of chlorine injected at the source node was reduced to 0.5 mg/l, the residual chlorine at majority of nodes in the network was within the range of 0.4 to 0.5 mg/l and the least value of 0.24 mg/l was obtained at nodes 6 and 7. Then the concentration of chlorine injected at the source node was further reduced to 0.2 mg/l and it is seen that the residual chlorine concentration in all the nodes is in the range of 0.1 mg/l to 0.2 mg/l, which is the desired condition. For the present network in the study, the optimum dosage of chlorine is 0.2 mg/l, to be injected at the source continuously.

4.2 Case study 2

In the present study, simulation of chlorine decay in a water distribution network was analysed for fixed and variable water demand situations. The details of simulation outputs obtained for fixed and variable demand situations are as follows:

Fixed demand situation: For the simulation of fixed demand situation, chlorine was injected at the tank with a concentration of 1 mg/l. Among the three situations simulated for fixed demand pattern (ie with maximum, minimum and average demand values), the decay of chlorine is lesser for the maximum demand situation and maximum for minimum demand situation. For the fixed minimum demand pattern, the temporal variation of chlorine in the selected pipes of the network, where the decay of chlorine is more predominant is shown in Figure 3(f).From the three situations analysed, it can be seen that the decay of residual chlorine is minimum for the fixed demand pattern. From Table 1, showing the summary of

the system performance for fixed demand pattern, it is found that in majority of the pipes (52 in number), the residual chlorine is high during maximum demand situation. Also, the chlorine level in none of the pipes is decreased below the limiting value of 0.1mg/l, whereas in minimum demand pattern, residual chlorine in most of the pipes (23 in number) is less than 0.1mg/l. This is due to the fact that when consumption is low, the velocity of flow in the pipes decreases. As a result, chlorine has got enough time to react with bulk fluid and hence the decaying of chlorine is more pronounced, which is indicated by a lower value of residual chlorine throughout the network.

Table 1. Summary of chlorine decay for fixed demand situation

Cl_2 dosage (mg/l)	Number of pipes								
	Maximum demand			Minimum demand			Average demand		
	P	O	A	P	O	A	P	O	A
2-1	1	1	1	1	1	1	1	1	1
1-0.4	52	50	52	24	24	24	38	38	38
0.3-0.1	9	9	9	16	14	14	14	12	13
< 0.1	0	2	0	20	23	23	9	11	10
P - Peak time (8am), O - Off peak time (3am), A - Average consumption time (6am)									

Variable demand situations: The simulation of chlorine decay was also studied for the variable demand conditions for three situations of chlorine injection at (i) source node (well) (ii) source node and intermediate nodes (iii) tank and spatial and temporal variation of chlorine in the pipes are shown in Figure 3(a) to Figure 3(e) and the results are tabulated in Table 2.

Table 2. Summary of chlorine decay in pipes for variable demand situation

Number of pipes						
Cl_2 dosage	Case 1: Chlorine injected in Well					
	1mg/l			2mg/l		
	P Col.1	O Col.2	A Col.3	P Col.4	O Col.5	A Col.6
2-1	-	-	-	1	1	1
1-0.4	16	16	15	35	39	37
0.3-0.1	25	25	26	12	11	11
< 0.1	21	21	21	14	11	13
Cl_2 dosage	Case 2: Chlorine injected at intermediate nodes					
	P		O		A	
2-1	2		2		1	
1-0.4	44		43		43	
0.3-0.1	16		17		16	
< 0.1	0		1		2	
Cl_2 dosage	Case 3: Chlorine injected in Tank					
	2 mg/l			1 mg/l		
	P	O	A	P	O	A
2-1	26	23	24	1	1	1
1-0.4	22	23	24	38	38	38

Number of pipes						
Cl₂ dosage	Case 1: Chlorine injected in Well					
	1mg/l			2mg/l		
	P Col.1	O Col.2	A Col.3	P Col.4	O Col.5	A Col.6
0.3-0.1	5	6	5	13	12	12
< 0.1	9	9	9	11	12	12

P - Peak time (8am), O - Off peak time (3am), A - Average consumption time (6am)

Figure 3 Temporal variation of residual chlorine in selected pipes in WDS of Kadinankulam Grama Panchayat (a) Case 1 (Chlorine injected at source is1mg/l) (b) Case 1 (Chlorine injected at source is 2mg/l), (c) Case2 (d) Case 3(Chlorine injected at tank is 2mg/l) (e) Case 3(Chlorine injected at tank is 1mg/l), (f) Fixed minimum demand
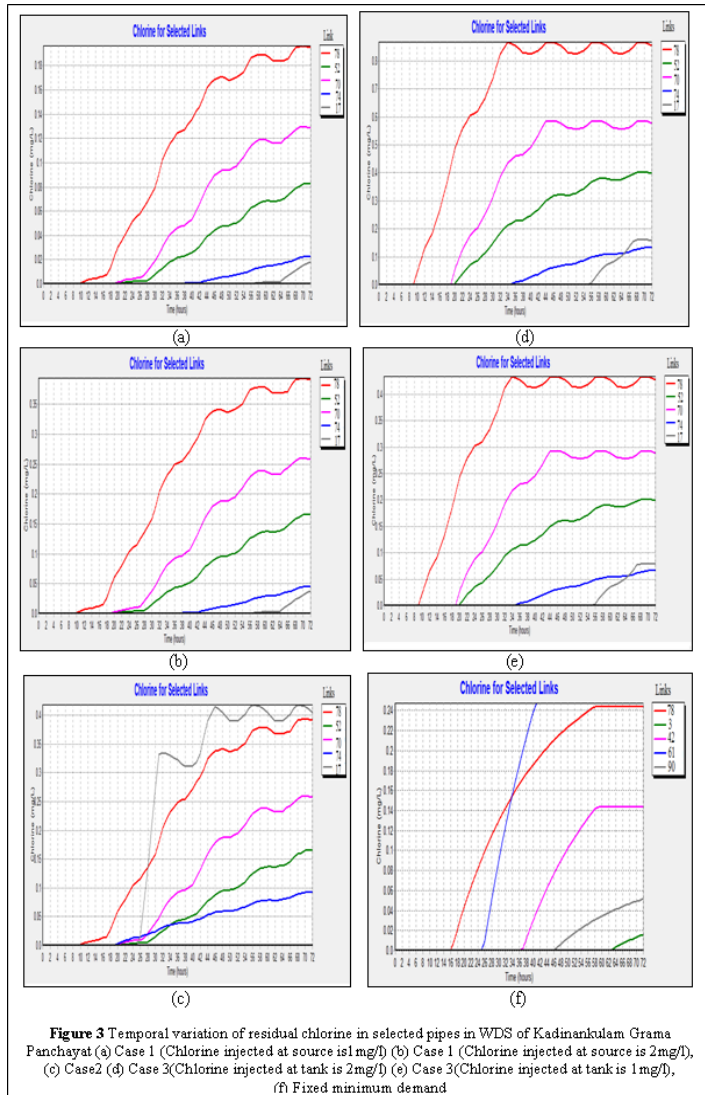
From the situation 1(chlorine injected at source only), from the Table, it can be seen that the residual chlorine in 22 pipes out of the total 62 pipes is less than 0.1 mg/l (desired value), which is not enough for proper disinfection. Hence the chlorine injected at the source node was increased to 2 mg/l. From Table 2, it can be seen that there is a significant increase of residual chlorine in all pipes but the concentration of chlorine at 14 pipes are still below the permissible value and is also evident from Figure 3(b).Therefore, in addition to the chlorine added at the source node, chlorine was injected continuously at intermediate nodes 9, 59 and 74. From the table it is found that chlorine

concentration at none of the pipes is less than 0.1 mg/l and is also seen in Figure 3(c).

 In majority of water distribution networks, the practice   of chlorination is done in overhead tank. Hence, the third case considered in the study is the injection of chlorine in overhead tank at a concentration of 2mg/l. It is seen that chlorine concentration at majority of pipes (26 pipes) is in the range of 2-1mg/l, which is considerably high and is also shown in Figure 3(d). Therefore, the concentration of injected chlorine was reduced to 1 mg/l. From Figure 3(e), it can be seen that only required amount of chlorine is available in majority of pipes and it is also evident from the Table 2, that the decay of residual chlorine is more pronounced during off-peak hours. Conversely, the decay of residual chlorine is less during peak hours, in which chlorine has got no time to react with bulk fluid in the water distribution network.

5. CONCLUSIONS

The simulation of decay of residual chlorine concentration in water distribution system was studied. The model was applied to two water distribution systems taken from literatures.

The specific conclusions from the study are as follows:

- In the first case study, only 0.2 mg/l of chlorine injected at the source node is enough for the simple WDS, under consideration in order to have sufficient residual chlorine throughout the network
- For fixed demand pattern (with minimum demand), the decaying process is more pronounced, since chlorine has got enough time to react with bulk fluid
- In the case of variable water demand for Kadinankulam WDS, the injection of chlorine with a concentration of   2 mg/l in the intermediate nodes, along with the source node is the best method for proper disinfection. When chlorine is injected in the overhead tank, a minimum concentration of 1mg/l is required for the proper disinfection in the system.

From the study it can be seen that the demand pattern, the initial concentration and point of injection of chlorine has a prominent role in maintaining the minimum desired residual chlorine in a water distribution system.

REFERENCES

i.   Andrei-Mugur Georgescu and Sanda-Carmen Georgescu (2012) Chlorine concentration decay in the Water Distribution System of a town with 50000 inhabitants
ii.   Kashfina Kapadia (2012) Modeling chlorine residuals in Water Distribution Network using EPANET 2 software
iii.   Lewis A. Rossman (2000) EPANET 2 Users Manual, U.S. Environmental Protection Agency, Cincinnati
iv.   Mohammed Shihab (2009) Simulation of Chlorine concentration in Mosul University's Distribution Network using EPANET
v.   Parameters of Water Quality (2001) Interpretation and Standards, U.S. Environmental Protection Agency
vi.   Pedro Castro and Mário Neves (2003) Chlorine Decay in Water Distribution Systems Case Study – Lousada Network

Anthropogenic Regulations Of Streamflow And Its Impacts- A Case Study From The Humid Tropical Zone, Kerala, India

George Abe[1]   E. J. James[2]

[1]Scientist & Head, CWRDM Sub Centre, Kottayam-686001, Kerala, India
[2] Distinguished Professor, Water Institute, Karunya University, Coimbatore-641 114, Tamil Nadu, India
Email: gb@cwrdm.org

ABSTRACT: *Hydroelectric Projects (HEPs) cause changes to flow regime of rivers. Changes in timings of flow, magnitude and duration of extreme flows, frequency and duration of high and low pulses and rate and frequency of water condition changes create a flow regime much different from the pre-regulated period. On the other hand, these storage structures help in flood moderation, summer flow augmentation and in meeting growing water demand in various sectors like agriculture, domestic water supply, industries, tourism and wetlands. Regulated release from HEPs is a major deciding factor of streamflow in Periyar and Muvattupuzha rivers in Central Kerala, Southern India. During the last four decades, three HEPs were commissioned in the Periyar river basin. The Idukki HEP (1976) is an interbasin water transfer to adjacent Muvattupuzha river basin, where as the Idamalayar (1987) and the Lower-Periyar (1997) HEPs are within basin (intrabasin) regulations. Time Series and hydrologic alteration analyses of streamflow shows that the interbasin water transfer under the Idukki HEP has worsened the situation in the Periyar river during the non-monsoon period. With the commissioning of Idamalayar and Lower-Periyar HEPs, flood moderation and leanflow augmentation improved considerably. The hydrologic alteration also increased with the degree of regulations. The tailrace water received in the Muvattupuzha river from the Idukki HEP caused an eco-surplus condition in the river. The non-monsoon flow in the river multiplied several folds, and the interbasin water transfer completely changed the unaltered flow regime.*
Keywords: Hydroelectric Projects, interbasin regulation, intrabasin regulation, streamflow, hydrologic alteration

1. INTRODUCTION

Hydroelectric projects (HEPs) play an important role in the power sector of Kerala State, India located in west coast. About sixty percent of the power requirements of the State are met from hydropower. Even though the undulating topography of the State offers a great potential for hydropower generation, only a small percentage of this potential is utilized by the State due to various reasons. The large storage structures under HEPs serve different sectors in the thickly populated State of Kerala (Population density varies between 2200 persons/sq km in the coastal lowlands to about 500 persons / sq km in the highlands). The demands from the domestic water supply schemes, agriculture, industries, inland navigation, tourism and wetlands

depend much on the downstream releases from HEPs in several regulated rivers of Kerala State.

Even though the releases after power generation is important for meeting water demands of multiple stake holders, the releases are purely based on the power demand and as a result the downstream releases on many occasions does not match with the demands. The concept of environmental flows is also not addressed properly in the regulated rivers. In this study an attempt is made to analyze streamflow data for different degrees of regulation so as to bring out the positive and negative impacts of regulated releases downstream of HEPs.

1.1   Study Area

Periyar River basin is located in the Central Kerala in the south west coast of India (Figure 1). Twelve reservoirs under seven HEPs in the Periyar river basin contribute to the major share of hydro electricity produced in the State.
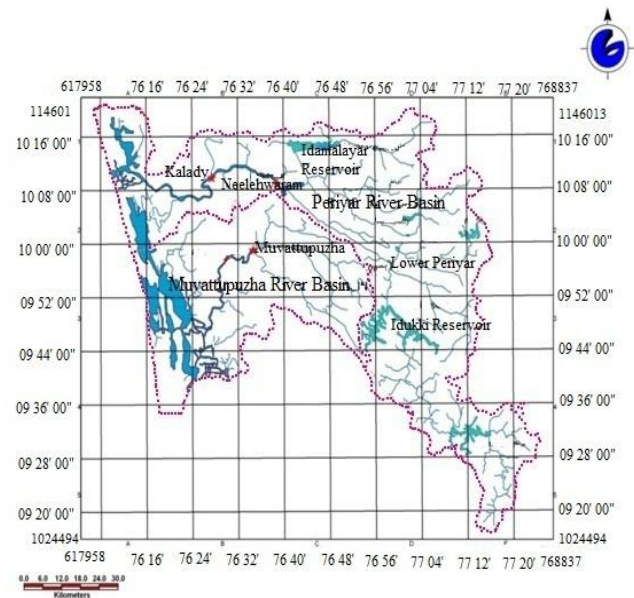
Figure 1. Location Map of the study area

The 244 km long Periyar river is the longest river in Kerala. The tailrace from the Idukki HEP, after harnessing power, is diverted to the Muvattupuzha river basin located on the southern side of the Periyar river basin. Because of the interbasin water transfer, the catchment of the Periyar river basin supplying water downstream is virtually 3665 sq. km where as the unaltered (natural) Periyar river basin catchment is 5398 sq km. The Idamalayar HEP (Idamalayar river is a branch of Periyar river), with an effective storage of 1017.8 million cubic meters and Lower Periyar H E Project (Periyar Main Stream) with an effective storage of 4.55 million cubic meters were subsequently commissioned in the Periyar river basin, which contribute to intrabasin regulations (Figure 1).

Vembanad wetlands *(a Ramsar site)*, Corporation of Cochin, and the fast growing industrial belt of Kerala are all located in

the lower reaches of the Periyar river. The water demands for two major irrigation projects [(Periyar Valley Irrigation Project (PVIP) and Idamalayar Irrigation Project (IIP)] are met from this river. About 48 water supply intakes [rural and urban schemes coming under Kerala Water Authority (KWA)] receive water from the Periyar river. Tourism and Inland water transport are other two sectors which depend on the Periyar River.

The Muvattupuzha river with a basin area of 1554 sq km is formed by the joining of three tributaries the Kothamangalam, the Kaliyar and the Thodupuzha. The Thodupuzha branch is the receptor of the tail water from the Moolamattom power house of the Idukki H E P. Since the power production from the Moolamattom power house is continuous throughout the year, a flow ranging from 19 cub m/sec to 45 cub m/sec is maintained in the river even in summer months.

1.2 Data for the Study

Stream flow data at two gauging stations (Neeleshwaram (1971-2010) (Central Water Commission, Government of India) and Muvattupuzha (Water Resources Department, Government of Kerala (1963-2009) were used to analyze conditions before and after commissioning H E projects.

2. MATERIAL AND METHODS

2.1 Time Series Analysis

The rainfall in the region is mainly confined to south-west (June-August) and north-east (September-November) monsoon periods. The average annual rainfall of the study area is 3000 mm, of which 60% is received during south-west monsoon, 25% is received during north-east monsoon and the remaining 15% in the non-monsoon season stretching from December to May. The water year for hydrologic studies is considered from 1 June to 31 May. An attempt was made to carry out time series analysis of streamflow to bring out the changes in flow regime due to the degrees of regulation by HEPs and diversion structures. The time series analysis was carried out for the six-monthly monsoon (June-November) and non-monsoon (December-May) periods. Three-monthly analysis was carried out considering south-west monsoon (June-August), north-east monsoon (September-November), first half of non-monsoon (December-February) and second half of non-monsoon (March-May) periods. Considering the importance of cropping periods of rice for water allocation, four-monthly time series was carried out for the first crop (Virippu, June-September) second crop (Mundakan, October-January) and the third crop (Puncha, February-May) periods. Analysis for smaller intervals such as weekly, ten-daily and monthly were done considering the increasing demands for sectors like domestic and industrial water supply. These finer details will help in quantifying the impacts, especially during the periods of water shortage.

2.2 Trend analysis of streamflow

Mann-Kendall trend analysis was also performed to bring out the significance of streamflow trends after commissioning of these large storage structures (Kendall, M.G (1975), Mann, H.B, (1945)). This test compares the relative magnitudes of sample data rather than the data values themselves. A Z value can be obtained from the test and can then be used to determine the significance of any trend in the data set. One benefit of this test is that the data need not conform to any particular distribution. Moreover, data reported as non-detects can be included by assigning them a common value that is smaller than the smallest measured value in the data set. When multiple data points exist for a single time period, the median value is used.

The trend is said to be decreasing if Z is negative and the computed probability is greater than the significance level. The trend is said to be increasing if the Z is positive and the computed probability is greater than the level of significance. If the computed probability is less than the level of significance, there is no trend. Different significance levels (99.9%, 99%, 95% and 90%) were chosen as the criteria for determining if a trend was present. 95% significance in a case means that if a trend is identified as significant (either positive or negative) that there is only a 5% (1 in 20) chance that the trend is actually not present. Conversely, it could also be said with 95% certainty that the trend is statistically significant (Bhutiyani, M. R. et.al 2008, Donald, H. Burn, 2004).

2.3 Hydrologic alteration analysis

The hydrologic changes due to interbasin (from one river basin to another) and intrabasin (within a river basin) regulations of stream flow are reflected in the shape and characteristics of hydrographs and or flow duration curves. Flood moderation and lean flow augmentation by the HEPs are some of the dominant impacts which can significantly alter aquatic life cycles (Kingsolving and Bain 1993). Along with moderated flood, and improved fair weather flow, other components of the hydrograph such as the timing and duration of low/high flows, the rate of change and the frequency of hydrograph rise/fall also contribute to the alterations in the aquatic life cycle (Richter et al. 1996; Poff et al. 1997; Dugger et al. 2002). The magnitude, frequency, duration, timing and rate of change of flow conditions are the five major components which control the ecological processes in a river (Poff et al. 1997).

The IHA is a suite of statistics developed by the US Nature Conservancy to assess the degree of hydrologic alteration caused by human activities. It consists of 67 parameters, which are subdivided into two groups-33 IHA parameters and 34 EFC (Environmental Flows Component) parameters. These hydrologic parameters were developed based on their ecological relevance and their ability to reflect human-induced changes in flow regimes across a broad range of influences including dam operations, water diversions etc. The 33 hydrological parameters are categorized into five groups addressing the magnitude, timing, frequency, duration, and rate of change. A common approach to assess hydrologic alteration involves a comparison of flow regimes between present

(impacted) and past (un-impacted) time periods (IHA User's Manual 2006).

3. RESULTS AND ANALYSIS

3.1 Time Series Analysis

The results of time series analysis for the stream gauge station at Neeleshwaram in the Periyar river and Muvattupuzha in Muvattupuzha river are detailed in this section. The results of time series analysis for the Neeleshwaram and Muvattupuzha gauging stations are given in Table 1 and Figure 2. Analyses of time series for smaller intervals are very much useful for summer months when there is a demand for freshwater from all sectors. Figures 2 shows the radar charts for weekly variations in streamflow and for standard deviation during the south-west monsoon (June to August) and second half of summer (March to May) in the Muvattupuzha river for different degrees of regulations.

Table 1. Mean streamflow for different time series- Neeleshwaram, Periyar river

Stream Gauge: Neeleshwaram	Mean streamflow in Million Cubic metres (M Cub m)										
	6 - Monthly Intervals		4 - Monthly Intervals (Based on cropping periods)			3 - Monthly Intervals					
	Season	Season				Monsoon	Monsoon	Half of Non-			
	Monsoon (Jun - Nov)	Non - monsoon (Dec - May)	Virippu (Jun - Sep)	Mundakan (Oct - Jan)	Puncha (Feb - May)	South - west Monsoon (Jun - Aug)	North - east Monsoon (Sep - Nov)	First Half of monsoon (Dec - Feb)	monsoon	Annual (Jun - May)	
Before Idukki	8734	550	7206	1775	303	6158	2576	275	275	9284	
After Idukki-B Idamalayar	6096	436	5066	1205	261	4310	1786	205	231	6532	
After Idamalayar	6116	946	4898	1540	624	4002	2114	418	528	7062	
After Lower Periyar	5963	1206	4533	1898	738	3505	2458	561	645	7169	

Figure 2. Time series of weekly mean flows for different degrees of regulation

(Muvattupuzha stream gauge, Muvattupuzha river)

3.2 Dependability Analysis

Figures 3 show the dependable flows at the Neeleshwaram gauging site during the monsoon and non-monsoon months. The reduction in downstream flows due to the interbasin diversion from the Periyar under the Idukki HEP, flood moderation and summer flow augmentation after intrabasin regulation by Idamalayar and Lower Periyar reservoirs are reflected in the figure.
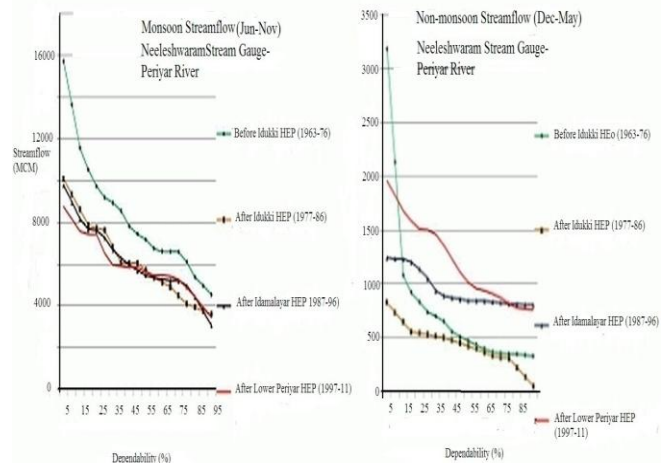
Figure 3. Dependable streamflow-Neeleshwaram gauging station-Periyar river

Muvattupuzha river basin, interbasin transfer from the Idukki HEP created an eco-surplus condition as detailed in Table 2.

The non-monsoon streamflow increased from 343 MCM to 1240 MCM - streamflow with 5% dependability - after receiving the tailrace from the Idukki HEP. Fifty percent reliable non-monsoon flows increased from 195 MCM to 948 MCM as seen from Table 2. The dependable non-monsoon flows in the Muvattupuzha river decreased after the diversion of water for irrigation at Malankara under the partially commissioned Muvattupuzha Valley Irrigation Project in 1994.

Table 2. Non-monsoon streamflows in the Muvattupuzha river

Stream Gauge: Muvattupuzha, River Basin : Muvattupuzha			
Based on 45 years of data between 64-65 to 2008-09			
Dependability (%)	Non-Monsoon Streamflow (December to May) in MCM		
	Before Idukki HEP (1963-1976)	After Idukki HEP-Before Malankara Diversion(MVIP) (1976-1994)	After Malankara Diversion (MVIP) (1995-2009)
5	343.3	1240.98	1402.92
10	337.98	1169.03	1257.24
20	327.73	1109.2	972.35
30	305.17	1054.83	783.34
40	245.94	964.6	774.32
50	194.89	948.05	770.65
60	167.19	906.84	760.53
70	157.98	835.22	720.21
80	113.63	754.81	692.96
90	54.77	700.46	628.32
95	25.46	667.26	590.76

3.3 Trend Analysis

Mann-Kendall trend analysis results for different time series (Periyar river) are shown in Table-3. The trend for all the time series was negative after interbasin water transfer, whereas the non-monsoon streamflow showed strong positive trend after the intrabasin regulations under the Idamalayar and Lower Periyar HEPs.

Table-3 Mann-Kendall trend analysis results for different time series-Periyar river

Time series	1971-86 Idukki Dam (1976)		1971-1996 Idukki Dam (1976), Idamalayar Dam (1987)		1971-2010 Idukki Dam (1976), Idamalayar Dam (1987), Lower Periyar dam (1997)	
	Test Z	Significance	Test Z	Significance	Test Z	Significance
Monsoon (Jun.-Nov.)	-1.42		-1.23		-1.44	
Non-Monsoon (Dec.-May)	-0.77		3.48	***	3.93	***
Virippu (Jun-Sept.)	-1.31		-1.36		-1.72	+
Mundakan (Oct.-Jan.)	-1.97	*	0.24		1.10	
Puncha (Feb.-May)	-0.44		2.73	**	3.62	***
S-W Monsoon (Jun.-Aug.)	-1.31		-1.77	+	-2.23	*
N-E Monsoon (Sept.-Nov.)	-2.19	*	0.15		-0.19	
Summer 1 (Dec.-Feb.)	-0.88		3.15	**	2.97	**
Summer-2 (Mar.-May)	-0.44		2.36	*	3.35	***
Annual	-1.64		-0.48		-0.59	

***   if trend at α = 0.001 level of significance, ** if trend at α = 0.01 level of sgnificance
*   if trend at α = 0.05 level of significance, + if trend at α = 0.1 level of significance

3.4 Hydrologic Alteration Analysis

The results of hydrologic alterations analysis for the Periyar and Muvattupuzha rivers (unaltered reference streamflow: before the Idukki HEP) are detailed in Figure 4. These figure gives the details of all the HA analysis carried out for 33 parameters in the middle category using streamflow before Idukki HEP as the reference streamflow regime. The hydrologic alterations (%) for all the parameters are shown for different degrees of regulation in the chart.
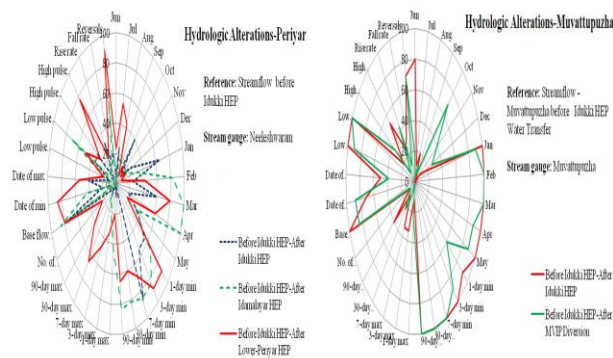
Figure 4. Hydrologic alterations- Periyar and Muvattupuzha rivers

4. CONCLUSIONS

The time series and trend analyses show that the interbasin water transfer from Idukki H E Project has worsened the situations in Periyar basin, especially during non-monsoon period. Studies conducted after the commissioning of Idukki HEP also report increased salinity intrusion and water quality deterioration in the downstream of the Periyar river due to reduced flow in summer months.

Improvement in intrabasin regulation with the commissioning of Idamalayar & Lower Periyar reservoirs helped flood moderation and summer flow augmentation in the downstream of the Periyar river. Improvement in reliable flows supported development of several water dependent sectors in the Periyar-Muvattupuzha system

The influence of interbasin and intrabasin water transfers in the flow regimes of the Periyar-Muvattupuzha river system was systematically studied using IHA model. The study shows that hydrologic alterations in the Periyar river increased with the increase in the degrees of regulation. The interbasin water transfer caused substantial alterations in several of the hydrologic indicators in the Muvattupuzha river compared to the cumulative impacts of intrabasin regulations in the Periyar river basin. Interbasin water transfer to the Muvattupuzha river created an eco-surplus condition as the river received an average flow of $45m^3/sec$ as diverted flow from the Periyar river basin. In both the Periyar and Muvattupuzha rivers, the low flow indicators were sensitive to regulations and showed considerable alterations when the degrees of regulation changed.

Construction and operation of reservoirs with multiple purpose of power generation, flood moderation, irrigation etc. invariably induces changes in the flow regime. The study shows that development of HEPs in the Periyar river basin changed the flow regime in Periyar and Muvattupuzha rivers. These alterations might have affected the aquatic and riparian flora and fauna. Indiscriminate sand mining from river beds and pollution mainly from the industrial belt also have added negatively to such alterations (Sreedharan Sreebha *et.al.* 2010). A recent fish survey conducted by Kurup et.al (2004) in the Periyar and Muvattupuzha rivers indicates that more than 50% of the ornamental/ food fish species are critically endangered or endangered. Scientific reservoir operation and river protection, taking into consideration the environmental flow requirements along with the freshwater demands from other stake holders, is required for maintaining sustainability of river basins in the bio-diversity rich humid tropical zone in the south west coast of India .

REFERENCES

i. Bhutiyani. M. R., Vishwas. S. Kale. and N. J. Pawar. (2008) "Changing streamflow patterns in the rivers of northwestern Himalaya: Implications of global warming in the 20th century", Current Science 95(5): 10 - 12.

ii. Donald H. Burn. and Mohamed A. Hag Elnur. (2002) "Detection of hydrologic trends and variability", Journal of Hydrology 255,107 – 122

iii. Dugger, K.M., Ryan, M. R., Galat, D.L., Reken, R.B., Smith, J.W. (2002) Reproductive success of the interior tem(Sterna antillarum) in relation to hydrology on the lower Mississippi River, River Research and Application 18 (2), 97-105

iv. Kendall. M.G (1975) "Rank correlation measures", Charles Gri_n, London, U K.

v. Kingsolving, A.D., Bain, M.B., (1993)"Fish assemblage recovery along a riverine disturbance gradient", Ecological Applications 3, 531-544

vi. Kurup. B.M., Radhakrishnan. K.V.and Manojkumar. T. G. (2004) "Biodiversity status of fishes inhibiting rivers of Kerala (South India) with special reference to endemism, threats and conservation measures", R.L. Welcomme and T Petr (editors), Proceedings of the second international symposium on the management of large rivers for fisheries 2:316.

vii. Mann. H.B,(1945) "Non-parametric tests against trend", Econometrica 13, 245 -259.

viii. Nature Conservancy (2006)"Indicators of Hydrologic Alteration, Version 7.1 Manual"

ix. Poff . N. L., Allan. J. D., Bain. M. B. , Karr. J. R., Prestegaard. K. L., Richter. B. D., Sparks. R. E., and Stromberg. J. C. (1997) "The natural flow regime: a paradigm for river conservation and restoration", BioScience, 47, 769 - 784.

x. Richter. B. D., Baumgartner. J.V., Powell. J., and Braun. D. P. (1996) "A method for assessing hydrologic alteration within ecosystems", Conservation Biology 10, 1163 - 1174.

xi. Sreedharan Sreebha and Damodaran Padmalal. (2010) "Environmental Impact Assessment of Sand Mining from the Small Catchment Rivers in the Southwestern Coast of India: A Case Study", Environmental Management, Online, October 2010.

EIA of Hydropower Project In Himachal Pradesh: An Analysis

Rajiv Ganguly[1], Veeresh Gali[1], Aman Thakur[1], Shubham Chopra[1]
[1]Department of Civil Engineering, Jaypee University of Information Technology, Waknaghat, Himachal Pradesh, India
Email: rajiv.ganguly@juit.ac.in

ABSTRACT :India is the 7th largest producer of hydroelectric power in the world accounting for 3.3 % of the world's total hydroelectric power and ranks 5th in terms of exploitable hydro-power energy. Himachal Pradesh (HP) is extremely rich in hydel resources. At national level, HP generates about twenty five percent of the gross hydropower produced. At present, there are 12 hydel power projects in HP generating a total of 7027 MW of hydel power. It has been estimated that about 21,244 MW of hydel power can be generated on the five perennial rivers. In this paper, an attempt is made to analyze the EIA of hydropower projects in HP considering the recent natural hazard in Uttarakhand and subsequent Supreme Court order to review all hydropower projects located in hilly areas. This is particularly important considering the geographical and topographical similarities between the two states. A typical 100 MW hydropower project located in Kullu district was considered for case study. Analyses of impacts were made during both construction and operational phases of the projects. An attempt was made to further analyze

National and International procedures on EIA of hydropower projects. Checklist and matrix methodologies were adopted to assess the impacts. New and relevant procedures were evaluated and appropriate remedial measures were suggested.

1. INTRODUCTION:

Environmental Impact Assessment (EIA) is a procedure used to examine the environmental consequences or impacts, both beneficial and adverse, of a proposed development project and to ensure that these effects are taken into account in project design. These impacts can include all relevant aspects of the natural, social, economic and human environment. The study therefore requires a multi-disciplinary approach and should be done very early at the feasibility stage of a project. An analysis of EIA of Hydropower Project in HP was carried out considering the recent natural hazards in Uttarakhand. In this context, honorable Supreme Court of India ordered to review EIA of hydropower projects present on Bhagirathi and Alakhnanda river and also for hydropower projects present in hilly areas. In this context, it was decided to analyze EIA of a typical hydropower project in HP, India. The main objectives of the paper involve analyzing EIA of Hydropower Project and suggest suitable remedial measures where necessary.

2. Impact Assessment Methodologies

In this project, following methodologies were used for determining essential environmental impacts by100MW Hydroelectric Power Project by Himachal Pradesh Power Corporation Ltd. (HPPCL): Interaction Matrix Methodology (Leopold et al., 1971) and Checklist Method (Anderson, 2000). The matrices and checklists prepared for the 100MW project, both during constructional and operational phase. The impacts considered were (a) Impact due to fish and wildlife due to environmental perturbations, (b) using checklist methodology for constructional phase and (c) using checklist methodology for operational phase

2.1 Rating of the Impacts

Impacts can be rated as major, minor and intermediate. Information expressed by means of ranks other than numerical values for magnitude and importance can be included in the impact scales associated with identification of an interaction. Scales have also been used to describe the probability of occurrence of an impact, with the scale ranging from low to intermediate to high probability of impact. The rating of impacts, both during constructional and operational phase, was carried out. Rating of impacts were given on scale of 1-10 with low (1-3), medium (4-7) and high (8-10)

2.2 Anticipated Environmental Impact and Mitigation Measures

The impacts can be categorized as follows:

Environmental Impact Due to:

(i) Project Location and design

The main adverse impact that the Project is likely to have on the environment, in terms of duration, extent, and severity, will be changes in the river hydrology, loss of agricultural and forestland, a decline in water quality, and resettlement, as outlined in the table below. Most of this impact will occur during project operation and is shown in Table 1.

Table 1. Primary Adverse Environmental and Social Impact of HEP

Features	Impact	Duration
Hydrology	Reduced river flow between barrage and tailrace outlet	Permanent
	Decline in river water quality	Permanent
Aquatic Ecosystems	Altered river ecosystem	Permanent
	Prevention of upstream fish movement	Permanent
Land resources	Loss of agricultural and forest land	Permanent
Social	Resettlement of households	Permanent

(ii) Resettlement

Since the project is a run-of-river type with trench weirs and hence no dam, no storage and therefore no submergence. Hence no dwellings, houses hamlets will be submerged. In fact, the area to be used for the Project is not populated; hence, no displacement or resettlement of population is involved. Only four villages are falling in affected zone. The field survey for demographic profile of affected villages revealed that in Pangi village, 11.8 ha private land will be affected. According to the land records and ground truth survey, 253 households in Niharni village of Kullu district are likely to be affected due to the acquisition of land/house/shops for project. Only a part of the land is being acquired from the 253 households and none of the landowners and only one household is being resettled from the area being acquired for the Project in the village.

2.3 Environmental Impact of Pre-Construction and Construction Activities

The construction of the Sainj HEP will involve the removal of trees at the project site, excavation work, the installation of equipment, and civil works related to the construction of a desilting chamber, forebay, penstock, powerhouse, and other related works. Standard construction impact, pertaining mainly to specific construction activities, site disturbance, spoil disposal, river flow disruption, and the influx of workers into the area, will occur.

The topography will change during construction as tunnels are excavated, buildings put up, and fills and cuts made to level the power channel and construction powerhouse, forebay, desilting chamber, and penstock. Surface features will change as trees and soil are removed at the HEP powerhouse, trench weir, tunnel construction site, and all along the ROW to facilitate construction. The most conspicuous impact on the surface topography will be in the hilly region along the reserve forest for HEP. The impact will be local but irreversible as the presence of the HEP changes the features along the ROW.

Laying grits, ramming and compaction would minimize dust emission from project's roads with regular water sprinkling. During construction, excavation of the HEP channel and the movement of vehicles carrying construction materials will give rise to dust particles, temporarily affecting air quality at the site. Spraying the excavation site with water will greatly reduce the dust emission. The ambient air quality recorded SPM concentration below the Central Pollution Control Board (CPCB) standard of $50\mu g/m^3$ for 24 hours for industrial areas. The level of gaseous air pollutants (SO_2 and NO_2) is also within limits. During major construction related activities, there will be marginal increase in the ambient air pollutants such as SPM, SO_2, and NO_2. However, with the construction of the trench weir, powerhouse, colonies, and other infrastructure facilities in the area, air quality will be affected during construction. The movement of heavy vehicles and operation of other construction equipment will also add to the amount of noxious gases released into the atmosphere. The concentration of these kinds of gases and dust emission, however, will be cleared daily as the area is located in a valley and gusty winds are common in the morning and evening hours. Land clearing, cutting, filling, and leveling may cause loss of vegetation, with irreversible impact on ecology.

Construction activities may disturb the fauna in the reserve forests and cause the animals to move elsewhere in the forest. Care will be taken not to disturb major wildlife habitat. Measures will include maintaining a greenbelt area around the project areas rich in vegetation. The extent of land acquired for the Project and the compensation to be given are dealt with separately in the social assessment report. Job opportunities for the local population during construction will give great impetus to the local economy. The issues related to resettlement and rehabilitation is discussed separately in the social assessment report. There are no archaeological, historical or cultural important sites in the alignments for the barrage and the powerhouse; hence, no impact is envisaged in this regard. Avoiding high-density areas, putting up proper traffic signs, providing proper access roads, and avoiding roadblocks will minimize traffic disturbance during construction. Construction of the proposed project may have the following impact on the health of local residents and the workforce. The execution of the integrated Sainj HEP and appurtenant works is to be carried out under contract in 48 months' time. Infrastructure facilities will be developed at the same time. When construction starts the labor force of skilled, semiskilled, and unskilled labor will be deployed, and at a given point in time, a workforce of 1,200 will be engaged. The skilled manpower of about 360 persons will be imported from other parts of country. The total construction time for the Project is about 4 years, which has the same processes as that of the Sainj project. At the peak of construction, there will be an estimated 1,200 workers, of which it is expected that 50% will be locally available. The domestic water requirement has been estimated as 70 liters per person per day. Thus, total incremental water requirements work out to 42,000 liters per day. It is assumed that about 80% of the water supplied will be generated as sewage. Thus, total quantum of sewage generated is expected to be of the order of 33,600 liters per day. Community latrines and oxidation ditches can be constructed for the treatment of sewage from the labor camp so that it does not pollute the river water.

A comprehensive socio-economic primary survey was carried-out in those villages where land is proposed to be acquired for the proposed Sainj hydroelectric project. As per the survey, the total affected population is of the order of 436 persons in 148 families. Males and females constitute about 54.36% and 40.82% of the total affected population respectively. About 39.45% of the project-affected population is illiterate without any schooling. The remaining population (60.55%) is either literate or is presently continuing with their education. Practically all the affected families reared domesticated animals for milk, meat, eggs and labor. Cows are mainly reared for their milk. It was observed that bulls are used extensively for ploughing the agricultural fields. No family was rendered homeless.

3. Environmental Impact Analysis

3.1 Meteorology

The climate of the project area is characterized by cool and dry climate. Meteorologically, the year can be divided into three distinct seasons. Winter season sets in from the month of October and continues till February, followed by summer season from March to June. The area receives rainfall under the influence of southwest monsoons over a period of three months from July to September. June is the hottest month of the year, with mean maximum and minimum monthly temperatures of the order of 32.9°C and 26.6°C respectively. January is the coldest month of the year. The annual average rainfall in the project area is 1459.2 mm. Majority of the annual rainfall is

received under the influence of southwest monsoons. During the period from January to April, winter precipitation occurs in association with the passage of western disturbances. The winter precipitation accounts for nearly 40% of the annual rainfall. Relative humidity is maxim (91%) during the monsoon months, while it is minimum (50%) in the summer months of April-May. Figure 1a illustrates the variation of temperature and Figure 1b illustrates the variation of rainfall at the project district over the entire year.

(a)

(b)
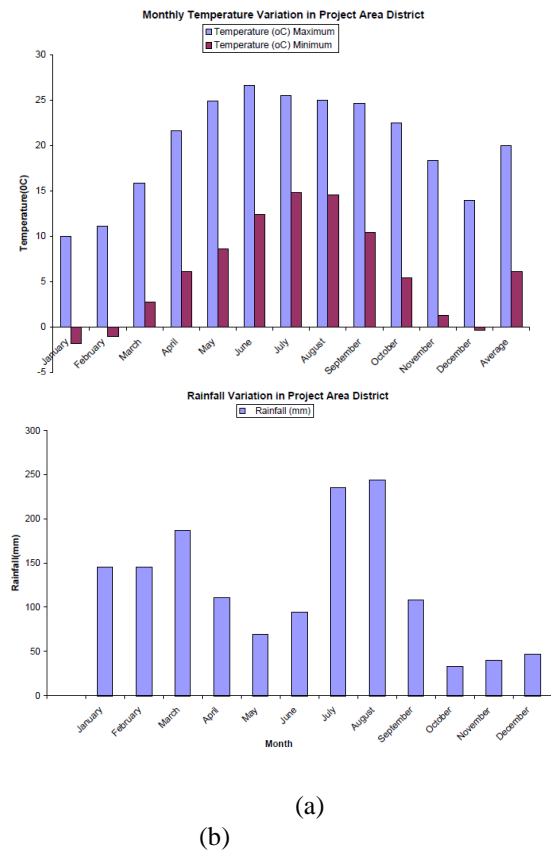
Figure 1. Meteorological Observations

3.2 Seismology

The project area falls in under the highest seismic zone in Western Himalayas as per IS: 1894: 2002 In the past, the region has been affected with a number of strong earthquakes.

3.3 Soil use

The soil in the study area is young like any other region of Himalayas. Soil on the slope above 30degrees, due to erosion and mass wasting processing, are generally shallow and usually have very thin surface horizons. As a part of field studies, soil samples from the catchment area were collected and analyzed for various physio-chemical parameters. The pH of soil at various sites lies within neutral range.

3.4 Land use Category

The major land use category in the study area is forestland,

which accounts for almost 82% of the study area. The other major category is barren land accounting for about 10% of the study area. The agriculture land accounts for about 3.3% of the study area. The areas under snow cover and water bodies accounted for about 2.8% and 2.4% respectively. The land-use patterns which fall under the study area (%) comprises of dense vegetation (40%), open vegetation (42%),forest area (82%), Agricultural land (3%) Barren land (10%) and water body (2%) and illustrated in Figure 1.
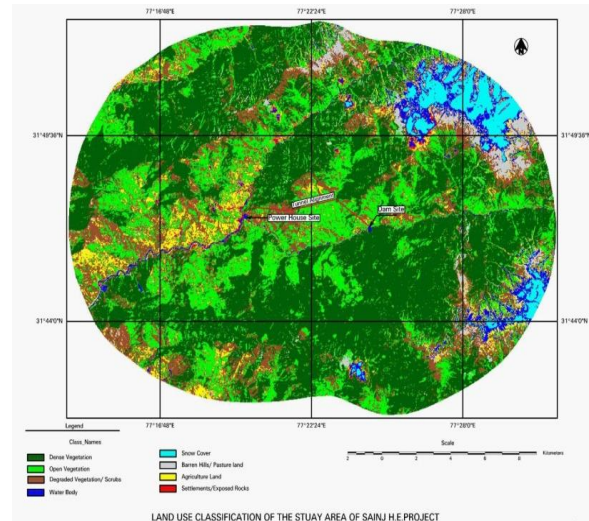
Figure 2. Land use Pattern

3.5 Water Resources

River Sainj is the major tributary of the river Beas, originating from west of Rakti Dhar at an elevation of +5500 m. The total catchment area of river Sainj intercepted at the barrage site is 408 km^2 of which 176 km^2 is permanently under snow (above elevation of 4250 m). The minimum flow for 90% dependable year is observed as 4.82 cumecs in the month of November.

3.6 Noise Environment

Baseline noise data has been measured for three seasons. The daytime equivalent noise level in summer and monsoon seasons at various sampling stations ranged from 32 to 45 dB (A), 34 to 46 dB (A). Likewise, daytime equivalent noise level in winter season ranged from 37.5 to 39.6 dB (A) at various sampling stations which were well within the permissible limit specified for residential area.

3.7 Ecological Aspects

The proposed project lies in the Sainj valley. The study area comes under Sainj, Forest Range and Jiwa Forest Range under the Great Himalayan National Park Conservation Area (GHNPCA).
Further, the proposed project lies in the vicinity of the Great Himalayan National Park (GHNP). The primates are represented by rhesus macaque (Macaca mulatta) and common langur (Presbytis entellus) and are found to occur between 1440m and 3420 m. Rare and endangered species have been

reported sited in the study area. The river Sainj and its tributaries have variety of cold water fishes dominated by trout. Conservation of freshwater fish is a great challenge because fishes use different habitats along the stretches of river including spawning, feeding and shelter (Allan and Flecker, 1993). In a river continuum fish show spatial and temporal variation depending on the water depth, current velocity, substrate, water discharge and physicochemical conditions (Angermeier and Karr, 1983).

3.8 Socio-economic Aspects

A comprehensive socio-economic primary survey was carried-out in those villages where land is proposed to be acquired for the proposed Sainj hydroelectric project. As per the survey, the total affected population is of the order of 436 persons in 148 families. Males and females constitute about 54.36% and 40.82% of the total affected population respectively. About 39.45% of the project-affected population is illiterate/ not going to school. The remaining population (60.55%) is either literate or is presently continuing with their education. Practically all the affected families reared domesticated animals for milk, meat, eggs and labour. Cows are mainly reared for their milk. It was observed that bulls are used extensively for ploughing the agricultural fields. No family was houseless. About 37% of the houses were electrified.

4. PREDICTION OF IMPACTS

4.1 Impacts on Water quality

a) Construction phase

Sewage from labour colony: The peak migrant population is likely to be of the order of 3,200. The quantum of sewage generated due to this population is expected to be of the order of 0.18 MLD. Even at minimum flow, sufficient dilution will occur thus, no significant impact on water quality of river Sainj is envisaged during construction phase.

Effluent from crushers and other sources: The effluent from the crushers and other sources, like conduit, tunnel, would contain high suspended solids. It is proposed to treat the effluents in settling tanks. Thus, no significant impact is envisaged.

b) Operation phase

Effluent from project colony: During operation phase, only a small number of O&M staff will reside in the colony. The sewage generated would be provided biological treatment before discharge.

4.2 Sediments

The proposed project is envisaged as a runoff the river scheme with a barrage. At regular intervals, the gates of the barrage shall be opened to flush the sediments. Thus, in the proposed project, sedimentation problems are not anticipated

4.3 Water Resources and downstream users

The river stretch downstream of the barrage site upto the confluence point of tail race discharge will have reduced flow for a length of about 8 km. In the intervening stretch, the flow shall be implemented by (i) releases of flushing discharges from desilting chamber, (ii) contribution of flow from various streams/nallahs in the confluence of tail race disposaland (iii) gates of barrage will remain open leading to continuous flow in the downstream river stretch during monsoon months. The river stretch downstream of the barrage site upto the confluence point of tailrace discharge (about 8 km) will have reduced flow i.e. 0.60 cumec. However, the flow will be augmented by contribution of flow from Kartol nallah (2.5 km downstream) joining the Sainj river on its right bank and other small khads joining the river from the left bank, which are Kotli, Khad (4 km downstream), Shana Khad (6 km downstream) and Nuhara Khad (7.5 km downstream) of the barrage. Thus, river Sainj will not be completely dry, in the intervening stretch. The reduction in flow or drying of the river in the intervening stretch is not likely to have any adverse impact on the downstream users. This is mainly because of the fact that settlements/ villages within this dry stretch are not dependent on the water of river Sainj, as the villagers use water of small streams or nallahs flowing adjacent to their habitation

4.4 Impact on Air Environment

Pollution due to fuel combustion: The major construction equipment would be operated through electricity. Therefore, fossil fuel combustion would be minimal. Diesel would be used only in contingency. Thus, no significant impact on ambient air quality is expected as a result of operation of various construction equipment. No significant impact is envisaged.

Emissions from various crushers: During crushing operations, there would be emissions of dust particles. Minimal impact is expected during construction phase. Therefore, commissioning of cyclone is suggested. Further, the labour camps would be located on the leeward side of the crusher with respect to predominant wind directions.

4.5 Impact on Noise Environment

The operation of construction equipment is likely to have insignificant impact on the ambient noise level. However, blasting can have adverse impact on wildlife, especially along the alignment of the tunnel portion.

4.6 Impacts on Land Environment

Impacts due to quarrying: In a hilly terrain, quarrying is normally done by cutting a face of the hill. A permanent scar is likely to be left, once quarrying activities are over. With the passage of time, they become a potential source of landslide. Thus it is necessary to implement appropriate slope stabilization and quarry reclaiming measures.

Impacts due to muck disposal: A large quantity of muck is expected to be generated as a result of tunnelling operations, construction of roads, etc. The same requires being suitably disposed. Normally, muck is deposited in low lying areas or depressions.

Impacts due to land acquisition: The total land to be acquired for the project is 56.763 hectares. A part of this land is required for labour camps, quarry sites, muck disposal storage of construction material, silting of construction equipment, which will be required temporarily and returned once the construction phase is over. Permanent acquisition of land is required for barrage axis, submergence area, project colony, etc.

Impacts due to land acquisition: The total land to be acquired for the project is 56.763 hectares. A part of this land is required for labour camps, quarry sites, muck disposal storage of construction material, siting of construction equipment, which will be required temporarily and returned once the construction phase is over. Permanent acquisition of land is required for barrage axis, submergence area, project colony, etc.

4.7 Impacts on Ecology

Terrestrial Ecology

Increased human interferences: A large population (3,200) is likely to congregate in the area during the project construction phase. This population residing in the area may use fuel wood (if no alternate fuel is provided). Therefore, alternate fuel should be provided to such population. Further, community kitchens should be provided using LPG or diesel as fuel. Acquisition of forest land: The total forest land to be acquired is about 47.993 ha. Disturbance to wildlife: The operation of various construction equipment and blasting is likely to generate noise. These activities can lead to some disturbance to wildlife population. Further, the project area does not fall in the migratory routes of animals.

Impacts on protected areas: During project operation phase, the accessibility to the area will improve due to construction of roads, which in turn may increase human interferences leading to marginal adverse impacts on the terrestrial ecosystem. Sainj Wildlife Sanctuary (SW S) and Great Himalayan National Park (GHNP)is located within the study area. However, no land of the SWS and GHNP is proposed to be acquired for the project.

Aquatic ecology

a) Construction phase

Due to construction of the proposed Sainj Hydroelectric Project, about 0.8 Mm3 of muck and debris would be generated at various construction sites. Based on the geological nature of the rock and engineering property of the soil, about 30% of the muck generated will be utilized as construction material. The remaining 70% would be dumped at designated sites.

b) Operation phase

The completion of Sainj Hydroelectric Project would bring about significant changes in the riverine ecology, as the river transforms from a fast-flowing water system to a quiescent lacustrine environment. Amongst the aquatic animals, it is the fish life which would be most affected. The migratory fish species, e.g. snow trout and brown trout are likely to be adversely affected due to obstruction created by the proposed barrage. With the completion of barrage, flow in the downstream stretch of the river would be reduced considerably more so during the lean period.

4.8 Impacts on Socio-Economic Environment

Impacts due to influx of labour force: During the construction phase a large labour force, including skilled, semi-skilled and un-skilled labour force of the order of about 3200 persons, is expected to immigrate into the project area. During the construction phase, the most important negative impact would be due to the temporary settling of labour force leading to filth, in terms of domestic wastewater, human waste, etc.

Economic impacts of the project: Apart from direct employment, the opportunities for indirect employment will alsobe generated which would provide great impetus to the economy of the local area. Various types of business like shops, food-stall, tea stalls, will set up. Besides a variety of suppliers, traders, transporters will concentrate here and benefit immensely as demand will increase significantly for almost all types of goods and services. The locals will avail these opportunities arising from the project and increase their income levels. With the increase in the income levels, there will be an improvement in the infrastructure facilities in the area.

Impacts due to land acquisition: Another most important deleterious impact during construction phase will be that, pertaining to land acquisition. About 56.763 ha of land proposed to be acquired for the proposed Sainj hydro-electric project. Of this about 8.77 ha is private land (un-irrigated land). It is observed that about 216 PAFs are likely to lose land (agricultural and/or homestead) in varying proportions.

5. MITIGATION MEASURES

Environmental impact mitigation measures are summarized in Table 3

Table 3. Impact Mitigation Measures

Features	Impact

Biophysical Impacts	1. Biological Diversity
	  2. Hydrologic Regimes
	    3.Fish Migration and river navigation
	    4. Reservoir sedimentation
	    5. Water Quality
	    6. Reservoir impoundment

| Socio-economic impacts | 7.Resettlement
8.Public Health
9. Landscape and cultural heritage |
|---|---|

5.1 Biophysical Impacts

Biological Diversity

The following are the major measures taken to avoid loss of biodiversity: (a) Understanding the influence of the project on the surrounding environment, and selection and implementation of appropriate conservation measures based on the environmental impact assessment. (b) Restricting the impacts on the ecosystem by constructing various types of structures underground. (c) Regeneration of vegetation by planting. (d) Conservation of a river ecosystem by maintaining flows capable of maintaining the river. (e) Implementing measures to prevent invasion of foreign species throughout the duration of projects ,including the construction period. Follow-up studies after the measures are taken for evaluation of their effectiveness.

5.2 Hydrological Regimes

The following are the major measures taken to mitigate the influence of changes in hydrological regime. Recovery of a river ecosystem by keeping flow rates required for river maintenance. Reservoir management considering the influence on local stakeholders. Raising and maintaining river levels by installing weirs around estuaries. Follow-up studies after the measures are taken and evaluation of effectiveness

5.3 Fish Migration and River Navigation

The following are the major measures taken to promote fish migration and to reduce mortality rates and damage to fish which pass through hydraulic turbines or spillways including installation of a fishway in an existing dam, and implementation of measures to attract fish with a sodium lamp. Also, installation of measures to direct fish at the intake (acoustic type, mercury lamp).

5.4 Reservoir Sedimentation

The following are the major measures taken to reduce or eliminate sediment flowing into reservoirs: (a) Reduction of sediment by constructing flood bypass tunnels going around a reservoir and (b) Construction of small-scale weirs to trap earth and subsequent removal by dredging.

5.5 Water Quality

The following are the major measures taken to improve water quality in reservoirs and downstream areas: (a) Temperature control considering the growth of fish by installing selective water intake facilities. (b) Reduction in water turbidity by selecting the operation of dams and constructing bypass tunnels. (c) Elimination the occurrence of abnormal odor or taste of the water in reservoirs by installing full thickness aeration and circulation facilities. (d) Reduction of outbreak of red tide in reservoirs by developing fresh water red tide treatment vessel. (e) Treatment of heavy metals discharged from copper mines located upstream of dam

5.6 Reservoir Impoundment

The following are measures taken to mitigate social and environmental impacts relating to impoundment of reservoirs: (a) Reductions in the scale of regulating reservoir levels and preservation of wetlands by maintaining appropriate water level. (b) Comparison of alternative reservoir water level reductions reflecting the results of environmental research.

5.7 Socio-Economic Impacts

Resettlement

The resettlement programs paying attention to the following points: (a) Securement of employment opportunities so that resettled people may have a sustainable livelihood. (b) Maintenance of social infrastructure (roads, water services, communication establishments, schools, hospitals, etc.) (c) Provision of sufficient information to communities and participation by the affected population in the resettlement process. (d) Information campaigns for community inhabitants continuous monitoring of water quality and health risk assessment can be conducted when a temporary increase in mercury concentration of fish was caused by impoundment of the reservoir.

Public Health

Deaths resulting from infectious diseases can be substantially reduced by improving various facilities including hospitals and community healthcare centres' after resettlement. Information campaigns for community inhabitants continuous monitoring of water quality and health risk assessment can be conducted when a temporary increase in mercury concentration of fish is caused by impoundment of the reservoir.

6.0 CONCLUSIONS

Hydropower is a well established technology that uses water without depleting it. It is the most reliable renewable energy and emits negligible greenhouse gases. Yet, there is occasionally debate on the negative social and environmental impacts caused by some hydropower projects. EIA certainly has a crucial role to play in addressing environmental issues surrounding project development and especially power projects. The integration of environment into development planning is the most important tool in achieving sustainable development for such hydropower projects. This paper attempts to summarize the Environmental Impact Assessment of

hydroelectric project taking a case of 100 MW Sainj Hydro Power Project, HPPCL located in Kullu district of Himachal Pradesh. Based on the Physico-Chemical and Socio-Economic data, various impacts of this project on environment are determined. We tried to enlist the differences in EIA procedures in the developed and developing countries. Different methodologies using Excel Sheets to enhance impact prediction have been worked upon. Appropriate adverse impact mitigation measures are proposed that can be followed in order to make the hydropower projects more environmental friendly.

REFERENCES:

i. *Allan JD, Flecker AS, (1993) Biodiversity conservation in running waters. BioScience 43: 32–43.*

ii. *Andersson K, (2000) Environmental Impact Assessment. Chalmers http://www.entek.chalmers.se/~anly/miljo/EIA.pdf*

iii. *Angermeier PL, Karr JL, (1983) Relationship between woody debris and fish habitat in a small warm water stream. Transactions of the American Fisheries Society 113: 716–726.*

iv. *Leopold LB, Clarke FE, Hanshaw BB, Balsley JR (1971) A procedure for evaluating Environmental Impact Assessment. Geological Survey Circular 645 http://eps.berkeley.edu/people/lunaleopold/(118)%20A%20Procedure%20for%20Evaluating%20Environmental%20Impact.pdf*

An Evolution Of Abiotic Factors In The Life Cycle Of Endaphis Aphidimyza (Zoophagous Cecidomyiids) In Ecological Parameters

Sanjay kumar Tripathi[1] and Ramesh Chandra[2]

[1]*Department of Biodiversity and Environment conservation, Atal Bihari Vajpaee Hindi Vishwavidyalay Bhopal M.P. (India) Email: tripathi.sk001@gmail.com*

[2]*Department of Biological Sciences, Mahatma Gandhi Chitrakoot Gramodaya Vishwavidyalay Distt. Satna, M.P 485780 (India) Email: rctmgcgv@gmail.com*

ABSTRACT:*Endaphis aphidimyza Shivpuje and Raodev is an endoparasitoid gall midge of black aphid Uroleucon gobonis of safflower. The experiment was conducted of safflower crop PVNS-12 In the field of Mahatma Gandhi Chitrakoot Gramodaya Vishwavidyalay Chitrakoot Satna (M.P.) after emergence mating was observed in the same day with in 7 to 10 hours. Zoophagous gall midge take rest after emergence on soil about 30 minutes then became active and they took flight landed after a few second on the plant and even the wall of the rearing pot. The male and female flies remain in copulation for few seconds to few minutes but only one male was success in approaching her. The genetilia of the male fly got entangled with the ovipositor of the female with the pointed head in opposite direction. The male and female flies remained in copulation for few seconds to few minutes. The size of container affects the mating process. The large size rearing containers resulted in somewhat better reproduction but presence of suitable mating sites seems more important than container size. The results of the mating concord with that of Grover and Kashyap (1988).The obsrvation of longivity nearly similar to Grover and Kashyap (1988). The paper is most important to balance the environment using environmental method of plant protection. Aphid has got adverse effect on the harvest and Zoophagous Cecidomyiids at cost of biotic and abiotic factors if support they are able to eat the hole population of aphid and also step forward in plant protection at the cost of environmental variables.*

1. INTRODUCTION:

The Cecidomyiidae family is one of the largest group of flies(Order: Diptera) whose midges generally known as gall midges (Cilbircioglu and Unal, 2009). Shivpuje and Raodev (1985) was described a new species *Endaphis* from Parbhani (M.S.). It is one of the important endoparasitoid gall midge of black aphid, *Urolucon gobonis Matsumura*. Morphology and life history of endoparasitoid gall midges were described by many scientist Kirkpatrick (1954), Mackauer & Foottit (1979), Firempong & Kumar (1975), Grover and Kashyap (1988), Tang et.al. (1994) & Gagne (1989) and Muratori et.al. (2009).The structure of cecidomyiids is comprises of Head, Anteena, Palpus, Thorex, Wing, Leg, Abdomen, Ovipositor (Aciculate, Lamilate) and Genetilia for the sake of present in vestigation abiotic factors namely Temperature. Humidity, Rainfall, Wind velocity in the life cycle of Zoophagous Cecidomyiids were taken one by one.The multivoltine gall midges adjust the numbr of generations according to climate and wheather conditions (Caresche & Wapshere, 1975, Gorden et.al. 1985 and Birch et.al 1992). The rearing of Zoophagous cecidomyiids the infested aphids *Uroleucon gobonis Matsmura* along with safflower(*Carthamus tinctorious Linn.*) plant were collected from Marathwada Agriculture university, Parbhani and brought to the research farm of Mahatma Gandhi Chitrakoot Gramodaya Vishwavidyalay Chitrakoot for rearing. The rearing of Zoophagous Cecidomyiids was done in different rearing cages according to needs. The lamp glass breeding cage 200mm-300mm-12'' with a diameter of 100mm in laboratory condition and cellophone muslin bag breeding in field condition for individual plants have been given the best results respectively. The rearing of aphid of safflower and the zoophagous cecidomyiids under organdy net proved better in field condition. There emergence and flight and sex-ratio were studied in depth. The occurrence of female biased sex –ratio has been repeatedly reported in various species of gall midged (Baxendale and Teetes, 1981; Matuszewski, 1982; McClay, 1996; Dorchin and Freidberg, 2004; Smith et.al.,2004; Mo and Liu,2007; Ogah et.al.,2010).Among biological control agents sex-ratio variation is widespread and can be attributed to wide range of casues (Ebbert, 1993; King,1987, 1993; Luck et.al.1993; Sabelis and Nagelkerke, 1993). In some midges species, males emerged earlier and searched for females Barnes, 1930; Summers, 1975; Yukawa and Sunose, 1976; Sone, 1986; Pivnick and Labbe, 1992.The sex-ratio of *Endaphis aphidimyza* is given in table 1.

2. MATHDOLOGY:

The abiotic factors namely Temperature, Humidity, Rainfall , Wind velocity were recorded at regional meterological laboratory Nagpur Maharashtra. The univariate and multivariate analysis were conducted to evaluate the effect of each factor separately with step up regression technique. The results of the different models are as given under.

The fallowing statistical tool were applied for evaluating abiotic factors

$$AM \ (X) = \sum f_i \ x_i \ / \ \sum f_i \ \text{...(i)}$$

$$Q1 = 1+(N/4-C/F) \ X_i \text{..................................(ii)}$$

$$Q2 = 1+ (N/2 \ -C/F) \ X_i \text{..................................(iii)}$$

$$Q3 = 1+ (3N \ /4 \ -C/F) \ X_i \text{..................................(iv)}$$

$$SD = \sum (Xi \ - \ X)^2 \ /N-1 \text{.................................(v)}$$

$$C.V = SD/ Mean \text{...(vi)}$$

Reg. coefficient (b) $== \sum xy / \sum x^2$

Reg. Equation

$$Y = a+b X \text{..(vii)}$$

$$A = Y-bX \text{..(viii)}$$

$$t = \text{Estimate} / \text{S.E.} \text{(Estimate)}\text{...(ix)}$$

3. RESULTS AND ANALYSIS

From this table it is evident that its emergence was highest in the month of January and it kept on decreasing in the month of March 2008. The sex-ratio was the female was dominated by male population. They were in the ratio of 44.4, 55.59 with effect from 7th January to 09/03/2008. The statistical analysis of the male and female is given below.

2008   2009
2010

Q1 =4.5   Q1 =7.25
Q1=22.5

Q2=10.5   Q2 =10.5
Q2=28

Q3 =16.75   Q3 =22.5
Q3=77.5

Mean (M,F) = 14.3   Mean (M,F) = 17.6
Mean (M,F)=68.25

Std Dev. = 13.98   Std. Dev. =16.5387

Table 3.1: Sex-ratio of *Endaphis aphidimyza* in 2007- 2008

| S. No. | Date | No. of midges emerged | | Total No. of emerged midges | Sex-ratio | |
		Male	Female		MALE : FEMALE	
1	07.01.2008	4	6	10	40	60
2	07.01.2008	6	5	11	54.54	45.45
3	07.01.2008	6	8	14	42.85	57.14
4	07.01.2008	6	9	15	40	60
5	08.01.2008	12	9	21	57.14	42.85
6	10.01.2008	11	14	25	44	56
7	10.01.2008	17	24	41	41.46	58.53
8	11.01.2008	10	12	22	45.45	54.54
9	12.01.2008	11	15	26	42.30	57.69
10	13.01.2008	12	18	30	40	60
11	15.01.2008	42	52	94	44.68	55.31
12	15.01.2008	41	59	100	41	59
13	16.01.2008	49	61	110	44.54	55.45
14	17.01.2008	23	27	50	46	54
15	18.01.2008	16	20	36	44.44	55.55
16	17.02.2008	10	5	15	66.66	33.33
17	17.02.2008	4	6	10	40	60
18	16.02.2008	3	4	7	42.85	57.14
19	08.03.2008	2	3	5	40	60
20	09.03.2008	1	1	2	50	50
Total		286	358	644	44.40	55.59

Average sex-ratio: 44.40 : 55.59 (4♂:5♀) i.e. (male: female)

Table 3.2: Sex-ratio of *Endaphis aphidimyza* in 2008 - 2009

| S. NO. | Date | No. of midges emerged | | Total No. of emerged midges | Sex-ratio | |
		Male	Female		MALE : FEMALE	
1	8.01.2009	4	6	10	40	60
2	7.01.2009	6	5	11	54.54	45.45
3	10.01.2009	7	8	15	46.66	53.33
4	12.01.2009	9	12	21	42.85	57.14

5	13.01.2009	12	13	25	48	52
6	14.01.2009	16	25	41	39.02	60.97
7	15.01.2009	53	77	130	40.76	59.23
8	16.01.2009	41	53	94	43.61	56.38
9	18.01.2009	43	57	100	43	57
10	19.01.2009	54	56	110	49.09	50.90
11	20.01.2009	24	26	50	48	52
12	21.01.2009	14	22	36	38.88	61.11
13	22.01.2009	18	24	42	42.85	57.14
14	22.01.2009	10	12	22	45.45	54.54
15	23.01.2009	11	13	24	45.83	54.16
16	24.01.2009	8	9	17	47.05	52.94
17	25.01.2009	8	13	21	38.09	61.90
18	25.01.2009	10	12	22	45.45	54.54
19	30.01.2009	3	2	5	60	60
20	30.01.2009	1		2	50	50
TOTAL		352	446	798	44.11	55.88

Average sex-ratio: 44 : 55 (4♂:5♀) i.e. (male: female)

Table 3.3: Sex-ratio of *Endaphis aphidimyza* in 2009 - 2010

| S. No. | Date | No. of midges emerged | | | Sex-ratio | |
		Male	Female	Total No. of emerged midges	MALE	FEMALE
1	11.01.2010	12	18	30	40	60
2	11.01.2010	18	24	42	42.85	57.14
3	13.01.2010	21	30	51	41.17	58.82
4	14.01.2010	13	16	29	44.82	55.17
5	13.01.2010	11	21	32	34.37	65.62
6	15.01.2010	17	25	42	40.47	59.52
7	16.01.2010	19	25	44	43.18	56.81
8	17.01.2010	20	26	46	43.47	56.52
9	18.01.2010	23	22	45	51.11	48.88
10	20.01.2010	21	26	47	44.68	55.31
11	12.02.2010	321	379	700	45.85	54.14
12	16.02.2010	182	193	375	48.53	51.46
13	16.02.2010	57	68	125	45.6	54
14	17.02.2010	64	76	140	45	54
15	18.02.2010	50	60	110	45	54
16	18.02.2010	90	110	200	45	55
17	19.02.2010	98	117	215	45	54.41
18	22.02.2010	72	78	150	48	52
19	22.02.2010	26	31	57	45.61	54.38
20	23.02.2010	15	20	35	42.85	57.14
TOTAL		1194	1321	2515	47.47	52.52

Average sex-ratio: 47: 52 (5♂:6♀) i.e., (male: female). w.e.f. from the years 2007 to 2010.

The analysis is based on pooled effect of independent variables namely temperature, humidity, rainfall and wind velocity and dependent variable sex ratio of zoophagous cecidomyiids w.e.f. from the years 2007 to 2010.

$$\overset{(ns)}{} \quad \overset{*}{} \quad \overset{**}{}$$
$$y = 154 - 14.7 \, x_1 - 0.97 \, x_2 + 84.7 \, x_3 + 87.4 \, x_4$$
$$SE : (8.044) \quad (1.270) \quad (36.95) \quad (25.31)$$
$$t : -1.82 \quad -0.76 \quad 2.29 \quad 3.45$$
$$R^2 = 0.641$$

3.1 TEMPERATURE

1. In abiotic conditions temperature x_1, humidity x_2, rainfall x_3 and wind velocity x_4 play a prolific role in sex ratio of zoophagous cecidomyiids commissioning. The analysis was accomplished with the aid of multivariate statistical analysis embedded with step - up statistical procedure. At the outset, sex ratio of zoophagous cecidomyiids was regressed with temperature. The regression equation is as given under :-

$$\overset{(ns)}{}$$
$$Y = 104 - 2.03 \, X_1$$
$$SE: \quad (9.350)$$
$$t: \quad -0.22$$
$$r^2 = 0.3$$

The analysis revealed that the effect of temperature remained non - significant at 5 per cent level of probability (t = -0.22). More vividly, unit change in temperature decreases the sex ratio of zoophagous cecidomyiids at the rate of (2.03). Temperature alone takes the responsibility of 0.3 per cent in the formation of sex ratio of zoophagous cecidomyiids pertaining to sex ratio. The correlation coefficient between sex ratio of zoophagous cecidomyiids and temperature remained 0.831 (Fig. : 1).

3.2 HUMIDITY

The regression equation indicated that humidity played an adverse effect on sex ratio of zoophagous cecidomyiids. A unit change in humidity per cent decreases the sex ratio formation by 2.03. The responsibility soldered by humidity came out to be 3.4 per cent. A positive correlation between humidity and sex ratio of zoophagous cecidomyiids (r =0.439) was observed (Fig. : 2).

$$\overset{(ns)}{}$$
$$Y = 104 - 2.03 \, X_2$$
$$SE: \quad (9.350)$$
$$t : \quad -0.79$$
$$r^2 = 0.34$$

3.3 RAINFALL

The third regression equation indicated the fact that higher is the rainfall more is the emergence of zoophagous cecidomyiids. One cm increase in the rainfall increases the sex ratio of zoophagous cecidomyiids by 78.8. A non - significant value of t and correlation coefficient r =0.102 indicates the facts that association between zoophagous cecidomyiids sex ratio and

rain fall is positive but non - significant. The responsibility of rain fall on zoophagous cecidomyiids sex ratio came out to be 14.1 per cent (Fig. : 3).

$$\begin{aligned} &\qquad\qquad\quad (ns)\\ Y &= -2.2 + 78.8\ x_3\\ SE &= \qquad (45.79)\\ t &= \qquad\quad 1.72\\ r^2 &= 0.141 \end{aligned}$$

3.4 WIND VELOCITY

The regression equation revealed the most important effect by wind velocity on the zoophagous cecidomyiids sex ratio formation. A unit change per km hour increase the sex ratio 87.2 and it is highly significant. The responsibility of wind velocity came out to be 43.5 percent on the sex ratio formation of zoophagous cecidomyiids. The correlation between zoophagous cecidomyiids sex ratio and wind velocity remained (r =0.02) (Fig. : 4).

$$\begin{aligned} &\qquad\qquad\quad ***\\ Y &= -105 + 87.2\ x_4\\ SE &= \qquad (23.45)\\ t &= \qquad\quad 3.72\\ r^2 &= 0.435 \end{aligned}$$

4 DISCUSSION:

The sex-ratio was 44.56 during the year 2008 as above the emergence of sex-ratio of *Endaphis aphidimyza* was the highest in the third week of February 2008 is February 2009 similar results were observed in the year 2007-2008 in the beginning of second week of February 2008 the sex-ratio was 45.55. During the year 2009 to 2010 the sex-ratio of *Endaphis aphidimyza* the male and female number where the highest 1075 (503 male + 572 female) in the month of February from 12th to 16th February 2010 the least number where in January (12+18). The emergence of the highest in this month and the sex-ratio was 49.51. The mean emergence of male was 14.3 with standard deviation 13.98 in the first quartile was observed that only 4.5 *Endaphis aphidimyza* was 4.5 and 50 percent 10.5 and 75 percent 16.75 was emerged in the year 2007 and 2008. During the year 2007 and 2008 female the emergence of *Endaphis aphidimyza* at q1 level was 5.25, 50 percent and 10.5, 75 percent 23.0 was observed the mean was17.9. It is evident from the graph that 25 to 40 the emergence was nill and similarly during 30 -50 the emergence was nil. The total number of midges emerged in the beginning where the highest fallowed by 20 to40, 40 to 60 and nil 60 to 80. It started increasing from 80 to 120 the mean was 32.2 and standard deviation was 32.32.

A polynomial of degree to was fitted and it was found that the correlation between male and emerged midges was .51. This clearly indicates a non significant emergence of midges (f=2.9338) the graph between male and emerged midges given figure no. 4. Non significant results were observed in case of female emergence midges (f=2.2569) was observed the correlation coefficient (r= .4571) indicated week emergence of female midges than the male. In the year 2008 and 2009 the q1

was 7.5 q2 10.5 and q322.5 mean was 17.6 and standard deviation 16.53 the population of the male was highest in the beginning and kept on decline till the number 30. between "30 to 40" emergence was nil and between 40 to 60 it was constant. Similarly during this year the female emergence was the highest in the beginning during the month of January and came down to nil between "30 to 50". However several ups and downs were observed in its emergence in the last week of February.

In case of female during the year 2008 and 2009 similar trained was observed. In this case q1 was 15.5 q2 23 and q3 48 mean emergence was 39.9 with standard deviation 37.73. A polynomial of degree to was fitted between male 2 and emerged midges the correlation coefficient r = .98 and f value of the model was non significant the model for analysis is given emerged midges is = -0.334819 + 2.3377535* male 2- 0.0035008* (male 2-17.6) A2. This model takes responsibility of 99.25 percent during the year 2009 and 2010 q1 was 22.5 q2 28 and q3 77.5 its mean was 63.25 and standard deviation it is 6.00 and the *Endaphis aphidimyza* emergence in the beginning was more and it started diminishing up to 200 it was nil between 200 to 350 in case of female midge. The midges were the highest and it came down to nil to 100 to 150 and also between 200to300. q1 was 17.25 q2 that is median equal to 22 and q3 = 70 mean was 57.5 and standard deviation 75. The emergence of midges showed similar trained but there was a improvement between 700 to 800. the models for male and female while fitting polynomial of degree to give the fallowing results.

Emerged midges 2 = 4.6028906 + 2.0683398* male 3 + 0.0004149* (male 3- 57.5) A2
Emerged midges 2 = - 3.92558 + 1.9259625* female 3- 0.0002521* (female 3-68.25) A2

From these results this may be safely concluded that those model give the best fit since 99.91 and 99.93 percent of variation in emergence of *Endaphis aphidimyza* midges by male and female are explained by them.

5 CONCLUSION:

From the above result this may be safely concluded that the emergence all the year with the effect from 2007 to 2010 is maximum in the middle of February up to the third week the structured model could explain 99.9 percent of the total variation.

From the above results this may be safely concluded that in *Endaphis aphidimyza* (Zoophagous Cecidomyiids) sex-ratio formation, there is negative effect of temperature and humidity whereas rainfall and wind velocity, their effect on the sex – ratio formation of Zoophagous Cecidomyiids remained positive. The rate of formation of Zoophagous Cecidomyiids sex-ratio was seen to be the highest in case of wind velocity followed by rainfall and adverse effect by humidity and temperature in case of a biotic Zoophagous Cecidomyiids sex-ratio formation environment.

REFERENCES:

i. Barnes, H.F. (1930). On some factors governing the emergence of gall midges (Diptera, Cecidomyiidae), Proc. Zool. Soc. Lond. 1930: 381 – 393.

ii. Baxendale FP, Teets GL. (1981) Production of unisexual progenies by the sorghum midge, Contarinia sorghicola. Annals of the Entomological Society of America, 74: 412-413

iii. Birch, M.L., J.W. Brewer, and O. Rohfritsch. (1992). Biology of Dasineura affinis (Cecidomyiidae) and influence of its gall on Viola odorata, pp. 171-184. In J.D. Shorthouse and O.Rohfritsch [eds.], Biology of insect – induced galls. Oxford University Press, New York.

iv. Caresche, L.A. and A. J. Wapshere.(1975).The chondrilla gall midge Cystiphora schmidti (Rübsaamen) (Diptera, Cecidomyiidae). II. Biology and host specificity. Bull. Entomol. Res. 65: 55-64.

v. Cilbircioglu C, Unal S. (2009). Gall midges (Diptera: Cecidomyiidae) in forest tree of Turkey. Journal of Agriculture and Urban Entomology, 25: 13-23.

vi. Dorchin N, Freidbrg A. (2004). Sex ratio in relation to season and host plant quality in a monogamous steming galling midge (Diptera : Cecidomyiidae), Ecological Entomology, 29: 677-684.

vii. Ebbert, M.A. (1993). Endosymbiotic sex-ratio distorters in insect and mites. In "Evolution and Diversity of sex –ratio in insect and Mites"(D.L. Wrensch and M.A. Ebbert, Eds.), pp.150 – 191. Chapman & Hall, New York.

viii. Firempong, S. & R. Kumar. (1975). Natural enemies of Toxoptera aurantii (Boy.) (Homoptera: Aphiddidae) on cocoa in Ghana. Bio. J. Linn. Soc. 7: 261 – 292.

ix. Gagne, R.J. (1989). The plant – feeding gall midges of North America. Cornell University Press, Ithaca, NY.

x. Ghule, B.D; A.B. Jagtap, V.S. Dhumal, and A. B. Deokar, (1986). Agriculture Research Station Jalgaon- 425001(India).

xi. Gordon, A. J., R.L., Kluge, and S. Neser. (1985). Effects of the gall midge, Zeuxidiplosis giardi (Diptera : Cecidomyiidae), on seedlings of St. John's Wort, Hypericum perforatum (Clusiaceae), pp. 743 – 748. In E.S. Delfosse [ed.], Proceedings, 6th International Symposium on Biological Control of Weeds, 19 – 25 August 1984. Agriculture Canada, Vancouver, Canada.

xii. Grover, P. and Vasantika, Kashyap. (1988). Biology of Endaphis aphidimyza (Shivpuje et.al) Cecid,Internationale, (IX): No.1

xiii. King, B.H. (1987), Offspring sex ratio in parasitoid wasp. Q.Rev Biol. 62, 367 – 396.

xiv. King, B.H. (1993). Sex ratio manipulation by parasitoid wasp. In "Evolution and Diversity of sex –ratio in insect and Mites" "(D.L. Wrensch and M.A. Ebbert, Eds.), pp.418-441 Chapman & Hall, New York.

xv. Kirkpatric, T..W. (1954). Notes on Pseudendaphis maculans Barnes, a cecidomyiid endoparasiteof aphids of Trinidad, B.W.I. Bull. Entomol. Res. 45: 777-781.

xvi. Luck, R.F., Stouthammer, R., and Nunney, L.P. (1993). Sex determination and sex –ratio patterns in parasitic hymenoptera. In "Evolution and Diversity of sex –ratio in insect and Mites" "(D.L. Wrensch and M.A. Ebbert, Eds.), pp.442-476 Chapman & Hall, New York.

xvii. Mackauer, M. and R. Foottit, (1979). A gall midge Endaphis species (Diptera: cecidomyiidae), as a gregarious aphid parasite. Canadian Entomologists ,111, 615-620.

xviii. Matuszewski B. (1982). Diptera I: Cecidomyiidae. In Animal cytogenetics. Insecta 3 (John B, ed). 91-137, Gebruder Borntraeger, Berlin, Germany.

xix. McClay AS. (1996) Unisexual broods in the gall midge Cystiphora sonchi (Bermi) (Diptera : Cecidomyiidae). Canadian Entomologist, 128: 775-776.

xx. Mo TL, Liu TX. (2007). Predation and life table of Feltiella acarisuga (Diptera : Cecidomyiidae) praying on eggs of Tetranychus urticae (Acari:Tetranychi). Environmental Entomology, 29: 195- 199.

xxi. Muratori, F. B. Gagne, R. J. and R.H. Messing, (2009). Ecological traits of a new aphid parasitoid, Endaphis fugitiva (Diptera : Cecidomyiidae),

and its potential for biological control of the banana aphid, Pentalonia nigronervosa (Hemiptera : Aphididae). Biological Control, (50): 185 – 193.

xxii. Ogah EO, Odebiyi JA, Ewete FK, et. al. (2010). Biology of the African rice gall midge, Orseolia orizivora (Diptera : Cecidomyiidae) and its incidence on wet season rice in Nigeria. International Journal of Tropical Insect Science, 30: 32 - 39

xxiii. Pivnick, K.A. and E. Labbe (1992). Emergence and calling rhythms, and mating behavior of the orange wheat blossom midge, Sitodiplosis mosellana (Gehin) (Diptera, Cecidomyiidae). Can. Entomol. 124: 501-507.

xxiv. Sabelis, M .W. and Nagelkerke, K. (1993). Sex allocation and pseudoarrhenotokey in phytoselid mites In "Evolution and Diversity of sex – ratio in insect and Mites" "(D.L. Wrensch and M.A. Ebbert, Eds.), pp. 512 - 541 Chapman & Hall, New York.

xxv. Shivpuje, P.R. and Raodev, A.K. (1985). A new species of parasitic gall midges from safflower aphid from India. Journal of Maharashtra Agric. Univ. 10 (1): 61 -63.

xxvi. Smith MAH, Wise IL, Lamb RG. (2004). Sex-ratio of Sitodiplosis mosellana (Diptera : Cecidomyiidae) implication for pest management in wheat (Poacae). Bullatin of Entomological research, 94:569 – 575.

xxvii. Sone, K. (1986). Ecological studies on the pine needle gall midge, Thecodiplosis Japonensis Uchida et Inouye (Diptera : Cecidomyiidae) I life history. Bull. For. & For. Prod. Res. Inst. 341: 1 – 25 (in Japanese with English Summary).

xxviii. Summers, C.G. (1975). Daily adult emergence in the sorghum midge, Contarinia sorghicola. Environ. Entomo. 4: 495 – 498.

xxix. Tang Y.Q; R.K. Yokomi and Gagne, R.J. (1994). Life history and description of Endaphis maculans (Diptera : Cecidomyiidae), an Endoparasitoid of Aphids in Florida and the Caribbean Basin. Ann, Entomol., Soc, America,87 : (5).

xxx. Tripathi, S.K. (2012) Ecological studies on Zoophagous Cecidomyiids (Cecidomyiidae: Diptera) A Ph.D Thesis Mahatma Gandhi Chitrakoot Gramodaya Vishwavidyalay Chitrakoot Satna (M.P.) India.

xxxi. Yukawa, J.and T. Sunose (1988). Midges galls of Niigata prefecture ((Diptera, Cecidomyiidae). Trans. Essa Entomol Soc. 66: 45 – 58 (in Japanese with English Summary).

g1 - Distribution of male
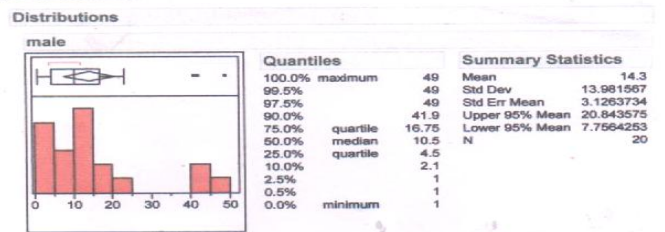
g1 - Distribution of female
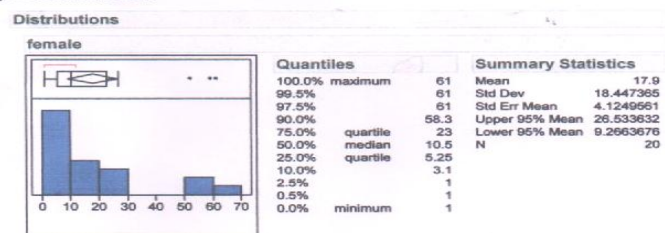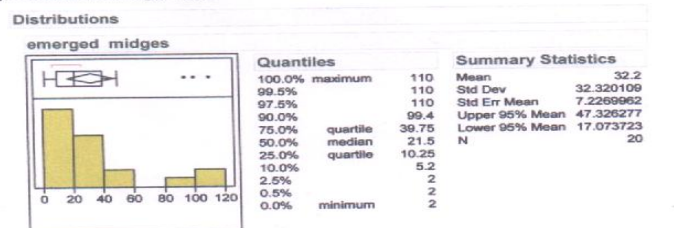
g1 - Distribution of emerged midges

g1 - Distribution of emerged midges

Distributions

emerged midges

Quantiles		
100.0%	maximum	130
99.5%		130
97.5%		130
90.0%		109
75.0%	quartile	48
50.0%	median	23
25.0%	quartile	15.5
10.0%		5.5
2.5%		2
0.5%		2
0.0%	minimum	2

Summary Statistics	
Mean	39.9
Std Dev	37.732995
Std Err Mean	8.4373543
Upper 95% Mean	57.559585
Lower 95% Mean	22.240415
N	20

g1 - Distribution of male 3

Distributions

male 3

Quantiles		
100.0%	maximum	321
99.5%		321
97.5%		321
90.0%		173.6
75.0%	quartile	70
50.0%	median	22
25.0%	quartile	17.25
10.0%		12.1
2.5%		11
0.5%		11
0.0%	minimum	11

Summary Statistics	
Mean	57.5
Std Dev	75.006316
Std Err Mean	16.771922
Upper 95% Mean	92.604036
Lower 95% Mean	22.395964
N	20

g1 - Distribution of female 2

Distributions

female 2

Quantiles		
100.0%	maximum	77
99.5%		77
97.5%		77
90.0%		56.9
75.0%	quartile	25.75
50.0%	median	13
25.0%	quartile	8.25
10.0%		2.3
2.5%		0
0.5%		0
0.0%	minimum	0

Summary Statistics	
Mean	22.25
Std Dev	21.437486
Std Err Mean	4.7935675
Upper 95% Mean	32.283052
Lower 95% Mean	12.216948
N	20

g1 - Distribution of female 3

Distributions

female 3

Quantiles		
100.0%	maximum	379
99.5%		379
97.5%		379
90.0%		185.4
75.0%	quartile	77.5
50.0%	median	28
25.0%	quartile	22.5
10.0%		18.2
2.5%		16
0.5%		16
0.0%	minimum	16

Summary Statistics	
Mean	68.25
Std Dev	86.006655
Std Err Mean	19.231673
Upper 95% Mean	108.50235
Lower 95% Mean	27.997646
N	20

g1 - Distribution of male 2

Distributions

male 2

Quantiles		
100.0%	maximum	54
99.5%		54
97.5%		54
90.0%		52
75.0%	quartile	22.5
50.0%	median	10.5
25.0%	quartile	7.25
10.0%		3.1
2.5%		1
0.5%		1
0.0%	minimum	1

Summary Statistics	
Mean	17.6
Std Dev	16.538313
Std Err Mean	3.6980792
Upper 95% Mean	25.340169
Lower 95% Mean	9.8598314
N	20

g1 - Distribution of emerged midges 2

Distributions

emerged midges 2

Quantiles		
100.0%	maximum	700
99.5%		700
97.5%		700
90.0%		359
75.0%	quartile	147.5
50.0%	median	49
25.0%	quartile	42
10.0%		30.2
2.5%		29
0.5%		29
0.0%	minimum	29

Summary Statistics	
Mean	125.75
Std Dev	160.9295
Std Err Mean	35.984929
Upper 95% Mean	201.06732
Lower 95% Mean	50.432678
N	20

2009 - 2010

Comparative Study Of Gamma Hydrograph And Synthetic Hydrograph Method For Flood Estimation Of Ungauged Catchment

Abhay Sharma[1]   Anugrah Singh[2]
[1]M. Tech Scholor, D.T.U., Delhi
[2]M. Tech Scholor, IIT, Roorkee
Email: sharmaabhay402@gmai.com,
anusingh0811@gmail.com

ABSTRACT:*Most of the small and medium sized catchments are ungauged as it is not economically feasible to make all the sites as gauged. In ungauged catchments, rainfall data of recent flood events in last 2-3 years is available. Regional methodology is most commonly used for flood estimation of ungauged catchments as inadequate data is available. Synthetic Unit Hydrograph (SUH) is a very reliable method for flood estimation of ungauged sites in which UH parameters (W_{50}, W_{75}, WR_{50}, WR_{75}, q_p, T_p, T_b) are calculated and UH is drawn through these calculated points using Hit and Trial method which is time consuming. Gamma Distribution function requires two inputs, Peak Discharge per unit area per unit effective depth and Time to Peak, to develop UH. Hit and Trial method is not required for developing Unit Hydrograph using Gamma Distribution Function (G.D.F.) as shape of the curve is known and area under the curve is always Unity. In this paper, GDF is used for calculation of UH parameters and peak of flood of 37 ungauged sites of India and results are compared with various SUH approaches. Results indicate that UH derived using GDF has shape most similar & Peak most near to actual data for all the sites as compared to all other methods. Flood peak using GDF and SUH method shows large variation.*
Keywords: Gamma Distribution Function, Ungauged catchments, Flood Estimation, Synthetic Unit Hydrograph

1. INTRODUCTION

Flood estimation for ungauged catchments cannot be done by usual methods of flood estimation like Rational method, Gumbel's method, etc because such methods require 10-15 years past hydrologic data. In ungauged (small or medium sized) sites very few or no rain gauges are installed and rainfall data available is inadequate. In such catchments, recent flood data of the past 3-4 rainfall events are convulated with geomorphologic parameters of the catchment to develop a reliable flood hydrograph. An alternative to this approach lies in the use of probability functions like gamma, beta etc to derive a flood hydrograph in a convenient and easy manner.

In this paper, gamma distribution function has been used for flood estimation studies in 37 catchments (area lying between w27-2297 km^2) located in hydrometerologically homogeneous subzones, Upper Narmada &Tapi Subzone and Chambal Subzone.

2. MATERIAL AND METHODS

a) DATA AVAILABE: Out of the 37 sites selected for flood estimation studies, data for site 863; Sakker River depicting basin characteristics and representative unit hydrograph parameters is shown below

BASIN CHARACTERISTICS					1-hour UH. Parameters						
Name	A	L	Lc	S	T_p	q_p	T_b	W_{50}	W_{75}	WR_{50}	WR_{75}
	Sq. km	Km	Km	m m/ m	hr	m3 / s / K m2	hr	h r	hr	h r	hr
Sa kk	211 0.8	1 6	90. 16	2.6 3	9. 5	0	27	4	2	2	0.8

b) METHOD USED FOR FLOOD ESTIMATION

- **Methodology used by Central Water Commission**

CWC has used Synthetic Hydrograph Method for flood estimation in ungauged sites. They developed regression equations relating UH parameters and geomorphologic parameters of the catchment, applicable for all the sites located in a particular homogeneous region.

- **Gamma Distribution Function**

The Unit hydrograph can be developed using the probability density functions like Weibull, Gumbel, Beta, Gamma functions etc. These functions have the benefit that area under these functions is always unity and shape of the distribution is also known.

Gamma hydrograph is developed using gamma distribution function defined as:

$$q(t) = \frac{e^{-\frac{t}{k}} * \left(\frac{t}{k}\right)^{n-1}}{k * \Gamma(n)}$$

(1)

Where k & n are scale and shape parameters of Gamma Distribution Function

Gamma function is used to develop unit hydrograph for the ungauged sites of a hydraulically homogenous region. In Gamma Unit Hydrograph, only two parameters; peak discharge per unit are per unit effective rainfall (Q_p/Area/Effective Rainfall) and Time to Peak (T_P) of a unit hydrograph of very small duration is required to develop the instantaneous unit hydrograph as compared to synthetic hydrograph method which requires q_p, T_P, T_b, W_{50}, W_{75}, WR_{50}, WR_{75} and simultaneous adjustment through these points to draw the Unit Hydrograph. Thus gamma hydrograph method is easy as compared to the synthetic hydrograph method used for estimation of flood hydrograph.

3. OBJECTIVE

a) Gamma unit hydrograph is compared with the synthetic hydrograph method used by CWC with representative unit hydrograph (actual data) parameters as reference to find the most appropriate Unit Hydrograph for the study area.

b) 50 year return flood hydrograph is developed for all 37 bridge sites using gamma hydrograph method.

c) A flood formula is developed for the peak of 50 year return flood developed by Gamma hydrograph.

4. RESULTS AND ANALYSIS

a) 1-Hour Unit Hydrograph parameters calculated using gamma hydrograph method and SUH method used by CWC:

Calculation of UH parameters for Sakker River-

Table 1: Representative Unit Hydrograph

Point	Time (hours)	X	Discharge (m³/sec)	Y
1		0		0
2	T_p-WR_{50}	7.5	$0.5Q_p$	460
3	T_p-WR_{75}	8.7	$0.75Q_p$	690
4	**T_p**	**9.5**	**Q_p**	**920**
5	T_p+(W_{75}-WR_{75})	10.7	$0.75Q_p$	690
6	Tp+(W_{50}-WR_{50})	12.4	$0.5Q_p$	460
7	T_b	27		0

Table 2: Synthetic UH by CWC method

Point	Time (hours)	X	Discharge (m³/sec)	Y
1		0		0
2	T_p-WR_{50}	8.54	$0.5Q_p$	312.85
3	T_p-WR_{75}	9.34	$0.75Q_p$	469.28
4	**T_p**	**10.9**	**Q_p**	**625.7**
5	T_p+(W_{75}-WR_{75})	12.77	$0.75Q_p$	469.28
6	Tp+(W_{50}-WR_{50})	13.98	$0.5Q_p$	312.85
7	T_b	25.6		0

Table 3: Gamma Hydrograph Method

T	T_p	q_p	qp (hr⁻¹)	b	n	K	IUH (hr⁻¹)	q= Q/A (m³/sec/km²)	Q FOR 1 hr UH
0	9.5	0.44	0.16		1.52	15.64	0.65	0.00	0.00	0.00
1							0.00	0.00	0.00	
2							0.00	0.00	0.01	
3							0.00	0.00	0.51	
4							0.00	0.01	7.44	
5							0.01	0.04	42.30	
6							0.04	0.12	136.62	
7							0.09	0.24	306.16	
8							0.13	0.36	529.18	
9							0.16	0.43	744.89	
10							0.16	0.44	881.19	
11							**0.14**	**0.38**	**896.43**	
12							0.10	0.29	799.54	
13							0.07	0.20	635.93	
14							0.05	0.13	457.74	
15							0.03	0.07	301.96	
16							0.01	0.04	184.52	
17							0.01	0.02	105.41	
18							0.00	0.01	56.73	
19							0.00	0.00	28.95	
20							0.00	0.00	14.08	
21							0.00	0.00	6.57	
22							0.00	0.00	2.95	
23							0.00	0.00	1.28	
24							0.00	0.00	0.53	
25							0.00	0.00	0.22	
26							0.00	0.00	0.09	
27							0.00	0.00	0.03	
28							0.00	0.00	0.01	
29							0.00	0.00	0.00	
30							0.00	0.00	0	

Using this method, calculated UH parameters for this site are: q_p=0.425 m³/sec/km², Q_p=896 m³/sec, T_p=10.0 hr, W_{50}=7.3 hr, WR_{50}=3.3 hr, W_{75}=4.0 hr & WR_{75}=2.3 hr
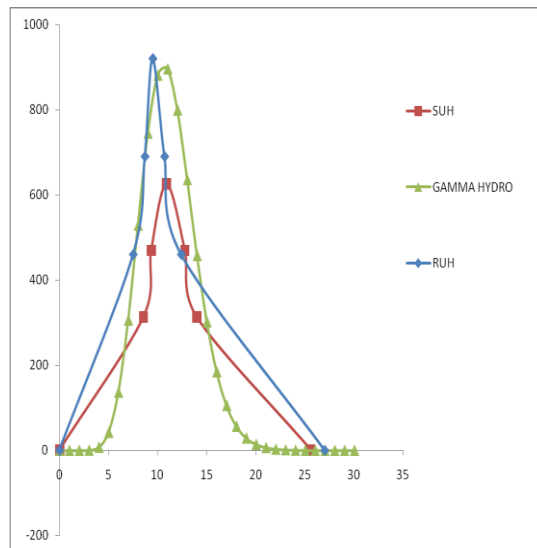
Figure 1: Unit Hydrograph using actual data, SUH method & Gamma Hydrograph Method

Table 4: q_p and T_p using GUH method and CWC's method

S.NO.	BRIDGE SITE	AREA	1 hour UH data by CWC Report		1 hr UH by G.I.U.H.	
		in km²	q_p	T_p	q_p	T_p
Sites of Upper Narmada and Tapi Subzone						
1	863	2110.85			0.425	10
2	644	989.80			0.318	9
3	802	945.23			0.356	9
4	578	676.00			0.479	7
5	625	535.41			0.426	8
6	249	518.67			0.316	8
7	394/2	348.92			0.392	7
8	557	343.17			0.406	8
9	787	321.16			0.781	5
Few Sites of Chambal Subzone						
10	39	145.45	0.77	2	0.594	3
11	51	140.43	0.55	4	0.549	3
12	44	108.78	0.82	2	0.77	3
13	495	66.3	0.62	4	0.486	5
14	406	47.44	1.02	2	0.982	2
15	1	44.75	0.89	2	1.074	2
16	306	43.77	0.86	2	0.447	2
17	118	41.44	0.96	1.5	0.701	2
18	35	39.52	0.67	3	0.713	3
19	77	26.18	1.13	1.5	0.71	2

b. Results of peak of 50 year return flood using SUH & Gamma Hydrograph method

Table 5: Peak of Hydrograph using CWC method and GUH approach

S. No.	BRIDGE SITE	AREA in km²	Qp OF 50-Year R.F.by CWC	Qp OF 50-Year R.F.by GUH
Few Sites of Upper Narmada and Tapi Subzone				
1	863	2110.85	9230.58	12335.9
2	644	989.8	3219.51	2886.5
3	802	945.23	5602.01	5579.66
4	578	676	3474.2	3910.56
5	625	535.41	3244.16	3098.78
6	249	518.67	3015.97	2648.08
7	394/2	348.92	1590	1422.07
8	557	343.17	2500	2203.35
9	787	321.16	1840.87	2361.59
Few Sites of Chambal Subzone				
10	39	145.45	983.31	886.97
11	51	140.43	1019.23	859.5
12	44	108.78	834.63	947.66
13	495	66.3	425.24	400.67
14	406	47.44	486.15	478.93
15	1	44.75	553.09	563.04
16	306	43.77	384.27	177.01
17	118	41.44	472.06	215.05
18	35	39.52	418.58	414.41
19	77	26.18	200.25	139.22

c. Comparison of regression equation developed by CWC and that developed for results of Gamma Hydrograph method

for Upper Narmada and Tapi Subzone-

Equation by CWC	Equation for results of GUH
$T_p = 0.995(L * L_c / S^{0.5})^{0.2654}$ $r^2=0.8908$	$q_p = 1.9227(T_p)^{-0.78701}$ $r^2 = 0.9297$
$q_p = 1.665(T_p)^{-0.71678}$ $r^2=0.8542$	$W_{50}=2.5937(q_p)^{-1.008}$ $r^2 = 0.9692$
$W_{50} = 1.9145(q_p)^{-1.2582}$ $r^2=0.940$	$WR_{50}=1.0497(q_p)^{-1.087}$ $r^2 = 0.8904$
$W_{75} = 1.1102(q_p)^{-1.1088}$ $r^2=0.8772$	$W_{75}=1.492(q_p)^{-1.1}$ $r^2 = 0.8949$
$WR_{50} = 0.7060(q_p)^{-1.3859}$ $r^2=0.8214$	$WR_{75} = 0.6793(q_p)^{-1.174}$ $r^2 = 0.8747$
$WR_{75} = 0.45314(q_p)^{-1.3916}$ $r^2=0.7627$	

d. Flood formula developed for sites of both the subzones using results of peak of 50 year return flood calculated using Gamma Hydrograph method

for Upper Narmada and Tapi Subzone-

$$Q_p= 0.8581 A^{0.929}L^{-0.187}L_c^{-0.063}S^{0.011}R_f^{1.022} \qquad r=0.99 \quad (2)$$

for Chambal Subzone-

$$Q_p= 17.20 A^{1.04} L^{-0.519} S^{0.186} R_f^{0.072} \qquad r=0.96 \quad (3)$$

5. CONCLUSIONS

a.   Peak of discharge of Gamma Unit Hydrograph is nearest to the Representative Unit Hydrograph value as compared regression method used. Results of GUH are about 5% lower than the actual values provided in the report i.e. very near to actual values as compared to Synthetic Unit Hydrograph method used by CWC whose peak value is very less compared to the observed values for the bridge site.

b.	Shape of the Gamma Unit Hydrograph is bell shaped which is generally the case and need not to be predicted because it depends on well known Gamma distribution function.

c.	Area of the Gamma distribution function is always unity and unit hydrograph is drawn with help of 2 parameters, peak discharge per unit area (q_p) and Time to peak (T_p) while SUH method is a hit and trial method in which unit hydrograph is fitted through calculated points, q_p, T_p, W_{50}, WR_{50}, W_{75} and WR_{75}.

d.	Gamma Hydrograph method is more accurate, simple and requires lesser calculation compared to the SUH method used by CWC for development of Unit Hydrograph.

e.	Regression equation developed for the calculated 1-Hour UH parameters using Gamma Hydrograph method without removing outliers has higher correlation coefficient than the equations developed by CWC for the subzones.

f.	There is high variation between the values of peak of 50-Year return flood between the results calculated by Gamma Hydrograph Method and the results available in CWC reports.

g.	Flood peak formulae developed using Gamma Hydrograph method shows very high multiple correlation coefficient and thus can be very accurately applied for the sites included in the homogeneous subzone

6. REFERENCES

i.	Ajward, M. H., & Muzik, I. (1999). A spatial hydrology model for flood estimation. Bridges. Vol. 10(40430), 188.

ii.	Al-Mashidani, G., Lal, P. B., & Mujda, M. F. (1978). A simple version of Gumbel's method for flood estimation. Hydrological Sciences Journal. Vol. 23 No. 3, 373-380

iii.	Aron, G., and White, E. L. (1982). Fitting a Gamma distribution over a synthetic unit hydrograph. Water Resources Bull. Vol. 18, No. 1, pp. 95-98.

iv.	Aziz, K., Rahman, A., Fang, G., Haddad, K., & Shrestha, S. (2010). Design flood estimation for ungauged catchments: Application of Artificial Neural Networks for eastern Australia. In World Environment and Water Resources Congress, ASCE, Providence, Rhodes Island, USA.

v.	Bhaskar, N. R., Parida, B. P., & Nayak, A. K. (1997). Flood estimation for ungauged catchments using the GIUH. Journal of water resources planning and management. Vol. 123 No. 4, pp:228-238..

vi.	Bhunya, P. K., Ghosh, N. C., Mishra, S. K., Ojha, C. S., & Berndtsson, R. 2005. Hybrid model for derivation of synthetic unit hydrograph. Journal of Hydrologic Engineering, Vol. 10 No. 6, pp:458-467

vii.	Bhunya, P. K., Mishra, S. K., & Berndtsson, R. (2003). Simplified two-parameter gamma distribution for derivation of synthetic unit hydrograph. Journal of Hydrologic Engineering. Vol. 8 No. 4, pp:226-230.

viii.	Central Water Commission India 2002. Flood estimation report for Upper Narmada & Tapi Subzone 3(c) a method based on unit hydrograph principles. Design Office Rep. No. 3/1980. Hydrology of small catchments Directorate, CWC, New Delhi, India.

ix.	Cleveland, T. G., He, X., Asquith, W. H., Fang, X., & Thompson, D. B. (2006). Instantaneous unit hydrograph evaluation for rainfall-runoff modeling of small watersheds in north and south central Texas. Journal of irrigation and drainage engineering. Vol. 132 No. 5, pp:479-485.

x.	Croley, I. I., & Thomas, E. (1980). Gamma synthetic hydrographs. Journal of Hydrology, Vol. 47 No. 1, pp:41-52.

xi.	Jeng, R. I., & Coon, G. C. (2003). True form of instantaneous unit hydrograph of linear reservoirs. Journal of irrigation and drainage engineering. Vol. 129 No. 1, pp: 11-17.

xii.	Jin, C. X. (1992). A deterministic gamma-type geomorphologic instantaneous unit hydrograph based on path types. Water resources research. Vol.28 No. 2, pp:479-486.

xiii.	Lee, K. T., & Yen, B. C. (1997). Geomorphology and kinematic-wave-based hydrograph derivation. Journal of Hydraulic Engineering. Vol. 123 No. 1, pp:73-80.

xiv.	Mair, A., & Fares, A. (2009). Assessing rainfall data homogeneity and estimating missing records in Mākaha valley, O 'ahu, Hawai 'i. Journal of Hydrologic Engineering. Vol. 15 No. 1, pp:61-66.

xv.	Nash, J. E. (1959). Systematic determination of unit hydrograph parameters. Journal of Geophysical Research. Vol.64 No.1, 111-115.

xvi.	Sahoo, B., Chatterjee, C., Raghuwanshi, N. S., Singh, R., & Kumar, R. (2006). Flood estimation by GIUH-based Clark and Nash models. Journal of Hydrologic Engineering. Vol. 11 No. 6, pp:515-525.

xvii.	Singh, S. K. (1998). Reconstructing a synthetic unit hydrograph into a Gamma distribution. In Proceeding of International conference on Integrated water Resources Management, Alexandria University, Egypt. pp. 104-110.

xviii.	Singh, S. K. (2000). Transmuting synthetic unit hydrographs into gamma distribution. Journal of Hydrologic engineering. Vol. 5 No. 4, pp:380-385.

xix.	Singh, S. K. (2005). Clark's and Espey's unit hydrographs vs the gamma unit hydrograph. Hydrological sciences journal. Vol. 50 No. 6

xx.	Singh, S. K. (2007). Use of gamma distribution/Nash model further simplified for runoff modeling. Journal of Hydrologic Engineering. Vol. 12 No. 2, pp:222-224.

xxi.	Singh, S. K. (2009). Time base as an invertible function of the parameters of gamma unit hydrograph. Journal of irrigation and drainage engineering. Vol. 135 No. 6, pp:802-805.

xxii.	Swamee, P. K., Ojha, C. S. P., & Abbas, A. (1995). Mean annual flood estimation. Journal of Water Resources Planning and Management. Vol. 121 No. 6, pp:403-407.

xxiii.	Wall, D. J., Kibler, D. F., Newton, D. W., & Herrin, J. C. (1987). Flood peak estimates from limited at-site historic data. Journal of Hydraulic Engineering. Vol. 113 No. 9, pp:1159-1174.

Impact Of Dem Grid Size On Estimation Of Flood Depth And Flood Level Using 1d-2d Coupled Flow Model

Pankaj Mani, Scientist D, CFMS, NIH, WALMI Complex, Phulwarisharif, Patna – 801505, Rakesh Kumar, Scientist F, SWHD, NIH, Roorkee
Jagadish Prasad Patra, Scientist B, SWHD, NIH, Roorkee

ABSTRACT: A hydrodynamic coupled 1-D and 2-D flow model has been developed in a rural terrain of northern India where an industrial plant has been proposed. The source of flooding in the area includes breach in canal in addition to local site rainfall for which flood simulation has been carried out. The design value of the local site rainfall is computed based on PMP value obtained from IMD and frequency analysis of daily rainfall of 6 raingauges in the area. The flow in canal and breach section has been simulated in 1-D flow model, MIKE 11 while the flow in floodplain and local site rainfall has been simulated in 2-D model, MIKE 21 and both are combined through MIKE FLOOD. Three cases of flood simulation has been carried out representing the floodplain by three different DEMs namely; DEM1, DEM2 and DEM3 of grid size of 180 m, 180 m and 10 m respectively. In DEM1, the floodplain is represented by 180 m grid size using the topographical information available in Survey of India (SOI) toposheet at 1: 50,000 scale. The detailed topographical maps (with CI <=1 m)/ surveys are available for selected areas only, mainly for the project sites. For the study area the topographical survey has been carried out at 2m CI and DEM

at 10 m regular grid (DEM3) has been generated from it. The DEM2 is generated by resampling the DEM3 at 180 m grid size to save computational time and computing resources. Hence, three cases of floodplain representation have been developed and the flood inundation depth and flood level due to rainfall estimates of 100 yr return period have been computed. The results are analyzed to study the effect of DEM grid size over the flood parameter. It is found that the inundation depth is increased while the flood level is decreased for finer DEM. This is due to better representations of ponds/ terrain irregularities in finer DEM. The presence of depressions in the area produces more flooding depth while it also provides larger storage causing the overall decrease in flood level. The impact of DEM grid size on computing resources has also been analysed.

Keywords: 2-D flow simulation, grid size, MIKE FLOOD

1. INTRODUCTION

The devastating nature of flood has acquired human attention and multi-stage and multi-dimensional approach since long has been practiced to minimize its impact over man and property. The approach includes structural measures like construction of reservoir and embankment etc and non structural measures like flood forecasting and flood plain regulation. The increasing population and limited land resources has compelled the people to encroach upon the floodplain. Under the climate change scenario not only the intense and frequent floods are observed but also the flood damages have increased manifolds. Hence, accurate and reliable information about flood characteristics have become the societal need to minimize the flood damages. The prediction of flood characteristics depends upon the computational tool as well as the quality of data input. Several advanced flood simulation tools; open source as well as commercial versions are available but the availability of input data is still scarce, particularly in developing countries. The predictions of the flood level and the flow velocity are the prerequisite in design of flood protection works as well as for formulating the flood plain regulation. Various river flow model has been developed which are capable of transforming the design floods to the flood level at the selected river cross sections. Recently, with the development in computational capability, 2-dimensional flood plain flow modeling is also widely practiced for this purpose. Rivers and floodplain topography are one of the major inputs for mathematical modeling of the flow in floodplain. The river is represented through cross sections and flow in river is simulated through 1-D flow model. The floodplain is represented though DEM at rectangular/ triangular grids and the flow within floodplain is simulated by 2-D flow model. Thus in the flow modeling the river cross section and DEM are the critical input influencing the flood hydraulics and the resultant areal extent of the simulated flood (Nicholas and Walling, 1997; Horritt and Bates, 2001a, Mani et al, 2014). A slight error in the model results may produce larger inundation due to low relief characteristics of floodplain (Bates and De Roo, 2000). Models obtained with global positioning system (GPS) or conventional

survey techniques have high accuracy and are suitable and easy to implement over small areas (Brasington et al., 2000). Several researchers has attempted to study the effect of spatial resolution on raster-based flood models (Werner, 2001; Horritt and Bates, 2001b). Casas et al (2006) reported that 1: 5000 contour based DTM overestimates the water surface elevation while the GPS-based DTM produces more realistic results. Sanders (2007) evaluated the performance of on-line DEMs for flood inundation modeling. The advancement in computing resources has increased the use of 2-D flow models. The availability of river cross section data is better in comparison to the availability of fine resolution representative DEM. Though several research have been carried out on 2-D flow simulation, quantifying the impact of grid size on flood characteristics are rarely noticed. The floodplains with uniform or gradual varying topography, though rarely found in nature, may be represented through a coarser DEM (large size grids). Most of the floodplains are marked with sudden topographical change due to natural or man-made activities like roads, buildings, dykes, ponds, drainage etc. The grid size of the DEM should be fine enough to represent the variation in the topography due to these terrain features. The paper represents the effect of grid size in simulating the floodplain in a rural terrain in northern India, where terrain features like canals and ponds are witnessed. The floodplain is accounted for by three different DEM representation; DEM1, DEM2 and DEM3 of grid size of 180 m, 180 m and 10 m respectively. In DEM1, the floodplain is represented by 180 m grid size using the topographical information available in Survey of India (SOI) toposheet at 1: 50,000 scale. This is the most commonly available data, particularly for developing countries like India, for generation of DEM. The available information in toposheets for bench marks, spot levels and contours (at 20 m contour interval (CI) for 1:50,000 scale) have been used for interpolation and sampling at 180 m regular grid interval. The detailed topographical maps (with CI <=1 m)/ surveys are available for selected areas only, mainly for the project sites. For the study area the topographical survey has been carried out at 2m CI and DEM at 10 m regular grid (DEM3) has been generated. The courser grid size in 2D flow simulation is selected to overcome constrains due to computer time and resources. The DEM2 is generated by resampling the DEM3 at 180 m grid size, thus the average representation of the floodplain topography is not due to data scarcity as in case of DEM1. Hence, three cases of floodplain representation has been developed and the flood inundation depth and flood level due to rainfall estimates of 100 yr return period have been computed using MIKE FLOOD. The results are analyzed to study the effect of DEM grid size over the flood parameter. It has been observed that the inundation depth is increased while the flood level is decreased for finer DEM. This is due to better representations of ponds/ terrain irregularities in finer DEM. The presence of depressions in the area produces more flooding depth while it also provides larger storage causing the overall decrease in flood level.

2. STUDY AREA

The study area is located in northern India where an industrial plant is proposed. The area is a flat terrain marked with absence of well defined natural drainage system in most of the part. A natural drainage exists in the northern part, while the plant site is in the adjacent southern catchment (Figure 1). The river course in the area is very narrow at several places and often causes floods when the heavy rainfall occurs in the catchment area. The branch canal B1 and feeder canal F1, both off-taking from the Main Canal M1, are running parallel and join together in their tail ends. The plant site is located on southern side of the branch canal B1 and feeder canal F1 at their tail end (Figure 1). The climate in the region can be classified into tropical desert & steppe, arid and hot which is mainly dry with very hot summer and cold winter except during monsoon season when moist air of oceanic origin penetrates into the region.
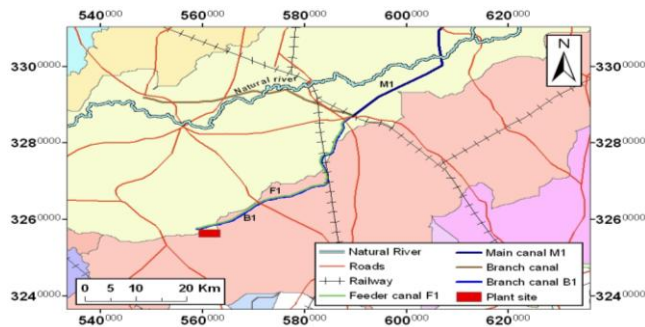
Figure 1 Location map of the study area. Polygons of different shades are the catchments. The plant site is close to ridge line of the catchment.

The DEM of the area is prepared by digitizing the contour lines, spot heights and bench marks from the Survey of India toposheets at 1:50,000 scale. The outlet point is selected on the stream grid near the plant site (Figure 2). The highest ground level is 253.5 m and is located in the north-east part of the catchment while the lowest elevation is 200 m in the south-west part. Probable maximum precipitation (PMP) has been obtained from India Meteorological Department for this catchment and synthetic unit hydrograph has been computed using geomorphological parameter of this catchment to estimate the PMF.
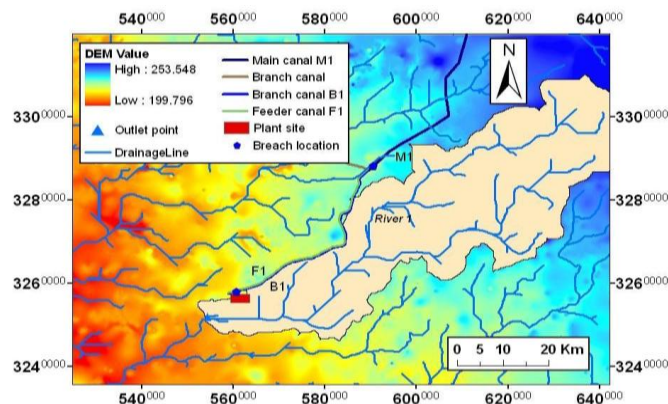
Figure 2 Drainage network extracted from DEM prepared by using the topographic information available in Survey of India toposheets at 1:50,000 scale

3. METHODOLOGY

The methodology adopted in the study mainly consists of estimation of design precipitation and flood, generation of three types of DEM based on topographical information and field survey data and development of flow model to compute the flow parameters. The flow model is used for assessing the impact of various DEM on flood inundation depth and flood elevation.

3.1. Rainfall design estimation

The Bureau of Indian Standards (IS:11223, 2004) for hydrologic design criteria states that design flood for carrying out flood submergence studies/ maximum flood level at an important structure is probable maximum precipitation (PMP)/ probable maximum flood (PMF). Further, the design guidelines specific to the type of the industrial plant being referred in this paper, also require that whichever of PMP/PMF or 1000 year return period rainfall/flood, whichever is higher should be considered as the design flood. Estimation of PMP and 1000 year return period rainfall are described as follows.

3.1.1. Probable maximum precipitation

The PMP of the study area has been obtained from India Meteorological Department (IMD). IMD provided the 1-day and 2-day PMP estimates with their temporal distributions and these are based on processing of long term rainfall data of various rain gauges in the region in accordance with the procedures mentioned in World Meteorological Organization (WMO) guidelines, WMO No. 332 (Kulkarni, 2011).

3.1.2. Estimation of 1000 year rainfall

The frequency analysis of 1-day and 2-day annual maximum rainfall values of the six raingauge stations lying within the study area has been carried out using the L-moments approach as described elsewhere (Hosking and Wallis, 1997; Kumar and Chatterjee, 2005; Kumar et al., 2003). Twelve frequency distributions viz. Extreme value (EV1), General extreme value (GEV), Logistic (LOS), Generalized logistic (GLO), Normal (NOR), Generalized Pareto (GPA), Generalized normal (GNO), Uniform (UNF), Exponential (EXP), Pearson Type-III (PT3), Kappa (KAP) and Wakeby (WAK) have been used to identify robust distributions for each of the six raingauges based on the L-moment ratio diagrams and the Zi-static criteria. The temporal distribution of PMP obtained from IMD has been used for distributing the rainfall of 1000 year return period into the rainfall hyetographs. The uncertainty in the rainfall estimate is described by inclusion of standard deviation (σ) in the computed value. Further, the effect of climate change (CC) is considered by increasing the rainfall by 15%. Figure 3 shows the PMP obtained from IMD, estimated rainfall for 1000 yr, 1000 yr + σ + CC.

3.2. Estimation of design flood

3.2.1. Probable maximum flood

For estimation of PMF, the unit hydrograph for the study area has been derived based on the method of synthetic unit hydrograph derivation developed by Central Water Commission (CWC) of India (1984). In this method relationships between physiographic characteristics of the catchments and the representative unit hydrograph parameters have been derived using the data of 40 gauged catchments varying in size from 25.26 to 2425.54 km^2, for the hydrometeorological homogeneous subzone covering the study area. For derivation of unit hydrograph for the study area, the DEM of the study area has been used and the physiographic characteristics of the catchment up to the plant site are computed as: area of catchment (A) = 2,190 km^2, equivalent stream slope (S) = 0.229 m/km and length of the main stream (L) = 131.56 km, using tools of ArcGIS. The regional relationships developed by CWC (1984) for estimating the regional unit hydrograph parameters are used. The design storm values computed from probable maximum precipitation (PMP) have been convoluted with the synthetic unit hydrograph and PMF hydrographs are estimated.
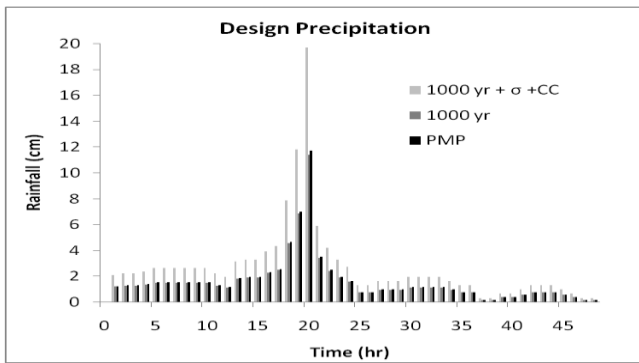
Figure 3 Design precipitations for the study area

3.2.2. Estimation of 1000 year flood

The average rainfall values of 1000 year return periods weighted by the thiessen weights of the six raingauges have been convoluted with the synthetic unit hydrograph derived for the study area and flood hydrographs for 1000 year return period are estimated. The estimated flood of PMF, 1000 yr and 1000 yr+σ+CC is shown in Figure 4.
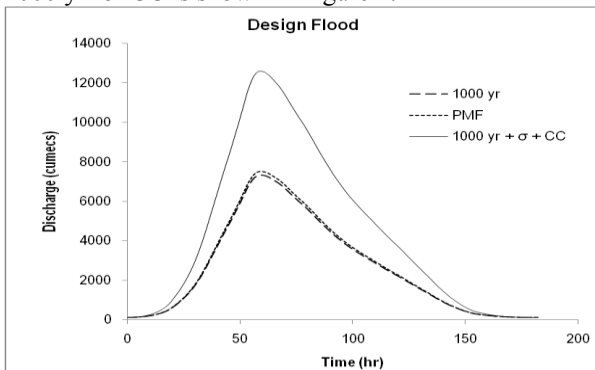
Figure 4 Design flood for the study area

3.3. Development of flow model

The various sources of flooding in and around the plant site include the spilling/ breaching of the main canal M1 and the branch canal B1 in addition to the catchment runoff routed to the site through the drainage network (catchment flooding) as evident from Figure 2. The flood resulting from the on-site rainfall is also included in the analysis. The canal and the river flow as well as the canal breach are simulated in MIKE 11 (1D flow) while the local site rainfall and flow over floodplain are simulated in MIKE 21 (2D flow). These 1D and 2D models are coupled together in MIKE FLOOD.

3.3.1. Governing equations for MIKE 11 and MIKE 21 models

MIKE FLOOD model is a dynamic coupling of 1-D MIKE 11 and 2-D MIKE 21 models (DHI 1997, 2000 & 2004). The MIKE 11 HD simulates the 1-D flow with the dynamic wave description by solving the vertically integrated equations of conservation of continuity and momentum (the 'Saint Venant' equations). These equations are as follows:

$$\frac{\partial Q}{\partial x} + \frac{\partial A}{\partial t} = q \qquad (1)$$

$$\frac{\partial Q}{\partial t} + \frac{\partial\left(\alpha\frac{Q^2}{A}\right)}{\partial x} + gA\frac{\partial h}{\partial x} + \frac{gQ|Q|}{C^2 AR} = 0 \qquad (2)$$

Where, Q = discharge, A = flow area, q = lateral inflow, h = stage above datum, C = Chezy resistance coefficient, R = hydraulic or resistance radius and α = momentum distribution coefficient. The solution of the equations of continuity and momentum is based on an implicit finite difference scheme, 6-point Abbott scheme.

MIKE 21 simulates unsteady 2-D flow in vertically homogeneous layer and uses the equations of conservation of mass and momentum to describe flow and water level variations:

$$\frac{\partial\xi}{\partial t} + \frac{\partial p}{\partial x} + \frac{\partial q}{\partial y} = \frac{\partial d}{\partial t} \qquad (3)$$

$$\frac{\partial p}{\partial t} + \frac{\partial}{\partial x}\left(\frac{p^2}{h}\right) + \frac{\partial}{\partial y}\left(\frac{pq}{h}\right) + gh\frac{\partial\xi}{\partial x} + \frac{gp\sqrt{p^2+q^2}}{C^2 h^2}$$
$$- \frac{1}{\rho_w}\left[\frac{\partial}{\partial x}(h\tau_{xx}) + \frac{\partial}{\partial y}(h\tau_{xy})\right] - \Omega_q - fVV_x + \frac{h}{\rho_w}\frac{\partial}{\partial x}(p_a) = 0 \qquad (4)$$

$$\frac{\partial q}{\partial t}+\frac{\partial}{\partial y}\left(\frac{q^2}{h}\right)+\frac{\partial}{\partial x}\left(\frac{pq}{h}\right)+gh\frac{\partial\xi}{\partial y}+\frac{gp\sqrt{p^2+q^2}}{C^2\cdot h^2}$$

$$-\frac{1}{\rho_w}\left[\frac{\partial}{\partial y}(h\tau_{yy})+\frac{\partial}{\partial x}(h\tau_{xy})\right]-\Omega_p-fVV_y+\frac{h}{\rho_w}\frac{\partial}{\partial xy}(p_a)=0$$

$$(5)$$

Where, $h(x,y,t)$ = water depth; $d(x,y,t)$ = time varying water depth; $\xi(x,y,t)$ = surface elevation; $p,q(x,y,t)$ = flux densities in x- and y- directions; $C(x,y)$ = Chezy resistance; g = acceleration due to gravity; $f(V)$ = wind friction factor; V, V_x, V_y (x,y,t) = wind speed and components in x- and y- direction; $\Omega(x,y)$ = Coriolis parameter, latitude dependent; $p_a(x,y,t)$ = atmospheric pressure; ρ_w = density of water; x,y = space coordinates; t = time; $\tau_{xx},\tau_{xy},\tau_{yy}$ = components of effective shear stress.

MIKE 21 HD makes use of a so-called Alternating Direction Implicit (ADI) technique to integrate the equations for mass and momentum conservation in the space-time domain. The equation matrices that result for each direction and each individual grid line are resolved by a Double Sweep (DS) algorithm.

3.3.2. Dam break simulation in MIKE 11

The flooding due to breach in the canals B1 has been simulated using Dambreak structure module of MIKE 11 flow model. The Dambreak structure is a composite structure composed of a structure representing the flow over the crest (crest flow structure) and another structure representing the breach of the dam. In this study, the flow through a dam breach is described in MIKE 11 through the use of a calculation method as implemented in National Weather Services (NWS) DAMBRK program. The NWS DAMBRK method uses two failure modes; Breach failure and Piping failure. The first of these uses a weir equation to determine the flow through the breach whereas the latter is based on the flow equation through an orifice.

Breach failure- The flow through the trapezoidal breach is given by

$$Q=c_v k_s\left[c_{weir}b\sqrt{g(h-h_b)}(h-h_b)+c_{slope}S\sqrt{g(h-h_b)}(h-h_b)^2\right]$$

$$(6)$$

Where b = width of the breach bottom; g = acceleration due to gravity; h = upstream water level (reservoir water level); h_b = level of breach bottom; S = side slope of breach; c_{weir} = weir coefficient for horizontal part (=0.546); c_{slope} = weir coefficient for slope part (=0.432); c_v = correction coefficient for approach sections. This coefficient compensates for the loss in energy due to the inflow contraction; k_s = correction coefficient due to submergence.
The weir coefficients have been made non-dimensional e.g.

$$c_{weir}\sqrt{g}=0.546430\sqrt{9.81(m/s^2)}=1.7115(m^{1/2}/s)$$

$$(7)$$

The correction coefficient for the approach section is determined through

$$c_v=1+\frac{c_B Q^2}{gW_R^2(h-h_{b,term})^2(h-h_b)}$$

$$(8)$$

Where c_B = non-dimensional coefficient (=0.74) termed as the Brater coefficient; W_R = reservoir width given by the undestroyed crest length; $h_{b,term}$ = the terminal level of the breach bottom, the minimum level in time series file. The submergence correction is determined through

$$k_s=\max\left(1-27.8\left(\frac{(h_{ds}-h_b)}{(h-h_b)}-0.67\right)^3,0\right)$$

$$(9)$$

where h_{ds} = downstream water level.

Piping failure - The flow through a piping failure is given by

$$Q=c_{orifice}A\sqrt{2g(h-\max(h_p,h_{ds}))}$$

$$(10)$$

where $c_{orifice}$ = orifice coefficient (=0.60); A = flow area in pipe is given by:

$$A=b(h_{pt}-h_b)+S(h_{pt}-h_b)^2;$$

$$(11)$$

h_{pt} = top of pipe; h_b = bottom of pipe; h_p = centerline of pipe given by $h_p=\dfrac{(h_{pt}+h_b)}{2}$

The pipe may collapse either due to the top of the pipe reaching the crest level or if the water level upstream is not high enough to maintain pipe flow. The criterion for the latter is given by:

$$h<\frac{3}{2}(h_{pt}-h_b)+h_b$$

$$(12)$$

Once the pipe has collapsed the flow is calculated based on the breach flow equations.

Crest flow - The flow over the crest of the dam is given by

$$Q = k_s c_{weir} b_c \sqrt{g(h-h_c)}(h-h_c)$$

(13)

where, h_c = the crest level; b_c = the remaining crest length (perpendicular to the flow) and the submergence correction given by

$$k_s = \max\left(1 - 27.8\left(\frac{(h_{ds}-h_c)}{(h-h_c)} - 0.67\right)^3, 0\right)$$

(14)

The failure moment may be defined in three ways: time in the form of a historic date and time; hours from start of simulation and the reservoir water level. Once the failure has initiated, the temporal development of the breach is defined from time series of breach parameters namely, the breach bottom, side slope and bottom width. In case of piping failure, time series also contains the upper level of the piping. Both the methods rely on the user specifying the full development of the breach geometry as a function of time. In the study, the breach geometry has been assigned based on the historical breach information obtained from the local project authority and published reports.

3.3.3. Schematization of drainage network and floodplain

The flow through the river, canals and breach in canal has been modeled in MIKE 11. The schematization of the drainage network and floodplain in MIKE FLOOD model setup is shown in Figure 5. The 1D model includes the main canal M1 from Chainage-0 m to Chainage-4155 m, and the branch canal B1 from Chainage-0 m to Chainage-48889.92 m. The main drainage lines of the catchment extracted from the DEM is named as River1 (from Chainage-0 m to Chainage-44070.5 m) in the network file. The cross sections for the canals are obtained from the project authority while it is extracted from DEM for the River1. As no observed river cross section is available, the accuracy of the derived cross section could not been estimated. However, the levels extracted from DEM corresponding to digitized spot levels and bench marks around the study area are compared to estimate the error of DEM. The error varies from -5.128 to 0.764 m while the average error is -0.189 m. The canal flow simulation at different breach locations are carried out to identify the critical location of the breach causing the severe flooding at the plant site. The locations at the tail end of the main canal M1 and near the plant site on the branch canal B1 are estimated to be the critical breach locations. The breach locations in the canals are incorporated in the network file as a lateral branch of 100 m length wherein a dam break structure is inserted in its mid point. SS_B1 is the breach location in the canal B1 at Chainage-46500 m while SS_M1 is the breach location in the canal M1 at Chainage-4000 m. The bathymetry of 426x331 grids of 180 m spacing is extracted from DEM and is used to develop 2D flow model in MIKE 21. In MIKEFLOOD the bathymetry is linked on either bank of the River1 while for

breach in the canals it is linked on the left bank only so that the entire flow is diverted towards the plant site.

MIKE 11 model has been calibrated for Manning's roughness coefficient 'n' (unit: sec/m$^{1/3}$) by the trial and error method using the designed discharge and full supply level (FSL) data for the canal obtained from the project authority. The root mean square error (RMSE) has been used as the performance index to select the optimum 'n' value. Figure 6 shows the designed and simulated FSL in B1. The values of 'n' in different canal sections are estimated in the range of 0.014 to 0.024. For the floodplain, the Manning's roughness coefficient of 0.05 (for floodplains with matured field crops and high grass, IS: 2912, 2004) has been assumed, as the terrain mainly consists of agricultural land.
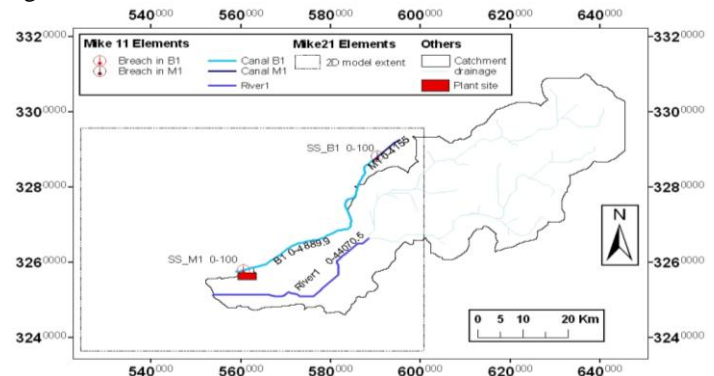
Figure 5 MIKE Flood model setup for the study area
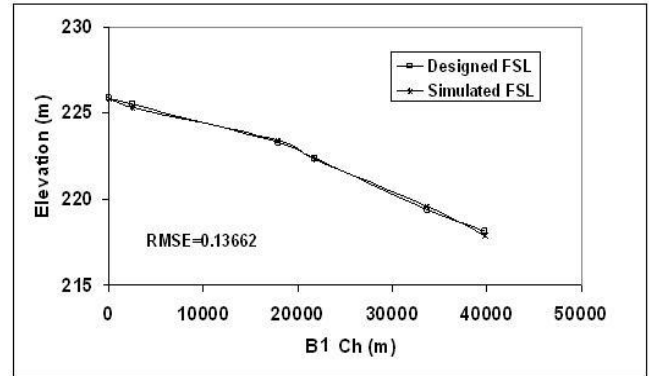
Figure 6 Designed and simulated FSL during calibration of MIKE 11 model

3.3.4. Canal breach parameters

Three breach parameters namely; breach width, breach time and breach level are required for modeling the development of a breach. In this study, breach due to piping is assumed under authorized full supply discharge (AFSD), which starts at FSL and develops till the water level in the canal reaches at the bottom level at that section. For the critical scenario, the breach due to overtopping of canal water under the bank full condition has been considered and therefore in this case, the initial breach level is the top level of the canal. The AFSD of the canal M1 and B1, obtained from the project authority, are 141 and 64 m^3/sec respectively. The bank full discharge for M1 and B1

has been computed using the conveyance equation for the trapezoidal section as 250 and 117 m^3/s, respectively. When failure of the canal B1 due to the bank full condition is simulated, the flow in the feeder canal F1 (with AFSD of 24 m^3/s) is also added to the discharge of B1. The trapezoidal shape of the breach section with side slope of 1:1 is assumed in the canal embankment considering it as an earthen dam. The size of the breach has been assumed as 300 m based on the information collected from the newspapers clips and concerned officials of State Irrigation Department about the maximum breach size. The breach time of 2 h has been assumed based on earthen dam failure criteria.

3.4. Development of digital elevation model

3.4.1. DEM1 (grid size 180 m based on toposheet information)

The entire study area is covered in 15 numbers of toposheets at 1: 50,000 scale have been used for digitizing the spot heights, contours and bench mark (BM). These levels have been interpolated to obtain the ground elevation at every square cell of 180 m size. The canal alignments are overlaid over it to include the canal profile in the DEM. Though the flow analysis of only two canals, B1 and M1 are performed in the model, the DEM includes the canal profile of other major canals and distributaries. This is to produce real terrain situation, as shown in Figure 7, which shows the DEM-1 of the study area and its extent used in MIKE FLOOD analysis, and to ensure that the flow of breached B1 near plant site is restricted by both the canals and thus would result into maximum inundation. Further, the cells along the drainage line are blocked to avoid double conveyance computation in 2D flow simulation as this flow has already been included in 1D flow computation. In MIKE FLOOD, the boundary cells along the DEM are assigned a higher value and no flow is allowed across these boundary cells. So, in the downstream reach, the boundaries are extended suitably to avoid back water flow to the point of interest. Hence, an extended area has been taken in the downstream reach, i.e. west and south boundary of the DEM as shown in Figure 8. In the upstream reach, the larger area has been selected to examine the movement of flow to the plant site either by catchment flooding or canal breaching. It consists of 426 columns and 331 rows having rectangular cells of 180 m grid size. Each cell contains the height of the ground in meter.
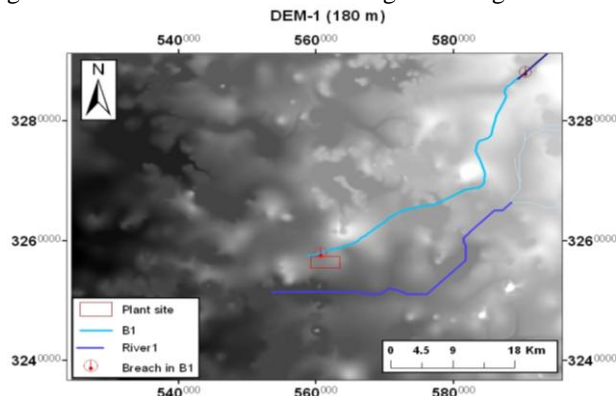
Figure 7: DEM 1 (180 m grid size) based on SOI toposheet height information
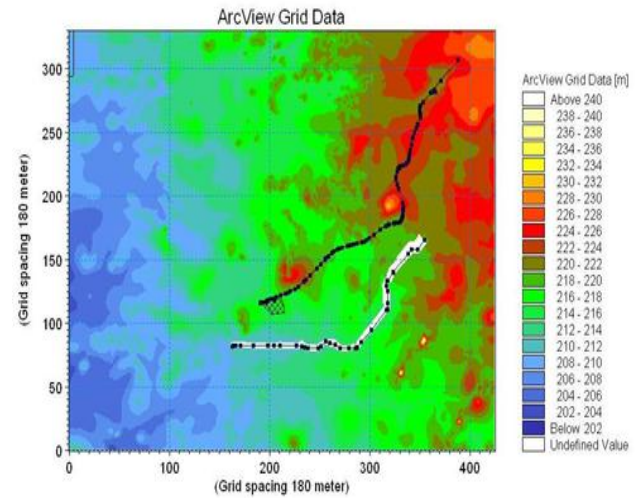
Figure 8: Bathymetry for DEM-1 in the MIKE FLOOD model setup.

3.4.2. DEM2 (grid size 180 m based on field survey)

The detailed topographical survey has been carried out in and around the plant site with CI < 1 m. This information is merged with the existing DEM1 to update the topographical details and DEM-2 with 180 m grid size has been developed as shown in Figure 9. Though the DEM has been updated with the detailed field survey information, grid size remains 180 m the number of grid points in this DEM is same as in case of DEM-1; i.e. 426 columns and 331 rows. The bathymetry for the DEM2 is shown in Figure 10.
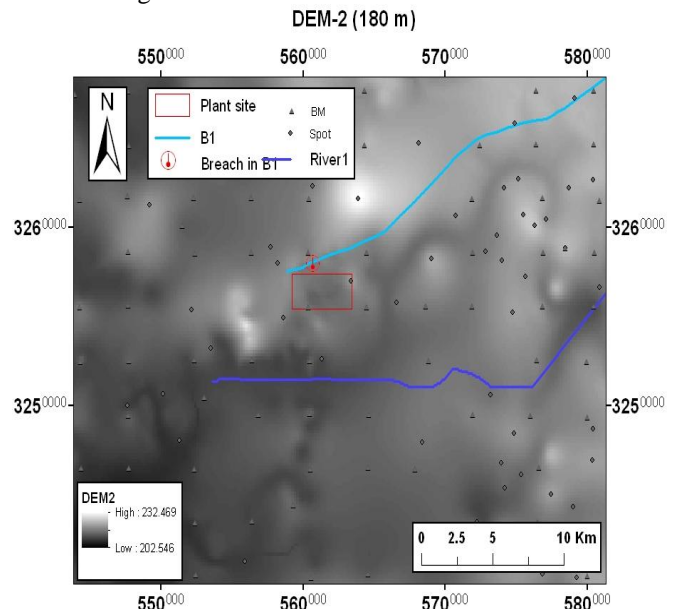
Figure 9: DEM 2 with 180 m grid size updated with detailed topographical survey.
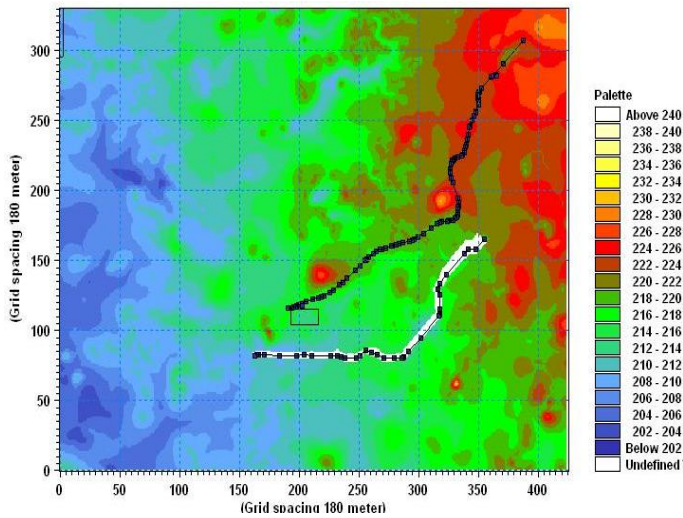
Figure 10: Bathymetry for DEM-2 in the MIKE FLOOD model setup.

3.4.3. DEM-3 (grid size 10 m based on field survey)

As the detailed field survey has been carried out in and around the plant site, the DEM of the area at 10 m grid size has been developed as shown in Figure 11. Further as the grid size is reduced to 10 m, the number of grid points has increased by 18x18 times. The increased grid points would require higher computer resources and time and therefore the extent of flood simulation is reduced to the plant boundary only. Figure 12 shows the bathymetry used in MIKE FLOOD for DEM-3. It may be observed that that no. of grids for DEM-1 and DEM 2 is 426 columns and 331 rows while for DEM-3 it is 676 columns and 801 rows, though the extent of simulation has been reduced.
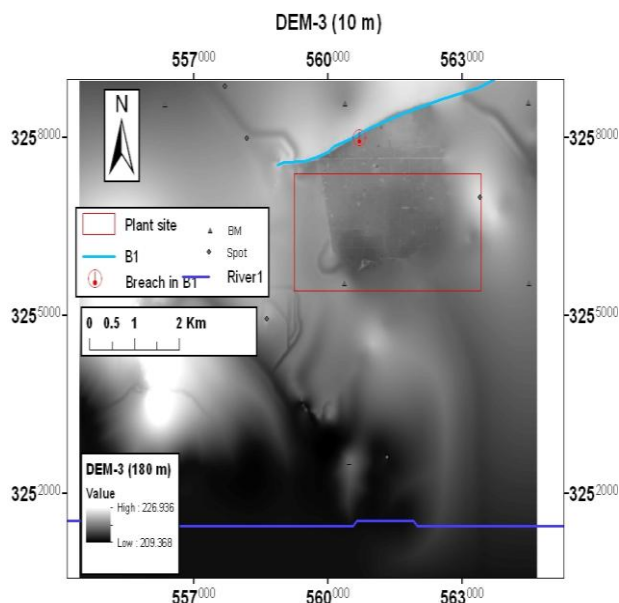
Figure 11: DEM 3 with 10 m grid size from detailed topographical survey.
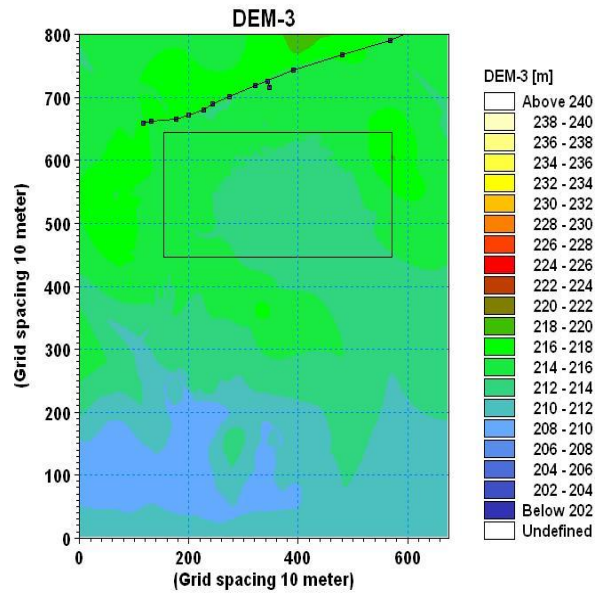
Figure 12: The bathymetry in the MIKE FLOOD model set up for for DEM-3

4. FLOW SIMULATION RESULTS AND ANALYSIS

To study the maximum flood level and inundation depth, the canals are assumed to breach under bank full condition while the flow in the river is corresponding to flood of 1000 yr $+\sigma$ + CC. The local rainfall of 1000 yr $+\sigma$ + CC over the plant site is also considered. The MIKE 11 setup remains the same while the M21 and thus MIKE FLOOD model is prepared separately for DEM1, DEM2 and DEM3. Thus three cases of flow model has been developed as summarized in Table-1.

Table 1: Flooding scenario and description of DEM

Case No.	Flooding Source & Condition			DEM		
	Local site Rainfall	Catchment flood	B1 Canal status	Name	Grid Size	Description/Source
Case-1	1000+σ+CC	1000+σ+CC	Bank Full flow with full breach	DEM1	180	Spot level & BM from toposheets
Case-2	1000+σ+CC	1000+σ+CC	Bank Full flow with full breach	DEM2	180	DEM1 updated with detailed topographical survey
Case-3	1000+σ+CC	1000+σ+CC	Bank Full flow with full breach	DEM3	10	Detailed topographical survey

The maximum flood elevation and inundation depth has been computed from the flow simulation results for each case of Case-1, Case-2 and Case3. The simulation result contains the time series of flood level and flood depth at all the grid. From this time series, the maximum flood depth and maximum flood

level are extracted at each grid. The maximum flood inundation depth and maximum flood level within plant site due to flood for Case-1, Case-2 and Case-3 are shown in Figure 13 and Figure 14 respectively. The figures show that the flood depth and flood elevation is not uniform within the plant site. This is due to non uniformity of ground level within the plant site. The mean, minimum and maximum flood depth/ levels within the plant site for each case are shown in Table-2.

Figure 13: Maximum flood depth (m) within plant site for various cases

Case-1

Case-2

Case-

Case-1

Case-2
Case-

3
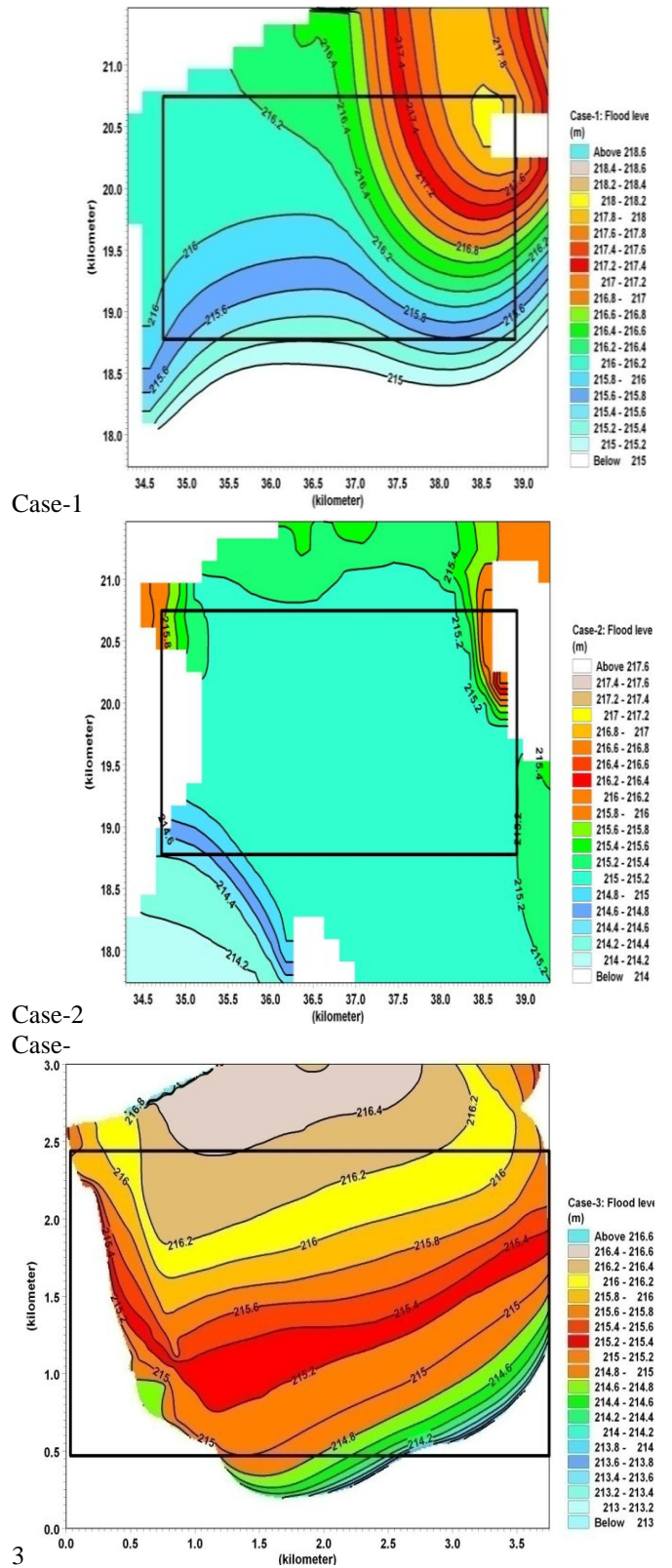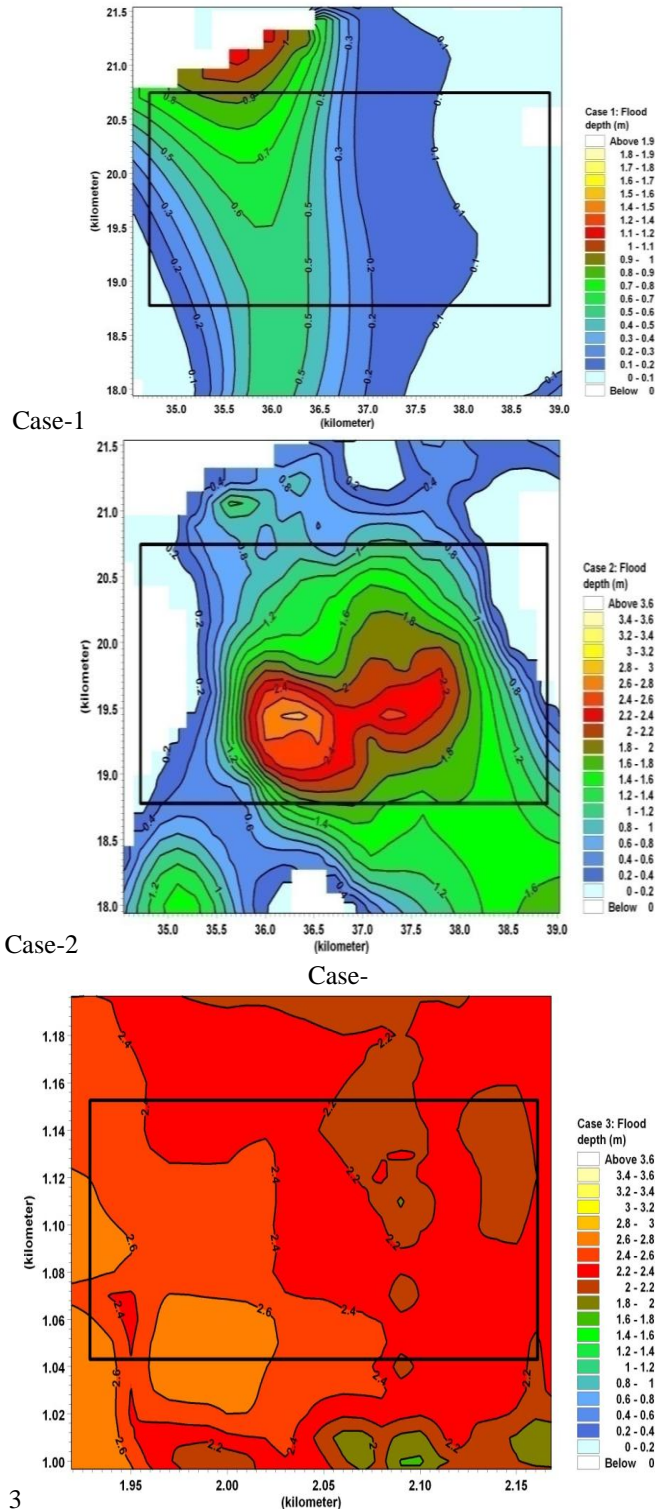
Figure 14: Maximum flood level (m) within plant site for various cases

Table-2: Inundation statistics for various cases of flooding

Case	DEM grid size	Flood elevation (m)			Inundation depth (m)		
		Minimum	Maximum	Average	Minimum	Maximum	Average
Case-1	180 m	215.34	218.06	216.3	0	0.92	0.32
Case-2	180 m	214.6	216.62	215.36	0	3.08	1.46
Case-3	10 m	213.3	216.41	215.49	0	3.32	1.72

From the table, it is observed that the maximum flood level reduces substantially when the detailed surveyed data are considered in preparation of DEM. On the other hand, appreciable increase in the maximum inundation depth is observed for DEM with detailed survey. The terrain representation through DEM is the critical input for the 2-D flood simulation. Various sources for generation of DEM include contours from standard topographical maps and detailed conventional survey of the area, DGPS survey and derived information through photogrammetric techniques from satellite/ ariel stereo-pairs. The contour interval in the standard topographical map is courser and therefore derived DEM may not adequately represent the terrain variability, particularly in the floodplains with low relief. The terrain vertical irregularity (mostly depression) smaller than half of the contour interval is not represented in the topographical maps. These depressions are the potential locations of flood storage which are ignored in the modeling. Hence, the contour based DEM overestimates the flood level while the inundation depths are underestimated. On the other hand, through detailed survey all the depressions are captured which provide additional storage for flood water and therefore the flood levels have reduced while the flood inundation depth increases as observed in Case-3. Further, the comparison of computing resources in three cases is shown in Table-3. For the courser grids of 180 m in Case-1 and Case-2, the computational time is about 2 hours while the computer space requirement is about 84 MB. When the grid size is reduced to 10 m, Case-3, the computation time is increased to 23.5 hours while the space requirement is increased to 444 MB. With 10 m grid size, though the number of grids has increased to 676 x 801 grids (instead of 426 x 331 grids in Case-1 and Case-2), the areal extent of simulation is only 5.42 ha in comparison to 1142 ha in case of Case-1 and Case-2.

Table-3: Impact of grid size on computing resource.

Case	DEM grid size	Computational extent		Computing resources	
		No. of grids Column x	Area (ha)	Memory (MB)	Time (Hr)
		Row			
Case-1	180 m	426 x 331	1142	84	2 hr
Case-2	180 m	426 x 331	1142	84	2 hr
Case-3	10 m	676 x 801	5.42	444	23.5

System configuration.: Intel(R) Core(TM), i7-2600 CPU@3.4GHz, 3.39 GHz, 2.85 GB of RAM

5. CONCLUSIONS

The flow simulation has been carried out with three DEMs; (i) 180 m grid size DEM derived from contours and spot level from 1:50,000 topographical maps, (ii) 180 m grid size DEM derived from detailed topographical survey and (iii) 10 m grid size DEM derived from detailed topographical survey. The flow conditions in three cases remained the same. It has been observed that the contour derived DEM (Case-1) overestimates the flood level while the inundation depth is underestimated. With the same grid size, when detailed topographical irregularities are included with DEM (Case-2), the estimates for the flood level and flood inundation depth improves. The base line estimates of flood level and inundation depth is considered when derived using the 10 m grid size DEM based on detailed topographical survey (Case-3). Thus though the finer grid size improves the estimation of flood characteristics, the source of DEM is also very significant. The source should be able to represent the terrain irregularities adequately. Further, when the detailed survey data is available, the reduction in grid size by 18 times (180 m to 10 m) improves the estimates of maximum flood level and maximum inundation depth by 20 cm and 24 cm respectively.

The impact of grid size on computing resource is significant. The courser grids consumes lesser storage and simulation time. The decrease in grid size by 18 times increases the computer storage by 5.3 times while the simulation time increases by about 12 times.

REFERENCES

i.   Bates PD, De Roo APJ. 2000. A simple raster-based model for flood inundation simulation. Journal of Hydrology 236: 54–77.
ii.   B.F. Sanders (2007) Evaluation of on-line DEMs for flood inundation modeling, Advances in Water Resources 30 (2007) 1831–1843
iii.   Brasington J, Rumsby BT, McVey RA. 2000. Monitoring and modelling morphological change in a braided gravel-bed river using high resolution GPS-based survey. Earth Surface Proceses and Landforms 25: 973–990.
iv.   Casas, A. Benito G., Thorndycraft V.R. and Rico M. (2006) The topographic data source of digital terrain models as a key element in the accuracy of hydraulic flood modeling, Earth Surface Processes and Landforms Earth Surf. Process. Landforms 31, 444–456 (2006) Published online in Wiley InterScience (www.interscience.wiley.com) DOI: 10.1002/esp.1278

v.   CWC (1984) Flood estimation report for upper Indo-Ganga plains (Subzone 1-e). Central Water Commission, New Delhi, India
vi.   DHI (1997) MIKE11 GIS Reference and User Manual. Danish Hydraulic Institute: Horsholm, Denmark.
vii.   DHI (2000) MIKE 21 User Guide. Danish Hydraulic Institute: Horsholm: Denmark.
viii.   DHI (2004) MIKEFLOOD 1D-2D Modelling User Manual. Danish Hydraulic Institute: Horsholm, Denmark.

ix.   Horritt MS, Bates PD. 2001a. Predicting floodplain inundation: rasted-based modelling versus the finite-element approach. Hydrological Processes 15(5): 825–842.

x.   IS:11223 (2004) Guidelines for fixing spillway capacity. Bureau of Indian Standards. New Delhi, India

xi.   Kulkarni, B. D., (2011) Generalized physical approach of estimating areal probable maximum precipitation (PMP) for plain region of the Godavari river basin (India), Journal of Spatial Hydrology Vol.2, No.2

xii.   Hosking J R M and Wallis J R (1997) Regional frequency analysis-an approach based on L-moments. Cambridge University Press, New York

xiii.   Kumar R and Chatterjee C (2005) Regional flood frequency analysis using L-moments for North Brahmaputra Region of India. Journal of Hydrologic Engineering, American Society of Civil Engineers, Vol. 10, No. 1, pp. 1-7

xiv.   Kumar R., Chatterjee C., Kumar S., Lohani A.K. and Singh R.D. (2003) Development of regional flood frequency relationships using L-moments for Middle Ganga Plains Subzone 1(f) of India, International Journal of Water Resources Management, Kluwer Academic Publishers, Netherlands, Vol. 17, No. 4, Pp. 243-257.

xv.   Mani P. Chatterjee C., Kumar R. (2014). Flood hazard assessment with multiparameter approach derived from coupled 1D and 2D hydrodynamic flow model, Natural Hazards, January 2014, Volume 70, Issue 2, pp 1553-1574.

xvi.   Nicholas AP, Walling DE. 1997. Modelling flood hydraulics and overbank deposition on river floodplains. Earth Surface Processes andLandforms 22: 59–77.

xvii.   Werner MGF. 2001. Impact of grid size in GIS based flood extent mapping using a 1D flow model. Physics and Chemistry of the Earth (B) 26(7–8): 517–522.

Flood Discharge Estimation In The Catchment Of Urbanized Lakes

Sumaiyah Tazyeen[1]   Shivakumar J Nyamathi[2]

[1]PG Student, Civil Engineering Department, UVCE, Bangalore University, Bangalore-560056, India

[2] Associate Professor, Civil Engineering Department, UVCE, Bangalore-560056, India

Email: sumaiyah_fz@yahoo.co.in   and shivakumarnyamathi@yahoo.com.

ABSTRACT: The number of the lakes in Bengaluru has fallen from 262 in 1960 to 81 in 1985 due to the rapid urbanization. As the catchment and command area becomes more urbanized, the impact of more impervious area, decreased potential for infiltration, and loss of natural depression storage has changed the response to runoff due to rainfall and thus the shape (peak and time base) of the resulting runoff hydrograph. For routing runoff through the lake, a flood hydrograph is determined.

The study area is Hulimavu lake situated in the south east part of Bengaluru of Pennar River Basin, Bellandur / Varthur Series and Madivala sub Series at an average elevation of 922 m above MSL with Latitude $12^0 52'5.88''$ N and Longitude $77^0 36'4.56''$ E. It is spread out in area of about 0.566 km^2 having a catchment area of 11.11 km^2. The lake area is being encroached for urban activities, decreasing the surcharge storage capacity thereby inundating downstream areas. Since the catchment is urbanised, the time to peak decreases, increasing the peak discharge.

1. INTRODUCTION:

A catchment's flood response to rainfall may have to be quantified for a variety of reasons. Among the most common are peak flow and flow volume estimation, flood duration, flood warning and the design of hydraulic structures. Flood estimation is inherently more difficult on smaller catchments than larger ones. Catchment characteristics, used in the estimation of flood parameters at ungauged sites, are more difficult to extract from smaller catchments; errors that escape detection will have a proportionally greater effect on the final estimate. Any flood estimation procedure in only as good as the data used in its construction. The relative deficiency of small, lowland, dry, permeable catchments in past analyses has so far meant that accepted procedures are less able to predict flood parameters accurately in such cases.

In general, estimation of floods can be done by empirical flood formulae, Envelope Curves, Rational Formula, Unit Hydrograph application and frequency analysis. For catchments with insufficient rainfall or corresponding concurrent runoff data, it is necessary to develop synthetic unit hydrograph. These are unit hydrographs constructed form basin characteristics. The Central Water Commission (CWC, 1986) recommends the use of the Flood Estimation Reports brought out for the various sub–zones in deriving the unit hydrograph for the region. These sub–zones have been demarcated on the basis of similar hydro – meteorological conditions and a list of the basins may be found. The design flood is estimated by application of the design storm rainfall to the synthetic hydrograph developed by the methods outlined in the report.

1.1.   Study area

The study area is Hulimavu lake (Fig 1) situated in the south east part of Bengaluru of Pennar River Basin, Bellandur / Varthur Series and Madivala sub Series at an average elevation of 922 m above MSL with Latitude $12^0 52'5.88''$ N and Longitude $77^0 36'4.56''$ E. It is spread out in area of about 0.566 km^2 having a catchment area of 11.11 km^2. The lake area is being encroached for urban activities, decreasing the surcharge storage capacity thereby inundating downstream areas. Since the catchment is urbanised, the time to peak decreases, increasing the peak discharge.
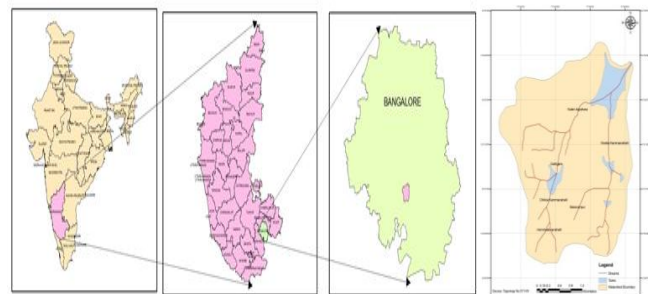

Fig 1: Location map of Study Area

In the past, this rain-fed water body was used as a storage pond primarily for agricultural purpose, fishing, drinking water source, etc., Rapid urbanization and change in the land use pattern in the surrounding vicinity has stressed the existing infrastructure facilities which has aggravated due to improper maintenance and lack of awareness. Raw sewage is getting mixed with rainwater and finding its way into the lake, polluting the groundwater. In addition, unhygienic activities are seen at several places on the foreshore of the lake and dumping of solid wastes into the lake. Change in land use pattern in the catchment area, modification in the original alignment and blockages in the inlet channels have reduced the runoff into the lake. This runoff gets diverted resulting in bringing raw sewage from un-sewered area. During peak monsoon, the water surcharges into low-lying residential areas.

2. METHODOLOGY

Flowchart gives the methodology for the Derivation of Flood hydrograph for the Study area (Fig 2).

1-hr Synthetic Unit hydrograph parameters for the derivation of Unit Hydrograph by Central Water Commission method are determined using the formulae given as

t_p =   Time from the center of rainfall excess (1.0 cm) in 1 hr unit duration to the UG peak in hours

t_r =   Unit rainfall duration adopted in specific study (hr)

T_m =   Time from the start of rise to the peak of the U.G (hr)

q_p =   Peak discharge of unit hydrograph per unit area in $m^3/s/$ sq. km

Q_p =   Peak discharge of unit hydrograph (m^3/s)

W_{50} =   Width of the U.H measured at 50% of peak discharge ordinates (hr)

W_{75} =   Width of the U.H measured at 75% of peak discharge ordinates (hr)

WR_{50} =   Width of the rising limb U.H of measured at 50% of peak discharge ordinate (hr)

WR_{75} =   Width of the rising limb of U.H measured at 75% of peak discharge ordinate (hr)

T_B =   Base width of unit hydrograph (hr)

A   =   Watershed area (km^2)

Table 1: Parameters of 1- hr Unit Hydrograph for Hulimavu Watershed

t_p	q_p	W_{50}	W_{75}	W_{R50}	W_{R75}	T_B	T_m	Q_p
(hr)	$m^3/s/km^2$	(hr)	(hr)	(hr)	(hr)	(hr)	(hr)	m^3/s
1.09	1.90	1.11	0.66	0.38	0.26	5.35	1.59	21.12

Once the unit hydrograph has been derived, the flood hydrograph is derived by the following steps.

2.1. Estimation of storm duration

The design storm duration is

$T_D = 1.1 \times t_p = 1.1 \times 1.09 = 1.2$ hrs

Adjusting the design storm duration to nearest one hour, the adopted design storm duration (T_D) is 2 hrs.

2.2. Estimation of point rainfall and areal rainfall

The point rainfall estimate for 50-yr return period and for duration of 24-hr is read against 50-yr 24-hr isopluvial map (Flood Estimation report for Kaveri Basin Subzone – 3(i)). The value of 50-yr 24-hr point rainfall is 16 cms. The design storm duration for the catchment is 2 hrs. The point rainfall estimate for 2 hrs was obtained by multiplying the 50-yr 24-hr point rainfall of 16 cms with the value of 0.53 read and interpolated from Section 4.2 of Flood Estimation report for Kaveri Basin Subzone – 3(i).

50-yr 2 hr point rainfall = 16 x 0.530 = 8.48 cm.

The above point rainfall estimate of 8.48 cm was multiplied by areal reduction factor of 0.98 corresponding to a catchment area of 11.11 km^2 and for design storm duration of 2 hrs as interpolated from Table A-3 (areal to point rainfall ratios as given in the Flood Estimation report for Kaveri Basin Subzone – 3(i)).

50-yr 2 hr areal rainfall = 8.48 x 0.98 = 8.31 cm.

Flowchart:
- Extraction of the catchment from Survey of India Topomap 57H/9C
- Determination of Physiographic parameters like Area, L, L_c Slope100
- Determination of 1-hr Synthetic Unit hydrograph parameters like q_p
- Drawing of a Synthetic Unit Hydrograph
- Estimation of Design Storm Duration T_D
- Estimation of Point rainfall and areal rainfall for Storm Duration T_D
- Distribution of Areal rainfall during the design storm duration T_D to obtain rainfall increments for unit duration intervals
- Estimation of rainfall excess units after subtraction of prescribed design loss rate from rainfall increments T
- Estimation of Baseflow
- Computation of design flood peak
- Computation of Design Flood Hydrograph

Table 2: Unit Hydrograph Ordinates of Hulimavu Watershed

W_{R50}= 0.366hr W_{R75}=0.26hr W_{50}=1.11hr
W_{75}=0.66hr   A=11.11 km^2

Sl No.	Time(hrs)	Trial 1 UHO, Q(m³/s)	(Q_n−Q_n+1)/2	Volume (4)*(n+1−n)*3600 (m³)	Depth (5)/Area (m)	Trial 2 UHO, Q(m³/s)	(Q_n−Q_n+1)/2	Volume (8)*(n+1−n)*3600 (m³)	Depth (9)/Area (m)
(1)	(2)	(3)	(4)	(5)	(6)	(7)	(8)	(9)	(10)
1	0	0				0			
2	R_B=1.2	10.56	5.28	22809.60	0.0020596	10.56	5.28	22809.60	0.0020596
3	R_M=1.32	15.84	13.20	5702.40	0.0005134	15.84	13.20	5702.40	0.0005134
4	t_m=1.6	21.12	18.48	18627.80	0.0016771	21.12	18.48	18627.80	0.0016771
5	F_M=1.98	15.84	18.48	25280.59	0.0022761	15.84	18.48	25280.59	0.0022761
6	F_B=2.31	10.56	13.20	15681.60	0.0014119	10.56	13.20	15681.60	0.0014119
7	3	6.75	8.66	21499.02	0.0019386	2.50	6.53	16220.52	0.0014604
8	4	2.75	4.75	17100.00	0.0015396	0.60	1.55	5580.00	0.0005024
9	5	0.50	1.63	5850.00	0.0005267	0.10	0.35	1260.00	0.0001134
10	T_B=5.35	0.00	0.25	315.00	2.836E05	0.00	0.05	63.00	5.672E06
					0.0119604				0.010014

Fig 3: Unit hydrograph of Hulimavu watershed

2.3. Time distribution of areal rainfall

The areal rainfall estimate for 50-yr 2 hr areal rainfall of 8.31 cm was distributed to give one hourly gross rainfall units by using the Distribution co-efficients for duration of 2 hrs from Table A-2: Time Distribution Co-efficients of Areal Rainfall (Flood Estimation report for Kaveri Basin Subzone – 3(i)) as under:

Table 3: Time Distribution of Areal Rainfall

Duration (hrs)	Distribution Co-efficients	Areal Storm Rainfall (cm)	1-hr Rainfall (cm)
(1)	(2)	(3)	(4)
2	1.0	8.31	1.66
1	0.8	6.65	6.65

Areal storm rainfall values in column (3) for durations of 2 and 1 hrs in column (1) were obtained by multiplying the 2-hr storm rainfall value of 8.31 cm with the distribution co-efficients in column (2) for respective durations. 1-hr rainfall units in column (4) were obtained by subtraction of successive values of storm rainfall from 1-hr onwards in column (3).

2.4. Estimation of rainfall excess units

Design loss rate of 0.50 cm/hr vide section 3.11 (Flood Estimation report for Kaveri Basin Subzone – 3(i)) is subtracted from 1-hr rainfall increments in column (4) of the Table 3 to obtain the 1-hr rainfall excess units as under:

Table 4: Rainfall Excess Units

Duration (hrs)	1-hr rainfall (cm)	Loss rate (cm/hr)	1-hr Rainfall Excess (cm)
(1)	(2)	(3)	(4)
1	6.65	0.5	6.15
2	1.66	0.5	1.16

2.5. Estimation of base flow

The design base flow rate vide section 3.12 (Flood Estimation report for Kaveri Basin Subzone – 3(i)) is 0.05 m³/s/sq km. Therefore, the total base flow for a catchment area of 11.11 km² = 11.11 x 0.05 = 0.56 m³/s.

2.6. Estimation of design flood (peak only)

The maximum discharge ordinate of unit hydrograph is 21.12 cumecs at 2 hrs. The maximum 1-hr rainfall excess unit of 6.15 cm was placed against the maximum discharge ordinate of 21.12 cumecs. Likewise the next lower rainfall excess unit was placed against the next lower unit hydrograph ordinate in the table 5 and so on. Summation of the products of columns (2) and (3) gives the total direct runoff to which base flow is added to get the maximum discharge.

Table 5: Direct Runoff

Time (hrs)	Unit hydrograph ordinate (m³/s)	1-hr rainfall excess (cm)	Direct runoff (m³/s)
(1)	(2)	(3)	(4)
1	15.84	1.16	18.41
2	21.12	6.15	129.85

		Total	148.26
		Base flow	0.55
		Total Peak Discharge	148.82

2.7. Computation of design flood hydrograph

The 1-hr Rainfall Excess sequence shown in column (3) of the Table-5 was reversed to obtain the critical sequence as shown in Table 6:

Table 6: Critical 1-hr Rainfall Excess (cm) sequence

Time (hrs)	Critical 1-hr Rainfall Excess (cm) sequence
1	6.15
2	1.16

3. RESULTS AND ANALYSIS

For computation of design flood hydrograph, the unit hydrograph ordinates for 1-hr interval were tabulated against time (hrs) as shown in table 7. The critical rainfall sequence of 1-hr rainfall excess units given in Table 6 were entered horizontally. The direct runoff resulting from each of the 1-hr rainfall excess units was obtained by multiplying the 1-hr rainfall excess unit with the unit hydrograph ordinates with a successive lag of 1-hr, since the unit duration of unit hydrograph is 1-hr. The direct runoffs were added horizontally to get the total direct runoff to which total base flow of 0.56 m^3/s was added to give the design flood hydrograph ordinates. The total discharge ordinates in column (7) were plotted against time in column (1) to get the design flood hydrograph as shown in the Figure-4.

Table 7: Flood Hydrograph Ordinates

Time (hrs)	UHO (cumecs)	1-hourly rainfall excess (cm)		Total Direct Runoff (cumecs)	Base flow (cumecs)	Total Flood flow (cumecs)
		6.15	1.16			
		Direct Runoff (cumecs)				
(1)	(2)	(3)	(4)	(5)	(6)	(7)
0	0	0.00	-	0.00	0.56	0.56
1	10.56	64.93	0.00	64.93	0.56	65.48
1.3	15.84	97.39	12.27	109.66	0.56	110.22
2	21.12	129.85	18.41	148.26	0.56	148.82
2.15	15.84	97.39	24.54	121.93	0.56	122.49
2.3	10.56	64.93	18.41	83.33	0.56	83.89
3	2.5	15.37	12.27	27.64	0.56	28.20
4	0.6	3.69	2.91	6.59	0.56	7.15
5	0.1	0.61	0.70	1.31	0.56	1.87
5.35	0	0.00	0.12	0.12	0.56	0.67
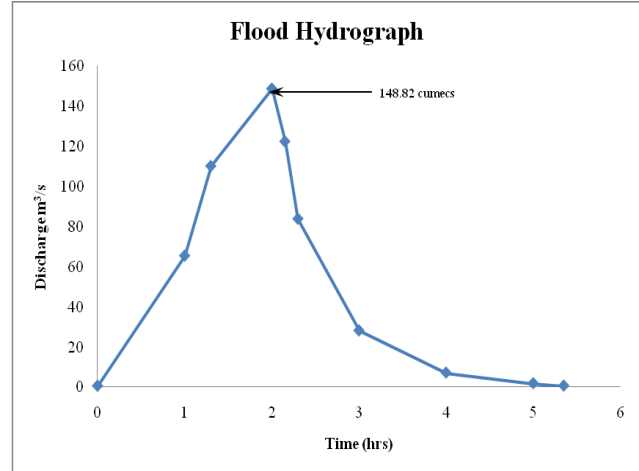
Fig 4: Flood hydrograph for the Hulimavu Watershed for 50-yr Return Period

The present paper deals with the estimation of 50-yr flood based on 50-yr design storm rainfall and Synthetic Unit Hydrograph. Besides, 25-yr and 100-yr flood can also be determined.

4. CONCLUSIONS

Peak discharges calculated from the empirical formulae namely Dickens, Ryve's, Inglis and Ali Nawaz Jung relates flood discharge to catchment areas only and effect of all other factors are included in a constant which is decided by the designer from his experience. Even intensity of the storm rainfall which is a prime factor responsible for the flood and which varies substantially from place to place is not included in the above formulae. A method of estimation of design flood peak of desired frequency knowing the physical characteristics of the catchments and design rainfall is recognised and a "systematic and sustained collection of hydro meteorological data of selected catchments in different climatic zones of India for evolution of a rational approach for determination of flood discharges" is recommended. The design discharge should be maximum flood on record for a period not less than 50 years. Where the requisite data is not available, the design flood should be decided based on the ground and meteorological characteristics obtained on the basis of design storm.

REFERENCES:

i.   Anil K. Gupta and Sreeja S. Nair (2011), "Urban floods in Bangalore and Chennai: risk management challenges and lessons for sustainable urban ecology", Current Science, Vol. 100, No. 11.

ii.   Anne K. Fleig and Donna Wilson (2013), "Flood estimation in small catchments (Report no. 60), Norwegian Water Resources and Energy Directorate, NORWAY.

iii.   CWC (1986). Flood estimation report for Kaveri basin subzone 3(i). Directorate of Hydrology (small Catchments), Central Water Commission, New Delhi.

iv.   Chow V. T., Handbook of Applied Hydrology, McGraw-Hill, New York, NY, USA, 1964.

v.   Curtis Weaver, J (2003), Methods for Estimating Peak Discharges and Unit Hydrographs for streams in the city of Charlotte and Mecklenburg County, North Carolina.

vi.   Iowa Storm water Management manual Version 2- December 5, 2008, 2C-7 Runoff Hydrograph Determination.

vii.   Jayaram Reddy P (2004). "A text book of Hydrology", 2nd Edition, Laxmi publication pvt limited, New Delhi.

viii.   National Programme on Technology Enhanced Learning, Indian Institute of Technology, Kharagpur, (2010), Module 2- The science of Surface and Ground water, Lesson 3- Rainfall-Runoff Relationships.

ix.   New Jersey Stormwater Best Management Practices Manual (2004), Chapter 5-Computing Stormwater Runoff Rates and Volumes.

x.   Ramachandra T. V and Pradeep P. Mujumdar (2009) "Urban Floods- Case study of Bangalore, Journal of the National Institute of Disaster Management", Vol.3, pp 1-98.

xi.   Scott A. Olson (2008), "Estimation of Flood Discharges at Selected Recurrence Intervals for Streams in New Hampshire", U.S. Geological Survey.

Flood Disasters In Uttarakhand – A Critical Assessment

Rajendra Chalisgaonkar

General Manager, Uttarakhand Project Development and Construction Corporation Ltd., Dehradun-248001, Uttarakhand.
E-mail: chalisgaonkar@yahoo.com

ABSTRACT:*India is one of the most densely populated countries in the world with over one billion people and it is vulnerable to numerous natural hazards, particularly earthquakes, floods, droughts, cyclones, and landslides. Uttarakhand was formed on November 9, 2000 to become the 27th State of India. It is predominantly a hilly State, having international boundaries with the People's Republic of China in the north and Nepal in the east. The monsoon in June 2013 arrived almost two weeks earlier than expected in Uttarakhand, cloud bursts and heavy to very heavy rainfall hit several parts of the higher reaches of the Himalayas. This unprecedented rainfall resulted in a sudden increase in water levels, giving rise to flash floods in the Mandakini, Alaknanda, Bhagirathi and other river basins, also causing extensive landslides at various locations. Continuous rains caused Chorabari Lake to rise and the Lake's weak moraine barrier gave way and a huge volume of water along with large boulders came down the channel to the east, devastating the towns of Kedarnath, Rambara, Gaurikund and others in its wake. The districts of Bageshwar, Chamoli, Pithoragarh, Rudraprayag and Uttarkashi were most affected. The paper discusses in detail the damages caused due to floods in the State, specially in Rudraprayag and Uttarkashi districts in Mandakini and Bhagirathi Valleys and reasons of damages and outlines the strategy for expanded monitoring of floods, improved mitigation measures, and effective communication with civil authorities and vulnerable populations to reduce loss of life in future flood events in the context of State of Uttarakhand.*

1.0   INTRODUCTION

Disasters are, probably, as old as mankind. Shaluf(2007) presents a detailed classification of disasters. The disasters have been classified into natural (resulting from natural forces), man-made (resulting from human-decisions), and hybrid (resulting from both natural and man-made causes). They further classify natural disasters into those resulting from the phenomena beneath the earth of the surface (e.g. earthquakes, tsunamis, volcanic eruptions etc.) and at the Earth's surface (landslides and avalanches). Then, there are disasters resulting from meteorological/hydrological phenomena (e.g. Windstorms: cyclones, hurricane, typhoons; tornados; floods, drought, heat wave), and biological phenomena (e.g. epidemics, infestations). Man-made disasters can further be classified into socio-technical and warfare disasters. The socio-technical disasters can occur in at least four types of situations i) technological (e.g. gas leakage, fire during an industrial activity), ii) transport failure (e.g. air crash, road/train accident etc.), iii) stadia and other public place failure (e.g. fire, structural collapse, crushing etc.), and iv) production failure (e.g. computer system failure, usage of defective product etc.). The warfare disasters are further classified into inter-state conflict and international conflict which can further include non-conventional (chemical, biological, nuclear) wars. Hybrid disasters are the result of natural forces and human actions (e.g. excessive deforestation causing soil erosion and subsequently heavy rain causing landslides; floodplain disasters). They also mention subsequent disasters which result from natural and/or man-made disaster (e.g. landslides and dam collapse following heavy rain and flooding).

In the last few years, India has witnessed many natural disasters (Tsunami, earthquakes, floods, cyclones etc.) and is at risk to man-made disasters (fire, stampedes, etc.) as well. These disasters, natural, man-made or hybrid, typically, result in a large number of casualties along with societal agony and a huge economic loss.

1.1   Flood Disasters

Floods are a serious problem in many river basins throughout the world, particularly in the monsoon and typhoon areas of South East Asia. In Asia as a whole, floods are said to destroy about 4 million hectares of crops every year and the lives of some 17 million people are affected. It has been estimated that annual flood losses in some countries are 40 times more today than they were in the 1950s. According to the Indian Government, one out of every 20 people in the nation is vulnerable to flooding and in China over 85 per cent of the population is concentrated on alluvial plains or basins along river courses which comprise one third of the total land area.

In recent years, floods seem to have been very much more destructive than usual. In 1978, India was struck by some of the worst floods in its history. Thousands of villages were flooded. Crops were damaged on millions of acres of farmland. Hundreds of people were drowned, millions were made homeless while damage to property and livestock is said to have run into billions of dollars. In 1981, China was also devastated by record floods. In July and August of that year, 53 cities, 580 towns, 2,600 factories and vast areas of agricultural land were submerged in Sichuan Province. Houses containing 1.6 million rooms were destroyed; 1,000 people were killed and nearly 30,000 injured; and the cost of the damage to property was estimated at over a billion dollars. That very same year, floods ravaged neighbouring Shaanzi Province – causing the death of 764 people, injuring 5,000 people, destroying 160,000 houses, washing away 230 villages and leaving 200,000 people homeless. In 2012, besides India, many countries have witnessed severe floods including China, Myanmar, Philippines, USA, etc.

The Himalayas are one of the youngest mountain ranges on earth and represent a high energy environment very much prone to natural disasters. High relief, steep slopes, complex geological structures with active tectonic processes and continued seismic activities, and a climate characterised by great seasonality in rainfall, all combine to make natural disasters, especially water-induced hazards, common phenomena. Flash floods are among the more devastating types of hazard as they occur rapidly with little lead time for warning, and transport tremendous amounts of water and debris at high velocity. Flash floods affect thousands of people in the Himalayan region every year – their lives, homes, and livelihoods – along with expensive infrastructure

In India, the continuing torrential rain on 16th August 2012 in the Rajasthan State wrecked havoc as the railway track got washed away near Nokhada railway station on Bikaner-Phalodi route. The fate of passengers of Jaisalmer-Lalgarh Express can be imagined by looking at Fig. 1, but surprisingly no casualty was reported in the accident. The heavy rains on 15th August 2014 filled the Sukhatal, Nainital and many buildings were partially submerged forcing the people to vacate their houses and take shelter at safety places.

Fig. 1 – Railway Track Washed Away

Fig. 2 – Sukhatal, Nainital on 15th Aug. 2014

2.0 FLOODS IN UTTARKASHI IN 2012

Uttarkashi district of Uttarakhand is situated on the banks of Bhagirathi at an altitude of 1352 m above the sea level. Most of the terrain is hilly and becomes inaccessible during landslides and snowfall. The Yamuna and the Ganga are the biggest rivers in Uttarkashi district. The incidents of Natural disaster like Cloud bursts, flash flood has happened before in this district. In the year 1978 and 1980 the district got affected by the could burst, followed by an earthquake in the 1991 which took 2000 lives, and 2002-03 major land slide tormented the people in the district.

In the worst tragedy to hit Uttarkashi in more than 30 years, a cloud burst in the middle of Friday night on 4th August 2012 triggered landslides and flash floods, which destroyed hundreds of homes in the Uttarkashi area. The cloud burst swept away bridges and a large chunk of the Gangotri national highway. 31 people lost their lives and at least 40 feared missing in the flash floods. Nearly 2000 people were affected in the floods and about 200 families were evacuated from low lying regions of Uttarkashi and moved to higher ground. Twenty three workers of the state-run UJVN Ltd Assi Ganga hydroelectric project, who went missing early in the morning of 4th August following a cloud burst in the upper hills of Uttarkashi district, were declared dead.

3.0 FLOOD DISASTER IN JUNE 2013 IN UTTARAKHAND

Uttarakhand comprises of 13 districts that are grouped into two regions: Kumaon and Garhwal, and has a total geographical area of 53,484 km². The economy of the State primarily depends on agriculture and tourism. The State is home to some of the most important pilgrimage centres known as the **Char-Dham**, i.e. the Gangotri, Yamunotri, Kedarnath and Badrinath. The monsoon in June 2013 arrived almost two weeks earlier than expected in Uttarakhand. Recent climate changes have had significant impact on high-mountain glacial environment. Rapid melting of snow/ice and heavy rainfall has resulted in the formation and expansion of moraine-dammed lakes, creating a potential danger from dammed lake outburst floods. On 16th and 17th June 2013, heavy rains together with moraine dammed lake (Chorabari Lake) burst caused flooding of Saraswati and Mandakini Rivers in Rudraprayag district of

Uttarakhand. Prolonged heavy down pour on 16 and 17 June 2013 resembled 'cloud burst' (except for amount of precipitation of 100 mm/h) type event in the Kedarnath valley and surrounding areas that damaged the banks of River Mandakini for 18 km between Kedarnath and Sonprayag, and completely washed away Gaurikund(1990m asl), Rambara(2740m asl) and Kedarnath(3546m asl) towns. The roads and footpath between Gaurikund and Kedarnath were also damaged. There are reports of loss of large number of human lives and damage to the property and livestock. The Chorabari Lake(3960m asl) also known as Gandhi Sarovar Lake is a snow melt and rain fed lake, located about 2 km upstream of Kedarnath town which is approximately 400 m long, 200 m wide having a depth of 15–20 m. The bursting of this lake led to its complete draining within 5–10 minutes as reported by the eye witnesses. The heavy rainfall together with melting of snow in the surrounding Chorabari Lake washed off both the banks of the Mandakini river causing massive devastation to the Kedarnath town. The meteorological observatory of Wadia Institute of Himalayan Geology, Dehradun at Chorabari Glacier camp recorded 210 mm rainfall in 12 hours between 15th June (5:00 p.m.) and 16th June (5:00 a.m.) 2013. On 16th June 2013 alone (from 5:00 a.m. to 5:00 p.m.), 115 mm rainfall was recorded, causing 325 mm rain in 24 hours.

The districts of Bageshwar, Chamoli, Pithoragarh, Rudraprayag and Uttarkashi were most affected. This region is one of the most important pilgrimage circuits in India. Since the disaster coincided with the peak tourist and pilgrimage season, it significantly increased the number of casualties, missing, and affected population. A total of 580 human lives were lost; over 5,200 people are reported missing; 4,200 villages were affected; 9,200 cattle/livestock were lost; about 3,320 houses were fully damaged; about 995 public buildings were damaged; close to 9,000 km of roads were affected; and 85 motor bridges and 140 bridle bridges were damaged. This event also left over 70,000 tourists and 100,000 local inhabitants stranded in the upper reaches of the State. Landslides and toe erosion by the sediment loaded rivers damaged roads/highways at many locations and washed away multiple bridges (steel girder, beam and suspension bridges). Traffic was disrupted along all national highways and link roads in the region, along with the disruption of telecommunication lines, all adding to the impact of the disaster. Many hotels, rest houses and shops around the temple in Kedarnath were completely destroyed. The before disaster and after disaster pictures shown in Fig. 3 are self-explanatory. The post-flood image on Bhuvan (ISRO'a geoportal) was acquired on 21th June, 2013. Zooming into the Kedar valley area highlights the disturbances and flooding that have occurred north of the region, including the emergence of a new stream (number 3 in the image) which has cut across a green patch. The water brought down a lot of debris towards Kedarnath and further down into the Mandakini river, causing the major disaster. Fig. 4 depicts the photographs of Kedarnath area before and after June 2013 disaster.

Before   After
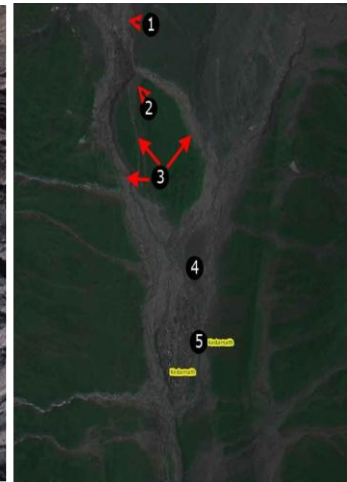
Before

1. Water comes from glacier in a single stream.
2. Large amount of debris lies on the path of this water.
3. Water moves down in two streams.
4. Water moves along in thin channels

After
1. The channel of water has now become broader.
2. The debris in its path has disappeared.
3. A new third stream of water has formed.
4. Large amount of water has moved into the area from all directions.
Devastated

Kedarnath settlement

3.1 Effect of Disaster in other Areas

Due to heavy precipitation on 16th – 17th June 2013 in the State of Uttarakhand, many rivers got unprecedented heavy floods, resulting in catastrophic destructions in the five hilly districts of the State resulting in heavy loss of life of people and animals, property and other infrastructural developments including Canals, Tube wells, Lift Canals, Flood protection Works, Pump Houses etc. of the State Irrigation Department and washed away several hectares of fertile agricultural land along the banks of the river. Fig. 5 shows the damaged view of famous Kalimath Temple during the disaster and its restoration after the disaster. Fig. 6 shows the confluence of river Mandakini and river Alaknanda before the disaster and rise in bed level near the confluence and shifting of confluence of river Mandakini and river Alaknanda at Rudraprayag after the disaster. Fig. 7 shows the erosion of river banks and damaged building in Tilwara and Sumari areas of Distt. Rudraprayag. Fig. 8 depicts three pictures of a bridge in different span of time in Uttarkashi town. Bank erosion and damaged buildings in Distt. Pithoragarh have been depicted in Fig. 9.
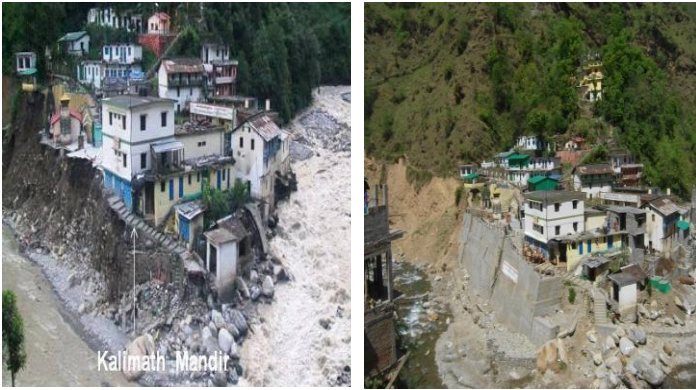
Fig. 5 – Damaged View of Kalimath Temple, Rudraprayag and View after Restoration

Fig. 6 – Confluence of river Mandakini and Alaknanda at Rudraprayag, before and after June 16, 2013 Disaster
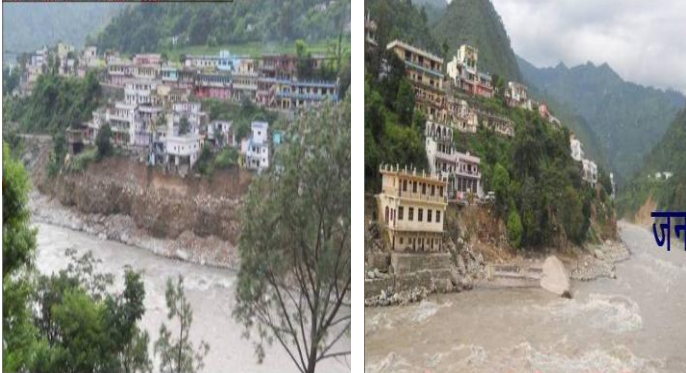
Fig. 7–Damages at Sumari and Tilwara, Distt. Rudraprayag in June 2013

Fig. 8–Damaged Bridge in Uttarkashi Town in June 2013

Fig. 9–Damages in Distt. Pithoragarh during flood of June 2013

4.0   NECESSITY OF REVISING THE GUIDELINES OF HYDRAULIC STRUCTURES

For the design of hydraulic structures and river training works e.g. bridges, barrages, culverts, groynes, guide bunds, revetments etc., a number of codes are referred to by the planners and designers. Bureau of Indian Standards(BIS) and Indian Road Congress(IRC) codes are being followed in the water resources sector and road sector respectively. These Indian codes/guidelines are treated almost like bible and the designers have hardly any freedom to deviate from the provisions made in the codes. Although the codes are being reviewed and updated from time to time, very little changes have been made in these codes/guidelines. However, fundamental changes in many of these codes/guidelines are needed in view of the recent developments in the disciplines like hydrology, hydraulic engineering, river mechanics and sediment transport. Understanding of river morphology and river mechanics is essentially needed for efficient planning, design, construction and maintenance of river training and scour protection and for formulation of the relevant codes accordingly. Mazumder(2005) has pointed out several deficiencies in the codes, issued by Indian Road Congress, New Delhi and Bureau of Indian Standards, New Delhi, related to hydraulic design of bridges, barrages, river training works etc.

5.0   FLOOD HAZARD MITIGATION: GOALS AND OBJECTIVES

The following goals articulate that commitment and provide a sense of direction to govern decisions and activities that may affect risk faced by the people residing in flood prone areas. While not all of the goals stated will be attainable in the short term, they nevertheless serve as a set of guiding principles by which future choices can be shaped. These goals will also set the framework as criteria for evaluating proposed mitigation actions.

5.1   Goal One: Reduce loss of life and personal injury from flooding

Its fundamental objective is to minimize the human loss and suffering resulting from terrestrial flooding events. This implies the need for enforcement of strict standards for siting and construction, as well as regulation of land uses and

development in flood-prone areas. Food hazard mapping(Fig. 10) is used to determine the areas susceptible to flooding when discharge of a stream exceeds the bank-full stage. Using historical data on river stages and discharge of previous floods, along with topographic data, maps can be constructed to show areas expected to be covered with floodwaters for various discharges or stages.
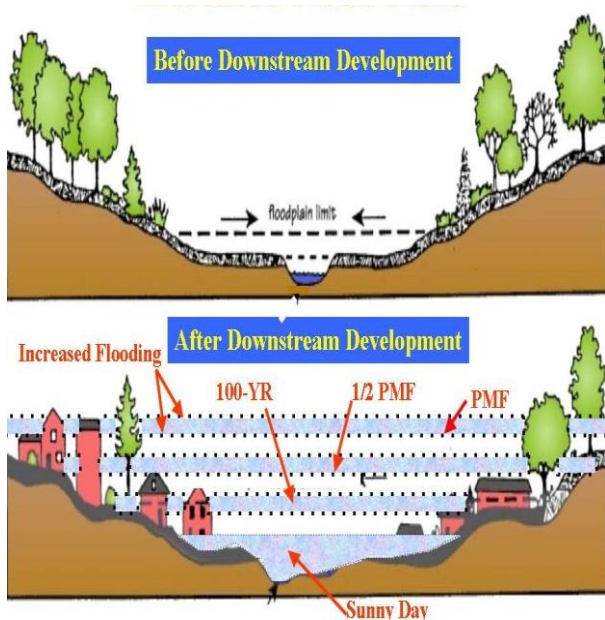
Fig. 10 – Flood Risks: Before and After Downstream Development in Flood Prone Areas

5.2 Goal Two: Reduce economic damages and social dislocation from flooding

This goal suggests a range of possible public actions, beginning with fundamental reforms of the planning and management of major public sector facilities management agencies. In this goal we aim to reduce the flooding-related costs of unwise government and private management practices. This Goal includes number of related Objectives:

• Reduce damages to existing development from flooding.
• Reduce damages to future development from flooding.
• Reduce damages to present and future development financed by public funds.
• Reduce public expense for response and recovery services following flood events
• Preserve, enhance and restore features of the natural environment.

5.3 Goal Three: Integrate effective flood hazard mitigation activities

This goal requires that the institutions planning, controlling and monitoring development be upgraded in their activities to assume Flood Hazard Mitigation functions. A major secondary focus of this goal will be to capacitate agencies and permitting

authorities in addressing the special needs of flood hazard mitigation.

• Incorporate Flood Hazard Standards in All Relevant Government Regulations
• Train Government Institutions and Staff in Flood Hazard Mitigation Standards.
• Provide Flood Hazard information to all property owners.

5.4 Goal Four: Develop a Flood Risk Management Cycle
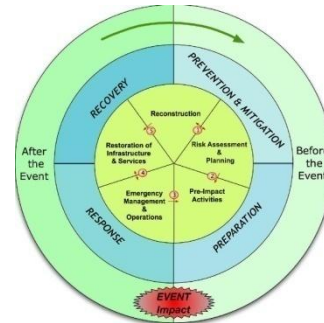
Fig. 11 – Flood Risk Management Cycle

Flood risk management cy[...]
flood risk management fo[...]
preparedness, including fl[...]
systems. Figure 11 presen[...]
management cycle. Statisti[...]
needed for formulating floo[...]
flood disaster management [...]
recovery phase in the schem[...]
be prepared on the basis of [...]
mitigate the effect of floods.[...]

6.0 CONCLUSION

Data from the past quarter of a century suggest that floods have exacted a significant toll on the human population when compared to other natural disasters, particularly in terms of the size of affected populations. However, human vulnerability to floods is increasing, in large part due to population growth, urbanisation, land use change, and climatological factors associated with an increase in extreme rainfall events. In future, the frequency and impact of floods on human populations can be expected to increase. Additional attention to preparedness and mitigation strategies, where the majority of floods occur, can lessen the impact of future flood events.

The State of Uttarakhand witnessed large scale destructions due to floods on 16th and 17th June 2013 and damaged infrastructural developments paralyzing the life in hilly districts. The paper has presented in detail the damages caused due to floods in the State, specially in Rudraprayag and Uttarkashi districts in Mandakini and Bhagirathi Valleys and reasons of damages and mitigation measures so that the damages due to floods can be minimized in future in the context of State of Uttarakhand. It is therefore essential to assess as precisely as possible the probability that a similar event occurs again in a given delay and it is therefore the need of the hour to prepare for the next floods, by engaging investigations and collecting the data that can improve the knowledge of the formation conditions of such phenomena.

7.0 REFERENCES

i. Chalisgaonkar R. et al(2002) "Emergency Preparedness for Dam Disaster Floods", National Seminar on Water & Environment -

Issues and Challenges, Indian Water Resources Society and WRDTC, IIT, Roorkee, October 12-13.

ii.   Chalisgaonkar R., Mukesh Mohan and Singh, Sanjay(2011) "Flood Hazard Mitigation-Issues and Challenges", Workshop on Disaster Remedial Measures & Impact on Roads and Infrastructure in Himalaya Region(DRMIRIHR), The Institution of Engineers(I), Uttarakhand State Centre, Dehradun, October 23.

iii.   Mazumder, S.K.(2005) "Training River near Hydraulic Structures", National Conference on Hydraulics and Water Resources Engg., HYDRO-2005, Indian Soc. for Hydraulics at SIT, Tumkur, Dec.8-9.

iv.   Purohit Jyoti and Suthar C. R.(2012) "Disasters Statistics in Indian Scenario in the Last Two Decade", International Journal of Scientific and Research Publications, Volume 2, Issue 5, May 2012

v.   Shaluf, Ibrahim Mohamed(2007),"Disaster types", Disaster Prevention and Management Journal, Vol. 16 Issue: 5.

vi.   (1989) "River behaviour, Management and Training", Publication No.204, Vol. I, Central Board of Irrigation and Power(CBI&P), New Delhi.

vii.   (1997) "Guidelines for Design and Construction of River Training Works for Road Bridges", IRC:89, The Indian Road Congress, New Delhi

viii. (2008) "National Guidelines for Flood Management", National Disaster Management Authority, New Delhi, January.

Best Practices On Flood Management Planning

Dr. Rajshree Kamat[1]   Vinay Kumar[2]
[1]Assistant Professor, Maulana Azad National Institute of Technology, Bhopal-462003, India
[2]M.Plan. III Sem. Department of Architecture & Planning, Maulana Azad National Institute of Technology, Bhopal-462003, India
Email: kamatrajshree@yahoo.co.in, +91 9179732524

ABSTRACT: *It is believed that most of the ancient civilizations were lost due to frequent floods. Thus it is necessary to discuss flood management practices on global level. Today, with rise in population and evolution of human societies, the degree of human intervention in nature is at pinnacle and one of the most hazardous impacts is climate change which can cause frequent floods throughout the globe. However, with advancement of science and technology, various flood protection measures are developed all around the globe but it is practically impossible to provide 100 per cent protection to flood prone areas from all kinds and magnitudes of floods. Also, it is not economically feasible to plan and design flood proof cities and to maintain them. Even our well planned urban cities are today suffering from urban floods. Flood forecasting can help mankind to survive tolerable to worst kind of floods. In this paper we discuss that the best practices of flood management are achieved through the combination of flood forecasting techniques and flood protection measures. As climate change is a dynamic process hence only structural measures like construction of reservoirs, parallel channel, embankments and diversion of flood water to water scarce areas, use of new construction materials etc. cannot prevent us from floods. We need the non-structural measures like the modernisation of flood forecasting network and its extension to other areas, automatic reservoir release information system, basin-wise integrated flood management approach, use of GIS system and remote sensing technologies to study the real time behaviour of climate, along with the techno legal amendments wherever required.*
Keywords: *Flood, climate, disaster, economic, magnitude, urban flooding.*

1. INTRODUCTION:

Earlier, floods were considered as natural disaster. Increasing interventions in nature by human activities results in change in climate which causes frequent flood and it becomes human induced disaster. Floods destroy human heritage and jeopardize sustainable development, which can be defined as "non-decreasing quality of life" (Kundzewicz 2002). Apart from social and economic impacts floods disturbs the network of interactions among organisms, and between organisms and their environment called as ecosystem (Schulze 2005). In comparison with other natural disasters worldwide (earthquakes, droughts, wind storms, volcanoes, landslides/avalanches, forest fires, technical disasters) floods have the largest damage potential of all and affect the largest number of people (Frank Friesecke 2004). Flooding causes over one third of the total estimated costs and is responsible for two-thirds of people affected by natural disasters (UN, 2004). During last two decades economic losses are tremendous compared to previous decades especially in developing countries. This is due to encroachment of flood plains with growing developmental and economical activities, rapid increase in population and urbanisation with centralisation etc. Apart from inadequate carrying capacity of river which is causing flood, flooding in cities, towns or urban areas is also a debateable topic. Urban floods occur due to heavy rainfall in short interval of time, encroachment of waterways, inadequate capacity of drainage system and lack of maintenance of the drainage infrastructure.

Structural measures for flood protection are in practice from a very long time and are found effective in many cases but with change in climate and dynamic behaviour of nature these practices become inadequate. Thus in order to maintain sustainable development we need the non-structural measures like the modernisation of flood forecasting network and its extension to other areas, automatic reservoir release information system, basin-wise integrated flood management approach, use of GIS system and remote sensing technologies to study the real time behaviour of climate, along with the techno legal amendments wherever required.

2. BEST PRACTICE ON FLOOD MANAGEMENT PLANNING:

2.1 STRUCTURAL MEASURES AND THEIR IMPACTS:

Flood events of the recent past have shown the vulnerability of the flood protecting structures and that of the emergency organisations in some cases. The performance of the defences could be extended successfully by appropriate countermeasures such as the erection of temporary heightening and supporting structures to avoid over-topping, to stability loss and hydraulic failure of the foundation soil of the defences. On the other hand, efficient dams and dykes cannot provide reliable safety against floods which exceed their designed capacities. Contrary to this, near dam or dyke-protected areas, a false sense of security is given to populations and properties encouraged locating on surrounding floodplains, thus causing disasters. Nevertheless, even after all the non-structural measures have been implemented there is still a natural risk of floods that might be reduced by means of technical flood protection. Different aspects of some of the important measures for flood management are enumerated below:

2.1.1 Dams, Reservoirs and Other Water Storages:
Dams, Reservoirs and other water storages which can be natural or man-made are effective means of reducing flood peaks in the river. Using these structures we cannot mitigate the risk of floods but the intensity and timing of the incoming flood can be delayed.
There are several problems associated with these structures, such as:
(i) Large dams and reservoirs have potential to contain huge damage.
(ii) If there is uncoordinated water release from multiple reservoirs at the same time then it may cause unnecessary flooding.

2.1.2 Embankments:
Embankments are the cheap, quick and most popular method of flood protection. Construction of embankments had been done from ancient period and now also used in many countries with improved construction material. Embankments confine the flood flows and prevent spilling, thereby reducing the damage.
Problems associated with use of embankments as flood protection measure:
(i) Erosion problem of embankment system.
(ii) It is not economically feasible to provide embankments for longer course of river.
(iii) Some embankments have, in certain reaches of the river, aggravated the flood problem by rising river bed levels, decreasing their carrying capacity, causing drainage congestion in the
Countryside and distorting the levels/gradient of the outfall points.

2.1.3 Channelization of rivers:
Channelization of rivers is used in the context of tackling the extensive meandering problems of the rivers, activating navigational channels and training these rivers into their original courses. While venturing to channelize rivers, thought must be given in allowing the river certain freedom to flow and right of way to pass its flood waters and silt load within its

natural waterway. There are several demerits and problems associated with river channelization such as:
(i) Loss of wetlands which are an excellent habitat for many forms of wildlife, and additionally serve as "filter" for much of the world's surface fresh water.
(ii) Channelization of rivers may cause increase in soil erosion and increase flooding downstream from the channelized area, as larger volumes of water traveling more rapidly than normal can reach choke points over a shorter period of time than they otherwise would, with a net effect of flood control in one area coming at the expense of greatly aggravated flooding in another.

2.1.4 Channel improvement:
The method of improving the channel by improving the hydraulic conditions of the river channels by desilting, dredging, lining etc., to enable the river to carry its discharges at lower levels or within its banks has been often advocated but adopted on a very limited extent because of its high cost and other problems.

2.1.5 Drainage improvement:
Basic causes of urban flooding are encroachment of waterways, inadequate capacity of drainage system to carry the storm water discharge within a reasonable period and lack of maintenance of the drainage infrastructure in our cities and towns. Thus, improvement of drainage by construction of new channels or improvement in the discharge capacity of the existing drainage system is recommended as an integral part of the flood management programme.
The main problem associated with this is that it is often difficult to distinguish between flood and drainage congestion situations. Stress should be made on improving the natural drainage system as construction of man-made drainage system to carry storm water discharge may not be economically feasible.

2.1.6 Diversion of Flood waters:
Floods can be controlled by redirecting excess water to purpose-built canals or floodway, which in turn divert the water to temporary holding ponds or other bodies of water where there is a lower risk or impact to flooding. This measure can be used to manage unusual floods around cities.

2.1.7 Flood Proofing:
Flood proofing consists of activities to modify buildings, their sites or contents to keep water out or to reduce the damage caused by water entry. Dry flood proofing consists of activities designed to keep water out of a building, i.e., the inside stays dry. Wet flood proofing consists of measures designed to limit the damage done by water, usually by using water resistant materials and construction techniques. New and existing structures can be flood proofed.
Some of the more common flood proofing measures includes:
(i) Backflow valves

(ii) Closures on doors, windows, stairwells and vents--they may be temporary or permanent

(iii) Elevating structures via landfill, walls, posts, piers, jacks and beams

(iv) Rearranging or protecting damageable property--e.g., relocates or raises utilities

(v) Ring walls and levees around structures and utilities

(vi) Sump pumps and sub-drains

(vii) Water resistant material; metal windows, doors and jambs; waterproof adhesives; sealants and floor drains.

2.1.8 Watershed Management:

A watershed is the divide between two drainage streams or rivers separating rainfall runoff into one or the other of the basins. In recent years, the term has been applied to mean the entirety of each of the basins, instead of just the divide between them (California Watershed Program). The Watershed Management measures comprises of prevention of soil erosion by developing and conserving the vegetative and soil covers as well as to carry out structural works such as check-dams, diversion canals, channel improvement etc. In the watershed management of upper catchment, land treatment through afforestation and grass land development practices should be supplemented by structural works for retarding the water velocity and arresting silt. The idea of "catching water where it falls" can be implemented by such measures as enhancing storage of water on the land surface, or underground, e.g. by infiltration (cf. Kundzewicz and Takeuchi 1999).

Even after implementation of structural flood protection measures it is practically impossible to provide 100 per cent protection to flood prone areas from all kinds and magnitudes of floods. Also, it is not economically feasible to plan and design flood proof cities and to maintain them. Even our well planned urban cities are today suffering from urban floods. As many structural flood protection measures are associated with several problems as discussed above hence a pragmatic approach in flood management is to provide a reasonable degree of protection against flood damages at economic cost through a combination of structural and non-structural measures.

2.2 FLOOD EMERGENCY:

2.2.1 Flood Preparedness Measures:

Flood preparedness plan is a series of sub-plans, including emergency response planning and training, raising public awareness, flood forecasting and warning, setting development policy, land use regulation, flood proofing, setting alternative plans, and local social structure strengthening.

Individual preparedness planning is based on raising public awareness. Realistic treatment of flooding related problems is a prerequisite for building confidence, as compared to pictures that may be portrayed by media and government officials. Confusion during evacuation, disruption of daily routine, strain on families removed from their homes, distress, altered social relationships, loss of feeling of security, personal vulnerability and many others are real psychological issues that need to be

addressed in this planning stage and treated as inevitable events and a quite normal behaviour.

2.2.2 Emergency Response Measures:

Emergency response can be considered as a series of sub-plans that address communication and public information management, search and rescue co-ordination, shelter management, stockpiling and distributing of food and supplies, contacting and requesting additional support, debris management, financial management, volunteers co-ordination and donations management.

The foundations of a flood emergency action are a mobilisation plan, comprehensive disaster plan and well-co-ordinated and trained flood fighting corps. Organisation and training of search and rescue teams are done locally, regionally or nationally but in real flood conditions, participation of volunteers, citizens and relatives is significant, thus requiring the co-ordination to develop as the action proceeds.

2.3 PUBLIC AWARENESS, PUBLIC PARTICIPATION AND INSURANCE:

2.3.1 Public awareness:

Problems associated with floods are often not sufficiently recognised and acknowledged. Communication plan to offer individuals an understanding of the nature and scope of these risks should be developed. Regional and municipal authorities will see to its continued and permanent implementation at the regional and local level in order to involve owners and administrators of properties, including organisations at levels of regions, districts, municipalities or individuals, and enable them to take preventive and protective actions by themselves and offer their opinions about the implementation of preventive measures for reduction of flood damages.

2.3.2 Direct public involvement:

All measures linked to public information and awareness raising are most effective when they involve participation at all levels. Public participation in decision-making is a cornerstone of successful implementation of integrated and comprehensive action plans, both to improve the quality and the implementation of the decisions, and to give the public the opportunity to express its concerns and to enable authorities to take due account of such concerns.

2.3.3 Flood Insurance:

Existence of appropriate scheme of insurance, that is distribution of risk and losses over a high number of people and long time, is an important component of flood preparedness strategies (Menzel and Kundzewicz 2003). Flood insurance is a complementary tool of hazard reduction. The purpose of flood insurance is to provide compensation for losses caused by flood when damages are not avoidable at acceptable cost. In most countries coverage is fragmented and property owners have to purchase different policies in order to insure against all major disasters.

Flood Insurance is more popular in developed countries and is difficult to implement in developing countries due to many

reasons. First, accurate flood zoning and depth-damage relationship have to be prepared to determine the risk of flood damage and corresponding premium. Second, insurance agencies are not well developed in the LDCs and these companies face the `adverse location' problem (Faisal, Kabir and Nishat 1999).

2.3.4 Rehabilitation Measures:

Post-flood management problems can be pre-planned. In order to achieve this, objective surveys need to be carried out during the flood for preparing the situation report covering human casualties and material damage. These surveys are needed for making decisions on the actions during the immediate emergency and in the period that follows. Later on, a thorough study needs to be made in order to perform a formal assessment of the damage.

Rehabilitation is providing services and facilities that will restore the former living standard and encourage adjustments to changes caused by the flood. Restoring morale is one of the most important factors in rehabilitation. Rehabilitation should be carried out separately for the flood victims and the disturbed public services.

2.4 LAND USE, ZONING AND RISK ASSESSMENT:

3.2.1 Flood Plain Zoning and Relocation:

With increase in population and spurt in economic development, more and more area has been occupied in the flood plains, mainly because of numerous advantages the proximity of river offers in developmental efforts (Rajshree K. and Ashutosh S. 2007). During heavy rainfalls, it is natural for a river to overflow its banks and spill into flood plains which are basically its domain. Thus it is the responsibility of governance system to delineate the flood plains to avoid any development activities in those areas and further relocate the damageable structures out of the flood plain. The hydrological effect of relocation is generally small, but could be significant if major flow obstructions are removed, in which case the channel capacity and routing criteria may be modified. The basic concept of flood plain zoning is to regulate land use in the flood plains in order to restrict the damage due to floods, while deriving maximum benefits from the same.

3.2.2 Risk Assessment:

Risk assessment is the determination of quantitative or qualitative value of risk related to a concrete situation and a recognized threat (also called hazard). It means improve knowledge concerning extent and evolution of floods and water related problems, simulate different high water incidences, study and compare zoning scenarios, and integrate this risk assessment, via identification and mapping of hazards and high-risk areas into land-use, emergency and rescue planning policies. Simultaneously, this would allow assessing effectiveness, thus priority of the flood protection measures along the whole longitudinal profile of a river, in view of informing the frontage population of the potential risks including remaining risks that occur, for example, as a result of a dam break. High level of risk combined with low levels of

coping mechanism result in major disruption of loss of lives and livelihood (Rajshree K. and Ashutosh S. 2007).

2.5 EARLY WARNING AND FLOOD FORECASTING SYSTEM:

2.5.1 Flood Forecasting:

The magnitude and severity of the floods, caused by excessive rainfall in the river catchments, depend upon the nature and extent of rainfall and the characteristics of the specific watersheds. For example, intense and shorter duration rainfall or cloud burst in small steep catchments or in hilly catchments results in flash floods of shorter time periods, whereas the heavy rainfall of longer duration in the large catchments may generate the floods which sustain for longer periods. Suitable real time flood forecasting techniques are required to forecast such floods. The accurate real time flood forecasts are required to be issued well in advance in order to provide sufficient time, known as lead time, for evacuating the people from the areas likely to be affected by the flood. The lead time available for flash flood forecasts are very small. It makes the implementation of evacuation plan very difficult during the flood.

The techniques available for real time flood forecasting may be broadly classified in four groups: (i) deterministic modelling, (ii) stochastic modelling, (iii) statistical modelling and (iv) computational techniques like Artificial Neural Network (ANN) and fuzzy logic.

The deterministic models are based on either index catchment models or conceptual catchment models. Such models tend to simulate the basin response to hydrological events and do not fully utilize information collected during an event. Further the deterministic models were originally developed for design studies, and their formulation has not been influenced by the need to incorporate hydrological information in real time. As a consequence, these models cannot readily be updated, and may prove difficult to re-initialize following telemetry or computer breakdowns. For example, a forecast from a conceptual model is often made of contributions from a number of stores (reservoirs), the contents of which have to be specified in order to initialize the model, which is clearly not practical in a real time context. The similar difficulties are also encountered in unit hydrograph models (which were primarily developed to meet design objectives) as the necessary separation of base-flow and storm runoff is difficult to invoke in real time. The inherent weaknesses of deterministic hydrological models for real time applications have provided to look into stochastic time series models with structures more suited to real time forecasting. The time series models and their applications to real time flow forecasting were evolved in 1970's and have been successfully applied for real time forecasting. The statistical models involve the development of the relationships correlating the flood characteristics of forecasting station and upstream gauging station considering the various other factors influencing the floods. The ANN and fuzzy logic based models, which have the potential for the real time flood forecasting, are capable of considering the inherent non-linear ties in the rainfall-runoff process.

2.5.2 Flood Warning:

Flood warning allows action to be taken to protect or remove damageable property. While flood forecasting is associated with gaining advance information for better system operation, flood warning is associated with advance information for protecting property. The principle effect is economic in that the damage function is altered by lowering potential damages when a warning is effective.

2.6 LEGAL AND INSTITUTIONAL ISSUES:

The primary responsibility of flood control lies with the governance system. To execute each phase of the disaster management cycle government has to frame policies and provide financial support. Following are the responsibilities of governance system:
(i) Constitutional provisions.
(ii) Formation of institutions/agencies/organisations at national, state, district as well as local level to deal with every phase of the disaster.
(iii) Formation of action plans and incorporates them with master plans if possible.
(iv) Funding of flood management schemes.
(v) Deployment of funds to deal with economic losses due to floods.
(vi) To deal with flooding problems between neighbouring countries.

2.6.1 Institutional framework and financial arrangements:
It is universally accepted that the national government with some degree of shared responsibility with regional or local authorities must bear the main responsibilities for managing disasters. The organisational structure needed for managing disasters is best founded on the existing government structure. It has been proven rather ineffective to create ad hoc arrangements for disaster purposes, as compared to a comprehensive body of legislation that should be enacted. One of the roles of government in formulating a flood policy is to draw attention to the hazards of life, health and property in those areas where flooding has occurred and will occur again.

Master planning tasks are usually shared between various levels of government having different authority and responsibility. State government usually develop technical guidelines, designate which watersheds are to be studied, prepare model ordinances, provide technical assistance to local agencies, and provide financial assistance.

2.6.2 Legislation:
Legislation that needs to be enacted in order to provide legal basis for implementation of storm water directives and programs should include:
(i) Provisions for storm water pollution control
(ii) Provisions for temporary storage of excess runoff
(iii) Provisions for disconnection of roof drains from sanitary sewers - provisions for floodplain zoning and regulation
(iv) Provisions for flood-proofing of buildings

(v) Provisions for development of a compatible and co-ordinated storm water drainage system.
(vi) Provisions for implementing the source control
The extent to which the basin-wide management approach can be applied will depend largely on the nature of the ownership of land (government or private) and the authority that can be imposed by the drainage agency over development.

Table 1: Organisational structure for managing disasters in India.

Constitutional Provisions:
• Regulation and development of inter-State rivers and river valleys to the extent to which such regulation and development under the control of the Union are declared by Parliament by law to be expedient in the public interest.
National Institutions/Agencies:
• National Disaster Management Authority (NDMA) • National Executive Committee (NEC) • National Disaster Response Force (NDRF) • National Institute of Disaster Management (NIDM) • The Central Flood Control Board (CFCB) • Central Water Commission (CWC) • Ganga Flood Control Commission/Ganga Flood Control Board • Brahmaputra Board/High Powered Review Board • India Meteorological Department • National Centre for Medium Range Weather Forecasting • National Remote Sensing Agency • National Flood Management Institute • River Basin Organisations-Interstate Coordination
State Level-Organisations:
• Disaster Management Departments/Commissioners • State Disaster Management Authority • State Executive Committee • State Flood Control Boards/State Flood Control Technical Advisory Committees • Irrigation/Water Resources/Flood Control Departments • District Disaster Management Authority • Local Authorities (Panchayati Raj Institutions (PRIs) and Urban Local Bodies (ULBs), such as municipal corporations, municipalities, district and cantonment boards and town planning authorities • State Disaster Response Force • Intra-state Multi-sectorial Coordination
Techno-economic Appraisal of Flood Management Schemes:
• Most of the state governments affected by floods have set up multi-disciplinary State Flood Control Technical Advisory Committees (TAC) for clearance of FM schemes before approval as per the procedure laid down by the Planning Commission. The TACs have representatives

from the concerned departments/organisations of the state as well as the central government.
Funding of Flood Management Schemes:
•   **Plans of Central Ministries/Departments** •   **State Plans** •   **Centrally sponsored/Central Sector Schemes** •   **District Planning and Development Council Funds** •   **Calamity Relief Fund** •   **National Flood Mitigation Project**
Flood Insurance:
•   **The CRF provides for gratuitous relief for survival of people affected by floods. It does not compensate them for the losses suffered by them during floods. Insurance against losses of lives and property in the flood is an important tool for transfer of risk compensating them for the losses suffered by them in floods. Flood insurance has not been adopted widely in India.**

2.7 ENVIRONMENTAL IMPACTS CAUSED BY FLOODING:

2.7.1 Water quality alteration:

The impact of floods has considerable environmental and health consequences, in particular given the very specific vulnerability of domestic water supplies and the physical infrastructure necessary for sanitation. The disruption of water distribution and sewage systems during floods contribute greatly to severe financial and health risks. Preventive measures should be taken to reduce possible adverse

effects of floods on these infrastructures. Alternative solutions should be planned and implemented to guarantee the operation of water distribution and sewage systems.

2.7.2 Environmental assessment:

Environmental flooding-related issues are numerous. Some of them are listed below:
(i) Mutual effects of agriculture and flooding
(ii) Migration disturbance in fish spawning areas
(iii) Protection of archaeological sites
(iv) Preservation of landscape and major trees
(v) Improvement of downgraded land
(vi) Avoiding sewerage effluents and limiting overflows
(vii) Avoiding damage to habitats in urban streams
(viii) Creating new habitats for wildlife
(ix) Developing green belt zones in flood plains
(x) Fostering and protecting the visual amenity of rivers and floodplains
(xi) Reducing risk of landslide and mud flows
Floods causes not only massive death but also social disruption, epidemic diseases and famine, which leave survivors dependent on relief. In recent years the health profession has developed new approaches and new mechanisms, referred to as disaster medicine or disaster health management.

2.7.3 Medical response to flood disasters:

Floods are very damaging to man and material (UNESCO, 1995). During a major flood many deaths, caused by drowning, may occur, mostly among the weaker sections of the population such as infants, elderly and sick. Immediate effects are not likely to last more than several days. Secondary effects are then likely to begin and more likely to last for a longer time, characterised by the emergence of communicable diseases, water-borne infections and food shortages. The diseases that are to be feared of are various diarrhoea diseases, acute respiratory infections, measles, tuberculosis and malnutrition.

It had long been believed that epidemics almost obligatory follow disasters. The truth is that diseases can be prevented by simple hygienic methods and should be kept under constant surveillance. The immediate medical response to a flood disaster consists of several elements: search and rescue, triage and tagging, disposal of the dead, and the management of the casualties and the medical supplies.
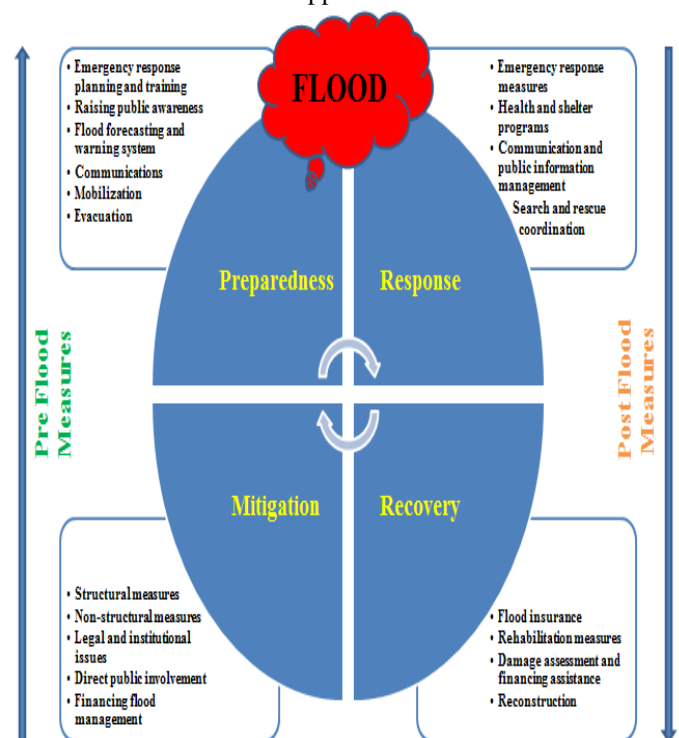
Figure 1: Flood Management Planning Cycle

3. CONCLUSION:

We can learn from the past experiences that using structural measures only low to medium magnitude of floods can be prevented. In order to deal with high magnitude floods non-structural measures plays a vital role. Thus best flood management practices can be achieved by the combination of structural and non-structural measures as same region can be hit by low to high magnitude of floods. If we consider structural measures as those that are directed at modifying the flood hazard then we can define non-structural measures as those that modify the impacts of the flood hazard. Structural measures keep the floods away from people and damageable property, non-structural measures keep the people and damageable property away from the floods. If all the structural

and non-structural measures as suggested here are adopted then the damages in case of the worst scenarios of flood, can be minimized up to a very great extent (Rajshree K., 2014). As there is lots of uncertainty and variation in climatic conditions during last two decades thus we cannot rely on either of the structural measures or the non-structural measures for the safety of mankind from disasters. We need a complete package of best available structural and non-structural measures in order to achieve best flood management practices.

REFERENCES:

i. Brooker, M.P (1985) The Ecological Effects of Channelization (The Impact of River Channelization). The Geographical Journal, 1985.

ii. Frank Friesecke (2004) Precautionary and Sustainable Flood Protection in Germany – Strategies and Instruments of Spatial Planning. 3rd FIG Regional Conference Jakarta, Indonesia, October 3-7, 2004.

iii. Government of India Planning Commission (2011) Report of Working Group on Flood Management and Region Specific Issues for XII Plan. New Delhi October, 2011.

iv. Ivan Andjelkovic (2001) Guidelines on Non-structural measures in urban flood management. IHP-V | technical documents in hydrology | no. 50 UNESCO, Paris, 2001.

v. I.M Faisala, M.R Kabir, A Nishat (1999) Non-structural flood mitigation measures for Dhaka City. Urban Water

vi. Volume 1, Issue 2, June 1999, Pages 145–153.

vii. Lucas Menzel, Zbigniew W. Kundzewicz (2003) Non-structural Flood Protection – A Challenge. International conference 'Towards natural flood reduction strategies', Warsaw, 6-13 September 2003.

viii. National Disaster Management Authority, Government of India (2008) National Disaster Management Guidelines (Management of Floods).

ix. Rajshree Kamat (2014), Planning and managing earthquake and flood prone towns, Stochastic Environmental Research and Risk Assessment, (DOI) 10.1007/s00477-014-0898-z.

x. Rajshree Kamat, Ashutosh Sharma (2007) Assessing flood hazard vulnerability of Hoshangabad town, Madhya Pradesh. Spatio-economic development record (Volume 14 No. 3, May-June 2007).

xi. R. D. Singh Real time flood forecasting - Indian experiences.

xii. Schulze et al. (2005), p.400.

xiii. Suhas P Wani and Kaushal K Garg Watershed Management Concept and Principles.

xiv. Zbigniew W. Kundzewicz (2002) Non-structural Flood Protection and Sustainability Water International Volume 27, Issue 1, 2002.

Scour Due To Water Jets In Cohesionless Sediments

Ankit Chakravarti[1], R.K. Jain[2], Z. Ahmad[3] and Umesh K. Singh[1]

[1]Research Scholar, Department of Civil Engineering, Hydraulic Engineering Section, IIT, Roorkee – 247667, India. **Email:** ankitchakravarti@gmail.com

[2]Asociate Professor, Department Civil Engineering, Govt. Engineering College, Chandkheda, Gandhinagar, 382 424, Gujarat, India. **Email:** rajkjain7@gmail.com

[3]Professor, Department of Civil Engineering, Hydraulic Engineering Section, IIT Roorkee – 247667, India. **Email**: zulfifce@gmail.com

ABSTRACT : The outflow of water jets from a reservoir or dam has usually high jet velocity which can lead to local scour at the downstream of hydraulic structures. The accurate estimation of location of dam foundation and assurance the stability of downstream structures is very important as far as the designing criteria of spillways are considered. The effects of submerged circular impingement water jets in case of cohesionless sediment were studied through laboratory experiments and theoretical analysis. Total eight laboratory experiments were carried out to study the characteristics of scour process under submerged circular vertical jets. The experiments involved jet diameters, sediment size, jet velocity and jet height from the bed level. Measurements were made for maximum dynamic and maximum static scour depth. It was found that the dynamic scour depth is much larger than the static scour depth in equilibrium state. The temporal variations of scour depth and maximum static scour depth have been also quantified.
Keywords: Hydraulics; Laboratory experiment; cohesionless sediment; scour; water jets

INTRODUCTION

Scour is the process of removal of loose sediment material from the bed and banks of a river or channel by the action of flowing water. Scour takes place in the vicinity of a hydraulic structure when the flow gets modified due to the presence of hydraulic structures in such a manner that there is an increase in the bed shear stress. When a submerged jet flows over a sediment bed, the local bed shear stress induced by the high velocity of the exceeds the bed shear stress for the initiation of sediment motion, which results in local scour downstream of hydraulic structures. Hence, due to the practical importance, the local scour process caused by water jets has been a topic of continued interest to the scientist, researchers and the design engineers as well.

Experience has shown that scouring can progressively undermine the foundations of hydraulic structures because complete protection against scouring is usually prohibitively expensive, the designer must therefore seek ways to guide and control the process so as to minimize the risk of failure. The scour of sand, gravels, and other materials, which are occurs in downstream of water resources structures due to submerged water jets is considerable importance because excessive scouring process my endanger the stability of the hydraulic structures such as culverts, gates, weirs, spillways and grade control structures etc. There are two types of scour profile geometries; firstly dynamic scour when the jet flow is in running condition and second one; is static scour when the final bed scour hole produced by the jet flow is stopped (Ansari et al. 2003). Most of the available methods for determination of maximum depth of scour under submerged water jets are applicable for steady flow conditions but water flows in the

river during a flood or high flood situation is unsteady water flow and discharge changes in it are quite rapid. Therefore, the temporal variation of scour depth also most important aspects for estimation of scour depth in case of unsteady flows (Kothyari et al., 1992a).

BRIEF LITRATURE REVIEW

Many researchers have performed laboratory experiments on scour process. The first experimental investigation on scour due to submerged vertical turbulent water jets in uniform sediments was performed by Rouse (1939). Since then a large number of researcher have been trying to carried out to study the scour downstream of hydraulic structures by using different types of water jets like horizontal water jets, vertical water jets, inclined water jets. The significant fundamental works and the problem of sediment bed response due to submerged water jets have been investigated by a number of researchers including those of Westrich and Kobus (1973), Rajaratnam (1982), Raudkivi (1990), Adribigbe and Rajaratnam (1996), Ansari et al. (2003), Rajaratnam and Mazurek (2003, 2005), Mazurek and Hossain (2007), Yeh et al. (2009), Chakravarti et al. (2013). Relationships have been developed by these investigators for the equilibrium scour depth as well as for shear stress distribution under the different jet flow and bed conditions. Westrich and Kobus (1973) studied the phenomenon of jet scour through experiments on a uniform sand bed with vertical submerged jet having different mean velocity, two types of nozzle diameter and two type of jet height. They found the scour volume first increases with jet height and then remain constant before decreasing again for given value of parameters. Rajaratnam (1982) studied erosion by planer, two-dimensional jets, primarily in the context of scour at hydraulic structures. Donoghue and Trajkovic (2001), Ansari et al. (2003), Mazurek and Hossain (2007) also studied the temporal variation of scour depth in cohesionless Sediments. Ansari et al. (2003) conducted laboratory based experimental study on scour under submerged circular vertical jets in both cohesive and cohesionless sediment material and identified the difference of scour hole profiles between these two sediment material. They found that more than 70% of the scour occurred in the first 30 minutes from the start of the experiment in case of cohesionless sediment (Ansari, 1999). Aderibigbe and Rajaratnam (1996) have investigated a laboratory experiment on the erosion of loose beds by submerged circular impinging vertical jets by using sand as a loose sediment beds for the erosion parameter less than five and investigated the variation of maximum depth of scour with impinging distance and found two major jet flow regimes i.e. strongly deflected and weekly deflected jet flow regimes. Donoghue and Trajkovic (2001) conducted experiment in cohesionless sediment to investigate the response of sand beds due to submerged circular vertical water jet. The experimental data was generated by larger diameter of jet, fine sediment and small jet impingement height from original bed level. They found that there is much larger difference in static and dynamic scour hole profile than that of previous experiments. Rajaratnam and Mazurek (2003) presents the laboratory based experimental study on erosion of cohesionless sand beds by circular water jets with a minimum tail water

depth. They found that the dynamic scour depth is about three times of static scour at the equilibrium state. The laboratory work conducted by Yeh et al. (2009) showed that the characteristic lengths of the scour profile in the equilibrium state were determined by modifying the empirical formulas proposed by Aderibigbe and Rajaratnam (1996). Maximum scour depth, scour hole radius and the ridge height were found to be a function of ratio of the jet exit to jet translation velocities. Chakravarti et al. (2013) conducted laboratory experiment under submerged circular vertical water jets in cohesionless sediment to study the temporal variation of scour depth, maximum static scour depth and maximum dynamic depth of scour have been analyzed.

The review presented above has revealed that scour under submerged circular vertical impinging water jets on movable bed is mainly a function of nozzle diameter, jet height, jet velocity, and sediment type. Therefore these variables are considered to study the scour process in cohesionless sediment. The main objective of the present study is to check the existing equations developed for estimation of temporal variation of scour depth, maximum static and maximum dynamic scour depth under submerged circular vertical impinging jets.

EXPERIMENTAL PROGRAM

A circular steel tank having diameter 1.25 m and depth 1.25 m, filled with the desired sediment up to a height of 0.80 m was used for the experiments on scour due to submerged circular vertical jets. The impinging jet was produced by a nozzle fitted at the end of circular supply pipe of diameter 0.0254 m. For each experimental run, the tank was filled by the desired sediment up to the height of 0.80 m, while the water was filled in the remaining 0.45 m height on the tank. The jet discharge was measured by calibrated Venturimeter fitted in the water supply pipe.

Material and method

The laboratory experiment were conducted using cohesionless sediment i.e. sand was used which has a median size, d_{50} equal to 0.24 mm and geometric standard deviation of 1.41. The experimental setup for scour due to submerged circular vertical impinging water jet is shown in Fig. 1. Experiments were conducted with two types of nozzle i.e. 12.5 and 8 mm diameter, at two jet heights i.e. 0.15 and 0.30 m from the original sediment bed level. Two jet velocities i.e. 7.19 and 5.12 m/s for 12.5 mm nozzle and 9.84 and 6.65 m/s for 8 mm nozzle were set in the experimentation. Total eight experimental runs were conducted to study the temporal variation of scour depth, maximum static and maximum dynamic scour depth.
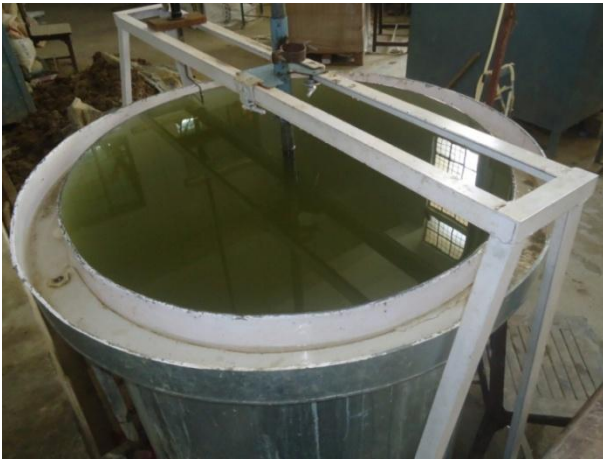
Fig. 1 Laboratory setup for submerged circular vertical water jets

In addition, the data available from the literature and those collected in the present investigation on scour under submerged circular vertical jets in cohesionless sediments were also compiled. Table 1 gives the range of data for present and previous investigation on scour under submerged vertical jet in cohesionless sediment.

Table 1: Range of data on scour under submerged vertical jet in cohesionless sediment for present and previous study

Investigators	Median size, d_{50} (mm)	Jet diameter, d_0 (mm)	Jet velocity, u_o (m/s)	Jet height, h_j (m)
Sarma (1967)	0.53 - 0.75	8.26-16.5	0.66-2.83	0.24
Wistrich and Kobus (1973)	1.5	20 - 40	0.7 - 3.7	0 - 0.82
Rajaratnam (1982)	1.2 - 2.38	9.8	2.99 - 4.6	0.14 - 0.28
Aderibigbe and Rajaratnam (1996)	0.88 - 2.42	4 - 12	2.65 - 4.45	0.004 - 0.523
Ansari et al. (2003)	0.27	8 - 12.5	1.3 - 5.75	0.15 - 0.30
Present study	0.25	8 - 12.5	5.12 - 9.84	0.15 - 0.30

Table 2 Parameter used for the experiments and characteristics of scour bed under submerged circular vertical jets

Run No.	Nozzle size d_o(m)	Jet height, h_j (m)	Velocity, u_o (m/s)	Dynamic Scour, d_{dms} (m)	Static Scour, d_{sms} (m)	(d_{dms}-d_{sms}) (m)
1	0.008	0.30	9.84	0.32	0.125	0.195
2	0.008	0.15	9.84	0.345	0.095	0.25
3	0.008	0.30	6.65	0.285	0.105	0.182
4	0.008	0.15	6.65	0.252	0.085	0.209
5	0.012.5	0.30	7.19	0.337	0.140	0.197
6	0.012.5	0.15	7.19	0.371	0.120	0.251
7	0.012.5	0.30	5.12	0.290	0.105	0.185
8	0.012.5	0.15	5.12	0.315	0.075	0.24

Measurements

In this experimental study the observation were taken for temporal variation of scour depth, maximum dynamic and maximum static depth of scour were taken using a simple point gauge relative to a fixed datum once the jet has been turned off and the suspended sediment particle has settled. The measurement of dynamic scour by jet was also taken using a simple point gauge relative to a fixed datum while the jet is in running condition.

ANALYSIS OF DATA AND DISCUSSION OF RESULTS

Temporal variation of scour depth in cohesionless sediments

The temporal variation of scour depth under submerged circular water jets revealed that more than 75 % of the depth of scour occurred during the first 30 minute form the start of experiment, a feature that was also noticed earlier by Clark (1962), Rajaratnam (1982) and Ansari et al. (2003). The temporal variation of maximum scour depth under submerged circular vertical jets can be expressed by Ansari et al. (2003) which can be describe as;

$$\frac{d_{ss}}{d_{sms}} = \left[\sin\left(\frac{\pi t}{2T_s} \right) \right]^{m_s}$$

(1)   Where d_{ss} = instantanious depth of scour at time t; T_s = time required to reach the maximum scour depth; d_{sms} = maximum scour depth at equilibrium in cohesionless sediments; and m_s is exponent. The temporal variation of maximum scour depth is presented in the dimensionless form for different conditions of experimental run as shown in Fig. 3. The agreement with equation may be noticed.

Sarma (1967), Westrich and Kobus (1973) and Rajaratuam (1982), Aderibigbe and Rajaratnam (1996) and Ansari et al. (2003), identified non-dimensional parameter used for describing the relationship for erosion parameter, E_c which can be expressed by the following equation;

$$E_c = u_o\left(\frac{d_o}{h_j} \right) \bigg/ \sqrt{\left(\frac{g d_{50} \Delta \rho_s}{\rho_f} \right)}$$

(2)

Where, d_o = diameter of nozzle, u_o = jet velocity, E_c = erosion parameter, h_j = height of jet from original bed level, g = acceleration due to gravity and $\Delta \rho_s / \rho_f$ is the relative

density defined by $(\rho_s - \rho_f / \rho_f)$, where ρ_s is the mass density of sediment, ρ_f is the mass density of water. Adribigbe and Rajaratnam (1996) proposed a equation to describe relationship between the two parameters was as follows;

$$\frac{d_{sms}}{h_j} = 1.26\left(E_c\right)^{0.11} - 1.0$$

(3)

The data of Sarma (1967), Westrich and Kobus (1973), Rajaratnam (1982), Aderibigbe and Rajaratnam (1996), Ansari et al. (2003) and the data collected during the present investigation were analyzed for the stability of the above mentioned non-dimensional variable in the relations for maximum depth of scour.
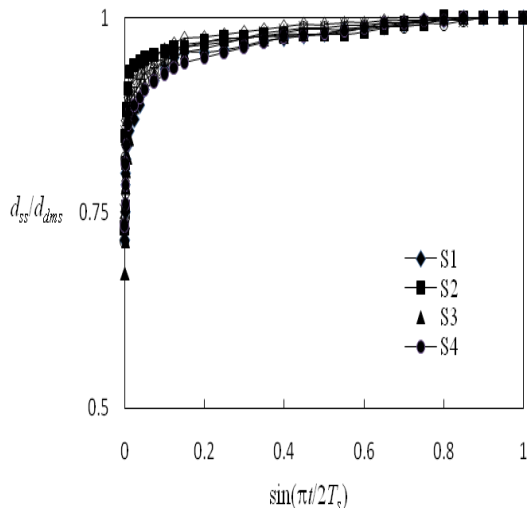
Fig. 2 Variation of d_{ss} / d_{sms} with $\sin(\pi t / 2T_s)$ here the notation S1, the first character S stands for cohesionless sediment and the second character 1 stands for the run number)

The plots of data between the variable E_c and d_{sms} / h_j described the variation in a better way as shown in Fig. 4. The erosion parameter E_c, originally proposed by Aderibigbe and Rajaratnam (1996) is found to be satisfactorily describing the variation of maximum scour depth under submerged circular vertical jet in cohesionless sediments for the present study as well.
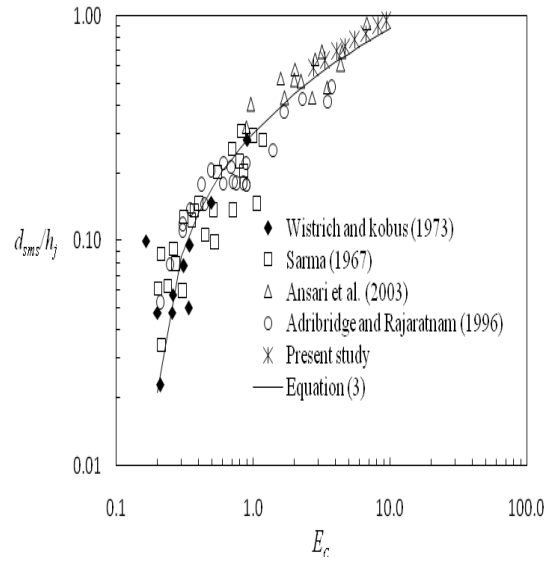
Fig. 3 Variation of maximum scour depth (d_{sms} / h_j) with erosion parameter (E_c) in cohesionless sediments

Maximum static and dynamic scour depth

In case of each experimental run the depths of dynamic and static scour was measured. Fig. 5 is prepared to show the variation of difference between dynamic and static scour depth against erosion parameter as described by Equation no. (2). It was found that this difference between scour depth increases linearly with the value of erosion parameter for the present data. However more experimental runs data should be analyzed to validate this variation.
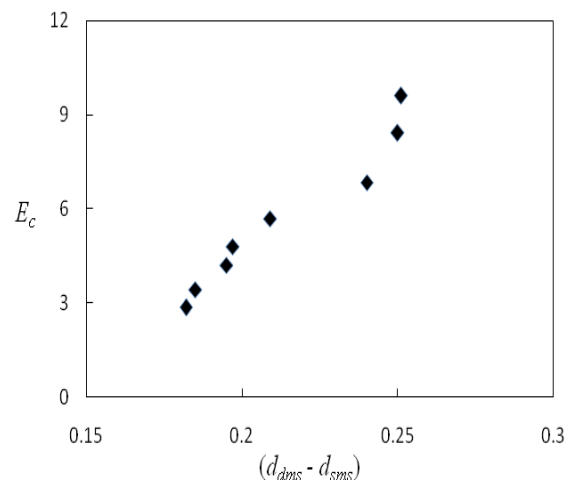
Fig. 4 Variation of difference between maximum dynamic (d_{dms}) and maximum static (d_{sms}) scour depth versus erosion parameter (E_c)

Conclusions

The experimental observations and analysis presented in this investigation on scour under submerged water jets in cohesionless sediment has established that the sediment size has a significant effect on size of scour hole produced by water

jets. The present study extends the range of existing experimental data by involving jet diameters, sediment size, jet velocity and jet distance from the bed level, resulting in much larger differences have been observed in between maximum dynamic and static scour depth than previous investigations. The erosion parameter (E_c) originally proposed by Aderibigbe and Rajaratnam (1996) is found to be satisfactorily describing the variation of maximum scour depth under submerged circular vertical jet in cohesionless sediments. The variation of difference between maximum dynamic and static scour depth against erosion parameter revealed that these differences increases linearly with the value of erosion parameter.

REFERENCES

i.   Aderibigbe, O. O., and Rajaratnam, N. (1996). "Erosion of loose beds by submerged circular impinging vertical turbulent jets." Journal of Hydraulic Research, IAHR, 34(1), 19–33.

ii.   Ansari, S.A., Kothyari, U.C., and Ranga Raju, K.G. (2003). "Influence of cohesion on scour under submerged circular vertical jet." Journal of Hydraulic Engineering, ASCE, 129(12), 1014-1019.

iii.   Chakravarti, A., Jain, R.K., and Kothyari, U.C. (2013). "Scour under submerged circular vertical jets in cohesionless sediment" ISH Journal of Hydraulic Engineering, Taylar and Francis Group. Vol. 20(1), pp 32-37.

iv.   Ansari, S.A. (1999). "Influence of cohesion on local scour." Ph.D Thesis, Department of Civil Engineering , IIT Roorkee.

v.   Clarke, F. R. W. (1962). "The action of submerged jets on movable material." Ph.D thesis, Imperial College, London.

vi.   Donoghue, T.O., Trajkovic, B., and Piggins J. (2001). "Sand bed response to submerged water jet." Proc., Eleventh Int. Offshore and Polar Engineering Conference, Stavanger, Norvey, June 17–22.

vii.   Kothyari, U. C., Garde, R. J. and Ranga Raju, K. G. (1992 a) "Temporal variation of scour around circular bridge piers." J. Hydraul. Eng., ASCE, 118(8): 1091-1106.

viii.   Mazurek, K. A., Tanvir Hossain. (2007). "Scour by jets in cohesionless and cohesive soils." Can .J. civ. Eng. vol.34, pp-744-751.

ix.   Rajaratnam, N. (1982). "Erosion by submerged circular jets." Journal of Hydraulic Division., ASCE, Vol.108, No. HY2, pp 262–267.

x.   Rajaratnam, N., and Mazurek, K.A. (2003). "Erosion of sand by circular impinging water jets with small tail water." Journal of Hydraulic Engineering, ASCE, Vol. 129(3), pp 225–229.

xi.   Rajaratnam, N., Mazurek K.A. (2005). "Impingement of circular turbulent jets on rough boundaries." Journal of Hydraulic Research, IAHR, vol. 43, No.6, pp 688-694.

xii.   Raudikivi, A. J. (1990). "Loose boundary hydraulics." 3rd Edition, Pergamon Press, Chap.9, New York, USA.

xiii.   Rouse, H. (1939). "Criteria for similarity in the transportation of sediment." Bulletin 20, University of Iowa, Iowa, USA, pp 33-49.

xiv.   Sarma, K.V.N. (1967). "Study of scour phenomenon and its functional form." Ph.D. Thesis, Indian Institute of Sciences, Banglore, India.

xv.   Westrich, B., and Kobus, H. (1973). "Erosion of a uniform sand bed by continuous and pulsating jets." Proc., 15th IAHR Congress, Istanbul, Turkey, 1, A13.1–A13.8.

xvi.   Yeh. Po-Hung, Kuang-An Chang., John Henriksen, Billy Edge., Peter Chang., Andrew Silver., and Abel Vargas. (2009). "Large-scale laboratory experiment on erosion of sand beds by moving circular vertical jets." Ocean Engineering vol. 36 pp 248-255.

Comparison Study On Discharge Prediction Approaches In Straightcompound Channels

ElloraPadhi[1]K.C.Patra[2]
[1]M.Tech Student, Dept. of Civil Engineering, National Institute of Technology, Rourkela, India.
[2]Professor, Dept. of Civil Engineering, National Institute of Technology, Rourkela, India
Email: ellora.padhi@yahoo.co.in,,prof_kcpatra@yahoo.com.

ABSTRACT: Due to the transfer of momentum at the junction of main channel and the adjoining floodplains the flow pattern in such a channel section becomes complicated. Many experiments are carried out to compute the velocity as well as boundary shear along the wetted perimeter of a straight compound channel to quantify the momentum transfer along the expected interfaces. This is helpful to evaluate the stage-discharge relationship for a compound channel more accurately. Discharge calculation can be done by using various hydraulic models. But the traditional discharge prediction models such as SCM, DCM and others fail to give accurate discharge as they don't consider the effect of momentum transfer. By considering the effect of transfer of momentum, some new models are being developed which makes discharge prediction more accurate than the traditional method. In this study the experimental data reported by other investigators are used through the hydraulic models such as the DCM, IDCM, MDCM and CES to evaluate the discharge estimation and the results are compared with the freshly observed experimental data. Besides the channel geometry, Manning's n is also dependant on the flow parameters. By varying the value of Manning's n with respect to depth of flow, the discharge is computed through MDCM and the percentage of error is found out. Modification to MDCM is applied to take care of the variation of n values.

Keywords:Discharge prediction, momentum transfer, IDCM, MDCM, CES.

1. INTRODUCTION

Prediction of discharge is one of the important works in river flow analysis. Discharge prediction is required to establish the stage discharge relationship in a channel which will be help full to the River Engineers for flood forecasting, bank protection etc. Discharge calculation is influenced by various hydraulic parameters as well as geometric parameters of the channel. For simple channel it is easy to compute the discharge, and it can be done using Manning's, Chazy's or Darcy-Weisbach's equation. But when it is required to calculate the discharge for overbank flows, the section becomes compound, then these equations do not give adequate answers. Investigations by the researchers have observed that the reason behind inaccurate discharge value is due to exchange of momentum. During flood, part of the river discharge is carried by the main channel and the rest is carried by the adjacent flood plains. The flow structure for such section is affected by large shear layers generated by the difference in velocities of water in the main

channel and the floodplain leading to the transfer of momentum between them.

In a compound channel formation of vortices at the junction of main channel and flood plain was first shown by Sellin (1964) and Zheleznvakov (1965). Wormleaton et al (1982) stated that the total dragging force on the main channel flow due to floodplain flow at the interfaces is equal to the accelerating force on the flood plain flow due to the main channel flow due to which transfer of momentum occurs. At lower depths of flow over the floodplain, momentum transfer takes place from the main channel to the floodplain resulting in decrement of the main channel velocity and discharge, while its floodplain components are being increased. And at higher depths of flow over the floodplains the process of momentum transfer is reverses, i.e. the momentum is supplied to the main channel from the floodplain and this momentum transfer makes the discharge prediction difficult. The effect of flow interaction between the floodplain and main channel for various depths of flow over floodplain should be adequately taken care, while calculating discharge in the compound channel. There are various traditional methods through which discharge can be estimated. Stephenson and Kolovopoulos (1990) discussed four different methods to evaluate the discharge prediction by considering variation of the shear stress between main channel and flood plain with respect to different flow conditions. Based on the previously published data, they predicted discharge and concluded that their 'area method' was the most reliable method in predicting discharge and that Prinos-Townsend (1984) equation gave better results for apparent shear stress at junction region of floodplain and main channel in a compound channel.

Ackers (1992) proposed a method by making some correction to the DCM named as coherence method (COHM). Patra (1999), and Patra and Kar (2000) proposed a variable interface plane of separation of compound channel which nullify the momentum transfer for a better estimate of discharge in straight compound river sections. Bousmar and Zech (1999) proposed a 1D model known as the exchange-discharge model (EDM) which is suitable for prediction of stage-discharge relationship as well as simulations of practical water-surface profile. The momentum transfer is calculated multiplying the velocity gradient at the interface with the mass discharge exchanged through this interface generated from the effect turbulence. Khatua and Patra (2007) carried out a series of laboratory tests for both smooth and rigid compound channels and a mathematical equation was developed using dimension analysis for evaluating the roughness coefficients. Huthoff et al (2008) parameterized the interface stress in terms of velocity of the main channel and floodplains. Later Khatua and Patra (2012) quantified momentum transfer in terms of interface length which makes discharge prediction more accurate. Apart from these one dimensional mathematical models, there is 1D software available such as HEC-RAS, ANN, MIKE 11 and CES that can be used suitably for discharge prediction in compound channels. The software use the DCM and or the other numerical approaches to estimate discharge that sometimes give quite unsatisfactory results. The aim of the present paper is to propose a modified DCM (MDCM) that can be good for all types of compound channels and roughness.

2. METHODOLOGY

2.1   Single Channel Method

It treats the channel cross-section as a whole channel without division to subsections. This method usually fails to give a good estimate of the stage-discharge relationship, as it over estimates the discharge.

$$Q = \frac{1}{n} * R^{2/3} S_o^{1/2}$$

(1)

Where Q= discharge, R=Hydraulic Radius, S_o=Bed slope of the channel.

2.2   Divide Channel Method

This method employs division of the compound channel into subsections i.e. the main channel (bank full) and floodplains (berms).The discharge is calculated for each sub sections considering the interfaces. Again, this method is modified into a few versions distinguishing each other by the way how they consider division line originating from the junction between main channel and the floodplain, ding the compound channel into sub-sections. This includes the horizontal interface, vertical interface, diagonal interface, curved interface, variable interface (Figure 1). However vertical interface and diagonal interface are the two methods which are commonly used. Discharge for each sub-section can be calculated by using the Eq. (2) given below.

$$Q = \sqrt{S_o} \left| \frac{1}{n_{mc}} A_{mc}^{\frac{5}{3}} P_{mc}^{-\frac{2}{3}} + \frac{1}{n_{fp}} A_{fp}^{\frac{5}{3}} P_{fp}^{-\frac{2}{3}} \right|$$

(2)

Where Q = Discharge through the compound channel, A_{mc} & A_{fp}= Area of the main channel and floodplain respectively, P_{mc} & P_{fp}= perimeter of the main channel and floodplain respectively, S_0= Bed slope of the channel, n_{mc} & n_{fp}= manning's co-efficient for main channel and flood plain respectively.
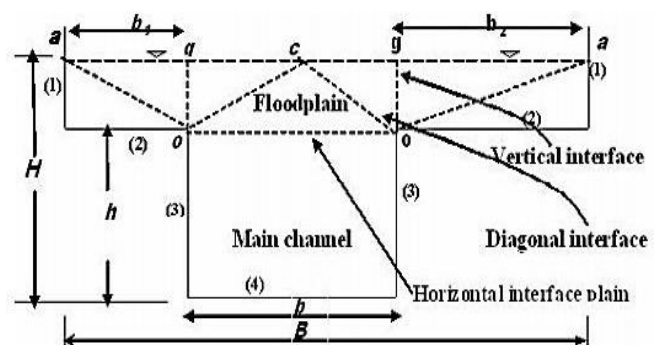

Figure 1. The vertical, horizontal, diagonal interfaces of a prismatic compound channel.

2.2.1   Vertical interface method

In this method the flood banks are separated from the main channel by means of vertical interface (Figure 1), but the interface length is not included in the calculation of wetted perimeter of either of the over bank flow or main channel flow as this interface is considered as a surface of zero shear stress and no momentum transfer takes place through junction of main channel and flood plain.

2.2.2   Diagonal Interface method

In this method a diagonal interface is considered from the top of the main channel bank to the centerline of the water surface. This interface is considered to be the surface of zero shear stress and due to that the length is not included in the calculation of wetted perimeter of the over bank flow and main channel flow. The problem with both the methods is, they overestimate the discharge to some extent.

2.3   Interacting Divide Channel Method

This method developed by Fredrik Huthoff in the year 2007. Here the channel is divided in to two parts by vertical interfaces and the effect of momentum transfer occurring at the junction of main channel and flood plain is considered in terms of interface stress (τ_{int}).The following equations have been developed to find out the velocity of the main channel as well as flood plain given as

$$\tau_{int} = \frac{1}{2}\gamma\rho\left(U_{mc}^2 - U_{fp}^2\right)$$

$$(3)$$

$$U_{mc}^2 = U_{mc,0}^2 - \frac{\frac{1}{2}\gamma N_{fp}\varepsilon_{mc}\left(U_{mc,0}^2 - U_{fp,0}^2\right)}{1+\frac{1}{2}\gamma\left(N_{fp}\varepsilon_{mc}+\varepsilon_{fp}\right)}$$

$$(4)$$

$$U_{fp}^2 = U_{fp,0}^2 + \frac{\frac{1}{2}\gamma\varepsilon_{fp}\left(U_{mc,0}^2 - U_{fp,0}^2\right)}{1+\frac{1}{2}\gamma\left(N_{fp}\varepsilon_{mc}+\varepsilon_{fp}\right)}$$

$$(5)$$

Where U_{mc} & U_{fp} are the velocities of main channel and the flood-plain respectively assumed steady and longitudinally uniform, γ = co-efficient of interface. N_{fp} = number of flood plains. $U_{mc,0}$ & $U_{fp,0}$ = velocities of the main channel and flood plain when $\gamma = 0$. τ_{int} = interface stress developed at the interface of the main channel and flood plain.

$$\varepsilon_{mc} = \frac{h_{int}}{f_{mc}P_{mc}}, \varepsilon_{fp} = \frac{h_{int}}{f_{fp}P_{fp}}$$

$$(6)$$

$$U_{mc,0}^2 = \frac{gR_{mc}S}{f_{mc}}, U_{fp,0}^2 = \frac{gR_{fp}S}{f_{fp}}$$

$$(7)$$

$$R_{mc} = \frac{A_{mc}}{P_{mc}}, R_{fp} = \frac{A_{fp}}{P_{fp}}$$

$$(8)$$

Where f_{mc} & f_{mc} are co-efficient of friction. P_{mc} & P_{fp} are the perimeter of the main channel and flood plain respectively.

A_{mc} & A_{fp} are the area for main channel and flood plain respectively. R_{mc} & R_{fp} are the hydraulic radius of main channel and flood plain respectively. h_{int} = difference between the water depth and the full bank level (Figure 2).
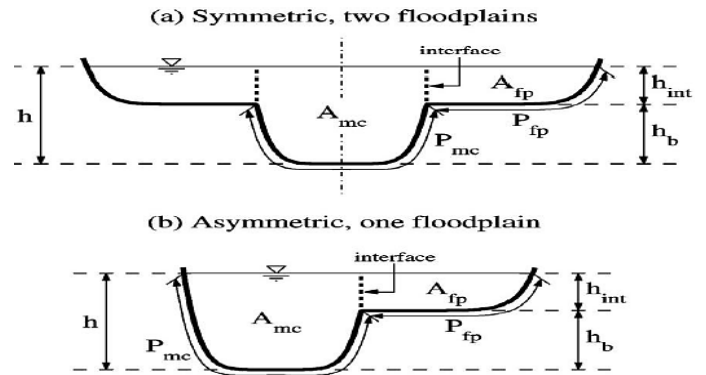
Figure 2. Cross section of a two-stage channel: (a) symmetric with two identical floodplains. (b) Asymmetric with oneside floodplain. (Hutoff 2007)

After finding out the velocities, discharge (Q) of the total section can be predicted through inter -acting divided channel method by using equation (9).

$$Q = A_{mc}U_{mc} + N_{fp}A_{fp}U_{fp}$$

$$(9)$$

The interface stress parameterization yields a set of model equations that is linear in the squared velocities, leading to an analytical solution" is a practical property of IDCM. When generalizing IDCM to compound channels with several numbers of compartments, this property is retained. This generalization is required as the interface co-efficient γhas either a universal value or an explicit dependency on the geometry as well as on the roughness of the nearby compartments. Based on the results from their study, Huthoff*et.al* has recommend a constant value of γ= 0 .020.

2.4   Modified divided channel method (MDCM).

This is another method developed by Khatua*et. al* (2012), which quantified the momentum transfer in terms of interface length. According to Wormleaton*et. al.* (1982), the total dragging force on the main channel flow due to floodplain flow at the interfaces is equal to the accelerating force on the floodplain flow due to the main channel flow due to which transfer of momentum occurs which makes the discharge prediction difficult. So for balancing the force, here the main channel boundary shear to be increased and that of the floodplain decreased suitably to account for main channel and floodplain flow interaction. Let X_{mc} = the interface length for inclusion in the main channel wetted perimeter and X_{fp} = the length of interface to be subtracted from the wetted perimeter of the floodplain termed as interaction length. So according to

this method, the value of X_{mc}, X_{fp} are found out from Equation (10) and Equation (11).

$$X_{mc} = \frac{100 P_{mc}}{(100 - \%S_{fp})[1+(\alpha-1)\beta]} - P_{mc}$$

(10)

$$X_{fp} = P_{fp} - \frac{100(\alpha-1)\beta}{(\%S_{fp})[1+(\alpha-1)\beta]} P_{fp}$$

(11)

Where α = width ratio = B/b; β = relative depth = $\frac{H-h}{H}$, b = width of main channel bottom; B = total width of compound channel; h = bank full depth; and H = total depth of flow. $\%S_{fp}$= percentage of shear force in the flood plains. Knowing $\%S_{fp}$ and the channel geometry, the interface lengths X_{mc} and X_{fp} are evaluated. Next, the discharges for the main channel and floodplain are calculated using Manning's equation and added together to give total discharge as

$$Q = \sqrt{S_o} \left[\frac{1}{n_{mc}} A_{mc}^{\frac{5}{3}} (P_{mc} + X_{mc})^{-\frac{2}{3}} + \frac{1}{n_{fp}} A_{fp}^{\frac{5}{3}} (P_{fp} + X_{fp})^{-\frac{2}{3}} \right]$$

(12)

Where S_o = bed slope of both main channel and floodplain (assumed to be the same in 1D models) and n_{mc}, n_{fp} = manning's co-efficient of main channel and floodplain subsections respectively. For rectangular channel and floodplains having homogeneous roughness (i.e., Manning's n value is equal for both the main channel and floodplains). $\%S_{fp}$is calculated from the equation (13), developed by Khatua&Patra(2012).

$$\%S_{fp} = 4.105 \left[\frac{100\beta(\alpha-1)}{1+\beta(\alpha-1)} \right]^{0.6917}$$

(13)

So by putting the value of %Sfp, the value of X_{mc} and X_{fp} can be calculated. After finding out the values of interface length the discharge of the straight compound channel can be estimated.

2.5   Conveyance estimation system (CES)

CES is a software tool which is used for estimation of flood and water levels in the rivers, watercourses and drainage channels. This software is being developed by the hydraulic engineers of United Kingdom.This involves roughness advisor, conveyance generator, uncertainty estimator, backwater module, afflux estimator etc.

The roughness advisor carries the information regarding the roughness values for a range of natural and man-made roughness types along with description and photographs related to that roughness. Based on the roughness information and cross section geometry the conveyance generator estimates the conveyance of the channel. By the help of**Lateral Distribution Method**(LDM) the conveyance is calculated. The general

expression for finding out depth averaged velocity through LDM is given below

$$\rho g S_o H - \rho \frac{f}{8} \sqrt{1+s^2} U_d^2 + \frac{\partial}{\partial y} \left[\rho \lambda H^2 \sqrt{\frac{f}{8}} U_d \frac{\partial U_d}{\partial y} \right] = 0$$

(14)

The uncertainty estimator gives some measure of the uncertainty associated with each predicted water level. The upper and lower values of the uncertainty estimator depend upon the upper and lower roughness values estimated from the roughness advisor. For gradually varied flow condition a code is used which is called as afflux generator. This code is helpful in finding out the afflux at upstream of the bridge and culvert at high flow condition. This code also provides longitudinal water surface profile.

Apart from these main tools, there is another tool named as afflux advisor which helps in quick calculation of afflux at simple culvert and bridge in a uniform flow condition. Like afflux generator, here also calculation is based on laboratory data as well as on field data but the problem with afflux advisor is it cannot provide longitudinal water surface profile. Water level, flow, rating curves, velocity, area, perimeter, Froude Number, Reynolds Number etc. are the available outputs with respect to given depth. Spatial distributions of velocity, boundary shear and shear velocity can also be obtained across the section through CES. Along with all above advantages there are some limitations of this software. It can only work with steady flow condition. It cannot work for sluice gates, weirs etc. Except within bridge and culvert it cannot consider super critical flow conditions.

3   DATA COLLECTION

Experimental discharge data has been collected from FCF (Large scale Flood channel facility created at Wallingford UK) series data(S-1, S-2, S-3, S-8, S-10) and Kinght&Demetriou (1983) (K&D-1, K&D-2, K&D-3) data with varying width ratio α (B/b). Stage discharge is calculated by using the Vertical Interface Method (DCM) as well as interacting divided channel method and Modified Divided Channel Method. The results of the all the methods are then compared with the actual discharge (observed discharge) of the collected data set.

4   RESULT AND DISCUSSION

4.1   Comparison of discharge prediction approaches

By using the given equations for all the above four models, discharge is being computed for both trapezoidal as well as rectangular straight prismatic channel with varying depth with different width ratio α (B/b). The graphs are plotted between relative depth (β) and percentage of error obtained from all four methods with respect to actual discharge (Figure 3(i)-3(viii)). The average absolute error for all four methods with respect to actual discharge is calculated and shown in table-1.

Figure 3(i)

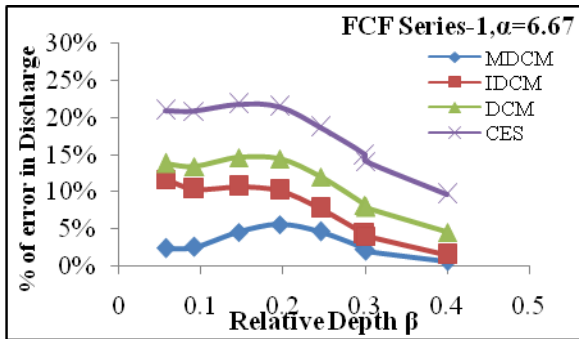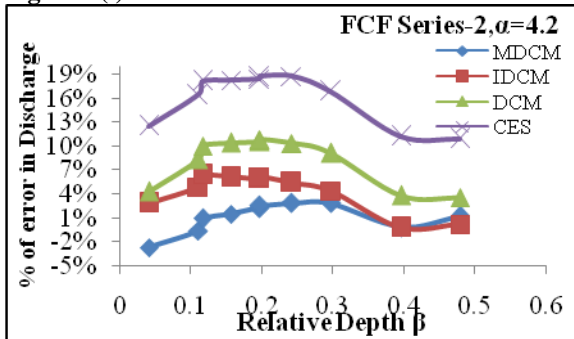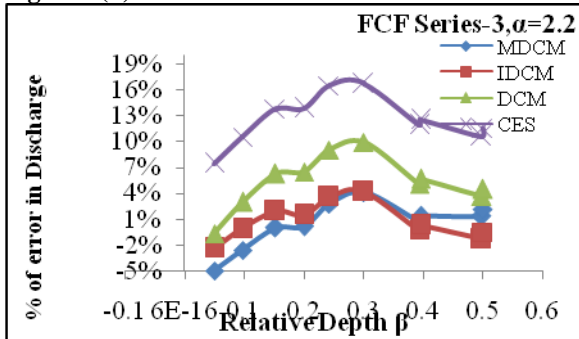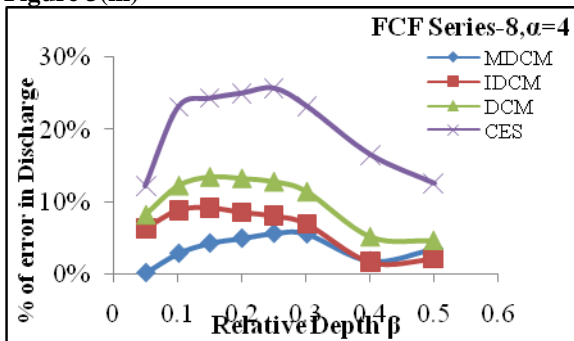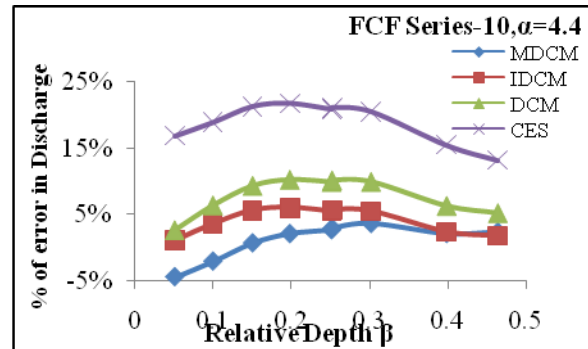Figure 3(ii)

Figure 3(iii)

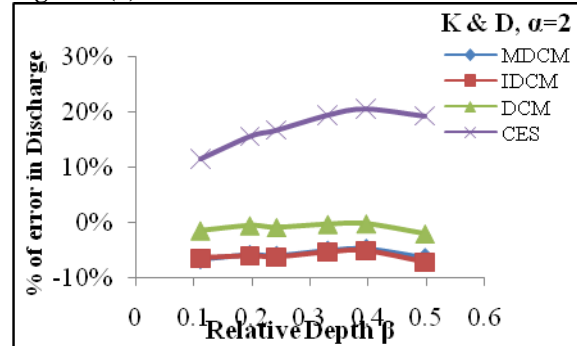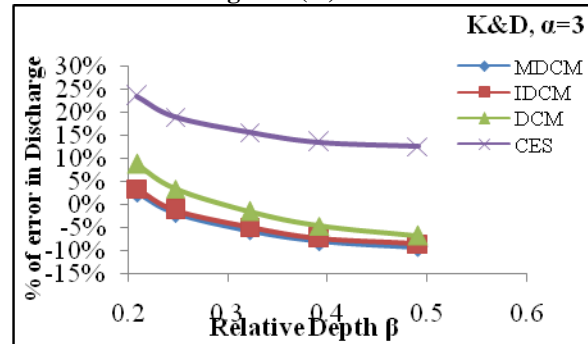
Figure 3(iv)

Figure 3(v)

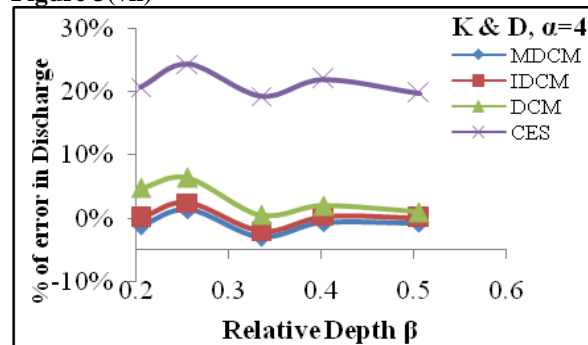

Figure 3(vi)

Figure 3(vii)

Figure 3(viii)

Figure 3(i) - Figure 3(viii) show the plots between the relative depth and % of error in discharge with respect to actual discharge.

Table-1 Average absolute error value

Average Absolute error	MDCM	IDCM	DCM	CES
	4.070955	5.782871	6.549618	14.50004

4.2 Effect of 'n' On MDCM

From the comparison study it is seen that MDCM is the best method among those four methods for predicting discharge by keep 'n' value constant with respect to surface roughness of the channel. Therefore in the present work all eight data sets are validated by MDCM for discharge prediction by changing the value of 'n' with respect to the depth of flow. From the calculation it is found that the MDCM is overestimating the discharge with a maximum error of 35% for lower depth of flow, while for higher depth of flow, the error has been reduced to 2%. So there is a large variation in error is occurring for all depth of flow. Therefore this method needs few modifications.

$\%S_{fp}$ is one of the influencing parameter in determining the discharge through MDCM and it is calculated by using equation(13), but it is valid for a constant value of manning's 'n'. So when the value of 'n' is changed for each depth of flow, it is no longer valid. Therefore on the basis of simulation of the experimental data an empirical factor (E_f) is multiplied to it. So the %S$_{fp}$ is now re written as

$$\%S_{fp} = \left(4.105\left[\frac{100\beta(\alpha-1)}{1+\beta(\alpha-1)}\right]^{0.6917}\right)E_f$$

(15)

Where $E_f = \left(1 + (0.25\beta + 1)^{(1-100\beta)}\right)$

So the value obtained from equation (15) has been put in the equation (10) and (11) to get the values of X_{mc} and X_{fp}. The discharge is again computed through the equation (12) and the results are compared actual discharge of experimental data sets. From the calculation it is found that the Revised MDCM is doing better discharge prediction with an average percentage of error of 4%. A graph is established between the actual discharge and predicted discharge through MDCM and Revised MDCM. After getting the results the graph is plotted between the actual discharge and the predicted discharge obtained through both MDCM and revised MDCM (Figure 4). From the Figure 4, it is clearly visible that Revised MDCM is doing better discharge prediction and it is almost equal to the actual discharge. Through Revised MDCM, and MDCM the discharge is calculated for all data sets by considering the variation in manning's n. So a linear relationship is established between the discharge obtained from these methods and the actual discharge obtained from each experimental run. The linear relationship is presented in Figure5(i)-5(ii).
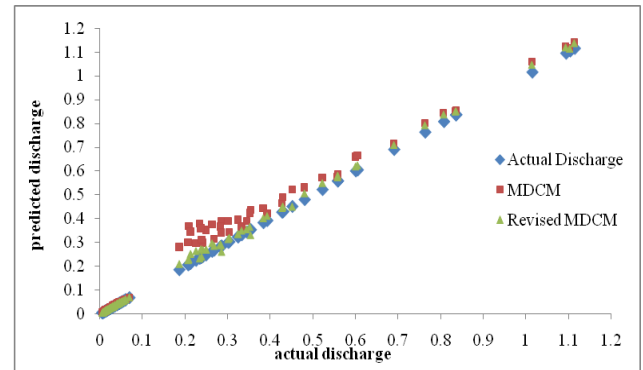
Figure 4. Graph plotted between actual discharge and predicted Discharge through MDCM and Revised MDCM.
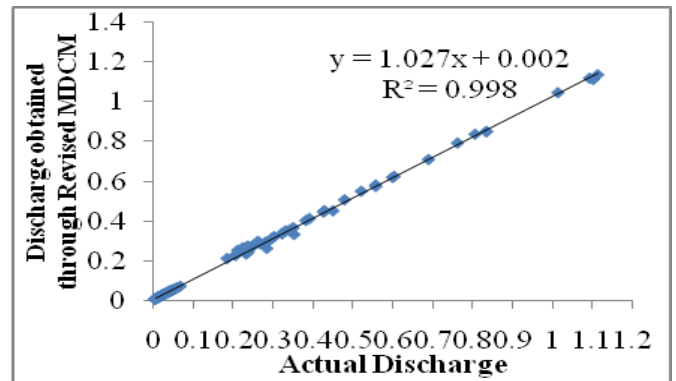
Figure 5(i)
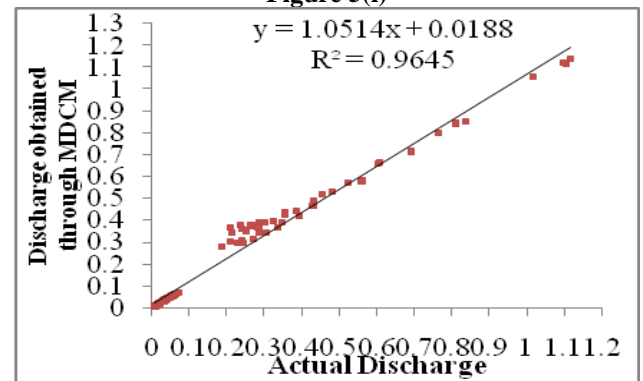
Figure 5(ii)

Figure 5(i) - Figure 5(ii) Correlation plot of actual discharge and Discharge predicted by Revised MDCM and MDCM respectively.

5. CONCLUSIONS

By considering channels with varying cross section and width ratio, discharge has been computed through three different methods. The results are compared with the actual data. From the comparison study we got that both IDCM and MDCM gives better discharge prediction as compared to DCM as both IDCM and MDCM considers the effect of momentum transfer at the junction of the main channel and the flood plain whereas DCM does not consider this effect. Between MDCM and IDCM, MDCM gives more accurate results and from the calculation point of view MDCM is much better than IDCM, as it has less number of computational steps for calculation of discharge which leads to less computational error.

By varying the values of Manning's n with respect to depth of flow, discharge is computed through MDCM. It is found that MDCM fails to predict the discharge for lower depth of flow. But at higher depth it works well. So modification is applied to MDCM. After modification discharge is again calculated through the revised MDCM and the results are compared with the experimental discharge data. It is found that the revised MDCM gives better discharge prediction as compared to MDCM with percentage of error of 4%. One of the limitations of the present study is that the work is applied to straight prismatic channels only, while its applicability to meandering channels needs to be incorporated and tested.

6. REFERENCES

i. Ackers, P. (1992). Hydraulic Design of Two Stage Channels. Proc. Inst. Civil.Engg., Waters. Maritime and Energy, December, Paper No. 9988, 247-257.

ii. Bousmar, D. and Zech, Y. (1999).Momentum transfer for practical flow computation in compound channels. J. Hydraul. Eng., (ASCE), 125(7), 696-706.

iii. Huthoff, F., Roos, P. C., Augustijn, D. C. M. andHulscher, S. J. M. H. (2008). Interacting divided channel method for compound channel flow. J. Hydraul. Eng., (ASCE), 134(8), 1158–1165.

iv. Khatua, K.K., Patra, K.C. (2007). Boundary Shear Stress Distribution in Compound Open Channel Flow. J. Hydraul. Eng., (ISH), 12 (3), 39-55.

v. Khatua, K.K., Patra, K.C., and Mohanty, P.K. (2012).Stage-Discharge Prediction for Straight and Smooth Compound Channels with Wide Floodplains. J. Hydraul. Eng. (ASCE) 138 (1), 93-99.

vi. Patra, K. and Kar, S. (2000). Flow Interaction of Meandering River with Floodplains. J. Hydraul. Eng., (ASCE) 126(8), 593–604.

vii. Sellin, R.H.J.,(1964), A Laboratory Investigation into the Interaction Between Flow in the Channel of a River and that of its Flood Plain, La Houille Blanche, No.7, pp.793-801.

viii. Stephenson, D. and Kolovopoulos, P. (1990).Effects of Momentum Transfer in Compound Channels. J. Hydraul. Eng., (ASCE), 116 (HY12), Paper No.25343, 1512-1522.

ix. Wormleaton, P. R., Allen, J. and Hadjipanos, P. (1982).Discharge Assessment in compound Channel Flow. J. Hydraul. Eng., (ASCE), 108(HY9), 975-994.

x. Zheleznyakov, G. V. (1965). Relative deficit of mean velocity of unstable river flow: Kinematic effect in river beds with floodplains. Proc.14th Congress of IAHR, Paris, France, 5, 144-148.

Boundary Shear Force Distribution Along Different Reaches Of A Highly Meandering Channel

Arpan Pradhan[1] Kishanjit K. Khatua[2] Saine S. Dash[3]
[1] Civil Engineering Dept., N.I.T. Rourkela, Rourkela 769008, India. Email: er.arpanpradhan@gmail.com
[2] Civil Engineering Dept., N.I.T. Rourkela, Rourkela 769008, India. Email: kkkhatua@yahoo.com
[3] Civil Engineering Dept., N.I.T. Rourkela, Rourkela 769008, India Email: sainedash@gmail.com

ABSTRACT: *Accurate assessment of boundary shear distribution is vital for governing various hydraulic problems, such as channel design, channel migration and interaction losses. Boundary shear stress being the tangential component of the hydrodynamic forces acting along the channel bed, boundary shear force is evaluated for the bed and side slopes of the channel. Distribution of boundary shear force along the wetted perimeter directly affects the flow structure. Hence the distribution of shear force between the channel bed, inner and outer walls are analysed for the complete meander path.*

In this paper, an experimental investigation has been carried out to compute shear stress distribution along the bed and side slopes at different cross-sections along a meandering path. The meander path is alienated into 13 sections, ranging from one bend apex to the next bend apex which changes its course at the cross-over. Bend apex is the position of maximum curvature while cross-over represents the section at which the sinuous channel changes its course. The results of the boundary shear distribution; along the bed, inner wall and outer wall are represented, which would give knowledge about the shear force sharing among them. As the longitudinal velocity remains higher in the inner wall than at the outer wall, consequently the shear force would be higher at the inner wall. As the meandering path changes its course, the shear force subsequently changes. Therefore these features can be considered by the engineers and researchers in the field of interaction losses, sediment erosion, deposition etc.

Keywords: boundary shear, shear force, bend apex, cross-over, meander path.

1. INTRODUCTION:

Water flowing in an open channel is opposed by resistance from the bed and side slopes of the channel. This force of resistance is apparently the boundary shear force. Boundary shear stress is the tangential component of the hydrodynamic forces acting along the channel bed. Flow characteristics of an open channel flow are directly dependent on the boundary shear force distribution along the wetted perimeter of the channel. Precise estimation of boundary shear force distribution is essential to deal with various hydraulic problems such as channel design, channel migration and interaction losses. Bed shear forces are useful for the study of bed load transfer where as wall shear forces presents a general view of channel migration pattern.

Rajaratnam and Ahmadi (1981) showed that the boundary shear stress reduces from the centre of the meandering channel toward the edge of the meandering channel. Then it sharply increases at the interface with the edges, afterwards it decreases and levels off for most of the width and finally decreases near the wall. They also concluded that the effect of the meandering channel is to reduce the boundary shear stress. Shear stress is highly affected by the secondary currents since according to Knight and Demetriou (1983), it increases where the secondary

currents flow towards the wall and decreases when they flow away from the wall. Many other aspects affect the boundary shear stress distribution across the channel. Knight, Yuan and Fares (1992) gives the experimental data of SERC-FCF about the boundary shear stress distributions in meandering channels through the path of one complete wave length. They also reported the experimental data on surface topography, velocity vectors, and turbulence for meandering channels. Khatua (2008) extended the work of Patra and Kar (2000) to meandering compound channels. Using five parameters, (sinuosity *Sr*, amplitude, relative depth, width ratio and aspect ratio) general equations representing the total shear force percentage carried by flood plain was presented. The proposed equations are simple, quite reliable and gave good results with the observed data for straight compound channel of Knight and Demetriou (1983) as well as for the meandering compound channel. Khatua (2010) reported the distribution of boundary shear force for highly meandering channels having distinctly different sinuosity and geometry. Based on the experimental results, the interrelationship between the boundary shear, sinuosity and geometry parameters has been shown.

In this paper, the boundary shear stress and shear force distribution along the bed and side slopes is examined throughout the meander path of a highly sinuous meandering channel of sinuosity 4.11. The shear stress and boundary shear force data are analyzed to find the shear force sharing among the bed and side slopes of the highly meandering path.

2. METHODOLOGY

2.1 Experimental Setup

For carrying out research in meandering channels, experimental setup was built in Fluid Mechanics and Hydraulics Laboratory of NIT Rourkela. A meandering channel is built inside a steel tilting flume of around 15m length as shown in figure 1. The bed and wall of channel was made with Perspex sheet (6 to 10 mm thick), having Manning's n value=0.01. The detailed geometric parameters of the meandering channel are illustrated in the following tabulation.

Sl. No.	Parameter	Description
1	Type of Channel	Simple Meandering
2	Flume Dimension	4.0m×15m×0.5m Long
3	Meandering Channel Geometry	Trapezoidal with side slopes 1:1
4	Type of Bed Surface	Rigid and Smooth Bed
5	Section of Channel	0.33m at Bottom and 0.46 m at Top
6	Bank Full Depth	0.065m
7	Bed Slope of the Channel	0.00040146
8	Sinuosity of the Channel	4.11
9	Amplitude of the Meandering Channel	1.555 m
10	Wave length of the Meandering Channel	2.162 m

Table-1: Details of Geometrical Parameters of the Meandering Channel

Figure 1. Photographs of the Experimental Channel

2.2 Position of Measurement

All the measurements are observed from the second bend apex to the next corresponding bend apex passing through the cross-over of the experimental meandering channel from the upstream end. Observations are recorded under steady and uniform conditions. A moving bridge arrangement is provided along the width of the channel of around 1.2m width by 4m length across the channel. The measuring instruments such as point gauges and Pitot tubes are arranged on the bridge such that each section along the meander path is accessible for measurements. A section at crossover perpendicular to both the inner and outer curves of the meandering channel is drawn and extended unto the extended bend apex line, as shown in figure 2. An angle of 120^0 is formed for both the curves. This is the cross-over angle or the arc angle. The curves are divided into 6 equal sections of 20^0 each to the centreline of the meandering channel. Channel sections are drawn along the width i.e. perpendicular lines drawn to both the curves from these points. Sections A and M are the bend apex sections while section G is the cross-over section. The sections A through M are considered for measurement of the boundary shear stress.
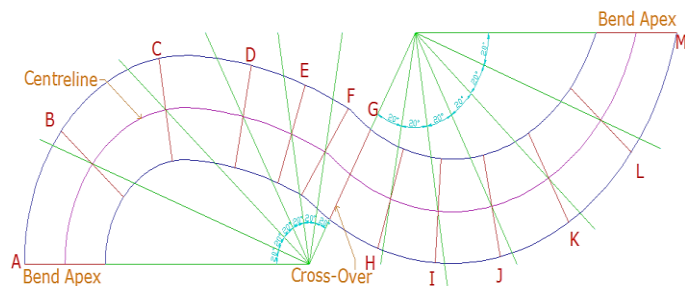
Figure 2. Plan Geometry of the Meandering Path.

A constant discharge of 5.2 x 10^{-3} m^3/s is maintained while taking the readings for the entire meandering path with the help of a rectangular notch incorporated at the start of the flume. Series of Pitot-tubes with moving bridge arrangement are made to measure the pressure difference at different grid points of the flow passage of the channel as shown in figure 3. The Pitot tube is used as Preston tube to find the shear stress at the channel bed and side slopes. The measurements are taken at different reaches along the meander path for every section. The lateral spacing of the grid points has been taken as 4cm on either side of the centreline. The measurements are taken at the bed of the channel and the side slopes at by 0.4H, 0.6H, and 0.8H from the bed. H here is the average depth of water at the every corresponding section along the meander path.
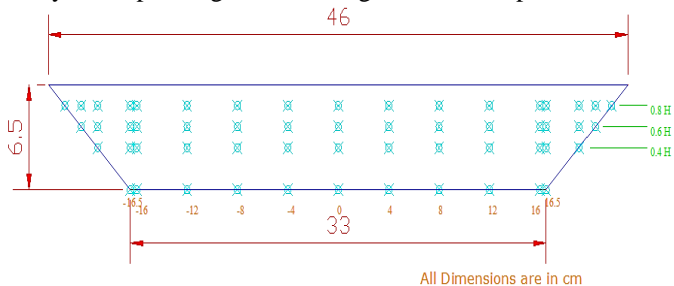
Figure 3. Grid Arrangement of Points for Shear Stress Measurement across the Channel Section.

2.3 Measurement of Boundary Shear Stress

Measurement of shear stress in open channel flow helps in understanding Shear bed load transport, momentum transfer, channel migration, etc. The shear forces at the bed are handy in the examination of bed load transfer whereas shear forces at the walls give a general overview of channel migration pattern. Although there are several methods to evaluate bed and wall shear, Preston-tube method being an indirect estimate, is broadly used for experimental observations.

Preston (1954) developed a simple technique for measuring local shear stress on smooth boundaries using a Pitot tube in contact with the surface. The method was based on the assumption of an inner law relating the boundary shear stress to the velocity distribution near the wall. Preston presented a non-dimensional relationship between the Preston tube differential pressure ΔP, and the boundary shear stress τ, of the form:

$$\left(\frac{\Delta P d^2}{4\rho \upsilon^2}\right) = F\left(\frac{\Delta P d^2}{4\rho \upsilon^2}\right)$$

$$(1)$$

where d is the outer diameter of the Preston tube, ρ is the density of the flow, υ is the kinematic viscosity of the fluid, and F is an empirical function. Patel (1965) further extended the research and his calibration is given in terms of two non dimensional parameters x^* and y^* which are used to convert pressure readings to boundary shear stress, where

$$x^* = \log_{10}\left(\frac{\Delta P d^2}{4\rho \upsilon^2}\right) \text{ and } y^* = \log_{10}\left(\frac{\Delta P d^2}{4\rho \upsilon^2}\right)$$

$$(2)$$

In the form

For $y^* < 1.5$ $y^* = 0.5x^* + 0.037$

$$(3)$$

For $1.5 < y^* < 3.5$ $y^* = 0.8287 - 0.1381x^* + 0.1437x^{*2} -$
0.006 x^{*3} (4)

and

For $3.5 < y^* < 5.3$ $x^* = y^* + 2\log_{10}(1.95y^* + 4.10)$

$$(5)$$

In the present case, all shear stress measurements are taken at all the thirteen sections throughout the meander path between the two bend apexes. The pressure readings were taken using pitot tubes along the predefined points across all the sections of the channel along the bed and side slopes. The manometers attached to the Pitot tubes provide the head difference between the dynamic and static pressures. The differential pressure is then calculated from the readings on the vertical manometer by,

$$\Delta P = \rho g \Delta h$$

$$(6)$$

where Δh is the difference between the two readings from the dynamic and static, g is the acceleration due to gravity and ρ is the density of water. Here the tube coefficient is taken as unit and the error due to turbulence is considered negligible.

Accordingly out of the equations 2-5, the appropriate one was chosen for computing the wall shear stress based on the range of x^* values. After that the shear stress value was integrated over the entire perimeter to calculate the total shear force per unit length normal to flow cross-section carried by the meandering section. The total shear thus computed was then compared with the resolved component of weight force of the liquid along the stream-wise direction to check the accuracy of the measurements.

3. RESULT AND ANALYSIS

3.1 Boundary Shear Stress Results

Boundary shear measurements are carried out at different sections from one bend apex to another bend apex through the cross-over. Total thirteen reaches of boundary shear measurements are carried out but shear stress plots for just five such sections are demonstrated. The figures 4.1 to 4.5 illustrate the boundary shear stress distributions across the channel bed and the side slopes at the inner and outer walls for five intermediate reaches, while the detailed values are shown by the contour plots in figure 5. The shear stress profiles along the rigid surface of the channel are represented by showing the stress curves perpendicular to all the three sides of the channel; namely the bed, the inner wall and the outer wall. Hence the figures give a clear demonstration about the boundary shear stress distribution throughout the channel section.
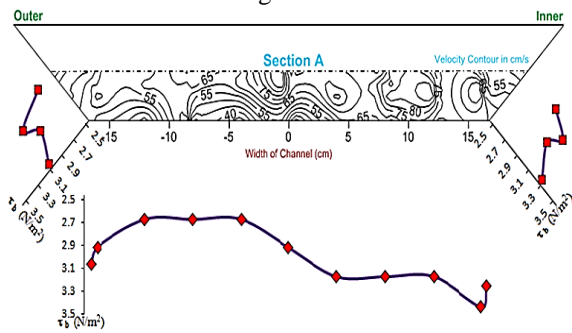
Figure 4.1
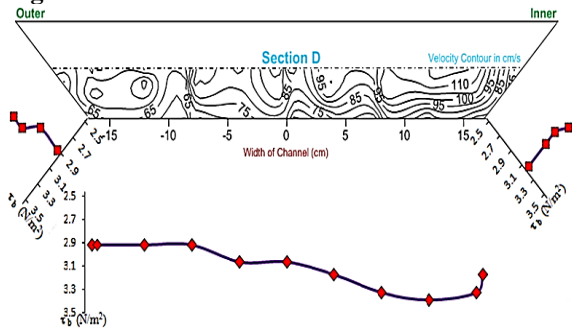
Figure 4.2
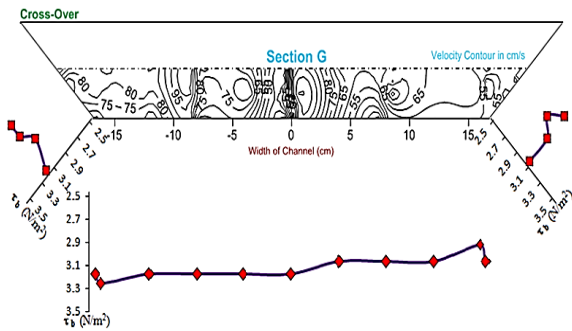
Figure 4.3
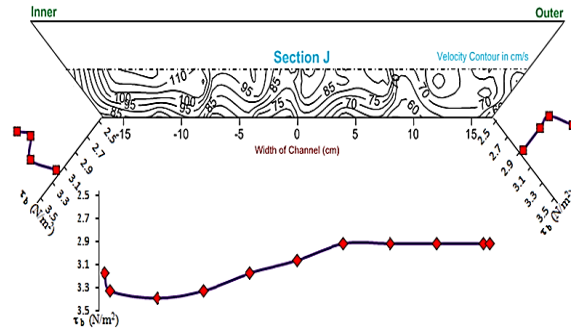
Figure 4.4
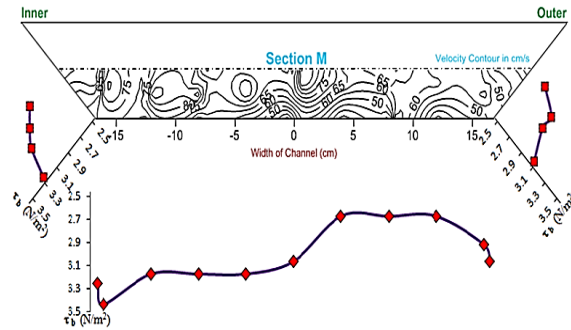
Figure 4.5

Figure 4. Boundary Shear Stress Plots across 5 intermediate sections along the Meander Path.
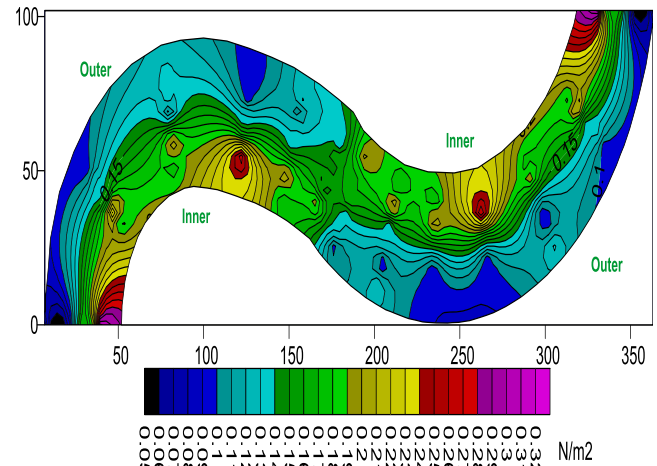
Figure 5. Contour Plot for Boundary Shear Stress along the Meander Path.

From the above boundary shear graphs it is observed that the highest shear stress at the inner bank of the section A is found to be around 3.44N/m^2, while a minimum of 2.67N/m^2 at the outer wall. The variation of shear stress in this section is seen to be erratic. At the corresponding sections before the cross-over, the shear stress although remaining higher towards the inner wall, the variation of shear stress between the inner and outer walls is observed to be gradual. At the cross-over section G, the variation of boundary shear stress is observed to be more or less uniform throughout the channel section. The shear stress value remains close to 3N/m^2. In the corresponding sections the

shear stress values reverse across the channel width, with the higher shear stress value remaining towards the inner wall.

3.2 Boundary Shear Force Distribution

Using the Preston tube technique, boundary shear stress is measured along the wetted perimeter of the channel at all the 13 different sections between one bend apex to the next bend apex. At every section, the boundary shear distribution plots were shown in figure 4. At each section the boundary shear stress is integrated over the wetted perimeter to get the shear force at the inner wall, outer wall and bed separately.

$$SF_{Inner} = \int_{Inner} \tau dp \tag{7}$$

$$SF_{Outer} = \int_{Outer} \tau dp \tag{8}$$

$$SF_{Bed} = \int_{Bed} \tau dp \tag{9}$$

$$SF_{Inner} + SF_{Bed} + SF_{Outer} = SF_T \tag{10}$$

Theoretically, $SF_T = \rho gAS$ (11)

SF representing the shear force, the total shear force is calculated by using the equation 4.4. The total theoretical shear force is calculated for each section by using equation 4.5. The total theoretical shear force is averaged and compared with the actual values. The error found between the values (which are less than 10%) is distributed proportionately among the bed and walls which give a new normalized value of shear force for the bed and walls.

The Table 2 depicts the shear force distribution and the percentage of sharing of normalized shear force at the inner wall, outer wall and the bed of the channel section from the averaged total theoretical shear force. After finding the shear force distribution in the inner wall, outer wall and bed, the boundary shear force distribution for the different sections are plotted and shown in figure 5 and 6.

Table 2. Shear Force Distribution for Meandering Channel at Different Reaches

Section	Flow Depth (in m)	$Area_{MC}$ (in m^2)	SF_{Inner} (in Nm/s)	SF_{bed} (in Nm/s)	SF_{Outer} (in Nm/s)	$SF_T{}'$ Experimental (in Nm/s)	SF_T Actual (in Nm/s)	SF_{Inner} as % of SF_T	SF_{Bed} as % of SF_T	SF_{Outer} as % of SF_T
A	0.035	0.012775	0.00690095	0.04039373	0.00450458	0.05179926	0.05029667	13.3224798	77.9813008	8.69621937
B	0.0377	0.01386229	0.00648843	0.04781314	0.00550344	0.05980501	0.05457745	10.849305	79.948384	9.20231096
C	0.0397	0.01467709	0.00696728	0.05045436	0.00470018	0.06212183	0.05778542	11.2155152	81.2184122	7.5660726
D	0.0415	0.01541725	0.00779788	0.05381132	0.00486157	0.06647077	0.06069951	11.7312916	80.9548561	7.31385231
E	0.044	0.016456	0.00782654	0.05026659	0.00340827	0.0615014	0.06478919	12.7257887	81.7324356	5.54177568
F	0.0422	0.01570684	0.00852204	0.05201762	0.00373357	0.06427323	0.06183966	13.2590836	80.9320131	5.80890329
G	0.04	0.0148	0.00553787	0.05042526	0.00705851	0.06302164	0.05826933	8.7872574	80.0126083	11.2001343
H	0.0373	0.01370029	0.00761981	0.04741461	0.00401603	0.05905044	0.05393964	12.903896	80.2950936	6.80101032
I	0.0363	0.01329669	0.00748323	0.04622744	0.00339398	0.05710465	0.05235062	13.1044107	80.9521422	5.94344712
J	0.0398	0.01471804	0.00905488	0.0522715	0.00461722	0.0659436	0.05794664	13.7312458	79.2669802	7.00177399
K	0.0354	0.01293516	0.00700224	0.04422857	0.00479621	0.05602702	0.05092724	12.497966	78.9415098	8.56052425
L	0.0361	0.01321621	0.00568623	0.04605451	0.00503772	0.05677846	0.05203376	10.0147723	81.1126371	8.87259066
M	0.0385	0.01418725	0.0066	0.04193355	0.00436462	0.05289463	0.05585686	12.4709341	79.2775215	8.25154446
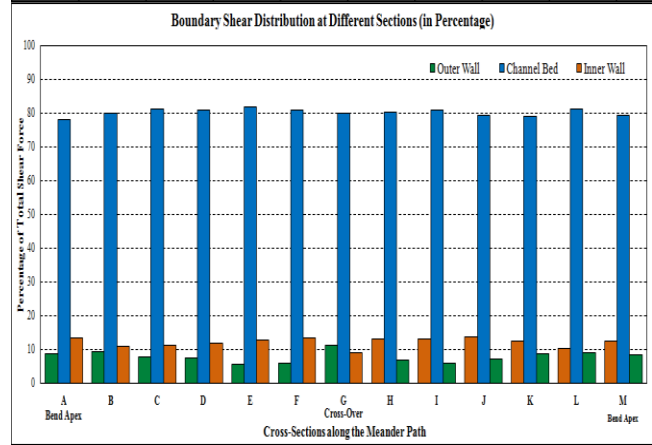
Figure 6. Boundary Shear Distribution at Different Sections (in percentage) – Separately
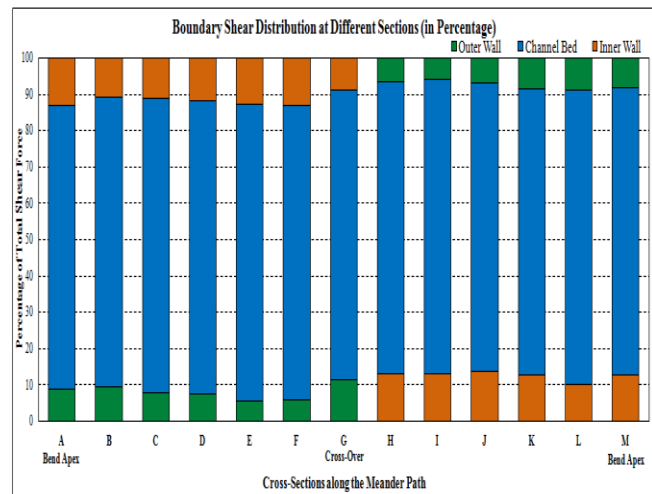
Figure 7. Boundary Shear Distribution at Different Sections (in percentage) – In one Column

From the figure 6 it is seen that, at the bend apex section A, the shear stress carried by the inner wall is more as compared to the outer wall. The inner wall carries about 13% of the total shear force while the outer wall carries about 8%. While going from reach to reach from the bend apex, as seen in figure 7 the shear carried by the inner wall decreases and reaches a minimum at

the cross-over (around 9% of the total shear force). Then the value goes on increasing towards the next bend apex. Similarly as seen in figure 7, at the outer wall, the shear force carried by the bend apex is less (about 8% of the total shear force) which first slightly decreases and then increases to reach maximum value at the cross-over (about 11% of the total shear force).On moving from the cross-over, the shear force at the outer wall starts decreasing and then somewhat increases towards the other bend apex. From figure 6, it is observed that there is a significant difference in the shear force sharing among the inner and outer walls of all the reaches. But, there is less variation among the inner and outer walls of the cross-over section G. Figure 6 demonstrates that the shear force carried by the bed of the channel throughout the meander path is found to remain more or less constant. The bed is observed to carry about 80% of the total shear force while the rest is being shared by the inner and outer walls.

4. CONCLUSIONS

The following conclusions can be presented in this work

1. The present research work is providing information for getting shear stress variation of a meandering channel of sinuosity more than 4.

2. An experimental investigation has been carried out to measure the boundary shear stress and shear force distribution along the bed and the side slopes of a highly meandering compound channel at different reaches along the meander path.

3. From the results of shear stress measurements it is found that the shear stress at the inner wall always remains higher as compared to that at the outer wall. The boundary shear stress distribution is prominent in the bend apex section while the difference gradually decreases on travelling from the bend apex to the cross-over. Boundary shear stress distribution at the cross-over section is found to be more or less uniform throughout.

4. The shear force carried by the inner wall is found to decreases up to the cross-over section and then goes on increasing. The shear force at the inner wall is also found to always remain higher than the shear force at the outer wall. The shear force carried by the bed of the all the channel section is found to be nearly uniform throughout the meander path.

5. From the shear force distribution results, the sharing among the inner and outer walls is not uniform at all reaches along the meander path. Whereas there is very less variation between the shear force sharing at inner and outer walls at the cross-over section.

6. The above observation can be applied in the study of hydraulic problems such as channel design, channel migration, interaction losses, erosion and depositional pattern study of a meandering channel. Bed shear forces which are useful for the study of bed load transfer and wall shear forces which represent a general view of channel migration pattern can be analysed.

5. ACKNOWLEDGEMENTS

REFERENCES:

i. Khatua, K. K. (2008), "Interaction of flow and estimation of discharge in two stage meandering compound channels". Thesis Presented to the National Institute of Technology, Rourkela, in partial fulfilment of the requirements for the Degree of Doctor of philosophy.

ii. Khatua, K.K. and Patra, K.C. (2010). Evaluation of boundary shear distribution in a meandering channel. Proceedings of ninth International Conference on Hydro-Scienceand Engineering, IIT Madras, Chennai, India, ICHE 2010, 74.

iii. Knight, D. W. (1981). "Boundary shear in smooth and rough channels." J. Hydraul. Div., Am. Soc. Civ. Eng., 107(7), 839–851.

iv. Knight D. W. and Demetriou J.D. (1983). "Floodplain and main channel flow interaction." J. Hydraul. Eng., ASCE, 109(8), 1073–92.

v. Knight, D.W.,Yuan,Y.M., and Fares, Y.R. (1992). "Boundary shear in meandering channels.",Proceedings of the Institution Symposium on Hydraulic research in nature and laboratory, Wuhan, China (1992) Paper No.11017, Vol. 118, Sept., pp. 151-159.

vi. Patel, V.C. (1965). "Calibration of the Preston tube and limitations on its use in pressure gradients.", Journal of Fluid Mechanics, 23(01), 185-208.

vii. Patra, K.C, and Kar, S. K. (2000). "Flow Interaction of Meandering River with Floodplains". Journal of Hydr. Engrg., ASCE, 126(8), 593–604.

viii. Pradhan, A. (2014). "Analysis of Flow along the Meander Path of Highly Sinuous Rigid Channel". Thesis Presented to the National Institute of Technology, Rourkela, in partial fulfilment of the requirements for the Degree of Master of Technology.

ix. Preston, J. (1954). "The determination of turbulent skin friction by means of Pitot tubes.", Journal of the Royal Aeronautical Society, 58(518), 109-121.

x. Rajaratnam, N., and Ahmadi, R.M. (1979). "Interaction between Main Channel and Flood Plain Flows." Journal of Hydraulic Division, ASCE,Vol..105, No. HY5, pp. 573-588.

Effect Of Cylindrical Staggered Vegetation On Roughness Prediction In An Open Channel

K. Panigrahi[1]   K.K.Khatua[2]   B. Naik[3]

[1]M.Tech (Research), Department of Civil Engineering, N.I.T. Rourkela, 769008, India
[2]Associate Professor, Department of Civil Engineering, N.I.T. Rourkela, 769008, India
[3]Ph. D. (scholar), Department of Civil Engineering, N.I.T. Rourkela, 769008, India
Email: *kajalpanigrahi@yahoo.in*

ABSTRACT:*A laboratory study to explore the effect of vegetation in terms of rigid cylindrical roughness on the hydraulics of flow in an open channel is presented. The study consists of flume experiments for flows with unsubmerged rigid cylindrical stems of a concentration and diameter arranged in a regular staggered configuration. Vegetation in an open channel retards the flow of water by causing a loss of energy through turbulence and by exerting additional drag*

forces on the moving liquid. Because of this complex nature, it is difficult to develop a flow model. Vertical profile of longitudinal velocity in vegetated channels reflects complex mechanics of flow vegetation interactions and determines the bulk flow velocity and flow rate. Velocity coefficient is found to vary with the non-dimensional hydraulic, geometric and surface parameters such relative depth ratio of water depth h to stem height hs, Reynolds's number (Re) and Froude's number (Fr) etc. Parameters determining the velocity distribution are discussed and results are summarised and presented. Graphs of velocity vs. hydraulic parameters are presented. In addition, vegetation characteristics were shown to influence the height of maximum velocity.

Key Words: Vegetative channel, cylindrical roughness, Manning's coefficient, Reynolds's number (Re) and Froude's number (Fr), Relative depth.

1. INTRODUCTION

The establishment of a satisfactory waterway for handling runoff from agricultural area is probably the most difficult problem encountered by the farmers in planning an economical and effective conservation system. While vegetated waterways have long been employed for terrace outlets, very little uses until recent years have been made of grasses in artificial waterways, but dependence has been placed more on the mechanical structures. So need for research of design of effective vegetated waterways is imminent. Design of effective vegetated waterways needs that various hydraulic characteristics of vegetated channels be studied. The most important hydraulic characteristic is the retardance coefficient mainly called as Manning's n. The retardance coefficient varies from vegetation to vegetation and also for the same vegetation it varies according to the stage of growth, depth of submergence etc. So effective design of grassed waterways needs a closely approximate value of retardance coefficient to be determined. If we underestimate the value of the roughness coefficient (n) then the canal section will be over designed as the low value of n will lead to high velocity and hence to high discharge capacity of the channel. Similarly if we overestimate the value of the retardance coefficient and use this value in design problems then we underestimate the discharge. The excess discharge therefore frequently spoils the downstream areas of channel by overtopping. This clearly indicates that the retardance coefficient of the grasses used for channel need to be determined before this value is used for the design purposes.

Vegetation in an open channel retards the flow of water by causing a loss of energy through turbulence and by exerting additional drag forces on the moving liquid. Because of this complex nature, it is difficult to develop a flow model. The scope of the present work includes determination of the various hydraulic characteristics i.e. resistance offered to the flow by the vegetation, protection offered by the channel bed and effect of the vegetation on the flow characteristics in the channel. In addition to the above mentioned points, other aspects like velocity distribution relations, Froude's number and Reynolds's number calculation and design of grass-lined channels are studied.

The degree of influence in a vegetative channel further depends on the other vegetation characteristics such as (a) vegetation species, (b) distribution, (c) flexibility, (d) degree of submergence and (e) the vegetation density (Abood et al. 2006). In a vegetative open channel flow, the average water velocity in the cross section tends to decrease at a higher rate, due to flow resistance from the stems and leaves of the vegetation which generally increases roughness of surfaces (Fishenich 2000). For calculating flow velocity, Manning's formula is generally used. It is also widely used in vegetated waterways to solve in related hydraulic applications. The formula states:

$$V = \frac{K}{n} R_h^{2/3} S^{1/2}$$

(1)

Where, V is the cross-sectional average velocity (L/T; m/s); K is a conversion factor of ($L^{1/3}$/T), 1 $m^{1/3}$/s for SI unit); n is the Gauckler–Manning coefficient (frequently called as Manning's roughness coefficient); R_h is the hydraulic radius ($L; m$)which is the ratio of cross sectional area of flow to wetted perimeter and S is the slope of the hydraulic grade line (= h_f /L), which is the same as the channel bed slope when the water depth is constant and h_f is called difference of hydraulic head across a cross section of channel of length L. Manning's roughness coefficient is found to vary largely in a vegetated waterway. It depends on depth of flow in the channel and slope of the channel; when the slope of the channel increases, roughness coefficients decreases (Diaz 2005).

The present study focuses on straight simple vegetated rectangular channel. New experiments have been conducted at the Hydraulics and Fluid mechanics Laboratory of Civil Engineering Department of National Institute of Technology, Rourkela to analyse the behaviour of flow effect due to rigid cylindrical vegetation.

2. MATERIALS AND METHODS

2.1 Experimental Setup

Experiments have been conducted in a straight simple rectangular channel with varying cross section built inside a metallic flume measuring 12 m long × .60 m width × 0.45 m depth and the aspect ratio is δ>5.00. Water was supplied through a centrifugal pump (a 15 hp) discharging into a RCC overhead tank. In the downstream end there lies a measuring tank followed by a sump which feed the water to the overhead tank through pumping. Water was supplied to the flume from an underground sump via an overhead tank by centrifugal pump (15 hp) and recirculated to the sump after flowing through the experimental channel and a downstream volumetric tank fitted with closure valves for calibration purpose. An adjustable vertical gate along with flow straighteners was provided in upstream section sufficiently ahead to reduce turbulence and velocity of approach in the flow near the initial section. At the downstream end another adjustable tail gate was provided to control the flow depth and maintain a uniform flow in the channel. A movable bridge was provided across the flume for both span wise and stream wise movements over the channel area so that each location on the plan of the experimental channel could be accessed for taking

measurements. The whole channel was fabricated by using 19 mm thick water resistant ply wood in the bed. Iron rods of diameter 6.5 mm, each raised to a height of 10 cm were pre-drilled into the plywood in a staggered pattern with spacing of 10 cm. Section of study with vegetation was limited to 6 m. Figure 1 represents the view of the experimental channel.

Point velocities were measured along verticals spread across the main channel so as to cover the width of entire cross section. Also at a number of horizontal layers in each vertical, point velocities were measured. Measurements were thus taken from mid-point of main channel to the left edge of the channel boundary. The lateral spacing of grid points over which After obtaining the point velocities at various grid points representing the cross section of whole rectangular channel flow, velocity contours were drawn. The velocity contours were drawn by normalizing the point velocities with the cross sectional means velocities for the respective overbank depth of flow.

Table-1: Hydraulic parameters for the experimental runs

Sl. no. of Runs	Discharge Q in m³/s	Depth H in m	Manning's n	Froude no. (Fr)	Reynolds' s no. (Re)
1	0.002345	0.017	0.021	0.648	3695.83
2	0.00287	0.018	0.022	0.622	4517.08
3	0.003638	0.021	0.024	0.618	5661.44
4	0.005287	0.029	0.025	0.563	8029.79
5	0.007255	0.033	0.026	0.548	10864.35
6	0.007898	0.041	0.029	0.504	11576.96
7	0.009327	0.051	0.035	0.430	13285.61
8	0.010264	0.060	0.042	0.363	14219.52
9	0.010711	0.067	0.048	0.322	14561.58
10	0.011206	0.075	0.054	0.288	14925.72

The new experimental results from rectangular vegetated channel are presented in this section. Velocity contours of cross sections without vegetation are shown in figure 2(a,b). From the figure it is seen that both at sections 2 and 4 the higher velocity contours occur at central region. The Stage~Discharge curve of the straight vegetated channel was plotted and shown in figure 3. Five cross sections are taken for the detail study purpose. Sections 1 and 5 are having 4 vegetations, section 3 consists of 5 vegetations, sections 2 and 4 do not consist of vegetation. The depth average velocity curves of two cross sections without vegetation (section-2 and section-4) and with vegetation (section-1, section-3 and section-5) of the experimental channel

measurements were taken was kept 5 cm inside the main channel. Velocity measurements were taken by pitot static tube (outside diameter 4.77 mm) and two piezometers fitted inside a transparent fibre block fixed to a wooden board, hung vertically at the edge of flume. The ends were open to atmosphere at one side and connected to total pressure hole and static hole of pitot tube by long transparent PVC tubes at other side. Steady uniform discharge was maintained during the running of the experiment and several runs were conducted. The discharge varied between 0.002345 m³/s to 0.013564 m³/s. Point depth average velocity were made at a depth of 0.4H from the bed in the main channel

11	0.012636	0.091	0.064	0.243	16142.68
12	0.013171	0.095	0.065	0.237	16654.79
13	0.013564	0.103	0.072	0.217	16812.13

are shown in the figure 4(a,b,c,d and e). From the figure it is seen that the vegetated cross sections are observed to have higher depth average velocities when compared to the cross sections without any cross sections in agreement with the depth average velocity curves. The curves of non-dimensional parameter i.e. Inverse Aspect Ratio Vs. Froude's Number, Reynolds's Number, Manning's n are shown in Figure 5(a,b and c) respectively. From the figure it is seen that the Froude's Number decreases as the Inverse Aspect Ratio increases while the Reynolds's Number increases alongwith the increase in Inverse Aspect Ratio. Again Manning's n is also seen to be rising according to the rise in Inverse Aspect Ratio.
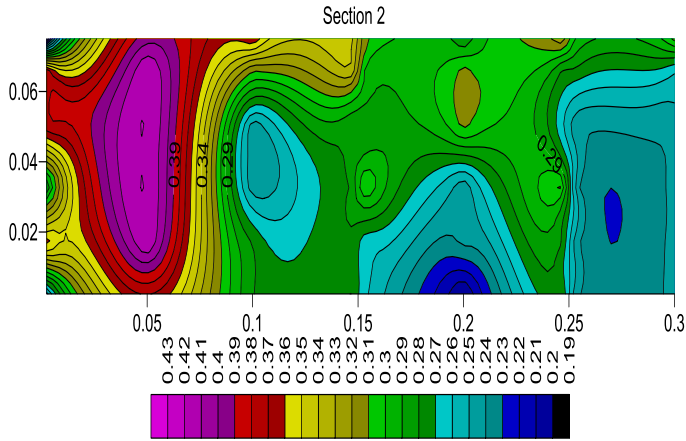
Figure-2(a): Velocity contour of section-2
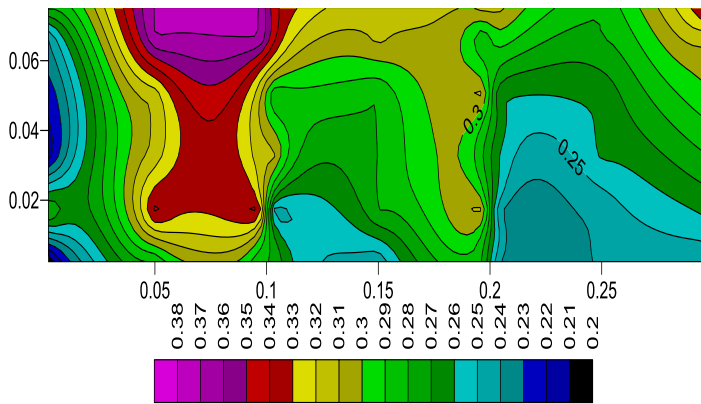
Figure-2(b): Velocity contour of section-4
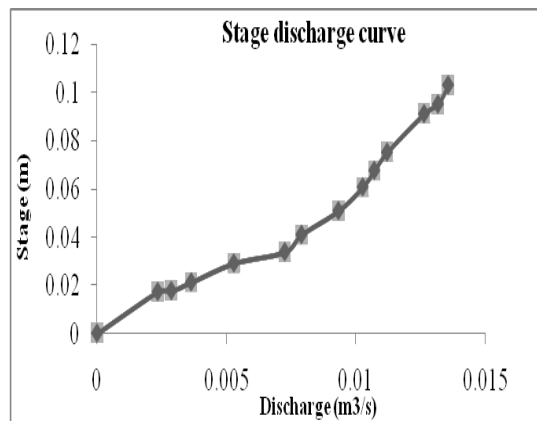
Figure-3: Stage~Discharge curve for the vegetated channel
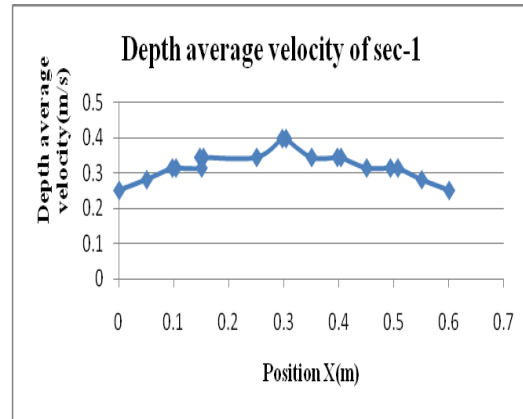
Figure-4(a): Depth average velocity curve of section-1 with 4 vegetations
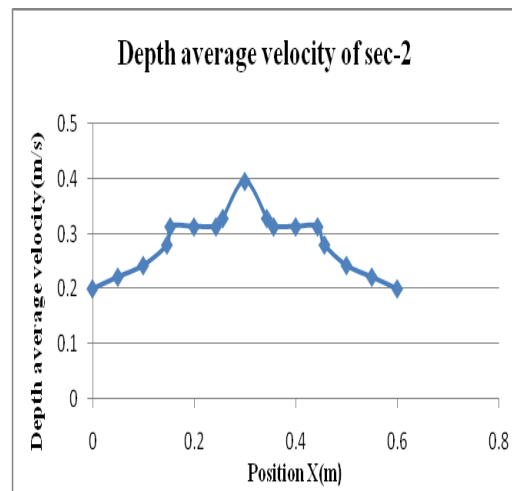
Figure-4(b): Depth average velocity of section-2 without vegetation
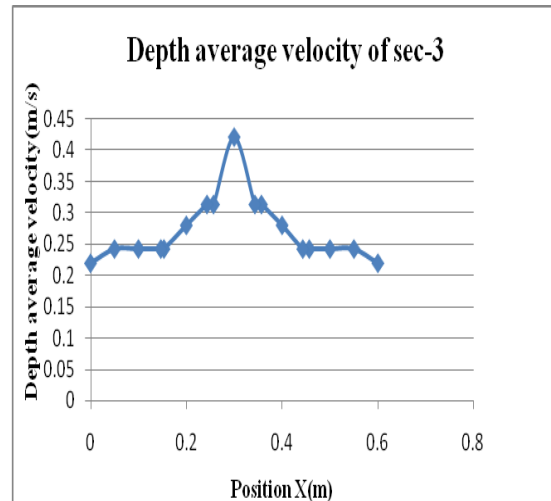
Figure-4(c): Depth average velocity curve of section-3 with 5 vegetations
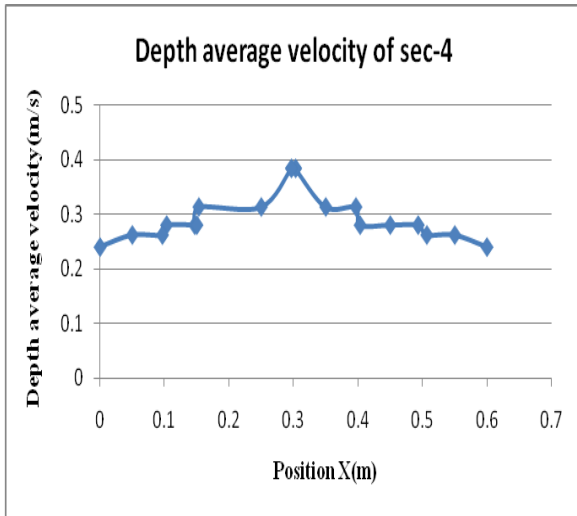
Figure-4(d): Depth average velocity curve of section-4 without vegetation

Figure-5(a): Froude's Number vs Inverse Aspect Ratio
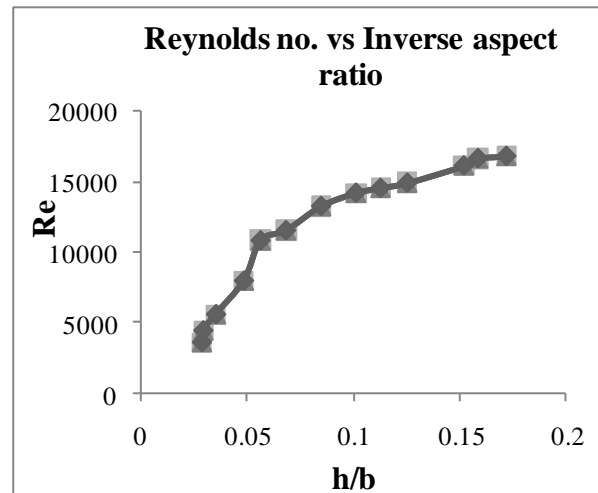
Figure-5(b): Reynolds's Number vs Inverse Aspect Ratio

Figure-4(e): Depth average velocity curve of section-5 with 4 vegetations
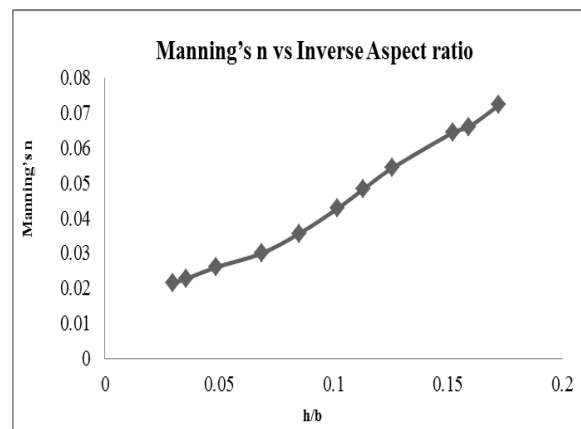
Figure-5(c): Reynolds's Number vs Inverse Aspect Ratio

4. CONCLUSIONS

Experiments are conducted to study the effect of flow variables for simple straight rectangular channel with rigid cylindrical vegetation arranged in a staggered pattern. From the velocity contours of the experimental channels, it is seen that both at sections 2 and 4 the higher velocity contours occur at central region. The vegetated cross sections are observed to have higher depth average velocities when compared to the cross sections without any cross sections in agreement with the depth average velocity curves. The nature of the Froude's Number and the Reynolds's Number are found to be exactly opposite when plotted against Inverse Aspect Ratio. The Froude's Number decreases as the Inverse Aspect Ratio increases while the Reynolds's Number increases alongwith the increase in Inverse Aspect Ratio. Again Manning's n is also seen to be rising according to the rise in Inverse Aspect Ratio.

5. REFERENCES

i.   B. Panigrahi, "Hydraulic Characteristics of Grass-Lined Channel," Unpublished M. Engineering. Thesis, Asian Institute of Technology, Bangkok, Thailand, Dec. 1987.

ii.   B. Panigrahi, B.P. Behera and S.D. Sharma, "Retardance coefficients for flow in vegetated waterways," J. of Indian Water Resources Society, Vol. 13, pp. 206-211, 1993

iii.   E. Žic1, M. Vranješ, N. Ožanić1 "Methods of roughness coefficient determination in natural riverbeds," in International symposium on water management and hydraulic engineering, 2009, Paper: A01.

iv.   E.Žic, "The roughness coefficient analysis on the example of Butoniga river bed in Istria," master's thesis in the making, Rijeka 2008

v.   F.C. Wu, H.W. Shen and Y.J. Chou, "Variation of roughness coefficient for un-submerged and submerged vegetation," J. of Hydraulics Engineering, ASCE, Vol. 125(9), pp. 934-942, 1999.

vi.   F. Maghdam and N. Kouwen, "Non-rigid, non-submerged vegetation roughness on flood plains," J. of Hydraulics Engineering, ASCE, Vol. 123(1), pp. 51-56, 1997.

vii.   J.C. Fishenich, "Resistance due to vegetation," EMRRP Technical Notes Collection (ERDC TN-EMRRP-SR-07), U.S. Army Engineer Research and Development Center,Vicksburg, MS, p. 9., 2000.

viii.   K.V.N.Sharma and S.R. Sasikantah, "Evaluation of Manning's n for steady and non-uniform flow," in Proc. Second Australian Conference on Hydraulics and Fluid Mechanics, 1965 pp. A177-A187.

ix.   M. Righetii and A. Armanini, "Flow resistance in open channel flows with sparsely distribution bushes," J. of Hydrology, Vol (269), pp. 55-64, 2002.

x.   M.M. Abood, B. Yusuf, T.A. Mohammed and A.H. Ghazali," Manning Roughness Coefficient for Grass-Lined Channel," Suranaree J. Sci. Technol., Vol.13(4), pp. 317-330, 2006.

xi.   M.W. Abdelsalam, F.A. Khattab, A.A. Khalifa and F.M. Bakry, "Flow capacity through wide and submerged vegetation channels," J. of Irrigation and Drainage, ASCE, Vol. 150(5), pp. 25-44, 1992.

xii.   M.A. Sadeghi, M.S. Bajestan and M. Saneie, "Experimental investigation on flow velocity variation in compound channel with son-submerged rigid vegetation in floodplain," World Applied Sciences J., Vol. 9 (5): 489-493, 2010.

xiii.   N. Kouwen and R.M. Li, "Biomechanics of vegetative channel linings, J. of Hydraulic Division," ASCE, Vol. 106 (HY 6), pp. 1085-1103, 1980.

xiv.   N. Kouwen and E.T. Unny, "Flexible roughness in open channels," J. of Hydraulics Division, ASCE, Vol. 99(5), pp.713-729, 1973.

xv.   N. Kouwen, "Effect of riparian vegetation on flow resistance and flood potential discussion," J. of Hydraulic Engineering ASCE, Vol. 126 (12), pp. 954, 2004.

xvi.   R.G. Diaz, "Analysis of Manning coefficient for small-depth flows on vegetated beds," Hydrological Processes, Vol. 19, pp. 3221-3233, 2005.

xvii.   R.N. Fenzl and J.R.Davis, "Hydraulic resistance relationships for surface flows in vegetated channels," Trans. of the ASAE, vol. 7(1), pp. 46-51 and pp.55, 1964.

xviii. R. Li and H.W. Shen, "Effect of tall vegetation on flow and sediment, J. of the Hydraulic Division," ASCE, Vol. 99 (HY 5), pp. 793-813, 1973.

xix.   S. Petryk and G. Bosmajian III, "Analysis of flow through vegetation, J. of the Hydraulic Division," Proc. ASCE, 1975, Vol. 101, (HY 7), pp. 871-884.

xx.   S.F. Shih and G.S. Rahi, "Seasonal variations of Manning's roughness coefficient in subtropical marsh," Trans. of ASAE, Vol. 25(1), pp. 116-119, 1982.

xxi.   T.Murota, M.Fukuhara, "Sato: Turbulence structure in vegetated open channel flows," J. of Hydro science and Hydraulic Engineering, Vol. 2 (1), pp. 47-61, 1984.

xxii.

xxiii.

An Improved Approach for Flow Prediction in Compound Open Channel Flowof Uniform Roughness

Pradhan Siprarani[1]Khatua Kishanjit K. [2]

[1]Ph.D. Research Scholar Departmentof Civil Engineering, N.I.T. Rourkela, India

[2]Associate Professor, Departmentof Civil Engineering, N.I.T. Rourkela, India.
Email: pradhan.siprarani@gmail.com,
512ce1006@nitrkl.ac.in.

ABSTRACT:*Most natural rivers consist of a main channel and the adjacent floodplains. The various subdivision methods fail to determine the discharge capacity in rivers with overbank flow because of the ignorance of the strong interaction between the main channel and the shallow floodplains. An experimental investigation is performed to study the effect of momentum transfer in terms of an apparent shear stress in rough and smooth compound channels for different hydraulic, geometric conditions and roughness ratios. A new method to calculate flow in compound channels is proposed. The approach is based on a new model on the momentum transfer coefficient at the vertical interface and the horizontal interface between adjacent flow compartments, typically between the main channel and floodplain of a two-stage channel. The new approach is found to give better results as compared to the other approaches when applied to the present experimental data sets, large channel of FCF data sets and some natural river data sets.*
Keywords: Compound Channels, Momentum Transfer coefficient, Stage-Discharge relationship, Apparent shear stress

1. INTRODUCTION

A major area of uncertainty in river channel analysis is that of accurately predicting the capability of river channels with floodplains, which are termed compound channels. Cross-sections of these compound channels are generally characterized by a deep main channel, bounded on one or both sides by a relatively shallow floodplain, which is rougher and has slower velocities than as compared to that of main channel. Due to interaction between the main channel and floodplains, there are bank of vertical vortices found in many experiments by Myers (1990), Knight and Shiono (1991), along the vertical interface between the main channel and the flood plain, which lead to extra resistance in terms of consumption a lot of energy. Due to this extra resistance, the prediction of stage-discharge curve become difficult and more difficult when there is large different roughness between the main channel and floodplain. There, flow structure and flow resistance become very complex and flow shows very strongly three-dimensional characteristics, see Knight (1999), Rameshwaran and Naden (2003).In predicting the flood-water level, conventional methods for estimating the discharge capacity of a compound channel have

been based on standard uniform flow formulas, such as Chezy, Manning, and Darcy-Weisbach equations, by either treating the cross section as a single channel or by dividing it horizontally, vertically, or diagonally into non interacting subareas. For divided channel methods, the total discharge is then obtained by adding the individual discharges in each subarea (Chow 1959; Shiono et al. 1999). However, if the compound section is treated as a single channel, the discharge capacity is underestimated; if the section is vertically divided into subsections of simple shape, the value obtained is a serious overestimation of capacity because the method fails to take account of the extra flow resistance resulting from momentum transfer (Myers and Brennan 1990). Knight and Hamed (1984) compared the accuracy of several subdivision methods for compound straight channels by including and excluding the vertical division line in determining the wetted perimeters of the main channel and the floodplains. However, their results show that the conventional calculation methods result in larger error. Apart from the case of the vertical division, Wormleaton et al. (1982) and Wormleaton and Hadjipanos (1985) also discussed the horizontal division through the junction point between the main channel and the floodplains. However, their studies also show that these subdivision methods cannot well assess the discharge in compound channels.For this type of channels, how to predict its stage-discharge curve is still fraught with difficulty.

This paper mainly focuses on the modeling of momentum transfer coefficient forthree-stage trapezoidal compound cross-section. The cross section is divided into vertically the main channel and floodplain, and floodplain. By separately calculating the apparent shear stress caused by lateral momentum exchange, the average velocity of each sub-section is derived via the balance of force. Using the subsection average velocity, the subsection discharge is estimated to develop the stage discharge relationship in compound channels. The UK Flood Channel Facility (UK-FCF) measured data have been used to verify the model.

2. THEORITICAL ANALYSIS

2.1Force balance analysis in compound channel sub sections

Following the work of Yang et al. (2014) andHuthoff et al. (2008), a step has been taken to present a simplified and modified approach for flow prediction in compound open channel flow. The analysis considered compound channel geometry as depicted in Fig. 1, consisting of a main channel with either two identical floodplains. When the water in the main channel over flows and inundates its floodplains, the momentum transfer takes place which is expressed in the form of apparent shear stresses acting on the horizontal interfacesbetween the upper and lower main channelsconsidered as horizontal apparent shear stress and on the vertical interface between the main channel and the floodplains as vertical apparent shear stresses. Hence, in this

present work, in dealing flow interaction phenomenon, the compound channel is considered to be divided into four sub sections, as shown in Fig.1.
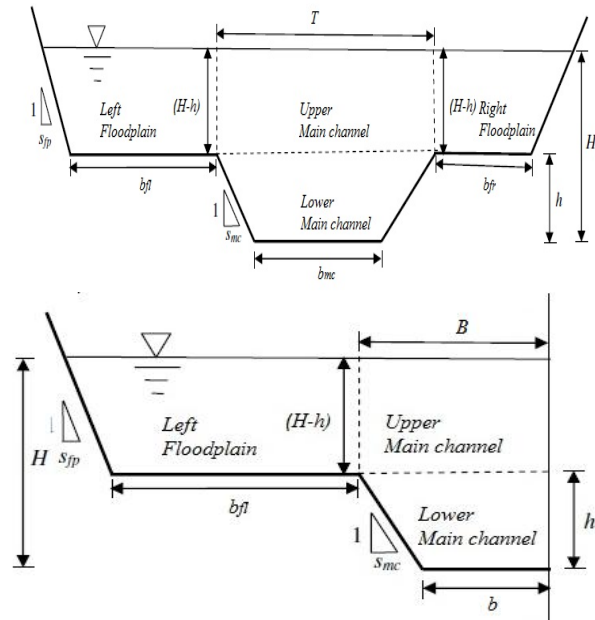
Figure.1 Cross section of compound channel(a)Symmetric with two identical floodplain(b_{fl}&b_{fr}) (b)Asymmetric with one floodplain (b_{fl})

The conceptual horizontal and vertical interfaces among the lower main channel, upper main channeland floodplain are assumed and denoted by broken lines.The present compound channel with subsections are analyzed based on the concept that for uniform flows, the force balance of water for a control volume with a unit length is the weight component equal to the sum of the total bed shear and the total apparent shear:

$$W_{fl} sin\theta = P_{fl}\tau_{fl} - (H - h)\tau_{\alpha flmu}$$

(1)

$$W_{mu} sin\theta = (H - h)\tau_{\alpha flmu} + (H - h)\tau_{\alpha frmu} + T\tau_{\alpha mlmu}$$

(2)

$$W_{fr} sin\theta = P_{fr}\tau_{fr} - (H - h)\tau_{\alpha frmu}$$

(3)

$$W_{ml} sin\theta = P_{ml}\tau_{ml} - T\tau_{\alpha mlmu}$$

(4)

where *W* is the weight per unit length of fluid and equals to *Aρg,A* is the area of subsection,*P* is the wetted perimeter, *ρ* is the water density; *g* is the gravitational acceleration; *sinθ* denoted as S_0 is the bed slope; *T* is the width of the horizontal interface between the upper and lower main channels; *τ_α*is the apparent shear stress, *(H-h)* is flow depths on vertical interfaces between the left and right floodplains and the upper main

channel, the subscripts f_l, f_r, m_l and m_u refer to the left flood plain, the right floodplain, lower and upper the main channel respectively. τ can be calculated with the Chezy equation for uniform flows.

2.2 Determination of the Sub sectional Solid Boundary Shear Stress

For uniform flows, the conventional flow resistance equations, such as the Chezy equation, are based on an assumption that the solid boundary shear stress is proportional to the square of the flow velocity which can be simplified by Manning's formula that the Chezy's constant (C) is equal to $C_i = \frac{1}{n_i} R_i^{1/6}$; where, n_i and R_i= Manning coefficient and hydraulic radius in Subsections i, respectively.

Then, the average shear stresses on each boundary are

$$\tau_{fl} = \frac{\rho g v_{fl}^2}{(\frac{1}{n_{fl}} R_{fl}^{\frac{1}{6}})^2} \quad \tau_{mc} = \frac{\rho g v_{mc}^2}{(\frac{1}{n_{mc}} R_{mc}^{\frac{1}{6}})^2} \quad \tau_{fr} = \frac{\rho g v_{fr}^2}{(\frac{1}{n_{fr}} R_{fr}^{\frac{1}{6}})^2}$$

(5)

where n_{fl}, n_{mc}, and n_{fr} are Manning's coefficients

2.3 Determination of Apparent Shear Stress

The apparent shear stresses on the vertical and horizontal interfaces are derived from the governing equations (1),(2),(3) &(4) as

$$\tau_{aflmu} = \frac{P_{fl}\tau_{fl} - \rho g A_{fl} S_0}{(H-h)}$$

(6)

$$\tau_{afrmu} = \frac{P_{fr}\tau_{fr} - \rho g A_{fr} S_0}{(H-h)}$$

(7)

$$\tau_{amlmu} = \frac{P_{ml}\tau_{ml} - \rho g A_{ml} S_0}{(H-h)}$$

(8)

Where $\tau_{aflmu}, \tau_{afrmu}$ and τ_{amlmu} are known as apparent shear stress in left vertical interface, right vertical interface and horizontal interface respectively.

2.4 Expression for Horizontal and Vertical Momentum Transfer Coefficients

Many investigators such as Knight and Demetriou (1983), and Wormleaton et al. (1982), conclude from a number of experiments that generally in compound channels, due to faster moving water in the upper main channel and the slower moving water on the floodplain, the lateral momentum transfer takes place in the vertical interfaces meanwhile the momentum

transfer also occurs in the horizontal interface that appears generally between the faster moving water in the upper main channel and the slower moving water in the lower main channel. As a result, the vertical apparent shear exists on the interface between the upper main channel and the floodplain, which generally accelerates the flow on the floodplain and resists the flow in the upper main channel. The horizontal apparent stress occurs on the interface between the upper and lower main channels, which generally accelerates the flow in the lower one and resists the flow in the upper one. According to Prandtl's momentum transfer theory and the similarity of velocity distribution, τ_{afl} and ε can be described as follows:

$$\tau_{aflmu} = \rho \varepsilon_{flmu} \frac{\partial u}{\partial z}$$

(9)

Where, ε_{flm2} = turbulent eddy viscosity coefficient; and z = vertical direction. Because the eddy viscosity is related to appropriate velocity and length scales, it is assumed that it may be expressed as

$$\varepsilon_{flmu} = \alpha_0 u h$$

(10)

where α_0 = certain dimensionless coefficient, and h = characteristic height in the vertical shear region between the left floodplain and upper main channels.
It is assumed that

$$h \propto h_z, \qquad u \propto \frac{v_{mu} + v_{fl}}{2} \frac{\partial u}{\partial z} \propto \frac{v_{mu} - v_{fl}}{h_z}$$

(11)

h_z = height of the vertical shear layer between the left floodplain and upper main channel. The apparent shear stress is derived from (9) and presented as:

$$\tau_{aflmu} = \rho \chi_{flmu} \frac{v_{mu} - v_{fl}}{2}$$

(12.a)

and

$$\tau_{afrmu} = \rho \chi_{frmu} \frac{v_{mu} - v_{fr}}{2}$$

(12.b)

in which χ_{flmu} and χ_{frmu} are defined as the dimensionless momentum transfer coefficient for the corresponding vertical interfaces, respectively.

Similarly, another apparent shear stress in horizontal interface is given by

$$\tau_{amlmu} = \rho \chi_{mlmu} \frac{v_{mu} - v_{ml}}{2}$$

(13)

in which χ_{mlmu} is defined as the dimensionless momentum transfer coefficient for the horizontal interface.

3. MODELLING OF MOMENTUM TRANSFER COEFFICIENTS

Figure 1(a&b) shows sketches of asymmetrical/ symmetrical compound sections, where H, h and $(H-h)$ are the main channel, bankfull and floodplain flow depths, b_{mc}, T and bf are the main channel bottom, main channel top and floodplain widths and S_{mc} the main channel bank slope. The best large-scale measurements for overbank flow in straight two-stage channels are considered those of FCF Phase- A of five series data(www.flowdata.bham.ac.uk). In Table 1, the geometrical characteristics of the FCF experiments are provided. All data series in Table 1 were obtained under steady uniform flow conditions. Figure 1(b) shows the similar dimensions of the symmetrical compound sections for the wider channel series.

Table-1 Details of FCF Series

Series No.	Manning's Roughness		B(m)	h(m)	b(m)	S_0	(B/b)	SS
	Main channel (mc)	Flood plain(fp)						
FCF Series 01	0.0099	0.0099	10.0	0.15	0.75	0.01027	6.67	1:1
FCF Series 02	0.0099	0.0099	6.3	0.15	0.75	0.01027	4.2	1:1
FCF Series 03	0.0099	0.0099	3.3	0.15	0.75	0.01027	2.2	1:1
FCF Series 08	0.0099	0.0099	6.6	0.15	0.75	0.01027	4.0	1:1
FCF Series 10	0.0099	0.0099	3.3	0.15	0.75	0.01027	4.4	1:1

*B is the total width of channel, h is the main channel depth, b is the half width of main channel, B/b is the width ratio, S_o is the bed slope of the channel and SS is the side slope of main channel

Relationship between momentum transfer coefficient and Relative flow depth

From the above discussed equations the momentum transfer coefficient for vertical and horizontal (χ_v and χ_h) interface simplified as

$$\chi_v = \frac{2(P_{fl}\tau_{fl} - \rho g A_{fl}S_0)}{\rho(v_{mu} - v_{fl})(H-h)} \; \text{or} \; \chi_v = \frac{2(P_{fl}\tau_{fl} - \rho g A_{fl}S_0)}{\rho(v_{mu} - v_{fl})(H-h)}$$

$$\text{(14.a)}$$

$$\chi_h = \frac{2(P_{ml}\tau_{ml} - \rho g A_{ml}S_0)}{\rho(v_{mu} - v_{ml})(H-h)}$$

$$\text{(14.b)}$$
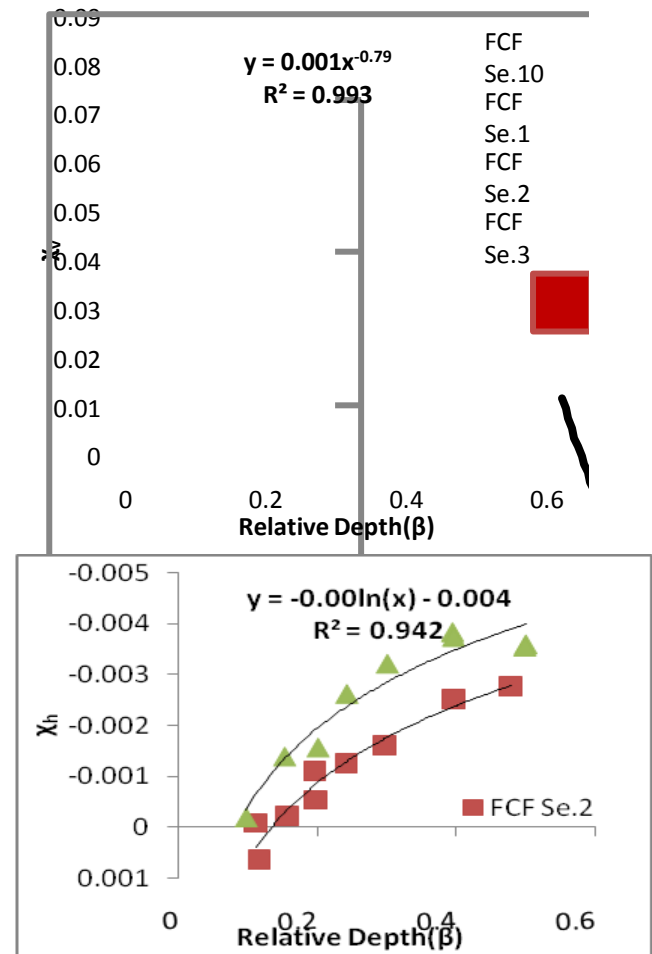
Figure. 2(a & b) variation of vertical and horizontal momentum transfer coefficient with different width ratio channel of SERC-FCF.

In the above Fig. 2(a), it is shown that the varying trends of the vertical momentum transfer coefficient (χ_v) with relative depth (β) for FCF Series 01-03, 08 and 10 are similar. For all the series, the momentum transfer coefficient generally decreases with increasing relative depth even if in case of horizontal momentum transfer coefficient (χ_h) shown in Fig.2(b).Hence, it is supposed that the momentum transfer coefficient to the relative depth, follows certain relationship. Figure 2 testifies that this is true for the SERC-FCF data which leads to the expressions given as

$$\chi_v = 0.0017\beta^{0.794}$$

$$\chi_h = -0.002\ln(\beta) - 0.0044$$

The above two expressions are modeled to finding out the vertical and horizontal momentum transfer coefficient for Large scale compound channels.

4. RESULT AND DISSCUSSION

Stage Discharge Relationship

For the experiments of FCF, Series 01, 02, and 03 with the same main channel width of 1.5 m and differentfloodplain widths of 4.1, 2.25, and 0.75 m, when derived expressions in equation 15(a&b) for χ_v and $\chi_h$are applied to in turn, the method gives good predictions of stage discharge curve as compare to other methods, as shown in Fig. 3(a). For Series 08 and 10, although they have different main channel side slope, they have the same floodplain and main channel widths as Series 02. Hence, when they are taken as the same momentum transfer coefficient as Series 01,02and 03, they also obtain very good predictions of the discharge, as shown in Fig.3 (b).

To obtain much more information on the effect of momentum transfer coefficients, χ, on the discharge, Q, numerical tests were further undertaken based on different series of FCF are considered, as shown in Fig.3 (a&b).
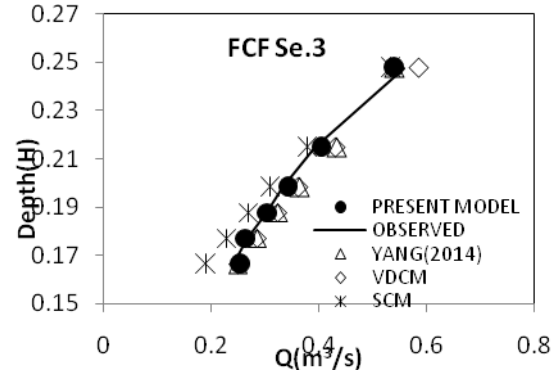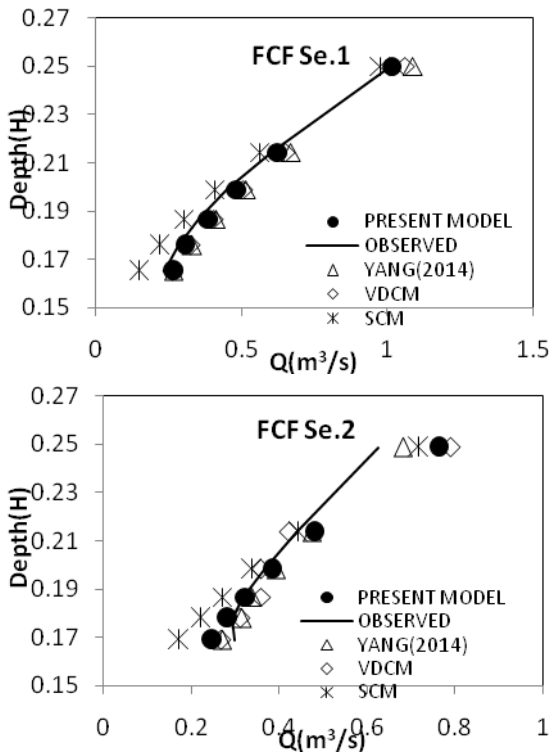
Figure.3 (a) Stage discharge curve for FCF Series 01, 02 and 03

Figure.3 (b) Stage discharge curve for FCF Series 08 and 10

Table-2 Errors in computation of discharge by different methods

	Mean Relative Error (%)			
	Present Model	Yang (2014)	VDCM	SCM
FCF Series 01	6.733646	13.1283	10.79343	15.87662
FCF Series 02	5.497665	6.545004	8.851232	15.75275
FCF Series 03	2.658443	6.639609	7.366103	10.54624

FCF Series 08	8.659591	15.82955	11.22988	12.90225
FCF Series 10	3.256716	8.004849	9.113598	12.81958

The computed discharge is well matched with the observed discharge by the present model shown in Fig. 3. However, the effect of momentum transfer is distinct for the prediction of discharge. From Table-2, the mean relative error is found lower in present method for the entire proposed Series of Large FCF channel. The minimum mean relative error for the present method is only 2.65% for (B/b)=2.2 of Series 03 whereas maximum is found 6.73% for (B/b) =6.67 of Series 01. The present approach has the smallest errors (see Table 2).

5.CONCLUSION

- The presented method is developed by using the momentum transfer coefficients which take account of the effect of the lateral momentum transfer between the floodplains and the upper main channel and of the vertical momentum transfer between the upper and lower main channels.

- The expressions are derived for vertical and horizontal momentum transfer coefficients by analyzing the experimental data of the SERC-FCF. For all the series considered, the momentum transfer coefficient generally decreaseswith increasing relative depth with a definite trend.

- Using the developed mathematical modelling for the momentum transfer coefficients ($\chi_v \& \chi_h$) the presented method has the advantage of being applicable to well deal with the apparent shear forces on the interfaces between the adjoining subareas by comparing with the other conventional divided channel methods. The discharge distribution and stage discharge relationship predictions of the method are verified against the large-scale compound channel data from the FCF at HR Wallingford. The results by the presented method give good agreement with experimental data.

- From the error analysis of the conventional methods, the accuracy of the present approach has been successfully examined to the experimental large channel FCF data sets with a minimum relative error of 2.65%.

- The expression for evaluating the momentum transfer coefficient should be validated in respect of accuracyby a vast number of experimental data and as well as natural river data. Again the problem is not resolved and to be studied further for an asymmetric compound channels.

REFERENCES:

i.   Chow, V.T.(1959). Open Channel Hydraulics.1st edn. McGraw-Hill Book Co., New York.

ii.   Huthoff, F., Roos, P. C., Augustijn, D. C. M., and Hulscher, S. J. M. H. (2008).Interacting divided channel method for compound channel flow. J. Hydraul. Eng., 10.1061/ (ASCE) 0733-9429(2008)134:8 (1158), 1158–1165.

iii.   Knight D. W. (1999). Flow mechanics and sediment transport in compound channels [J]. International Journal of Sediment Research, 14(2): 217-236.

iv.   Knight, D.W., and Demetriou, J. D. (1983). Flood plain and main channel flow interaction. J. Hydraul. Eng., 10.1061/(ASCE)0733-9429(1983)109:8(1073), 1073–1092.

v.   Knight, D.W., Hamed, M.E. (1984). Boundary shears in symmetrical compound channels. Journal of Hydraulic Eng., ASCE, 110(10), 1412–1430.

vi.   Myers, W.R.C. and Brennan, E.K.(1990). Flow Resistance in Compound Channel. Journal of Hydraulic Research 28(2): 141–155.

vii.   Myers, W.R.C., Brennan, E.K. (1990). Flow resistance in compound channel. J. Hydraulic Res., IAHR, 28(2), 141–155.

viii.   Rameshwaran P. and Naden P. S. (2003). Three-dimensional numerical simulation of compound channel flows [J]. Journal of Hydraulic Engineering, ASCE, 129(8): 645-652.

ix.   Shiono, K. and Knight, D.W.(1991) .Turbulent open-channel flows with variable depth across the channel. Journal of Fluid Mechanics 222, 617–646.

x.   Wormleaton, P. R., Allen, J., and Hadjipanos, P. (1982). "Discharge assessment in compound channel flow." J. Hydraul. Div., 108(9), 975–994.

xi.   Wormleaton, P. R., and Hadjipanos, P. (1985). Flow distribution in compound channels. J. Hydraul. Eng., 10.1061/ (ASCE) 0733-9429(1985) 111:2(357), 357–361.

xii.   Yang, K.Y., Cao, S.Y., Liu, X. N. (2014). Stage-Discharge Prediction in Compound Channels. J. Hydraul. Eng.10.1061/(ASCE)HY.1943-7900.0000834.21(4): 353–361

Morpho-Hydrodynamic Modelling Of Subarnarekha River

V. Parmar[1]R. Khosa[1]   R. Maheswaran[1]
[1]Department of Civil Engineering, Indian Institute of Technology, HauzKhas, New Delhi–110016, INDIA.
Email: vilakshnaparmar@gmail.com

ABSTRACT: Subarnarekha is an East flowing drainage feature that originates near Ranchi, Jharkhand. The river banks of Subarnarekha have witnessed significant levels of retreat along some reaches. Also, the basin is known to be prone to recurrent floodsthus necessitating extensive river training and other flood management works. For scientific and rational flood mitigation, an understanding of the morphological behavior of the river is indeed imperative. River morphology is concerned with the structure and form of rivers and its evolution in time is influenced by factors that include flow characteristics, sediment characteristics and bed and bank characteristics.

In the present study, the morphological setup of River Subarnarekha has been used to develop a hydrodynamic model of the river. The model is calibrated and validated for the period from 1990 to 2013 using split sample validation test. In the study, global values of Manning's n were found to be 0.035 which is reasonable for alluvial stratum.

Keywords:Morphological model, Hydrodynamic Model, Subarnarekha River

1. INTRODUCTION

River systems are highly dynamic natural systems and their morphometric features are constantly evolving in time at rates that may range from the very slow – on geologic time scales – to rather very rapid – a change that is more in the character and in the form of sudden catastrophic avulsions. Expectedly, considering the vast range of time scales over which river morphology is known to have evolved historically, there do exist a diverse set of triggering mechanisms, natural as well as anthropogenic, that operate at corresponding spatial and temporal scales and accordingly shape the basin drainage system. The major processes responsible for the formation and evolution of rivers are indeed a complex interplay of weather and long term climate, basin morphological characteristics, hydrodynamic characteristics of basin, hydrologic runoff and flood propagation patterns, characteristics of the basin pedosphere and deeper regolith, upland erosion, sediment transport and deposition. Accordingly, recognition of this fundamental reality of nature necessitates an objective morphological study that captures the extensive scale of the underlying dynamics of the basin drainage network system.

Much research on morphological modelling has been done in past few decades and these studies have followed two different approaches namely (i) studies based on remote sensing and cartographic techniques (see, for example Roy N. et al., 2007; Sinha et al., 2008; Jain S. K. et al., 2013) and (ii) studies based on development of an extensive hydrodynamic model to investigate its effects on various river characteristics like sediment transport, plan form, and bank profile (Sharma N., 2012).

The present study aims to develop a hydrodynamic model for the Subarnarekha River which is one of the longest east flowing drainage feature in the region and originates near Piska-Nagri, near Ranchi, Jharkhand. The total length of the river, till its outfall into Bay of Bengal at Kirtania port, is 395 km. Over this short traverse to the sea, Subarnarekha River shows distinctive morphological features such as meandering and braiding. River bank retreat has been observed along some reaches and there are reports of portions of numerous villages having disappeared as a result. Some of the affected regions that face a serious threat include Bhogarai, Baliapal and Jaleswar blocks. As part of river training and bank reinforcement efforts, though some of the more vulnerable stretches have been reinforced with boulders and metal, the river, however, has started eroding some of the other unprotected bank segments thus necessitating a detailed morphological evaluation of the river.

Historically, Subarnarekha has been the subject of intense scientific scrutiny and include the study by Yarrakula K. et al. (2010) wherein the latter authors combined GIS and remote sensing techniques with a hydrodynamic modelling approach for the purpose of developing a flood forecasting model and inundation map of the study reach. Maiti (2013) also carried out a study of coastal morphodynamics of Subarnarekha estuary using integrated cartographic and field techniques.

In the current study, an attempt is made to develop a hydrodynamic model of the river system using MIKE 11. The model seeks to obtain those governing flow parameters along the channel profile that are deemed to have a significant influence on some of the other characteristics of river system.

2. MATERIAL AND METHODS
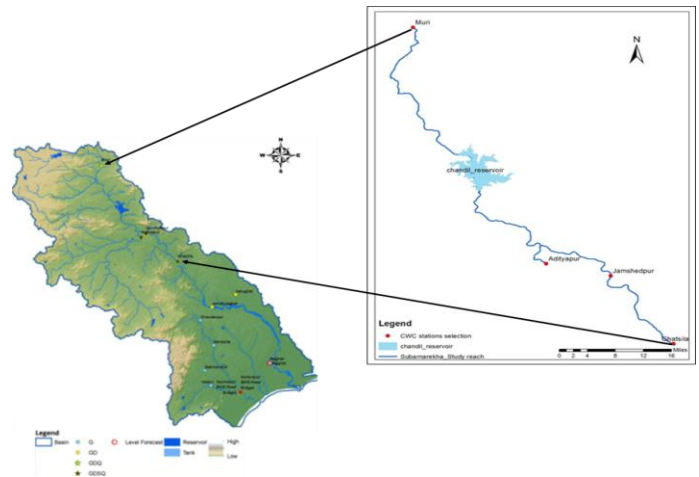
2.1 Study Area

Figure 1. Subarnarekha basin (left) and Study Area opted (right).

The reach of Subarnarekha chosen for the present study is from Muri to Ghatsila in Jharkhand and was essentially dictated by limitations on account of data availability. Central Water Commission (Ministry of Water Resources, GoI) operates three hydrometric stations at Muri, Jamshedpur and Ghatsila, out of which the first is a Gauge and Discharge (GD) station and the latter two are Gauge, Discharge, Sediment and Water Quality (GDSQ) stations. The study reach has a tributary joining it from Adityapur and the reach also features a major reservoir impoundment at the Chandil dam site which supports irrigation along with municipal and industrial demands. These supplies are carried from Chandil reservoir by two canal systems namely (i) right bank canal; and (ii) left bank canal.

2.2 Data Acquisition

Separate terrain models were constructed from ASTER GDEM (30m x 30m), SRTM DEM (90m x 90m) and CARTOSAT DEM (30m x 30m) which were downloaded from USGS and Bhuvan respectively. The hydro observation data was downloaded from Water Resources Information System (WRIS, MoWR). The downloaded data sets included the cross-section data, gauge and discharge data and sediment data for the reach.

2.3 Methodology

To obtain the river network, basin delineation was carried out using the Arc SWAT Automatic Watershed Delineator with the threedigital terrain models ASTER, SRTM and CARTOSAT and evaluated for accuracy by inter-comparison on Google Earth.All the three DEMs produced similar results. But the SRTM DEM results are used in the analysis.Only cross sections at three gauge sites, Muri, Adityapur and Ghatsila, were available. All the other cross sections were interpolated and compared with Google earth elevation profiles.Chandil dam was also included as a structure in the network. The diversion from the reservoir was assumed to be constant and equal to 70% of the annual water diversion from the dam for drinking and irrigation purposes (17.625m^3/s). Also, 30% of the water diverted is assumed to be coming back as return flows.There were two open boundaries in the study reach. At the upstream boundary (Muri) the inflow type boundary was taken. The discharge data time series available from WRIS at Muri was taken as input. At the downstream boundary (at Ghatsila) the Q-h typeboundary is defined. Thepoint source inflow boundary is assumed where tributary from Adityapur meets study reach, and TS discharge at Adityapur was taken as input.

Split sample validation technique has been used for calibration and validation. The calibration and validation was done for both water level and flow at Jamshedpur and Ghatsila. This was carried out in two samples. For sample I, calibration was done for period 11/1/1989 to 12/31/2005 and validation for period 1/1/2006 to 1/31/2013. For sample II, calibration was performed for period 1/1/1998 to 1/31/2013 and validation for period 11/1/1989 to 12/31/1997. The model performance was evaluated using performance indices like coefficient of determination (R^2) and Nash-Sutcliffe Efficiency Index.

3. RESULTS AND ANALYSIS

3.1 Calibration of the Model Set Up

In the process of calibration, the values of Manning's n were adjusted to bring the modeled water level and discharges at Jamshedpur and Ghatsila closer to the observed values at those locations. The calibrated global manning's n value was found to be 0.035. The performance indices for this value at different check stations are given in table 1 and 2 for sample I and II respectively. Thesevalues are suggestive of a satisfactory model performance.

Table 1. Performance Indices for calibration for sample I

	Water Level At Jamshedpur	Water level At Ghatsila	Flow at Jamshedpur	Flow at Ghatsila
Nash-Sutcliffe Efficienc	0.856	0.922	0.639	0.662

y				
Coefficient of determination, R^2	0.745	0.924	0.803	0.857
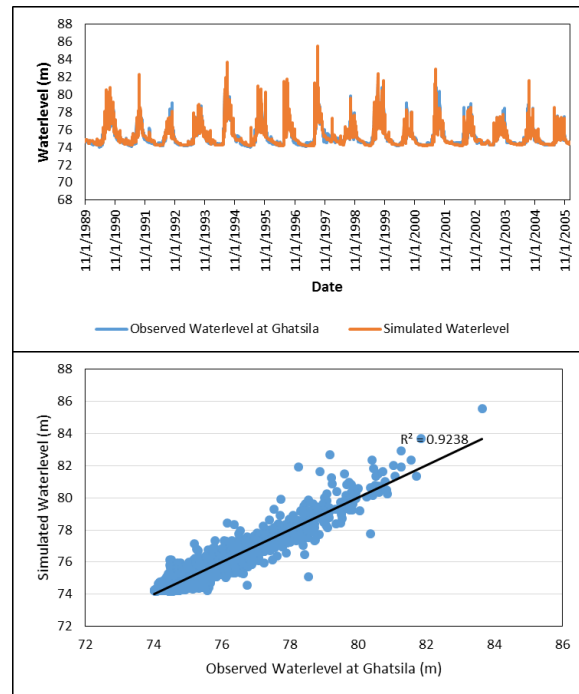
Figure 2. Time series plot (left) and scatter plot (right) for calibration of sample I at Ghatsila.

Table 2. Performance Indices for calibration for sample II

	Water Level At Jamshedpur	Water level At Ghatsila	Flow at Jamshedpur	Flow at Ghatsila
Nash-Sutcliffe Efficiency	0.852	0.908	0.700	0.613
Coefficient of determination, R^2	0.733	0.906	0.833	0.859
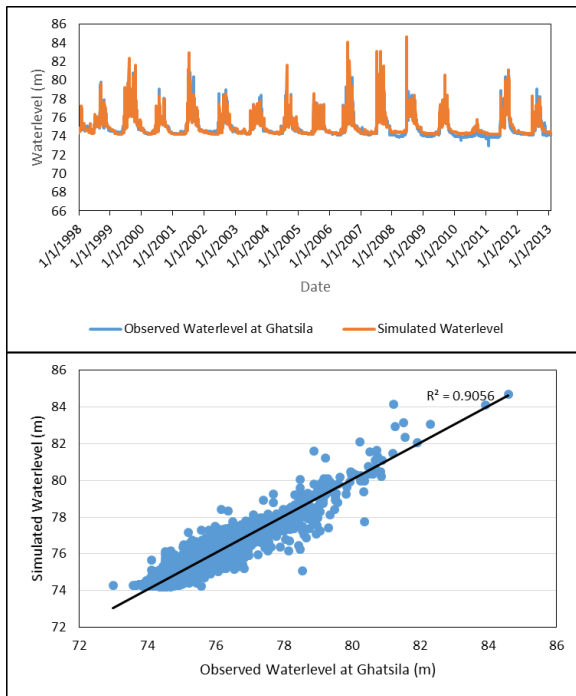
Figure 3. Time series plot (left) and scatter plot (right) for calibration of sample II at Ghatsila.

Figure 4. Time series plot (left) and scatter plot (right) for validation of sample I at Ghatsila.

3.2 Validation of the model

The calibrated hydrodynamic model was used to validate the discharge and water level for the period from 1st January 2006 to 31st January 2013 for sample I, and from 1st November 1989 to 31st December 1997 for sample II. The simulated flows and water levels of the mentioned period were compared with the actual observed values and the corresponding performance indices for validation period are presented in table 3 and 4 for sample I and II respectively.

Table 3. Performance Indices for validation for sample I

	Water Level At Jamshedpur	Water level At Ghatsila	Flow at Jamshedpur	Flow at Ghatsila
Nash-Sutcliffe Efficiency	0.846	0.909	0.706	0.601
Coefficient of determination, R^2	0.702	0.916	0.817	0.864
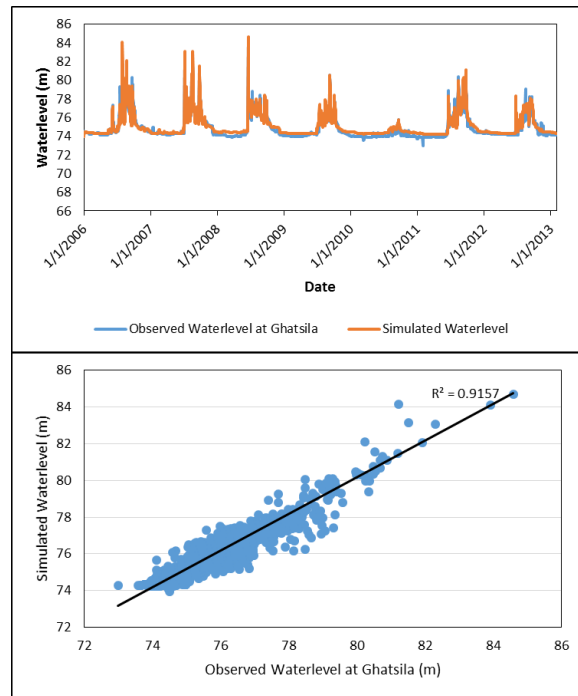
Table 4. Performance Indices for validation for sample II

	Water Level At Jamshedpur	Water level At Ghatsila	Flow at Jamshedpur	Flow at Ghatsila
Nash-Sutcliffe Efficiency	0.854	0.931	0.610	0.676
Coefficient of determination, R^2	0.730	0.933	0.776	0.862
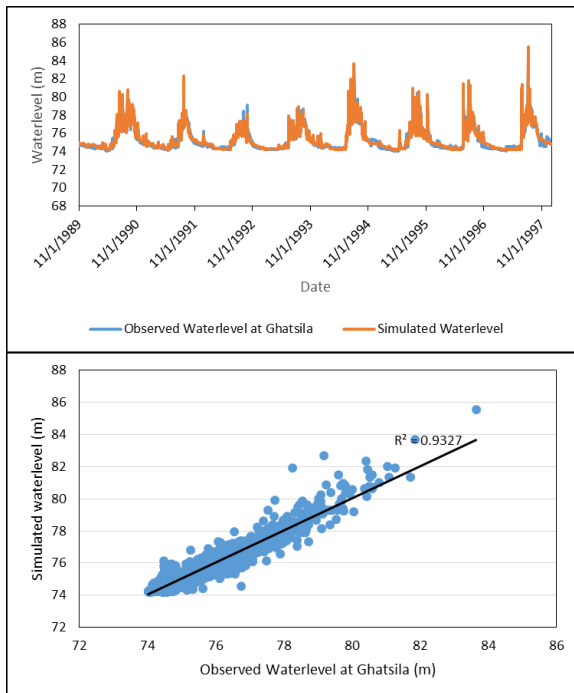
Figure 5. Time series plot (left) and scatter plot (right) for validation of sample I at Ghatsila.

4. CONCLUSIONS

The study as described in the foregoing sections has described the development of a validated MIKE 11 hydrodynamic model in order to study the flow transport characteristics of Subarnarekha River. The results show that the developed model is performing satisfactorily for a calibrated global value of Manning's n equal to 0.035, which is within feasible range of Manning's n for alluvial stratum.

As is seen from the available results, the model performance is reasonably good in period of high flows, like in 1997 and 2007 when floods were experienced in the river system. But, there is an observed discrepancy between flow values at time of low flows, which may be the result of assumptions made regarding the specification of the hydraulic attributes of Chandil Dam and diversions from the system. This was a necessity for reasons of non-availability of the required details.

5. CAVEATS

Hydrodynamic modeling of flood propagation in river Subarnarekha is based on the numerical solution of the 1-D St. Venant's equations. These equations are derived based on certain fundamental assumptions and may often represent a highly idealized physical system and these idealizations do indeed influence the quality of model simulations.

Further, limitations on account of the dataquality as well as its availabilityhave the potential to affect the quality of model results and, understandably, the results presented herein reflect these constraints.

Specifically, the present study could not employ actual river cross-sections at the required intervals. Instead, interpolated cross-sections were used in the model development. Additionally, non availability of data on (i) geometric and hydraulic attributes of Chandil Dam and reservoir; (ii) reservoir diversions; (iii)representative estimates of irrigation return flows, as diffused contribution from irrigated command areas, would also have similarly impacted the quality of simulations.

REFERENCES:

i.   Department of Water Resources Development and Management, Indian Institute of Technology Roorkee, 2012, "Study Of Brahmaputra River Erosion and Its Control".

ii.   Jain V., Tandon S. K., Sinha R., 2012, Application of modern geomorphic concepts for understanding the spatio-temporal complexity of the large Ganga river dispersal system, Current Science, Vol. 10.

iii.   Jan S. Ribberink, Mathematical modelling of one-dimensional morphological changes in rivers with non-uniform sediment.

iv.   Lahiri S. K., Sinha R., 2012, Tectonic controls on the morphodynamics of the Brahmaputra River system in the upper Assam valley, India, Geomorphology, Elsevier.

v.   Leopold, L. B., & Wolman, M. G. (1957). River channel patterns: braided, meandering, and straight (pp. 37-86). Washington, DC: US Government Printing Office.

vi.   Maiti, S., & Bhattacharya, A. K. (2009). Shoreline change analysis and its application to prediction: a remote sensing and statistics based approach. Marine Geology, 257(1), 11-23.

vii.   Mosselman E., 1995, A review of mathematical models of river planform changes, Earth Surface Processes and Landforms, BGRG, Vol.20.

viii.   Mosselman E., 1998, Morphological modelling of rivers with erodible banks, Hydrological Processes, Hydrol. Process. 12, 1357-1370.

ix.   National Institute of Hydrology, 2013, "Morphological Study of Ghagra River".

x.   National Institute of Hydrology, 2013, "Morphological Study of Satluj River".

xi.   Rinaldi M., Mengoni B., Luppi L., Darby S.E., Mosselman E., 2008, Numerical simulation of hydrodynamics and bank erosion in a river bend, Water Resources Research, Vol. 44.

xii.   Roy, N., & Sinha, R. (2007). Understanding confluence dynamics in the alluvial Ganga–Ramganga valley, India: an integrated approach using geomorphology and hydrology. Geomorphology, 92(3), 182-197.

xiii.   Sinha, R., & Ghosh, S. (2012). Understanding dynamics of large rivers aided by satellite remote sensing: a case study from Lower Ganga plains, India. Geocarto International, 27(3), 207-219.

xiv.   Yarrakula, K., Deb, D., &Samanta, B. (2010). Hydrodynamic modeling of Subarnarekha River and its floodplain using remote sensing and GIS techniques. Journal of Scientific & Industrial Research, 69(7), 529-536.

Morpho-Hydrodynamic Modelling Of Kosi River

V. Parmar[1]   R. Khosa[1]   R. Maheswaran[1]
[1] Department of Civil Engineering, Indian Institute of
Technology, Hauz Khas, New Delhi–110016, INDIA.
Email: vilakshnaparmar@gmail.com

ABSTRACT: *River Kosi is well-known for its course instability besides being prone to frequent avulsions. As a consequence, the plains of North Bihar are exposed to regular destructive episodes of inundation from the flood waters of this vagrant river bringing great misery in the Northern Bihar plains. To design viable mitigation strategies that are based on sound scientific understanding of the underlying processes, it is imperative to study and understand the morphology of the river which is commonly understood to be largely influenced by factors that include the temporal history of hydrodynamic attributes of the prevailing streamflow regime like water level and associated flow velocity.*

In the present study the hydrodynamic modelling of River Kosi has been attempted from Chatara in Nepal to Baltara in Bihar. MIKE 11 platform has been used to develop, calibrate and validate the hydrodynamic model of the river system for the period from 1990 to 2002. The study also accommodates the contributions to streamflows from the intervening catchment of the modeled reach. Examination of performance indices which shows that model simulations are reasonably realistic when compared with the observed streamflow values. The global values of Manning's n was estimated to be 0.021 and is deemed to be within acceptable limits.

Keywords: Morphological model, Hydrodynamic Model, Kosi River

1. INTRODUCTION

Kosi River, also known as Saptakoshi, is one of the major tributaries of Ganga river system and originates from the major confluence of seven rivers Indravati, Sun Kosi, Tama Kosi, Likhu Kosi, Dudh Kosi, Arun Kosi and Tamar Kosi near north of Chatara George in Nepal. The upper catchment of the river system lies in Nepal and Tibet and carries the privilege of having six of the ten highest mountain peaks of the world including, Mount Everest and Mount Kanchenjunga. The river enters India near Hanuman Nagar in Nepal where it branches into a complex mesh of sinuous channels and, in the process, forming one of the world's biggest alluvial mega fans. The main stem of Kosi has its point of confluence with river Ganga near Kursela in Bihar. Kosi basin has huge variation in its elevation profile having two distinct topographical features. On one hand, it boasts of some of the world's highest peaks in its upper reach (in Nepal) and, on the other hand, flows in vast flat flood plains when it enters Bihar, India.

The Kosi basin lies between 85° to 87° 21' east longitudes and 25° 25' to 26° 48' north latitudes of the country. Other than the main river the Kosi, the Adhwara, the Baghmati, the Kareha, the Balan, the Kamla and the Lakhandal form some of the major river flowing in this sub-basin. The sub-basin completely falls in the Bihar state.

Over the last 250 years, Kosi has reportedly shifted its course carving, in the process, a 120 km wide swathe with the general sweep being from East to West. Kosi River is vulnerable to frequent, but catastrophic avulsions that inevitably lead to it shifting its course. As a consequence, the plains of North Bihar are exposed to regular destructive episodes of inundation from the flood waters of this vagrant river and appropriately earning the epithet Sorrow of Bihar. The two major upheavals recorded in the course of Kosi River were in 1936 after Bihar earthquake (in 1934) and the avulsion in 2008 after breaching its embankments near Kusaha. In 1963 a barrage was constructed over the river to regulate Kosi and, in order to check its lateral movement as well as for flood control, embankments on both sides of the river were constructed, five to sixteen km apart. Presumably, on account of a relentless deposition of its silt load along its course, the Kosi bed levels have attained a higher profile than the natural surface levels of land beyond the embankments.

Many studies have been done on Kosi sub basin in the past decades. Singh et al., 1993 observed a depositional model for the Kosi megafan while Sinha, 1995, in his study of sedimentological characteristics of the alluvial sediments in the interfan area between the Gandak and Kosi megafan in the north Bihar plains, found clayey silt and silty clay as the two most dominant units in flood plain sediments. Kosi has been a constant challenge in north Bihar in terms of long and recurring flood hazards which have also been a research focus of numerous studies. For example, the flooding problem and analysis of flood hydrology of Kosi has been attempted using Analytical Hierarchy Process (AHP) by Sinha et al., 2008 who also attempted a GIS-based flood risk mapping. Sinha, 2009, presented an account of Kusaha avulsion of 2008 based on a detailed study of satellite images and followed it up by an enunciation of strategies for integrated management of the Kosi basin.

Following an objective review of the aforementioned and related literature (for example Roy et al., 2007, Sinha et al., 2008, Sharma N., 2012, and Jain et al., 2013) it is averred that an extensive morpho-hydrodynamic evaluation of the Kosi basin is an urgent necessity and, accordingly, the in the study described hereafter in the following sections, an attempt is made to develop, calibrate and validate a hydrodynamic model using MIKE 11 (DHI) for the river system to obtain the flow parameters along the channel profile.

2. MATERIAL AND METHODS

2.1 Study Area
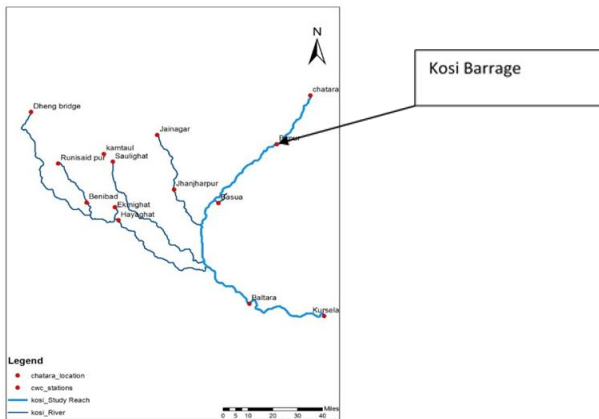
Figure 1. Area selected for study.

The reach of Kosi chosen for the present study is from Chatara in Nepal to Baltara in Bihar and is depicted in Figure 1. The study was limited to Baltara as no data was available for the downstream reach of Kosi upto Kursela (Bihar) which is also the confluence point of the latter river with Ganga.

2.2 Data Acquisition

Separate terrain models were constructed from ASTER GDEM (30m x 30m), SRTM DEM (90m x 90m) and CARTOSAT DEM (30m x 30m) which were downloaded from USGS and Bhuvan respectively.

While discharge data was available from Central Water Commission (CWC) for some of the stations distributed across the study basin, however, flow data was available only for one site along the main stem of Kosi at Baltara station. The rest of the data requirement was taken care of using the SWAT model simulations of Ganga River Basin developed at IIT Delhi as part of the Ganga River Basin Management Plan study being carried out by the consortium of seven IITs.

2.3 Methodology

Hydrodynamic modelling is a part of morphological model. It is necessary to study the flow of water in a river to analyze its morpho-dynamics. The hydrodynamic model was setup in MIKE 11 for the reach from Chatara to Baltara including the Kosi barrage.

The SRTM, ASTER and CARTOSAT DEM of Kosi region were delineated using Arc SWAT Automatic Watershed Delineator to obtain the river network. The resulting channels and basin were then validated with Google Earth. Surveyed

cross-section data were not available and were indirectly extracted from Google Earth by developing an elevation API at intervals of 5 km which were found to compare well with those developed from ASTER DEM using HEC GEO-RAS.

Kosi barrage, included in the study area, is located near Birpur. No data was available for barrage structure nor were data available pertaining to releases downstream into river and canal diversions made from the barrage. The diversions from the barrage were indirectly computed by estimating crop water requirement in its designated command based on the knowledge that the principal crops grown include mainly rice, wheat, soybean, potato and peanut. The time series of canal diversions thus derived is presented for a period of one year in Figure 2 out of which return flows were fixed at a single benchmark figure of 30% of the total water diverted.
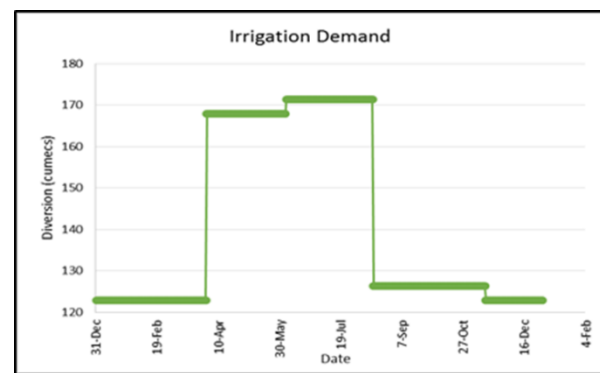
Figure 2. Assumed diversion for Irrigation.

This research assumed two open boundaries for the study reach. An inflow type boundary condition was imposed at the upstream extremity of the study reach at Chatara which was in the form of a simulated flow hydrograph and obtained from SWAT model runs. For the downstream boundary at Baltara, a Q-h type boundary condition was specified. Additionally, point source inflow boundary conditions are also assumed where four tributaries have their confluence points with the study reach of Kosi. The flow values from CWC discharge data at the nearby station are taken to be the input from the streams into study reach. Also, for whole reach, surface runoff and base flow contribution were also taken from the SWAT model.

The calibration and validation was done for flow values at Baltara. In this study, calibration and validation was done using Split sample validation technique. In first sample calibration is done for period 1990 to 1998 and validation for period 1999 to 2002. In second sample calibration is done from 1995 to 2002 and validation for 1991 to 1994. The model performance was assessed using performance indices like coefficient of determination (R^2) and Nash-Sutcliffe Efficiency.

3. RESULTS AND ANALYSIS

3.1 Calibration of the Model Set Up

The hydrodynamic model developed was calibrated using data for the period 1st January 1991 to 31st December 1998 (for sample I) and from 1st January 1995 to 31st December 2002 (for sample II). As part of the calibration process, trial values of Manning's roughness, n, were adjusted to bring the modeled discharge at certain locations closer to the observed values at these locations and a global 'n' value equal to 0.021 was adopted. The performance indices corresponding to this value at different check stations are given in table 1 and are suggestive of a model performance that is acceptable.

Table 1. Performance Indices for calibration at Baltara

	Sample I	Sample II
Nash-Sutcliffe Efficiency	0.787	0.727
Coefficient of determination, R^2	0.821	0.781
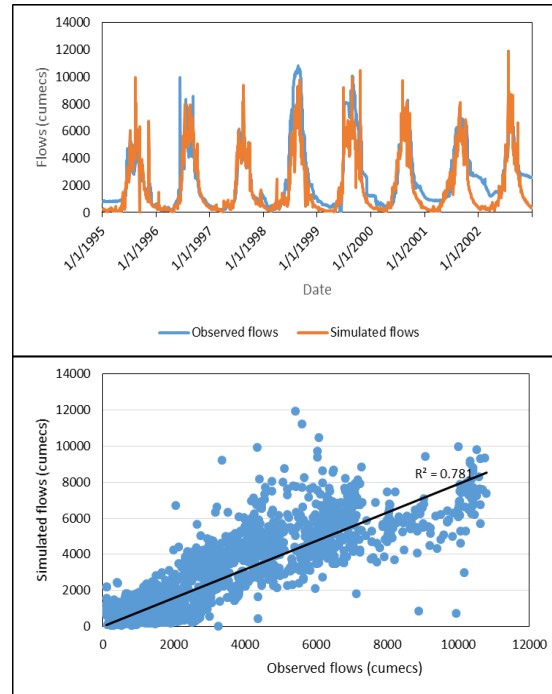
Figure 3. Time series plot (left) and scatter plot (right) for calibration of sample I at Baltara.

Figure 4. Time series plot (left) and scatter plot (right) for calibration of sample II at Baltara.

3.2 Validation of the model

The validation of the calibrated hydrodynamic model was done for the period from 1st January 1999 to 31st December 2002 (for sample I) and from 1st January 1990 to 31st December 1994 (for sample II) and the corresponding performance indices, as presented in table 2, indicate a reasonable performance. However, an examination of accompanying Figure 5 shows that while the model appears to perform well when simulating high flows, but, in contrast, the model performance is markedly below par when simulating low flows at Baltara and this may be attributed to (i) use of indirect estimates of actual canal diversions from Kosi Barrage; and (ii) lack of clarity regarding the specific nature of hydraulic control exercised by Kosi Barrage with regard to downstream releases. Such an assertion seems reasonable based on the observation that low flows simulation was significantly better when validation was done for an identified location just upstream of the barrage (refer table 3).
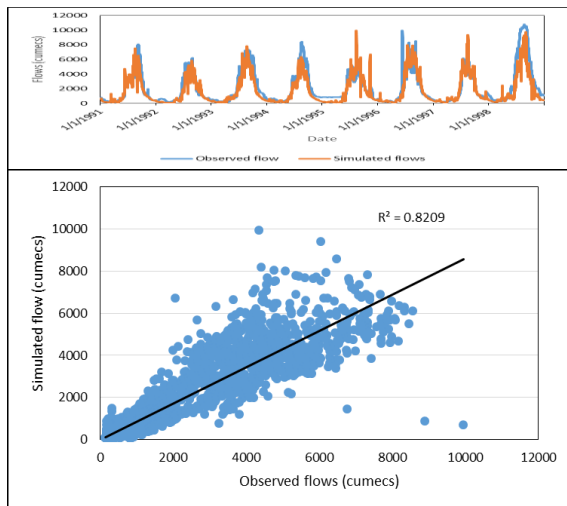
Table 2. Performance Indices for validation at Baltara

	Sample I	Sample II
Nash-Sutcliffe Efficiency	0.678	0.816
Coefficient of determination, R^2	0.788	0.870
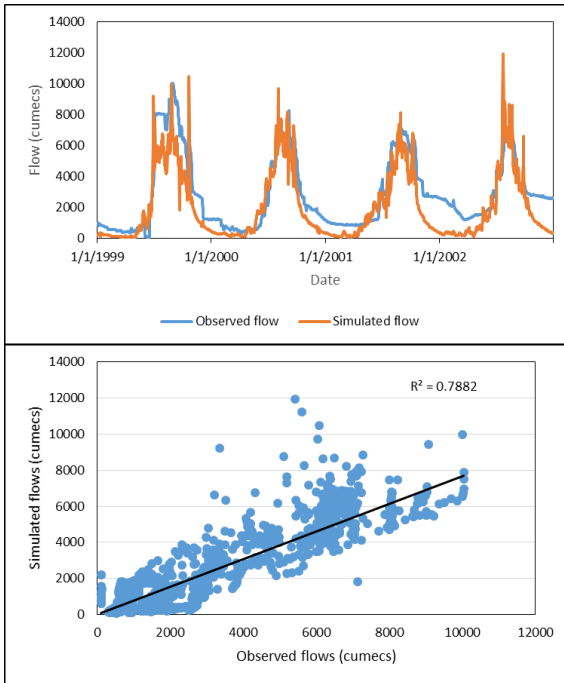
Figure 5. Time series plot (left) and scatter plot (right) for validation of sample I at Baltara.
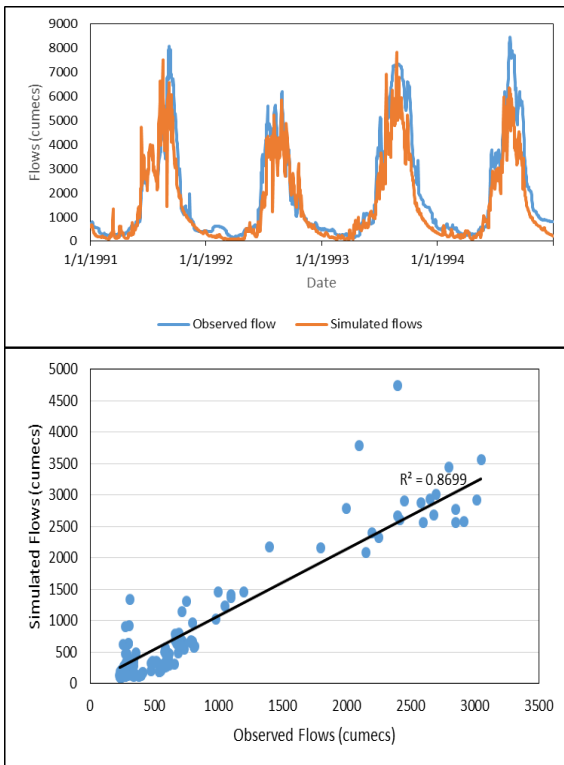
Figure 6. Time series plot (left) and scatter plot (right) for validation of sample II at Baltara.

Table 3. Performance Indices for validation just upstream of barrage

	Sample I	Sample II
Nash-Sutcliffe Efficiency	0.956	0.965
Coefficient of determination, R^2	0.958	0.964

4. CONCLUSIONS

Kosi River shows a very curious behavior in its morphodynamics. Also, the river is highly flood prone. Thus, the thorough study of the river characteristics are needful. In this study, the hydrodynamic modelling was done to determine the flood characteristics of the river. MIKE 11 hydrodynamic model was developed, calibrated and validated to study the flow characteristics of the river. The results show that the developed model is performing satisfactorily. The calibrated global value of Manning's n was found to be 0.021 which is reasonable for alluvial stratum.

There are differences in the results that can be attributed to the assumptions made in defining abstractions and cross sectional data.

5. CAVEATS

Hydrodynamic modeling of river Kosi is done on MIKE 11 platform which is based on the numerical solution of the 1-D St. Venant's equations. These equations are derived based on certain fundamental assumptions and may often represent a highly idealized physical system and these idealizations do indeed influence the quality of model simulations.

Further, there are limitations on account of the data quality as well as its availability. The results presented herein reflect these constraints.

Specifically, the present study could not employ actual river cross-sections due to unavailability of data. Additionally, the results are also affected by the limitation of data of (i) geometric and hydraulic attributes of Kosi barrage; (ii) diversions from the system; (iii) inflows (taken from SWAT model), would also have similarly impacted the quality of simulations.

REFERENCES:

i.   Chakraborty, T., Kar, R., Ghosh, P., & Basu, S. (2010). Kosi megafan: Historical records, geomorphology and the recent avulsion of the Kosi River. Quaternary International, 227(2), 143-160.
ii.   Department of Water Resources Development and Management, Indian Institute of Technology Roorkee, 2012, "Study Of Brahmaputra River Erosion and Its Control".

iii.   *Gahtak A., 2009, Geospatial Technology in Humanitarian Mapping – A Case Study of Kosi River Floods: 2008, India, 10th ESRI India user conference 2009.*

iv.   *Jain V., Tandon S. K., Sinha R., 2012, Application of modern geomorphic concepts for understanding the spatio-temporal complexity of the large Ganga river dispersal system, Current Science, Vol. 10.*

v.   *Jan S. Ribberink, Mathematical modelling of one-dimensional morphological changes in rivers with non-uniform sediment.*

vi.   *Lahiri S. K., Sinha R., 2012, Tectonic controls on the morphodynamics of the Brahmaputra River system in the upper Assam valley, India, Geomorphology, Elsevier.*

vii.   *Leopold, L. B., & Wolman, M. G. (1957). River channel patterns: braided, meandering, and straight (pp. 37-86). Washington, DC: US Government Printing Office.*

viii.   *Mosselman E., 1995, A review of mathematical models of river planform changes, Earth Surface Processes and Landforms, BGRG, Vol.20.*

ix.   *Mosselman E., 1998, Morphological modelling of rivers with erodible banks, Hydrological Processes, Hydrol. Process. 12, 1357-1370.*

x.   *National Institute of Hydrology, 2013, "Morphological Study of Ghagra River".*

xi.   *National Institute of Hydrology, 2013, "Morphological Study of Satluj River".*

xii.   *Rinaldi M., Mengoni B., Luppi L., Darby S.E., Mosselman E., 2008, Numerical simulation of hydrodynamics and bank erosion in a river bend, Water Resources Research, Vol. 44.*

xiii.   *Roy, N., & Sinha, R. (2007). Understanding confluence dynamics in the alluvial Ganga–Ramganga valley, India: an integrated approach using geomorphology and hydrology. Geomorphology, 92(3), 182-197.*

xiv.   *Singh H., Parkash B. and Gohain K., 1993, Facies analysis of the Kosi megafan deposits, Sedimentary Geology,85, 87-113, Elsevier*

xv.   *Sinha R., 1995, Sedimentology of Quaternary Alluvial Deposits of the Gandak-Kosi interfan, Northern Bihar Plains, Journal Geological Society of India Vol.46.*

xvi.   *Sinha R., Bapalu G.V., Singh L.K. , Rath B., 2008, Flood Risk Analysis in the Kosi River Basin, North Bihar Using Multi-Parametric Approach of Analytical Hierarchy Process (AHP), J. Indian Soc. Remote Sens.*

xvii.   *Sinha R., 2009, Dynamics of a River System-the Case of the Kosi River in North Bihar, e-Journal Earth Science India Vol.2 (I).*

xviii.   *Sinha, R., & Ghosh, S. (2012). Understanding dynamics of large rivers aided by satellite remote sensing: a case study from Lower Ganga plains, India. Geocarto International, 27(3), 207-219.*

River Bank Erosion And Retreat Model

V. Parmar[1]   R. Khosa[1]   R. Maheswaran[1]

[1] *Department of Civil Engineering, Indian Institute of Technology, Hauz Khas, New Delhi–110016, INDIA.*
Email: vilakshnaparmar@gmail.com

ABSTRACT: *River bank erosion is an emerging concern in alluvial river systems for its egregious impacts on riparian morphology leading eventually to loss that has ramifications across socio-politico-economic domains. Bank erosion also has the potential to compromise structural integrity and stability of constructed features and thereby enhancing a river's potential to shift course. River banks are also acknowledged as one of the most vulnerable geologic features as bank stability is at an enhanced risk of compromise on account of its perpetual exposure to the persistent action of various destabilizing natural and anthropogenic causes namely hydraulic characteristics of flow, channel characteristics, underlying geology of the banks, bank profiles, human activities and role of flora and fauna on the banks or in its vicinity etc. These and other related issues makes a scientific study of the underlying physical phenomena imperative when planning appropriate bank protection and related mitigation strategies.*

In the present study, a bank erosion model is developed to estimate the rate of bank erosion and the associated likely changes in the bank profile over time. While there are numerous mechanisms that could potentially cause banks to retreat, the present model, however, is developed based on a consideration of the effect of fluvial erosion, erosion due to seepage forces, cantilever failure and slope failure mechanisms.

Keywords: Bank erosion, bank retreat, fluvial erosion, seepage erosion.

1. INTRODUCTION

The observed widespread bank erosion that is witnessed in the alluvial rivers is a growing concern as there are inevitable accompanying consequences such as destruction of riverine habitats, loss of fertile land, damage to floodplain structures, increased downstream sedimentation, loss of life and property and more (Mosselman et al., 1995).

River bank erosion has been a major problem downstream of the confluence of Kosi with River Ganga. Instability of the river banks is an important concern as it affects the nearby lands, stability of the structures and may gradually cause shifting of the river course. The reach between Sahibganj and Rajmahal (both in Jharkhand) on River Ganga has been particularly vulnerable having lost almost 100m of the flood plain to the river due to sheer bank retreat and thereby necessitating an urgent implementation of river bank protection measures and, importantly, a scientific study of the bank retreat phenomenon therefore becomes imperative.

1.1 Bank Erosion Mechanism

River banks are most vulnerable geologic features as they are constantly under the effect of different forces that have the collective potential to compromise structural integrity of the banks and, therefore, seriously affecting bank stability as a result. River bank failure occurs when these forces exceed the cohesive forces that hold the bank material together. Rate of bank retreat depends upon flow characteristics, channel characteristics, geo-material composition of the banks, changes in the neighborhood, etc. There are many mechanisms which are responsible for bank retreat and some of the important ones include fluvial erosion, slope failure, seepage erosion, erosion caused by runoff, cantilever failure, tectonic failure etc.

Over the past decades, several studies have been conducted to explain the mechanism of bank erosion and predict the bank

retreat rate. These researches assumed fluvial erosion as a key factor affecting the bank retreat mechanism (JunQiang et al., 2014). Past work on the development of bank erosion models that are based on the effect of fluvial erosion and geotechnical failure include Osman and Thorne, 1988; Darby et al., 2002; Duan, 2005; and Midgley et al., 2012. Seepage mechanism is also an important factor that affects bank stability and has been incorporated in studies by Crosta and di Prisco, 1999; and Fox et al., 2013. In recognition of the effect of different plan forms of a river on bank retreat rat, models have been proposed to study the morphological behavior of meandering channels by Ikeda et al., 1981; and Nagata et al., 2000 including others. However, a review of related literature reveals that the effort to develop an extensive bank erosion model has on the whole been rather tepid.

To fill this glaring gap, the present study presents the development of a bank erosion model that considers the effect of the four major processes namely fluvial erosion, slope failure, seepage and cantilever failure as a framework to define the bank retreat mechanism and eventually leading to an estimate of the rate of shift in the bank over a given time horizon and further, in the process, yielding the expected profile of the bank as it evolves over the given time reference.

2. MODEL DESCRIPTION

The present model is developed to understand the effect of different processes on the rate of bank erosion and retreat occurring in a composite bank profile. In the methodology presented, the following assumptions have been made:

1) Bank material is composite and stratified.
2) Each stratum is uniform and homogeneous.
3) Slope of bank is steeper as compare to slope of channel.
4) Shear stresses along the bank vary linearly with the bank height.
5) Concentration of the suspended sediment varies linearly vertically along the bank.
6) The hydraulic gradient varies linearly along the seepage face.
7) Surface of slope failure is assumed to be planar.
8) All the eroded material is assumed to be washed out.

2.1 Fluvial Erosion

Fluvial erosion is the erosion caused due to flow of water. This erosion depends upon the prevailing flow velocities and corresponding water level in the river. The two dominant mechanisms at work include (i) entrainment of bank material; and (ii) deposition of suspended sediment on the bank and, accordingly, the net erosion occurring is the difference of erosion and deposition taking place. If, in a given time interval, the rate of entrainment of bank material exceeds the rate of

deposition, bank erosion is an inevitable consequence. The above mechanisms are summarized below.

FLUVIAL ENTRAINMENT

Sediment particles on the river banks will become entrained in the flow on account of the impinging forces associated with it. There will be a component of weight force and cohesive force which will try to bind the sediment with the bank. The amount of sediment that will be pulled out from the banks in a time Δt can be calculated as follows.

Consider an erodible river bank with slope angle of β. Then the forces acting on a particle having diameter d can be evaluated as given below.
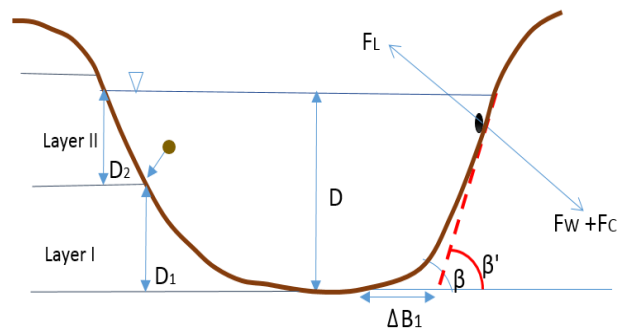
Figure 1. Diagram representing fluvial erosion mechanism.

Component of weight force acting normal to the bank on the particle can be expressed as,

$$Fw = \frac{\pi}{6} d^3 (\gamma_s - \gamma_w) \cos \beta \cos \alpha \qquad (1)$$

where, α is channel slope; γ_s is unit weight of bank material; γ_w is unit weight of water.

For cohesive bank material, cohesion force can be given as

$$F_c = c \pi d^2 \qquad (2)$$

where, c is coefficient of cohesion (N/m²).

Sediment on the bank will be subjected to lift force due to flow of water. Lift force will cause a pulling action on the sediment. If this force exceeds the binding force of the particle sediment will entrain. The lift force can be expressed as,

$$F_L = C_L' \frac{\pi}{4} d^2 \frac{\rho u_b^{*2}}{2} \qquad (3)$$

where,

$$C_L' = C_L \frac{\ln^2(0.35d/K_s)}{K^2}$$

C_L is coefficient of lift force and depends upon the Reynolds number.

u_b^* is the near bank shear velocity.

K_s is roughness height and can be taken equal to mean size of the diameter of sand grain.

K is von Karman constant.

The resultant force acting on the sediment particle in the direction of its movement may be expressed as

$$F_R = F_L - (F_W + F_C)$$

And the rate of particle entrainment may be computed from

$$E = (1 - \eta) \sqrt{\frac{3C_L'}{4\gamma_s}} \sqrt{\tau_0} (1 - \frac{y}{D} - \frac{\tau_c}{\tau_0})^{1/2} \qquad (4)$$

where,

η is porosity of the bank material.

τ_0 is shear stress at toe of the bank.

τ_c is critical shear stress of the bank.

DEPOSITION

The rate of spontaneous deposition of particles on banks can be given as,

$$D = V_S . C_b . \cos\beta \qquad (5)$$

where,

C_b is concentration of the sediment near bank at level b from the bed.

Vs is settling velocity and can be expressed as

$$V_S = \sqrt{\frac{4(\rho_s - \rho)gd}{3C_D\rho}}$$

where,

C_D is coefficient of drag and depends on Reynolds number. Then,

$$D = K_2 C_0 (1 - \frac{y}{D}) \qquad (6)$$

where,

$$K_2 = \sqrt{\frac{4(\rho_s - \rho)gd}{3C_D\rho}} * \cos\beta$$

Net rate of erosion of particles from the bank can be given as (E-D).

Volumetric rate of erosion ξ, can be given as, (Duan, 2005)

$$\xi = \frac{(E - D)}{(1 - \eta)} \qquad (7)$$

Total rate of erosion of composite bank thus can be obtained and change in the bank profile can be estimated.

2.2 Seepage erosion

For an effluent river reach, the groundwater head near bank is higher than the water level in the river. In this case there will be a force on the bank material on account of seepage which will tend to destabilize the bank profile along the seepage face. In this mechanism, weight force and seepage force will be driving forces and resistance will be due to the shear strength of soil.

The seepage force is given by,

$$J = iY_w A \qquad (8)$$

And the seepage erosion rate may be calculated as follows (refer figure 2).

Consider a sediment particle of diameter d, on the seepage face of the bank. Then forces acting on this particle will be seepage force and a component of weight force which will tend to push the sediment particle out of the bank and cohesion force and friction force which will try to keep the particle intact. The movement of particle will occur when this driving force exceeds resisting force.
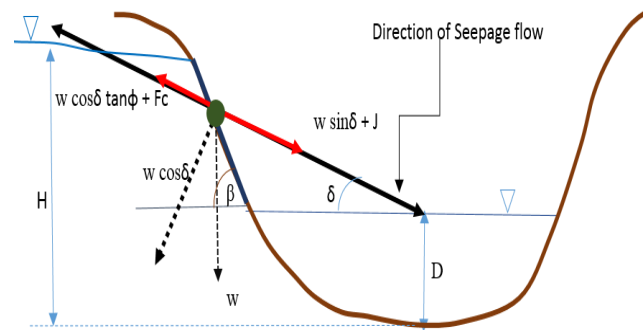
Figure 2. Force diagram for seepage erosion rate.

Let due to this imbalance in force, the particle travel distance d (equal to the diameter of the particle) with velocity say, v_{seep}.

Applying momentum conservation, the value of v_{seep} can be calculated and is given by:

$$v_{seep} = \sqrt{\frac{6\gamma'}{\rho_s} \left\{ \frac{d}{6} (\sin\delta - \cos\delta \tan\emptyset) + \frac{1}{\gamma'} (iY_w - c) \right\}^{\frac{1}{}}} \quad (9)$$

where,

$i = \tan^{-1}\delta$

γ' is the submerged unit weight of bank material

c is coefficient of cohesion

Φ is the friction angle of the soil

If δ_{max} = maximum seepage gradient, then the net erosion due to seepage then can be calculated by integrating the rate of erosion from 0 to δ_{max}. Then net erosion volumetric rate can be computed as,

$$E_{seep} = (1-\eta) \int_0^{(H-D)} \sqrt{\frac{6\gamma'}{\rho_s} \left\{ \frac{d}{6} (\sin\delta - \cos\delta \tan\emptyset) + \frac{1}{\gamma'} (\tan\delta \, \gamma_w - c) \right\}^{1/2}} \, d \quad (10)$$

The solution of Eq. (10) will give the net seepage erosion rate.

At equilibrium, $\tau = \tau_c$

The angle of failure can be computed by calculating the force required to stabilize the soil. Since contribution of cohesion will remain same, the net normal force required to provide shear strength to the soil is calculated. Accordingly, the width of bank shift can be computed and is given as,

$$\Delta B_2 = (H - D) \left\{ \frac{1}{\tan \beta''} - \frac{1}{\tan \beta} \right\} \quad (11)$$

2.3 Cantilever Failure

Cantilever failure may be observed if Δt is less than the time of bank failure, It is understood that the aforementioned twin erosion mechanisms namely (i) fluvial erosion and (ii) seepage erosion will occur up to a particular depth of the bank. It is also expected that the soil above the zone of erosion will present as an overhanging but, importantly, a weak element against tensile stresses leading inevitably to cracking and eventually to a failure mechanism known widely as cantilever failure.
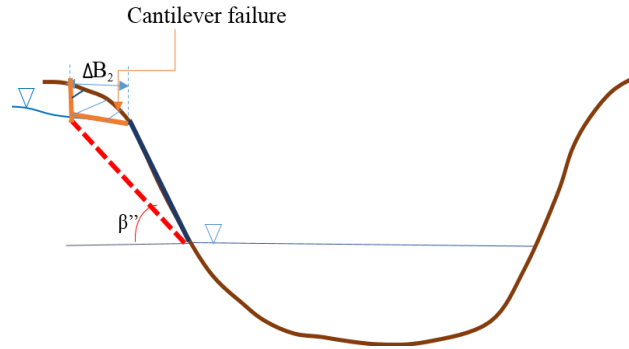
Figure 3. Mechanism of cantilever failure.

Understandably, cohesive forces will oppose the downward movement of the soil mass on account of its weight and if the net weight force is more than the shear strength of the soil, the mass will fail. The width of failure can be assumed to be approximately equal to the width of failure due to seepage erosion, i.e. ΔB_2.

2.4 Slope failure

The river bank geometry will change in time Δt and will be accompanied by a change in the bank slope. Continuous scouring of river bank can lead to a progressively steepening bank slope rendering the newer slope profile relatively less stable. In order to acquire a stable slope profile, therefore, a slope mass failure is indeed implied. In this study a planar failure plane is assumed and is a reasonable hypothesis when bank slopes are steep. In contrast, for gently sloping banks, curved failure surfaces may be assumed (Osman and Thorne, 1988).

From a rational point of view, a slope is likely to experience failure when the driving force exceeds the resisting force. The destabilizing force is essentially due to weight component along the failure plane. The resisting force is the shear strength of soil which depends upon the cohesion and angle of friction of the soil. The mechanism of slope failure is represented in Figure 4.

The forces that manifest in such a scenario may be estimated for various bank slope angles β that may vary over a defined range starting from angle β' and eventually to the steepest safe slope which will also be the slope of failure, β'''.
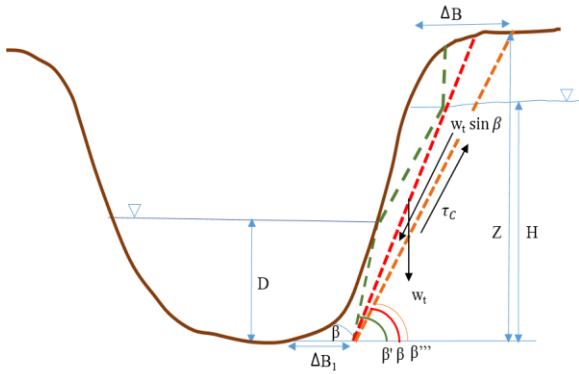
Figure 4. Representation of slope failure mechanism.

Also, the width of bank failure can be computed as:

$$\Delta B = \left(\frac{Z}{\tan \beta'''} - \frac{Z}{\tan \beta} \right) \tag{12}$$

Thus, rate of bank retreat ΔB may be estimated and represents the shift that would have occurred over a time interval Δt. The results also yield the snapshot bank profile likely to be attained at the culmination of the designated time interval of interest, Δt.

3. RESULTS

The model developed using above mentioned sets of equations was tested for the case study of bank retreat of a bend at Goodwin creek, Mississippi done by Lai et al., 2014 for which the latter authors developed a multilayer cohesive bank retreat model. The data used in the study was used to analyze the performance of the model presented in this paper. For implementation of the model, some reasonable assumptions had to be made with regards to parameters for which data was not available.

For the analysis, XS-6 data was used to obtain the preliminary result and the various attributes of bank profile considered are as given in table1. Groundwater level was assumed in this study to be at elevation of 82.3 m while the water level of the river is assumed to remain constant at 82 m. The bed was assumed to be at an elevation of 79.6 m while the top of the bank is at an elevation of 84.3 m.

Table 1. Geotechnical properties of bank profile (Lai et al., 2014)

	Depth below ground surface (m)	d_{50} (mm)	γ_{sat} (kN/m^3)	Φ ($^\circ$)	c (kPa)	η
Layer I	0-0.5	0.0625	16.9	33.1	1.41	0.489
Layer II	0.5-1.7	0.0625	19.3	28.1	2.70	0.489
Layer III	1.7-3.2	0.0625	19.9	27.0	6.30	0.380
Layer IV	3.2-4.7	2	21.0	35.0	1.00	0.320

The retreat of top width of the bank till December, 1996, as predicted by the model for the above datasets, was found to be 0.4116 m and are of a similar order of magnitude as the results obtained by Lai et al., 1996, as shown in figure 5.

Based on the comparison as above, it is averred that the bank retreat model developed in the present study is working satisfactorily under the assumptions made. The analysis also gives rate of fluvial erosion equal to 0.00744 m^3/s while no mass failure of bank was observed in model in period from March, 1996 to December, 1996.
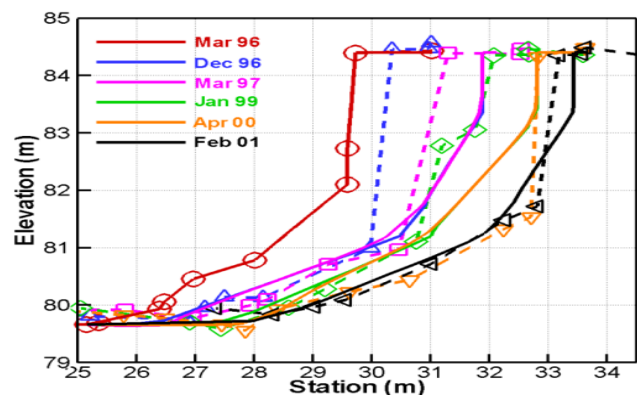
Figure 5. The changes in bank profile at XS-6 (Lai et al., 2014).

The analysis for longer time period could not be done under these sets of assumptions.

4. CONCLUSION

The study was done to develop a process based model for the bank erosion in alluvial rivers. The model development also aimed to account for seepage erosion of river banks in view of its increased risk especially in places where a high groundwater table is encountered.

The model has been tested for the case study of Goodwin Creek, Mississippi and the results show that model is performing reasonably well. In order to derive the bank profile as it develops over time, analysis requires specification of the

time series of river water levels as well as ground water levels. Detailed inputs are also required to evaluate the final performance of the model.

The model is yet to be improved for the prediction of the bank profile after occurrence of each episode of erosion.

The model assumes that the eroded material is washed away after each erosion process while in a more general case, a suitable material depositional model has also got to be specified.

REFERENCES:

i.   Crosta, G., & Prisco, C. D. (1999). On slope instability induced by seepage erosion. Canadian Geotechnical Journal, 36(6), 1056-1073.
ii.   Darby, S. E., Alabyan, A. M., & Van de Wiel, M. J. (2002). Numerical simulation of bank erosion and channel migration in meandering rivers. Water Resources Research, 38(9), 2-1.
iii.   Duan, J. G. (2005). Analytical approach to calculate rate of bank erosion. Journal of hydraulic engineering, 131(11), 980-990.
iv.   Fox, G. A., & Felice, R. G. (2014). Bank undercutting and tension failure by groundwater seepage: predicting failure mechanisms. Earth Surface Processes and Landforms, 39(6), 758-765.
v.   Ikeda, S., Parker, G., & Sawai, K. (1981). Bend theory of river meanders. Part 1. Linear development. Journal of Fluid Mechanics, 112, 363-377.
vi.   Lai, Y. G., Thomas, R. E., Ozeren, Y., Simon, A., Greimann, B. P., & Wu, K. (2014). Modeling of multilayer cohesive bank erosion with a coupled bank stability and mobile-bed model. Geomorphology.
vii.   Midgley, T. L., Fox, G. A., & Heeren, D. M. (2012). Evaluation of the bank stability and toe erosion model (BSTEM) for predicting lateral retreat on composite streambanks. Geomorphology, 145, 107-114.
viii.   Mosselman, E. (1995). A review of mathematical models of river planform changes. Earth Surface Processes and Landforms, 20(7), 661-670.
ix.   Nagata, N., Hosoda, T., & Muramoto, Y. (2000). Numerical analysis of river channel processes with bank erosion. Journal of Hydraulic Engineering, 126(4), 243-252.
x.   Osman, A. M., & Thorne, C. R. (1988). Riverbank stability analysis. I: Theory. Journal of Hydraulic Engineering, 114(2), 134-150.
xi.   Xia, J., Zong, Q., Zhang, Y., Xu, Q., & Li, X. (2014). Prediction of recent bank retreat processes at typical sections in the Jingjiang Reach. Science China Technological Sciences, 1-10.

Sediment Transport In Irrigated Channel And Influence Of Infiltration On Aggradation

Kapil Rohilla[1]   K.S. Hari Prasad [2]
[1] Research scholar, Department of Civil Engineering, Indian Institute of Technology Roorkee, Roorkee 247667, India
[2] Professor, Department of Civil Engineering, Indian Institute of Technology Roorkee, Roorkee 247667, India
Email: **rohilla21@gmail.com**
Email: Suryafce@Iitr.Ernet.in

ABSTRACT: *Aggradation   occurs when the equilibrium of an irrigated channel is distributed in such a manner that either the sediment carrying capacity of the irrigation channel is reduced or the rate of supply of sediment is increased over and above the carrying capacity of the irrigation channel. The primary objective of the present study is to provide an experimental procedure for the prediction of transient bed and water surfaces profiles and the effect of infiltration on aggradation. For this purpose, here two types of study are performed. In the first case, aggradation is done without considering the infiltration (under saturated condition), on the other hand, aggradation is done unsaturated condition for considering the effect of infiltration. The results shows that more deposition was occurred in case of unsaturated condition as compared to saturated condition. The infiltration of channel bed was found to be the main factors controlling the depth of aggradation of channel bed of sand.*
Keywords: Sediment transport, Infiltration, Irrigated channel, aggradation, carrying capacity

1. INTRODUCTION

Numerical simulation of flow and sediment transport in the irrigated channels is of practical importance in agriculture. The application of plant nutrients with irrigation water is an efficient and cost-effective method of fertilizer application to enhance crop production and reduce or eliminate potential environmental problems related to conventional application methods. Fertilizer and nutrients essential to crops are attached to the soil surface and transported along the irrigated channel by the irrigation flow. To optimize nutrient delivery to crops requires accurate predictions of flow and sediment transport in irrigation channels. As water infiltrates, flow rates decrease linearly along the irrigated channel. Brown et al. (1988) proposed that sediment deposition along the furrow perimeter creates a low-permeability seal that increases the soil water tension at the furrow perimeter. The stress, in act, increases deposition and stabilizes the seal. This self-perpetuating process stabilizes the furrow perimeter and decreases the erodibility of the soil with time.

The kinematic-wave model and zero-inertia model was commonly used for flow routing in early studies. Such models are stable and efficient for prismatic channels. These studies showed that the zero-inertia model is applicable with negligible errors for surface irrigation flow of small Reynolds numbers, and the kinematic-wave model is more applicable to channels of steeper slopes. However, these models neglected fluid acceleration, and thus, their accuracy are limited for unsteady flows. Several sediment transport models have been developed for channel irrigation flows (Lu et al. 1987; Strelkoff and Bjorneberg 2001;Bjorneberg et al. 2006). Zhang et al. (2012) developed a numerical model to simulate unsteady flow, sediment transport, and infiltration in irrigation furrows using the modified St. Venant equations. They considered the density of sediment-laden flow as a spatial variable. Two types of flume experiments were performed in the laboratory. The first series of experimental runs has a clear-water condition without

feeding sediment at the flume entrance and another was with feeding sediments. The transport capacity for fine-grained sediment was determined by the modified Laursen formula. The correlation coefficient between the sediment discharge per unit width and the tractive shear stress found to be 0.883, without sediment feeding and in case of volumetric sediment concentration and the tractive shear stress was less than 0.707. This indicates that the volumetric sediment concentration is less correlated with the tractive shear stress than the sediment discharge per unit width. The present model well simulated the advance time and flow hydrograph as compare to sediment discharge. For the sediment discharge study more refined formula should be practiced.

1.1 Aggradation Process

When man made or natural changes disturb the equilibrium of an irrigated channel in such a way that either the sediment carrying capacity of the irrigation channel is reduced or the incoming sediment load is greater than the carrying capacity of the channel, graduation take place. When relatively clear water is drawn from an alluvial stream in equilibrium for irrigation or water supply purpose aggradation occurs downstream of the point of secession.

2. EXPERIMENTAL SET-UP

The experiments were conducted in a 46cm wide, 100cm deep and 18 m long recirculatory tilting flume located in the hydraulics laboratory of Indian institute of technology, Roorkee. The flume was provided with glass side wall. The recirculatory system consisted of a rectangular tank sloped bottom to collect the sediment laden flow from the downstream end of the flume. A 25-H.P.pump was connected to the tank and a supply pipe for maintaining the recirculation. The discharge was controlled by a valve. A floating wooden wave suppressor provided at the entrance of the flume for damping the disturbances at the free surface. Rails made from metallic tube provided on the top offside walls. A movable carriage with a pointer gauge having at least count of 0.01 cm was mounted on a carriage which could move on the rails. This was applied for recording water surface and bed profiles. An adjustable gate at the downstream end of the flume was used to control the depth of flow in the flume.

Figure 1. A view of the experimental flume.

2.1 Sediment Gradation: Sieve analysis test is performed to determine the characteristics of the sediment used.

The sediment used in this work is the sand from Ganga River. The size of the sediment used to obtain from the sieve analysis is found to be d_{50}=0. 32mm. The sand was filled in the flume up to a depth of 35 cm and leveled parallel to the rails. The sand forming the bed and injected material had a median sieve diameter of 0.32 mm and geometric standard deviation of 1.39. The grain size distribution curve of the sand is shown in Fig.2. The specific gravity of the sand was 2.65.

Figure 2. Sieve Analysis

3. EXPERIMENTAL PROCEDURE

3.1 Experimental Procedure: In this section, a brief explanation of the procedure followed is given. Experiments were conducted in which the sediment was injected at the upstream end and the aggradation downstream studied. Detailed measurement of the bed and water surface profiles at various times were taken; these were useful in the study of sediment

transport and resistance to flow under non-uniform flow condition, apart from providing the basic data on aggradation.

In these experiments the flume was filled with sediment as mentioned earlier and then was given the desired slope. The recirculatory system was then filled with water and pump started. The valve was slowly adjusted to give specified discharge and uniform flow was obtained by adjusting the tailgate at the downstream end of the flume and allowing the bed to adjust. Because of the effect of entrance and exit conditions on the flow, about 3 m length of the flume at the upstream and downstream ends was not considered in assessing the uniformity of the flow. Uniform flow condition was considered to be obtained when the measured bed and water surface profiles were parallel to each other. After the uniform flow was established the bed and water surface profiles at measured at various sections along the irrigated channel. After the uniform to be obtained, the sediment was injected at the upstream end and the aggradation downstream studied. when sediment was injected at the upstream end as shown in (Fig.3). The carrying capacity of irrigatd channel was reduced. Consequently deposition (aggradation) took place along thelength of irrigated channel. The same procedure was followed in both studies. Here two types of study were performed. In the first case, aggradation was done without considering the infiltration (under saturated conditions), on the other hand, aggradation was done unsaturated (drybed) condition for considering the effect of infiltration.The concentration of the total sediment load was measured at the downstream end of the flume. The samples were collected by a sampler (Fig.1) Which discharged the sand, water mixing into a collector. The sampler collects the total load at the downstream of the channel. Minimum of 8-10 samples were collected at an interval of 10 minutes. The contents of the collector for each sample were filtered through filter paper. The material was dried in an oven, then the weight on chemical balance and concentration in gm/litre for each sample determined. From these data average concentration was determined for each run.

Figure 3. Transient bed and water surfaces, profiles in sand bed.

Figure 4. Uniform flow in the flume for the study.

4.1 Time of experiment

The aggradation is measured along the length of flume at regular time interval t = 60,75, 120 minutes.

5. RESULTS AND DISCUSSION

5.1. Effect of infiltration on Aggradation: The effect of infiltration on aggradation is investigated with flow conditions (Q = 9.6 l/sec, y = 5.0 cm, d_{50}= 0.32 mm). The aggradation is measured along the length of the flume at regular time interval t = 60,75 and 120 minutes respectively. Maximum depth of deposition was occurring in the upstream of the irrigated channel. Transient bed and water surface profiles in irrigated channel are shown in figures (5).
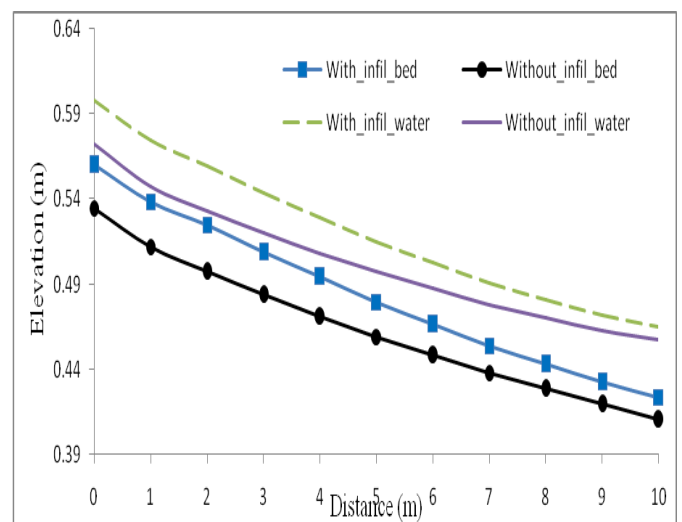
Figure 5. Transient bed and water surfaces, profiles in the sand bed for 60 minutes.

Aggradation without infiltration resulted in decreased bed elevation as compared to bed elevation computed by with infiltration. Also, infiltration is found to be the primary parameter which impacts both bed elevation and water elevation.
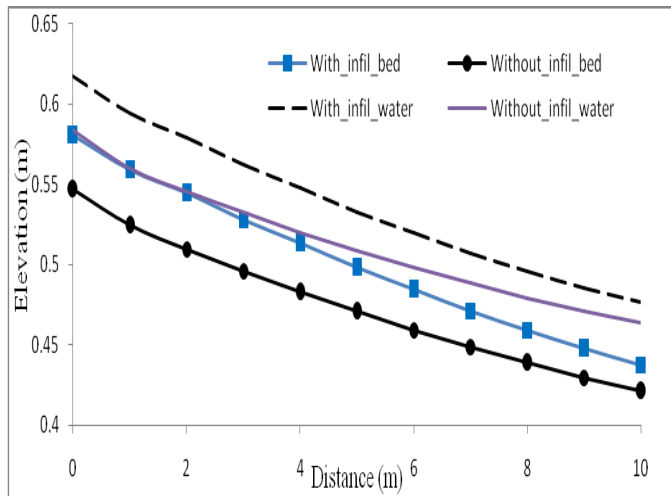
Figure 6. Transient bed and water surfaces, profiles in the sand bed for 75 minutes.

When the duration was 60 minutes the corresponding bed and water surface elevation with infiltration was found to be 0.56m and 0.60m. However, in cases without infiltration values of bed and water surface elevation were 0.53m and 0.57m respectively.
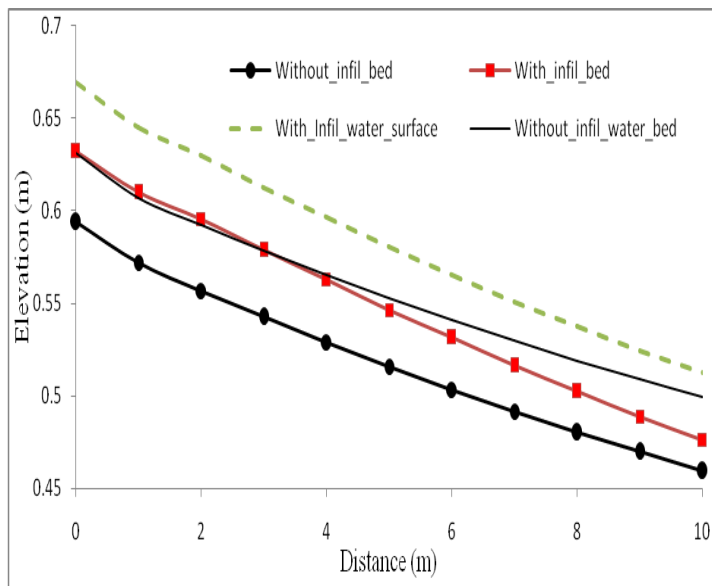
Figure 7. Transient bed and water surfaces, profiles in the sand bed for 120 minutes.

6. CONCLUSIONS

1. Infiltration influenced the bed elevation and water elevation during aggradation effectively.

2. However, bed and water elevation were increased during the infiltration. Compared to the without infiltration case (saturated condition for 60 minutes), Maximum bed and water surface elevation were found to be 0.53m and 0.57m. However, when the infiltration case (unsaturated condition for 60 minutes), corresponding maximum bed and water surface elevation were found to be 0.56m and 0.60m. Similar pattern were followed by other duration of transient bed and water surfaces, profiles eq. 75, 120 minutes.

3.   Aggradation without infiltration resulted in decreased bed elevation as compared to bed elevation measured by with infiltration. Also, infiltration is found to be the primary parameter which impacts both bed elevation and water elevation.

4. Due to infiltration (during unsaturated condition) tractive force is reduced, which is the primary force caused increased bed and water elevation. However, in the case of saturated condition tractive force may be greater than unsaturated condition.

7. REFERENCES

i.   Abbasi F, et al. (2003) Overland water flow and solute transport: model development and field-data analysis. Journal Irrigation Drainage Engineering 129(2): 71 – 81

ii.   Abderrezzak KE, Paquier A (2009) One-dimensional numerical modeling of sediment transport and bed deformation in open channels. Water Resources Research 45:W05404, 10.1029/2008WR007134

iii. Alcrudo F, Garcia-Navarro P, Saviron JM (1992) Flux difference splitting for 1D open channel flow equations. Int. J. Numerical Methods Fluids 14: 1009–1018

iv.   Bhallamudi S, chaudhry H (1991) Numerical modeling of aggradation and degradation in alluvial channels. Journal Hydraulic Engineering 117(9): 1145-1162

v.   Bjorneberg DL, Westermann DT, Aase JK, Clemmens AJ, Strelkoff T S (2006) Sediment and phosphorus transport in irrigation furrows. Journal Environmental Quality 35 (3): 786 –794

vi.   Brown MJ, Kemper WD, Trout TJ, Humpherys AS (1988) Sediment, erosion and water intake in furrows. Irrigation Science 9(1): 45-55

vii. Carsel RF, Parrish RS (1988) Developing joint probility distributions of soil water retention characteristics. Water Resources Research 24(5): 755-769

viii. Celia MA, Bouloutas TE, Zabra R (1990) A general mass-conservative numerical solution for the unsaturated flow equation. Water Resources Research 26(7):1483-1496

ix.   Chaudhry MH, (1987) Applied hydraulic transients. 2nd Ed., Van Nostrand Reinhold Co., New York, N.Y.

x.   Gill MA (1983a) Diffusion model for aggrading channels." Journal Hydraulic Research 21(5): 355-367

xi.   Jaramillo WF, Jain SC (1984) Aggradation and degradation of alluvial channel beds. Journal Hydraulic Engineering 110(8): 1072-1085

xii. Kothyari UC, Jain RK (2010) Experimental and numerical investigations on degradation of channel bed of cohesive sediment mixtures. Water Resources Research 46(W12534): 1-15

xiii. Park I, Jain SC (1986) River-bed profiles with imposed sediment load. Journal Hydraulic Engineering 112(4), 267-279

xiv. Segeren AG, Trout TJ (1991) Hydraulic resistance of soil surface seals in irrigated furrows. Soil Sci. Soc. Am. J. 55, 640–646

xv.   Shobha Ram, Hari Prasad KS, Gairola A, Jose MK, Trivedi MK (2006) Estimation of border- strip soil hydraulic parameters. Journal Irrigation Drainage Engineering 138(6): 493–502

xvi.   Singh V, Bhallamudi SM (1996) Complete hydrodynamic border irrigation model. Journal Irrigation Drainage Engineering 122(4):189–197

xvii.   Soni JP, Garde RJ, Raju KGR (1980) Aggradation in streams due to overloading. Journal Hydraulic Divison(ASCE) 106(1): 117-132

xviii.   Strelkoff T, Souza F 1984) Modeling effect of depth on furrow infiltration. Journal Irrigation Drainage Engineering 110(4): 375 – 387

xix.   Strelkoff TS, Clemmens AJ (2005) Transport capacity for eroded silts in irrigation furrows. Journal Hydraulic Engineering 131(10): 921 – 926

xx.   Trout TJ (1996) Furrow irrigation erosion and sedimentation: On-field distribution. Trans. ASAE 39, 1717–1723

xxi.   Trout TJ (1999) Sediment transport in irrigation furrows.10th international soil conservation organization meeting held may 24-29 at purdue university and USDA-ARS National soil erosion research laboratory

xxii.   Trout TJ, Neibling WH (1993) Erosion and sedimentation processes on irrigated fields. Journal Irrigation Drainage Engineering 119(6): 947-963

xxiii.   Zhang H, Kahawita R (1987) Nonlinear model for aggradation in alluvial channels. Journal Hydraulic Engineering 113(3): 353-369

xxiv.   Zhang S, Duan J, Strelkoff T, Bautista E (2012) Simulation of Unsteady Flow and Soil Erosionin Irrigation Furrows. Journal Hydraulic Engineering 138(4): 294-303

Roughness Variation In A Meandeirng Compound Channel

Saine S. Dash[1] Kishanjit K. Khatua[2] Arpan Pradhan[3]
[1] Civil Engineering Dept., N.I.T. Rourkela, Rourkela 769008, India Email: sainedash@gmail.com
[2] Civil Engineering Dept., N.I.T. Rourkela, Rourkela 769008, India. Email: kkkhatua@yahoo.com
[3]Civil Engineering Dept., N.I.T. Rourkela, Rourkela 769008, India. Email: er.arpanpradhan@gmail.com

ABSTRACT:*This paper presents a new relationship between the roughness variations for meandering compound channels under uniform flow conditions. So as to derive such a formula, a large data base involving plane-bed experiments was compiled from previous investigations and analyzed. Comparisons between the data and different existing predictive formulas for the bed roughness obtained from the literature were also made. There is no accepted standard equation for predicting roughness coefficient in meandering compound channel. This is mainly because of the lack of an effective approach for describing the roughness of the surface. A relationship with the Shields parameter only, which is commonly proposed, appeared to be insufficient. The roughness was also found to be a function of flow and channel parameters. Mainly in research work the one dimensional analysis is to select a value of n depending on the channel surface roughness and take it as uniform for the entire surface for all depths of flow. The influences of all the parameters are assumed to be taken into a single value of n. The larger the value of n, the higher is the loss of energy within the flow. Although much research has been done on Manning's n, for straight simple channels, very little has been done concerning the roughness values for meandering channels and channel with floodplains. An investigation concerning roughness variation with depths ranging from in bank to the over bank flow, spreading the water to floodplains formeandering compound channels is presented. The new empirical equation that was developed which yields the best results for all conditions investigated.*
Keywords: Manning's n, Flow Parameters, Channel Parameters, Meandering Channels with flood plains

1. INTRODUCTION:

Rivers are a natural quality of our scenery and shape of an integral part of the water cycle. As such they are at the mercy of the prevailing weather conditions. Under normal conditions flow in a river remains within the main channel. Occasionally they become inundated with excessive volumes of water and pass out onto the surrounding areas. Normally this is a harmless event as natural channels have a floodplain designed to cope with this increase in flow. However, flooding is classified as a natural disaster, and extreme events can be catastrophic. Rivers being the lifeblood of any civilization have traditionally been regarded as a major natural resource for the growth and the prosperity of the nations or states through which they traverse. The perennial supply of good quantity and quality of water along with a host of other benefits such as fertile and plain landmasses constituting the floodplains suitable for growth of crops and fodder, water connectivity to major cities both intra state and interstate etc. have made the rivers very attractive destination for dense population to settle on their floodplains.

The discharge prediction approaches in a meandering compound channel are totally different from a straight compound channel followed by Sellin (1964) and Shino et al. (1999), Patra and Kar (2004), Patra and Khatua (2006), Khatua et al. (2012).Due to different geometrical shape and flow parameters the study in a meandering compound channel are more complicated than straight compound channels. So In a meandering river, distribution of flow and velocity play a major role in relation to practical problems such as flood protection, flood plain management, bank protection, navigation, water intakes and sediment transport depositional patterns. To prediction of flow in a meandering compound channel, the experimental facilities, instrumentation and computer models have been gradually improved in the world. Extensive research has already been conducted using simple and complex type

channels such as the study was being carried out by Ikeda & Parker (1989).

Our present study attempts to justify the computational hydraulics analyses of meandering compound channels with formulation of equation for roughness coefficient and hence the discharge. A simple but reliable prediction technique for estimating roughness of a compound channel is highly necessary for field engineers, designers and researchers. Experiments are conducted to examine the variation of roughness coefficients of a meandering compound channel with different parameters. In addition to the experimental data sets with other data sets of meandering channels of investigators are collected to formulate the mathematical model.

To formulate a generalized model to predict stage discharge relationships in a meandering compound channel, here the data series of meandering compound channels of same geometry but with different sinuosities are used for the present study. The meandering compound channels which are now considered for the study which has consisted of different sinuosities. The sinuosities are 1.00, 1.11 & 1.41respectively. All the meandering channels are having same dimension i.e. width =330mm and depth =65mm. The details of the analysis of the other four channels can also be found from Mohanty et.al 2012, 2013, and Patnaik et.al 2012. This study focuses on modeling the stage discharge relationships for meandering compound channels in relation to roughness coefficients.

2. METHODOLOGY

2.1 Experimental Setup

For carrying out research in meandering channels, experimental setup was built in Fluid Mechanics and Hydraulics Laboratory of NIT Rourkela. Both the straight compound channel and meandering compound channel have same main channel dimensions and same width of total floodplains. The cross section of the main channel in both cases is trapezoidal in shape with bottom width (2b) dimension of 330mm, height (h) of 65 mm and side slope value of 1V:1H. The overall width of floodplains (2B) in case of straight channel is 395cm with symmetric floodplain of width (B) lying on either side of center of the main channel. However though total width of left and right floodplains in case of meandering compound channel is still 395cm but due to meandering nature of the channel path, floodplains on left and right are of unequal width. Flow analysis in straight and meandering compound channels with wide floodplains being the primary aim of the research, experiments were planned to study both type of compound channels keeping the geometry and surface roughness constant. Accordingly only rigid bed channels were designed for both straight and meandering compound channels, by using the Perspex Sheets (6 to 10 mm thick and having Manning's n value=0.01) for creating the desired physical flow domain. All the experiments in straight and meandering compound channel

were to be done under subcritical flow conditions. Accordingly the flume was given a mild bed slope of value of 0.0011 so that water could flow in the inside channels under gravity. For imparting this desired slope, the flume was tilted by operating the gear mechanism on trial basis. The traverse bridge with the point gauge (least count 0.1mm) was moved back and forth along the channel length measuring the depth of water at some predetermined points and hence the difference in water surface elevation in a given length, say 1m. All the channels were sine generated curves (Fig.1 shows the experimental setup, Fig.2 shows the plan view of Meandering Channel (Top) & Flow Section (Side) represents the dimensions of channel with test section respectively and Fig.3 shows the test section of meandering channel).

Measuring devices like pointer gauges having least count of 0.1 mm were used to measure the flow depths. A large rectangular notch of 4m wide has been provided at the upstream end to monitor the continuous discharge passing through the channels. All the observations were recorded at the central bend apex of the meandering channels. The details of geometrical parameters and hydraulic parameters of meandering compound channels are given in Table 1.

Table-1: Details of Geometrical Parameters of the Meandering Compound Channel

Sl. No.	Parameter	Description
1	Flume Dimension	15m×4m×0.5m
2	Meandering Channel Geometry	Trapezoidal with side slopes 1:1
3	Type of Bed Surface	Rigid and Smooth Bed
4	Section of Main Channel	0.33m at Bottom and 0.46 m at Top
5	Bank Full Depth of main Channel	0.65m
6	Top Width of Compound Section	3.95m
7	Bed Slope of the Channel	0.0011
8	Sinuosity of the Channel	1,1.11,1.41
9	Types of Flood Plain	Unsymmetrical
10	Types of Main Channel Path	Sine generate curve
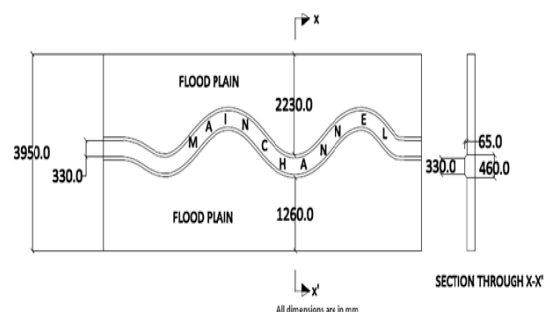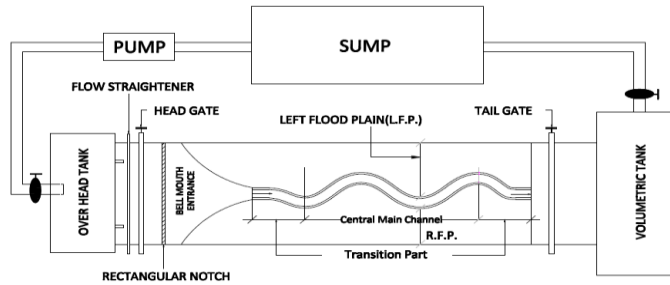
Figure 1. Experimental Setup of Meandering Compound Channel
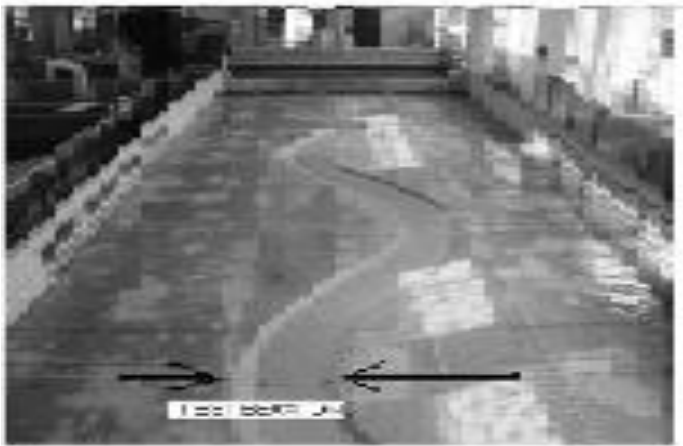
Figure 2. Plan view of Meandering Channel (Top) & Flow Section (Side)

2.2 Measurement of Roughness Coefficient in a Meandering Compound Channel

Measurement of roughness in an open channel flow helps in measuring of stage-discharge relationship in meandering compound channel. Previously some investigators gives some different formula to calculate the roughness at different conditions which are explain at below, such as

Cowan (1959) developed a procedure for estimating the effects of some factors to determine the value of *n* for a channel. This equation provides much more flexibility and accuracy than can be achieved using Chow (1959) in isolation. The value of *n* may be computed by

$$n = (n_b + n_1 + n_2 + n_3 + n_4)m$$

$$(1)$$

Where, n_b is the base value of *n* for a uniform, smooth and straight channel in natural materials, n_1 is the correction factor for the effect of surface irregularities, n_2 is the value for variations in shape and size of the channel cross section, n_3 is the value for obstructions, n_4 is the value for vegetation and flow conditions, m is the a correction factor for meandering of the channel.

Toebes and Sooky (1967) carried out series of experiments in small scale flume has 7.3m long by 1.18m wide and of low sinuosity (1.09). To determine the overall conveyance of meandering channels as a function of stage is given by

$$\frac{f'}{f} = 1.0 + 6.89 R \qquad \text{For s=1.1}$$

$$(2)$$

Where, R = Hydraulic radius in meters.
f = friction factor

Shino, Al-Romaih and Knight (1999) here discharge measurement for meandering compound channel were carried out with various effects of bed slope, water depth and sinuosity of meandering channel. Here, maintaining different longitudinal slope (0.001, 0.002, and 0.0005) with keeping Sinuosity 1.37 constant for experimentation. It was found that the channel discharge increased with an increase in bed slope and it decreased with increase in sinuosity for the same channel. The simple mathematical equation is given below,

$$S = 10\left(\frac{f}{8}\right)^{\frac{1}{2}}$$

$$(3)$$

Where, S=Sinuosity of the Channel

Khatua and Patra (2012) carried out a series of laboratory tests for smooth and rigid meandering channels whose Sinuosity is 1, 1.44, 1.91 with both rectangular and trapezoidal cross section is considered. Here also developed numerical equation using dimension analysis to evaluate Manning's *n* for meandering compound channel and validate with different investigator paper.

$$n = \frac{S_r v^{0.72} S^{0.07} m^{0.29}}{7k\alpha g^{0.86} R^{1.2}}$$

$$(4)$$

Where, R is the hydraulic radius, v is the viscosity, g is the gravitational acceleration, S is the bed slope, S_r is the sinuosity, α is the aspect ratio, k is a constant of value 0.001.

3. EXPERIMENTAL RESULT AND ANALYSIS

The experimental data sets analysis of meandering compound channels are studied. From the experimental results and literature study, it is seen that the investigators such as Shino, Al-Romaih and Knight (1999), Khatua et.al (2012), Moharana and Khatua (2014) proposed models to predict roughness coefficients and justify the dependency of flow parameters. In the present study we considered taking three non-dimensional influencing parameters into our considerations. Those are Depth ratio (β), Reynolds Number (Re) and Froude's number (Fr) respectively.

The dependency of roughness coefficient in terms of Manning's n with their best functional relationships has been found out from different plots. The variation of roughness co-efficient in terms of Manning's n with depth ratio is plotted in Fig (3.a). It is seen that, as sinuosity increases, Manning's n also increases. In high depth of flow depth ratio is increase as sinuosity increases. It means the depth ratio is directly proportional to the Manning's n. Then the Reynolds no vs. Manning's n are plotted for all the meandering compound channels and show in Fig (3.b).It is seen that Manning's n decreases with Reynolds increase. Because for straight channel and low sinuous channels, the loss of energy is less for higher depth of flow but higher sinuous channel, Manning's n increase with Reynolds number. In the third case, we tried to find the effect of gravity on evaluation of resistance of a meandering channel. Therefore, Manning's n values are plotted with different Froude's no F_r in Fig (3.c). It is seen that Manning's n decreases with Froude's no increases for both lower sinuous channel as well as higher sinuous channel. This may be due to the fact that Froude's number is directly proportional to mean velocity and at the same time Manning's n is inversely proportional to mean velocity. Due to this reason Manning's n decreases with successive increment of Froude's number.
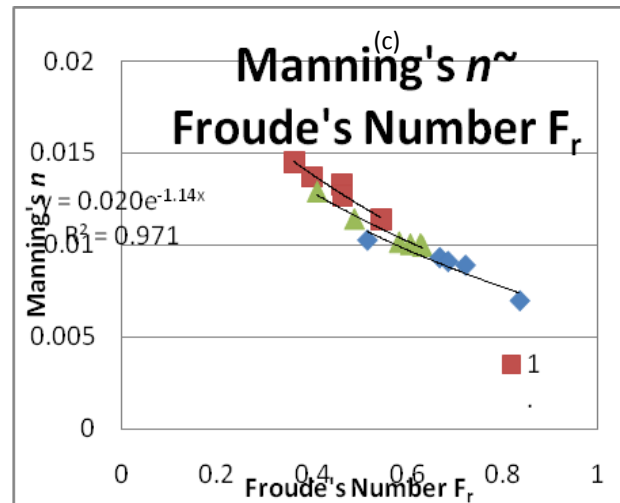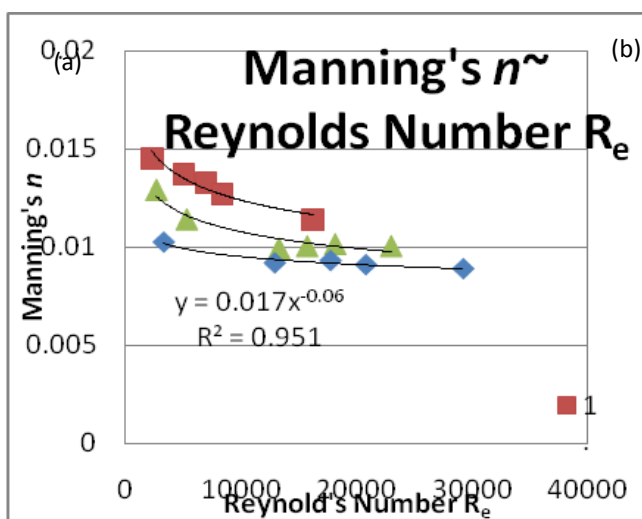
Figure 3. (a to c) Comparison of Manning's n with different subsequent flow parameters.

4. MODEL DEVELOPMENT

In this work, the STASTICA Software tool is applied for formulation of the mathematical model to predict roughness coefficients in terms of Manning's n in meandering compound channel. The Multiple Linear Regression analysis (MLR) is applied where the dependencies of roughness coefficient on different parameters which are related. Therefore all the variables here are divided into two categories i.e. dependent and independent variables. At first the variation of the non-dimensional variables in relation to Manning's n are plotted and the best fit curve are obtained. The functional relationships which are providing the maximum coefficient of determination are fixed for each dependency parameter with Manning's n. The dependency of roughness and the best functional relationships have been found out from different plots from the experimental data sets. The functional relationship of Manning's n can be written as

$$n = f\left(\beta,\, Re,\, Fr\right)$$

$$(5)$$

By analysed the above plots, corresponding best functional relationships of roughness coefficients with different non-dimensional geometric and hydraulic parameters are found out are represented as f_1, f_2, and f_3 respectively. The best functional relationships obtained are

$$n = f_2\left(R_e\right)$$
$$f_2 = A_2\left(R_e\right)^{-0.065}$$

$$(6)$$

$$n = f_3\left(F_r\right)$$

$$f_3 = A_3 e^{C_2 R_e}$$

$$(7)$$

$$n = f_1(\beta)$$
$$f_1 = A_1 \ln(\beta) + C_1$$

$$(8)$$

Where A_1, A_2, A_3, c_1 and c_2, are proportionality coefficients. From the above graphs it's shown that R^2 value for all the relationships are very high and varies from 0.92 to 0.98. By using the above relationships we develop the equation for predicting Manning's n. All the dependent variables are taken in Y-axis and observed Manning's n value which the independent variables are taken in X-axis. After applying the Multiple Linear Regression Analysis using STASTICA, the unstandardized coefficients are found out and tabulated in Table 2.

Table 3: Unstandardized Coefficient by Multiple Linear Regression Analysis

	Coefficients	Standard Error
Constants	-0.056208811	0.00615
R_e	10.82751792	1.072983
F_r	-0.816703287	0.65856
β	-2.099595359	0.751763

By applying multiple linear regression, here we found R^2 =0.94. As described previously, the functional relationship for Manning's n with all the independent variables are written as,

$$n = f(f_1, f_2, f_3)$$

After diverting in separate functional group for each non-dimensional parameter, the equation for roughness coefficients is presented as

$$n = -0.0562 + 10.827 f_1 - 0.8167 f_2 - 2.099 f_3$$

$$(9)$$

Now putting the individual values of functions f_1, f_2 and f_3 from equations (5), equation (9) is now modified and the final expression compiling the individual functional relationships of each independent variable is given by

$$n = -0.071(1 - 2.61 \operatorname{Re}^{-0.065} + 0.23 e^{-1.141 Fr} + 0.086 \ln(\beta)$$

$$(10)$$

After then by putting the different dependent variables from the above graph equation (9) then it will give a relation in a modified equation (10) in accurate linear form. At this point roughness of meandering compound channel gives a better

result means actual vs. predicted graph in fig (4) is given below, which shows the efficacy of the developed model.
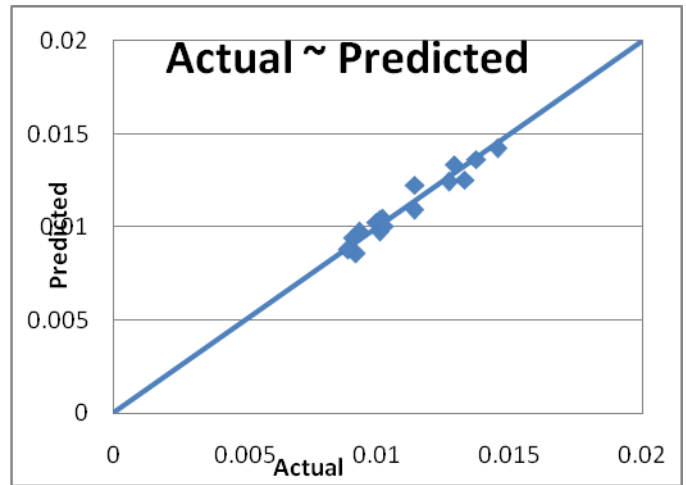
Figure 4. Actual vs. Predicted valuein meandering compound channels

5. CONCLUSION

On the basis of the present experimental investigation supported by mathematical modeling in smooth, rigid sinusoidal channels, the following conclusions are drawn.
1. For meandering compound channels of different sinuosity, Manning's n increases with increase of sinuosity at increase the depth of flow.
2. Manning's n is found to vary with Reynolds (R_e) no and Froude's no (F_r). Manning's n increase with Reynolds number (R_e) and decreases with Froude's no F_r.
3. A Mathematical Model has been proposed for predicting roughness coefficients of meandering compound channel for different geometry, sinuosity and flow conditions.
4. Regression analysis has been carried out to formulate a mathematical model to predict roughness coefficient in meandering compound channel. The model is found to give good result with the experimental findings.
5. The accuracy of models has also been studied and the R^2=0.94 are found for meandering compound channel. By using this model the roughness coefficient means Manning's n of any meandering compound channel of sinuosity i.e. Sr>1.41 can easily be evaluated.

6. ACKNOWLEDGEMENTS

REFERENCES:

i. Cowan W. L. (1956), "Estimating Hydraulic roughness Coefficients", Agric. Engg, 37, 473-475.

ii. Ikeda S., Parker G. and Kimura Y.(1988), "Stable Width and Depth of Straight Gravel Rivers With heterogeneous Bed Materials", Water Resources Research, Vol. 24, No. 5, pp. 713-722, May.

iii. Khatua K.K., Patra K.C., Nayak P.(2012), "Meandering effect for evaluation of roughness coefficients in open channel flow", 6th inter. conf. on river basin management, WIT Transactions on Ecology and the Environment (ISSN 1743-3541), CMEM, WIT Press. 146(6):213-227.

iv. Mohanty, P.K., Dash,S.S. and Khatua,K.K. (2012), "Flow Investigations in a Wide Meandering Compound Channel". International Journal of Hydraulic Engineering 1(6) 83-94.

v. Nayak, Pinaki. (2010) "Meandering effect for evaluation of roughness coefficients and boundary shear distribution in open channel flow". M.Tech Thesis NIT, Rourkela.

vi. Patnaik, M., Patra.K.C., Khatua, K.K., Mohanty, L. (2012), "Modelling Boundary Shear Stress in Highly Sinuous Meandering Channels", ISH Journal of Hydraulic Engineering, Taylor & Francis.

vii. Patra, K.C., Kar, S. K. and Bhattacharya A. K. (2004), "Flow and Velocity Distribution in Meandering Compound Channels", Jour. of Hydraulic Engg., ASCE, 130 (5), 398.

viii. Patra, K.C., and Khatua, K. K. (2006), "Energy loss and discharge estimation in two stage meandering and straight compound channel", EWRI of ASCE and IIT Kanpur,

ix. Saine S. Dash, K.K.Khatua, P.KMohanty (2013), "Energy loss for a highly Meandering open Channel Flow" Res. J. Engineering Sci.,Vol. 2(4), 22-27.

x. Saine S. Dash, K.K.Khatua, P.KMohanty (2013), "Factors influencing the prediction of resistance in a meandering channel" ,International Journal of Scientific & Engineering Research, Volume 4, Issue 5.

xi. Sellin R. H. J. (1961), "A Study of the Interaction between Flow in the Channel of a River and that over its Floodplain", Ph. D Thesis, University of Bristol, England.

xii. Sellin, R. H. J. (1964), "A Laboratory Investigation into the Interaction between the Flow in the Channel of a River and that over its Floodplain", La. Houille Blanche.

xiii. Shiono K., Al-Romaih IS., and Knight D. W., (1999), "Stage-discharge assessment in compound meandering channels", Journal of Hydraulic Engineering, ASCE, 125 (1), 66- 77.

xiv. Toebes G. H.,Sooky A. A.(1967), "Hydraulics of Meandering Rivers with Floodplains", Journal of Waterways and Harbours Div., ASCE, Vol. 93.

Empirical Formulation of Flow Characteristics In Trapezoidal Channels

S. Gandhi[1] and R. P. Singh[2]

[1] Assistant Professor, Department of Civil Engineering, Jaypee University of Engineering & Technology, Guna (M.P.) India. E-mail: sumit.gandhi@juet.ac.in

[2] Professor, Department of Civil Engineering, Motilal Nehru National Institute of Technology, Allahabad (UP), India. E-mail: singh_ram_pal@yahoo.com

ABSTRACT: Empirical relations for hydraulic jump characteristics, viz. sequent depth ratio (Y_2/Y_1), efficiency of jump (E_2/E_1) and relative length of jump (L_j/Y_1) in trapezoidal channel with/without appurtenances are developed by introducing dimensionless Reynolds number, and neglecting the frictional effect for approach Froude number (varied between 2 to 10 under different conditions). Developed empirical models were also validated and compared with acquired experimental data as well as with literature data. Close fitness of the empirical models with appurtenances under varying dimensions, positions of baffle blocks provides accurate prediction of same for higher value of Froude number.

Keywords: Trapezoidal channel, Hydraulic jump, Energy dissipation, Reynolds number, Baffles.

1. INTRODUCTION

Transition of rapidly varied flow in an open channel from supercritical to subcritical within short distance, is of considerable importance in many practical problems to control high energy, especially when $F_{r1}>2$. Hydraulic jump in trapezoidal channels possesses different characteristics. Compared to prismatic channels, such channels with appurtenances not only modify the hydraulic jump characteristics but also effect significantly the formation of symmetric flows. Moreover, the flow with baffle blocks arrangements are useful to control the hydraulic jump when there is deficiency of tail water depth to form a good jump, and the places where there is design constraints in order to reduce the basin length.

2. THEORY

Hydraulic jump formation in horizontal trapezoidal channel is one of the challenging problems in hydraulic engineering as noted by Rajaratnam (1968) and Hager (1992). Diskin (1961) obtained a theoretical equation for the sequent depth ratio in trapezoidal channels and showed that the sequent depth is smaller than that for a rectangular channel. In the reviews of Rajaratnam (1967) and Hager (1992) only few investigators considered the internal structure of the flow in the jump and there is scarcity of analytical and experimental studies on trapezoidal channel. Wanoschek and Hager (1989) performed an experimental study on the characteristics of hydraulic jump in a trapezoidal channel with side slope 1:1, and observed that the sloping side walls caused a significant reduction in the sequent depth as well as increase in the energy loss and the length of jump.

Recently Afzal and Bushra (2002) analyzed the axial flow structure of turbulent hydraulic jump, based on the solution for trapezoidal channel (that includes rectangular and triangular channels as special cases) has been obtained for the surface profile of the hydraulic jump. According to them overall length L_j is of the order of roller length L_r of the hydraulic jump. Jamil and Khan (2008) proposed models for sequent depth ratio and relative energy loss on the basis of theoretical study of hydraulic jump for different side slopes and compared well with Silvester (1964) result.

$$F_{r1}^2\left[4+4n\left(2+n+n\frac{Y_2}{Y}+\frac{Y_2}{Y_1}\right)\right]-\left[2+\frac{8Y_2^3}{3Y_1^3}n+\frac{2}{3}n\left(\frac{Y_2^2}{Y_1^2}+\frac{Y_2}{Y_1}\right)+\frac{Y_2}{Y_1}\right]=0$$

(1)

$$\frac{E_2}{E_1} = 1 - \frac{\left(1 + 0.5 F_{r1}^2\right) - \left[\frac{Y_2}{Y_1} + \left\{F_{r1}^2 \frac{(1+n)^2}{2\left(1 + n\frac{Y_2}{Y_1^2}\right)\frac{Y_2^2}{Y_1^2}}\right\}\right]}{\left(1 + 0.5 F_{r1}^2\right)}$$

(2)

where, n = zY_1/b, z is side slope and b is bottom width of channel.

Omid (1996) studied the trapezoidal channel with side slope varied from 0.5:1 to 2:1 and observed that the sloping side walls cause reduction in the sequent depth, and increase in the energy loss as well as the length of jump. Experimental investigations have also been reported by Ohtsu (1976) and Wanoschek and Hager (1989). The experimental results of Press (1961) were analysed by Wanoschek and Hager (1989) and they developed an empirical relation for $L_j/(Y_2-Y_1)$, whereas Ohtsu (1976) correlated the length of hydraulic jump 'L$_j$' with energy loss. Based on the solution for trapezoidal channels, Afzal and Bushra (2002) have analyzed the axial flow structure of turbulent hydraulic jump to study the surface profile of jump. As per Afzal and Bushra (2002), the roller length 'L$_r$' is of the order of overall length 'L$_j$' of the hydraulic jump. Esmaeeli (2005) developed a theoretical equation for the sequent depth ratio and relative length of jump by using multiple regression analysis for trapezoidal channel section as:

$$\frac{Y_2}{Y_1} = 0.288 - 0.0708\frac{L_j}{Y_1} + 1.54 F_{r1}$$

(3)

$$\frac{L_j}{Y_1} = -2.3 + F_{r1}\left(5.01 + 0.381\theta\right) + 1.818\frac{Y_2}{Y_1}z$$

(4)

3. EXPERIMENTAL SET-UP AND METHODOLOGY

In order to understand various flow characteristics, the experiments were carried out in trapezoidal (with & without baffle) channels. The set up consists of a constant head tank of volume $3.6 \times 3.6 \times 3$ m^3, water reaches to the inlet tank of volume $0.43 \times 0.31 \times 0.80$ m^3 through the connecting pipe of diameter 10 cm provided with regulating valve. The upstream face of inlet regulating gate is covered by stilling basin of length 3 m and width 0.3 m to prevent side wave reflection and surface undulation so that a stabilized flow is available at the inlet of main channel. Parallel rails were mounted at the top of the side walls for sliding of pointer gauge to measure the depth at different positions along the length and across the width of the main channel. Number of experiments for different values of approach Froude number (varying between 2 to 10) using sharp edged regulating gates (both upstream and downstream) and feeding pipe with valve were performed.

4. DIMENSIONAL ANALYSIS

The important variables affecting the jump pattern and energy dissipation can be expressed as:
f (Y$_1$, Y$_2$, V$_1$, V$_2$, L$_j$, E$_L$, μ, g, ρ, ε) = 0

(5)

Using Buckingham's π-theorem and treating Y$_1$, g and μ as repeating variables, the following dimensionless groups are developed:

$$f\left(\frac{Y_2}{Y_1}, \frac{E_2}{E_1}, \frac{L_j}{Y_1}, \frac{V_1^2}{gY_1}, \frac{\rho V_1 Y_1}{\mu}, \frac{x_{bi}}{L_{bt}}, \frac{nW_b}{b}, \frac{h_b}{L_{bb}}, \frac{\varepsilon}{Y_1}\right) = 0$$

(6)

From the analysis of experimental results, it is observed that all the three hydraulic jump characteristics namely Y$_2$/Y$_1$, E$_2$/E$_1$ and L$_j$/Y$_1$ in different channel conditions are function of approach Froude number, Reynold's number and dimension and position of baffle blocks.

$$f\left(\frac{V_1^2}{gY_1}, \frac{\rho V_1 Y_1}{\mu}\right) \quad \text{For Trapezoidal Channel}$$

(7)

$$f\left(\frac{V_1^2}{gY_1}, \frac{\rho V_1 Y_1}{\mu}, \frac{x_{bi}}{L_{bt}}, \frac{nW_b}{b}, \frac{h_b}{L_{bb}}\right) \quad \text{For Trapezoidal Channel}$$
with Baffle Blocks   (8)

Using linear fitting of the experimental data for jump characteristics and the dimensionless groups, the following empirical model for Y$_2$/Y$_1$, E$_2$/E$_1$ and L$_j$/Y$_1$ were developed:

Trapezoidal Channel

$$\frac{Y_2}{Y_1} = 35860\left(\frac{F_{r1}^2}{R_{e1}}\right) + 1.4911 \qquad (R^2$$
$$= 0.990) \qquad (9)$$

$$\frac{E_2}{E_1} = -8.5608\left(\frac{F_{r1}^{0.05}}{R_{e1}^{0.01}}\right) + 8.4344 \qquad (R^2$$
$$= 0.9819) \qquad (10)$$

$$\frac{L_j}{Y_1} = 970218\left(\frac{F_{r1}^{1.5}}{R_{e1}}\right) + 2.915 \qquad (R^2$$
$$= 0.9868) \qquad (11)$$

Trapezoidal
$$(R^2 = 0.9955) \qquad \text{Channel with Baffle Blocks}$$

$$\frac{Y_2}{Y_1} = 1242.15\left[\left(\frac{F_{r1}^2}{R_{e1}}\right)\left(\frac{x_{bi}}{L_{bt}}\right)\left(\frac{nW_b}{b}\right)\left(\frac{h_b}{L_{bb}}\right)\right] + 1.7438$$

(12)

$$\frac{E_2}{E_1} = -0.0181\left[\left(\frac{F_{r1}^{0.3}}{R_{e1}^{0.01}}\right)\left(\frac{x_{bi}}{L_{bt}}\right)\left(\frac{nW_b}{b}\right)\left(\frac{h_b}{L_{bb}}\right)\right] + 1.0668$$
$$(R^2 = 0.9376) \qquad (13)$$

$$\frac{L_j}{Y_1} = 38692.5\left[\left(\frac{F_{r1}^{1.5}}{R_{e1}}\right)\left(\frac{x_{bi}}{L_{bt}}\right)\left(\frac{nW_b}{b}\right)\left(\frac{h_b}{L_{bb}}\right)\right] + 5.6924$$
$$(R^2 = 0.956) \qquad (14)$$

5. RESULTS: DATA ANALYSIS

The variation of all the three hydraulic jump characteristics with Froude number was observed in trapezoidal channel under different conditions of channel arrangements, i.e. without baffle, with 2 baffles (series 1) and with 1 baffle (series 2 and series 3) of different dimensions. The experimental results for flow variation of the entire hydraulic jump characteristics with approach Froude number are shown through combined plots in Figures 1 to 3.

Figure 1 shows a linear variation of sequent depth ratio (Y_2/Y_1) against Froude number (F_{r1}) for all three types of channel arrangements. From the figure 1, close data shows that the symmetrical jump pattern is formed at lower values of Froude numbers ranging between 2 to 6. However, at higher values of F_{r1}, more scattering of data points is observed due to asymmetric jump. Similar pattern of symmetric jump formation has been reported by Iwao and Youichi (2001) at lower Froude number ranging between 1.5 to 2.5 and becomes asymmetric at higher F_{r1} due to high surface turbulence. R^2 value of 0.84, 0.86, 0.8 and 0.85 respectively for four channel conditions show scattering of data at higher F_{r1}. Significant increment in Y_2/Y_1 is observed after providing 2 baffle blocks (series 1) in comparison with simple channel with no baffle blocks. There is 29% increment in the value of Y_2/Y_1 at $F_{r1} = 10$ after providing 1 baffle block (series 3), however comparatively less increment in sequent depth ratio is obtained with 2 baffle blocks (series 1) and 1 baffle blocks (series 2) arrangements. It is also clear from the figure that at higher Froude number effect of baffle blocks for all the three series of channel conditions are quite significant. On the other hand, when baffle blocks of series 1 and 2 are provided, 10% and 2 % increments in Y_2/Y_1 are observed at all approach Froude numbers. Therefore, it can be concluded that baffles of higher width are more effective for better hydraulic jump pattern.
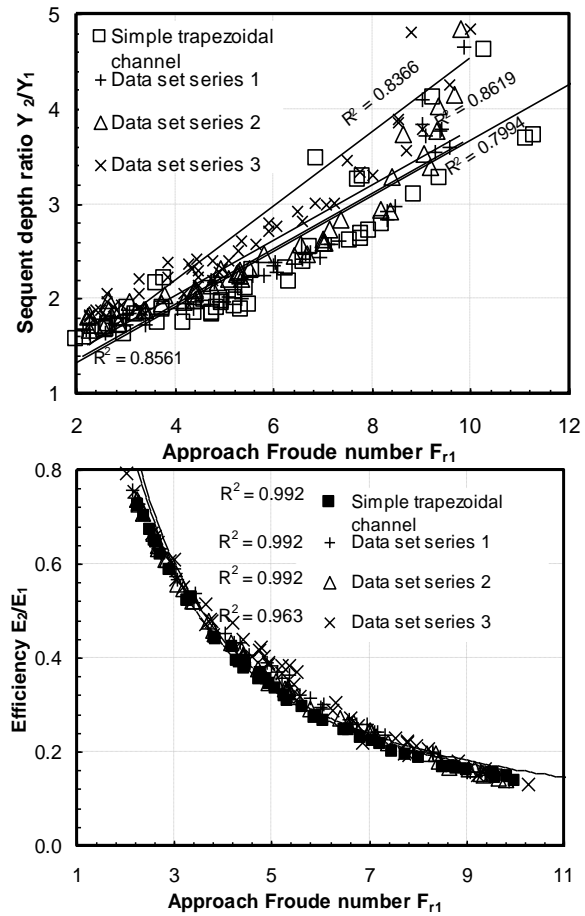
Figure 1. Variation of sequent depth ratio
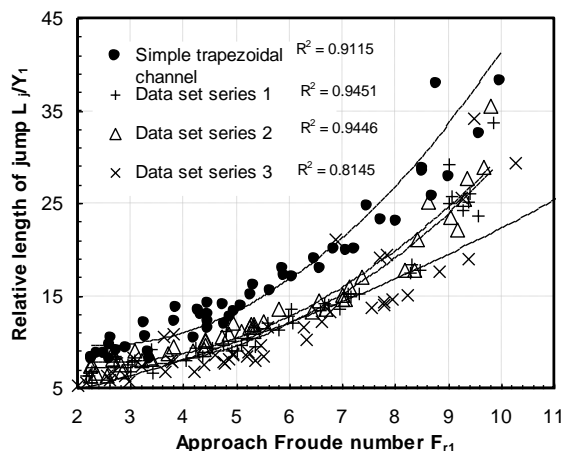
Figure 2. Variation of efficiency of jump against approach Froude number against approach Froude number

Figure 3. Variation of relative length of jump against approach Froude number

Figure 2 shows a decreasing trend of efficiency (E_2/E_1) against the approach Froude number (F_{r1}) varied between 2 to 10 for all the four types of channel arrangements. From the figure 4.64, It is seen that efficiency of jump is increased by an amount of 7% at $F_{r1} = 2$ and 10% at $F_{r1} = 10$ when baffle blocks of series 3

arrangement are provided in comparison to simple trapezoidal channel, whereas the increase in efficiency is only 3% at $F_{r1} = 2$ for series 2 and series 1 experiments. At $F_{r1} = 10$, the increase in efficiency is 6 % and 4 % for series 2 and series 1 respectively. Therefore, it is concluded that efficiency is more when single baffle of higher width than the rest of the other two arrangements (i.e. series 1 and series 2).

Figure 3 shows a non-linear variation of relative length of jump (L_j/Y_1) against approach Froude number (F_{r1}) varied between 2 to 10 for all the four types of channel arrangements. About 26% and 43% reduction in L_j/Y_1 is seen at $F_{r1} = 2$ and 10 respectively with baffle blocks of series 3 arrangement than the simple trapezoidal channel, whereas 12% and 8% reduction in L_j/Y_1 is observed with series 2 and series 1 baffle block arrangements in comparison to simple trapezoidal channel at $F_{r1} = 2$ and 10 respectively. Thus, it may be concluded that single baffle block of higher width provided at the centre is more effective in reducing the relative length of jump than the simple and the other two trapezoidal channel arrangements (series 2 and series 1). Omid et al (2008), Afzal & Bushra (2002) and Esmaeeli et al (2005) have also reported the similar experimental results by varying the side slopes. It is therefore, concluded that the dimension of series 1 and series 2 baffle blocks may be modified to obtain the maximum reduction in relative length of jump.

6. RESULTS: VALIDATION

6.1 Sequent Depth Ratio (Y_2/Y_1)

Figure 4 shows linear variation of sequent depth ratio (Y_2/Y_1) against approach Froude number (F_{r1}) for trapezoidal channel. Linear model of Eq. (9) were fit for the present experimental data and Mathur (1965) data with R^2 value 0.94 and 0.88. The deviation between the two lines obtained may be attributed to the reason that Mathur (1965) considered side slope 0.25:1, whereas in present study it is 1.73:1. Figure 5 shows difference in variation between Y_2/Y_1 computed using Esmaeeli (2005) [Eq. (3)], Jamil (2008) [Eq. (1)] and presented model [Eq. (9)], it shows values obtained through presented model [Eq. (9)] lying between the results of Jamil (2008) and Esmaeeli (2005). The deviation between Eq. (9) and the results of other two authors may be explained on the basis that Esmaeeli developed his relation assuming sequent depth ratio depends upon relative length of jump and approach Froude number, which in turn depends on the side slope of the channel, whereas Jamil (2008) had given his model assuming trapezoidal channel with bed slope. Figure 6 shows the comparison of experimental result of Omid et al (2008) for trapezoidal and rectangular channel and the present model [Eq. (9)]. The deviation between the two result can be explained on the basis of experimental conditions that Omid et al (2008) had given his experimental result with side slope 1.5:1 and diverging angle of 5°, whereas in present case side slope is 1.73:1 and divergence angle is 0°. His experimental result also compared in the present model

showing sequent depth ratio always more than the trapezoidal channel at all F_{r1}, which were also explained by other authors [Afzal and Bushra (2002) and Wanoschek and Hager (1989)].
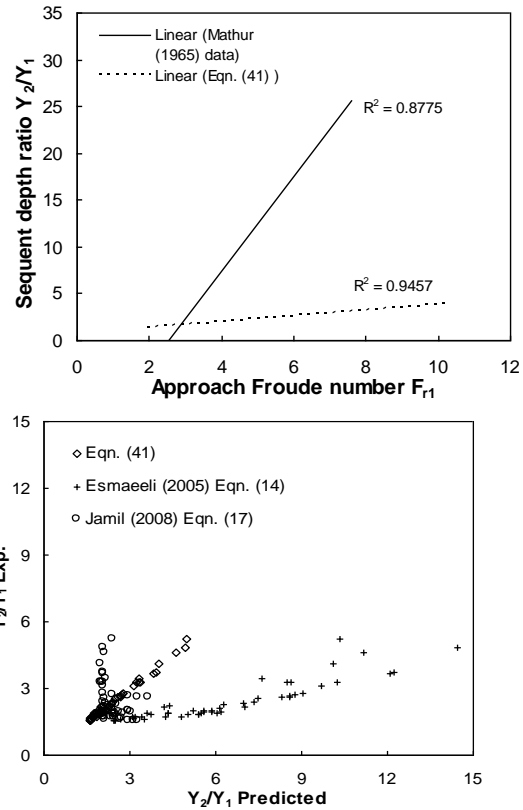
Figure 4. Testing of Eq. (9) with Mathur (1965)

Figure 5. Comparison of Eq. (9) with other data for sequent depth ratio data for sequent depth ratio

6.2 Efficiency of Jump (E_2/E_1)

Figure 7 shows non-linear variation of efficiency (E_2/E_1) against approach Froude number (F_{r1}). Linear model of Eq. (10) were fit for the present experimental data and Mohd. Jamil (2008) data for testing. R^2 value for Jamil (2008) data shows some scattering, attributed to the experimental condition of providing bed slope, whereas in present case it is kept horizontal. Figure 8 shows the comparison of experimental and predicted E_2/E_1 values using Jamil (2008) model [Eq. (2)] and the present model [Eq. (10)] close to each other; proves to be satisfactory prediction of E_2/E_1. Figure 9 shows comparison of experimental E_2/E_1 values of Omid et al (2008) for trapezoidal and rectangular channel with the predicted values for trapezoidal channel; indicates that values obtained are close to each other at all values of F_{r1}. Similarly, Omid et al (2008) experimental result for rectangular channel is also shown to compare the E_2/E_1 values between two types of channel.

Figure 8. Comparison of experimental
Figure 9. Comparison of present experimental
data with Eqs. (10) and (2). Omid et al (2008) data.

Figure 6. Comparison of Y_2/Y_1 between   Figure 7. Comparison of Eq.
(10) with Eq. (2)   experimental results with Omid et. al (2008)
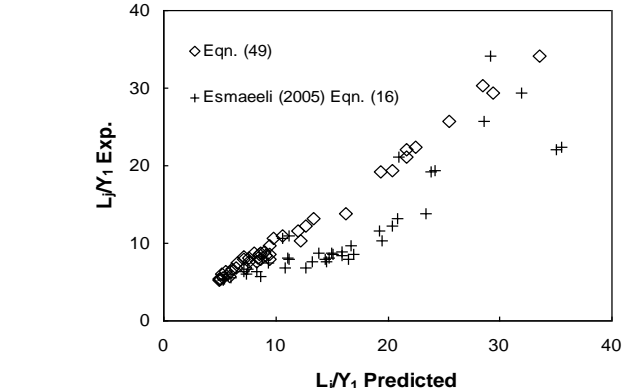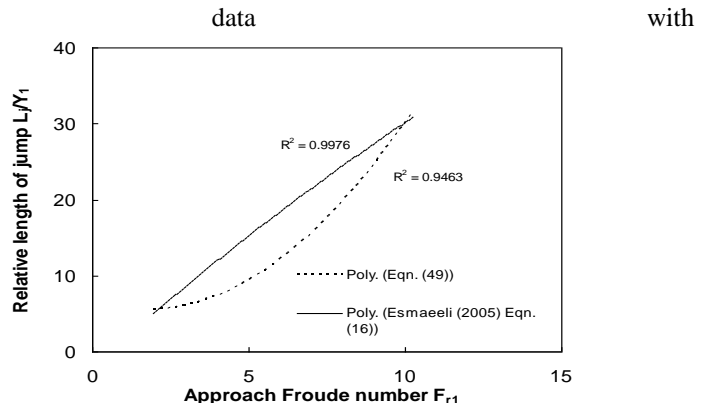
Figure 10. Testing of Eq. (14) with
Figure 11. Comparison of experimental
Esmaeeli (2005) [Eq. (4)].and Eq. (14) & Eq. (4)
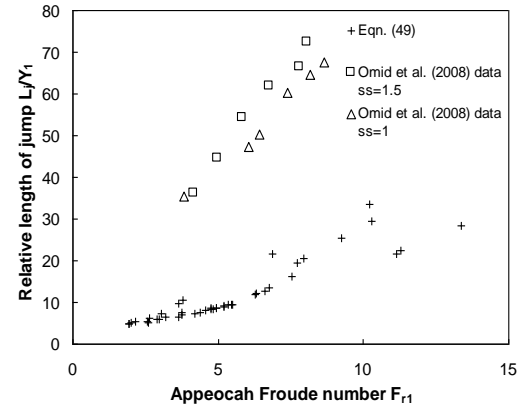
data

Figure 12. Comparison of experimental data with Omid et al (2008) data.

6.3 Relative Length of Jump (L_j/Y_1)

Figure 10 shows non-linear variation of relative length of jump (L_j/Y_1) against approach Froude number (F_{r1}). Linear model of Eq. (11) were fit for the experimental data and Esmaeeli (2005) data with R^2 values of 0.95 and 0.99 respectively, showing large deviation at low approach Froude number and becomes closer at $F_{r1} = 9$. R^2 value of 0.99 shows Esmaeeli (2005) data are much better fitted in present model. Figure 11 shows the comparison of L_j/Y_1 between experimental and predicted values using Eq. (11) and Eq. (4) indicates good agreement between the two at lower Froude number and scattering at higher Froude number; this may be attributed to the effect of different side slope is more significant at higher Froude number as Esmaeeli (2005) considered different side slope. Figure 12 shows comparison of experimental L_j/Y_1 experimental values of Omid et al (2008) with the predicted value using Eq. (11). Result of Eq. (11) and Omid et al (2008) data obtained with side slope 1.5 and 1.0 showing large deviation between the two values. It is therefore concluded that presented model vary in comparison to the existing models and experimental results, which may prove insignificant for the prediction of L_j/Y_1.

7. CONCLUSION

In trapezoidal channel almost all empirical models for Y_2/Y_1, E_2/E_1 and L_j/Y_1 have been compared and observed well with the results of Mathur (1965) Jamil (2008), Esmaeeli (2005) and Omid et al (2008), indicates the accuracy of the developed models in present study. Model presented for trapezoidal channel with appurtenances also shows good R^2 values and hence observed significant in describing the jump characteristics as well as in dissipating energy as compared to the trapezoidal channel without appurtenances. Hence, it can be concluded that these models are suitable for varying dimensions and positions of baffle blocks.

NOTATIONS

b	= bottom width of trapezoidal channel (m)
E_1	= energy per unit weight at section 1 (before the jump) (m)
E_2	= energy per unit weight at section 2 (after the jump) (m)
F_{r1}	= approach Froude number (-)
h_b	= height of baffle (m)
L_{bb}	= length of baffle at base (m)
L_{bt}	= length of baffle at top (m)
L_j	= length of jump (m)
n	= number of baffle blocks (-)
n_1	= zY_1/b
R_{e1}	= Reynold's number (-)
s	= spacing between baffle and channel (m)
ss	= side slope of trapezoidal channel
W_b	= width of baffle (m)
x_{bi}	= position of baffle from inlet gate (m)
z	= side slope
Y_2/Y_1	= sequent depth ratio
E_2/E_1	= efficiency of jump
E_L/Y_1	= relative energy loss
L_j/Y_1	= relative length of jump
ρ	= density of water (Kg/m^3)
μ	= dynamic viscosity of water (Ns/m^2)
ε	= surface roughness (m)
θ	= side slope angle

REFERENCES

i.   Afzal. N., Bushra. A. (2002). "Structure of Turbulent Hydraulic Jump in a Trapezoidal Channel", J. Hydraulic Research, 40 (2), 205 – 214.

ii.   Diksin, M. H. (1961). "Hydraulic Jump in Trapezoidal Channels", J. Water Power, 13, 12 – 17.

iii. Esmaeeli, V. M. (2005). "Modeling Hydraulic Jumps with Artificial Neural Networks", J. Water Management, 158 (WM2), 65 – 70.

iv.   Hager, W. H. (1985). "Hydraulic Jump in Non-Prismatic Rectangular Channels", J. Recherches Hydrauliques, 23 (1), 21 – 34.

v.   Hager, W. H., and Damei, L. (1992). "Sill-Controlled Energy Dissipater", J. Hydraulic Research, 30 (2), 165 – 181.

vi.   Iwao, O., Youichi, Y., and Hiroshi, G. (2001). "Hydraulic condition for undular-jump formation", Journal of Hydraulic Research, 39 (2), 203 - 209.

vii. Jamil, M. & Khan, S. A. (2008). "Theoretical Study of Hydraulic Jump in Trapezoidal Channel Section", J. Institution of Engineers (India), 89, 28 – 32.

viii. Mathur, A. K. (1965). "Hydraulic Jump in Open Prismatic Channel", M.Tech Thesis, Department of Civil Engineering, University of Roorkee, Roorkee, India.

ix.   Noor, A and Bushra, A., (2002). "Structure of The Turbulent Hydraulic Jump In A Trapezoidal Channel", J. of Hydraulic Research, 40 (2), 205 – 214.

x.   Omid, M. H. (1996). "Hydraulic Jump in a Trapezoidal Channel", Iranian Journal of Agricultural Science, 28 (3), 113 – 121.

xi.   Omid, M. H. Esmaeeli M., and Narayanan R. (2008). "Gradually Expanding Hydraulic Jump in a Trapezoidal Channel", J. Hydraulic Research, 45 (4), 512 – 518.

xii.   Ohtsu, I. (1976). "Free Hydraulic Jump and Submerged Hydraulic Jump in Trapezoidal and Rectangular Channels", Trans. JSCE, 8, 122 - 125.

xiii.   Press, M. J. (1961). "The Hydraulic Jump", Engineering Honors Thesis, University of Western Australia, Nodlands, Australia.

xiv.   Rajaratnam, N., and Subramanya, K. (1968). "Profile of Hydraulic Jump", Proc. ASCE, J. Hydraulics Division, 94 (HY3), 663 – 673.

xv.   Ranga Raju, K. G., Mittal, M. K., Verma, M. S., and Ganeshan, V. R. (1980). "Analysis of Flow over Baffle Blocks and End Sills', J. Hydraulics Research, 18 (3), 227 – 241.

xvi.   Stahl, H., and Hager, W. H. (1999). "Hydraulic Jump in Circular Pipes", Canadian J. Civil Engineering, 26, 368 – 373.

xvii.   Wanoschek, R., and Hager, W. H. (1989). "Hydraulic Jump in Trapezoidal Channel", J. Hydraulic Research, 27 (3), 429 – 446.

xviii.   Wu, S. and Rajaratnam, N. (1996). "Transition From Hydraulic Jump To Open Channel Flow", J. Hydraulic Engineering, 122 (9), 526 – 528.

Study Of Bed Load Transport

Sumit Gandhi[1], Dushyant Pal[2], Manvender Singh[3], Harshit Jain[4]

Assistant Professor, Department of Civil Engineering
[2,3,4]B.Tech Graduates, Department of Civil Engineering
Jaypee University of Engineering & Technology, Guna (M.P.), 473226, India
Email: sumit.gandhi@juet.ac.in, dushyantpal7@gmail.com, msmohit91@gmail.com, gini0207@gmail.com

ABSTRACT*: Present study deals with the bed load transport and shear stress with uniform and non-uniform sediments in open channel under different experimental conditions. Effort has been made to analyse extensive experimental results in comparison with the existing theories given by the various eminent researchers for both the types of sediment materials. Extensive experimental work is presented in terms of data analysis and comparison. Empirical relations are proposed using Buckingham-π theorem in terms of dimensionless shear stress and bed load transport parameter and are compared and vaidated with Meunier (2006) and Roorkee's approach [i.e. Gilbert (1914), Pazis & Graf, Paintal (1977), Misri et. al (1984), Ranga Raju & R. J. Garde (1986)] for both uniform and non uniform sediment material.*
Keywords: Bed load, Shear stress, Uniform & Non-uniform sediments, Empirical modeling.

1. INTRODUCTION

When the average shear stress on the bed of a channel exceeds the critical stress for the bed materials then bed load transportation take place. Sediment moves in three different modes; as contact load in which sediments move by rolling or sliding along the bed but they do not leave contact with the bed; as saltation load in which sediments move by hopping and bouncing along the bed and; as suspended load in which the material moving in the suspension in a fluid, being kept in suspension by the turbulent fluctuations. Study of the bed load movement for a hydraulic engineer is important because they come across various type of the problems (land erosion, silting of reservoir, degradation, aggradations, silt excluders, silt extractors etc.) related to alluvial rivers and channels. The bed load movement mainly depends upon the velocity of flow, size of the sediments, type of the bed material (uniform and non-uniform), τ'_* and $\emptyset_b$. The problems associated with the sediments are varied and complex.

Present study deals with the study of bed load transport and the effort has been made to verify analytical and empirical relations. The experimental results are compared with the Meunier (2006) and Roorkee's method (1986) for different bed materials (uniform and non uniform). Relations have been developed for bed load transport between dimensionless shear stress and bed load transport parameter for both uniform and non uniform bed material.

2. THEORY

Du Boys (1879) was the first to propose a bed load empirical relation and subsequently it is used by many investigators. He assumed that the bed material moves in a series of layers parallel to the bed, the velocity of each layer varying linearly from a maximum for the top layer on the bed surface to zero from the lowest layer at some depth.

$$\emptyset_b = A \, (\tau_o - \tau_{oc}) \, \tau_o$$

(1)

were $A = \gamma_s \Delta h \Delta V / 2\tau_{oc}^2$, Δh the thickness of each layer, ΔV is the velocity of second layer from the bottom.

Meyer-Peter and Muller (1948) proposed a relation for $\emptyset = 8(\tau'_* - 0.047)^{3/2}$. According to Meyer-Peter and Muller, sediment transport is zero when $\tau'_* = 0.047$. Thus the quantity $(\tau'_* - 0.047)$ may be interpreted as the effective excess shear stress causing bed load transport.

Meunier et. al (2006) has given emphasis on mean velocity of flow for bed load movement and proposed the graphical result for the bed load per unit width. Use of a logarithmic pattern fails to explain velocity profile and to estimate the shear velocity of flow. Shield (1936) also proposed the equation for bed load transport, which was based on a range of sediment size from 1.56 mm to 2.47 mm only and unable to explain the phenomenon for higher sediment sizes.

Ashida and Michue (1972) proposed

$$q_B = 17(\tau_O - \tau_{Oc})\left(\sqrt{\tau_O} - \sqrt{\tau_{Oc}}\right) \text{ for } \qquad \tau_O = 0.05$$
(2)

Engelund and Fredsoe (1976) proposed
$$q_B = 18.74(\tau_O - \tau_{Oc})\left(\sqrt{\tau_O} - 0.7\sqrt{\tau_{Oc}}\right) \text{ for } \quad \tau_O = 0.05$$
(3)

Fernandez and Van (1976) proposed
$$q_B = 5.7(\tau_O - \tau_{Oc})^{3/2} \text{ for } \qquad \tau_O = 0.037 - 0.0455$$
(4)

Parker (1979) proposed new relation for dimensionless critical shear stress $\tau_* = 0.03$ as
$$q_B = 11.2(\tau_O)^{1.5}\left[1 - {\tau_{Oc}}/{\tau_O}\right]^{4.5}$$
(5)

Misri et al.(1984) and Samaga et al.(1986) at the University of Roorkee develops a relationship between $\emptyset_b$ and τ_*' for sediment size ranging from 0.49 mm to 4.94 mm as:

$$\emptyset_b = 4.6 \text{X} 10^7 {\tau_*'}^8 \qquad \text{for } \tau_*' \leq 0.065$$
(6)

$$\text{and } \emptyset_b = \frac{8.5\tau_*'^{1.8}}{\left(1 + 5.95 \text{X} 10^{-6} \tau_*'^{-4.6}\right)^{1.43}} \quad \text{for } \tau_*' \geq 0.065$$

$$\text{Also, } \emptyset_b = \frac{q_b}{\gamma_s}\sqrt{\frac{\rho}{\theta}}$$
(7)

Einstein (1942) was the first to attempt a semi theoretical solution, he assumed that there is no existence of critical shear stress and sediment particles moves only if lift force becomes greater than submerged weight (for non-uniform bed material only) of particle. Also, probability of re-deposition of sediment particles on the stream bed is possible and the step length is entirely dependent on the sediment size. He proposed following equation:

$$\emptyset_b = \frac{i_B q_B}{i_b \gamma_s}\sqrt{\frac{\rho}{\theta}}$$
(8)

Same equation used by Roorkee's approach [i.e. Gilbert (1914), Pazis & Graf, Paintal (1977), Misri et. al (1984), Ranga Raju & R. J. Garde (1986)] for non-uniform sediments but the steps involved for the calculation of $\emptyset_b$ were different from that of Einstein (1942) approach. Misri et. al (1984) have collected extensive data on partial bed load transport in a laboratory flume using sediment mixtures with size ranging from 0.07 mm to 40 mm.

Patricia et. al (1989) computes the sequences of trajectories of individual saltating sediments as well as concentration of moving sediments that the flow can support. Bed load transport (particle velocity, bed load sediment concentration, and the height of the bed load layer) can be determined from their model. They proposed a curve as in Fig. 1 between $\emptyset_b$ and τ_*' for uniform sediments which gave relatively accurate results as compared to other results.
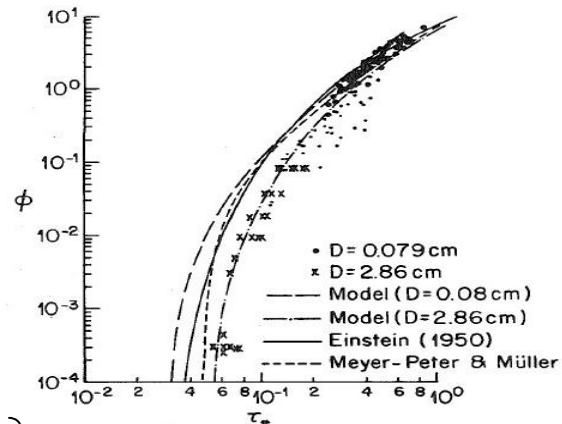
Figure 1. Variation of $\emptyset_b$ and τ_*.

3. EXPERIMENTAL SET-UP AND METHODOLOGY

Experimental studies are carried out on an experimental system involving a rectangular channel of dimension 5m × 0.2m × 0.25m. The setup consists of a constant head tank from where the water reaches to the inlet tank through feeding pipe provided with regulating valve. Sharp edge regulating gate at the inlet is provided to prevent side wave reflection and surface undulation so that a stabilized flow is available at the inlet of main channel. Also, controlling gate at the end of channel is provided to maintain certain volume of water and sediment concentration in the main channel. Parallel rails were mounted at the top of side walls for sliding of pointer gauge in order to measure depth at different positions along the length and across the width of the main channel. The experimental set-up and instrument were shown in Fig. 2.

Figure 2 (a). Showing the Experimental Setup
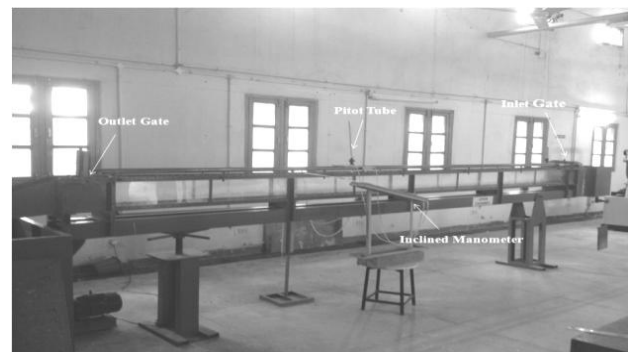
Figure 2 (b). Channel with Bed Material

Numbers of runs for the different values of the velocity ranging from 0.2 m/s to 0.8 m/s for different bed materials (uniform and non-uniform) were conducted and velocity of flow, depth of flow and bed laod moved were measured. The bed load coming from the channel is collected in the sediment baskets located at the downstream part of the channel and weighed after its proper drying. Bed material used in the channel is composed of uniform and non-uniform graded material respectively for different cases. The arithmetic mean sizes 'd' of sediments used are 2.36 mm and 10 mm (for uniform sediments) and 0.87 mm to 12.5 mm (for non-uniform sediments).

Observations were collected for the variaion of bed load per unit width (kg/m/sec) for different mean velocity of flow for uniform and non-uniform sediments. Bed load transport parameter '$\emptyset_b$' and dimensionless shear stress 'τ'_*' were then calculated from the above measurement. Results are used; to compare with Meunier (2006) and Roorkee's approach (1986) [i.e. Gilbert (1914), Pazis & Graf, Paintal (1977), Misri et. al (1984), Ranga Raju & R. J. Garde (1986)]; and to carryout empirical modeling for obtained data.

4. DIMENSINOAL ANALYSIS AND EMPIRICAL MODELING

Based on the theory of bed load transport and applying the concept of contact load (sediment moves by rolling or sliding along the bed but don't leave the bed) saltation load (sediment moves by hopping and bouncing) and suspended load (material moves in suspension being kept in suspension by the turbulent fluctuations), the important variables affecting bed load are q_b, γ_s, γ_f, d, D, V, N, R, S, μ, g, and F_e. Using Buckingham π-Method and treating d, v and γ_f as reapting variables; following π terms were developed.

$$f\left(\frac{q_b}{du}, \frac{\gamma_s}{\gamma_f}, \frac{R}{d}, \frac{gd}{u^2}, \frac{u\mu}{\gamma_f D^2}, \frac{D}{d}, S, N\right) = 0$$

(9)

Under dimensional form, the equation for dimensionless shear stress in terms of bed load transport parameter for uniform and non-uniform sediment material is transformed to:

$\tau^{*'} = 0.1860\ \emptyset_b^{\ 0.2071}$ ($R^2 = 0.9209$)   (For uniform bed material)   (10)

$\tau^{*'} = 0.2577\ \emptyset_b^{\ 0.2132}$ ($R^2 = 0.9894$)
$\tau^{*'} = 0.1027\ \emptyset_b^{\ 0.1934}$ ($R^2 = 0.9104$)   (For non-uniform bed material)   (11)
$\tau^{*'} = 0.1407\ \emptyset_b^{\ 0.239}$ ($R^2 = 0.9724$)
$\tau^{*'} = 0.1202\ \emptyset_b^{\ 0.1797}$ ($R^2 = 0.697$)
(12)

5. ANALYSIS OF DATA

5.1 Uniform Sediment

Fig. 3 shows the Bed load transport rate per unit width as a function of the average velocity 'U' for the uniform sediments of the size d = 2.36 mm. Results are compared with Roorkee approach (1986) and Mayer-Peter (1948) results. It is clear from the plot that experimental data meet with the other theoretical approach, also in all the three cases R^2 value is nearly equal to 1 show regression line meets the data well.

Fig. 4 shows approximately a similar pattern of bed load transport rate of uniform bed material (d = 10 mm) as compared to Roorkee approach (1986). Gap between both the plots is attributed to the varying experimental conditions. Roorkee approach is based on experimental conditions in which they varied most of the parameters like velocity, slope of the channel etc. whereas in present study constant bed slope is considered and surface was rigid and boundaries were smooth. Using Roorkee's equations for bed load transport rate, the value coming out to be very low on the other hand it is quit higher for the present case at particular mean velocity. It is clear from the figure that about 75% of data points are lying within ± 10% limit of the best fitted curve and about 25% of the data points are seen deviated may be because of inaccurate measurements.
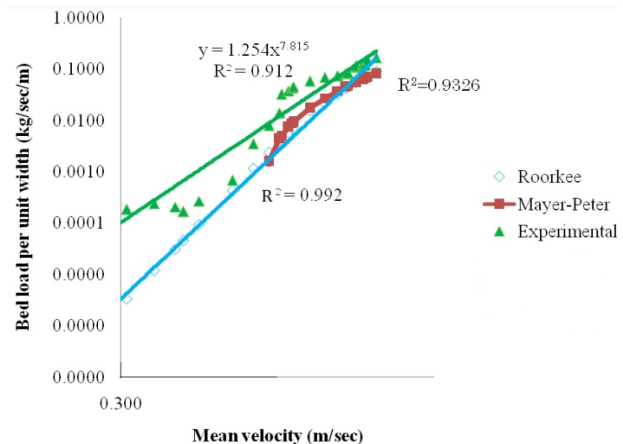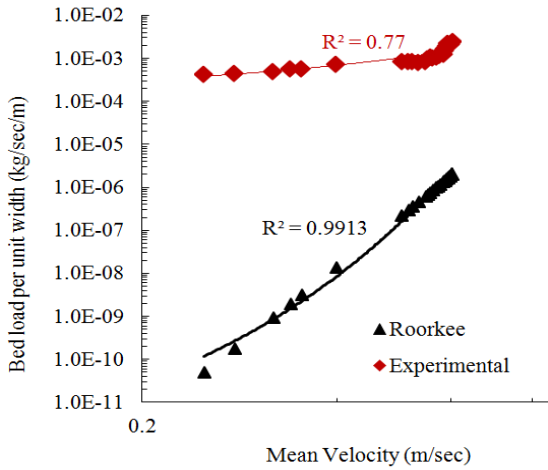
Figure 3. Bed load transport rate Vs
Figure 4. Bed load transport rate Vs
mean velocity (d = 2.36mm) mean velocity (d = 10mm)

5.2 Non-Uniform Sediment

Fig. 5 – Fig. 7 shows a variation of bed load transport rate against the mean velocity, R^2 values of the power fit shows good correlation between bed load transport rate and the mean velocity. Roorkee approach is based on various experimental results in which they varied velocity, slope of the channel, different bed material, channel setup of 16 m X 0.75 m X 0.48 m. In present study constant bed slope and with only one material composition is taken uder consideration where bed surface was rigid and boundaries were smooth. Using Roorkee equations for bed load transport rate, the rate was found to be very low on the other hand in present case it is high at same mean velocity.

Fig. 5 shows a plot of experimental bed load movement per unit width with respect to the mean velocity with R^2 values 0.935. For the measured velocity and the arithmetic mean size of non-uniform bed material, bed load movement per unit width were calculated for Roorkee and Meunier approach and compared with experimental data. As it can be seen from the graph the result follows the same pattern with good R^2 values 0.980 and 0.960 respectively for both the authors. Variation can be attributed to sediments sizes; it is 0.87 mm – 12.5 mm for present case and 0.07 mm – 40 mm for authors' case.

Fig. 6 shows the same variation as above for bed load movement per unit width against mean velocity with R^2 values 0.939. Others authors' plots are also obtained by same procedure as explained above and the variation are explained again on the basis of same reason for different experimental and boundary conditions. This plot is drawn as a result of Run 2 to verify above mentioned behavior and verification of other authors results.

Fig. 7 shows a plot of bed load movement per unit width for present experimental data and with respect to the mean velocity and compared to Roorkee (1986) and Meunier (2006) result for size ranges between 0.07 mm – 20 mm which is different from run 1 and run 2 above. For this run R^2 values 0.975 against 0.972 and 0.961 for other authors. It can be seen from the graph the result follows the same pattern in all the three different studies. Reason for the variation in the result is same explained above.
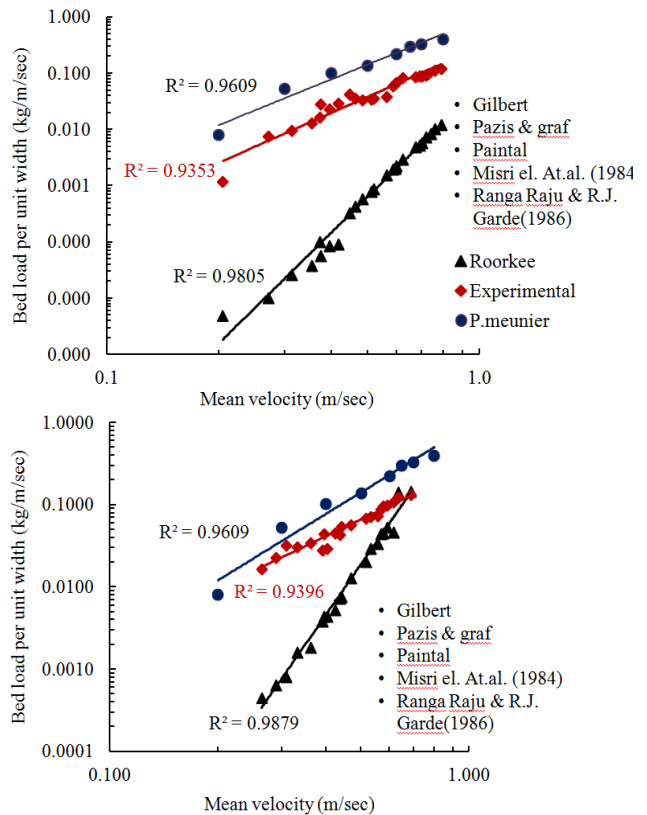
Figure 5. Bed load transport rate Vs mean
Figure 6. Bed load transport rate Vs mean   velocity for
non-uniform bed material (Run 1).   velocity for non-uniform bed material (Run 2).
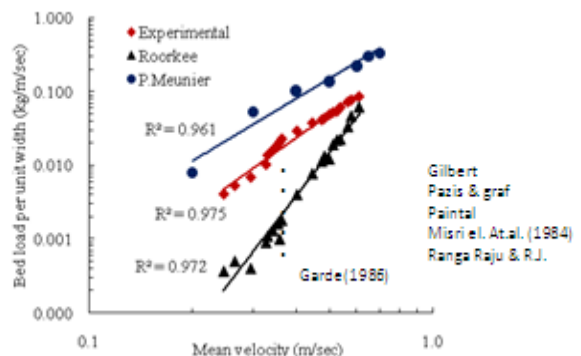
Figure 7. Bed load transport rate Vs mean velocity for non-uniform bed material (Run 3)
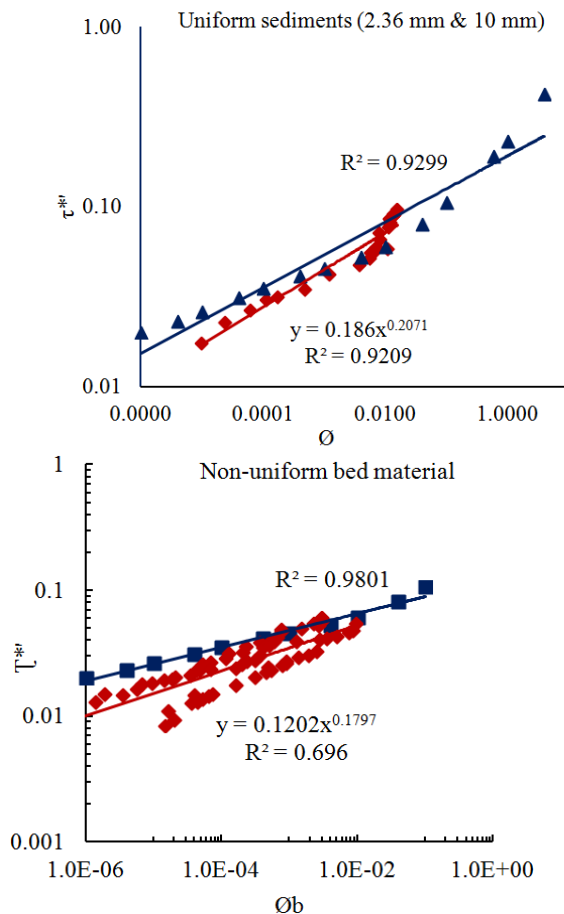
Figure 8. $\tau^{*\prime}$ and $\varnothing_b$ for uniform

Figure 9. $\tau^{*\prime}$ and $\varnothing_b$ for non-uniform bed mate bed material (Combined)

6. RESULTS AND DISCUSSION

6.1 Uniform Sediment (2.36 mm and 10 mm)

Fig. 8 shows the combined variation of dimensionless shear stress with the bed load transport parameter for uniform sediment size of 2.36 mm and 10 mm for experimental data and Roorkee's data. It is clear that similar pattern is seen in both the cases. The value of $R^2 = 0.920$ [eqn. (10)] shows good relation between $\varnothing_b$ and $\tau^{*\prime}$. It is also proved from $R^2 = 0.929$ for Roorkee's approach (1984, 86) that the same amount of deviation is seen from the respective fitted line.

6.2 Non-Uniform Sediments (0.87 mm – 12.5 mm)

Fig. 9 shows combined plot of dimensionless shear stress with the bed load transport parameter for non-uniform sediment

sizes for all the three runs mentioned above. Experimental results were compared with Meunier (2006) and Roorkee's approach (1984, 86) and discussed well about the deviations and its suitability for field applicability. The variations among different plots attributed to the varying experimental conditions like velocity, boundary conditions, bed slope, sediments sizes, etc.

For run 1 variation of dimensionless shear stress with the bed load transport parameter is observed with $R^2 = 0.989$ (eqn. 11) nearly equal to one indicates, the empirical relation [$\tau^{*\prime}= 0.2577\ \varnothing_b{}^{0.2132}$] developed defines well the phenomenon and suitable for particular range of sediment size. Run 2 also shows similar variation with $R^2 = 0.910$ (eqn. 11) for correlating the two parameters of the present experimental phenomenon. Variation can be attributed to different sediment size; in present case size varies between 0.87 mm – 12.5 mm were as in case of Roorkee's approach it varies between 0.07 mm – 40 mm. In run 3 small gap is obtained between experimental and Roorkee's methods due to the different sediment material composition and varying boundary conditions. The value of $R^2 = 0.972$ (eqn. 11) nearly equal to one shows regression line meets the data well and the relation proposed $\tau^{*\prime} = 0.1407\ \varnothing_b{}^{0.239}$ (eqn. 11) holds good for particular range of experimental condition.

Fig. 9 shows combined representation of data and empirical relation [$\tau^{*\prime} = 0.1202\ \varnothing_b{}^{0.1797}$] (eqn. 12) for non-uniform size sediments with $R^2 = 0.696$. It shows the deviation of data points from the regression line and with the Roorkee's approach, due to the small range of sediment size for present case (i.e. 0.87 mm - 12.5 mm) and large range of sediment size for Roorkke's approach (0.07 mm – 40 mm). On the other hand present study have been made with constant bed slope (bed surface was made rigid); boundaries were smooth with single and mixed sediment compositions.

7. CONCLUSION

Variation for bed load transport rate per unit width as a function of the average velocity 'U' for the uniform sediments size d = 2.36 mm shows experimental data meet the theoretical approach made by Mayer-Peter and Roorkee approach. In all cases R^2 value is close to one, shows regression line meets the data well. Similar plot for uniform bed material (d = 10 mm) compared to Roorkee approach shows gap between the plots, due to the varying experimental conditions. It is clear that about 75% of data points are lying within ± 10% limit of the best fitted curve.

Results obtained for variation between dimensionless shear stress with the bed load transport parameters for uniform and non-uniform (run1, run2 and run3) sediments show good agreement with Roorkee approach with R^2 value close to 1. As a concluding remark empirical model has been proposed, these

holds good for present experimental conditions and satisfying with the other authors result.

NOMENCLATURE

A	=	Cross-section area
D	=	Sieve diameter
d	=	Sediment diameter
i_b	=	Fraction of bed sedimet of a given range
i_B	=	Fraction of bed load of a given range
N	=	Rugosity/Manning-Strickler coefficient
Q	=	Discharge
q_b	=	Fraction of bed sediment discharge of a given range
q_B	=	Fraction of bed load discharge of a given range
R^2	=	Coefficient of determination
S	=	Bed slope
γ_s	=	Unit weight of solid
γ_f	=	Unit weight of fluid
ρ_s	=	Mass density of sediment
ρ_f	=	Mass density of fluid
$\emptyset_b$	=	Bed load transport parameter
τ'_*	=	Dimensionless shear stress
µ	=	Dynamic viscosity of water
T_o	=	Shear stress
T_{oc}	=	Critical shear stress

REFERENCES

i.   Ashida K, Michiue M (1972). 'Study On Hydraulic Resistance And Bedload Transport Rate In Alluvial Streams', Transactions, Japan Soc. Civil Eng., 206: 59-69.

ii.   Du Boys (1879). 'Le Rohene et les rivieres a lit affouillable Annales des Ponts et Chaussees', Seerie 5, Vol. 18, 141-195.

iii.   Einstein, H. A. (1942). 'Formulas for The Transportation Of Bed-Load', Trans., ASCE. 107, 561-597.

iv.   Einstein, H. A. (1950). 'The Bed Load Function for Sediment Transportation In Open Channel Flows', Tech. Bulletin No. 1026, U.S.D.A., Soil Conserv. Service, 1-71.

v.   Engelund F, Fredsoe J (1976). 'A Sediment Transport Model For Straight Alluvial Channels'. Nordic Hydrol., 7: 293-306. Fernandez LR, van Beek R (1976). 'Erosion and Transport Of Bedload Sediment', J. Hydraulic Res., 14(2): 127-144.

vi.   Gilbert, G. K. (1914). 'The transportation of de´bris by running water, U.S., Geological Survey', Prof. 86-263.

vii.   Graf. W (1971). 'Hydraulics of Sediment Transport', McGraw-Hill Series In: Water Resource and Environmental Engineering.

viii. Meyer-Peter, E. and R. Muller (1948). 'Formula for Bed Load Transport', Proc. IAHR, 2nd congress Stockholm.

ix.   Misri R. L., R. J. Garde and K. G. Ranga Raju (1984). 'Bed Load Transport of Coarse Non Uniform Sediment', JHD, Proc. ASCE, 110 (3), 312-328.

x.   Meunier P, F Metivier, E Lejeunesse (2006), 'Flow pattern and sediment transport in a braided river': The ''torrent de St Pierre''.

xi.   Patricia L. Wiberg1 and J. Dungan Smith2 (1989). 'Model for Calculating Bed Load Transport of Sediment', Journal of Hydraulic Engineering, 115, 1, 101-123.

xii.   Parker G (1979). 'Hydraulic Geometry of Active Gravel Rivers', J. Hydraulic Eng., 105(9):1185-1201.

xiii. Pazis G. C. and W. H. Graf (1977). 'Weak sediment transport', J. Hydraulic Divison, ASCE, 103, 799–802.

xiv.   R. J. Garde, K.G. Ranga Raju (2000). 'Mechanics of Sediment Transportation and Alluvial Stream Problems', New Delhi: New Age International, P. 262. ISBN 978-81-224-1270-3.

xv.   Samaga B. R., K. G. Ranga Raju and R. J. Garde (1986). 'Bed Load Transport of Sediment Mixture', JHE Proc. ASCE, 112 (11), 1003-1017.

Computation Of Regime Depth In Alluvial And Gravelly Rivers – A Comparison

Rajendra Chalisgaonkar [1], Manish S. Sant [2] and Pratibha S. Sant [2]

[1]Superintending Engineer, Irrigation Department, Dehradun-248001, Uttarakhand.

[2]Assistant Engineer, Irrigation Department, Roorkee-247667, Uttarakhand.

E-mail: chalisgaonkar@yahoo.com

ABSTRACT: *Estimation of scour is necessary for economic and safe design of hydraulic structures. An accurate estimation of regime/scour depth below stream-bed during design is important since this determines the foundation levels of all elements of hydraulic structures such as pier, abutment, guide bund, spur, groynes, etc. Lacey's method of estimating regime depth of flow in loose bed alluvial rivers, recommended for design by the Indian Road Congress and Indian Railways has been used in alluvial and non alluvial rivers. Recently, questions have been raised about its application to rivers in gravelly or bouldery strata, as the bed slopes in the hilly regions are very steep which create tremendous velocities and bed materials being unable to stand such velocities are scoured and transported down the river. These carry very heavy charge of coarse sand, shingle and boulders. Silt factor plays vital role in this as the foundation level depends upon soil strata underneath. Small changes in foundation play a crucial role in the design of hydraulic structures and thus affect the cost and completion of the structures. The scour depth computations in hilly or sub-hilly terrains is yet to be incorporated in the prevailing methods as yet the Indian Standards have not been published on the same and field engineers and other design consultants keep computing the scour depth using the formulae, which have been developed for alluvial rivers. In this paper, the Authors have tried to compute the scour depth for different discharges using the Lacey's regime formulae and the formulae suggested for gravelly terrains up to 500cumec and above 500cumec and the results have been presented in the paper. The authors have recommended that some large scale model studies be conducted to establish the scour predicted by the formulae suggested for computing scour depth in hilly and sub-hilly terrains.*

1.0 INTRODUCTION

Rivers flow downhill with their power derived from gravity. A river flowing through deposits can be characterised as alluvial and non-alluvial rivers. An alluvial river carries alluvial soils such as silt along with water while non-alluvial river carries non alluvial soil such as loam, clay, hard soil, boulders, etc. These non-alluvial rivers also known as bouldery rivers in hilly terrains. Estimation of scour in hydraulic structure is extremely important as it helps in deciding their foundation level. Estimation of scour is necessary for economic and safe design of hydraulic structures, as under estimation of scour may result in failure of the structure, whereas over-estimation will lead to more excavation, larger size and increase in cost of structure besides it will require more time to construct the structure.

Lacey's method of estimating regime depth of flow in loose bed alluvial rivers was developed by Lacey(1929) and Inglis(1944) and is mainly based on observations made in canals in India and Pakistan. This method is commonly used in India for estimation of scour depth in alluvial rivers, and is recommended for design by the Indian Road Congress and Indian Railways. However the same formulae are being used in estimating the regime depth in non-alluvial rivers including hilly terrains, as no sufficient literature is available on the subject. Lacey's method has several limitations as it ignores many important parameters, namely, geometric, hydrologic, hydraulic, flow, sediment transport, properties of foundation materials etc. The bed slopes in the hilly regions are very steep which create tremendous velocities and bed materials being unable to stand such velocities are scoured and transported down the river. These carry very heavy charge of coarse sand, shingle and boulders. Due to high flood in June 2014, the State of Uttarakhand has witnessed large scale destructions in the State and many cities/towns have been washed out/severely damaged resulting in loss of life and property. In order to construct the flood protection/anti-erosion works along the various rivers, the authors tried to collect the information on estimating the regime depth in bouldery strata so that the flood protection/anti erosion structures can be constructed to safeguard the life and property of the people. It has come to the notice that yet the Indian Standards have not been published on the estimation of scour depth computations in hilly or sub-hilly terrains and field engineers and other design consultants keep computing the scour depth using the formulae, which have been developed for alluvial rivers. However Researchers Hey(1986), Sen(1997), Mazumder(2004) and others has conducted some studies on the non-alluvial rivers and have provided some formulae for computing scour depth in hilly and sub hilly terrains. Authors have tried to compute the scour depth for different discharges using the Laceys regime formulae and the formulae suggested for gravelly terrains up to 500 cumec and

above 500 cumec and the results have been presented in the paper.

2.0 ESTIMATION OF SCOUR DEPTH

2.1 Alluvial rivers

2.1.1 Lacey–Inglis method

During the early 20th century Lacey(1929) analysed data from stable irrigation channels flowing through loose sandy material in the Indo-Gangetic plain. These channels used to carry relatively less bed load since in the upstream reach of the channel a sediment excluder or ejector was provided. The analysis of field data gave the following two relations for depth (or hydraulic radius) R and perimeter (or width) P of the channel:

$$R = 0.47(Q/f)^{1/3}$$

(1)

$$P = 4.75\sqrt{Q}$$

(2)

Here R is the normal scour depth in m below the design flood level, Q the design flood discharge in cumec and f the Lacey's silt factor related to the median size of bed material d_{50} by the equation:

$$f = 1.76\sqrt{d}_{50}$$

(3)

Where d_{50} is median size of bed material in mm.

Inglis(1944) collected data from seventeen bridges on alluvial rivers in India and found that maximum scour depth below the highest flood level (HFL), D_{se}, when expressed in terms of computed depth of flow in the river R using Eq.1 gave

$$D_{se} = K.R$$

(4)

where K varied from 1·76 to 2·59 with a mean value of 2·09. Hence, according to Inglis

$$D_{se} = 2·0 \quad R$$

(5)

According to the Indian Road Congress(IRC 1998 & 2000) for natural channels flowing in alluvium the mean depth of scour below flood level can be calculated using the Lacey's formula

$$R = 1.34\left(\frac{q^2}{f}\right)^{1/3}$$

(6)

Where R is the mean scour depth in m below the design flood level, q the design flood discharge intensity in cumec/m allowing for concentration of flow, f the Lacey's silt factor.

Initially Lacey's equations (1) and (2) were meant for constant discharge flowing through channels in loose non-cohesive material having the bed material size in the range 0.13 to 0.43

mm. Later, an analysis of data from some rivers in India flowing through Indo-Gangetic plain, it was stated that these equations also apply to meandering rivers at the bankful stage. The bankful discharge was defined by Inglis(1947) as 2/3 to 3/4 of the flood discharge, and it was basically the maximum discharge that the main river channel, excluding flood plain, carried. The bankful discharge has a return period of about 1.6 to 2 years. In the context of scouring around bridges and hydraulic structures, the designer applies these equations for a flood discharge of 50 to 100 year return period which is much greater than the bankful discharge.

2.2 Non alluvial (Gravelly or Bouldery) Rivers

Due to non – availability of literature in non-alluvial or boulder rivers, the Lacey's formulae which were developed for alluvial rivers flowing through loose sandy material in the Indo-Gangetic plain are still being adopted for calculating the regime depth in non-alluvial or Boulder Rivers. However, the following formulae, for average diameter of bed material upto 400 mm, have been developed by the researchers to estimate the scour depth in gravelly or boulder terrains, but they have not been adopted yet, universally to estimate the scour depth:

2.2.1 For Discharge up to 500cumec

On the basis of studies conducted, R. D. Hey(1986) gave the following formula to predict the scour depth:

$$R = 0.22Q^{0.37}d_{50}^{-0.11}$$

(7)

Where R is regime depth below the HFL in m, d_{50} is median size of bed material in mm and Q is a total discharge in the river in cumec.

2.2.2 For Discharge more than 500cumec

For designing hydraulic structures such as barrages, bridges etc. across large gravelly and bouldery rivers, the expected depth of scour during flood is required to be predicted. Although some studies have been carried out in European rivers, the formulae so derived vary considerably. Moreover, those studies were mostly carried out in relatively small rivers. Indian rivers of large magnitude, flowing over gravelly and boulder beds in the Himalayan and sub-Himalayan regions, need more accurate studies and analysis. The data collected by Central Water Commission (CWC) on gauge and discharge observation stations all over India was analysed and P. Sen(1997) developed a following simple formula for scour, or regime depth in large gravelly and bouldery rivers, when the discharge in the river is more than 500cumec:

$$R = 0.2q^{0.855}d_{50}^{-0.3}$$

(8)

Where R regime depth below the HFL in m, d_{50} is median size of bed material in mm and q is the intensity of discharge in the river in cumec/m.

3.0 VARIATION OF REGIME DEPTH WITH SIZE OF BED MATERIAL IN BOULDERY TERRAINS

3.1 Discharge in the river less than 500cumec

The effect of sediment on scour depth that is transported by river is studied with average diameter of bed material. To observe the effect of average diameter of bed material on scour depth in boulder regions, graphs between scour depth and average diameter of bed material plotted for 50cumec to 500cumec discharges have been depicted in Fig.1. The formula suggested by R.D. Hey has been used to predict the scour depth in boulder terrains, when the discharge varies from 50cumec to 500cumec.

The perusal of Fig. 1 clearly indicates that in the initial phase, when the median size of bed material increases from 4.75mm to 40mm, there is a large reduction in the value of scour depth and as the median size of bed material increases further from 40mm, the normal scour depth does not have much variation for all discharges.
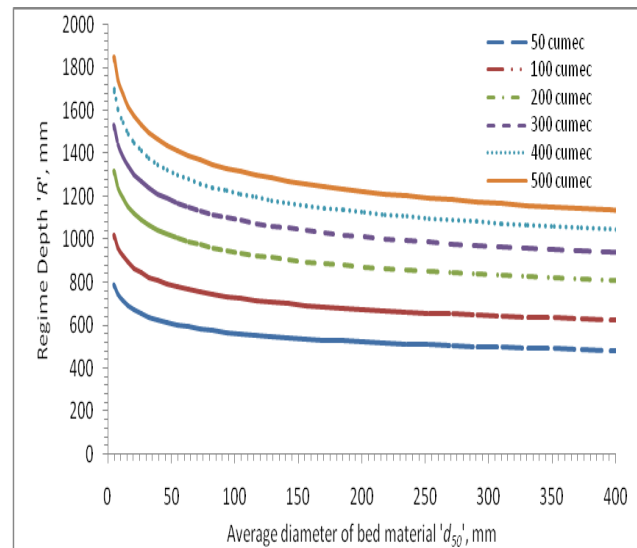
Figure 1. Variation of scour depth with average diameter of bed material for different discharges using formulae suggested by R D Hey

3.2 Discharge in the river above 500cumec

The study the effect of average diameter of bed material on scour depth in the boulder regions, when the rivers carry a discharge of 500cumec or more, the formula suggested by P. Sen(1997) has been used to predict the scour depth in boulder terrains for discharges more than 500 cumec. Since the formula suggested by P. Sen uses the intensity of discharge 'q', water way of 80m for all the discharges i.e. for 500cumec to 5000cumec, has been adopted to compute the scour depth in the boulder regions. The graphs between scour depth and average

diameter of bed material plotted for 500cumec to 5000cumec discharges have been depicted in Fig. 2.
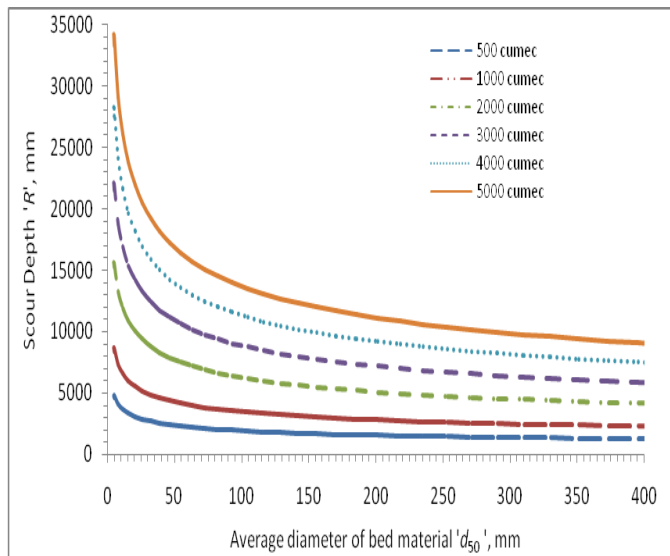
Figure 2. Variation of scour depth with average diameter of bed material for different discharges using R D Hey equation of scour depth

The perusal of Fig. 2 also indicates that in the initial phase, when the median size of bed material increases from 4.75mm to 160mm, there is a large reduction in the value of scour depth estimated by the formula suggested by P. Sen and as the median size of bed material increases further from 160mm, the normal scour depth does not have much variation for all discharges.

4.0   VARIATION OF REGIME DEPTH WITH SILT FACTOR – A COMPARISON

4.1 Discharge in the river less than 500cumec

Generally the effect of sediment on scour depth that is transported by river is studied with help of silt factor given by Lacey's. To compare the results, Lacey's and R. D. Hey formulae were used to compute the regime depth for different values of silt factor and different discharges ranging from 50cumec to 500cumec. The results obtained have been depicted below in Fig.3.
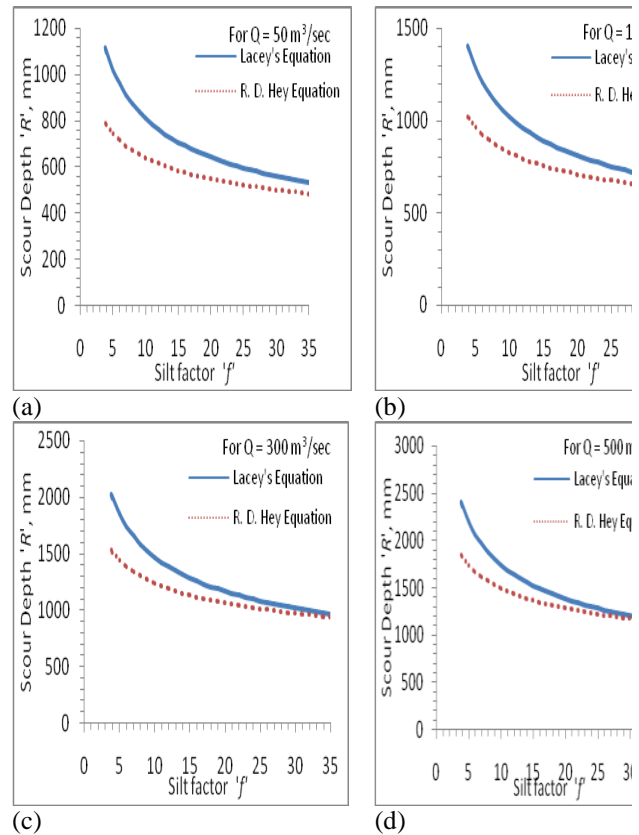
Figure 3. Variation of scour depth with silt factor (upto 500cumec discharge)

The perusal of Fig. 3 clearly indicates that the scour depth predicted by Lacey's formulae is more than the one obtained from the formula given by R. D. Hey. However, it has also been observed that in the initial phase, when the silt factor increases from 1 to 10, there is a large reduction in the value of scour depth and as the silt factor increases further from 10, the normal scour depth does not have much variation for all discharges.

4.2 Discharge in the river more than 500cumec

4.2.1 Width of Waterway as 80m

To compare the results, Lacey's and P. Sen formulae were used to compute the regime depth for different values of silt factor and different discharges ranging from 500cumec to 5000cumec. Since the formula suggested by P. Sen uses the intensity of discharge 'q', water way of 80m for all the discharges i.e. for 500cumec to 5000cumec, has been adopted to compute the scour depth. In order to compare the results, Lacey's equation (Eq.6), based on intensity of discharge has been used to compute the scour depth. The results obtained have been depicted below in Fig. 4.
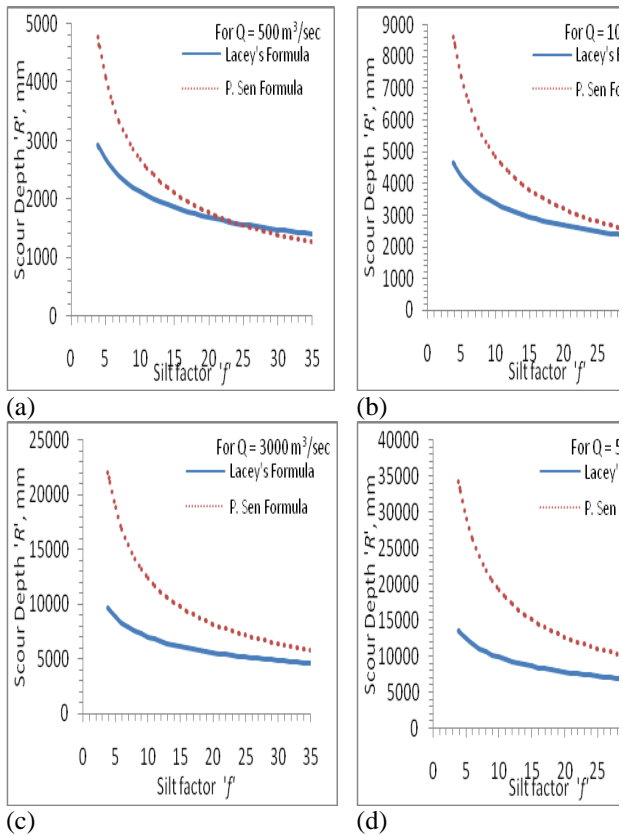
Figure 4. Variation of scour depth with silt factor (Discharge more than 500cumec and Water way as 80m)

The perusal of Fig. 4 indicates that the scour depth predicted by P. Sen formulae is more than the one obtained from the formula given by Lacey's. However, it has also been observed that for discharges up 1000cumec, when the value of silt factor is more than 25, the scour depth obtained by the methods is nearly equal. It can also be seen that in the initial phase, when the silt factor increases from 1 to 15, there is a large reduction in the value of scour depth in case of scour depth prediction by P. Sen formula; where as in case of Lacey's formula the variation is not much as compared to P. Sen formula. However, as the silt factor increases further from 15, the normal scour depth does not have much variation for all discharges.

4.2.2 Width of Waterway as 150m

Water way, assumed in estimating the scour depth was increased to 150m and the effects of silt factor on scour depth for discharges ranging from 500cumec to 5000cumec were studied and are
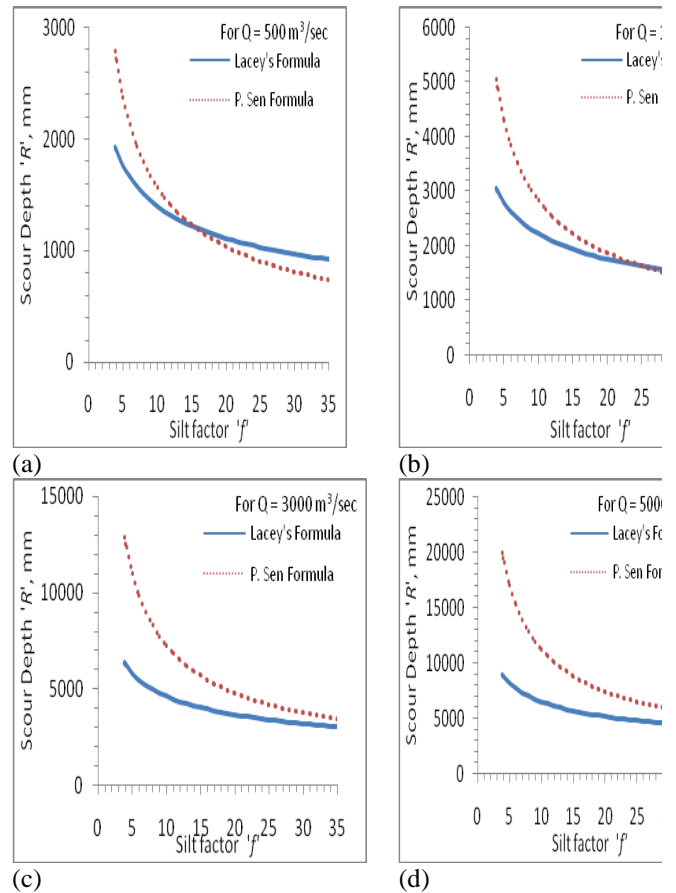
Figure 5. Variation of scour depth with silt factor (Discharge more than 500cumec and Water way as 150m)

plotted in Fig. 5. It can be observed from Fig. 5 that since the value of scour depth inversely varies with the water way, as the water way increases the scour depth reduces substantially. However the trend remains the same as has been observed in Fig. 4.

5.0   LIMITATIONS OF METHOD

5.1 Lacey's Method

Lacey's regime equations were developed in India on the basis of extensive data collected from stable canals in the Bari Doab areas in West Punjab (now in Pakistan). But they have several limitations. Scour estimated by indiscriminate use of Lacey's regime equations, irrespective of river behaviour (Mazumder, 2004), river plan and bed forms (Garde, 2000), properties of river bed materials, geometry of the bridge piers and abutments and the approach channel geometry etc. may substantially differ from actual one. Some of the limitations of Lacey's model adopted by IRC/IS/RDSO for finding scour depth in bridge piers and abutments are as:

- The Lacey–Inglis method is meant for non-cohesive sandy material with mean sediment size of about 0.15 mm to 0.43 mm.

- It cannot be used for estimating the scour depth in Gravelly and Bouldery terrains.
- It does not consider many of the important parameters, e.g. flow shallowness; geometry, length & alignment of piers and abutments; incoming sediment load and debris; size, shape and non-uniformity of sediments etc.
- Lacey's R-value is applicable for steady flow in fine incoherent alluvial soils only
- Lacey's silt factor (*f*) depends on many other parameters besides mean size of sediment *d*.
- It neglects the morphology of a river-its various plan and bed forms.
- Lacey's theory is applicable for canal flow, which is steady, continuous and for a prolonged period. It can at best be used for finding approximate general scour depth, but definitely not for localized scour depth around bridge piers and abutments governed by several other parameters.
- Sediment transport principles and scouring processes under live bed and clear water conditions are totally ignored in Lacey's method of scour estimation.

5.2 R. D. Hey's Method

- R. D. Hey's method can only be used for estimating the scour depth up to the design discharge of 500cumec.
- Silt factor used in the formula is based on Lacey's silt factor, which has its own limitations.
- The results obtained are yet to be authenticated with more studies.

5.3 P. Sen's Method

- P. Sen's method can only be used for estimating the scour depth, when the discharge in the river is more than 500cumec.
- Silt factor used in the formula is based on Lacey's silt factor, which has its own limitations.
- Values of scour depth obtained from the formula are on the higher side and the results are yet to be authenticated with more studies.

6.0   CONCLUSIONS

The paper has presented the comparison of values of scour depth in alluvial and non-alluvial rivers using Lacey's method and R. D Hey and P. Sen's formulae. It has been seen that the Lacey–Inglis method is basically empirical and essentially gives total scour below HFL in the case of meandering rivers in flood plain in sandy material. It is based on data from only seventeen bridges -a relatively small number. The Lacey–Inglis method is meant for non-cohesive sandy material with mean sediment size of about 0·15 mm to 0·43 mm and having the geometric standard deviation of the bed material about 1·4 to 1·8. However, the method is being used extensively by field engineers for estimating the scour depth in alluvial and non-alluvial rivers. The formulae suggested by R. D. Hey and P.

Sen for estimating the scour depth in non-alluvial (Gravelly) rivers does not give results in uniformity. Until and unless mores studies are conducted on the behaviour of rivers in Gravelly and Bouldery terrains and they are validated, the results obtained from the formulae suggested by R. D hey and P. Sen be used with caution, because when R. D. Hey's formula is used it gives lower values in comparison to Lacey's method up to 500cumec discharge and the values obtained from P. Sen's formula are very high in comparison to the values obtained from Lacey's method for the same values.

7.0   REFERENCES

i. Garde, R.J. and RangaRaju, K.G.(2000) "Mechanics of Sediment Transport and Alluvial Stream Problems" 3rd Edition, New Age Int. Pub. Pvt. Ltd., New Delhi.

ii. Hey, R. D., and Thorne, C. R.(1986) "Stable channels with mobile gravel beds." J. Hydraulic. Div., 112(8), 671–689.

iii. Inglis, C.C.(1944) "Maximum depth of scour at heads of guide banks, groynes, pier noses and downstream of bridges", Annual Report (Technical), CWPRS, Pune.

iv. Inglis, C.C.(1947) "Meanders and their bearing on river training." Proc., Institution of Civil Engineers, Maritime and Waterways Paper No. 7.

v. Lacey, G.(1929) "Stable channels in alluviums". Journal Institution of Engineers, Paper No. 4736, 229.

vi. Mazumder, S.K.(1971) "Discussion on Scour around bridge piers" by Govind Rao, Journal of the Institution of Engineers (India), Vol. 51(5).

vii. Mazumder, S.K.(2004) "Scour in Bouldery Bed – Proposed Formula", Written discussion on Paper No. 508 by R. K. Dhiman, Journal of Indian Road Congress, Vol 65(3).

viii. Mazumder, S.K.(2007) "Limitations of Lacey's Theory for Estimation of Bridge Scour", Proc. of Hydraulics & Water Resources HYDRO2007, Indian Society for Hydraulics and VSNIT, Surat,.21-22 Dec.

ix. Mazumder, S.K. and Yashpal Kumar(2005) "Estimation of Scour in Bridge Piers on Alluvial Non- Cohesive Soil by different methods", IRC Highway Research Bulletin. Oct., 2006.

x. Sen, P.(1997) "Depth of scour in gravelly and bouldery rivers", Journal of the Institution of Engineers (India) Civil Engineering Division, vol. 77, pp. 209-214.

xi. -----------------(1989) "Guidelines for hydraulic design of barrages and weirs", Part 1-Alluvial reaches IS:6966, Bureau of Indian Standards, Water Resources Department, New Delhi.

Characteristics Of Scour Holes Developed Around The Bridge Piers Placed In Staggered Arrangement

Dr. Mubeen Beg[1]

[1]*Associate Professor, Department of Civil Engineering, Z. H. College of Engineering and Technology, AMU, Aligarh,202003, U.P. India, E-mail:* raisbeg2013@gmail.com

ABSTRACT : Owing to rapid urbanization and increased traffic volume, it is often needed to construct new bridges across the rivers in the proximity of the already existing bridge where the scour process will be quite different from one which occurs around a single pier. The work reported herein is concerned with a carefully controlled extensive experimental study of local scour around a group of bridge piers placed in staggered arrangement in uniform sediment at varied pier spacing under steady uniform flow clear water scour conditions at flow intensity equal to 0.95. As the scour hole characteristics are important in determining the extent of countermeasures needed to prevent/control scour at piers, the objective of present study is to investigate the effect of mutual interference of bridge piers placed in staggered arrangement on the characteristics of scour holes developed around the piers. The data on various characteristics of scour holes are collected, processed and analyzed. Present study reveals that the piers placed in staggered arrangement at close proximity have considerable mutual interference effect on scour hole characteristics which may lead to bridge failure, if pier group effect is ignored and bridge piers are designed merely as an isolated pier. The maximum effect of mutual interference occurs at relative pier spacing $X_C/b = 10$ and minimum effect at relative pier spacing $X_C/b \geq 40$.

***Keywords*:** *Local scour, bridge pier, pier spacing, scour hole, experimental*

1. INTRODUCTION

Scour is the process of lowering of river-bed around an obstruction due to removal of the bed material by erosive action of flowing water. In case of local scour the lowering of the riverbed occurs in the vicinity of the structure. In spite of significant amount of research on single pier scour, failure of many bridges has rekindled interest in furthering understanding of the pier group scour.

1.1 Local scour at group of bridge piers

In case of scour around group of piers, the presence of piers can generate a complex interaction in the hydrodynamic characteristics of the flow field near the piers themselves and therefore, lead to the occurrence and development of a scour process that is quite different from one which occurs around a single pier.

Local scour around a single bridge pier is affected by a large number of inter-dependant variables. The flow, sediment, pier characteristics and time are the main variables affecting this phenomenon. As a consequence of extensive research by several investigators on the phenomenon of local scour around a single bridge pier, a large number of design relationships have been bequeathed to the bridge designer. Notwithstanding this, many bridges still suffer damage by local scour. This is due to more intense complexities due to the mutual interaction of piers group. It indicates that in addition to the variables affecting local scour around a single pier, spacing of piers and pattern of piers' placement in the riverbed also affect the scour depth and scour hole characteristics around group of piers. One of the patterns of piers placement may have staggeed arrangement (Figure 1). Timonoff (1929), Garde. (1961), Basak *et. al.* (1975), Hannah (1978), Elliot, K.R. And Baker, C.J. (1985), El-Taher, R.M. (1984, 85), Shah (1988), Kothyari, U.C., (1989), Breusers and Raudkivi (1991), Garde, *et. al.* (1995), Vittal *et. al.* (1994), Babaeyan-Koopaei and Valentine (1999) and Mubeen Beg (2008) have made some studies on scour around group of piers.

Hannah (1978) carried out detailed investigation on local scour at groups of cylindrical piles with steady and uniform flow and clear-water condition. The mechanisms involved in the scouring process at piers group placed in tandem arrangement were identical as reinforcing, sheltering, vortex shedding.

(i) Reinforcing

It causes increased scour depths at the front pier. Bed material is continuously lifted from the base of the hole by the flow, which is not, however, capable of removing this material from the scour hole. When the downstream pier is so placed that the scour holes overlap, the bed level is lowered at the rear of the upstream scour hole. It is, thus, easier for the flow to remove material from this hole and it deepens. As the pier separation increases, the reinforcing effect decreases gradually and disappears when the maximum bed level between the piers returns to the undisturbed bed level.

(ii) Sheltering

The presence of an upstream pier can cause a reduction in effective approach velocity for downstream pier. This reduction weakens the effect of horseshoe vortex and thereby reduces scour at the downstream pier. A second form of sheltering occurs if the material scoured from the upstream pier is deposited on the bed in front of the downstream pier. Flow is then deflected up from the bed near the downstream pier, which reduces the horseshoe vortex strength. As pier separation increases, the velocity deficit in the wake of the upstream pier disappears and the sheltering effect decreases. All the studies of scour around pier groups substantiate the existence of sheltering mechanism for small angles of attack.

(iii) Vortex shedding

Vortices shed from an upstream pier are convected downstream. When a second pier is so placed close to one of the vortex shedding paths, the vortices assist in lifting the material from the scour hole. The scouring potential of the shed vortex is a function of its convection speed and of the distance between the path and the affected pier. This effect, therefore, decreases more rapidly for piers in line with the flow than for those at angles of attack which place downstream piers on the paths traced by vortices shed by upstream pier.

(iv) Horseshoe vortex compression

When piles are placed transverse to the flow, each will have, except at very close spacing, its own horseshoe vortex. As pile spacing is decreased, the inner arms of the horseshoe vortices will be compressed. This causes velocities within the arms to increase with a consequent increase in scour depths. This compression also exists for piles in staggered arrangement.

2. EXPERIMENTAL PROGRAMME

Experiments were conducted in the Department of Civil Engineering, Z.H. College of Engineering and Technology, AMU, Aligarh, U.P., India. 33 mm galvanized steel circular cylindrical piers were used in present study. As shown in figure 1, two of the three pier models were set on upstream across the flume at right angles to the flow direction at a fixed centre to centre lateral spacing between the piers Z_c/b, where Z_c is the center to center lateral spacing between the upstream piers and b is the diameter of the pier model. The third pier model was located on downstream along the bisector of the upstream pier models at varied clear longitudinal pier spacing X_c/b = 5, 10, 15, 20, 25, 30, 35, 40, 50, 60, 70, 80 and 90, where x is the center to center distance between the upstream and downstream pier models along the length of the flume and b is the diameter of the pier model. The lateral centre to centre pier spacing Z_c/b was set at 9 because at this lateral pier spacing, the scour holes at piers are found to be free from the effect of lateral mutual interference and only the interference of the downstream pier remains to affect the scour depth at upstream piers.
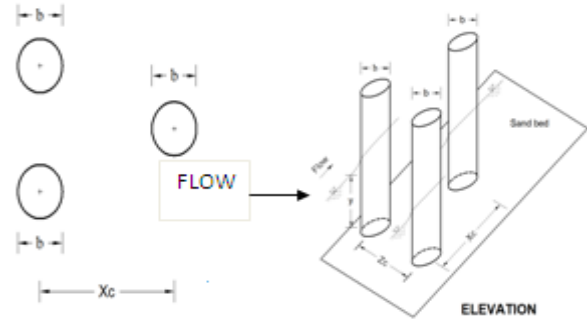
Figure- 1. Piers of same size in placed in staggered arrangement

Tables 1 and 2 give the flow, sediment and pier parameters used in experiments.

Table 1. Properties of sediment and piers used in present study.

$D_{84.1}$ (Mm)	D_{1} 5.9 (M m)	D_{5} 0 (M M m)	Geo.-standard dev.σ_G (mm)	Specific Gravity S_s	Pier size used Circular Piers	Angle Of Repose ϕ	U/U_C
1.03	0.73	0.95	1.187	2.65	33mm	32°	0.95

Table 2. Computed mean flow parameters.

Discharge (m³/s)	Depth Of Flow y (mm) $_0$	Mean Velocity U (m/s)	Threshold Velocity U (m/s)	Froude No. F $_{fr}$	Critical Froude No. F_{rc}	Average energy slope S_0
0.04141	140.0	0.391	0.4127	0.3328	0.35028	0.001

Since in present study clear-water experiments were conducted using coarse sediment of 0.95 mm median diameter, duration of 10 hours was considered adequate

To form a basis for analyzing results on group of piers placed in staggered arrangement, a series of experiments on 33 mm diameter single pier was also performed.

Each experiment commenced from a condition of still water at the predetermined flow depth over a leveled bed surface. The time of start of initial movement of sediment, and of water surface establishment were recorded. On the completion of the experimental run, the water supply to the flume was gradually stopped and the water from the flume was drained off carefully so that the scour holes and the scour patterns around the piers developed by the flow were not disturbed.

3. DATA COLLECTION

Detailed experimental data during the experimental runs and after experimental runs were collected The dynamic scour depths at the nose of piers were measured and recorded during the entire experimental runs at suitable interval of time. However, as each experimental run was over, scoured area around the piers was surveyed with point gauge and detailed static scour measurements were made and recorded. The length of scour holes at front and rear faces of upstream and downstream piers, width of scour holes at front faces of upstream and downstream piers, the areal extent of scour around the piers and the length of sediment deposition on rear face of upstream and downstream piers were measured and recorded. Photographs of scour holes and areal extent of scour were taken as shown in figure 2.

Figure- 2. Scour and deposition patterns around piers placed in staggered arrangement at varied pier spacing
(A) X_c/b=50   (B) X_c/b=60

4. RESULTS AND DISCUSSION

The data on various characteristics of scour holes collected during and after the experimental runs are then processed and analyzed as under.

4.1Scour hole dimensions

Since the knowledge of scour hole dimensions is vital in determining the extent of countermeasures needed to prevent/control scour at piers, various parameters explained as under using present experimental data are determined

4.1.1 Length of scour holes

The variation of length of scour holes at the front and rear face of upstream and downstream piers against pier spacing 'X_c/b' is shown in figure 3. As evident from figure 3, the length of scour hole at front face of upstream piers increases upto $X_c/b \leq 10$ due to reinforcing effect of downstream pier but, this effect diminishes thereafter, and as a result, scour hole length remains constant upto X_c/b=90.

As shown in figure 3, the length of scour hole at front face of downstream pier increases as X_c/b increases and reaches to a maximum value at X_c/b=10. The occurrence of maxima in the length of scour hole at this pier spacing can be attributed to the maximum enhancement in the strength of horseshoe vortex caused by the flow approaching towards downstream pier at 45° (*i.e.*, 22.5°+22.5°) angle of attack. At X_c/b>10 the length of scour hole at the front face of downstream pier decreases and reaches to a minimum value at ' X_c/b=60'. The reason for this decrease is the shielding effect of wakes developed at the downstream end of upstream piers and also to the diminishing effect of the angle of attack being less than 30º (*i.e.*, total angle produced at pier spacings Z_c/b=9 and X_c/b=60).

Figure- 3. Variation of length of scour hole at front faces of upstream and downstream piers placed in staggered arrangement with pier spacing 'X_c /b'.

At 60< X_c /b≤90, the length of scour hole at the upstream face of downstream pier remains constant which indicates the diminishing state of the shielding effect of upstream piers wakes and the disappearance of effect of angle of attack because of it being less than 7.5º.

4.1.2 Width of scour holes

The scour hole widths at the upstream face of piers relative to the scour hole width at an isolated pier are plotted against pier spacing 'X_c/b' as shown in figure.4. This variation shows that the scour hole width at upstream piers 'w_1/b' (where 'w_1' is the horizontal distance normal to the flow direction along the noses of the upstream piers and measured between the outer edges of upstream piers scour holes) remains constant over the entire range of pier spacing except at 'X_c/b' upto 10 which indicates that the reinforcing effect of downstream pier beyond pier spacing, X_c/b=10, does not significantly affect the relative width of scour holes.
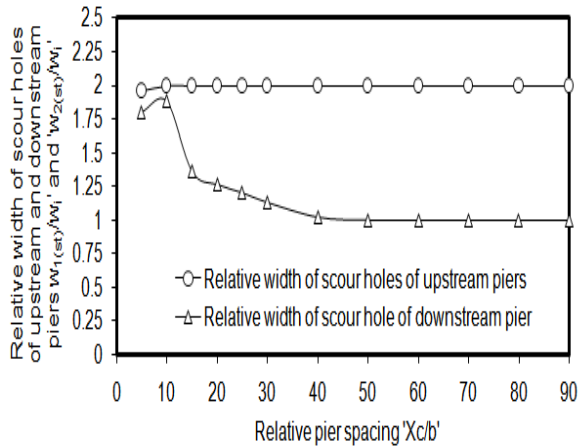
Figure- 4. Variation of relative width of scour hole of upstream and downstream piers placed in staggered arrangement $w_{1(st)}/w_i$ and $w_{2(st)}/w_i$ with pier spacing 'X_c /b' (where $w_{1(st)}$= width of upstream piers scour hole, $w_{2(st)}$ = width of downstream pier scour hole and w_i= width of an isolated pier scour hole).

However, the scour hole width of downstream pier relative to the upstream piers '$w_{2(st)}/w_{1(st)}$' (where, '$w_{2(st)}$' and '$w_{1(st)}$' are the horizontal distances measured normal to the direction of flow and through the noses of the downstream and upstream piers respectively and between the outer edges of scour holes of upstream and downstream piers) at front face of downstream pier, increases as the pier spacing increases and approaches to a maximum at pier spacing $X_c/b=10$. This increase in scour hole width indicates the dominance of the effect of angle of attack of flow approaching from upstream piers towards the downstream pier. As the pier spacing 'X_c/b' exceeds 10, there occurs a steep reduction in the scour hole width at front face of downstream pier and this trend continues upto pier spacing $X_c/b=15$. This decrease in the width of scour hole 'w_2/b' is due to a sudden decrease in the magnitude of angle of attack. At $15<X_c/b\leq50$, the downstream scour hole width '$w_{2(st)}/b$' further decreases due to further reduction in the magnitude of angle of attack at these pier spacings. Beyond $X_c/b=50$, the effective angle of attack of flow falls below 7.5° at which it has no effect on the scour hole width '$w_{2(st)}/b$'. As a result the downstream pier becomes free from all the effects and its scour hole width 'w_2/b' remains constant at $50<X_c/b<90$.

The downstream scour hole widths with respect to upstream scour hole widths '$w_{2(st)}/w_{1(st)}$' are plotted against pier spacing 'X_c/b' and are shown in figure 5. The value of '$w_{2(st)}/w_{1(st)}$' increases as pier spacing increases and reaches to a maximum at pier spacing $X_c/b=10$. This maxima at $X_c/b=10$, occurs due to approachment of flow from upstream piers to the downstream pier at 45° angle of attack which has maximum impact on local scour (Hannah, 1978).

At $10<X_c/b<15$, there is a steep reduction in the values of '$w_{2(st)}/w_{1(st)}$' which can be explained mainly due to two reasons. First reason is the shielding effect of wakes

of upstream piers and the second reason is the steep reduction in the angle of attack of flow approaching to the downstream pier. At $15<X_c/b<40$, there is a gradual decrease in the values of 'w_2/w_1'. This gradual decrease can be attributed to a decrease in the effect of angle of attack at increasing 'X_c/b'.
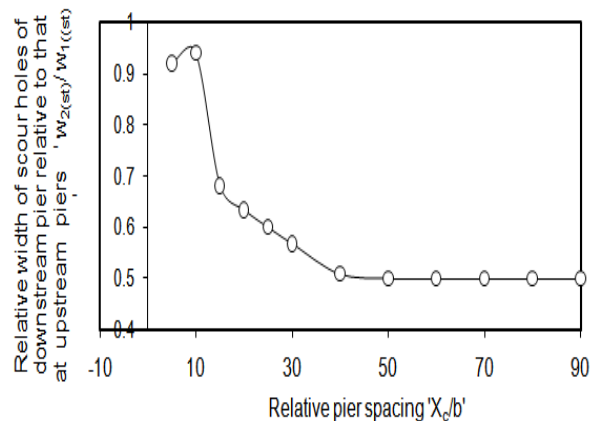
Figure- 5. Variation of width of scour hole of downstream pier relative to the scour hole width of upstream piers placed in staggered arrangement '$w_{2(st)}/w_{1(st)}$' with pier spacing x_c/b (where $w_{1(st)}$ and $w_{2(st)}$ are width of scour hole of upstream and downstream piers respectively).

At $40<X_c/b<90$, the value of 'w_2/w_1' remain constant which indicates the disappearance of shielding effect of upstream piers and effect of angle of attack on downstream pier at these pier spacings.

4.1.3 Variation scour extent with pier spacing

Using the scour data collected in this study, areal extents of scour around the three staggered piers are plotted as shown in figures 6 and 7. Overlapping of areal extents around upstream and downstream piers at pier spacing '$X_c/b=40$' as shown in figure 6. indicates the existence of the effect of mutual interference of piers. It can, however, be seen in figure 7. that the areal extents of scour become independent of each other at pier spacing $X_c/b\geq60$ which implies that the three piers have become free from the effect of mutual interference.
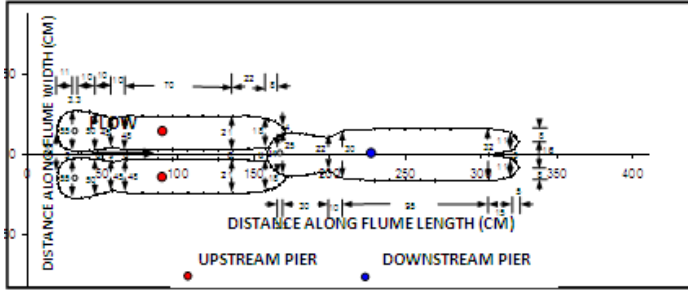
Figure 6. Areal extent of scour around upstream and downstream piers placed in staggered arrangement at $X_c/b=50$
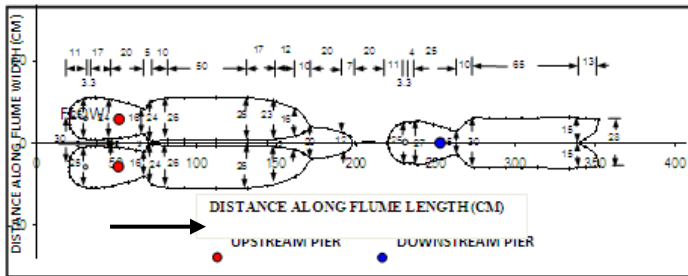
Figure 7. Areal extent of scour around upstream and downstream piers placed in staggered arrangement at $X_c/b=60$

4.1.4 Variation of sediment deposition at rear face of upstream and downstream piers

Figure 8 shows the variation in the length of sediment deposition at the rear faces of upstream and downstream piers with pier spacing X_c/b. A decreasing trend in the average values of length of deposition at the downstream side of piers can be noticed in figure 8. The reason for this decreasing trend can be explained by the fact that as the pier spacing X_c/b increases, the flow pattern at the downstream end of upstream and downstream piers changes due to the altering interaction of flow with piers and the sediment bed.
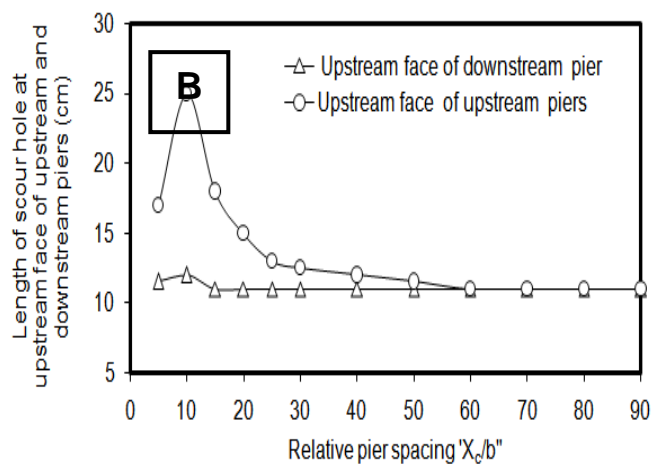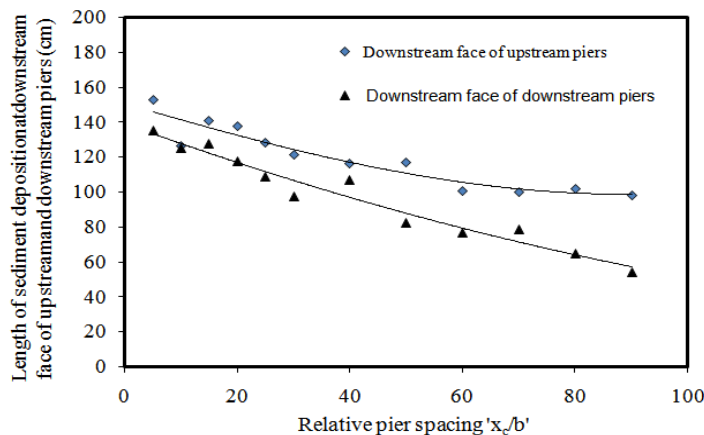

Figure 8. variation of length of sediment deposition at rear faces of upstream and downstream piers placed in staggered arrangement with pier spacing x_c/b.

5. CONCLUSIONS

The length of scour holes at front faces of upstream and downstream piers is maximum at $X_c/b=10$ and at $X_c/b>10$ it decreases and reaches to a minimum value at ' X_c/b'=60. Beyond X_c/b'=60, the length of scour hole at the upstream face of downstream pier remains constant which indicates disappearance of effect of mutual interference of upstream and downstream piers.

The width of scour holes at the front faces of upstream piers remain constant over the entire range of pier spacing except 'upto X_c/b'=10 which indicates that the reinforcing effect of downstream pier beyond pier spacing, $X_c/b=10$, does not significantly affect the relative width of scour holes.

The scour hole width at front face of downstream pier, is maximum at $X_c/b=10$. At $10< X_c/b≤ 15$ a steep reduction in the scour hole width at front face of downstream pier occurs. However, at $15<X_c/b≤60$, the downstream scour hole width decreases gradually. Beyond $X_c/b =60$, the downstream pier becomes free from mutual interference effects.

Upto pier spacing '$X_c/b=50$' areal extents of scour around upstream and downstream piers overlap each other which indicates the existence of the effect of mutual interference of piers. Beyond $X_c/b=50$ the areal extents of scour start becoming independent of each other which implies that upstream and downstream piers have become free from the effect of mutual interference.

Based on the results achieved in this study, it can be concluded that the downstream pier should be placed at $X_c/b =60$ since, at this pier spacing, the mutual interference effect of upstream piers and downstream pier on local scour, is negligible.

REFERENCES

I.   Babaeyan-Koopaei, K. and Valentine, E. M. (1999). Bridge pier scour in self-formed laboratory channels, the XXVIII IAHR Congress, p. 22-27

ii.   Basak, V. Baslamish, Y. and Ergun, O. (1975). Maximum equilibrium scour depth around linear-axis square cross–section pier groups, report No. 583, State hydraulic works, Ankara, Turkey, (in Turkish).

III.   Breusers, H.N.C. and Raudkivi, A.J. (1991). Scouring, Hydraulic Structure Manual, I.A.H.R., Balkema, Rotterdam, Netherlands.

IV.   Elliot, K.R. and Baker, C.J. (1985). Effect of Pier spacing on scour around bridge piers, Journal of Hydraulics Divn., Proc. ASCE, Vol. 111, No. 7, p. 1105-1109.

V.   El-Taher, R.M. (1984). Experimental study on the interaction between a pair of circular cylinders normal to a uniform shear flow, J. Wind Eng. Ind. Aerodyn. 17, p. 117-132.

VI.   El-Taher, R.M. (1985). Flow around two parallel circular cylinders in a linear shear flow. J. Wind Engg. Ind. Aerodyn. Vol. 21, p. 251-272.

vii.   Garde, R.J. (1961). Local bed variation at bridge piers in alluvial channels, University of Roorkee research journal, Vol. 4, No. 1,

viii. Garde, R.J. and Kothyari, U.C. (1995). State of art report on scour around bridge Piers, Pune, India.

IX.   Hannah, C.R. (1978). Scour at pile groups, University of Canterbury, N.Z., Civil Engineering Research Rep. No. 78-3, 92.

x.   Kothyari, U.C. (1989). Scour around bridge piers, Ph.D. Thesis, Univ. of Roorkee, Roorkee, India.

xi.   11. Melville, B.W. And Chiew, Y.M. (1999). Time scale for local scour at bridge piers, J. Of Hydr. Engrg., Asce, 125(1), p. 59-65.

XII.   Mubeen Beg, (2008). Effect of Mutual interference of bridge piers on local scour, PhD Thesis, Department of Civil Engineering, Aligarh Muslim University, Aligarh, India.

xiii. Shah, B.P. (1988). Interference effects on scour depth around bridge piers, M.Tech. Thesis, Department of Civil Engineering, Indian Institute of Technology, Kanpur, India.

xiv.   Timonoff, V.E. (1929). Experiments on the spacing of bridge piers in the case of parallel bridges, Hydraulic laboratory practice, edited by J.R. Freeman, Am. Soc. of mech. engrs. New York.

xv.   Vittal, N., Kothyari, U.C. and Haghighat, M. (1994). Clear water scour around bridge piers Group, J. Hydr. Engrg, ASCE, 120(11), p. 1309-1318.

Assessment Of Waterways For Series Of Multiple Bridges Across A River Floodplain

Arun Kumar[1], Dr. R.G. Patil[2], V.K. Barodiya[3] and M. N. Singh[4]

[1]*River Hydraulics Division, CWPRS, Khadakwasla, Pune-411024, India*

[2]*River Hydraulics Division, CWPRS, Khadakwasla, Pune-411024, India*

[3]*River Hydraulics Division, CWPRS, Khadakwasla, Pune-411024, India*

[4]*River Engineering Group, CWPRS, Khadakwasla, Pune-411024, India*

Email: ak_cwprs@yahoo.co.in, rsrgp@rediffmail.com, barodiyavk@gmail.com, mns19542003@yahoo.co.in

ABSTRACT:*The afflux and back water effects are mainly the function of linear waterway provided for the bridges across the rivers. The determination of waterway requires adequate hydrologic/hydraulic data collections and proper investigations. Waterway is governed principally by the design peak flood discharge which can be computed by several methods. Generally, waterway is computed based on the Lacey's regime theory and actual waterway to be provided under a bridge may substantially differ from Lacey's waterway, depending on the topographic condition. For a new bridge, one can provide waterway as per the detailed hydrologic, topographic and hydraulic investigations. But for the existing bridges, to accommodate extra discharge, bridge is required to be widened. The designers then require to assess the foundation levels and widening of the existing bridges. In such case, the modification for a single bridge is rather simple. However, in case of series of multiple bridges across river floodplain, determination of waterways is complex as percentage of discharge passing in each bridge during inundation may not be assessed properly. These difficulties can be overwhelmed by the physical model studies. This paper describes the assessment of waterway for series of multiple bridges using physical model studies conducted at CWPRS.*

Key Words: Tel river, Udanti river, Waterway, scour, piers, Bhawani Patna, Khariar.

1.   INTRODUCTION

Nine major rivers (Indus, Ganga, Brahmaputra, Narmada, Tapi, Godavari, Mahanadi, Krishna and Kavery) along with their numerous tributaries make up the river system of India. Large numbers of road and railway bridges exist over these rivers and new ones are being constructed for better and faster communication and connectivity throughout the country. The rivers are either straight or meandering or braided. In some cases, they are in transitionary phase having parallel multiple channels. Theoretically, the site for river crossing is generally selected at a place where the river is straight and is flowing through a single channel. However, avoiding bends, parallel multiple channels and various other difficult river conditions may not be an easy task. The land acquisition and general road alignment problems are also faced by the engineers. The highway engineers have to find a trade-off between the difficulties and try to find an optimal solution while minimizing the overall cost of the bridge. Engineers build bridge across main channel, resort to closing smaller parallel channels and divert the flow into a main channel. This involves provision of costly river training and management structures. Due care shall be taken to understand the river behavior after the closure of the minor channels. This procedure requires thorough knowledge of river behavior and training structures. As an alternative, engineers resort to provision of small bridges/culverts on parallel channels avoiding costly and technically complicated closure/diversion structures. This method provides for a river crossing, generally for average annual flood. It is considered to be cost effective, as it involves construction of smaller individually separate low cost bridges/culverts based on local technology and materials.

This method is fraught with possibility of river outflanking due to change in morphology. In majority of cases, the later type of multiple parallel bridges are existing which get submerged during high flood flow in the river. As the funds are made available, engineers propose to build all weather bridge by raising the road top level above the high flood level. However, the old bridges lack sufficient water way and have shallow founding levels. They need to be provided with additional water way at a place along the length, where it is most effectively utilizable. After that the founding levels have to be assessed by computing the flow intensity. If in case, the present foundation is insufficient, then the bridges are to be constructed from foundation or else, existing bridge water way and road top level could only be increased.

These assessments could be best done using hydraulic models. A case study of multiple bridge extension is presented here to bring to the fore the problems faced by the engineers and solution adopted to solve the problems.

Multiple crossings (six numbers) in the form of bridges and culvert existed across river Tel immediately after the confluence of river Udanti along the Bhawanipatna - Khariar road in Odisha. River Udanti join river Tel at about a distance of 600 m before the series of crossings. River Tel is having multiple channels at the point where the crossings have been constructed. The road top level of bridge across main channel has been raised in recent past and seems to have sufficient water way also. However, three bridges/culverts on Bhawanipatna side and two bridges on Khariar side have low road top level and the water way is also insufficient. Physical model studies were carried out at CWPRS, Pune for determining the adequacy of waterway, founding level of piers, location of opening etc. which are elaborated in this paper.

2. WATERWAY COMPUTATION

The waterway is one of the important parameters to be decided while designing any bridge across a river. The value of waterway provided depends on many factors including discharge, slope of river, type of bed materials, alignment of bridge structure, etc. The underestimated value may result in high afflux and intense flow through the openings. Further, it may result in higher scour around piers and foundation failure. However, on the other hand the overestimation of waterway may result into slack flow, planform changes in the river course and very rarely lead to outflanking of bridge structure. In view of this, bridge engineers are required to estimate the waterway with due care and assess the same using physical models depending on the importance of the structure involved. The waterway is estimated based on empirical formulas derived among others by Meyer's, Talbot, Lacey's (Bruce, 2009), railway

practice (IRS, 2003). The details of these formulae are presented briefly for information.

2.1 Myers Formula

American railroad engineer E. T. C. Myers developed the first formula for waterway area. The Myers formula was first published in the Proceedings of the Engineers Club of Philadelphia in 1879 (Bruce, 2007). The Myers formula is:

$$A = C\,D \tag{1}$$

in which A = waterway area (ft2); D = drainage area (acres); and C = a coefficient with recommended values of 1.0 as a minimum for flat country, 1.6 for hilly compact ground, and 4.0 as a minimum for mountainous and rocky country.

Meyers developed his formula from observations of structures in the general vicinity of the railway line. However, the Myers formula does not appear to have been widely adopted by highway engineers (Bruce, 2007).

2.2 Talbot Formula

In 1887, Professor A. N. Talbot of the University of Illinois proposed a new formula for waterway area (Bruce, 2009):

$$A = C\,D^{3/4} \tag{2}$$

in which,
A = area of waterway (ft^2);
D = drainage area (acres) and
C = a coefficient.

The Talbot formula differed from the Myers only in the value of the exponent of the drainage area. Talbot concluded that judgment must be the main dependence, the formula being a guide to it. On a road already constructed the C may be determined for the character of surface along that line by comparing the formula with the high-water mark of a known drainage area. Experience and observation on similar water-courses is the most valuable guide.

2.3 Laceys's Method

Lacey (CBIP 204, 1989) has correlated stable widths of canals with discharge over wide range and has found a general equation:

$$P = W = 4.83\,Q^{1/2} \tag{3}$$

Where,
Q is design flood discharge in m³/s
P is Wetted perimeter in metres
W is linear waterway in metres (In case of wide rivers, P is practically equal to W, the surface width)

Rivers of braided pattern are however known to be wider than Lacey width. On the other hand, in case of incised rivers, the actual width can be shorter than Lacey width. Generally, the Lacey width formula gives better fit for alluvial rivers in flood plains. The equation is widely used for Indian rivers.

2.4 Railway Practice

According to railway bridge substructure code (CBIP 204, 1989), effective waterway for bridges on alluvial rivers should normally be equal to width given by the Lacey formula

$$P = W = 1.1811 \, C \, Q^{0.5}$$

$$(4)$$

Where
Q is design flood discharge in m³/s
P is Wetted perimeter in metres
W is linear waterway in metres (In case of large rivers, P is practically equal to W, the surface width)
Wherein, the value of C should normally have a value of 2.76. The formula then becomes same as given by Lacey, i.e.,

$$P = W = 4.83 \, Q^{1/2}$$

$$(5)$$

The value of 'C' may vary from 2.5 to 3.5 according to local conditions depending upon bed slope and bed material (IRS, 2003).

2.5   Allowance for pier thickness

In fixing the bridge waterway, obstruction caused by the piers should be adequately provided. The present railway practice is to assume an active waterway equal to the length of the span from centre to centre of adjacent piers, less twice the width of pier-foundation wells. Smaller the spans, greater will be number of piers and hence, the obstruction, requiring greater allowance in working out the waterway. Similarly, since the end spans are partially obstructed by the training works, an extra span is generally provided to make for the loss of waterway.

3   MULTIPLE BRIDGES ON RIVER TEL

A major high level bridge having linear waterway of 480 m was constructed across river Tel near Turkel on Bhawani Patna-Khariar road (SH16) in Orissa (Figure 1). There are two low level bridges and one causeway on Bhawani Patna side; and two low level bridges on Khariar side of this main bridge.

Just about 600 m upstream of these bridges, river Udanti joins the river Tel. During the floods of year 2006, the approach embankments on Bhawani Patna side got washed away and the low level bridges on either side of the main Tel bridge were over topped by the flood water. The Government of Odisha had proposed to undertake improvement of the Bhawani Patna – Khariar road on SH16 having a length of 70 km with the financial assistance from the World Bank. Hence, the authorities decided to modify the low level bridges on either side of main Tel river bridge to make the SH 16 an all-weather road. However, designers were ambiguous about the waterway and its spatial variation. In addition, as the minor bridges had old foundations and designers were unaware about its adequacy given the limited input of waterway and discharge intensity in the absence of model studies. A model study was conducted at CWPRS to resolve these issues of waterway and adequacy of foundation.
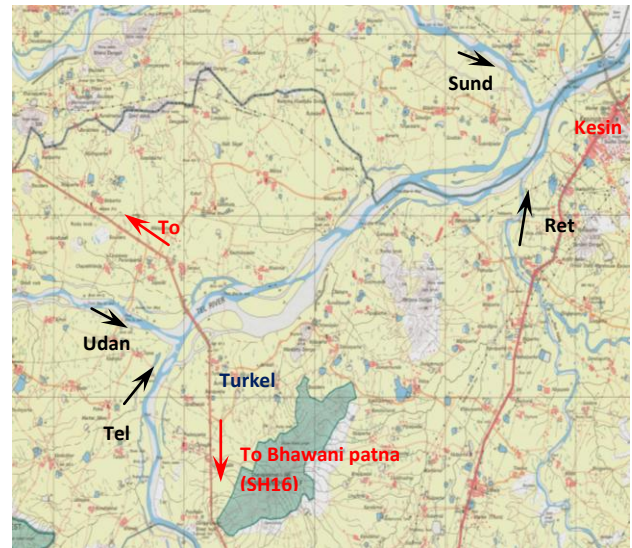
Fig.1: Index Plan

3.1 The Model

Froudian physical model to a scale of 1:200 Horizontal and 1:50 Vertical with rigid bed was constructed at CWPRS, Pune for the above study. The river reach of 5 km upstream to 3.5 km downstream of Tel river bridge and 2.5 km upstream along Udanti river from its confluence with Tel river was reproduced in model. The existing major and minor bridges including pipe culvert were also reproduced in the model. The details of bridges/culvert are given in Table 1.

Two inlet channels, one for Tel river and the other for Udanti river were also constructed. For measurement of discharges, thin plate weirs (Rehbock weir) were installed in both the inlet channels as per the codal specifications (ISO 1438, 2008). A system of gates were installed at the downstream end of the model for maintaining the tail water level at 3 km downstream of the bridge. At upstream end near the mouth of Tel and

Udanti rivers, a grid wall was constructed to avoid turbulent flow and uneven distribution of flow in to the rivers at its mouth.

Table 1: Details of Existing Bridges

	Bhawani Patna side			Main Bridge	Khariar Side	
Bridge Nos.	1	2	3	4	5	6
Location, (Km)	27/600	27/800 (Pipe Culvert)	27/850	28/400	28/900	29/400
Existing span, (m)	7 x 9.2	10 x 1.2ϕ	9 x 9.2	2 x 9.9 +1 x 24.37 +1 x 34.9 +10 x 40.85	4 x 9.2	2 x 9.2
Existing waterway, (m)	58.2	12	75.2	480.5	33.2	16.4
Existing FRL, (R.L., m)	191.217	188.322	190.504	195.985	190.978	191.217
Existing foundation level, (R.L., m)	182.634	182.634	182.634	173.671	183.13	182.307

The design discharge of Udanti river for a structure upstream of confluence was reported to be 6,400 m^3/s; similarly, it was 15,500 m^3/s for Tel river at the bridge site. In view of this, the discharge distribution of Tel and Udanti river upstream of the confluence was computed as 58.71% and 41.29 % of 15,500 m^3/s respectively. The gauge discharge data in respect of the tail water levels were not available at a point in the reach, which was reproduced in the model. However, the tail water data was available at Kesinga which is about 16 km downstream of the bridge site. The tail water variation at 3 km downstream of the bridge was derived from the available data at Kesinga gauing site by simulating the design discharge in one dimensional mathematical model (HEC-RAS). The tail water variation for Kesinga gauge site and 3 km downstream of bridge site is presented in Figure 2.

Fig. 2: Gauge –Discharge Curve at Kesinga and 3 Km Downstream of Bridge Site
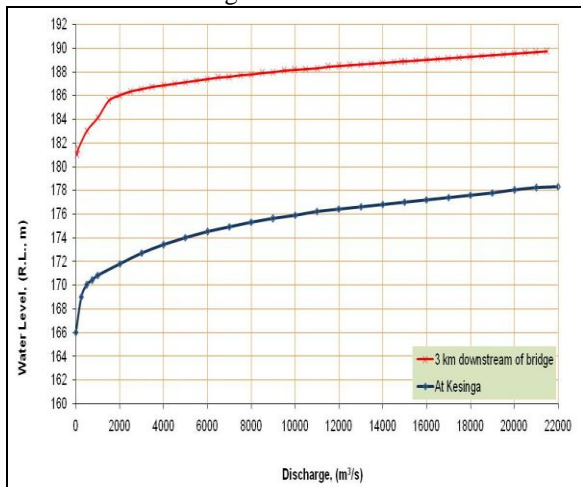
The equivalent discharges as discussed in the above para were passed through the river mouths of Tel and Udanti. Tail water level as indicated in Figure 2 was maintained at the downstream point of the model.

As reported by the project authorities, a discharge of 16,000 m^3/s in river Tel was observed in the year 2006. This discharge was considered for proving the model. The discharge of 16,000 m^3/s was distributed corresponding to 58.71% in river Tel and 41.29 % in river Udanti. Corresponding model discharges as per the model scales were passed through each limbs of the river model. The corresponding tail water level as per Figure 2 was also maintained at 3 km downstream of bridge site. After attaining steady condition, the water levels at bridge site was noted. The water level observed at prototype and on physical model at main Tel bridge is presented in Table 2.

Table 2: Comparison of Water Level Observed at Prototype and on Physical Model at Main Tel Bridge

Discharge, (m^3/s)			Water Level, (R.L., m)	
Tel river at upstream of bridge	Udanti river	Total at downstream of bridge	Prototype (observed)	Physical model
9,394	6,606	16,000	191.90	191.83

From the above table, it can be seen that the water level obtained from physical model matches fairly well with the observed value of prototype. Hence, it was assumed that the model was validated and "proved".

3.2 Experiments under existing condition

3.2.1 With the model set up as discussed in the above para, the model was run for the design discharge of 15,500 m^3/s and 11,625 m^3/s (75 % of design discharge). The corresponding tail water levels for these discharges were maintained at 3 km downstream of bridge site as per the tail water rating curve (Figure 2). The velocity, depth, angle of flow in the vicinity of bridges was observed. The percentage of discharge passing through each bridge and culvert under existing condition were computed and are given in Table 3. All the minor bridges as well as pipe culvert were seen submerged except main Tel bridge, indicating inadequacy in the height of bridges and waterways for these discharges. In addition, an orifice flow was also noticed at bridge No. 3 (on Bhawani Patna side). Photo 1 show generalized flow pattern near bridge site for discharge of 15,500 m^3/s, under existing condition**.**

Table 3: Percentage of Discharge Passing Through the Existing Bridges

Discharge, (m^3/s)	Bhawani Patna side (%)	Bridge 4	Khariar side (%)

	Bridge 1 27/600	Bridge 2 Pipe Culvert 27/800	Spill portion (Over topping)	Bridge 3 27/850	Main bridge 28/400	Bridge 5 28/900	Bridge 6 29/400
15,500	2.72	0.32	12.77	5.62	76.89	1.43	0.23
11,625	3.39	0.54	6.87	6.64	81.34	1.02	0.23
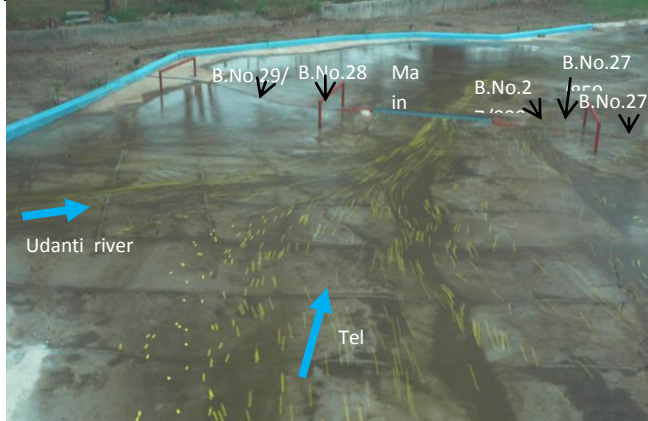
Photo 1: Generalized Flow Pattern Near Bridges at Turkel (Discharge – 15,500 M^3/S, Under Existing Condition)

3.2.2 The discharge passing in each span of the bridges /culvert was computed based on the measured average velocity at each bay. With the known clear vent area of each bridge, the discharges in each bridge/ culvert were computed. After summing up, the discharges passing through all the bridges and culvert, discharge of 1,979 m^3/s was computed as a surplus discharge out of the total discharge of 15,500 m^3/s. The surplus discharge was treated as overflow discharge over the approach bund. To accommodate this surplus discharge through the bridge vent including a free board of 1.5 m, the waterways of minor individual bridges/culvert are to be increased except for the main Tel bridge. Redistribution of surplus discharge is a complex procedure, as it involves factors such as flow pattern, slack flows, parallel flow near bridges, increased intensity in a particular bridge, etc. While redistributing the waterway, it was assumed that the flow condition/ flow intensity through individual openings would remain same. This assumption entails increasing the waterway of each bridge/culvert in the proportion of discharges passing in each opening in the existing condition. Otherwise, the discharge redistribution would have posed a difficult flow condition which could have compromised the structural safety of the bridge and approach roads. With this requirement, the waterways of individual minor bridges/culvert were increased. However, Bridge No. 27/800 (culvert) and 27/850 were very close by and were joined together. The details of modified bridges are given in Table 4.

Table 4: Details of Modified Bridges

	Bhawani Patna side			Main Bridge	Khariar Side	
Bridge Nos.	1	2	3	4	5	6
Location, (Km)	27/600	27/800 (culvert)	27/850	28/400	28/900	29/400
Span, (m)	7 x 9.2	8 x 32.2 (2 and 3 are combined)		2 x 9.9 +1 x 24.37 +1 x 34.9 +10 x 40.85	4 x 9.2	2 x 32.2

Waterway, (m)	58.2	240	480.5	33.2	60
FRL, (R.L., m)	192.989	194.939	195.985	192.989	192.989

3.3 Studies with modified bridges

The waterways for the minor bridges were increased based on the flow pattern, discharge intensity and as per the empirical formula to accommodate the surplus overspill discharge of 1,979 m^3/s which is discussed in the above para. After reproducing the extra waterway and modifying the formation level of minor bridges on the model, the model was run for the discharges as specified in the existing condition (para 3.2). Under this condition, the model studies indicated that the waterways provided for each bridge is adequate and no submergence of bridges during high floods was noticed. The flow conditions were also favourable. The generalized flow patterns are shown in Photo 2. The discharge distribution passing through modified bridges are given in Table 5. There was 0.6 m reduction in the water level at upstream of bridge site as compared to the existing condition. Based on the maximum discharge intensity of each bridge, the corresponding founding levels were computed using generally accepted empirical formula. It was seen that the foundation levels of all the minor bridges were inadequate and hence, it was decided to dismantle the minor bridges for reconstructing the same with proposed increased waterway and deeper founding levels.

Table 5: Percentage of Discharge Passing Through the Modified Bridges

Discharge, (m^3/s)	Bhawani Patna side, (%)		Main bridge, (%)	Khariar side, (%)	
Location	Bridge 1 27/600	Bridge 2 & 3 27/800-850	Bridge 4 28/400	Bridge 5 28/900	Bridge 6 29/400
15,500	4.06	21.39	72.01	1.66	0.80
11,625	2.46	19.28	76.16	1.38	0.72

Photo 2: Generalized Flow Pattern Near Bridges at Turkel

(Discharge – 15,500 M^3/S, Under Modified Design of Minor Bridges)
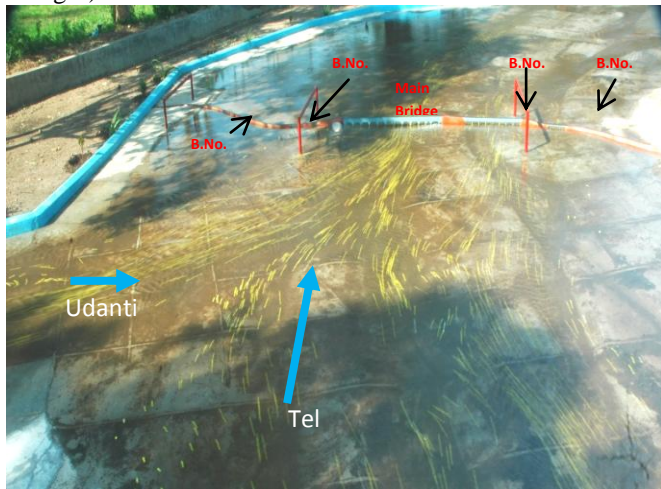
4 CONCLUSION

Reallocation of waterways for series of multiple bridges across a multiple channels of river is a complex procedure and for this purpose, a physical model is a good tool to obtain optimum solution. In the present case study, it was found that the waterway of the existing minor bridges was inadequate and hence it was modified based on the assumption that the discharge distribution would remain same as in case of existing conditions. The experiments conducted proved that the waterway provided for the modified minor bridges was adequate. The experiments also showed that there would be a reduction of 0.6 m in the afflux on upstream of bridges and accordingly, road top level was also decided.

ACKNOWLEDGEMENT

REFERENCES

i.   Bruce M. McEnroe (2007) – Report on 'Sizing of highway culverts and bridges: ahistorical review of methods and criteria', University of Kansas,
ii.   Bruce M. McEnroe, ASCE (2009) - Hydrologic Design of Bridges and Culverts: A Historical Review World Environmental and Water Resources Congress 2009: Great Rivers History Great Rivers History.
iii.   CBI & P (1989) "River Behaviour, Management and Training, Pub. No. 204 Vol. 1".
iv.   Chow, Ven Te -"Open Channel Hydraulics", McGraw – Hill Book Company.
v.   IRC 78:2000 -" Standard Specifications and Code of Practice for Road Bridges, Section VII – Foundations and Substructure (Second Revision)".
vi.   IRC: SP:13 (2004) – "Guide lines for design of small bridges and culverts"
vii.   IRC 5:1998 – "Standard specification and code of practice for road bridges.
viii.   ISO 1438 (2008) – Hydrometry – Open channel flow measurement using thin-plate weir
ix.   IRS (2003) – Code of practice for the design of sub-structures and foundation of bridges, RDSO, Lucknow.
x.   Mazumder S.K. (2009)- "Determination of waterway under a bridge in Himalayan region - some case studies", Journal of the Indian Roads Congress, July-September 2009

Vortex Power Concept For Local Scour Around Non- Uniform Oblong Bridge Piers

G. Veerappadevaru[1], Abhijeetkumar[2], Abhishekdey[3] and T. Gangadharaiah[4]

[1]Associate Professor, Department of Civil Engineering, Siddaganga Institute of Technology, Tumkur-572103 Karnataka State, India.   Email: gv_devaru@yahoo.com (author for correspondence)

[2]Undergraduate Student, Department of Civil Engineering, Siddaganga Institute of Technology, , Tumkur-572103 Karnataka State, India. Email: kumarabhijeet48@gmail.com

[3]Undergraduate Student, Department of Civil Engineering, Siddaganga Institute of Technology, , Tumkur-572103 Karnataka State, India. Email: abhishekdey1992@gmail.com

[4]Professor Emeritus, Department of Civil Engineering, Siddaganga Institute of Technology, Tumkur-572103 Karnataka State, India. Email: tganga1939@gmail.com

ABSTRACT : Bridges built across rivers flowing on soft soil strata needs a deeper foundation for its supporting structures like piers and abutments. Adaptation of non-uniform shaped piers and abutments are needed for their stability and safety. Predication of local scour depth around non-uniform piers is necessity for their safe foundation design. Piers with pile cap supported by group of piles are considered as one such non-uniform pier. The vortex power concept developed for uniform piers is modified by introducing equivalent width for non-uniform piers and used to predict its local score depth. The experiments were conducted to find the depth of local scour around round nosed (oblong) piers having a pile cap supported by group of piles. The experimental data available in literature along with present data confirms the valid usage of vortex power concept for prediction of local scour depth around non-uniform piers.
Keywords: Bridge pier, local scour, vortex, river engineering

1. MECHANISM OF SCOURING PROCESS

Flow separation occurs at the corner of pier with the river bed. The vortices are formed in the separated flow zone. The interaction of these vortices with the sediment bed leads to dislodging of sediment grain and transporting them downstream, thus causing local scour. Vortices exist in pairs

and these pairs may be designated as the primary vortex and the secondary vortex. The primary vortex occurs near the bridge pier frontal surface and the secondary vortex behind the primary vortex. The removal of sediment and deepening of the scour hole are mainly due to the primary vortex. The secondary vortex mostly maintains the slope of the scoured hole surface by transporting the dislodged sediment sideways. The separation between the primary vortex and the secondary vortex are visible in the form of ridge line. The primary vortex lies below the ridge line and the secondary vortex above the ridge line. The down flow along the pier surface and curving of incoming flow into scour hole are the cause for the vortex formation. An obstruction like the surfaces of caisson top or the pile cap arrest part of the down flow on the projected portion of the pier surface. The remaining part of the down flow moves further downward towards the sediment bed, forming vortex at their junction point as suggested by Veerappadevaru et al. (2011) and Gangadharaiah and Muzzammil (1985).

1.1 Vortex power concept applied to local scour around non-uniform oblong piers

Power available in the primary vortex P_v formulated by Veerappadevaru et al. (2011) as:

$$P_v = \rho \pi D_v N D_e V^2 \tag{1}$$

Where ρ is mass density of water, D_v is the size of primary vortex, N is rotational speed of the primary vortex, D_e is equivalent width of pier and V is the average velocity of flow at level of primary vortex in the sour hole. P_c is the power consumed in dislodging and transporting the sediment grain from the scour hole. An expression for P_c is written as:

$$P_c = 2/3 \, \pi \, D_v D_e \, (\rho_s - \rho) \, g d_{50} V_{*c} \tag{2}$$

Where ρ_s is mass density of sediment grain, g is the acceleration due to gravity, d_{50} is the median size of sediment in the scour hole and V_{*c} is the critical shear velocity of size d_{50} which is computed based on shield's critical shear stress criteria at equilibrium state as:

$$P_v = P_c \tag{3}$$

Substituting the relations obtained from experiments on vortex size D_v and vortex rotational speed N, an expression for score depth relation is written as:

$$F_{De} \; \alpha \; (h + h_s)/D_e \tag{4}$$

Where F_{De} is defined as flow parameter and is written as:

$$F_{De} = q \,/\, \{(D_e^2 h) \, ((\rho_s - \rho)/\rho) \, g d_{50} V_{*c}\}^{1/3} \tag{5}$$

Where q is discharge intensity, h is depth of flow and h_s is scour depth measured from bed level to deepest portion of score hole. The constant of proportionality in equation (4) is obtained by their experimental results and also using the experimental data available in literature by Veerappadevaru et al. (2011) as:

$$F_{De} = 0.48((h + h_s)/D_e) \tag{6}$$

The measurement of scour level is made with respect to water surface. The length parameter $(D_e^2 h)^{1/3}$ was obtained from the theory. This length parameter was first introduced by Unger and Hager (2007) in their analysis of scour data.

The equivalent width D_e is defined as the ratio of frontal projected area taken up to Y_{max} for pier on pile cap supported by group of piles. When the pier pile cap level lowered or raised with respect to Y_{max} the scour depth decreases and the expression for Y_{max} is written as:

$$\frac{b}{(D_c^2 h)^{1/3}} = 0.204 \frac{(Y_{max} + T)}{(D_p^2 h)^{1/3}} + 0.0446 \tag{7}$$

With $R^2 = 0.89$

Where D_p is the width of pile cap, D_c is the diameter of caisson pier, Y_{max} is the position of pile cap level which results in maximum scour level, b is the vertical width of the deep scour hole and T is thickness of pile cap. These relations are obtained by Veerappadevaru et al. (2011) using their results and experimental data available in literature. The value of $R^2 = 0.89$ represents the statistical correlation coefficient value.

2. EXPERIMENTAL SETUP AND PROCEDURE

The scour studies were conducted in a 5.5 m long trapezoidal flume having a cross section of 1.0 m wide and 0.3m deep. The trapezoidal flume had rigid sand banks and mobile sand bed. The sand banks were made rigid by applying cement mortar slurry. The median size of sand was $d_{50} = 0.52$mm, having geometric standard deviation $\sigma_g = 1.912$. The flow was allowed into the river tray from the overhead tank. Water was allowed to flow into the flume through a stone screen of 20cm width extended up to the width of the flume and height from bed level to the top of the sand bank. Stone pebble mat was placed behind the stone screen on sand bed to avoid erosion. Sediment trap was provided at the downstream end of the flume. Measurement of discharge was carried out through a 90º V-notch provided at the end of the flume. The experimental setup and the pier geometry with piles on a pile cap are shown in Figures 1 and 2.

Figure1. Front view of experminatal set up

Figure2. Oblongpeirwithpilecapsupported by piles

Table 1. The following experimental results were collected at the end of
10 hours for pier on pile cap supported by array of piles

Pier position with respect to bed level cm	Depth of flow (h) mm	Scour depth (h_s) mm	Equivalent width (D_e) mm	Projected width (b) cm
-12	80	16	75	1.15
-9	80	14	63.75	1.15
-6	80	12	52.5	1.15
-3	80	10	41.25	1.15
0	80	7.6	30	1.15
3	80	11	30	1.15
6	80	21	30	1.15
9	80	26	30	1.15
12	80	33	30	1.15

Here Y_{max} is measured from bed level to top of pile cap. It is negative (- ve) when the pile cap is above bed level and positive (+ ve) when the pile cap is below bed level.

4. ANALYSIS OF RESULTS

The equivalent width D_e was calculated for all the positions of caisson top with respect to bed level to determine the actual contact area with the flow field from free surface up to Y_{max} below bed level. The power concept is used for non-uniform piers to show the variation of scour depth $(h + h_s)/D_e$ against

the flow parameter F_{De}. The equivalent width was also calculated for the data available in the literature and plots were drawn between $(h + h_s)/D_e$ and F_{De} to check the validity of the power concept for the non-uniform piers.

An enveloping line is drawn which has a relation as $(h + h_s)/D_e$ = 0.57 F_{De}. It can be inferred from the plots that the experimental data agree well with the literature data when diameter of caisson (D_c) is replaced by equivalent diameter (D_e) of the frontal pier surface. Hence, the validity of the power concept agrees for the case of oblong piers and oblong piers with piles supported on a pile cap.
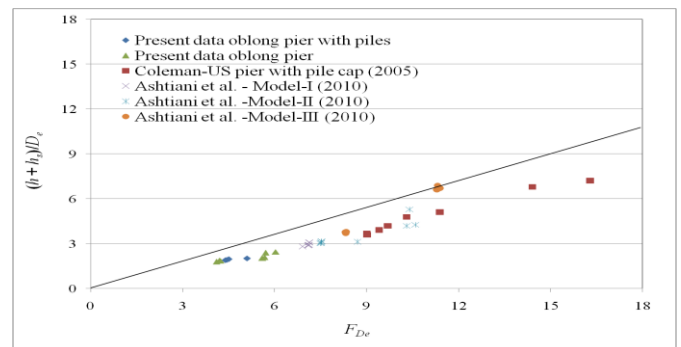
Figure 3. Showing the relation between $(h + h_s)/D_e$ and F_{De} for the literature data as well as for the present investigation.

5. DISCUSSION OF RESULTS AND CONCLUSIONS

Most of the previous works to predict the scour depth were carried out for uniform piers. Hence, little was known regarding the behaviour of non-uniform piers. Melville and Raudkivi (1996) initiated a method to predict the scour depth for non-uniform piers. This involved a number of empirical equations using experimental investigations. Veerappadevaru et al. (2011) developed the vortex power concept to predict the scour depth for pier with caisson when caisson top located at bed level. This power concept was extended for the cases when the pile cap top level is located above and below the bed level. It was observed that, large scatter in the plot is due to the position of PT (Pile cap Top), which is not considered in the analysis. To account the effect of PT position on the scour depth, the concept of equivalent diameter is formulated. This is based on the ratio of projected area of non-uniform pier above Y_{max} to the depth measured from free surface. Using this equivalent diameter in vortex power concept suggested by Veerappadevaru et al. the prediction of scour depth for non-uniform oblong piers is carried out. It was observed that $(h + h_s)/D_e$ against F_{De} based on vortex power concept shows a linear relation for oblong piers and oblong pier on pile cap supported by an array of piles. The analysis of the results revealed that in addition to the pier geometry and relative position of PT (Pile cap Top) with respect to bed level, the projected width 'b' is the dominant factor for the progress of local scour. The enveloping curve was taken for design

purposes to predict the maximum scour depth from free surface. An equation for enveloping line is written as $(h + h_s)/D_e = 0.57 \ F_{De}$. The scour depth measurements were taken from the free surface because the bed level is not constant during floods and hence scour depths are fairly reliable. The magnitude of proportionality constant is changed from 0.48 for uniform piers to 0.57 for non-uniform piers, having ablong in shape mounted on pile cap supported by group of piles.

REFERENCES

i.   Ataie-Ashtiani, B., Baratian-Ghorghi, Z., Behesti, A. A. (2010). Experimental investigation of clear-water local scour of compound piers. J. Hydraulic Eng. ASCE, 136(6), 343-351.

ii.   Coleman, S. E. (2005). Clear-water local scour at complex piers. J. Hydraulic Eng. 131(4) 330- 334.

iii.   Gangadharaiah, T., Muzzammil, M. (1985). Vortex strength approach for bridge pier scour predictions. Second International workshop on alluvial river problems. University of Roorkee, Proc. 151-158.

iv.   Melville, B. W., Raudkivi, A. J. (1996). Effects of foundation geometry on bridge pier scour. J. Hydraulic Eng. 122(4), 203-209.

v.   Unger, J. and Hager, W. H. (2007). Down-flow and horseshoe vortex characteristics of sediment embedded bridge piers. J. Exp. Fluids. 42, 1-19.

vi.   Veerappadevaru, G., Gangadharaiah. T. and Jagadeesh, T. R. (2011). Vortex scouring process around bridge pier with a caisson. J. Hydraulic Res., IAHR, 49 (3), 378-383.

Study Of Sediment Concentration Distribution In Vortex Settling Basin Considering Three Dimensional Flow

Mujib Ahmad Ansari[1] and Mohd Athar[2]

[1]Associate Professor, Department of Civil Engineering, Zakir Husain College of Engineering and Technology, Aligarh Muslim University Aligarh, 202002, U.P., India. (Corresponding author)

[2]Professor, Department of Civil Engineering, Zakir Husain College of Engineering and Technology, Aligarh Muslim University Aligarh, 202002, U.P., India.

Email: mujibansari68@gmail.com, mujibansari_68@yahoo.com

ABSTRACT : In present study an attempt has been made to study the distribution of suspended sediment concentration within the vortex settling basin by considering three dimensional velocity distribution. The governing equation for variation of sediment mass concentration is solved numerically by using an unconditionally stable second order accurate Crank-Nicholson type of implicit finite difference scheme. Values of components of velocity appearing in sediment mass equation are measured by three dimensional Programmable Electromagnetic Liquid Velocity Meter. Sediment diffusion coefficients used in sediment mass equation are computed by using experimental data of velocity components in r, θ and z-directions collected in the present study. The equivalent finite difference form of governing equation is solved with the Gauss-elimination method by making use of the appropriate boundary conditions. A reasonable agreement is found to exist between the experimental values of sediment concentration and its values computed using the proposed method.

1. INTRODUCTION

Information regarding the variation of sediment concentration within the vortex basin is useful in the determination of sediment removal efficiency of the vortex settling basin. Also this information can be used in evolving an efficient vortex settling basin that is more efficient in removing the sediment particle from its flow. Only a few studies are available regarding variation of sediment concentration in a vortex basin.

Julien (1986) developed relationships for the suspended sediment concentration profiles in a steady Rankine vortex. He considered that with rotation of fluid with very fine sediment in a circular path, vortex is formed and the sediment concentration gradient gradually builds up across the vortex. A diffusive flux proportional but opposite to the centrifugal flux is induced. Equilibrium is reached when two fluxes are equal. At this stage, the sum of all forces i.e. pressure, centrifugal as well as viscous force reduces to zero and the sediment particles attain a limit velocity in radial direction.

Julien (1986) also conducted experiment to verify his result for the sediment concentration distribution using very fine silts with 0.053 mm $\leq$ d_{50} $\leq$ 0.0074 mm and obtained the theoretical concentration profiles in a Rankine combined vortex. The sediment concentration profile depended on three major factors viz., diffusion, friction and centrifugal force exerted on small particles.

Vatistas (1989) conducted studies on development of fine silt concentration caused by the influence of a prevailing combined vortex. The sediment concentration profiles obtained by Julien (1986) were found to be in good agreement with results obtained in the study of Vatistas (1989). However the values of ε_r used for computations were different to those used by Julien (1986).

Athar (2000) and Athar et al.(2007) theoretically developed the following sediment diffusion equation in polar coordinate system by considering the inflow and outflow of the sediment flux through various faces of an elementary parallelopiped.

$$\frac{1}{r} \frac{\partial}{\partial r}(r\,v_r\,c) + \frac{1}{r} \frac{\partial}{\partial \theta}(v_\theta\,c) + \frac{\partial}{\partial z}(v_z\,c) = \frac{1}{r} \frac{\partial}{\partial r}\left(\varepsilon_r\,r\,\frac{\partial c}{\partial r}\right) +$$

$$\frac{1}{r^2} \frac{\partial}{\partial \theta}\left(\varepsilon_\theta \; \frac{\partial c}{\partial \theta}\right) + \frac{\partial}{\partial z}\left(\varepsilon_z \; \frac{\partial}{\partial z}\right) + \frac{\partial}{\partial z}\left(\omega_o c\right)$$

(1)

They solved the above equation numerically by using an unconditionally stable second order Crank-Nicholson type of implicit finite difference scheme by assuming that the vertical components of velocity is significant only near the centre of the vortex settling basin and considered only radial and tangential velocities.

No detailed investigation is however, available on study of suspended sediment concentration in vortex settling basin by considering tangential, radial and vertical velocity components. Thus there is a need to collect such information for evolving more efficient vortex basin.

2. EXPERIMENTAL PROGRAMME

2.1 Measurement of velocity components in the vortex basin

The equipment used for measurement of velocity components namely PEMS simultaneously measures the components of velocity in three mutually perpendicular directions at the point in the flow where its probes are fixed. The vortex basin was first divided into six circular segments. These were further subdivided into eight angular segments as shown in Fig.1(a). The 3D assembly of PEMS probes was fixed with specially designed vertical gauge and the whole assembly was mounted on the horizontal circular railing fixed over the vortex basin. The PEMS probes could be moved horizontally as well as vertically up and down. For measuring the velocity components, the PEMS moved to five different levels along the intersection points (*i.e.* nodal points) of the annular and the angular lines as shown in Fig. 1(a). Electrodes in the PEMS probes were so oriented that the PEMS measured the velocity components in radial, tangential and vertical directions at the point where it was fixed. The probes were also connected with the two PEMS main cassette that directly display the observations. Next, steady flow was established in the vortex settling basin by allowing known inflow and operating the tailgate and outlet valve for establishing known underflow-flushing discharge. Radial, tangential and vertical velocities were measured next by fixing the PEMS probes at desired locations and orienting its probe in requisite directions.
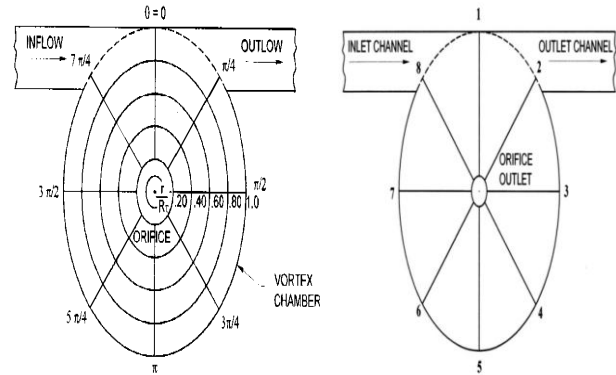
1(a)   1(b)

Figure 1. Sectorisation of vortex settling basin

Detailed measurements on velocity components have been made on vortex settling basin. Data for velocities have been collected for inflow discharge of 0.012m³/s. The water abstraction ratio was maintained at 10 per cent, as on this abstraction ratio the sediment removal efficiency for the model was the maximum (Athat et al. 2002). The diameter ratio and width ratio were kept as 9.91 and 4.87 respectively as on these ratios the removal efficiency of the model was the maximum Ansari (2008) and Ansari et al. (2013). During the flow, the velocity components were observed at all nodal points within the vortex basin.

2.2 Measurement of sediment concentration in the vortex basin

The steady flow in the vortex settling basin was first established as described earlier for given inflow discharge and abstraction ratio. Sediment load as per the Engelund-Hansen transport capacity was fed into the inflow using the sand feeder as suggested by Athar et al (2002). After about 15 minutes of feeding the sediment into the inflow, the observations were taken for sediment concentration of the flow in vortex basin. Following procedure was adopted for the same.

Separate samples of sediment-laden water were withdrawn from the vortex basin from those locations where the radial, tangential and vertical velocities were measured. Care was taken to withdraw the sample from given location in tangential direction at a velocity, which was equal to the measured tangential velocity there. Pre-calibrated orifice-meter and centrifugal pump were provided on delivery pipe and these were carefully operated for this purpose.

Sediment feeding into the inflow was continued while samples were being taken for measurement of sediment concentration. For a given sample the sediment-laden flow was collected through a rubber tube in a collector. The collected sample from the collector was filtered through a thick filter paper. The filtered material was dried in the oven and was weighed on a

chemical balance and concentration in parts per million (ppm) for each sample was determined. Variation of sediment concentration in vortex basin was observed by taking the samples as mentioned above at all those locations where velocity components were measured for inflow discharge of 0.012m³/s. The water abstraction ratio was maintained at 10 per cent, as on this abstraction ratio the sediment removal efficiency for the model was the maximum. The diameter ratio and width ratio were kept as 9.91 and 4.87 respectively as on these ratios the sediment removal efficiency of the model was the maximum.

3. ANALYSIS OF DATA, RESULTS AND DISCUSSION

3.1 Numerical scheme for solution of governing equation for sediment concentration

The analytical solution of Equation (1) is available only for simplified situations and these are not valid in the case of vortex settling basin in actual practice. Numerical solution is therefore attempted by using the unconditionally stable Crank-Nicholson implicit finite difference scheme.

3.2 Non-Dimensional Form of the Governing Equation

Equation for variation of sediment mass concentration *viz.* Equation (1) is a parabolic partial differential equation. The order of magnitude of various terms appearing in Equation (1) could be largely different in problems involving real data. However it is considered that the order of magnitude of various terms in non-dimensional form of the equation will not vary much from each other. The non-dimensional variables are defined below:

$$C = \frac{c}{C_i}, \qquad R = \frac{r}{R_L}, \qquad Z = \frac{z}{h_p},$$

$$\omega = \frac{\omega_O}{\omega_f R_L}, \qquad V_R = \frac{v_r}{\omega_f R_L},$$

$$V_\theta = \frac{v_\theta}{\omega_f R_L}, \quad V_Z = \frac{v_z}{\omega_f R_L}, \quad \varepsilon_R = \frac{\varepsilon_r}{\omega_f R_L^2},$$

$$\varepsilon_Z = \frac{\varepsilon_z}{\omega_f R_L^2} \qquad (2)$$

Here R_L is the characteristic length which is taken as equal to the radius of the vortex basin and ω_f is the reciprocal of characteristic time (also called characteristic frequency) and it is defined as $Q_i / (A_i R_L)$. Where Q_i is the inlet discharge, and A_i is the cross-sectional area of the inlet channel. The term $\omega_f R_L$ is equivalent to V_i. Substituting the values of variables from Equation (2) into Equation (1) and after simplification we can get the following equation.

$$\varepsilon_R \frac{\partial^2 C}{\partial R^2} + \frac{\partial C}{\partial R}\left(\frac{\varepsilon_R}{R} - V_R + \frac{\partial \varepsilon_R}{\partial R}\right) + \frac{\varepsilon_\theta}{R^2}\frac{\partial^2 C}{\partial \theta^2} + \frac{\partial C}{\partial \theta}\left(-\frac{V_\theta}{R} + \frac{\partial \varepsilon_\theta}{R^2 \partial \theta}\right) +$$

$$\left(\frac{R_L}{h_p}\right)^2 \varepsilon_Z \frac{\partial^2 C}{\partial Z^2} + \left(\frac{R_L}{h_p}\right)\frac{\partial C}{\partial Z}\left\{\omega - V_Z + \left(\frac{R_L}{h_p}\right)\frac{\partial \varepsilon_Z}{\partial Z}\right\}$$

$$+ C\left\{-\frac{V_R}{R} - \frac{\partial V_R}{\partial R} - \frac{1}{R}\frac{\partial V_\theta}{\partial \theta} - \left(\frac{R_L}{h_p}\right)\frac{\partial V_Z}{\partial Z}\right\} = 0 \qquad (3)$$

Solution of Equation (3) will give the non-dimensional values of the unknowns involved *i.e.* the sediment concentration values at the computational grid points. These are multiplied by the scaling parameters to obtain the results in dimensional form.

3.3 Finite difference scheme

A centred finite difference scheme is used for first order partial derivatives and the scheme of Crank–Nicholson is used for second order partial derivatives. Here ΔR, $\Delta \theta$ and ΔZ are the computational grid sizes in r, θ and z directions respectively. The solution grid adopted in $r - \theta - z$ co-ordinate system is shown in Fig. 2. Using this finite difference technique, each term of Equation (3) is converted into the equivalent finite difference form to get second order accuracy.
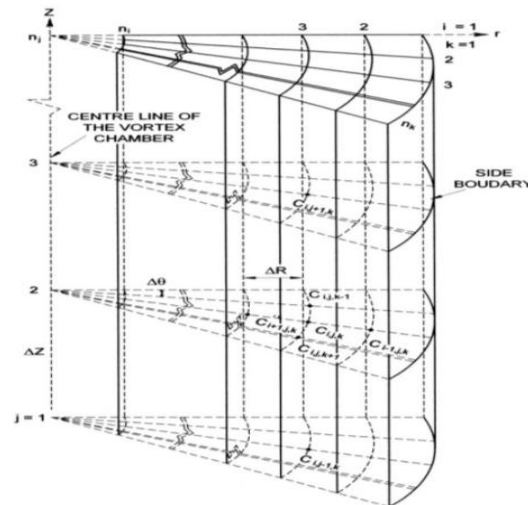
Figure 2. Computational grid in r-θ-z co-ordinate system

The subscript i, j, k denote the position of computational nodes in r, θ and z directions respectively with i and $k = 1$ occurring at the inflow section as shown in Fig. 2 and j =1 at bottom of the basin. Substituting the values of these differential equivalents in Equation (3) to get second order accuracy, the resulting equation is written for all the computational nodes of the finite difference grid. Nevertheless, it can not be solved by itself, as the number of unknowns it contains is larger than the

number of equations. The unknowns at various computational nodes are determined using the boundary conditions described at inlet, water surface and bottom.

Subsequent to making use of the boundary conditions mentioned above the number of unknowns remaining in the system of equation become equal to the number of equations. The coefficients of these equations when collected together result in the formation of an unsymmetrical banded matrix of coefficients.

This system of equation can be written as below

$$[\ CO\ ]\ [\ C\ ]\ =\ [\ RO\ ] \tag{4}$$

Here CO is the square matrix of coefficients, the order of which is equal to the number of unknowns, C is the vector of unknowns and RO is the vector values of elements, which are known. The system of matrices represented by Equation (4) can be solved by using Gauss-elimination method for computation of the unknowns *i.e.* sediment concentration values at various nodal points within the vortex basin.

3.4 Sediment diffusion coefficients

Information on sediment diffusion coefficients is required while making the computations for the distribution of suspended concentration within the vortex basin. Athar (2000) and Athar et al. (2003) considered that value of the velocity gradient along the direction of velocity itself would provide a good measure of the shear velocity in that particular direction. Hence following functional relationships are assumed for ε_r, ε_θ and ε_z respectively.

$$\varepsilon_r = f\left(\frac{\partial v_r}{\partial r}\right),\ \varepsilon_\theta = f\left(\frac{\partial v_\theta}{\partial \theta}\right)\ \text{and}\ \varepsilon_z = f\left(\frac{\partial v_z}{\partial z}\right) \tag{5}$$

3.5 Variation of suspended sediment concentration within the vortex settling basin

The present finite difference scheme to solve the partial differential equation governing the variation of sediment concentration in the vortex settling basin is applied herein to obtain the concentration of suspended sediment when boundary

conditions and sediment diffusion coefficients   and   , the values of velocity components in tangential, radial and vertical directions appearing in the sediment mass equation are known. The values of velocity components in all the three directions at various nodal points within the vortex basin were measured using three-dimensional electromagnetic liquid velocity meter. Functional relationships for determination of diffusion coefficients were empirically derived. A trial and error procedure is used to ascertain the values of these coefficients appearing in these equations. Through the method of trial such values of the coefficients were adopted, which

produced best match between the computed and observed variation of concentration of suspended sediment within the vortex basin.

The following relations were thus obtained for the diffusion coefficients.

$$=\qquad\qquad,\ \varepsilon_\theta\ =\qquad 3.02,$$

$$=\qquad 2.36\ *\qquad\qquad (6)$$

Values of other parameters used for this purpose were   ,   = 0.33 and   = 0.55.

It is to be mentioned that values of   and   smaller than those listed above did not produce different results; hence the above mentioned values were adopted for use in further

3(a)   3(b)
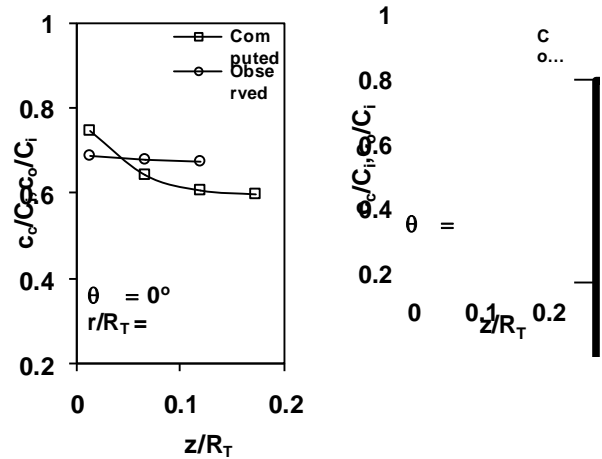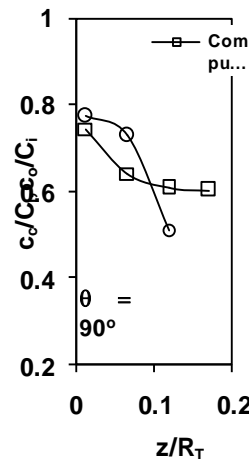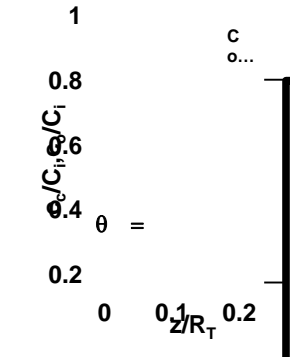
3(c)   3(d)
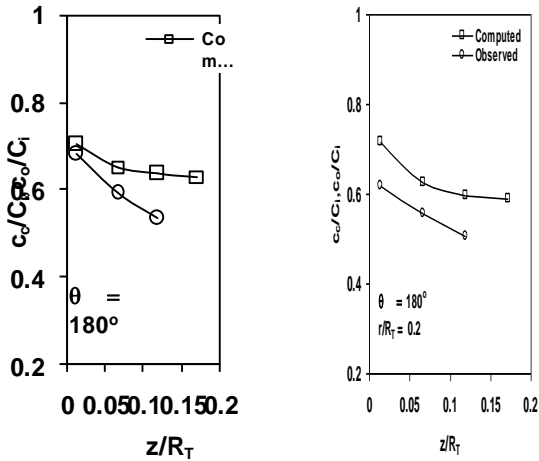
3(e)   3(f)

Figure 3. Variation of sediment concentration along vertical direction for different θ values

computations. It is to be further mentioned that the velocity components in tangential, radial and vertical directions at various nodal points, sediment concentration in the flow in the inlet channel, dimensions of inlet and outlet channels, vortex settling basin and inlet and outlet flow rates are the inputs to the numerical scheme for the computation of the sediment concentration.

The concentration of suspended sediment within the vortex settling basin at a number of nodal points as shown in Fig. 1(a) was computed. The property of mass conservation of the numerical scheme used herein was verified by comparing the quantity of sediment inflows to the basin with the sum of computed sediment storage within the vortex basin and computed sediment outflows from the basin over a given period of time.

Figures 3(a) to 3(f) illustrate the variation of non-dimensional sediment concentrations c_c/C_i & c_o/C_i with non-dimensional depth parameter z/R_T. A close study of these plots revealed that the sediment concentration is indeed found to increase with the flow depth measured downward from water surface. Similar trends are obtained for both computed and observed sediment concentration.

Non-dimensional computed sediment concentration for different -values was plotted along each basin diameter marked in Fig. 1(b). These plots are depicted here for the purpose of illustration (Figs.4(a) to 4(c)). A close study of these plots revealed that there is significant variation in sediment concentration along the vertical as well as along radial direction. The maximum value of sediment concentration was obtained at the periphery and minimum at the orifice outlet.
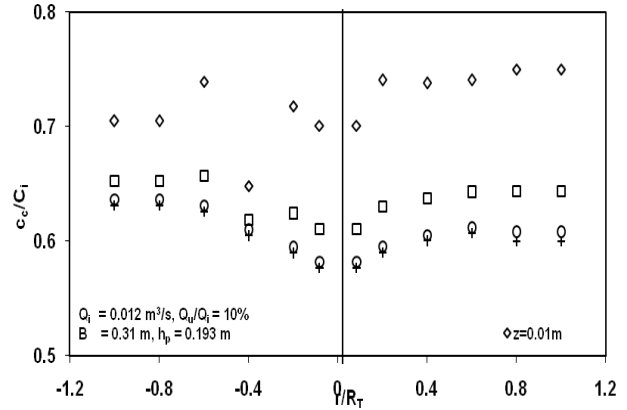
Figure 4(a). Variation of sediment concentration along basin diameter 1 – 5
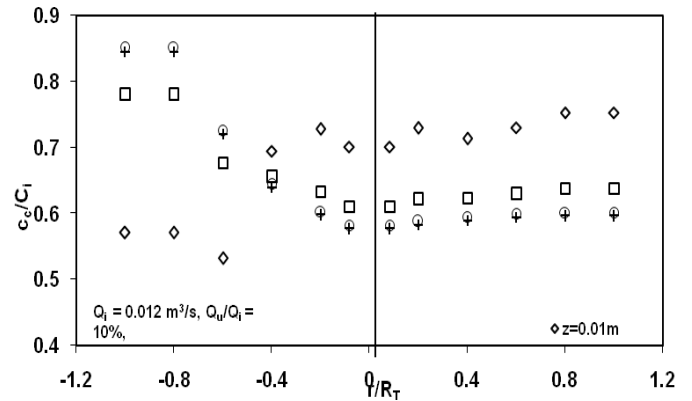
Figure 4(b). Variation of sediment concentration along basin diameter 2 – 6
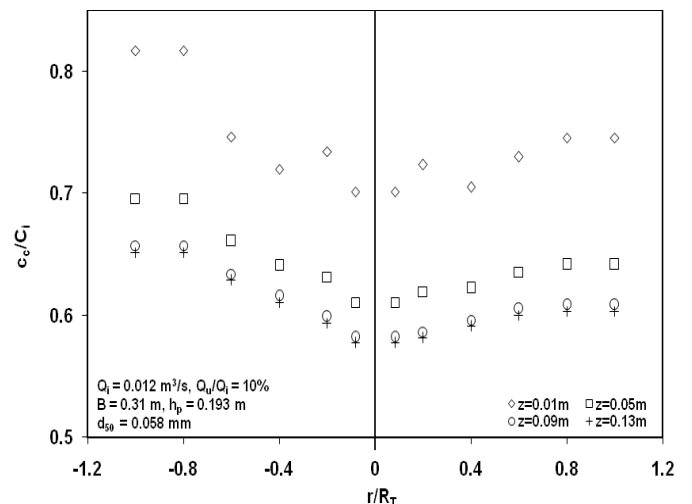
Figure 4(c). Variation of sediment concentration along basin diameter 3 – 7

4. CONCLUSIONS

The governing equation for variation of sediment mass concentration *viz.* Equation (1) is solved numerically by using an unconditionally stable second order Crank-Nicholson type of implicit finite difference scheme. Values of tangential, radial and vertical components of velocity to be used in numerical solution of Equation (1) are measured by three-dimensional Electromagnetic Liquid Velocity Meter.

The equivalent finite difference form of Equation (1) is solved with the Gauss-Elimination method by making use of the appropriate boundary conditions. A satisfactory agreement is found to exist between thus computed and observed values of sediment concentration. Empirically derived relations given as Equation (6) are used for the computation of sediment diffusion coefficients appearing in Equation (1).

Within the vortex settling basin there is significant variation in sediment concentration along the vertical as well as along radial direction. Sediment concentration is found to increase with the flow depth measured downward from water surface. The maximum value of sediment concentration was obtained at the periphery and minimum at the orifice outlet.

REFERENCES

i.   Ansari, MA 2008 *Performance evaluation of vortex settling basins*. Doctoral thesis, Department of Civil Engineering, Aligarh Muslim University, Aligarh, U.P. India

ii.   Ansari MA, Athar M 2013 *Design parameters of vortex settling basin*. Proceedings of the ICE – Water Management 166(5): 262–271

iii.   Athar M 2000 *Study of vortex chamber* Doctoral thesis, submitted for the award of the degree to the Civil Engineering Department IIT Roorkee Roorkee India

iv.   Athar M, Kothyari UC, Garde RJ 2002 *Sediment removal efficiency of vortex chamber type sediment extractor*. J. Hydraul. Eng. 128(12): 1051–1059

v.   Athar M 2007, *Sediment Concentration Distribution in Vortex Chambers*. JHE The Indian Society for Hydraulics 13(3): 15-38

vi.   Athar M, Kothyari UC, Garde RJ 2003 *Distribution of Sediment Concentration in the Vortex Chamber Type Sediment Extractor*. JHR Proc. IAHR 41(4): 427-438

vii.   Julien PY 1986 *Concentration of Very Fine Silts in a Steady Vortex*. JHR, Proc. IAHR 24(4): 255-264

viii. Vatistas GH 1989 *Analysis of Fine Particles Concentration in a Combined Vortex* JHR Proc. IAHR 27(3): 417-426

NOTATIONS

B	=	Bed width of the inlet channel
C	=	Non-dimensional concentration
c	=	Concentration in parts per million
C_i	=	Concentration in parts per million at inlet of settling basin
D_T	=	Diameter of the vortex-settling basin
d_{50}	=	Median size of the sediment particles
d_u	=	Diameter of the under flow outlet orifice
g	=	Gravitational acceleration
h_p	=	Depth of flow at the periphery of the vortex settling basin
n_i, n_j, n_k	=	Total number of computational nodes along r, θ and z directions
Q_u	=	Discharge through underflow outlet
Q_u/Q_i	=	Water abstraction ratio
R	=	Dimensionless radial spacing
R_T	=	Radius of the vortex settling basin
S_T	=	Bottom slope of the vortex settling basin
V_r, V_θ, V_Z	=	Dimensionless velocity components along radial, tangential and vertical directions
v_r, v_θ, v_z	=	Components of the velocity along radial, tangential and vertical directions
Z	=	Non-dimensional vertical coordinate
z	=	Depth in the basin measured from the bottom of basin
Z_h	=	Difference between the bed levels of vortex settling basin and overflow outlet channels
α	=	Weighting coefficient
$\varepsilon_r, \varepsilon_\theta, \varepsilon_z$	=	Diffusion coefficients along r, θ and z directions
$\varepsilon_R, \varepsilon_\Theta, \varepsilon_Z$	=	Non-Dimensional Diffusion coefficients along r, θ and z directions
ω	=	Angular velocity of forced vortex
ω_o	=	Fall velocity of the sediment particle
r, θ, z	=	Cylindrical polar co-ordinate system
$\delta r, \delta \theta, \delta z$	=	Increments along r, θ, z directions

Optimal Discharge Of Pumps Supplying Water To A Common Delivery Point From Different Sources

Dr. P. S. Mahar[1] and Dr. R. P. Singh[2]

1.   Professor and Head, Civil Engg. Deptt., College of Technology, GBPUA&T Pantnagar, 263145, Distt. Udham Singh Nagar (Uttarakhand), India
Email: pooransmahar@yahoo.co.in
2.   Professor, Irrig. and Drain. Engg. Deptt., College of Technology, GBPUA&T Pantnagar, 263145, Distt. Udham Singh Nagar (Uttarakhand), India
Email: rajprasin1@rediffmail.com

ABSTRACT : In present age of depleting water resources and increasing demand due to high population growth, it may be required to pump water from different sources to meet the demand. The sources of water may have different conditions like availability of water, elevation and distance to the delivery point. The energy consumption of the pump depends on the operating pressure, and discharge and its corresponding efficiency. The special characteristic of a centrifugal pump is that its efficiency is maximum for particular values of discharge and pressure. Therefore, it is important that a pump should be operated at its maximum efficiency when the pump is running at constant load. When the load on the pump is varying, it should be operated in higher efficiency range to save energy. In this study, a nonlinear optimization model is developed to maximize the total discharge of the pumps supplying water from different sources. The constraints are represented by the characteristic curves of the centrifugal pumps and the system head curves. The equations representing the efficiency of the pumps have been also used as constraints in the developed optimization model. The pump characteristics curves equation were obtained by using the performance data related to discharge, head, power and efficiency of centrifugal pump. The system head curve equations were developed by considering the difference between the elevation of water sources and delivery point, frictional head loss and velocity head for the pipe lines supplying water in the system. The head developed by pumps and the system head requirements were related as constraint equations The developed model results in obtaining the optimal operating conditions of different pumps by maximizing the discharge and minimizing the energy consumption for the known data related to the water sources and performance of the pump. Example problems have been solved by using LINGO software to illustrate the applicability of the developed optimization model. The application of the developed model will be helpful in pumping water from different sources for domestic and/or irrigation supplies.
Key words: Characteristic curves, system head curve, parallel connection, centrifugal pumps, nonlinear optimization, optimal discharge.

1. INTRODUCTION

In many situations, the pumping of water from a single source may not meet the increasing demand of water for different uses like domestic, irrigation, industrial etc. In such cases the water has to be supplied from more than one source like river, canal, groundwater, lake/pond etc. These sources of water may be at different locations and altitude. If the sources of water are located at lower altitude than the delivery point, centrifugal pumps are required to transport water from the source to the delivery point. In these cases, different pumps located at different sources discharge to a common delivery point connected through pipelines making a parallel connection of pumps. The capability of pump to discharge water over a certain elevation is represented by the characteristic curves showing relationship between pressure head, power and efficiency with the discharge (Church and Lal, 1973). The pumps should be preferably operated at high value of efficiency to consume the minimum energy resulting in the maximum discharge. The operating conditions to achieve this condition can be decided with the help of the characteristic curves and the system head curve (Mahar and Singh, 2014). The system head curves for different locations will vary according to elevation difference, length and diameter of pipes. Further, the pumps may be identical or different type. This creates the scope of optimizing the operating conditions of pumps for conjunctive use of water. This paper presents a nonlinear optimization model to maximize the total discharge of two identical pumps with available performance data having parallel connection to supply water from two different sources.

2. METHODOLOGY

2.1 Pump Characteristic Curves

The characteristic curves of the centrifugal pumps are prepared from the performance test data supplied by manufacturers to represent the relationship among discharge, pressure head, and efficiency (Punmia et al., 2010). The head-discharge curve of a pump can be represented as:

$$H = a_0 + a_1 Q + a_2 Q^2 \qquad (1)$$

Where H is the pump head (m); Q is the pump discharge (L/s); a_0, a_1 and a_2 are constants. Similarly the efficiency-discharge curve for a pump can be represented as:

$$\eta = b_0 + b_1 Q + b_2 Q^2 \qquad (2)$$

Where η is the efficiency of the pump, (percent); b_0, b_1 and b_2 are constants.

2.2 System Head Curve

The system head curve represents the elevation difference between the source and the delivery point and the frictional energy losses in the pipeline carrying water. The system head curve for a pump can be represented by neglecting minor losses as: $HS = S + hf \qquad (3)$

Where HS is the system head (m), S is the static head (m); hf is frictional head loss in the total length of the pipe (m). The value of hf can be calculated using the Darcy-Weisbach equation as:

$$hf = \frac{8 \times 10^{-6} \, f \, L Q^2}{\pi^2 \, g \, D^5} \qquad (4)$$

Where, f is friction factor (dimensionless); L is the length of the pipe through which discharge Q of the pump is flowing (m); g is the acceleration due to gravity (m/s^2); and D is the inside diameter of the pipe (m).

2.3 Optimization Model

The objective of the proposed optimization model is to maximize the total discharge of two identical centrifugal pumps having discharge Q1 and Q2. The constraints can be represented by the characteristic curves representing head-discharge and efficiency-discharge separately for both the pumps. Similarly, the system head curves for both the sources can be written as constraints. Thus, the nonlinear optimization model can be written as:

Maximize: $Z = Q1 + Q2$ $\qquad\qquad$ (5)

s. t.

$$H1 = a_0 + a_1 Q1 + a_2 Q1^2 \qquad (6)$$

$$H2 = a_0 + a_1 Q2 + a_2 Q2^2 \qquad (7)$$

$$HS1 = S1 + \frac{8 \times 10^{-6} \, f \, L1 Q1^2}{\pi^2 \, g \, D1^5} \qquad (8)$$

$$HS2 = S2 + \frac{8 \times 10^{-6} \, f \, L2 (Q1 + Q2)^2}{\pi^2 \, g \, D2^5} \qquad (9)$$

$$\eta1 = b_0 + b_1 Q1 + b_2 Q1^2 \qquad (10)$$

$$\eta2 = b_0 + b_1 Q2 + b_2 Q2^2 \qquad (11)$$

$$H1 \geq HS1 \qquad (12)$$

$$H2 \geq HS2 \qquad (13)$$

$$H1 - H2 \leq S1 - S2 + \frac{8 \times 10^{-6} \, f \, L1 Q1^2}{\pi^2 \, g \, D1^5} \qquad (14)$$

$$\eta1, \eta2 \geq \eta r \qquad (15)$$

$$Q1, Q2 \geq 0 \qquad (16)$$

Equations 6 and 7 are the head-discharge relationships for two identical pumps delivering discharge Q1 and Q2 from sources 1 and 2, respectively. The values of a_0, a_1 and a_2 are same in both the equations as the pumps are identical. Equation 8 represents

the system head relationship for the first pump having static lift of S1 from the first source to the delivery point discharging Q1 through the pipe of diameter D1 and length L1 upto the junction point where second pump is adding discharging Q2 from the second source. Equation 9 represents the system head relationship for the second pump having static lift of S2 from the second source to the delivery point with a total discharge of (Q1+Q2) through the pipe having length L2 and diameter D2. Here, it has been assumed that the second source is at a higher elevation as compared to the first source. Equations 10 and 11 are the efficiency-discharge relationships for two identical pumps delivering discharge Q1 and Q2 from sources 1 and 2, respectively. The values of b_0, b_1 and b_2 are same in both the equations as the pumps are identical. Equation 14 represents the condition of pressure compatibility at the junction point. In equation 15, hr represents the desired/recommended efficiency of the pumps.

3. EXAMPLE PROBLEM AND DISCUSSION

The applicability of the developed nonlinear optimization model is presented with the help of the following example problem.

3.1 Example Problem

Water has to be supplied from two sources A and B by using two identical centrifugal pumps to a common delivery point as shown in Fig. 1. The elevation difference between the delivery point and the sources A and B are 10m and 5m, respectively. The length and diameter of pipeline between the pumps are 100 m and 30 cm, respectively. The length and diameter of the pipe between the pump at source B and delivery point are 200m and 45cm respectively. The friction factor for both pipes is assume d as 0.03. The value of hr was taken as 60 %.
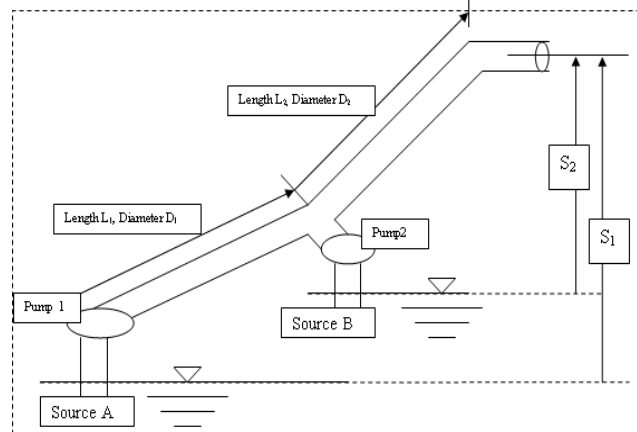
Fig. 1 Schematic diagram for two pumps supplying water from two sources

The pump characteristics data are given in Table 1 (Punmia et al., 2010).

Table 1. Pump Characteristic data

Discharge (L/s)	Head (m)	Efficiency (%)
0	20	0
8	18.6	48
16	16.7	69
24	14	75
32	10.9	70
40	7.4	60
48	3.6	47

3.2 Solution

Using Excel the constants of Equation 1 were obtained as: a_0 = 20.083, a_1 = - 0.1598, and a_2 = - 0.0039. Similarly, the constants of Equation 2 were obtained as: b_0 = 6.2381, b_1 = 5.0446 and b_2 = - 0.0897. In the optimization model described by equations 5 through 16, the given values were substituted to obtain the values of Q1 and Q2. The optimization model was solved using LINGO 8.0 software (LINDO Systems Inc., 2003) in demo mode. The values of Q1 and Q2 were obtained as 33.7 and 41.9 L/s, respectively. The efficiency of the pumps A and B were obtained as 74.4 and 60 percent, respectively. The effect of hr on the optimal solution is shown in Table 2 as sensitivity analysis. It can be seen from Table 2 that the discharge and efficiency of the pump at source A are nearly constant with the efficiency being nearly at the peak for all values of hr. However, the efficiency and discharge of the pump at source B is affected with change in the value of hr. Further, the optimal value of total discharge is decreasing when both the pumps are required to operate at higher efficiency. This is due to the nonlinear nature of the efficiency-discharge curve and thus causing more discharge for the pump at source B having lower static head. Thus, it can be concluded that the minimum recommended efficiency of the pumps should be appropriately considered to obtain the combined discharge.

Table 2. Effect of desired efficiency on optimal solution

Desired efficiency (%)	Efficiency of Pump1 (%)	Efficiency of Pump2 (%)	Discharge of Pump1 (L/s)	Discharge of Pump2 (L/s)	Optimal total discharge (L/s)
40	74.4	52.6	33.67	44.67	78.34
50	74.4	52.6	33.67	44.67	78.34
60	74.4	60.0	33.69	41.95	75.64
70	74.3	70.0	33.74	37.05	70.79

4. CONCLUSIONS

A nonlinear optimization model is developed to maximize the discharge of two identical pumps connected in parallel and supplying water from two different sources using the characteristic equations of the pumps and system head equations as constraints. The minimum desired efficiency of the pumps affects the optimal solution. The developed model will be helpful to the field engineers working in the departments of water supply and irrigation.

5. REFERENCES

i.   Church, A. H. and Lal, J. (1973). Centrifugal pumps and blowers. Metropolitan Book Co. Pvt. Ltd. Delhi -6, India.
ii.   LINDO (2003). Demo LINGO Release 8.0, LINDO System, Inc., Chicago.
iii. Punmia, B. C., Jain, A. K. and Jain, A. K. (2010). Water supply engineering, Laxmi Publications (P) Ltd. New Delhi, India.
iv.Mahar, P. S. and Singh, R. P. (2014). "Optimal design of pumping mains considering pump characteristics". Journal of Pipeline Systems Engineering and Practice, Vol. 5 (1) p.p. 04013010-1,6.

A Delta Wing Protected Bridge Pier Under Steady And Unsteady Flows

Vikas Garg[1]   Baldev Setia[2]   D V S Verma[3]
[1]Professor & Head, Civil Engineering Department, University of Petroleum & Energy Studies, Dehradun 248007, India
vgarg@ddn.upes.ac.in
[2]Professor, Civil Engineering Department, National Institute of Technology, Kurukshetra
Email: setia_b@rediffmail.com
[2]Professor, Civil Engineering Department, PDM College of Engineering, Bhadurgarh
Email: dvs_verma@yahoo.co.in

ABSTRACT : Among the three facets of bridge pier scour, namely prediction, mechanism and protection, there is a significant thrust on devising means and techniques to prevent or at least reduce scour. The present paper is the result of an experimental study carried out to check the efficacy of a delta like wing to protect a bridge pier against local scour. The delta wing is installed on the upstream of pier and works on the principle of modification of flow so as

to cause scour away from the pier and deposit the sediment near the pier. The study was conducted by employing a delta wing of size 1.75D: 1.5D: 0.5D on a circular glass cylinder of diameter 6.2 cm. Experiments were run in a water channel under steady as well as unsteady flows to include both, clear water scour and live bed scour. Unsteadiness of flow was attained by varying the discharge in nine to eleven discrete steps, first in an increasing and then in a decreasing manner. The discharge intensity was increased from 0.02 m³/sec/m in the first step to 0.065 m³/sec/m in the fifth or sixth step, usually in time durations of 30 minutes each. The discharge was then made to retrack its journey back to the lowest value in the ninth or eleventh step. For a prismatic laboratory channel, this implied a proportional variation in the depth of flow and velocity as well. The discharge pattern thus resembled a more or less unskewed flood hydrograph. It is worthwhile to note that the maximum scour depth does not correspond to the peak discharge but lags behind the peak discharge and velocity by a time step to reach the peak. Thereafter, the scour depth decreases indicating the deposition of suspended sediment and reduced scour activity. It was observed that during the last phase of experimental run, through the flow conditions revert to those in the initial step, yet the scour depth does not decrease proportionally. Scour depth with and without the use of delta wing has been compared and presented. The delta wing is device which is capable of reducing scour and the performance is comparable to devices such as, a group of piles or a slot through the pier. However, the delta wing has its limitations as it has a tendency to record more scour when the flow is not aligned to the pier.

Keywords: Scour, Horse shoe vortex, Passive device, hydrographic run

1. INTRODUCTION:

Bridges are the integral part of the transportation network of a country. Failure of an important bridge can lead to a big loss of life and material. Failure of bridges is attributed to either structural or hydraulic factors. Scour around a bridge pier is one of the major possible causes of hydraulic failures of a bridge. Bridge piers in a flow cause a horizontal constriction of flow. The local scour around bridge piers depends strongly on the geometry of the pier. The basic mechanism causing local scour at piers is the down-flow at the upstream face of the pier and formation of Horse Shoe vortices at the base. The horseshoe vortex is responsible scrapping sediment from in front of the pier and releasing it downstream of the pier. The prevention or reduction of local scour has also been a subject of importance along with the studies on scour prediction and scour protection. The genesis of the geometry and mechanism of a particular protection device is to counter the ill-effects of the scouring horseshoe vortex by not allowing this vortex to grow or by retaining and confining the vortex on an impenetrable

rigid   surface.
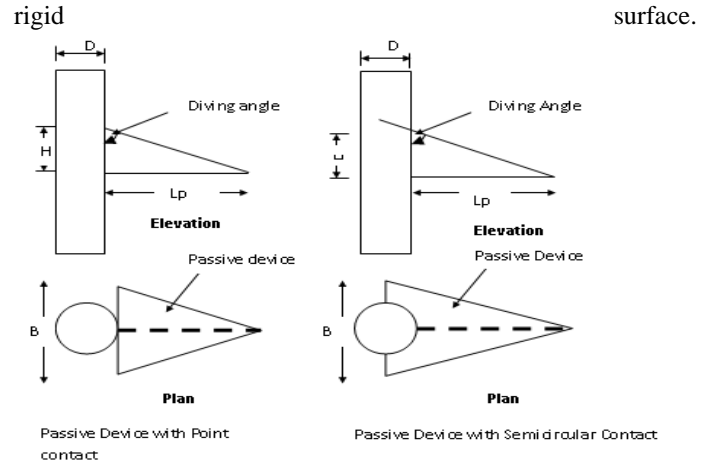
Figure 1: Definition Sketch of Delta - Wing - Like - Passive Device
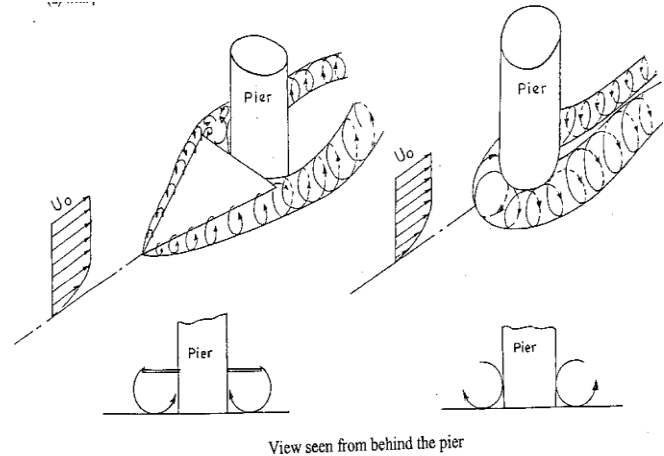
Figure 2: Mechanism of Delta - Wing - Like - Passive Device

A delta wing like passive device henceforth referred to as a passive device is attached to the leading edge of pier model to prevent scouring at a cylindrical pier shown in figure 1. The device
has its origin in the aerodynamics for prevention of scour by channelizing the strength of horseshoe vortex. Concept of Delta - Wing - Like - Passive Device was employed successfully by Gupta (1987), T.D. Nghien (1988), Setia (1997) at Indian Institute of Technology, Kanpur. Its geometrical shape is characterized by an isosceles triangle planform and a thin vertical spinal rib attached on the bottom side of it along its line of symmetry. The vortices generated by a well-known delta wing are utilized as a scour protection device in the present study. The two leading edge stream wise vortices generated by delta wing with its upstream tip pointing upward wrap towards each other and move to downstream side. These vortices are formed on the upper side of delta wing. When the delta wing is tilted to point downward, the vortices are generated below the wing, wrap towards each other and move to the downstream

side. This forms the basis for using a delta wing as a scour protection device. A suitable delta wing like plate attached to leading edge of a pier junction can modify hydro dynamically the primary horse shoe vortex as shown in Figure 2.

2. EXPERIMENTAL SET UP:

Experiments were carried out under uniform flow conditions at incipient velocity (Approx. 20 - 21 cm/sec) for clear water scour and velocity was varied for hydrographic run. In order to minimize the effect of depth of flow on scouring, the ratio of depth of flow to diameter of the pier, h/D was kept more than 2.5 based on the recommendation of Ettema (1980), Chiew (1992). The depth of flow was maintained 16 cm to 17 cm while Froude Number was maintained 0.15 to 0.18. Reynold Number is taken less than 2000 because flow condition was kept laminar (Re = 1300 to 1600). Experimental run was kept for 300 minutes for steady flow and for unsteady flow 330 minutes.

3. RESULTS AND DISCUSSION:

In this study, experimentation was carried out on the passive device around circular bridge pier for clear water scour as well as for live bed scour. During this study, effect of Variation of Dimensions of Passive Device with point contact and semicircular contact is discussed for clear water scour and in the form of hydrographic run.

3.1 Effect of dimensions of passive device on maximum scour depth:

A passive device is fabricated with a triangular plate and a web or flow splitter is provided at the center of triangular plate below the triangular portion on the upstream face of bridge pier. The geometry of passive device was chosen for point and semicircular contact around circular pier. Point Contact touched the pier at midpoint of base width, whereas for semicircular contact, it engulfed the bridge pier up to the front half of bridge pier. Figure 1 shows the positions of both passive device and semicircular contact with bridge pier. Both the passive devices were provided at the upstream face of bridge pier wherever opposite to the direction of flow to check their efficacy against scour. Point contact and semicircular contact of the passive devices were discussed in clear water condition as well as hydrographic run.

3.2 Point contact under clear water condition:

Experiments were conducted by varying length, base width of triangular plan form and for different web height of passive device for clear water condition.

3.2.1 Length of passive device

The length of passive device is the length of the diagonal of the splitter web running from the upstream face of the cylindrical pier to the pointed end of the device for point contact. This dimension of passive device was varied from 1.0D to 2.5D in increments of 0.25D while the base width and web height were held constant at 1.5D and 0.5D, respectively. After performing experimentation, the length of 1.75D was considered as the optimum length for the passive device. Figure 3 shows there is not substantial increase in performance potential after length of 1.75D. The separation zone extends up to a distance of 1.75D in the upstream side of bridge pier (Setia, 1997). Hence any scour prevention device, which is expected to provide the protection against scour by modifying the flow, should extend at least up to the separation zone i.e. 1.75D. Thus the length of 1.75D for the passive device is also in agreement with the flow separation zone around a circular bridge pier.
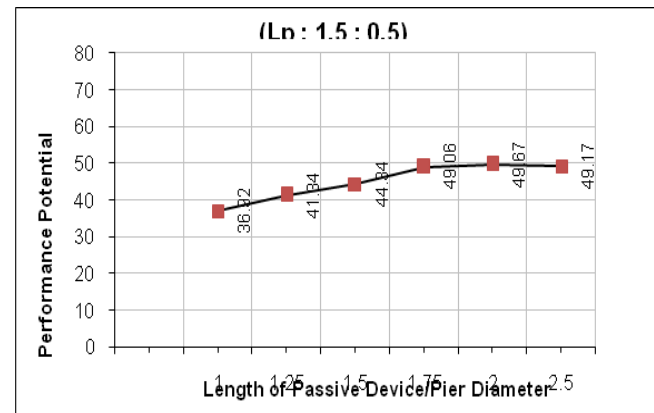
Figure 3: Effect of Length of Passive Device (Point contact) on Performance Potential

3.2.2 Width of passive device

The base or shoulder width is the dimensions of the device measured transverse to the flow at the position of its point of contact with the cylinder. A number of experiments were conducted by varying base width from 1.0D to 2.5D with an increment of 0.5D while the length and web height were held constant at 1.75D and 0.5D, respectively. It was observed that as the width of the device goes on increasing from 1.0D to 2.5D, the scour depth goes on decreasing consequently beyond 1.5D there is a marginal decrease in scour depth upto 2.5D. Figure 4 shows that the largest difference lies among the values is less than 0.6D. Then the base width of passive device of 1.5D was chosen in which maximum scour depth of 0.54D was noted around bridge pier.
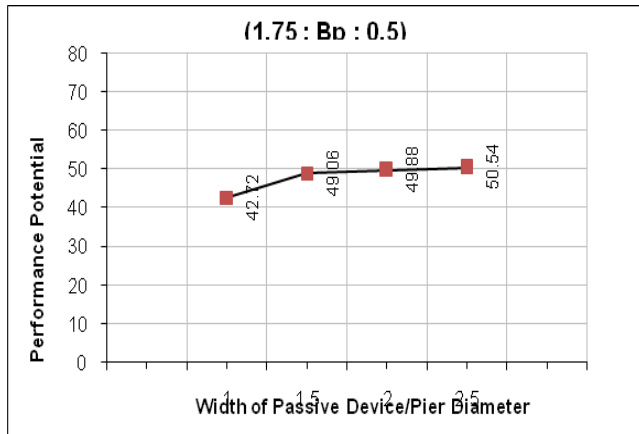
Figure 4: Effect of Width of Passive Device (Point contact) on Performance Potential

3.2.3 Web height of passive device

A thin vertical spinal rib is attached to triangular portion of delta wing on the bottom side along the line of symmetry is termed as web of the device. It provides the negative angle of attack to delta-wing and also prevents interaction between the two leading edge vortex sheets. This web is a triangular plate, having minimum height at the base and maximum height at the vertex of the triangular delta wing. The height of the web which touched the base of the delta wing was varied for the experiments under this set maintaining, the web height at the vertex of the triangular planform is zero. To find out the effect of web height variation form 0.1D to 1.0D with an increment of 0.1D while the length and base width were held constant at 1.75D and 1.5D, respectively.

In general, maximum depth of scour reduces gradually as height of web increases but after a certain height of web, maximum scour depth starts increasing. The scour depth at very small web heights, the device shields the effect of the horse shoe vortex as a partial triangular plate placed on or near the sediment bed upstream of the pier. The increase in scour depth at higher values of web height is due to larger obstruction to flow offered by the pier with passive device in such a position. This way the base angle at the nose of the device goes on increasing, gradually drifting it towards an unstreamlined shape. Thus web height of 0.5D was adopted which results into a scour depth of 0.54D shown in Figure 5.
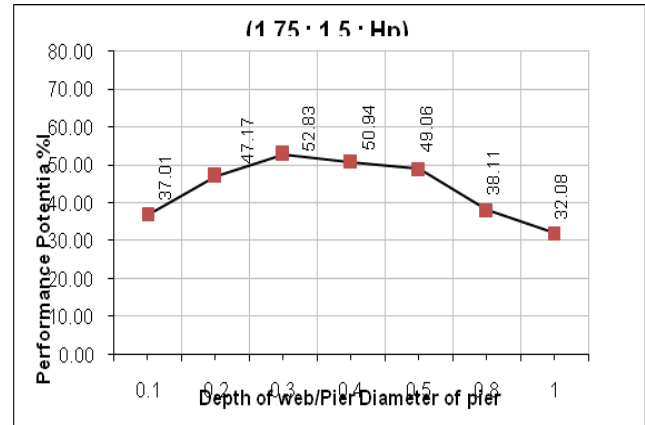
Figure 5: Effect of web height of Passive Device (Point contact) on Performance Potential

Optimum dimensions of delta wing like passive device Lp: Bp: Hp:: 1.75D: 1.5D: 0.5D were selected which provides maximum reduction of scour depth and performance potential of 49.06% for point contact at circular bridge pier with reference to an unprotected pier.

3.3 Semicircular contact under clear water condition:

Experiments with a similar scheme were conducted for a semicircular contact of the passive device on a circular pier. The length of passive device is the length of the diagonal of the splitter web running from the upstream face which is engulfed in semicircular portion of bridge pier of to the pointed end of the device. The base or shoulder width is the dimensions of the device measured transverse to the flow at the position for semicircular contact it is designated so at the level of an imaginary plane passing through the center of Pier. On similar reasoning of point contact, the length and base width of passive device 1.75D and 1.5D was considered as optimum length and base width for semicircular contact also. The variation of scour depth was done with base width of 1.5D for length as 1.75D and web height from 0.1D to 1.0D shown in figure 6. The effectiveness of the protection device in terms of performance potential for semi-circular passive device of size Lp: Bp: Hp :: 1.75D: 1.5D: 0.5D is 64.30% with reference to the scour of an unprotected circular bridge pier. This size of passive device proves to be providing maximum efficacy against scour fitted with semicircular contact at a circular bridge pier.

3.4 Comparison between point and semicircular contact for circular pier:

A comparison of performance potential for point contact and semi circular contact devices for length and base width of delta as 1.75D and 1.5D and for different web depth varying from 0.1D to 1D is shown in Figure 6. It can be clearly seen from the

figure that semicircular contact device around a cylindrical pier protects more than a point contact device in almost all the cases. A Passive device having length of 1.75D, base width of 1.5D and web height of 0.5D provides a performance potential of 49.06% and 64.30% for point contact and semicircular contact, respectively.
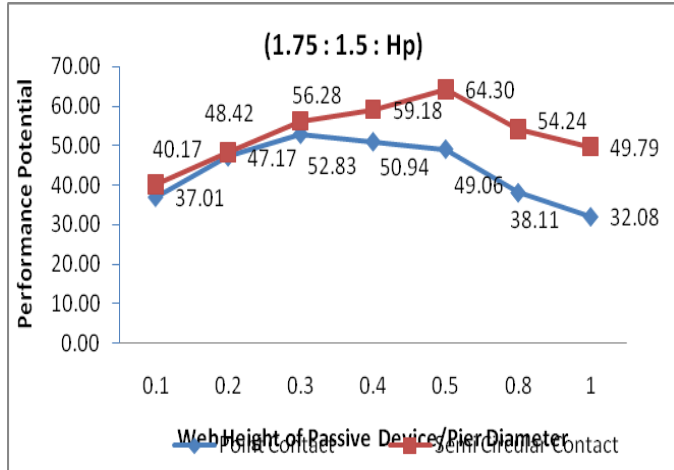
4. HYDROGRAPHIC RUN:

Effect of unsteady flow was investigated to simulate somewhat natural conditions in the form of hydrographic run. Flow in the form of a simulated symmetric single peaked hydrograph was offered on to a circular bridge pier protected by an optimum passive device for point contact as well as for semicircular contact.

4.1 Point Contact under Hydrographic Conditions:

A single peaked hydrographic discharge was simulated by varying velocity from 16 cm/sec to 28 cm/sec in five increments at interval of 30 minutes each and decreased back to 16 cm/sec in further five decrements at same time interval (Figure 7). Initially very less scour depth of the order of 0.12D was recorded corresponding to flow velocity of 16 cm/sec after the attack of flow for 30 minutes duration. Thereafter the scour depth showed an increase on account of increase in the velocity at every 30 minutes interval. The peak value of 0.74 D was observed at seventh interval (sixth increment) corresponding to flow velocity of 27 cm/sec. Interestingly, the peak value did not appear at sixth interval which is at highest velocity of 28 cm/sec. Performance potential of the device was observed 30% in live bed scour. The reason can be attributed to probably the less time interval (30 minutes) allowed for the flow to attack.
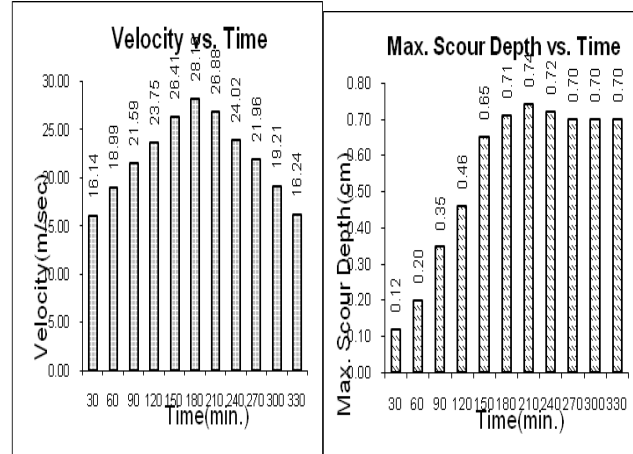
Figure 7: Hydrographic Run for Delta Wing Like Passive Device (Point Contact)
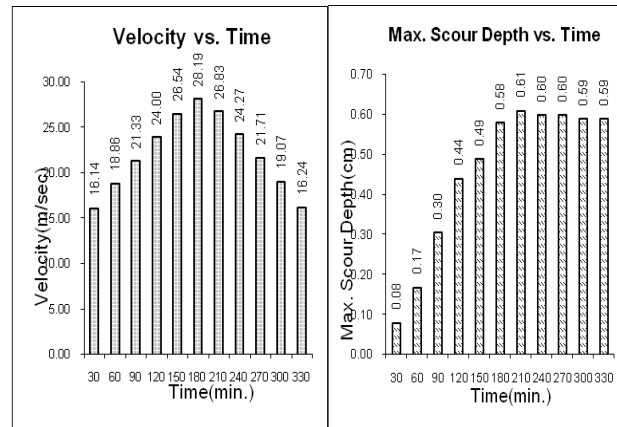
Figure 8.17: Hydrographic Run for Delta Wing Like Passive Device

Figure 8: Hydrographic Run for Delta Wing Like Passive Device (Semi Circular Contact)

4.2 Semicircular contact under hydrographic conditions:

On similar lines the hydrographic flow was offered to passive device with semicircular contact with velocity ranging from 16 cm/sec to 28 cm/sec and back to 16 cm/sec in 10 regular intervals of 30 minutes each. Similar trend of the variation in scour depth was observed as for a point contact but the performance potential of the device in semicircular contact was found to be about 38% which is 8% lesser than the performance potential of point contact. This observation clearly indicates that the effectiveness of semicircular contact is more as compare to point contact. The reason for this higher efficacy can be attributed to the fact that a semicircular contact offers higher sheltering around the bridge pier in comparison to point contact.

5. CONCLUSIONS:

The delta wing like passive device is having its origin from aerodynamics. The genesis of the geometry and mechanism of a particular protection device is to counter the ill-effects of the scouring horseshoe vortex by not allowing this vortex to grow or by retaining and confining the vortex on an impenetrable rigid surface. A detailed investigation into various features of the device has helped in drawing the following conclusions.

I.   The optimum dimensions of passive device namely length (L_p), base(B_p) and web height(H_p) have been selected as 1.75, 1.5 and 0.5 times the diameter or size of pier for circular bridge pier.

II.   The passive for optimum dimensions reduce scour by 49.06% and 64.24% for point contact and semicircular contact, with respect to an unprotected cylindrical pier under uniform flow conditions for 300 minutes durational run.

III.   A comparative study was also carried out in between point and semicircular contact, and then semicircular contact of passive device with the bridge pier performs better than point contact.

IV.   Hydrographic run was carried out for point contact of passive device which is able to reduce scour 30% in comparison to unprotected bridge pier. In case of semicircular contact, passive device reduces scour about 38% on the upstream side of bridge pier.

V.   Semicircular contact performs better than point contact. Because semicircular contact offers higher sheltering around the bridge pier in comparison to point contact.

VI.   The device is also sensitive to its particular location. Any change in its location, vertically or horizontally, affects its performance.

REFERENCES

i. A.K. and Gangadharaiah, T. (1992), "Local Scour Protection by a Delta-Wing Like Passive Device.", Proc. of the VIII congress of APD-IAHR,Vol.. II, CWPRS, Pune, India

ii.   Chiew, Y.M. (1992), "Scour Protection at Bridge Piers" J. Hydr. Engg., ASCE, 118(9),1260-1269.

iii. Gupta, A.K. and Shanna, S.c. (1989), "On the Mechanism of Horseshoe Vortex Modification by a Passive Device." Proceeding of the Fourth Asian Congress of Fluid Mechanics, Hong Kong. Pp A150-A153.

iv. Ettema, R. (1980). Scour at Bridge Piers. University of Aukland, School of Engineering, Report No. 216.

v. Garde, R.J. (1995), "Scour Around Bridge Piers," ISH-News,VoI.. 4, No.2, Indian Society for Hydraulics, CWPRS, Pune, India

vi.   Garde, R.J. (1995). Scour Around Bridge Pier. ISH-News, Vol.4, No.2, Indian Society for Hydraulic Research, CWPRS, Pune, India.

vii.   Setia, Baldev (1997). Scour around Bridge Piers: Mechanism and Protection. Ph.D. Thesis, Department of Civil Engineering, Indian Institute of Technology, Kanpur, India.

viii.   T.D.Nghien (January, 1988). "Laboratory investigation of scour reduction near   bridge pier by delta-wing-like passive device". M.Tech.Thesis, I.I.T Kampus, India.

Explicit Equation For Sediment Threshold

ShriRam
[1]Associate Professor, Department of Civil Engineering,
M.M.M.U.T., Gorakhpur-273010 (U.P.)
Email:src_gkp@rediffmail.com

ABSTRACT : The Shields diagram remains the most widely used criterion even today for incipient motion of sediment. However, its implicit nature makes its applications rather inconvenient. In this paper, an explicit equation of different investigators has been presented in a tabular form which may be beneficial for further study. An explicit equation has been derived on the basis of Madsen and Grant (1976) approach and an explicit equation has been recommended to be used for the computation of critical shear velocity and thus sediment critical velocity for cohesion-less sediments and steady uniform flow condition as well as it is also useful to calculate shear stress over sloping bed.
Keywords: sediment transport; incipient motion; Shields diagram; Critical shear velocity; sediment fluid parameter.

1.   INTRODUCTION

The initiation or ceasing of motion of sediment particles is involved in many geomorphic and hydraulic problems including stream stability and scour at highway bridges, sediment transport, erosion, slope stability, stable channel design, and design of riprap. These problems can only be handled when the threshold of sediment motion is fully understood. Beginning of motion can be related to either shear stress on the grains or the fluid velocity in the vicinity of the grains. When the grains are at incipient motion, these values are called the critical shear stress or critical velocity. The choice of shear stress or velocity depends on: (i) Which is easier to determine in the field; (ii) The precision with which the critical value is known or can be determined for the particle size; (iii) The type of problem.

In sediment transport analysis most equations use critical shear stress. In stable channel design either critical shear stress or critical velocity is used; whereas, in rip-rap design critical velocity is generally used. The average shear stress on the bed/boundary is given by $\tau_0 = \gamma RS$, where γ is the unit weight of water, R is the hydraulic radius, and S is the slope of the energy grade line. In wide channels (width equal to or greater than 10 times the depth) $R \approx h$, the depth of flow. Other relations give the shear stress in terms of the velocity of flow.

Water flowing over a bed of sediment forces that tends to more or entrain the particles. The forces that resist the entraining action of the flowing water differ depending upon the properties of bed material. For coarse sediments such as sands and gravels, the resisting forces relate mainly to the weight of

the particle, its position relative to other particles, and the form of bed roughness. For cohesive bed material (generally silts and clays) , chemical bonding between particles resisting the beginning of motion.

When the forces of the flowing water (as measured by the sheer stress or velocity) are less than some critical value, the bed material of a channel remains motionless. Then, the alluvial bed can be considered as immobile, but when the shear stress or velocity remains motionless. Then, the alluvial bed can be considered as immobile. But when the shear stress or velocity over the bed attains or exceeds its critical value, particle movement is difficult in nature. The most dependable data available have resulted from the laboratory experiments.

The sediment threshold or beginning of motion is difficult to define. This difficulty is a consequence of a phenomenon that is random in time and space. When the shear stress is near to its critical value, it is possible to observe a few particles moving on the channel bottom. The time history of the movement of a particle involves long rest periods. In fact, it is difficult long rest periods. In fact, it is difficult to conclude that particle motion has begun, Kramer (1935) and Buffington (1999) has proposed four levels of motion of bed materials.**(i)None; (ii) Weak movement** – only a few particles are in motion on the bed. The grains moving on one square centimetre of the bed surface can be counted. **(iii) Medium movement**- the grains of the mean diameter begin to more. The motion is not local in character but the bed continues to be flame; and **(iv) General Movement**- All mixture is in motion; the movement is occurring in all parts of the bed at all times. It is sufficiently vigorous to change the bed configuration.

When the hydrodynamic forces acting on a grain of sediment have reached a value that, if increased even slightly the grain will more, critical or threshold conditions are said to have been reached, under Critical conditions the hydrodynamic forces acting upon a grain are just balanced by the resisting force of the particle. In this paper, on the basis of Shields (1936) theory, and Madsen and Grant (1976) theory based on non-dimensional number. i.e. sediment-fluid parameter an explicit form of equation has been developed. It may not be sufficient to determine the average value of the critical shear stress or velocity because both quantities are fluctuating. For the same mean values, they may have larger values that act for a sufficient long enough time to cause a particle to move. In addition, the forces on the particle resulting from the flowing water, waves, and seepage into or out of the bed or banks affect the beginning of motion. Finally an explicit equation has been developed.

2.   SHIELDS DIAGRAM

Shields (1936) was one of the first who applied similarity approach to sediment studies. Since there are many uncertainties in turbulent flows and loose boundary materials, it is very difficult to formulate critical shear stress analytically. Shields then turned to a similarity approach or dimensional analysis to arrive at two important dimensionless variables: Shields dimensionless shear stress,

$$\theta_{cr} = \frac{\tau}{(s-1)\rho g d} \tag{1}$$

and   particle   Reynolds   number,
$$Re_* = \frac{u_* d}{v} \tag{2}$$

where τ_0 = bed shear stress, s = specific gravity of the sediment, ρ = specific gravity of water, g = acceleration due to gravity, d = sediment diameter, $u_* = \sqrt{\tau_0/\rho}$ = shear velocity, v = Kinematic viscosity of water.

Introducing the critical shear stress, τ_{0c}, Shields claimed that when a sediment particle is about to move, the following dynamic similarity law must be true,

$$\frac{\tau_{oc}}{(s-1)\rho g d} = f\left(\frac{u_{*c} \cdot d}{v}\right) \tag{3}$$

In which $u_{*c} = \sqrt{\tau_{oc}/\rho}$ Shields' determined equation (3) experimentally, as shown in Figure 1. The Shields' diagram expresses a relation between the critical mobility Shields' parameter (θ_{cr}) and the hydraulic condition on the bed, which is represented by a dimensionless parameter i.e. particle Reynolds number ($Re_* = u_* d/v$). This particle Reynolds number is based on grain size and shear velocity. The threshold of motion will occur when the mobility Shields' parameter (θ_c) is greater than the critical mobility Shields' parameter, θ_{cr}.
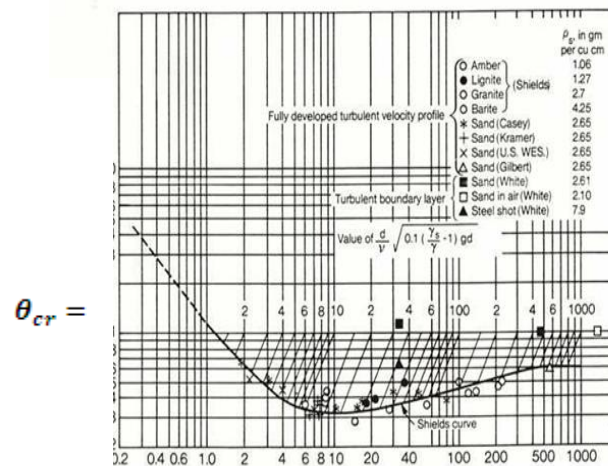
figure-1 Shields diagram for Sediment Threshold

Boundary Reynolds number, $Re_* = \frac{u_* d}{v}$

[**Note:** There are two striking things about Figure-1 i.e. (i)-there is considerable scatter in the data points, and (ii)- Shields had no data for Re_* less than about 2 or greater than 600]

These parameter can be expressed by:

$$\theta_{cr} = \frac{\tau_{oc}}{(s-1)\rho gd} = \frac{u_{*c}^2}{(s-1)gd} \qquad \qquad 4(a)$$

and,

$$Re_{*c} = \frac{u_{*c}d}{v} \qquad \qquad 4(b)$$

$$\theta = \frac{\tau_o}{(s-1)\rho gd} = \frac{u_*^2}{(s-1)gd} \qquad \qquad 4(c)$$

where,

$$u_* = \sqrt{ghs} \qquad \qquad 4(d)$$

The use of Shields' diagram is not appropriate for practical purpose because the u_* value appears in both axes of the diagram and can be only solved by trial and error. With the wide applications of numerical modelling, a mathematical expression for equation (4) is necessary. This imperfection of the Shields' diagram can be eliminated by introducing the particle parameter, d_*, which is represented by (Yalin,1977);

$$d_* = \left(\frac{Re_*^2}{\theta}\right)^{1/3} = d\left[\frac{(s-1)d}{v^2}\right]^{1/3} \qquad (5)$$

3. EXISTING EXPLICIT EQUATIONS FOR SEDIMENT THRESHOLD

In 1930's Shields conducted a number of experiments in Berlin and found that there was a narrow band of demarcation between motion and no motion of bed particles, corresponding to sediment threshold. He presented these on a curve (Figure 1) of θ versus Re_*. A slight problem with this is that the fluid velocity (in the form of shear velocity) occurs in both quantities. Thus it is more reasonable to introduce the dimensionless grain size, d_*

Here, we can observe, the meaning of, d_*. If we take a common value of $s = 2.65, g = 9.81\ m^2/s, v = 1 \times 10^{-6} m^2/s$ at $20°C$, then we can obtain $d_* = d \times 25000$ in units of meters. If $\emptyset$ is specified in terms of millimetres then we have $d_* \approx 25d$, and so hence for a range of different particle sizes. we can have a value of d_* as.

d(mm)	0.004	0.04	0.40	4.00	40.00
d_*	0.10	1.00	10.00	100.00	40.00

So, on the basis of Shields' results we obtain results for sediment threshold, giving the critical value θ_{cr};

$$\theta_{cr} = 0.13 d_*^{-0.392} - \exp\left(-0.015 d_*^2\right) + 0.045\left(1 - \exp(-0.068 d_*)\right) \qquad (6)$$

For a small particles there appears to be a linear relationship, while for a large particles the critical shear stress, based on Shields laboratory experiments, approaches a constant value of about 0.045. A simple algebraic expression that of its Shields' curve closely was proposed by Soulsby and Whitehouse(1997):

$$\theta_{cr} = \frac{0.24}{d_*} + 0.055[1 - \exp(-0.02 d_*)] \qquad (7)$$

However, using more recent data, Soulsby (1997) observed much smaller values for θ_{cr} when $d_* < 2$. Thus he proposed a modification of Eq(7).

$$\theta_{cr} = \frac{0.30}{1 + 1.2 d_*} + 0.055[1 - \exp(-0.02 d_*)] \qquad (8)$$

It is, however, difficult to define the exact threshold of sediment transport from the incipient motion regime where a few particles on the bed surface motion which corresponds to a well defined and reproducible transition from occasional motion to general motion of the uppermost particles. In order to avoid trial and error solutions, alternative parameters are proposed by some researchers allowing direct computation of the critical shear velocity (or stress) through the entrainment function, θ_{cr}, without recourse to an iterative procedure. Some of the existing explicit formula and functions proposed for Shields' type diagram are given in Table-1.

Table-1 Explicit Empirical Equations for the Shields Diagram

S.No.	Researchers	Equation
1.	Bonnefille (1963)	$\theta_{cr} = \begin{cases} 0.118 d_*^{-0.468}; & d_* < 2.33 \\ 0.137 d_*^{-0.648}; & 2.33 \le d_* < 9.15 \\ 0.063 d_*^{-0.298}; & 9.15 \le d_* < 15.28 \\ 0.9 d_*^{0.424}; & 15.285 \le d_* < 58.3 \end{cases}$
2.	Brownlie(1981)	$\theta_{cr} = 0.22\beta + 0.06 \times 10^{-7.7\beta}, \beta = \left[\frac{d_*}{v}\left((s-1)g d_*\right)^{0.5}\right]^{-0.60}$
3.	Chien and Wan(1983)	$\theta_{cr} = \begin{cases} 0.126 d_*^{-0.44}; & d_* < 1.5 \\ 0.131 d_*^{-0.55}; & 1.5 \le d_* < 10.0 \\ 0.0685 d_*^{0.27}; & 10 \le d_* < 20 \\ 0.0173 d_*^{0.19}; & 20 \le d_* < 40 \\ 0.0115 d_*^{0.30}; & 40 \le d_* < 150 \\ 0.052; & d_* \ge 150 \end{cases}$
4.	van Rijn(1984)	$\theta_{cr} = \begin{cases} 0.24 d_*^{-1.00}; & d_* < 4.0 \\ 0.14 d_*^{-0.64}; & 4.0 \le d_* < 10.0 \\ 0.04 d_*^{0.10}; & 10 \le d_* < 20 \\ 0.013 d_*^{0.28}; & 20 \le d_* < 150 \\ 0.055; & d_* \ge 150 \end{cases}$

5.	Guo(1990)	$\theta_{cr} = 0.1R_*^{-0.667} + 0.054[1 - \exp(-0.1R_*^{0.52})];$ where, $R_* = \dfrac{d_s}{v}[0.1(s-1)g\,d_s]^{0.50}$
6.	Guo(1990)	$\theta_{cr} = 0.23d_*^{-1.0} + 0.054[1 - \exp(-0.0435d_*^{0.85})];$
7.	Paphitis(2001)	$\theta_{cr} = \dfrac{0.273}{1 + 1.2d_*} + 0.046[1 - 0.576\exp(-0.02d_*)];$ $0.01 < Re_* < 10^4$
8.	Hager and Oliveto(2002)	$\theta_{cr} = \begin{cases} 0.12d_*^{-0.50}; & d_* < 10 \\ 0.026d_*^{0.167}; & 10 \le d_* < 150 \\ 0.06; & d_* \ge 150 \end{cases}$
9.	Shippard and Renna(2005)	$\theta_{cr} = \begin{cases} 0.25 + 0.1d_*^{0.50}; & 0.1 \le d_* < 3 \\ 0.023d_* - 0.000378d_*\ln d_* - 0.005\ ; & 3 \le d_* < 150 \\ 0.0575; & d_* \ge 150 \end{cases}$
10.	Cao et al. (2006)	$\theta_{cr} = \begin{cases} 0.1414R_d^{-0.2306}; & R_d \le 6.61 \\ \dfrac{[1 + (0.0223R_d)^{2.8358}]^{0.3542}}{3.0946R_d^{0.6769}}; & 6.6 \le R_d < 282.84 \\ 0.045; & R_d \ge 282.84 \end{cases}$

4. DATA SOURCE FOR STUDY

The different data used in the present study are from experiments that were undertaken in flumes with parallel side-walls under steady uniform flows over cohesionless sediment bed. The sediments used in these study include a variety of natural and artificial grains of quartz and near-quartz densities and coals in beds consisting of nearly uniform grain sizes. The data compiled had their threshold/incipient conditions established either : (i) some form of visual definition; or (ii) from the extrapolation of transport rates to either zero or a low reference value. Table-2 summarises all the sources utilized such as sediment material and fluid involved in the experiments. A total of 223 independent data set are used.

TABLE-2 Data sources, sedimentary material used for Investigations and Ambient Fluid for Experiments included in the analysis undertaken as part of present investigation.

S.No.	Data Source for Comparison	Material/fluid
1.	Gilbert (1914)	Sand/water
2.	USWES (1935)	Sand/water
3.	Cosey (1935)	Sand/water
4.	Kramer (1935)	Sand/water
5.	Shields (1936)	Sand, granite, fragments/water
6.	White (1970)	Sand, crushed silica, lead glass spheres/water
7.	Rao and Sitaram (1999)	Sand/water
8.	Dancey et al. (2002)	Spherical glass bead/water
9.	Marsh et al. (2004)	Sand/water

5. COMPARISON OF CRITICAL SHEAR VELOCITY PREDICTION

Some of most widely used methods as given in Table-3 has been compared with the data of different investigators as given in Table-2. The ability of each of the above methods in predicting incipient motion are tested against the experimental data of different investigators of Table-2, and the correlation coefficients (R^2), slope of lines of best fit (i.e. slope), and root mean squared errors (RMSE) are given in Table-3. The correlation coefficients for Bonnefille (1963); Chien and Wan (1983); van Rijn (1984); Soulsby (1997); Soulsby and Whitehouse (1997); Paphitis (2001); Hager and Oliveto (2002); Sheppard and Renna (2005), and Cao et al. (2006) are approximately same. Paphitis (2001) method has a high R^2, a slope near unity, and a low RMSE. The low RMSE of Paphitis (2001) method shows that it predicts U_{*c} values consistently close to the experimental values.

TABLE-3 Comparison of Different Methods of Predicting Incipient Motion

S.No.	Author/Investigator	R^2	RMSE	Slope
1.	Bonnefille (1963)	0.8667	0.01234	1.162
2.	Chien and Wan (1983)	0.8589	0.01268	1.1578
3.	van Rijn (1984)	0.8437	0.01360	1.2163
4.	Soulsby (1997)	0.8490	0.01310	1.181
5.	Soulsby and Whitehouse (1997)	0.8586	0.01260	1.1590
6.	Paphitis (2001)	0.8678	0.01058	1.0726
7.	Hager and Oliveto (2002)	0.8606	*0.01456*	1.182
8.	Sheppard and Renna (2005)	0.861	0.0148	1.2386
9.	Cao et al. (2006)	0.868	0.0107	1.0693

Note : The RMSE is a measure of the deviation of the prediction from the line of perfect agreement (i.e. slope of 1)

6. DEVELOPMENT OF NEW EQUATION

Shields (1936) who studied the initial motion of sediment in steady flow on a flat bed. Shields offered this relationship as

$$\theta_{cr} = \frac{\tau_{oc}}{(s-1)\rho g d} = f\left(\frac{u_{*c}d}{v}\right) \qquad (9)$$

where, θ_{cr} = Shield's critical parameter; τ_{oc} = bottom shear stress; ρ = density of the fluid; s = specific gravity of sediment; d = grain size of the sediment; g = acceleation due

to gravity; and $\theta_{cr} =$ the ratio of the shear atress acting on a unit area of the bed to the submerged weight of particles in that same area.

The two parameters in the Shield's diagram i.e. θ_{cr} and Re_*, both depend on the flow characteristics and the friction velocity, u_*, appears in both the axes and hence θ_{cr} in Eq. (9) is implicit, and τ_{oc} needs to be iterated. To overcome this weakness, new variable i.e. $s_* = d[(s-1)gd]^{1/2}/(4v)$ is introduced to rewrite Eq. (9) explicitly as $\theta_{cr} = F(s_*)$ because Re_* is also a function of s_* i.e.

$$\frac{u_* d}{v} = \left[\frac{\tau_{oc}}{(\rho_s - \rho_w)gd} \times \frac{g(\rho_s - \rho_w)d^3}{\rho \cdot v}\right]^{0.50} \qquad (10)$$

From which we obtain $s_* = g_1(u_* d/v)$ or $(u_* d/v) = g_2(s_*)$. Thus, finally the modified Shields' criterion, $\theta_{cr} = G(s_*)$, may be approximated as, Madsen et al. (1976) converted the Shields diagram into the diagram showing the relation between the critical Shields' parameter, θ_{cr}, and the so-called sediment fluid parameter, s_*

$$s_* = \frac{d[(s-1)gd]^{1/2}}{4v} \qquad (11)$$

$$\theta_{cr} =$$
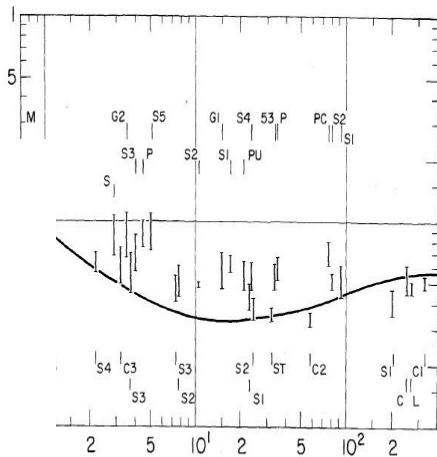
Fig   **dsen and Grant (1976) diagram**

The Madsen et al. (1976) diagram is shown in Figure.2. The solution by this method also require graphical interpolation. Hence always chances of human error. Thus for this graphical presentation between θ_{cr} and s_* following equations are obtained.

$$\theta_{cr} = 0.101s_*^{-2.687}; \, for \, s_* < 0.80 \qquad\qquad s_* = \frac{d[(s-1)gd]^{1/2}}{4v}$$

$$\theta_{cr} = 0.119s_*^{-0.667} + 0.0551[1 - \exp(-0.0504s_*^{0.664})]; \, for \, s_* < 300 \qquad 12(b)$$
$$\theta_{cr} = 0.0551; \, for \, s_* \geq 300 \qquad 12(c)$$

However, for very fine grain sizes, Eq (12) greatly over predicts the data. Force consideration by Bagnold (1959) showed that θ_{cr} cannot exceed a value of about 0.30, because this exerts a sufficient force on the grains to overcome the weight of every grain in the topmost layer of the bed. A correction to account for this has been made to Eq. (12) to give an improved threshold bed shear stress formula i.e.

$$\theta_{cr} = \frac{0.307}{1 + 3.03s_*^{0.667}} + 0.055[1 - \exp(-0.0504s_*^{0.667})]; \qquad (13)$$

It must be noted that Eqs. (12) and (13) apply to the threshold of motion on an initially flat horizontal bed. If the bed is rippled, these results i.e. Eqns. (12) and (13) apply to only to the skin friction component of the bed shear stress. Eqns (12) and (13) both give an approximately constant value of $\theta_{cr} = 0.0551$ for larger grain size i.e. $s_* \geq 300$.

This value of, θ_{cr} i.e. Eq.(14) does not take slope into effect. The equation (13) can be also used for computation of θ_{cr} at an angle of, β, in the longitudinal direction. i.e.

$$\theta_{cr,\beta} = \cos\beta\left(1 - \frac{\tan\beta}{\tan\phi}\right)\theta_{cr} \qquad (14)$$

where, ϕ = angle of repose of soil; and β = slope of bed in longitudinal direction.
The kinematic viscosity coefficient for the above equations can be used as:
$$v = [1.14 - 0.0013(T-15) + 0.000681(T-15)^2] \times 10^{-6}\, m^2/s \qquad (15)$$
where, T= temperature in $^\circ$C.

7. CONCLUSIONS:
In the present paper, explicit equation for sediment threshold in terms of sediment-fluid parameter (s_*) has been proposed for uniform non cohesive sediment (Eqns 13 and 14) for horizontal bed which can be also used for longitudinal sloping bed i.e. Eq. (15). The present form of equation can be used for all range of Re_* i.e. without any limitations. Thus this equation seems to be better than the all other equations available and presented in this paper.

8. REFERENCES

i.   Beffington, J.M. (1999). "The legend of A.F. Shields", Jr. of Hydraulic Engg., ASCE, 125(4), 376-387.
ii.   Cao,Z,Pender,G,Ming.J.(2006), "Explicit formulation of the Shields diagram for incipient motion of sediments."Jr. of Hydraulic Engg, ASCE, 132(10) pp. 1097-1099.
    Oliveto,G. (2002), "Shields entrainment ulics", ASCE,128(5),538-542.

iv.   Kramer,H.(1935), "Sand Mixtures and sand movement in fluvial models", Transitions,ASCE-100,798-878.

v.   Paphitis,D.(2001),   "Sediment   movement   under unidirectional flows: an assessment of empirical threshold curves", coastal Eng., 43,227-245/

vi.   Bonnefille, R. (1963) "Essais de synthese des lois de debut d'entrainment des sediment sous I'action d'un courant en regime uniform". Bukk – Du CREC, No. 5, Chatou.

vii.   Brownlie, W.R. (1981), "Prediction of flow depth and sediment discharge in open channels."Report No. KH-R-43A, Keck laboratory of Hydraulics and Water Resources, California Institute of Technology, Pasadena California.

viii.   Chien, N, Wan, Z.H. (1983), "Mechanics of sediment movement", Science Publication, Beizing (in Chinese).

ix.   Cao, Z, Pender, G., Meng, J. (2006), "Explicit formulation of Shields' diagram for incipient motion of sediment", Jr. Hydr. Engg., 132 (10), pp: 1097-1099.

x.   Gua, J. (1990), "Basic laws of sediment transport", Technical Report, Shanxi Provincial Natural Science Foundation, Taiyuan, Shanxi Province, China (in Chinese).

xi.   Kunhle, R. (1993), "Incipient motion of sand-gravel sediment mixtures", Jr. Hydr. Engg., 119 (12), pp: 1400-1415.

xii.   Madsen, O.S., and Grant, W.D. (1976), "Sediment transport in the coastal environment", Rep. No. 209, Ralph M. Parsons Laboratory, Massa Chusettes Institute of Technology, Cambridge, Massachussettes.

xiii.   Madsen, O.S., (1999), "Sediment transport on the shelf", Proc. Coastal Sediments, Proc. Coastal sediments;. 99 Short Term Course Notes.

xiv.   Paphitis, D. (2001), "Sediment movement under unidirectional flows": an assessment of empirical threshold curves, Coastal Engg., 43, pp: 227-245.

xv.   Raudkivi, A.J. (1990), "Loose boundary hydraulics", 3rd Edn. Pergamon, Tarrytown, N.Y.

xvi.   Shields, A.F. (1936), "Application of similarity principles and turbulence research to bed-load movement, vol. 26", Mittilungen der Preussischen Versuchsan stalt fur Wasserfaund Schiffban, Berlin, Germany, pp: 5-24.

xvii.   Soulsby, R.L., and Whitehouse, R.J.S. (1997), "Threshold of sediment motion in coastal environments", Proc. of Combined Australian coastal Engineering and port conference, Christ church, New Zealand, pp: 149-154.

xviii. Chaurasia,ShriRam (2005), "Sediment Threshold – An Overview", Proc. of Hydro – 2005, Tumkur, Karnataka, pp : 645-655.

xix.   Shri ram, (2001), "Explicit equation for Sediment Threshold" HYDRO-2011 at SVNIT, Surat, Dec 29-31,2011 pp.110-120.

xx.   Sheppard, D. Max., Renna, Rick (2005), "Florida Bridge Scour Mannual". Florida Deptt. of Trans., 605 Suwannee Street, Tallahassee, F.L. 32399-0450.

xxi.   van Rijn, L.C. (1984), "Sediment transport, part-I": Jr. Hydr. Engg. 110 (10), pp: 1431-1456.

xxii.   Yalin, M.S., and Karahan, E. (1979), "Inception of sediment transport", Jr. Hydr. Div., 105 (11), pp: 1433-1443.

Turbulence Statistics In Wake Zone Of Pier Founded In Clay-Gravel Cohesive Sediment

Ajay Kumar[1]   Rajesh K. Jain[2]   Umesh C. Kothyari[3]
[1]Senior Scientist, ICAR Research Complex for Eastern Region, Patna, 800 014, India
[2]Associate Professor and Head, Department of Civil Engineering, Govt. Engineering College, Chandkheda, Gandhinagar, 382 424, India
[3]Ex Professor, Department of Civil Engineering, Indian Institute of Technology, Roorkee, 247667, India
Email: ajaykumar1001@gmail.com

ABSTRACT: *Results of turbulence statistics, measured through acoustic Doppler velocimeter (ADV), in wake zone of pier founded in clay-gravel cohesive sediment bed are presented. Sediment bed material used was consisting of mixture of clay and gravel. Clay was added to gravel in percentage varying from 20 to 60 % by weight. Three dimensional velocity and turbulence statistics were collected inside and outside of scour hole around a pier at 10 locations of 4 azimuthal planes (i.e. at θ = 0, 30, 60 and 90°) in wake zone of the pier and 3 azimuthal planes (i.e. at θ = 120, 150 and 180°) in upstream side of the pier. Turbulence intensities and Reynolds stresses reduced, as one moved from nearer the pier towards the downstream in wake zone. The maximum value of turbulent kinetic energy is observed to occur in the scour hole (i.e. for z/h < 0) predominantly at radial distance r_0 = 40 mm in the various azimuthal planes in almost all the runs. Quadrant analysis indicates that ejection and sweep are mainly responsible for sediment detachment and its transport in the scour process. Keywords: River flow, Turbulence statistics, Wake zone, Scour, ADV, Cohesive sediment, Sediment transport*

1. INTRODUCTION

Scouring by river flow is a natural phenomenon which occurs as a part of the morphological changes of rivers. It is further intensified by increased turbulence and forces that develop in the flowing water due to the obstruction in river flow in the presence of hydraulic structures. These structures are exposed to the interaction among flow characteristics, turbulence statistics and river bed material causing sediment detachment and transport and finally resulting into scour. Although the cost of repair of damaged infrastructure due to scouring and riverbed erosion is often significant, the indirect environmental costs of such events can be even greater.

Three dimensional flow field and turbulence statistics around pier and a strong interaction with the erodible bed sediments makes the process of scour around piers a complex phenomenon. Therefore, prediction of shape, size and magnitude of scour at piers are of prime importance to hydraulic engineers, planners and environmentalists. Comprehensive understanding of the turbulence statistics helps

in more precise prediction of depth of scour (Coleman and Melville, 2001). The turbulence statistics within the scour hole around the pier founded in cohesionless sediment is well explored in recent past (Graf and Istiarto, 2002; Dey and Raikar, 2007). However the land surfaces and river bed material frequently consist of mixture of cohesive as well as cohesionless sediments like mixtures of sand, gravel and clay etc. (Jain and Kothyari, 2009). The phenomenon of river bed scour around piers becomes further complex when piers are founded in such cohesive sediments. The experiments revealed that the process of scour as well as depth, shape, and geometry of scour hole developed in such cohesive sediment were significantly different from that of cohesionless sediments (Kothyari et al., 2014). Study of three-dimensional flow characteristics within the scour hole around circular uniform and compound piers are also useful in modeling the scour process and developing new measures for protection against scour around piers (Kumar and Kothyari, 2012).

Kumar et al. (2011a) presented flow characteristics over scoured bed in wake zone of pier founded in clay-sand-gravel sediment mixtures. However the present study has been taken up to investigate flow and turbulence statistics by using an acoustic Doppler velocimeter (ADV) over scoured bed in wake sediments.
zone of a pier founded in channel bed consisting of clay-gravel

2. MATERIAL METHODS

The details of experiments are given in Kumar et al. (2011b) and Kumar (2011), however same is repeated here for completeness. Experiments have been conducted in a tilting flume ($16 \times 0.75 \times 0.5$ m) located in the Hydraulic Engineering laboratory of Civil Engineering Department, Indian Institute of Technology, Roorkee. The channel has a test section of 6.0 m length, 0.75 m width and 0.16 m depth starting at a distance of 5.5 m from channel entrance. Observations made at constant bed slope of flume, $S_o = 2.5 \times 10^{-3}$ are reported herein. The discharge (Q) in the flume was provided by a constant head overhead tank. The measurement of discharge is made volumetrically with the help of a tank provided at the end of the channel. The clay material used has a median size equal to 0.052 mm, while gravel has a median size of 3.1 mm. The clay has liquid limit $W_L = 27.75$ %, plastic limit $W_P = 21.59$ % and plasticity index $PI = 6.16$ %, optimum moisture content $OMC = 12$ % and maximum dry density $(\gamma_d)_{max} = 19.03$ kN/m^3. As per IS-1498 (1970), the clay used by us was classified as CL i.e. clay with low plasticity.

2.1 Experimental procedure

For preparation of channel bed, the accurately weighed clay powder, gravel and already computed moisture (water) were mixed thoroughly thereafter covered with polythene and left for 24 hours for uniform distribution of the moisture. The sediment was mixed thoroughly again and filled in the test section and compacted by a dynamic compaction method

(Kothyari and Jain, 2008). Thus a plain sediment bed with 0.16 m thickness was prepared. Desired discharge was allowed into the channel through the inlet pipe. Flow parameters corresponding to the scour condition around the pier were recorded. Scour depth was measured with the help of electronic profile recorder PV09 manufactured by Delft Hydraulics Laboratory, Delft, The Netherlands.

The ADV measurements were taken after the development of equilibrium scoured bed around a circular pier having diameter 114 mm (Figure 1). The instantaneous three-dimensional velocity and turbulence characteristics in wake zone and upstream of the pier were measured. Measurements for mean velocities, turbulence intensities and Reynolds stresses were taken. A cylindrical polar coordinate system is used to represent the flow and turbulence characteristics. The time-averaged velocity components in (r, θ, z) are represented by (u, v, w) whose corresponding fluctuations are ($u^{'}, v^{'}, w^{'}$). The positive directions of u, v and w are stream-wise, outward and upward, respectively. In order to present the distance of different ADV measuring locations with respect to pier periphery, radial distance is given by $r_0 = r - 0.5b$, where r is the distance from centre of the pier to the point of location of measurement by an ADV, b is the diameter of pier. It means that $r_0 = 0$ represents pier boundary.

Measurements were taken in 7 vertical planes at the horizontal interval of 30^0 creating 10 locations in wake zone of pier (0, 30, 60 and 90^0) and 3 locations in upstream of the pier (120, 150 and 180^0). The ADV observations were taken in all 4 runs in clay-gravel mixtures (with 20, 40, 50 and 60% clay). However results from one such run namely GC5.6 (clay-gravel mixture having 20% clay) is discussed herein in detail. The summary of hydraulic parameters for the run used are given in Table 1 where S_o is channel bed slope, Q is discharge, h is approach flow depth, U_o is point mean velocity, d is maximum depth of scour, W is antecedent moisture content and e is void ratio. Clear water conditions existed in the approach flow during the present investigation.

Figure 1. Data measurement by an ADV

Table 1. Summary of hydraulic parameters

Run No.	S_o	Q (m³/s)	h (m)	U_O (m/s)	d (m)	W (%)	e
GC5.6	5.4×10^{-3}	0.088	0.096	1.16	0.08	15.18	0.26

3. RESULTS AND ANALYSIS

The discussion on variation of time averaged velocity in stream-wise direction, turbulent intensities, Reynolds stresses and turbulent kinetic energy observed in various planes is presented below. Lastly, the discussion on quadrant analysis is presented.

3.1 Vertical distribution of stream-wise velocity, turbulence intensity and Reynolds stresses

The measurements around the pier in scour hole were made in various azimuthal planes i.e. $\theta = 0°$, $30°$, $60°$, $90°$, $120°$, and $180°$ in clockwise direction from wake zone of the pier to its upstream nose at radial distances of $r_0 = 40, 70, 90, 100, 140, 190$ and 650 mm.

The stream-wise velocity u is observed to have smaller value at $0°$ plane and thereafter it increases as we move in clockwise direction within the wake region till $\theta = 60°$. However u values near the bed is minimum at $\theta = 120$ to $180°$. The vertical distribution of turbulence intensities (Figure 3) reveals that maximum value of turbulence intensities are recorded near about initial bed level and thereafter it decreases towards the water surface at all locations except in 0^0 plane where maximum turbulence intensities are found to occur near the water surface. The magnitude of Reynolds stresses (Figure 4) is

maximum between $z/h = 0$ to -0.4 and they reduces if this value is increased or reduced beyond this range.

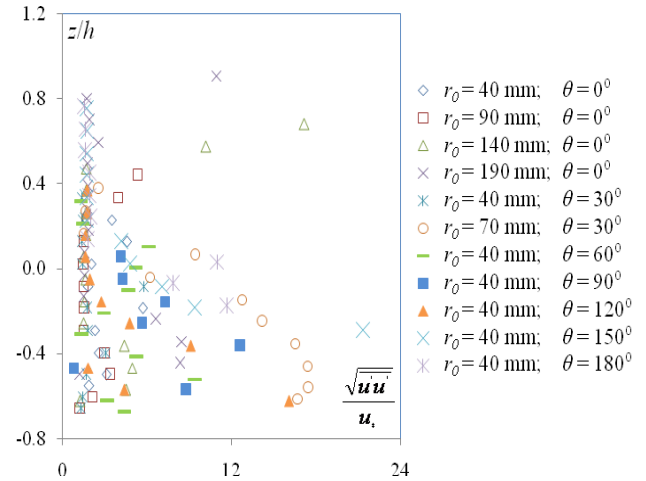**Figure 2.** Normalized profiles of turbulence intensities component $\sqrt{\overline{u'u'}}$ measured around the pier in scour hole for experimental run GC5.6
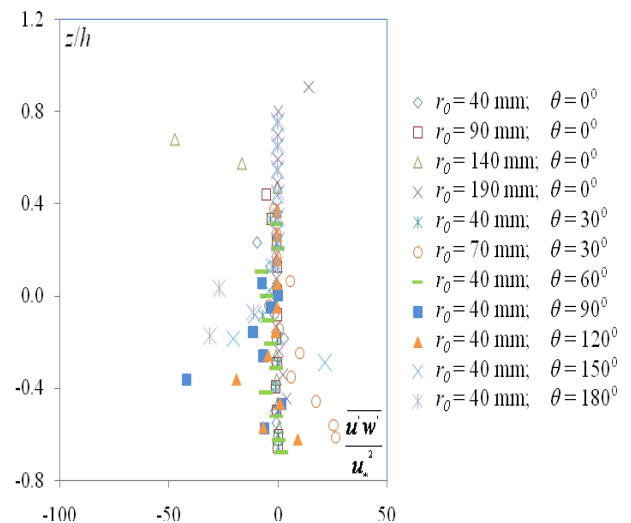
Figure 3. Normalized profiles of Reynolds stresses component $\overline{u'w'}$ measured around the pier in scour hole for experimental run GC5.6

3.1.2 Turbulent kinetic energy

The turbulent kinetic energy, k can be expressed as

$$k = \frac{1}{2}\left(\overline{u'u'} + \overline{v'v'} + \overline{w'w'}\right)$$

(1)

where, time-averaged velocity components in (r, θ, z) are represented by (u, v, w) whose corresponding fluctuations are (u', v', w').

The value of k is normalized using the square of shear velocity i.e. u_*^2. The turbulent kinetic energy is qualitative representation of turbulence fluctuations in the flow within the scour hole. The variation of turbulent kinetic energy across the flow depth in various azimuthal planes in the scour hole shows maximum value of turbulent kinetic energy is observed to occur in the scour hole (i.e. for $z/h < 0$) (Figure 4).
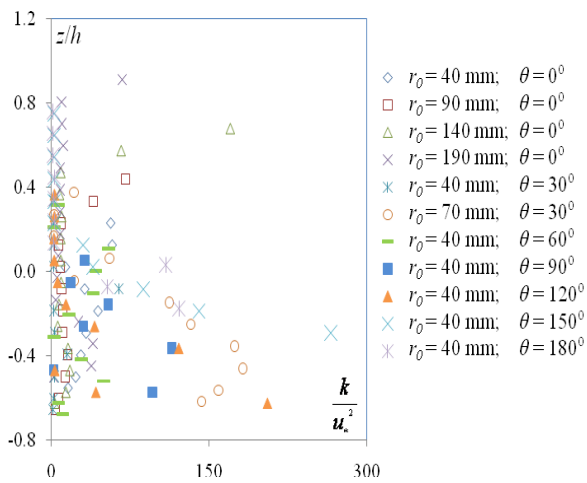
Figure 4. Normalized profiles of turbulent kinetic energy measured around the pier in scour hole for experimental run GC5.6

This result indicates that maximum turbulence fluctuations occur in the flow within the scour hole near the pier. Further away from the scour hole i.e. when $r_0 > 40$ mm, in various azimuthal planes, fairly uniform and much smaller value of turbulent kinetic energy is observed. Kumar (2007) also observed maximum value of k near the pier in the wake zone and its value reduces as one moves away from the pier.

In comparison to most of the experimental runs in cohesive sediment bed, the experimental run in cohesionless sediment bed recorded relatively more uniform distribution of turbulent kinetic energy (except azimuthal plane $\theta = 0^0$). In a few runs, however the value of k is observed above the original bed level (i.e. for $z/h > 0$) is noticeable.

In some experimental runs the maximum value of turbulent kinetic energy is recorded near the scoured bed in azimuthal plane $\theta = 150$ to 180^0. This may be attributed to reverse flow condition at these locations. In general relatively more uniform

distribution of normalized turbulent kinetic energy is noticed for $z/h > 0$ in all the azimuthal planes (except $\theta = 0^0$) in almost all the runs.

3.2 Quadrant analysis

For performing the quadrant analysis the stream-wise fluctuating velocity $u' = u - \overline{u}$ and the vertical fluctuating velocity $w' = w - \overline{w}$ are decomposed following their sign using explore V software (Nortek, 2000). Only those data having average signal to noise ratio =17 and average correlation coefficient larger than 70% were considered in the decomposition of velocity. A code is developed in FORTRAN-90 to obtain the contribution of outward interaction, ejection, inward interaction and sweep events out of whole data for a particular z/h value. $S_{i,H}$ indicatively defines occurrence probabilities of a particular event, the same is obtained using the code developed herein. The occurrence probability for each event over the entire flow depth in wake zone of pier in one experimental runs GC5.6 was made. The results presented herein were derived by performing computations taking all the events with $H = 0$.

3.2.1 Run GC5.6

Figure 5 shows the contribution of bursting events in azimuthal plane $\theta = 0^o$ at four locations in case of scour hole formed in clay-gravel mixture. The highest value of occurrence probabilities $S_{i,H}$ was found for ejection between $z/h = -0.3$ to -0.1 at all locations i.e., at $r_0 = 40, 90, 140$ and 190 mm in this azimuthal plane. Its value however reduces as one moves either towards scoured bed or water surface. Maximum value of $S_{i,H}$ is recorded near about initial bed level in the case of sweep also in $\theta = 0^o$ plane (Figure 3). The outward and inward interactions have maximum value at lower most level and decreases near initial bed level. Their values further increase towards the water surface. The larger value of outward and inward interaction as observed in the lower most measurement layer supports the finding of Nelson et al. (1995), since it denotes a potential for near bed flow to transport more sediments than elsewhere in water column. Above analysis indicates that comparatively ejection and sweep are mainly responsible for sediment detachment and its transport in the scour process.
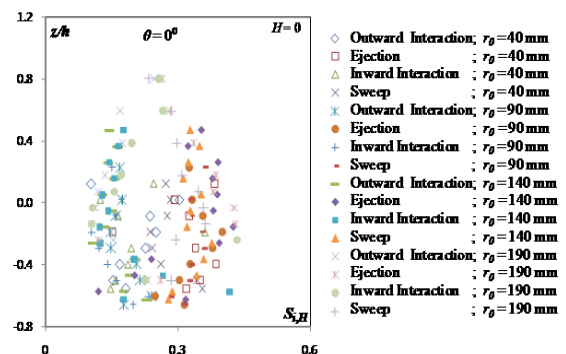
Figure 5. Distribution of bursting events at various locations in wake zone of the pier at
azimuthal plane $\theta = 0^o$ for experimental run GC5.6

4. CONCLUSIONS

The vertical distribution of turbulence intensities reveals that maximum value of turbulence intensities are recorded near about initial bed level and thereafter it decreases towards the water surface at all locations except in 0^0 plane where maximum turbulence intensities are found to occur near the water surface. The magnitude of Reynolds stresses is maximum between z/h = 0 to -0.4 and they reduces if this value is increased or reduced beyond this range. The result indicates that maximum turbulence fluctuations occur in the flow within the scour hole near the pier. Further away from the scour hole i.e. when $r_0 > 40$ mm, in various azimuthal planes, fairly uniform and much smaller value of turbulent kinetic energy is observed. The highest value of occurrence probabilities $S_{i,H}$ was found for ejection between z/h = -0.3 to -0.1 at all locations i.e., at r_0 = 40, 90, 140 and 190 mm in this azimuthal plane. Its value however reduces as one moves either towards scoured bed or water surface. Maximum value of $S_{i,H}$ is recorded near about initial bed level in the case of sweep also in $\theta = 0^o$ plane. Above analysis indicates that comparatively ejection and sweep are mainly responsible for sediment detachment and its transport in the scour process.

REFERENCES

i.   Coleman, SE and Melville, BW (2001) Case study: New Zealand bridge-scour experiences. Journal of Hydraulic Engineering (ASCE) 127(7): 535-546

ii.   Dey, S and Raikar, VR (2007) Characteristics of loose rough boundary streams at near threshold. Journal of Hydraulic Engineering (ASCE) 133(3): 288-304

iii.   Graf, WH and Istiarto, I (2002) Flow pattern in the scour hole around a cylinder. Journal of Hydraulic Research (IAHR) 40 (1): 13-20

iv.   Jain, RK and Kothyari, UC (2009) Cohesion influences on erosion and bed load transport. Water Resources Research: 45, W06410 DOI:10.1029/2008WR007044 W06410

v.   Kothyari, UC and Jain, RK (2008) Influence of Cohesion on Incipient Motion Condition of Sediment Mixtures. Water Resources Research: 44, W04410 DOI: 10.1029/2007WR006326

vi.   Kothyari, UC, Kumar, A and Jain, RK (2014) Influence of cohesion on river bed scour in wake region of piers. Journal of Hydraulic Engineering (ASCE) 140(1): 1-13

vii.   Kumar, A (2007) Scour around circular compound bridge piers. Ph. D. Thesis, Department of Civil Engineering, Indian Institute of Technology, Roorkee, India, 237pp

viii.   Kumar, A (2011). Scour around circular piers founded in clay-sand-gravel sediment mixtures. Ph. D. Thesis, Department of Civil Engineering, Indian Institute of Technology, Roorkee, India, 182pp

ix.   Kumar, A and Kothyari, UC (2012) Three-dimensional flow characteristics within the scour hole around circular uniform and compound piers. Journal of Hydraulic Engineering (ASCE) 138(5): 420-429

x.   Kumar, A, Jain, RK and Kothyari, UC (2011a) Flow characteristics in wake zone of a pier founded in clay-sand-gravel mixture. 34th IAHR World Congress -Balance and Uncertainty, June 26 – July 1, 2011, Brisbane, Australia

xi.   Kumar, A, Jain, RK and Kothyari, U.C. (2011b) Flow characteristics at a pier in scoured bed of clay-gravel sediment. In Hydraulics and Water Resources, Patel, PL, Manekar, VL, Yadav, SM and Timbadiya, PV (Eds.), Elite Pub. House

xii.   Nelson, JM, Shreve, RL, Mclean, SR and Drake, TG (1995) Role of near bed turbulent structure in the bed load transport and bed form mechanism. Water Resources Research, Vol. 31, 2071-2086

xiii.   Nortek (2000) Nortek 10 MHz Velocimeter: Operations Manual. NDV Operations Manual, Document No., N3000-100/Rev.b/10.08.2000

Impact of Sand Mining On River-Aquifer Interactions

Mathew K. Jose[1], P. Dhote[2], T. C. Mohan[3], C. P. Kumar[4]
[13] National Institute of Hydrology, Regional Centre, Belgaum, Karnataka-590019, India
[2] National Institute of Technology, Suratkal, Karnataka, India
[4] National Institute of Hydrology,Roorkee, Uttarakhand-247667, India
Email:mathewkjose@gmail.com

Abstract: *Because of increased human activities within the riverine environment, a number of rivers in India are under tremendous stress. Sand extraction from river bed and flood plains is in an ever-increasing phase due to burgeoning demand for construction grade sand. The consequences of continuous sand removal from river bed are of serious nature. In-stream mining of sand can lead to irreversible damages to the river as well as the adjoining aquifer systems. However, it may be noted that scientific studies pertaining to various aspects of environmental effects of sand mining are meager. Besides the river system itself, impact of river sand mining on the adjoining aquifer systems are to be investigated as groundwater is an important source for drinking and irrigation. In the presented paper an effort has been made to analyse impact of sand mining on the aquifer system by considering a case study. Sand mining activities, and subsequent environmental degradations have been reported in the case of a number of rivers in India. The case study presented here on the impact of sand mining on aquifer system is applicable for a chosen stretch of the River Manjira (Godavari River Basin) in Nizamabad District of Telangana State. The effects have been investigated by studying the river-aquifer interaction aspects by formulating a groundwater model of the region of interest covering the river reaches with sand mining activities. Analyses of impact of river sand mining on the aquifer system in terms of water level changes, has been carried out for different scenarios arising out of sand mining activities. Results correlating changed river*

profiles due to sand removal, river stages, and groundwater levels have been presented in the paper.

Keywords: Aquifer system, groundwater, interaction, sand mining, environmental impact

1. INTRODUCTION

In India, as a result of faster rates of development, creation of infrastructural facilities is rapidly growing. Construction grade sand is one of the pre-requisites for such activities. This causes undue stress on many river systems due to increased rates of sand extraction. It is, however, known that large-scale extraction of sand and pebbles from river beds is one of the most serious stresses on the river environment (Rovira et al. 2005; Kondolf 1994). It can lead to irreversible damage to the river environment (Weeks et al. 2003; Hemalatha et al. 2005). Studies have been carried out in the past in various parts of the world regarding river sand mining (Bull and Scott 1974; Collins and Dunne 1987; Sandecki 1989; Kondolf and Swanson 1993; Poulin et al. 1994; Kondolf 1997; Rinaldi et al. 2005; Jia and Luo 2007; Erskine 2008, Sreebha and Padmalal 2011). Excessive sand mining activities can destroy riverine vegetation, cause erosion, pollute water sources and reduce the diversity of animals supported by these woodlands habitats (Ashraf et al. 2011; Erskine et al.1985; Rinaldi et al. 2005). There are cases reported by investigators highlighting adverse effects of sand mining on the river ecosystems as well as adjoining aquifer systems (Padmalal et al. 2008, APGWD 2009). It is now well established that indiscriminate sand mining activities could be responsible for considerable environmental damage to aquifer systems besides the river ecosystem itself (Kondolf 1997; Leeuw et al. 2010). Nevertheless, in India such kind of investigations is yet to gather momentum. Want of appropriate scientific feedback and results on the subject in our country, decision making processes related to sand mining are mostly empirical in nature. Therefore, site-specific scientific investigations on the impact of river sand mining are to be carried out to facilitate sustainable levels of sand extraction from river systems (Malaysian Dep of Irrigation & Drainage 2009). In this context, mining of sand from the beds and flood plains of many rivers in the Andhra/ Telangana region is reported to have been causing environmental damages including depletion in the surrounding aquifer systems. This paper presents a case study from Nizamabad district of Telangana state wherein the interaction aspects of river-aquifer system (Sanz et al., 2011) is investigated visa-a-vis impact of sand mining on groundwater levels.

1.1 Description of Study Area
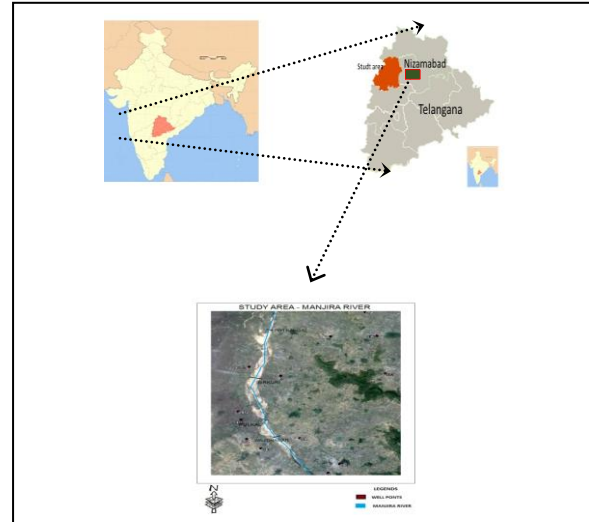
The study area falls within the catchment of River Manjira in Nizamabad district of Telangana state. Contained within the Godavari river system, Manjira river basin has a catchment area of about 11,000 sq km. Two sand mining reaches have been identified along the left and right banks of River Manjira at Birukur and Pulkal respectively (Ref: SI Toposheet No. 56F/15). The selected river stretches are located at downstream of a reservoir (Nizam Sagar) bound by latitudes 18° 05' N & 19° 00' N and longitudes 77° 40' & 78° 37' E respectively. Forest cover in the region is about 22%. The area receives a normal annual rainfall of about 1036 mm of which 74% received during the SW monsoon season (June-October). The annual potential evapotranspiration (PET) is about 1591 mm.

Figure 1: Location of Study area on River Manjira in Distric Nizamabad (Telangana State)

Figure 2: An in-stream sand mining location on R Manjira at Wajidnagar (Nizamabad)

Ground water occurs under various geological formations. Its occurrence and movement are governed by nature of geological formations, the porosity, fracturing and joint systems in rocks. It may be observed that 85% of state geographical area is covered by hard rocks, feasible for bore wells, 10% by

sedimentary formations, which are generally semi consolidated in nature, suitable for dug wells and tube wells (APGWD 1976). About 5% area is alluvial formations, favorable for filter points and tube wells along the river reaches. The discharge of an open well may vary between 30,000 to 50,000 lpd in the area (APGWD 2011). In alluvial formations all along the river course, filter points (shallow bore-wells) and infiltration galleries are developed for irrigation and water supply respectively with very good yield.

Though alluvium occupies only about 5% of geographical area, these areas yield nearly 40% of ground water that is used chiefly to irrigate paddy fields (APGWD 2011). As there are no perennial streams in the region, groundwater is the dependent source for all water requirements. Clearly, these are compelling facts that lead to serious investigations regarding the impact of sand mining on groundwater resources, besides that on river system itself. With the reduction or absence of sand layers in these alluvial areas due to sand mining, storage has been observed to be gradually reduced leading to increased runoff from the rainfall received. Further, analysis of water level data indicates that the base flow contribution from aquifer to river system has been on the rise as a result of reversal of flow gradients.

2. MATERIAL AND METHODS

The aquifer modelling methodology (Anderson and Woessner, 1992). has been used to assess the impact of sand mining on groundwater. Data concerning ground water levels, water quality, rainfall, stage-discharge as well as hydrogeological parameters were collected and processed to facilitate simulation of aquifer system for various stress conditions and sand removal options. The study has employed a methodology consisting of (i) field investigation methods, (ii) laboratory analyses of water samples and river bed load samples, (iii) river hydraulics modelling using HEC-RAS (Brunner, 2010) and (iv) groundwater aquifer simulation techniques. A conceptual groundwater model for the river-aquifer system of the study area has been formulated, and simulations of scenarios under different stresses are generated using the MODFLOW code (McDonald and Harbaugh 1988). The aspects of sand mining versus riverine environment are described in a separate paper. This paper deals with the aquifer conditions under the influence of various scenarios / stress conditions in the modelled area.

The interaction characteristics have been analysed by simulating heads in the domain by employing the developed groundwater model for various stage conditions in the river. A few scenarios have been predefined depending upon the condition of the river based upon varying degrees of sand mining activity, land use practices in the surroundings and groundwater usage pattern in order to ascertain the river-aquifer interaction aspects. Thus, the following possibilities of the river channel arising out of sand mining activities have been considered, namely, widening of the river channel, deepened of

the river channel, a combined effect of both widening plus deepening of the river channel as well as changes in groundwater pumping rates. Stress periods consisting of pre-monsoon, monsoon and post-monsoon periods have been considered for simulations.

3. RESULTS AND ANALYSIS

A discussion on the results and inferences are presented based on field investigations and modelling studies. A three dimensional groundwater model (MODFLOW) has been calibrated for the study area and analyses performed using the simulation results.

3.1 Discretization and Boundary Conditions

The discretised model has 90 rows, 95columns, and 4 layers for the finite difference grid. The grid dimesions are: 25 km along the columns, 27km along the rows with 60m depth. The study area is characterized by granite and patches of alluvial soil composed of sand and clay. Lateral extension of alluvium varies between 0.2 to 3 km from the river banks. Aquifer thickness is about 17 m.
Site map has georeferenced with known coordinates. Natural ridge line exist at the eastern boundary. Therefore, all the cells of eastern boundary are kept as inactive. Cells of fourth layer are inactive as it constitutes the impermeable strata and forms the lower boundary of the model.
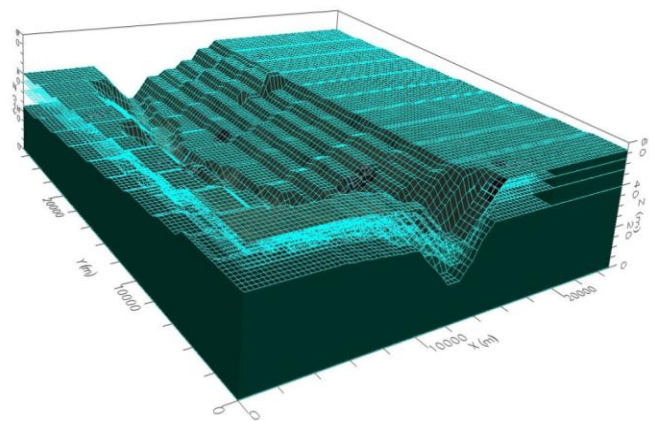
Figure 3: The three dimensional discretized model domain of the study area

The elevation goes on decreasing from south to north. Also, there is a slope towards the river channel from eastern and western boundaries. Longitudinal profile of Manjira River varies from 368 msl at upstream side to 348 msl at downstream side. Considering 328 msl as datum for the model domain, all other elevations have been reduced to model elevations to facilitate simulations. Observation data from 22 observation

wells have been collected and used for calibration and validation of the model.
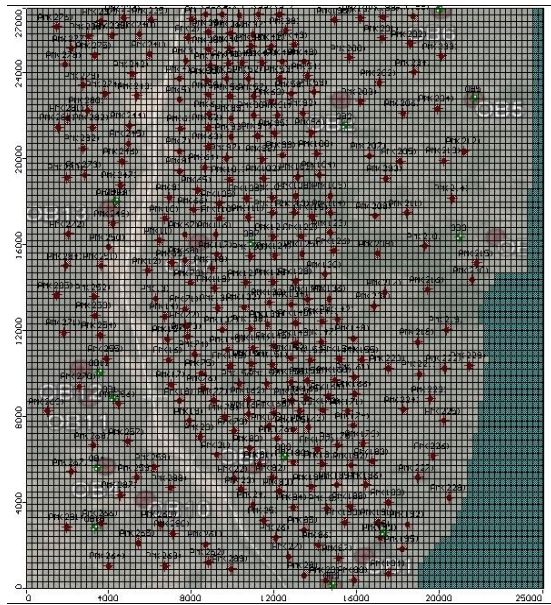
Figure 4: A planar view of the grided domain of the study area with wells

The calibration parameters like hydraulic conductivity, storage coefficient and rainfall recharge are given in Tables 3.1, 3.2 & 3.33 respectively.

Table 3.1: Calibrated conductivity

Soil Type	Initial Conductivity (m/s)			Calibrated Conductivity (m/s)		
	Kx	Ky	Kz	Kx	Ky	Kz
Sand	6.9E-4	6.9E-4	6.9E-4	6.9E-5	6.9E-5	6.9E-6
Clay	10E-10	10E-10	10E-6	10E-10	10E-10	10E-6
Granite	10E-8	10E-8	10E-8	10E-8	10E-8	10E-11

Table 3.2: Calibrated storage characteristics

Soil Type	Initial Storage Characteristics			Calibrated Storage Characteristics		
	Sy	Ss	n_{eff}	Sy	Ss	n_{eff}
Alluvium (sand/clay)	0.2	2.8E-5	0.15	0.2	2.8E-5	0.15
Granite	0.03	2.8E-5	0.15	0.003	2.8E-5	0.15

Table 3.3: Calibrated rainfall recharge

Soil Type	Initial rainfall recharge	Calibrated rainfall recharge
Alluvium (sand/clay)	22 % of precipitation	16 % of precipitation

It is found that groundwater flow is generally in the south to north direction, and also towards river reaches. Analysis of seasonal variation in river-aquifer fluxes indicates gains to the aquifer system during the post and pre-monsoon periods while the aquifer is contributing during the wet season. The general nature of the river-aquifer interaction is clear from Table 3.4.

Table 3.4: Typical values fluxes indicating river-aquifer interaction in the study area

Months	River-aquifer Interaction fluxes	
	m^3/day	m^3/s
August 2010	-34220.4	-0.396
November 2010	-6666	-0.077
February 2011	+49476.1	+0.572
May 2011	+60134	+0.695

During the rainy season (monsoon) there is no irrigation, and agricultural activity (dominated by paddy) solely depends upon rainfall. The negative flux during this period indicates that aquifer is losing and river is gaining as the regional water table is elevated compared to the river stage. However, during the dry season (pre monsoon) water table tends to deplete and hydraulic gradients reverse. Thus, river starts contributing to the aquifer system and helps to sustain the availability of groundwater. It may be noticed that, indiscriminate mining of river bed can cause further lowering of the water table within

the river channel and flood plains resulting in less flux or no contribution to the aquifer system.

The calibrated model has been used to isolate effects of sand mining for various scenarios on groundwater levels at different river reaches. Four river reaches with sand mining activities namely, Wajidnagar, Pulkal, Birkur, and Pothangal have been considered for the investigations. The results of these different scenarios are tabulated in the tables 3.5, 3.6 and 3.7 respectively for three distinct cases of widening of river channel, deepening of river channel, and widening plus deepening of river along with increased groundwater extraction rate.

Table 3.5: Case1: Widening of river channel

River reach	Effect on left bank of river		Effect in right bank of river	
	Extension (km)	Maximum groundwater level depletion (m)	Extension (km)	Maximum groundwater level depletion (m)
Wajidnagar	3.6	1.53	3.1	2.1
Pulkal	2.3	2.5	4.2	1.5
Birkur	-	-	3.4	2.2
Pothangal	2.3	1.67	3.6	3.5

In the first scenario width of river channel is increased by 25 %. There is depletion in groundwater levels right from upstream Wajidnagar to downstream Pothangal. Maximum groundwater depletion found to be 3.5 m at right bank of Pothangal and effect extends up to 3.6 km. There is no groundwater depletion at left bank of Birkur.

Table 3.6: Case2: Deepening of river channel

River reach	Effect on left bank of river		Effect in right bank of river	
	Extension (km)	Maximum groundwater level depletion (m)	Extension (km)	Maximum groundwater level depletion (m)
Wajidnagar	3.6	4.1	3.1	4.7
Pulkal	2.3	5.8	4.2	5.1
Birkur	0.5	4.7	3.4	4.6
Pothangal	2.3	6.8	3.6	6.5

River channel is deepened by 4m in the second scenario. Groundwater level depletion is more as compare to widening. Groundwater level depletion found to be in left bank of Birkur as it was not the case in widening scenario. Maximum groundwater level depletion is found to be 6.8 m at left bank of Pothangal.

Table 3.7: Case3: Widening plus deepening of riverl & increased groundwater extraction rate

River reach	Effect on left bank of river		Effect in right bank of river	
	Extension (km)	Maximum groundwater level depletion (m)	Extension (km)	Maximum groundwater level depletion (m)
Wajidnagar	3.6	4.6	3.1	4.7
Pulkal	2.3	7.1	4.4	5.1
Birkur	2.6	4.8	3.4	4.6
Pothangal	2.6	6.8	3.6	6.5

In the third case, a combination different conditions is applied, where river channel is widened, deepened and groundwater extraction rate is increased by 25 %. Groundwater level depletion is marginally higher as compared to both widening and deepening scenarios. However, it may be observed that deepening of river channel by means of sand mining has greater impact. Overall, it is found that there is not much variation as far as case 2 (channel deepening) and case 3 (combined effect) are concerned. Therefore, marginal increment in channel widening and extraction of groundwater in the adjoining aquifer (of the tune of 25%) has not apparently influenced considerable depletion of groundwater levels in the aquifer system in comparison to the channel deepening situation. It is further observed that there is an increase in groundwater depletion rate in the upstream to downstream direction.
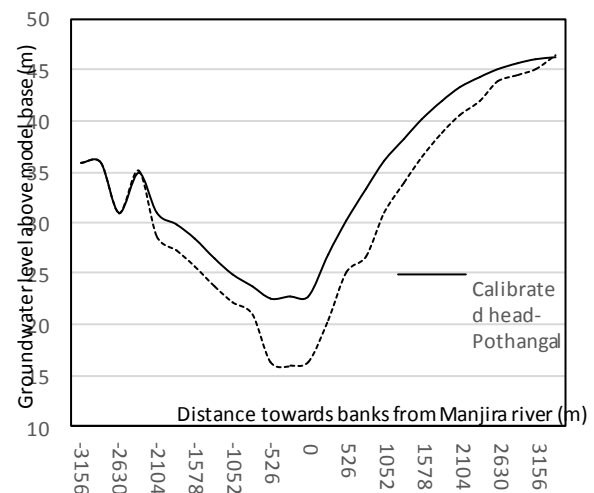

Figure 5: Effects of widening & deepening of river channel and increase in groundwater extraction rate at Pothangal

CONCLUSION

Results from a case study of river-aquifer interaction in the backdrop of in-stream sand mining activities on a stretch of river Manjira in the district of Nizamabad, Telangana has been presented. As mentioned earlier, the study employed (i) field investigation methods, (ii) laboratory analyses, (iii) river hydraulics modeling, and (iv) groundwater aquifer simulation techniques. The prognostic projections of various possible scenarios facilitate specific understanding of river aquifer interaction characteristics. Sustainability of the river as well as aquifer has to be maintained while removing bed load material from the river. Maintaining sustainable limits of groundwater levels in the adjoining aquifer system is important to ensure dependability on well discharges to support agriculture and domestic requirements. Site-specific guidelines based on the inferences of the study can be of use while framing policies for sustainable levels of sand mining and regulating such activities with a view to environmental protection.

ACKNOWLEDGEMENTS

REFERENCES

i.   Anderson P.M. and Woessner W.W. (1992) Applied Groundwater Modelling- Simulation of Flow and Advective Transport, Academic press, 143p.

ii.   APGWD (2009) Report on Hydrogeological Surveys for feasibility of sand mining impact on Ground water regime for Chennur site on R. Godavari, SGWD Nirmal, Adilabad.

iii. APGWD (1976) Report of hydrogeological surveys for delineation of valley fills along River Manjira and Godavari in Nizamabad District, SGWD Nizamabad.

iv.   APGWD(2011) Dynamic groundwater resources of Nizamabad District AP for 2008-09, Nizamabad.

v.   Ashraf M A, Maah M J, Yusoff I, Wajid A and Mahmood K (2011) Sand mining effects, causes and concerns: A case study from Bestari Jaya, Selangor, Peninsular Malaysia, Sci. Res. & Essays, 6(6), 1216-1231.

vi.   Brunner G A (2010) HEC-RAS River Analysis System, US army Corps of Engineers, Hydrologic Engineering Centre, p790.

vii. Bull W B and Scott K M (1974) Impact of mining gravel from urban stream beds in the southwestern United States, Geology 2: 171-174.

viii. Collins B D and Dunne T (1987) Assessing the effects of gravel harvesting on river morphology and sediment transport: a guide for planners. Report to State of Washington, Department of Ecology, Olympia.

ix.   David Sanz, S Castano et al (2011) Modelling aquifer river interactions under the influence of groundwater abstraction in Mancha Oriental System (SE Spain), Hydrology Journal, 19, 475-487.

x.   Department of Irrigation and Drainage (2009) River Sand Mining Management guideline, Malaysia.

xi.   Erskine W D (2008) Channel incision and sand compartmentalisation in an Australian sandstone drainage basin subject to high flood variability. Proc. "Sediment dynamics in changing environments", IAHS Publ. No.325, 1-8.

xii. Erskine W D, Geary P M and Outhet D N (1985) Potential impacts of sand and gravel extraction on the Hunter River, New South Wales. Austral. Geog. Studies 23: 71-86.

xiii. Hemalatha A C, Chandrakanth M G and Nagaraj N (2005) Effect of Sand Mining on Groundwater Depletion, International R & D Conference of the Central Board of Irrigation and Power, Bangalore, Karnataka.

xiv. Jia L and Luo Z (2007) Impacts of the large amount of sand mining on riverbed morphology and tidal dynamics in lower reaches and delta of the Dongjiang river , Journal of Geographical Science, 17, 197–211.

xv.   Kondolf, G.M. (1997) Hungry Water: effects of dam and gravel mining on river channels, Environmental Management, 21, 533-551.

xvi. Kondolf GM (1994) Geomorphic and environmental effects of instream gravel mining, Landuse & Urban Planning, 28, 225-243.

xvii. Kondolf G M and Swanson M L (1993) Channel adjustments to reservoir construction and instream gravel mining, California. Environ Geol Water Sci 21: 256-269.

xviii. Leeuw J D, Shankman D, Wu G, De Boer W F, Burnham J, He Q, Yesou H and Xiao J (2010) Strategic assessment of the magnitude and impacts of sand mining in Poyang Lake, China, Reg Environ Change, 10, 95–102.

xix. McDonald M G and Harbaugh A W (1988) A Modular Three-Dimensional Finite Difference Groundwater Flow Model, Techniques of Water-Resour. Investgn. , US Geological Survey, Book 6 Ch. A1.

xx.   Padmalal, D et al (2008) Environmental effects of river sand mining: A case from southwest coast of India, Environ. Geol, 54, 879-889.

xxi. Paulin R, Pakalnis R C and Sinding K(1994) Aggregate resources: production and environmental constraints. Environ Geol 23: 221-227.

xxii. Rinaldi M, Wyzga B and Surian N (2005) Effects of sediment mining on channel morphology and environment in alluvial rivers. River Research and Application 21: 805–828

xxiii. Rovira A, Batalla RJ and Sala M (2005) Response of a river sediment budget after historical gravel mining in the lower Tordera, NE Spain, River Research & Application, 21, 829–847

xxiv. Sandecki M (1989) Aggregate mining in river systems. Calif Geol 42: 88-94

xxv. Sreebha S and Padmalal D (2011) Environmental Impact Assessment Of Sand Mining From The Small Catchment Rivers In The Southwestern Coast Of India: A Case Study, Environ. Manage., 47(1), 130-140.

xxvi. Weeks J M, Sims I, Lawson C and Harrison D J (2003) River mining: assessment of the ecological effects of river mining in the Rio Minho and Yallahs rivers, Jamaica, British Geol. Survey Report, CR/03/162N.

Effect Of Conjunctive Use On Waterlogging In Lower Gandak Basin Of Bihar

Biswajit Chakravorty, N.G. Pandey and Sanjay Kumar
Scientist, Centre for Flood Management Studies, National Institute of Hydrology
WALMI Complex, Phulwari Sharif, Patna–801505, Bihar, India E-mail: biswajitnih@gmail.com

ABSTRACT : The effect of conjunctive use of surface and groundwater on waterlogging scenario in the Habibpur region of lower Gandak command in India is investigated through simulation technique based on the groundwater flow package MODFLOW. A groundwater flow model is developed for the region to simulate groundwater behavior taking into account the surface and groundwater interaction under various external stresses. The calibrated model is used to simulate the extent of waterlogging under increased crop area coverage and utilization of groundwater potential of the area. Results show that increase in cropped area coverage has positive impact in reducing the waterlogged area. The increased use of groundwater potential during non-monsoon period further lowers the groundwater table. It induces condition for more areal recharge and thereby reduction of waterlogged area. Thus, both options may be effectively used for better planning, management and reduction of waterlogged area in lower Gandak command.
Keywords: Conjunctive Use, Waterlogging, MODFLOW.

1. INTRODUCTION

The lower Gandak basin has the problem of excess surface water during *Kharif* season (July to October) due to flood in Gandak river and release of excess water through its canal system. Flat topography alongwith poor drainage leads to waterlogging conditions in the area. These conditions make *Kharif* cultivation difficult. During *Rabi* (November to February) and *Garma* or summer seasons (March to June), flow in the river reduces and at the same time due to greater utilization of canal water in the upper reaches, lower Gandak command receives negligible water from the canal system. Therefore, agricultural activity of the area suffers in all three cropping seasons of the year. The study investigates effects of conjunctive use of surface and groundwater on waterlogging scenarios. In the present study, a groundwater flow model is developed incorporating the use of maximum cultivable area and using the groundwater potential to investigate its effect on waterlogging conditions. In the process of model development, groundwater fluctuation for each cropping season is modelled using MODFLOW (McDonald and Harbaugh, 1988) package. The simulation is carried out for un-steady flow for an irregularly shaped flow system and combination of unconfined leaky confined aquifer system. The external stresses such as pumpage from wells, areal recharge, evapotranspiration and river/canal aquifer interaction are considered during simulation.

Conjunctive use of surface and groundwater has been the subject of much research (Young et al., 1972; Bredhoeft et al., 1983; O'Mara et al., 1984; Onta et al., 1991; Matsukawa et al., 1992 and Reichard, 1995). Flores et al.(1978) examined a stream connected aquifer system for optimal water management. Bredhoeft et al. (1983) examined the extent of groundwater being developed as insurance against period of low streamflow. Tsur (1990) studied the stabilization role of groundwater and its economic benefits when surface water supplies are uncertain. Haken et al. (1998) developed a management model to determine optimal water allocation policies for time variant surface and groundwater supplies in a hypothetical system. However, these studies do not investigate the effects of conjunctive use on waterlogging conditions.

2. STUDY AREA

The study area is a part of lower Gandak basin. The index map of the study area is shown in Figure 1. The area falls in Vaishali and south of Muzaffarpur districts in the state of Bihar. The river Gandak forms the western boundary of the area. Vaishali Branch Canal (VBC) bounds its eastern side. Habibpur sub-distributory is an off take from VBC and is in the middle of the study area. The area lies between the latitudes of 25°56′ and 26°05′ N and longitudes of 84°57′ and 85°08′ E and is estimated to be 181.6 km^2. The area is relatively flat with maximum ground elevation of 56.27 m in the north-east and minimum of 50.90 m above mean sea level (MSL) near the Gandak river. The average annual precipitation of the area is 1168 mm of which 10% occurs during *Garma* (hot weather), 85% occurs during *Kharif* and only 5% occurs during *Rabi* season. The temperature is high during April to June. The highest temperature goes up to 40°C in the month of June and the lowest to 13.5°C during January.
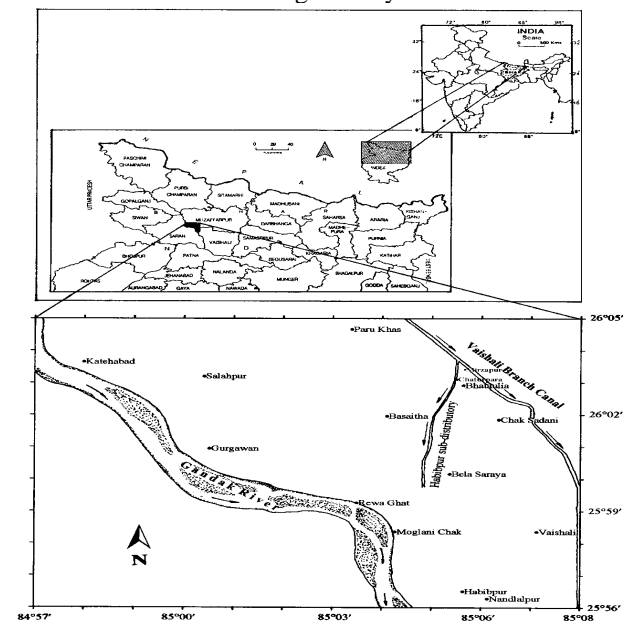

Figure 1. Index map of the study area.

Paddy is the main crop in the area. Maize and wheat are other important cereal crops. Besides this, pulses, oil seeds and some cash crops such as sugarcane and tobacco are also grown. The cropped area during 1991-92 were 16%, 60% and 60% of the total area during *Garma, Kharif* and *Rabi* seasons respectively.

Flow in Gandak river is the main source of water supply for irrigation of the region. The discharge of the river is diverted at Valmikinagar to three main canals namely Main Western Canal (MWC), Nepal Western Canal (NWC) and Tirhut main canal or Eastern Main Canal (EMC). Vaishali Branch canal (VBC) which forms the eastern boundary of the study area takes off at 554 RD (1 RD = 1000 feet) of Tirhut Main Canal. Habibpur sub-distributory takes off at 138.2 RD of VBC. Habibpur sub-distributory provides irrigation facility through 18 outlets. As these canal networks are fed through diversion of river flows, they carry water mainly during *Kharif* season and have insufficient water for irrigation during other two cropping seasons. To supplement uncertainties in surface water supplies farmers use groundwater in a limited way to meet irrigation requirements during these two seasons although plenty groundwater is available (Central Ground Water Board (CGWB), 1993) at shallow depths.

3. MODELING TOOL

MODFLOW package simulates groundwater fluctuation of each cropping season of the year and allows to study the waterlogging scenario of the area. The mathematical background of MODFLOW describes three-dimensional partial differential equation governing unsteady movement of groundwater of constant density through porous earth material under equilibrium condition in a heterogeneous anisotropic medium by:

$$\frac{\partial}{\partial x}\left(K_{xx}\frac{\partial h}{\partial x}\right) + \frac{\partial}{\partial y}\left(K_{yy}\frac{\partial h}{\partial y}\right) + \frac{\partial}{\partial z}\left(K_{zz}\frac{\partial h}{\partial z}\right) - W = S_s\frac{\partial h}{\partial t} \quad (1)$$

Where,

K_{xx}, K_{yy}, K_{zz} : hydraulic conductivity along major axes [LT^{-1}],

h : potentiometric head [L],

W : volumetric flux per unit volume and represents sources and/or sinks of water [T^{-1}],

S_s : specific storage of the porous material [L^{-1}] and,

t : time [T].

This equation of groundwater flow together with specification of flow conditions at the boundaries of an aquifer system and specification of initial head conditions constitute a mathematical model of groundwater flow.

4. MODEL INPUTS

The study area of 20 km X 16 km is divided into 100 X 80 equal sizes gridal network i.e. 8,000 cells having a cell dimension of 200 m X 200 m. The number of active cells in the model domain is 4540 having an area of 181.6 km^2. Three layers are considered in the model based on the sub-surface geology of the area. The average thickness of first, second and the third layers are 15 m, 15 m and 50 m consisting of fine sand, clay mixed with sand and sand respectively. Most of the wells are shallow wells tapping the first layer unconfined in nature and a few deep tubewells (state tubewells) tapping the deeper zones in the third layer semi-confined in nature. The aquifer in the study area can thus be considered as *unconfined to semi confined aquifer system*.

4.1 Hydraulic properties

Vaisali district report (CGWB, 1993) indicates that the transmissivity (T) of the aquifer increases towards north-east direction and decreases towards south-west direction. The transmissivity values are in the range of 400-700 m^2/day with specific yield (S_y) and coefficient of storage (S) as 12-20% and 0.15 respectively. Since location specific input parameters were not available, representative values of hydraulic conductivity and specific storage for different aquifer materials for three layer aquifer system were taken from standard literature (Krusman, 1991 and Boonstra, 1989). The input value of `K' for first, second and third layer are taken as 10.0 m/day, 1.0 m/day and 25.0 m/day with specific storage values of 0.01/m, 0.002/m and 0.0001/m. These values were modified during the process of calibration of the model, if needed. The vertical hydraulic conductivity is taken as 1/20 times the horizontal hydraulic conductivity uniformly distributed over the area.

4.2 Estimation of stresses

Three stress periods with a duration of four months each coinciding with three cropping seasons of the year namely *Garma (*March to June), *Kharif* (July to Oct.) and *Rabi* (Nov. to Feb.) are considered in the model. Stresses in a groundwater system are usually due to outflow from the aquifer or inflow into the aquifer. In the study domain, the components of outflow consist of pumpage from aquifer, evapotranspiration, rivers and boundaries. The inflow components consist of recharge from rainfall, irrigation return flow and from boundaries etc. The outflow from the aquifer is defined as discharge and inflow is termed as recharge.

4.2.1 Estimation of Discharge

In the model, 800 tubewells pumping from first and third layer with discharge of 25 m^3/day for each well was taken during *Garma* and *Rabi* seasons (WALMI, 1993).

Potential Evapotranspiration (ET$_o$) values pertaining to the study area are taken from the average ET$_o$ values available for two nearby locations viz. Muzaffarpur and Patna (Hargreaves, 1985). These values were used for estimation of crop water requirements (Doorenbos et al., 1977, 1979) for different crops.

By dividing the consumptive use of the dominant crop in particular season throughout its base period evapotranspiration values for the cropped area in the model domain are calculated as 5.31 mm/day, 3.66 mm/day and 3.02 mm/day during *Garma, Kharif* and *Rabi* seasons respectively. The root zone depth is taken as 2.0 m. For the uncropped area the input `ET' values (i.e soil evaporation) are taken as 50% of the ET of the cropped area. This is simply a rational assumption, which may require to be modified during calibration. Outflow through boundaries is taken care by the model depending on the river/canal stages and the head in the boundary.

4.2.2 Estimation of Recharge

Areal recharge through rainfall and irrigation return flow due to spreading of water on the field through 18 outlets of the Habibpur sub-distributary each having a discharge of 2,160 m^3/day is considered as external recharge. Recharge due to inflow from river/canal and head dependent boundaries would be taken care by the model automatically depending on the heads in the boundaries. The areal recharge due to rainfall is taken as 20% of rainfall occurring in a particular season as starting values. However, the recharge is expected to be more during *Kharif* season due to occurrence of maximum rainfall (85%) and flat topography of the area. The quantum of recharge may go as high as 35%–40% of the rainfall. Therefore, the percentage of recharge in a particular season would be calibrated.

4.3 Initial and boundary conditions

The *Garma* season was taken as the initial condition. Observed daily watertable data for one year for four locations at Mirzapur, Chaturpara, Bhataulia and Chak Sadani were available. Since, observed water table data were scanty, additional wells were assumed adjacent to the river Gandak having fluctuation of water table elevation same as that of the stage of Gandak river. This provided better starting value of initial water table conditions at every cell.

West and east side of the study area is bounded by Gandak river and VBC flowing from north to south. The VBC and Habibpur sub-distributary are considered as streams having flow for all 120 days in *Kharif* season and only 40-45 days during *Rabi* season. Flow between the stream and the groundwater system is estimated using the following formula:

$$QRIV = CRIV(HRIV - h_{i,j,k}); \quad CRIV = \frac{k.L.W}{M} \quad (2)$$

where,
QRIV = flow between the stream and the aquifer [L^3T^{-1}],
CRIV = hydraulic conductance of the stream-aquifer interaction [L^2T^{-1}],
HRIV = head in the river [L],

$h_{I,j,k}$ = head at the node in the cell underlying the stream reach [L],
k = hydraulic conductance of river bed [L T^{-1}]
L = length of the reach contained in the river cell [L]
W = width of the river [L]
M = thickness of the river bed material [L]

Hydraulic conductance value of stream-bed material is assumed as 0.04 m/day. This assumption is based on the available exit resistance of water through streambed of rivers. Thickness of the bed material is taken as 2.0 m for river and 0.25 m for canals. The average width of Gandak river in the model domain, VBC and Habibpur sub-distributary are 750 m, 10 m and 4 m respectively. The cell length is 200 m. Values of `QRIV' for other cells are computed from the slope of the river-bed and canal by linear interpolation. Details of computations for different data types used as input to the `river package' are given in table 1.

Table 1. Details of river parameters considered in the `River package' in the model.

Stress Period	Entry (North)		Exit (South)		CRIV (m²/day)
	Stage (m)	River bed elevation (m)	Stage (m)	River bed elevation (m)	
Gandak river					
Garma	151.50		150.00		CRIV value for: Gandak = 3,000 m²/day, VBC = 320 m²/day and HSD = 117 m²/day.
Kharif	153.50	148.00	152.00	146.50	
Rabi	152.50		151.00		
Vaishali branch canal (VBC)					
Garma	155.31		152.20		
Kharif	156.65	155.31	153.54	152.20	Gradient of: Gandak = 1:15,000 VBC = 1:8,000 and HSD = 1:4,500.
Rabi	155.72		152.61		
Habibpur sub-distributary (HSD)					
Garma	155.24		154.42		
Kharif	156.33	155.24	155.41	154.42 (Last point)	
Rabi	155.40		154.63		

North and south side of the study domain did not have any conventional hydrological boundaries. These two sides were considered as General Head Boundaries (GHB).

5. CALIBRATION OF THE MODEL

The model was simulated with initial and boundary conditions, input values of aquifer parameters and external stresses. During initial run, the difference between the observed and computed water table elevation for three stress periods were noticeable and thus minor calibrations of aquifer parameters and/or stresses became necessary. During calibration, minor modifications of initial values of hydraulic conductivity, evapotranspiration and rainfall recharge were done considering the prevailing conditions in the area for three stress periods. The computed water table elevations obtained with the calibrated parameters show a close agreement with the observed water table elevations as shown in Figure 2. The model efficiency for Garma, Kharif and Rabi seasons are more than 90%.
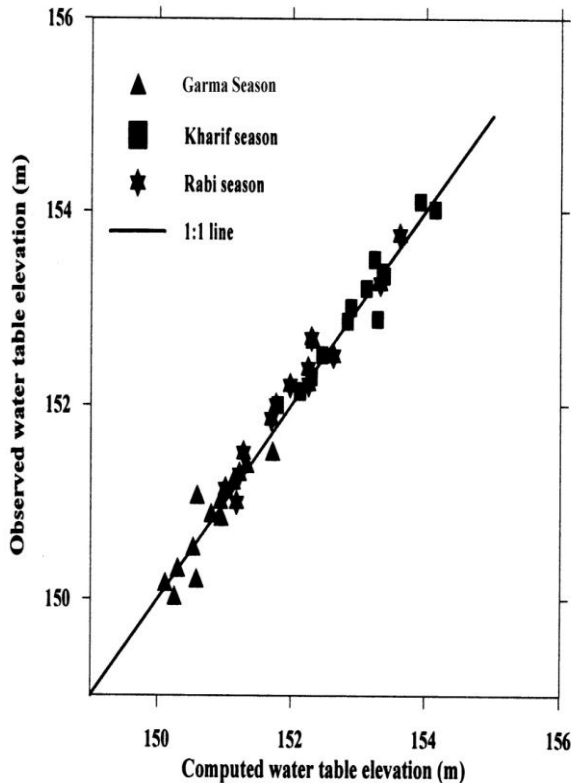
Figure 2. Computed versus observed water table elevations obtained after calibration of MODFLOW for Garma, Kharif and Rabi seasons.

The calibrated value of the hydraulic conductivity for first, second and third layers were 5m/day, 1m/day and 20 m/day respectively. The initial rainfall recharge of 1.655 mm/day (20% of rainfall) during *Kharif* season was modified to 4.137 mm/day. The evapotranspiration during *Garma* and *Kharif*

were calibrated to 6.37mm/day and 4.39 mm/day respectively for the cropped area.

6. ANALYSIS AND RESULTS

6.1 *Garma* season

The water balance computed by the model at the end of *Garma* season indicates that the river Gandak feeds the aquifer to the extent of 1300 m^3/day as well as gains marginally. There is inflow and outflow through GHB. The evapotranspiration is quite high (505,253 m^3/day from the whole area) which can only be met out of the aquifer storage. Thus, there is net depletion in water table. The computed depth to water table contours demarcate the waterlogged (< 2.0 m below ground level (bgl)) and non-waterlogged (> 2.0 m bgl) areas as shown in Figure 3. Although extent of waterlogged area is 104.8 km^2, but the areas for which depth to water table is less than 1.0 m bgl is only 15.8 km^2 with no surface waterlogging. It means, considerable area in the model domain has shallow water table. These are the prospective areas that can be brought under suitable cropping pattern within an acceptable limit.
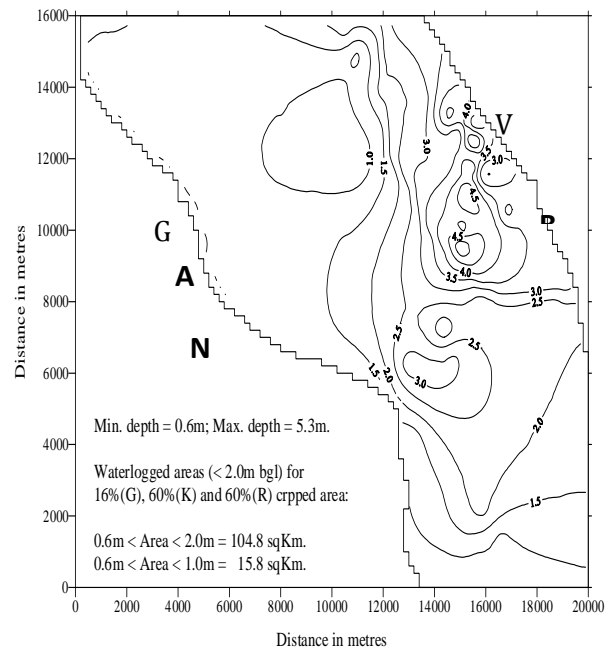
Figure 3. Depth to water table contours (m) at the end of *Garma* season.

6.2 *Kharif* season

The initial condition of *Kharif* season is the groundwater table elevation at the end of *Garma* season. The water balance shows that during *Kharif* season the components of river leakage from Gandak, areal recharge and inflow from GHB have the magnitude of 55018 m^3/day, 781493 m^3/day and 10523 m^3/day

respectively. The ET component is 528620 m^3/day. There is net recharge to the groundwater table. From the computed depth to water table contours, the extent of waterlogged area (< 2.0 m bgl) is 128.2 km^2. The areas for which the depth to water table is less than 1.0 m bgl is 83.8 km^2 with surface waterlogging (< 0.0 m) is 45.6 km^2. It means, considerable area in the model domain remains under surface waterlogging condition. The depth to water table contours also show emergence of waterlogged areas near Vaishali Branch Canal and Habibpur sub-distributary during *Kharif* season since the canal operates for all 120 days.

6.3 *Rabi* season

The water balance shows high outflow through ET (375688 m^3/day) whereas the total inflow due to river leakage, recharge and GHB is only 20%. Thus, there would be depletion of the aquifer storage and the water table would go down. From the computed depth to water table contours, the extent of waterlogged area (< 2.0 m bgl) is 86.4 km^2 and the areas for which the depth to water table is less than 1.0 m bgl is 52.2 km^2 with surface waterlogging (< 0.0 m) is 1.5 km^2 only.

The extent of waterlogged area could however be reduced considerably if cropped area is increased for all three seasons. At the same time, the CGWB report of Vaishali district (1993) indicates under-utilization of groundwater resources to an extent less than 50%. So, lot of irrigation potential in the area still remains to be explored. The model would help in planning futuristic groundwater surface water developmental activity in the area and its impact on the overall groundwater regime. The model can conveniently be used for any kind of water resources developmental activity which would incorporate change in cropped area, cropping pattern, change in rainfall and change in the stages of Gandak river, canal.

The objective of any conjunctive use model is to utilize water resources available in the area (surface and groundwater) so as to increase the water availability for irrigation. The present study has an additional objective of reducing waterlogged areas through increased water use during dry season. The calibrated model gives the scenario of waterlogged areas for the year 1991-92. The model is utilised to investigate the waterlogging scenarios for: i) increased the cropped area in all three cropping seasons to an acceptable limit and/or ii) utilization of maximum groundwater potential to meet the net irrigation requirement (NIR) of crops in different seasons of the year. These two conditions can help in lowering of water table inducing more areal recharge thereby reducing waterlogged area. The developed model can be an excellent tool to predict waterlogging scenarios by adopting these options. The model would thusbe used to investigate the waterlogging scenarios for both the options for three depths to water tables viz. i) < 2.0 m bgl, ii) < 1.0 m bgl and iii) 0.0 m bgl (i.e. surface waterlogging) so as to maximize areas under cultivation adopting suitable cropping pattern.

The existing percentage crop coverage during 1991-92 was 16% during *Garma*, 60% during *Kharif* and 60% during *Rabi*. The model has been used to predict the waterlogging scenario for projected crop areas in a phased manner upto 35% during *Garma*, 80% during *Kharif* and 80% during *Rabi* utilizing groundwater potential during *Garma* and *Rabi* season. One such scenario for three seasons with and without utilizing groundwater potential for two sets of crop coverage is depicted in Figure 4. The overall improvement in the waterlogging scenario for the projected area is shown in table 2.
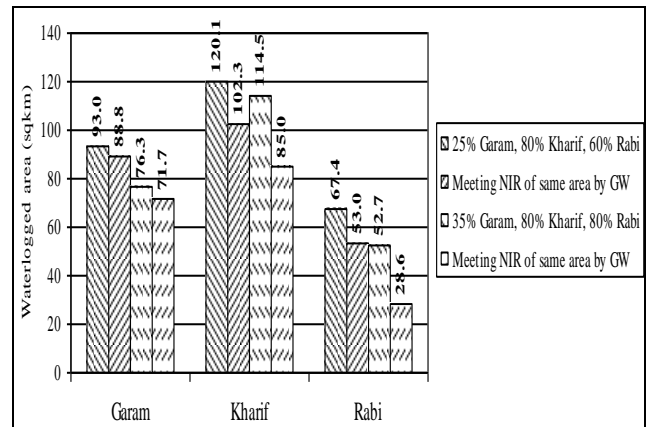
Figure 4: Effect of groundwater utilization on waterlogged areas (< 2.0m bgl).

Table 2: Improvement in waterlogging scenario for the projected area.

Depth to water table (m bgl)	Existing walerlogged area (91-92) (sqkm)			Walerlogged area Utilizing groundwater potential (sqkm)		
	Garma	Kharif	Rabi	Garma	Kharif	Rabi
Less than 2.0m	104.8	128.2	86.4	71.7	85.0	28.6
Less than 1.0m	15.8	83.8	52.2	5.5	44.1	16.8
Surface Waterlogging	Nil	45.6	1.5	Nil	19.8	0.1

7. CONCLUSIONS

The developed model provides an insight to various futuristic scenarios under different situations. The model is used to predict the extent of waterlogging under increased cropped area coverage and utilizing groundwater potential for irrigation during *Rabi* and *Garma* seasons. The model results show positive impacts on reduction of waterlogging under increased cultivable area. Utilizing groundwater potential to meet the

irrigation requirements of crops during *Garma* and *Rabi* seasons would provide assured irrigation to crops and also help in lowering of water table. This would facilitate greater areal recharge during *Kharif* season and reduce the extent of waterlogging in all three seasons. Thus, conjunctive use would result in reduction of waterlogged areas and greater agricultural productivity in the region.

REFERENCES

i.   Boonstra, J. 1989, SATEM: Selected aquifer test evaluation methods, ILRI publication 48, Wageningen, The Netherlands.

ii.   Bredehoeft, J. D., and R. A. Young. 1983. Conjunctive use of groundwater and surface water for irrigated agriculture: Risk aversion, Water Resources Research 19(5): 1111-1121.

iii.   Central Ground Water Board (CGWB). 1993. Hydrogeology and groundwater resources of Vaishali district, Bihar. Technical report no. 103, series 'D'.

iv.   Doorenbos, J., W.O Pruitt. et.al. 1977. FAO Irrigation and drainage paper-24, Guidelines for predicting crop water requirements. Food and Agriculture Organization of the United Nations.

v.   Doorenbos, J., A.H. Kassam et.al. 1979. FAO, Irrigation and drainage paper-33, Yield response to water, Food and Agriculture Organization of the United Nations.

vi.   Flores, E. Z., A. L. Gutjair, and L. W. Gelhar. 1978. A stochastic model of the operation of a stream-aquifer system, Water Resources Research 14(1): 30-38.

vii.   Haken, B., and M. A. Marino. 1998. Joint management of surface and ground water supplies, Ground Water 37(2): 214 – 222.

viii.   Hargreaves, G.N., U.K. Prasad,, and Sumani, Z.A. et.al. 1985. A crop water evaluation manual for India. The international Irrigation center, Utah State University, USA: 85-86.

ix.   Kruseman, G.P. and N. A. de Ridder. 1991. Analysis and evaluation of pumping test data, ILRI publication 47, Wageningen, The Netherlands: 13 – 25.

x.   Matsukawa, J., B. A. Finney, and R. Willis. 1992. Conjunctive use planning in Mad river basin, California, Journal of Water Resources Planning and Management, ASCE 118(2): 115-132.

xi.   McDonald, M. G., and A. W. Harbaugh. 1988. A Modular three-dimensional finite-difference groundwater flow model - Techniques of water resources investigations of the United States Geological Survey. Book. 6, Chap. A1, U. S. Geological Survey.

xii.   O'Mara, G. T., and J. H. Duloy. 1984. Modeling efficient water allocation in a conjunctive use regime: The Indus basin of Pakistan, Water Resources Research 20(11): 1489-1498.

xiii.   Onta, P. R., A. D. Gupta, and R. Harboe. 1991. Multistep planning model for conjunctive use of surface and groundwater resources. Journal of Water Resources Planning and Management, ASCE 117(6): 662-678.

xiv.   Reichard, E. G. 1995. Groundwater-Surface water management with stochastic surface water supplies. Water Resources Research 31(11): 2845-2865.

xv.   Tsur, Y. 1990. The stabilization role of groundwater when surface water supplies are uncertain: The implication for groundwater development. Water Resources Research 26(5): 811-818.

xvi.   WALMI, CWRS and IIMI Sri Lanka. 1993. Research on conjunctive management of surface and groundwater for irrigation in the lower reaches of Gandak Command.

xvii.   Young, R. A., and J. D. Bredehoeft. 1972. Digital computer simulation for solving management problems of conjunctive groundwater and surface water systems. Water Resources Research 8(3): 533-556.

Identification Of Unknown Pollution Sources In Groundwater Aquifer Using Ann-Ga Based Simulation-Optimization Model

T. Borah[1]   R.K. Bhattacharjya[2]

[1]*Jorhat Engineering College, Jorhat, Assam, India*
[2]*Indian Institute of Technology Guwahati, Guwahati- 781039, Assam, India*
Email*: rkbc@iitg.ernet.in*

ABSTRACT : Identification of unknown pollution sources is an important and challenging task for the engineers working on pollution management of a groundwater aquifer. The locations and transient magnitude of contaminant sources can be identified using inverse optimization techniques. In this approach, an error function is formulated which is minimized using an optimization algorithm. The error function is basically the difference between the simulated and observed contaminant concentration at observation locations. The simulated concentration can be calculated using aquifer simulation model. As such there is a need to incorporate the aquifer simulation model with the optimization model. The performance of the source identification model is highly related to the aquifer simulation model. Incorporation of sophisticated numerical simulation model will give better performance, but the model will be more computationally expensive. The computational efficiency of the model can be achieved using approximate simulation model. In this study, we have used ANN model to simulate the aquifer process. The ANN model is linked with the optimization model for predicting unknown pollution sources. The performance of the model has been evaluated using illustrative study areas.
***Keywords:** Pollution, Aquifer, Optimization, Artificial Neural Networks, Genetic Algorithms*

1. INTRODUCTION:

The requirement of freshwater is increasing day by day due to the alarming growth of population and substantial industrial and agricultural development. Due to the increased demands of freshwater, overexploitation of groundwater becomes unavoidable in many parts of the world, specifically for the regions away from the surface water sources. As a result of overexploitation, groundwater table has been depleted substantially in many parts of the world. Apart from depletion of groundwater table, the overexploitation of groundwater has also exaggerated the problem of groundwater contamination as more and more contaminants reach the well point due to the increased flow towards the well. The groundwater may be contaminated by various point and nonpoint sources of pollutants. Some of the common groundwater pollution sources are intensive use of fertilizers, herbicides, pesticides, disposal of human and industrial waste, natural pollution sources of minerals like fluoride, arsenic, iron, *etc*. This leads in increase

in concentration of contaminants at the well locations. Once groundwater gets polluted, it is difficult and uneconomical too to restore its quality again. Moreover, in many situations, the sources of pollution are not known explicitly. As such, there is a need to develop methodologies to identify the unknown groundwater pollution sources so that appropriate management strategies can be adopted for sustainable exploitation of the aquifer (National Research Council 1990). The contamination of groundwater has been addressed by numerous researchers from different corners of the world (Deninger, 1970; Kleinecke, 1971;; Maddock, 1972; Frind and Pinder, 1973; Hefez, 1975; Alley *et al.,* 1976; Mahar and Datta, 2000, 2001; Das and Datta, 2000; Montas*et al.,* 2000; Nunes*et al*., 2004;Yeh*et al*., 2007; Dhar and Datta, 2007; Chandalavada and Datta, 2008; Kollat*et al*., 2011; Dhar and Datta,2009; Chandalavada*et al*., 2011; Prakash and Datta, 2013).

The groundwater pollution source can be characterized by its location, magnitude, and duration of activity. The pollutant observed at an observation well may be caused by the pollution sources of more than one locations. Further, at each potential location, magnitude of source flux may vary and may also operate with different disposal period. This is really a difficult task to identify the true combination of pollution sources from the innumerable combinations. Unknown groundwater pollution sources can be identified using inverse optimization technique. In this technique an error function is defined which minimizes the absolute differences between simulated and actual contaminant concentration at few observation locations. The actual concentration can be observed at the field. On the other hand, the simulated concentration can be obtained using aquifer simulation model. Therefore it is necessary to incorporate the aquifer simulation model with the optimization model. It can be viewed that for calculation of objective function value, it is necessary to simulate the aquifer process. Thus the methodology is known as simulation-optimization problem. The incorporation of aquifer simulation model with the optimization model makes the problem a very difficult one. The process is complex and time consuming too. Incorporation of numerical simulation model with the optimization model makes the problem a very time consuming one. Computational time can be reduced by using approximate simulation model.

In this paper, for reduction of computational time, ANN model is used to simulate the flow and transport processes of aquifer. The ANN model is then linked with optimization model for solving groundwater pollution source identification problem. ANN model can simulate the flow and transport processes very quickly and has also the capability to simulate complicated real world groundwater simulation model. As such, the linking ANN model with the optimization model has facilitated to solve complicated real world source identification problem. In this study, we have developed a simulation-optimization model using ANN as the approximate simulator of groundwater aquifer process. The ANN model is linked externally with the inverse optimization model which has been solved using direct

search method and genetic algorithms. Performance of the methodology is evaluated and compared with the embedded optimization approach. The approach is computationally less extensive. It takes up to few hours to solve a source identification problem of a medium scale groundwater aquifer. It may be mentioned here that use of numerical simulation model takes around few days of computational time to solve the same problem. The performance of the model is evaluated using the two illustrative study areas.

2. MATERIAL AND METHODS

For finding the unknown pollution sources, the inverse optimization model minimizes the difference between simulated and the observed concentration of contaminants at observation wells. The error function can be written as,

$$Minimize\, err = \sum_{t=1}^{T} \sum_{n=1}^{N} (OC_t^n - SC_t^n)^2$$

The err is a function of magnitude of pollution sources. OC_t^n is the observed concentration at n[th] well location fort^{th} time steps; SC_t^n is the simulated concentration at n[th] observed location for t^{th}time steps; N is total number of observation wells and T is the total time steps. The observed concentration is the concentration measured at the observation wells. The simulated concentration can be obtained using the aquifer simulation model, which basically solves the governing partial differential flow and transport equations. As such, the aquifer simulation model has to be executed for calculating the objective function value. This can be done by linking the aquifer simulation model with the optimization model. As simulation model is linked with the optimization model, the methodology is known as simulation-optimization model. We have used ANN model to simulate the flow and transport processes in aquifer. The simulation-optimization methodology can be explained using the schematic diagram presented in Fig. 1.
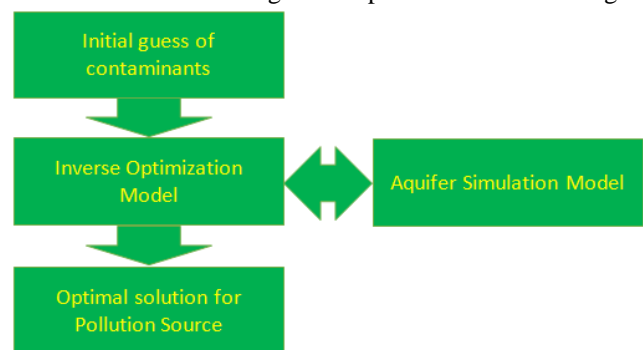

Fig.1. Schematic representation of Simulation-Optimization methodology

The algorithm starts with the supply of initial guesses of contaminants at probable source locations. The source values are supplied to the inverse optimization model. For calculating objective function value for the given sources, the inverse model calls the aquifer simulation model. The source values are

then updated by the inverse model. The iterations between optimization model and aquifer simulation model continue till termination criteria are not satisfied.

2.1 Study area

The performance of the developed model has been evaluated using two illustrative study areas. We have used the study area considered by Mahar and Datta (2000) to evaluate the relative efficiency of the model. This is a rectangular shaped confined aquifer. To show the field applicability of the developed model, another bigger study area with irregular boundary is also considered in this study area.

2.1.1 First study area

The problem considered by Mahar and Datta (2000) is initially considered here for evaluating the performance of the proposed models (Fig. 2). The hypothetical confined aquifer has an area of 1.04 km2 (1.3 km× 0.8 km) and is homogeneous and isotropic. In this study area, the boundary condition of the aquifer is considered as time invariant. The aquifer has fixed head boundary condition in the east and in the west sides, whereas the north and the south boundaries of the aquifer have no flow boundary. In the east side of the aquifer, the hydraulic head is varying from 100.00m to 99.58m. On the other hand, in the west side of the aquifer, the hydraulic head is varying from 88.00m to 87.72m. The aquifer is simulated for single layer in the computational grid. There are 8 rows and 13 columns. The study area is discritized into 100m x 100m. Inside the aquifer, the initial head is considered as 100 m. There are three pollutant sources in the aquifer which have been designated as S1, S2 and S3. The concentration values at S1 locations are 47 gm/sec, 15 gm/sec, 37 gm/sec and 0 gm/sec for four time steps. Similarly concentration for S2 source location are 30 gm/sec, 58.80 gm/sec, 0 gm/sec, 35 gm/sec whereas the source S3 is inactive throughout the simulation period. The initial contaminant concentration for the entire aquifer is 100 ppm. The parameters used in the simulation are; horizontal hydraulic conductivity ($K_{xx} = K_{yy}$) of 0.0002 m/s, porosity (η) of 0.25, longitudinal dispersivity (α_L) of 40.0m, transverse dispersivity (α_T) of 9.6 m and storativity (S) of 0.002. There are eight observation wells which have been designated as W1, W2, W3, W4, W5, W6, W7 and W8. The aquifer has only a single pumping well (P) which is located at the centre of the study area. The pumping rates are shown in Table 1. The flow and transport simulation are made for 5 years considering time interval of 3 months. At the time of simulating the transport process, out of three pollutant sources, only two are considered as active while other one is taken as inactive.

2.1.2 Second Study area

Fig. 3. Illustrative second study area

The proposed model is applied in a bigger area as shown in Fig. 3 to show the field applicability of the model. The size of the second study area is approximately 17.346 km^2. The west and south sides of the aquifer are bounded by the rivers. As such, constant head boundary is considered in these two sides. The other two boundaries, i.e., the north and the east sides have no flow boundary. The boundary condition of the aquifer is considered as time invariant. There are five contaminant sources in the aquifer which have been designated as S1, S2, S3, S4 and S5. The concentration values assigned for these five locations at S1, S2, S3, S4 and S5 are 908.42 gm/sec, 1130.50 gm/sec, 653.35 gm/sec, 902.13 gm/sec, 721.25 gm/sec; 644.02 gm/sec, 1023.87 gm/sec, 1139.88 gm/sec, 781.09 gm/sec, 889.77 gm/sec; 0 gm/sec for all the time steps; 0gm/sec,1024.16 gm/sec, 652.05 gm/sec, 1117.45 gm/sec, 987.08 gm/sec, 0gm/sec,0gm/sec,1104.82 gm/sec, 639.93 gm/sec respectively. The initial contaminant concentration for the entire aquifer is 200 ppm. There are four pumping wells in the study area which has been marked as P1, P2, P3 and P4. The pumping rate assigned for different stress periods are

Table 1. Pumping rate at the wellfor the first study area

Pumping rate (m^3/day)			
Time step	First study area	Time step	First study area
1	273.02	11	163.29
2	163.29	12	327.45
3	327.45	13	273.02
4	163.29	14	163.29
5	273.02	15	381.02
6	327.45	16	217.72
7	163.29	17	273.02
8	273.02	18	163.29
9	381.02	19	327.45
10	217.72	20	217.72

shown in Table 2. There are eight observation wells which are designated as W1, W2, W3, W4, W5, W6, W7 and W8. The flow and transport simulation are done for 5 years considering time step of 3 months. The hydraulic parameters for this study area are considered as same as the first study area.

2.2 Development of simulation-optimization methodology

In order to achieve efficiency in computational time, ANN model is proposed to simulate flow and transport processes in aquifer. Initially, the inverse model is solved using direct search (DS) optimization algorithm. The approach can be named as ANN-DS mode. The model is also solving using genetic algorithms (GA). This approach is designated as ANN-GA model. The ANN model is developed using ANN toolbox available in Matlab which is then used to calculate the objection function value of the source identification optimization model. The ANN simulator is repeatedly called by the optimization model to evaluate the error function. The iterative process is continued until termination criteria are not satisfied.

2.3 Development of ANN model

We have used single hidden layer standard feed-forward network and the network is trained using back propagation algorithm. The data required for training the ANN model is generated by using Groundwater Modeling System (GMS) model. For solving the source identification problem, we need to find out the simulated concentration at the observation locations. The objective of the simulation model is to predict the concentration at observation wells. Thus the output from the ANN model is the concentration at the observation wells at different time steps. The pollutant sources in the aquifer are the input to the ANN model. There are eight observation wells in both the study areas. Thus we have developed eight different ANN models for predicting concentration at observation wells, i.e. each ANN model will predict the concentration of a particular observation well only. The problem is now much smaller with input to the ANN model is the source fluxes at source locations, which is equal to 60. The output from the ANN model is the concentration at the observation wells, which is equal to 20. The ANN architecture for the first study area is therefore 60-HN-20. Where HN is the number of hidden neurons. The optimal number of hidden neurons required has been calculated using trial and error method. An experiment is also conducted to obtain the other parameters of the ANN models. In the second study area, there are five pollution sources and simulation is performed for five years at an interval of three months. As such, total input to the ANN model is equal to 100. The outputs from the ANN model are the concentrations for the entire simulation period at an observation well. As such, the total output of the ANN model is equal to 20. The ANN architecture for the second study area is 100-HN-20, where HN is the hidden neurons. For this study area also, an experiment has been conducted to find out the number of

hidden neurons and other model parameters for optimal performance of the model. Based on the experimental study we have used 65 hidden neurons for the second study area. Around 2000 data are generated using the GMS model for training and validation of the ANN model. Out of the 2000 patterns, 60% is used to train the networks and 20% each is for validation and prediction of the model.

3. RESULTS AND ANALYSIS

3.1 Performance of the ANN model for first study area

The performance of the ANN model as an approximate simulator of the flow and transport processes in grounwater aquifer is evaluated on the basis of three stastical criteria, *i.e.* average absolute relative error (AARE), threshold statistics (TS) and coefficient of correlation (R). The ANN results are compared with the results obtained using GMS model.Fig. 4 shows the scatter plots for observation well 1 at first time steps. It can be observed that the linear fit line makes an angle approximatly equal to 45° with the x-axis and coefficient of correlation value is 0.99. The x-axis of the plot represents the predicted concentration by the ANN model and y-axis represents the concentration simulated by the GMS model. This shows that the ANN prediction is quite good. It can be observed from the figure that, the ANN prediction and GMS simulation results are almost similar for these wells. These show that that ANN model has high predicting capablity in simulating the flow and transport processes in groundwater aquifer. Fig. 5 shows the breakthrough curve generated for first study area by using ANN and GMS models. It is observed in the figure that the breakthrough curves are comparable and follow the same pattern.Initially,the performance of the model is evaluated for error free data, i.e. the model is trained using the data generated using the GMS model. The performance of the model is evaluated on using average absolute relative error

Table 2. Pumping rate at the wellfor the second study area
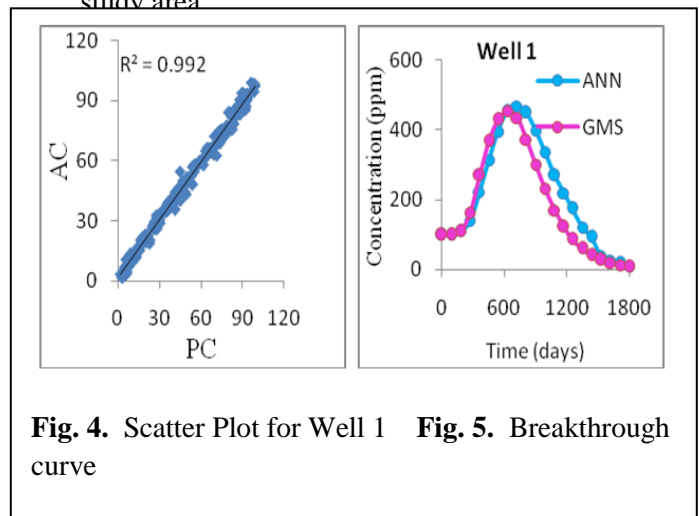

Fig. 4. Scatter Plot for Well 1   **Fig. 5.** Breakthrough curve

(AARE), threshold statistics (TSx) and coefficient of correlation (R) criteria. The AARE and R values for the first observation well at first time step is 3.93 and 0.985 respectively. For the second time step, the AARE and R values are 2.26 and 0.997 respectively. These values are quite encouraging and show the good predicting capability of the ANN model. For the other observation wells also, the value of AARE and R values are quite encouraging. The performance of the model is also superior in terms of TSx statistics. We have also checked the model performancewhile trained using erroneous data.The performance of the model while trained using erroneous data generated using mean zero and sigma 0.05 is also evaluated using TSx statistics for *x*value of 5, 10, 20, 30, 40 and 50. The average values of TS5, TS10, TS20, TS30, TS40 and TS50 are 82.52%, 91.42%, 94.04%, 95.86%, 96.92% and 97.30% respectively. It means ARE value of 82.52% pattern are less than 5%; 91.42% pattern are less than 10%; 94.04% pattern are less than 20%; 95.86% pattern are less than 30%; 96.92% pattern are less than 40% and 97.30% pattern are less than 50%. This evaluation shows that the performance of the model does not degrade much while trained using erroneous data.

3.2 *Performance of the ANN model for second study area*
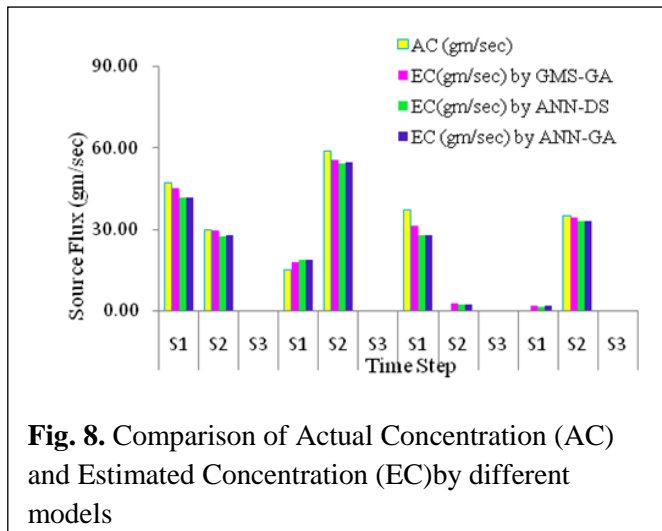
Fig. 8. Comparison of Actual Concentration (AC) and Estimated Concentration (EC)by different models

Fig.6 shows the scatter plots for an observation well. It can be observed that the ANN prediction and GMS simulation results are almost the same. Therefore, it can be concluded that the developed ANN model has high predicting capability in simulating the flow and transport processes of groundwater aquifer. Fig. 7 shows the comparison between the ANN simulation and the GMS simulation in terms of breakthrough curvefor well 1. It can be seen from the figure that the both the curves are comparable and the results are intuitively as expected.We have also checked the performance of the model with erroneous data for second study area and same treand have been observed as first study area.
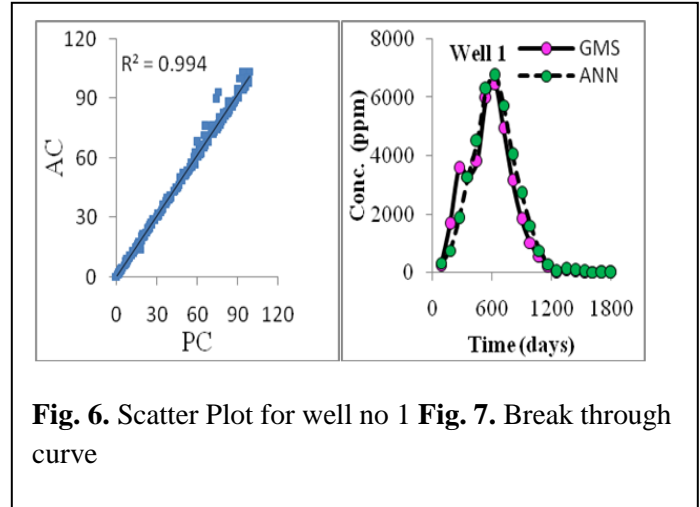
Fig. 6. Scatter Plot for well no 1 **Fig. 7.** Break through curve

3.3 Performance of ANN based simulation-optimization model for first study area

The proposed inverse models, i.e. ANN-DS and ANN-GA are utilized to obtain the unknown pollution sources of first study area. The results obtained by ANN-DS and ANN-GA models have been compared with the actual source concentration and the results obtained using GMS-GA model. In case of GMS-GA model, the GMS simulator is linked to the inverse optimization model. It can be observed from the Fig. 8 that concentration estimated by ANN-GA model is superior to ANN-DS model whereas the concentration estimated by GMS-GA methodology is more closer to the actual concentration. The concentration estimated by ANN-DS and ANN-GA models for first time step is 41.48 gm/sec and 41.67 gm/sec respectively whereas concentration estimated by GMS-GA model is 45.29 gm/sec, which is more closed to the actual concentration. The actual concentration is 47 gm/sec. This shows that ANN-GA model is slightly better than ANN-DS model and GMS-GA model is significantly better than both ANN-GA and ANN-DS model. For the other time steps also same trend have been observed. Thus for this study area, it can be conclude that GMS-GA model is better than ANN-DS and ANN-GA model in predicting the unknown pollution sources of the aquifer.

3.4 Performance of ANN based simulation-optimization model for second study area

The ANN based simulation-optimization model is also applied to the second study area to evaluate the applicability of the method on larger aquifer system. The unknown source flux obtained by ANN-DS and ANN-GA models are compared with the actual source flux value and also with the results obtained using GMS-GA model. It can be observed that the concentration predicted by the ANN-DS and ANN-GA model is almost similar whereas GMS-GA model is closer to the actual concentration. The actual value at source S1 for first time step is 908.42 gm/sec. The concentration predicted by

GMS-GA model is 990.72 gm/sec whereas the concentrations predicted by ANN-DS and ANN-GA models are 1027.06 gm/sec and 1027.40 gm/sec respectively. Similarly for the S2 source location, the actual concentration at time step 1 is 644.02 gm/sec whereas concentration predicted by GMS-GA, ANN-DS and ANN-GA are 771.30 gm/sec, 886.42 gm/sec and 818.54 gm/sec respectively. For the other sources and time steps also the concentration predicted by GMS-GA is better than the ANN-DS and ANN-GA model. But the concentration predicted by ANN-GA is slightly better than ANN-DS model. Fig.9 shows the comparison of these methodologies using bar diagram.

Fig.9. Actual and predicted source fluxes obtained by different model for second study area

We have also conducted an analysis to evaluate the efficiency of the models in terms of computational time requirement. Table 3 shows comparison of the objective function value and computational time requirement for GMS-GA, ANN-DS and ANN-GA methods for both the study areas. It may be observed from the table that for the first study area, the time required for solving the problem by GMS-GA model is 2 days 1 hour 15 minutes and 24 seconds. On the other hand the times required by ANN-DS and ANN-GA models are 2 hours 15 minutes 49 seconds and 2 hours 48 minutes 43 seconds respectively. This clearly shows that GMS-GA model is computationally less efficient than ANN-DS and ANN-GA models. For the second study area, time required by GMS-GA model to solve the problem is 5 days 1 hou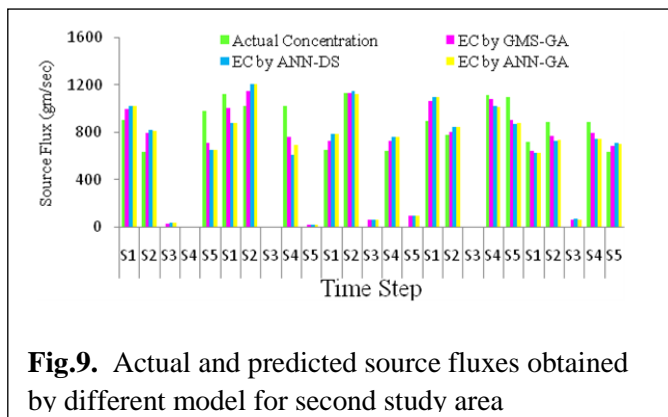r 54 minutes and 45 seconds. On the other hand the times required by ANN-DS and ANN-GA models are 4 hours 56 seconds and 4 hours 9 seconds respectively. This also shows that GMS-GA model is computationally less efficient thanANN-DS and ANN-GA models. Further it can be observed from the table that ANN-DS and ANN-GA models are less efficient in predicting the unknown sources than GMS-GA model. Thus it can be concluded that ANN-DS and ANN-GA models are computationally more efficient than GMS-GA model but inferior in terms of prediction capabilities of unknown pollution sources. In summary, it can be concluded that in terms of predicting capability GMS-GA model is more efficient than ANN-GA and ANN-DS model. However, in terms of computational time requirement, ANN-GA and ANN-DS is more efficient than GMS-GA model.

Table 3. Comparative evaluation of the models in terms of computational time

| Models | First Study area | | | Second Study area | |
	Obj. funct. value	Time DD HH MM SS	Obj. funct. value	Time DD HH MM SS	
GMS-GA	1.34E-06	02:01:15:24	1.340E-06	05:01:5	
ANN-DS	2.33E-04	00:02:15:49	3.160E-04	00:04:(	

4. CONCLUSIONS

This paper presents two linked simulation-optimization models for optimal identification of unknown groundwater pollution sources. In the first model, the artificial neural network (ANN) is linked with the direct search (DS) based optimization model. In the second approach, ANN model is linked externally with GA based optimization model for solving source identification problem. The main advantage of ANN-DS and ANN-GA models is that it takes only few hours to solve a relatively medium scale source identification problem of medium scale aquifer system. This approach drastically reduces the computational time of the simulation-optimization model. The problem which was solved in few days using GMS-GA approach can now be solved in few hours. However, most of the time, it yields only the near optimal solution. The main drawback is that the quality of the solution is inferior as compared to GMS-GA model.

REFERENCES:

i. Alley, W.M., Aguado, E., and Remson, I. (1976). 'Aquifer management under transient and steady state conditions.' Water Resour. bull., 12(5), 963-972.

ii. Chadalavada, S., and Datta, B. (2008), 'Dynamic Optimal Monitoring Network Design for Transient Transport of Pollutants in Groundwater Aquifers.' Water Resour. Management, 22(6), 651-670.

iii. Chadalavada, S., Datta, B. and Naidu, R. (2011), 'Uncertainty based optimal monitoring network design for a chlorinated hydrocarbon contaminated site.' Environ. Monit. Assess., 173, 929-940.

iv. Das, A., and Datta, B. (2000), 'Optimization Based Solution of Density Dependent Seawater Intrusion in Coastal Aquifers.' J. Hydrol. Engg., ASCE, 5(1), 82-89.

v. Deninger, R.A. (1970), 'System analysis of water supply systems.' Water Resour. Bull., 6(4), 573-579.

vi. Dhar, A. and B. Datta, B. (2007), 'Multiobjective Design of Dynamic Monitoring Networks for Detection of Groundwater Pollution.' Water Resour. Plng. and Mgmt., 133(4), 329-338.

vii. Dhar, A.,and Datta, B. (2009), 'Logic based design of groundwater monitoring network for redundancy reduction.' J. Water Resour. Plng. and Mgmt. (ASCE), Vol 136 (1), 88-94.

viii. Frind, E.O. and Pinder G. F. (1973), 'Galerkin solution of the inverse problem for aquifer transmissivity.' Water Resour. Res., 9(5), 1397-1410.

ix. Hefez, E.,Shimar V., Bear J. (1975), 'Identifying the parameters of an aquifer cell model.' Water Resour. Res., 11(6), 993-1004.

x. Kleinecke, D. (1971), 'Use of linear programming for estimating geohydrologic parameters of groundwater basins.' Water Resour. Res., 7(2), 367-374.

xi. Kollat, J. B., Reed, P. M., & Maxwell, R. (2011), 'Many-objective groundwater monitoring network design using bias-aware ensemble kalman

filtering, evolutionary optimization, and visual analytics.' Water Resour. Res., 47, W02529.

xii. Maddock III, T. (1972), 'Algebraic technological function from a simulation model.' Water Resour. Res., 8(1), 129-134.

xiii. Mahar, P.S., and Datta, B. (2000), 'Identification of Pollution Sources in Transient Groundwater Systems.' Water Resources Management, 14(3), 209-227.

xiv. Mahar, P.S., and Datta, B. (2001), 'Optimal Identification of Ground-Water Pollution Sources and Parameter Estimation.' J. Water Resour. Plng. And Mgmt., ASCE, 127(1), 20-29.

xv. Montas, H.J., Mohtar, R.H., Hassan, A.E. and AlKhal, F.A. (2000), 'Heuristic Space-Time Design of Monitoring Wells for Contaminant Plume Characterization in Stochastic Flow Fields.' J. Cont. Hydrol., 43(3-4), 271-301.

xvi. Yeh, H.D., Chang, T.H. and Lin, Y.C. (2007), 'Groundwater Contaminant Source Identification by a Hybrid Heuristic Approach.' Water Resour. Res., 43(9), 1-16.

Assessment Of Ground Water Potential Zones In Bankura-1,Saltora,Chatna Blocks Of Bankura District Of West Bengal Using Remote Sensing & Gis

Raktim Biswas[1], S.Bhattacharyya[2], K.Adhikari[3]
[1] Research Scholar, Civil Engineering Department, NIT Durgapur, India
[2]Prof.,Civil Engineering Department, NIT Durgapur, Indi a[3]Assossiate Prof., Earth & Environmental Studies Department, NIT Durgapur, India
Email:[1.] raktim.biswas6215@gmail.com, [2]sb_recdgp@yahoo.com, [3]k_adh@yahoo.com

ABSTRACT: *Ground water has emerged as an important source to meet the water requirement of various sectors of the world including the major consumers of water like irrigation, domestic and industries. And so its demand is increasing with time due to rapid urbanisation, industrialisation and population explosion. The sustainable development and management of ground water resources requires quantitative assessment based on scientific principles. The present study has been undertaken to demarcate the Ground Water Recharge Potential Zones using Geographical Information System (GIS) approach. This approach is used in this study to demarcate the ground water potential zones of Bankura-1, Saltora&Chatna blocks of Bankura district of West Bengal. In order to do this, various thematic maps such as Land use-Land cover, Soil Type, Geology, Hydrogeology, Lineament Density, Drainage Density, Slope & Auto-flow zone were integrated in TNT MIPS Pro environment and the Multi-Criteria Analysis Method has been used in the present study. During Multi-Criteria Analysis the weightage has been given for each thematic map and the scores were assigned to each parameter of the thematic maps according to relevance to ground water recharge potential. Scoring was done in the context of Analytical Hierarchy Process (AHP). The ground water potential zones were generated in terms of Good, Moderate, Poor grades with Ground Water Potential Index (GWPI) values lying in the ranges of 7-9,4-6,1-3 respectively.*
Keywords: GIS, Ground Water, Multi-Criteria Analysis Method, AHP, GWPI.

1.INTRODUCTION:

Ground water is one of the most precious natural resources which supports human civilization in different aspects like economic development, ecological diversity and hygiene of living beings. With its varied intrinsic qualities (e.g. consistent temperature, widespread, continuous and spatial availability, excellent natural quality, limited vulnerability to contamination, low development cost and reliability against draught), it has come up as an inevitable source of water supplies in all climatic conditions of urban and rural areas of developed and developing countries (Todd and Mays 2005). Out of 37 M km^3 of fresh water estimated to be present on the earth, around 22% forms as ground water which in-turn makes around 97% of all liquid fresh water potentially available for human purpose (Foster 1998). In our country more than 90% of the rural and nearly 30% of urban demography rely on ground water for fulfilment of their drinking and house-hold requirement (Obi Reddy et al. 1996). Therefore, ground water studies have become important not only for targeting ground water potential zone but for subsequent monitoring and conserving this ever vital resource. In order to locate aquifer, its physiographic characteristics and the quality of available ground water in a catchment or a river basin, test drilling/ stratigraphy analysis are the most reliable and standard conventional method but it comes out to be very costly, time consuming and hence requirement of skilled personnel (Sander et al.1996). But remote sensing with integrated GIS technology with its advantage of spatial, spectral and temporal availability of data covering large and inaccessible areas with a short duration of time, it has proven as a useful technique for the assessment, monitoring and sustainable management of ground water resources (Engman and Gurney 1991, Jha et al. 2007).

2.STUDY AREA:

Bankura district of West Bengal in Eastern India has been facing an acute water shortage problem for both irrigation and domestic purposes over the past few decades. Every year in summer season most of the water surfaces dry up causing therefore a serious water deficit for the above both sectors. Again because of uncertain nature of the South-West monsoon in India, the availability of surface water resources cannot be ensured in appropriate quantity at required time period.Hence the majority of irrigated cropland in the district is being cultivated with the aid of ground water acquired from masonry dug wells and hand tube wells. However, the unrestricted pumping of ground water has resulted in ground water level declination in a considerable parts of the study area. Dug wells and hand pumps become inoperative every year during the dry period and thereby resulting acute water problem in the study

area.The region (Bankura-1,Saltora,Chatna) is located in Bankura district in the western part of the state West Bengal and included in the area known as "Rarh" in Bengal.The four corners of the study area are : upper left 86°41'40"E and 23°37'06"N, lower left : 86°41'40"E and 23°08'31"N, upper right: 87°07'43"E and 23°37'38"N and lower right: 87°07'43"E and 23°38'31"N. The tropic of cancer passes almost middle through the district and the river Damodorflows the northern boundary of the study area as well as the district.The study area is bounded by the SOI topographic sheets 73 M/2, 73 M/3, 73 M/4, 73 I/14,73 I/15, 73 I/16.It is paradoxical that though the area lies in sub-humid zone having total annual rainfall of 1300 mm to 1400 mm; cultivators are largely dependent on the uncertain onset of monsoon. Drought constitute major hazard in the area.So, the main aim of the present study was to assess ground water potential in the three blocks (namely Bankura -1,Shaltora, Chatna) in Bankura district of West Bengal by considering suitable thematic layers that have direct and indirect influence over the ground water occurrence using GIS technique.

Figure 1. Location of Study Area

3. DATA AND METHODOLOGY

3.1.Generation of Thematic Layers

For demarcation of ground water potential in the study area a multi parametric dataset comprising satellite data and conventional maps were used.DEM (Digital Elevation Model) was collected from ASTER DEM from USGS, from which slope map, drainage density map were prepared in TNT MIPS Pro environment. Conventional maps like survey of India (SOI)

topographic sheets were collected from Geological Survey of India (GSI), Govt. of India, Kolkata. All the six toposheets covering the study area at 1:50,000 scale were scanned separately and were Geo-referenced and subsequently mosaicked to form a single image and transferred to GIS environment to be prepared as study area boundary thematic layer. The thematic layers of geology and hydrogeology and lineament density, auto-flow buffer zone were prepared from existing hydrogeology map obtained from NRDMS Bankura, Govt. of West Bengal by the same process. The soil layer was prepared by digitizing the soil mapobtained from the NBSS and LUP, Govt. of India, Nagpur at 1:2,50,000 scale. And finally land use/land cover map was prepared with the help of LU/LC image obtained from BHUVAN website of ISRO. The projection type was used "polyconic" with the spheroid and datum as "WGS-84". All these thematic maps and their features were subsequently given weightage and finally were run into Multi Criteria Analysis under GIS environment to obtain finally the ground water potential index map. The thematic maps were further modified by applying cartography in TNT MIPS Pro environment for the final representation.
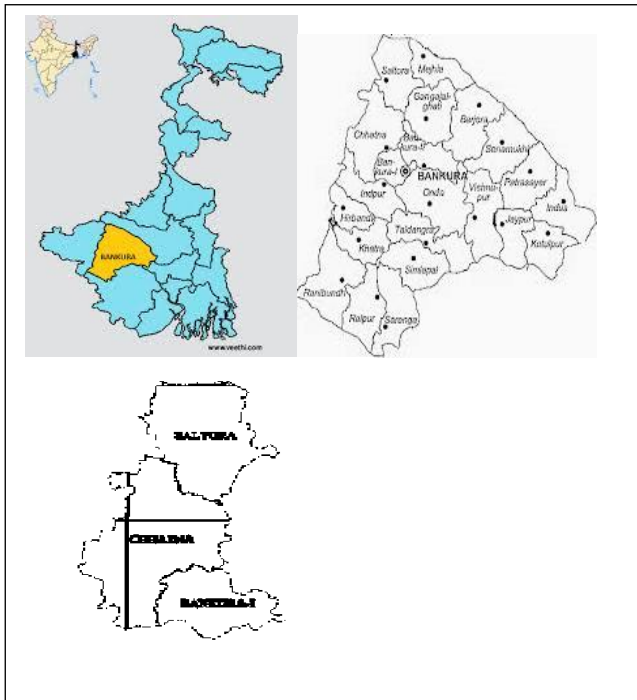

Figure 2. DEM & Topographic Study Area
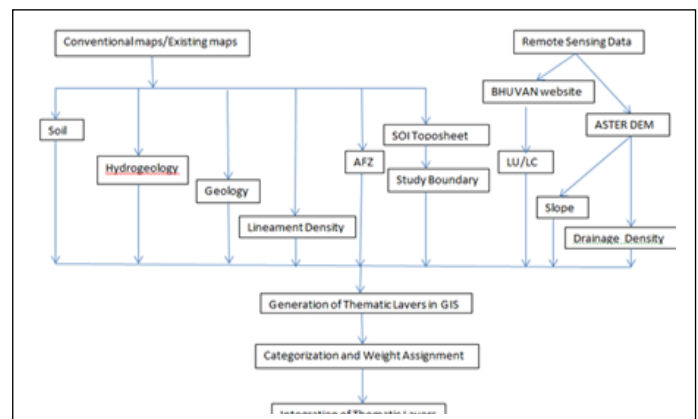
Flowchart 1.Groundwater Potential Assessment using integrated Remote Sensing and GIS technique.

3.2. Integration of Thematic Layers:

Thematic layers of geology, hydrogeology, soil, slope, drainage density, lineament density and auto flow buffer zone were used for the delineation a ground water potential zone in the study area. All of these thematic layers were integrated in TNT MIPS Pro software. The weights of the different themes were assigned on a scale of 1-5 based on their influence on the ground water potential. Different features of each themes were assigned on a scale of 1-9 according to their relative influence on ground water potential. Based on this scale, a qualitative evaluation of different features of a given theme was performed with: poor (weight=1-1.5); moderate (weight =2-3.5); good (weight=4-4.5); very good (weight= 6-7.5) and excellent (weight=8-9). For the evaluation of weights for different layers and each features of the individual thematic layer, questionnaires were prepared and were given to several experts (geologist and hydro-geologist) in India as well as abroad, including local geologists.The weights were then finalised considering the weights suggested by various experts and those used in earlier studies as well as local experience. Thereafter,a pairwise comparison matrix were constructed using the Saaty's Analytical Hierarchy Process (Saaty 1980) to calculate normalized weights for individual theme and their features.

To demarcate a ground water potential zone all the eight thematic layers after assigning weights were integrated with TNT MIPS Pro software. The total weights of the integrated layers were derived from the following equation to obtain Ground Water Potential Index (Rao and Briz-Kishore 1991).

$$GWPI=[(DD_w)(DD_{wi})+(SL_w)(SL_{wi})+(HG_w)(HG_{wi})+(ST_w)(ST_{wi})+(GG_w)(GG_{wi})+(LD_w)(LD_{wi})+(LC_w)(LC_{wi})+\quad(AFZ_w)(AFZ_{wi})]$$
(1)

Where GWPI=Ground Water Potential Index, DD=Drainage Density, SL=Slope, HG=Hydro-geology, ST=Soil, GG=Geology, LD=Lineament Density, LC=Land Cover, AFZ=Auto Flow Zone. Subscripts 'w' and 'wi' refer to normalized weight of theme and the normalize weight of individual feature of a theme, respectively.GWPI is a dimensionless quantity that helps in indexing probable ground water prospecting zones in the area.

4. Thematic Layers of (Bankura-1, Saltora,Chatna)

4.1. Geology

The greater portion of the area consists of a rolling country covered by laterite and alluvium. While metamorphic or

gneissose rocks are found to the extreme west, to the east there is a wide plain of recent alluvium. The Gondwana system is represented in the northern portion of the area, south of the Damodar& between Mejia and Biharinath Hill.
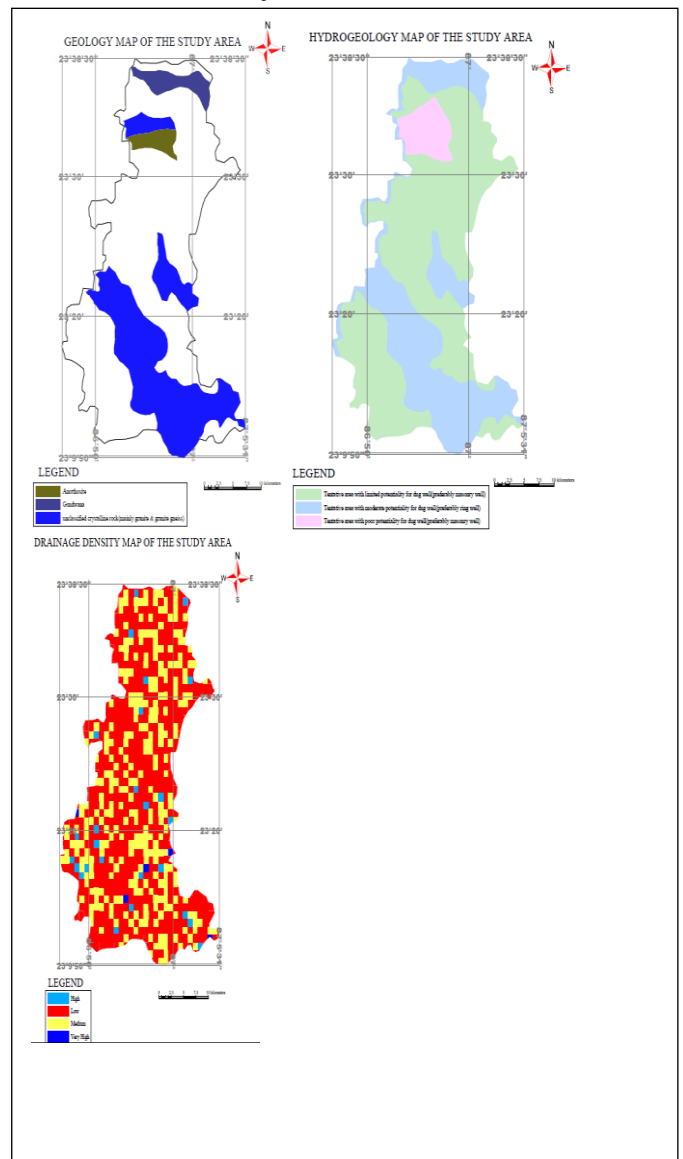
Figure 3: Geology Map, Hydrogeology Map, Drainage Density Map

4.2. Hydrogeology

Hydro-geologically the study area is classified as tentative area with limited potentiality for dug well (preferably masonry well, and tentative area with moderate potentiality for dug well (preferably ring well) and tentative area with poor potentiality for dug well (preferably masonry wee).

4.3. Drainage Density

The surfaceDrainage Density is an inverse function of permeability. There are four drainage density classes like high, very high, low and medium. Low and medium drainage density are given higher weightage than the rest two. The drainage density map is processed from DEM obtain from ASTERDEM. The drainage length of the study area was divided by a uniform square grid (1.5/1.5 km.).

4.4. Lineament density

The Lineament Density map was prepared by scanning the hard copy hydro-geology map obtain from NRDMS Bankura and subsequently processing in the GIS environment. Lineament Density was prepared as DD and was classified as low, moderate, high and very high.
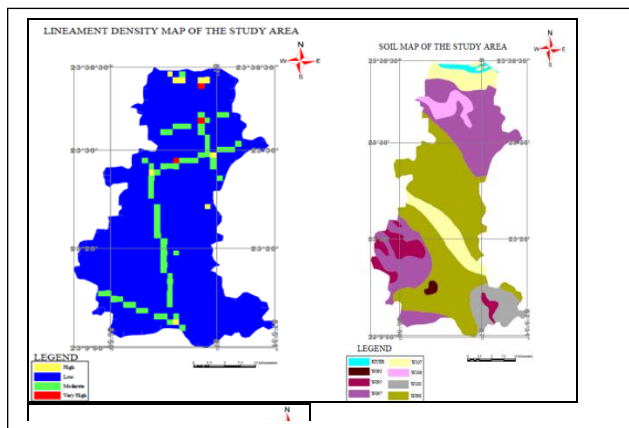
Figure 4: Lineament Density Map, Soil Map, LU/LC Map

4.5. Soil

Soil map is collected from NBSS and LUP Nagpur and the hard copy map was scanned and geo-reference with respect to study area and converted to thematic map and applied the necessary cartography. The soils in the map are:
W093-shallow,exclusively drained, gravely loam.
W095-Shallow, moderately well drained, course loam.
W097- Very deep, in perfectly drained, fine soil.
W098- Very deep, moderately well drained, fine loamy soil
W100-very deep, moderately well drained, fine loamy
W106-very deep, well drained, fine loamy soil
W107-very deep, well drained, coarse loamy soil

4.6. Land use/ Land cover

Land use/ Land cover map was prepared from the land use/ land cover map of BHUVAN website of ISRO, Govt. of India& processed in the software. The prominent land use/ land cover classes were deciduous forest and agricultural plantation and river stream invariably in the study area and river stream and reserved lack pond in the Northern and Lower middle portion of the study area. Urban and built-up rural are scantily distributedthroughout study area.

4.7. Slope

Slope map was prepared from DEM by processing it in the GIS software. The slope zonation for the entire study area gives four different classes of slope ranging 1°-4°.
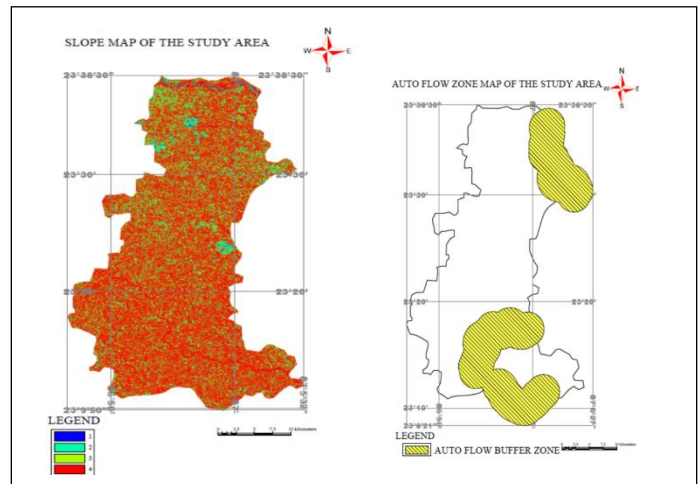
Figure 5. Slope Map, Auto-Flow Zone Map

4.8.Auto Flow Buffer Zone

Here auto flow zone demarcated by two hatched portion which is in the North-West of the study area in the vicinity of Damodar and the Southern area of the study area in the vicinity of Darokeshwar and Kangsaboti reservoir. About 1-2 km^2 area was taken as buffer zone .

5. Weight assignment and GIS based-modelling

The normalized weights of the individual themes and their different features were obtained through the Saaty's analytical hierarchy process. The weights that were assigned to different themes are presented in table- 1 and the process of obtaining of normalized weights of themes is presented in table 2. The weights assigned to different features of the individual themes and their normalized weights are presented in table-3.The process of obtaining normalized weights for different features are similar as above. But finally for the weight assignment an importance was given to experts from where questionnaires werecollected , whereas Saaty's analytical hierarchy process gives us an idea about the range of the weights to be assigned. After weight assignment, all data were integrated by multi-citeria analysis process in the software which takes into account the geoformulagiven by eqn. 1

Table 1. Weights of eight themes of Ground Water potential Zoning

Theme	Weight
Drainage Density	5
Slope	4.5
Hydrogeology	3.5
Soil Type	3
Geology	2.75
Lineament Density	2.5
Land Use/Land Cover	2
Auto Flow Buffer Zone	1.5

Table 2.(Pair-wise comparison matrix of eight thematic layers)

Theme	DD	SL	HG	ST	GG	LD	LC	AFZ	Geometric mean	Normalized weights
DD	5/5	5/4.5	5/3.5	5/3	5/2.75	5/2.5	5/2	5/1.5	1.73	0.19
SL	4.5/5	4.5/4.5	4.5/3.5	4.5/3	4.5/2.75	4.5/2.5	4.5/2	4.5/1.5	1.56	0.17
HG	3.5/5	3.5/4.5	3.5/3.5	3.5/3	3.5/2.75	3.5/2.5	3.5/2	3.5//1.5	1.21	0.13
ST	3/5	3/4.5	3/3.5	3/3	3/2.75	3/2.5	3/2	3//1.5	1.05	0.12
GG	2.75/5	2.75/4.5	2.75/3.5	2.75/3	2.75/2.75	2.75/2.5	2.75/2	2.75/1.5	1.53	0.17
LD	2.5/5	2.5/4.5	2.5/3.5	2.5/3	2.5/2.75	2.5/2.5	2.5/2	2.5/1.5	0.86	0.09
LC	2/5	2/4.5	2/3.5	2/3	2/2.75	2/2.5	2/2	2/1.5	0.69	0.08
AFZ	1.5/5	1.5/4.5	1.5/3.5	1.5/3	1.5/2.75	1.5/2.5	1.5/2	1.5/1.5	0.52	0.06
Total									9.15	1.01

Table 3. Normalized weightage of individual features

Theme	Class	Weight Assigned	Normalized Weight
Drainage Density	Low Drainage Density	4	0.4
	Medium Drainage Density	3	0.3
	High Drainage Density	2	0.2
	Very Hig Drainage Density	1	0.1
Slope	1° (Low)	4	0.4
	2° (Moderate)	3	0.3
	3° (High)	2	0.2
	4° (Very High)	1	0.1
Hydrogeology	Tentative area with limited potentiality for dug well (preferably masonry well)	1	0.19
	Tentative area with moderate potentiality for dug well (preferably ring well)	3	0.60
	Tentative area with poor potentiality for dug well (preferably masonry well)	1	0.19
Soil Type	River	8	0.23
	W093	1	0.03
	W095	6	0.164
	W097	7	0.197
	W098	5	0.142
	W100	4	0.086
	W106	3	0.086
	W107	2	0.052
Geology	Anorthosite	3	0.395
	Gondwana	2	0.208
	Unclassified crystalline rock (mainly granite & granite gneiss)	3	0.395
Lineament Density	Very high	4	0.4
	High	3	0.3
	Moderate	2	0.2
	Low	1	0.1
Land Cover	River & stream	8	0.23
	Reservoir, lake & pond	7	0.197
	Deciduous forest	6	0.164
	Scrub forest	5	0.142
	Agricultural plantation	4	0.086
	Scrub land	3	0.086
	Built up rural	2	0.052
	Urban	1	0.03
Auto flow buffer zone	Auto flow buffer zone	2	2

6. Ground Water Potential Zoning:

After proper running the geoformulae mention above in the scripts icon of the TNT MIPS main menu under "8 bit unsigned" mode. It yields ground water potential index (GWPI) ranging from 1-9 where GWPI value 1-3 is classified as poor, GEPI value 4-6 is classified as moderate, GWPI value 7-9 is classified as good. Though no bore- hole and pumping test were made by the result directly validate the data.The moderate zone falls in the middle and South-Western portion of the study area where is little traces of water resource and finally poor zone lies in the region in the North far from Damodar flat land where rock type or schist, phylite, granite gneiss, and unclassified crystalized rock occurred.

Also in the Southern portion above Darokeswar river region to West-Southern portion of the study area falls in this zone were some rocky out crop is present.
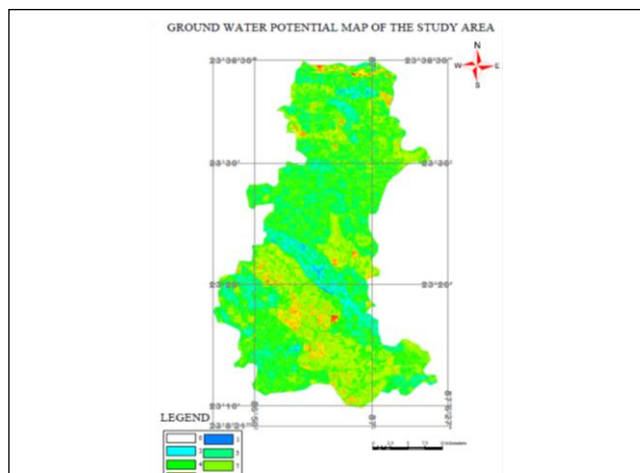

GROUND WATER POTENTIAL MAP OF THE STUDY AREA

Figure 6. Ground Water Potential Map

7.Conclusion :

As seen from the map GWPI is maximum ; from 7 to 9 in the regions of Damodar&Darokeswar river & their vicinity area.And GWPI is of 4 to 6 in the middle & south western portions of the study area.And finally, GWPI is 1 & 2 in the north far from Damodar flatland where some rock types occur. Also in the southern portion above Darokeswar river region where some rocky outcrop is present. And it validates the corresponding soil, geology, hydrogeological conditions of the area. In conclusion, we can interpret that we can suggest NallaBund , Check Dam or even Percolation tank for the area having high GWPI value, Recharge pit & Recharge shaft in the region having low GWPI value ; from 1 to 4.We can validate this suggestion because nalah bunds and check dams are constructed across bigger streams and in areas having gentler slopes which is the above high potential area. Percolation tanks, which are based on principles similar to those of nalah bunds suitable for highly permeable zone as above and recharge pit & shaft in the shallow aquifer zones as mentioned.

REFERENCES

i.   "A Survey of Methods for Groundwater Recharge in Arid and Semi-arid Regions" , UNEP/DEWA/RS.02-2 , Division of Early Warning and Assessment United Nations Environment Programme , NESCO , Nairobi , Kenya.

ii.   BasavarajHutti, Nijagunappa. R , Environmental Science Department, Gulbarga University, "Identification of Groundwater Potential Zone using Geoinformatics in Ghataprabha basin, North Karnataka, India. "International Journal of Geomatics and Geosciences volume 2, no 1, 2011."

iii.   Guide on Artificial Recharge to Ground Water" ,Central Ground Water Board , Ministry of Water Resources , New Delhi, may2000.

iv.   Jha M.K, Mal B. C. AgFE Department, I.I.T.Kharagpur,V.M.Chowdary,, I.I.T. Kharagpur." Integrated Remote Sensing and GIS-based approach for assessing Groundwater potential in West Medinipurdistrict,West Bengal, India ." International Journal of Remote Sensing Vol. 30, No. 1,10 January 2009, 231–250.

v.   Manual on Artificial Recharge of Ground Water" , Ministry of Water Resources , Central Ground Water Board , Faridabad, September 2007.

vi.   Official Web site of BankuraDistrict , Govt. of West Bengal, Official Web site of NRDMS Bankura, Govt. of West Bengal.Ravi Shankar MN & Mohan G, Department of Earth Sciences , Indian In- stitute of Technology Bombay, Powai, Mumbai 400 076, India.

vii.   "A GIS based hydrogeomorphic approach for identification of site-sp e cific artificial-recharge techniques in the Deccan Volcanic Province"J.Earth Syst. Sci.114, No.5, October 2005, pp.505–514.

viii.   Report of the Group for Suggesting New and Alternate Methods of Ground Water Resources Assessment" , Central Ground Water Board, Ministry of Water Resources, Government of India , Faridabad, October, 2009.

ix.   Shahid S.,.Nath S.K, Department of Geology & Geophysics, Indian Institute of Technology, Kharagpur, J.Roy, Regional Remote Sensing Service Center, Kharagpur. "Ground water potential modelling in a soft rock area using a GIS".Int. J.RemoteSensing , 2000,vol.21,no.9,1919 –1924.

Modified Ghyben-Herzberg Theory Based Saltwater Intrusion Modelling For Two Pumping Well System Using Density Dependent Flow Correction Factors

Selva Balaji M[1] and Anirban Dhar[2]
[1]*Research Scholar Department of Civil Engineering, Indian Institute of Technology Kharagpur, Kharagpur-721302, India*
selva191@gmaill.com,
[2] *Assistant Professor, Department of Civil Engineering, Indian Institute of Technology Kharagpur, Kharagpur-721302, India*
anirban@civil.iitkgp.ernet.in

ABSTRACT: *Modelling saltwater intrusion and optimization of pumping operation without contaminating the pumping wells in coastal aquifers require either computationally expensive density dependent numerical simulations in regional scale, or use of analytical solutions based on sharp interface assumption. Analytical solutions for critical pumping rates and saltwater toe intrusion location provided by Strack (1976), for sharp interface between freshwater and saltwater without mixing zone based on continuous single-potential for interface groundwater flow. Strack (1976) analytical solution is less tedious computationally, but overestimates the intrusion of saltwater wedge toe. Pool and Carrera (2011) empirically derived a correction factor for Strack (1976) solution in confined aquifer with single pumping well by comparing density dependent numerical simulations of non-dimensional flow and transport equation with analytical solution. We extend the analysis to two pumping well system by numerically modelling density dependent flow for homogenous, isotropic, confined aquifer and comparing the saltwater toe and critical pumping rates with analytical solution for two pumping well system. Analytical expression based on Strack's potential developed using stagnation point approach for two pumping wells arranged in a line perpendicular to the coastline. Analytical solutions obtained for critical discharge and toe location of the interface of the second well by using fixed discharge for the well nearby coastal boundary. Numerical simulations done using SEAWAT for the critical discharges obtained from the analytical approach and the result are compared. By using non-dimensional transverse dispersivity a correction for the analytical toe location provided.*

Keywords: Flow through Porous Media, Density Dependent flow, Coastal Aquifer, Seawater Intrusion

1. INTRODUCTION:

Coastal population is heavily dependent on the groundwater resources for its drinking water and agricultural needs. Saline water intrusion problem due to density dependent flow is a major threat to the pumping well systems with the fluctuations in the aquifer recharge associated with climate change.

Excessive pumping of groundwater by the pumping wells impacts the equilibrium between the regional freshwater flux and the intruding seawater. Remediation of the pumping wells after the seawater intrusion is economically costly and time consuming process. So, it is essential to plan the pumping well location and pumping rates to prevent the seawater intrusion. Pumping rates can be optimized by linked optimization algorithm (Dhar and Datta, 2009) with the solution for saltwater intrusion.

Saltwater intrusion modeled by sharp interface approach by assuming the there will not be any mixing between freshwater and seawater, and density dependent approach by assuming dispersive mixing between freshwater and seawater. Analytical solutions based on the sharp interface approach are more suitable to optimization models, due to its computational efficiency over density dependent approach. Density dependent approach is more accurate since it takes the mixing into account by solving coupled groundwater flow and salt transport equations numerically. However, density dependent numerical modeling is computationally expensive due to coupled nature of flow and salt transport equations (Datta et al., 2009). Strack (1976) provided analytical solution for critical pumping rates for single well using single, continuous potential for seaward side of the interface as well as freshwater side.

Cheng et al. (2000) extended Strack's analytical solutions for multiple well systems for pumping well optimization without saltwater entering the pumping wells. Several researchers extended the applicability of Strack's potential for pumping well optimization. Pool and Carrera (2011) provided a buoyancy correction factor for the error introduced by sharp interface solution with a non-dimensional parameter based on transverse dispersivity and aquifer depth of the confined aquifer. They provided correction factor by comparing density dependent numerical solution with Strack's analytical solution for single well. The present study sought to explore the possibility of density dependent correction for analytical solution of in a two well pumping system with both wells are located in the same line which is perpendicular to the coastline.

2. METHODOLOGY

An analytical solution for critical pumping rate and toe location of two wells in a same line which is perpendicular to coastline is provided and compared with the density dependent numerical solution based on Strack's stagnation point approach. The pumping rate for the well nearby the coastline is fixed at a minimum pumping rate and the critical discharge of the second pumping well is found. Analytical solution is then compared with the numerically solved toe location for different transverse dispersivity values and aquifer depths.

2.1. Analytical Solution for Sharp Interface

A confined aquifer with uniform aquifer thickness b and constant freshwater flux q_f is considered as shown in Figure 1. Steady sharp fresh water-seawater interface approximation as per Ghyben-Herzberg theory (i.e., without mixing) the depth of the interface is given by, $\xi = h_f / \varepsilon$, where h_f is the (freshwater) piezometric head and ε is the density reference or buoyancy factor given by $\varepsilon = (\rho_s - \rho_f)/\rho_f$.

Strack introduced single, continuous potential for both fresh groundwater zone (zone-I) and freshwater saltwater interface for aquifers with homogeneous and isotropic hydraulic conductivities. The expression for Strack's potential in a confined aquifer is given as,

$$\Phi = \begin{cases} b\varepsilon[\xi - (d - \dfrac{b}{2})] & \text{for } Zone\ I \\ \dfrac{1}{2}\varepsilon[\xi - (d - b)]^2 & \text{for } Zone\ II \end{cases}$$

(1)

Where,
b - aquifer thickness,
d- height mean sea level from the aquifer impervious datum.

The Strack's potential at the toe location for a confined aquifer is given by,

$$\Phi_{toe} = \frac{1}{2}\varepsilon\,b^2$$

(2)

For two fully penetrating wells located in (x_{w1}, y_{w1}) and (x_{w2}, y_{w2}) expression for potential,

$$\Phi = \frac{q_f b}{K}x + \frac{Q_1}{4\pi K}\ln\left[\frac{(x-x_{w1})^2+(y-y_{w1})^2}{(x+x_{w1})^2+(y-y_{w1})^2}\right] + \frac{Q_2}{4\pi K}\ln\left[\frac{(x-x_{w2})^2+(y-y_{w2})^2}{(x+x_{w2})^2+(y-y_{w2})^2}\right]$$

(3)

Where,

q_f - is the uniform freshwater outflow rate in [L/T],
K - hydraulic conductivity [L/T],
Q1 and Q2 are the pumping rates of well 1 and well 2 respectively.
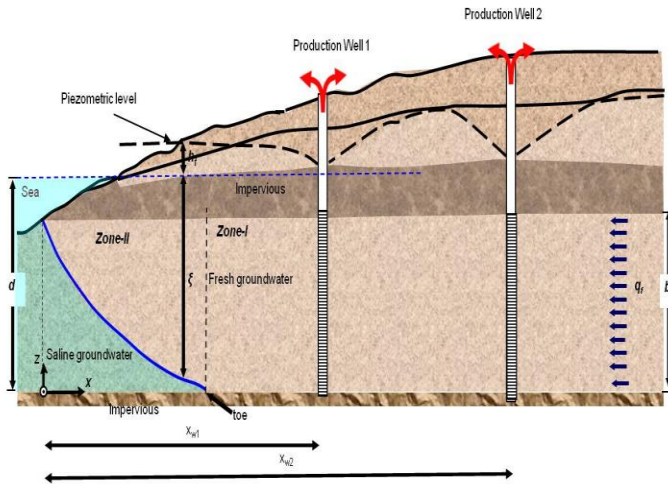
Figure 1. Cross-sectional view of a typical coastal confined aquifer with two wells in the same cross-section

For two well toe location (x_{toe}, y_{toe}) can be determined from Strack's potential as (Cheng et al., 2000)

$$\Phi_{toe} = \frac{q_f b}{K} x_{toe} + \frac{Q_1}{4\pi K} \ln\left[\frac{(x_{toe} - x_{w1})^2 + (y_{toe} - y_{w1})^2}{(x_{toe} + x_{w1})^2 + (y_{toe} - y_{w1})^2}\right]$$
$$+ \frac{Q_2}{4\pi K} \ln\left[\frac{(x_{toe} - x_{w2})^2 + (y_{toe} - y_{w2})^2}{(x_{toe} + x_{w2})^2 + (y_{toe} - y_{w2})^2}\right]$$
(4)

By assuming x-axis passes through the wells the above expression can be written as (Park and Aral, 2004),

$$\Phi_{toe} = \frac{q_f b}{K} x_{toe} + \frac{Q_1}{2\pi K} \ln\left[\frac{x_{toe} - x_{w1}}{x_{toe} + x_{w1}}\right] + \frac{Q_2}{2\pi K} \ln\left[\frac{x_{toe} - x_{w2}}{x_{toe} + x_{w2}}\right]$$
(5)

Non-dimensional form of the Strack potential is givenn as,

$$\Phi_{toe}^* = x_{toe}^* + \frac{Q_1^*}{2\pi} \ln\left[\frac{x_{toe}^* \delta - 1}{x_{toe}^* \delta + 1}\right] + \frac{Q_2^*}{2\pi} \ln\left[\frac{x_{toe}^* - 1}{x_{toe}^* + 1}\right]$$
(6)

Where,

$$x_{toe}^* = \frac{x_{toe}}{x_{w2}} ; \qquad \Phi_{toe}^* = \frac{K\Phi_{toe}}{q_f b x_{w2}} ;$$

$$Q_1^* = \frac{Q_1^*}{q_f b x_{w2}} ;$$

$$Q_2^* = \frac{Q_2^*}{q_f b x_{w2}} ; \qquad \delta = \frac{x_{w2}}{x_{w1}} ;$$

$$b^* = \frac{b}{x_{w2}^2} .$$
(7)

There is a local maximum of the potential at the stagnation point where the water enters low-potential region surrounding wells (Cheng et al., 2000). Local maximum of the potential can be expressed as,

$$F_1\left(x^*, Q_2^*\right) \equiv \frac{\partial \Phi^*}{\partial x^*} = 0 .$$
(8)

By considering a constant safe pumping rate for the well nearby the coastal boundary the expression for local maximum and Strack potential becomes functions of x^* and Q_2^*. At the critical location the difference between Φ_{toe}^* and Φ^* should be minimum.

$$F_2\left(x^*, Q_2^*\right) \equiv \Phi_{toe}^* - x^* + \frac{Q_1^*}{2\pi} \ln\left[\frac{x^* \delta - 1}{x^* \delta + 1}\right] + \frac{Q_2^*}{2\pi} \ln\left[\frac{x^* - 1}{x^* + 1}\right]$$
(9)

Both the functions can be minimized by minimizing summation of their squares. The objective function can be written as,

$$g_1 \equiv Minimization\left[F_1^2 + F_2^2\right]$$
(10)

Maximum allowable toe intrusion, minimum pumping rates are given as constraints.

Constraints:

$$x^* > 0; \qquad x^* < \frac{1}{\delta}; \qquad Q_2^* > Q_{min}^*$$
(11)

Present study considered fixed δ, b^* with different aquifer depths (table 1). Non-dimensional toe location from the analytical solution based optimization is defined as (x_{toe}^{a*}).

2.2. Numerical Modeling for Density Dependent Dispersive Mixing

Density dependent dispersive mixing zone is modeled by numerically solving groundwater flow and salt transport equations simultaneous by coupling them with the relationship between density and salt concentration. Numerical modeling is done by using variable density, fully saturated, finite difference based density dependent program SEAWAT

(Langevin et al. 2003). SEAWAT code consists of MODFLOW and MT3DMS for solving groundwater flow and transport equations respectively. A finite, confined, coastal aquifer (1200 x 2400 in XY plane) with two fully penetrating wells simulated numerically. Numerical domain and the boundary conditions are defined as given in Figure 2. The wells are placed in a way that they are symmetric about x-axis and only one half of the domain considered for modeling. Pool and Carrera (2011) correction for buoyancy factor is dependent on transverse dispersivity and aquifer thickness. So simulations are done for

different transverse dispersivity (α_T) values and aquifer depths (b).

Table 1. Parameters used in numerical simulations

Parameters	Value
b	25, 30, 35 m
δ	1.5
b^*	0.075
Q_1	60 m^3/day
α_L	10 m
α_T	0.1, 0.25, 0.5, 1.0, 2.0, 3.0, 10.0 m
K	10 m/day
D_m	8.6E-5 m^2/day
q_f	0.025 m/day

Discharge for the well1 is fixed at 60 m^3/day and the critical discharge Q_2^c and corresponding toe locations x_{toe} are found as explained in the previous section. Numerical simulations are done with
with the critical pumping rates obtained from analytical solution.
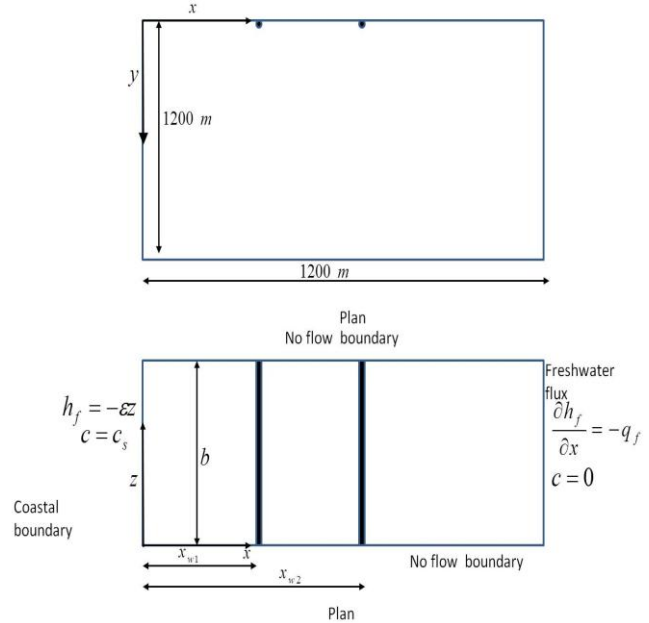
Figure 2. Schematic diagram of domain used for numerical modeling with boundary conditions

3. RESULTS AND DISCUSSIONS

The toe location for the analytical solution (x_{toe}^{a*}) based on stagnation point and numerical simulations are compared. Salt concentration contours corresponding to 0.5 kg/m^3 (500 ppm) takes as the representative contour for the toe location (Figure 3). The concentration is chosen based on maximum allowable salt concentration for safe drinking water. From the comparison it is clearly evident that toe location (x_{toe}^{a*}) based on analytical solution is over estimated. Saltwater intrusion toe location is increasing with the decrease in transverse dispersivity.

From regression analysis it is found that analytical toe location (x_{toe}^{a*}) and non-dimensional toe location from the numerical simulation (x_{toe}^{n*}) can be related using non-dimensional parameter based on transverse dispersivity and aquifer depths (Figure 4). A correction factor based on the non-dimensional transverse dispersivity is provided. The correction equation for the toe location given as,

$$x_{toe}^{n*} = x_{toe}^{a*}\left[1-\left(\frac{\alpha_T}{b}\right)^{0.3}\right] \quad (12)$$
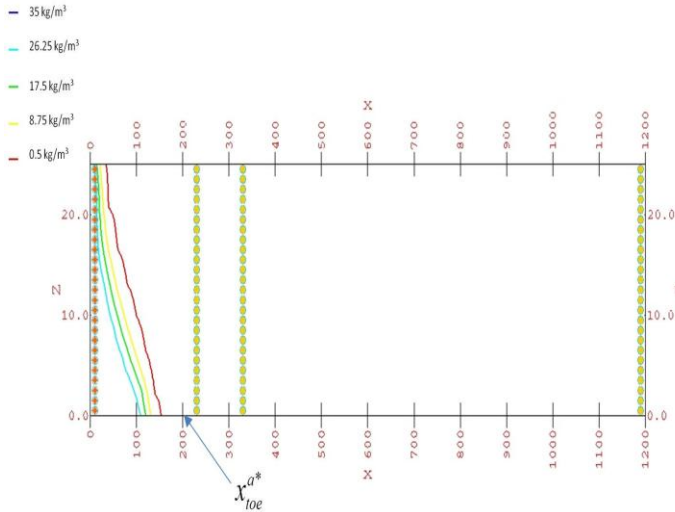
Figure 3. Saltwater intrusion contours for aquifer depth 30m and transverse dispersivity 0.1 m
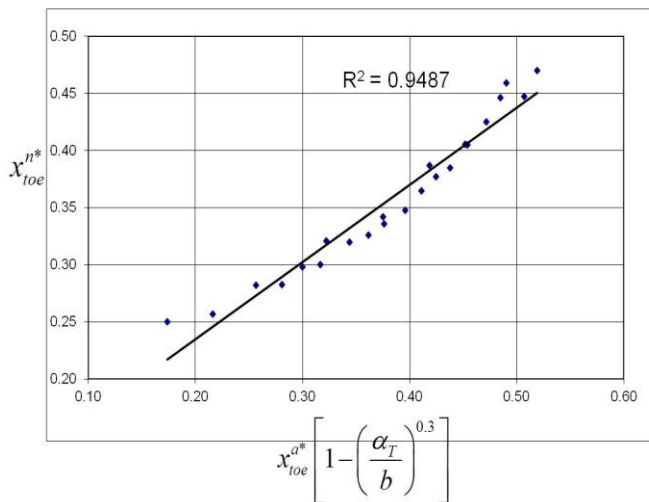
Figure 4. Regression obtained with application of correction for analytical non-dimensional toe location

4. CONCLUSIONS

An analytical expression for the saltwater intrusion is derived based on stagnation point has been derived for two well pumping system with the wells located on a line perpendicular to the coastline. An confined aquifer with two fully penetrating pumping wells, is assumed to be homogeneous and isotropic for hydraulic conductivies. Strack's (1976) analytical solution for single well flow in a coastal aquifer has been extended for two wells and the non-dimensionalised. Non-dimensional parameters related to distance between the two pumping wells (δ), distance between the farther pumping well and coast line (b^*), non-dimensial pumping rates and strack's potential at toe $\left(\Phi_{toe}^*\right)$ controls the saltwater intrusion.

Analytical solution used to find critical pumping rate for the second well Q_2^c by optimization and numerical simulation done for the critical discharges to estimate the error introduced by sharp interface solution. A correction factor obtained by regression analysis using non-dimensional transverse dispersivity and it is in good agreement with the numerical toe location. Similar analysis needed for multiple pumping wells with anisotropic aquifers can be taken up for future study. Sensitivity of the correction factor to the non-dimensional parameters needed to be analysed in future.

REFERENCES:

i.   Cheng, AH-D, D Halhal, A Naji, and D Ouazar (2000) Pumping optimization in saltwater-intruded coastal aquifers. Water Resources Research 36(8): 2155–2166.

ii.   Datta B, Vennalakanti H, Dhar A (2009) Modeling and control of saltwater intrusion in a coastal aquifer of Andhra Pradesh, India. Journal of Hydro-Environment Research 3(3): 148-159.

iii.   Dhar A, Datta B, (2009) Saltwater Intrusion Management of Coastal Aquifers. I: Linked Simulation-Optimization. Journal of Hydrologic Engineering 14(12): 1263-1272.

iv.   Langevin, CD, WB Shoemaker, and W Guo (2003) MODFLOW–2000, the U.S. Geological Survey modular groundwater model—Documentation of the SEAWAT–2000 version with the variable density flow process (VDF) and the integrated MT3Dms transport process (IMT). U.S. Geological Survey: Open-File Report 03–426.

v.   Park, CH, and MM Aral (2004) Multi-objective optimization of pumping rates and well placement in coastal aquifers. Journal of Hydrology 290(1/2): 80–99.

vi.   Pool, M, and J Carrera (2011) A correction factor to account for mixing in Ghyben-Herzberg and critical pumping rate approximations of seawater intrusion in coastal aquifers. Water Resources Research 47: W05506, doi:10.1029/2010WR010256.

vii.   Strack, ODL (1976) A single-potential solution for regional interface problems in coastal aquifers. Water Resources Research 12: 1165–1174.

Simulation – Optimization Using Differential Evolution to Assess Aquifer System Parameters

M.Vidhya[1]   A.K. Rastogi[2]
[1]M. Tech Student, Department of Civil Engineering, Indian Institute of Technology Bombay, Mumbai 400076, India
[2] Professor, Department of Civil Engineering, Indian Institute of technology Bombay, Mumbai 400076, India
Email: vidhya.munu@gmail.com

ABSTRACT: *Planning and management of groundwater is essential for sustained utilization of groundwater for agricultural, industrial, municipal and rural sectors. It is realized through simulation-optimization modelling where system parameters are often evaluated through inverse modelling. Conventional numerical techniques are often not suitable for obtaining optimal solutions due to non linear, non-convex and non differentiable nature of the objective function. Evolutionary algorithms in the recent past are developed to solve complex non-linear combinatorial optimization problems. Some of the evolutionary algorithms with extensive application in water resources engineering are*

genetic algorithm (GA), simulated annealing (SA), particle swarm optimization (PSO), ant colony optimization (ACO) and differential evolution (DE). Of these DE is relatively of more recent origin and is yet to be tested extensively in groundwater hydrology. In this study therefore focus is on differential evolution for parameter estimation through inverse modelling where unknown parameters are assessed by matching the state variable that are observed and simulated. The FEM model is used to find simulation head for the synthetic aquifer problem and these reference heads are used for parameter assessments. Sensitivity of the head values to applicable variations in different boundary conditions, aquifer parameters and inflow outflow conditions are examined. The model is verified by performing adequacy check using mass balance. Optimization model was developed using DE to estimate the parameters of the aquifer system using reference heads generated from the FEM model. Parameter structure identification is also performed using the developed DE optimization model and ascertained an aquifer model structure that is appropriate for the problem. Different strategies of DE are implemented and the strategy where best individuals are used for finding difference vector is found to be the optimal strategy for the present study. From the results it can be concluded that DE is capable of estimating the system parameters reliably and efficiently with less intricacies.

Keywords: Finite element method, parameter estimation, inverse modelling, Differential evolution

1. INTRODUCTION

Water is an essential resource without which mankind cannot survive in the world. The utilization of this resource has to be properly planned. The rapid decline in hydraulic head due to excessive pumping, contamination of groundwater due to industrial activities, saltwater intrusion into aquifers are the important problems that world faces today. Proper management activities such as remediation of contaminated aquifers, prevention from excessive pumping, prediction of contaminants movement, recharge location are some of the necessary

requirement. Groundwater modeling plays an important role in planned usages of this resource without causing the unacceptable lowering of water table. In the recent past the development of models has become essential for predicting different groundwater flow parameters like groundwater head, velocity of flow and decline in head after some
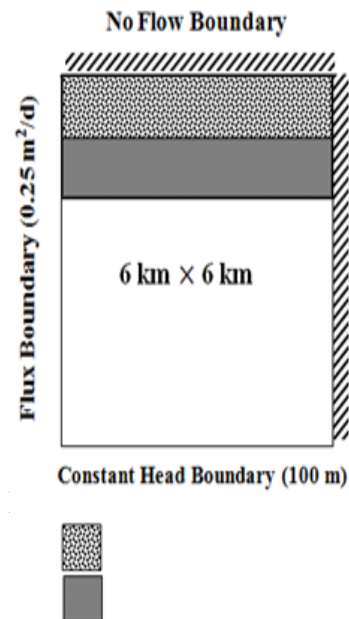
specified period involving properties of aquifer (transmissivity, storativity), etc. More recently aquifer remediation and contaminants prediction too involve extensive application of subsurface flow models.

The partial differential equation that governs the groundwater flow is being solved using numerical techniques to obtain the unknown state variable (groundwater head of the system). Numerical methods like Finite element, Finite difference and Boundary element method are most commonly used methods. In this study Finite element method is adopted for simulating the head values.

Inverse modelling as defined by Franssen et al. (2009) refers to the process of gathering information on the model and/or its parameters from measurements of what is being modeled. They also stated that it is also termed as history matching, scanning or tomography, amongst other synonyms. Groundwater models are mostly distributed parameter models in which the parameters used can be normally computed from the field test at certain location.

The inverse problem aims at the optimal determination of the aquifer parameters by the observation of state variables collected over a period of time and space domain. For an aquifer having homogeneity of parameters, the number of observation is usually finite and limited and the space domain is continuous, whereas in a heterogeneous aquifer the dimension of the parameter involved is theoretically infinite. In an heterogeneous case, the aquifer is first parameterized using FEM or FDM, in which the aquifer is subdivided into several sub regions with each sub regions characterized by a constant parameter and in this process the number of parameters is reduced so that, the estimation of the parameters in heterogeneous case is practically possible.

2. PROBLEM FORMULATION

A confined aquifer problem is chosen from Huggi and Rastogi (2009). The confined aquifer domain (refer Figure 1(a)) has area of 36 km^2 and it has been discretized using 49 nodes and 72 linear triangular elements (refer Figure 1(d)). The northern and eastern sides of the domain are impervious whereas in the southern of the domain, a constant head 100 m is maintained. The transmissivity value in the aquifer varies with space as shown in Figure 1(c). There are two pumping wells of magnitude 1200m^3/d and 800m^3/d located at node 24 and node 33 respectively as shown in Figure 1(b). The flux boundary

inflow on the left side of the domain is of magnitude 0.25 m²/d. There is consideration of aquitard recharge at the rate of 0.00015 m/d and 0.00025 m/d from the two strips on the northern side of the domain respectively and the storativity value of the aquifer is 0.001.

In this example the impervious boundary on two sides may represent the hillock or water divide. The variations in the aquitard recharge rate may be due to the variation in the hydraulic conductivity of the aquitard whereas the constant head boundary represents the presence of a reservoir or river on the southern side of the domain. Flux boundary may result from a canal on the western boundary with known canal seepage entering the system. The domain considered is applicable to the actual field conditions except for its regular shape (Huggi and Rastogi 2009).
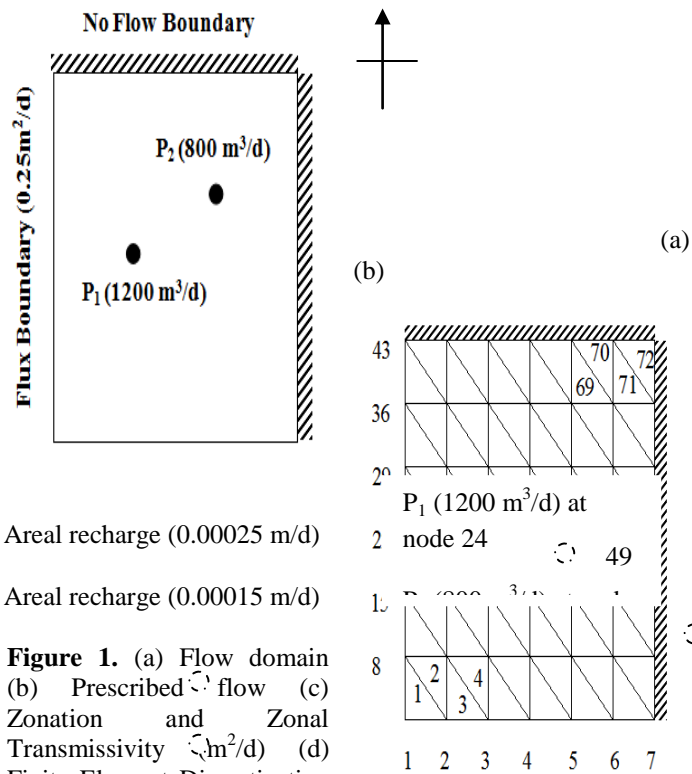
Areal recharge (0.00025 m/d)

Areal recharge (0.00015 m/d)

Figure 1. (a) Flow domain (b) Prescribed flow (c) Zonation and Zonal Transmissivity (m²/d) (d) Finite Element Discretization (Huggi and Rastogi 2009)

3. DIFFERENTIAL EVOLUTION

Differential evolution is a meta-heuristic method developed by Storn and Price in 1995. Unlike classical optimization method (gradient descent, quasi-newton methods) DE can be used for non-differentiable o Nodes varying from 1 to 49 nethod is simple, powerful and easier to implement. In this method, a population set is maintained and new individual solutions are created by performing *difference* operation on the existing population set. The new individuals replace the old population

only if the fitness value of new solution is higher than the old solution.

Differential evolution algorithm is easier to follow as considered below

(a) **Initialization of solution**: Population set is initially generated randomly with upper and lower bounds specified.

(b) **Finding trial individuals**: Trial individuals are computed for each individual in the population set using the condition,

$$\omega = \beta + F.\delta$$

(3.1)

Where β is base vector

F is constant of differentiation

δ is difference vector

(c) **Updating population**: Selection of individual is done by two steps.

(i) First, with crossover probability of C_r the individuals are inherited. With crossover probability of C_r, inherit the new trial individual(ω_j).

$$\omega_j = \begin{cases} \omega_j & if\ rand_j \le C_r, \\ ind_j & otherwise \end{cases}$$

(3.2)

Where ind_j is the old trial individual,

$$rand_j \in [0,1]$$

$$C_r \in [0,1]$$

(ii) Secondly the inherited individuals are evaluated using fitness function and are updated in the population set if fitness function of new individuals is higher than the existing old individuals.

$$Fit = \frac{1}{1+f}$$

(c)

$$ind = \begin{cases} \omega & if\ f(\omega) \le f(ind) \\ ind & otherwise \end{cases}$$

(3.4)

Where f is objective function

Fit is fitness function

Repeat steps (b) and (c) until the convergence condition is satisfied.

The standard form for defining the strategies is DE/x/y/z. x represents the vector to be perturbed, y represents the number of difference vectors involved in the perturbation and z indicates the type of crossover. The vector to be perturbed can be either the best of the previous iteration solutions or the

randomly chosen vector and similarly the number of difference vectors can be 1 or 2. Finally the type of crossover can be either exponential or binomial. In the present study five strategies are used where only binomial crossover is followed. The five strategies are described below

(a) DE/rand/1/bin : $\omega_1 = \xi_1 + F.(\xi_2 - \xi_3)$

(b) DE/rand/2/bin : $\omega_1 = \xi_1 + F.(\xi_2 - \xi_3) + F.(\xi_4 - \xi_5)$

(c) DE/best/1/bin : $\omega_1 = \xi_{best} + F.(\xi_1 - \xi_2)$

(d) DE/best/2/bin : $\omega_1 = \xi_{best} + F.(\xi_1 - \xi_2) + F.(\xi_3 - \xi_4)$

(e) DE/rand-best/1/bin : $\omega_1 = \xi_1 + F.(\xi_{best} - \xi_2) + F.(\xi_3 - \xi_4)$

The results of simulation and optimization model and their validations are discussed in the next chapter.

4. RESULTS AND DISCUSSION

The steady state head is computed without considering pumping wells. The groundwater head values are plotted as surface plot and contour plot. (Figure 2 (a) and (b))
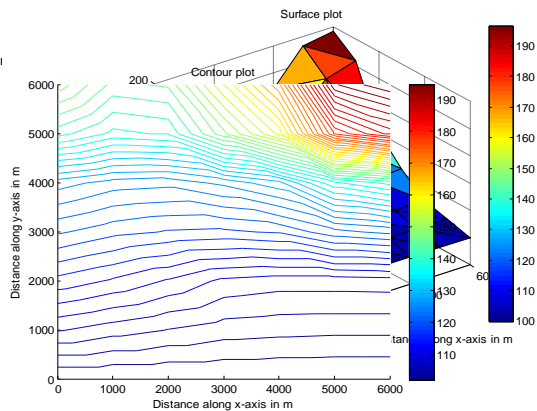
(a)   (b)

Figure 2. (a) Surface plot of Steady state head distribution and (b) Contour plot for Steady state head distribution

The surface plot and contour plot of steady state head distribution of confined heterogeneous isotropic aquifer shows that head values decreases from northern side where aquitard recharges are present towards southern side where constant head boundary is present. From this it is understood that the flow direction is towards constant head boundary. The highest head value is observed at the northeastern side of the domain due to the presence of aquitard recharge.

After the commencement of pumping, the head values are noted at different intervals of time, after 50 days, 100 days, 200 days, 500 days and 1000 days. It was observed that the head

values decreases with time, but at later stage it reaches steady state. The decrease in head with time is due to the withdrawal of water from pumping wells. Let us take an observation well for illustration, in observation well 49, the head value for all rates of pumping just after the pumping commenced is about 196 m, but after 1000 days of pumping, the head value decreases to 185.71 m for pumping rate (P_1) of 1000 m^3/d. Whereas for pumping rate (P_1) of 3000 m^3/d, head decreases to 154.01 m. This shows that initially just after the pumping is commenced head values are almost same for different pumping rates, but with respect to time it decreases significantly for increase in the pumping rates due to excessive withdrawal of water.

As the recharge rate increases, the head also increases (Table 1), but the head values decreases with time (Table 2) since there is continuous withdrawal from pumping wells and outflow through the constant head boundary. The chosen range of aquitard recharge rates can be corroborated by referring to McMahon et al. (2011).

Table 1. Head values for different aquitard recharges values at node 49 after 50 days

Days	Observation well 26 (m)	Observation well 49 (m)
50	113.9227	196.6538
100	111.8386	196.661
200	109.8456	194.786
500	107.6717	187.2776
1000	106.6964	182.5439

Table 2. Head Values at observation wells 26 and 49 for different time interval

Aquitard recharge, m/d	Head values, m
0.00025 and 0.00015	196.6538
0.000125 and 0.000075 (1/2 fold)	151.3157
0.0000625 and 0.0000375 (1/4 fold)	128.6461
0.00050 and 0.00030 (2 fold)	287.3292

The governing equation of groundwater flow is primarily based upon the concept of mass balance over a nodal control volume. Since the governing equation holds for all the nodes of the flow domain, therefore a correct solution should satisfy the total (or global) mass balance for the aquifer system. Therefore mass balance is a definite check towards the adequacy of solution obtained from the developed model. An error of 2.25% is obtained and hence the mass balance check validates the developed model. This error is due to approximations in the numerical scheme and is generally acceptable in groundwater

flow modelling, since parameter uncertainty to real aquifer is normally higher than the above balance error.

The developed FEM model was coupled with optimization model to obtain the system parameters optimally. In developing the optimization model differential evolution (DE) method is adopted. Using DE the parameters are estimated and compared with the true parameters. There are three tuning parameters in DE, constant of crossover, constant of differentiation and transversal steps. These parameters are tuned and the optimal values obtained for constant of crossover, constant of differentiation and transversal steps are 0.6, 0.5 and 15 respectively.

The transmissivity values are estimated by defining the other parameters known. For steady state condition with 14 observation wells and for population size of 100, C_r value of 0.6, F value of 0.5, the transmissivity values are estimated and are listed in Table 3. The chosen lower and upper bounds on the transmissivity values are 1 and 180 m^2/d respectively.

Table 3. Estimated transmissivity values in steady state using DE

Zone	Estimated transmissivity (m^2/d)	Actual transmissivity for synthetic aquifer (m^2/d)
1	150.20	150
2	49.86	50
3	15.04	15
4	4.99	5

For C_r value of 0.6 and F value of 0.5 the aquitard recharge values are estimated. It was observed that both the estimated parameters and assumed parameters are same and hence it can be revealed that the developed model could estimate parameters with greater accuracy. Similarly the estimated boundary inflow (0.25 m^2/d) matches exactly with the true value (0.25 m^2/d) and hence it was realized that DE optimizer is capable of estimating the exact parameter values.

Zones	Model structure								
	1	2	3	4	5	6	7	8	9
Zone 1	149.78	65.23	179.16	171.46	150.5	129.42	162.50	167.08	4.99
Zone 2	50.01		31.58	30.74	52.70	27.98	170.12	55.64	15.07
Zone 3	14.98		8.94	179.99	9.81	3.49	39.60	7.78	50.02
Zone 4	5						141.45		149.90
Zone 5							44.76		148.82
Zone 6							16.86		
Zone 7							51.37		
Zone 8							14.98		
Zone 9							4.92		
SSHR	0.01	2956.43	1092.46	2555.10	94.73	390.15	3.4787	77.85	0.03
Rank	1	9	7	8	5	6	3	4	2

The transmissivity, aquitard recharge, boundary flux and storativity values are estimated collectively and listed in Table 4. Hence the number of decision variables considered is 8.

Parameters	Estimated parameters							
	Transmissivity values				Storativity, S	Aquitard recharge, R_1 (m/d)	Aquitard recharge, R_2 (m/d)	Boundary flux (m^2/d)
	T_1 (m^2/d)	T_2 (m^2/d)	T_3 (m^2/d)	T_4 (m^2/d)				
Estimated parameters (with time period of 10 days)	150.07	50.02	15	5	0.001	0.00025	0.00015	0.25
Estimated parameters (with time period of 25 days)	150.08	50.03	15.01	5	0.001	0.00025	0.00015	0.25
Estimated parameters (with time period of 50 days)	150.03	50.01	15	5	0.001	0.00025	0.00015	0.25
True parameters	150	50	15	5	0.001	0.00025	0.00015	0.25

Table 4. Estimation of parameters collectively using DE

The computational time for estimating the parameters collectively is 254.75, 384.99 and 602.86 seconds for time period of 10, 25 and 50 days. The number of function evaluations for time period of 10, 25 and 50 days are 319, 326 and 329 respectively. The number of function evaluations vary only slightly, however computational time increases proportionally with increase in time period. DE optimizer could estimate the collective parameters (8 decision variables) accurately even for lesser time periods. The variation between estimated and true parameters is diminutive. Hence in solving

real aquifer problem it is beneficial to collect head data for smaller time periods rather than collecting yearly data.

The optimal number of parameters needed for a representative model is often not evident, and in many ways model complexity is ultimately determined by the objectives of that model (Hunt et al. 2007). Various aquifer model structures with different zonation pattern are considered. SSHR is computed for the nine chosen zonation pattern (Table 5). It is expected that the original model will give the least SSHR if inverse solutions are reliable.

Table 5. Zone wise optimal transmissivity values for different model structure using DE

In developing the model, the model structure pattern 1 was used for estimating the parameters which is corroborated by the model with minimum SSHR value. This analysis therefore suggests that in field problem best conceptual aquifer model can be identified by inverse modelling which is often a difficult task due to difficulty in drawing the correct zonation pattern identified with distinct parameters.

In the present study five different strategies of DE are examined to evaluate the optimal transmissivity distribution in the aquifer. Among five strategies, DE/best/1 performs better compared to other strategies with lesser computational time (8.811s), less number of iterations (24) and better quality solution (Minimum objective value of 0.0002). Hence it can be concluded that for this problem DE/best/1 is the appropriate strategy to be used for estimating the optimal transmissivity values.

The reliability of parameter estimates can be investigated by using the variance-covariance matrix for the final estimated parameters (Bard 1974). Generally the parameter with smaller variance indicates good estimate while larger variance represents insensitive parameter (Huggi and Rastogi 2009). It was observed that for zone 4 the variance is lesser (0.0001) compared to variances of other zones. Hence the parameter estimation for zone 4 is more reliable. In general all variances are quite small and indicate reliable assessment of all the four transmissivity parameters.

5. CONCLUSION

The surface and contour plots obtained from the simulation model give a clear picture of the distribution of head over the aquifer domain. The simulation model is validated through the mass balance check. Optimization model was developed using DE and was coupled with the simulation model to estimate various groundwater parameters optimally. From the results it was found that differential evolution could estimate the parameters reliably and accurately.

REFERENCES:

i. Bard, Y. Non linear parameter estimation. *Academic Orlado, FL, 341* (1974)

ii. Franssen, Hendricks H.J. and Kinzelbach, W., Ensemble Kalman filtering versus sequential self-calibration for inverse modelling of dynamic groundwater flow systems. *Journal of Hydrology 365 , 261–274* (2009)

iii. Huggi, V.P. and Rastogi, A.K. Estimation of system parameters in groundwater systems. *VDM Verlag, Germany* (2009)

iv. Hunt, R.J., J. Doherty, and M.J Tonkin. Are models too simple ? Arguments for increased parameterization. *Groundwater, 45(3), 254-262* (2007)

v. McMahon et al. A Comparison of recharge rates in aquifers of the United States based on groundwater – age data. *Hydrogeology Journal 19: 779-800* (2011)

Modeling Solute Transport Through Porous Media With Scale Dependent Dispersion

Teodrose Atnafu Abgaze[1], P. K. Sharma[2] and Deepak Swami[3]
[1,3]Research Scholar and [2]Associate Professor
Department of Civil Engineering, Indian Institute of Technology, Roorkee
Email: drpksharma07@gmail.com

ABSTRACT : *In this study, an attempt has been made to study the behavior of breakthrough curves in both layered and mixed heterogeneous soil by conducting experiments in long soil column. Sodium chloride has been used as conservative tracer in the experiment. Advective dispersive transport equation including equilibrium sorption and first order degradation coefficients are used for solute transport through mobile-immobile porous media. Implicit finite difference numerical method has been used to solve the governing equations for solute concentration. Both linear and asymptotic distance dependent dispersion functions are used to describe the scale effect and to simulate experimental breakthrough curves. Also, a comparative study has been done among distance dependent and constant dispersion models, while simulating the experimental data of solute transport through soil column. Results of experimental breakthrough curves indicate that the behavior of observed breakthrough curves are approximately similar in both case of layered and mixed soil, while earlier arrival of solute concentration is obtained in case of mixed soil. It means that the types of heterogeneity of the soil media affect the behavior of solute concentration. Finally, it is also shown that asymptotic dispersion model simulate the observed experimental data better as comparison to constant and linear distance dependent dispersion model.*
Keywords: Reactive transport; Numerical method; Distance dependent dispersion model.

1. INTRODUCTION:

Groundwater contamination occurs when man-made products such as gasoline, oil, road salts and chemicals get into the

groundwater and cause it to become unsafe and unfit for human use. Waste materials from the land's surface can move through the soil and end up in the groundwater. Ground water can become contaminated from point source pollution that comes from a single source, such as a factory or wastewater treatment plants. Fertilizers and pesticides, surface runoff, septic wastes, and household wastes are the various source of non-point pollution. Sometimes leaching of wastes from land fills or discharge of industrial wastes to the soil without treatment also affects ground water. Different chemicals like chloride, arsenic; Fluoride etc are dissolved in the water. Polluted ground water is difficult to purify. Different types of contaminant have different transport properties and depend on the size of grain of porous medium. Drinking contaminated groundwater can have serious health effects. Diseases such as hepatitis and dysentery may be caused by contamination from septic tank waste. Poisoning may be caused by toxins that have leached into well water supplies. Wildlife can also be harmed by contaminated groundwater. Therefore, it is very essential to study the transport mechanisms of chemicals through subsurface porous media so that health risk can be avoided. Various laboratory experiments were performed to understand the physiochemical reaction of solute in porous medium.

For understanding the process of transport of contaminants through porous media, several mathematical models have been developed (Lapidus and Amundson, 1952; Bear, 1979 and Valocchi, 1985) with constant dispersivity, which is a measure of the dispersive properties of the porous media. In recent years, several authors such as Sudicky and Cherry (1979), Pickens and Grisak (1981) and David Logan (1996) had suggested that the dispersivity is not a constant parameter but depends on the mean travel distance or distance along the movement of contaminant transport in porous media. Also, they suggested that the dispersivity can be linear, parabolic, asymptotic and exponential function of mean travel distance in the subsurface porous media. Yates (1990 and 1992) obtained one-dimensional analytical solution for uniform flow with constant concentration or constant flux boundary conditions and for a linear or exponentially increasing dispersion coefficient. Sudicky et al. (1985) studied under controlled laboratory conditions, for transport of non reactive solute with the help of injection a tracer into a thin layer of soil by silt layers on all sides. Tailing of the breakthrough curves occurred due to diffusive exchange of tracer between the strata in the layered system. Hassanizadesh and Gray (1987) studied experimentally and established observations in a porous media, that the relation between velocity of fluid and pressure head gradient does not depends on high rates of flow of fluids. Flow at high velocity, the non linear dependence of interfacial drag forces on the flow velocity had been shown to give rise to non-linear behavior. Chrysikopoulos et al. (1990) conducted experiments to derive the first order solution of one-dimensional equation of advection-dispersion with spatially variable of retardation factor. They described the transport of sorbing but in that case non reacting solutes in porous

formations which is homogenous hydraulically and heterogeneous geochemically. Sternberg et al. (1994) did experiments in three homogeneous, linear, non uniform porous media. The columns were connected end to end horizontally to make it a heterogeneously porous media. Heterogeneous porous medium studied dispersion during two phase miscible flow in a composed of homogeneous layers with different permeability heterogeneous porous medium abilities. Huang et al. (1995) conducted laboratory tracer experiments in a long soil column which is filled with the homogeneous and heterogeneous material to investigate solute transport through column during steady saturated flow. Kau et al. (1997-1998) conducted experiments in laboratory to understand the process of sorption and desorption of fluoride in kaolin natural soil. The pH value decides the amount of fluoride sorption within 24 hrs. Experiments proved that several factors affect the degree of immobilization of fluoride. Li and Brusseau (2000) elaborated mathematical model using two major approaches to incorporate heterogeneous rate-limited mass transfer. Two approaches are used to evaluate potential in experiment and model formulation. It was observed that mean transport behavior for systems with field-scale heterogeneity did not influence the heterogeneity in the local scale mass transfer. Peter and Smith (2001) studied the ADE (Advection-Dispersion Equation) under various configurations and conditions with the help of TR model. It was observed that the solution of transition region model (TR model) become almost same as the solution of the standard ADE model with correct boundary conditions. Hsu (2004) performed experiments on the stochastic analysis of flow. Experiments were also performed to understand the phenomenon of solute transport. Perturbation theory for low-order approximations of velocity covariance described the flow and solute transport.

Xu and Hu (2004) adopted an Eulerian perturbation approach and conducted experiment on it. They defined the moment for solute transport in a fractured medium which is non stationary. The conceptualized fractured medium was explained with the help of dual-porosity model. The flow and contaminant transport in fractured media by the dual continuum model. Huang et al. (2006) analyzed the solute in 12.5 m long homogeneous and heterogeneous soil column. They performed experiments to test the non-Fickian dispersion theory of FADE. With transport scale for homogeneous column it was found that, with increase in heterogeneous column the dispersion coefficient increases exponentially. Dispersion coefficient was much more significant in the heterogeneous media. Wang and Huang (2011) employed Monte Carlo simulation method to describe the sensitivity of flow and solute transport to the behavior of highly heterogeneous and non- stationary random permeability fields characterized by truncated fractional levy motion. Fallico et al. (2012) conducted the experiments to analyze and compare the scaling behavior of the hydro-dispersion for some different sandy soils for some different sandy soils in laboratory conducted the experiments to describe the scaling behavior of the hydro-dispersion. Dispersion was a

key processes controlling transport of solutes in porous media. Leij et al. (2012) presented a dual-advection equation to describe the transport of solute in structured or layered porous media. Various non-zero flow rates in two different pore domains with linear transport of solute between them were adopted. The advection-dispersion equation played an important role in the phenomenon of solute transfer and also for transport in a mobile and immobile model. From above literature reviews, it has been seen that solute transport experiment in very long heterogeneous porous media has not been done. Therefore, the present study is focused on solute transport in long heterogeneous soil column experiments.

The main objective of the present study is to perform experiments and study the behavior of solute transport in saturated long soil columns which is placed horizontally. Soil columns are heterogeneous, which contains both layered and mixed soil for different size of soil. Observed experimental breakthrough curves are compared for both cases of layered and mixed heterogeneous soil column experiments. Developed numerical model has been used to simulate the experimental breakthrough curves using constant, linear and asymptotic dispersion models.

2. EXPERIMENTAL SETUP

Figures 1a and 1b represent the line diagram of soil column experiments in the lab. Different combination of soil materials are filled in the first soil column experiment as shown in Figure 1a. It means that soil samples of different material such as gravel, coarse sand, fine sand, silt, natural soil and fine sand are filled in layered in the soil column. In the second part of the soil column experiment as shown in Figure 1b, mixed soil of different soil materials are filled in the column. Both set up of layered soil and mixed soil placed in the soil column experiments behave as heterogeneous media. Actual photograph of experimental model long soil column is shown in Figure 2.
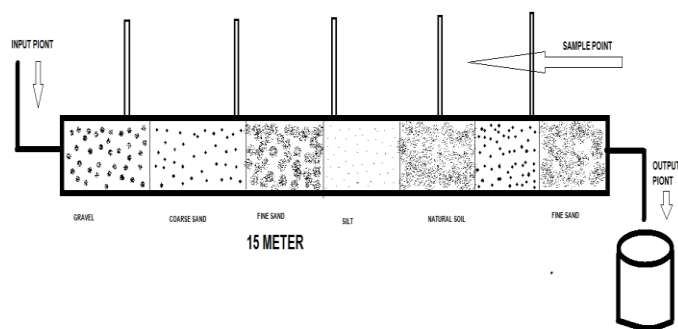
Figure 1a: Line diagram of experimental set-up for heterogeneous medium for layered soils
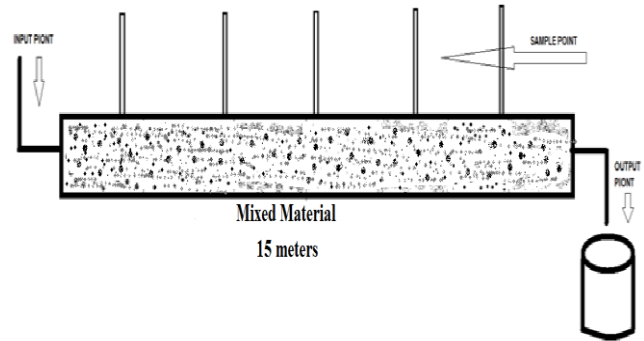
Figure 1b: Line diagram of experimental set-up for heterogeneous medium for mixed soils

Figure 2 Experimental Set-ups for Heterogeneous Medium

2.1 Experimental Procedure

The length of the column is taken 1500 cm and diameter of the column is 15.24 cm, espectively. The soil column is heterogeneous in nature and is filled with coarse, fine, natural soil, silt and gravels in periodical layers. 300 liter of storage tank in which solution is made was placed near to the column. The experiments are conducted using heterogeneous soil columns, which contained negligible organic content. For sample collection at regular intervals, entire column length was divided in 5 equally distributed distances of 300 cm, afterward the column was saturated slowly by flowing tap water continuously for 72 hrs. To avoid leakage through joints, high quality sealant was applied to joints of the column. The head gradient was introduced by maintaining varying head at input, while keeping output head constant. For a known concentration of solute tracer was introduced in the column from storage tank. Several sets of samples were collected at time of 1 hr interval. Chloride testing was done by silver nitrate titration method. In the titration method 50ml volume of sample is taken and 1ml potassium chromate indicator was mixed, and then titrated with silver nitrate till red brick color appeared. Pulse type boundary condition, was considered in experiment.

2.2 Physical Properties of Soil Media

Figure 3 shows the different types of soil media such as coarse sand, silt, gravel etc. The particle size distribution for all the materials was done to estimate the mean grain size (D_{50}). Figures 4a and 4b represent the grain size distribution curve for different soil media used in the experiment. Table 1 show the estimated value of physical properties of soil media such as coarse sand, gravel, fine sand, natural soil, silt and mixed soil.

Figure 3 Different types of soil media contained in the containers.

Figure 4a Grain size distribution curve of different soil media

Figure 4b Grain size distribution curve of mix soil media

Table 1: Results of sieve analysis for coarse sand

Material	Density (gm/cc)	Hydraulic Conductivity	Porosity	D_{10}	D_{30}	D_{50}	D_{60}	C_c	C_u
Silt	1.63	Order of 10^{-8}	0.40	0.026	0.048	0.058	0.076	1.16	2.92
Fine Sand	1.82	Order of 10^{-2}	0.32	0.37	0.68	0.75	0.8	1.56	2.16
Coarse Sand	1.50	Order of 10^{-1}	0.28	0.25	0.68	0.91	0.96	1.93	3.84
Natural Soil	1.42	Order of 10^{-5}	0.33	0.11	0.25	0.35	0.42	1.35	3.82
Gravel	1.65	Order of 10^{-1}	0.42	3.6	4.7	6	6.4	0.96	1.78
Mix Material	2.11	Order of 10^{-4}	0.38	0.11	0.33	0.9	1.1	0.9	10

3. OBSERVED BREAKTHROUGH CURVES IN LAYERED AND MIXED SOIL

Figures 5-7 represent the behavior of observed experimental breakthrough curves through layered and mixed heterogeneous soil media, respectively. The experimental breakthrough curves are predicted at 300 cm, 900cm and 1500 cm down gradient distance in the flow direction during experiment. The observed value of solute concentration for chloride has been compared for both cases of layered soil and mixed soil media. The behaviors of breakthrough curves are similar in both cases of soil media, but the magnitude of solute concentration is not same for higher transport time. It is also, known that the different types of soil strata affect the value of hydraulic conductivity within the soil media. The physical properties of the soil affect the transport of solute through heterogeneous media. Dispersion is a key process controlling transport of solute in heterogeneous porous medium. Long tailing is also observed in breakthrough curves during large transport time. It indicates that the some magnitude of solute is remained in immobile zone. Velocity also plays an important role in the diffusion process. The steady-state conditions describe the function for the solute behavior. Dispersivity is also defined as the ratio of dispersion coefficient to the effective pore water velocity. Hence, solute transport in soil and groundwater is generally affected by a large number of physical, chemical and microbial processes and medium properties.
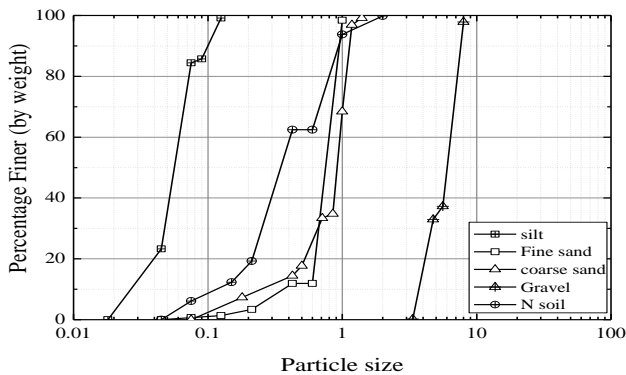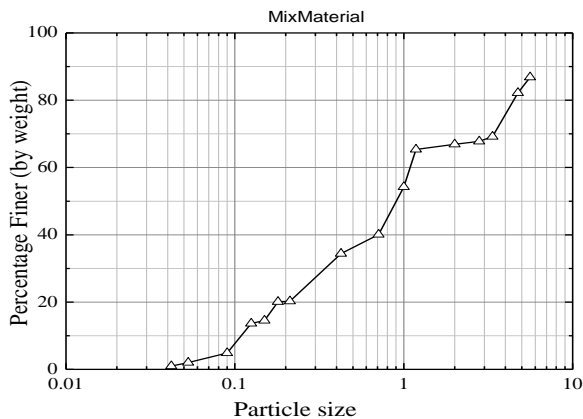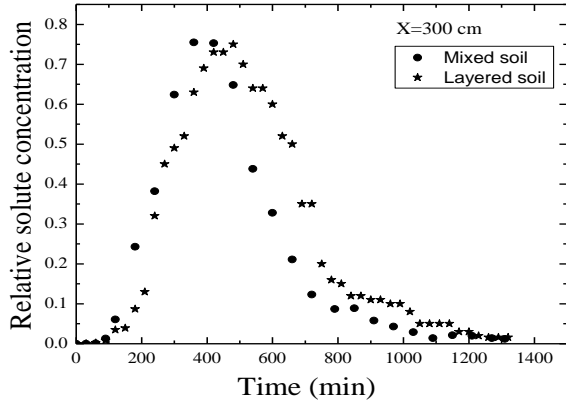
Figure 5 Break through curves of experimental data for chloride at 300cm distance in heterogeneous soil.
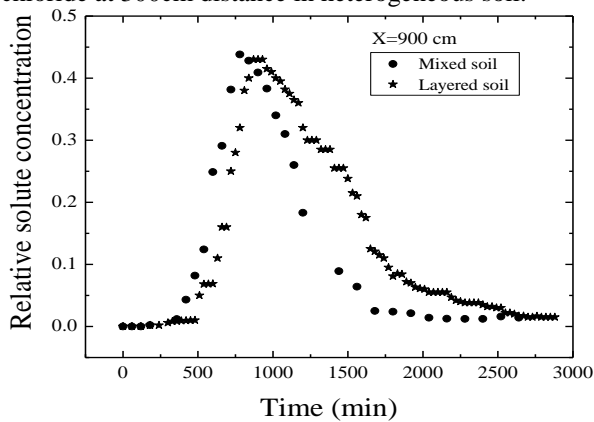

Figure 6 Break through curves of experimental data for chloride at 900cm distance in heterogeneous soil.
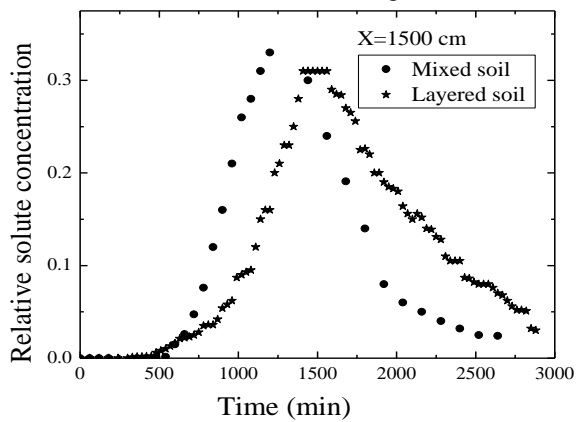

Figure 7 Break through curves of experimental data for chloride at 1500cm distance in heterogeneous soil.

4 GOVERNING EQUATION

Mobile-immobile model (MIM) separates the porous medium into mobile and immobile regions. It is assumed that advection-dispersion equation is used for mobile region, and solute exchange between mobile and immobile regions can be described as a first-order process. The porous medium is also partitioned into two fractions of adsorption sites which equilibrate instantaneously with the mobile and immobile liquid regions. The solute adsorption by the solid phase is described with a linear isotherm, and the solute degradation in both the liquid and solid phases is assumed to be a first-order process. Based on the above conceptual model, MIM for reactive transport under steady state flow is given by the following expressions (van Genuchten and Wagenet, 1989):

$$\left(\theta_m + f\rho K_d\right)\frac{\partial C_m}{\partial t} = \theta_m \frac{\partial}{\partial x}\left(D(x)\frac{\partial C_m}{\partial x}\right) - V_m\theta_m\frac{\partial C_m}{\partial x} - w\left(C_m - C_{im}\right) - \left(\theta_m\mu_{lm} + f\rho K_d\mu_{sm}\right)C_m$$

(1)

$$\left(\theta_{im} + (1-f)\rho K_d\right)\frac{\partial C_{im}}{\partial t} = w\left(C_m - C_{im}\right) - \left(\theta_{im}\mu_{lim} + (1-f)\rho K_d\mu_{sim}\right)C_{im}$$

(2)

where θ_m and θ_{im} are water contents in the mobile and immobile regions, respectively, and $\theta_m + \theta_{im} = \theta$; θ is the total water content of the soil media, C_m and C_{im} are solute concentrations in the mobile and immobile regions (ML^{-3}), respectively; V_m is mobile pore-water velocity (LT^{-1}) and $V_m\theta_m$ is equal to flow rate, q (LT^{-1}); w is the first-order mass transfer coefficient (T^{-1}); f and (1 − f) represent fractions of adsorption sites that equilibrate instantaneously with the mobile and immobile regions, respectively; ρ is bulk density of the porous medium (ML^{-3}); K_d is distribution coefficient for the linear sorption process (M^{-1} L^3); μ_{lm} and μ_{lim} are the first-order decay coefficients for degradation of solute in the mobile and immobile regions (T^{-1}), respectively; μ_{sm} and μ_{sim} are the first-order decay coefficients for degradation of solute in the mobile and immobile adsorbed solid phases (T^{-1}), respectively; x is spatial coordinate (L); t is time (T); $D(x)$ is the hydrodynamic dispersion coefficient in the mobile region (L^2 T^{-1}).

The dispersivity is generally considered as constant in case of mobile-immobile model (MIM) with constant dispersion, while in case of scale dependent dispersion, the dispersivity is considered as function of distance (Yates, 1990). However, Picken and Grisak (1981) and Yates (1990) have shown that the dispersivity (α) can be considered as a function of linear and asymptotic function of distance (x). At laboratory scale, distance (x) is the length of soil column experiments. The linear distance-dependent dispersivity increases with distance without bounds, while the asymptotic distance-dependent dispersivity initially increases with distance and ultimately approaches an asymptotic value. The linear distance- dependent dispersion coefficient, as given by Yates (1990) is:

$$D(x) = \alpha(x)V_m = k\,x\,V_m$$

where $\alpha(x)$ the distance-dependent dispersivity, k is the slope of the dispersivity-distance relationship (dimensionless), x is distance from the source and V_m is mean pore water velocity. Asymptotic dispersivity can be written as:

$$D(x) = \alpha(x)V_m = a\left(1 - \frac{b}{x+b}\right)V_m$$

where a is the asymptotic dispersivity value (L) and b is a characteristic distance (L), which determine the travel distance for the dispersivity to reach half of the asymptotic value.

4.1 Development of numerical model and its application

An implicit finite difference formulation of Equations 1 and 2 can be written as:

$$A_1 \frac{C_{mi}^{l+1} - C_{mi}^{l}}{\Delta t} = \frac{\theta_m}{\Delta x^2}\left(\frac{D_{i+1} + D_i}{2}\right)C_{mi+1} - \frac{\theta_m}{\Delta x^2}\left(\frac{D_{i+1} + 2D_i + D_{i-1}}{2}\right)C_{mi} + \frac{\theta_m}{\Delta x^2}\left(\frac{D_i + D_{i-1}}{2}\right)C_{mi-1} -$$

$$V_m \theta_m \frac{C_{mi+1}^{l+1} - C_{mi-1}^{l+1}}{\Delta x} - w\left(C_{mi}^{l+1} - C_{imi}^{l+1}\right) - A_2 C_{mi}^{l+1}$$

(4)

$$A_3 \frac{C_{imi}^{l+1} - C_{imi}^{l}}{\partial t} = w\left(C_{mi}^{l+1} - C_{imi}^{l+1}\right) - A_4 C_{imi}^{l+1}$$

(5)

where defined coefficients are

$$A_1 = \left(\theta_m + f\rho K_d\right)$$

(6a)

$$A_2 = \left(\theta_m \mu_{lm} + f\rho K_d \mu_{sm}\right)$$

(6b)

$$A_3 = \left(\theta_{im} + (1-f)\rho K_d\right) \quad A_4 = \left(\theta_{im}\mu_{lim} + (1-f)\rho K_d \mu_{sim}\right)$$

(6c)

and i represents the grid number; l represents the known time; $l+1$ represents the unknown time level; Δx represents the grid size along the length of domain; and Δt represents computational time step.

Following initial conditions have been used:

$$C_m(x,0) = C_{im}(x,0) = 0$$

$$\left.\frac{\partial C_m(x,t)}{\partial x}\right|_{x=L} = 0$$

The constant concentration type boundary condition is

$$C_m(0,t) = C_0$$

Pulse type boundary condition is:

$C_m(0,t)=C_0$ for $t \le t_0$

(7d)

$C_m(0,t)=0$ for $t > t_0$

(7e)

where C_0 is initial injected solute concentration at inlet of the soil media (M/L^3) and t_0 is the pulse time (T). Thomas algorithm is used to solve the set of linear simultaneous

equations. Numerical model is used to predict temporal and spatial solute concentration with constant, linear and asymptotic distance dependent dispersivity. Following input parameters i.e., constant dispersivity α =2m, linear distance coefficient, k=0.1, asymptotic distance dependent dispersivity, a=2.5 m, b=5 m, flow rate, q=0.04 m/d, θ_m =0.3, θ_{im} =0.1, mass transfer coefficient, w=0.01 per day are used during simulation. Figure 2 represents the temporal concentration profile predicted at down gradient distance of 5m and 20 m in flow direction. The behaviors of temporal concentration profiles are different among constant, linear and asymptotic distance dependent dispersivity. Early arrival of solute concentration has been obtained in case of constant dispersivity as compared to both linear and asymptotic value of dispersivity. Similarly, behaviors of spatial solute concentration profiles are different for constant, linear and asymptotic distance dependent dispersivity as shown in Figure 9. In case of constant dispersivity (MIMC), the value of solute concentration is smaller at small distance and its value is higher at large travel distance.
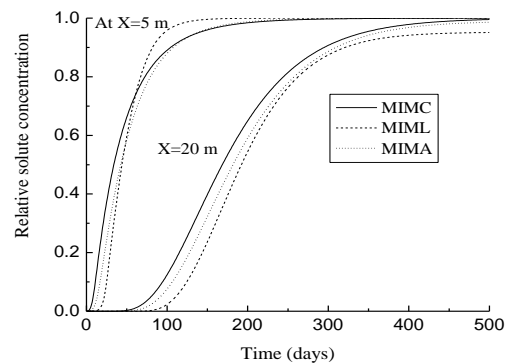

Figure 8 Temporal concentration profiles predicted at 5m and 20 m down gradient distance with constant, linear and asymptotic distance dependent dispersivity.
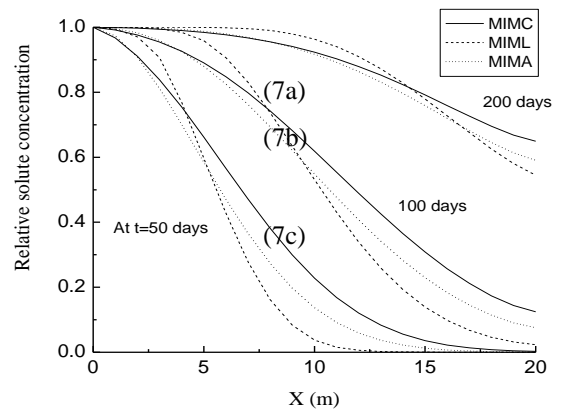

Figure 9 Spatial concentration profiles predicted at different transport time with constant, linear and asymptotic distance dependent dispersivity.

5. SIMULATION OF EXPERIMENTAL BREAKTHROUGH

The numerical model is used to simulate the observed experimental breakthrough curves predicted at different distances of 300cm, 900cm and 1500cm in the flow direction. Figures 9-11 show the observed experimental breakthrough curves and numerically simulated results at different distances in the flow direction. Following parameters i.e., flow rate, q=0.42 cm/min, θ_m =0.34, θ_{im} =0.04, mass transfer coefficient, w=2.42 E-05 per min, dispersivity, α =82.46 cm, linear distance dependent coefficient, k=0.0824, asymptotic distance dependent coefficients, a=82.74 cm, b=148.56 cm are used during simulation. Firstly, we simulated observed experimental data at 1500 cm down gradient distance using mobile immobile constant, linear and asymptotic distance dependent dispersivity as shown in Figure 9. Thus, via best fit simulation of observed breakthrough curve, the value of mass transfer coefficient, constant dispersivity, linear and asymptotic distance dependent parameters have been estimated. Performance of simulations are evaluated by considering root mean square error (RMSE), Nash-Sutcliffe efficiency coefficient (NSE) and coefficient of determination (R^2) are used for finding efficiency of simulations as described by Equations 8(a-c).

$$RMSE = \sqrt{\frac{1}{n}\sum_{i=1}^{n}(C_{iobs}-C_{isim})^2}$$
(8a)

$$R^2 = \left(\frac{\sum_{i=1}^{n}(C_{iobs}-\overline{C}_{iobs})(C_{isim}-\overline{C}_{isim})}{\sqrt{\sum_{i=1}^{n}(C_{iobs}-\overline{C}_{iobs})^2}\sqrt{\sum_{i=1}^{n}(C_{isim}-\overline{C}_{isim})^2}} \right)^2$$
(8b)

$$NSE = 1 - \frac{\sum_{i=1}^{n}(C_{iobs}-C_{isim})^2}{\sum_{i=1}^{n}(C_{iobs}-\overline{C}_{iobs})^2}$$
(8c)

where C_{iobs} and C_{isim} are ith observed and simulated concentration, respectively, $\overline{C}_{iobs}$ and $\overline{C}_{isim}$ are the mean of observed and simulated concentration respectively. N is the number representing total observations taken at any particular observational point.

Computed values of root mean square error, coefficient of determination and Nash-Sutcliffe efficiency coefficient is shown in Table 2 for mobile immobile model with constant, linear and asymptotic distance dependent dispersivity (i.e., MIMC, MIML and MIMA). The estimated values of R^2= 0.907,

RMSE=0.035, NSE =0.896 in case of MIMC, R^2= 0.984, RMSE=0.017, NSE =0.976 in case of MIML, R^2= 0.99, RMSE=0.011, NSE =0.99 in case of MIMA are obtained for simulated breakthrough curve in Figure 9. It is seen that the value of R^2 and NSE is higher for the case of asymptotic dispersivity model (MIMA) as compared to both constant dispersivity (MIMC) and linear distance dependent (MIML) models. Similarly, to evaluate the performance of simulation of breakthrough curve observed at 300 cm and 900 cm down gradient distances (Figures 10 and 11), the estimated value of R^2, RMSE, and NSE is shown in Table 2. The simulation results of experimental breakthrough curves indicates that the MIMC and MIML models could not give the best fit of observed data and also over estimate the value of dispersivity. Finally, results indicated that the asymptotic (MIMA) model gives best fit of observed data of experimental breakthrough curves in long heterogeneous soil column experiment.
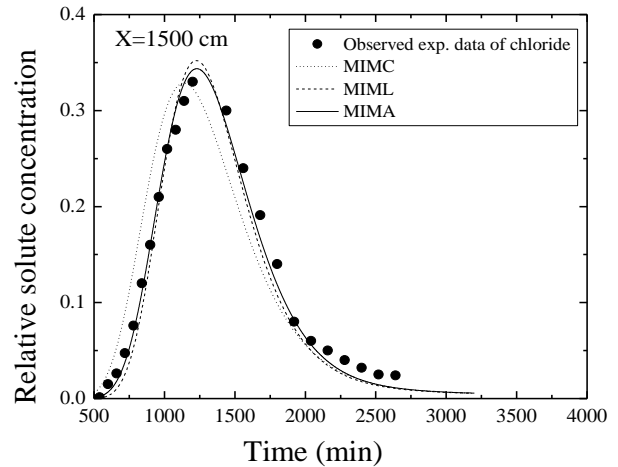

Figure 9 Simulated breakthrough curve of experimental data of chloride at 1500 cm
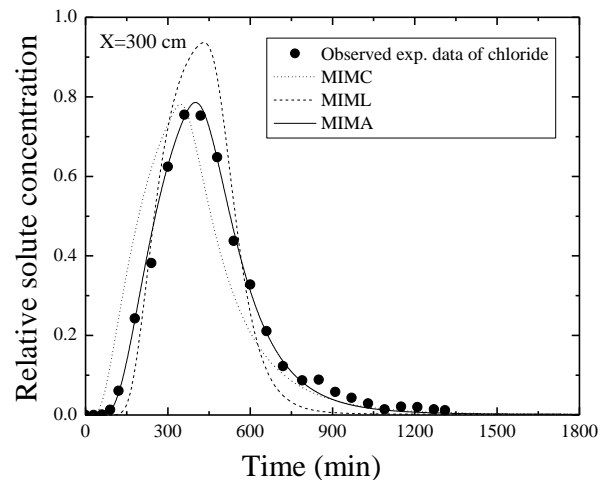

Figure 10 Simulated breakthrough curve of experimental data of chloride at 300 cm .
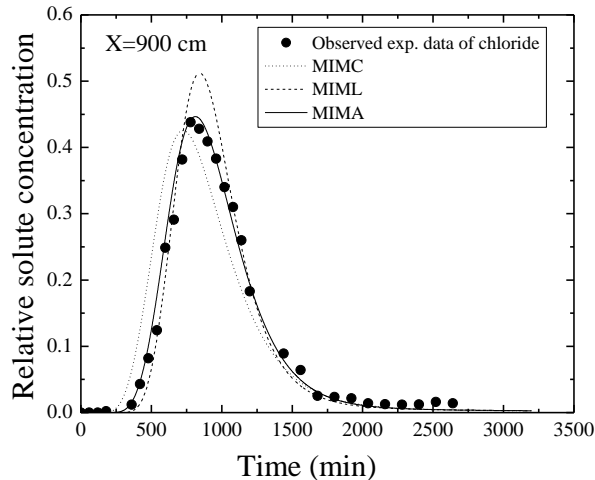
Figure 11 Simulated breakthrough curve of experimental data of chloride at 900 cm.

Table 2 estimated values of R^2, *RMSE* and Nash Sutcliffe coefficients (*NSE*)

Distance (cm)	MIMC			MIML			MIMA		
	RMSE	R^2	*NSE*	RMSE	R^2	*NSE*	RMSE	R^2	*NSE*
300	0.102	0.84	0.83	0.081	0.97	0.89	0.019	0.99	0.99
900	0.061	0.848	0.843	0.031	0.986	0.959	0.018	0.988	0.986
1500	0.035	0.907	0.896	0.017	0.984	0.976	0.011	0.99	0.99

6. SUMMARY AND CONCLUSIONS

In this study, experiments were conducted in the laboratory to understand the behavior of solute transport through horizontal heterogeneous long soil column filled with filled with layered and mixed soil media. Chloride was used as conservative tracer in the experiments. Observed experimental break through curves have been predicted at different distance in flow direction. Breakthrough curve for non-reactive solute shows early appearance due to strong dispersion in layered soil as compared to mixed. Long tailing is also observed due to presence of solute in porous space. It is also seen that the stratification i.e., layered and mixed soil media affect the behavior of predicted breakthrough curves in long heterogeneous soil column experiments. The behaviors of breakthrough curves are very irregular and exhibited extensive tailing. It means that the variation of pore velocity in heterogeneous porous media is much larger as compared to homogeneous porous media. It means that the large variation of hydraulic conductivity increase the dispersion of solute in heterogeneous porous media.

Finally, it is also shown that the MIMA model gives the best fit curve of experimental breakthrough curve in long heterogeneous soil column experiment as compared to both MIC and MIML models. Thus MIMA model is efficient to capture the evolution distance dependent dispersion behavior. Hence asymptotic dispersivity can be useful for describing solute transport in long heterogeneous porous media.

REFERENCES:

i.   Bear, J. (1979). "Hydraulics of groundwater." McGraw-Hill, NewYork.
ii.   Chrysikopoulos, C. V., Kitanidis, P. K., & Roberts, P. V. (1990). "Analysis of one-dimensional solute transport through porous media with spatially variable retardation factor." Water Resources Research, 26(3), 437-446.
iii.   David Logan, J. (1996). "Solute transport in porous media with scale-dependent dispersion and periodic boundary conditions." Journal of Hydrology, 184(3), 261-276.
iv.   Fallico, C., Chidichimo, F., and Straface, S., (2012). "Solute dispersion in porous media at different transport velocities and distances." Int. Water Tech. J. (2), 100-109.
v.   Hassanizadeh, S. M., & Gray, W. G. (1987). "High velocity flow in porous media." Transport in Porous Media, 2(6), 521-531.
vi.   Huang, K., Toride, N., & Van Genuchten, M. T. (1995). "Experimental investigation of solute transport in large, homogeneous and heterogeneous, saturated soil columns." Transport in Porous Media, 18(3), 283-302.
vii.   Huang, G., Huang, Q., & Zhan, H. (2006). "Evidence of one-dimensional scale-dependent fractional advection–dispersion." J. of contam. Hydrol., 85(1), 53-71.
viii.   Kau, P. M. H., Smith, D. W., & Binning, P. (1997). "Fluoride retention by kaolin clay." J. of contam hydrol., 28(3), 267-288.
ix.   Kau, P. M. H., Smith, D. W., & Binning, P. (1998). "Experimental sorption of fluoride by kaolinite and bentonite." Geoderma, 84(1), 89-108.
x.   Lapidus, L., & Amundson, N. R. (1952). "Mathematics of adsorption in beds. VI. The effect of longitudinal diffusion in ion exchange and chromatographic columns." J. of Physical Chemistry, 56(8), 984-988.
xi.   Li, Z., & Brusseau, M. L. (2000). "Nonideal transport of reactive solutes in heterogeneous porous media: 6. Microscopic and macroscopic approaches for incorporating heterogeneous rate-limited mass transfer." Water Resour. Res., 36(10), 2853-2867.
xii.   Leij, F. J., Toride, N., Field, M. S., & Sciortino, A. (2012). "Solute transport in dual-permeability porous media." Water Resour. Res., 48(4).
xiii.   Pickens, J. F., and Grisak, G. E. (1981). "Scale-dependent dispersion in a stratified granular aquifer." Water Resour. Res., 17, 1191-1211.
xiv.   Peters G. P., and Smith, D. W. , (2001) "Numerical study of boundary conditions for solute transport through porous medium." Int. J. Numer. Anal. Meth. Geomech. 25, 629-650.
xv.   Sternberg, S. P., & Greenkorn, R. A. (1994). An experimental investigation of dispersion in layered porous media. Transp.in porous media, 15(1), 15-30.
xvi.   Sudicky, E. A., and Cherry, J. A. (1979). "Field observations of tracer dispersion under natural flow conditions in an unconfined sandy aquifer." Water Pollut. Res. Can. 14, 1-17.
xvii.   Sudicky, E.A., Gillhamand, R.W., Frind, E.O. (1985) "Experimental investigation of solute transport in Stratified porous media 1.The non reactive case" Water resource research 21: 1043-1050
xviii.   Valocchi, A. J. (1985). "Validity of the local equilibrium assumption for modeling sorbing solute transport through homogeneous soils." Water Resour. Res., 21(6), 808-820.
xix.   Van Genuchten, M. T., & Wagenet, R. J. (1989). "Two-site/two-region models for pesticide transport and degradation: Theoretical development and analytical solutions." Soil Science Society of America Journal, 53(5), 1303-1310.
xx.   Wang, K., & Huang, G. (2011). "Impact of Hydraulic Conductivity on Solute Transport in Highly Heterogeneous Aquifer." In Computer and

Computing Technologies in Agriculture IV (pp. 643-655). Springer Berlin Heidelberg.

xxi.   Xu, J., & Hu, B. X. (2004). "A numerical Eulerian method of moment for solute transport in a nonstationary dual-porosity medium." Adv. in water resour., 27(3), 207-222.

xxii.   Yates, S. R. (1990). "An analytical solution for one-dimensional transport in heterogeneous porous media." Water Resour. Res., 26(10), 2331-2338.

xxiii.   Yates, S. R. (1992). "An analytical solution for one-dimensional transport in porous media with an exponential dispersion function." Water Resour. Res., 28(8), 2149-2154.

Estimation And Detection Of Multipath Noise In The Reservoir Bathymetry Data Using Wavelet

Anjali Ghadage[1]   Selva Balan[2]   Sushama Shelke[3]

[1]Student, NBN SSOE, Pune-411041, India
[2] Chief research officer, CWPRS khadakwasla, Pune-411024, India
[3]Professor, NBN SSOE, Pune-411041, India
Email: anjali.ghadage@gmail.com

ABSTRACT : *Bathymetric data is depth values of reservoir. Bathymetric data is useful for hydrographic survey, volume calculation and 3D plot generation. Echo sounder collects bathymetric data using ultrasonic waves. Multipath noise gets added during reflection of ultrasonic waves from bottom of reservoir in SONAR system. Bathymetric data taken from SONAR is not accurate because multipath noise gets added and there is need to remove multipath noise. By applying wavelet packet decomposing (WPD) method multipath noise is removed. Then after removing multipath noise for 3D visualization of bathymetric data Triangulated Irregular Network (TIN) and regression method are used.*
Keywords: Bathymetric data, Multipath Noise, WPD, TIN, Regression.

1. INTRODUCTION:

Mountains occupy 24% of the global land surface area and are home to 12% of the world's population. About 10% of the world's population depends directly on the use of mountain resources for their livelihoods and wellbeing and an estimated 40% depends indirectly on them for water, hydroelectricity, timber, biodiversity, niche products, mineral resources, recreation and flood control.

Reservoirs are a major part of the usable surface water resources They are used for multiple purposes, including water supply, recreation, flood control, sports fishery, industrial purposes, and hydroelectric-power generation.

Accumulation of sediment is one of the most serious factors that threaten aquatic environments such as reservoirs, lakes and ponds. Sedimentation causes some lakes, ponds and reservoirs to be filled and polluted within a short time. It also causes loss of area and volume, and reduces the lifespan of facilities. Due to sediment accumulation reflection of ultrasonic waves adds multipath noises in ultrasonic data.

Multipath noise is removed using WPD. Wavelet packet decomposing method is based on the wavelet packet decomposition (WPD) and the selection of the so–called "best basis" in the sense of some criteria. It has been shown that an orthogonal wavelet basis is particularly adapted to discriminate signal and noise: the latter is represented by small coefficients on the wavelet domain.

In that case, the "Hard-Thresholding" of the lowest coefficients leads to a noise reduction. In this paper, we use the bathymetric data acquired by multi-beam echo-sounder s. This paper mainly studies the TIN and ANN algorithms to seafloor terrain modelling. In TIN, we first divide the large amount of data in survey area into several blocks and construct Delaunay triangulations in sub-blocks individually, and then merge the sub-triangulations in a regressive order to obtain an integrated triangulation mesh. And in ANN algorithm regression methods are used for 3D visualization.

In order to store more water in reservoirs, lakes and ponds, prevent water pollution, protect water sources and extend the service life of these facilities, it is important to know the current topographic conditions and any changes in the capacities of these facilities. The study identified changes in water volume of the some reservoir, as a result of sedimentation over a 25-year period, by comparing topographic and bathymetric data.

2. MATERIAL AND METHODS

2.1   Data Collection

A Personal Computer was connected to the Sonar through a serial data cable to access the operating system of the instrument and to download the data for post processing applications. Geographical Positioning System (GPS) was connected to the Sonar using a standard data cable, so that GPS readings were generated in conjunction with instrument's echo sounding functions to create full XYZ hydrographic data using Sonar software package.

2.2   Wavelet Packet Decomposing Method

When SONAR transmit sonar wave it should be reflect from bottom surface of reservoir but due to sediment accumulation multi path noise gets added and sonar waves reflect from or between sediment layer so algorithm have to develop to remove multipath noise which gets added in bathymetric data.

The method is based on the wavelet packet decomposition (WPD) and the selection of the so–called "best basis" in the sense of some criteria (e.g., entropy). It has been shown that an orthogonal wavelet basis is particularly adapted to discriminate signal and noise. : The latter is represented by small coefficients on the wavelet domain. In that case, the "Hard Thresholding" of the lowest coefficients leads to a noise reduction.

WPD–based denoising method consists in:

• Projecting the signal on an orthogonal wavelet basis and selecting the entropy–based best basis.
• Eliminating lowest coefficients by Hard Thresholding,
• Projecting back remaining coefficients to the original space with the inverse unitary WPD transform.

2.3 TIN Algorithm

Triangulated Irregular Networks algorithm consists of following steps:

A. Topological Relations of TIN Establishing
Compared with the simple data structure of Grid, the data structure of TIN is much more complex. Topological relations allow data structures of TIN are classified into: point structure, surface structure, point-surface structure, edge structure and edge-surface structure.

B. Survey Area Splitting
It is unacceptable to construct the Delaunay triangulation with the huge amount of data points directly. A proper way is splitting the survey area into several sub-blocks first, and then constructing Delaunay triangulations individually.

C. Delaunay Triangulation Construction
The algorithms of Delaunay triangulation construction can be divided into several groups: divide & conquer, incremental insertion, incremental construction, sweeping and high-dimensional embedding. We adopt the incremental insertion algorithm for Delaunay triangulation for reasons of its simplicity, robustness and acceptable speed.

D. Sub-triangulations Merging
Sub-triangulations are merged in reverse order of splitting, that means merge the leaf nodes in binary tree in descending order according to the level.

2.4 Regression Method

Polynomial models have the advantages of being simple, familiar in their properties, and reasonably flexible for following data trends. They are also robust with respect to changes in the location and scale of the data. However, polynomial models may be poor predictors of new values. They oscillate between data points, especially as the degree is increased to improve the fit. Asymptotically, they follow power functions, leading to inaccuracies when extrapolating other long-term trends. Choosing a polynomial model is often a trade-off between a simple description of overall data trends and the accuracy of predictions made from the model.

3. RESULTS AND ANALYSIS

All experiments were carried out using MATLAB 9.0 simulations.

A.   Original Bathymetric Data and Data after WPD

Bathymetric data is depth value data for reservoir or lack which is in XYZ co-ordinate form. Table 1 shows original bathymetric data which does not give smooth points of bottom lack or reservoir surface.

Table 1. Bathymetric Data

X	Y	Z
689505.8	1254012	-4.03
689506.6	1254013	-4.46
689506.9	1254014	-4.23
689507.6	1254015	-4.55
689508	1254015	-4.51
689508.4	1254016	-4.5
689509.3	1254017	-4.48
689509.6	1254018	-2.22
689510	1254019	-2.22
689510.3	1254019	-2.23
689511.1	1254021	-2.22
689511.4	1254022	-2.2
689511.8	1254022	-2.19
689512.3	1254024	-5.92
689512.7	1254024	-10.92
689513.2	1254025	-12.72
689513.6	1254026	-3.6
689514.3	1254027	-4.06
689514.7	1254028	-3.52
689515.2	1254028	-3.88
689515.7	1254029	-3.63
689516.7	1254031	-3.89
689517.2	1254031	-15.36
689517.7	1254032	-3.68
689518.3	1254033	-3.85

Table 2 consists of data after applying wavelet packet decomposing method. Data after WPD gives smooth points of bottom lack or reservoir surface.

Table 2. Bathymetric data after WPD

X	Y	Z

689507.6	1254015	-4.32
689507.6	1254015	-4.29
689507.6	1254015	-4.26
689507.6	1254015	-4.24
689507.8	1254016	-4.24
689507.9	1254016	-4.24
689508.2	1254017	-4.25
689508.5	1254017	-4.27
689508.9	1254018	-4.3
689509.4	1254019	-4.33
689510	1254020	-4.37
689510.5	1254021	-4.4
689511.1	1254022	-4.43
689511.7	1254023	-4.49
689512.4	1254024	-4.58
689513.1	1254025	-4.74
689513.9	1254026	-4.93
689514.7	1254027	-5.13
689515.4	1254029	-5.34
689516.2	1254030	-5.55
689516.8	1254031	-5.72
689517.4	1254032	-5.83
689517.7	1254032	-5.81
689517.7	1254032	-5.62
689517.5	1254032	-5.3

B. *Original Bathymetric Data Plot and plot after WPD*

Bathymetric data is plotted using TIN algorithm in MATLAB software. Figure 1 shows plot of bathymetric data. And after applying WPD data is plotted using TIN algorithm which is shown in figure 2.

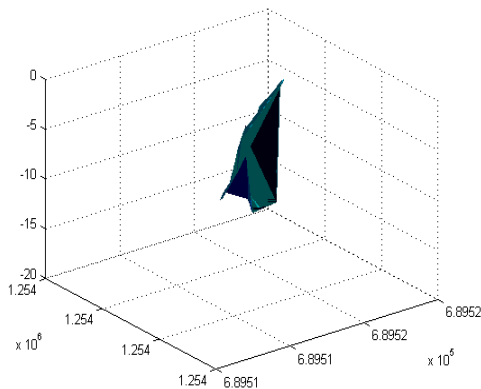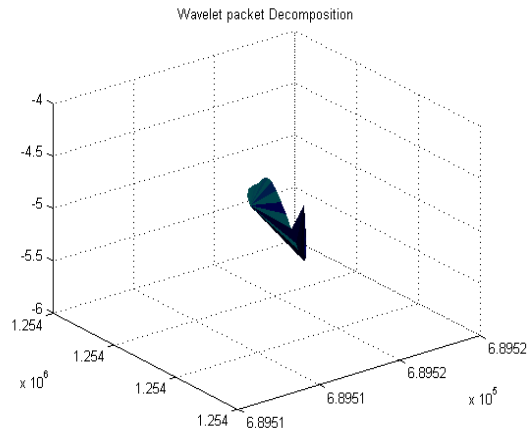**Figure 1.**Original Bathymetric Data Plot

Figure 2. Plot of Data after WPD

C. *Original Bathymetric Data regression and plot after WPD*

Bathymetric data is plotted using regression method in MATLAB software. Figure 3 shows plot of bathymetric data. And after applying WPD data is plotted using regression method which is shown in figure 4.
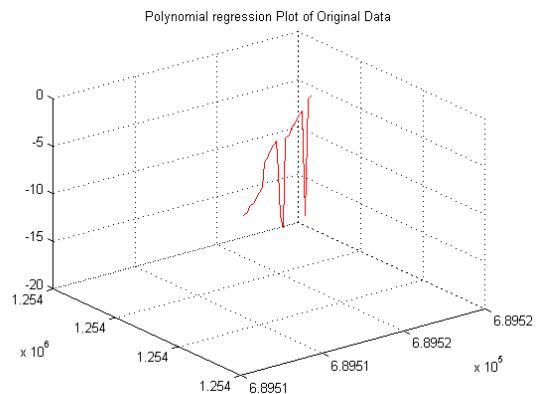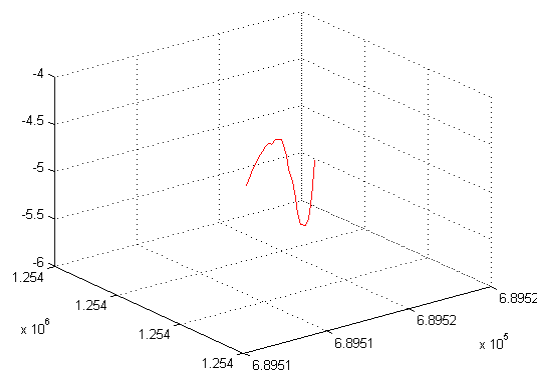

Figure 3. Original Bathymetric Data Regression Plot

Figure 4. Regression Plot Bathymetric Data after WPD

4. CONCLUSIONS

Multipath is one of the most important error sources in the echo reflection so that bathymetric data contains multipath noise. By applying wavelet packet decomposing method multipath noise in underwater bathymetry data is removed. After filtering bathymetric data set, image is reconstructed using Triangulated Irregular Network (TIN) and Regression method using MATLAB software.

REFERENCES:

i. Dan Lu, Haisen Li, Yukuo Wei, TongxiShen, "An Improved Merging Algorithm for Delaunay Meshing on 3D Visualization Multibeam Bathymetric Data", Proceedings of the 2010 IEEE International Conference on Information and Automation, pp. 1171-1176, June, 2010.

ii. Demetris Koutsoyiannis, "Climate change, the Hurst phenomenon, and hydrological statistics", Hydrological Sciences–Journal–des Sciences Hydrologiques, pp. 1-24, February, 2003.

iii. Hassen M. Yesuf, Tena ,Alamirew, Assefa M. Melesse and Mohammed Assen, "Bathymetric Mapping for Lake Hardibo in Northeast Ethiopia Using Sonar", International Journal of Water Sciences, pp.1-9, August, 2012.

iv. Mohd Ansor Bin Yusof, Shahid Kabir, "Underwater Communication Systems: A Review", Progress In Electromagnetics Research Symposium Proceedings, Marrakesh, Morocco, pp.803-807, March, 2011.

v. Padmavathi, Subashini, Muthu Kumar and Suresh Kumar Thakur, "Performance analysis of Non Linear Filtering Algorithms for underwater images" , (IJCSIS) International Journal of Computer Science and Information Security, Vol.6, No. 2, pp. 232-238, June, 2009.

vi. Pierre Cervenka and Christian de Moustier, "Post processing and Corrections of Bathymetry Derived from Sidescan Sonar Systems: Application with SeaMARC II", IEEE Journal of Oceanic Engineering, Vol.19, No. 4, pp. 619-629, October 1994.

vii. Sang-Ki Moon, Nam C. Woo, Kwang S. Lee, "Statistical analysis of hydrographs and water-table fluctuation to estimate groundwater recharge", Journal of Hydrology, pp. 198–209, December, 2004

viii. Schild, "The case of the Hindu Kush–Himalayas: ICIMOD's position on climate change and mountain systems", Mountain Research and Development, March, 2008.

ix. Shamik Tiwari, Ajay Kumar Singh, V.P. Shukla, "Statistical Moments based Noise Classification using Feed Forward Back Propagation Neural Network", International Journal of Computer Applications , Volume 18– No.2, pp.36-40, March 2011.

Investigationof Fractal Behaviour In Precipitation For Three Different Climatic Regionsin India

Arvind Kumar Bairwa, Rakesh Khosa and Maheswaran
Department of Civil Engineering,
Indian Institute of Technology Delhi
New Delhi-110016
maheswaran27@yahoo.co.in

ABSTRACT: *In developing countries, there is a crucial necessity of high resolution meteorological information to cater for the needs of studies related to urban hydrology where it is required to study the hydrological response at smaller spatial and temporal scales. This study investigates presence of Fractal (scaling) behaviour in precipitation of Bangalore, Palam (Delhi), Safdarjung (Delhi) and Hyderabad.In the present work, fractal behaviour in precipitation has been examined using two methods namely (i) conventional statistical moments (SMs), and (ii) Probability Weighted moments (PWMs).Analysis reveals that the SMs approach suggests existence of a simple scaling behaviour in the precipitation data whereas PWMs approach revealed evidence of multi-scaling behaviour. The presence of scaling behaviour of rainfall observed in the above three significantly different climatic regions, Delhi (subtropical), Bangalore (tropical savanna) & Hyderabad (tropical dry and wet) seems to suggest the general suitability of the fractal-scaling theory for transforming rainfall across the time-scales.*
Keywords: fractals, scaling, rainfall.

1. Introduction

The climate of India is monsoonal in rhythm and character. The nature of Indian precipitation is distinctly different from many locations mainly due to monsoon effect. India experiences a tropical monsoon type of climate where about three fourth of total rainfall is concentrated within four months(June to September).The recent study by Goswami et al.,2006 of a large central Indian region used analyses of daily rainfall data from 1803 stations (1951-2000)and found significant increase in frequency and magnitude of high intensity rain events (>100 mm/day) and significant decrease in frequency of light and moderate events (>5 and <100 mm/day).Hence, there is an urgent need of high-resolution meteorological information to cater for the new focus on the hydrological response at smaller spatial and temporal scalesand also to aid in the studies related to urbanization.

Recent advances in the fractalsconcept offer new perspective in the analysis and modelling of several physical and geophysical processes. Analysis of the fractal (or scaling) behaviour of the hydrological process over a wide range of scales may lead to a better understanding of strongly irregular fluctuations of a process such as rainfall. In the past, Gupta and Waymire (1990) assessed the scaling behaviour of the rainfall by studying the

variations of the ordinary product moments or conventional Statistical moments (SMs).Based on scaling properties in rainfall, Yu et al.,(2004) constructed a regional rainfall intensity formulas using forty-six rain gauge stations over northern Taiwan.Kumar et al., (1994) presented a statistically robust approach based on probability weight moments(PWMs) to assess the presence of simple scaling in geophysical processes. Their study revealed that the scale free (scale-invariance)behaviour in the rainfall phenomenon often sheds light on the genesis of the phenomenon and there by reduces the complexity of models and their inference, and allows one to get the information from one scale to another. Even though there have been many other studies (Gupta and Waymire (1993), SivaKumar (2000), Veneziano and Langousis (2010)) investigating the scaling behaviour of rainfall across the globe, there has been much less work done for indian regions. Therefore, the purpose of this study is to investigate Fractal (or scaling) behaviour of rainfall in India for distinctly different climatic regions.

2. Data Collection

Numerical analysis was performed on annual maximum rainfall series on 4 meteorological stations in India. The data was obtained from the INDIA METEROLOGICAL DEPARTMENT (IMD). The four stations were selected based on record length, and availability of current datasets (refer Table 1).

Table 1 Data used in the study.

Station	Years	Record Length	Duration
HYDERABAD	1993 - 2008	16 years	Hourly
BANGLORE	1969 - 2003	33 years	Hourly
DELHI - SAFDARJUNG	1969 - 1998	30 years	Hourly
DELHI-PALAM	1969 - 1999	33 years	Hourly

3. Methodology

Fractal-Scaling theory (Gupta & Waymire,1990):

- Let $\{I_d\}$ and $\{I_{\lambda d}\}$ are annual maximum rainfall intensity (AMRI) series for rainfall duration d and λd respectively.
- The random variable $\{I_d\}$ and $\{I_{\lambda d}\}$ have the scaling properties as

$$I_{\lambda d} \overset{\Delta}{=} \lambda^{\alpha} I_d$$

where equality $\overset{\Delta}{=}$ is understood in the sense of equality of probability distributions, and α represents the scaling exponent (INFORMATION CARRYING ELEMENT). This property is usually referred to as 'simple-scaling in the strict sense' (Gupta and Waymire, 1990).

If $I_{\lambda d}$ has finite moments, $E(I_{\lambda d}^q)$ of the order q; then the strict sense simple scaling in Eq. (1) implies that $I_{\lambda d}^q$ and $(\lambda^{\alpha} I_d)^q$ have the same probability distribution. Therefore, they have the same moments, i.e.

$$E(I_{\lambda d}^q) = \left(\lambda^{\alpha_q}\right) E(I_d^q)$$
(2)

where α_q represents the scaling exponent of order q, Eq. (2) can be transformed into:

$$\log E\left(I_{\lambda d}^q\right) = \log\left(\lambda^{\alpha_q} E\left(I_d^q\right)\right) \tag{3}$$

$$\log E\left(I_{\lambda d}^q\right) = \log E(I_d^q) + \alpha_q \log(\lambda) \tag{4}$$

The scaling exponents α_q can be estimated from the slope of linear regression relationships between the log-transformed values of moment $\log E\left(I_{\lambda d}^q\right)$ and scale parameters log λ for various orders of moment q.This property is often referred (eq.2) as 'wide sense simple scaling'. If the above linear relationship does not exist, the multi-scaling approach has to be considered (Gupta and Waymire, 1990).

3.1Scaling analysis using probability weight moments (PWMs)

Probability Weight Moment (PWM), defined byGreenwood et al. (1979), assumes I_d as a Random variable, F_{I_d} represents cumulative distribution function (CDF) of I_d.
$y = y (F_{I_d})$ denotes the inverse form of CDF F_{I_d}.

$$M^{i,j,k} = E\left[I^i F_{I_d}{}^j (1 - F_{I_d})^k\right]$$
$$= \int_0^1 I^i F_{I_d}{}^j (1 - F_{I_d})^k dF_{I_d} \tag{5}$$

Where i, j, k are the real numbers, and $M_{1,n,o} = M_n$, PWM (β-type) is used in this study.

$$M_n = E\left[IF_{I_d}^n\right] = \int_0^1 y F_{I_d}^n dF_{I_d}$$

where $y = y\left(F_{I_d}\right)$, n is the order of PWMs of I_d and $I_{\lambda d}$ denoted as M_n^d and $M_n^{\lambda d}$ and λ is the scale factor have the scaling relationship as

$$M_n^{\lambda d} = \lambda^\beta M_n^d \tag{6}$$

$$\log M_n^{\lambda d} = \beta \log \lambda + \log M_n^d \tag{7}$$

From above Eq. (7), using the PWM to assess the scaling property has the following properties. The scaling exponent β can be estimated as the slope value of linear regression relationships between the log-transformed values of PWM $\log M_n^{\lambda d}$ and logλ for various orders of PWMs (n).

4. Case Study

A detailed analysis for only one case study (Palam Station) is presented here for brevity. For this station, the conventional statistical moments (SMs) of orders q=1 to q=4 and the Probability weight moments (PWMs) of orders n=0 through n=3 were computed. The nth order PWM, when n=0, is equal to the first-order conventional moments, which is basically the mean. Fig. 1shows the four conventional SMs (i.e. q= 1,2, 3, 4) plotted against the duration. To determine the nature of scaling (i.e., simple or multi), the variations in the values of the scaling exponents (q) were studied. The estimated values of the scaling exponent, the order of the conventional SMs(q)and $R^2$are given in Table 2.It can be seen that nearly a perfect linear relationship prevails between the exponents and the order (q)of the conventional SMs (Fig.2). This satisfies both the conditions imposed by equation (1).Thus, based upon the scaling behaviour of the conventional SMs, the annual maximum rainfall series are showing simple scaling behaviour. Similarly, the plots between the four PWMs order (i.e. n= 0, 1, 2, 3) against the duration (hr) are shown in Fig. 3. In contrary to SMs analysis, the analysis based on PWMs show that the annual maximum rainfall series are showing multi-scaling behaviour (indicated by the change of slope at 9 hr duration in the Fig.3).The analysis of the Fig.3 indicate that the relationships between PWMs and durations are linear having two different slopes with a breaking point at the 9h duration this property indicates transition in storm dynamics. Therefore, in this case we have two scaling exponents, $\beta_a (1hr - 9hr)$ and $\beta_b (9hr - 24hr)$. Figure 4 shows the scaling exponents corresponding to these two regimes. Similar results were obtained for other three stations where the SMs show simple scaling and PWMs analysis show multi scaling behaviour.

The above analysis clearly shows the presence of scaling in the rainfall in these areas. However, the debate whether the scaling is a single or multi scaling is still open and depends in the method used for estimation. There have been many propositions on the use of PWMs due to the following advantages (i) estimates of the PWMs are more robust than the conventional SMs (Kumar et al. (1994), Pandey (1998)), (ii) the estimation of higher-order conventional moments is significantly influenced by the presence of some large observations in the data series and consequently, the inferences based upon the conventional moments could be misleading. However, the inferences obtained from the PWMs are less affected by the extreme observations of the rainfall series. Therefore, the inferences obtained from the scaling analysis based on PWMs have been considered more reliable and more investigation are required to prove the same.
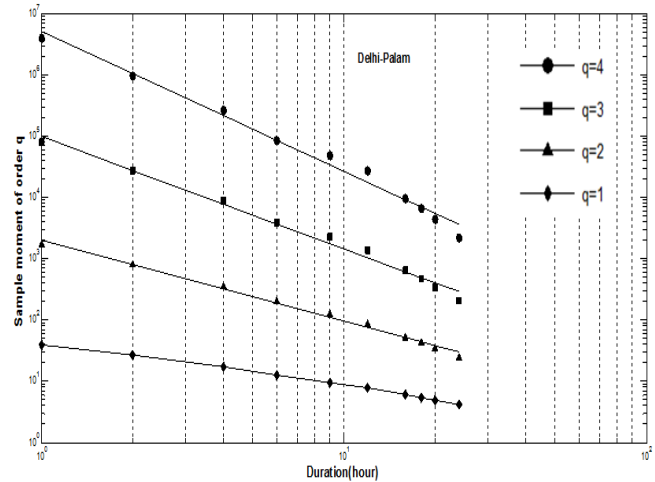
Fig.1 .Log-Log plots of Conventional SMs of order *q* versus durations.
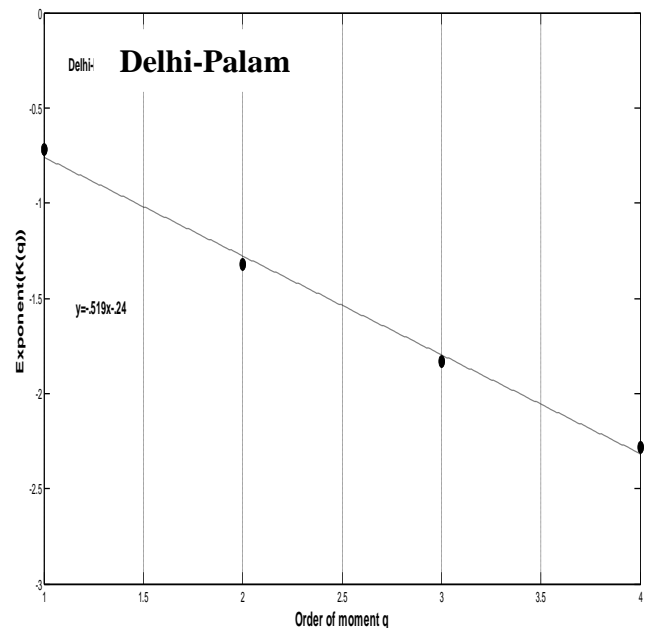
Fig.2Relationship between scaling exponentsand order of moment q(1,2,3,4).

Order of moments (q)	Palam α_q	Palam R^2
1	-0.72	0.9942
2	-1.32	0.9925
3	-1.83	0.9899
4	-2.28	0.9866

Order of moments(n)	β_a (1-9) hr	β_b (9-24) hr	R^2 (1-9) hr	R^2 (9-24) hr
0	-0.620	-0.867	0.9977	0.9975
1	-0.592	-0.854	0.9981	0.9964
2	-0.557	-0.820	0.9980	0.9956
3	-0.544	-0.840	0.9977	0.9947

Delhi-Palam
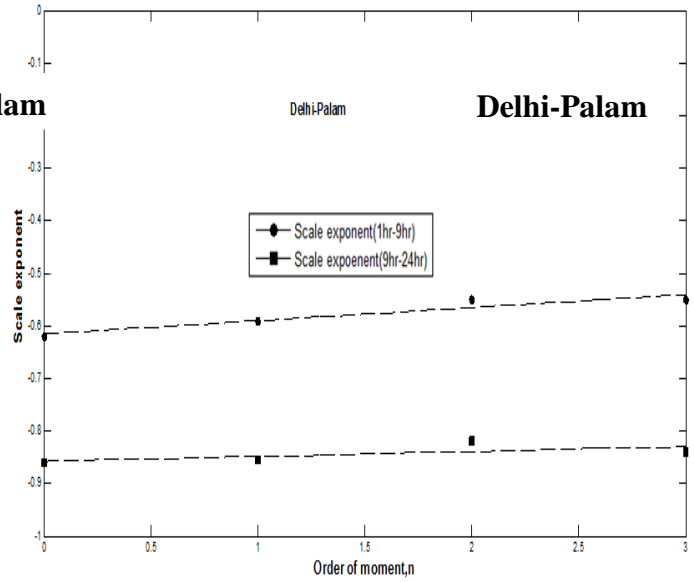
Fig.4. Relationship between scaling exponentsand order of moment n(0,1,2,3).
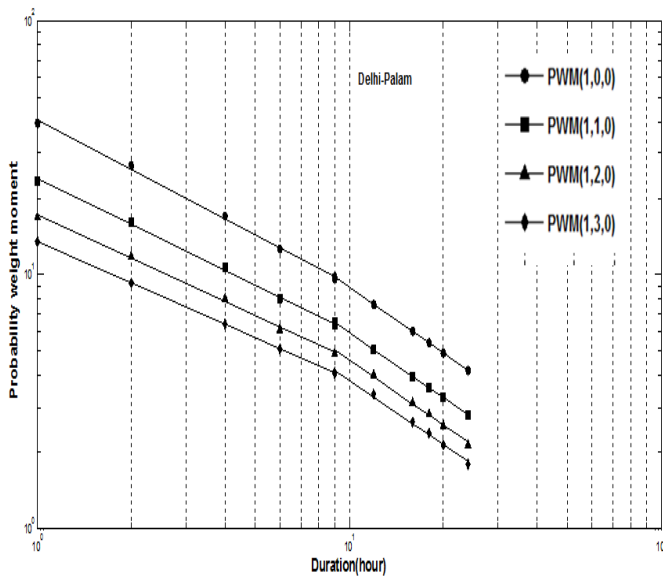
Fig.3.Log-Log plots of PWMs of order n versus durations.

Table 2 The values of the Conventional moment scaling function α_q for Palam station.

Table 3 The values of the PWM moment scaling function β for Palam station.

5. Conclusions

1)   The analysis of the rainfall in the four stations show the presence of Fractal behaviour.

2)   Conventional statistical moments(SMs) shows a simple scaling behaviour within 1-hour to 1-day for all the stations whereas PWM scale analysis shows the multi-scaling behaviour within (1hr-2hr) to (2hr-24hr) for the Bangalore,Delhi-Safdarjung and Hyderabad whereas Delhi-Palam is showing multi-scaling behaviour within (1hr-9hr) to (9hr-24hr) of the annual extreme rainfalls. This change in slope in the PWM analysis signifies the existence of two scaling regimes. These important findings enable the development of the methods for estimating annual extreme rainfalls for these stations based on the statistical moment of the selected rainfall series.

3)   The benefit of using the principles of the scaling is that it allows transformation of rainfall data from one time scale to another &reduces the amount of parameter required to compute the quantiles.

4)   Future work stemming from this can be to develop scaling relationship across different time scales to derive the IDF curves.

5)   Also, more investigations can be done in showing the superiority of the PWMs over SMs in estimating the scaling exponents.

6.References

i.   Gupta, V. K., & Waymire, E. (1990). Multiscaling Properties of Spatial Rainfall And River Flow Distributions. Journal Of Geophysical Research: Atmospheres (1984–2012), 95(D3), 1999-2009.

ii.   Gupta, V. K., & Waymire, E. C. (1993). A Statistical Analysis Of Mesoscale Rainfall As A Random Cascade. Journal Of Applied Meteorology, 32(2), 251-267.

iii.   Pandey, G. R. (1998). Assessment Of Scaling Behavior Of Regional Floods. Journal Of Hydrologic Engineering, 3(3), 169-173.

iv.   Kumar, P., Guttorp, P., & Foufoula-Georgiou, E. (1994). A Probability-Weighted Moment Test To Assess Simple Scaling. Stochastic Hydrology And Hydraulics,8(3), 173-183.

v.   Yu, P. S., Yang, T. C., & Lin, C. S. (2004). Regional Rainfall Intensity Formulas Based On Scaling Property Of Rainfall. Journal Of Hydrology, 295(1), 108-123.

vi.   Sivakumar, B. (2000). Fractal Analysis Of Rainfall Observed In Two Different Climatic Regions. Hydrological Sciences Journal, 45(5), 727-738.

vii.   Veneziano, D., & Langousis, A. (2010). Scaling And Fractals In Hydrology.Advances In Data-Based Approaches For Hydrologic Modeling And Forecasting. World Scientific, Singapore.

viii.   Greenwood, Landwehr, J.M., Matalas, N.C., & Wallis, J.R., (1979). Probability weighted moments: definition and relation to parameters of several distributions expressible in inverse form.Water Resour. Res. 15(5), 1049–1054.

Prediction Of Streamflow At Ungauged Sites In Mahanadi River Basin Using Regional Flow Duration Curves

Nruthya. K[1]   V. V. Srinivas [2]

[1] Research Scholar, Dept. of Civil Engineering, Indian Institute of Science, Bangalore-560 012, India.

[2]Associate Professor, Dept. of Civil Engineering, Indian Institute of Science, Bangalore-560 012, India.

Email: nruthya.kishore@gmail.com, vvs@civil.iisc.ernet.in

ABSTRACT: *Accurate information on streamflows is of prime importance for planning as well as monitoring of water resources schemes related to hydro power, water supply, irrigation, flood control, maintaining ecosystem. Engineers encounter challenges when streamflow data are either unavailable or inadequate at target locations. To address these challenges, there have been efforts to develop methodologies that facilitate prediction of streamflow at ungauged sites. Conventionally, time intensive and data exhaustive rainfall-runoff models are used to arrive at streamflow at ungauged sites. Most recent studies show improved methods based on regionalization using Flow Duration Curves (FDCs). A FDC is a graphical representation of streamflow variability, which is constructed as a plot between flow values and their corresponding exceedance probabilities that are determined using a plotting position formula. It provides information on the percentage of time any specified magnitude of streamflow is equaled or exceeded. The present study assesses the effectiveness of a method, which uses FDC to predict streamflow, by application to catchments in Mahanadi river basin, India. The method involves (i) development of regression relationships between chosen quantiles (percentile flows) and attributes of catchments in the study area, (ii) use of the relationships to construct regional FDC for the ungauged site, and (iii) use of a sequential generation technique to decode information in FDC to construct streamflow time series for the ungauged site. Attributes that have been considered for the analysis include variables representing hydrology, climatology, topography, land-use/land-cover and soil of catchments in the study area. Effectiveness of the presented methodology is assessed using leave-one-out cross validation. Results indicate that the method performs fairly well.*

Keywords: Flow duration curve, sequential generation technique, Mahanadi river basin

1. INTRODUCTION

Long term streamflow records are necessary for various locations in river basins for use in design of water resources projects and for water management. Most often data are either unavailable or inadequate at sites considered for planning water resources projects. A simple method to predict streamflow is area ratio method proposed by Stedinger et al. (1993), which may not be always effective. Conventionally

rainfall-runoff models are used to predict streamflow at ungauged sites. They need extensive data and are time intensive. Recent studies propose use of improved methods for streamflow prediction based on regional Flow Duration Curves (FDCs). A FDC is a graphical representation of streamflow variability at a site without time sequence component, as it is constructed as a plot between flow values and their corresponding exceedance probabilities. Information on time sequence is necessary to predict time series of streamflow from FDC for a site. Hughes and Smakhtin (1996), Mohamoud (2008) and Shu et al. (2012) have developed procedures to predict streamflow time series at ungauged sites using FDCs. Those procedures involve prediction of FDCs at target (ungauged) site and use of it as the basis to construct streamflow time series. Castellarin et al. (2004) provides a review of procedures for predicting FDCs at target (ungauged) site, which use information transferred from gauged sites in the study area. The present study assesses effectiveness of a FDC based method proposed by Mohamoud (2008) for predicting streamflow at ungauged locations in Mahanadi river basin, India.

2. METHODOLOGY

2.1. Construction of flow duration curves at gauged sites

Flow duration curves can be constructed non-parametrically using streamflow records (data) corresponding to different time scales (e.g., daily, weekly, monthly). Conventional practice for construction involves (i) arranging the data in descending order, (ii) ranking the data, (iii) identifying plotting position (exceedance probability) corresponding to each data point using Weibull plotting position (WPP) formula, and (iv) plotting data as points in two-dimensional space of flow magnitude and exceedance probability and joining them by a smooth curve. Exceedance probability (P) is estimated using WPP as,

$$P\left(X \geq x_m\right) = \frac{m}{n+1}$$

(1)

Where X is the random variable being analyzed, x_m is the data point corresponding to rank m, and n is the total number of data points. The streamflow values corresponding to various exceedance probabilities constitute quantiles.

2.2. Construction of flow duration curves at ungauged sites using regression relationships

Flow duration curves can be constructed for an ungauged site by substituting attributes corresponding to catchment of the ungauged site in regression relationships developed between streamflow quantiles and catchment attributes corresponding to all the gauged sites in the study area. In this study fifteen regression relationships were developed, each corresponding to

one of the 15 fixed percentage points (P=0.001, 0.005, 0.01, 0.05, 0.1, 0.2, 0.3, 0.4, 0.5, 0.6, 0.7, 0.8, 0.9, 0.95, and 0.99).

To develop regression relationship corresponding to a quantile, irredundant catchment related attributes that are reasonably well correlated with the quantile were identified. Following this, a best subset regression analysis was performed to identify potential catchment related attributes for developing regression relation to estimate the quantile. The relationship appears as,

$$X = a \times Y_1^{b} \times Y_2^{c} \times Y_3^{d} ...,$$

(2)

Where, $Y_1, Y_2, Y_3...$ are the potential attributes and X denotes quantile; $a, b, c, d...$ are the model parameters. The above equation is logarithmically transformed to equation (3) so that the standard multiple variable linear regression technique can be applied.

$$\ln X = \ln a + b \ln Y_1 + c \ln Y_2 + d \ln Y_3 ...,$$

(3)

Regression relationships thus developed corresponding to each of the 15 percentage points (exceedance probabilities) yield corresponding quantile estimates. As the number of percentage points (15) is limited, there is a need to interpolate quantile estimates at points in between the 15 percentage points. Mohamoud (2008) suggested use of sequential generation technique to interpolate estimates.

The data length at the site gives the number of ranked percentile flows to be considered, out of which 15 are predicted quantiles. The sequential generation for any segment is given by

$$x_{r_{k+1}} = x_{r_k} - \frac{X_{r_k} - X_{r_n}}{r_n - r_k}$$

(4)

Where, $x_{r_{k+1}}$ is the first sequentially estimated unknown percentile flow within the segment, X_{r_k} is the known percentile flow at the upper end of the segment starting point, X_{r_n} is a known percentage flow at the lower end of the segment end point, and r_k and r_n are their respective ranks. $x_{r_k} = X_{r_k}$ when calculating the first unknown percentile flow within each segment and the ratio $\frac{X_{r_k} - X_{r_n}}{r_n - r_k}$ is constant within each segment. This technique iteratively estimates the next percentile flow using the percentile flow estimated in the previous step. This technique is repeated at all other segments to arrive at the complete flow duration curve at the ungauged site.

2.3. Construction of streamflow time series at ungauged sites

The complete streamflow time series is constructed at the ungauged site using the complete FDC generated at the ungauged site. This is accomplished by restructuring the predicted FDC values using streamflow time sequence from a neighboring gauged site. The neighboring gauging site is considered to be the source site and the ungauged site as the destination site. Hughes and Smakhtin (1996) suggested that the source site can either be the nearest site in the same river, its tributaries or site in the adjacent streams. The catchments are assumed to be receiving similar precipitation and having similar streamflow generating mechanism. Thus ascertaining that if there are high flows at source site, there will be high flows at destination site and vice versa. The restructuring procedure sorts the predicted FDC and the streamflow time series from the source site by magnitude. Both source and destination sites have date and magnitude columns sorted in magnitude order. The predicted FDC magnitude column is copied to the magnitude column of the streamflow time series column of the source site without disturbing the date column. Once copied, the two columns are re-sorted, using the date column. This results in time series of the predicted streamflow at the ungauged site (Mohamoud, 2008).

2.4. Evaluation method

To test effectiveness of method in predicting FDCs at ungauged sites, leave one out cross-validation experiment was performed. One site at a time was considered to be pseudo ungauged and information corresponding to remaining gauged sites in the study area was utilized to develop regression relationships between flow quantiles and catchment related attributes. Quantiles corresponding to the ungauged site were predicted by substituting attributes corresponding to catchment of the ungauged site in the developed regression relationships. The predicted quantiles are compared with true quantiles corresponding to the pseudo ungauged site (estimated using observed data), and the error was quantified in terms of four performance measures: Nash Sutcliffe error (NSE), Relative-bias (R-bias) and Relative Root Mean Square Error (RRMSE) and Coefficient of Determination (R^2).

$$NSE = 1 - \frac{\sum_{i=1}^{N}(O_i - P_i)^2}{\sum_{i=1}^{N}(O_i - \bar{O})^2}$$

(5)

$$R\text{-bias} = \frac{1}{N}\sum_{i=1}^{N}\left(\frac{O_i - P_i}{O_i}\right) \times 100$$

(6)

$$R\text{-RMSE} = \sqrt{\frac{1}{N}\sum_{i=1}^{N}\left(\frac{O_i - P_i}{O_i}\right)^2} \times 100$$

(7)

$$R^2 = \frac{\left[\sum_{i=1}^{N}(O_i - \bar{O})(P_i - \bar{P})\right]^2}{\sum_{i=1}^{N}(O_i - \bar{O})^2 \sum_{i=1}^{N}(P_i - \bar{P})^2}$$

(8)

Where O_i and P_i are the observed and predicted values; $\bar{O}$ and $\bar{P}$ are observed and predicted mean; N is the data length. Optimal performance corresponds to NSE=1, R-bias=0, RRMSE=0 and R^2=1.

3. CASE STUDY

Effectiveness of the methodology presented in section 2 in predicting FDC and streamflow time series for ungauged sites is evaluated by application to data pertaining to catchments of 17 gauges in Mahanadi river basin, India (Fig. 1). Locations of the gauges that are part of the network of Central Water Commission (CWC), India, are shown in Fig. 1. The river basin extends over 1,41,600 km² area, which is bounded in the North by Central India hills, in the South and East by the Eastern Ghats and in the West by Maikala hill range. Significant part of the basin is in Chhattisgarh and Orissa states, and some part of it lies in Madhya Pradesh, Jharkhand and Maharashtra states. Except for a dam (Hirakud) located in lower reaches of the basin, flows in rest of the basin are largely uncontrolled. The basin receives a significant part of its annual rainfall from south-west monsoon that extends over the period June-September.

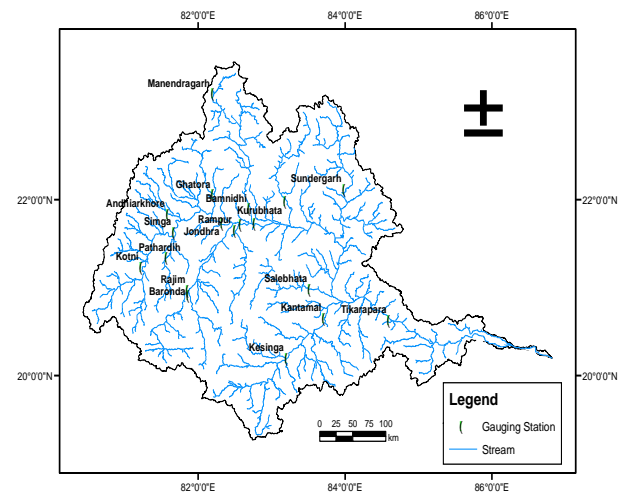**Fig 1.** Study area and location of gauges

For use in the analysis, daily streamflow records corresponding to the 17 gauges were available from CWC for the period 1971 to 2010. Further, daily gridded rainfall data over the period 1971 to 2005 were available for the study area at 0.25^o resolution from Pai et al. (2014). Daily temperature data over a period 1901 to 2009 were available at 0.5^o resolution from

Harris et al. (2014). Morphological characteristics of the catchments were determined by processing Shuttle Radar Topography Mission (SRTM) Digital Elevation Model (DEM) data having 90m spatial resolution in ArcGIS framework.

An inventory of 33 catchment characteristics was prepared. The characteristics related to geomorphology, climate, soil and Land Use Land Cover (LULC) of catchments in Mahanadi basin. They include catchment area (sq km), length of main channel (km), compactness coefficient, drainage density (km/km^2), stream frequency (/km^2), circularity ratio, elongation ratio, form factor, total stream length (km), minimum elevation (m), maximum elevation (m), mean elevation (m), median elevation (m), mean slope(%), main channel slope (%), difference between mean and minimum elevation (m), relief (m), perimeter (km), number of streams, elevation of highest point of catchment divide, elevation of outlet, length of the longest channel (basin length)(km), mean annual precipitation (mm), maximum temperature ($^\circ$ C), minimum temperature ($^\circ$ C) , hydraulic conductivity (cm/hr), built up area (%), agriculture land (%), forest land (%), grassland area (%), water body (%). Latitude and longitude of catchment centroid were also considered as attributes, because geographically nearby catchments could exhibit similar flow response due to similarities in the causative precipitation events.

For each of the 17 catchments, flow quantiles corresponding to 15 exceedance probabilities (*P*=0.001, 0.005, 0.01, 0.05, 0.1, 0.2, 0.3, 0.4, 0.5, 0.6, 0.7, 0.8, 0.9, 0.95, and 0.99) were computed using WPP formula (equation (1)). The FDCs constructed for the catchments are shown in Fig. 2.
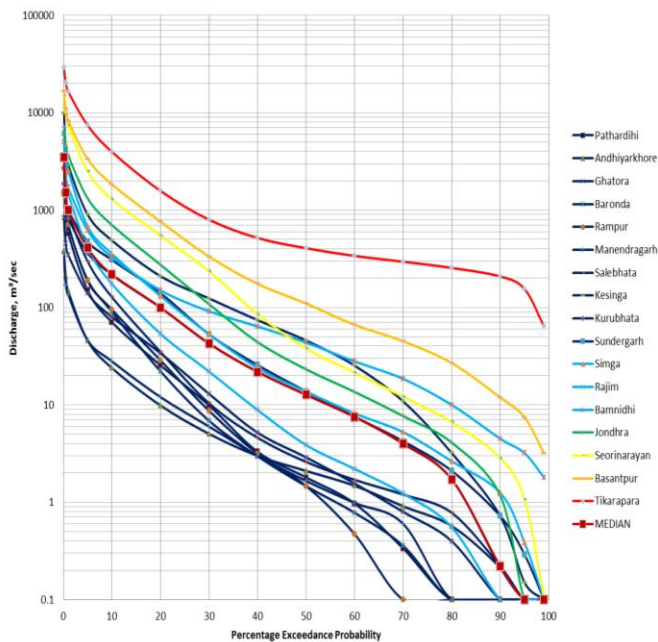

Fig 2. FDCs for gauges considered in Mahanadi basin. Median FDC across sub-catchments is show as 'Median'

Flow quantiles corresponding to ungauged sites are predicted using regression based method as discussed in the foregoing section. For the analysis, catchment characteristics that were irredundant among themselves, but significantly correlated with the individual flow quantiles were determined, and referred to as attributes (predictors). The identified attributes were catchment area (CA), latitude (Lat), built up area (BA), grassland area (GA), elongation ratio (ER), minimum elevation (Min E), median elevation (Med E), elevation difference (E Diff) and relief. Regression relationship for each flow quantile is a distinct association of the most influential combination of attributes with the representative quantile as shown in Table.2.

The method was calibrated utilizing data corresponding to all the 17 sites. Following this, the method was validated by performing leave one out cross-validation experiment. One site at a time was considered to be ungauged and FDC corresponding to that site was then determined using regression relationships as described in section 2.4. Performance of the method in both calibration (Cal) and validation (Val) was examined based in results presented in Table 1.

The presented methodology was applied to predict streamflows at pseudo ungauged sites in the Mahanadi basin.. The quantiles are predicted using the regression relationships developed using the information from the other 16 sites. The attributes considered and regression model parameters for various exceedance probabilities corresponding to the case where Sundergarh was considered to be pseudo ungauged site are shown in Table.2. The comparison of the observed and estimated FDC is made in Fig.3.

Table 1. Performance of regression based method in predicting quantiles

| P (%)	NSE Cal	NSE Val	RRMSE Cal	RRMSE Val	R-BIAS Cal	R-BIAS Val	R-Square Cal	R-Square Val
0.1	0.948	0.898	46.480	57.254	-7.302	-10.002	0.979	0.968
0.5	0.973	0.941	35.038	42.745	-4.315	-6.178	0.992	0.986
1	0.987	0.972	33.444	40.861	-3.757	-5.033	0.995	0.992
5	0.992	0.987	33.828	45.106	-4.280	-7.790	0.996	0.995
10	0.992	0.988	37.039	49.546	-5.305	-9.950	0.994	0.992
20	0.984	0.963	28.447	39.170	-3.725	-6.404	0.991	0.985
30	0.991	0.986	29.827	43.764	-4.148	-7.751	0.991	0.987
40	0.980	0.965	48.652	66.932	-9.006	-12.698	0.984	0.977
50	0.966	0.935	58.337	78.771	-12.560	-17.073	0.985	0.975
60	0.821	0.605	52.606	71.393	-11.565	-13.727	0.968	0.875
70	0.747	0.483	69.015	105.126	-15.808	-23.977	0.971	0.857
80	0.913	0.469	60.089	76.897	-14.686	-14.768	0.997	0.914
90	0.780	0.192	80.960	119.085	-21.529	-32.399	0.998	0.932
95	0.682	0.014	131.511	208.970	-47.166	-83.064	0.998	0.799
99	0.557	-0.043	173.999	341.563	-60.122	-122.476	0.998	0.229
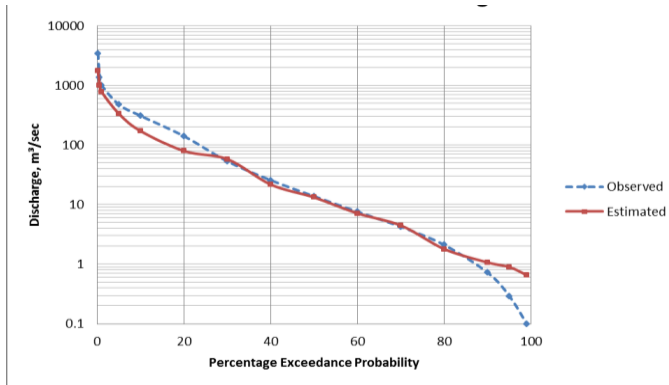
Fig 3. Comparison of observed and estimated FDC for Sundergarh site

Table 2. Regression models and their parameters corresponding to Sundergarh site

P (%)	Attributes			Model parameters				
				a	b	c	d	e
0.1	CA	Lat		28.691	0.793	-9.014		
0.5	CA	Lat		18.610	0.907	-6.276		
1	CA	Lat		12.867	0.945	-4.628		
5	CA	BA		-3.842	1.071	-0.089		
10	CA	BA		-4.456	1.070	-0.079		
20	CA	Med E	GA	-8.372	1.109	0.497	0.034	
30	CA	Med E	GA	-13.012	1.171	1.092	0.129	
40	CA	E Diff	GA	-10.640	1.096	0.665	0.383	
50	CA	E Diff	GA	-11.783	1.115	0.735	0.460	
60	CA	ER	E Diff	BA	-15.126	1.121	-1.113	1.427	0.439
70	CA	ER	E Diff	BA	-18.081	1.185	-1.205	1.826	0.549
80	CA	ER	E Diff	BA	-21.079	1.434	-2.262	1.682	0.573
90	CA	Min E	Med E	BA	-16.217	1.063	-3.253	4.247	0.434
95	CA	Min E	Med E	Relief	-10.210	1.072	-4.543	5.552	-1.322
99	CA	Min E	Med E	Relief	-3.990	0.609	-4.834	5.133	-1.079

The intermediate quantiles are estimated by sequential generation of values, as mentioned in section 2.3. Kurubhata is used as the source site to reconstruct time series for Sundergarh the destination site. Kurubhata was chosen as the source site, as it is geographical neighbour to the destination site. The time sequence component along with magnitude of flows for the source site and the predicted flow magnitude sequence (using FDC) for the destination site were used to reconstruct the time series for Sundergarh. The comparison of observed and predicted time series in represented in Fig.4. The figure indicates that the method performs fairly well in capturing the

flow pattern and variability. Extreme flow values were however not predicted satisfactorily. Error in predicting flood corresponding to the year 1997 was quite significant, as the flow magnitude (7000m³/sec) was exceptionally large. Inability to model such extremes could be attributed to inadequate number of predictor-quantile relationships corresponding to high exceedance probabilities.
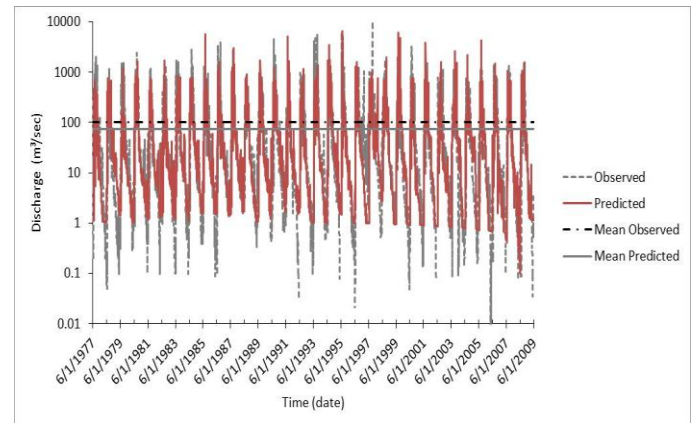

Fig 4. Observed and predicted time series comparison for site Sundergarh

4. SUMMARY AND CONCLUSIONS

Effectiveness of a FDC based method was evaluated in predicting streamflow at ungauged locations in Mahanadi river basin, India. Results indicated the method performs fairly well in capturing the flow pattern and variability. Extreme flow values were however not predicted satisfactorily. Further research is necessary on other river basins to strengthen the conclusions drawn based on the present study. Also, there is a need for developing effective methodologies for prediction of streamflows at ungauged sites.

REFERENCES:

i.   Castellarin A, G Galeati, L Brandimarte, A Montanari, and A Brath (2004a) Regional flow-duration curves: reliability for ungauged basins. Advances in Water Resources, 27(10), 953-965

ii.   Harris I, Jones P.D, Osborn, TJ and Lister DH (2014) Updated high-resolution grids of monthly climatic observations – the CRU TS3.10 Dataset. Int. J. Climatol, 34: 623–642

iii. Mohamoud Y M (2008) Prediction of Daily Flow Duration Curves and Streamflow for Ungauged Catchments Using Regional Flow Duration Curves. Hydrological Sciences Journal, 53(4), 706-724

iv.   Pai DS, Latha Sridhar, Rajeevan M, Sreejith OP, Satbhai NS and Mukhopadhyay B (2014): Development of a new high spatial resolution (0.25° X 0.25°)Long period (1901-2010) daily gridded rainfall data set over India and its comparison with existing data sets over the region. MAUSAM, 65, 1(January 2014), pp1-18

v.   Shu C, and TBMJ Ouarda (2012) Improved methods for daily streamflow estimates at ungauged sites, Water Resour. Res, 48, W02523

vi.Smakhtin VY, DA Hughes, and E Creuse-Naudin (1997) Regionalization of daily flow characteristics in part of the Eastern Cape, South Africa. Hydrological Sciences Journal,42(6), 919-936

vii.Stedinger JR, RM Vogel, and E Foufoula-Georgiou (1993) Frequency analysis of extreme events. In Handbook of Hydrology, edited by D. Maidment, pp. 18.1–18.66, McGraw-Hill, New York.

Snow and Glacier Melt Runoff Modeling At Tosh Watershed and Parbati Sub-Basin

R.J. Soni[1]   B.P. Rathore[2]   I.M. Bahuguna[2]   H.M. Patel[3]

[1]*P.G student, Department of Civil Engineering, The M.S. University of Baroda, Vadodara (390001), India*
[2]*Scientist, Space Applications Centre, Ahmedabad (380015), India*
[3]*Professor and Head, Dept. of Civil Engineering, The M.S. University of Baroda,Vadodara (390001), India*
Email*: ravijsoni@outlook.com*

ABSTRACT:*Snowmelt is not only a beneficiary source of water but also a calamitous source of water. Accurate estimation of the volume of water stored in the snowpack and its release is essential to predict the flow during the snowmelt period. Snow & glacier melt study has kindled a new hope to woo the usable water which is the lifeline of the living world. The gist of this study is to invent and develop a model for pragmatic purposes. Snow & glacier melt runoff modeling is carried out using remote sensing and GIS techniques. Computation of melt factor has been done by using reflectance images remotely. It can sense and show reflectance of snow and ice changes with their density. For making the model more potent, a great inventiveness and skill is applied and used to it. River catchments are distributed into small cells using grid to increase the efficiency of the model. For developing the model AWiFS data are used for the computation of the streamflow. Aster DEM to extrapolate temperature to each grid cell, NDSI images to estimate spatial and temporal distribution of snowcover extent and Reflectance images to compute melt factor are used. Using degree day method, the snow & glacier melt runoff model is developed at Tosh watershed and is validated at Parbati sub-basin. For simulating the model on 10-daly basis, satellite, meteorological and hydrological data are applied. The model shows the high workability efficiency on the both basins while considering its simulation periods.*
Key words: Snow, Glacier, Modeling, Toshwatershed, Parbati sub-basin, Streamflow, 10-Daily.

1.   INTRODUCTION:

Only 1% of the world's water is usable to us. About 97% is salty sea water and 2%is frozen in snow and glaciers and polar ice caps. As 1% is insufficient to overcome the causes of water scarcity which vary from natural causes such as climate change and draught to human causes such as demand over stripping supply, population growth, water quality and   resource allocation.So studies on mountain glaciers and snow are welcomed.The pious peaks of the Himalayas are known as the water towers of Asia providing drops of elixir to quench the parched plains and to satisfy the scorching throats of the living world. They store a significant quantity of fresh water which is found in the concentrated form of seasonal snow cover and glaciers outside the polar realm. Indeed, they have the capacity for supplying 86,000,000 cubic meters of water annually to Asia's seven great rivers.Western Himalayan Riverscombine into the Indus Basin, of which the Indus River is the largest. The Indus begins in Tibet at the confluence of Sengge and Gar river and flows southwest through India and then through Pakistan to the Arabian Sea. It is fed by the Jhelum, the Chenab, the Ravi, the Beas and the Sutlej River, among others.In western Himalayas,the temperature is lesser due to higher altitude as well as latitude and as a consequence the snowline in the western Himalaya is at a lower altitude than the eastern Himalaya. As distance from the sea is greater, both annual and diurnal range of temperature is greater in the western Himalayas. So it receives lesser precipitation than eastern Himalayas Anil Bose et al(2013). As in western Himalayas, the snowmelt commences in March, the snow line starts receding upwards and by the end of June to an altitude of 4,500m Vajja Hari Prasad, et al. (2006). Changes in climate have drastic repercussions on the entire earth and have affected more dramatically on the Himalayan glaciers. These glaciers are more susceptible to climate changedue to their latitudinal and altitudinal position and other interrelated processes. These processes need detailed multidisciplinary investigations and have opened a new venue for estimating the runoff with the help of different models. These models require the fundamental variables which directly affect the melt process.

For snowmelt runoff modeling, the two pragmatic approaches are accessible. They are energy balance approach and degree-day method. In comparison to the energy balance approach, degree day approach is more practicable and needs minimum parameters for simulating snow & glacier melt runoff. It is widely used due to its being less complicated. The energy exchange at snowpack surface can be explained by four major components. They are shortwave radiation exchange and heat exchange, convective heat transfer and adventive heat transfer. These radiations exchange and heat transfer can be estimated if information on various parameters as cloud covers, albedo, wind, cloud temperature and dew point temperature are known Anderson et al. (1976). Information on these parameters is normally not available; therefore, degree-day approach is used for operational forecasting Quick et al.(1988).Precipitation and temperature are the major factors for generating runoff in mountainous regions which are covered with snow and glaciers. Precipitation falls either in the form of liquid (rain) at lower latitude and altitude or in the form of solid (snow) at higher latitude and altitude. When rainfall occurs, runoff is estimated by subtracting various types of water losses. In case of snow fall, snow remains static for quite sometime and it requires certain amount of temperature to convert it into liquid and then to set the process of runoff.

2. DEVELOPMENT OF THE SNOW AND GLACIER MELT RUNOFF MODEL:

Model is designed to simulate and forecast streamflow in mountain basins where snowmelt is a major runoff factor. To develop the model different remote sensing and GIS techniques are used. Catchments are distributed using grid.Model works on NDSI to estimate snow cover and on reflectance to estimate melt factor.From time to time, runoff generated from snow and glacier melt and also from rainfall is computed using the following equation, inspired from Martinec et al. (1975):

$$Q = \sum_{i=1}^{n} \{ C_1\{a(T*G)\} + C_2(P*B) + C_3\{a(T*S)\}\} * \frac{10000}{86400}(1-K) + Q_{last}*K \quad (1)$$

Where, Q = Average 10-Daily runoff (m^3/s), C_1 = Runoff coefficient for glaciated areas, C_2 = Runoff coefficient for non-snow and non-glaciated areas, C_3 = Runoff coefficient for seasonal snow covered areas, a = Melt-factor (cm °C^{-1} d^{-1}), T =Average 10-daily degree days (°C. d), G = Grid cell area of glaciers, permanent and 10-daily snow (km^2), S = Grid cell area of 10-daily snow (km^2), P = Average 10-daily rainfall (cm), B = Grid cell area without snow/glacial cover (km^2), Factor 10000/86400 is required for conversion of units from cmkm^{2}d^{-1} tom^{3}s^{-1}, K= recession coefficient, Q$_{last}$= last average 10-daily discharge, n= No of cells.

3. STUDY AREA AND GRID DISCRETIZATION:

The Himalayas "abode of the snow" is a mountain range in Asia separating the Plains of the Indian subcontinent from the Tibetan plateau. It encompasses about 15,000 glaciers, which store about 12,000 km3 (3000 cubic miles) of fresh water. Himachal Pradesh has prospered and flourished in the lap of Himalayas. The perennial rivers are worthy of growth and development of Himachal Pradesh. All the devotional effort for growth goes to two reverent rivers-Parbati and Beas.

Figure 1.
Parbati sub-basinand Tosh watershed, Himachal Pradesh

Parbati River is in the Parbati valley in Himachal Pradesh, Northern India that flows into the Beas River at Bhuntar, some 10 km south of Kullu. It rises from the Man Talai glacier below the Pin Parbati and flows in a gradual curve from north-northwest to west-southwest past the important temple town of Manikaran. Parbati sub-basin is situated in the western Himalayan region. It is also a part of Sutluj basin. Throughout the year, a part of this basin is covered with snow and glaciers. It is continuously fed by melting of high altitude snowfields and glaciers. Indeed, this basin is sub divided in to various watersheds. Tosh watershed is one of the significant and substantial watersheds of Parbati sub-basin. As being part and participle of Parbati sub-basin and having the same features and characteristics, it represents the similar hydrologic processes as that of the whole Parbati sub-basin. In short, it is the representative of Parbati sub-basin.Figure 1 shows the study area and river network of Parbati sub-basin and Tosh watershed with their latitude and longitude. Parbati sub-basin covers the area of 1773 km^2. Elevation range of this catchment is 1110 m to 6597 m. Tosh watershed covers the area of 329 km^{2}which is a part of Parbati sub-basin.Tosh watershed is situated at higher elevation.
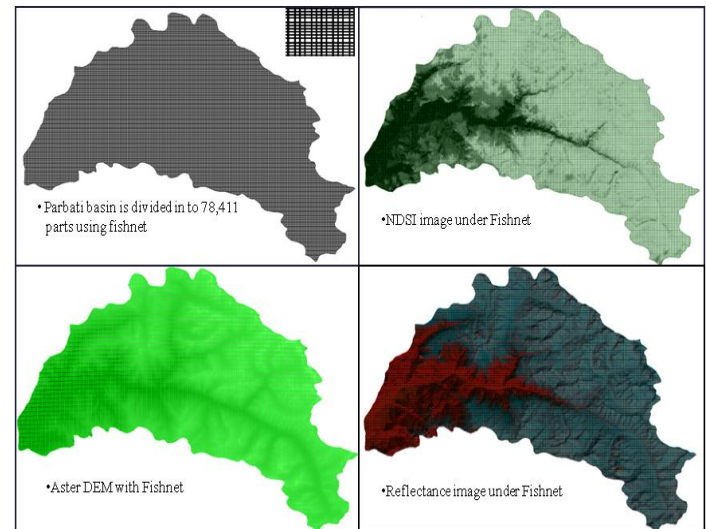
Figure 2. Distribution of the Parbati sub-basin

The main aim of this study is to distribute area, NDSI, reflectance and DEM of the basin. Using ARC GIS 9.3, distribution of the Tosh watershed (329 Km^2) and Parbati sub-basin (1773 km^2) is done by fabricating a grid of the same size and laying it over the catchments. So consequently, the catchments are distributed into a number of small grid cells. In this way, the Tosh watershed and Parbati sub-basin are divided respectively in to 90,236 and 78,411 cells. For Tosh watershed, the area of cells 0.0046 km^2 while for the Parbati sub-basin is 0.0228 Km^2. So it can be said that for Tosh watershed area of cell is smaller than the AWiFS resolution andfor Parbati sub-basin area of cell is equal to3- pixel resolution of the AWiFS. Figure 2 shows distribution of Parbati sub-basin.

4. DATA USED:

4.1 Satellite data:

The Advanced Wide Field Sensor (AWiFS) data have been used for this study. It provides a spatial resolution of 56 m and covering a swath of 740 Km. to cover this wide swath, the AWIFS camera is split into two separate electrooptic modules, AWiFS-A and AWiFS-B. Because of its large swath the repetivity of the AWiFS is 5 days. These data are imported from NRSC (National Remote Sensing Centre), H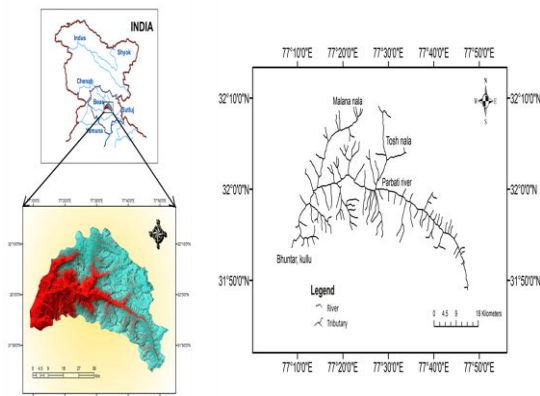yderabad. Reflectance, NDSI images are generated using NDSI algorithmKulkarni et al. (2006). Advanced Space born Thermal emission and Reflection radiometer (ASTER) sensor is one of the five remote sensory devices on board the Terra satellite launched into the Earth's orbit by NASA in 1999. ASTER GDEM (Global Digital Elevation Model) is the global DEM created using ASTER.

4.2 Meteorological data:

Surface variables like precipitation and temperature are to be highlighted for estimation of runoff in snow & glacier covered area. Indeed precipitation is said to be any product of the condensation of atmospheric water vapour that falls under gravity while the changes in air temperature in the atmosphere which take place due to dynamic processes should both be taken in to account. These significant parameters which have high contribution in snow & glacier melt runoff have been taken from Bhuntar, Kullu District of Himachal Pradesh for this present study. For clarity, maximum and minimum air temperatures and precipitation data from 2004-2005 available in daily format are converted in to 10-daily format specifically for utilizing and for fulfilling the requirementsof the model.

4.3 Hydrological data:

For the calibration period of the model at Tosh watershed, the discharge data are collected from the U/s of the confluence of both Tosh Nala and Parbati River. For the validation period of the model at Parbati sub-basin, the discharge data are collected from the D/s of the Parbati sub-basin near the dam site. These places are the focal and centric points where total discharge is collected from both the catchments.

5. MODEL PARAMETERS:

5.1 Temperature:

Daily maximum and minimum temperature dataare used from 2004-2005. From the available maximum and minimum daily temperature data, average daily temperature data are calculated and finally converted in to 10-daily format.Then they are extrapolated to each cell of the grid by overlaying it on Aster DEM using temperature lapse rate Martinec et al, (1975).

5.2 Snow cover area and Precipitation:

Model itself estimates snow cover area using NDSI. Catchmentsare distributed in to small cells and each cell has its own NDSI value. Principally, NDSI value varies from -1 to 1. The value $>= 0.4$ indicates snow cover area (SCA) while the value < 0.4 indicates snow free area (SFA)Model has capacity to sense whether the cell area is under snow cover or snow free area as shown in table. It takes the threshold values of NDSI that means model senses all the grid cell area which has NDSI value greater than or equal to 0.4, considering as snow cover area Kulkarni et al.(2006).

Available precipitation data of Bhuntar meteorological station are extrapolated to the mean hypsometric altitudes of the respective grid cell. There are two forms of precipitation: Rain and Snowfall. Critical temperature (T_{crit}) determines whether the measured precipitation is either rain or snow. Model gives an output from each grid cell whether it is snowmelt-runoff, rainfall-runoff or the mixture of both. This model output is dependent on critical temperature, occurrence of an event (rain fall/snowfall) and whether it is SCA or SFA.

5.3 Melt factor:

Model computes both reflectance based melt factor and field based melt factor (using degree-days). In this study, the melt factor parameter is calculated by model itself by using reflectance value of each cell. Reflectance changes with the changes in density of snow/glacier (Reflectance decreases with increment in density of snow/glacier). The threshold values of reflectance are adjusted with the density of new snow, damp snow, settled snow, depth hoar, wind packed snow, very wet snow and firn and glacier ice. Using below empirical equation Martinec et al(1975), melt factor is computed of all cells:

$$a = 1.1 * \frac{(density\ of\ snow)}{(density\ of\ water)} \quad (2)$$

5.4 Runoff coefficients:

Runoff coefficient shows difference between the available water volume (snowmelt + rainfall) and the outflow from the basin.Runoff coefficient of rainindicates the percentage of rainfall converted to runoff. It is found 0 to 0.72forTosh watershed and 0 to 0.84for Parbati sub-basin. Runoff coefficients of snow/glacier indicate the percentage of snowfall converted to runoff.These coefficients are found 0.21 to 0.78for Tosh watershed and they are 0.13 to 0.69for Parbati sub-basin. These coefficients have been calibrated using observed runoff on a 10-dailybasis.

5.5 Recession coefficient:

Recession coefficient indicates the fraction of discharge contribution from last day's discharge of snowmelt on a current day. In this study, observed daily discharges are plotted on log-log scale and the slope of the best fit line is determined as the recession coefficient. It is calibrated on 10-daily basis. It varies

from 0.73 to 1 for Tosh watershed and 0.64 to 1 for Parbati sub-basin.

6. RESULTS AND DISCUSSIONS:

Model is developed at the Tosh watershed and executed at Parbati sub-basin for 2004-2005. After applying the model at the Tosh watershed, training of the model is done using the available field data for calibration. The best match simulation is adopted. After this procedure, model is executed at Parbati sub-basin. Model is developed and validated on the 10-daily basis using degree day approach.
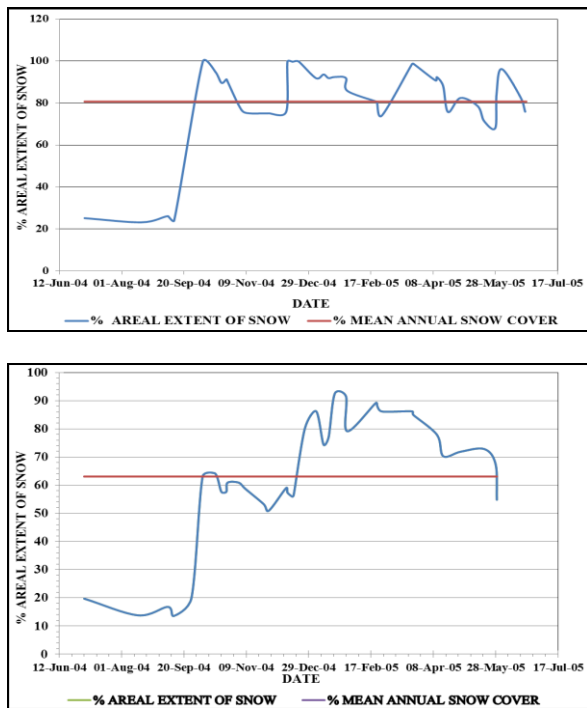
6.1 Snow cover area:

Figure 3. Areal extent of snow of Tosh watershed and Parbati sub-basin, 2004-2005

Table 1. Snow cover pattern for year 2004-2005

No	Catchment	Minimum SCA (%)	Maximum SCA (%)	Annual mean SCA (%)
1	Tosh	23.16(17, Aug 04)	99.82(21, Dec 04)	80.25
2	Parbati	13.56(12, Sep 04)	92.53 (19, Jan 05)	63.06

From thetable 1, it can be inferred that the snow cover in the Tosh watershed and Parbati sub-basin is maximum in winter while it is minimum in monsoon on the 10-daily basis using AWifs data.Geographically, Tosh watershed is situated at

higher elevation so in winter it is found that this watershed area is almost covered with snow. As some part of Parbati sub-basin is situated at lower elevation so in winter onlythis lower elevated part is found without snow. For Tosh watershed and Parbati sub-basinmaximum snow cover areas are respectively found 99.82% and 92.53%. Minimum snow cover for both Tosh watershed and Parbati sub-basin are respectively: 23.16% and 13.56%.Mean annual snow cover for both Tosh watershed and Parbatisub-basin are: 80.25 % and 63.06 % respectively.

6.2 Efficiency of the model:

Efficiency of model is derived by computing coefficient of determination (R^2) and (%) volume difference (D_v) using below equations Martinec et al.(1975):

$$R^2 = 1 - \frac{\sum_{i=1}^{n}(Q_i - Q')^2}{\sum_{i=1}^{n}(Q_i - \bar{Q})^2}$$

(3)

$$Dv\ (\%) = \frac{V_R - V_R'}{V_R} * 100$$

(4)

Where, R^2 = Coefficient of determination, Q_i = Measured 10-daily discharge, Q'_i = Simulated 10-daily discharge, $\bar{Q}$ = Average daily discharge for the simulation year or simulation season, n = Number of 10-daily discharge values, D_V= (%) Volume Difference between the total observedand simulated runoff, V_R = Observed 10- daily runoff volume,V_R'= Simulated 10-daily runoff volume.
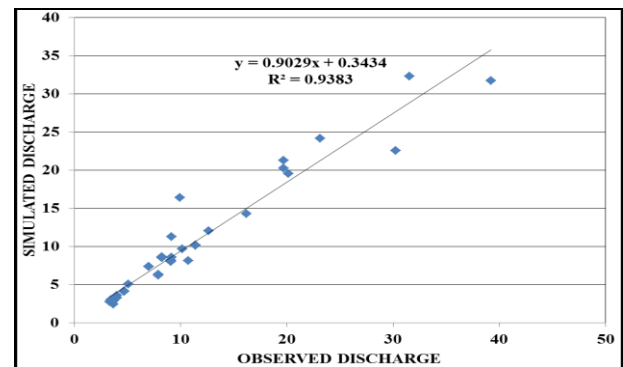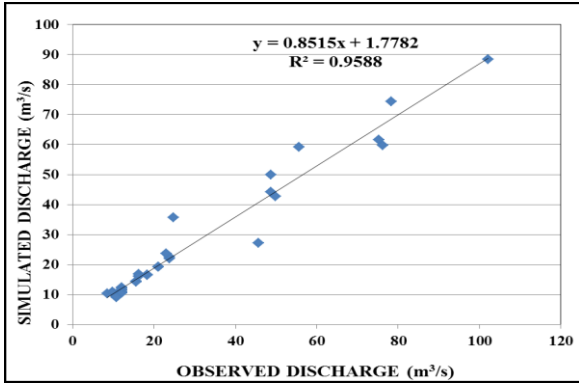
Figure 4. Coefficient of regression for Tosh watershed and Parbati sub-basin

Figure 5. Comparisons of simulated and observed discharge for Tosh watershed and Parbati sub-basin

Figure 5 shows coefficient of regression and comparison between observed and simulated discharge for both the catchments. It also shows that except monsoon, best match is found between observed and simulated discharge.

Table 2. Accuracy criteria of model

Catchment	Year	Coefficient ofdetermination (R^2)	Volume difference (D_v) (%)	Coefficient of regression (Graph)
Tosh watershed	2004-05	0.91	8.82	0.938
Parbati sub-basin	2004-05	0.92	5.44	0.958

The table 2 and figure 4 comprehensively show that forTosh watershed, co-efficient of determination (R^2) is derived 0.91, Volume difference (D_v) is derived 8.82%, and coefficient of regression from graph is derived 0.938. For Parbati sub-basin, co-efficient of determination (R^2) is derived 0.92, Volume difference (D_v) is derived 5.44%, and coefficient of regression from graph is derived 0.93.

7.   CONCLUSION:

Snow and glacier melt runoff modeling at Tosh watershed and Parbati sub-basin is done precisely integrating space based and in-situ data using degree-day method.Parameters such as melt factor, runoff coefficients and recession coefficient for the model are derived from satellite, topographic and hydro-meteorological data.

During winter, high elevated catchment, Tosh watershed is found to be almost covered with snow. As the Parbati basin's elevation range is high so some part of the sub-basin is found without snow. For both the catchments, the least snow cover is found in the season of monsoon. Temperature and precipitation are found major factors in contributing runoff.Temperature datasuggest that the winter season exists normally and the melt season starts from March and ends in June. Precipitation occurs normally in July, August, September and October. However, some isolated precipitation is also observed in other months as this study area is mountainous region.Runoff due to rain is noted high during monsoon while it is very low in winter. Runoff generated from snow and glaciers is noted high in summer and monsoon than winter and autumn.By using grid of smaller size cells, physical processes can be represented easily and the results are found to be accurate and reliable. Indirect way of estimating the melt factor using the threshold values of reflectance is found to be very successful and convenient in AWiFS satellite data as it calculates melt factor remotely.From the simulation results of both catchments, it is found that simulated discharges are fairly matching with the observed discharges. The coefficient of determinations, % volume differences and coefficient of regressions for Tosh watershed and Parbati sub-basin indicate that themodel is efficient and has high potential for application of snow and glacier prediction.
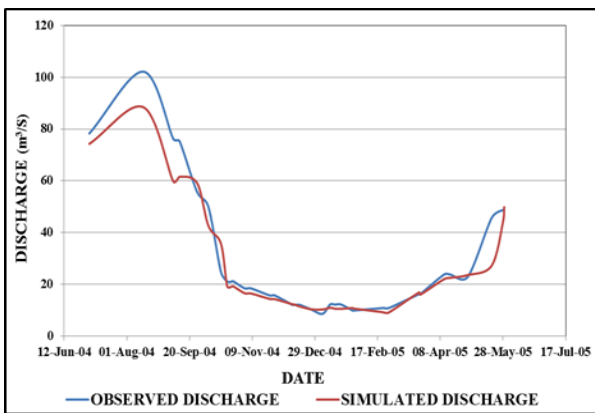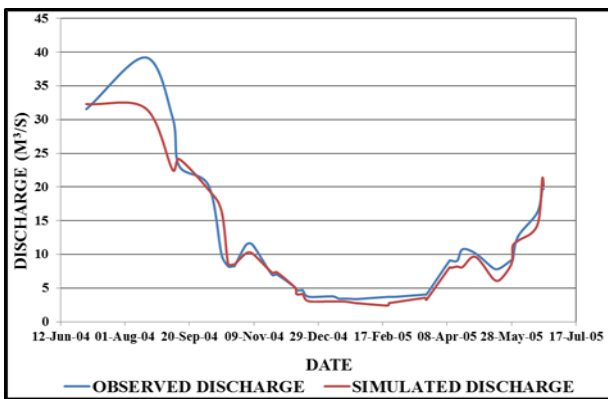
8.   REFERENCES:

i.   Aggarwal, S. P., Thakur, K. P., Nikam, B. R. and Garg, V. (2014) integrated approach for snowmelt runoff estimation using temperature index model. remote sensing and GIS. Current Science, 106 (3), 397-407.

ii.   Anderson, E.A (1976).National river Forecastsystem-snow accumulation and ablation model, NOAA Tech. Memo.NWS Hydro-17, US Dept. of Commerce,Silver Spring, USA.

iii.   Arora, M., Rathore, D.S. and Singh, R.D. (2010) Estimation of melt contribution to total streamflow in River Bhagirathi and River DhauliGanga at Loharinag Pala and Tapovan Vishnugad project sites. J. water Resources and protection, 2, 636-643.

iv.   Bose, A. (2013). Comparison of Eastern and Western Himalayas. Indian Geography, http://www.importantindia.com/4310/compare-western-and-eastern-himalayas/

v.   Harshburger, B. j., Walden, V. p., Humes, K.S, Moore, B.C., Blondford, T.R. and Rango, A. (2012) Generation of ansemble streamflow forecasts using an enhanced version of the snowmelt runoff model. Journal of American water resources Association, 48(4):643-655.

vi.   Kulkarni, A. V., Randhawa, S. S., Rathore, B. P., Bahuguna, I. M. and Sood R. K. (2002)Snow and Glacier Melt Runoff Model to Estimate Hydropower Potential, Journal of the Indian Society of Remote Sensing, 30(4):220-228.

vii.   Kulkarni, A. V., Singh S. k., Mathur, P. and Mishra, V. D. (2006) Algorithm to monitor snow cover using AWiFS dataof RESOURCESAT-1 for the Himalayan region, International Journal of Remote Sensing, 27(12):2449-2557.

viii.   Martinec, j. (1975) Snowmelt runoff model for stream flow forecast, Nordic Hydrology, 84, 197-219.

ix.   Prasad, V. H. and Roy, P. S. (2005) Estimation of Snowmelt Runoff in Beas Basin, India, Geocarto International, 20(2).

x.   Quick, M.C. and Pipes, A. (1988).High mountain snowmelt and application to runoff forecasting, Proc. of Workshopon Snow Hydrology, held atManali from Nov. 23-26,1988, ppIV1-32.

xi.   Singh, p, S.K and Kumar, N. (1997) Estimation of snow and glacier melt contributing to the Chenab River, western Himalaya, Mountain Research and development, 17(1):49-56.21.

Crop Water Assessment Of Plain And Hilly Region Using Modelling Techniques

Pritha Banik[1]   N.K. Tiwari[2]   Subodh Ranjan[3]

[1]Assistant Professor, Bharat Institute of Technology, Meerut-250103, India

[2]Associate Professor, National Institute of Technology, Kurukshetra-136119, India

[3]Professor, National Institute of Technology, Kurukshetra-136119, India

Email: rbrimibanik@gmail.com, [2]nand_nitk@rediffmail.com, [3]sranjan@nitkkr.ac.in

ABSTRACT : *This paper investigates the potential of meteorological data to model the crop water requirement of plain and hilly region using field data. CROPWAT model is used in this study which was developed by the FAO Land and Water Development Division. A dataset consisting of 2007 to 2011 each for maximum temperature, minimum temperature, relative humidity, sunshine hour, wind speed and rainfall taken from Central Soil Salinity Research Institute Karnal and Meteorological Centre, Dehradun for the plain and hilly region were used for this analysis. Besides, information on crop and soil were collected from different literature review. After putting all the input parameters it calculates reference evapotranspiration, crop evapotranspiration and irrigation requirement for the plain and hilly region. Although so many studies have been reported on Crop water assessment by CROPWAT model but every studies are very much conventional and conservative and no one has carried out a comparative studies in totality for crop of different seasons of varied topographical regions besides no comparative evaluation for Crop water assessment has been made between CROPWAT model and any other credible method. To achieve these objectives, comparison of crop water requirement is made between plain and hilly region for rice and wheat crop to meet the irrigation demand of crops for sustainable development of agriculture. Results were found that reference evapotranspiration of rice and wheat crop is more for the plain region as compared to the hilly region while crop evapotranspiration of rice crop is more for the hilly region as compared to plain region and for wheat crop it is more for the plain region as compared to the hilly region. Irrigation requirement of rice and wheat crop is more for the plain region as compared to the hilly region.*

Keywords: Reference evapotranspiration, crop evapotranspiration, irrigation requirement, CROPWAT model, meteorological data

1. INTRODUCTION

Since agriculture is the major user of water, improving agricultural water management is essential. Efficient agricultural water management requires reliable estimation of crop water requirement. Crop water requirements are normally expressed by the rate of evapotranspiration (ET) in mm/ day. The global consumption of water is doubling every 20 years, more than twice the rate of human population growth. A Food and Agriculture organization estimate puts that 70-80 per cent of the increase in food demand between 2000 and 2030 will have to be met by irrigation. Irrigated agriculture is practiced on about 300 million hectares only or 20 per cent of the cultivable area (Food and Agriculture Organization, 2010), but contributing substantially with more than 40 per cent of world's food production. Irrigation can reduce the risks associated with the unpredictable nature of rain fed agriculture in dry regions. Irrigated agriculture offers great potential for economic growth and poverty reduction. The measurement of ET from a crop surface is a very difficult and time consuming task. A large number of more or less empirical methods have been developed over the last 50 years by numerous scientists and specialists worldwide to estimate evapotranspiration from different climatic variables like Thornthwaite method, Hargreaves method, Turc method, Blaney Criddle method, Modified Penman method, Penman-Monteith method etc. To evaluate the performance of these methods under different climatological conditions, a major study was undertaken under the auspices of the Committee on Irrigation Water Requirements of the American Society of Civil Engineers (ASCE). They said that

these methods either underestimate or overestimate the evapotranspiration except Penman-Monteith method. They recommended the FAO Penman-Monteith method as the sole standard method for computation of evapotranspiration. India have different topographical region. It is necessary to know the crop water requirements for different regions to meet the irrigation demand and for sustainable development of agriculture. One of the major practices adopted by the researchers for water requirement of crops is modeling. For determination of crop evapotranspiration and yield responses to water, CROPWAT model is used which was developed by the FAO (Food and Agriculture Organization) Land and Water Development Division. Based on FAO Penman-Monteith method CROPWAT model has been developed. It requires some input meteorological parameter like maximum temperature, minimum temperature, relative humidity, sunshine hour, wind speed. After putting all the input parameters it calculates reference evapotranspiration, crop evapotranspiration and irrigation requirement for the plain and hilly region.

2. MATERIAL AND METHODS

In this study, CROPWAT model is selected for the computation of crop water requirement and irrigation requirement of plain and hilly region for rice and wheat crop. CROPWAT 8.0 can calculate reference evapotranspiration using only maximum and minimum temperature, sunshine hour, rainfall, relative humidity, wind speed etc. Researchers proposed several methods to determine evapotranspiration out of which the Penman-Monteith Method (FAO 1998) has been recommended as the appropriate combination method to determine the crop water requirements from climatic data on temperature, humidity, sunshine and wind speed.

The climate module is selected by clicking on the "Climate/ET$_o$" icon in the module bar located on the left of the main CROPWAT window. The data window opens with the default data type (monthly / decade / daily values); it is possible to quickly change to another data type by using the drop down menu from the "New" button on the toolbar. The module is primary for data input, requiring information on the meteorological station together with climatic data. After checking the data for possible errors, climate/ET$_o$ data is saved by selecting the "Save" button on the toolbar or the "File" > "Save" menu item.

The rain module is selected by clicking on the "Rain" icon in the module bar located on the left of the main CROPWAT window. The data window opens with the default data type (daily / decade / monthly values); it is possible to quickly change to another data type by using the drop down menu from the "New" button on the toolbar. Once the window is open with the suitable data type, rainfall data is typed and the input is checked. The rain module includes calculations producing effective rainfall. Rainfall data is saved after input of one set of

data is completed. To do so, "Save" button on the toolbar is selected or the "File" > "Save" menu item.

The crop module is selected by clicking on the "Crop" icon in the module bar located on the left of the main CROPWAT window. The data window opens with the default data type (non-rice / rice crop); it is possible to quickly change to the other data type by using the drop down menu from the "New" button on the toolbar. Data required differ in case of non-rice or a rice crop. In case of non-rice crop, crop name, planting date, crop coefficient (K_c), stages length, rooting depth, critical depletion fraction (p), yield response factor (K_y) are necessary.

The soil module is selected by clicking on the "Soil" icon in the module bar located on the left of the main CROPWAT window. The Soil module is essentially data input, requiring the general soil data like Total Available Water (TAW), maximum infiltration rate, maximum rooting depth, initial soil moisture depletion. In case of rice calculation, additional soil data are required like drainable porosity, critical depletion for puddle cracking, water availability at planting, maximum water depth. Soil data is saved after input of one set of data is completed. To do so, "Save" button on the toolbar is selected or the "File" > "Save" menu item.

Calculation of the CWR is carried out by calling up successively the appropriate climate and rainfall data sets, together with the crop files and the corresponding planting dates. In case of CWR calculation of rice, soil data are also required. The CWR module is selected by clicking on the "CWR" icon in the module bar located on the left of the main CROPWAT window. Data on climate/ET$_o$, rainfall, crop and soil are required. If not all data are available, CROPWAT will produce a warning and close the CWR module. The CWR module includes calculations, producing the irrigation water requirement of the crop on a decadal basis.

3. RESULTS AND ANALYSIS

The results obtained by CROPWAT 8.0 software are tabulated below:

Table 1. ET$_o$, ET$_c$ and IR values of rice crop for plain region[1]

Year	ET$_o$ (mm/day)	ET$_c$ (mm/decade)	IR (mm/decade)
2007	4.59	698	693.3
2008	4.02	628.6	550.3
2009	4.86	750.6	882.5
2010	4.12	632.7	453
2011	4.17	637.8	682.2

---

[1] In Table 1, 2 , 3 and 4 ET$_0$, ET$_c$ and IR represents the reference evapotranspiration, crop evapotranspiration and irrigation requirement respectively.

Table 2. ET_o, ET_c and IR values of rice crop for hilly region[1]

Year	ET_o (mm/day)	ET_c (mm/decade)	IR (mm/decade)
2007	4.06	756.5	427.7
2008	3.31	650.4	263.2
2009	3.95	741.9	377.6
2010	3.57	659.2	367.4
2011	3.48	665.3	250.4

Table 3. ET_o, ET_c and IR values of wheat crop for plain region[1]

Year	ET_o (mm/day)	ET_c (mm/decade)	IR (mm/decade)
2007	2.85	309.5	211.6
2008	2.71	305.2	296.5
2009	2.86	311.6	287.2
2010	2.78	292.5	267.8
2011	2.60	284	231

Table 4. ET_o, ET_c and IR values of wheat crop for hilly region[1]

Year	ET_o (mm/day)	ET_c (mm/decade)	IR (mm/decade)
2007	3.30	278	164.2
2008	2.59	223.5	183.5
2009	2.72	240.8	194.1
2010	2.71	231.3	175
2011	2.49	215.6	145.9

Now comparison is made between reference evapotranspiration, crop evapotranspiration and irrigation requirement of rice and wheat crop for the plain and hilly region. In Figure 1 and Figure 2 black line and dotted line represents the reference evapotranspiration of plain and hilly region respectively. In Figure 3 black and grey color represents the ET_c of rice crop for plain region and hilly region respectively. In Figure 4 grey and black color represents the ET_c of plain and hilly region respectively for wheat crop. In Figure 5 black and grey color represents the irrigation requirement of plain and hilly region respectively for rice crop. In Figure 6 grey and black color represents the irrigation requirement of plain and hilly region respectively for wheat crop.
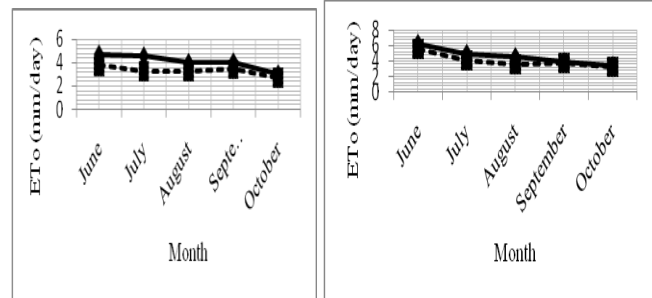
3.1 Comparison of reference evapotranspiration (ET_o) of rice crop

Figure 1. Comparison of ET_o of plain and hilly region of the year 2007, 2008, 2009, 2010 and 2011 respectively

3.2 Comparison of reference evapotranspiration (ET_o) of wheat crop

Figure 2. Comparison of ET$_o$ of plain and hilly region of the year 2007, 2008, 2009, 2010 and 2011 respectively

3.3 Comparison of crop evapotranspiration (ET$_c$) of rice crop

Figure 3. Comparison of ET$_c$ of plain and hilly region of the year 2007, 2008, 2009, 2010 and 2011 respectively

3.4 Comparison of crop evapotranspiration (ET$_c$) of wheat crop

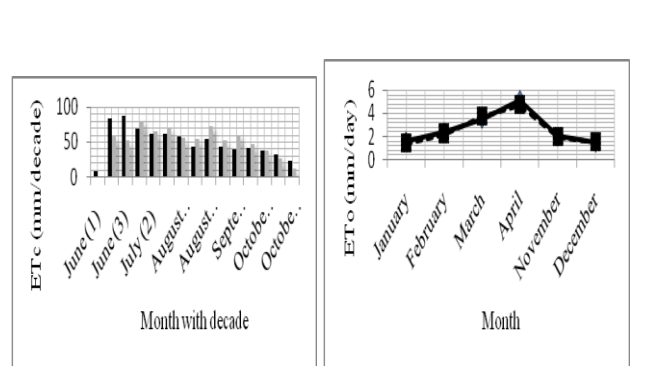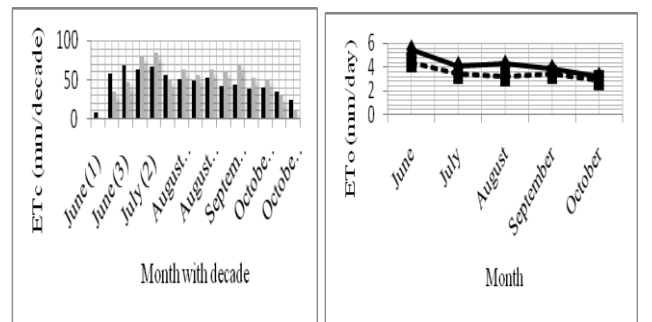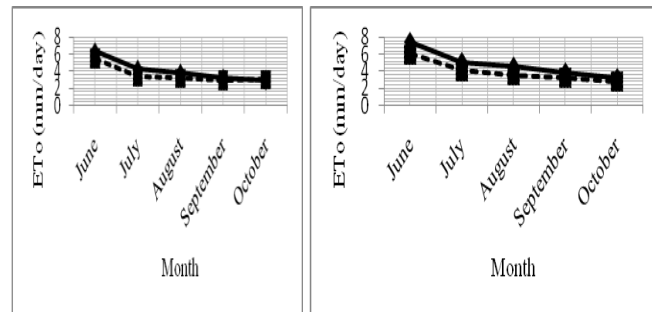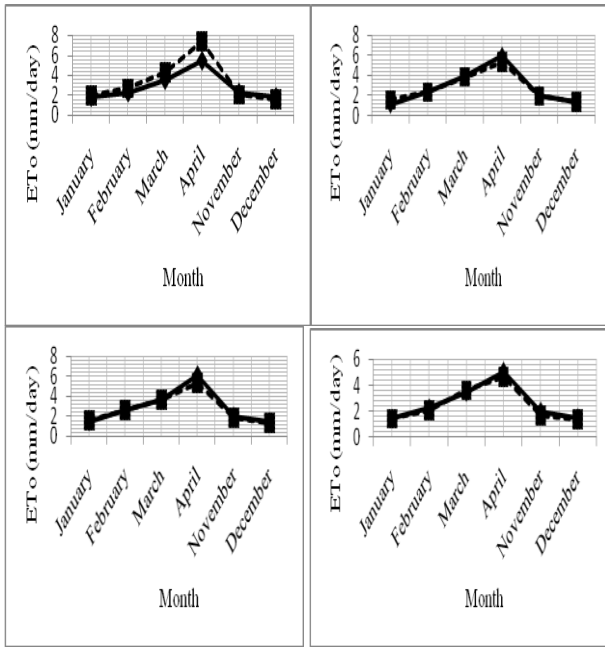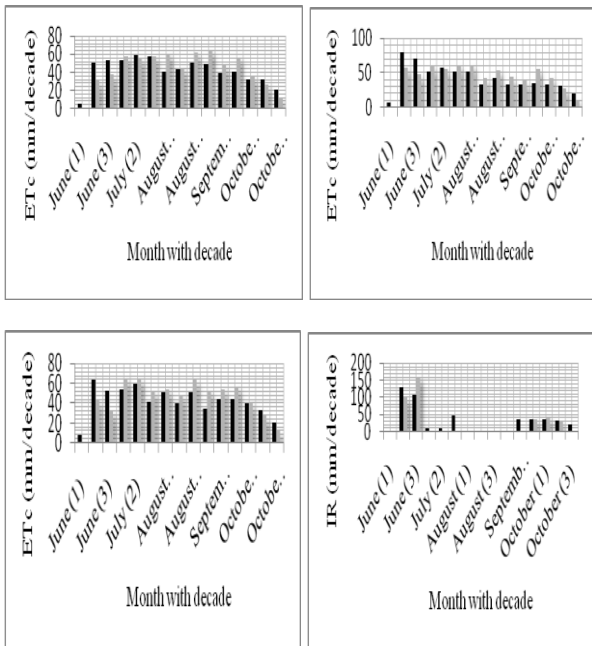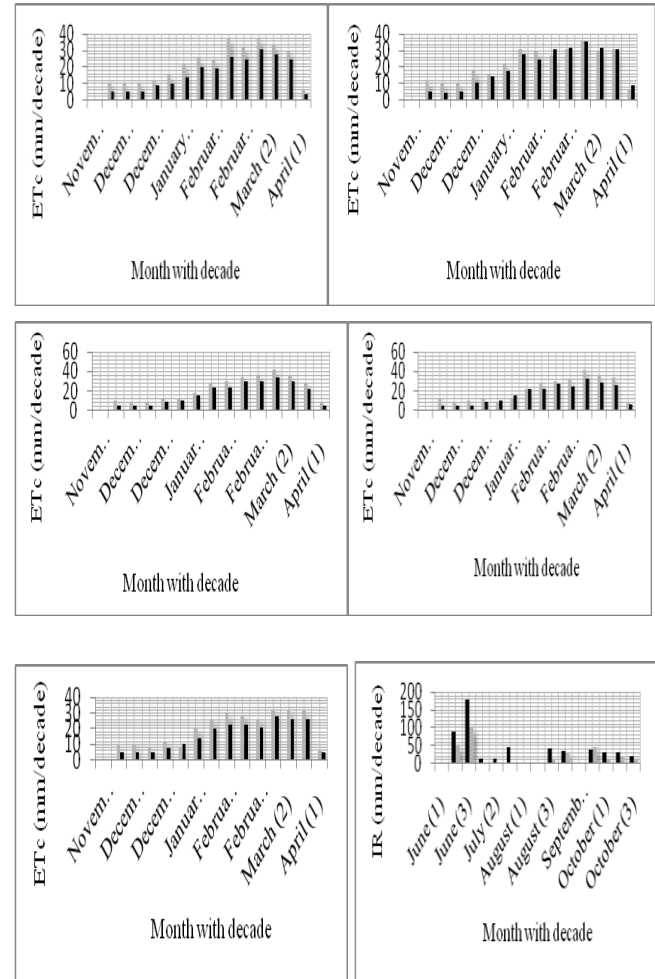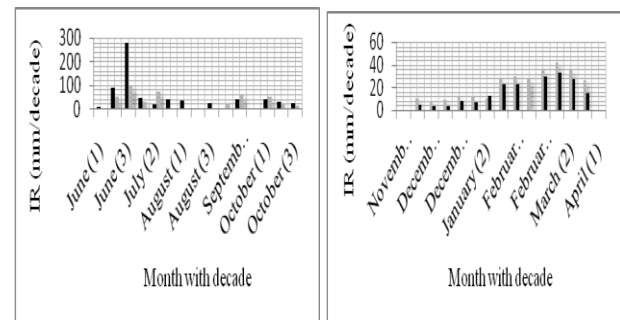**Figure 4.** Comparison of ET$_c$ of plain and hilly region of the year 2007, 2008, 2009, 2010 and 2011 respectively

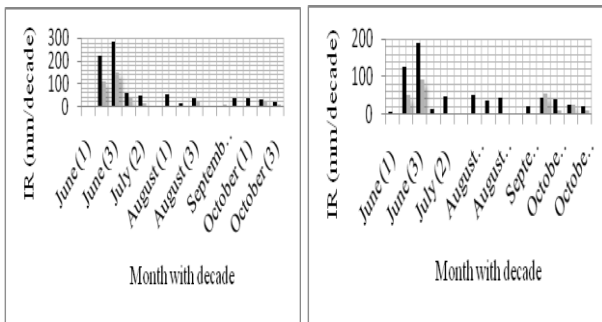### 3.5 Comparison of irrigation requirement (IR) of rice crop

Figure 5. Comparison of irrigation requirement of plain and hilly region of the year 2007, 2008, 2009, 2010 and 2011 respectively

3.6 Comparison of irrigation requirement (IR) of wheat crop
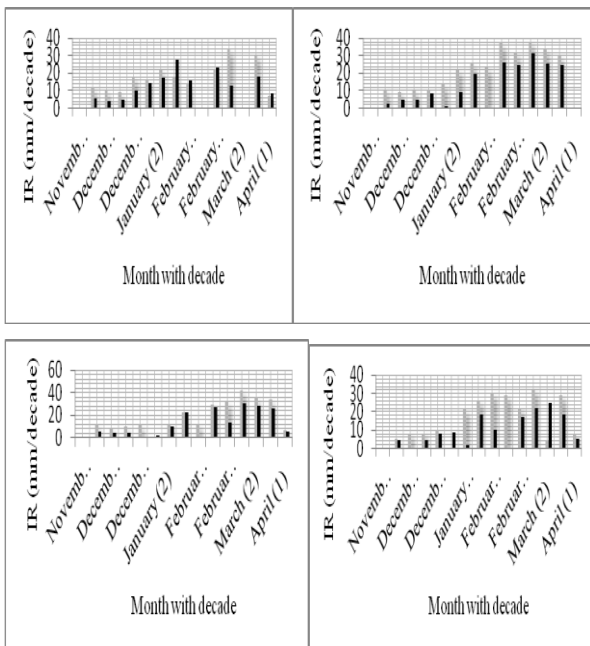

Figure 6. Comparison of irrigation requirement of plain and hilly region of the year 2007, 2008, 2009, 2010 and 2011 respectively

From the above graphs (Figure 1) it has been observed that reference evapotranspiration of rice crop is more for the plain region as compared to the hilly region. Because temperature and sunshine hour was maximum during these periods for the plain region as compared to the hilly region. From Figure 2 it is again observed that reference evapotranspiration of wheat crop is also more for the plain region as compared to the hilly region due to the maximum temperature and sunshine hour during the period of 2007 to 2011. Then again from Figure 3 it is observed that crop evapotranspiration of rice crop is more for the hilly region as compared to the plain region. It was observed that temperature and sunshine hour was maximum for the Karnal region during the period of 2007-2011 as compared to the

Dehradun region. It was also observed that effective rainfall was less for the Karnal region during that period as compared to Dehradun region. From Figure 4 it is observed that crop evapotranspiration (ET_c) of wheat crop is more for the plain region as compared to the Dehradun region during the period of 2007 to 2011. It was observed that temperature and sunshine hour was minimum in Karnal region during Rabi season as compared to Dehradun region. It was also observed that effective rainfall was less in Karnal region as compared to Dehradun region during Rabi season. From Figure 5 and Figure 6 it is observed that irrigation requirement of rice and wheat crop is more for the plain region as compared to the hilly region. It was observed that there was less effective rainfall in Karnal region as compared to the Dehradun region during Kharif season. So irrigation requirement for Karnal region was more as compared to Dehradun region.

4. CONCLUSIONS

It was found that reference evapotranspiration of rice and wheat crop is more for the plain region as compared to the hilly region. Crop evapotranspiration of rice crop is found more for the hilly region as compared to plain region whereas for wheat crop it was more for plain region as compared to hilly region. Irrigation requirement of rice and wheat crop is more for the plain region as compared to the hilly region.

REFERENCES:

i.   Abdalla N M, Xiuju Z, Ishag A. Hussein, G Estimating reference evapotranspiration using CROPWAT model at Guixi Jiangxi province. State Key Laboratory of Hydrology and Water Resources and Hydraulic Engineering, Hohai University, Nanjing.

ii.   Adeniran K A, Amodu M F, Amodu M O, Adeniji F A (2010) Water requirements of some selected crops in Kampe dam irrigation project. Australian Journal of Agricultural Engineering 1(4):119-125.

iii.   Allen R G, Pereira L S, Raes D, Smith M Crop evapotranspiration: guidelines for computing crop water requirements. FAO Irrigation and Drainage Paper No. 56.

iv.   Arku A Y, Musa S M, Mofoke A L E (2012) Determination of water requirements for irrigating Hibiscus (Rosa Sinensis) in Maiduguri Metropolis. Journal of Applied Hytotechnology in Environmental Sanitation 1(1):37-42.

v.   Arulkar K P, Hiwase S S (2008) Evaluation of crop evapotraspiration for rice (kharif) in Nagpur district. Agric Sci Digest 28 (2):149 – 150.

vi.   Chatterjee S K, Banerjee S, Bose M (2012) Climate Change impact on crop water requirement in Ganga river basin, West Bengal, India. 3rdInternational Conference on Biology, Environment and Chemistry Vol. 46.

vii.   Das P, Gupta S (2007) Ground water information booklet, Karnal district, Haryana. Ministry of Water Resources, Central Ground Water Board, Government of India.

viii.   DIOP M Analysis of crop water use in Senegal with the CROPWAT model. CEEPA, University of Pretoria.

ix.   Durand W Assessing the impact of climate change on crop water use in South Africa. ARC-Grain Crops Institute, Potchefstroom, Private Bag X1251, 2520 Republic of South Africa.

x.   Eid H M, Marsafawy S M, Ouda S A Assessing the impact of climate on crop water needs in Egypt: the CROPWAT analysis of three districts in Egypt. Soil, Water & Environment Research Institute (SWERI), Agricultural Research Center, Egypt.

xi.   FAO Corporate Document Repository. Irrigation water management: irrigation water needs. Natural Resources Management and Environment Department.

xii.   Harrington L W, Fujisaka S, Morris M L, Hobbs P R, Sharma H C, Singh R P, Chaudhary M K, Dhiman S D (1992) Wheat and rice in Karnal and Kurukshetra districts, Haryana, India: farmer's practices, problems and an agenda for action. Haryana Agricultural University, Indian Council for Agricultural Research.

xiii.   Hunink J E, Droogers P (2011) Climate change impact assessment on crop production in Uzbekistan. World Bank Study on Reducing Vulnerability to Climate Change in Europe and Central Asia (ECA) Agricultural Systems.

xiv.   Karanja F K CROPWAT model analysis of crop water use in six districts in Kenya. Department of Meteorology, University of Nairobi.

Development of Design Criteria For Sizing Of Break Pressure Tanks

N.N. Sontake[1]   **A.D. Ghare[2]**
R.N. Ingle[3]

[1]Research scholar, Department of Civil Engineering, Visvesvaraya National Institute of Technology, Nagpur, 440 010, India, Email:
nitinsontake@gmail.com

[2]Associate Professor, Department of Civil Engineering, Visvesvaraya National Institute of Technology, Nagpur, 440 010, India, Email:
adghare@yahoo.co.in

[3]Professor (Retd.), Department of Civil Engineering, Visvesvaraya National Institute of Technology, Nagpur,   440 010, India, Email:
rningle@gmail.com

ABSTRACT : For transporting large quantity of water from one source to another location at a long distance, large sized pipes are used. Water may be transported by gravity or by pumping. For economic considerations, these pipelines are laid following the ground level profile. In some situations, the longitudinal profile of pipeline may be highly undulating in nature. Installation of Break Pressure Tank (BPT) at the proper location on such pipelines provides a good solution to control pressure in the pipeline within desirable limit. In this paper, an attempt has been made to develop design criteria for sizing of BPT. The pipeline on downstream of BPT is classified into two different categories depending on profile of the pipeline. Flow in the pumping main is analyzed under unsteady conditions for both the categories. Expressions for variation of velocity, rise in water level in BPT have been derived and represented in the form of curves. The application of the expressions derived for computation of variation in velocity and rise in water level in BPT has been demonstrated.
Keywords: Unsteady flow; Pump pipe system; Break pressure tank

1. INTRODUCTION:

Large and long pipes are used for transporting water from one location to another location at long distance. In water supply scheme, pumps are generally used to transport water at higher locations, while potential energy stored in the water in the form of gravity is used to transport water at lower locations. Accordingly the pipe systems are categorized as gravity pipe system and pump pipe system. From the considerations of economy and convenience in construction, the pipelines are laid along the ground level profile. In some cases the ground level profile is highly undulating, design of pipelines in such cases becomes critical due to large variation of pressure along the pipelines. BPT, which are open to atmosphere are provided in long pipelines either to reduce the pressure or to avoid negative pressure. The sizes of BPT under various situations are governed by the pipeline profile and generally provided at high summits in the pipeline profile. Johnson (1977) highlighted the importance of providing BPT in the closed pipe system, if the topography or elevation of ground changes abruptly. Blackwell (1979) conducted series of dynamic tests on possible restraint systems for domestic BPT to check the stability against earthquake. Jordon (1984) discussed importance of providing a BPT to reduce high pressure in gravity pipe system having large elevation difference between inlet and outlet. Ingle (1993) developed guidelines for sizing of BPT. Niskanen (2003) developed an arbitrary design criterion for BPT and discussed the significance of providing BPT at various locations. Brown (2006) highlighted the significance and importance of providing BPT in many practical situations. McNabola et al. (2011) investigated a hydro-BPT project and assessed the technical and economic feasibility of the energy recoverable from BPT's.

In this paper an attempt has been made to develop the design criteria for sizing of BPT by considering various pipeline profiles. The pipeline on downstream side of BPT is classified into two different categories depending on the nature of ground profile. In first category, the nature of ground is continuously sloping. The pipeline in this case will be laid following the ground profile to achieve the economy. In such systems, during no flow condition water is drained out and pipeline remains empty. During the operation of system, the water level in BPT starts rising and at the same time starts filling the empty pipeline. Rise in water level in BPT continues till it attain a steady state condition and will remain stationary at that position, hence water level in BPT will never rise above the steady state value. BPT of nominal size should be provided when the nature of ground is continuously sloping. In the second category, the topography or elevation of ground changes abruptly. If the pipeline is laid following such profile, the longitudinal profile of pipeline will be in the form inverted siphon (Fig.1). During no operation condition the water will remain in the pipeline upto the level of outlet of BPT in stagnant condition. During operation of pipeline, if the size of BPT is not adequate it will overflow as the rate of rise of water level will not become zero when it reaches the steady state value. Dynamics of fluid flow through pipe system should be considered to determine the maximum rise in water level and the size of BPT.
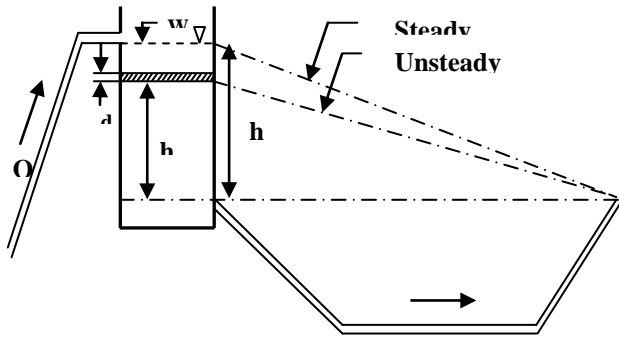
Figure 1. Inverted siphon type pipeline profile

2. EQUATIONS GOVERNING THE FLOW IN THE SYSTEM:

As shown in figure (1), when the steady state discharge from the pump starts filling the BPT, the water level in BPT starts rising gradually and develops head. This developed head will push the stagnant water in the inverted siphon portion of the pipeline. The principle of conservation of mass and momentum can be used to derive the equations describing this unsteady flow. Applying Continuity equation for unsteady flow (figure 1),

Inflow – Outflow = Change in the control volume per unit time

$$Q_0 - A \times V = A_T \frac{dh}{dt}$$

Bernoulli's equation for unsteady flow of incompressible fluid is given by

Total head at inlet = Total head at outlet + Friction head loss + Acceleration head

$$Z_1 + \frac{\rho_1}{w} + \frac{V_1^2}{2g} = Z_2 + \frac{\rho_2}{w} + \frac{V_2^2}{2g} + h_f + h_a$$

or, $$h = F \times V^2 + \frac{L}{g} \frac{dV}{dt}$$

where, $$F = \left(1 + \frac{fL}{D}\right) \frac{1}{2g}$$

Equations (1) to (3) govern the flow in the pipeline from BPT to outlet, with the boundary condition that at $t=0$, $V=0$ and $h=0$ and at steady state $t=\infty$ and $V=V_0$ and $h=h_0$, an expression for V and h are obtained in terms of time. Differentiating equation (3) with respect to t and substituting the value of $\frac{dh}{dt}$ in equation (1), and rearranging the terms, a second order non linear differential equation in terms of V is obtained and its general solution is not possible. To obtain the general solution an approximation is made by replacing the variable V by its

average value $\frac{1}{2}V_0$ in the coefficient of the term of $\frac{dv}{dt}$. The final form of equation obtained is,

$$\frac{d^2 V}{dt^2} + a_1 \frac{dv}{dt} + a_2 V = a_3$$

where, $$a_1 = \frac{FV_0 g}{L} \qquad a_2 = \frac{Ag}{A_T L} \qquad a_3 = \frac{Q_0 g}{A_T L}$$

Equation (5) being linear in nature, its general solution can be obtained. The auxiliary equation corresponding to this equation is,

$$m^2 + a_1 m + a_2 = 0$$

Depending on the values of coefficient a_1 and a_2, the values of roots m i.e. m_1 and m_2 can be real or complex. Therefore, the solution of equation (5) can be categorized into different cases.

3. ANALYSIS AND DISCUSSION ON CASES:

In all the cases, to derive the expression for variation velocity (V) and rise in water level (h) with time the roots of auxiliary equation and constants of integration are expressed in term of critical area of BPT (A_{Tc}) which is defined as, minimum area required for asymptotic solution for h. When $a_1^2 > 4a_2$ (Case – I), roots m_1 and m_2 are real and different. The general solution for equation (5) and values of roots are,

$$(1)$$

$$V_1 = C_1 e^{m_1 t} + C_2 e^{m_2 t} + \frac{a_3}{a_2}$$

$$m_1 = \frac{FV_0 g}{2L}\left[-1 + \sqrt{1 - \frac{A_{Tc}}{A_T}}\right] \qquad (2)$$

$$m_2 = \frac{FV_0 g}{2L}\left[-1 - \sqrt{1 - \frac{A_{Tc}}{A_T}}\right] \qquad (3)$$

$$(4)$$

where, $$A_{Tc} = \frac{4AL}{F^2 V_0^2 g}$$

To evaluate the constants C_1 and C_2, applying boundary conditions, at $t = 0$, $V = 0$ and $h = 0$, equations (8) and (3) gives,

$$C_1 = V_0 \left[\frac{\frac{1}{2}\left(-1 - \sqrt{1 - \frac{A_{Tc}}{A_T}}\right)}{\sqrt{1 - \frac{A_{Tc}}{A_T}}}\right]$$

$$(12)$$

$$C_2 = V_0 \left[\frac{\frac{1}{2}\left(1 - \sqrt{1 - \frac{A_{T_C}}{A_T}}\right)}{\sqrt{1 - \frac{A_{T_C}}{A_T}}} \right] \quad (13)$$

Substituting the values of C_1 and C_2 in equation (8), the variation of velocity in BPT with time is given by,

$$V_1 = C_1 e^{m_1 t} + C_2 e^{m_2 t} + V_0 \quad (14)$$

Substituting the values of V_1 from equation (14) in equation (3), the variation of rise in water level in BPT with time is given by,

$$h_1 = \left[\frac{L}{g} \times C_1 \times \left(m_1 e^{m_1 t}\right) + C_2 \times \left(m_2 e^{m_2 t}\right) \right] + F\left[C_1 e^{m_1 t} + C_2 e^{m_2 t} + V_0\right]^2 \quad (15)$$

Similarly, when $a_1^2 = 4a_2$ (Case-II), roots m_3 and m_4 are real and equal, the constants of integration C_3 and C_4 are different. When $a_1^2 < 4a_2$ (Case-III), roots m_5 and m_6 are complex numbers, the constants of integration C_5 and C_6 are different. If

$$A_T \le \frac{4AL}{F^2 V_0^2 g} \quad (\text{ Case – I and II}),$$ the velocity in the pipeline

will approach Steady state value V_0 asymptotically and water level in BPT will also approach its steady state level asymptotically. Therefore, water level in BPT will never rise above its steady state value. For Case – III, the general solution for equation (5) and the values of roots (m_5 and m_6) are obtained. By applying boundary conditions at $t = 0$, $V = 0$ and $h = 0$, constants of integration (C_5 and C_6) are worked out. Thus final variables obtained are as follows,

$$V_3 = [C_5 Cos \omega t + C_6 Sin \omega t]e^{-\beta t} + \frac{a_0}{a_2} \quad (16)$$

$$m_5 = \beta + I\omega, \quad m_6 = \beta - I\omega \quad (17)$$

$$\beta = \frac{-a_1}{2}, \quad \omega = I\left[\frac{\sqrt{a_1^2 - 4a_2}}{2}\right] \quad (18)$$

where,

$$C_5 = -V_0, \quad C_6 = \frac{-V_0}{\sqrt{1 - \frac{A_{T_C}}{A_T}}} \quad (19)$$

$$\left[-V_0 Cos\left[\frac{\sqrt{a_1^2 - 4a_2}}{2}\right]t + \left(\frac{-V_0 Sin\left[\frac{\sqrt{a_1^2 - 4a_2}}{2}\right]t}{\sqrt{1 - \frac{A_{T_C}}{A_T}}}\right)\right]e^{\frac{-a_1}{2}t} + V_0 \quad (20)$$

Substituting the values of C_5 and C_6 in equation (16), the variation of velocity in BPT with time is given by

$$h_3 = \frac{L}{G}\left[(C_5 \cos \omega t + C_6 \sin \omega t)e^{-\beta t}(-\beta) + (-C_5 \sin \omega t + C_6 \cos \omega t)e^{-\beta t}\right] + F\left[(C_5 \cos \omega t + c_6 \sin \omega t)e^{-\beta t} + V_0\right]^2 \quad (21)$$

Substituting the values of V_3 from equation (20) in equation (3), the variation of rise in water level in BPT with time is given by, Equation (21) contain trigonometric functions, indicating oscillatory behavior of water level in BPT hence the maximum oscillation point can suitably be used to find out the maximum increase in water level in BPT.

4. APPLICATION OF DERIVED EXPRESSIONS:

To demonstrate the application of various expressions derived to determine the increase in velocity and rise in water level in BPT i.e. design of BPT, an illustrative example has been considered. As discussed in previous paragraphs, if profile of pipeline is continuously slopping; nominal size of BPT can be provided. When the pipeline profile is in the form of inverted siphon, rise in water level in BPT can be determined by using expressions derived. In the considered example, the gravity raw main or pipeline profile from BPT to water treatment plant is in the form of inverted siphon. Silent features of the raw water gravity main are as follows: $L = 50000$ m, $d = 1500$ mm $Q_0 = 1.3$ m³/s, $h_f = 14.68$ m, $A = 1.767$ m², $V_0 = 0.730$ m/s, $F = 27.20$ s²/m and $g = 9.81$ m/s².

By using equation (11), the area of BPT needed to be provided is 90 m². Steady state velocity (0.73 m/s) and maximum water level reached in the BPT (14.68 m) is obtained asymptotically for case – I and II as represented in figure (2) and (3). For economic design, the area of BPT can be reduced below the critical area of BPT. Thus, solution to case – III; shows that when the area of BPT calculated by equation (11) is reduced further upto 30%, the velocity and water level corresponding to that velocity in the BPT increase gradually and reach its maximum value as shown in figure (4) and (5). Considerable time is required to achieve the steady state velocity and steady state water level. Therefore, equation (20) and (21) can suitably be used to calculate maximum increase in velocity and rise in water level in BPT.
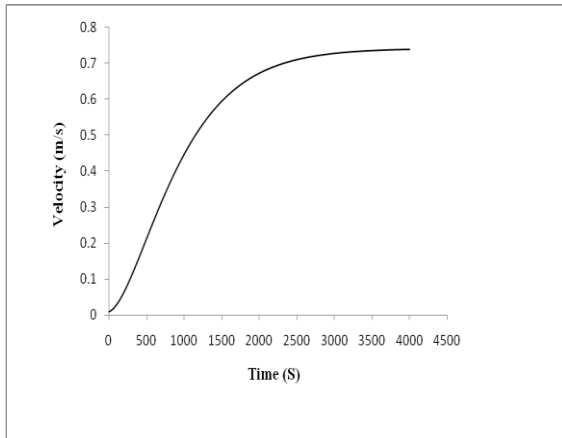
Figure 2. Variation in velocity with time for Case – I.
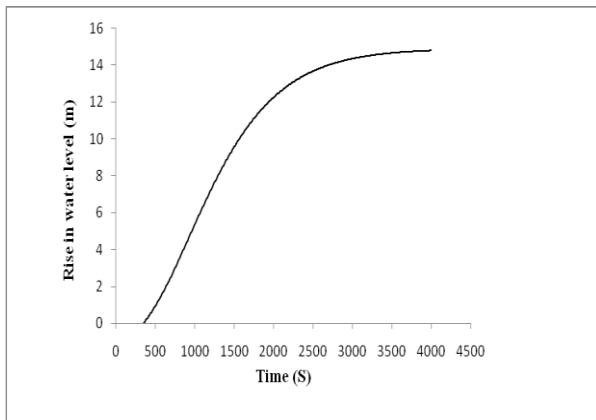
Figure 3. Variation in water level with time for Case – I.
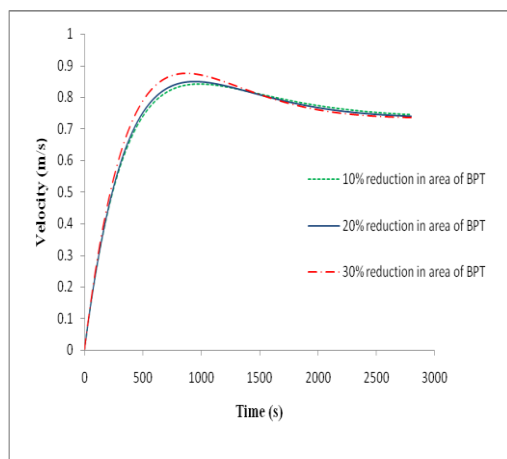
Figure 4. Variation in velocity with percentage reduction in critical area of BPT
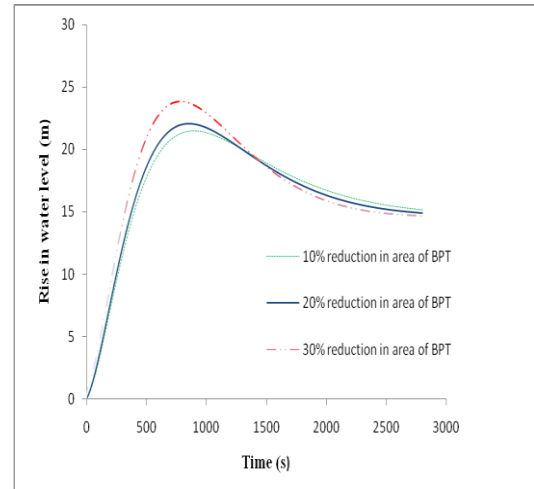
Figure 5. Variation in rise in water level with percentage reduction in critical area of BPT

5. CONCLUSIONS:

Analysis has been carried out for unsteady condition for the flow of water in the pump-pipe system provided with BPT, in which gravity pipe line downstream of BPT is in the form of inverted siphon. Based on the analysis, following conclusions have been drawn.

1.   The minimum area of BPT, defined as critical area of BPT (A_{T_C}) required for the condition of water level not shooting above the steady state water level in BPT, is given by equation (11).

2.   Expressions for velocity (V) i.e. V_1, V_2 and water level (h) i.e. h_1, h_2 in BPT in terms of time (t), have been derived for the Case-I and II, where the cross sectional area of BPT is greater than the critical area of BPT for Case – I and the cross sectional area of BPT is equal to the critical area of BPT for Case –II. In both the cases, V and h approach their steady state values asymptotically.

3.   Expressions for velocity in pipe (V) i.e. V_3 and water level (h) i.e. h_3 in BPT in terms of time, have been derived for the Case-III, where cross sectional area of BPT is reduced upto 30% than the critical area of BPT. V and h showed the oscillatory pattern.

NOTATIONS:

i) L = Length of pipeline
ii) d = Internal diameter of pipe
iii) Q_0 = Steady discharge in pipeline
iv) h_f = Maximum frictional loss
v) h_a = Acceleration head
vi) A = Cross sectional area of pipe
vii) V = Velocity in the pipeline
viii) V_0 = Steady state velocity in pipeline
ix) F = Coefficient in friction loss formula
x) g = Gravitational acceleration

xi)   h = height of water level above outlet of BPT
xii)   t = Time
xiii) $A_{T=}$ Cross sectional area of BPT
xiv) WL = Water level

REFERENCES:

i.   Blackwell, F.N. (1979) A Study of the Earthquake Resistance of Domestic Break Pressure Tanks. Bulletin of the New Zealand National Society for Earthquake Engineering, 12(3), 168-173.

ii.   Brown, L. (2006) Understanding Gravity-Flow Pipelines Water Flow, Air Locks and Siphons. Livestock, Watering Factsheet, British Columbia, Ministry of Agriculture and Lands, Order No. 590.304-5.

iii.   Ingle, R.N. (1993) Development of Guidelines for Sizing of Break Pressure Tank, proceedings of Afro-Asian Conference-II, organized by Indian Water Works Association, at Mumbai, 5.2.1-5.2.5.

iv.   Johnson, Carl R. (1977) Standards and Procedures for the Design of Water Supply Systems in Rural Areas of Nepal and Bhutan. University Press, Tribhuvan University, Kathmandu.

v.   Jordon, T.D. Jr. (1984) Handbook of Gravity-Flow Water System for Small Communities. A reference manual for surveying, designing, and constructing gravity flow water system, government of Nepal, 52-73.

vi.   Kirmeyer, G. J., Friedman, M., Martel, K., Howie, D., LeChevallier, M., Abbaszadegan, M., Karim, M., Funk, J. & Harbour, J. (2001) Pathogen Intrusion into the Distribution System. AWWA Research Foundation and the American Water Works Association, Denver, CO.

vii.   McNobola, A., Coughlan, P. & Williams, A. P. (2011) The Technical & Economic Feasibility of Energy Recovery in Water Supply Networks. Renewable Energy and Power Quality Journal, 9.

viii.   Niskanen, Matthew A. (2003) The Design, Construction, and Maintenance of a Gravity-Fed Water System in the Dominican Republic. M.Sc. thesis, Department of Civil Engineering, Michigan Technological University.

Effective Drought Index Based Evaluation Of Meteorological Drought Characterisitcs In Bundelkhand Region Of Central India

T. Thomas[1*]   R. K. Jaiswal[2]   R. V. Galkate[1]   N. C. Ghosh[3]

[1]Scientist-D, National Institute of Hydrology, WALMI Campus, Bhopal-462017, India

[2]Scientist-C, National Institute of Hydrology, WALMI Campus, Bhopal-462017, India

[3]Scientist-G, National Institute of Hydrology, Jalvigyan Bhavan, Roorkee-247667, India

Email: thomas_nih@yahoo.com

ABSTRACT :Water resources management in arid and semi-arid regions is a hydrologically challenging proposition for the decision makers and planners as they are more susceptible to drought. The Bundelkhand region is under the limelight due to continuous droughts resulting in acute water scarcity leading to large-scale out-migration of people. The effective drought index (EDI) developed by Byun and Wilhite, (1999) based on the concept of effective precipitation with a time-dependent reduction function has been used to analyze the meteorological drought characteristics in the Bundelkhand. The average drought frequency varies between 1 in 3 years and 1 in 5 years. The average drought intensity in Sagar district (Madhya Pradesh) varies between -0.93 at Banda and -1.15 at Khurai whereas in Jhansi district (Uttar Pradesh) it varies between -0.73 at Garotha and -1.43 at Pachwara. The spatio-temporal variation of drought has been studied using ILWIS 3.6. It has been observed the area under mild drought increased from 2% (mild drought) in July 2007 to 81% (mild drought) and 2% (moderate drought) in August 2007 due to the deficient rainfall. The drought situation further worsened in September 2007 with almost the entire Bundelkhand reeling under drought with 77.5% (mild drought), 14.3% (moderate drought), and 0.1% (severe drought). The spatio-temporal analysis of EDI based drought characteristics can be used effectively for drought monitoring to identify the problematic areas within the region, so that timely drought relief measures can be more focused towards these areas during periods of crisis.

Keywords: Drought, drought index, EDI, Bundelkhand, spatio-temporal

1. INTRODUCTION

Drought is an unavoidable and unpredictable phenomenon both in its occurrence and duration and therefore preparation against droughts, through proper planning are key elements for minimizing their adverse impacts to a great extent, for which effective drought monitoring systems and drought management plans need to be developed. Drought remains a major disaster causing enormous damages to people, environment and economy, despite making considerable progress in its monitoring, forecasting and mitigation. The available estimates on drought impacts suggest that, during the period 1900–2013, 642 drought events were reported across the world resulting in death of about 12 billion people and affecting over 2 billion (EM-DAT, 2014) as shown in Table 1. The total economic damages have been estimated at USD135 billion. The main focus of the drought management should be towards catering the vulnerable regions with provision of adequate water supply

to various stakeholders during periods of water crisis. In India, almost one-sixth geographical area is drought prone mainly the arid, semi-arid and sub-humid regions. Therefore drought mitigation measures including development of early warning and forecasting systems, building resilience of the societies and adaptation mechanisms and capacity building is necessary (Calow et al., 2010; Clarke et al., 2012; Falkenmark and Rockström, 2008; GFDRR, 2011; Mishra and Singh, 2010; Msangi, 2004; Sehmi and Kundzewicz, 1997; Tøttrup et al., 2012; UNISDR, 2004 and 2010; Vicento-Serrano et al., 2012; World Bank and GFDRR, 2010). Of all the 20th century natural hazards, droughts have had the greatest detrimental impact (Bruce, 1994; Obasi, 1994). In recent years, widespread droughts have

Table 1. Overview of number of droughts and their impact across the world during 1900–2013

Continent	# of events	# of people killed	# of people affected	Damage (×103 USD)
Africa	291	847143	362225799	2920593
Americas	134	77	69505391	50471139
Asia	153	9663389	1707836029	44251865
Europe	42	1200002	15488769	25481309
Oceania	22	660	8034019	12303000
Total	642	11711271	2163090007	135427906

Source: EM-DAT: The International Disaster Database. Centre for Research on the Epidemiology of Disasters-CRED

been observed affecting large areas in Europe, Africa, Asia, Australia, South America, Central America, and North America (Le Comte, 1995; Le Comte, 1994). Zargar et al. 2011 conducted a comprehensive review of 74 operational drought indices. Masih et al. (2014) in his recent work conducted a review of droughts in African continent and concluded that the African continent is likely to face extreme and widespread droughts in future and stressed the need for integrated approaches in drought mitigation. Drought indicators have been used to effectively evaluate the meteorological, agricultural, and hydrological drought characteristics universally. The drought index is defined as an index which is related to some of the cumulative effects of a prolonged and abnormal moisture deficiency (World Meteorological Organization, 1975). The operationally used meteorological indicators include

Standardized Precipitation Index (SPI; McKee et al., 1993) and the Palmer Drought Severity Index (PSDI; Palmer, 1965), both of which are useful for agricultural drought monitoring (Mishra and Singh, 2010). Heim 2002 carried out a review of the 20th century drought indices used in the United States for evaluation of meteorological, agricultural, and hydrological drought characteristics. Mishra and Singh (2010) carried out a detailed review of fundamental drought concepts, drought indices and relation between droughts and large scale climate indices. They concluded that drought is best characterized by multiple climatological and hydrological parameters. Sepulcre-Canto et al. (2012) developed a combined indicator to detect agricultural droughts in Europe wherein they combined the Standardised Precipitation Index (SPI) and the anomalies of soil moisture and absorbed photsynthetically active radiation at the European level to classify the drought situation based on a classification scheme composed of three warning levels viz., watch, warning and alert.

Smakhtin (2004) reviewed the existing indices developed for monitoring and quantitative assessment of droughts and analysed their applicability for drought prediction and management in the specific context of South Asia. Byun and Kim (2010) compared the performances of the effective drought index (EDI) with the SPI for the drought monitoring data accumulated over 200-year period from 1807 to 2006 for Seoul, Korea. The results confirmed that the EDI was more efficient than the SPI in assessing both short and long-term droughts. Morid et al. (2006) compared the performances of seven drought indices namely, deciles index (DI), percent of normal (PN), standard precipitation index (SPI), China-Z index (CZI), modified CZI (MCZI), Z-Score and effective drought index (EDI) for drought monitoring in the Tehran province of Iran. The concluded SPI and EDI were able to detect the onset of drought including its spatial and temporal variation consistently, and recommended them for operational drought monitoring. The EDI was found to be more responsive to the emerging drought and performed better. In view of the effective performance of EDI as compared to the other available indices, the EDI has been used to evaluate the meteorological drought characteristics in Bundelkhand.

1.1 Study area

Bundelkhand is a cultural-geographic region in Central India bounded by Vindhyan Plateau in south, Yamuna river in north, Ken river in east and rivers Betwa and Pahuj in west and remains administratively divided between Uttar Pradesh (U.P.) and

Madhya Pradesh (M.P.). The Bundelkhand region comprises of six districts in M.P. viz., Sagar, Damoh, Chhatarpur, Tikamgarh, Panna and Datia and seven districts in U.P. viz., Jhansi, Lalitpur, Jalaun, Hamirpur, Banda, Mahoba and Chitrakoot. The topography comprises of gently-sloping uplands, distinguished by barren hilly terrain. The region lies between 23° 8′ N to 26° 30′ N latitude and 78° 11′ E to 81° 30′ E longitude with a total area of 71,619 sq. km. About 82% of the population is dependent on agriculture. The region receives average annual rainfall varying between 514.4 mm to 1260.1 mm, 90% of which occurs during the south-west monsoon from mid-June to early-October, but most of it is lost to runoff owing to very few irrigation schemes. In general, the rainfall pattern of this region is erratic and uncertain with very high variability. This region is bounded on all the four sides by rivers, viz. the Yamuna, the Narmada, the Chambal and the Tons. The principal rivers draining the region are Sindh, Betwa, Ken, Bagahin, Tons, Pahuj, Dhasan and Chambal. While the Yamuna flows from west to east, its first order tributaries, Betwa, Ken, Sindh, Pahuj, Gharara, Bagain and Paisuni flow from south to north. The entire drainage forms a part of Ganga basin and region generally slopes from south to north. The elevations in the area range from 600 m above mean sea level (amsl) in southern part to 150 m amsl near the Yamuna. The map showing the study area is given in Figure 1.

Figure 1. Index map of Bundelkhand

2. MATERIAL AND METHODS

The effective drought index (EDI) developed by Byun and Wilhite, 1999 can used to analyze the drought severity and drought duration. The EDI is based on the concept of effective precipitation (EP), which is the summation of daily precipitation with a time-dependent reduction function. It is a function of the precipitation needed for a return to normal (PRN) condition, signifying the precipitation necessary for recovery from accumulated deficit since the beginning of a drought. Three more additional indexes are also used to complement EP. The each day's mean of EP i.e. MEP, shows the climatological characteristics of precipitation as a water resource for an area. The deviation of EP from the MEP i.e. DEP, shows the variation of EP and the third index is the standardized value of DEP i.e. SEP. By using these three indexes, consecutive days of negative SEP, which depicts the onset, termination, and duration of a water deficit period is categorized. With the duration of the water deficit being categorized, four additional indexes that show drought severity can be calculated viz., accumulation of consecutive negative SEP, which shows the duration and severity of precipitation deficit; accumulated precipitation deficit, which shows precipitation departure from the normal; precipitation for the return to normal (PRN); and EDI, a standardized index used to assess drought severity. The EDI has is considered to be more precise for identification of drought duration and useful in monitoring an ongoing drought.

The first step in the analysis is the computation of EP, a function of summed values of daily precipitation with a time-dependent reduction function. Similarly, for a monthly time step, it is defined as the current month's rainfall and weighted rai ⌃ ll   d ⌃ d preceding period. To represent daily depleti Bundelkhand   rces, the EP is computed by next three equations as given,

$$EP_i = \sum_{m=1}^{i} P_m^{\frac{-m}{i}}$$
$$(1)$$

$$EP_i = \sum_{n=1}^{i} \left[\frac{\left(\sum_{m=1}^{n} P_m \right)}{n} \right]$$
$$(2)$$

$$EP_i = \sum_{m=1}^{i} \left[a(i - m + 1) \frac{P_m}{\sum_{n=1}^{i} n} \right]$$
$$(3)$$
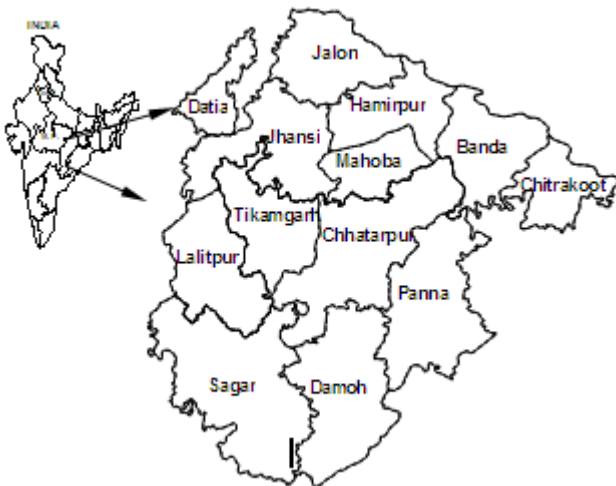
where, i = duration of summation (DS), P_m = precipitation of m days before, a = constant [if i is 365, 100 is used as a value of a].

The second equation which is commonly used for the computations is derived from the concept that the precipitation m days before is added to total water resources as a form of average precipitation of m days. The choice of the best equation remains an unsolved problem because many parameters, like topography, soil characteristics, ability to keep water in reservoirs, air temperature, humidity, and wind speed, must be considered precisely together to represent the depletion of water resources in nature by runoff and evapotranspiration.

Once the daily EP of a station is computed, a series of calculations can be made to highlight different characteristics of the station's water resources. EP needs to be compared to climatological data, and because precipitation at most stations has a strong annual variation, EPs are averaged along the day number (by calendar day). The MEP which illustrates the climatological characteristics of water resources, is computed in the next step. But, since a strong daily variation of MEP is not helpful for practical use, a 5-day running mean is applied. The DEP is then computed, which shows the deficiency or surplus of water resources for a particular date and place.

$$DEP = MEP - EP$$

$$(4)$$

The next step involves the calculation of the standardized value of DEP i.e. the SEP

$$SEP = \frac{DEP}{ST(EP)}$$

$$(5)$$

where, SEP denotes the standard deviation of each day's EP. Here too, each date's (each calendar day's) standard deviation is used in incorporating a 5-day running mean to smooth daily variation. SEP enables the comparison of drought severity at different locations regardless of climatic differences. Because negative values of DEP or SEP denote below normal precipitation, periods of consecutive negative values in DEP and SEP denote consecutive drier periods than normal. Therefore a dry duration is defined as the period of consecutive negative values of SEP. The accumulated precipitation deficit (APD_j) is calculated by a simple accumulation of precipitation deficit as given by,

$$APD_j = \sum_{n=1}^{j} P_n - AVG_i$$

$$(6)$$

where, AVG_j is the averaged daily precipitation of the date for many years during a pre-defined DS. The EP function is not used in APD. The APD is useful because users are more accustomed to precipitation accumulation than to the EP. The APD is the best of all indexes when used to compare drought damages in same climatic conditions.

Negative values of DEP can be calculated directly to convert it to the 1-day precipitation needed for a return to normal condition (PRN_j). The precipitation needed for a return to normal condition (PRN_j) is calculated as given by,

$$PRN_j = \frac{DEP_j}{\sum_{i=1}^{j}(1/n)}$$

$$(7)$$

PRN_{400} shows the needed precipitation for recovery from the deficit accumulated during the last 400 days, in which daily depletion of water resources is taken into account. PRN_{365} is more important, since if PRN_{365} is positive, all other drought indexes are not calculated, in spite of accumulated water deficit. The APD and PRN are superior to EDI in the description of drought intensity. Since APD and PRN depend on the background climatology, EDI is often needed for universal drought assessment. It is expressed as:

$$EDI_j = \frac{PRN_j}{Std(PRN_j)}$$

$$(8)$$

Similar to the SPI, the EDI values are standardized, which allows drought severity at two or more locations to be compared regardless of their climatic differences. The EDI varies from -2.5 to +2.5. The EDI has thresholds indicating the range of wetness from extreme drought to extremely wet conditions. The 'drought range' of the EDI indicates extreme drought conditions at EDI < -2.5, severe drought at -1.5 > EDI > -2.49 and moderate drought at -0.7 > EDI > -1.49. Near normal conditions are indicated by -0.69 < EDI < 0.69. The major problem associated with the EDI in its original form is that it is based on daily precipitation data. However, Smakhtin and Hughes, (2004) developed EDI application with monthly data. Many studies in the United States has revealed that the EDI was the best index in assessing drought severity worldwide and PRN was the best suited for limited areas in a timely manner. The EDI can be used to assess the water deficit as well as water surplus. The problems associated with lack of water resources can be assessed, monitored, and predicted more objectively and quantitatively for the effective water resources management objectives.

3. RESULTS AND ANALYSIS

The EDI and all the related indices have been estimated for each of the development blocks of all the thirteen districts of Bundelkhand. The temporal variation of the EDI has been studied based on the plots of the time series of the EDI. These plots highlight the periods of droughts as well periods of water surplus. The temporal variation of the EDI at Sagar and Chattarpur are given in Figure 2 and Figure 3 respectively. The drought classification based on EDI suggests that most the blocks in Bundelkhand faced recurrent droughts since 2002 with drought severity varying between moderate to extreme during this period. The drought characteristics including the drought severity, drought duration, drought intensity and the onset and termination of drought have been determined for all the blocks in the Bundelkhand region based on the EDI. The analysis revealed that the average frequency of drought varies between 1 in 3 years and 1 in 5 years.
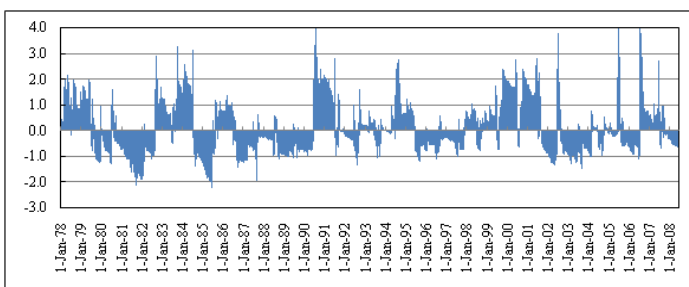

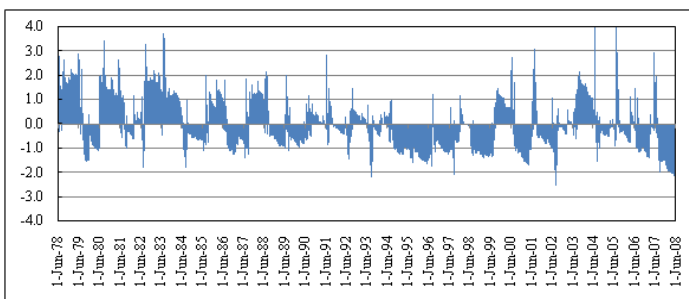**Figure 2.** Temporal variation of EDI in Sagar block of Sagar district

Figure 3. Temporal variation of EDI in Laundi block of Chattarpur district

The EDI based drought characterisitcs have been computed for all the blocks in Sagar district. The drought characterisitcs at Garhakota block of Sagar district is given in Table 2. The drought of maximum duration of 14 months occurred during

August 2007 to September 2008 with a maximum severity of -14.87 and drought intensity of -1.06. Similarly, the next major drought event occured in

Table 2. EDI based drought charactersitics at Garhakota in Sagar district

Name of block	Onset of drought	Termination of drought	Duration (months)	Severity	Intensity
Garhakota	Sep-1995	Dec-1995	4	-3.54	-0.89
	Feb-1996	Jun-1996	5	-4.13	-0.83
	Sep-2001	Apr-2002	8	-9.16	-1.15
	Sep-2002	May-2003	9	-8.86	-0.98
	Jul-2003	Aug-2003	2	-1.70	-0.85
	Oct-2005	Oct-2005	1	-0.71	-0.71
	Jan-2006	Jun-2006	6	-5.16	-0.86
	Aug-2007	Sep-2008	14	-14.87	-1.06
	Feb-2009	Mar-2009	2	-1.46	-0.73
	Apr-2010	Jun-2010	3	-2.56	-0.85
	Aug-2010	Aug-2010	1	-1.11	-1.11

2002-03 which had been another prominent drought year with a duration of 9 months during September 2002 to May 2003; severity of -8.86 and intensity of -0.98. The other years during which drought was expereinced in Garhakota block include 1995, 1996, 2001, 2005, 2006, 2009 and 2010. Similar analysis have been performed for all the blocks and it has been observed that most of the blocks experienced droughts of varying severities and intensities during 2002-03 and 2007-08. This is also susbtantiated by the reduction in food production, loss of livestock and large scale out-migration during these years.

After the computation of drought characteristics including the drought severity, duration and intensity at all the blocks in each district, the summary of the EDI based drought characteristics have been computed for each district. The summary of the drought characteristics in Sagar district is given in Table 3. It has been observed that the average drought intensity in Sagar district varies between   -0.93 at Banda to -1.15 at Khurai. The variation of the average drought intensity is given in Figure 4. Similarly the variation of the total number of drought events, total drought duration and total drought severity in Sagar district is given in Figure 4. In Sagar distirct, Deori block faced the maximum total drought duration of 102 months followed by 101 months at Rehli.

Table 3. EDI based drought charactersitics of Sagar district

| S. No	Name of block	Number of drought events	Total drought duration (months)	Total drought severity	Average drought intensity
1.	Band	19	80	-74.88	-0.93
2.	Bina	16	64	-62.55	-0.97
3.	Deori	17	102	-108.22	-1.06
4.	Garhat	11	55	-53.26	-0.97
5.	Jaisin	15	63	-65.45	-1.03
6.	Kesli	10	53	-54.55	-1.03
7.	Khura	16	92	-105.68	-1.15
8.	Malth	12	74	-84.76	-1.13
9.	Rahat	12	76	-82.87	-1.09
10.	Rehli	18	101	-96.78	-0.96
11.	Sagar	23	99	-104.84	-1.06
12.	Shahg	15	54	-50.91	-0.95
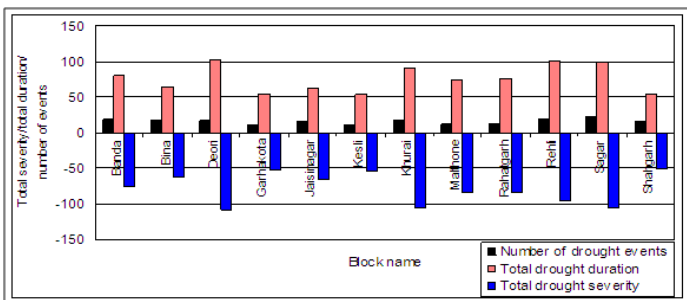
Figure 4. Variation of EDI based drought characteristics in Sagar district

However the maximum total severity of -108.22 has been observed at Deori followed by -105.68 and -104.84 at Khurai and Sagar respectively. The variation of the total number of drought events, total drought duration and total drought severity in each of the blocks in Chattarpur district is given in Figure 5. The summary of the EDI based drought characteristics in Chattarpur district is given in Table 4. In Chattarpur district, Buxwaha block faced the maximum total drought duration of 115 months with a maximum total severity of -123.73 followed by Chattarpur block with a total drought duration of 106 months and total severity of -120.08 during the

period of analysis from 1978-2010. It has been observed that the average drought intensity at the various blocks in Chattarpur district is much higher than that in Sagar district.
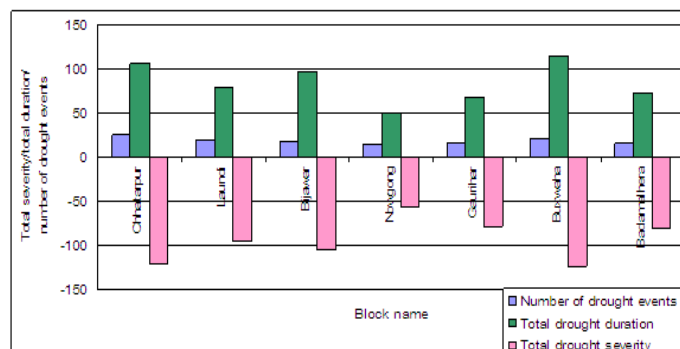
Figure 5. Variation of EDI based drought characteristics in Chattarpur district

Table 4. EDI based drought charactersitics in Chhatarpur district

S. No	Name of block	Frequency of drought events (number)	Total drought duration	Total drought severity	Average drought intensity
1.	Chhatarpur	26	106	-120.08	-1.13
2.	Laundi	18	78	-92.39	-1.18
3.	Bijawar	18	97	-105.32	-1.09
4.	Nowgong	15	51	-56.08	-1.10
5.	Gaurihar	16	68	-78.51	-1.15
6.	Buxwaha	20	115	-123.73	-1.08
7.	Badamalhera	15	72	-78.82	-1.09

The spatial variation of the drought characteristics based on the EDI has been carried out for Bundelkhand region for some of the identified drought years. The analysis was performed using ILWIS 3.6 for the successive months during the monsoon seasons of 2002-03 and 2007-08. The spatial variation of drought during the monsoon of 2002-03 and the area falling under various drought classes are given in Figure 6 and the histogram details of the same are given in Table 5. It has been observed that during June 2002, 7.75% of the total area was under mild droughts which considerably increased to 87.32% under various drought classes namely, mild (20.67%), moderate

(47.13%), severe (9.18%) and 10.33% under extreme droughts during July 2002. The severity of the droughts thereafter decreased in August with 66.62% area under mild drought and 33.03% under normal conditions. In September 2002, situation improved further with 92.64% under normal conditions. Similarly the spatial and temporal variation of drought characteristics during 2007-08 along with the area under various drought classes is given in Table 6. It has been observed that during 2007-08, only 2% of the area had been under mild drought during July 2007, which increased to 81.05% (mild

1.	Extreme	0.00	10.33	0.00	0.00
2.	Severe	0.10	9.18	0.01	0.00
3.	Moderate	0.04	47.13	0.34	0.02
4.	Mild	7.75	20.67	66.62	7.34
5.	No drought	92.2	12.68	33.03	92.64

drought) and 2.02 (moderate drought) in August 2007. Due to lack of sufficient precipitation, the drought situation further worsened in September 2007 with almost entire area (92%) reeling under the effects of drought viz., moderate drought (14.34%), mild drought (77.52%) and severe drought (0.05%).

Table 6. Spatial and temporal variation of EDI during 2007-08 in Bundelkhand

S. No	Drought severity	Percentage of area under different severity classes (%)			
		Jun-07	Jul-07	Aug-07	Sep-07
1.	Extreme	0.00	0.00	0.00	0.00
2.	Severe	0.00	0.00	0.01	0.05
3.	Moderate	0.00	0.02	2.02	14.34
4.	Mild	0.02	2.13	81.05	77.52
5.	No drought	99.98	78.68	16.92	8.09

4. CONCLUSIONS

The evaluation of meteorological drought characteristics has been carried out in Bundelkhand based on the EDI which is a comparatively one of the best techniques available for drought monitoring and preparation of drought management plans. The frequency of occurrence of drought in Bundelkhand varies between 1 in 3 years to 1 in 5 years, which require detailed planning to solve the problems of the region. Also there are considerable variations in the drought severities and drought durations in various
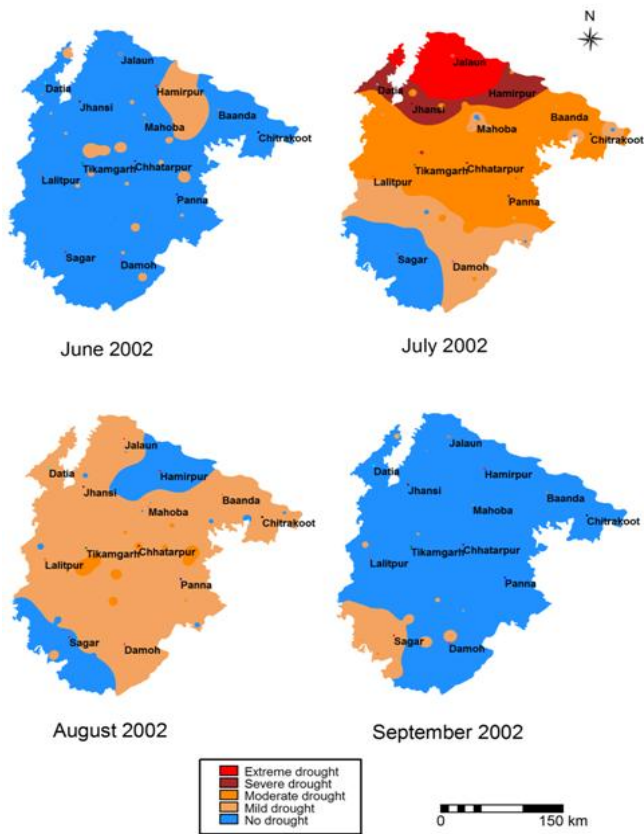

Figure 6. Spatio-temporal variation of drought during 2002-03

Table 5. Spatial and temporal variation of EDI during 2002-03 in Bundelkhand

S. No	Drought severity	Percentage of area under different severity classes (%)			
		Jun-02	Jul-02	Aug-02	Sep-02

districts of Bundelkhand. The analysis of the spatial and temporal variation of the drought revealed that each drought event has its own distinct footprint. The study demonstrated that the EDI can effectively be used to monitor the spatial and temporal variation of drought and its progression and withdrawal during different months of a water year. This helps to give a better understanding of the zones/areas reeling under drought conditions, so that all necessary efforts can be channelized towards these affected areas. The frequent occurrences of drought particularly during the last decade clearly indicates that rain-fed agriculture is almost impossible without the provision of adequate supplementary irrigation calling for a proactive drought management strategy to cope up with the frequent drought scenario. The holistic approach of integrated water resources management (IWRM) can be adopted towards the management of the natural resources including water by the active involvement of all concerned stakeholders.

REFERENCES

i.   Bruce JP (1994) Natural disaster reduction and global change. Bull. Am. Meteorol. Soc. 75: 1831–1835.

ii.   Byun HR, Wilhite DA (1999) Objective quantification of drought severity and duration. Journal of Climate 12: 2747-2756.

iii.   Byun HR, Kim DW (2010) Economics of drought and drought preparedness in a climate change context. Options Méditerranéennes, No. 95.

iv.   Calow RC, Macdonald AM, Nicol AL, Robins NS (2010) Ground water security and drought in Africa: linking availability, access and demand. Ground Water 48: 246–256.

v.   Clarke CL, Shackleton SE, Powell M (2012) Climate change perceptions, drought responses and views on carbon farming amongst commercial livestock and game farmers in the semiarid Great Fish River Valley, Eastern Cape province, South Africa. Afr. J. Range For. Sci. 29: 13–23.

vi.   Falkenmark M, Rockström J (2008) Building resilience to drought in desertification-prone savannas in sub-Saharan Africa: the water perspective. Nat. Resour. Forum 32: 93–102.

vii.   GFDRR (Global Facility for Disaster Reduction and Recovery): Disaster risk management programs for priority countries. Washington DC, World Bank.

viii.   Le Comte D (1994) Weather highlights around the world. Weatherwise 47: 23–26.

ix.   Le Comte D (1995) Weather highlights around the world. Weatherwise 48: 20–22.

x.   Masih I, Maskey S, Mussa FEF, Trambauer P (2014) A review of droughts in African continent: a geospatial and long-term perspective. Hydrol. Earth Syst. Sci. Discuss 11:, 2679-2718.

xi.   McKee TB, Doesken NJ, Kleist J (1993) The relationship of drought frequency and duration to time scales. Proceedings of the 8th Conference of Applied Climatology, Anaheim, CA, Am. Meterol. Soc. 179–184.

xii.   Mishra AK, Singh VP (2010) A review of drought concepts. Journal of Hydrology 391: 202-216.

xiii.   Morid S, Smakhtin VU, Moghaddasi M (2006) Comparison of seven meteorological indices for drought monitoring in Iran, Int. J. Climatol. 26: 971–985.

xiv.   Msangi JP (2004) Drought hazard and desertification management in the dry lands of Southern Africa. Environ. Monit. Assess. 99: 75–87.

xv.   Obasi GOP (1994) WMO's role in the international decade for natural disaster reduction. Bull. Am. Meteorol. Soc. 75(9): 1655–1661.

xvi.   Palmer WC (1965) Meteorological drought. US Weather Bureau, Research Paper No. 45.

xvii.   Sehmi NS, Kundzewicz ZW (1997) Water, drought and desertification in Africa, sustainability of water resources under increasing uncertainty. Proceedings of International Symposium of the Fifth Scientific Assembly of the International Association of Hydrological Sciences IAHS, Rabat, Morocco, 57–65.

xviii.   Sepulcre-Canto G, Horion S, Singleton A, Carrao H, Vogt J (2012) Development of a combined drought indicator to detect agricultural drought in Europe. Nat. Hazards Earth Syst. Sci. 12: 3519-3531.

xix.   Smakhtin VU, Hughes DA (2004) Review, automated estimation and analysis of drought indices in south Asia, Working Paper 83, Colombo, Sri Lanka. International Water Management Institute.

xx.   Tøttrup AP, Klaassen RHG, Kristensen MW, Strandberg R, Vardanis Y, Lindström Å, Rahbek C, Alerstam T, Thorup K (2012) Drought in Africa caused delayed arrival of European songbirds. Science 338: 1307.

xxi.   UNISDR (United Nations International Strategy for Disaster Reduction) (2004) Living with risk: a global review of disaster reduction initiatives, UNISDR, Geneva, Switzerland.

xxii.   UNISDR (United Nations International Strategy for Disaster Reduction) (2010) Declaration of the second African Ministerial Conference on Disaster Risk Reduction, Nairobi, Kenya.

xxiii.   Vicente-Serrano SM, Beguería S, Gimeno L, Eklundh L, Giuliani G, Weston D, El-Kenawy A, López-Moreno J I, Nieto R, Ayenew T, Konte D, Ardö J, Pegram GGS (2012) Challenges for drought mitigation in Africa: the potential use of geospatial data and drought information systems. Appl. Geogr. 34: 471–486.

xxiv.   World Bank, GFDRR (2010) Report on the status of disaster risk reduction in Sub-Saharan Africa, The World Bank, Washington DC.

xxv.   World Meteorological Organization (1975) Drought and agriculture. WMO Note 138, Publ. WMO-392, Geneva, Switzerland.

Rainfall Runoff Model Development Under Regulated River Flow Condition

R.V. Galkate[1], R.K. Jasiwal[1], T. Thomas[1], T.R. Nayak[1]

1.   Scientist, National Institute of Hydrology, Regional Centre, WALMI Campus, Bhopal-462016.
Corresponding Author Email:
rgalkate@yahoo.co.in

ABSTRACT : Observed discharge is one the crucial and common input parameter required in rainfall runoff model development and importantly, it should be the true representative runoff of that river basin. When the stream flow regime is regulated, it needs to be modified or corrected before setting up the rainfall runoff models. To examine the fact, the study was carried out in the Kharun river, a tributary of Seonath river in Chhattisgarh state having strongly

regulated flow regime. The non-regulated flow time series at Patherdihi was simulated from the regulated observed flow at Patherdihi G/D site by developing Kharun river basin model in Mike Basin software using the information on storages, addition, diversion and return flows from irrigation, etc. The MIKE 11 NAM rainfall runoff models were developed under regulated flow condition and non-regulated (virgin) flow conditions. Accuracy of the models were examined on the basis of coefficient of determination (R^2), Efficiency Index (EI), Sum of Square of Error (SSE) and percentage difference between observed and simulated discharge. When the model was developed under non-regulated condition, the R^2 value increased from 0.78 to 0.858, Efficiency Index increased from 0.71 to 0.86 and the difference between observed and simulated discharge reduced from 6.2 to 3.5% and the SSE of the model was found reduced by 25% indicating improved agreement between simulated and observed runoff. The model accuracy was seen higher when the model was developed using the non-regulated flow data. It could be concluded that the rainfall runoff model simulation using regulated flow data as an input may lead to inaccurate simulation of river flow.

Key Words: Rainfall runoff modelling, NAM Model, Mike Basin model, regulated flow, non regulated (virgin) flow.

1. INTRODUCTION

Rainfall-runoff modelling is simplified representation of real world system, and consists of a set of simultaneous equations or logical set of operation contained within a computer programme with the aim of simulating the end result of hydrological cycle, which is runoff. Hydrologic models especially simple rainfall-runoff models are widely used in understanding and quantifying the impacts of land use changes and to provide information that can be used in land-use decision making (Shoemkar et al., 1997). Various models have been developed by many researchers to study the rainfall-runoff relationship in engineering research and practices. The widely known rainfall-runoff models identified are the Rational method (Mcpherson, 1964), Soil Conservation Services (SCS) Curve Number method (Maidment, 1993), and Green-Ampt method (Green, 1911). The rainfall-runoff modelling is an important tool to deal with various practical problems in water sector such as water resources assessment, design of engineering channels, flood forecasting, predicting population incidents and many other purposes. Water resources development and management in the river basin can be planned by making use of appropriate model. Nash (1958) prepared a conceptual rainfall runoff models by routing a unit inflow through the reservoirs. Kumbhare and Rastogi (1984) tested the Nash conceptual model (1958). Pathak et al. (1984) developed a model to predict runoff volume from small watershed to simulate daily monthly and annual runoff volume. Kumar and Rastogi (1989) developed a mathematical model of the instantaneous unit hydrograph based on time area histogram for

a small watershed at Pantnagar. Mishra and Singh (1998) and Mishra (2000) have worked on SCS Curve Number method.

Rainfall runoff modeling forms an important component of hydrological studies and observed discharge is one the common input required in rainfall runoff modeling techniques to simulate, calibrate and validate the model. Therefore, for model development, the observed discharge data should be the true representative runoff of that river basin. However, when there exists the storage or diversion works on a stream, the flow in the downstream channel is regulated by structures and does not represent the true discharge hence it need to be modified or corrected before setting up the model. The present study has been carried out in the Kharun river, a tributary of Seonath river in Chhattisgarh state to examine the accuracy of the rainfall runoff model when developed under regulated flow condition and non-regulated (virgin) flow condition. The MIKE 11 NAM rainfall runoff model was developed using 15 years observed flow data of Patherdihi G/D site having catchment area 2442 km^2 on Kharun river. The flow regime in Kharun at Patherdihi site is regulated and strongly influenced by regulation operations associated with water transfer from Ravishankarsagar reservoir (on Mahanadi river) into the river and its supply for various usages through the series of anicuts. The non-regulated flow time series at Patherdihi was simulated from the regulated observed flow at Patherdihi by developing Kharun river basin model in MIKE BASIN software using the information on storages, addition, diversion and return flows from irrigation, etc. The MIKE 11 NAM rainfall runoff model was developed under both regulated and non-regulated flow conditions situation and their results were compared.

2. MATERIAL AND METHODOS

Kharun is one of the important tributary of Seonath river basin, a sub-basin of Mahanadi river Chhattisgarh state. The catchment area of Kharun river basin is 4112 km^2. This region is characterized by dense forests at some regions, severe soil erosion and increasing water demands for industries and irrigation. The average annual rainfall in the region is about 1022 mm. The onset of monsoon is usually from July and the season extends up to September, with monsoon peaking during July and August. The Kharun river basin is situated between 20°38' N to 21°36'N Latitude and 81°20' to 81°55'E Longtitude. It originates from Petechua in the south-east of the Durg district and after traversing 129 km through Durg, Raipur and Dhamtari districts, joins Seonath river near Somnath in Raipur district. The index map showing location of Kharun river is given in Figure 1.

Figure 1: Index map showing location of Kharun river in Chhattisgarh

Various researchers have conducted studies to analyze hydrological behavior of river under natural virgin and regulated condition. Maheshwari, et al. (1992) studied the changes in flow regime in term of floods and low flow characteristics of the Murray river in Australia due to increased diversions, construction of dams, weirs and levees and changes in operational procedures using a model developed by the Murray–Darling Basin Commission. McCartney, et al. (2013) in his report summarized the findings of a literature review conducted to find evidence of the flow regulating functions of the major ecosystems in the Zambezi River Basin in South Africa. Kharun is originally an intermittent river having flow during monsoon season and 2-3 months thereafter. To meet the various demands, Kharun is supplemented from Ravishankarsagar reservoir on Mahanadi river to meet the domestic water demand of Raipur city and railways and industrial water demand of Urla and Silthara industrial area (Galkate, et al., 2012). Thus the flow regime in Kharun at Patherdihi site is regulated and strongly influenced by regulation operations associated with it.

Development of rainfall runoff model for regulated flow regime is a big challenge. The flow data needs to be corrected for water transfer effects, storage effects and the diversion of flow and return flow before developing model. Thus the flow data at Patherdihi G/D site on Kharun river, which was considered to be the regulated flow was used to develop rainfall runoff model under regulated and non-regulated (virgin) condition both. First the non-regulated flow time series at Patherdihi was simulated from the regulated observed flow by developing Kharun river basin model in Mike Basin software using the information on storages, addition, diversion and return flows from irrigation,

etc. The Kharun River Basin lelling under both regulated and virgin flow conditions was carried out using MIKE 11 NAM model and results were compared.

2.1 Estimation of non-regulated (virgin) flow

Runoff representing the response of a catchment to precipitation reflects the integrated effect of a wide range of catchment, climate and precipitation characteristics. True runoff is therefore stream flow in the natural condition that is without human intervention. Such as a stream flow unaffected by works of man, such as structure for storage and diversion works on a stream is called virgin flow also called non-regulated flow. When there exists the inter basin transfer, storage or diversion works on a stream, the flow in the downstream channel is affected by structures and hence does not represent the true runoff unless corrected for water transfer effects, storage effects and the diversion of flow and return flow. The complex water transfer system associated with Kharun river flow due to addition of water from Ravishankarsagar reservoir and diversion of water from series of anicuts is shown through schematic in Figure 2.

The water from Ravishankarsagar reservoir is being released into Kharun river from Mahanadi Feeder Canal (*MFC*) through Deorani Jethani Nala. The Mandhar Branch Canal (*MBC*) a major distributor of Mahanadi Main Canal (*MMC*) directly releases water into Kharun river. The water transferred into Kharun river is utilized to meet various water demands like domestic water demand of Raipur city, industrial water demand, water supply for railways and other water demands. The irrigation water supplied through Mahanadi Main Canal (*MMC*) and Tandula Main Canal (*TMC*) in Kharun catchment area also joins the river in the form return flow and has significant contribution to the river flow. In present study the observed flow data of Patherdihi G/d site of CWC was used for the analysis. The flow data in Kharun at Patherdihi could be considered as the highly regulated and influenced due to the associated regulation operations. In order to estimate non-regulated or virgin flow time series using the regulated observed flow at Patherdihi, the Kharun river basin model was developed in Mike Basin software. The data of water releases and diversions at all locations were collected from Water Resources Department, Govt. of Chhattisgarh, Raipur and used in the model. The existing water transfer setup of Kharun river basin was simulated in Mike Basin Model and is shown in Figure 3. Mike Basin is a network model in which the river and their tributaries are represented by network of branches and nodes. The river system is represented in model by digitized river network which can be generated directly in Arc Map 9.1 (DHI. 2003).
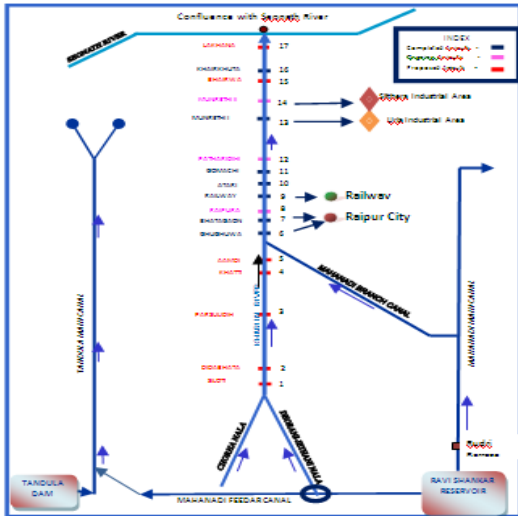
Figure 2: Schematic of Kharun rivers water transfer system

Figure 3: Kharun River Basin Model setup in MIKE BASIN for the estimation of virgin flow

For estimation of virgin flow or non-regulated flow time series at Patherdihi following equations were developed after critically observing the field conditions and existing setup of the Kharun river basin. These equations were then applied in the MIKE BASIN Model and the virgin flow time series at Patherdihi was simulated which was then used to develop rainfall runoff model. Virgin flow or non-regulated flow time series was calculated by accounting the water diverted and added into the Kharun river basin as shown in equation no 1, 2 and 3.

$$Q_{Obs\,virgin} = Q_{Obs\,reguleted} - Q_{Added} + Q_{Diverted} \tag{1}$$

$$Q_{Added} = Q_{MFC} + Q_{MBC} + RF_{TMC} + RF_{MMC} \tag{2}$$

$$Q_{Diverted} = Q_{TO\,Raipur + Railway + Nistar} \tag{3}$$

Where

$Q_{obs\,virgin}$	= Virgin flow at Patherdihi G/D site
$Q_{obs\,regulated}$	= Actual observed flow at Patherdihi G/D site
Q_{MFC}	= Flow from Mahanadi Feeder Canal through Deorani Jethani Nala
Q_{MBC}	= Flow from Mandhar Branch Canal
RF_{TMC}	= Return flow from Tandula Canal System
RF_{MMC}	= Return flow from Mahanadi Main Canal System.
$Q_{Diverted}$	= Water diverted from Raipur city supply, railway and for the purpose of nistari

2.2 Rainfall runoff (RR) modelling

Present study envisages development of rainfall-runoff models in Kharun River using MIKE 11 NAM Model under regulated and non-regulated flow conditions both. The catchment area of Kharun river basin up to Patherdihi is 2442 km^2. A view of Kharun river basin, location of rain gauge stations and gauge discharge sites are shown in Figure 4.

Figure 4: Map of Kharun river basin

2.2.1 Input data

Rainfall and evapotranspiration data are the important inputs used in rainfall-runoff modeling as the runoff volume of a stream is mainly controlled by amount of rainfall and evapotranspiration. Daily rainfall data of 8 rain gauge stations Bhatagaon, Bhilai, Chhati, Gurur, Kurud, Patan, Raipur, Selud were used for NAM model development. Meteorological data like, temperature, sunshine hours, evaporation, wind velocity and humidity were used for estimation of evapotranspiration (*ETo*) by applying Modified Penman Method (1963). Observed flow or discharge data is the very important inputs used in rainfall-runoff modeling. The rainfall runoff modelling was carried out by developing two separate models, first one under regulated flow condition using the observed daily flow data at Patherdihi G/D site and second one under non-regulated flow condition using Mike Basin simulated virgin flow data.

2.2.2 NAM Rainfall runoff model

NAM is the abbreviation of the Danish "Nedbor-Afstromnings-model", meaning precipitation-runoff-model. MIKE11 NAM is professional engineering software developed by Danish Hydraulic Institute (DHI), Denmark. It is deterministic, lumped and conceptual rainfall-runoff model that operates by continuously accounting for the moisture content in three different and mutually interrelated storages that represent overland flow, interflow and base flow (DHI 2003). The physical processes involved for runoff simulation in the model are shown in Figure 5. Fleming (1975); Kjelstrom and Moffat (1981); Kjelstrom (1998), Arcelus (2001), Shamsudin and Hashim (2002) and many other researchers have carried out rainfall runoff modeling studies using MIKE 11 NAM model.

NAM is prepared with 9 parameters, representing surface zone, root zone and ground water storage. U_{max} denotes the upper limit of the amount of water in the surface storage. The soil moisture in the root zone, a soil layer below the surface from which the vegetation can draw water for transpiration, is represented as lower zone storage, L. L_{max} denotes the upper limit of the amount of water in this storage. Evapotranspiration demands are first met at the potential rate from the surface storage. When the surface storage, U spills, i.e. when $U > U_{max}$, the excess water P_N give rise to overland flow as well as to infiltration. Q_{OF} denotes the part of P_N that contributes to overland flow. The interflow contribution, Q_{IF}, is assumed to be proportional to U and to vary linearly with the relative moisture content of the lower zone storage. The interflow is routed through two linear reservoirs in series with the same time constant C_{K1K2}. The overland flow routing is also based on the linear reservoir concept but with a variable time constant. The amount of infiltrating water, G recharging the groundwater storage depends on the soil moisture content in the root zone. The base flow, BF from the groundwater storage is calculated as the outflow from a linear reservoir with time constant C_{KBF}.

2.2.3 Model calibration and validation

MIKE 11 NAM models were setup to carry out rainfall runoff modeling in Kharun river basin at Patherdihi G/d site having average annual rainfall 1147 mm. For development of model under regulated flow condition, the input information of daily rainfall, observed daily flow data and potential evapotranspiration for the period of 15 years from 1993 to 2007 was used. However For development of model under non-regulated flow condition, the input information of daily rainfall, Mike Basin simulated virgin flow data as an observed flow for similar period was used.

The NAM parameters were applied and model was then calibrated, validated and tested for assessing its suitability in selected sub-basin. Calibration is a development of standardizing predicted values, using deviations from observed values for a particular area to derive correction factors that can be applied to generate predicted values that are consistent with the observed values. Such empirical corrections are common in modeling, and it is understood that every hydrologic model should be tested against observed data, preferably from the river basin under study, to understand the level of reliability of the model (Linsley 1982, Melching 1995). NAM rainfall runoff model was calibrated for 8 years period from 1993 to 2000. The model output simulation results during calibration were checked for coefficient of determination (R^2) value and graphically analyzed for degree of agreement between simulated and observed runoff. The model parameters were again adjusted one by one using trial and error method to obtain the set of best fit model parameters.
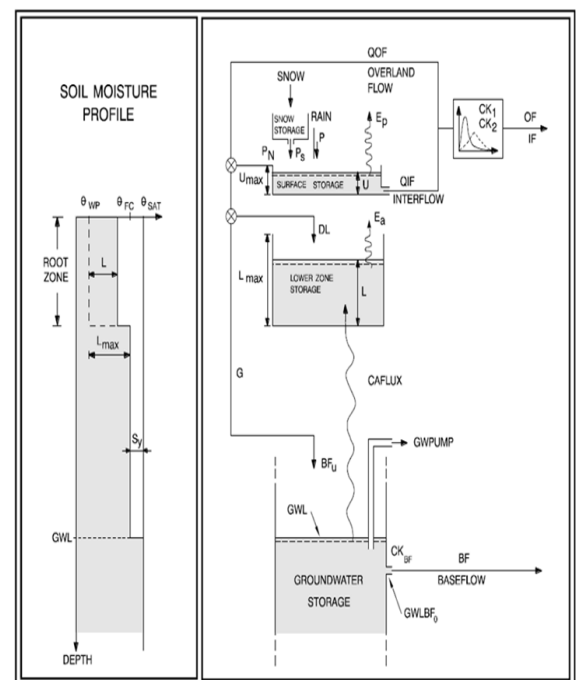

Figure 5: Process of NAM Model

Model validation tests the ability of the model to estimate runoff for periods outside that used to calibrate the model. Once the calibration of a model is completed, it becomes necessary to check that the calibrated parameter values which can be used satisfactorily to simulate events, for the period other than those used for the calibration (Sorooshian et. al., 1983). The MIKE 11 NAM model was validated for the remaining period of 7 years from 2001 to 2007. During validation the set of model parameters obtained during the calibration were used to simulate runoff. The output of the model was checked to verify the capability of the model to simulate the runoff for the extended period of time. The model calibration and validation processes were performed for both cases of modelling i.e. under regulated and non-regulated flow condition.

3. RESULTS AND DISCUSSION

The MIKE11 NAM Model calculates the average rainfall of the study area using weights of the station. In this study the weights of the influencing raingauge station of the study area were identified using Thiessen Polygon application. From the analysis it was observed that average seasonal and annual rainfall in the study area was 1059 and 1077 indicating that the major part of annual rainfall is due to south west monsoon. The monthly rainfall distribution in Kharun basin is shown in Figure 6. Average evapotranspiration (ETo) in the study area was 1548 mm and the ETo during monsoon and non-monsoon seasons were 503 mm and 1045 mm respectively.

Before starting the model development, the reliability of rainfall data was tested by plotting the annual rainfall against the annual regulated and virgin runoff as shown in Figure 7. The correlation coefficient (R^2) for virgin and regulated flow was 0.7745 and 0.77 respectively showing good correlation between rainfall and runoff. Two straight line graphs thus obtained were overlapping, shown the linear relation between rainfall and observed runoff and concluded that the data was consistent to be used further in rainfall-runoff modeling.
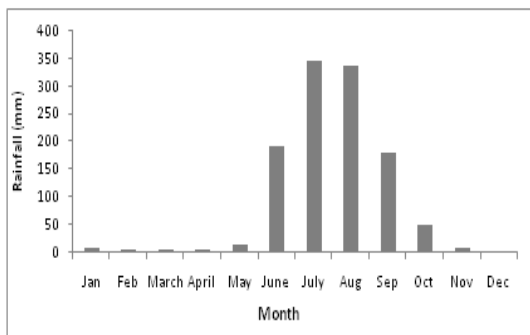

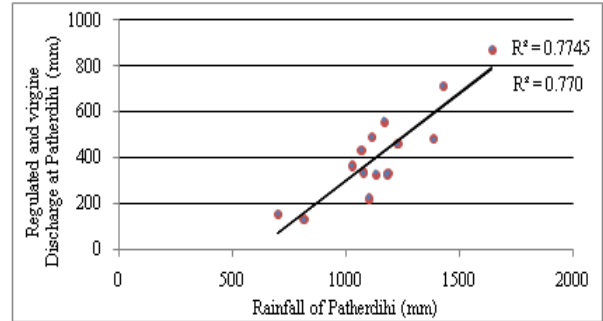**Figure 6:** Rainfall distribution in Kharun basin

Figure 7: Graph showing linear relation between rainfall and regulated and regulated runoff

The MIKE11 NAM model was setup for the Patherdihi G/d site of Kharun river with all input information and calibrated and validated to obtain the set of best fit model parameters which could simulate runoff with high degree of agreement with observed runoff. The set of model parameters were obtained after model calibration and validation under both non-regulated (virgin) and regulated condition as shown in Table 1. The model parameters were observed within their specified range.

The runoff hydrographs for selected period under both non-regulated (virgin) and regulated condition are shown in Figure 8 and 9 respectively. The difference between NAM simulated runoff under non-regulated (virgin) and regulated conditions could not be demarcated clearly. The shapes of the hydrographs of observed and simulated runoff were matching well for almost all the runoff events under both conditions. However, it could be seen that the matching between the observed and simulated runoff was found higher in case of model developed under virgin condition. It can also be seen that the time of beginning and termination of observed and simulated runoff events were matching well whereas the amplification in peak values of runoff events were matching with moderate accuracy. Thus NAM model was found suitable for Kharun river basin for simulation of runoff.

Table 1: Final calibrated model parameters value and range of the NAM Model

Parameter	Description	Parameter Range	Values of the RR Model Parameters	
			Virgin (Non-Reg. flow)	Regulated
U_{max}	Maximum water content in surface storage	10 − 40	40.00	35.00
L_{max}	Maximum water content in lower zone/root storage	100 − 480	299.00	352.00

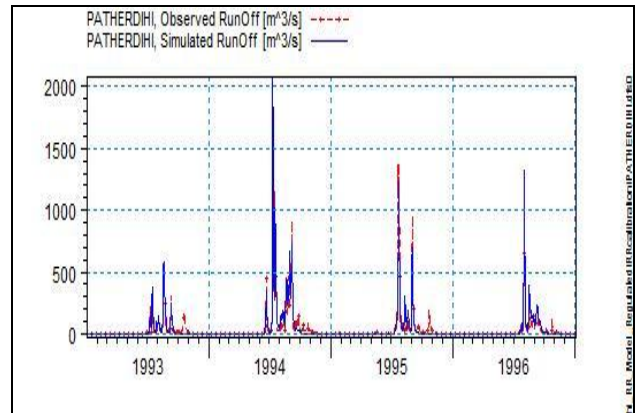|				
C_{QOF}	Overland flow coefficient	0.1 – 1.0	0.85	0.94
C_{KIF}	Interflow drainage constant	200 – 1000	799.00	824.00
C_{K1K2}	Time constant for overland flow and interflow	10 – 50	38.80	38.60
T_{OF}	overland flow threshold	0 – 0.99	0.304	0.314
T_{IF}	Interflow threshold	0 – 0.99	0.566	0.163
TG	Groundwater recharge threshold	0 – 0.99	0.926	0.609
C_{KBF}	Timing constant for base flow	300 – 4000	300.00	1838

Figure 9: Observed and simulated runoff hydrograph during under Regulated Flow condition

Table 2: Accuracy criteria to evaluate model performance

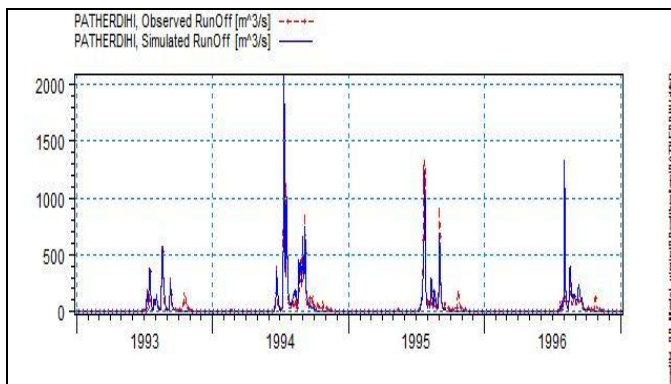| Test of Accuracy	Non-Regulated (Virgin flow)	Regulated Flow
coefficient of determination (R^2)	0.858	0.78
% difference between observed and simulated discharge	3.5 %	6.2 %
Sum of Square of Error (SSE)	4813323	6488005
Efficiency Index (EI),	0.86	0.77

Figure 8: Observed and simulated runoff hydrograph during under Virgin Flow condition

The comparison of results used for evaluation of model simulation capability based on accuracy criteria are given in Table 2. It clearly indicated the model performance under both non-regulated (virgin) and regulated condition.

Accuracy of the model was examined on the basis of coefficient of determination (R^2), Efficiency Index (EI), Sum of Square of Error (SSE) and percentage difference between observed and simulated discharge and compared under regulated and non-regulated flow conditions. It was observed that the R^2 value was increased from 0.78 to 0.858, Efficiency Index was increased from 0.77 to 0.86 and the difference between observed, simulated discharge was reduced from 6.2 to 3.5% and the SSE of the model was found reduced by 25% when model developed under non-regulated (virgin) flow condition indicating good agreement between simulated and observed catchment runoff in terms of the peak flows with respect to timing, rate and volume.

The results indicated that the model accuracy was higher when the model was developed using the non-regulated observed discharge data. It could be concluded that the rainfall runoff model simulation using regulated flow data as an input may lead to inaccurate simulation of river flow which may result in vagueness in water resources planning, thus the observed discharge has to be corrected for various effects like storage, diversions, return flows and other regulation operation associated with the river system to generate non-regulated flow (or virgin flow) to be further used as a model input information.

CONCLISIONS

The rainfall-runoff modelling is used as an important tool to deal with various practical problems in hydrology and water resources development and management, hence it need to develop with high accuracy. The MIKE 11 NAM rainfall runoff model was found efficient and performing well and simulating runoff with high accuracy in Kharun basin. It was proved to be the quick to setup, accurate in runoff simulation and to handle huge data. From the study it could be summarized that, whenever the rainfall-runoff model has to be developed for the river having regulated flow regime due to storage, diversions,

return flows and other regulation operation, it must be developed using virgin flow data set as an input observed data, otherwise it may lead to inaccurate simulation of river flow which may result in vagueness in water resources planning based on it. Mike Basin software was found very useful in river basin model simulation and to simulate virgin flow.

REFERENCES

i.   Arcelus EA (2001) Coupling two hydrological models to compute runoff in ungauged basins. Project Report, National Directorate of Hydrography, Ministry of Transport and Public Works of Uruguay.

ii.   Danish Hydraulic Institute (2003) MIKE BASIN: Rainfall-runoff modeling reference manual. DHI, Denmark,

iii.   Fleming G (1975) Computer simulation techniques in hydrology. Elsevier, New York, 239-252.

iv.   Galkate RV, Mehta P, Jaiswal RK, Thomas T (2012) Water availability assessment in Kharun river under regulated and virgin flow conditions using MIKE BASIN. National Symposium on water Resources Management is Changing Environment (WARMICE-2012), February 8-9, 2012, National Institute of Hydrology, Roorkee.

v.   Green WH and Ampt GA (1911) Studies on soil physics: The flow of air and water through soils. Journal of Agriculture Science, V 4: 1-24.

vi.   Kjelstrom LC (1998) Methods for estimating selected Flow-Duration and Flood-Frequency characteristics at un-gauged sites in central Idaho. Water-Resources Investigations Report, U. S. Geological Survey, Boise, Idaho.

vii.   Kjelstrom LC and Moffat RL (1981) A Method for estimating Flood-Frequency parameters for streams in Idaho. Open-File Report, U. S. Geological Survey, Boise, Idaho.

viii.   Kumar and Rastogi (1989) Determination of direct runoff from a small agricultural watershed. Journal of Agricultural Engineering, vol. 26, 223-228.

ix.   Kumbhare PS and Rastogi RA (1984) Determination of surface runoff from Himalayan watershed using two-parameter conceptual model. 2^{1st} Annual Convocation of ISAE, IARI, New Delhi.

x.   Linsley RL (1982) Rainfall-runoff models - an overview in Rainfall-runoff relationship. Proceedings of the International Symposium on Rainfall-Runoff Modeling, May 18-21, 3-22.

xi.   Maheshwari BL, Walker KF and McMahon TA (1995) Effects of regulation on the flow regime of the river Murray, Australia. Regulated Rivers: Research and Management, 10: 15–38, doi: 10.1002/rrr.3450100103.

xii.   Maidment DR (1993) Handbook of Hydrology. 1st Edition. McGraw Hill, NewYork.

xiii.   McCartney M, Cai X and Smakhtin V (2013) Evaluating the flow regulating functions of natural ecosystems in the Zambezi River Basin. Colombo, Sri Lanka. International Water Management Institute (IWMI), IWMI Research Report 148, 59p, doi:10.5337/2013.206.

xiv.   McPherson MB (1964) Some notes on the Rational method of storm drain design, Tech. Memo. No.6. ASCE, Water Resources Research Program, Harvard University, Cambridge.

xv.   Melching CS (1995) Reliability estimation. In: Computer models of watershed hydrology. Water Resources, Littleton CO, 69-118.

xvi.   Mishra SK (2000) A modified SCS-CN based hydrologic model. National Institute of Hydrology Report, TR(BR)-2.

xvii.   Mishra SK and Singh VP (1998) Another look at 'SCS-CN' method. J. Hydrology Engg., vol. 4, no. 3, ASCE, 257-264.

xviii. Nash (1958) Determination of runoff from rainfall'', Institute of Civil Engineering, Proc., vol. 10, 163-184.

xix.   Pathak P, Swaify SA, Murty VVN and Sudi R (1984) Runoff model for small semi-arid watersheds. 21st Annual Convocation of ISAE, IARI, New Delhi.

xx.   Shamsudin S and Hashim N (2002) Rainfall-Runoff simulation using MIKE 11 NAM. Journal of Civil Engineering, vol. 15, no. 2, 1-13.

xxi.   Shoemaker L, Lahlou M, Bryer M, Kumar D and Kratt K (1997) Compendium of tools for watershed assessment and TMDL development U.S. Environmental Protection Agency, EPA841-B-97-006.

xxii.   Sorooshian S, Gupta VK and Fulton JL (1983) Evaluation of maximum likelihood parameter estimation techniques for conceptual rainfall-runoff models – influence of calibration data variability and length on model credibility. Water Resources Research, 19(1): 251-259.

2d And 3d Analysis Of A Diapgragm Wall Type Berthing Structure Under Static Loading

Yajnheswaran.B[1] Ranjan[2] Dr.Subba Rao[3]

[1]Research Scholar, Department of Applied Mechanics and Hydraulics, National Institute of Technology Karnataka, Surathkal-575025, Mangalore, India
[2] PG Student, Department of Applied Mechanics and Hydraulics, National Institute of Technology Karnataka, Surathkal-575 025, Mangalore, India
[3]Professor, Department of Applied Mechanics and Hydraulics, National Institute of Technology Karnataka, Surathkal-575 025, Mangalore, India

ABSTRACT : Berthing structures are constructed in ports and harbours to provide facilities for berthing and mooring of vessels, loading and unloading of cargo and for embarking and disembarking of passengers and vehicles. Diaphragm walls and anchor rods are sometimes provided to support open berth structures in marine soils .The diaphragm walls are subjected to loads due to the soil layer on one side of the structure. In case of dredging, additional lateral loads are derived from landside earth pressure. In this paper, the deep draft berth of new mangalore port supported with diaphragm wall as shown in Fig.1 is analysed for the loads. The analysis is done using the finite element software PLAXIS 2D and PLAXIS 3D Foundation. The displacement, and bending moment of diaphragm wall of the berthing structure is found due with and without anchor, and the results of the cases are compared. In the case of static loading of the structure, the extreme displacement, and bending moment, of the diaphragm wall is found to be about 0.0734 m, 24936knm/m, in the 2D analysis, and 3D analysis shows 0.0693m.,23550knm/m, respectively. When anchor located at 0m,the displacement, bending moment, reduced to 0.0226m, 11990knm/m, respectively.
Keywords: Diaphragm Wall, Anchor rod, Seismic Analysis, Static loads.

1. INTRODUCTION:

Berthing structures are constructed in ports and harbours to provide facilities for berthing and mooring of vessels, loading and unloading of cargo and for embarking and disembarking of passengers and vehicles. Diaphragm walls and anchor rods are sometimes provided to support open berth structures in marine soils . In this study the behavior of the diaphragm wall and tie

rod anchors subjected to static load is analyzed. By the accurate estimation of the deflection and bending moments induced in diaphragm wall, more cost effective construction procedures may be implemented. Construction of piles and diaphragm wall supporting open type berthing structure on marine soils results in development of time dependent vertical and horizontal sub soil displacement. Where the land side forms an approach to the berthing structure the sub soil displacement may generate axial and lateral loads on the piles and diaphragm walls. Sometimes the lateral loading may lead to structural distress or failure of the structures. Hence the study of effect of lateral loading on the piles and diaphragm wall supported berthing structure is necessary.

Tie rod anchors may be provided in order to strengthen the structure and to resist the lateral loads and reduce the deflection to a large extent. The use of tie rod anchors in berthing structures will reduce the bending moment and lateral deflection and thus the required cross sectional area of the pile and the amount of reinforcement can be reduced resulting in an economical design of the structure.

The mechanism of an anchored wall is complex since the ground, wall and anchors must interact and work together in order to resist earth pressure loads and surcharges developing during and after construction, and restrict deformations to acceptable values. As the wall deflects toward the excavation under the lateral loading, the anchor stretches and initiates the load transfer in the fixed zone. The fixity imposed on the anchorage by the soil restraints further wall deflection. This movement is further controlled if anchors are prestressed.

In the present study the analysis of diaphragm wall is carried out using software PLAXIS 2D and PLAXIS 3D. The diaphragm wall is analysed in the presence and absence of anchor rod. The variation of displacement, and bending moments of the wall throughout the depth is plotted. The extreme displacements and bending moments of the wall are found out for the varying locations of anchor rod to find out the optimum location of the anchor rod. Finally the results obtained from PLAXIS 2D and PLAXIS 3D are compared

1.1 Details of berthing structure and soil data:

The cross section of deep draft berth is shown in Fig.1. The tie rod anchor is inclined at an angle of 45°. The dredge level is from -10 m to -17 m. Hard rock is found at a depth of -30 m. The vertical length of the model is 34.5 m. The chart datum is at 0 m. The width of the berthing structure is 33 m. The berth is supported by a diaphragm wall and 4 rows of 1000mm diameter piles. The piles are terminated at a depth of 30 m. the dredge depth is -10m near the diaphragm wall and -17 m near the first pile as shown in Fig1. In addition, anchor rods are also provided at every 2.5 m.c/c in longer direction.

The different soil layers present in the borehole : fine sand 4.5m to 0m., Medium sand 0m to -6m, Black to bluish clay -6 m to -10 m, Medium sand -10 m to -12 black to bluish clay -12 m to -18 coarse sand -18 m to - 25m are considered for the analysis.
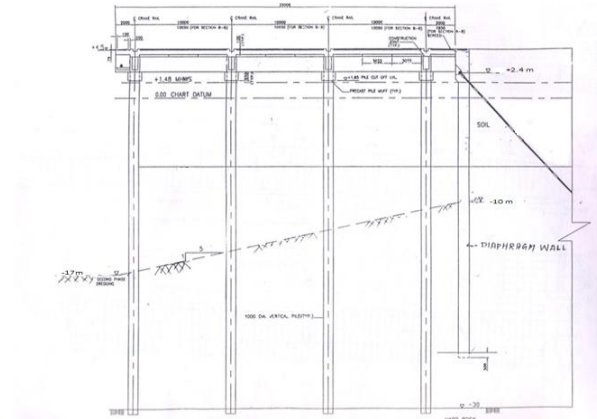

Fig 1:Cross section of Deep Draft Berth of New Mangalore Port

1.2. Loads acting on the structure:

Surcharge- A uniform surcharge of 50 kN/m2 acting on top of the soil and structure. Uniform load of 50 kN/m2 is considered for the analysis because the berth was designed for the load.

Water Pressure- Water pressure acting on the diaphragm wall due to the phreatic level. Since the water level on both the sides of the diaphragm wall is considered to be at the same height in this analysis, differential water pressure is zero.

Self weight – The structural members such as slabs, beams, diaphragm wall and piles are assumed of having a density of 25 kN/m2. PLAXIS 3D accounts for selfweight based on the geometric dimensions (length, depth and breadth) and densities of the structural elements.

Software- The berthing structure is analysed by using finite element softwares PLAXIS 2D AND PLAXIS 3D for static loading considering only the dead loads and live loads acting on the structure. In this study, the entire berthing structure is analyzed, but the forces and moments which are induced only in the diaphragm wall are considered and the variation of the same with the depth of wall are plotted. Finally a comparative study has been made between 2D and 3D analyses.

1.3 Model

The cross section of the model is prepared in the PLAXIS Input window. In2D analysis a plane strain model is used for geometries with a (more or less) uniform cross section and corresponding stress state and loading scheme over a certain length perpendicular to the cross section (z-direction).

Displacements and strains in z-direction are assumed to be zero. However, normal stresses in z-direction are fully taken into account.

To carry out a finite element analysis using PLAXIS 3D, the user has to create a finite element model and specify the material properties and boundary conditions. This is done in the Input program. To set up a three dimensional finite element model, the user must create a two-dimensional geometry model composed of points, lines and other components in the x-z plane. Later the model is extended into three dimension by means of workplanes.The generation of an appropriate finite element mesh and the generation of properties and boundary conditions on an element level is automatically performed by the PLAXIS mesh generator based on the input of the geometry model. Users may also customize the finite element mesh in order to gain optimum performance.The model includes soil strata and structural elements. The length and depth of the model is taken as 66m and 29.5m respectively. The diaphragm wall is modelled as a single panel. The length of the panel is taken as 5m. The diaphragm wall is provided with anchors at a spacing of 2.5 m. In this analysis equivalent sheet pile walls are modeled as beam column elements and soil strata is represented by 15 nodded triangular elements of elastic-plastic Mohr-Coulomb model.
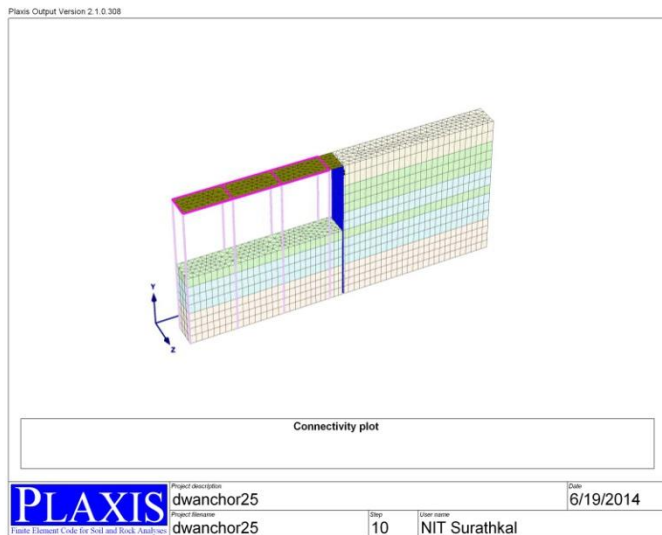

Fig 3: Model of berthing structure in PLAXIS 3D

2.0. STATIC ANALYSIS

The static analysis is carried out for the following cases.Analysis of diaphragm wall in loaded condition in the absence of anchor rod.Analysis of diaphragm wall for varying locations of anchor rod.The different parameters to be inputted into the PLAXIS software include the structural details of the different elements and also the properties of the different soil layers. All the details to be inputted are collected from NMPT.

Table 1. Input Parameters of structural elements

Material	Model	Axial ratio modulus	Rigidity modulus	poisons
Pile	Elastic	4.552E7	5.570E6	0.15
Diaphragm wall	Elastic	1.775E7	6.544E7	0.15
Beam	Elastic	1.775E7	5.324E5	0.15
Rod anchor	Elastic	2.080E10		

Table 2.Input Parameters of soil properties

Material	Model	Young's nodulus	γ_{sat}	N(Nue)	C_{ref}	Φ (phi)
fine sand	Elastic	80000	18.0	0.3	0.5	30.0
medium sand	Elastic	70000	18.0	0.3	0.45	30.0
marine clay	Elastic	20000	18.0	0.49	17.0	0.0
coarse sand	Elastic	60000	18.0	0.25	0.4	30.0

3. RESULTS AND ANALYSIS

3.1 Static analysis-2D

3.1.1 Analysis of diaphragm wall in loaded condition in the absence of anchor rod.

The extreme total displacement in this case was found to be around 0.07342 m. The diaphragm wall in the absence of anchor rod behaves like a cantilever beam with the bottom end fixed. In a cantilever beam, the maximum displacement occurs at the free end which in this case is the top of the wall. So the maximum displacement of 0.07342 m n this case occurs at the top of the diaphragm wall. The variation of displacement of the diaphragm wall with increasing depth of the diaphragm wall is shown in Fig.4.

The variation of bending moment in the diaphragm wall is shown in Fig 5. The extreme value is obtained at the bottom of the diaphragm wall. The bending moment value is dependent on the value of shear force. So the bending moment is zero at the top. The maximum bending moment is obtained at the bottom of the diaphragm wall. The maximum value of bending moment which is obtained at the bottom of the diaphragm wall is 24936 kNm/m.
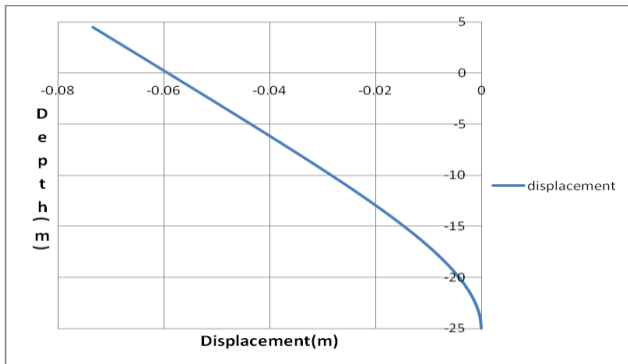
Fig.4 : Variation of displacement of diaphragm wall in static analysis when no anchor is present
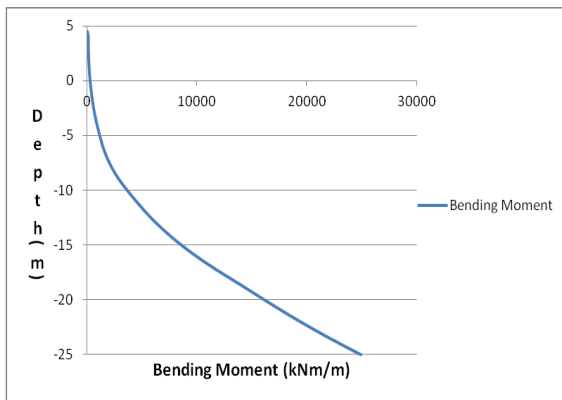

Fig.5: Variation of Bending moments in diaphragm wall in static analysis   when no anchor is present

3.1.2   Analysis of diaphragm wall for varying locations of anchor rod.

The anchor rod is placed at different locations and its effect on the displacement of the diaphragm wall is studied to find the most suitable one. The different locations considered in the analysis are:
i.   At the surface of the structure, at 4.5 m
ii.   At the water table, at 0 m
iii.   At the different soil levels, at 2.5 m, -6m and -10 m
Diaphragm wall acts like a propped cantilever. When the anchor is placed at 4.5 m, it acts like a propped cantilever beam. with bottom fixed and support at the top. So the maximum displacement occurs at the middle with bulging. When the anchor is at 2.5 m, the maximum deflection at the middle is reduced. The anchor position when it is shifted to 0 m, the bulging is still reduced but the wall deflects to the other side. The anchor position when at -6 m, the diaphragm wall deflection is almost same in both the directions. When the anchor position is shifted to -10 m, the deflection pattern of diaphragm wall is almost similar to that without anchor except

that the deflection is considerably reduced at -10 m. It is shown in Fig.6.
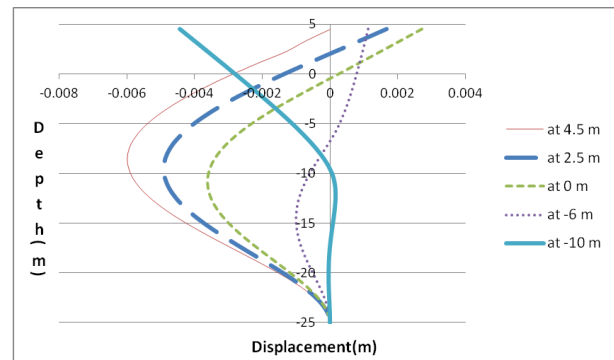
Fig 6 : Depth Vs displacement graph of diaphragm wall in static analysis for varying locations of anchor rod

The variation of bending moment is shown here in Fig.7. The bending moment is initially 0 at the top of the diaphragm wall for the normal case when there is no anchor rod present. At the position where the anchor is placed, the bending moment value increases in the positive direction due to load being taken up by anchor.

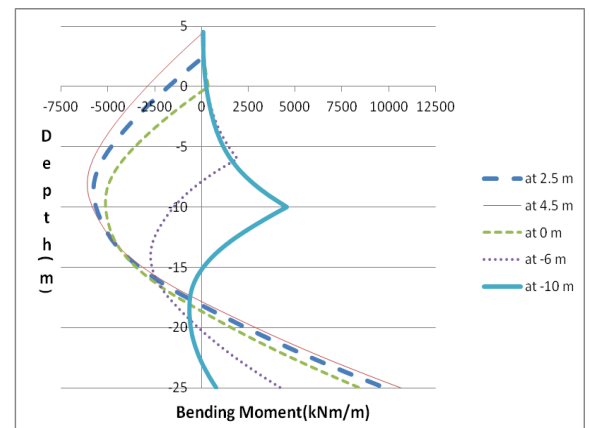Fig.7: Depth Vs Bending Moment of diaphragm wall in static analysis for varying locations of anchor rod

Table 3. Values of Displacement and Bending moment for varying locations of anchor

	4.5m	2.5m	0 m	-6m	-10m.
Total displacement(m)	0.00599	0.00492	0.00362	0.0013	0.00444
Extreme shear force in(kn)	1720	1650	1530	-1160	-1210

Extreme bending moment(knm/m)	-10710	-9800	-8440	-4200	-4560

3.2 static analysis by- 3D

3.2.1 Analysis of diaphragm wall in loaded condition in the absence of anchor rod.

The extreme total displacement in this case was found to be around 0.0693 m. The diaphragm wall in the absence of anchor rod behaves like a cantilever beam with the bottom end fixed. In a cantilever beam, the maximum displacement of 0.0693 m occurs at the free end which in this case is at the top of the wall. The displacement of the diaphragm wall is zero at the bottom. The variation of displacement of the diaphragm all increasing depth of the diaphragm wall is shown in Fig 8.

The variation of bending moment in the diaphragm wall is shown in Fig 9. The extreme value is obtained at the bottom of the diaphragm wall. The bending moment value is dependent on the value of shear force. So the bending moment is zero at the top. The maximum bending moment is obtained at the bottom of the diaphragm wall. The maximum value of bending moment which is obtained at the bottom of the diaphragm wall is 23553 kNm/m.
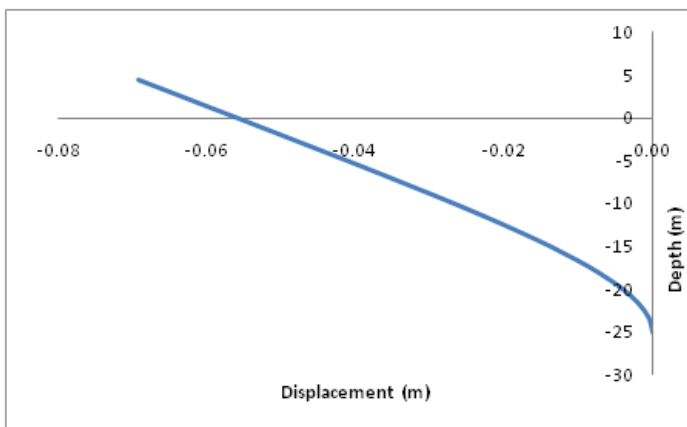

Fig 8 : Variation of displacement of diaphragm wall in static analysis when no anchor is present (Extreme value: --0.0693 m)

Fig 9: Variation of Bending moments in diaphragm wall in static analysis when no anchor is present (Extreme value: 23553 kN-m/m)

3.2.2 Analysis of diaphragm wall for varying locations of anchor rod using PLAXIS 3D.

The simulation of the construction of diaphragm wall supported berthing structure is a complex problem. It involves many stages such as installation of wall, excavation of soil, installation of anchor rod , applying of surcharge load etc. In PLAXIS these construction stages are modelled using staged construction technique (phases). The construction phase in which the diaphragm wall performance is critical(maximum displacement, bending moment and shear force) is considered and the variation of displacement and bending moment is plotted for the critical phase . Generally diaphragm wall supported excavations are provided with anchors to limit the deflection of wall. So in this study the performance of diaphragm wall provided with anchors has been carried out.The anchor rod is placed at different locations and its effect on the displacement and bending moment of the diaphragm wall is studied to find the most optimum location for the installation of anchor rod. The different locations considered in the analysis are:

i. At the surface of the structure, at 4.5 m

ii. At the water table, at 0 m

iii. At the different soil levels, at 2.5 m, -6 m and -10 m

Fig 10 : Variation of Displacement with depth for the diaphragm wall for different anchor rod locations for critical phase

Diaphragm wall acts like a cantilever. From Fig. 10,it is clear that the maximum displacement of the wall occurs at the free end i. e at +4.5 m. From the graph it is seen that the maximum displacement in the wall occurs before the installation of anchor rod for all the cases. The variation of displacement is

almost linear till -10 m then it is parabola. From the graph, it is clear that the maximum displacement occurs when the anchor is at -10 m.
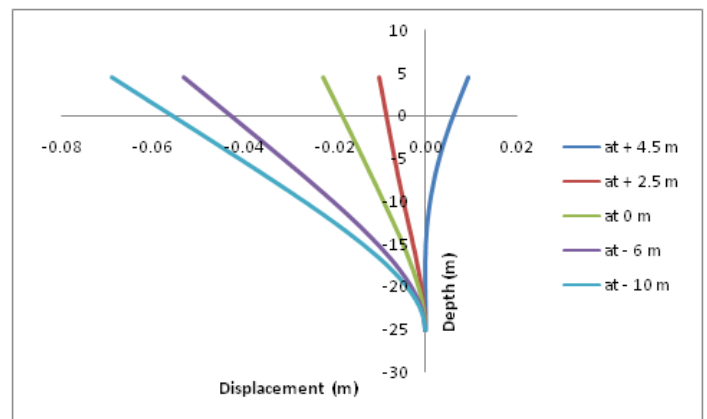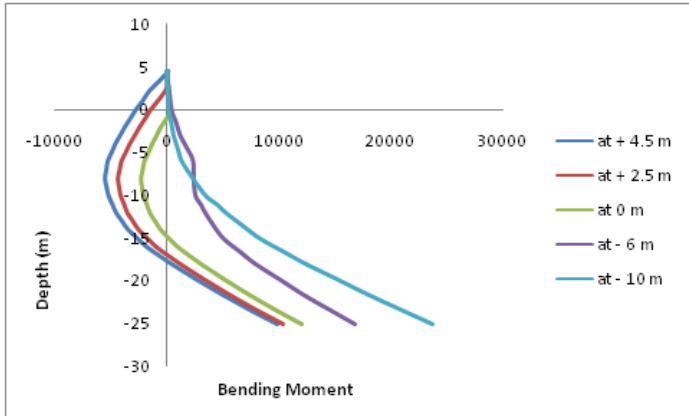

Fig 11: Variation of Bending moment with depth for the diaphragm wall for different anchor rod locations for critical phase

The variation of bending moment is shown here in Fig 11. The bending moment is initially zero at the top of the diaphragm wall for all the anchor locations. At the position where the anchor is placed, the bending moment value increases in the negative direction(hogging bending moment) which is caused due to the prestressing of ground anchor. The bending moment increases in the positive direction after -10m depth, this is due the presence of passive earth pressure. The maximum value of positive bending moment is obtained when the anchor is placed at - 10 m.

Table 4. Values of Displacement and Bending moment for varying locations of anchor obtained from PLAXIS 3D for critical phase.

	+4.5 m	+2.5 m	0 m	-6 m	-10 m
Total Displacement (mm)	9.5 Phase 3	- 10.3 Phase 3	- 22.6 Phase 3	- 53.3 Phase 4	- 69.22 Phase 5
Bending Moment (kN-m/m)	9900 Phase 7	10040 Phase 7	11990 Phase 6	18100 Phase 4	23710 Phase 5

3.2.3 Comparison between PLAXIS 2D AND PLAXIS 3D results

Table 5.The displacement,and bending moment obtained in PLAXIS 2D and PLAXIS 3D.

	PLAXIS 2D		PLAXIS 3D	
	Displacement(m)	Bending moment (kN-m/m)	Displacement(m)	Bending moment (kN-m/m)
Without Anchor	0.07342	24936	0.0693	23553
With anchor	0.0362	8440	0.0226	11990

4. CONCLUSIONS

From 2D analysis it is found the case without no anchor , the maximum displacement of the diaphragm wall is -73.2mm and bending moment is 24936knm/m whereas when an anchor is provided at an elevation of +0.0 m, the maximum displacement of the diaphragm wall is reduced to -36.2mm which occurs at + 4.5 m and bending moment is reduced to 8440knm/m at bottom most depth of diaphragm wall. The displacement is reduced 49,3% and the bending moment is reduced 33.84% when the anchor is provided at +0.0m.   From 3D analysis the displacement of diaphragm wall in the case no anchor   is 69.3mm and with anchor it is reduced to 22.6mm and bending moment is reduced from 23553knm/m to 11990knm/m. The displacement is reduced to 32.61% and the bending moment is reduced 50.9% when the anchor is provided at +0.0m. from this study it is found that the presence of anchor has a significant impact on the stability of diaphragm wall type berthing structure. Similarly the location of anchor is also have an important role in controlling the displacement, moment and the forces on structure.

REFERENCES:

i.   Akhlaghi, T. and Neishapouri, M. (2008), "An investigation into the pseudostatic analyses of the Kitayama dam using FE simulation and observed earthquake-induced deformations", 14th World conference on earthquake engineering, October 12-17, Beijing, China

ii.   Arindam Dey. (2011), "Calibration of a PLAXIS Finite Element Dynamic Model:Effect of Domain Width and Meshing Schemes/AES", Third Indian Young Geotechnical Engineers Conference (3IYGEC), Indian Geotechnical Society, 25 - 26 March, p.127-132

iii.   Atsushi Nozu, Koji Ichii, and Takahiro Sugano. (2004), "Seismic design of port structures", Journal of Japan Association for Earthquake Engineering, Vol.4, No.3 (Special Issue)

iv.   Cilingir, U., Haigh, S. K., Madabhushi, S.P.G. and X, Zeng. (2011) " Seismic behaviour of anchored quay walls with dry backfill", Geomechanics and Geoengineering: An International Journal, Vol. 6, No. 3, September, p.227–235

v.   Deepankar Choudhury, and Syed Mohd. Ahmad. (2007) , "Design of waterfront retaining wall for the passive case under earthquake and tsunami", Science Direct, Applied Ocean Research, p.p 37–44

vi.   Dimitrios C. Konstantakos, Andrew J. Whittle and Bernhard Scharner (2004), "Control of ground movements for a multi-level-anchored diaphragm wall during excavation ", Proceedings of Fifth International Conference on case histories in geotechnical engineering New York, NY, April 13-17,2004.

vii.   Everaars M.J.C. and Peters M.G.J.M. (2013), " Finite Element Modelling of D-wall Supported Excavations", Proceedings of the 18th International Conference on Soil Mechanics and Geotechnical Engineering, Paris 2013.

viii.   Kasinathan Muthukkumaran,and Ranganathan Sundaravadivelu. (20007) , "Numerical modeling of dredging effect on berthing structure", Acta Geotechnical, p.249–259

ix.   Madhuri S, Sannasiraj,S. A., Sundaravadivelu, R. (2005), "Effect of soil structure interaction on the seismic analysis of berthing structures", ArabianCoast

x.   Mojtaba Heidari, and Mahmoud Hassanlou Rad .(2008), "Static and Dynamic Behavior Analysis of Neka Dry Dock Walls, A Case Study", 14th World Conference on Earthquake Engineering, October 12-17, Beijing, China

xi.   Osorio,P., Odenbreit, C. and Vrouwenvelder, T (2010), "Structural reliability analysis of quay walls with steel sheet piles", PIANC MMX Congress Liverpool UK

xii.   Premalatha, P. V. (2009). "Analysing the Optimum Length of Tierod Anchors for a Berthing Structure", Indian Geotechnical Society, Chennai chapter

xiii.   Richard, N. Hwang ., Tsung-Yeh Lee ., Chung-Ren Chou , and Ting-Chiun Su.(2012), "Evaluation of performance of diaphragm walls by wall deflection paths", Journal of geoengineering, Vol. 7, No. 1, April, pp. 001-012

xiv.   Sangseom Jeong , Donghee Seo. (2004), "Analysis of tieback walls using proposed P–y curves for coupled soil spring", Science direct, pp.443-456

xv.   Sitharam.,T .G., Naveen James.,and K .Ganesha Raj.(2012) , "A study on seismicity and seismic hazard for Karnataka State", Journal of earth science systems 121, No. 2, April, p. 475–490

xvi.   Subha, I. P (2012), "Behaviour of an open type berthing structure under earthquake condition-a numerical approach",IJERA, Vol. 2, Issue 1, Jan-Feb, pp.036-040

xvii.   Tschuchnigg F. (2010), "Optimization of a deep foundation with diaphragm wall panels employing 3D FE analysis", Computational Geotechnics Group, Graz University of Technology, Austria.

Approachesof Total Sediment Transport Of Alluvial River:The State Of The Art

Sahita I. Waikhom[1] Dr. S. M. Yadav[2]

[1]Research Scholar (Associate Prof.), Civil Engineering Department, Government Engineering College, Surat-395001, Gujarat, India
[2] Prof., Civil Engineering Department, SardarVallabhbhai National Institute of Technology, Surat-395001, Gujarat, India
Email: siwgecs@gmail.com

ABSTRACT : Alluvial streams invariably carry sediment with water. The stability of a stream is closely linked with the sediment transport rate.Knowledge of Sediment Transport Rate or "Sediment Transport Capacity" is necessary for in-depth study of many alluvial-river processes, like flooding which is significant for design and operation of hydraulic structures, like dams. Sediment transported by a stream is a function of flow, fluid and sediment characteristics. Correct prediction of transport capacity of streams is challenged by mainly two facts: dynamic nature of rivers with complex flow conditions and correlation of flume observations and result with natural streams. Moreover these developed relationships cannot be applied uniformly to all the streams. Du Boys, Einstein and Van Rijn have developed various approaches for finding Bed Load, Suspended Load and Total Load transport rate. The total sediment transported can be computed by considering the total load either as sum of suspended load and bed load or measured load and unmeasured load. Such methods areknown as microscopic methods, e.g. Einstein's method. In "modified Einstein methods", such as Colby and Hembree's, the original predictive Einstein function has been modified to a non predictive function for the estimation of unmeasured load based on measured suspended load for predicting total bed-material load. Some researchers argue that the process of suspension is an advanced stage of traction along the bed, therefore total sediment transported should be related primarily to the shear parameter and distinctions need not be made between bed load and suspended load. These methods, described as macroscopic method, are based on dimensional analysis, intuition or complete empiricism. Most of these methods use a single representative size for the entire mixture ignoring the possibility of partial transport. Researchers like Laursen, Ackers and White, Engelund-Hansen, Yang, etc., believed in this approach. The present study discuss the findings, suitability and limitations of various sediment transport formulas in predicting total sediment transport rate of alluvial stream.

Keywords:Sediment Transport Rate, Total sediment transport approaches, Suitability and Limitations of sediment transport approaches.

1. INTRODUCTION

Sediment transport in natural rivers has been widely studied in the past few decades and there are many theoretical or empirical formulas based on many concepts like probabilistic and stochastic,dimensionally homogeneousstream power (Particle size and shear velocity)unit stream power,numerical modelling, regression analysis etc.that can be used with reasonable accuracy to predict the transport rate of an alluvial river. Some comparative studies have been done to test the predictability of various sediment transport methods covering a wide range of flow conditions and sediment types. But, the accuracy of computational sediment transport models has remained a "challenging question" still. Every formula has its own requirements and limitations. In the present paper, only the total load transport rate is discussed.The total load is the sum of the bed load, suspended load and wash load. In flume experiments, except in special cases, wash load is absent and total load is considered to be the bed-material load. On the other hand, in natural streams wash load is invariably present and the total load is the summation of the bed-material load and the wash load. Further, it is difficult to separate out the wash load from the measured total load. Thus the difference in the nature of laboratory and field data, as mentioned above, makes it difficult to unify the total load data collected in the laboratory and predicted in the field. But a majority of the total load relationships are based mainly on flume data and river data in which wash load is excluded from the measured total load and as such these relationships can be expected to yield the bed-material load.Thus the total load carried by the stream is the sum of suspended load and bed load transported per unit time per unit width of channel. Suspended load and bed-load can be calculated for different fractions of the bed material and added to get the total load. For many morphological studies such refined calculations may not be needed. If all size fractions are moving these methods can also be used for fraction wise sediment transport, however the results are approximate because coarser particles are not included in these methods.

2.METHODS FOR FINDING TOTAL SEDIMENT.

The methods of computation of the total sediment transport rate can be broadly classified into two categories as: i) Microscopic Methods and ii) Macroscopic Methods.

2.1Microscopic method

In thismethod, the total sediment load is subdivided either into suspended load and bed load or into measured load and unmeasured load. Since the suspended sediment sampler cannot sample the entire depth of the stream, some suspended load and the bed load remain un-sampled. This is designated as unmeasured load. Addition of the measured and the unmeasured load gives the total load.Einstein (1950), Colby and Hembree(1955), Bagnold (1966),Hsieh W. Shen and Gary S. Hung(1983),Van Rijn (1984 a,1984b), Samaga et al.(1986 a,

1986 b) and Swamee and Ojha (1991) are some of the microscopic approachesreviewed through literature. The salient features of these investigations and the final relationship are given in Table 1.

Table 1: Total load (bed material load) equation proposed byResearchers (Microscopic Approaches)

Sr. No.	Researchers	Year	Formula
1	Einstein	1950	$q_b = \phi . \gamma_s \left(g\, \Delta d_s^{\,3} \right)^{0.5}$ $q_s = \dfrac{\gamma_s}{100} 11.6\, u'_* \, C_{2d} 2d \left\{ 2.3 log \left(\dfrac{30.2\, Dx}{d_{65}} \right) \right.$
2	Bagnold	1966	$q_t = q_{bw} + q_{sw} = \dfrac{\gamma_s - \gamma}{\gamma} \tau V$
3	Van Rijn	1984a,b	$q^*_b = 0.53(s-1)^{0.5} g^{0.5} d_s^{\,1.5} D_*^{\,-0.3} T^{2.1}\ if\ T$ $q^*_b = 0.1(s-1)^{0.5} g^{0.5} d_s^{\,1.5} D_*^{\,-0.3} T^{2.1}\ if\ T$
4	Samaga .et al	1986	$\Phi_{bi} = 3.62 \times 10^7 (\tau'_{*i})^8$ for $\tau'_{*i} \le 0.065$ $\Phi_{bi} = 8.5(\tau'_{*i})^{1.8}/$ $[1 + 5.95 \times 10^{-6} 10_i\ (\tau'_{*i})^{-4.7}]^{1.45}$ $\tau'_{*i} > 0.065$
5	Swamee and Ojha's	1991	$\Phi_{Bs} = \dfrac{q_B}{\gamma_s\,(\rho_s/\rho_f - 1)^{1/2} g^{1/2} d_s^{\,3/2}}$ and $\Phi_{Ss} = \dfrac{q_s}{(\rho_s/\rho_f - 1)^{1/2} g^{1/2} d_s^{\,3/2}}$
6	Wu Wang and Jia	2000	$q^*_k = \emptyset_{bk}\, P_{bk} \sqrt{ \left(\dfrac{\gamma_s}{\gamma} - 1 \right) g\, d^3 }_k$ and $q_{si} = \emptyset_{si} \sqrt{\Delta g D_i^{\,3}}$

2.2 Macroscopic method

In macroscopic methods the total sediment transport rate is primarily related to the shear parameter and no clear distinction is made between bed load and suspended load, since some of the researchers believe that the process of suspension is an advanced stage of traction along the bed. The relationships proposed under this category are based on dimensional analysis, intuition, or complete empiricism. Essentially, most of these methods use a single representative size for the entire mixture and thereby ignore the possibility of partial

transport.Laursen(1958),Garde and Albertson (1958),Garde and Dattatri (1963),Colby (1963),Bishop, Simons and Richardson's Method(1965),Engelund and Hansen's (1967),Graf and Acaroglu (1968),The Toffaleti (1968),Graf (1971),Shen and Hung (1972),Engelund-Hansen (1972),Ackers and White's (1973),White et al. (1973),Yang(1984),Brownlie (1981),Karim and Kennedy (1990),Shu-Qing Yang and Siow-Yong Lim(2003), S. K. Sinnakaudan et.al (2006)are some of the researchers whose sediment transport function comes under macroscopic approaches as observed in literature. The salient features of these investigations and the final relationship are given in Table 2.

Table 2: Total load (bed material load) equation proposed by Researchers (Microscopic Approaches)

Sr. No	Researchers	Year	Formula
1	Laursen	1958	$C = 10^4 \sum_{i=1}^{n} i_b \left(\dfrac{D_{si}}{d}\right)^{7/6} \left[\dfrac{V^2}{58\, Y_C D_{si}(S_g}\right.$
2	Garde and Albertson	1958	$\dfrac{u_* D}{v}\, \dfrac{1}{C_v^{1/3}} = f\left(\dfrac{D}{d}\dfrac{1}{\eta}\right)^{1.5}$
3	Garde and Dattatri	1963	$q_T / (\gamma_s u_* d) = f(\tau_*)$ or $q_T / (\gamma_s u_* d) = 16.6(\tau_*)^{4.0}$
4	Colby	1963	$g_s = A(V - V_C)^5\, 0.67$
5	Bishop, Simons and Richardson's	1965	$\Phi_T = \dfrac{q_T}{\rho_s (\rho_s/\rho_f - 1)^{1/2}\, g^{3/2}\, d_s^{3/2}}$
6	Engelund and Hansen	1967	$\varnothing = \dfrac{q_t}{\gamma_s}\left[\left(\dfrac{\gamma_s-\gamma}{\gamma}\right)gd^3\right]^{-1/2}$
7	Graf and Acaroglu	1968	$q_T / (\gamma_s u_* d) = 10.39(\tau_*)^{2.02}$
8	Toffaleti	1968	$g_{ssL} = M\, \dfrac{(R/11.24)^{1+n_v-0.756z} - (2d_m)^{1+n}}{1+n_v-0.756z}$ $g_{ssM} = M\, \dfrac{(R/11.24)^{0.244z}\,[(R/2.5)^{1}}{1+n}$ $g_{ssU} = M\, \dfrac{(\frac{R}{11.24})^{0.244z}(\frac{R}{2.5})^{0.5z}[R^{1+n_v-1.5z}}{1+n_v-1.5z}$ $g_{sb} = M\,(2d_m)^{1+n_v-0.756z}$ $g_s = g_{ssL} + g_{ssM} + g_{ssU} + g_{sb}$
9	Graf	1971	$\Phi = 10.39(\Psi)^{-2.52}$
10	Shen and Hung	1972	Log C_t = -107,404.45938164 + 324,214.74734085Y - 326,309.58908739Y^2 + 109,503.87232539Y^3
11	Engelund-Hansen	1972	$g_s = 0.05\, \gamma_s V^2 \sqrt{\dfrac{d_{50}}{g(\frac{\gamma_s}{\gamma}-1)}} \left[\dfrac{\tau_0}{(\gamma_s-\gamma)d_{50}}\right]^{3/2}$
12	Ackers and White's	1973	$G_{gr} = C\left(\dfrac{F_{gr}}{A} - 1\right)^m$ $F_{gr} = u_*^{n} gd\left[\left(\dfrac{\gamma_S}{\gamma} - \right)gd\right]^{-1/}$ $d_{gr} = d\left[\dfrac{g\left(\frac{\gamma_S}{\gamma}-1\right)}{v^2}\right]^{1/3}$
13	White et al	1973	Graphical solution
14	Yang Approach	1973,1979,1984	$\log C_t = 5.435 - 0.286 \log \dfrac{\omega d_m}{v}$ $\left(1.799 - 0.409 \log \dfrac{\omega d_m}{v} - 0.3\right.$ for sand $d_m < 2$mm $\log C_t = 6.681 - 0.633 \log \dfrac{\omega d_m}{v}$ $\left(2.784 - 0.305 \log \dfrac{\omega d_m}{v} - 0.28\right.$
15	Brownlie	1981	$\overline{C_T} = 7115 C_F\left[\dfrac{U}{\sqrt{\frac{\Delta\gamma_s}{\rho_f}d}} - \dfrac{U_{cr}}{\sqrt{\frac{\Delta\gamma_s}{\rho_f}d}}\right.$
16	Karim and Kennedy	1990	$\log \dfrac{q_s}{(1.65g\, d^3{}_{50})^{1/2}} = -2.279 + 2.972 \log \dfrac{v}{(1.65g\, d_{50})^{1/2}} +$ 1.060 $\log \dfrac{v}{(1.65g\, d_{50})^{1/2}}\, \log \dfrac{u_*}{(1.65}$
17	Shu-Qing Yang and Siow-Yong Lim	2003	$g_t = k\left(\dfrac{\gamma_s}{\gamma_s-\gamma}\right)\tau_0\left(\dfrac{u_*' - u_{*c}^2}{\omega}\right)$

| 18 | S. K. Sinnakaudan et. Al | 2006 | $C_v = 1.811 * 10^{-4} \left(\dfrac{VS_o}{\omega_o}\right)^{0.293}$ (|

The summary of the various total bed material load equation developed by many researchers and the applicability ranges are presented in Table 3and 4.

Table 3:Transport Functions and their approaches (Microscopic)

Sr. No	Researchers	Year	Approaches/ Basic Concept	Applicable to particle size(mm)
1	Einstein	1950	Probabilistic and Stochastic (Complex computation using a large number of graphs)	greater than or equal to 0.065
2	Bagnold	1966	Energy exchange(Stream power)Analytical Equations, Dimensionally homogeneous	greater than or equal to 0.015
3	Van Rijn	1984a,b	Numerical modelling, Regression analysis	0.2 to 2.0 for bed load and 0.1 to 0.5 for suspended load
4	Samaga .et al	1986	Modification of Einstein 1950 function	greater than or equal to 0.065
5	Swamee and Ojha's	1991	Empirical relation	Nonuniform sediment size
6	Wu Wang and Jia	2000	Probabilistic , Stochastic and Regression analysis	0.088 to 28.7mm

Table 4:Transport Functions and their approaches (Macroscopic)

Sr. No	Researchers	Year	Approaches/ Basic Concept	Applicable to particle size(mm)
1	Laursen Bed-Material Load Formula	1958	Empirical relation based critical bed shear stress(functions of stream and sediment characteristics)	Coarse silt to very coarse sand range.
2	Garde and Albertson	1958	Based on Laursen 1958	Coarse silt to very coarse sand range.
3	Garde and Dattatri	1963	-	0.011 mm to 0.93 mm
4	Colby	1963	Einstein's (1950) bedload function as a guide	sand-size 0. 1 to 0.8 mm.
5	Bishop,Simonsand	1965	-	-

Sr. No	Researchers	Year	Approaches/ Basic Concept	Applicable to particle size(mm)
	Richardson's			
6	Engelund and Hansen	1967	Potential energy	0.19 to0.93 mm
7	Graf and Acaroglu	1968	-	-
8	Toffaleti	1968	Modification of Einstein 1950 function. Probabilistic (breaks load into vertical zones, representing two dimensional sediment transport)	Sediment size as small as 0.095 mm but works best for medium sand to coarse gravel range (0.25mm to 32mm)
9	Graf	1971	-	-
10	Shen and Hung	1972	Regression approach	-
11	Engelund-Hansen	1972	Bagnold's Stream power (Particle size and shear stress)	Very coarse silt to very coarse sand range.(0.065 to 2.0 Sand transport)
12	Ackers and White's	1973	Stream power (Particle size and shear velocity)	0.04 to 4 mm
13	White et al	1973	-	-
14	Yang Approach	1973,1979,1984	Unit stream power	Sand2.0 to 10.0 mm gravel transport
15	Brownlie	1982	Regression	-
16	Karim and Kennedy	1990	Non linear Regression approach	-
17	Shu-Qing Yang and Siow-Yong Lim	2003	-	-
18	S. K. Sinnakaudan et. Al	2006	Multi linear Regression approach	0.37–4.0 mm

3. COMPARITIVE EVALUATION OF SEDIMENT TRANSPORT FUNCTION

White, Milli, and Crabe (1975) reviewed and compared sediment transport theories based on over 1,000 flume experimentsand 260 field measurements.It isobserved from comparisons (considering only total load functions)that Ackers and White's (1973) equation is themost accurate, followed by Engelund and Hansen's (1972), Einstein's (1950),Bishop, Simons, and Richardson's (I965), Toffaleti's (1969), Bagnold's (1966)

Yang and Molinas (1982)tested seven total-load formulas (Ackers and White 1973; Colby and Hembree1955; Engelund and Hansen 1967; Maddock 1967; Shen and Hung 1972;Yang 1973; Yang 1979) for six river stations, bed materials of whichare characterized by sand-range sediment. Yang concluded that the predictorsproposed by Ackers and White, Engelund and Hansen, and Yang arefar more reliable than the

others and also shown theoretically that bedload and suspended load,as well as total load, are directly related to unit stream power.

Shen and Hung (1983) compared suspended-sediment discharges computed using the modified (Colby and Hembree1955) and remodified (Shen and Hung 1983) Einstein predictors withthe measured values for three large natural rivers, and concluded that theirnew remodified Einstein procedure was found to yield better results than themodified Einstein procedure.

Lau and Krishnappan (1985) also tested fiveformulas (Ackers and White 1973, Einstein 1950, Bagnold 1966, Lau andKrishnappan 1985,Yang 1976) using their laboratory sediment-discharge data.The Ackers and White formula was found to predict the sediment dischargereasonably well for the range of flows tested. All the other formulas were found to overpredict the sediment discharge, the Einstein method gave the highest values, and Bagnold's predictionswere between Einstein's and Yang's.

Van Rijn(1984) developed and testedhis formulas as well as the Ackers and White (1973), the Meyer-Peter andMueller (1948), the Engelund and Hansen (1967) and the Yang (1973) formulasusing extensive flume and field data. It was concluded that althoughhis formulas' predictions were the best among those tested, total-load predictionswith accuracies less than a factor of two cannot be achieved due toinaccuracies in various controlling parameters.

Nakato (1987) tested five sediment-discharge formulas,including those of Ackers and White (1973), Engelund and Fredsoe (1976),Engelund and Hansen (1967), Inglis and Lacey (Inglis 1968), and Toffaleti(1969), for a reach of the San Dieguito River that was studied by the NRCCommittee, and compared the results with those computed by Chang (1984)using the Graf formula (1971). The largest discrepancy,amounting to more than one-hundred-fold, was found between theGraf and Toffaleti formulas.

TatsuakiNakato(1990)tested eleven existing, sediment-transport formulas against thefield data measured at two United States Geological Survey (USGS) gauging stationsalong the Sacramento River in California, whose bed-material sizes are classifiedas those ranging from fine sand to coarse gravel. TheAckers-White formula failed to predict total-load discharges only in two casesout of the 29 flow events (ButteCity). Engelund-Hansenformula was able to predict sediment dischargesfor all the flow events. Except for four data points, slight overpredictions by Karim's total-loadformula are observed. BecauseKarim's formula is for the total load, an overprediction against the measuredsuspendedsediment discharge is expected.Van Rijn's suspended-load predictorresulted in a wide range of scatters. Yang's (1973) predictions of the total-load discharges seem to bevery close to

the measured suspended-load discharges at a higher range ofq$_{sm}$; however, they are seen to be much greater at a lower range of q$_{sm}$. Both the Toffaleti and Yang formulas were able to predict sedimentdischarges for all the flow events.

R. L. Misri, R. J. Gardeand K. G. Ranga Raju(1984) observed thatEinstein's bed load function does not accurately predict the transportrates of individual fractions in a mixture and this is primarily becausehis correction for sheltering effect is at variance with experimentaldata.

Weiming Wu, Sam S.Y. Wang and YafeiJia (2000)formulas have been tested against a wide range of laboratory and field data consisting 1859 sets of uniformbed-material load data selected from Brownlie's (1981)data collection by limiting the standard deviation of bed material less than 1.2 and the Shields parameter $\theta > 0.055$ and comparedwith several other existing empirical methods. Comparison of the calculated and measured transport rates was done along with testing of three widely used bed-material load transport formulas developed by Engelund and Hanson (1967), Ackers and White (1973), and Yang (1973, 1984) using the same data set .It was found that the newly proposed formulas provide very good results.

P. Van der Scheer,J.S. Ribberink and A. Blom (2002)studied behaviour of transport formulas and verification with data was also studied. Among the selected formulae, the formula of Wu et al. (2000) found to be the best formula to predict transport ofnon-uniform sediment. The formula has large validity ranges due to the largeamount of data that was used for the original calibration of the formula. The formulashows stable behaviour concerning the transport rate and the transport composition.Even outside the validity ranges of the formula, it gives good predictions.

5. LIMITATIONS AND SUITABILITY

Yalin (1977) gives an extensive discussion aboutEinstein bed load function. Herein a brief description of Yalin's argument is given:
"Einstein assumes that the average jump length, L, is constant and equal to100ds. However, no experimental evidence or theoretical justification is given insupport of this assumption. In fact available evidence suggests that jump lengthincreases with increasing dimensionless shear stress. Van Rijn (1984a) has alsoshown that L/d$_s$ varies with particle size and flow shear stress.

Einstein considers the time interval, T proportional to d_s/ω, and in his statementthere appears to be no relation between T and turbulence characteristics. Yalinshows that T, which is a property of the frequency of the jumps, must depend onthe turbulence parameters and should be proportional to d_s/u_*.

Engelund and Hansen's (1967) derivation is directly based on bed load transportphenomenon. Their fundamental postulation

that in the case of a dune bed, the movingparticles are elevated to a height comparable to the dune height is essentially applicable whenonly bed load particles are involved. However, Engelund and Hansen used this assumptionfor developing total load equation, which includes both bed and suspended loads.Engelund and Hansen also assumed that the particle velocity, for the whole sedimentmaterial in transport, is proportional to the bed shear velocity. This assumption is againmostly applicable to the bed load particles and cannot be considered as a good descriptionfor the velocity of suspended solids. In general the velocity of suspended particles in thedirection of the flow, is closely proportional to the velocity of the surrounding fluid. **Garde and Ranga Raju (1985)** also stated that the mechanism conceived by Engelund and Hansen does notdescribe the physical processes of suspended load transport adequately. Also, Engelund and Hansen's did not consider the effect ofviscous forces on the transportation of sediment particles.

Toffaleti (1969)did not offer either experimental evidence or theoretical explanation tosupport the validity of bed load equation. Hence,Toffaleti'sprocedure should be carefully used for predicting transport rates of bed load, especially inthose natural rivers or laboratory flumes where the flow is carrying only bed load or themajor part of the moving material is bed load, i.e. for rivers with low energy gradients.In fact,Toffaleti's model is only applicable to sand transport, i.e. particles in range0.065mm to 2.0mm which are mostly transported in suspension.

Rijn (1984a) suggested that the proposed expressions of bed load concentration andtransport rate, are applicable to the sand grains with diameterbetween 0.2mm and 2.0mm. However, in natural streams with high energy slope, bedloads mostly include gravel particles, which are greater than 2.0mm in diameter.**Rijn's (1984b)** expression of suspended load is applicable to theranges of natural streams where the bed shear stresses are big enough to lift sandparticles with diameter larger than 0.5mm into the suspension mode.

Although **Samaga et al(1986)** relate the transport rate of bed load particles to bed shearstress due to grain roughness, suspended load transport is related to the overall bed shearstress. This is consistent with natural conditions, where both the grain and bed formroughness are effective in production of turbulence which is responsible for suspension.In general the Samaga et al method lacks simplicity and uses several parameters correction factors to be read from a number of tables and graphs. This not only makescomputations difficult but reduces the accuracy of calculations at each stage. Such aprocedure is very time consuming for engineering applications.

6. CONCLUSIONS

For the transportation of fine sand, the best predictions were consistently obtained using the proposed total load formula and Yang's unit stream power equation. Especially when fine sands were transported under high velocitycondition these two approaches indicated very satisfactory predictions (with scores upto 100%) and are hence recommended for similar conditions.

Depending on the hydraulic conditions, Engelund and Hansen's theory producedvery variable results, from over-prediction for the cases of movement of small particlesunder high velocity conditions to under-estimation for the transportation of mediumsands in the laboratory flume studies of Samaga et al. This suggests that Engelund andHansen's theory should be used with caution.

Despite the complicated procedure and large number of correction factors adopted,the established theory of Einstein failed to produce satisfactory predictions in most ofthe applied cases and always over-estimated the transport rates. In particular, Einstein'sprocedure is not recommended for application to particles smaller than 0.15mm indiameter.

The Samaga et al procedure tends to under-estimate the sediment discharges,especially for fine bed material. Even for Samaga et al data, thisprocedure underestimatedboth bed and suspended load transport rates.

Toffaleti's procedure may not be used for predicting bed load, especially whenthe flow is carrying only bed load or the major part of the moving sediment is bed load. As such,Toffaleti's model is only applicable to sand transport, i.e. particles in the range of 0.065mm to 2.0mm which are mostly transported in suspension (Habibi, 1994).

The total load theory of Ackers and White produced satisfactory results,especially for the transportation of fine to medium sands. However, in application tohigh velocity conditions, Ackers and White's equation over-predicted the transport ratesand resulted in unsatisfactory scores.

Rijn's expression for bed load transport is valid only for the sediment particles in the range of 0.2mm to 2.0mm, which covers transportation of sand grains. However, innatural streams with high energy slope, bed loads mostly include gravel particles,which are greater than 2.0mm in diameter. For these conditions Rijn's theory is notapplicable. On the other hand, Rijn's expression for suspended load is applicable onlyto sand particles in the range of 0.1mm to 0.5mm. Again this equation does not coverthose ranges of natural streams where the bed shear stresses are large enough to liftsand particles with diameters larger than 0.5mm into the suspension mode.

Yang showed that dimensionless unit stream power (DUSP) is the best parameter to be correlated with the total sediment concentration. This is probably the most valuable finding of Yang over two decades of investigation. Theoretically, DUSP

contains the particle characteristics including size, shape and density, as well as the flow parameters including mean velocity and energy slope.

REFERENCES:

i. Ackers, P. and white, W.R. (1973), "Sediment transport: A new approach and analysis", J. of Hydraulics Division, ASCE, 99(HY11), pp.2041–2060.

ii. Bagnold, R.A. (1966), "An approach to the sediment transport problem from general physics", U.S. Geological Survey Professional Paper 422-J.

iii. Bishop, A. A. Simons, D. B. and Richardson, E. V. (1965), "Total Bed Material Transport", Proc. ASCE, Vol. 91, No.HY2, March, pp. 175-19.

iv. Brownlie, W.R. (1981), "Compilation of fluvial channel data: laboratory and field", Rep. No. KH-R-43B, W.M. Keck Lab. of Hydr. and Water Resources, California Institute of Technology, Pasadena, Calif.

v. Colby, B.R. and Hembree, C.H. (1955), "Computations of Sediment Discharge, Niobrara River near Cody, Nebraska". US Geological Survey Water Supply Paper 1357.

vi. Colby, B.R. (1963), Fluvial sediments – a summary of source, transportation, deposition, and measurement of sediment discharge, United States Geological Survey Bulletin 1181A

vii. Einstein, H.A. (1950). The Bed Load Function in Open Channel Flows. United States Department of Agriculture, Soil Conservation Service, Technical Bulletin No. 1026.

viii. Engelund F. and Hansen (1967), Hydraulic resistance of alluvial streams (Closure to discussion), Proceedings of the American Society of Civil Engineers, Journal of the Hydraulics Division, Volume 93. No.4. pp 287 – 296.

ix. Engelund, F. and Hansen, E. (1972),A Monograph on Sediment Transport in Alluvial Streams, TekniskForlag, Copenhagen, Denmark.

x. Garde, R. J., Bondurant, D. C. and Albertson, M. L. (1958), Discussion of Laursen (1958), JHD, Proc. ASCE, vol.84, No.H

xi. Garde, R.J. and J. Dattatri (1963), Investigations of the Total Sediment Discharge of Alluvial Streams. University of Roorkee Research Journal, Roorkee (India), Vol. VI, No. II,

xii. Garde R. J. and Ranga Raju K. G. (1985), Mechanics of Sediment Transportation and Alluvial Problems, Wiley Eastern Limited, New Delhi, 2nd edition.

xiii. Graf, W.H. and E.R. Acaroglu(1968). Sediment Transport in Conveyance System. Bulletin of International Association of Scientific Hydrology, Vol. 13, No. 2,

xiv. Graf W.H. (1971), Hydraulics of sediment transport, McGraw Hill, New York.

xv. Karim, M.F., and J.F. Kennedy (1990).Means of Coupled Velocity and Sediment-Discharge Relationships for Rivers, Journal of Hydraulic Engineering, ASCE, vol.116, no. 8, pp 973-996.

xvi. Laursen, E.M. (1958). The total sediment load of streams. Journal of Hydraulic Division, ASCE 84(HY1): 1-36.

xvii. Misri, R.L., Ranga Raju, K.G. and Garde, R.J. (1984). Bed load transport of coarse non uniform sediments, J. of Hydraulic Engineering, ASCE, Vol.110, No.3, pp.312–328.

xviii. M. Habibi, (1994), Sediment transport estimation methods in river systems University of Wollongong.

xix. Nakato, T. (1990). "Tests of Selected Sediment Transport Formulas," J. Hydr. ASCE, Vol. 116, No. 3, pp. 362-379.

xx. Samaga, B. R., Ranga Raju, K. G., and Garde, R. J. (1986 a). "Bed load transport of sediment mixtures." J. Hydr. Engrg., ASCE, 112(11), 1003-1018.

xxi. Samaga, B.R., Ranga Raju, K.G. and Garde R.J. (1986 b). Suspended load transport rate of sediment mixture, J. of Hydraulic Engineering, No.11, pp.1019–1038.

xxii. Shen, H.W., and C.S. Hung (1972). "An Engineering Approach to Total Bed-Material Load byRegression Analysis," Proceedings of the Sedimentation Symposium, ch. 14, pp. 14-1 through 14-1 7.

xxiii. Shu-Qing Yang and Siow-Yong Lim (2003), Total load transport formula for flow in Alluvial channels, Journal of hydraulic engineering, Vol. 129, pg 68-72, ASCE, ISSN 0733-9429/2003

xxiv. Swamee P.K and Ojha P. C (1991) Bed-load and suspended-load transport of non-uniform sediments,Journal of hydraulic engineering, vol.117, ASCE, ISSN 0733-9429/91/0006-pp No. 25868.

xxv. S. K. Sinnakaudan, A. Ab Ghani, M. S. S. Ahmad and N. A. Zakaria, (2006),Multiple Linear Regression Model for Total Bed Material Load Prediction, Journal of Hydraulic Engineering, Vol. 132, No. 5, ASCE, ISSN 0733-9429/2006/5-521–528.

xxvi. Toffaleti, F.B. (1968). A procedure for computation of the total river sand discharge and detailed distribution, bed to surface, Technical Report No.5, US Army Corps of Engineers, Vicksburg, Miss.

xxvii. Toffaleti F. B. (1969), Definitive computations of sand discharge in rivers,Proceedings of the American Society of Civil Engineers, Volume 95, No. HY1.

xxviii. Van Rijn, L.C. (1984 a). Sediment transport, part I: bed load transport, J. Hydr. Engi., ASCE, Vol 110, No. HY10, 1431–1456.

xxix. Van Rijn, L.C. (1984 b). Sediment transport, part II: suspended load transport, J. Hydr. Engi., ASCE, Vol 110, No. HY10, 1431–1456

xxx. White, W.R., H. Milli and A.D. Crabbe1973.. Sediment Transport: An Appraisal of Available Methods. Vol. 2, Report No. INT 119, Hydraulics Research Station, Wallingford, England, Nov.

xxxi. White, W. R., Milli, H., and Crabbe, A. D. (1975). "Sediment Transport Theories: Review," Proc. Inst, of Civil Engineers, London, England, Part 2, Vol. 59, pp.265-292.

xxxii. Wu W. Wang S.S.Y. and Jia Y. (2000), Non-uniform sediment transport in alluvial rivers,Journal of Hydraulic Research, IAHR, Vol..38, No6

xxxiii. Yalin, M.S. (1972), Mechanics of Sediment Transport, Pergamon Press.

xxxiv. Yang, C.T., 1979. Unit stream power equations for total load. J. Hydrol., 40: 123--138.

xxxv. Yang C.T. (1984), Unit Stream Power Equation for Gravel, Journal of Hydraulic Engineering, ASCE, vol. 1 10, no. 12, pp. 1783-1 797.

xxxvi. Yalin M.S. (1992), River Mechanics, Oxford, Pergamon Press

xxxvii. Yang C.T. (2002), Sediment Transport and Stream Power, International Journal of Sediment Research, vol. 17, no. 1, Beijing, China, pp. 3 1-38.